CONF-9508133--

PROCEEDINGS

COAL LIQUEFACTION AND GAS CONVERSION CONTRACTORS REVIEW CONFERENCE

Westin William Penn Hotel
Pittsburgh, Pennsylvania

August 29–31, 1995

Sponsored by: The U.S. Department of Energy
Pittsburgh Energy Technology Center

DISCLAIMER

TABLE OF CONTENTS

DIRECT LIQUEFACTION

INDIRECT LIQUEFACTION

GAS CONVERSION

AR - LIQUEFACTION

DIRECT LIQUEFACTION

RATIONALE FOR CONTINUING R&D IN DIRECT COAL CONVERSION TO PRODUCE HIGH QUALITY TRANSPORTATION FUELS

R.D. Srivastava and H.G. McIlvried
Burns and Roe Services Corporation
P.O. Box 18288
Pittsburgh, PA 15236
D. Gray and G.C. Tomlinson
The Mitre Corporation
McLean, VA 22102
E.B. Klunder
Pittsburgh Energy Technology Center
Pittsburgh, PA 15236

ABSTRACT

For the foreseeable future, liquid hydrocarbon fuels will play a significant role in the transportation sector of both the United States and the world. Factors favoring these fuels include convenience, high energy density, and the vast existing infrastructure for their production and use. At present the U.S. consumes about 26% of the world supply of petroleum, but this situation is expected to change because of declining domestic production and increasing competition for imports from countries with developing economies. A scenario and time frame are developed in which declining world resources will generate a shortfall in petroleum supply that can be alleviated in part by utilizing the abundant domestic coal resource base. One option is direct coal conversion to liquid transportation fuels. Continued R&D in coal conversion technology will result in improved technical readiness that can significantly reduce costs so that synfuels can compete economically in a time frame to address the shortfall.

BACKGROUND

The United States continues to rely heavily on liquid fuels for transportation, and, in spite of the strong interest in using alternative fuels, hydrocarbon liquids will continue to play a significant role in our energy future. This is primarily because of their convenience, high energy density, and the enormous infrastructure in place for their production, distribution, and end-use. Currently, the U.S. consumes about 17.5 million barrels per day (BPD) of oil (about 35 quads/yr - 1 quad/yr equals approximately 500,000 BPD). Of this, 75% is used by the transportation sector.

Current domestic crude production is 6.6 million BPD, having steadily declined from 9 million BPD ten years ago at a decline rate of about 3%/yr. Currently, the U.S. imports over 50% of its petroleum, and the Energy Information Administration (EIA)[1] predicts that this will increase to 68% by the year 2010.
The U.S. currently uses 26% of the world's total petroleum production. Even if this percentage were to remain constant, a signif-

icant shortfall in the petroleum supply in the U.S. is likely to occur because of declining domestic production. Because of competition from rapid economic development worldwide, the U.S. may not be able to import sufficient oil to meet future demand.

Coal resources in the U.S. are enormous. EIA estimates total reserves at 1.7 trillion short tons. Coal represents an inexpensive, domestic resource that can be used as a feedstock to produce clean, high-quality transportation fuels in an environmentally sound manner.

The Department of Energy (DOE) Fossil Fuel Energy's R&D program has been largely responsible for technological improvements in coal liquefaction in the U.S. The goal of the DOE program is to develop and demonstrate coal liquefaction technology that is competitive with crude oil at $25-30/bbl in 1993 dollars. The purpose of this program is to reduce vulnerability to energy supply disruptions, to create new high wage jobs, and to do this while respecting the environment.

THE WORLD ENERGY PICTURE

At the last World Energy Congress meeting in 1992[2], MITRE presented a world energy demand model that was used to estimate total commercial world energy demand to the year 2100. If energy use efficiency does not improve, estimated world demand will reach 2,090 quads by 2100. If energy conversion and end-use efficiencies continue to improve, the world's commercial energy demand will be reduced from 2,090 quads in the no-efficiency-improvement case to about 1,050 quads in 2100. However, even with efficiency improvements, world energy demand will still increase three-fold over the present level of 350 quads per year.

The question is whether this demand can be satisfied with known energy resources. To answer this, the world resources of oil and natural gas must be determined. The United States Geological Survey[3] estimates the world's ultimate resource of conventional oil as 1.7 trillion barrels (about 10,000 quads). Estimates for natural gas are less certain; therefore, a range was assumed: 10,000-20,000 trillion cubic feet[4] (TCF) (10,000-20,000 quads).

Figure 1 shows resource depletion curves. By 2100 oil will be essentially depleted, and natural gas will either be depleted or in rapid decline. Although not shown on the figure, coal availability worldwide is enormous. Estimates range from 45,000 quads[5] for proved reserves to 240,000 quads[6] for the total resource, between 500 and 2000 years supply at current usage rates.

The estimated conventional fossil energy resource and the postulated world energy demand scenario can be combined to produce a world energy demand/supply scenario as shown in Figure 2. In this scenario, it is assumed that oil, gas, and present day nuclear use follow the depletion curves shown, coal use remains constant at the present level, and hydroelectric power supply triples between now

and the year 2100. The area designated as "21st Century" represents the energy shortfall. In this constant coal use scenario, the shortfall will have to be supplied by advanced nuclear energy technologies and renewable or sustainable energy technologies.

Figure 2 shows that before the year 2030, and perhaps as early as 2010, the demand on world oil is such that supply cannot keep pace, and the world oil supply starts to decline. This scenario is optimistic, since it assumes that world oil use is essentially constant from the present to 2030. However, world oil use is actually increasing, so that the imbalance of oil supply and demand will occur before 2030. If the world energy demand scenario presented above is credible, then the world may have less than 30 years before a significant shortfall in conventional liquid fuel supplies occurs.

THE UNITED STATES ENERGY PERSPECTIVE

Let us now concentrate on the situation in the U.S. The U.S. annually produces about 17 quads of domestic crude oil and natural gas liquids (NGL), and this production is declining. Figure 3 shows a resource depletion scenario from the present to the year 2100 for oil, natural gas, and power from current nuclear plants (nuclear energy from current technologies is assumed to phase out over the time period shown). It is evident from Figure 3 that the declining domestic energy supply, especially liquid fuels, must be made up by expanding petroleum imports or by increasing the use of our domestic coal reserves.

The ability of the U.S. to import oil may be limited. Two import scenarios which may be applied to the U.S. energy situation from now until 2050 are (1) the U.S. will continue to consume 26% of total world petroleum and (2) the U.S. will import a fraction of the world's oil that is proportional to the U.S. GDP compared to the world GDP. In both cases, the supply of oil to the U.S. declines early in the next century.

Two U.S. demand scenarios may be considered. The higher demand scenario is from the EIA, and the essentially constant demand scenario is from the MITRE energy model. Depending on which scenario is selected, a shortfall in petroleum supply (domestic production plus imports) begins somewhere in the 2005-2015 time period and becomes significant by 2010-2030. The probable shortfall is between 1 and 3.5 million BPD in 2030. This is illustrated in Figure 4.

MEETING THE SUPPLY SHORTFALL

One alternative to meet this supply shortfall is to produce liquid fuels from coal. In direct liquefaction, coal reacts with hydrogen in a hydrogen donor solvent vehicle to produce a distillate product that can be refined into liquid transportation fuels. The product from direct coal liquefaction is easy to refine because it is an all-distillate, low sulfur and nitrogen liquid. Transportation

fuels that meet the strict environmental regulations expected to be in force in the next century can be made from domestic coals.

If coal conversion is to play a significant role in alleviating the liquid fuel supply problem before the year 2030, then the liquefaction technologies must be in a state of readiness for commercial deployment about 15 years earlier, because lead times for the introduction of new energy technologies are on the order of 10 to 15 years, even after the technologies are technically ready for commercial deployment. Although direct liquefaction technology has undergone very significant improvements over the past decade and achieved a high level of technical readiness, it is still not cost competitive. Therefore, continuing R&D is needed to reduce costs to meet the target of 2015 for the start of commercial deployment. Further R&D can achieve additional process improvements to permit earlier introduction of coal-derived transportation fuels into the marketplace.

Current liquefaction program activities cover all aspects of technology development from basic and exploratory research through bench-scale operations to proof-of-concept (POC) demonstration. The four integrated elements of the direct liquefaction program are development of the catalytic two-stage direct liquefaction process, coprocessing development, advanced liquefaction concepts development, and POC (3 ton/day) testing of promising technologies.

To help identify the high-cost elements of direct coal liquefaction, DOE contracted with Bechtel[7] to develop a conceptual commercial design of a direct coal liquefaction facility to produce hydrotreated distillate products from either bituminous or subbituminous coal. The Bechtel design, which represents the current state of the art for direct liquefaction, yielded a cost of about $34/bbl of crude oil equivalent (COE). Although higher than the present world oil price (WOP) of about $17/bbl, this cost is significantly lower than earlier estimates of $40-50/bbl because of process improvements from the R&D undertaken over the last decade. Because direct liquefaction technology is still evolving and additional process improvements are expected, costs will decrease further as improvements are incorporated.

THE IMPACT OF CONTINUING R&D ON DIRECT COAL LIQUEFACTION COSTS

Table 1 shows the elements of cost for the baseline direct liquefaction conceptual commercial plant and the estimated reduction in cost that can be achieved by further R&D. Areas of most importance in reducing costs include decreasing capital investment, improving product yields, and reducing catalyst cost.

Several opportunities are available for reducing capital investment, such as increasing space velocity to reduce the number of liquefaction reactor trains and improving H_2 production. Replacing the current ebullated bed reactors with slurry reactors decreases the COE cost by about $1-2/bbl. By employing advanced technologies now under development, the capital cost of H_2 production can be

decreased by an estimated 12% with a resulting decrease in the COE cost of about $1/bbl.

Product quality improvement is equally important. One way to do this is to increase the yield of products boiling below 850°F. An increase of 10% in these products will decrease the COE cost by about $3/bbl. Catalyst costs are a significant contributor to product costs. If 90% of the catalyst can be recovered and reused, the COE cost will be reduced by about $2/bbl.

The high probability of achieving the improvements discussed above suggests that a $6/bbl decrease in the COE price to about $28/bbl is readily achievable. The R&D strategy is to concentrate efforts over the next few years in the high potential areas listed above. With no further R&D, direct coal liquids will remain at the Bechtel baseline cost of about $34/bbl of COE, and coal liquids would not be competitive with petroleum until 2030. With continued R&D, the cost of direct liquids will be reduced to about $28/bbl ($0.67/gal) and be competitive in 2017, 13 years earlier.

STRATEGY FOR DEVELOPING A COMMERCIAL COAL LIQUEFACTION INDUSTRY

Once cost competitiveness is achieved, the next step is to achieve commercialization. Initial pioneering production of coal-derived transportation fuels will require a capital expenditure of $3.8 to $4.6 billion for each plant to produce about 70,000 BPD of liquid fuels; it may require five to seven years to achieve full production. Because of the costs involved, coal-derived liquid fuels will probably not make a major contribution to the nation's transportation fuel needs until a significant imbalance between crude oil supply and demand occurs, expected sometime between 2015 and 2030.

The liquefaction plants to produce coal-derived fuels will be designed to meet the highest standards for environmental compliance. The transportation fuels produced by coal liquefaction technologies will be environmentally superior to their petroleum-derived counterparts and will be capable of meeting all requirements of the 1990 Clean Air Act Amendments. Coal liquefaction technologies can also be utilized to co-convert wastes, such as plastics, to environmentally acceptable fuels.

The key to commercialization will be integration with the existing petroleum refining/distribution infrastructure. In achieving commercialization, two intermediate technologies are important. The first is coprocessing of petroleum-derived wastes (plastics, tires, waste oil) with coal. Development of this technology is being driven by dwindling landfill availability and increases in tipping fees. These additional incentives may permit early implementation of this technology. The second technology is coprocessing of coal with heavy petroleum resids or oils. This technology is seen as being commercially feasible as a mid-term option and is likely to account for the first production of coal-based transportation fuels in existing petroleum refineries.

THE CONTRIBUTION OF DIRECT COAL LIQUEFACTION TO THE U.S. ECONOMY

If construction of coal liquefaction plants can be initiated in the year 2012, one million BPD capacity could be in place by 2030. Although direct coal liquefaction would only provide a portion of the energy mix needed to address the U.S. shortfall, production of high quality transportation fuels from U.S. coal will constitute a new and growing domestic industry that will employ engineering and construction personnel, plant operators, coal miners, and related workers. An estimated 333,000 jobs would be created by a one million BPD industry.

Demonstrating the ability to produce coal-derived transportation fuels at $28/bbl by the year 2010 could have the effect of moderating the world oil price at $28/bbl from 2017 onwards with consequent savings to the U.S. economy of up to $200 billion (1993 dollars) between 2015 and 2030. An R&D program that can reduce dependence on oil imports, help in providing national energy security, provide domestic jobs, and save $200 billion in balance of payments is a sound investment in the nation's future.

CARBON DIOXIDE EMISSIONS

Concern has been expressed that increased coal use will result in excessive emissions of carbon dioxide into the atmosphere, thereby exacerbating the potential for global warming. Figure 5 shows the energy mix that will result in no further increase in annual carbon dioxide emissions in the U.S. over the present. This figure shows that, because of the decrease in oil and gas, coal use can be increased substantially after 2015 with no net increase in annual carbon dioxide emissions. Coal use can be increased by about 7 quads over present consumption by 2030 with no further increase in carbon dioxide emissions. If this amount of coal were used for production of liquid fuels, about two million BPD of coal-derived fuels could be produced.

CONCLUSION

Because of the long-term nature of the market opportunity and the consequent long wait for return on investment, without government participation, private industry is unlikely to fund these activities. Therefore, continued government support for laboratory, bench, and POC activities is essential to continue the development of transportation fuels from coal.

The analysis presented in this paper clearly shows that the world will need substantial amounts of "new" energy to continue economic progress in the next century. The U.S. has the opportunity to develop coal liquids technology that will help ensure our continued economic prosperity by creating a new industry with highly skilled jobs and providing opportunity for export of U.S. technology on the world market without compromising environmental quality.

References

1. Energy Information Administration, "Annual Energy Outlook 1995," January 1995.
2. Gouse, S.W., D.Gray, G.C. Tomlinson, D.L. Morrison, "Potential World Development through 2100: The Impacts on Energy Demand, Resources, and the Environment," World Energy Council Journal, December 1992.
3. USGS, 14th World Petroleum Congress, Norway, May 1994.
4. Masters, C.D., "Oil and Gas - Where in the World and Why?" 8th V.E. McKelvey Forum on Mineral and Energy Resources, Houston, TX, February 1992.
5. World Resources Institute, "People and the Environment," Oxford University Press, 1994.
6. Institute of Gas Technology, "World Reserves Survey 1987," 1989.
7. Bechtel and Amoco, "Direct Coal Liquefaction Baseline Design and System Analysis," report prepared for DOE under Contract DE-AC22-90PC89857, March 1993.

Table 1. Estimated Cost Impact of Continued R&D on Direct Liquefaction

Cost Elements, $MM	Baseline 28,776 tpd	Increased Space Velocity	Improvement in Yield	Catalyst Recovery & Recycle	Improvement in Hydrogen Production
Coal Handling	222	222	226	226	226
Liquefaction	941	762	762	822	822
Gas Cleanup/Byprd Rec.	297	297	297	297	297
Product Hydrotreating	107	107	113	113	113
ROSE Unit	46	46	43	43	43
Gasification	334	334	342	342	302
Air Separation	244	244	250	250	220
ISBL Field Cost	2192	2013	2034	2094	2024
OSBL Field Cost	978	978	981	978	968
Total Field Cost	3170	2991	3015	3072	2992
Total Capital	3889	3669	3699	3768	3670
Refined Product Cost, $/bbl					
Capital*	23.61	22.25	20.37	20.77	20.23
Coal	7.84	7.85	7.51	7.51	7.51
Catalyst	2.57	2.58	2.33	0.23	0.23
Natural Gas	3.59	3.45	2.90	2.74	2.69
Labor	1.66	1.67	1.51	1.51	1.51
Other O&M	0.33	0.33	0.29	0.29	0.30
By-Product Credits	(4.18)	(4.05)	(3.43)	(3.29)	(3.25)
RSP	35.42	34.08	31.48	29.76	29.22
Quality Premium	(1.19)	(1.19)	(1.19)	(1.19)	(1.19)
COE	34.23	32.89	30.29	28.57	28.03
Plant Output, million bbl/yr	24.16	24.16	26.58	26.58	26.58

*Includes maintenance materials, taxes, and insurance.

Figure 1

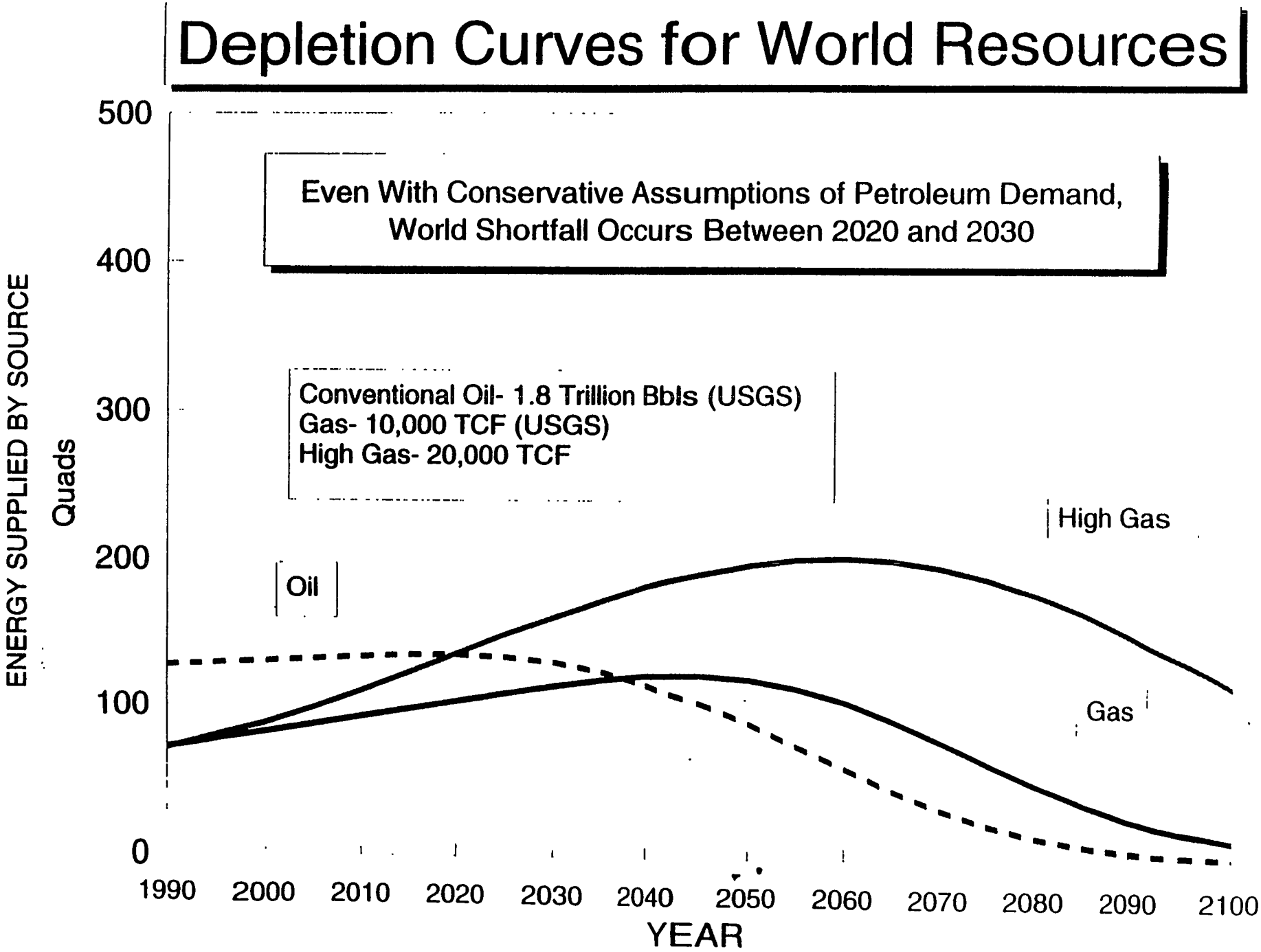
Depletion Curves for World Resources
Even With Conservative Assumptions of Petroleum Demand,
World Shortfall Occurs Between 2020 and 2030
Conventional Oil- 1.8 Trillion Bbls (USGS)
Gas- 10,000 TCF (USGS)
High Gas- 20,000 TCF
High Gas
Oil
Gas
ENERGY SUPPLIED BY SOURCE
Quads
500
400
300
200
100
0
1990
2000
2010
2020
2030
2040
2050
2060
2070
2080
2090
2100
YEAR

Figure 2

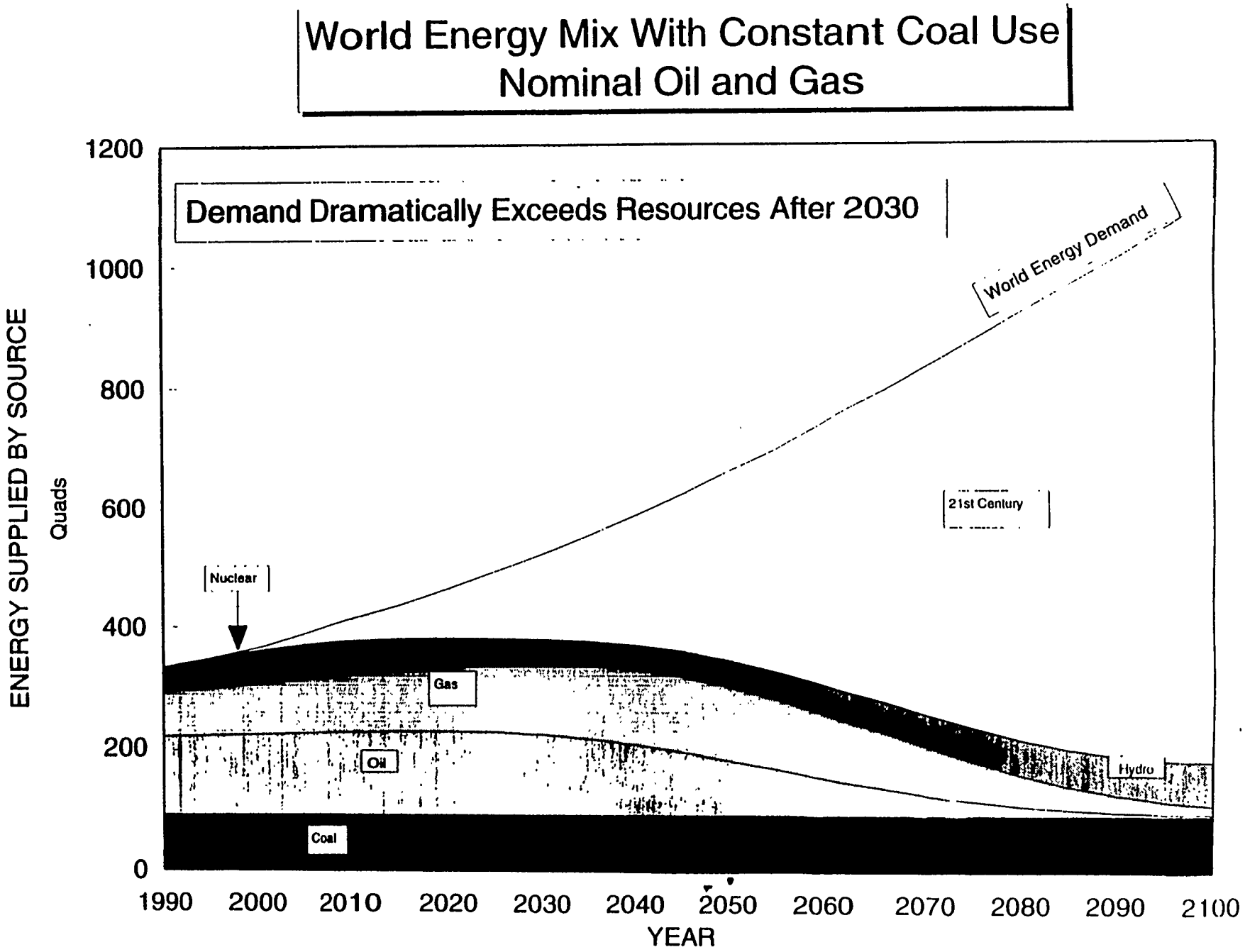
World Energy Mix With Constant Coal Use
Nominal Oil and Gas
Demand Dramatically Exceeds Resources After 2030
ENERGY SUPPLIED BY SOURCE
Quads
1200
1000
800
600
400
200
0
World Energy Demand
21st Century
Nuclear
Gas
Oil
Coal
Hydro
1990
2000
2010
2020
2030
2040
2050
2060
2070
2080
2090
2100
YEAR

Figure 3

Projected U.S. Energy Production

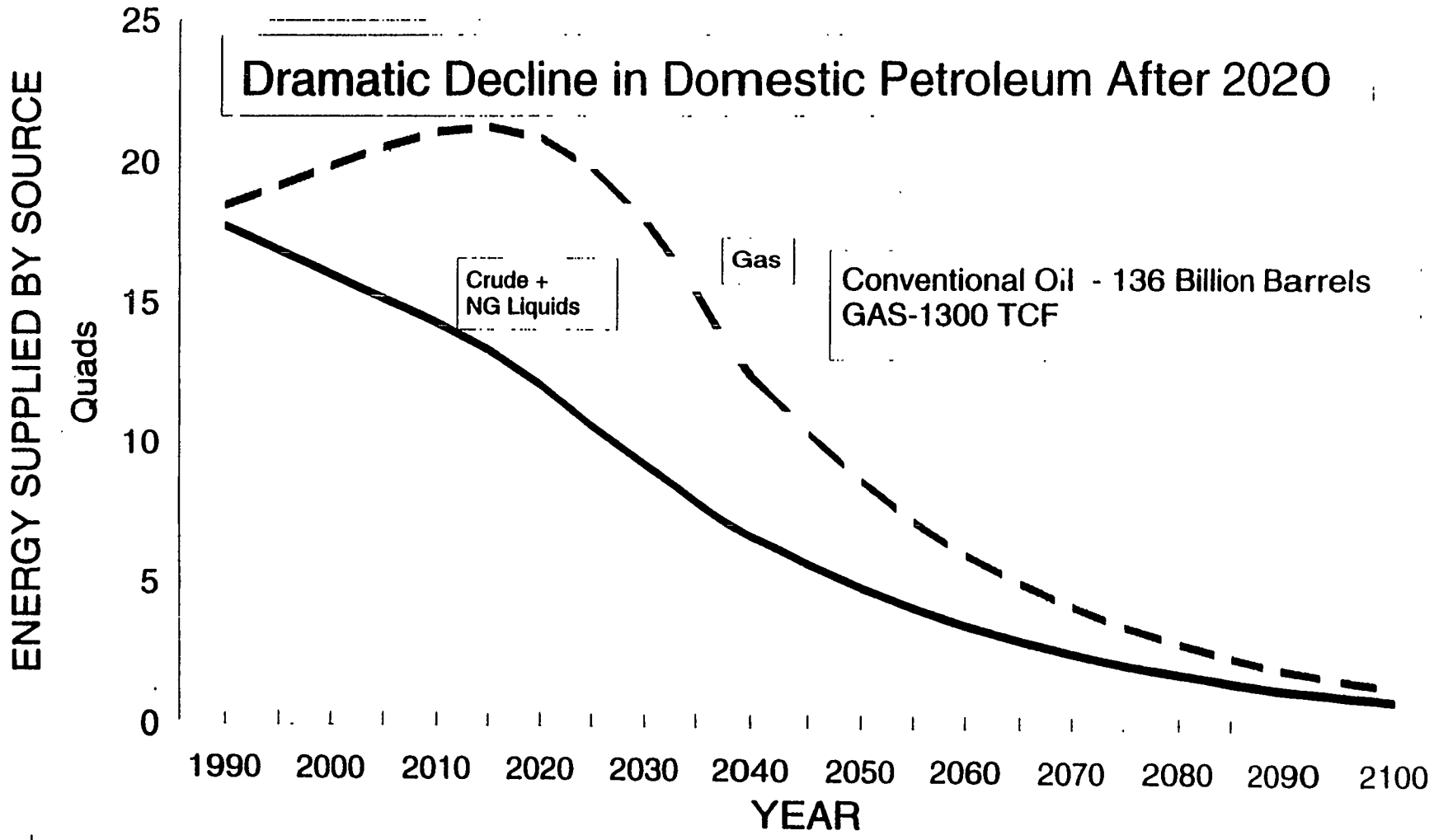

EIA Projections to 2010 Followed By MITRE Projection Of Resource Depletion

Figure 4

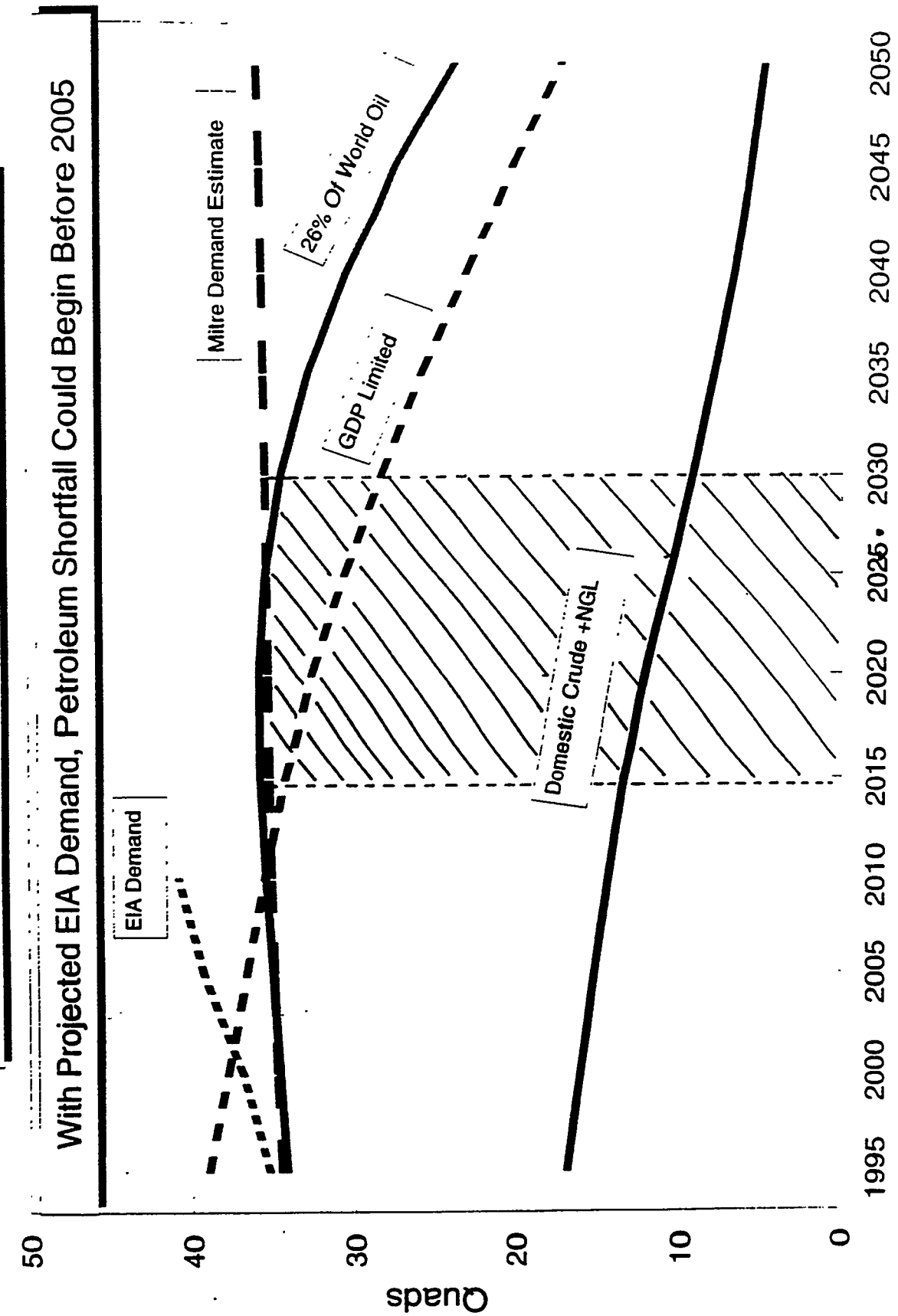
U.S. Oil Supply And Demand Scenarios
With Projected EIA Demand, Petroleum Shortfall Could Begin Before 2005
EIA Demand
Mitre Demand Estimate
26% Of World Oil
GDP Limited
Domestic Crude +NGL
Quads
50
40
30
20
10
0
1995
2000
2005
2010
2015
2020
2025
2030
2035
2040
2045
2050
Year

Figure 5

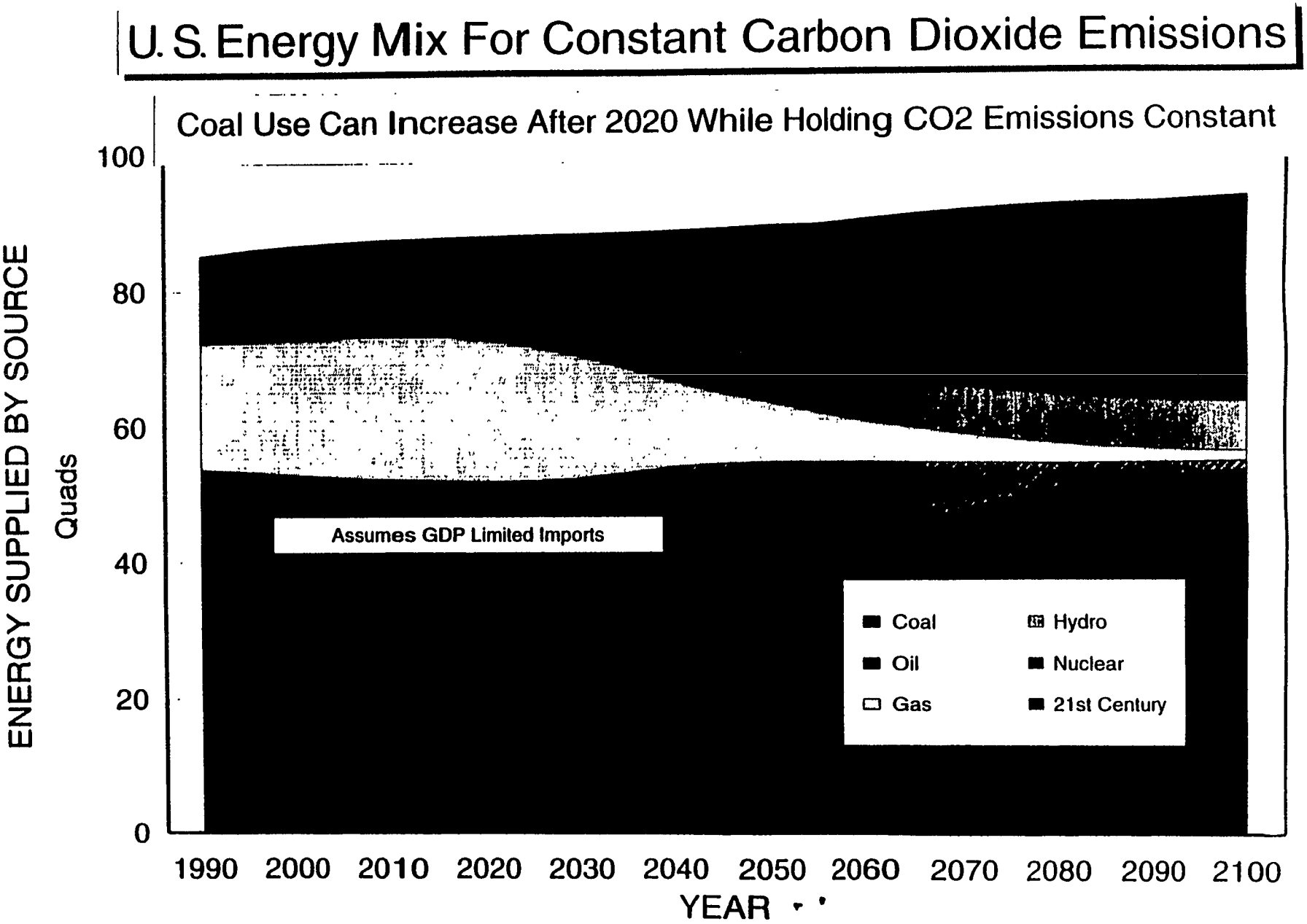
U. S. Energy Mix For Constant Carbon Dioxide Emissions
Coal Use Can Increase After 2020 While Holding CO2 Emissions Constant
ENERGY SUPPLIED BY SOURCE
Quads
100
80
60
40
20
0
Assumes GDP Limited Imports
Coal
Oil
Gas
Hydro
Nuclear
21st Century
1990
2000
2010
2020
2030
2040
2050
2060
2070
2080
2090
2100
YEAR

CASE STUDIES ON DIRECT LIQUEFACTION OF LOW RANK WYOMING COAL

Paul Adler, Sheldon J. Kramer and Syamal K Poddar
(Bechtel Corporation, San Francisco, CA)

CONTRACT NUMBER: DE-AC22-90PC89857

PERIOD OF PERFORMANCE; April, 1993 to February 15, 1995

ABSTRACT

Previous Studies have developed process designs, costs, and economics for the direct liquefaction of Illinois No. 6 and Wyoming Black Thunder coals at mine-mouth plants. This investigation concerns two case studies related to the liquefaction of Wyoming Black Thunder coal. The first study showed that reducing the coal liquefaction reactor design pressure from 3300 to 1000 psig could reduce the crude oil equivalent price by 2.1 $/bbl provided equivalent performing catalysts can be developed. The second one showed that incentives may exist for locating a facility that liquefies Wyoming coal on the Gulf Coast because of lower construction costs and higher labor productivity. These incentives are dependent upon the relative values of the cost of shipping the coal to the Gulf Coast and the increased product revenues that may be obtained by distributing the liquid products among several nearby refineries.

INTRODUCTION

This study is an extension of DOE Contract Number DE-AC22-90PC89857 (which started in 1990) in which several process designs and economics were developed for direct coal liquefaction facilities processing Illinois No. 6 coal at a mine-mouth location in southern Illinois[1-5]. ASPEN process flowsheet simulation (PFS) models also were developed for the Baseline design case and the following optional cases:

- Additional coal cleaning by heavy media separation
- Additional coal cleaning by heavy media separation and spherical agglomeration
- Thermal-catalytic liquefaction reactor configuration
- Catalytic-catalytic liquefaction reaction configuration with vent gas separation
- Fluid coking as a alternate vacuum bottoms processing option
- Hydrogen production by steam reforming of natural gas
- Addition of a naphtha reforming plant

As the above designs were being developed, additional pilot plant data became available from the advanced coal liquefaction facility at Wilsonville, Alabama. Thus, the contract was extended to develop a design, economics and an ASPEN PFS model for an Improved Baseline case based on this higher space velocity data[4,5]. An additional case based on this Improved Baseline design also was developed which produced the required hydrogen by steam reforming of natural gas rather than by coal gasification.

In April, 1993, this contract was modified to develop two designs, economics and ASPEN PLUS simulation models for a direct liquefaction facility processing a low rank, sub-bituminous Black

Thunder coal at a mine-mouth plant located near Gillette Wyoming. The results for the base case design with hydrogen production by coal gasification and for one where hydrogen is produced by steam reforming of natural gas have been reported[6-8].

This paper reports on the results of two case studies based on the low rank coal liquefaction design. The first study considers the hypothetical effects on the design and economics of reducing the design pressure of the coal liquefaction reactors from 3300 psig to 2000 psig and to 1000 psig. The second one considers the effects of relocating the plant from Gillette, Wyoming to the Louisiana Gulf Coast.

LOW RANK COAL PROCESS DESIGN

Table I shows the properties of the low rank coal from the Black Thunder mine which was used in this study. HRI Inc. developed the process design for the high pressure coal liquefaction reactor section utilizing a two-stage ebulated-bed catalytic reactor system[9]. This design is based on data from Wilsonville pilot plant runs 262E and 263J[7-9]. The coal liquefaction reactors have a design pressure of 3300 psig although the first stage reactors operate at 3100 psig.

Figure 1 is a simplified block flow diagram of the main processing area for the entire base case design. Not shown in this figure are the air separation plant, sulfur recovery plant, phenol recovery plant, and other offsite plants. Run of Mine coal enters the complex through the coal screening, crushing and grinding plant (Plant 1) where partial drying is achieved in the presence of a nitrogen purge. Coal containing 6.3 wt% ash (MF) is further dried to a moisture level of 2.0 wt% in a slurry drier (Plant 1.4) before entering the coal liquefaction plant (Plant 2).

The light products from the coal liquefaction plant are sent to the gas plant (Plant 3) to separate the fuel gas, propane and mixed butanes. The C5-350 F stream goes to the naphtha hydrotreater (Plant 4). The 350-850 F fraction from Plant 2 goes to the gas oil hydrotreater (Plant 5). Hydrogen is produced by coal gasification in Plant 9. The bottoms from the coal liquefaction plant goes to a Kerr-McGee Rose-SR unit (Plant 8) which produces an extract stream that is recycled back to Plant 2 and an ash concentrate stream that goes to the gasification section of Plant 9. The oxygen required by the Texaco gasification section of Plant 9 is produced in the air separation plant (Plant 10).

The hydrogen purge from Plant 2 is recovered by the hydrogen purification plant (Plant 6) which is a combination of membrane and PSA units. The purified hydrogen goes to Plants 2 and 5. Sulfur is produced in a sulfur recovery plant (Plant 11). The sour water collected from the various plants is sent through an ammonia recovery plant (Plant 38) before going either to the coal gasification plant or to the phenol recovery plant (Plant 39) followed by a waste water treatment plant (Plant 34).

Table II shows the major input and output flows from the plant on a stream day basis. From 24,952 tons/day of dry ROM coal from the Black Thunder mine, this plant produces 67,312 bbls/day of C4+ hydrocarbons. The naphtha is only 10% of the C5+ liquids production (naphtha, distillates and gas oil). In addition, this plant produces significant amount of byproducts; 167 tons/day of ammonia, 127 tons/day of liquid sulfur, and 45 tons/day of mixed phenols.

EFFECT OF LIQUEFACTION REACTOR DESIGN PRESSURE

Direct coal liquefaction is a capital intensive process as has been demonstrated in numerous previous studies. For the above described low rank coal liquefaction design, the costs associated with the coal liquefaction plant are about 28% of the installed field costs (total ISBL and OSBL costs) of the liquefaction facility. A good portion of these costs can be attributed to the cost of the large thick-walled high pressure reactors, other high pressure vessels, and the compressors required to supply the high pressure hydrogen-rich gas. Therefore, this study was made to determine the incentives for conducting catalyst and process research to develop coal liquefaction catalysts which will operate at lower pressures.

Since these catalysts do not yet exist and insufficient thermodynamic, kinetic and hydrodynamic data are available for a complete and detailed study, this is a somewhat hypothetical study. Therefore, the following assumptions were made.

- The kinetics of the coal liquefaction reaction remains unchanged as a function of pressure.
- The coal liquefaction reaction product distribution and product composition are independent of the coal liquefaction pressure.
- Most stream compositions are independent of the coal liquefaction pressure.
- The cost of the new coal liquefaction catalysts which will operate at low pressure are the same as those which are used in the base low rank coal design case.
- There is no effect of coal liquefaction pressure on either the design or cost of the OSBL plants.
- There is no net effect of coal liquefaction pressure on the total utilities consumed by the entire facility. This is a conservative assumption that will underestimate the cost savings of lower liquefaction reactor pressures because less power is required to compress the make-up hydrogen and pump the liquids into the liquefaction reactors.

Besides the major effect of reaction pressure on the cost of the coal liquefaction plant, the coal liquefaction pressure may have a small effect on the cost of some of the other processing plants.

Plants 1 and 1.4 - The Coal Crushing, Grinding and Drying Plants -- The coal liquefaction pressure has no effect on these plants.

Plant 3 - The Gas Plant -- This plant uses lean oil absorption at 200 psig to recover light hydrocarbons from several gas streams. Since this pressure is well below the lowest coal liquefaction reactor design pressure of 1000 psig which is being studied, the coal liquefaction pressure has no effect on this plant.

Plant 4 - The Naphtha Hydrotreater -- The naphtha hydrotreater reactor operates at about 1000 psig. The naphtha feed comes from either intermediate storage or the low pressure fractionation section of Plant 2 and has to be pumped up to reactor pressure. The make-up hydrogen comes from either the Plant 3 (gas plant) or Plant 9 (coal gasification plant), and consequently, is independent of the coal liquefaction reactor pressure. In either case, these make-up hydrogen streams have to be compressed to the naphtha hydrotreater reactor pressure. Therefore, there is no effect of liquefaction reactor pressure on this plant.

Plant 5 - The Gas Oil Hydrotreater -- The gas-oil hydrotreater reactor operates at about 2600 psig. The distillate and gas oil feeds come from either intermediate storage or the low pressure fractionation section of Plant 2 and have to be pumped up to reactor pressure. The make-up hydrogen comes from either Plant 2 (coal liquefaction plant), Plant 3 (gas plant), or Plant 9 (hydrogen production by coal

gasification plant). The make-up hydrogen streams from Plants 3 and 9 always have to be compressed to the gas oil hydrotreater reactor pressure. Only when the coal liquefaction reactor pressure is below the gas oil hydrotreater reactor pressure does the hydrogen-rich stream from the coal liquefaction plant require compression. Thus, for the coal liquefaction reactor pressure cases at 1000 and 2000 psig, an additional make-up hydrogen-rich gas compressor is needed. Consequently, the ISBL cost of Plant 5 increases as the liquefaction reaction pressure decreases.

Plant 6 - The Hydrogen Purification Plant -- The hydrogen purification plant has two major sections. The first section is a high pressure section which recovers hydrogen by membrane permeation from the high pressure purge gas from the coal liquefaction and gas oil hydrotreating plants. In this section, the key parameter for the hydrogen separation is the pressure difference across the membranes. The second section is a low pressure section which recovers hydrogen by pressure swing adsorption (PSA) from the lower pressure purge gas from the coal liquefaction, naphtha hydrotreating, gas oil hydrotreating, and gas plants. The cost of this section of the plant is independent of the liquefaction reaction pressure. However, the overall cost of Plant 6 does vary with liquefaction pressure. As the liquefaction reaction pressure decreases, so does the ISBL cost of this plant.

Plant 8 - The ROSE-SR Critical Solvent Deashing Plant - The feed to this plant comes from the bottom of the vacuum tower of Plant 2. Consequently, the coal liquefaction pressure has no effect on this plant.

Plant 9 - The Hydrogen Production by Coal Gasification Plant -- The cost of the hydrogen production by coal gasification plant is independent of the liquefaction reaction pressure except for the final hydrogen compressor. This machine compresses the product hydrogen going to Plants 2 and 6. Thus, the cost of this plant decreases as the liquefaction reaction pressure decreases only because a smaller compressor is required to supply that portion going to Plant 2.

Table III compares the fourth quarter 1993 capital costs of an Nth plant for the entire low rank coal liquefaction reactor complex at three liquefaction reactor design pressures; 3300, 2000 and 1000 psig. As the liquefaction reactor design pressure drops from 3300 psig to 1000 psig, the field cost of Plant 2 drops by 245 MM$ to 547 MM$; a decrease of about 31%. This corresponds to a drop in the total installed cost of the entire complex of 324 MM$ to 3368 MM$. However, this is only a drop of 8.8% in the cost of the entire coal liquefaction complex because so much of the cost of the facility is in either the other ISBL plants or the OSBL plants.

Figure 2 graphically shows the amount of COE reduction for the three cases. At a coal liquefaction reactor design pressure of 2000 psig, the crude oil equivalent (COE) price is about 1.3 $/bbl less than that at the 3300 psig liquefaction reactor design pressure. At a coal liquefaction reactor design pressure of 1000 psig, the COE price is about 2.1 $/bbl below that at the 3300 psig liquefaction reactor design pressure of the base case. This corresponds to about a 6.5% reduction of the COE when going from a 3300 psig to a 1000 psig liquefaction reactor design pressure.

Thus, there is a significant economic incentive for continuing catalyst and process research to lower the reaction pressure for direct coal liquefaction. Because of the large costs associated with all the other plants in the complex, the cost reduction is not as great as would be expected when only the coal liquefaction plant is considered. However, the savings could be more significant when considering the integration of a coal liquefaction facility into an existing petroleum refinery because the other processing plants and offsite facilities could already be available.

EFFECT OF PLANT LOCATION

A study was undertaken to determine the effect of relocating the base case coal liquefaction plant from the Wyoming mine-mouth location to a Gulf Coast location because of lower labor and operating costs. Construction costs are lower on the Gulf Coast as a consequence of the lower labor costs and higher productivity. Furthermore, there are more petroleum refineries in the area which allows the distribution of the products among several of them so that each of them can take maximum advantage of the coal liquids. Also, the option of several potential customers creates a more competitive market which, over the long term, could result in higher sales prices.

Table IV compares some cost differences between the Wyoming mine-mouth location and the Gulf Coast location. The average 1994 operator wage rate on the Gulf Coast is 12.00 $/hr which is significantly less than the 18.50 $/hr in Wyoming. Also, the overhead factor for worker benefits on the Gulf Coast is only 1.25 compared to a 1.40 factor in Wyoming. Construction and supervisory labor costs also are lower by a similar ratio.

Utility costs also are lower on the Gulf Coast. Fuel gas is about 10% less expensive. Raw water is significantly less expensive. It is only 20 cents per thousand gallons compared to $2.50 per thousand gallons at the Wyoming mine-mouth location.

The above lower labor and utility costs and a more skilled labor force on the Gulf Coast results in a lower installed plant cost at the Gulf Coast than in Wyoming. The design of the Gulf Coast plant essentially is the same as that of the base Wyoming plant with the 3300 psig coal liquefaction reactor design pressure. However, in order to save on coal transportation costs, Plant 1 still is located in Wyoming to crush and dry the ROM Black Thunder coal from 27.0 wt% moisture to 12.9 wt% moisture. It was assumed that drying the coal to 12.9 wt% moisture prior to shipping has no effect on its reactivity. Table V compares the costs of the Gulf Coast and Wyoming coal liquefaction plants in fourth quarter 1993 dollars. The installed cost of the Gulf Coast plant is 369 MM$ or 10% less than that of the Wyoming location.

The Bechtel transportation department estimated the cost of transporting the Black Thunder coal from the mine to the plant located on the Louisiana Gulf Coast along the Mississippi River to be 15 $/ton in large rail cars carrying over 100 tons per car. However, in actual practice this will be a negotiated price, and can vary. Therefore, in the subsequent economic analysis, a range of coal transportation costs will be studied.

In the Gulf Coast case, the ash will be returned to the mine for disposal in the same manner as is done in the base Wyoming case. Since the ash from the gasifier is in a vitrified state, it does not have to be shipped in closed containers and can be returned to the mine for disposal in the same railroad cars that are used to transport the coal to the Gulf Coast. Hence, the ash transportation cost will be the same as the coal transportation cost. In the Gulf Coast case, the ash disposal cost was assumed to be half that of the Wyoming case because the ash already is in the transportation mode from being shipped to the mine and will be handled by the same equipment used to ship the coal.

PIMS LP models were used to determine values for the coal liquefaction products. For the original study, a LP model of a typical mid-west refinery located in PADD II processing 150,000 bbls/day of crude was developed[5]. This model was developed before all the ramifications of the 1990 Clean Air Act Amendments were known and understood. Studies using this model showed that Wilsonville coal liquids were, on the average, 1.07 times more valuable to the refinery than the crude oil mix when the refinery was constrained to make the same product slate. Thus, by definition, the coal

liquefaction products were said to have a syncrude premium factor (SCP) of 1.07. This 1.07 SCP was used for the economic evaluation of the base low rank coal case at the Wyoming location[6-8].

Petroleum refineries located along the Gulf Coast are in PADD III and are configured differently than those in the mid-west. These refineries generally contain more heavy ends processing, such as gas oil hydrocracking and delayed coking units. Another LP model was constructed to represent a typical PADD III refinery processing 150,000 bbls/day of an average PADD III crude mix [8]. Unlike the LP model of the PADD II refinery, this model contains processing units that are capable of producing reformulated gasoline and low sulfur diesel fuel. Six cases were studied, a base case that processed no coal liquids and five cases that processed various amounts of coal liquids. When the refinery was forced to process all the coal liquids produced by the liquefaction plant, the same SCP value of 1.07 was obtained. However, as the amount of available coal liquids was reduced, the SCP value increased. When the refinery processed 50% of the total coal liquids production, the SCP increased to 1.15; at 25% of the coal liquids production, it increased to 1.20; and when the refinery only processed 1,000 bbls/day of the coal liquids, the SCP increased to 1.25.

Because there is a concentration of petroleum refineries along the Gulf coast, the coal liquefaction facility has a larger possible customer base with an increased likelihood of distributing the products among several refineries. Thus, the liquefaction plant could increase its product revenue by distributing the coal liquids among several customers who would be willing to pay more for a portion of the production than a single buyer would pay for the entire amount. Economic evaluations were made at both the low and high SCP values of 1,07 and 1.25 to bracket the effect of the SCP value.

Although the LP models used to determine the SCP values are rigorous models, the calculated SCP values are much less rigorous because of several uncertainties. For example, the behavior of the coal liquids in the PIMS LP model was estimated based on limited published properties and processing data of similar coal liquids. Additional data are needed to better determine the behavior of these materials when processed in mixtures with conventional petroleum derived materials. Currently, a "Refining and End Use Study of Coal Liquids" is in progress to obtain such processing data for both direct and indirect coal liquids. Coal liquids from the POC facility are being upgraded mixed with conventional petroleum intermediates, and the results will be used to improve the LP models. Secondly, the LP models used in this study represented typical PADD II and PADD III petroleum refineries. Markedly different results could be obtained when models of specific refineries are used because each one has different unit capacities and processing constraints.

Finally, in the following economic calculations for both cases, no transportation costs for the coal liquids were assumed. Inclusion of liquids transportation coast will lower the product revenues, and correspondingly, the calculated COEs. However, if the liquids transportation costs are different, then this omission will favor that case with the lower costs. This omission should favor the Gulf Coast location because of the proximity of more refineries and the availability of water transport. However, the magnitude of this omission cannot be calculated without knowing specific locations, refineries and means of transportation.

Figure 3 shows the effect of the coal transportation cost on the COE difference between the Gulf Coast and Wyoming locations for the lowest and highest syncrude premium values. At the lowest syncrude premium value of 1.07, the Gulf Coast location is more favorable when the coal transportation cost is less than about 9.0 $/ton. Above a coal transportation cost of 9.0 $/ton, it is better to locate the plant in Wyoming. However, when the syncrude premium has a value of 1.25, the Gulf Coast location is more favorable when the coal transportation cost is less than 20 $/ton. At the estimated 15 $/ton coal transportation cost and a 1.25 SCP value, the COE is lower by 2.4 $/bbl at the

CONCLUSIONS AND RECOMMENDATIONS

An engineering study to determine the effect lowering the design pressure of the coal liquefaction reactors from 3300 to 1000 psig showed that the crude oil equivalent price could be reduced by about 2.1 $/bbl in a grass-roots plant. However, larger savings could be realized when integrating a coal liquefaction facility into an existing petroleum refinery. Thus, there is a significant economic incentive for continuing catalyst and process research to lower the reaction pressure for direct coal liquefaction.

Another study showed that incentives may exist for constructing a facility to liquefy Black Thunder coal on the Gulf Coast rather than at a mine-mouth location in Wyoming. The amount of which depends on the relative cost of shipping the coal to the Gulf Coast and the increased product revenues that may be obtained by distributing the liquid products among several nearby refineries. LP studies suggest that the coal liquids are more valuable when distributed among several refineries. However, additional data are needed to better determine the behavior of coal liquids when they are processed in mixtures with conventional petroleum derived materials

ACKNOWLEDGMENT

Bechtel, along with Amoco who was the main subcontractor for the initial portion of this study, expresses their appreciation to the DOE for both financial funding and technical guidance.

REFERENCES

1. Poddar, S. K., Basu, A. and Kramer, S. J., "A Baseline Design Study on Two Stage Direct Coal Liquefaction", Pittsburgh Coal Conference, Pittsburgh, PA, October 14, 1991.
2. Poddar, S. K., Habash, S. N., Kramer, S. J., Basu, A. and Schachtschneider, A. B., "Baseline Design and System Analysis for Direct Coal Liquefaction - Capital Cost and Economics", DOE/Proceedings of the Liquefaction Contractors' Review Conference, September 22-24, 1992.
3. Poddar, S. K., Habash, S. N., Kramer, S. J., Basu, A. and Myers, T. E., "Capital Cost and Economics of the Two Stage Direct Coal Liquefaction Plant", Pittsburgh Coal Conference, Pittsburgh, PA, October 12-16, 1992.
4. Poddar, S. K., Kramer, S. J. and Basu, A., "Direct Coal Liquefaction - Capital Cost and Economics for Improved Baseline Design", DOE/Proceedings of The Coal Liquefaction and Gas Conversion Contractors' Review Conference, September 27-29, 1993.
5. "Final Report on Baseline and Improved Baseline", DOE Contract DE-AC22-90PC89857, Final Report, March 1993.
6. Poddar, S. K., Adler, P and Kramer, S. J., "Direct Coal Liquefaction - Capital Cost and Economics for Low rank Coal Design", DOE/Proceedings of The Coal Liquefaction and Gas Conversion Contractors' Review Conference, September 7-9, 1994.
7. Poddar, S. K. and Klunder, E. B. "Economics of Direct Liquefaction of Subbituminous Coal from Black Thunder Mine", DOE/PETC/AIST-NEDO Joint Technical Meeting on Coal Liquefaction, Albuquerque, NM, September 26-30, 1994
8. "Final Report on Design, Capital Cost and Economics for the Low Rank Coal Study", DOE Contract DE-AC22-90PC89857, Final Report, February 1995.
9. HRI Report "DOE Direct Coal Liquefaction Baseline Design and Systems Analysis Low Rank Coal Liquefaction Study", September 1993.

Figure 1

SIMPLIFIED BLOCK FLOW DIAGRAM

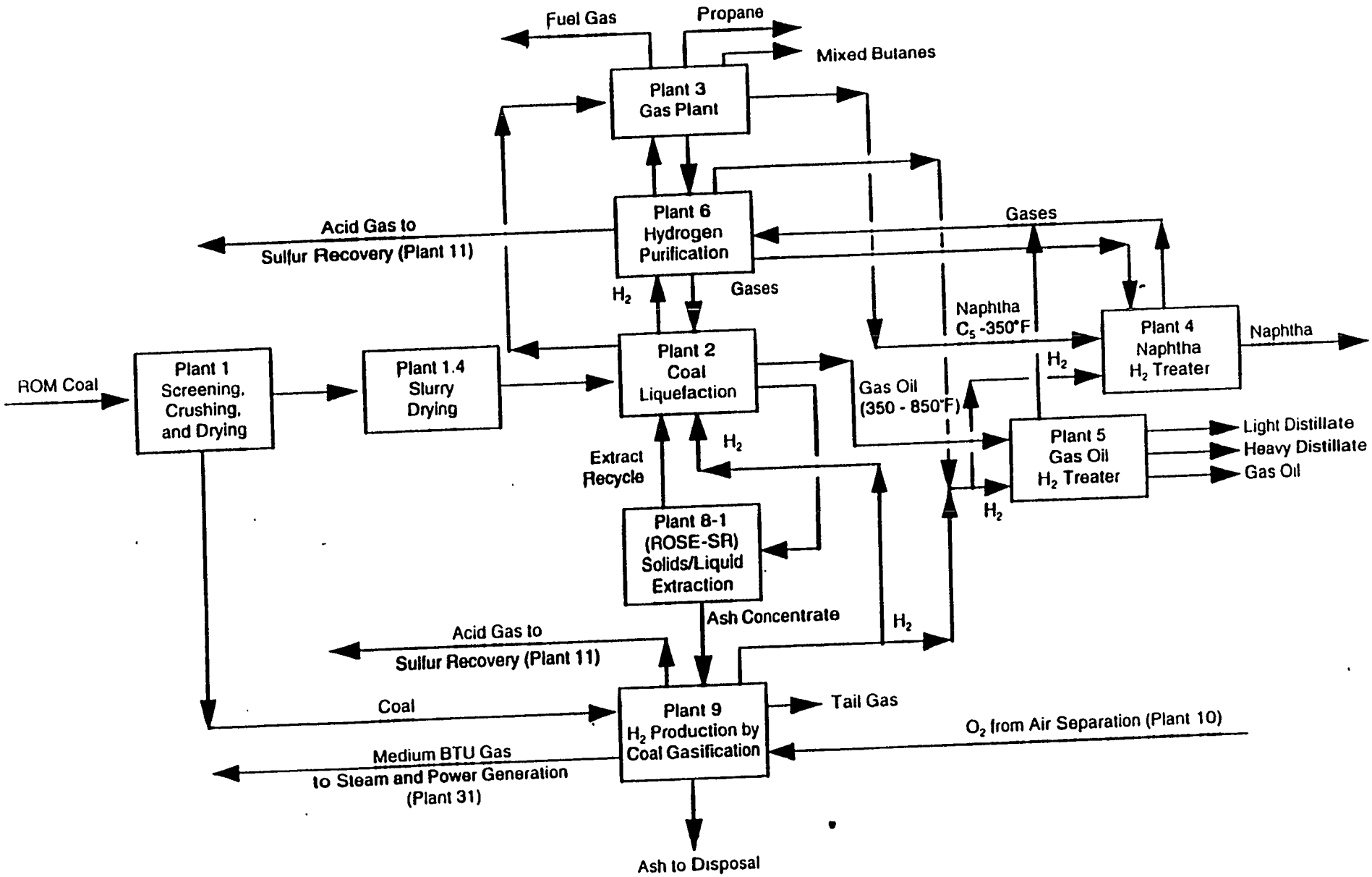

Figure 2
COE Reduction vs. Liquefaction Reactor Pressure

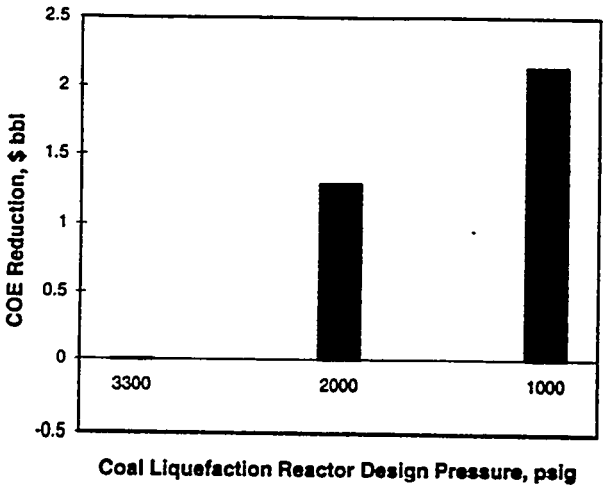

Figure 3
Effect of Coal Transportation Cost on the COE
Difference Between the Gulf Coast and Wyoming Locations

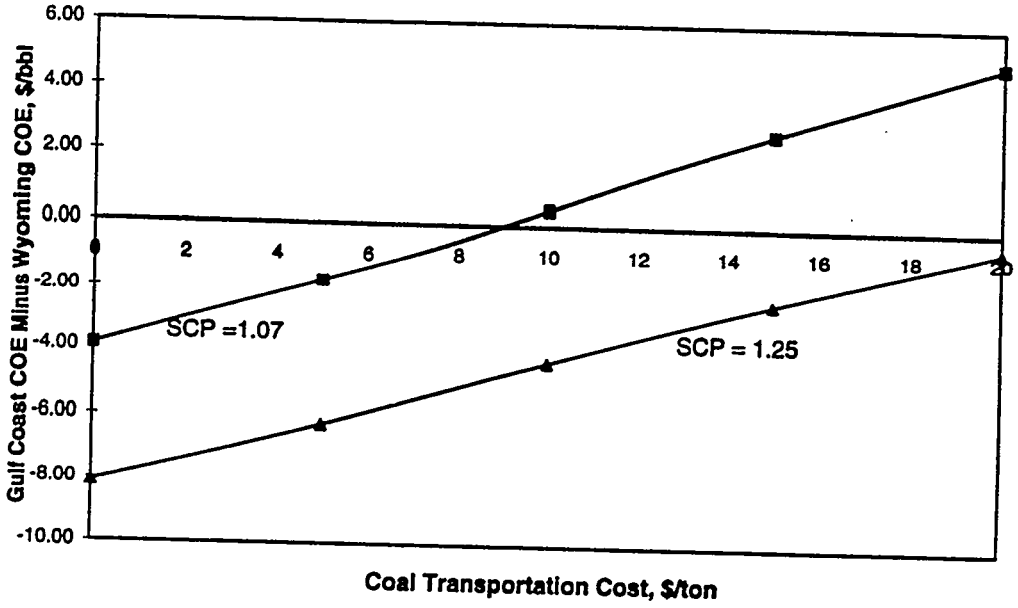

TABLE I

Properties of the Low Rank Coal from the Black Thunder Mine

Proximate Analysis (wt%)	
Volatile Matter	32.6
Fixed Carbon	35.8
Ash	4.6
Moisture	27.0
Total	100.0
Ultimate Analysis (wt% Dry Basis)	
Carbon	68.5
Hydrogen	4.8
Sulfur	0.5
Nitrogen	1.0
Ash	6.3
Oxygen (by difference)	18.9
Total	100.0

File: DOE895/Tab1

TABLE II

Major Plant Inputs, Outputs and Economic Parameters for the Base Low Rank Coal Design Case

ROM Coal Feed Rate, TSD (MF)	24952
Slag Production Rate, TSD (MF)	1659
Natural Gas Rate, MMMBTUs/SD	109.6
Raw Water Make-up, MMGSD	12.641
Naphtha Production, BSD	13063
Light Distillate Production, BSD	6610
Heavy Distillate Production, BSD	24167
Gas Oil Production, BSD	21221
Liquid Propane Production, BSD	4268
Mixed Butanes Production, BSD	2251
Total C3+ Hydrocarbons, BSD	71580
Total C4+ Hydrocarbons, BSD	67312
Ammonia Production, TSD	167
Phenol Production, TSD	45
Sulfur Production, TSD	127
No. of Operators and Boardmen	430
Total Installed Capital, $MM (4th Quarter 1993)	3692.1
Catalyst and Chemicals, $MM	80.0

File. DOE895/Tab2

TABLE III

Capital Costs for the Low Rank Coal Liquefaction Complex as a Function of Liquefaction Reactor Design Pressure

Liquefaction Reactor Design Pressure, psig	3300	2000	1000
Plant Field Costs			
Plant 2 - Coal Liquefaction Plant	792	664	547
Other ISBL Plants	1206	1187	1175
Total ISBL Plants	1998	1851	1722
OSBL Plant Costs	841	841	841
Total ISBL and OSBL Plant Costs	2839	2692	2563
Home Office, Fees and Contigency	853	805	805
Total Installed Plant Cost	3692	3498	3368

All costs are fourth quarter 1993 costs for the Nth plant.

File: DOE895/Tab3

TABLE IV

Comparison Between the Wyoming and the Gulf Coast Locations

	Wyoming	Gulf Coast
Labor		
Operator Pay Rate, $/hr	18.50	12.00
Labor Overhead Factor	1.40	1.25
Utility Costs		
Fuel Gas, $/MMBTUs	2.00	1.82
Raw Water, $/Mgals	2.50	0.20
Transportation Costs		
Coal, $/ton	0.00	Variable
Ash, $/ton	0.00	Variable
Ash Disposal Cost, $/ton	5.00	2.50
Plant Located in PADD	II	III
Syncrude Premium	1.07	1.07 to 1.25

All costs are first quarter 1994 costs.

File:DOE895/Tab4&5

TABLE V

Comparison of Plant Costs Between the Wyoming and the Gulf Coast Locations

	Wyoming	Gulf Coast
ISBL Plant Field Costs, MM$	1998	1769
OSBL Plant Field Costs, MM$	841	776
Total ISBL and OSBL, MM$	2839	2545
Home Office, Fees and Contingency, MM$	853	778
Total Installed Plant Cost, MM$	3692	3323

All costs are fourth quarter 1993 costs for the Nth plant.

File:DOE895/Tab4&5

THE DIRECT LIQUEFACTION PROOF OF CONCEPT PROGRAM

Alfred G. Comolli
L.K. (Theo) Lee
Vivek R. Pradhan
Robert H. Stalzer

P.O. Box 6047
New York & Puritan Avenues
Lawrenceville, NJ 08648

Sponsored By

The U.S. DOE-PETC
Hydrocarbon Technologies, Inc.
Kerr-McGee Corporation

Presented At

COAL LIQUEFACTION AND GAS CONVERSION CONTRACTORS REVIEW CONFERENCE
Western William Penn Hotel
Pittsburgh, PA

AUGUST 29 - 31, 1995

The Direct Liquefaction Proof-of-Concept Program
Coal Liquefaction and Gas Conversion Contractors
Review Conference, Pittsburgh, PA
August 29-31, 1995

ABSTRACT

The goal of the Proof of Concept (POC) Program is to develop Direct Coal Liquefaction and associated transitional technologies towards commercial readiness for economically producing premium liquid fuels from coal in an environmentally acceptable manner. The program focuses on developing the two-stage liquefaction (TSL) process by utilizing geographically strategic feedstocks, commercially feasible catalysts, new prototype equipment, and testing co-processing or alternate feedstocks and improved process configurations.

Other high priority objectives include dispersed catalyst studies, demonstrating low rank coal liquefaction without solids deposition, improving distillate yields on a unit reactor volume basis, demonstrating ebullated bed operations while obtaining scale-up data, demonstrating optimum catalyst consumption using new concepts (e.g. regeneration, cascading), producing premium products through on-line hydrotreating, demonstrating improved hydrogen utilization for low rank coals using novel heteroatom removal methods, defining and demonstrating two-stage product properties for upgrading; demonstrating efficient and economic solid separation methods, examining the merits of integrated coal cleaning, demonstrating co-processing, studying interactions between the preheater and first and second-stage reactors, improving process operability by testing and incorporating advanced equipment and instrumentation, and demonstrating operation with alternate coal feedstocks.

During the past two years two major PDU Proof of Concept runs were completed. POC-1 with Illinois No. 6 coal and POC-2 with Black Thunder sub-bituminous coal. Results from these operations are continuing under review and the products are being further refined and upgraded. This paper will update the results from these operations and discuss future plans for the POC program.

The Direct Liquefaction Proof-of-Concept Program
Hydrocarbon Technologies, Inc. (HTI)
Lawrenceville, New Jersey 08648

INTRODUCTION

Coal is the most abundant fossil fuel resource of the United States. The technology for its conversion to liquid transportation fuels such as gasoline, kerosine, and diesel is being continually improved at Hydrocarbon Technologies, Inc. (HTI). The state-of-art direct coal liquefaction process has brought down the crude equivalent price of coal liquids to about $30.00 a barrel from over $70 a barrel by the technologies existing in the early 70s. The most widely researched technology today is the Catalytic Two Stage Liquefaction Process (CTSL$^+$), invented by Hydrocarbon Research, Inc. during the late 80s. The Catalytic Two Stage Liquefaction Process is an advanced direct coal liquefaction process that utilizes a low temperature first stage to foster hydrogenation in the presence of a nickel molybdenum ebullated bed catalyst and a higher temperature second stage to increase conversion and heteroatom removal. A preferred mode of operation developed at the Bench Scale is with extinction recycle of the 700°F$^+$ fraction to produce a premium quality light distillate product. The CTSL™ technology is also environmentally benign. Most of the R & D work on CTSL was funded by the U.S. Department of Energy during the last decade. The U.S. DOE also co-sponsored a demonstration program at the Proof-of-Concept (POC) scale for the CTSL™ Technology during the last three years at Hydrocarbon Technologies, Inc. As a result of this, extensive modifications were made to HTI's 4.0 TPD Process Development Unit incorporating equipment from Wilsonville Advanced Coal Liquefaction Facility and upgrades in the period from December 1992 into October 1993. This created a unique POC unit consisting of two ebullated bed reactors plus an on-line hydrotreater and three modes of solid separation: vacuum distillation, ROSE-SR℠, a pressure filtration. Two long duration process demonstration runs were accomplished during 1993 and 1994. POC Run 1 evaluated the liquefaction behavior of a bituminous coal from Illinois No. 6 seam, Crown II mine. POC Run 2 demonstrated the performance using a sub-bituminous coal from Wyoming Black Thunder mine, followed by several days of co-liquefaction operations of coal with plastics and waste tire rubber.

PROGRAM OBJECTIVES

The overall objective of the Proof of Concept (POC) Program is to develop Direct Coal Liquefaction and associated transitional technologies towards commercial readiness for economically producing premium liquid fuels from coal in an environmentally acceptable manner. The program focuses on developing the two-stage liquefaction (TSL) process by utilizing geographically strategic feedstocks, commercially feasible catalysts, new prototype equipment, and testing co-processing or alternate feedstocks and improved process configurations. Other high priority objectives include:

- dispersed catalyst studies, demonstrating low rank coal liquefaction without solids deposition, improving distillate yields on a unit reactor volume basis, and demonstrating ebullated bed operations while obtaining scale-up date.
- demonstrate optimum catalyst consumption using new concepts (e.g. regeneration, cascading), produce premium products through on-line hydrotreating, demonstrate improved hydrogen utilization for low rank coals using novel heteroatom removal methods.
- define and demonstrate two-stage product properties for upgrading, demonstrate efficient and economic solid separation methods, examine the merits of integrated coal cleaning.
- demonstrate co-processing, study interactions between the preheater and first and second-stage reactors, improve process operability by testing and incorporating advanced equipment and instrumentation, and to demonstrate operation with alternate coal feedstocks.

PROCESSING CONFIGURATION

The Proof of Concept Facility consists of several distinct process units, a Coal Handling System, Two Ebullated-Bed Reactors in series, an On-Line Hydrotreater, Separation and Pressure Let-Down System, Scrubbing and Oil-Water Separation, Flash Vessels and Atmospheric and Vacuum Distillation Equipment a ROSE-SR℠ and U.S. Filter Solid Liquid Separation Systems and Produce Storage. The heart of POC reaction section is two ebullated bed reactors employing an extrudate hydroprocessing catalyst. Ebullated bed reactors offer several advantages as a well back-mixed reactor, it provides a uniform temperature and a control of exothermic heat of reactions. It also provides a facility for on-line catalyst replacement. The POC Process Development Unit (PDU) processes about 3 tons a day of coal producing about 15 barrels per day of clean distillate liquid product and can operate with or without solids containing recycle solvent. The ROSE-SR℠ unit and On-Line Hydrotreater were added along with other improvements to the equipment and control systems prior to the CTSL™ Process Scale-Up with Illinois #6 Bituminous Coal. *Figure 1* shows a schematic of the process.

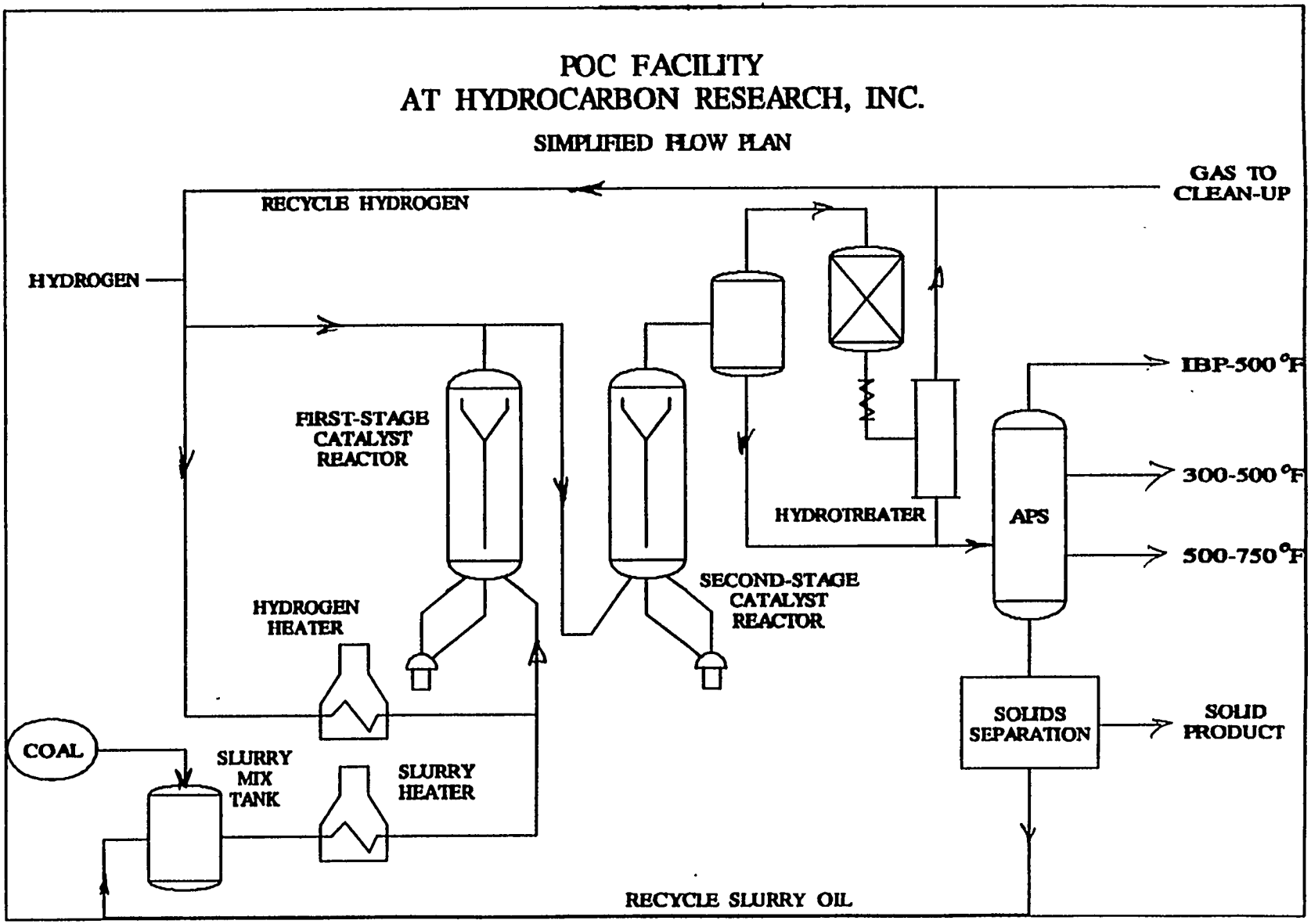
POC FACILITY
AT HYDROCARBON RESEARCH, INC.
SIMPLIFIED FLOW PLAN
GAS TO CLEAN-UP
RECYCLE HYDROGEN
HYDROGEN
FIRST-STAGE CATALYST REACTOR
HYDROTREATER
APS
IBP-500 °F
300-500 °F
500-750 °F
SECOND-STAGE CATALYST REACTOR
HYDROGEN HEATER
SOLIDS SEPARATION
SOLID PRODUCT
COAL
SLURRY MIX TANK
SLURRY HEATER
RECYCLE SLURRY OIL

Figure 1

INSPECTION OF FEED COALS

Illinois No. 6 Crown II mine coal is a high volatile bituminous coal with high mineral matter and sulfur contents, while Wyoming Black Thunder mine is a lower rank coal with high oxygen and low sulfur contents. The analysis of these two coal feedstocks is shown in *Table 1.*

Table 1. Analysis of Feed Coals in POC Program

Coal	Illinois No. 6 Crown II Mine	Wyoming Black Thunder Mine
Moisture (as-received), w%	15.2	28.2
Ash (dry basis), w%	9.5	6.7
Elemental Analysis, w% Dry		
Carbon	70.3	70.2
Hydrogen	5.2	5.1
Nitrogen	1.5	1.0
Sulfur	4.0	0.3
Oxygen (by difference)	5.5	16.7
H/C Ratio	0.89	0.88

RESULTS AND ACCOMPLISHMENTS

POC-Run1

The main objective of POC-1 was to scale-up the CTSL™ process with Illinois No. 6 coal in the extinction recycle mode to produce an all distillate slate of products. This was the culmination of a ten year effort devoted to the development and scale-up of the two stage low - high temperature sequencing ebullated bed process. Alternate goals were to confirm new equipment operability, to collect data in the CTSL™ mode for comparison with the existing data base, to collect 2500 gallons of distillate for downstream refining studies and to evaluate the ROSE-SR and U.S. Filter systems. Following is a list of the several run conditions and variables studied. *Table 2* shows the actual conditions and set points. Hydrotreater was bypassed during most of the operation.

TABLE 2. POC-01 Operating Summary
Illinois No. 6 Crown II Mine Coal
Akzo AO-60 1/16" Extrudate Catalysts

Condition Period No.	1 13-19	2 20-26	3 27-32	3B 41-44A	4 A/B 47-50	4C 54-57	5 58
Recycle Mode	Ashy	<-----	Solid	Free	-------	-->	
Space Velocity [Kg mf coal/h/m^3 reactor]	304	320	464	464	432	464	448
Solvent/Coal Ratio	1.2	1.25	1.26	1.39	1.4	1.0	1.1
First Stage							
Temp deg C	409	408	413	410	413	413	413
Cat. Repl. Rate [kg/ton mf coal]	0.3	0.8	0.8	0.8	0	0	0
Second Stage							
Temp deg C	426	432	435	432	433	438	440
Cat. Repl. Rate [Kg/ton mf coal]	0.5	1.5	1.5	1.5	1.5	0	0

During the run POC-01, Illinois No. 6 coal was successfully converted to light distillate liquids with low heteroatom (N, S, and O) contents. Throughout the entire 57 day operation, coal conversion (based on quinoline solubility) was high, in the range of 94.7 to 95.4 w% of moisture-ash free (maf) coal. Removal of organic sulfur and nitrogen was also high *(Table 7)*. A major portion of the converted coal was in the form of distillate liquids. The C^4-524°C distillate yield was in the range of 72.8 to 75.1 w% maf coal. When the process severity was reduced by increasing the space velocity from about 320 to 460 Kg/h/m^3 reactor, the distillate yields dropped down to about 70% and further to below 60% when on-line periodic catalyst replacement was terminated. The overall process performance from POC-01 is summarized in *Table 3.* The typical distribution of light distillates and their properties are shown in *Table 6a.* As shown in this Table, a typical total distillate product from POC-01 is characterized by its low nitrogen and sulfur contents, and high hydrogen contents and API gravity.

POC-Run 2

The main objective of POC-2 was to scale-up the CTSL extinction recycle process on sub-bituminous coal including on-line hydrotreating of the IBP-343°C distillate. Of major concern was whether or not calcium-carbon deposits would occur as has been evident in other low rank coal processes. *Table 3* shows the operating plan and conditions. An additional objective of major importance was the addition of nine days of operation to study the co-liquefaction of plastics with coal and waste tire rubber and coal. This was a scale-up from microautoclave and one liter reactors to a 3 ton/day unit.

TABLE 3. POC-01 PROCESS PERFORMANCE
Coal: Illinois No. 6 Crown II Mine (10.4 w% Dry Ash)
Catalyst: Akzo AO-60 1/16" NiMo Extrudates in both Reactors

Process Conditions Period/s	1 18-20	2 24-26	3B 42-43	4B	4C
Recycle Type	Ashy	<-----	Ash-free	------	--->
Process Performance					
Chemical H^+ Consumption, W% MAF	7.1	7.1	6.1	5.9	5.3
Coal Conversion, W% MAF	95.6	95.0	94.7	95.1	95.4
524 C+ Conversion, W% MAF	86.6	86.6	83.0	78.0	76.0
Desulfurization (Organic), W%	98.0	97.7	96.0	94.4	94.0
Denitrogenation, W%	86.0	82.5	78.2	75.9	78.0
C^4-524°C Distillates, W% MAF	72.8	74.2	70.64	63.2	58.8
Deasher Performance					
Deasher	<--	------	ROSE-SR	----	-->
Energy Rejection, %	25.2	16.5	12.8	22.5	33.0
Deasher Coal Conversion, W% MAF	95.7	95.1	95.2	95.2	94.9

TABLE 4. POC-02 Catalytic Two-Stage Liquefaction of Wyoming Black Thunder Coal

Condition No.	1	2	3	4
Period No.	1-15	16-22	23-33	34-36
Feed Composition Ratio	Coal 1.2/1	Coal 1.2/1	Coal 1.2-1.5/1	Coal 1.2/1
Temperatures K-1/K-2, °C K-3 Hydrotreating, °C	 400/435 370	 413/443 372	 432/446 382	 432/446 382
Space Velocity, $Kg/hr/m^3$	320	320-480	640	640
Catalyst Replacement, kg/ton maf Coal K-1 K-2	 0.5 1.0	 0.5 1.0	 0.8 1.3	 0.8 1.3
Recycle Mode	Ashy	Ashy	Ashy	Ashy
Other				Molyvan 150 ppm

As mentioned earlier, Wyoming Sub-bituminous Black Thunder mine coal was processed during POC-02 during the first 36 days of operations, with an in-line hydrotreater. The operating conditions are summarized in *Table 4.* POC-2 was a very successful scale-up of the CTSL processing of sub-bituminous coal producing high yields of clean hydrotreated distillate at space velocities as projected by Bench-Scale Testing. The typical process performance for POC-02 operations is summarized in *Table 5.*

TABLE 5. POC-02 PERFORMANCE

Condition	1	2	4A	4B
Hydrogen Consumption	8.6	8.3	6.9	8.1
Coal Conversion	90	92.6	91.8	93.5
Resid Conversion	86	84	84	82
C^4 - 343°C Net Distillate	58	54	56	49
C^4 - 524°C Distillate	66	62	56.6	57.5
Deasher Performance				
Organic Rejection, %	24.3	22.0	12.7	13.8
Deasher Rejection, %	23.1	21.0	12.0	13.6

As shown in Table above, the high oxygen-containing lower rank sub-bituminous coal exhibited a lower degree of conversion, 90 to 93.5 w% maf coal, and yields higher amounts of light hydrocarbon gases and water. The light premium distillate yield was 66% maf at coal space velocity of 320, and reduced to about 57% maf at a higher space velocity of 640 kg/h/m^3 reactor. The typical overall process performance for POC-02 operations is summarized in *Table 7.* The quality of distillates obtained from POC-02 was excellent as a result of an in-line hydrotreater. As summarized in *Table 6b,* for a typical POC-02 Condition, high proportion of the distillate was lighter than 343°C and had less than 40 ppm nitrogen, 10 ppm sulfur, and high H/C atomic ratios.

TABLE 6a. QUALITY OF THE PREMIUM DISTILLATE PRODUCTS FROM POC-01 OPERATIONS

Boiling Fraction	Distribution, W%	API Gravity	S, ppm	N, ppm	H/C Atomic Ratio
IBP-177°C	25.5	51.4	4.1	88	1.97
177-288°C	43.7	27.7	77	146	1.71
288-343°C	25.6	20.6	94	187	1.63
343°C+	5.2	16.3	652	263	1.54
Whole Product	100.0	33.4	153	240	1.75

TABLE 6b. QUALITY OF THE PREMIUM DISTILLATE PRODUCTS FROM POC-02 OPERATIONS

Boiling Fraction	Distribution, W%	API Gravity	S, ppm	N, ppm	H/C Atomic Ratio
IBP-177°C	32.8	56.4	1	5	1.94
177-288°C	51.3	32.1	1	30	1.71
288-343°C	13.9	24.6	9	38	1.61
343°C$^+$	2.0	19.1	40	81	1.56
Whole Product	100.0	36.2	5	21	1.78

TABLE 7. OVERALL SUMMARY OF CTSL™ PROCESSING AT PROOF-OF-CONCEPT SCALE

COAL TYPE	ILLINOIS NO. 6 (BITUMINOUS COAL)	BLACK THUNDER MINE (SUB-BITUMINOUS COAL)
PDU OPERATION	POC-01	POC-02
SOLIDS-SEPARATION	ROSE-SR™	ROSE-SR™
RECYCLE TYPE	Ash-free	Ashy
SPACE VELOCITY Kg/hr/m^3(Stage)	310	460
Reactor K-1 Temperature, °C	407	413
Reactor K-2 Temperature, °C	432	445
Backpressure, MPa	6.8	6.8
Process Performance		
Overall Material Balance, W%	98.1	100.3
Coal Conversion, W% maf	95.0	92.6
524°C$^+$ Resid Conversion, w% maf	86.6	84.0
C4-524°C Distillate Yield, w% maf	74.2	62.0
C4-524°C, Barrels/Ton maf coal	5.0	4.1
Hydrodesulfurization, %	97.7	96.5
Hydrodenitrogenation, %	82.5	95.5
Hydrogen Consumption, w% maf	7.1	8.3
C4-343,°C Distillate Quality		
API Gravity	33.4	35.8
Nitrogen, ppm	153	40
Sulfur, ppm	240	5
H/C Atomic Ratio	1.75	1.80
Deasher Performance		
Organic Rejection, w% maf	15.2	22.0
Energy Rejection, w% maf	16.5	21.0

POC-2 Plastics and Rubber Co-Processing with Coal

In the closing condition of Run POC-2, pulverized waste tires and mixed plastics were processed with coal at 3 tons/day to produce products, to study scale-up and to highlight process problems. Operations were sustained for several days with 25% tire rubber - 75% coal and 30% plastic and 70% coal. The component ratio of the plastics was 50% High Density Polyethylene, 35% polystyrene and 15% polyethylene terephtalate. A total of 15 tons of plastics, coal and used tires and coal were converted to light (180-650°F) distillate of less than 10 ppm sulfur and 25 ppm nitrogen and cetane index over 40 thus demonstrating the feasibility of processing wastes with coal and defining areas requiring further R&D.

PLANS

The POC program is being modified to include a series of 9 continuous Bench Scale Runs examining variant co-liquefaction schemes and optional POC Runs for scale-up and demonstration. The POC schedule shows nine Bench-Scale runs occurring from July, 1995 through June, 1997 with two POC-PDU runs in fiscal 1998, December through May.

TITLE : REFINING AND END USE STUDY OF COAL LIQUIDS I — PILOT PLANT STUDIES

AUTHORS: J. Erwin and D. S. Moulton

ORGANIZATION: SOUTHWEST RESEARCH INSTITUTE

CONTRACT: DE-AC22-93PC91029

PERIOD OF PERFORMANCE: 11/1/93 to 9/30/97

1. Abstract

The Office of Fossil Energy, Pittsburgh Energy Technology Center is examining the ways in which coal liquids may best be integrated into the refinery of the 2000 - 2015 time frame and what performance and emission properties will prevail among the slate of fuels produced. The study consists of a Basic Program administered by Bechtel Group, Inc. to build a linear programming refinery model and provide processing and fuel properties data through subcontractors Southwest Research Institute, Amoco Oil R&D, and M.W. Kellogg Company. The model will be used in an Option 1 to devise a slate of test fuels meeting advanced specifications, which will be produced and tested for physical ASTM-type properties, engine performance, and vehicle emissions. Three coal liquids will be included: a direct liquid from bituminous coal, another from subbituminous, and a Fischer-Tropsch indirect liquefaction product. This paper reports the work to date on fractions of the first direct liquid including naphtha hydrotreating, heavy distillate hydrotreating, FCC of the heavy distillate hydrotreater products. Also reported are the first stages of work on the indirect liquefaction wax including feed preparation and FCC tests of blends with petroleum FCC feed.

2. Project Overview and Objective

What is the best way to integrate coal liquids into the refining industry of the future (2000 - 2017 time frame)? The answer to this question, the supporting data, and related fuel utilization issues are the subject of *Refining and End Use Study of Coal Liquids*. In sequence with the companion paper," - II, Linear Programming Analysis", this paper will review the work to date in the project. With Bechtel Group as prime contractor managing the project and performing the refinery modeling, Southwest Research Institute, Amoco Oil R & D, and M.W. Kellogg Company are studying the unit operations uniquely affected by introducing a yet-to-be-determined optimum concentration of coal liquids in the crude stream of a modern refinery. Further project overview is provided in Paper II.

Both direct and indirect liquids are being studied. Feed and product properties, processing requirements & behavior, refining economics, and fuel performance and emissions are objectives of the project. An overview of the work is given in Figure 1. The arrows represent the flow of materials and information through the stages of the work. The optimization of concentrations and product recipes is discussed in Paper II, while the individual unit operations studied to date under the heading of "processing" in Figure 1 are discussed here.

3. Refining Scheme

The coal liquids, direct or indirect, are produced outside the petroleum refinery. The approach adopted in the *End Use Study* is to make the least perturbation of the existing refining process by mixing the coal feedstocks with the crude oil entering the refinery; except that for indirect liquids, maximum benefit of their paraffinic nature would be made by distilling them separately and sending appropriate boiling range cuts to individual refinery units most suited for them.

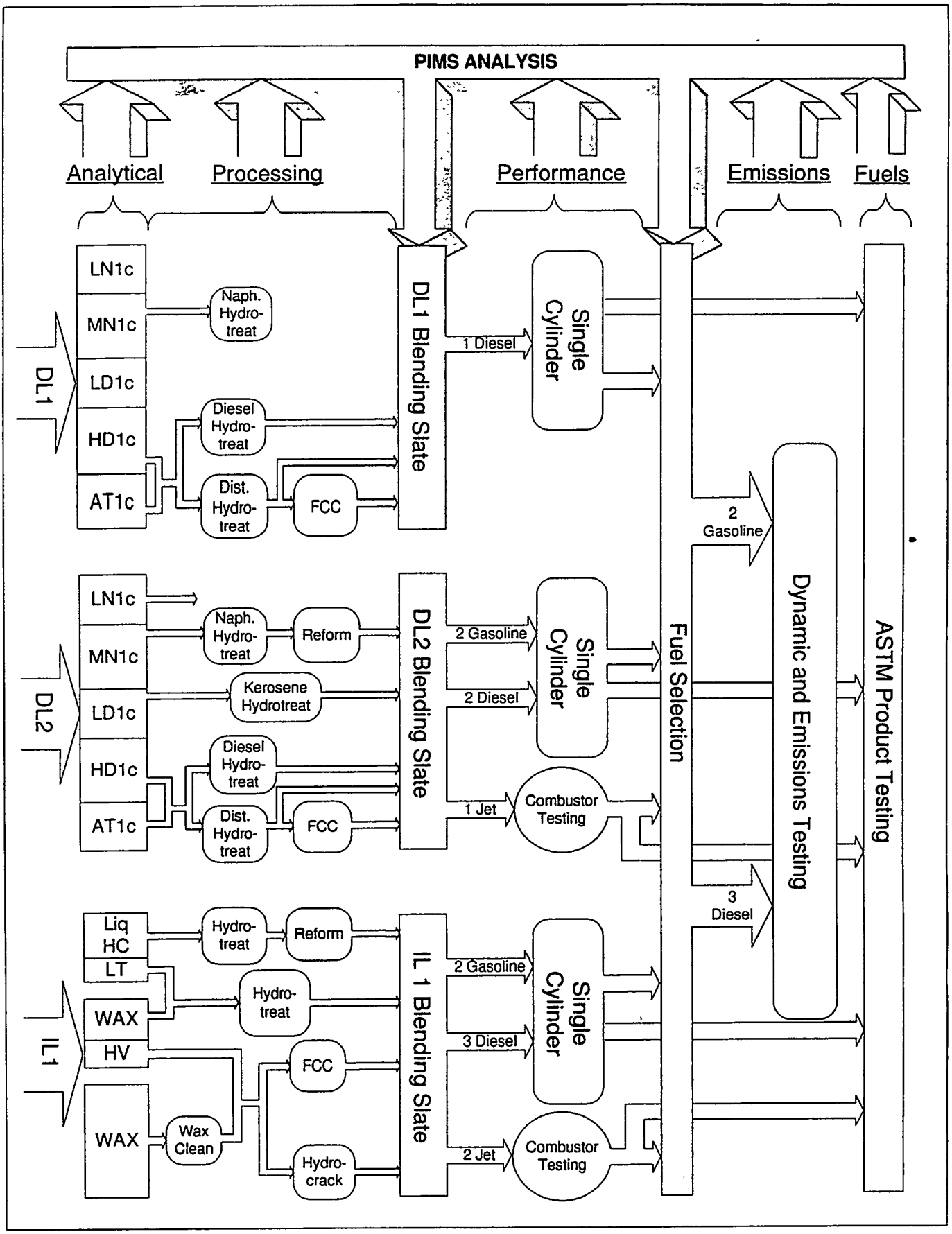

Figure 1. Overview of End-Use Study

Figure 2 shows the refining scheme selected for the study. Only proven technologies were considered for inclusion in the Bechtel refinery model and then only units needed for the slate of fuels being considered in the future time frame: two grades of conventional and reformulated gasolines, three grades of diesel (& low aromatics diesel for the IL1), jet A. Other refinery products (fuel oil, asphalt, gases, etc.) are considered in the computer modeling to satisfy the mass balance.

In the sections below, the hydrogenation of the naphtha stream for reforming, hydrogenation of the heavy distillate for FCC feed and product blending, fluid catalytic cracking of the heavy distillate, and indirect wax processing to date will be discussed. The work thus far concerns coal feeds DL1 and IL1 described below.

4. Direct Liquid Feedstock

The coal liquid feedstock, DL1, was produced by HRI, Inc. in the DOE Close Coupled, Two-Stage PDU plant during Proof of Concept Run 1 from Illinois #6 coal, a bituminous feed. Operations were arranged to recycle 750°F$^+$ material to extinction and to omit the in-line hydrotreating. At Southwest Research Institute, the full-boiling material was distilled into four fractions: light naphtha, medium naphtha, light distillate and heavy distillate according to the atmospheric split shown on Figure 2. The 7% atmospheric bottoms was allowed to remain with the heavy distillate as a matter of practicality. In the future, a subbituminous feed will liquefied for study in the program as DL2.

5. Naphtha Hydrotreating

Naphtha hydrotreating is an integral part of the preparation of the refinery streams blended into gasoline. The objectives of the test of DL1 naphtha were to:

- reduce the sulfur content to less than 0.5 ppm by weight to protect the reforming catalyst
- reduce the nitrogen content to less than 0.5 ppm by weight
- increase the hydrogen content of the naphtha
- obtain process data and operating efficiency data at various operating conditions.

The pilot plant of the DOE Alternative Fuel Center at Southwest Research Institute was configured for hydrogenation: feedstock is pumped from a weighing tank, heated to 400°F in a feed preheater, and passed to the reactor. On the way to the feed heater, make-up and recycle streams of high pressure (770 - 1400 psig) hydrogen join the feedstock. The make-up hydrogen flowrate was set at 10 SCFH and the recycle was held constant at 20 SCFH. The aggregate hydrogen flows constituted a gas contacting rate of 2208 - 4258 SCFB. The reactor is composed of two stages- a 3.5 liter guard bed, followed by a 4.0 liter reactor. The reactor is packed with an equilibrium nickel-molybdenum catalyst, Criterion HDN-60. The processed feedstock is cooled and depressurized after leaving the reactor first in a high, then a low, pressure separator. Hydrogen gas is recovered in the high pressure separator, scrubbed, and returned to the reactor. For the coal liquid naphtha, which was in short supply, a smaller (one-eighth scale) reactor was used for the test matrix.

During the course of the experiment, pressures, temperatures, and flow rates were varied over a matrix of conditions selected to achieve the experimental objectives of the naphtha hydrogenation while still considering typical refinery conditions. The matrix of conditions is shown in Figure 3. System conditions were monitored, and when sufficiently stabilized, a sample was drawn from the low pressure separator outlet. The specific gravity was measured with a density meter and hydrogen content was determined by ASTM D 3701, broadband NMR method. A stripper column was not used during the run in order to conserve DL1 feedstock, instead, the samples were caustic washed to remove H_2S and submitted for nitrogen (by

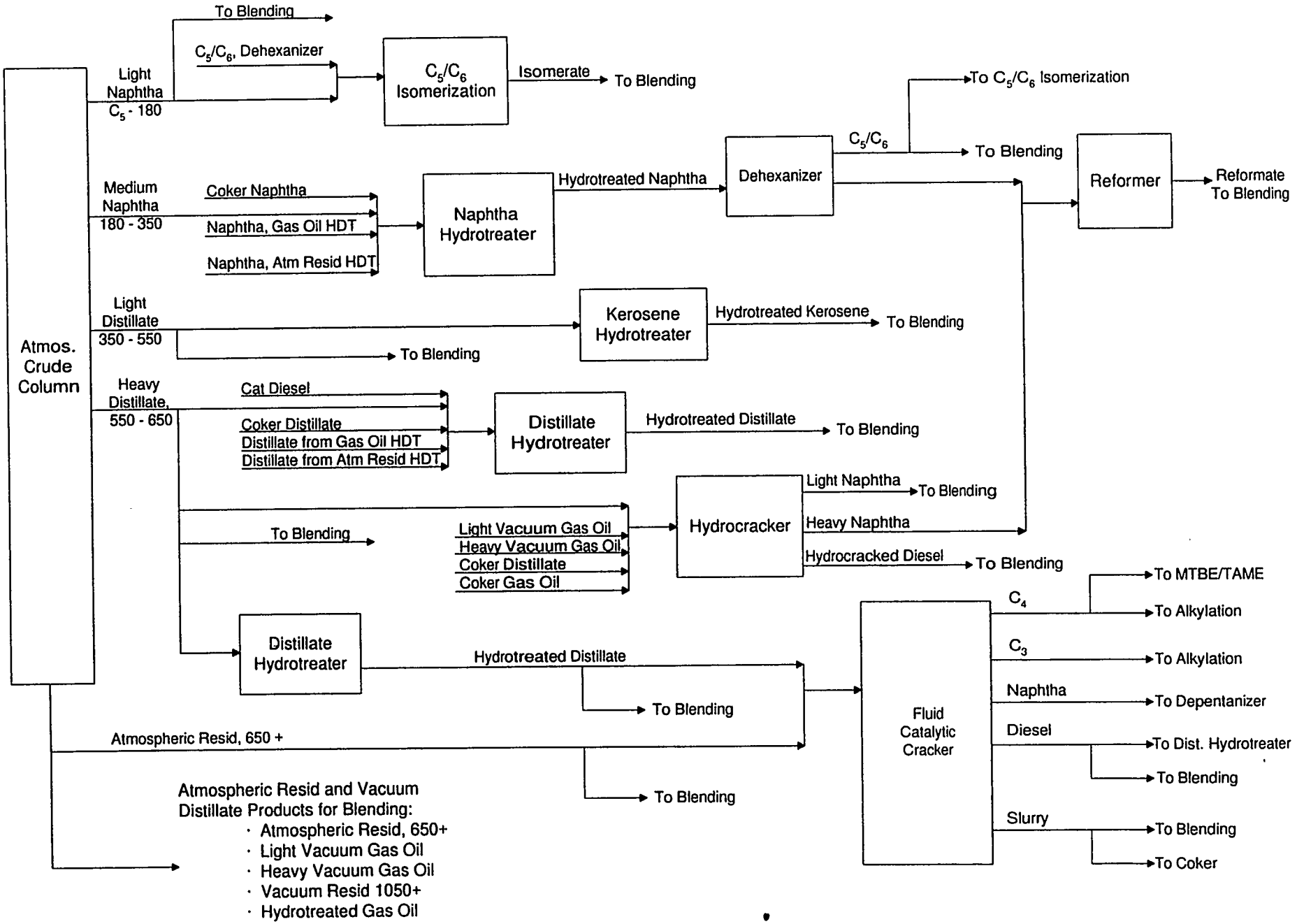

Figure 2. PIMS Refinery Model

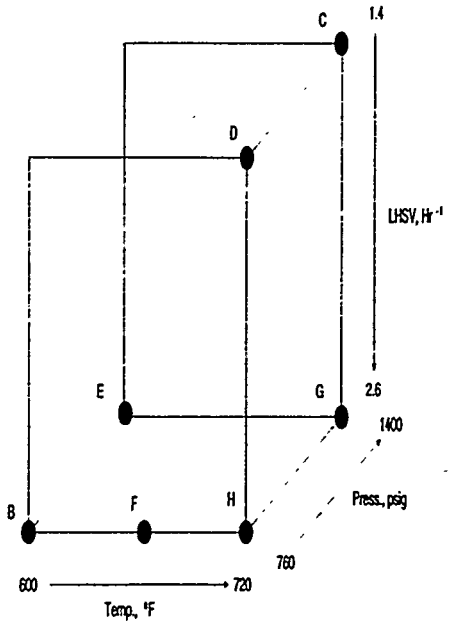

Figure 3. Experimental Matrix for DL1 Naphtha Hydrotreating

chemiluminescence, Antek) and hydrogen content (D 3701) analyses. This sampling method precluded measuring sulfur content of the product. Gas samples were also taken from the vent sample port for gas chromatographic analyses.

Three feedstocks were used in the naphtha hydrotreating. The first was a petroleum feedstock which was selected in consultation with Amoco as a typical refinery naphtha normally used as hydrotreater feedstock. The second experimental feed was the neat DL1 naphtha fraction. The third feedstock was a blend of 67% petroleum naphtha/33% coal naphtha (by volume).

The test sequence began with the petroleum feedstock at the low severity condition A. At steady state (determined by reaching constant density and hydrogen contents), a product sample was drawn at this and each subsequent condition. The petroleum feed was tested first to provide a benchmark for the PIMS library data and to perform startup on a more abundant feed to conserve DL1 naphtha. The neat coal liquid was then introduced at the low severity condition B. The temperature, pressure, and residence time were increased to the high severity level C, and a sample was drawn and tested to assure that the nitrogen was below 0.5 PPM. Once this had been established, the neat coal liquid was tested at five additional conditions with varying pressure, temperature, and flow rate at severities between the two extremes, B and C. The petroleum/coal liquid blend was then tested at three conditions (I, J, and K) and the petroleum feedstock was reintroduced as the process was brought back to its initial, low severity condition L. Comparison of this last test condition to the first shows whether there has been significant catalyst de-activation.

Experimental Results: The test conditions and measurements are summarized in Table 1. There is a narrow range of product properties; e.g., for the neat coal naphtha, the density differs by only 0.008 gm/ml and the hydrogen content differs by 0.37 wt% between the extremes of process severity. The hydrotreating produced good hydrodenitrogenation, with product nitrogen values at or below the target (values marked <1).

The wire frame representation of the experimental matrix in Figure 3 illustrates which direct comparisons may be made between sample points sharing common values of two test parameters, but differing in the third. Table 2 compares points differing in only one parameter, and presents the effects of increasing pressure, temperature, and flow rate. Pressure influenced the hydrogenation more strongly than temperature or flowrate in the ranges studied. The hydrogen content increased by an average of 0.22% wt when the

Table 1. Naphtha Hydrotreating Summary							
SAMPLE#	Feed Type	Avgerage Processing			Density g/mL	H2 Wt% NMR	Nitrogen PPMW
		Deg F	Psig	LHSV			
Coal	Feed DL1 Naphtha				0.794	13.62	219
Petrol	Feed Petr				0.767	13.95	<1
A	Petr	599	770	2.6	0.765	14.06	<1
B	DL1	596	770	2.7	0.787	13.89	3
C	DL1	723	1397	1.4	0.780	14.21	<1
D	DL1	722	762	1.4	0.784	13.84	2
E	DL1	602	1397	2.7	0.786	13.98	<1
F	DL1	656	762	2.7	0.786	13.97	<1
G	DL1	720	1396	2.7	0.782	14.13	3
H	DL1	718	762	2.8	0.788	13.94	3
I	Blend	722	764	1.5	0.768	14.25	10
J	Blend	722	1400	1.3	0.761	14.80	<1
K	Blend	603	766	2.6	0.771	14.12	<1
L	Petr	607	768	2.7	0.771	13.34	<1
M	Petr	721	772	1.5	0.760	14.39	<1

pressure was increased from 770 to 1400 psig. The pressure also had the greatest effect on density, decreasing the density by an average of -0.0037 gm/ml when the pressure was increased from 770 to 1400 psig. The changes in specific gravity generally confirmed the change in hydrogen content. Increasing the temperature from 600° to 720°F consistently increased the hydrogen content, but reducing the LHSV from 2.7 to 1.4 hr^{-1} increased the hydrogen content only at high pressure (1400 psi). At low pressure (770 psi) the hydrogen content decreased.

Table 2. Naphtha Hydrotreating Main Effects					
Effect	Sample Points	Effect on H_2	Effect on SG	Average Effect on H_2	Avgerage Effect on SG
Temperature (600 to 720°F)	B to H E to G	+0.05% +0.15%	+0.001 -0.004	+0.010%	-0.0015
Pressure (770 to 1400 psig)	B to E H to G D to C	+0.09 +0.19 +0.37	-0.001 -0.006 -0.004	+0.22%	-0.0037
LHSV (1.4 to 2.7 hr-1)	C to G D to H	-0.08 +0.10	+0.002 +0.004	+0.01%	+0.003

There is a three step progression in temperature between points B, F, and H. The points share a common pressure (770 psig) and LHSV (2.7 hr^{-1}). In this case, the consumption of hydrogen is greater and the specific gravity is lower at the intermediate temperature, point F. This would suggest that there may be a critical temperature between 600 and 720°F where the processing efficiency is maximum. The higher temperatures favor the reverse or dehydrogenation reactions arriving at the hydrogen concentration dictated by thermodynamic equilibrium. The effect of high naphthenes concentration in the feed probably caused some dehydrogenation, locally, at hot spots within the reactor during operation in the low hydrogen pressure and high temperature part of the matrix.

The experimental results show that the catalyst lost activity during the sequence of experiments. Aromatics hydrogenation and heteroatom removal in a petroleum feed were observed before and after the sequence to indicate whether a major activity loss, which could complicate the modeling effort, had occurred. Activity reduction can come from the high temperature levels of the most severe points of the present matrix without regard to the specific feedstocks. The usual measure of catalyst deactivation (the change in temperature required to restore product quality) was simulated with points L and M by raising the temperature on the petroleum feedstock, and indeed, an increase in conversion was observed.

The selection of the experimental matrix was influenced by the expected increase in processing severity over current refinery practice that would be expected in the time frame of interest to the current study. The naphtha results indicate that the increase in severity went too far, and caused little improvement in product quality and may have contributed to catalyst deactivation. Considering that the matrix was developed with guidance from the literature of earlier coal liquid processing experiments, the current coal liquid was much more readily upgraded than was expected.

6. Distillate Hydrotreating

Hydrogenation of heavier fractions is practiced to increase hydrogen content and thereby improve the yield of valuable components, as well as to remove impurities that are unacceptable in fuels and which are damaging to downstream processing. The objectives of the test of DL1 heavy distillate were to:

- reduce the sulfur content to less than 380 ppmw
- reduce the nitrogen content to less than 380 ppmw
- increase the hydrogen content to 12 wt% or higher for FCC pretreatment
- reduce aromatics content, improving ignition quality
- obtain process data and operating efficiency data at various operating conditions.

The pilot plant hydrotreating configuration was identical to the one used in the naphtha processing. The hydrogen was circulated at a slightly greater flow rate than in the naphtha processing: make-up hydrogen was set at 12 SCFH and the recycle hydrogen was set at 24 SCFH. The make-up hydrogen varied from 1084 to 2981 SCFB, and the recycle hydrogen was added at between 2167 and 5961 SCFB. Pressures, temperatures, and flow rates were adjusted to attain 17 different conditions, A through Q in Figure 4. The operating conditions were varied between a low severity condition, set to match current refinery practice, and a high severity condition sufficient to reduce the sulfur and nitrogen contents of the treated distillate well below 380 ppmw to obtain storage stability. Pressures were varied between 700 psig and 1350 psig. Temperatures were varied from 620 to 688°F. The LHSV was also varied between 0.8 and 2.2 hr^{-1}.

Three feedstocks were used in the distillate hydrotreating. The first was a petroleum gas oil with properties to match the DL1 heavy distillate (within practical availability). The second was the DL1 heavy distillate fraction. The third was a blend of the two: 67% petroleum distillate/ 33% coal heavy distillate (by volume). The hydrotreating was done according to the test sequence depicted in the wire frame drawing of Figure 4.

The test sequence began with the petroleum feedstock at the low severity condition A. A sample was drawn at this and each subsequent condition. The neat coal liquid was then introduced at the low severity condition B. The temperature, pressure, and residence time were then increased to the high severity Condition C, and a sample was drawn and tested to assure the nitrogen was below 380 PPM. After several adjustments, this was established. The neat coal liquid was tested at nine additional conditions with varying pressure, temperature, and flow rate at severities between the two extremes of Conditions B and C. The petroleum/coal liquid blend was then tested at three conditions (M, N, and O), and the petroleum feedstock was reintroduced as the process was brought back to its initial, low severity condition P. Comparison of this last test condition to the first showed whether there had been significant catalyst deactivation, and this was checked by increasing the severity on the petroleum feedstock to Condition Q.

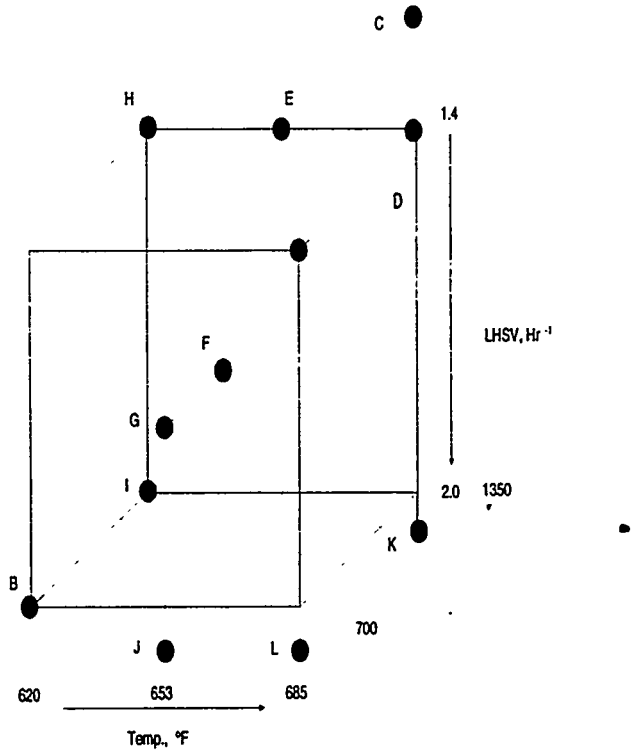

Figure 4. Experimental Matrix for DL1 Heavy Distillate Hydrotreating

Experimental Results: The test set points and the data collected are summarized in Table 3. The hydrogen content of the processed DL1 distillate consistently fell above 12 wt%, satisfying the test objective. The exception was Condition L, whose high flow rate made the condition effectively less severe than point B. Multiple tests of the hydrogen content showed an *average* hydrogen content of the product of 11.98 wt%. The range of product properties for the coal distillate was narrower than it was in the naphtha processing. The density differed by only 0.006 gm/ml and the hydrogen content differed by 0.24% wt between the extremes of process severity.

The hydrotreating step reduced sulfur and nitrogen in the DL1 heavy distillate below the 380 ppmw criterion required for product stability. Table 4 compares points differing in only one parameter, and presents the main, average effects of increasing pressure, temperature, and flow rate from the low to the high value of each parameter. As with the naphtha hydrotreating, the most influential control parameter was an increase in pressure from 700 to 1350 psig, which resulted in the predominant effect of increasing the hydrogen content by 0.105 wt%. An increase in hydrogen content was usually, but not always, accompanied by a

Table 3. Distillate Hydrotreating Summary							
SAMPLE #	Feed Type	Avgerage Processing			Density	H2 Wt%	Nitrogen
		Deg F	Psig	LHSV	g/mL	NMR	PPMW
Coal Dist	DL1Feed				0.919	11.87	590
Petrol	Petr Feed				0.868	12.22	109
A	Petr	619	700	1.9	0.851	13.20	<1
B	DL1	624	700	2.0	0.914	12.06	351
C	DL1	687	1350	0.8	0.909	12.23	2
D	DL1	688	1350	1.3	0.913	12.14	44
E	DL1	649	1345	1.4	0.913	12.14	115
F	DL1	654	1025	1.4	0.914	12.09	218
G	DL1	650	700	1.4	0.915	12.07	300
H	DL1	620	1345	1.4	0.913	12.17	238
I	DL1	622	1351	2.0	0.914	12.20	303
J	DL1	653	700	2.2	0.914	12.13	355
K	DL1	684	1351	2.1	0.911	12.10	129
L	DL1	685	700	2.2	0.915	11.98	321
M	Blend	686	699	2.0	0.875	12.57	53
N	Blend	685	1351	0.7	0.859	13.08	<1
O	Blend	618	700	1.9	0.876	12.55	119
P	Petr	620	699	1.9	0.854	12.87	53
Q	Petr	652	700	1.4	0.847	12.80	11

decrease in density, but over the narrow range of the data, no inference about resulting hydrocarbon composition should be made. There is an occasional inconsistency between these two effects. Increasing either the temperature (from 620 to 688°F) or LHSV (from 1.4 to 2.7 hr^{-1}) changed the hydrogen content and specific gravity by lesser amounts, and in inconsistent ways. A decrease in the LHSV should not decrease the hydrogen content. This information suggests that the variation within the data (analytical precision and randomness) is obscuring the effects caused by varying the process conditions over a limited range of severity.

7. Discussion of Hydrogenation Experiments

Regression analyses were performed on the data from both the naphtha and the distillate hydrotreater experiments. Predictive linear models of the specific gravity and hydrogen fraction were generated in a form relating these product properties linearly to the three operating parameters. This permitted a simplified model using a single plotting parameter, an index of hydrogenation severity. The severity term, S, is the

Table 4. Distillate Hydrotreating Main Effects					
Effect	Points	Effect on H_2	Effect on SG	Average Effect on H_2	Average Effect on SG
Temperature (620 to 688°F)	H to D I to K	-0.03% -0.10%	0 -0.003	-0.0125%	-0.0015
Pressure (700 to 1350 psig)	B to I G to E	+0.14% +0.07%	0 -0.002	+0.105%	-0.001
LHSV (1.4 to 2 hr-1)	H to I D to K	+0.03% -0.04%	-0.001 -0.002	-0.005%	-0.0015

combination of the controllable operating parameters: S = P·T/LHSV. In general, as the pressure, temperature, or processing duration (1/LHSV) increases, the products are processed more fully, whether for desulfurization, denitrogenation, or hydrogenation. Consequently, as the severity term increases, the hydrogen content should increase and the specific gravity decrease. Figure 5 shows the increase in hydrogen content (relative to the feedstock) for the naphtha and distillate hydrotreater runs. The figure shows a linear relationship between the hydrogen content and the severity term, considering the uncertainty in the data. The scatter in the data does not obscure the strong correlation. The same holds true for the specific gravity vs. severity.

The correlation coefficient, r^2, which is one measure of the goodness of fit of a model to data, was calculated for the severity model and a linear polynomial (e.g. $SG = a_0 + a_1 T + a_2 P + a_3 LHSV$) with terms comprised of the individual operating parameters as shown in Table 5. The numbers show that the severity model has a slightly stronger correlation to the data than the linear model.

Table 5. Comparison of Correlation Coefficients for Distillate Hydrotreating		
Property	R^2 (P,T,LHSV)	R^2 (Severity)
H_2 Wt%	0.37	0.52
Specific Gravity	0.59	0.59

8. Distillate FCC

Fluid catalytic cracking (FCC) of higher-boiling fractions of crude oil increases the value of heavy feedstocks and balances the product blending pool by providing gasoline blending components. In this unit process, feedstock is preheated before injection into the bottom of a vertical, fluidized bed reactor containing the finely divided , zeolite cracking catalyst. Steam and reactor gases transport the vaporized feed and catalyst up the riser and out to another vessel, the regenerator, where product gases are separated from the catalyst. The catalyst is valved into a lower vessel freed of deposited coke by combustion air before being recycled to the riser. The most significant operating parameters are catalyst to oil ratio and operating temperatures, while measured variables of interest include gasoline yield, gasoline octanes, and "coke make".

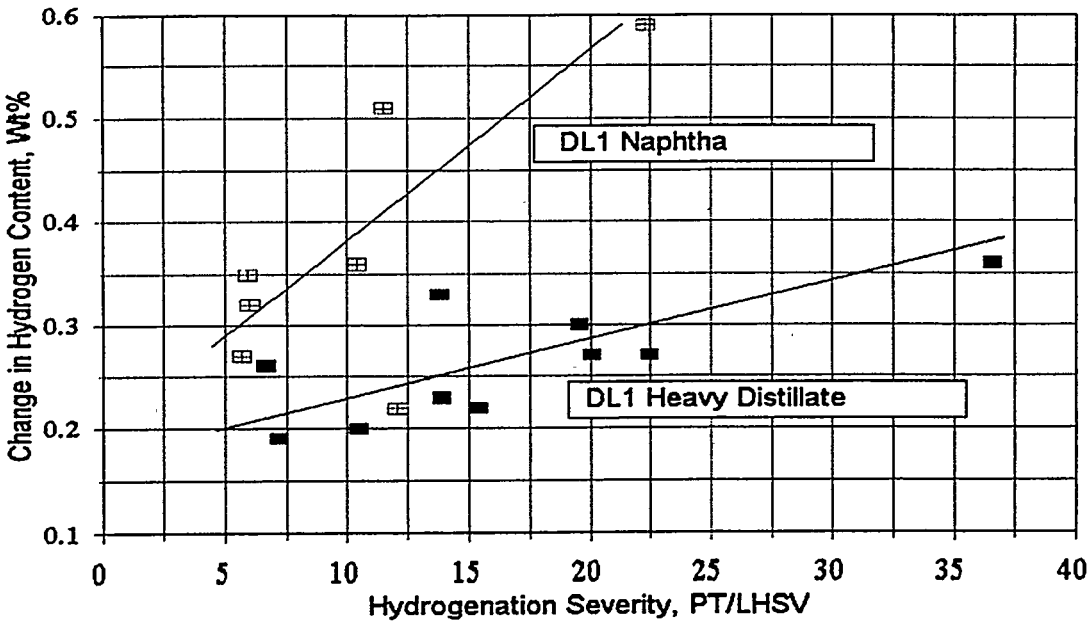

Figure 5. Hydrotreating Severity

The experiments performed at M.W. Kellogg Company were in two parts:

- Microactivity Tests (MAT) similar to ASTM D 3907 on the following:

IDENTITY	DESCRIPTION
DL1 Neat Heavy Distillate	550°F+ fraction of DL1
HTR Dist Product J	Slightly hydrotreated heavy distillate
HTR Dist Product R	Highest severity heavy distillate
HTR Dist Product C	Severely hydrotreated heavy distillate
Petroleum Gas oil	Matched boiling range
Blend	50:50 (vol) DL1 Dist & Petr Gas Oil

- Pilot plant FCC tests on:

IDENTITY	DESCRIPTION
Petroleum Gas Oil	Matched boiling range
DL1 HTR Dist Product C	Severly hydrotreated 550°F+ fraction of DL1
Blend	33:67 (vol) DL1 Dist & Petr Gas Oil

A MAT test apparatus consists of a glass reaction tube containing 3 to 7 grams of prepared FCC catalyst in a two-zone furnace (970°F) and syringe injector delivering 1 ml over a 30-second time span.

The procedure includes a nitrogen flush after injection then GC analysis of the product gases. The liquid product is also analyzed by GC to determine conversion to gasoline (yield) and to estimate octane number. The carbon on the catalyst is determined by measuring CO_2 production upon burnoff. A mass balance accounting for >95% of the material is required for a successful run. The MAT test runs provided:

- Yield over a range of conversions for each liquid
- Gasoline composition of one product of each feed
- Octane numbers of selected products showing effect of hydrotreating.

The results of the MAT testing are interpreted through plots of conversion to gasoline and coke yield such as in Figure 6, which shows both parameters as a function of catalyst to oil ratio. For three materials of varied hydrotreating severity, the overall effect of hydrogen content on gasoline yield is shown in Figure 7. The line for "potential gasoline" also takes into account C3 and C4 olefins plus butane, which are used in alkylation and ether production to the benefit of gasoline. This desireable effect is directly from the molecular structure of the coal-derived component. The range of hydrotreating severity increased the gasoline yield from 52 to 65 Wt% as a linear function of hydrogen concentration.

The pilot plant runs are summarized in Table 6 for the three liquids tested. The catalyst rates averaged 48.2 pounds per hour of Vektor-50 FCC catalyst from Conoco while oil rates were ~0.47 pounds per hour. Riser outlet pressure was 35 psig. Other data appear in the table. All three feedstocks ran well with little filter plugging propensities, which bodes well for the test fuel production run in Option 1.

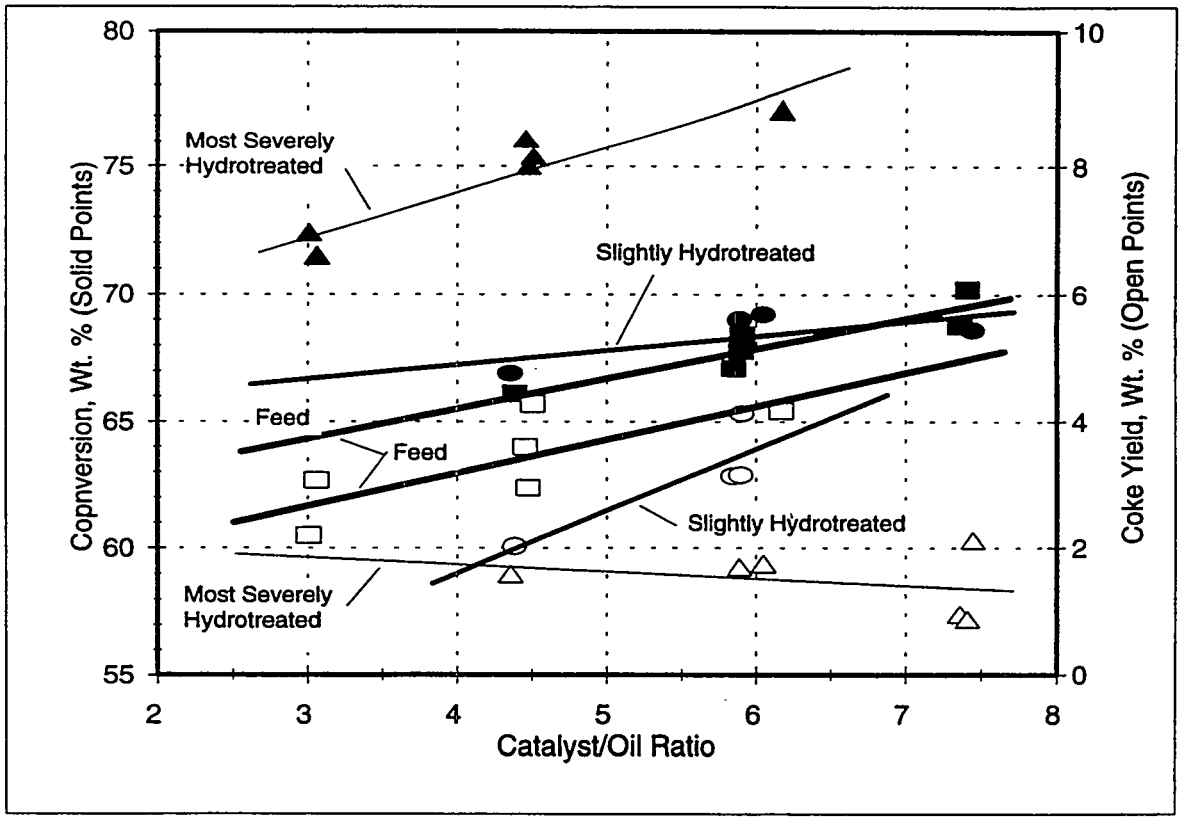

Figure 6.. FCC Performance of Hydrotreated DL1 Heavy Distillate

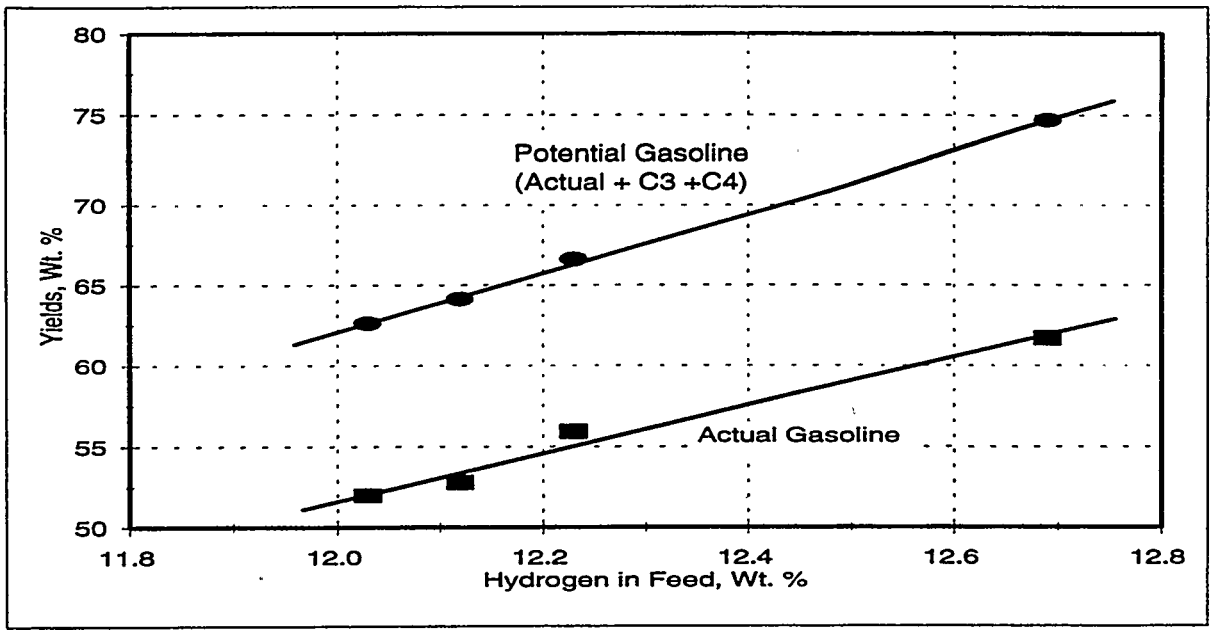

Figure 7. Effect of Distillate Hydrogen Content on Gasoline Yield

Table 6. DL1 Heavy Distillate FCC Pilot Plant Operations Summary			
Run Number	1	2	3
Feed	Gas Oil	DL1 Dist	Blend
Catalyst/Oil Ratio	12.2	12.2	12.0
Temperatures			
Feed Preheat	212	212	214
Catalyst Inlet	1265	1253	1252
Riser Average	984	987	983
Material Balance			
Closure, Wt%	98.50	98.49	98.46
Conversion, Wt%	74.13	74.20	73.18
C2 & Lighter	3.34	2.03	2.83
C3 & C4	15.37	13.73	15.02
C5 - 430°F	50.52	55.17	51.01
430°F$^+$	25.87	25.80	26.82
Coke	4.90	3.27	4.32
Octanes			
Engine RON/MON	91.0/80.3	91.0/80.0	90.7/80.2
GC RON/MON	93.2/81.1	92.8/81.0	90.7/80.7

Compared to the petroleum stock, the coal liquid made much less coke and nongasoline products. The lower coke make would require far more conversion than would yield the optimum product distribution (maximum gasoline). In practice this indicates the need for an auxiliary fuel to supply adequate energy in the regenerator to keep the FCC unit in heat balance at the required temperatures. The required heat inputs at optimum yields were calculated for each material for use in optimizing the LP refinery model.

9. Indirect Wax Processing

As shown in Figure 1, the sequence of steps applied to the upgrading and integration of Indirect Liquid 1 (IL1) differs from the sequence for the DLs, because of the nature of the Fischer-Tropsch product. Air Products and Chemicals produced the IL1 feedstock in the DOE Alternative Fuels Process Development Unit (PDU) at LaPorte, Texas during tests to check the hydrodynamics of the unit. In the PDU an artificial coal gasification syngas is conducted through a slurry of high activity iron oxide catalyst, which polymerizes the methane and the paraffin products of polymerization. The overflow from the slurry reactor enters several stages of separation to return catalyst and low molecular weight paraffins to the reactor. Product paraffins leave the process as a stream of hydrocarbons liquid at room temperature, a light wax slurry, and a heavy wax, which is solid at room temperature. There are traces of olefins and oxygenates made during the reaction. There is also an aqueous effluent.

Feed Preparation: The first step in the investigation was reconstituting the fractions of interest for processing experiments. As a test of hydrodynamics, it was not a concern to preclude incidental catalyst release with the heavy wax. Catalyst cannot leave with light wax and hydrocarbon liquid, because they are condensed from vapor when they are discharged. Since the iron-based catalyst would interfere with downstream processing experiments and would not be present in a commercial production wax, a clean up step was added in which the 5 Wt% iron was reduced below 500 ppmw.

After lab-scale experimentation, a technique was implemented at Southwest Research Institute to remove nearly 99.9 Wt % of the catalyst while not skewing the hydrocarbon distribution of the heavy wax. Approximately 20 V% catalyst containing wax was dissolved in Isopar M™ solvent at 250°F and sent through 1.5 micron cellulose filter paper in a plate and frame filter press. The Isopar M solvent was removed by two-pass distillation in a wiped film pilot plant under vacuum. The next step was removing the 20 Wt% 650°F$^+$ material contained in the light wax for recombination with the clean heavy wax. Each portion of this heavy fraction of the light wax was mixed with four parts clean heavy wax to reconstitute the as-produced 650°F$^+$ portion of the PDU product for further experiments.

Fluid Catalytic Cracking Experiments: At Amoco Oil R&D, FCC pilot plant runs were made at 20 and 40 Wt% wax concentration in conventional petroleum FCC feed from the Amoco Whiting, IN refinery. The catalyst (also used at M.W. Kellogg) was fed at ~2 pounds per hour. Liquid feed was about 0.22 pounds per hour. Other operating data as well as pilot plant results appear in Table 7.

Table 7. IL1 FCC Pilot Plant Operations Summary			
Run Number	1	2	3
Feed	FCC Petr.	20 Wt%	40 Wt%
Catalyst/Oil Ratio	9.43	9.57	8.88
Temperatures			
Feed Preheat	394	393	394
Riser Average	953	953	952
Material Balance			
Closure, Wt%	100.04	100.00	100.01
Conversion, V%	71.52	75.44	79.98
C2 & Lighter	2.14	2.04	1.79
C3 & C4	14.05	15.84	17.43
C5 - 430°F	51.37	53.32	56.36
430°F+	28.78	25.05	20.69
Coke	3.68	3.76	3.75
Octanes			
	88.2/79.6	86.6/78.8	86.7/79.2

Initial runs with the wax blends exhibited injector nozzle plugging from coke buildup. The plugging was determined to come from composition, rather than catalyst fines. Boring out the injector nozzle from 0.02" to 0.04" allowed the pilot plant to run successfully on both blends. Analysis of the data show that the incremental naphtha yields were 82 V% for the 40% blend and 75 V% for the 20% blend *versus* 62 V% for the petroleum FCC feed. The incremental C4+ olefins yield was 18 Wt% for both wax blends compared to 10 Wt% for the petroleum. The results indicate that the cycle oil produced is very light and that very little of the more troublesome decant oil is produced.

Incremental product values, using a 1994 price structure, show the LaPorte FT wax/gas oil blend products to be worth three dollars per barrel more than the gas oil cracked products alone. This is principally because of the greater naphtha yield and because of the valuable light olefins. Compared to previous work on fixed bed FT wax cracked products, there was only a one octane number debit compared to the petroleum-only case, while there was a 4 octane number debit for similar fixed bed products. Also the coke make was 75% higher with IL1 than fixed bed FT wax processing.

10. Summary and Future Work

The *End Use Study* is nearing the completion of its pilot plant analysis of DL1 fractions and will soon begin work on DL2. In fact, the DL2 feedstock, POC-2 from subbituminous coal, is being fractionated now. The unexpectedly superior properties of DL1 resulted in hugher than necessary processing severities, which resulted in narrow ranges of product properties from naphtha and heavy distillate hydrotreating. Operating conditions in subsequent experimental matrices will be broadened accordingly.

The naphtha hydrotreating showed good denitrogenation and readily met the specification of ½ ppmw needed to protect modern reforming catalysts. Similar results were observed in special testing for sulfur. Good agreement between hydrogen concentration increase and density decrease (except at two experimental points) indicated that the feed resisted dehydrogenation by reverse reactions which tend toward the concentration of aromatics favored by in thermodynamic equilibrium.

The heavy distillate hydrotreating achieved 90 - 97 Wt% hydrodenitrogenation, well below the target production concentration of 380 ppmw. Limited tests showed similar results for sulfur. Hydrogen addition was readily achieved. Observed catalyst deactivation probably arose from temperature excursions as shown by increased treatment of the petroleum stock upon increasing reactor temperature. Byproduct hydrogen sulfide can be removed by stripping with nitrogen gas to obtain a stable product.

FCC pilot plant and MAT tests showed that gasoline yields increase from 52 to 62 Wt% when the DL1 distillate is severely hydrotreated. Coke production was low indicating that extra heat would be needed to balance cracking operations at the optimum conditions for gasoline production. The indications were that all the products were good gasoline producers and would be unlikely to foul catalysts. Octane numbers produced were comparable to petroleum and the effect of hydrotreating was to make a small increase with increasing hydrogen content. The prospects for the production run of blend components from cracking of DL1 heavy distillate is favorable.

Work on IL1 is at an early stage. Reconstitution of the heavy wax fraction by cleaning and distillation is complete. FCC pilot plant testing of 20 and 40 Wt% blends of the resulting heavy wax showed better performance in cracking than comparable fixed bed FT wax feeds. A 75 Wt% higher coke production was observed for IL1 over a similar fixed bed FT feed. Calculations showed a three dollar per barrel premium of IL1 heavy wax blends over the matched petroleum feed from increased naphtha production and the higher proportion of valuable light olefins. This value was attained with only a small reduction in octane numbers of the FT blend's naphtha *versus* the petroleum naphtha. In all the IL1 would make a valuable FCC feed.

11. Acknowledgements

The authors wish to acknowledge the DOE Program Manager, Dr. Shelby Rogers and the Bechtel Project Director, Mr. Samuel Tam and Project Manager, Mr. Clifford Lowe for their insightful operation of the research program. The use of the DOE Alternative Fuel Center pilot plant is greatly appreciated, NREL Program Managers, Messrs. Brent Bailey and Christopher Colucci. The work at M. W. Kellogg Company was reported and performed by W.A. Cronkright, M.I. Schlossman and P.J. Shires and their laboratory staff. The processing and analyses at Southwest Research Institute were performed by C.C. Cover, D.L. Hetrick, P. M. Rainwater, and G. R. Segura.

The investigators for indirect coal product processing at Amoco were J. A. Mahoney and M.M. Schwartz. The feedstock preparation effort at Southwest Research Institute was led by Mr. D.E. Ketchum with processing by J.L. Merold and J.P. Montgomery.

TITLE: **REFINING AND END USE STUDY OF COAL LIQUIDS II - LINEAR PROGRAMMING ANALYSIS**

AUTHORS: Cliff Lowe and Sam Tam

ORGANIZATION: Bechtel Group, Inc.

CONTRACT: DE-AC22-93PC91029

PERIOD OF PERFORMANCE: 11/1/93 to 9/30/97

1.0 Abstract

A DOE-funded study is underway to determine the optimum refinery processing schemes for producing transportation fuels that will meet CAAA regulations from direct and indirect coal liquids. The study consists of three major parts: pilot plant testing of critical upgrading processes, linear programming analysis of different processing schemes, and engine emission testing of final products.

Currently, fractions of a direct coal liquid produced from bituminous coal are being tested in sequence of pilot plant upgrading processes. This work is discussed in a separate paper.

The linear programming model, which is the subject of this paper, has been completed for the petroleum refinery and is being modified to handle coal liquids based on the pilot plant test results. Preliminary coal liquid evaluation studies indicate that, if a refinery expansion scenario is adopted, then the marginal value of the coal liquid (over the base petroleum crude) is $3-4/bbl.

2.0 Project Overview And Objective

Bechtel, with Southwest Research Institute, Amoco Corp., and the M.W. Kellogg Co. as subcontractors, began a study on November 1, 1993, for the U.S. Department of Energy's (DOE's) Pittsburgh Energy Technology Center (PETC) to determine the most cost effective and suitable combination of petroleum refinery processes needed to make specification transportation fuels or blending stocks from direct and indirect coal liquefaction product liquids.

A key objective is to determine the most desirable ways of integrating coal liquefaction liquids into existing petroleum refineries to produce transportation fuels meeting current and future, e.g. year 2000 and beyond, Clean Air Act Amendment (CAAA) standards. An integral part of the above objective is to test the fuels produced and compare them with appropriate ASTM fuels. The comparison will include engine tests to ascertain compliance of the fuel slate with CAAA and other applicable fuel quality and performance standards.

Three types of coal liquids will be examined in this study: (1) direct coal liquids from a bituminous coal, (2) direct coal liquids from a sub-bituminous coal, and

(3) indirect coal liquids (Fischer-Tropsch). The two direct coal liquids were produced by hydrogenation in the HRI Proof-of-Concept (POC) pilot plant. The indirect coal liquids (distillate and wax portions) were produced in the DOE-AFPDU (Alternate Fuels Process Development Unit) at La Porte, Texas.

The final part of the project includes a detailed economic evaluation of the cost of processing the coal liquids to their optimum products. The study reflects costs for operations using state of the art refinery technology; no capital costs for building new refineries is considered. Some modifications or additions to the existing refinery may be included if they are economically justified. Economy of scale dictates the minimum amount of coal liquid feedstock that should be processed.

To enhance management of the study, the work has been divided into two parts, the Basic Program and Option 1.

BASIC PROGRAM

The objectives of the Basic Program are to:

- Characterize the coal liquids
- Develop an optimized refinery configuration for processing indirect and direct coal liquids
- Conduct pilot plant tests on the critical upgrading processes
- Develop a LP refinery model with the Process Industry Modeling System (PIMS) software.

The work has been divided into six tasks.

Task 1 - Development of a detailed project management plan for the Basic Program
Task 2 - Characterization of the three coal liquid feeds supplied by DOE
Task 3 - Optimization of refinery processing configurations by linear programming
Task 4 - Pilot plant analysis of critical refinery process units to determine yield, product quality and cost assumptions. Petroleum cuts, neat coal liquids, and coal liquids/petroleum blends will be processed through the following process units: reforming, naphtha and distillate hydrotreating, catalytic cracking and hydrocracking.
Task 5 - Development of the project management plan for Option 1
Task 6 - Project management of the Basic Program and Option 1

OPTION 1

The objectives of Option 1 are to:

- Confirm the validity of the optimization work of the Basic Program
- Produce large quantities of liquid transportation fuel blending stocks
- Conduct engine emission tests

- Determine the value and the processing costs of the coal liquids

This will be done by processing the coal liquids and petroleum blends under the optimized conditions indicated by the results obtained in Task 4 , blending and characterizing the product liquids, and running engine emission tests of the blends. Option 1 has been divided into three tasks.

Task 1 - Based on the pilot plant and linear programming optimization work of the Basic Program, production runs of pilot plants (hydrotreating, reforming, catalytic cracking, and hydrocracking) will be conducted to produce sufficient quantities for blending and engine testing.
Task 2 - The pilot plant products will be blended, characterized, and engine tested
Task 3 - An economic analysis will be conducted to determine the value of processing the coal liquids through the existing refinery

3.0 Linear Programming Model

A model was developed using the Bechtel PIMS (Process Industry Modeling System) linear programming software to simulate a generic Midwest (PADD II) petroleum refinery of the future[1].

This "petroleum-only" version of the model aimed to establish the size and complexity of the refinery after the year 2000 and prior to the introduction of coal liquids. It should be noted that no assumption was made on when a plant will be built to produce coal liquids, except that it will be after the year 2000. The year 2000 was chosen because it is the latest year where fuel property and emission standards have been set by the Environmental Protection Agency. The model assumes the refinery has been modified to accept crudes that are heavier in gravity and higher in sulfur than today's average crude mix. In addition, the refinery has also been modified to produce a product slate of transportation fuels of the future (i.e. 40% reformulated gasolines with advance specifications). This model will in turn be used as a basis for determining the optimum scheme for processing coal liquids in a petroleum refinery.

3.1 Refinery Expansion Scenario

A refinery expansion scenario was chosen as the basis for evaluating the three coal liquids that are being examined in this study. The refinery expansion scenario is a reasonable assumption because:

- No grass roots refineries will be built in the future for economic and environmental reasons.
- As small or uneconomical refineries shutdown, larger and more complex refineries will be expanded to meet consumption.

- Coal liquids will have the highest value when credit is given for capital avoidance. In an expansion, the use of higher quality coal liquids will allow for lower capital expenditures.

The first step in developing this expansion scenario was to establish a base refinery configuration. This configuration, which is called Case 1, represents how the refinery would look prior to expansion.

The Case 1 refinery has the following characteristics:

- Nominal crude feed rate is 150,000 BPD .
- Crude is heavier and higher in sulfur than current average PADD II crudes.
- Unit capacities are adjusted from 1993 PADD II average capacities.
- All process units are running at capacity.
- Product slate and specifications are based on year 2000 estimates and the EPA Complex Model.

Case 2 or the expansion scenario, involves expanding the Case 1 refinery based on the following assumptions:

- Nominal feed rate is increased to 200,000 BPD by increasing product demand by 33.3% (over Case 1). The increase in feed consists of either additional crude or coal liquids.
- Process units are added or expanded as economically warranted. Capital costs are charged for expansion costs above Case 1 capacities.
- The product slate is the same as for Case 1.
- The crude feedstock is the same as for Case 1.

Figure 1 shows the differences between the two cases. Except as noted, the coal liquids will be evaluated under the Case 2 - expansion allowed scenario.

3.2 Initial coal liquid pilot plant data

The Direct Coal Liquid 1 (DL1) heavy distillate hydrotreating pilot plant tests conducted by SwRI provided treated samples produced under a number of different conditions. Three of these samples (treated under mild, medium and high severity conditions) and an untreated sample were sent to M.W. Kellogg for catalytic cracking tests. This section of the report describes how the results from the SwRI and Kellogg tests were used in the LP model to decide on the optimum processing sequence.

The procedure used was to take the raw test data and develop yields, consumptions, and product properties for hydrotreating and catalytic cracking the DL1 heavy distillate. These yields, consumptions, and properties were then entered into the LP model and the refinery operations were optimized.

Heavy Distillate Hydrotreating

Input to the model for the three samples that were sent to Kellogg was developed as follows:

- Hydrogen consumptions were estimated for the three samples based on hydrogen uptake and heteroatom removal.
- Volumetric yields were adjusted to achieve a weight balance for each condition.
- Distinct liquid product streams were created for each severity level.
- Capital costs and utilities (per barrel) were assumed to be the same for each severity level, thus giving an advantage to the high severity case.

Catalytic Cracking

Data for the model for the three treated and one untreated samples were developed as follows:

- Volumetric yields were calculated for the four coal liquids based on Kellogg weight based yield data.
- For each product cut range (naphtha, diesel, etc.) the properties were assumed to be the same regardless of the feed type.
- Fuel usage was adjusted based on coke yield for each feed type to achieve a heat balanced operation.

The results from the above work are summarized in the table below. It shows that, as expected, as hydrotreating severity increases, the hydrogen consumption and distillate yield increase, and the specific gravity decreases. The gasoline yields from catalytic cracking increase as the hydrogen content of the hydrotreater product increases.

Distillate Hydrotreating				
Severity		Low	Medium	High
Pressure, psig		700	1350	1800
Temperature, °F		653	687	730
LHSV		2.2	0.8	0.9
Hydrogen Consumption, SCF/bbl		212	286	565
Distillate yield, volume %		100.15	100.49	101.69
Product specific gravity		0.914	0.909	0.887
Catalytic Cracking				
Feed hydrotreating severity	Neat	Low	Medium	High
C5-430, volume % of feed	63.6	63.8	66.9	73.7
Fuel usage, MMBtu/bbl	0.200	0.200	0.203	0.264

Operating fuel usage is an adjustment to achieve a heat balanced yield.

3.3 Preliminary coal liquid evaluation studies

3.3.1 Distillate hydrotreating/catalytic cracking

A diagram showing the possible processing options for the DL1 heavy distillate is shown in Figure 2. This shows that the program is allowed to choose the most economical path for processing the heavy distillate. Each path has advantages and disadvantages.

1. Sending the neat heavy distillate to diesel/fuel oil blending avoids the capital and operating costs of hydrotreating and cat cracking, but the product has a lower value than gasoline. In addition, the neat liquid may not meet diesel specifications even after blending with higher quality material.

2. Hydrotreating the heavy distillate before sending it to blending may allow it to meet specifications, but there are significant costs and, again, the blended product has a low value.

3. Cat cracking the neat heavy distillate avoids the costs of hydrotreating and results in higher value gasoline blendstock, but the cat cracking yields are lower than the yields with hydrotreated feeds.

4. Cat cracking the hydrotreated heavy distillate is the most expensive option from a capital and operating standpoint. The higher gasoline yields, however, may compensate for these costs.

A run was made in which 50,000 bbl/day of DL1 were fed into refinery under the Case 2 - refinery expansion scenario. An analysis showed that 90 percent of the neat heavy distillate bypassed the distillate hydrotreater and was sent to the catalytic cracker (option 3 above). This is because the improved cat cracker yields from the hydrotreated feeds are not enough to compensate for the additional hydro-treating capital costs. Seven percent of the neat heavy distillate was sent directly to diesel blending. The remaining three percent was hydrotreated (at medium severity) and then blended into the diesel pool.

3.3.2 Feedstock value determination

In determining the value of different feedstocks such as coal liquids, it is important to understand the term *objective function*. *Objective function* is a linear programming term defined as follows:

Objective Function = Revenues - Purchases - Utilities - Capital charges

The linear program maximizes the objective function based on the constraints set by the model.

Using a method similar to the one used for the alternate crude feedstocks, the value of the coal liquids was determined by using the linear programming model. The first step was to run the model without any coal liquid feed. This

was followed by forcing a given amount of the coal liquid into the model at zero value. The coal liquid value is the change in objective function divided by the amount of coal liquid feed. The end result is such that when this value for the coal liquid is used in the model , the objective function will be the same as for the zero coal liquid case.

3.3.3 Preliminary coal liquid value determination

Figure 3 shows the results of the coal liquid evaluation work. With the base petroleum crude set at $18/bbl, the DL1 coal liquid had a value varying from 21 to 22 $/bbl, depending on the amount of coal liquid fed into the refinery. Under closer inspection, this coal liquid margin of $3-4/bbl is due to a combination of capital avoidance and lower feedstock (crude, butanes, methanol, etc.) volumes.

The capital avoidance portion of the margin is distributed into a number of areas. In comparison with the Case 2 run with zero coal liquid, there is:

- Less cat cracking (less resid to process)
- Less alkylation (less olefins from cat cracking)
- Less kerosene/distillate treating (higher quality CL distillate allows bypassing)
- More naphtha HDT/reforming (more light material in CL)
- Less low value product

At 50,000 BPD of coal liquid, the $3.25/bbl margin over the base petroleum crude is broken down as follows:

	$/bbl	
Capital avoidance -	1.48	
Utility charge	(0.10)	
Additional feedstock avoidance	2.79	(less total feedstock is required with coal liquids)
Additional product	(0.92)	
Total	3.25	

Figure 4 shows the significance of capital avoidance. For the Case 2 - expansion allowed scenario, the daily capital charges are plotted versus increasing amounts of coal liquid. This shows that at zero coal liquid, the daily capital charges would be approximately $274,000. This falls steadily to $193,000 when 60,000 BPD of coal liquids are processed. This $81,000 savings is directly due to the characteristics of the DL1 coal liquid.

3.3.4 Expansion vs. no expansion allowed

The DL1 coal liquid was also evaluated under the Case 1 - no expansion scenario. Here, the coal liquid displaced a portion of the 150,000 BPD of crude. The results are shown in Figure 5. The coal liquid margin is significantly lower, 0.50 to 1.20

$/bbl. This is because the model is much more restricted in the number of ways it can process the coal liquid. In particular, there is no credit for capital avoidance.

3.3.5 Effect of new pilot plant data

Prior to the experimental work detailed in section 3.2, direct coal liquid yields, properties, etc. were estimated based on preliminary DL1 characterization work and yields and properties from previous coal liquid upgrading studies. These studies in turn were based on using coal liquid feedstocks from early liquefaction processes such as Solvent Refined Coal (SRC) and Exxon Donor Solvent (EDS). These liquids are significantly inferior in quality to DL1 and, thus, require more extensive upgrading than DL1 requires.

These yield and property estimates were used in the model and several runs were made to determine the coal liquid values at several feed rates.

Figure 6 compares the results from these LP runs to the results from the runs made with the new pilot plant data. The lower curve is the coal liquid values with the original estimates for yields, properties, etc. The upper curve is the values based on the new data. This shows that using the pilot plant data results in about a $1/bbl increase in coal liquid value. This increased value emphasizes the higher quality of DL1 over the coal liquids of earlier generations. In particular, DL1 does not require costly heavy distillate hydrotreating.

4.0 Summary

The linear programming model of a generic PADD II refinery was used to make preliminary evaluations of the DL1 coal liquid. The evaluations were made using the assumption that the coal liquids could fulfill the incremental feedstock requirements in a refinery expansion scenario. The results showed that:

- The DL1 coal liquid margin ranged from $3-4/bbl depending on the amount of coal liquid fed into the refinery. A significant portion of this margin is due to the avoidance of capital expenditures when coal liquids are used.
- In a case scenario where no expansion is allowed and all refinery process unit capacities are fixed, the margin falls to 0.5-1.2 $/bbl.
- Incorporation of the recent pilot plant test data into the model resulted in 1.0 $/bbl increase in the coal liquid margin over the value using literature data. This increase reflects the higher quality of the DL1 coal liquid over previous coal liquids.

5.0 References

1. "Petroleum Refinery Linear Programming Model Design Basis", DOE Contract No. DE-AC22-93PC91029, Topical Report, March, 1995.

6.0 Acknowledgments

Bechtel, along with the Southwest Research Institute, Amoco Corp. and the M.W. Kellogg Co., would like to express their appreciation to the Department of Energy for their financial support and technical assistance.

Figure 1 - Base and Expansion Scenarios

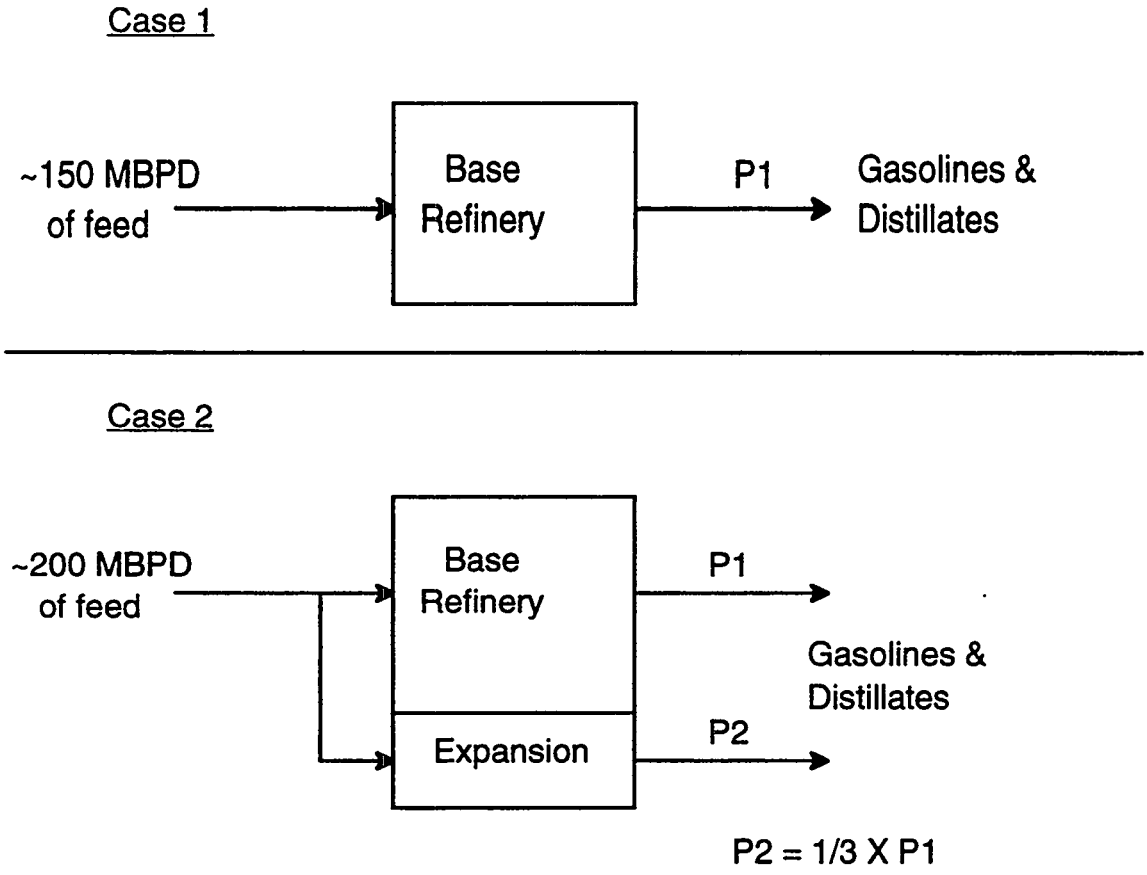

Figure 2
Heavy Distillate Hydrotreating/Catalytic Cracking

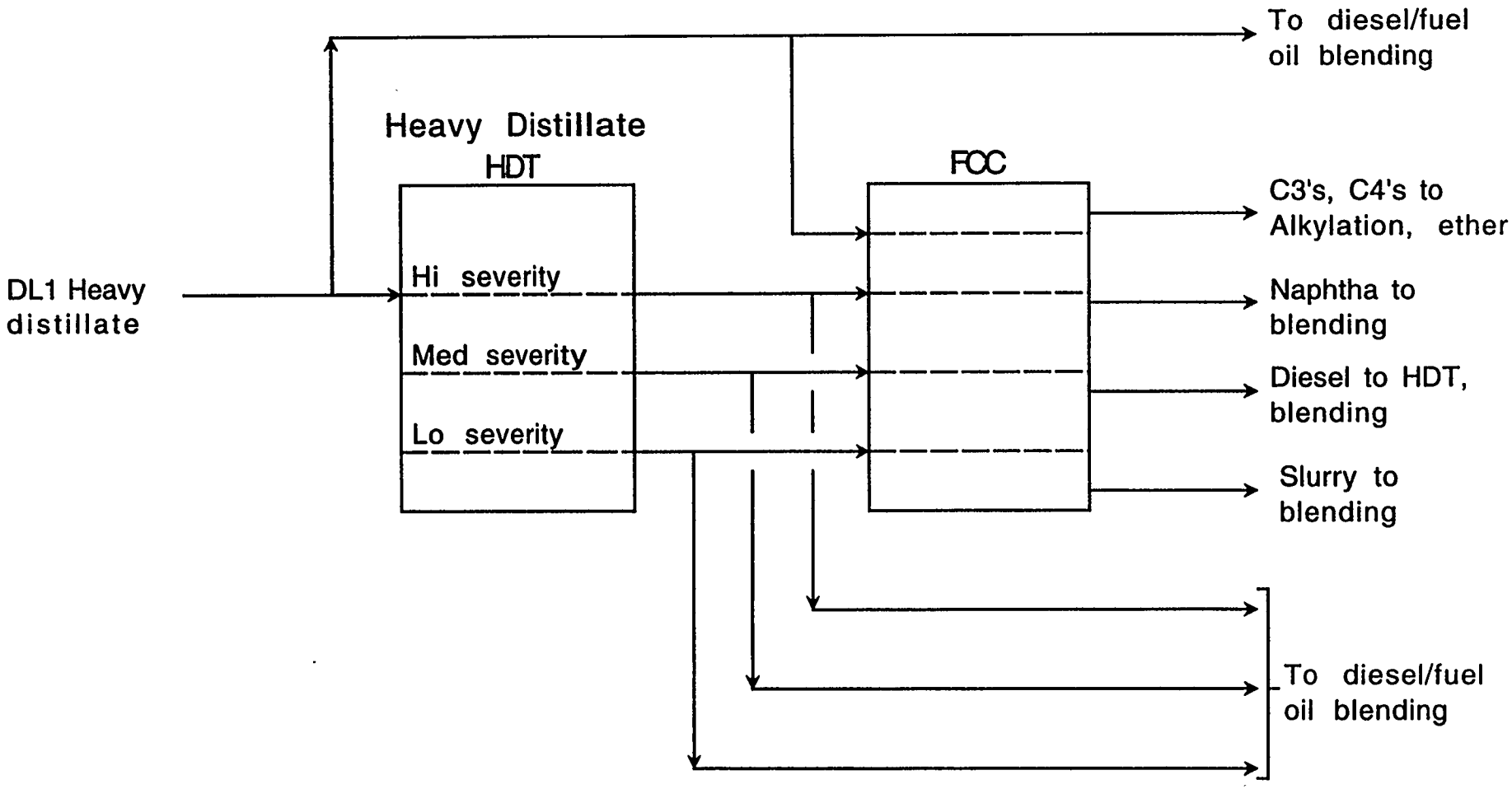

Figure 3
DL1 Coal Liquid Value

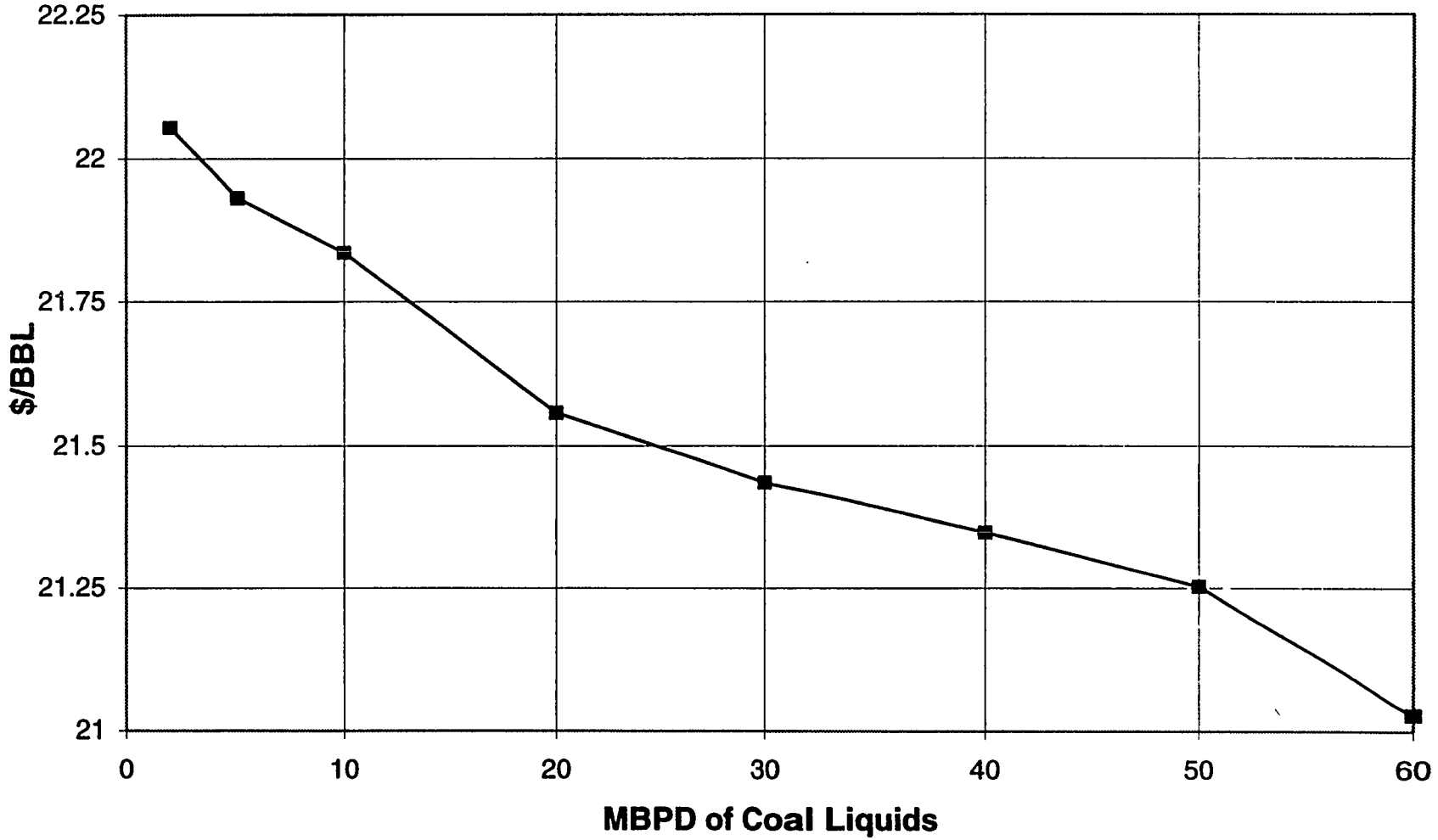

Figure 4
Capital Expenditures

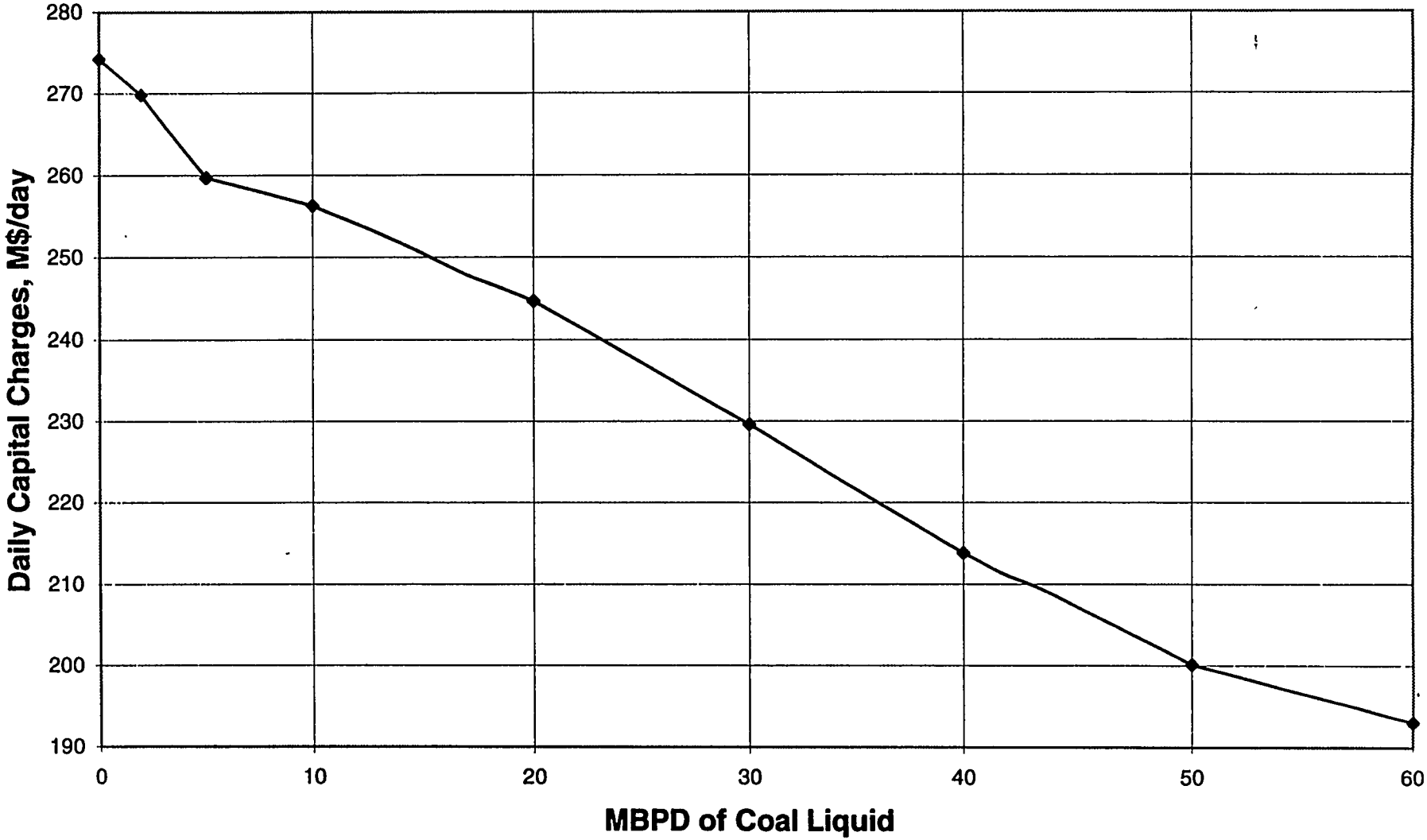

Figure 5
DL1 Coal Liquid Value
Expansion vs. No Expansion

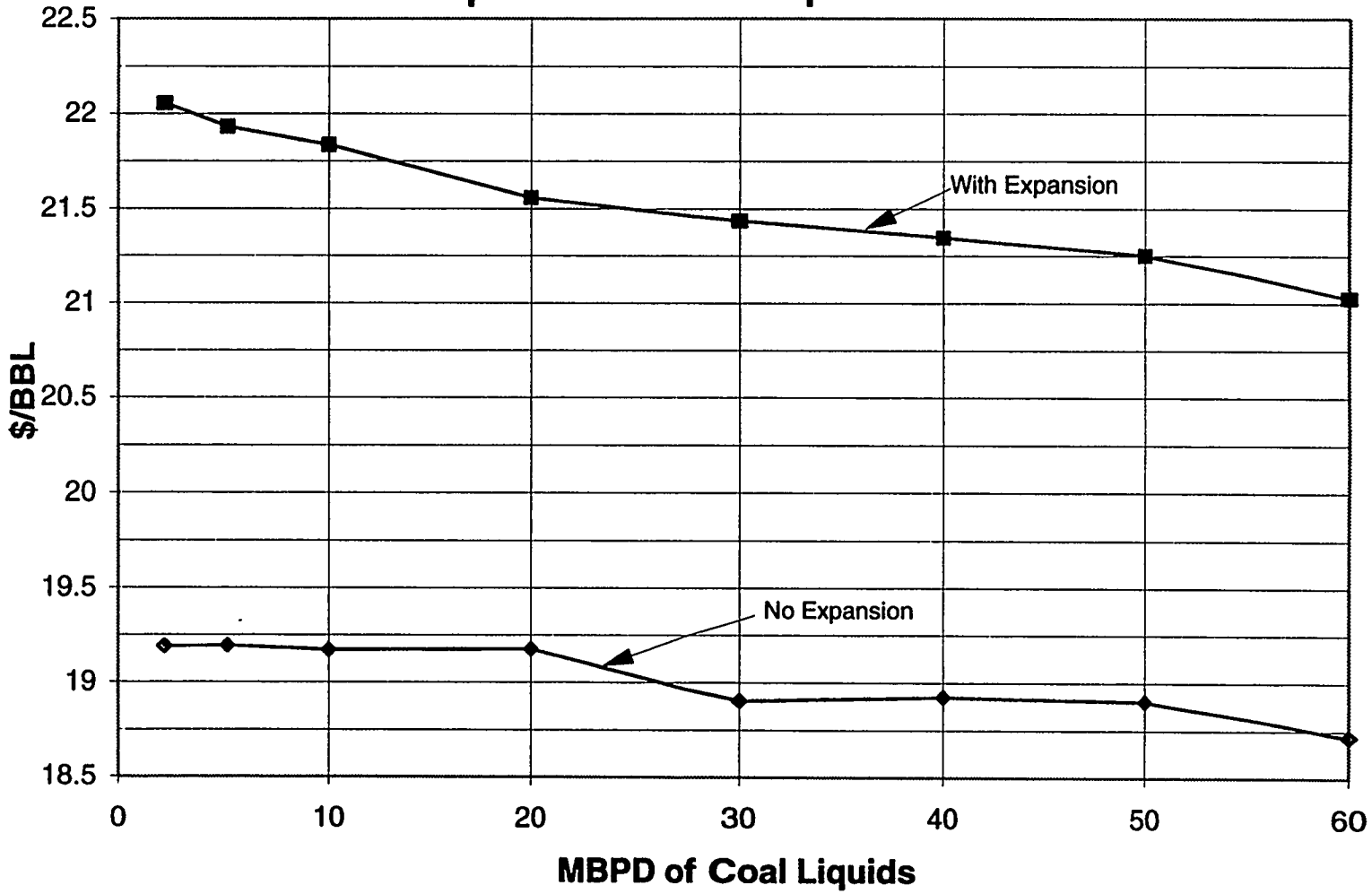

Figure 6
DL1 Coal Liquid Value
Effect of Pilot Plant Data

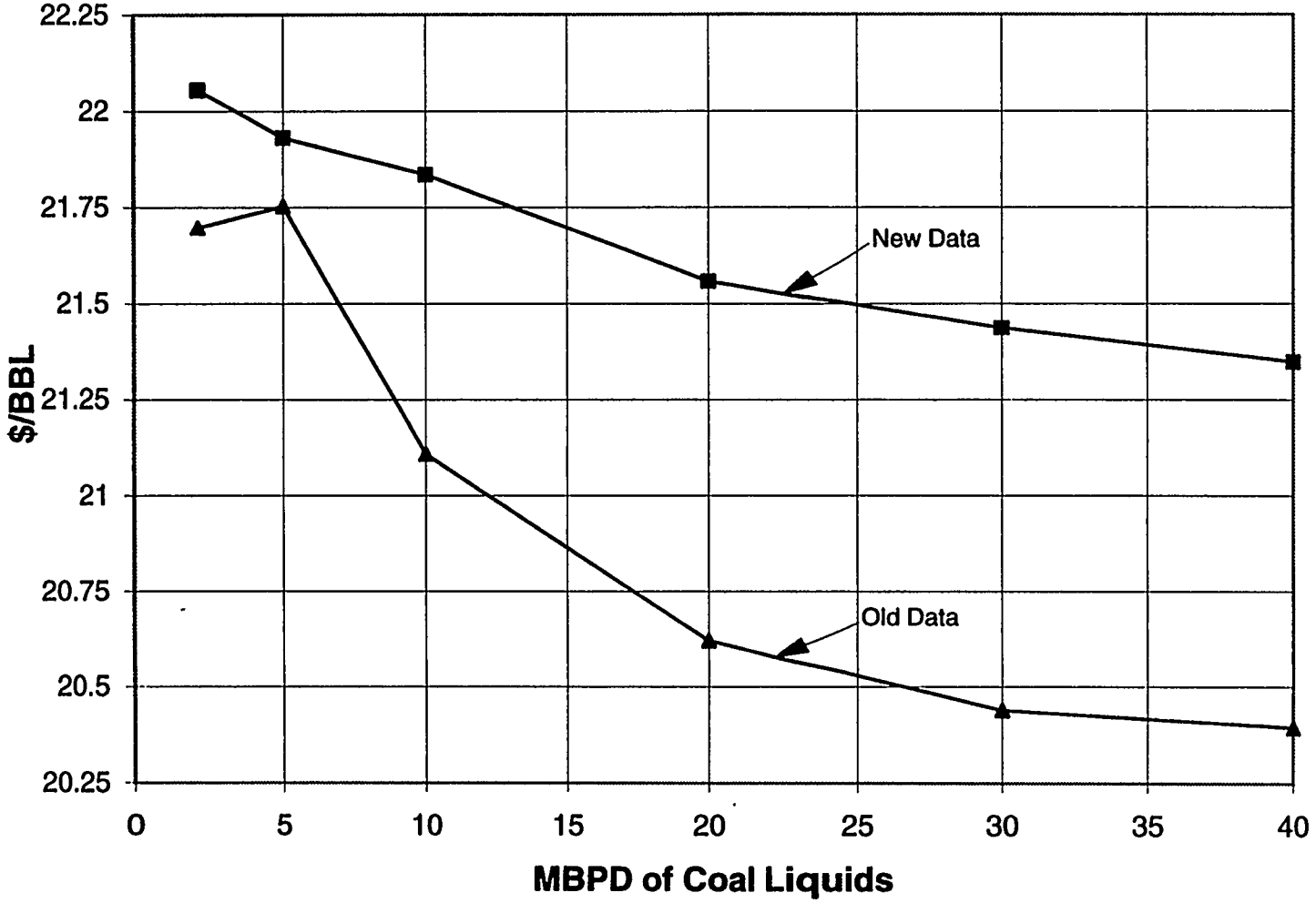

Title: **HYDROTREATING OF COAL-DERIVED LIQUIDS***

Authors: Stephen E. Lott, Frances V. Stohl, Kathleen V. Diegert, David C. Goodnow, John B. Oelfke

Organization: Sandia National Laboratories, Albuquerque, NM 87185-0709

Contract No.: Sandia's work was funded by the U. S. Department of Energy under contract DE-AC04-94AL85000.

Period of Performance: October 1992 -

Objective: To develop a database relating hydrotreating parameters to feed and product quality by experimentally evaluating options for hydrotreating whole coal liquids, distillate cuts of coal liquids, petroleum, and blends of coal liquids with petroleum.

Accomplishments: The objective of Sandia's refining of coal-derived liquids project is to determine the relationship between hydrotreating conditions and product characteristics for liquids produced using current technology. The coal-derived liquids used in this work were produced in HTI's (formerly HRI) first proof-of-concept run using Illinois #6 coal. Samples of the whole coal liquid product, distillate fractions of this liquid, and Criterion HDN-60 catalyst were obtained from Southwest Research Inc. Hydrotreating experiments were performed using a continuous operation, unattended, microflow reactor system. A factorial experimental design with three variables (temperature, (310°C to 388°C), space velocity (1 to 3 g/h/cm^3(cat)), pressure (500 to 1000 psig H_2)) was being used in this work. Sulfur and nitrogen contents of the hydrotreated products were determined using an Antek 7000 Sulfur and Nitrogen Analyzer with an automatic sampler. Small samples (about 7 to 22 g depending on the liquid hourly space velocity) were collected periodically at each of the test conditions evaluated during the course of the run. Several conditions were repeated so the effects of catalyst deactivation could be determined. Nitrogen and sulfur contents of the hydrotreated products were monitored during the run to ensure that activity was lined out at each set of reaction conditions. Two large batches (about 875 ml) of hydrotreated product were collected at the end of the run for more detailed characterization. The total amount of reaction time for this run was about 32 days (excluding down time). Results of hydrotreating the whole coal liquid showed that nitrogen values in the products ranged from 549 ppm at 310°C, 3 g/h/cm^3(cat), 500 psig H_2 to <15 ppm at 388°C, 1 g/h/cm^3(cat), 1000 psig H_2. Sulfur values were very low for all conditions ranging from about 0 to 20 ppm.

Plans: Ongoing work includes characterizing products from the run with whole coal liquid, completing the statistical analysis of the data, and performing a hydrotreating run with the kerosene fraction of the whole coal liquid. Future work will involve evaluating hydrotreating conditions for additional distillate fractions of this liquid, as well as a petroleum feedstock, and blends of the coal-liquids and petroleum.

Sandia Project Team: Frances V. Stohl, Stephen E. Lott, Kathleen V. Diegert, David C. Goodnow, John B. Oelfke

INTRODUCTION

DOE/PETC's refining of coal liquids program is aimed at determining the most cost effective combination of existing refinery processes and blending options necessary to upgrade direct and indirect coal liquids into transportation fuels that meet year 2000 specifications. A main reason for this program is that coal liquefaction processing has improved significantly since the last refining evaluation was done by Sullivan and Frumkin (1) at Chevron in the early 1980s. In addition, a recent publication by Zhou, Marano and Winschel (2) indicates that blending coal liquids with petroleum may allow refiners to produce specification products with less refining than if each fraction was processed separately. Sandia's role in this program is to develop a database relating hydrotreating parameters to feed and product quality by experimentally evaluating options for hydrotreating whole coal liquids, distillate cuts of coal liquids, petroleum, and blends of coal liquids with petroleum. Sandia's project is unique because our small-scale, continuous operation flow reactor system enables us to evaluate many hydrotreating options in a cost effective manner while keeping waste production to a minimum. Sandia's project is integrated with other program participants including participants in the Refining and End-Use of Coal Liquids Study project (Bechtel, Southwest Research Inc. (SwRI), Amoco, M. W. Kellogg), Hydrocarbon Technology Inc. (HTI, formerly HRI) the MITRE Corporation, and PETC. Sandia's data will be used by other program participants in refinery linear programming models to identify the most cost effective options for introducing and processing coal liquids in a refinery. This paper will cover results obtained from hydrotreating whole coal liquid product from HTI's first proof of concept run with Illinois #6 coal.

EXPERIMENTAL PROCEDURES

Sandia's experimental procedures included using a factorial experimental design, hydrotreating the whole coal-derived liquid, characterizing the feeds and hydrotreated products, and reporting results to other program participants.

Continuous Operation Reactor System: Sandia's hydrotreating studies are being performed using a continuous operation, trickle-bed, microflow reactor system. The system has all required safety features to enable it to be operated unattended. The capabilities of this reactor system include catalyst loadings up to 25 cm^3, liquid flow rates from 0.05 to 4 cm^3/min, gas flows for hydrogen and nitrogen up to 2 l/min, gas flows for H_2S/H_2 up to 0.5 l/min, maximum temperature of 620°C, and a maximum pressure of 1800 psig. The reactor volume is 59 cm^3. Four samples can be collected automatically during unattended operation. For liquid hourly space velocities (LHSV) of 1 and 3 g/h/cm^3(cat), samples would weigh about 7 and 22 g respectively.

Factorial Experimental Design: Based on experience, three parameters were chosen for the factorial experimental design (Figure 1): temperature, pressure, and LHSV. The ranges of hydrotreating conditions used with the design were temperatures of 310 to 388°C, pressures of 500 to 1000 psig H_2, and LHSVs from 1 to 3 g/h/cm^3(cat). Evaluation of the first set of hydrotreating conditions (388°C, 500 psig H_2, 1 g/h/cm^3(cat)) was repeated once during the run and once at the end of the run so that effects of catalyst deactivation could be determined. Prior to the use of the testing using the factorial experimental design, two additional sets of reaction conditions were evaluated to see the effects of high pressure and temperature: 388°C, 1500 psig H_2, 1 g/h/cm^3(cat) and 362°C, 1500 psig H_2, 1 g/h/cm^3(cat).

Reactor Feeds and Catalyst: Sandia received (from SwRI) a sample of fresh Criterion HDN-60 catalyst and about 3.5 gallons of whole coal liquid product that was produced in HTI's first proof-of-concept run using Illinois #6 coal. The whole coal liquid product was collected when HTI's third stage reactor was not on line and while catalyst replacement was being used. Sandia's reactor was loaded with 10g of fresh catalyst that was sulfided in situ using temperature staging. The presulfiding procedure consisted of heating the catalyst to 177°C under He, starting the flow of a 10 mol% H_2S/H_2 mixture and maintaining 177°C for 1 hour. The catalyst was then heated to 288°C under flowing H_2S/H_2 and maintained at 288°C for 1 hour. Next the catalyst was heated to 404°C under flowing H_2S, the temperature was maintained at 404°C for 1 hour. H_2S flow was stopped and H_2 flow started.

Figure 1: Factorial experimental design (temperature = °C, LHSV = g/h/cm^3(cat), pressure = psig)

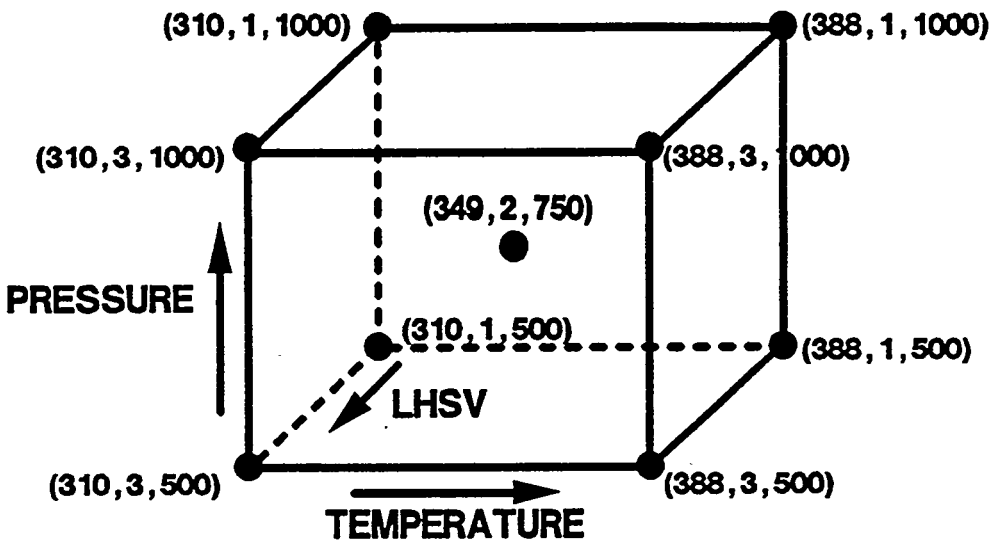

Analytical Procedures: Small samples were collected either manually or automatically throughout the run. Nitrogen and sulfur analyses were used to determine when line out was achieved at each reaction condition. These analyses were performed using an Antek 7000 Sulfur & Nitrogen Analyzer with an automatic sampler. Standards were prepared using phenanthridine for nitrogen, thianthrene for sulfur, toluene for the solvent, and four to five dilutions. Standards were measured at least twice and a polynomial fit of the intensity versus concentration data was used for analysis of unknowns.

RESULTS AND DISCUSSION

Analyses of the whole coal liquid by HTI, SwRI, and Sandia are shown in Table 1. SwRI used their measured specific gravity. Sandia used 0.9 g/ml for the first and second samples. Data for the second sample was also calculated using SwRI's specific gravity to show the effect of different values. Results show some variability but indicate the whole coal liquid has about 600 ppm nitrogen and 400 ppm sulfur.

Table 1. Sulfur and nitrogen analyses of whole coal liquid. Specific gravities used: HTI unknown; SwRI = 0.8628 g/ml; Sandia = 0.9 g/ml (except as noted).

HTI		SwRI		Sandia	
N	S	N	S	N	S
581	345	529	405	616	428
				621	399
				649*	417*

* Same data as second analysis but calculated with specific gravity = 0.8628.

The first condition used in the run was 388°C, 1500 psig H_2, and LHSV = 1 g/h/cm^3(cat). This condition was chosen to line out the freshly sulfided catalyst and to evaluate high severity conditions as a check on parameters for the factorial experimental design. Product analyses showed no detectable nitrogen or sulfur. Therefore, temperature was decreased to 362°C with pressure and LHSV remaining the same. At this condition, nitrogen and sulfur contents of the hydrotreated products were still very low (less than 5 ppm). Since hydrogen pressure is the most restrictive variable in a refinery and because low pressure gives more versatility for processing, the maximum pressure used in the factorial experimental design was decreased to 1000 psig H_2. In addition, the lower limit for temperature was also decreased. The goal was to have as broad a range of parameters as possible without decreasing sensitivity to the parameters. The order in which the various conditions were evaluated is shown in Figure 2.

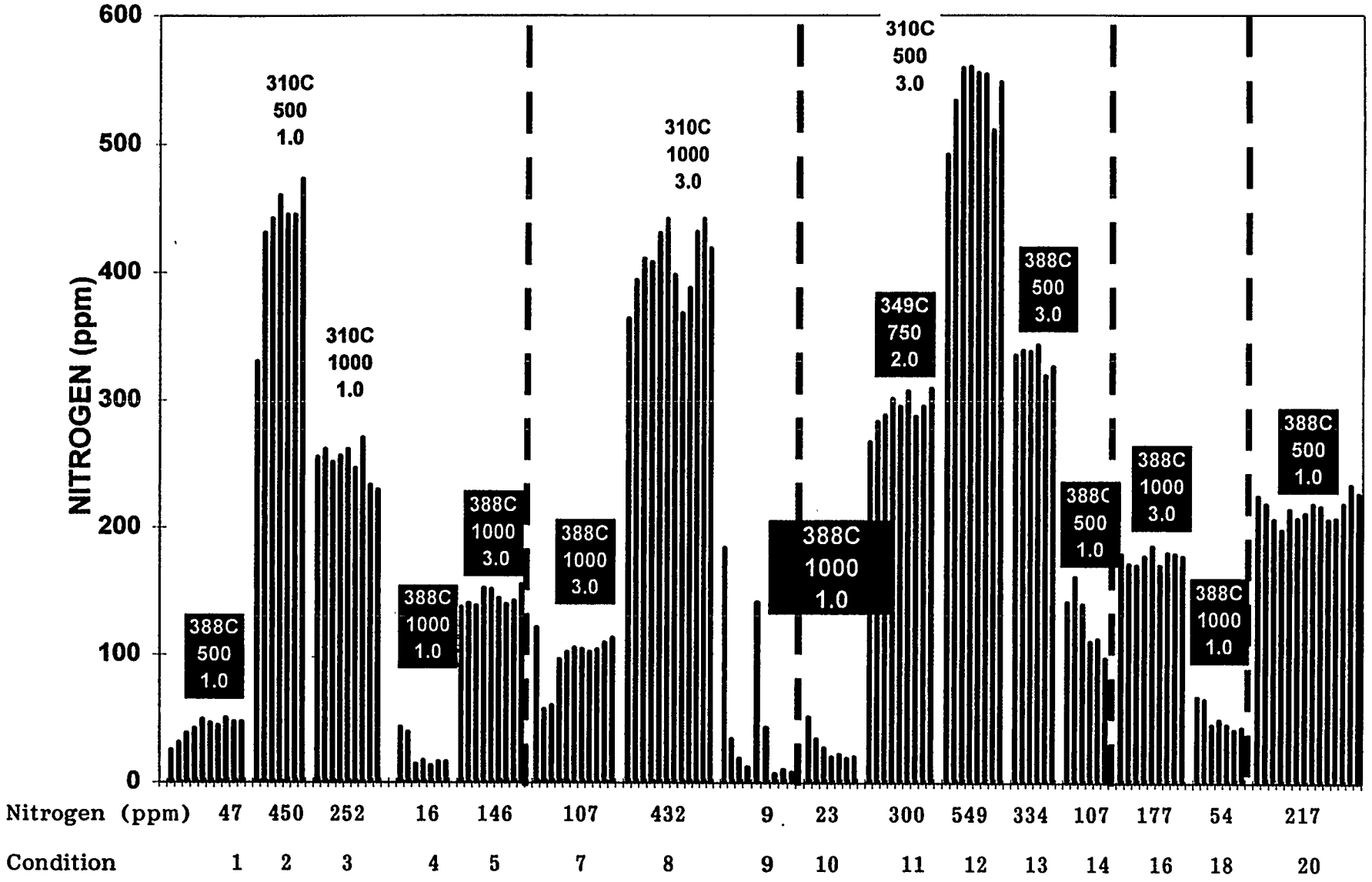

Figure 2. Nitrogen (ppm) vs reaction conditions. Temperature (^{o}C), Pressure (psig), LHSV g/h/cm^{3}(catalyst). Dashed line = Reactor Shutdown

Figure 2 shows the nitrogen contents for all samples that were obtained at the various processing conditions. Results were considered lined out when temperature, pressure and LHSV were relatively constant, and the nitrogen and sulfur results were relatively constant. Only nitrogen results that were relatively constant were used to calculate the average values at that condition. The average nitrogen contents and standard deviations are shown along the X-axis. In addition, the order in which conditions were evaluated is also shown. No data is shown for conditions 6 or 15 because the reactor went down before there were enough data points for analysis. Sample 17 was a large batch (about 890 ml) of hydrotreated product collected at the same condition used for sample 16 (388°C, 1000 psig H_2, 3 g/h/cm^3(cat)). Sample 19 was a large batch (865 ml) collected at the same condition as sample 18 (388°C, 1000 psig H_2, and 1 g/h/cm^3(cat)). These large batches were collected so that there would be enough hydrotreated product for additional analyses. Sample 17 had 151 ppm nitrogen, which is a little lower than sample 16, which had 178 ppm nitrogen. Samples 19 and 18 had similar nitrogen contents, 42 and 44 ppm respectively. Both samples 17 and 19 had <7 ppm sulfur.

Figure 3: Average nitrogen values (ppm) with standard deviations.

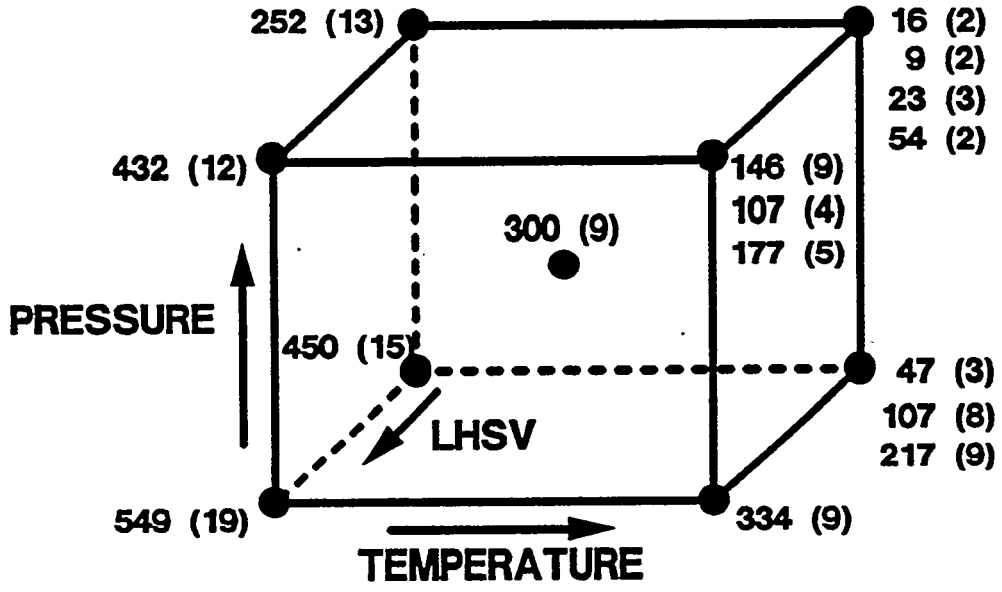

Figure 3 shows nitrogen contents as related to the conditions for the experimental design. Multiple values at a given condition show effects of catalyst deactivation. The total amount of reaction time (excluding down time) for this run was just over 32 days. Comparison of results for conditions 1 and 20 shows the effects of catalyst deactivation. Figure 4 shows the sulfur contents for the conditions of the factorial experimental design.

Figure 4: Average sulfur values (ppm) with standard deviations.

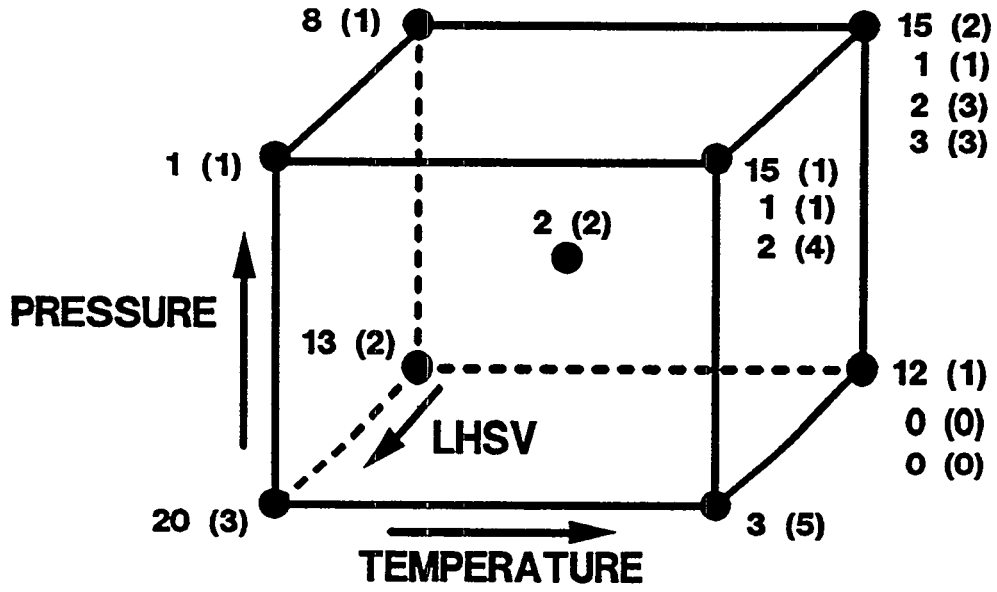

CONCLUSIONS AND FUTURE WORK

Results of this work show that good denitrogenation and good desulfurization can be obtained under relatively mild conditions with coal liquids from current processes. At the lowest severity condition, there is only about 10% nitrogen removal, whereas at the highest severity condition, there is about 97% nitrogen removal. Sulfur removal is good over the whole range of conditions and is greater than 95%. Ongoing and future work will involve additional characterization of reaction products by techniques such as distillation, PONA or PIONA analyses, density determinations, and proton NMR for hydrogen distributions. Results will be corrected for catalyst deactivation and analyzed statistically to determine the effects of process conditions on product quality. Future hydrotreating experiments will be performed with distillate fractions of this coal liquid and with coal-derived liquids from subbituminous coal.

* Acknowledgment: This work was supported by the U. S. Department of Energy at Sandia National Laboratories under contract DE-AC04-94-AL85000.

References:

1) Sullivan, R. F., Frumkin, H. A., ACS Div. of Fuel Chem. Preprints 31(2), 325, 1986.
2) Zhou, P.-Z., Marano, J. J., Winschel, R. A., ACS Div. of Fuel Chem. Preprints 37(4), 1847, 1992.

CATALYTIC MULTI-STAGE LIQUEFACTION OF COAL AT HTI
Bench-Scale Studies in Coal/Waste Plastics Coprocessing

DOE Contract No. DE-AC22-93PC92147

(December 8, 1992-September 30, 1995)

V.R. Pradhan
L.K. Lee
R.H. Stalzer
E.S. Johanson
A.G. Comolli

Hydrocarbon Technologies, Inc.
P.O. Box 6047
New York & Puritan Avenues
Lawrenceville, NJ 08648

COAL AND GAS CONVERSION CONTRACTORS' REVIEW CONFERENCE

AUGUST 29-31,1995

INTRODUCTION

The development of Catalytic Multi-Stage Liquefaction (CMSL) at HTI has focused on both bituminous and sub-bituminous coals using laboratory, bench and PDU scale operations. The crude oil equivalent cost of liquid fuels from coal has been curtailed to about $30 per barrel, thus achieving over 30% reduction in the price that was evaluated for the liquefaction technologies demonstrated in the late seventies and early eighties. Contrary to the common belief, the new generation of catalytic multistage coal liquefaction process is environmentally very benign and can produce clean, premium distillates with a very low (< 10 ppm) heteroatoms content. The HTI Staff has been involved over the years in process development and has made the following significant improvements in the CMSL processing of coals:

- Staging coal liquefaction reactions
- Lower temperature and higher residence times
- Heavier (343°C+) boiling recycle solvents preferred
- Low-High temperature mode of operation in catalytic processing
- Coal concentration in feed slurries increased from ca. 30 W% to ca. 53 W%
- Deep coal cleaning improved feedstock quality for liquefaction
- Continuous sulfating for low-rank, low-sulfur coals
- In-Line hydrotreating for product quality improvement
- Use of synthesis gas in first stage instead of pure H_2 improved net hydrogen utilization
- Interstage separation of light products (343°C-) with in-line hydrotreating improved process performance significantly
- Use of ashy recycle, containing unreacted coal, 343°C+ resid, and inerts, improved overall coal and resid conversion

A 24 month program (extended to September 30, 1995) to study novel concepts, using a continuous bench scale Catalytic Multi-Stage unit (30 kg coal/day), has been initiated since December, 1992. This program consists of ten bench-scale operations supported by Laboratory Studies, Modelling, Process Simulation and Economic Assessments. The Catalytic Multi-Stage Liquefaction is a continuation of the second generation of Catalytic Two-Stage Liquefaction approach, which results in high coal and resid conversions, and liquid yields using a low/high temperature approach. This paper covers work performed between October 1994 - August 1995, especially results obtained from the microautoclave support activities and the bench-scale operations for runs CMSL-08 and CMSL-09, during which, coal and the plastic components of municipal solid wastes (MSW) such as high density polyethylene (HDPE), polypropylene (PP), polystyrene (PS), and polythylene terphthlate (PET) were coprocessed.

Coal/Waste Plastics Coprocessing: Increasing problems associated with waste disposal have combined with the recognition that some raw materials exist in limited supply to dramatically increase interest in recycling. Recycling of paperboard, glass, and metal are technically straightforward and these materials are now commonly recycled in many areas around the world. Recycling of plastics presents greater technical challenges, primarily due to the differences in the chemical compositions/properties of various types of plastics. Some of the low-cost bulk plastics such as HDPE, PP, PS, and PVC find their way into advanced recycling/conversion processes that convert these plastics to petrochemicals further refinement of which could lead to isolation of monomers for plastics production or other high quality hydrocarbon products such as transportation fuels and lubricants. Used automobile tires, the main source of waste rubber, pose another environmental challenge. Most of the 200 million used tires that are discarded in the United States every

year, end up in stockpiles or landfills, although recently some use of these used tires are also reported in the power generation facilities. Other reported methods of recycling the scrap tires are based on pyrolysis which results in low thermal efficiency and also poor selectivity to liquid fuels.

Why process recyclable wastes such as plastics and used rubber tires together with coal? Well, coal is an abundantly available fossil fuel source with low hydrogen contents. The cost of hydrogen is a significant portion of the total cost of converting coal to refined transportation fuels such as gasoline, kerosene, and diesel via the state-of-the-art conversion technology. These municipal solid waste components such as plastics or hydrocarbon oil in used tires are relatively richer in hydrogen contents than coal. Thus, using these as a part of the feed in coal liquefaction would significantly reduce the cost of hydrogen production. There also seems to be a distinct advantage in processing plastics/rubber waste in a liquid phase or slurry mode under conditions much milder than those used in pyrolytic methods of conversion. Coal as a component of the feed mixture can thus provide not only a way to liquefy these waste stream, but can also act as a "mitigator" in maintaining the overall composition/properties of the combined feedstock more uniform. This mediator role of coal is very crucial for any waste-stream conversion/recycling process because the waste streams, depending on the location of the source, are going to inherently differ in their compositions. Thus, it appears to be practical to co-process the most abundantly available fossil fuel, coal, with hydrogen-rich, though in homogeneous in composition/properties, waste streams. The results obtained during the seven days of operation of the Proof-of-Concept Run No. 2 (POC-02) at HTI, using combined feeds of coal/plastics and coal/rubber, were very encouraging and established the technical as well as the operational feasibility of such combined processing. It also warranted further studies and process development efforts to optimize the coprocessing of coal with either waste plastics or used tire rubber to realize a commercially feasible plant operation.

OBJECTIVES

The overall objective of this 24 month Bench Scale study is to produce liquid fuels from direct coal liquefaction at a cost that is competitive with conventional fuels. This objective is to be accomplished with cumulative improvements through:

- Improvements in the effectiveness, use and to lower the costs of catalysts.
- Investigation of coal pretreatment and low temperature hydrogenation.
- Evaluation of hydrogen sources and improve hydrogen management to reduce the cost of liquid fuels to less than $30/bbl.
- Improvements in the quality and acceptability of fuels from direct liquefaction, addressing concerns of 1990 Clean Air Amendment.
- Evaluation of coals of national interest and identify coals that have a good potential for easy liquefaction at mild conditions.
- Improvement in process energy efficiency and reduce carbon oxide emissions during processing.

- Screening of new concepts using continuous bench-scale units prior to the higher costs "Proof of Concept" demonstration.
- Providing input/feedback for the "Proof of Concept" demonstration program.
- Improvements in the overall process economics and environmental acceptability of coal conversion processes by utilizing low quality, cheap, and otherwise-hard-to-convert hydrocarbon feedstocks such as waste plastics, waste tire rubber, and heavy resids.

PROJECT STATUS

Microautoclave studies conducted during this reporting period include catalyst screening tests in supported of the bench operations CMSL-08 and CMSL-09. Additional tests were performed to evaluate the reactivity of different plastics, commonly found in municipal waste, and co-processing with coal under typical liquefaction conditions. The development of novel iron and molybdenum based dispersed catalysts, which can enhance the cracking of waste plastics.

A total of four bench scale operations, Runs CMSL-7 to 10, were carried out during this reporting period. The effect of lower pressure was evaluated in CMSL-07 replacing hydrogen by a mixture of syngas in the first stage of a two stage coal liquefaction operations. The co-liquefaction of coal and plastics was studied in Runs CMSL-8 and 9. In CMSL-8 a mixture of co-mingled plastics (or HDPE) was processed with Illinois No. 6 Coal from Crown II Mine in a Catalytic/Thermal configuration. Following Run CMSL-08, the combined processing of plastics with a sub-bituminous Wyoming coal (Black Thunder coal) was evaluated in a three stage configuration in Run CMSL-9. Both these runs involving waste plastics, varying from 25-50 W% of feed, were carried out under relatively high space velocities ranging from 480 to 640 $Kg/h/M^3$ reactor volume. The last test of the CMSL program, Run CMSL-10, is in progress at the time this paper was prepared. The objective of CMSL-10 is to further evaluate the activity of iron and molybdenum based catalysts using Black Thunder coal (without any waste plastics) in a configuration similar to Run CMSL-9. The process performance of using Molyvan-A, a HTI iron based catalyst and a combination of these two catalysts will be compared in CMSL-10.

This paper discusses results obtained from Runs CMSL-8 and 9 only. Results from the other runs will be presented in the Contractors' review Meeting to be held in August.

ACCOMPLISHMENTS AND CONCLUSIONS

The following major accomplishments and conclusions can be drawn from work completed during this reporting period (October, 1994 to June, 1995):

1. In coal only operations, the conversion of coal was as high as 96% for Illinois No. 6 and Black Thunder coal. The corresponding C_4-524°C distillate yields of over 75% and 65% (maf basis) were obtained at relatively high space velocity.

2. Dispersed catalysts were found to be effective in improving the hydroconversion of coal and co-mingled plastics.

3. As compared with the coal only operations, co-liquefaction of coal and co-mingled plastics (20-50%) seemed to give as much as 15% more distillate of lighter quality, less C_1-C_3 gas make and lower hydrogen consumption.

4. Direct coupled in-line hydrotreating produced premium quality coal liquids containing 10-20 ppm of sulfur and as low as 10 ppm of nitrogen in processing both Illinois No.6 Crown II Mine and Wyoming Black Thunder Mine coals.

LABORATORY SCALE SUPPORT STUDIES

The laboratory scale support studies consisted of preparation and testing of different novel dispersed iron and molybdenum based catalysts for direct coal liquefaction and coal/plastics coprocessing. Microautoclave tests were also conducted to investigate the reactivity of various polymers that are found in MSW under typical coal liquefaction conditions. Studies were also carried out to determine the type of feed preparation section handling needed for plastics in the combined feed with coal. These also included a couple of off-line pumping tests for combined coal/plastics feeds, with 33 and 50 w% mixed plastics, to determine the effects of adding plastics to a coal/recycle solvent slurry in terms of its viscosity and other flow-related properties.

For CMSL-08, the laboratory support consisted of experiments, conducted in relation to the pre-reactor handling (mixing/dissolution and pumping) of the coal/solvent/plastic mixtures. In essence, two dissolution tests were conducted at 33 and 50 W% co-mingled plastics and remaining Illinois No. 6 Crown II mine coal (ca. 5 % moisture). The Tank-4 material, the oil used during the start-up and operations of the PDU Run POC-02, was used as solvent for dissolution. The Tank-4 material contained mostly petroleum-derived oils and small amounts of coal liquids obtained during POC-02. Thus, all compositions and ratios to be used during CMSL-08 were simulated in these tests. The approach used was to make, at room temperature, a slurry of coal and solvent, heating it to about 200-250°C and then adding co-mingled plastics to the slurry at that temperature. After allowing the plastics in slurry about 30-60 minutes at temperature, the hot mixture was observed to be fluid, homogeneous, and free of any lumps. Upon cooling down to room temperature, the mixture took an appearance of a plasticized and grainy filter cake material. This approach is certainly different from that employed successfully during the POC-02 run, although the new approach is less complicated as it will need only one pre-mix tank at high temperatures (200-220°C) instead of three (as during POC-02) and would also make the foaming problem due to moisture in coal more manageable. As a

result, this was the approach that was followed for the pre-reactor handling of the coal/plastics with recycle solvent during CMSL-08 bench run. The off-line pumping tests, carried out both at 33% and 50% plastics in the feed, using the hot slurry mix tank at 220°C, successfully demonstrated the pumpability of the feed mixtures.

The microautoclave tests using pre-dissolved/pre-mixed feed, carried out under conditions similar to those corresponding to the bench run, indicated as high as 92 W% maf conversion for coal+ plastics combined feed (@ 33% plastics) while the conversion was 90 W% maf (@ 50% plastics), both based on THF solubility of the products (Figure 1). These values were much higher than those obtained earlier (75-82 W% range) in the microautoclave tests that used the separately added coal and plastics feed. Thus, a distinct advantage is seen here in using the pre-dissolved/pre-mixed coal/plastics/solvent mixtures for the actual reaction studies. The reaction of HDPE and polystyrene (50/50 w/w%) mixture was carried out in the microautoclaves (20 cc) in the presence of dispersed acidic catalysts, HTI-I and HTI-II, at typical coal conversion process conditions. The results (Figure 2) indicate about 98-99 W% conversion of the plastics (which are mostly THF insoluble before reaction) into liquids (light, free flowing) and gases (C_1-C_5). Based on the difference in the reactor weights before and after reactions, the gas yields are estimated to be between 10-12 W% and the rest is light liquid (THF solubles). Further analysis of THF soluble products indicated that it was completely soluble in cyclohexane. This result seems to be very encouraging considering that the other laboratories working on the plastics hydrocracking/depolymerization have been using a strongly acidic and more expensive zeolites (HZSM-5 or Y-Zeolite) for this reaction. Both the catalyst additives, indicated above, have been developed in-house at HTI. In order to verify this result and also search for optimum conversion conditions, additional microautoclave tests were conducted under "coal liquefaction conditions".

Activity of molybdenum and iron based catalysts are also evaluated for coal dissolution. At similar Mo concentration, Molyvan-A seems to be slightly more active (5-7%) than Molyvan-L. The iron based catalyst, HTI-II, at higher concentration had a similar activity as the Molyvan-L, as shown in Figure 3.

Bench Scale Operations

The bench scale operations consisted of two continuous runs, CMSL-08 and CMSL-09, carried out in HTI's integrated unit 227, for a combined total of 64 days of operation on either coal-only or coal/plastics combined feed. The Bench Run CMSL-08 was a 22 day long operation to study the coprocessing of a bituminous Illinois No. 6 coal with 25-33 % mixed plastics consisting of 50% HDPE, 35% PS, and 15% PET. Bench Run CMSL-09 was a 40 day long operation, with last 12 days on a combined feed of coal and 33-50 w% plastics which consisted of about 40% HDPE, 33% PP, and 27% PS. The detailed run plans (operating conditions) for both CMSL-08 and CMSL-09 are summarized in Tables 4 and 5, respectively.

Bench Run CMSL-08

The bench-run CMSL-08 was successfully carried out for 22 continuous days spread over five conditions to investigate the effects of co-liquefying the primary plastic constituents of the municipal solid waste on the CMSL Process performance. This bench run was a follow-up of the earlier exploratory work Hydrocarbon Research, Inc. had carried out in the PDU scale continuous operations during the DOE sponsored POC-02 PDU run. During this bench run, the conditions were chosen to seek for the optimum set of operating severity/catalysis for converting plastics together with Illinois No. 6 coal. Although the work at the larger scale

demonstrated the operational and technical feasibility of the coprocessing of this type, the interpretation of the results was clouded by the fact that the continuous operation was never under solvent-balance, i.e., employed significant proportions of the external make-up oil as a part of the recycle stream for the process. A conscious effort was made to maintain the process under a net positive solvent-balance during the continuous bench operations CMSL-08, thereby minimizing any intrusive effects of an external make-up oil. The first stage reactor was provided with both the supported Ni-Mo/Alumina extrudate and the dispersed sulfated iron-molybdenum catalysts to ensure sufficient activity for the depolymerization of plastics in this stage while the second stage reactor was a back-mixed thermal reactor with no supported catalyst but with the dispersed catalyst, carried over from the first stage.

The overall process performance during the five work-up (Steady-State) periods of CMSL-08 is summarized in Figures 4 to 6. The first two run conditions, Conditions 1 and 2 at feed space velocity of 480 Kg/h/m^3 reactor, compared on one-to-one basis, the process performance, product yields and quality between the 'coal-only' feed and the 'coal and mixed-plastic (25 W%)' combined feed (mixed-plastic part of feed was 50 W% HDPE, 35 W% polystyrene, and 15 W%, PET). These two conditions established that performance with coal-plastics co-liquefaction was very similar, in terms of conversions and product yields, to direct coal liquefaction, with much improved hydrogen efficiency. Condition 1, with coal-only feed, resulted in about 96% total conversion, 91% resid conversion, and 72% distillate yield (all maf basis); the light gas yield and hydrogen consumption were high (11.4 and 7.5% maf respectively), Condition 2, with 25 W% co-mingled plastics in the feed with coal, resulted in about 96% total conversion, over 85% resid conversion, and 71% distillate yield; thus the overall performance was maintained despite the batch deactivation of the first stage supported catalyst. The light gas yield and hydrogen consumption were also lower during Condition 2 (9% and 6.9% maf respectively).

Condition 3, with higher feed space velocity of 640 Kg/h/m^3, higher K-2 temperature, and 25 W% mixed plastics in feed, resulted in a drop in distillate yields and 524°C$^+$ resid yield. The solvent-to-feed ratio had to be increased during transition to Condition 4 with 33 W% mixed plastics in the feed and a space velocity of 480 Kg/h/m^3. Due to the compensating effects of increased catalyst age (deactivation) in K-1 and reduced space velocity during this condition as compared to the previous one, process performance was maintained. The light gas formation and the hydrogen consumption were lower during Condition 4, probably as a result of the increased plastics concentration in the feed. The last run condition, Condition 5, was similar to Condition 4 in terms of feed space velocity and reactor temperatures although instead of using mixed plastics, pure HDPE alone was used at 33 W% of feed. The overall process performance deteriorated steeply during Condition 5, with distillate yield just over 50 W% maf and resid conversion of 62 W% maf. Overall operations during this run were smooth, except for a few feed pump interruptions. The material balance was excellent (an average for the whole run was 100 W%) and the net recycle solvent-balance was also positive throughout the run.

Bench Run CMSL-09

The objective of CMSL-09 was to evaluate the activity of molybdenum and iron based catalysts for coal liquefaction, as well as for co-liquefaction of coal and plastics. Similar to CMSL-08, CMSL-09 was conducted in a two-stage configuration with an in-line hydrotreater. The feed coal was from Wyoming Black Thunder Mine. The run started in a coal only operation mode. This mode extended over 6 conditions and switched to coal and plastic feed for the remaining 3 conditions. Two levels of con-mingled plastics loadings, 33 and 50 W%, were evaluated in Conditions 7 and 9, while the remaining plastics condition was in HDPE only. A feed space velocity of 640 kg/h/m^3 was maintained throughout the entire run. Results of this run are given in Figures 7 to 9. The relative activity of fresh, a mixture of fresh and recycle (only) molybdenum catalysts were

evaluated in Conditions 1 to 3. The distillate yield decreased gradually from the initial level of 66.6 W% to 62.2 W%, while 50% of the fresh Mo catalyst was replaced by recycled catalyst and further reduced to 60 W% when all Mo catalysts were recycled catalysts. A high coal conversion of 95.2 to 95.8 W% was maintained up to 50% of the fresh Mo catalyst was being replaced. At all recycled Mo mode of operation, the coal conversion dropped to 92 W%. The yield of C_1-C_3 gases and consumption of hydrogen in the "All Recycled" were 1.5 and 1%, respectively, lower than the "All Fresh" case.

During Condition 7, 33 W% of coal was replaced by a mixture of (HDPE/PP/PS) synthesized plastics. The distillate yield increased from low 60% in the case of coal only to 75.4%. This high liquid yield was still observed with 50% of plastics in the feed. The poorer process performance, lower THF and 524°C$^+$ conversions, suggested the HDPE was less reactive than PP and PS. Results from this run confirms that co-liquefaction improve the overall process performance by giving higher liquid yield, lower C_1-C^3 gas make a consuming less hydrogen.

Product Quality from Bench Operations

The separator overhead oil products from CMSL-08 and CMSL-09 represent the net light distillate stream from the process. The overhead stream, which is essentially the liquids boiling between an initial boiling point of about 60°C and 370°C, represents a combination of hot separator (O-1) overhead and continuous atmospheric still (N-1 CAS) overhead streams which passes through an in-line hydrotreating unit, K-3. The product stream from K-3 is designated as the overall SOH (Separator OverHead) product. The other liquid part of the distillate comes from the IBP to 524°C boiling fraction of the pressure filter liquid (PFL) or the vacuum still overheads (VSOH), which are used to constitute recycle solvent, depending upon what is used for solid separation of the CAS bottoms. The properties of Separator OverHeads for CMSL-08 and CMSL-09 from their respective work-up Periods are shown in Figures 3 and 4.

As shown in Table 3, the API gravities and H/C atomic ratios of the SOH oil from CMSL-08 have been high (35-38, and 1.73-1.82 respectively), especially for the coal/plastics coprocessing Conditions. The quality of the distillates is also premium, with less than 10 ppm nitrogen and between 5-15 ppm sulfur contents. The sharp increase in the naphtha (IBP-177°C) fraction during the coprocessing conditions indicates a significant contribution from the plastics part the feed. It was also found that a significant contribution to the resid (524°C$^+$) fraction in the product oil was made by the partially or incompletely degraded/depolymerized HDPE. This finding was based upon the waxy nature (solubility behavior) of the pressure filter liquid and the significant rise in both the resid content and API gravity of the heavier oil product when plastic part of the feed was switched over from co-mingled plastics to pure HDPE alone with coal.

Similar findings with regards to the SOH distillate oil properties have been made (Table 4) for CMSL-09. The API gravities (an indication of paraffinic character) of the distillate increased significantly in going from the "coal-only" conditions to "coal/plastics" conditions (from about 32-37 to 40-44). The H/C ratios also improved simultaneously during the transition. The light boiling naphtha (IBP-177°C) fraction increased significantly during the coprocessing conditions, except for the condition that coprocessed coal with HDPE alone, instead of mixed plastics. The sulfur and nitrogen contents of the distillate products have been very low in general, and even lower for the coal/plastics coprocessing conditions.

Thus, both CMSL-08 and CMSL-09 were very successful bench runs from the technical as well as the operational standpoints. A net positive solvent balance (excess production of 343°C$^+$ oil over what is needed

for recycle) was obtained for all the operating periods of both these bench runs. Over 22 days of continuous operation was completed without any major issues/interruptions for CMSL-08 (17 days on coal/plastics coprocessing) while CMSL-09 lasted for 41 days of continuous operation (12 days on coal/plastics coprocessing). Samples of different process streams were also obtained for the Consol, Inc. for property characterization/assessment.

These bench runs not only succeeded in providing insights into combined processing of coal with MSW plastics but also indicated the type of reaction severity, reactor configuration, and catalysts needed for achieving near-optimum process performance. The overall process performance, using plastics in the feed with both coals independently, was much better with an improved hydrogen utilization, a significant benefit one strives to derive from the plastics part of the feed in such coprocessing. Secondly, more so with a sub-bituminous coal (CMSL-09), it was found that plastics had synergistic effects on coal conversion in terms of improving the C_4-524°C premium distillate yields. The presence of an in-line hydrotreater during both the bench operations resulted in light distillate liquids containing as less as 10-25 ppm nitrogen and sulfur. Indeed, it is strongly believed that, because of all the positive effects of coprocessing waste plastics with coal, the economics of coal liquefaction will improve significantly. More importantly, such coprocessing technology would allow re-use of a very valuable hydrocarbon source (waste plastics) into the energy stream, in an environmentally benign manner.

FUTURE PLANS

Run CMSL-10 is scheduled to end during the last week of June. Detailed product characterization will be performed in July and August. Technical and economic assessment of process improvements obtained during this program is under way and scheduled to complete in August. Also, preparation of the final report has been initiated in May aiming to have a draft report for the project in mid-September.

TABLE 1 CMSL-08 RUN PLAN

Coal: Illinois No. 6 Crown II Mine
Plastics: HDPE, 50%; PS, 35%; PET, 15%
1st Stage Catalyst: Akzo Ao-Go Extrudate
Hydrotreater: Criterion C-411 Catalyst

Period	Condition	Description
1-6	1	Coal only; Space Velocity of 480 kg/h/m^3
7-11	2	Coal + mingled Plastics, same condition as Condition 1
12-16	3	Coal + 25% Co-mingled Plastics, 25% increase in space velocity
17-20	4	Same condition as Condition 3, with 33% Co-mingled plastics
20-22	5	Same as Condition 4, with 33% HDPE

TABLE 2 CMSL-09 RUN PLAN

Coal: Black Thunder
Plastics: HDPE, 40%; PP, 33%; PS, 27%
Hydrotreater Catalyst: Criterion C-411 Catalyst

Period	Condition	Discription
1-5	1	Coal only; Fresh Mo only
10-14	3	Coal only; Fresh & Recycle Mo
15-19	4	Coal only; Recycle Mo only
20-24	5	Coal only; Repeat of Condition 3
25-29	6	Coal only; Mo and Fe based catalysts (with recycle)
30-34	7	Coal & Plastics; same as Condition 6
35-38	8	Coal & HDPE; Mo and Fe based catalysts (no recycle)
39-41	9	Coal & Plastics; Mo and Fe based catalysts (no recycle)

TABLE 3. PROPERTIES OF THE SEPARATOR OVERHEAD DISTILLATES FOR BENCH RUN CMSL-08					
Run Condition	1	2	3	4	5
Work-Up Period	6	11	16	20	22
W% Plastics in Feed	0	25	25	33	33
Gravity, API	35.4	36.4	37.7	37.6	35.4
IBP, °C	59	79	57	64	77
FBP, °C	366	379	379	377	399
IBP-177°C, w%	28.2	37.1	47.5	37.5	31.6
177-260°C, w%	31.8	22.2	20.9	23.4	24.2
260-343°C, w%	34.3	33.1	24.6	32.4	32.7
343°C$^+$, 2%	5.7	7.6	7.0	6.7	11.5
H/C Ratio	1.79	1.78	1.73	1.78	1.82
Sulfur, ppm	6	16	5	115	10
Nitrogen, ppm	<1	8	<1	5	4

TABLE 4. PROPERTIES OF THE SEPARATOR OVERHEAD DISTILLATES FOR BENCH RUN CMSL-09						
Run Condition	1	3	4	7	8	9
Work-Up Period	5	15	19	34	38	41
W% Plastics in Feed	0	0	0	33	33	50
Gravity, API	37.5	34.5	34.2	39.4	39.9	43.8
IBP,°C	59	61	61	57	72	57
FBP,°C	357	376	379	365	379	379
IBP-177°, w%	35.8	33.1	33.5	43.4	28.2	48.3
177-260°C, w%	23.0	29.8	28.6	24.5	27.6	20.4
260-343°C, w%	32.7	29.9	29.9	26.6	33.3	24.2
343°C$^+$,w%	8.5	7.2	8.0	5.5	10.9	7.1
H/C Ratio	1.81	1.72	1.72	1.76	1.87	1.82
Sulfur, ppm	7	15	9	9	17	34
Nitrogen, ppm	<1	36	61	47	24	10

Figure 1

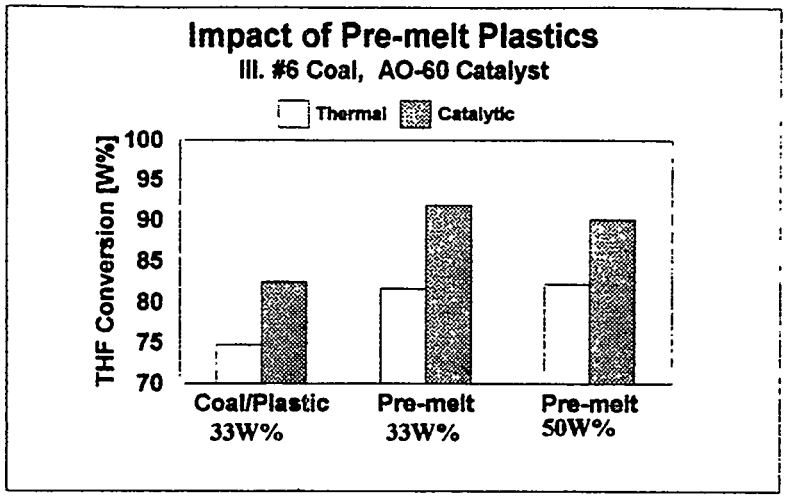

Figure 2

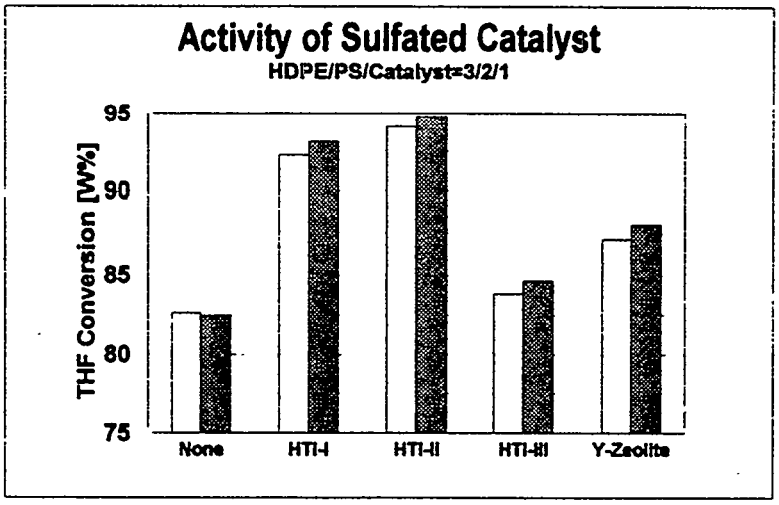

Figure 3

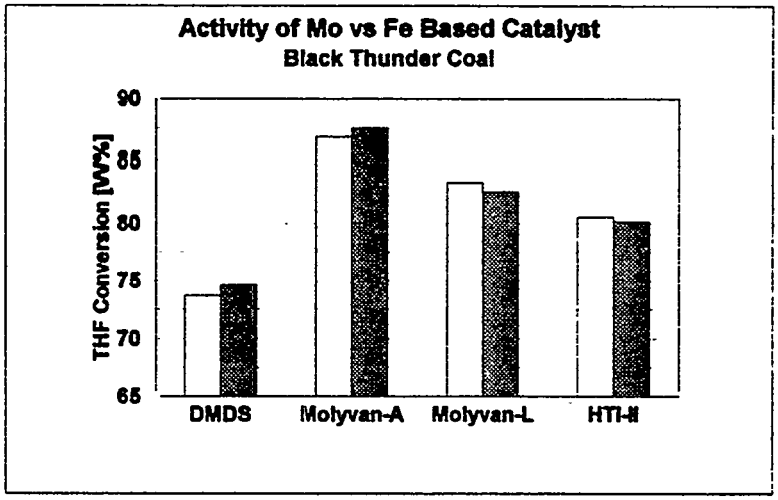

Figure 4

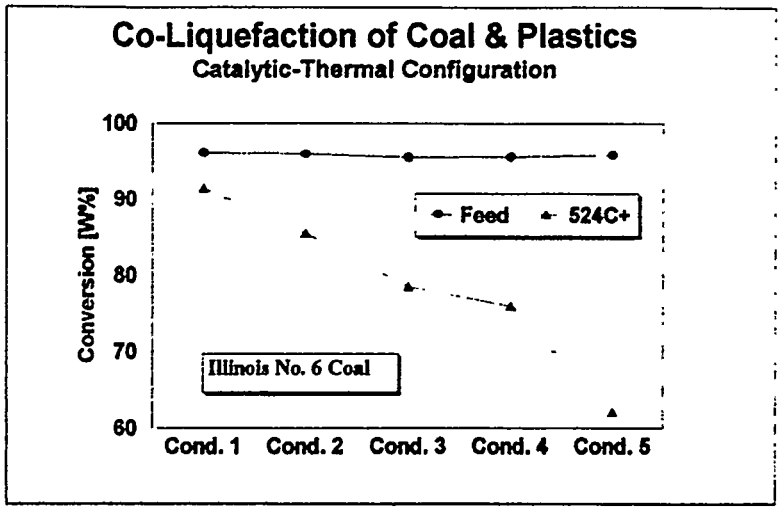

Figure 5

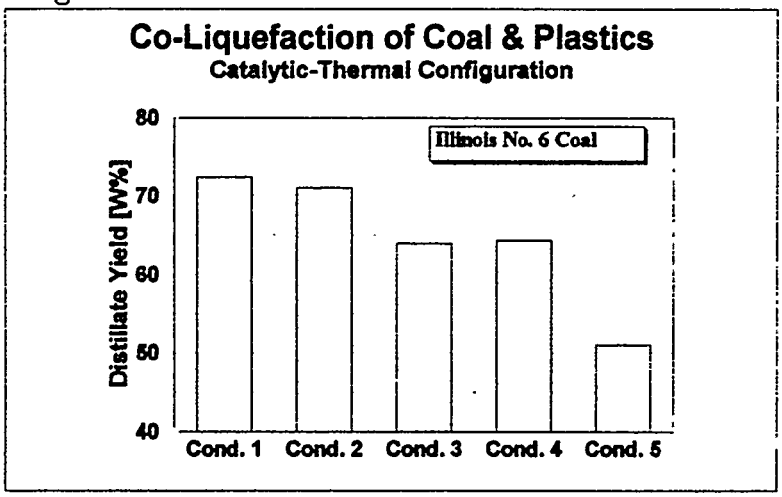

Figure 6

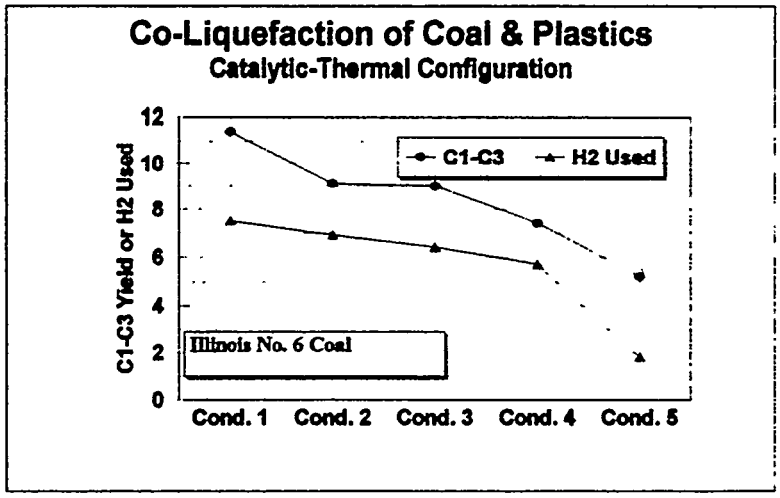

Figure 7

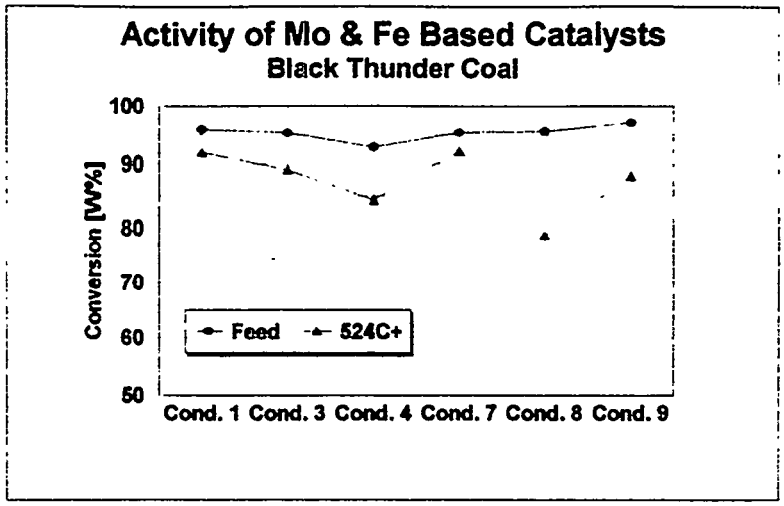

Figure 8

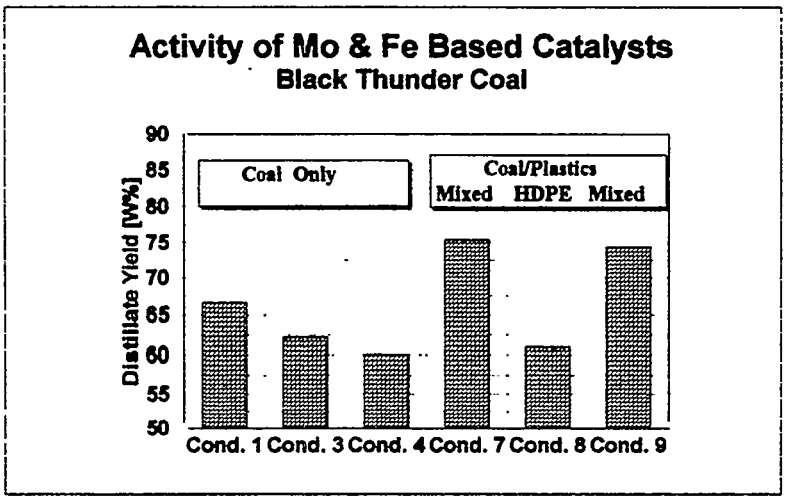

Figure 9

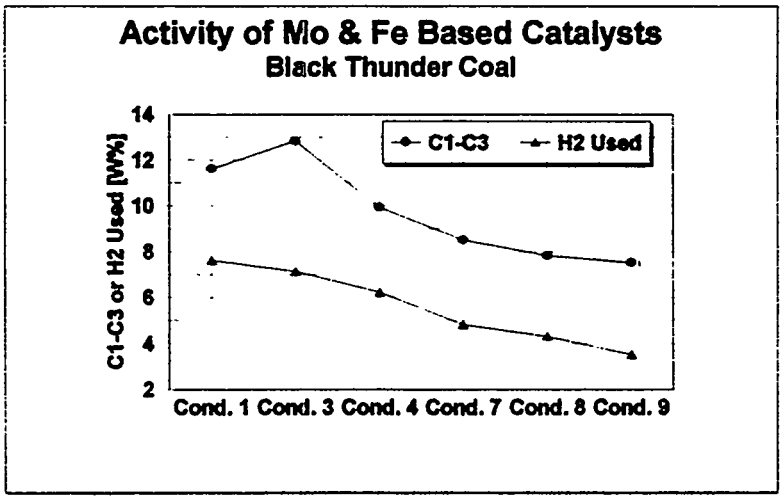

COAL LIQUEFACTION AND GAS CONVERSION CONTRACTORS
REVIEW CONFERENCE

August 29-31, 1995
Pittsburgh, PA

Continuous Bench-Scale Slurry Catalyst Testing
Direct Coal Liquefaction of Rawhide Sub-bituminous Coal

Contract Number DE-AC22-94PC94051
Covering Operations from June 1994 - December 1994

R. F. Bauman
L. A. Coless
S. M. Davis
M. C. Poole
M. Y. Wen

Introduction

In 1992, the Department of Energy (DOE) sponsored research to demonstrate a dispersed catalyst system using a combination of molybdenum and iron precursors for direct coal liquefaction. This dispersed catalyst system was successfully demonstrated using Black Thunder sub-bituminous coal at Wilsonville, Alabama by Southern Electric International, Inc. The DOE sponsored research continues at Exxon Research and Development Laboratories (ERDL).

A six month continuous bench-scale program using ERDL's Recycle Coal Liquefaction Unit (RCLU) is planned, three months in 1994 and three months in 1995. The initial conditions in RCLU reflect experience gained from the Wilsonville facility in their Test Run 263. Rawhide sub-bituminous coal which is similar to the Black Thunder coal tested at Wilsonville was used as the feed coal. A slate of five dispersed catalysts for direct coal liquefaction of Rawhide sub-bituminous coal has been tested. Throughout the experiments, the molybdenum addition rate was held constant at 100 wppm while the iron oxide addition rate was varied from 0.25 to 1.0 weight percent (dry coal basis). This report covers the 1994 operations and accomplishments.

Objective

The objective of this project taken from the Statement of Work (DE-AC22-94PC94051) is to test advanced and novel slurry phase catalysts for direct coal liquefaction. These novel slurry phase catalysts were developed in other DOE sponsored research programs. The properties of the catalysts are presented in Table 1. A number of such catalysts have shown initial promise in laboratory-scale research, typically by experimentation in small batch autoclaves. The efficacy and application of these catalysts is expected to be strongly dependent upon the process steps and overall configuration envisioned for a particular liquefaction process. The most favorable catalysts and relevant approaches must be evaluated in a continuous flow bench-scale facility in order to define and verify the steady-state product yield structures in response to operating parameters and process changes.

In order to help guide the research effort a set of goals was targeted. A summary of the major project goals as listed in DOE's Statement of Work is presented below:

- Demonstrate mechanical operability of continuous bench unit.
- Verify suitability of system design, including use of plug flow reactors.
- Define suitable catalyst screening conditions.
- Test three iron catalysts.
- Test two molybdenum catalysts.
- Conduct limited optimization studies.
- Obtain mass and elemental balances for chosen data periods.
- Define product yield structures for chosen data periods.

Table 1
Properties of Slurry Catalysts

Catalyst	Particle Size, Microns	Surface Area, m^2/g	Bulk Density, g/cm^3	Physical Form	Composition wt %
NANOCAT® Superfine Iron Oxide (SFIO)	0.003	250	0.05	Reddish-brown powder	100 % Fe_2O_3
Bayferrox PK 5210 Technical Iron Oxide	0.020	123	n/a	Reddish-brown powder	100 % Fe_2O_3
Bailey Iron Oxide	96 wt%<44	n/a	n/a	Reddish-brown powder	100 % Fe_2O_3
MOLYVAN L, Molybdenum containing lubricant	n/a	n/a	1.08	Dark green liquid	8.1 % Mo
MOLYVAN A, Molybdenum containing powder	5 to 10	n/a	1.58	Yellow-orange powder	30.0 % Mo
Ammonium heptamolybdate	n/a	n/a	2.50	White powder	54.3 % Mo

Process Overview and Simplified Process Flow Plan

The Recycle Coal Liquefaction Unit (RCLU) is located at the Exxon Research and Development Labs in Baton Rouge, Louisiana. RCLU is a highly automated, highly instrumented pilot plant designed to process 34 kg (75 lbs.) of coal per day. It has redundant computer control and data acquisition systems allowing for efficient trouble shooting, data analysis and material balance calculations. Over the years, RCLU has been re-configured many times to meet specific data requirements for coal and heavy hydrocarbon conversion. Hence, RCLU is versatile and easy to re-configure. RCLU has been a very reliable tool in the past, with many runs over 1000 continuous hours. An overview of the process is described below and a simplified process flow plan is presented in Figure 1.

Slurry Mixing

In this process, coal, make-up catalysts, recycle solvent and recycle bottoms are prepared in 6 to 8 hour batches in the mix tank to form a homogeneous feed slurry. The

equipment in the slurry mix area are the mix tank, spared recirculation pumps, the coal/bottoms bin and the solvent tank. The mix tank is totally enclosed to prevent dust and vapors from entering the process streams. The slurry temperature is typically held around 135- 143 °C (275-290 °F) to ensure an easily pumpable slurry. The pressure is held at atmospheric or slightly above during non-charging periods. However, a vacuum can be drawn on the solvent tank to aid during feed charging. The tank is equipped with a mixer to mix the coal, bottoms, solvent and catalyst. The feed slurry is further mixed by the recirculation pump.

Slurry Feed

The slurry feed section is used to provide continuous slurry flow to the liquefaction reactors. The major equipment in the area include the feed tank, spared recirculation pumps, and high pressure feed pumps. Periodically, the feed tank is charged with a fresh batch of slurry from the mix tank. The slurry is continuously mixed and recirculated to ensure a homogeneous slurry in the feed tank. The high pressure pumps are used to pump a slip-stream of slurry from the recirculation loop to the liquefaction reactors. Typical holding tank operating conditions are 135- 143 °C (275-290 °F) and atmospheric pressure.

Liquefaction Reactors

The liquefaction reactor system consists of a pretreater and two reactors in series and their associated sandbaths. The pretreater consists of two or three 25 mm (1") ϕ 316 stainless steel pipes and each reactor consists of four or six 25 mm (1") ϕ 316 stainless steel pipes. The reactor pipes are 1.22 m (4 ft) in length and are connected by 9.5 mm (3/8") ϕ 316 stainless steel tubing. The reactors operate in an upflow mode and are capable of having interstage hydrogen addition. The sandbaths are electrically heated and are used to control the reactor temperatures.

The slurry is pumped from the feed tank to the pretreater at a rate of 3.6 to 5.5 kg/hr (8 to 12 lbs/hr). The purpose of the pretreater is to activate the catalyst by sulfiding the iron oxide. The catalyst is activated by treat gas containing 10 volume percent H_2S in H_2. The activated slurry leaving the pretreater is blended with pure H_2 treat gas before it is fed to the first stage reactor. Most of the coal is converted to liquid hydrocarbons and gas via a combination of thermal and catalytic processes in the two liquefaction reactors.

The residence time within the pretreater and each reactor can be varied by varying slurry feed rate or by varying the number of reactor pipes in each sandbath. The nominal residence time of the pretreater ranges from 20 to 30 minutes while the nominal residence time of each reactor ranges from 40 to 55 minutes. The pretreater and liquefaction reactors operate at 17.2 Mpa (2500 psig). The pretreater operates between 296 - 302 °C (565 - 575 °F) while the liquefaction reactors operate between 427 - 454 °C (800 - 850 °F). A slight exotherm exists in the first two tubes of the first stage reactor. Otherwise, the reactors operate close to isothermal operation and have minimal pressure drop.

High Pressure Separations

RCLU uses high pressure separation vessels to separate the heaviest fraction of the reactor product from the lighter fraction. The high pressure separations consist of both hot and cold separators operating at slightly below reactor pressure. The hot separator is used to split the reactor effluent into two streams; an overhead stream consisting of gases, water and light oil and an underflow stream consisting of heavy oil and mineral matter. The overhead stream from the hot separator passes through two heat exchangers before entering the cold separator. The exchangers cool the stream, thus condensing some of the light oils which are captured in the cold separator. The hot separator underflow stream proceeds to the bottoms stripper where it is stripped with the offgas from the cold separator. The cold separator underflow stream proceeds to fractionation.

Bottoms Stripping

The bottoms stripper separates nominally 1000 °F- hydrocarbons from heavier hydrocarbons and mineral matter (bottoms). Bottoms are periodically withdrawn into a bucket and allowed to cool and solidify. The bottoms is then crushed and a fraction is recycled to the mix tank. The overhead gas and the stripped hydrocarbons are cooled before going to fractionation.

Fractionation

The cold separator underflow stream and the bottoms stripper overhead stream are combined in the fractionator feed surge tank. The product gas passes through several flowmeters before the stream is released to the flare vent. A slipstream of the gas is sent to an online process gas chromatograph (GC) system after the flowmeters. The GC system samples the product gas continuously and analyzes the stream for H_2, H_2O, CO, CO_2, N_2, H_2S, O_2, C_1, C_2, C_3, C_4 and C_5+. The information from the product gas flowmeters and GC system are used to develop daily online material balance closures and later for the complete data workup.

The liquid is pumped from the fractionator feed surge tank to a preheater before it is fed to the fractionator. The fractionator is designed to split the nominally 1000 °F- stream into two components, solvent (also called VGO) and light oil (naphtha/distillate). The heavier component has an initial boiling point (IBP) between 550 °F and 650 °F depending upon tower temperatures. The lighter component has a C_5 IBP. The tower underflow stream is periodically removed and partially recycled to the mix tank. The overhead stream is condensed, refluxed and periodically removed.

Operations Synopsis

Operations were initiated in August, 1994 following a period of about 2 months of equipment modifications, pressure testing and instrument calibrations. During the period

of August 7, 1994 to October 29, 1994, twenty-four yield periods were successfully completed. Below is a synopsis of the pilot plant operations.

Typically, the ash content of the recycle bottoms stream provides a good indication of coal conversion level. As the coal conversion levels off the unit approaches steady state operations. The analytical tests for bottoms ash content showed that the first set of yields periods were not at steady state. Since the analytical ash tests cannot be conducted daily, screening ash tests were used to determine if the operations were near steady state. However, the initial screening tests were inaccurate and needed to be revised because of incomplete ashing. The revised screening ash tests gave similar results to the analytical ash tests.

During the third balance of condition 1 (YP411) the feed tank scale malfunctioned. The coal slurry feed rates were calculated from the mix tank weights because of the problems with the feed tank scale. The measured material balance was poor for this period. However, the other data was more than adequate for reliable data reconciliation.

Molyvan A was used for conditions 2A, 2B and 3 because Molyvan L was not available. The operations for condition 2A were smooth.

Several computer boards went bad during condition 2B after completing the second yield period (YP416). The control programs were not operating for several hours, but the boards were changed in time to avoid shutting down the unit. The conditions were allowed to stabilize for 30 hours before collecting data for the third yield period of condition 2B (YP418).

A slight tuning problem with the first stage reactor temperature was experienced during condition 3. The temperature profile was sinusoidal with swings of 2.8 °C (5 °F). The controls were re-tuned before condition 4 to reduce the temperature swings.

The first stage reactor heaters were shutdown temporarily during the third yield period of condition 4 (YP424) due to a low pressure alarm. The low pressure alarm was set off by plugged lines. Once the lines were unplugged the heater operations returned to normal. However, the average reactor temperature was 2.8 °C (5 °F) low for YP424. Otherwise operations were smooth for condition 4.

During condition 5, the first stage reactor thermocouple relays went bad. The thermocouples were reading 2.8 °C (5 °F) low during the first two yield periods of condition 5 (YP425 & YP426). The average sand bath temperatures were substituted for the average reactor tube temperatures of YP425 & YP426. After the thermocouple relays were replaced, the difference between the average sand bath and the average reactor tube temperatures was within 0.3 °C (0.5 °F) for the remaining yield periods (YP427-YP433).

One of the two dry test meters that measures the product off gas rate gave inaccurate readings for condition 6 and subsequently was taken out of service before condition 7. Therefore, the product off gas rate was based only on one dry test meter

rather than the average of two. The yield periods for condition 6 were collected before approaching steady state because of the limited supply of Mach 1 catalyst.

The second dry test meter became unreliable during condition 7. A restriction in the second dry test meter caused a high pressure drop across the flow meter. Consequently, the upstream roots meter was adversely affected by this high pressure drop. The roots meter gave an erroneously low reading for the product off gas rate because it did not correct the flow rate for the higher pressure condition. Since the feed gas and product gas rates were nearly constant for the previous two conditions the product off gas rate for condition 7 was approximated based on the product off gas rates for conditions 5 & 6. The approximations were fairly good since the reconciliation program made only slight adjustments to the product off gas rates.

Material Balancing and Analyses Procedures

Material balances are based on a 24 hour operating period at constant conditions. Ideally, the conditions are at or near steady state before a yield period (material balance period) is initiated. There is a compromise between the number of conditions and the approach to steady state for a given amount of operating time. For these experiments, some approach to steady state was sacrificed for maximizing the number of operating conditions. The yield periods were initiated when the bottoms conversion started to level off.

From past experience at Exxon, the ash content of recycle bottoms provides a good indication of coal conversion level with known feed coal ash content. In typical bottoms recycle pilot plant operations, the ash content of the recycle bottoms are monitored daily in a screening test. The final ash content in the recycle bottoms is conducted by the analytical labs several weeks later. The procedure for both tests are essentially the same. The main differences are that the analytical tests are automated and use a different purge gas. The ash content of bottoms are measured in duplicate by combustion of small samples of bottoms at 950°C for at least three hours. The average ash content of bottoms and known feed coal ash content are input to a computer model with an equation built in assuming 100% ash balance. The model calculates DAF coal conversions and data are plotted daily to monitor the trend of new conditions vs. the previous conditions. In a typical case, a significant change in the coal conversion is observed in the first few days after starting a new condition. The coal conversion gradually levels off in about 3-5 days after the change to the new condition. The yield periods are initiated when the bottoms ash content begins to level off. The screening tests compare well with the analytical lab tests.

Material balances are conducted after a yield period is complete. RCLU utilizes two levels of material balancing. The first level is on-line material balancing and the second level is material balancing that utilizes data reconciliation techniques. The on-line material balances are often completed within 24 hours after the end of the yield period. They are

used to guide unit operations, identify data acquisition problems, and provide preliminary product yields leading to the determination of subsequent run conditions.

The raw data and process variables of each yield period are stored in the RCLU computer system. The on-line material balancing program retrieves these raw data from the RCLU computer system along with input data from unit engineers to calculate the overall material balance, DAF coal conversion, hydrogen consumption, and gaseous and distillate yields for each yield period. The input data from unit engineers include moisture and ash contents of feed coal, and percents of $1000°F^+$ material in the recycle solvent and $1000°F^-$ material in the recycle bottoms. In order to cross-check the data, balances and yields are calculated using three different slurry feed bases. If balances are poor or yields deviate substantially from the expected then the weights and analyses are re-checked for errors. If no errors are found, an investigation is initiated to determine possible unit material losses and/or errors in data acquisition.

The second level of material balancing utilizes the results of the on-line material balances as well as elemental analyses of each feed and product stream, and simulated distillation by gas chromatography (GCD) analyses of hydrocarbon streams. The reconciled balances are usually not finalized until at least three weeks after the end of a given yield period. Reconciled balances are considered the finalized results and are the results most often reported. Once finalized, reconciled results are used to compare the effects of process variables and/or catalysts on product yields and product distribution.

In order to reconcile the data, a mainframe computer program which utilizes geometric programming techniques is used to adjust the data to comply with a set of constraint equations. The objective of data reconciliation is to legitimately adjust data values to balance elemental weights of feed and product streams. Data is therefore adjusted by taking into account the reliability of each data measurement. Those variables which have poor reliability are preferentially changed in order to achieve data consistency. Neither the constraint equations nor variable reliabilities are changed from yield period to yield period.

Data reconciliation is an iterative procedure that is designed to be used only when "as-measured" balances are good. Typically, data reconciliation requires that the total material balances are between 98 and 102%. However, material balances between 95 and 102% are tolerable. If the balances do not meet the above criterion, the data is re-analyzed for obvious errors and suspect samples are resubmitted for analyses.

Data from any single reconciled yield period should not be used in data comparisons due to operational variations. Rather, the results from several yield periods (≥ 3) at one condition should be used for comparison purposes.

Results and Discussion

Eight conditions were tested during the 1994 operations, covering the impact of solvent to coal ratio, time-temperature trade off, and type and make-up rate of iron oxide catalyst as shown in Table 2. The molybdenum make-up rate remained constant throughout the experiments. However, the source of molybdenum was varied. A summary of the operating conditions are presented in Table 3. Three 24 hour balances (yield periods) were performed at each condition. A summary of the reconciled yields and overall conversion are presented in Table 4. The values shown in Tables 3 & 4 are the average values at each condition.

Table 2
Summary of Experimental Design

Condition	Comment	Yield Periods of Interest
1	Initial conditions.	409-411
2A	Reduced solvent to coal ratio compared with initial conditions.	412-414
2B	Reduced H_2S treat rate compared with conditions 1 and 2A.	415, 416, 418
3	Increased first stage reactor temperature and increased mass flow rate compared with previous conditions.	419-421
4	Switched from Bailey iron oxide to Bayferrox PK5210 iron oxide catalyst.	422-424
5	Reduced iron oxide addition rate from 1.0 to 0.25 wt% on dry coal.	425-427
6	Switched from Bayferrox PK5210 to Mach 1-Nanocat SFIO catalyst.	428-430
7	Switched from organic to inorganic source for molybdenum catalyst and switched back to Bayferrox PK5210 iron oxide.	431-433

Table 3
Summary of Test Conditions

Condition	Fe_2O_3 Type	Fe_2O_3 wt %	Mo Type	S/C: B/C	H_2S as S wt %	NRT, min.	Reactor Temperatur 1st °C (°F)	2nd °C (°F)
1	Bailey	1.03	Org.	1.07:0.85	5.8	49	430.6 (807.0)	450.6 (843.0)
2A	Bailey	0.99	Org.	0.94:0.71	6.0	53	431.1 (808.0)	451.1 (844.0)
2B	Bailey	1.00	Org.	0.90:0.75	2.7	50	431.3 (808.3)	449.3 (840.7)
3	Bailey	1.02	Org.	0.95:0.79	3.4	41	441.3 (826.3)	450.0 (842.0)
4	Bayferrox	1.00	Org.	0.94:0.76	3.3	41	439.3 (822.7)	449.6 (841.3)
5	Bayferrox	0.25	Org.	0.91:0.80	3.0	41	441.5 (826.7)	450.6 (843.0)
6	Mach 1	0.26	Org.	0.91:0.83	3.1	42	440.9 (825.7)	450.4 (842.7)
7	Bayferrox	0.26	Inor.	0.98:0.85	3.1	41	440.9 (825.7)	450.0 (842.0)

Table 4
Summary of Reconciled Yields and Conversion,
(wt% Based on Dry Ash-Free Coal)

Condition	Yield Period	H_2	C_1-C_4	C_5-350	350-650	650-1000	Conversion
1	409-411	-6.12	15.34	14.48	33.93	9.06	88.56
2A	412-414	-6.11	14.51	13.54	32.55	13.57	89.26
2B	415-418	-5.77	13.69	12.86	31.35	14.87	88.60
3	419-421	-5.76	13.31	12.30	29.61	14.59	86.88
4	422-424	-5.43	12.48	12.71	31.33	13.70	85.62
5	425-427	-5.76	14.08	12.24	31.22	13.54	87.01
6	428-430	-5.46	12.82	11.66	30.69	14.67	85.19
7	431-433	-5.65	12.61	12.27	32.14	12.57	85.74

General Observations

In general, catalyst changes had very small impact on performance. Of all of the changes tested, one process change, reducing the recycle ratio had the most striking impact. Apparently, recycle ratio has more impact on performance than catalyst over the range of the tests. It may be that the constant addition of 100 wppm molybdenum is masking other changes, such as type and amount of iron catalyst addition rate. Discussions with PETC have indicated to us that the constant molybdenum addition rate was specified based on results at Wilsonville.

Reduced Recycle

The impact of reduced recycle is shown by comparing condition 1 with 2A. The total recycle was reduced from 1.92 to 1.65 on dry ash free (DAF) coal. The result was a significant shift towards a heavier product slate, and higher conversion.

Reduced Sulfur Addition Rate

The impact of reduced sulfur addition rate is shown by comparing condition 2A and 2B. The result was a small reduction in gas yields and hydrogen consumption. No other statistically significant changes were observed. While statistically significant, a small systematic error in the feed gas or product gas sulfur content may have clouded the data. Thus our interpretation of the test result is that the reduction in sulfur had no significant impact on yields or conversion.

Increased Stage 1 Temperature and Mass Velocity

The impact of increasing the first stage reactor temperature and the mass velocity can be seen by comparing condition 3 with 2B. Conversion and liquid yields dropped. Conversion went from 88.60 to 86.88 wt % on DAF coal. C_5-1000°F dropped from 59.1 to 56.5 wt% DAF coal. The temperature and mass velocity were increased to make the impact of a better catalyst easier to detect.

Changed Iron Oxide Catalyst

The impact of iron catalyst type, Bailey vs. Bayferrox is shown by comparing conditions 3 and 4. There was an unintended drop in the first stage reactor temperature of about 2 °C during condition 4, otherwise, conditions were held nominally constant. Conversion, gas yield, and hydrogen consumption all dropped significantly. As with all of these tests, the molybdenum addition rate was held steady at 100 wppm on dry coal. Liquid yields held their own and gas selectivity (100 x C_1 to C_4 yield/total conversion) decreased. Directionally this seems to indicate that an improved iron catalyst could lead to a more selective liquefaction process.

Reduced Iron Oxide Addition Rate

The impact of reducing the iron oxide addition rate from 1.0 to 0.25 wt% DAF coal is shown by comparing condition 4 and 5. The temperature control was improved during condition 5, resulting in an apparent increase of 2 °C in the first reactor stage temperature. The most notable changes were a significant increase in conversion, gas yield, and hydrogen consumption. Conversion increased from 85.62 to 87.01 wt%, C_1 to C_4 increased from 12.48 to 14.08, and hydrogen consumption increased from 5.43 to 5.76 wt % on DAF coal, all statistically significant. Liquid yields remained steady. Notionally, the small increase in temperature may have contributed to the small but significant increase in conversion, while the reduction in catalyst may have lead to the deterioration in gas/liquid selectivity (100 x C_1 to C_4/C_1 to 1000 °F).

Changed Iron Oxide Catalyst

The impact of iron catalyst type, Bayferrox vs. Mach 1 are shown by comparing conditions 5 vs. 6. The results were small, but significant drops in conversion, C_1 to C_4, and hydrogen consumption. Conversion dropped from 87.0 to 85.2 wt% DAF coal, while C_5 to 537.7°C (1000°F) liquid yields held steady at 57.0 wt % on DAF coal.

Changed Molybdenum Source

The impact of changing the Molybdenum source from Organic, Molybdenum Van L, to inorganic, ammonium heptamolybdate is shown by comparing conditions 5 and 7. The change resulted in a significant drop in conversion, from 87.0 to 85.7, and lower C_1 to C_4 from 14.1 to 12.6. Even though conversion and gas yields dropped in going from the organic to the inorganic molybdenum source, selectivity to liquids improved.

Figure 1
Schematic Flow Plan of RCLU Pilot Plant

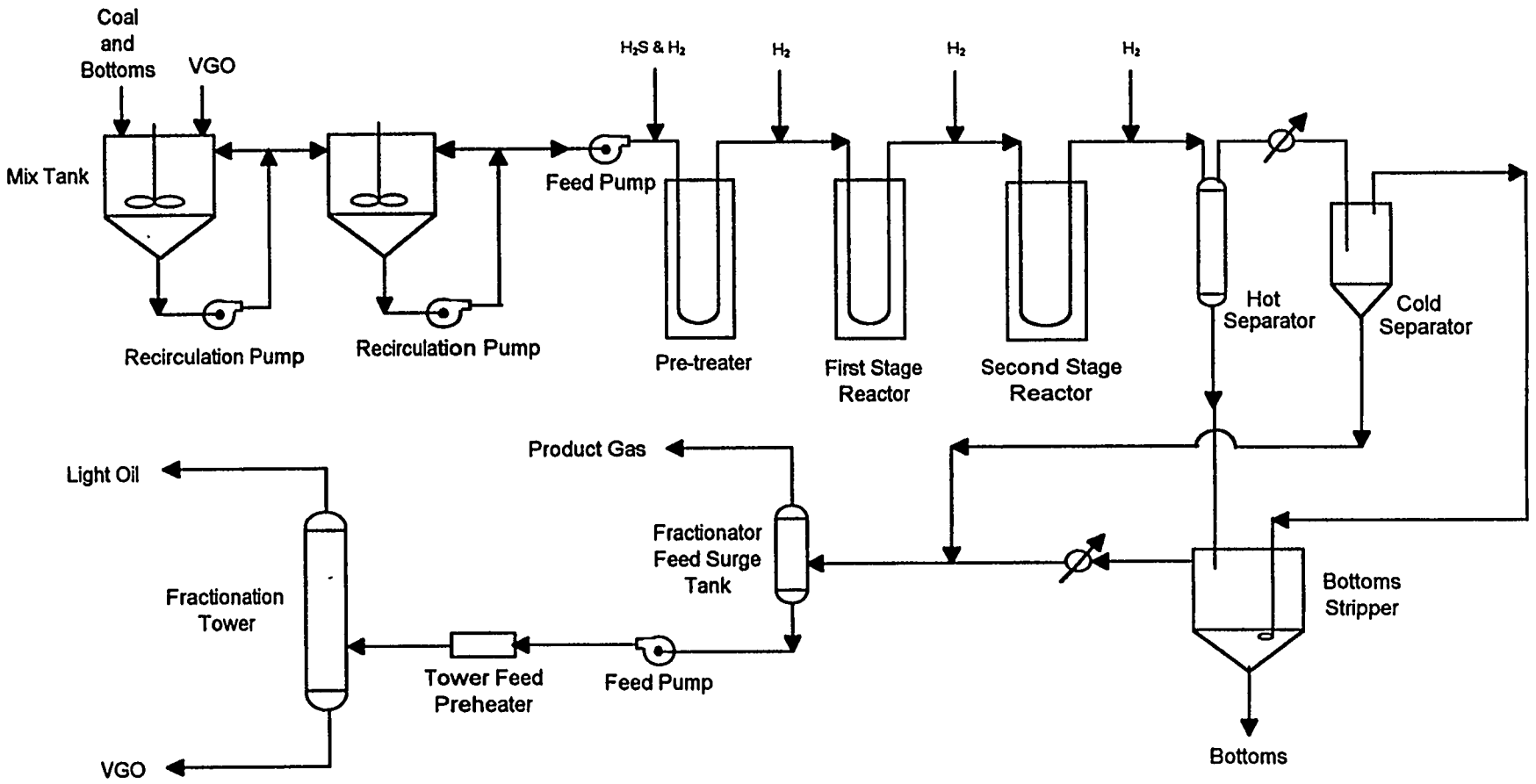

ADVANCED PROCESS CONCEPTS FOR DIRECT COAL LIQUEFACTION

Richard Anderson[1], Frank Derbyshire[1], Ed Givens[1], Todd Hager[1], Geoff Kimber[1], James Lim[1], Frank Burke[2], Mike Lancet[2], Gary Robbins[2], Dick Winschel[2], Howard Stephens[3], Richard Kottenstette[3], Mike Peluso[4]

[1] University of Kentucky Center for Applied Energy Research, 3572 Iron Works Pike, Lexington, KY 40511-8433;

[2] CONSOL Inc., Research & Development, 4000 Brownsville Road, Library, PA 15129-9566;

Sandia National Labs., Division 6212, 1515 Eubank SE, Albuquerque, NM 87123;

[4] LDP Associates, 32 Albert E. Bonacci Drive, Hamilton Square, NJ 08690

Contract Number: DE-AC22-91PC91040

Period of Performance: 28th August, 1991 to 25th August, 1995

Introduction

The Advanced Concepts Program was initiated by the Department of Energy in 1991 to promote the development of new and emerging technology concepts that have the potential, alone or in combination, to significantly reduce the cost of producing liquid fuels by the direct liquefaction of coal. Among other efforts, the advanced 2-stage liquefaction technologies that were developed at Wilsonville over the past 10 years and by the former Hyrocarbon Research Inc., HRI (now Hydrocarbon Technology Inc., HTI) have contributed significantly toward decreasing the cost of producing gasoline from coal. However, given the low cost of petroleum crude, direct liquefaction is still not an economically viable process. The DoE objectives are to further reduce the cost of coal liquefaction to a more competitive level. The approach has been to develop a long term strategy, in which certain promising liquefaction concepts, that have been identified mainly through fundamental studies, are subjected to technical and economic evaluation on a progressively increasing scale of experimentation, and with progressive integration into a complete process configuration. At each stage, depending upon their merit, research on any particular concept may be continued, modified or abandoned.

One of the contracts awarded under this program has involved a collaborative research and development effort between the University of Kentucky Center for Applied Energy Research (CAER), CONSOL, Inc., LDP Associates and SANDIA National Laboratories, beginning in August 1991. The project has involved two principal stages: the evaluation of individual process concepts, followed by the integrated testing of those concepts that were judged to warrant further investigation. The results obtained in each of these stages have been reported to this meeting (1,2). In both stages, individual and integrated concepts were tested and assessed in small-scale laboratory experiments. In a future phase of the research, it is intended that the more promising concepts will be subjected to more detailed testing in a larger-scale continuous unit.

In this project, the primary focus is on the use of low-rank coal feedstocks. A particular strength is the use of process-derived liquids rather than model compound solvents. Although this stratagem has created some difficulties in experimental operation and in the interpretation of data, it has lent additional credibility to the results.

The original concepts are illustrated in Figure 1, where they are shown on a schematic of the Wilsonville pilot plant operation. Wilsonville operating data have been used to define a base case scenario using run #263J, and Wilsonville process materials have been used in experimental work. The CAER has investigated: low severity CO pretreatment of coal for oxygen rejection, increasing coal reactivity and inhibiting the propensity for regressive reactions; the application of more active, low-cost, Fe and Mo dispersed catalysts; and the possible use of fluid coking for solids rejection, and to generate an overhead product for recycle. CONSOL has investigated: oil agglomeration for coal ash rejection, for the possible rejection of ash in the recycled resid, and for catalyst addition and recovery; and distillate dewaxing to remove naphthenes and paraffins, and to generate an improved quality feed for recycle distillate hydrogenation. At Sandia, research has been concerned with the production of active hydrogen donor distillate solvent fractions, produced by the hydrogenation of dewaxed distillates and by fluid coking, via low severity reaction with $H_2/CO/H_2O$ mixtures, using hydrous metal oxide and other catalysts. The technical and economic evaluation of the experimental data, and the impact on liquefaction process economics was made by LDP Associates.

For reasons that have been described in the Final Technical Report for this project, the concepts of low severity coal pretreatment and fluid coking were found not to offer sufficient incentives for continued work. The remaining concepts are still considered to be viable prospects for reducing the cost of coal liquids and have formed the basis of a proposal for continued development in a second phase project. The current status of these concepts is described in this paper.

Dispersed Catalyst Development

It has been shown that suitable dispersed catalysts can enhance the rate and extent of conversion of both subbituminous and bituminous coals, and that their presence is essential to the continuous processing of low-rank coals. A successful demonstration of the liquefaction of a low-rank coal in a continuous operation was achieved at Wilsonville in Runs 263J, when operating in a "thermal"-catalytic mode with the addition of a dispersed Fe + Mo catalyst to the first stage. However, the high cost of the molybdenum catalyst precursor used in that run (Molyvan L), combined with the fact that the catalyst is ultimately purged from the system, creates a considerable incentive to identify lower cost catalysts with comparable activity. In this research, efforts at the CAER have been directed to improving the activity of iron-based catalysts through the co-addition of Mo or other metals, while attempting to minimize catalyst cost. Two basic approaches were employed: the impregnation of the catalyst precursor on the feed coal, and the introduction of the catalyst in the form of nanometer size particles.

Development of Standard Microautoclave Tests

In order to relate the performance of the experimental systems to the base case, it became necessary to develop a standard laboratory scale test that could be used to compare different catalysts and other concepts with the base case. Since the base case operated with a process generated recycle solvent, it was decided to use a similar solvent in order to closely simulate the conditions in Run 263J. The recycle solvent contained about equal parts of 566°C- distillate and 566°C+ resid, along with about 20% recycled solids consisting of approximately equal parts of unconverted coal and mineral matter. A significant amount of the iron and molybdenum catalysts had accumulated in this stream and were present as pyrrhotite and molybdenum sulfide, respectively. The first challenge in developing a representative test was to understand how the solvents behaved and affected coal liquefaction.

Liquefaction of Black Thunder Wyodak coal in the microautoclaves consistently gave tetrahydrofuran (THF) conversions in excess of 100%, suggesting that the insoluble organic matter (IOM) in the recycle solvent was solubilized during reaction. It was eventually found that the solvent contained an easily converted THF insoluble fraction, and it became apparent that this same situation also held for other Wilsonville solvents that were evaluated.

Another difficulty with plant-derived recycle solvents was the presence of the recycled catalyst. The contribution of these background catalysts to the overall reaction did not become apparent until other results were obtained using solvents from different Wilsonville runs. The conversion of Black Thunder Wyodak coal in solvents that contained recycled Mo, in addition to the Fe that was present in all these solvents, was always significantly greater than in solvents which contained only iron. The activity of the background Mo was very high and masked the activity of freshly added catalysts, complicating efforts to develop a simulated 1st-stage catalyst screening test.

Standard test conditions to simulated the first stage resid conversion in microautoclaves were defined as 440°C for 22 min with 1000 psig cold hydrogen. The solvent to coal ratio was the same as used in Run 263J, namely 2.33 parts of solvent to 1.0 part of dry coal. However, it is to be noted that the 566°C+ resid conversion was actually higher than observed at Wilsonville. The resid conversion values obtained under the test conditions, with the 1 wt % Fe_2O_3 and 100 ppm Mo (as Molyvan L) base case catalyst, as used in Run 263J, was 30-32 wt %, versus a target value of 24 wt %. The significant activity of the recycled Mo became apparent when using a Mo-free recycle solvent (V-131B) from Run 258K, which gave resid conversions of only 17-18 wt %. The same results also showed quite clearly that the activity of the recycled iron (pyrrhotite) was considerably less than that of the Mo component. Further, equivalent resid conversions could only be achieved

with fresh Mo catalyst by adding twice the amount of metal that was present in the recycle solvent. In all these cases, fresh iron as iron oxide was added with the Mo. It was later found that the activity of freshly added Mo was considerably enhanced in the absence of any fresh iron, or as finally realized, was actually less inhibited. Although the inhibiting effect of iron has not been widely studied, the present results suggest that iron oxide, sulfate and nitrate can all inhibit the Mo activity while pyrrhotite has a negligible effect.

Impregnated Catalysts

The development of the base case (see later) showed that the cost of the dispersed Fe + Mo catalyst used in Run 263 is quite substantial. Most of this cost can be attributed to the cost of the Mo precursor, Molyvan L, which is an oil-soluble molybdenum organophosphorodithioate. A considerable amount of effort was thus directed towards identifying lower cost Mo precursors that could be added to the coal by impregnation as water-soluble salts, thereby eliminating the need for expensive oil-soluble catalyst precursors. A range of catalyst impregnated coals was prepared with impregnated Fe and Mo salts, alone and in combination. The outcome of this research showed that, for the Fe-Mo system, the catalyst concentration is the most important variable with respect to determining catalyst activity. It was also found that the metals could be impregnated on as little as 10% of the coal and perform just as well as if they were dispersed over the whole coal. This approach has been referred to as the Vector impregnation method, and it can offer a number of economic and technical advantages: less water is added with consequently less of an energy burden for subsequent drying; the amount of coal handling for the catalyst impregnation step is greatly reduced; and the technique allows more flexibility in plant design. The effectiveness of the Vector method also points to the fact that the catalyst must function primarily through the solvent phase, rather than act directly on the coal.

The addition of Fe and Mo as ferrous sulfate and ammonium molybdate by catalyst impregnation, at the same concentrations as in the base case, can substantially reduce the cost of the dispersed catalyst from ~$2.60/bbl gasoline to ~$1.10/bbl gasoline. More than half of the remaining catalyst cost (~$0.60/bbl gasoline) is attributable to the addition of the ferrous sulfate that was used. For this reason, attention was then given to the possibility of either eliminating or reducing the concentration of iron. As already mentioned, in the first-stage screening test, the activity of freshly added Mo was clearly improved in the absence of added Fe. In fact, the level of activity upon the addition of 500 ppm of impregnated Mo was found to approach that of the highly active recycled Mo at 450 ppm, although it must be stated that the two systems were not strictly comparable. Assuming then that Mo alone will give a performance equivalent to that of the Fe-Mo catalyst at the same Mo concentration, the cost of the dispersed catalyst can be further reduced to about ~$0.40/bbl gasoline, which is even less than the cost of the iron oxide in the base case.

Another interesting outcome of this project was to establish that the activity of the dispersed Mo catalysts is promoted by the presence of small amounts of nickel, as is already known for supported NiMo catalysts, where the Ni is believed to inhibit the growth of Mo crystallites. Co-impregnating coal with Ni and Mo, both in the presence and absence of Fe, repeatedly gave higher coal conversions while continuing to give resid conversions and distillate yields that were equal to those obtained in the Ni-free system. Since the influence of Ni in increasing conversion is similar to the effect of Fe, it may be possible to substitute Ni for Fe at a considerably lower concentration and reduced cost. For most of the catalysts that were tested, the Mo/Ni molar ratio was 4/1. The cost of adding this level of Ni to 100 ppm Mo, with no added Fe, would be only $0.03/bbl gasoline, which is still less than the cost of the 1% iron oxide used in the base case.

Sulfated Hematites

The second family of catalysts that was investigated was small particle sulfated hematites that are prepared by the base precipitation of solutions of iron salts. Other researchers have reported that particulate sulfated-hematites, as well as various metal promoted ones, can be exceptionally active in coal liquefaction. Other potential advantages of using this form of catalyst is that high dispersions can be achieved and maintained during processing. A series of sulfated hematites was prepared and tested in this project. The results were somewhat scattered, with no obvious pattern. Some catalysts exhibited exceptional activity, and others produced resid conversions that were significantly less than obtained in the base case.

A preliminary process and economic evaluation for the preparation of this type of catalyst showed that the cost of a Mo-promoted hematite, used at a level equivalent to the Fe and Mo concentrations in the base case, and with a distillate product yield equal to that of the base case, would cost about ~$1.90/bbl gasoline. Reducing the Fe content by half while maintaining the same 100 ppm Mo level decreases the cost of the catalyst to ~$1.20/bbl gasoline. Additional process benefits that could be derived from using these catalyst could further reduce that cost. Based upon the positive results that have been observed in this work and elsewhere, it is considered that this approach deserves further attention.

Solvent Quality Improvement: Distillate Dewaxing/Hydrogenation

Solvent dewaxing was examined by CONSOL as a means of improving coal liquefaction economics through solvent quality upgrading. Coal liquids, and subbituminous coal liquids in particular, contain a paraffinic wax component. Because of their relative inertness, paraffins tend to concentrate in the recycle solvent over time. These aliphatic materials dilute the hydrogen donors in the process recycle solvent, and are poor physical solvents for the coal reaction products. Therefore, they can impair the dissolution and upgrading of low rank coals. The purpose of dewaxing is to remove these paraffinic materials from the recycle distillate in the coal liquefaction process, as their presence is detrimental to solvent quality. The removal of the paraffins as a wax stream reduces the burden on the reactors to crack them to light distillate products, with the economic advantage that the reduced reactor burden may translate into higher reactor throughput. The gas production and hydrogen consumption that must accompany the paraffin cracking are thus avoided.

Three dewaxing schemes were evaluated for potential use in removing the wax from the recycle solvent. The features and benefits of each of these dewaxing routes are summarized below.

Ketone Dewaxing

In ketone dewaxing, which is a commercially proven technology, all or part of the heavy distillate stream is dewaxed in a ketone-based solvent. The extent of dewaxing is readily controlled by the choice of conditions. The dewaxed distillate is then recycled, either directly or after hydrogenation, to the first stage liquefaction reactor. The wax product may be purified and sold as a high-value by-product, or it could be converted to product distillate in an fluid catalytic cracking (FCC) unit.

Ketone dewaxing of the Wilsonville Run 262E V-1074 heavy distillate was tested with acetone, methyl ethyl ketone (MEK), toluene and various mixtures of these at temperatures from -35 °C to 0 °C. The degree of dewaxing was found to be a function of solvent composition and temperature. It was found that the solvent quality of the dewaxed distillate improved rapidly with dewaxing up

to ~20 wt % wax removal and then levelled off. The effect of the improved solvent quality on Black Thunder coal liquefaction was to increase the coal conversion from 87 wt % to 90 wt % when dewaxed distillate was substituted for the untreated distillate in the Wilsonville Run 262E solvent (5-min microautoclave tests at 824 °F, 1.5 S/C, 1500 psig of cold H_2). However, some of this increase may be due to the higher proportion of H-donors to coal, since the same overall solvent to coal ratio was used in microautoclave tests with the original and dewaxed solvents. It was also found that hydrogenation of the dewaxed distillate at SANDIA further improved coal conversion to 91 wt %.

A clean wax by-product, similar to commercial petroleum based waxes, is produced by de-oiling the slack wax that is removed from coal-derived distillate. The slack wax properties indicate that it should be an excellent feedstock to produce high yields of light products in an FCC unit.

There are several advantages of improving the recycle distillate solvent quality. An increase in single pass coal conversion from 87 to 91 wt % could result in about a 6 wt % decrease in rejected organics and a similarly improved product yield. Other prospective advantages of improved solvent quality are that it could allow operation at lower severity conditions than in the base case (lower temperature, pressure, residence time) while maintaining current levels of performance. Alternately, it could facilitate operation at higher severity conditions by countering retrograde reactions (increases in coal conversion of ~4 wt % were obtained at reaction temperatures that were ~30°C higher than in the base case) and improve throughput. Economic benefits can also be gained from either the sale of the clean by-product wax, or the increased distillate yield that is obtained upon cracking the crude wax.

Liquid Extraction Dewaxing

An alternative to ketone dewaxing is the process of liquid extraction using N-methylpyrrolidone (NMP), furfural or similar selective solvents. This is also a commercially proven technology that is used for the removal of aromatics from paraffinic lube oils but not for paraffin removal from aromatic-rich distillates.

In laboratory experiments, NMP and furfural were used at ambient temperatures to extract the aromatics from the heavy distillate fraction of the recycle solvent. It was found that the slack wax yield is greater (>40 wt % vs ~20 wt %), but the wax is of lower quality than that from ketone dewaxing. The extracted material is also more aromatic than the ketone dewaxed distillate (~30% aromatic hydrogen vs ~20%), and it is difficult to completely remove the extraction solvent. In terms of solvent quality, the aromatic fraction performs similarly to the feed distillate. However, hydrogenation of the aromatic fraction, which should be facile, is expected to improve solvent quality.

The advantage of liquid extraction is that it can be conducted at moderately elevated temperatures (40 - 90°C) and atmospheric pressure. The process operating costs have been estimated by LDP Associates to be lower than those of ketone dewaxing. It is considered that, with subsequent hydrogenation of the dewaxed distillate, coal conversion improvements should be similar to those obtained by ketone dewaxing plus hydrogenation, with similar associated cost benefits.

Thermal Dewaxing

Thermal dewaxing presents a third possible route to solvent quality improvement. In this process, all or part of heavy distillate stream is heated to elevated temperatures for a short time to preferentially thermally crack paraffins and naphthenes. The light cracked product is removed as net product and the aromatic-rich heavy distillate is recycled to the liquefaction reactor with or without prior hydrogenation.

Thermal dewaxing was tested by heating the heavy distillate to over 480°C for five minutes. Significant findings are: the dewaxed oil yield was ~75 wt % and the gas yield was <5 wt % at 495°C, and lower; the dewaxed material was more aromatic than most ketone dewaxed distillates (~25% aromatic protons in 495°C dewaxed distillate); and hydrogenating the dewaxed (495°C) distillate produced an improved liquefaction solvent (Black Thunder coal conversion increased by 2 wt % when this hydrogenated thermally dewaxed distillate was substituted for untreated distillate in recycle solvent).

The advantages of this approach are that: it involves a very simple process flow sheet; the process is the same as the "satcracking" process developed by the British Coal Corporation; and it should be easy to demonstrate in bench-scale continuous unit. The net outcome is that waxes are converted to distillable oils and gases, and a highly aromatic distillate is produced that should be readily hydrogenated (in a separate hydrogenation reactor or in the first stage liquefaction reactor) to produce a superior donor solvent with similar benefits to those demonstrated for the other dewaxing methods.

Agglomeration and Coal Cleaning

Coal agglomeration has been studied by CONSOL as a potential means of mineral matter rejection and catalyst incorporation with the goal of improving liquefaction economics by increasing yields and lowering catalyst requirements. A specific advantage is that the agglomerating oil is process-derived. Several agglomeration scenarios are presented to summarize this work. These scenarios include: agglomeration at natural pH; agglomeration of low-rank coal at natural pH, after pretreatment; agglomeration of low-rank coal at low pH; and splitting the feed coal, based on ash content, for liquefaction and gasification.

There are three basic issues to be addressed in developing agglomeration as an integrated component of a coal liquefaction process: the agglomeration performance at a given set of conditions; the cost of agglomeration at those conditions; and the liquefaction benefit and economic value of the agglomeration.

The first of these can be answered by a number of definitive laboratory experiments, the results of which are described below. The latter two issues deal more directly with development and scale-up of the process, and will be addressed more specifically in the proposed second phase of the project.

Agglomeration at Natural pH

It has been shown that coals ranging in rank from lignite through bituminous can be reduced in ash content by up to two thirds. This performance can be achieved under the following conditions: natural pH or minor adjustment to pH ≈6-8; an oil dosage of ca. 15 to 35%; 50-65 °C; and a coal slurry concentration of 20-43%.

The process can use sour water, whose low pH may enhance ash rejection for some coals. Any dissolved salts in the separated water could be fed to a gasifier of the Texaco type. All organics, most iron, and any pre-impregnated catalyst are retained with the coal. Hence, if this is deemed to be advantageous, catalyst can be added to the coal or part of the coal by impregnation before coal cleaning by oil agglomeration. Also, when using sour water, some silica and ≈50% of the sodium is rejected from low-rank coals. In no case is there any loss of coal reactivity.

The advantages of coal cleaning by oil agglomeration are: coal can be recovered following any aqueous pretreatment procedure; the lower ash content feed reduces slurry viscosity and can allow a reduction in solvent/coal ratio, or a higher rate of ashy recycle and reduction in the size of the ROSE-SR unit. Increasing the amount of the ashy recycle stream has another advantage in that more of the disposable catalyst will also be recycled, reducing the make-up of fresh catalyst. The dissolution of salts when using sour water may also lower the exposure of the second stage supported catalyst to poisons (especially the Na present in low-rank coals), resulting in lower catalyst replacement rate.

In one process scenario, coal is slurried with waste sour water from liquefaction and recycled water, and agglomerated with process-derived heavy distillate. The agglomerates are rinsed over screens, blown with air to remove surface moisture, and sent to liquefaction. Additional drying prior to liquefaction is optional and depends on other factors (i.e., it is not a requirement of agglomeration). A slipstream of the agglomerate rinse water with ash is used to slurry ash concentrate and coal for Texaco gasification. The remaining agglomerate rinse water with ash is treated to remove solids, and then recycled for slurrying coal and rinsing agglomerates. Any additional water requirement would be met by gasification sour water, and any excess agglomeration waste water would go to water treatment. Because liquefaction is a net producer of water, both from coal drying, and from hydrogenation, it is anticipated that there will be an adequate water supply for agglomeration. The cost of water use and treatment will be minimized by using waste streams wherever possible.

Agglomeration of Coal at Natural pH after Coal Pretreatment

As noted, in addition to cleaning untreated coal, oil agglomeration is well suited to the recovery of coal from any aqueous coal pretreatment step. It has been demonstrated that ash can be rejected following CO-H_2O-pretreatment, and after two types of catalyst impregnation.

This concept differs from that of untreated coal recovery by agglomeration at natural pH in that aqueous coal slurry from a pretreatment step is agglomerated, instead of using sour water to slurry the coal. The concept is not restricted to any particular pretreatment. Sour water might be useable in the pretreatment and agglomeration steps.

Agglomeration of Low-Rank Coal at Low pH

By using low pH conditions, it has been shown that coals ranging in rank from lignite through subbituminous can be reduced in ash content by up to three quarters. This performance can be achieved under the following conditions: pH of 1 or 2 adjusted using H_2SO_4; an oil dosage of 21 to 54%; 50°C; and a coal slurry concentration of 20 to 43%. The use of sour water could be of benefit as its low pH may reduce the acid requirement. As with the process using sour water only, any dissolved salts in the separated water can be fed to a Texaco gasifier. All organics, and most iron are retained with the coal. A pre-impregnated catalyst may also be retained although this has yet to be confirmed. Some silica and ≈90% of the Na, K, Ca, Mg are rejected from low-rank coals, and there is no loss of coal reactivity due to cleaning.

The advantages of coal cleaning by oil agglomeration at low pH are essentially the same as already described for oil agglomeration at natural pH.

Splitting of Feed Coal Quality for Liquefaction and Gasification

The potential for physical cleaning of several coals (Black Thunder, Burning Star 2, and Martin Lake) was assessed by float/sink tests, and by column flotation (Black Thunder only).

Segregation of the feed coal into a lower ash cleaned coal product that can be fed to liquefaction and a higher ash reject that can be gasified to produce hydrogen was shown to be a potentially attractive option to improve liquefaction economics: both ash and inert macerals are concentrated in the intended gasifier feed, while the lower ash content, more reactive coal is liquefied.

Economic and Technical Assessment

A basis for the technical and economic assessment of the experimental results obtained with the new process concepts was developed from the technical data for the Wilsonville pilot plant operation, material balance period #263J, Figure 1. During Wilsonville Runs #262 & 263, the pilot plant operated in the so-called hybrid ("thermal" - catalytic) mode with Black Thunder subbituminous coal, and with dispersed iron and molybdenum catalysts added to the first reaction stage and a supported nickel-molybdenum catalyst in the second-stage reactor.

An all-distillate product base case was formulated in which resid extinction was achieved in the system via a reduction in reactor space velocities, assuming first order reaction kinetics. It was anticipated that the distillates produced from liquefaction experiments in the present program might differ from those obtained at Wilsonville during Run#263J. As a result, all liquefaction distillates are assumed to be upgraded to a common basis (all-gasoline finished product) so that consistent comparisons are assured.

The base case conceptual commercial plant is a facility located at a mine-mouth Wyoming location. The hydrogen needed for liquefaction is generated by water slurry gasification of ash concentrate from the ROSE unit and of fresh coal. Light hydrocarbon gases produced during liquefaction and upgrading are used to close the fuel gas balance. Any excess gas is used to generate hydrogen via the steam reforming process. It is assumed that the electricity needed to operate the plant can be purchased from a nearby utility power plant. The capital and operating cost estimates for the Base case were developed using the relevant portions of previous liquefaction plant studies, as well as in-house information.

The base case plant converts 17,929 t/d of Black Thunder coal (dry basis) into 68,100 bbl/d of gasoline product. An additional 5,204 t/d of coal is gasified in order to meet hydrogen requirements. Overall coal conversion is 92%. The per pass conversion of resid plus IOM in the first and second stage reactors is approximately 23.5% and 18%, respectively. A high process solvent to coal ratio of 2.33 is employed since significant quantities of both IOM and ash are recirculated. Recycled ash is approximately 3.3 times the quantity of ash rejected from the process via the ash concentrate. The ash recirculation rate results in a 3.3 concentration effect for both the Mo and Fe dispersed catalysts. As a result, the effective concentration of Mo on coal to liquefaction is approximately 450 ppm at the Base case fresh addition level of 100 ppm.

A once-through first stage reactor design has been assumed. Four reactor trains in parallel are required to process the 17,929 t/d of coal. The first stage reactor is refractory lined in order to maximize the cross sectional area per reactor. Reactor gas rates were determined based on the

estimated average reactor partial pressures which existed during Wilsonville Run #263J and the recycle hydrogen gas purity. Actual reactor residence times and space velocities were also based on estimates from the Run #263J operation with appropriate corrections for the required resid plus IOM conversion level. Organic rejection (i.e. resid, insoluble organic material or IOM, and deashing solvent) from the liquefaction process amounts to 14.5% on a dry coal basis.

Significant investment cost areas include the liquefaction reaction system, vacuum fractionation system, the hydrogen recovery and recycle system, the makeup hydrogen generation system and the upgrading system. The hydrogen production system represents the dominant investment cost. Offsite unit investment costs are widely distributed among the various units. Working capital, start-up costs and the costs of initial catalyst and chemicals adds an additional 10% to the total capital requirement of $3.842 billion. Assuming a capital charge factor of 15%, the annualized capital costs are $26.45 per barrel of gasoline product.

Total operating costs are approximately $20/bbl of gasoline product inclusive of a $1/bbl. credit for ammonia, sulfur and phenol byproducts. The significance of liquefaction system additives and purchased electrical power costs and the relative insignificance of coal cost is noteworthy. Liquefaction additives costs are approximately $5.20/bbl. of gasoline, with the iron and molybdenum dispersed catalysts accounting for more than half of this total. Coal costs are low because of the low $5/ton, wet mine-mouth price for Black Thunder coal. On this basis, assuming a capital charge factor of 15%, the Base case required gasoline product selling price is $46.46/bbl. [Note. The price is quoted for gasoline and not crude oil equivalent.]

Case Analyses of Selected Advanced Concepts

The base case data has been used by LDP ASSOCIATES to evaluate the impact of three of the concepts that have been under investigation, and to develop a modified base case. Laboratory scale experimental data has been evaluated to determine the prospective gains in terms of increased product yield per unit of coal feed, and reduced solvent recycle rate and liquefaction system additive costs.

Addition of Dispersed Catalyst by Coal Impregnation with Water-Soluble Salts

As pointed out in the base case the cost of dispersed iron and molybdenum catalysts accounts for almost $3/bbl. of the gasoline product selling price. A significant portion of this cost results from the use of an expensive molybdenum source, the oil soluble Molyvan L. At $3.20/lb. and an 8.1 wt.% molybdenum concentration, the cost per pound of Mo is $39.50. By using a molybdenum salt such as ammonium octamolybdate (available in tonnage quantities), the raw material cost per pound of Mo could be reduced to $7.30. Even with the additional processing costs for preparing the salt solution, impregnating a small portion of the feed coal to liquefaction, and driving off the extra water added to the coal, the cost of the impregnated Mo is still only about 25% of the cost of using Molyvan L. Further, when using a water-soluble Mo source in this way, the cost drops below the cost of using particulate iron oxide at the base case dosage level of 1 wt.% Fe on dry coal. Therefore, unless dispersed iron catalysts in conjunction with Mo confer a level of catalytic activity that is not attainable with Mo alone, the use of Fe is questionable. Other advantages can be anticipated if this proves to be the case: using iron at a 1 wt.% level adds to the ash in the liquefaction system and increases the organic rejection due to the assumed constant solids content of the ash concentrate. For the purposes of this assessment, the addition of the iron catalyst was assumed to be unnecessary.

Oil Agglomeration at Low pH

The experimental results indicate that the oil agglomeration at low pH can remove approximately 50% of the ash in Black Thunder coal. The reduction of ash in the feed coal will reduce organic rejection during solids separation thereby increasing the potential product yield. It will also reduce the ash recirculation rate within the process while still maintaining the same catalyst recycle enhancement factor as in the base case. In effect, front end ash removal purges useless inerts from the system. Through oil agglomeration at low pH, potential supported catalyst poisons, such as calcium, sodium, magnesium and potassium are also removed. For this assessment it has been assumed that the second stage reactor supported catalyst replacement rate can be reduced by 30%.

The oil agglomeration process is well-suited for the preparation of the feed coal: distillate recycle solvent can be used as the agglomerating agent; sour water can be used as make-up water to the system; and the slurry reject of solids and dissolved salts can be utilized in the gasification slurry mixing systems. In fact, the dissolved salts may even act as catalysts in the gasification process. Of course, the use of oil agglomeration will add capital and operating costs to the overall process. The capital cost for low pH oil agglomeration is expected to be approximately $60 million, and the cost of the sulfuric acid could also be significant.

Distillate Solvent Quality Improvement

It is proposed that three process steps will be used to treat the waxy distillate recycle solvent: solvent extraction, solvent dewaxing and hydrotreating. In combination, these processes effectively remove and recover the waxy material from the distillate solvent and enhance its donor solvent capabilities. Both solvent extraction and solvent dewaxing are commercial processes used in the petroleum refining industry.

The objectives of applying these three processes are: to reduce the distillate solvent recycle while improving its quality; to recover a valuable by-product wax; and to increased the potential product yield via coal conversion improvement. It is estimated that the wax yield is 4 wt % on coal. However, this wax accumulates in the distillate recycle solvent until the rate of its removal by cracking is equal to its production rate. Based on the Wilsonville Run#263 data, the wax concentration in the distillate recycle solvent is estimated to be approximately 24 wt %. Therefore, the removal of a substantial portion of the wax significantly reduces the distillate solvent recycle rate. The wax that is removed and recovered has a current estimated selling price (34¢/lb.), more than double that of gasoline. The ability of the wax market to absorb the significant quantity of wax produced by a commercial size plant is a key consideration.

The solvent extraction process is used upstream of the solvent dewaxing process as a means of significantly reducing the feed rate to, and therefore the cost of, the much more expensive solvent dewaxing process. In the solvent extraction process, a solvent such as furfural or NMP, is used to absorb aromatics from the feed stream. The paraffinic wax is not absorbed and passes through the unit. For the modified base case, approximately 70% of the distillate solvent feed to the extraction unit is absorbed, thereby reducing the solvent dewaxing unit feedrate by a factor of 3. In the solvent dewaxing process, the paraffinic wax is separated from the feed stream by chilling, precipitation and filtration in the presence of a suitable solvent such as MEK. When wax production is desired, a three stage filtration system is used. In addition, a wax finishing step is also required.

Conventional fixed bed hydrotreating is used to make the final improvement in distillate solvent quality. For the modified base case, a single train system operating at conditions favorable for hydrogenation of the aromatics (340 to 400°C & 1800 psig) is anticipated. It is also assumed that full dewaxing and hydrotreating of the distillate recycle solvent will improve coal conversion by 3

percentage points. Such an improvement further increases the potential product yield and reduces the IOM recycle rate.

Combined Impact of Selected Concepts: Modified Base case

The benefits of reduced feed ash and improved coal conversion are evident. While the solids concentration in the ash concentrate remains the same, organic rejection is reduced to 8.5% on dry coal. At the same time, the recycle solvent rate is reduced by 20% because the removal of the wax, lower feed ash and higher coal conversion. The recirculation of the Mo catalyst remains at the same 3.3 factor as in the base case. In order to achieve the higher product yield, the required per pass resid plus IOM conversion increases in both reaction stages. Since reaction temperatures are not changed, this increased conversion is achieved by reducing the space velocity (predicted by first order kinetics) by approximately 15% versus the base case. Although reactor space velocities are lower, this is partially offset by the lower recycle rate, such that the reactor volume, and hence cost, is only slightly increased.

In this configuration the gasoline production rate increases by 4.5%, while a significant quantity of the valuable wax by-product is also produced, and the C4+ product yield increases to greater than 65 wt % on dry coal. Hydrogen consumption increases in proportion to the increased production rate. Because of the significant decrease in organic rejection, additional gasification of coal is required to close the hydrogen balance. The total electrical power requirement for the modified base case increases by approximately 12% due to increased gasification quantities and the requirements of the added units.

Process unit investment increases by $432 million due to the added units and the increased gasification requirements, and total capital required increases by $520 million over the base case. The net operating costs drop by approximately $140 million/year due to the lower liquefaction system additive costs and the significant impact of by-product wax revenue. If a 15% capital charge factor is used, the required gasoline product selling price is $41.82/bbl or $4.64/bbl lower than in the base case.

References

1. Derbyshire, F, Givens, E, Burke, F, Winschel, R, Lancet, M, Stephens, H, Kottenstette, R, Peluso, M "Improved Coal Liquefaction through Enhanced Recycle Distillate Quality", DoE Contractors' Review Conference, Pittsburgh, PA, 28-29 Sept., 1993

2. Anderson, R, Derbyshire, F, Givens, E, Hager, T, Kimber, G, Lim, J, Burke, F, Lancet, M, Robbins, G, Winschel, R, Stephens, H, Kottenstette, R, Peluso, M "Advanced Process Concepts for Coal Liquefaction: Process Simulation Testing", DoE Coal liquefaction and Gas Conversion Contractors' Review Conference, Pittsburgh, PA, 7-8th September, 1994.

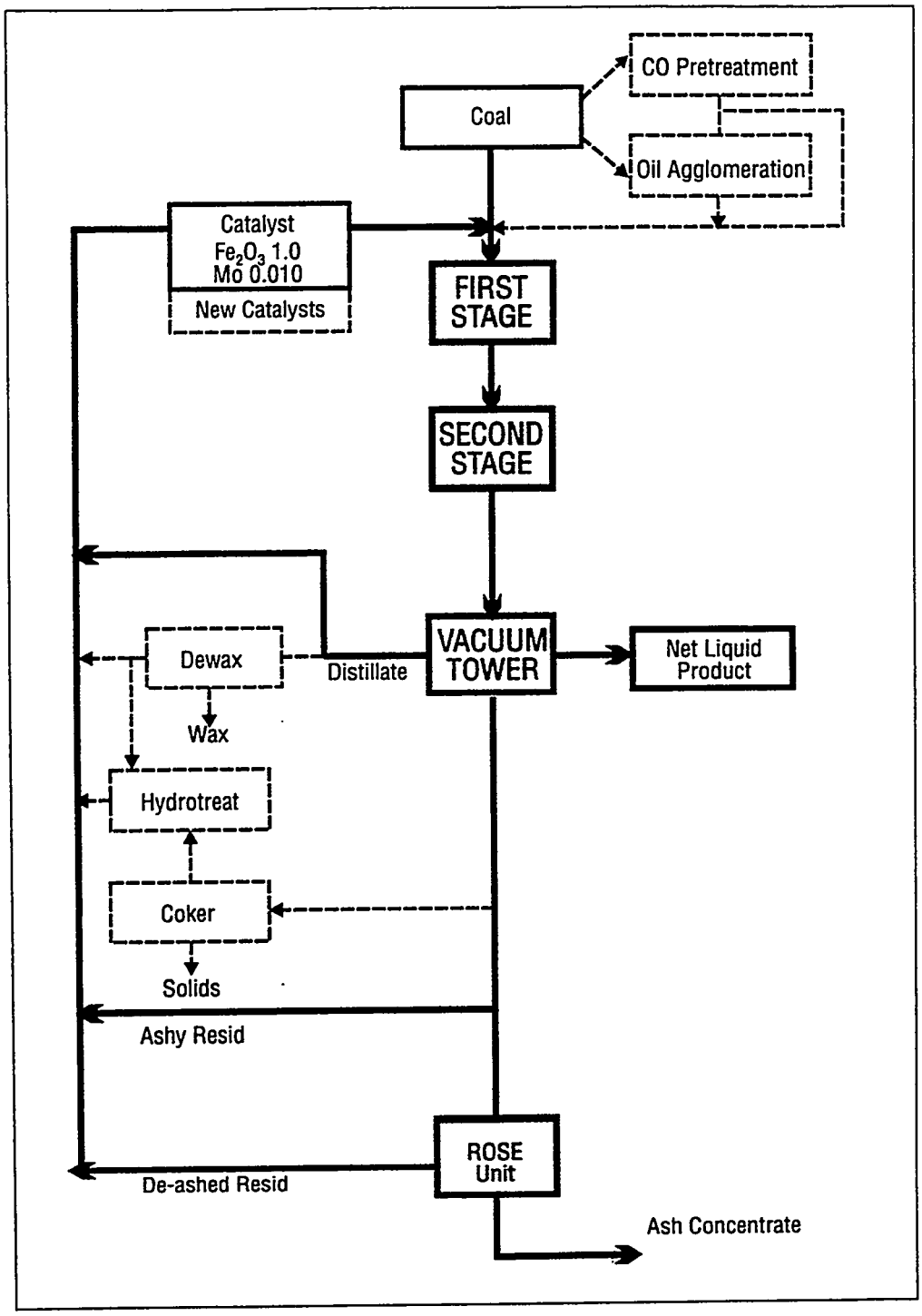

Figure 1. Advanced Concepts Shown on Schematic of All-Distillate Mode Operation, Wilsonville Pilot Plant Operation

TECHNOLOGY FOR ADVANCED LIQUEFACTION PROCESSES: COAL/WASTE COPROCESSING STUDIES

Anthony V. Cugini, Kurt S. Rothenberger, Michael V. Ciocco, Donald Krastman, Raymond Bernarding, Theodore Jordan, John Erinc*, and Christine McCreary*

U.S. Department of Energy, Pittsburgh Energy Technology Center
Pittsburgh, PA 15206-0940

* Gilbert Commonwealth, Inc.

PROJECT OVERVIEW AND INTRODUCTION:

The efforts in this project are directed toward three areas: (1) novel catalyst (supported and unsupported) research and development, (2) study and optimization of major operating parameters (specifically pressure), and (3) coal/waste coprocessing.

The novel catalyst research and development activity has involved testing supported catalysts, dispersed catalysts, and use of catalyst testing units to investigate the effects of operating parameters (the second area) with both supported and unsupported catalysts. Several supported catalysts were tested in a simulated first stage coal liquefaction application at 404°C during this performance period. A Ni-Mo hydrous titanate catalyst on an Amocat support prepared by Sandia National Laboratories was tested. Other baseline experiments using AO-60 and Amocat, both Ni-Mo/Al_2O_3 supported catalysts, were also made. These experiments were short duration (approximately 12 days) and monitored the initial activity of the catalysts. The results of these tests indicate that the Sandia catalyst performed as well as the commercially prepared catalysts. Future tests are planned with other Sandia preparations. The dispersed catalysts tested include sulfated iron oxide, Bayferrox iron oxide (iron oxide from Miles, Inc.), and Bailey iron oxide (micronized iron oxide from Bailey, Inc.). The effects of space velocity, temperature, and solvent-to-coal ratio on coal liquefaction activity with the dispersed catalysts were investigated. A comparison of the coal liquefaction activity of these catalysts relative to iron catalysts tested earlier, including FeOOH-impregnated coal, was made.

The potential for reducing pressure in coal liquefaction using various combinations of dispersed catalysts and donor solvents are being investigated. To date, the efforts have focused on microautoclave experiments. The results of the microautoclave efforts are reported in the "Liquefaction Chemistry and Kinetics: Hydrogen Utilization Studies" project discussion. Future plans are to extend the microautoclave efforts to semi-batch and continuous tests.

As part of the U.S. Department of Energy (DOE) Fossil Energy program, the Pittsburgh Energy Technology Center (PETC) recently initiated research in coal waste coprocessing. The objective of this project is to explore and facilitate development of processes that will economically convert, into liquid fuel feedstock, a combination of any or all of the following; coal, rubber, plastics, heavy oil, waste oil, and paper. The effort to date has centered on the combined processing of coal and heavy oil (coal-oil coprocessing), coal and plastics, and a smaller effort with coal and rubber. The initial

effort with coal and plastics has focused on the reactivity of coal/plastics mixtures and the operability of processes that utilize these feedstocks. This paper summarizes the coal/waste coprocessing efforts. The early stages of this work have been presented at a Symposium at the American Chemical Society National Meeting[1] and recently at the Ninth Annual Consortium for Fossil Energy Technical Meeting[2].

EXPERIMENTAL SECTION

Materials Liquefaction experiments were conducted with -200-mesh Black Thunder mine coal (Wyodak-Anderson seam, Campbell County, WY). High-density polyethylene (PE), melting point 135°C, density 0.96 g/mL, was manufactured by Solvay Polymers. Polystyrene (PS), melting point 95°C, was manufactured by BASF. Poly(ethylene terephthalate) (PET), melting point 215 C, density 1.4 g/mL, was manufactured by Hoescht Celanese as IMPET EKX-105. All plastics were supplied to PETC by HTI, formerly HRI, as 3.2-mm (1/8-in) extrudates. A mildly hydrogenated (9% hydrogen) fluid catalytic cracking (FCC) decant oil, obtained as the 340-510°C (650-950°F) fraction from run POC-1 on the proof-of-concept coal liquefaction unit at HTI, was used as a vehicle in the coal-waste coprocessing experiments. Aged Akzo AO-60 Ni-Mo/Al_2O_3 catalyst was obtained from run POC-1 at HTI.

Reactions Microautoclave reactions were conducted in 42-mL cylindrical, stainless-steel batch reactors constructed at PETC. The base conditions of the reactions were 2:1 hydrogenated FCC decant oil vehicle : coal-plastics mixture, one hour at 430°C, 7 MPa (1000 psi) cold hydrogen gas pressure, and 0.6 g aged Akzo AO-60 catalyst, although variations in time, temperature, and catalyst composition were also made. During workup, the reactor contents were sonicated in tetrahydrofuran (THF) for 30 minutes and subsequently filtered through a 0.45-micron filter under 40 psi nitrogen gas pressure. The THF soluble material was stripped of solvent on a rotary evaporator and re-extracted with heptane to produce a heptane soluble fraction. Conversion was calculated from the measured mass of insolubles adjusted for catalyst and coal mineral matter, based on the mass of plastic and MAF coal. The mass of the catalyst was also adjusted for the presence of entrained oil in the material as determined in a separate extraction step. The PE and PET plastics showed no significant solubility in either THF or heptane under the workup conditions used. PS did show appreciable solubility in THF, rendering those conversion calculations meaningless.

Semi-batch (batch slurry, flow-through gas) reactions were performed in a 1-L stirred-tank reactor system. The feed charge consisted of 350 g of slurry that typically consisted of a 2:1 ratio of vehicle:feed with 30 g aged AO-60 catalyst. The experiments were done at temperatures of 430-460°C under 17.5 MPa (2500 psi) hydrogen gas pressure flowing at a rate of 1.9 L/min (4 SCF/h). The products were characterized in terms of gas yield and composition, solubility in heptane and THF, and 450°C conversion [conversion of all material distilling above 450° C (850° F), including MAF coal, plastics, and 450°C+ oil, to material distilling below 450°C].

Continuous mode catalytic liquefaction experiments were conducted in a computer controlled 1-L bench-scale unit. The unit is a once-through system without recycle. A typical charge consisted of a vehicle:feed mixture of 70/30 at an overall slurry feed rate of 146 g/h. The catalyst, 35 g of aged AO-60, was contained in an annular basket surrounding the stirrer to simulate the action in an

ebullated bed. The coprocessing experiments were done at reactor temperatures of 400-460°C under 17.5 MPa (2500 psi) of a 97% H_2 / 3% H_2S gas mixture flowing at a rate of 2.4 L/min (5 SCF/h). The products were characterized by distillation into three fractions - those boiling below 340°C (650°F), between 340-450°C (650°F-850°F), and above 450°C (850°F).

Gas Analyses Microautoclave reactor gas samples were collected at the completion of each run. Hydrogen consumption was calculated, based on the difference between initial and final (cold) gas pressure as adjusted for product gas composition. Semi-batch unit gas samples were collected once during the run (tail gas), and at its completion (flash gas). Hydrogen consumption was calculated based on the assumption that the tail gas sample was representative of the gas make throughout the run.

Viscosity Measurements Viscosity measurements were made to obtain data on feed mixtures in support of continuous unit operations. These measurements were conducted on a CANNON Model MV 8000 rotational viscometer equipped with an optional heating jacket and spindle capable of measuring viscosities as high as 500,000 cP at temperatures up to 260°C. The sample holder was loaded with 10.5 mL of material and tests were conducted over the temperature range corresponding to actual operating conditions. Viscosities were also measured over a series of sheer rates, again corresponding to unit operating conditions. Regressions indicated that the oil-coal-plastics mixtures are well represented as power law fluids, i.e. viscosity is proportional to shear rate raised to some power.

RESULTS AND DISCUSSION

Feed Slurry Rheology Studies The rheological properties of the feed slurry for coprocessing will be a significant factor in determining the pumpability and feed system requirements (e.g., pressure drop) of the slurry. Measurements of viscosity and flow properties will be used to develop a database to compare the feed requirements of systems using different types of hydrocarbon wastes.

The effect of plastic component type on viscosity was evaluated with HRI-L800 (a hydrotreated decant oil obtained from HTI, Inc.) oil as the solvent. Three major components were investigated: high density polyethylene (HDPE), polystyrene (PS), and polyethylene terephthalate (PET).

Figure 1 shows the effect of component type (including a commingled plastic mixture of 50% HDPE, 35% PS, and 15% PET) on slurry viscosity. The HDPE resulted in the highest viscosity, and the viscosity of the commingled system was intermediate between that of the HDPE and the PS systems. PET was not successfully tested, since it was not possible to obtain a single phase mixture with PET and oil. To successfully use PET a second plastic component, either PS or HDPE, has been required. It is unclear whether a synergy is observed with the commingled system with respect to viscosity. However, it is clear that a benefit is observed with the commingled system with respect to being able to obtain a single phase containing PET.

Figure 2 presents the effect of varying the relative amounts of coal and the commingled plastics mixture while maintaining a 70/30 oil-to-solids ratio. The HTI oil and Black Thunder (BT) subbituminous coal were used with the plastics mixture (HTI oil/BT/plastics) in these measurements.

As shown in Figure 2, increasing the plastics content at the expense of the coal results in higher slurry viscosities. Figure 3 shows the effect of commingled plastics addition in the oil/plastics (no coal) system. As expected, the viscosity increases with increasing plastics content.

In separate tests, no significant difference was observed between BT and Illinois No. 6 coal. However, there did appear to be a dependence of viscosity on solvent type. Differences were observed between use of North Slope ATB, Wilsonville V-1074 heavy distillate, and the HRI L-800 oil.

From continuous experiments that were conducted on the PETC bench-scale liquefaction units, two observations were made regarding the needs for pumping slurries containing plastics. The high viscosity of the mixture requires high temperature and head pressure during pumping. However, if the viscosity becomes too low and the feed rate is low, settling of the suspended coal becomes significant and plugging will occur.

Waste Coprocessing Reactivity Studies Microautoclave studies were conducted to determine the conditions required to convert the plastics, especially HDPE. At 430°C both PS and PET were easily converted to heptane soluble products. However, no significant conversion of HDPE was observed at this condition. Table I summarizes the results of the microautoclave tests. For the most part, the conversions observed in mixed plastics with coal systems indicated that the plastics were compatible with coal. There was one exception, however; it appears that the presence of coal (and in several cases an aromatic solvent) inhibited the conversion of HDPE. Only at higher temperatures was significant HDPE conversion observed in the presence of coal.

Experiments were also made with semi-batch reactors. For the most part, the observations from microautoclave experiments were also evident in the semi-batch reactors. The difficulty of converting HDPE was also observed in the semi-batch reactors.

Two separate continuous experiments (with 9 run conditions) on coal/waste coprocessing (over 100 hours) were successfully conducted on one of the PETC bench-scale units with Black Thunder subbituminous coal and commingled plastic. The major accomplishments of these experiments were determining the proper operating envelope for processing coal/waste slurries and confirming high HDPE conversion. In selecting the proper feed temperature, both high and low viscosity effects (refer to Task 1) had to be addressed. The catalyst used in the continuous tests was a supported NiMo on alumina, AO-60. It is worth noting that HDPE conversion was observed at elevated temperature with a hydrogenation catalyst (and no specific cracking catalyst). Table II summarizes the conditions used for the continuous experiments.

POC-Scale and Bench-Scale Coprocessing Product Analysis The HTI POC-2 (a proof of concept run of coal/waste coprocessing at HTI, Inc.) and CMSL-08 (a bench-scale test of coal/waste coprocessing at HTI, Inc.) samples have been subjected to an extensive suite of analytical techniques, with the goals of determining (1) what is the fate of the plastic materials; (2) how the presence of plastics and coal affects the processing of each of these components; and (3) whether the traditional measurements of process efficiency, such as conversion, are applicable to mixed coal-waste systems. Analyses include low voltage high-resolution mass spectrometry (LVHRMS),

nuclear magnetic resonance (NMR), infrared spectroscopy (IR), potentiometric titration, and electron paramagnetic resonance (EPR) spectroscopy.

Low-voltage, High-resolution Mass Spectrometry LVHRMS results were obtained from POC-2 samples SP-3 (naphtha stabilized bottoms), SP-4 (atmospheric still bottoms), and SP-5 (vacuum still overhead) samples for run periods 36(coal-only), 43(coal+plastic), and 45(coal+rubber). The data follow a logical progression of increasing average molecular weight and degree of condensation and decreasing hydrogen-to-carbon ratio, as the sampling points varied from SP-3 (naphtha stabilized bottoms) to SP-4 (atmospheric still bottoms) to SP-5 (vacuum still overhead). The three SP-3 samples ranged in average molecular weight from 130 to 170, while the three SP-4 samples ranged from 195 to 215 and the three SP-5 from 220 to 230.

The most dramatic observation from the LVHRMS data is a dominant C_2-benzene peak in the spectrum of SP-3, period 43. This peak is more than twice as intense as the next most prevalent signal. It is attributed to ethylbenzene from depolymerization and hydrogenation of polystyrene in the plastics mix. The assignment is supported by analogous results from coupled gas chromatography - mass spectrometry analysis.

Nuclear Magnetic Resonance Spectroscopy NMR spectra were obtained for the SP-3 (naphtha stabilized bottoms), SP-4 (atmospheric still bottoms), and SP-5 (vacuum still overhead) samples for run periods 36, 43, and 45.

For a given run period, carbon aromaticity follows the sequence SP-3 < SP-4 < SP-5. In fact, the correlation is strong enough that none of the SP-5 samples has a carbon aromaticity less than any of the SP-4 samples, none of which exhibit carbon aromaticities less than any of the SP-3 samples. This is consistent with expectations of increased aromaticity as the distillation cuts become heavier. Within a given sample point, the carbon aromaticity always increases (or stays the same) in the order period 36 < period 45 < period 43. This is more likely related to the aromatic products of PS and PET plastic degradation, and to the presence of hydrogenated decant oil added as make up solvent in the coprocessing run periods.

Fourier Transform Infrared Spectroscopy FTIR spectra were recorded of the SP-27 (ROSE bottoms) product from periods 36 and 43. The results provide strong evidence of polyethylene in the ROSE bottoms product. The period 43 sample showed polyethylene aliphatic C-H and CH_2 bands at 2910, 2850, 1460 and 720 cm^{-1}. Based on period 43 results alone, it was not clear whether the bands were due to polyethylene or waxy material from the coal. However, these bands were much less prevalent in the period 36 product. A difference spectrum between the period 43 and 36 samples compared very well with the major bands in a neat polyethylene sample. These data do not indicate how much of the polyethylene is being removed, or whether the polyethylene that was removed had undergone any cracking. However, they do indicate that at least some of the polyethylene is not converting and is being removed in the ROSE extraction step.

SUMMARY AND CONCLUSIONS

Individually, plastics degrade as reported in the literature, and products rapidly hydrogenate to

saturation. HDPE generally requires more severe conditions for conversion to solubles than either PS or PET. The traditional solvent extraction methods for evaluating coal conversion are not particularly appropriate for plastics. The feed PS was found to be soluble in THF. It is quite possible that in cases where no HDPE conversion was observed (by THF solubility analysis) that, in fact, the HDPE chain was broken down, just not sufficiently for solvent extraction.

Less hydrogen may be required to produce saturated products from plastics (if gas production can be minimized), since the average waste plastic stream is less aromatic than coal. However, under traditional liquefaction conditions, each C-C bond scission still consumes one molecule of H_2, because any olefinic products formed as a result of depolymerization rapidly hydrogenate to saturates. This is particularly true with PE, which tends to degrade randomly along the polymer chain.

In the two-component and multicomponent microautoclave tests, THF solubles could be reasonably well predicted from the behavior of the individual components under similar conditions. However, the heptane solubles were greater than that predicted by the assumption of individual behavior. This may be indicative of some type of synergistic behavior in coliquefaction of coal with plastics. Further work in this area will be done, including investigating the addition of polypropylene.

The viscosity of coal-plastics mixtures increases significantly as the plastics concentration increases. PE seems to have the greatest influence on viscosity. Higher temperatures were required to pump the mixture when the composition was raised from 25% to 50% plastics. Control of viscosity by control of temperature was the key to successful operation of continuous mode coprocessing. Future investigations in continuous operations of the effect of solvent type and plastics concentrations will be done.

DISCLAIMER

Reference in this report to any specific commercial product, process, or service is to facilitate understanding and does not necessarily imply its endorsement or favoring by the United States Department of Energy.

REFERENCES

1. Rothenberger, K.S., Cugini, A.V., Ciocco, M.V., Anderson, R.R., and Veloski, G.V., Am. Chem. Soc., Div. of Fuel Chemistry, Prep., Vol. 40(1), 38-43(1995).

2. To be presented at the 9th Technical Meeting of the Consortium for Fossil Fuel Liquefaction Science.

TABLE I: SUMMARY OF MICROAUTOCLAVE REACTION CONDITIONS AND RESULTS

Experiment	Feed Mixture (%) Coal	PE	PS	PET	Vh:F[1]	Catal	Time min.	Temp. (°C)	Conv. % THF	Hept	H_2cons (mmol)
Single-Component Reactions											
I	100	0	0	0	2:1	AO-60	60	430	83	51	50
II	0	100	0	0	1:1	AO-60	60	430	-19	-19	28
III	0	100	0	0	2:1	AO-60	30	465	79	76	75
IV	0	0	100	0	2:1	none	60	430	94	77	N/A
V	0	0	100	0	2:1	AO-60	60	430	98	98	N/A
VI	0	0	100	0	2:1	AO-60	60	430	97	96	54
VII	0	0	0	100	2:1	AO-60	60	430	93	86	N/A
Two-Component Reactions											
VIII	33	67	0	0	1:1	AO-60	60	430	28	26	38
IX	50	50	0	0	6.6:1	HTO	60	430	36	27	41
X	50	50	0	0	6.6:1	HTO	60	430	34	24	39
XI	0	67	33	0	1:1	AO-60	60	430	36	36	N/A
XII	0	67	0	33	1:1	AO-60	60	430	35	35	46
Multicomponent Reactions											
XIII	70	15	10	5	2:1	AO-60	60	445	71	37	73
XIV	70	15	10	5	2:1	AO-60	120	445	48	13	N/A
XV	70	15	10	5	2:1	Fe-S	120	445	67	26	N/A
XVI	50	25	16	9	2:1	AO-60	60	430	65	57	54
XVII	50	25	16	9	2:1	AO-60	60	430	63	56	49

[1] 2:1 Vehicle:Feed (Vh:F) represented 6.6g vehicle : 3.3g feed; 1:1 Vh:F = 3.3g vehicle : 3.3g feed; 6.5:1 Vh:F = 6.6g vehicle : 1g feed

Table II. Summary of Continuous Test Conditions

Test:	I	II	III	IV	V	VI	VII	VIII	IX
Coal:	Black Thunder	Black Thunder	Black Thunder	Black Thunder	Black Thunder	Black Thunder	Black Thunder	Black Thunder	Black Thunder
Wt% Coal:	22.5%	22.5%	22.5%	22.5%	15.0%	22.5%	20.0%	15.0%	22.5%
Wt% Plastics:	7.5%	7.5%	7.5%	7.5%	15.0%	7.5%	10.0%	15.0%	7.5%
Wt% HDPE	50%	50%	50%	50%	50%	50%	50%	50%	60%
Wt% PS	35%	35%	35%	35%	35%	35%	35%	35%	40%
Wt% PET	15%	15%	15%	15%	15%	15%	15%	15%	0%
Temperature (degree C):	430	430	430	430	430	430	430	430	460
Feed Rate(g/h):	198	142	162	167	117	146	146	146	146

Figure 1. Effect of Plastics Type on Viscosity

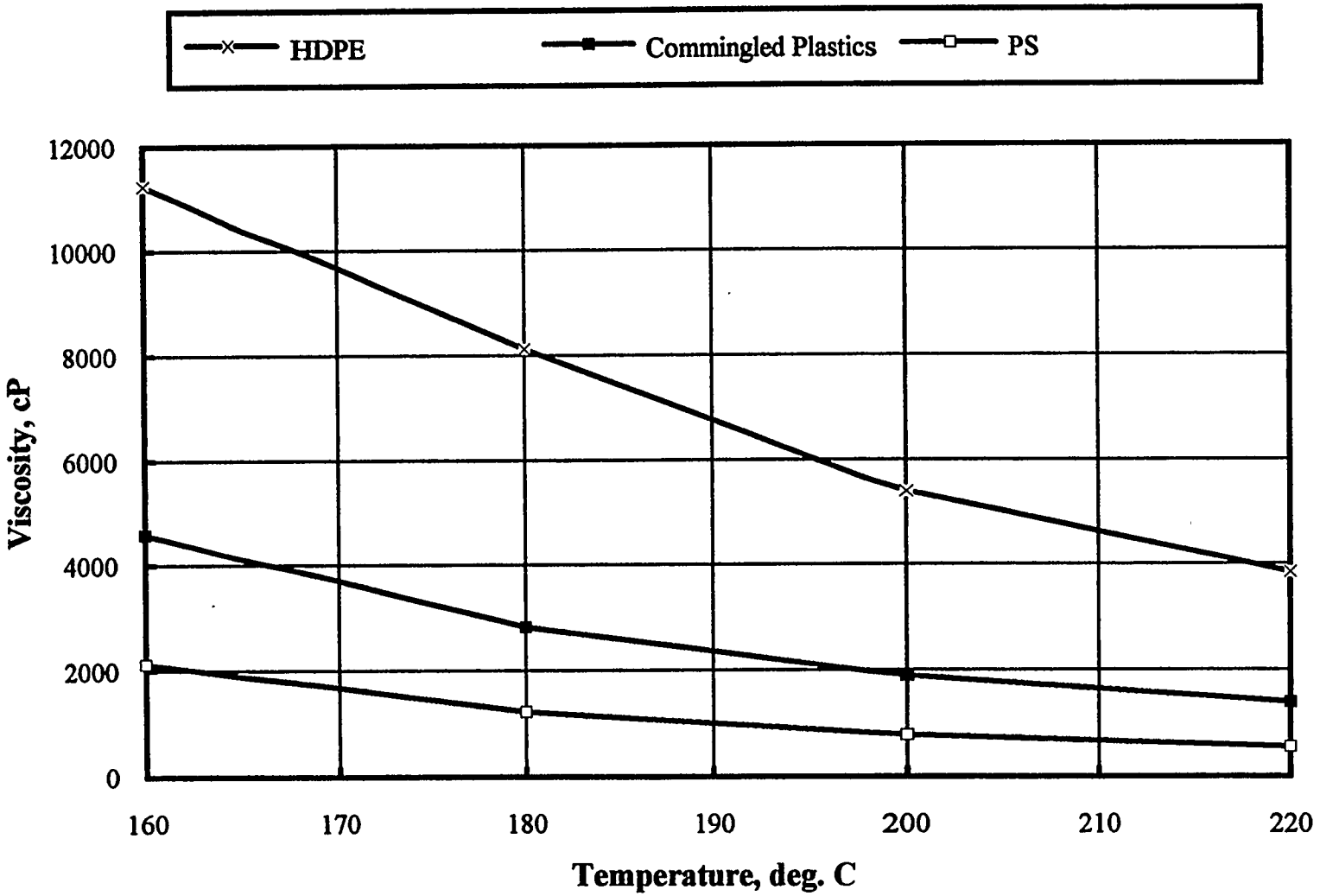

Commingled Plastics Mixture: 50% HDPE, 35% PS, 15%PET

Figure 2. Effect of Coal to Plastics (C:P) Ratio on Viscosity

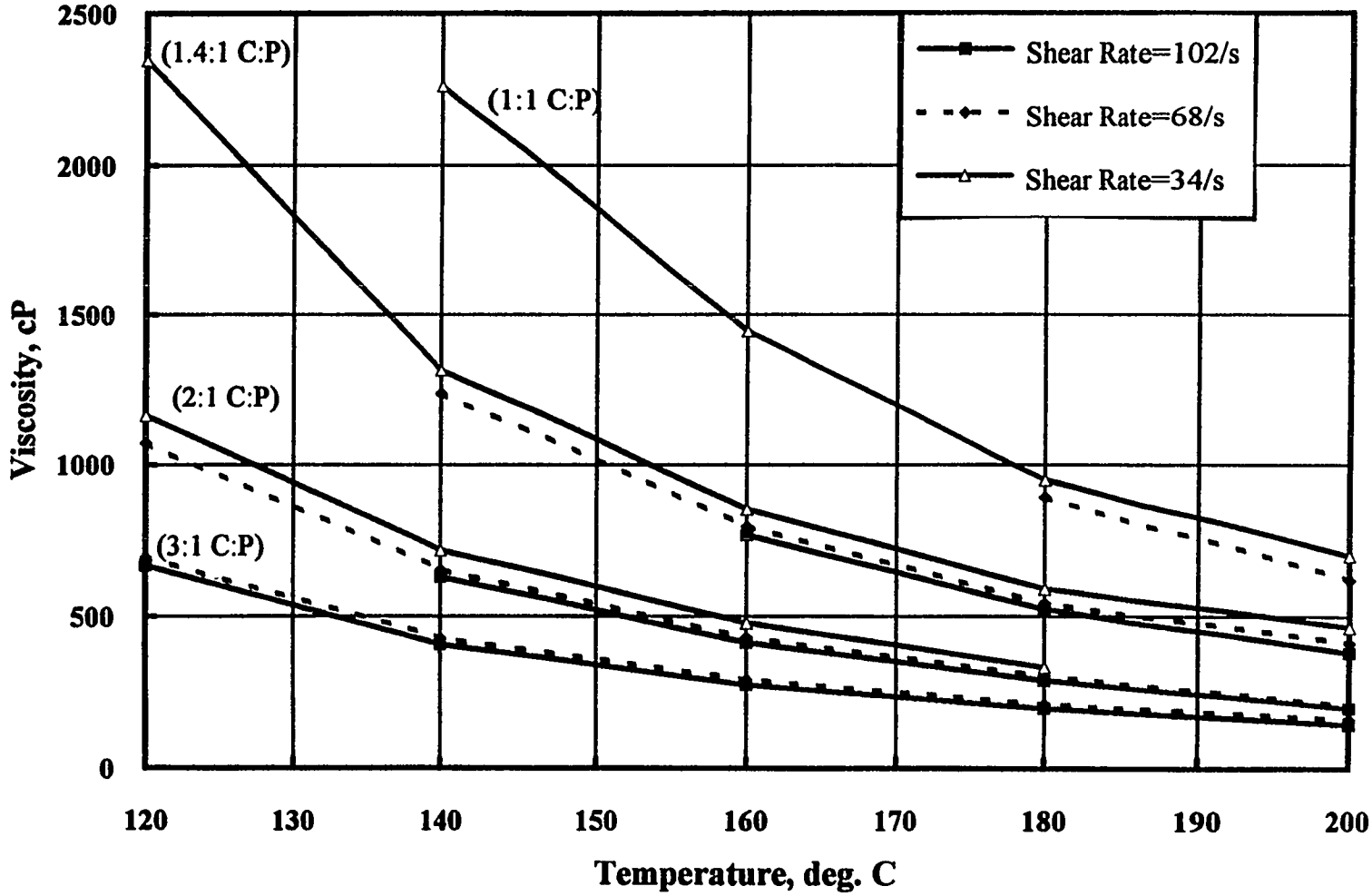

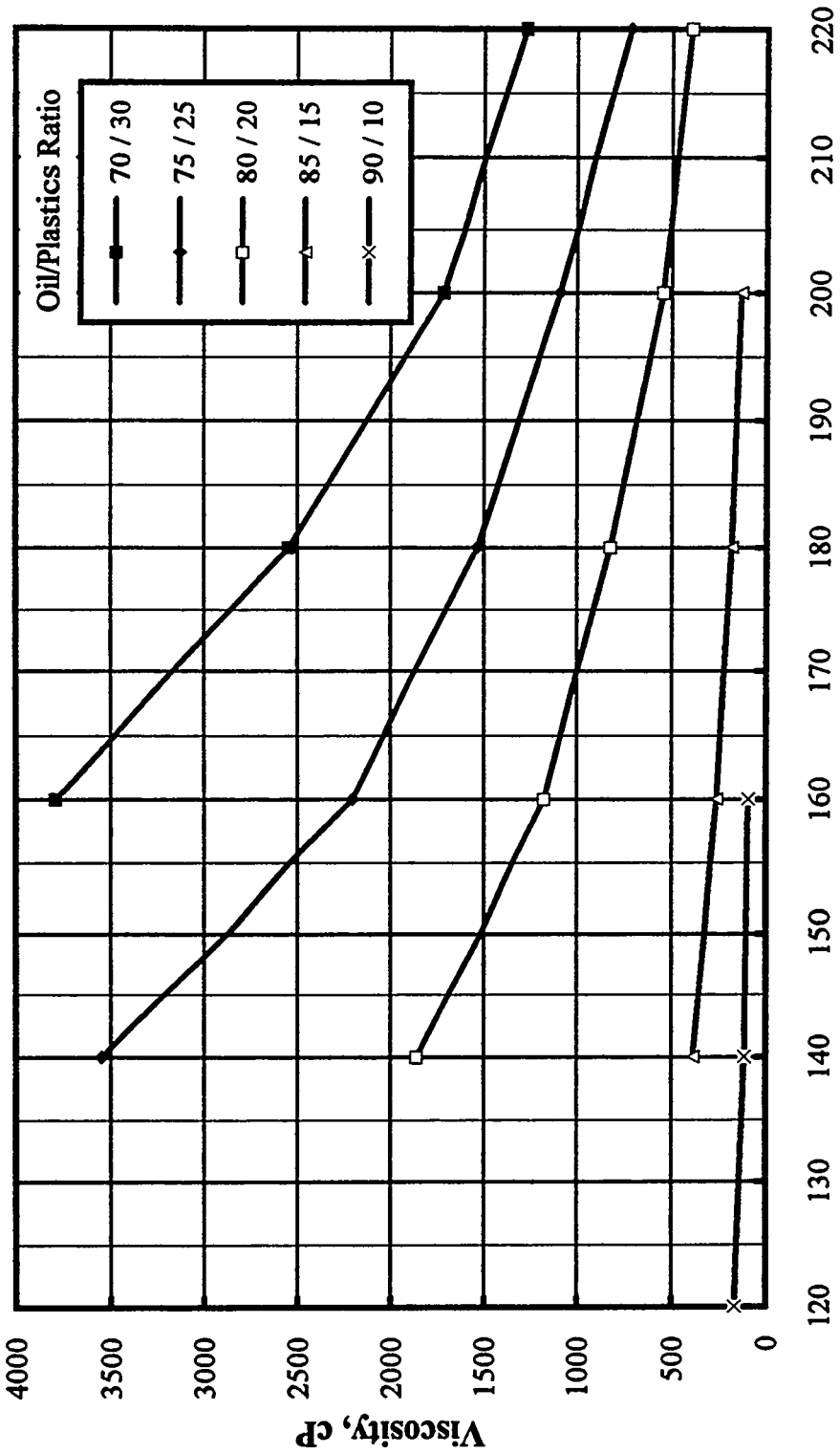

Figure 3. Effect of Plastics Content on Viscosity using HRI L800 Oil and Commingled Plastics

TITLE: Characteristics of Process Oils from HTI Coal/Plastics Co-Liquefaction Runs

PI (AUTHORS): G. A. Robbins, S. D. Brandes, R. A. Winschel, F. P. Burke

INSTITUTION/ORGANIZATION: CONSOL Inc., Research and Development Department

CONTRACT NUMBER: DE-AC22-94PC93054

PERIOD OF PERFORMANCE: June 30, 1994 - June 30, 1997

OBJECTIVE:
The objective of this project is to provide timely analytical support to DOE's liquefaction development effort. Specific objectives of the work reported here are:

- to determine the fate of the plastics feedstocks, relative to coal-only operation;
- to determine the conversion of the feedstocks;
- to determine the product streams to which the feedstocks are converted (bottoms vs. distillate);
- to determine interactions of feedstocks;
- to determine how use of plastics feedstocks affect product quality; and
- to determine to what degree property differences reflect feedstock differences vs. other (process) condition changes, such as unit operations, space velocity, and catalyst age.

ACCOMPLISHMENTS AND CONCLUSIONS:
Introduction
During a few operating periods of Run POC-2, HTI co-liquefied mixed plastics with coal, and tire rubber with coal. Although steady-state operation was not achieved during these brief test periods, the results indicated that a liquefaction plant could operate with these waste materials as feedstocks. CONSOL analyzed 65 process stream samples from coal-only and coal/waste portions of the run. Some results obtained from characterization of samples from Run POC-2 coal/plastics operation are:[1,2]

1. Polystyrene (PS) products were identified and quantified in distillate product oil.

2. Incompletely converted high-density polyethylene (HDPE) was found as tetrahydrofuran (THF)-insoluble material in the ash-free-resid recycle stream. It was unclear to what extent this material was present in the ROSE bottoms stream. Unusual solubility behavior seems to be associated with HDPE-derived material in resid-containing streams. The broad implication is that HDPE was not completely converted in the liquefaction process.

3. The unusual presence of a product-oil sediment raised questions about the stability of the product oil.

5. Analytical issues were identified including how to identify and quantify HDPE, the appropriateness of coal liquefaction work-up procedures to

coal/plastics liquefaction, and how to measure the extent of plastics liquefaction.

Along with the analytical difficulties, the brevity of the coal/plastics liquefaction period in Run POC-2 prevented these issues from being resolved. To better evaluate these issues, Run CMSL-8 was performed at a smaller scale and over a longer period than Run POC-2. There were other differences too, such as reactor and temperature configuration and the feed coal used. However, the plant operated in solvent balance, which did not occur during the coal/plastics portion of Run POC-2. Solvent-balanced operation in Run CMSL-8 meant that samples, material balances, and performance results from Run CMSL-8 were representative of operation with the coal/plastics feedstocks. Coal/HDPE liquefaction was tested in Run CMSL-8, in addition to coal/mixed plastics liquefaction. The background and results from characterization of Run CMSL-8 process oil samples is presented below.

HTI Run CMSL-8 Background

A diagram of HTI's bench unit 227 as configured for Run CMSL-8 (also known as Run 227-85) is shown in Figure 1.[3] CONSOL analyzed feed samples, and samples from sample points 4 through 7, representing recycle and product streams. The operating conditions and process performance summary for the run are given in Table 1.[3] Operating performance was good early in the run, but as the run continued, the catalyst age increased, and the concentration of polyethylene in the feed was increased. The resid conversion decreased as the run progressed. Several adjustments were made to process conditions after period 16 to maintain performance and operability. Notable events were: the change from coal operation in period 6 to 75% coal and 25% mixed plastics prior to period 11; the increase in second-stage reactor temperature from 830 to 850 °F, an increase in first-stage space velocity from 30 to 40 lb dry feed/hr/ft^3 reactor prior to period 16; the increase in mixed plastics concentration to 33%, decrease in space velocity from 40 to 30 lb dry feed/hr/ft^3 reactor, and increase in dispersed Mo catalyst concentration from 100 to 200 ppm, prior to period 20; and, prior to period 22, the switch from 33% mixed plastics to 33% HDPE. Over the duration of the run, the supported catalyst reached an age of 966 lb dry feed/lb cat. Samples received as either period 22 or period 23 samples were considered to represent material balance period 22.

Analyses Performed

A brief description of the Run CMSL-8 samples and analyses conducted as CONSOL's baseline characterization is provided in Table 2. In this paper, the samples will be referred to by the abbreviations given in Table 2, e.g., SOH for the product oil, PFL for the recycle liquid, and PFC for the bottoms stream. The baseline analytical methods can be applied to many different kinds of samples, can be performed quickly, and have proven to be suitable for liquefaction process stream characterization. In addition to the routine laboratory analyses, non-routine characterization (such as FTIR characterization of certain samples) was performed, based on the Run POC-2 sample experience. Several samples were selected for specialized analyses, such as plasma desorption mass spectrometry (PDMS) and field ionization mass spectrometry (FIMS).

SOH Product Characteristics and Effects of On-line Hydrotreating

The separator overheads (SOHs) from periods 6 and 11 through 23 were consistently low in aromatic hydrogen and high in paraffinic hydrogen content (Figure 2). There was a small increase in paraffinic hydrogen from periods 16 to 20 to 23

coincident with increases in the HDPE concentration in the feed (8.75 to 11.5 to 33 wt % dry feed in those periods). There was no change in paraffinic hydrogen content from period 6 (coal-only) to period 11 (coal/mixed plastics). However, a substantially lower paraffinic hydrogen content was observed when the on-line hydrotreater was by-passed in period 9. This indicates that, because of extensive upgrading in the hydrotreater, the paraffinic hydrogen content of the SOH may be relatively insensitive to other process changes. The product oil (SOH) sample from period 9, in which the on-line hydrotreater was by-passed, is much poorer in quality than the SOHs produced with the hydrotreater in place. Differences included: medium brown in color vs. colorless, presence of a "coal liquid" odor, more aromatic, less paraffinic, and considerably higher phenolic -OH concentration (Figure 2). The effects of hydrotreating observed in this run were greater than those observed in Run POC-2.[1] This may be because the distillate hydrotreated in Run CMSL-8 is a thermal distillate, and the distillate of Run POC-2 came from a catalytic reactor.

Gas chromatography-mass spectrometry (GC-MS) total ion chromatograms of SOH samples (Figure 3) show that replacing a portion of the coal with mixed plastics (from period 6 to period 11) and the switch from mixed plastics to HDPE (from period 11 to period 22) increased the concentrations of n-paraffins in the SOHs, and shifted the n-paraffins to higher molecular weight. Thus, HDPE appears to be an important source of the n-paraffins in the SOHs produced after period 6.. Two peaks corresponding to ethylbenzene and cumene (isopropylbenzene) are marked in Figure 3. These components are polystyrene (PS) liquefaction products. Cumene was not found in the coal-only period SOH, and ethylbenzene was present at about 1% concentration in the coal-only and coal/HDPE periods 6 and 23. ^{1}H-NMR results indicate that PS products persisted in the SOH product from the coal/HDPE period. In the NMR spectra of the SOHs, ethylbenzene features are nonexistent in the coal period SOH, quite prominent in the coal/mixed plastics period SOHs, and observable, but small, in the coal/HDPE period SOH.

The PS products were quantified by GC-MS and ^{1}H-NMR (Table 3). The area of the ethylbenzene and cumene peaks, as a percentage of the total ion chromatogram was used to estimate the concentration of these components in the SOHs. The alkylbenzene concentration of the SOHs was estimated (as ethylbenzene) by integration of the ^{1}H-NMR peak near 7.1 ppm. Based on these estimates, ethylbenzene and cumene constitute about 8-15 wt % of the coal/mixed plastic period SOHs (with the HTU in use), less than 1 wt % of the coal/HDPE period SOH, and about 2 wt % or less of the coal period SOH. When the hydrotreater was by-passed with the coal/mixed plastics feed, the concentration increased to about 15 to 23 wt % of the SOH. Approximately 50% of the PS fed to the process can be accounted for as these alkylbenzene products (with the hydrotreater operating).

HDPE in Recycle and Resid Samples

The PFLs from the coal/plastics periods 11, 16, 20, and 22 contained 15 to 30 wt % THF insolubles. These insolubles were tan with white specks early in the run and dark brown later in the run. The presence of THF insolubles in the PFL is a unique feature of coal/plastics processing. PFLs from coal-only operations (including period 6 of this run) typically contain little or no THF-insoluble material. The FTIR spectra of insolubles from coal/plastics periods 11 and 22 were similar and indicated that they are polyethylene-like material (Figure 4). PFL 850 °F$^+$ distillation bottoms from two of three coal/mixed-plastics periods separated into two solid phases upon cooling; none of the other PFL resids behaved in this way. The two phases differed in physical characteristics and

color. Diffuse reflectance FTIR (Figure 4) was used to examine both phases of one of the resids. The upper phase appeared to be predominantly plastic derived (much of it PE), and the lower phase is predominantly coal derived. The spectrum of the upper brown phase indicated primarily aliphatic hydrocarbons with PE-like features. Aromatic hydrocarbon peaks also were significant, but no features indicated the presence of heteroatomic functional groups. The spectrum of the lower black phase showed more intense aromatic hydrocarbon peaks than did the upper phase, and a significant amount of aliphatic hydrocarbon in the lower phase, but no distinctive PE-like features. The spectrum of the lower phase also contains prominent peaks from heteroatomic functionality, perhaps N-H and O-H.

Samples of both PFL resid phases, along with other samples from Run CMSL-8, also were characterized by field-ionization mass spectrometry (FIMS) at SRI International.[4-6] The pyrolysis profiles are shown in Figures 5a-b and the FIMS spectra in Figures 5c-h. Volatilization of each sample was nearly complete. The pyrolysis profiles show that HDPE pyrolyses to low molecular weight components at about 430 °C (Figure 5a), and that the THF-insoluble sample from the period 22 PFL is nearly all HDPE (Figure 5b). In the mass spectra, the HDPE pyrolysis products are lower in molecular weight and generally distinct from the coal-derived resid components (Figure 5c-h). These spectra also confirm the identification of the period 22 PFL THF insolubles as nearly pure HDPE (Figure 5c-d), and show that HDPE is present to varying degrees in the other samples from coal/plastic operating periods (Figure 5c-h). The plastic layer (Figure 5g) contains more HDPE than the corresponding coal layer (Figure 5h). Furthermore, the odd/even mass ratio is higher for the coal layer, suggesting that it contains more heteroatomic species. This is consistent with the FTIR results. A simple quantitation method was tried with the FIMS data (Table 4), and it appears to work fairly well (to the extent determinable at this stage). This method is compared with another method below.

In Table 5, the results of two methods for estimating the concentration of HDPE in liquefaction process streams are compared. In the first method, the THF-insoluble content of a PFL sample was measured and assumed to be unconverted HDPE. In the second method, a linear relationship between the HDPE concentration and the number average molecular weight (M_N) determined by FIMS was assumed. The methods for this limited sample set agree quite well. The FIMS approach offers the potential to quantify the amount of unconverted HDPE present in the bottoms (PFC) stream. This would allow a more accurate determination of HDPE conversion than is presently available.

Conversion of HDPE During Run CMSL-8

CONSOL and others have found indications that high-density polyethylene (HDPE) is less reactive than coal and other plastics feedstocks toward liquefaction at conventional liquefaction conditions. Since adequate conversion of HDPE is an important factor in the development of coal/plastics coprocessing, it is important to know the conversion of the HDPE during Run CMSL-8 and other coal/plastics coprocessing runs. Upper limits for both single-pass and overall conversions of HDPE during Run CMSL-8 were estimated (Table 6). It was assumed that: 1) the HTI unit was operating at steady-state, 2) that the PFL THF-insolubles are HDPE, and 3) that there was no unconverted HDPE in the PFC. During Run CMSL-8, PFL was both the recycle liquid (Figure 1) and a liquid product. Overall conversion is a measure of fresh HDPE which is not present as unconverted HDPE in the net products; in overall HDPE conversion, recycled HDPE is considered an internal stream and does not need to be explicitly accounted

for. The single-pass conversion of HDPE is a measure of the disappearance of both the recycled and fresh HDPE fed (recycled HDPE is explicitly accounted for).

The conversion calculations require material balance data for the HTI run periods,[3] and an estimate of the amount of HDPE in the pressure-filter liquid (PFL). Details of the method used are provided elsewhere.[7] These results (Table 6) represent an upper limit for conversion, because the HDPE concentration in the pressure-filter cake (PFC) product could not be determined. The overall conversion of HDPE ranged from 40-80% during the run (Table 6), lower than the 90-95% coal conversion and 80-85% resid conversion typically observed for coal liquefaction. The single-pass HDPE conversions averaged around 25%. Both overall and single-pass conversions were lowest during period 16, after an increase in second-stage reactor temperature and space velocity. Measures taken by HTI to improve performance after period 16, such as reducing the space velocity and doubling the dispersed Mo catalyst concentration, restored the conversions observed in period 11. The single-pass HDPE conversion in period 22 was much higher at about 50%. Measures that HTI took to maintain operability in that period of the run when HDPE and coal were fed seemed to provide the high single-pass conversion, and high overall conversion of HDPE.

Conclusions

The major conclusions from characterization of Run CMSL-8 samples are listed below.

- PS products are identifiable and quantifiable in the SOH distillate product from coal/mixed plastics co-liquefaction.
- HDPE appears to be an important source of n-paraffins in the SOHs from coal/plastics co-liquefaction.
- The SOH sample from period 9 in which the on-line hydrotreater was by-passed was much poorer in quality than the SOHs produced with the hydrotreater in operation.
- Identification of some PS and polyethylene terephthalate (PET) products in the SOHs may be masked by highly effective on-line hydrotreating. Addition of a hydrotreater feed sample point, or of more off-line hydrotreater reference periods may help in identification of plastics liquefaction components in the SOHs.
- Incompletely converted HDPE constituted 15 to 30 wt % of the PFL recycle streams, and was found as THF insolubles; virtually no THF insolubles were present in the coal-only period PFL.
- Phase separation in some PFL distillation resids indicates that HDPE products have complex phase behavior.
- HDPE conversions were estimated to be ca. 80 % overall, and ca. 25 % single-pass, and the conversions were responsive to changes in process conditions.
- THF insolubility is currently the best way to separate HPDE in liquid samples which contain no other solids.
- FTIR is useful for the identification of HDPE products.
- FIMS allows distinction of coal-derived material and HDPE-derived material in process stream samples. Quantification of HDPE seems possible using the FIMS technique, but additional development is needed.

PLANS:

CONSOL Support to DOE Coal/Plastics Co-Liquefaction Development

We will do similar sample collection, distribution, and characterization work for future runs. Specialized analyses will supplement baseline characterization techniques. Additional analytical work, such as method development and evaluation, will be performed, as needed, to address key issues in coal/waste coprocessing. This will include evaluation of methods for characterization of plastic liquefaction products. Additional work could include development of alternative liquefaction work-up schemes to accommodate plastic components which are not amenable to conventional coal liquefaction work-up schemes. It is anticipated that at some future point, a distillate product oil from coal/waste co-liquefaction will be selected by DOE for a full set of product inspection tests. CONSOL will assist DOE in conducting these tests.

ACKNOWLEDGEMENTS:

The assistance of several individuals is greatly appreciated. These include Lorna Schlutz, Sophia Heunisch, and Dave Olson at CONSOL R&D, Vivek Pradhan at HTI, Udaya Rao and Kurt Rothenberger at DOE/PETC, John Larsen at Lehigh University, and Ripu Malhotra at SRI.

REFERENCES:

1. Robbins, G. A.; Brandes, S. D.; Winschel, R. A.; Burke, F. P. "A Characterization and Evaluation of Coal Liquefaction Process Streams, Quarterly Technical Progress Report October 1 through December 31, 1994", DOE/PC 93054-10, May 1995.

2. Robbins, G. A.; Winschel, R. A.; Burke, F. P. "Characterization of Coal/Waste Coprocessing Samples from HRI Run POC-2", Prepr. Am. Chem. Soc., Div. Fuel Chem., 40 (1) 1995, Anaheim, CA, April 2-7, 1995, pp. 92-96.

3. Pradhan, V. R. "Run CMSL-8, Evaluation of Coal-Plastics Co-Liquefaction in CTSL Mode", Draft HTI Report, January, 1995.

4. Larsen, J. W.; Lapucha, A. R. "Coal Liquefaction Process Streams Characterization and Evaluation, The Application of ^{252}Cf-Plasma Desorption Mass Spectrometry to Analysis of Direct Coal Liquefaction Heavy Products", DOE/PC 89883-58, October 1992.

5. Malhotra, R.; McMillen, D. F. "Coal Liquefaction Process Streams Characterization and Evaluation, Characterization of Coal Liquids by Field Ionization Mass Spectrometry and Iodotrimethylsilane Derivatization", DOE PC 89883-39, January 1992.

6. Malhotra, R.; McMillen, D. F. "Coal Liquefaction Process Streams Characterization and Evaluation, FIMS Analysis for Direct Coal Liquefaction Process Streams", DOE/PC 89883-91, March 1994.

7. "A Characterization and Evaluation of Coal Liquefaction Process Streams", Status Report for April 1 through 30, 1995, DOE/PC 93054-13, May 26, 1995.

TABLE 1. RUN CONDITIONS AND PROCESS PERFORMANCE SUMMARY FOR HTI RUN CMSL-8 (227-85)

Condition	1	2	3	4	5
Period No.	6	11(b)	16	20	22
Hours of Run (End of Period)	144	264	384	480	528
wt % Plastics in Feed (a)	0	25	25	33	33
Stage 1 Cat. Age, lb Feed/lb Cat	252	457	711	884	966
Stage 1 Feed Space Velocity lb Feed/hr/ft^3 Reactor Vol.	32.2	29.6	39	30.1(c)	29.6
Oils/Solids Ratio	1.5	1.6	1.8	2.1	1.9
Temperature, °F					
Stage 1	810	810	810	810	810
Stage 2	830	830	850	850	850
HTU	715	715	715	715	715
Dispersed Mo Concentration, ppm of Dry Feed	100	100	100	200(c)	200
Total Material Recovery, % (Gross)	102.2	98.4	96.7	101.2	99.6
Estimated Normalized Yields, wt % MAF Feed					
C_1-C_3 in Gases	11.35	9.14	9.02	7.41	5.17
C_4-C_7 in Gases	4.81	3.27	3.41	3.17	3.27
IBP-350 °F	15.86	20.48	19.00	17.63	8.80
350-500 °F	17.99	12.57	8.59	11.16	7.60
500-650 °F	21.14	19.85	12.27	16.88	10.72
650-850 °F	10.18	11.84	15.18	11.54	14.24
850-975 °F	2.29	2.94	5.60	4.22	6.43
975 °F	4.74	10.53	17.15	19.67	33.83
Unconverted Feed	3.90	4.07	4.50	4.40	4.22
Water	9.04	7.34	6.90	5.92	4.85
COx	0.67	0.80	0.86	0.57	0.16
NH_3	1.50	1.08	1.04	0.82	0.27
H_2S	3.98	2.98	2.84	2.52	2.24
Hydrogen Consumption	7.46	6.91	6.35	5.71	1.80
Process Performance					
Feed Conversion, wt % MAF Feed	96.10	95.90	95.50	95.60	95.80
975 °F$^+$ Conversion, wt % MAF Feed	91.40	85.40	78.40	75.90	62.00
C_4-975 °F Distillates, wt % MAF Feed	72.30	71.00	64.00	64.40	51.00
Hydrogen Efficiency, lb Dist/lb H_2	9.69	10.27	10.08	11.28	28.33

Feeds:
Illinois No. 6 Crown II Mine coal, HDPE, Polystyrene, and PET
Back Pressure: 2500 psig

Catalysts:
K-1: Shell 317 Supported + Dispersed Sulfated Fe/Mo Oxide (100 ppm Mo)
K-2: Only Dispersed Sulfated Fe/Mo Oxide Introduced in Feed to K-1
Hydrotreater: HRI-6135 (Criterion C-411 Trilobe)

(a) Conditions 2-4 used a 50/35/15 w/wt % ratio of HDPE/PS/PET; Condition 5 used HDPE alone w/coal.

(b) Although not specifically listed here, in period 9 the on-line hydrotreater (HTU) was by-passed; otherwise conditions were the same as in period 11.

(c) The total space velocity was reduced from 40 to 30 beginning in Period 18 as a result of operating difficulties at higher space velocities; the dispersed catalyst addition rate also was increased from 100 ppm Mo to 200 ppm Mo beginning in Period 19 to improve process performance.

TABLE 2. CONSOL ANALYSES OF SAMPLES
FROM HTI COAL/PLASTICS CO-LIQUEFACTION RUN CMSL-8

Sample Description; Name (Abbrev.); Sample Point	Periods	Technique & Information Sought (Refer to Key)
Product Distillate; Separator Overheads (SOH); SP-4	6,9,11,16,20,23	A,B,C
Recycle Oil; Pressure Filter Liquid (PFL); SP-6	6,11,16,20,22	A,E,F,G; THF Extract - B; THF Insols - D; Dist. - A,B,E; Resid - G; Resid THF Extract - A,B,H
Solid Residue; Pressure Filter Cake (PFC); SP-7	6,11,16,20,22	G; THF Extract -A,B,H

KEY TO TECHNIQUES AND INFORMATION SOUGHT:

A = ^{1}H-NMR for hydrogen distribution (7 classes), aromaticity (degree of hydrogenation), paraffinicity, hydrogen donors
B = FTIR in THF solution for phenolic -OH content
C = GC-MS for composition, carbon numbers of paraffins
D = special analyses
E = microautoclave test with standard coal for donor solvent quality
F = 850°F distillation for distillate content
G = THF extraction and ash for resid, ash and IOM content, for coal and resid conversion
H = solvent fractionation (oils, asphaltenes, preasphaltenes) for resid composition.

TABLE 3. QUANTITATION OF POLYSTYRENE LIQUEFACTION PRODUCTS IN SOH PRODUCT OILS FROM HTI RUN CMSL-8

Period	Analysis by GC-MS, Area % of SOH Total Ion Chromatogram			Analysis by ^{1}H-NMR	wt % PS in Dry Feed	SOH Yield, wt % of Dry Feed	EB+IPB by GC-MS, as wt % of PS Fed	EB by ^{1}H-NMR, as wt % of PS Fed
	Ethylbenzene, Ret. Time ca. 16.7 min.	Cumene (Isopropylbenzene), Ret. Time ca. 21.8 min.	Total, Area % (assumed to equal wt % of SOH)	As Ethylbenzene, wt % from Integration of Peak at 7.1 ppm				
6 (Coal)	0.55	-	0.55	-	0	50.06	- (b)	-
11 (Coal/Mixed Plastics)	6.53	1.91	8.4	8.8	8.75	47.65	45.7	47.9
16 (Coal/Mixed Plastics)	8.32	3.38	11.7	15.1	8.75	33.52	44.8	57.8
20 (Coal/Mixed Plastics)	6.94	2.01	9.0	12.1	11.55	43.28	33.7	45.3
23 (Coal/HDPE)	1.38	0.29	1.7	3.4	0	25.29	(c)	(d)
9 (Coal/Mixed Plastics - HTU Off-line)	13.52	4.03	17.6	15.4 (a)	8.75	35.02	70.4	61.6

(a) Assumed 11 wt % H in SOH for NMR estimate, other periods used wt % H reported by HTI.[3]
(b) Represents 0.3 wt % of dry coal fed; equivalent to 3.1 wt % of PS fed in period 11.
(c) Represents 0.6 wt % of dry coal fed; equivalent to 3.7 wt % of PS fed in period 20.
(d) Represents 1.2 wt % of dry coal fed; equivalent to 7.4 wt % of PS fed in period 20.

TABLE 4. ESTIMATION OF HDPE CONCENTRATION WITH FIMS DATA

Sample	FIMS M_N, Da	FIMS M_W, Da	Estimate of wt % HDPE[a]	M_W/M_N
HDPE	154	558	100	3.6
PFL 22 THFI[b]	184	662	93	3.6
PFC 22	304	591	66	1.9
PFL 22	329	493	14[c] (61[d])	1.5
PFL 11 Resid Top Layer	404	627	44	1.6
PFL 11 Resid Bottom Layer	466	580	30	1.2
THF-Soluble Coal Resids[4,5]	600	710	-	1.2

Note: FIMS analyses were performed by R. Malhotra, at SRI International.

(a) It was assumed that wt % HDPE is linearly related to M_N, and that M_N = 154 Da for 100% HDPE, and M_N = 600 Da for 100% coal resid.[4,5]
(b) THFI = THF insolubles.
(c) It was assumed that M_N = 515 Da for the non-HDPE portion of the sample, rather than 600 Da, as in the other samples. This value was calculated from 21.1 wt % of the THF-soluble PFL as 850 °F$^-$ distillate with an assumed M_N = 200 Da, and 78.9 wt % of the THF-soluble PFL as 850 °F$^+$ resid with an assumed M_N = 600 Da.
(d) Value if uncorrected for 850 °F$^-$ distillate.

TABLE 5. COMPARISON OF METHODS TO ESTIMATE HDPE CONCENTRATION

Sample	Estimate of HDPE as THF Insolubles, wt % of Sample		Estimate of wt % HDPE, Based on M_N
	From Whole Sample	From Resid	
PFL 22 THFI	100	-	93
PFL 22	18.6	15.8	14
PFL 11 Resid Top Layer	-	-	44
PFL 11 Resid Bottom Layer	-	-	30
PFL 11	20.0	20.3	23[a]

(a) Calculated from wt % HDPE in each resid layer, the wt % of each layer in the resid (66.7 wt % top layer, 33.3 wt % bottom layer), and 59.3 wt % resid in the PFL.

TABLE 6. OVERALL AND SINGLE-PASS CONVERSIONS OF HDPE DURING HTI RUN CMSL-8

Period	wt % HDPE in PFL [a]	Overall Conversion, % [b]	Single-Pass Conversion, % [b]
Using THF insolubles in whole PFL as estimate for HDPE in PFL:			
11	20.0	80.7	23.2
16	30.4	44.6	9.1
20	14.5	71.6	26.2
22	18.6	73.9	49.5
Using THF insolubles in PFL resid as estimate for HDPE in PFL:			
11	20.3	80.5	22.9
16	37.4	32.0	5.9
20	16.5	67.7	22.9
22	15.8	77.8	53.3

(a) Assuming that THF insolubles in PFL are unconverted HDPE.
(b) Calculations are described in Reference 7.

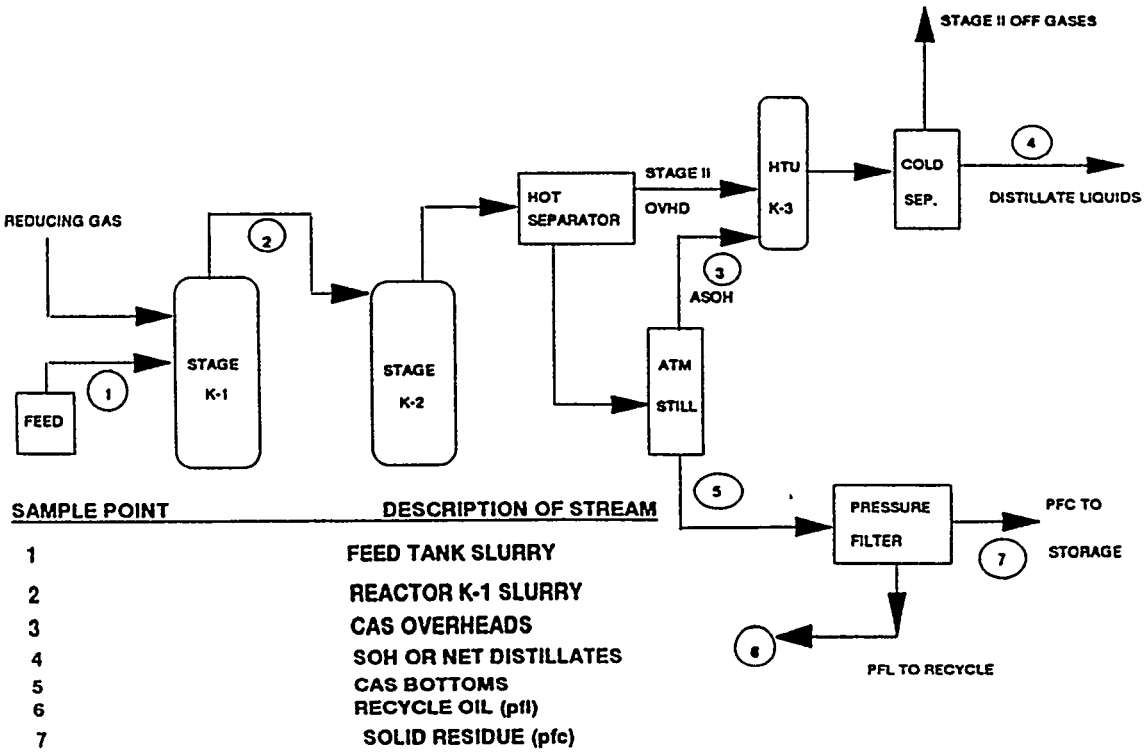

Figure 1. Simplified Plant Diagram for HTI Run CMSL-8.
(Source: Reference 3)

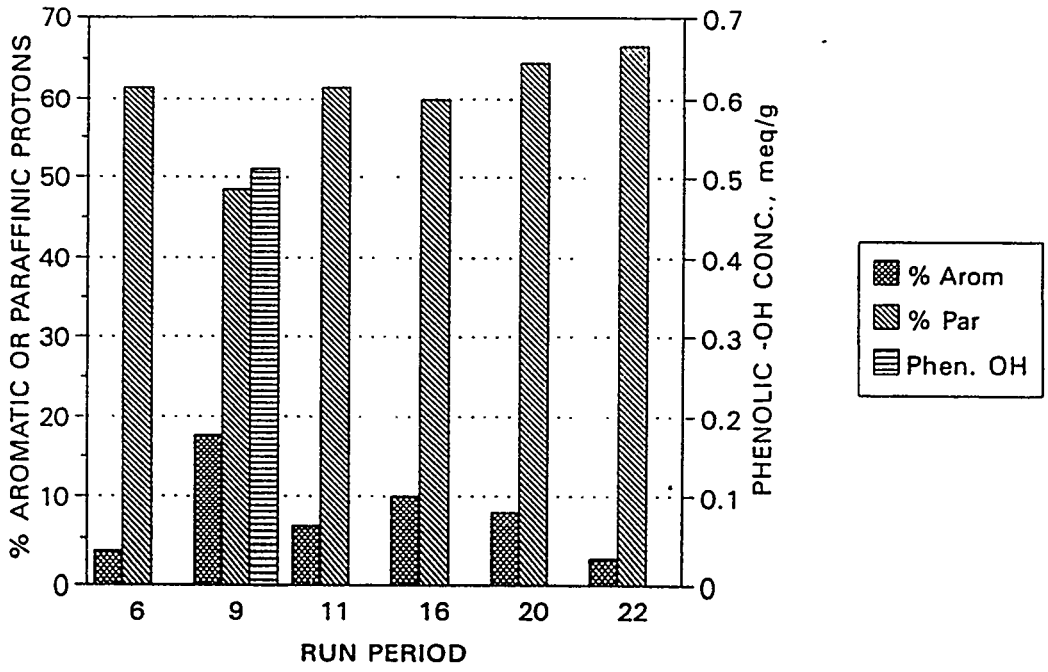

Figure 2. Characteristics of SOH Samples from Run CMSL-8.

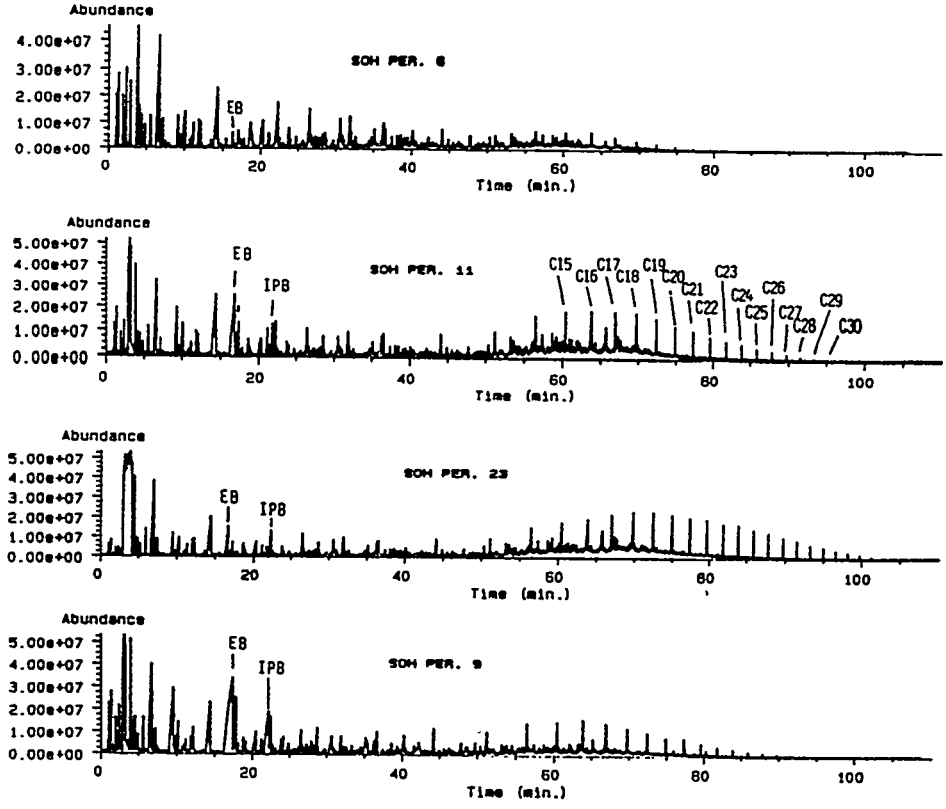

Figure 3. Gas Chromatography-Mass Spectrometry (GC-MS) Total Ion Chromatograms of Selected SOH Samples from Run CMSL-8.

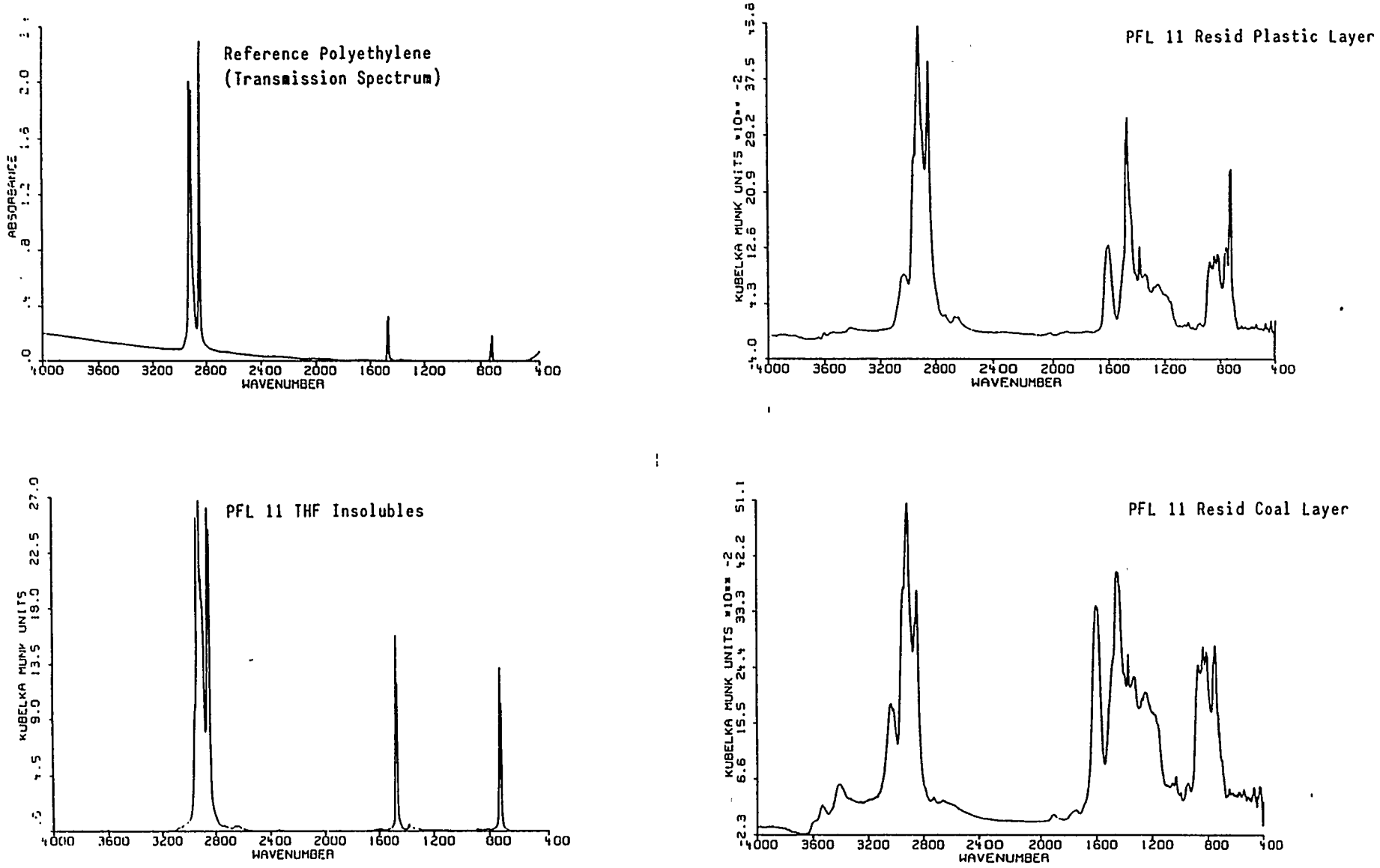

Figure 4. Fourier-Transform Infrared (FTIR) Spectra of Reference Polyethylene and Selected Run CMSL-8 Samples.

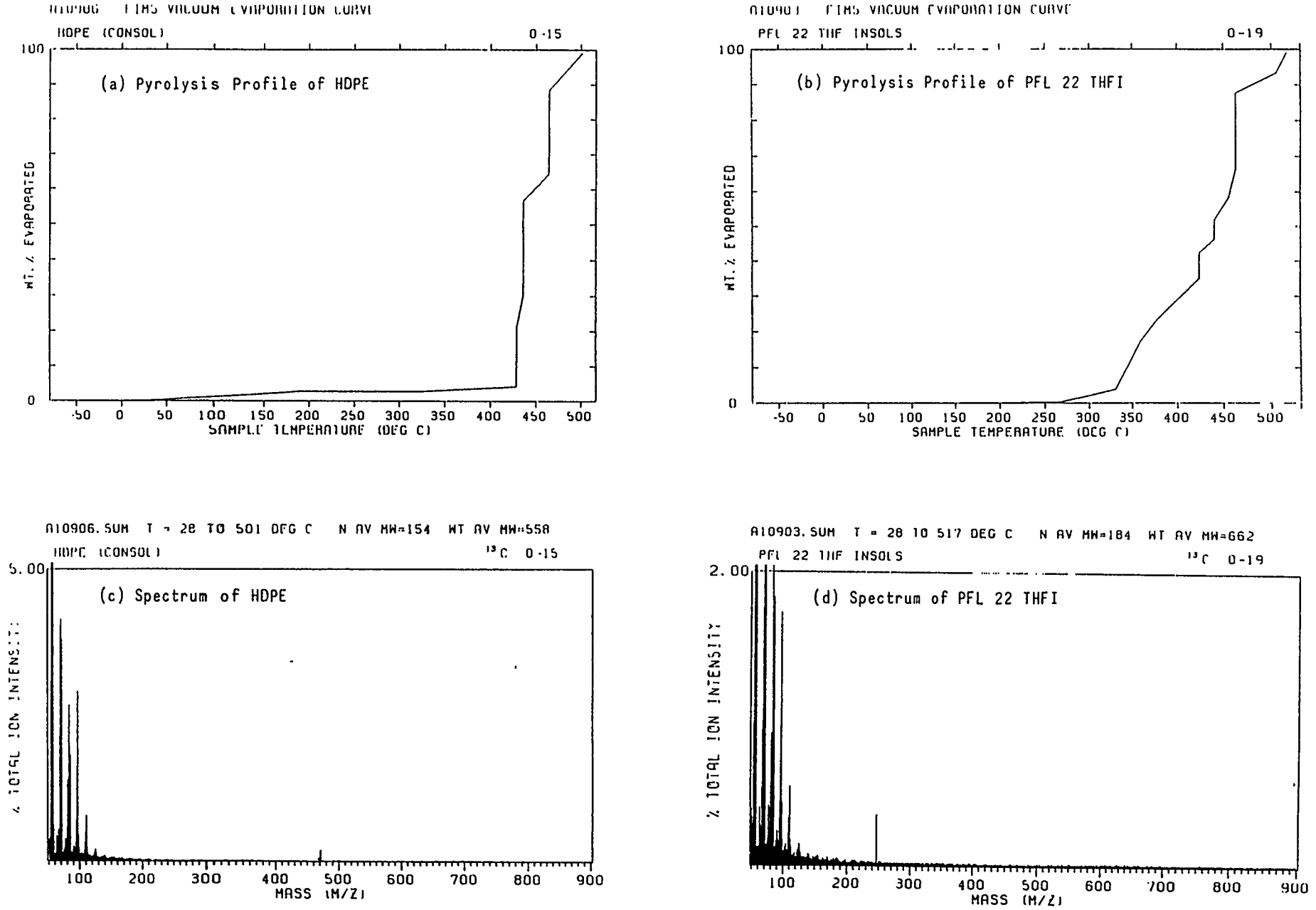

Figure 5. Pyrolysis Profiles and Field-Ionization Mass Spectrometry (FIMS) Spectra of Selected Run CMSL-8 Samples.

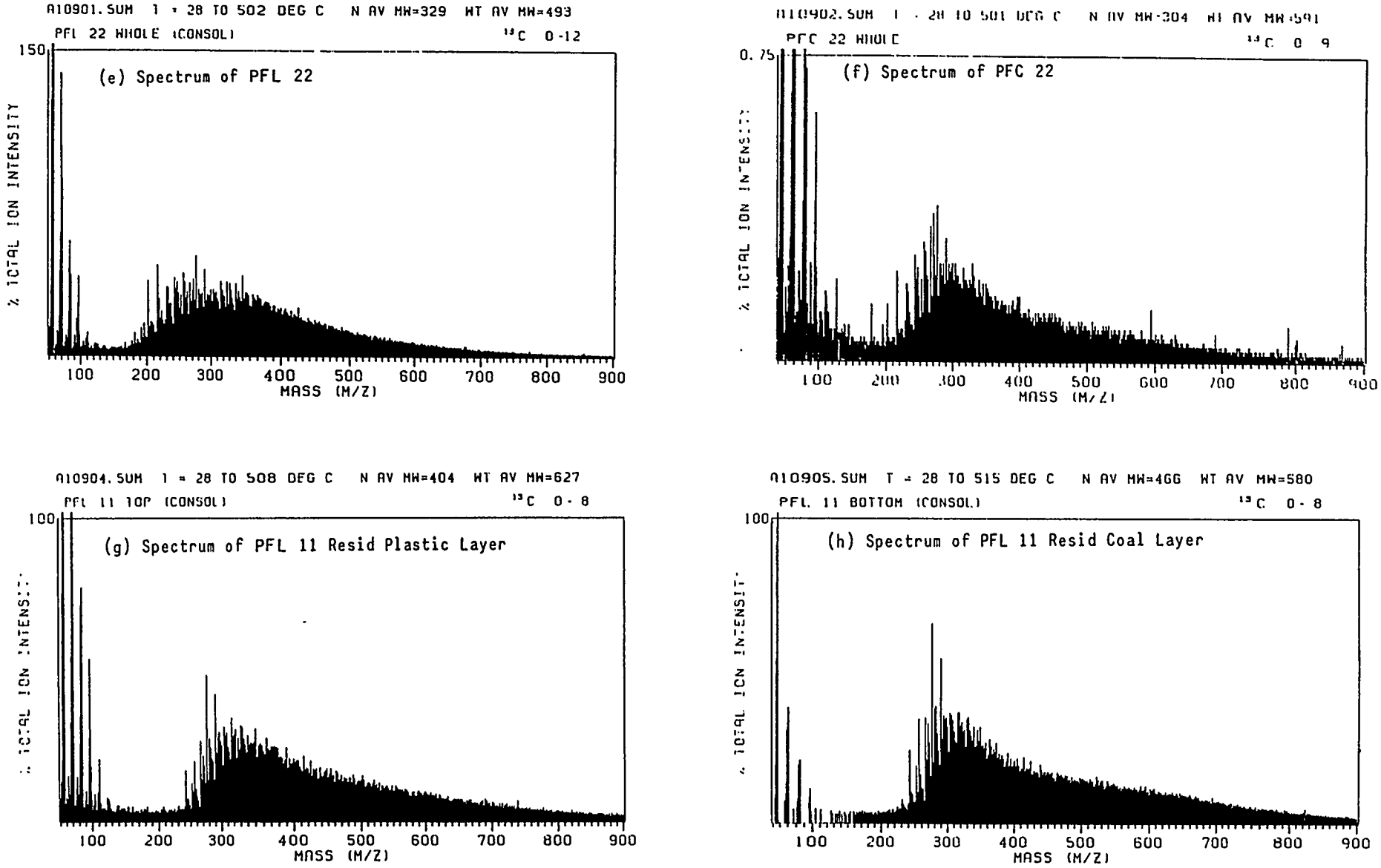

Figure 5 (Continued). Pyrolysis Profiles and Field-Ionization Mass Spectrometry (FIMS) Spectra of Selected Run CMSL-8 Samples.

SOLVENT RECYCLABILITY IN A MULTISTEP DIRECT LIQUEFACTION PROCESS

Melanie D. Hetland and John R. Rindt

Energy & Environmental Research Center
University of North Dakota
PO Box 9018
Grand Forks, North Dakota 58202-9018

Grant No. DE-FG22-94PC94050
July 14, 1994 - November 30, 1995

INTRODUCTION

Direct liquefaction research at the Energy & Environmental Research Center (EERC) has, for a number of years, concentrated on developing a direct liquefaction process specifically for low-rank coals (LRCs) through the use of hydrogen-donating solvents and solvents similar to coal-derived liquids, the water/gas shift reaction, and lower-severity reaction conditions. The underlying assumption of all of the research was that advantage could be taken of the reactivity and specific qualities of LRCs to produce a tetrahydrofuran (THF)-soluble material that might be easier to upgrade than the soluble residuum produced during direct liquefaction of high-rank coals. A multistep approach was taken to produce the THF-soluble material, consisting of 1) preconversion treatment to prepare the coal for solubilization, 2) solubilization of the coal in the solvent, and 3) polishing to complete solubilization of the remaining material. The product of these three steps can then be upgraded during a traditional hydrotreatment step.

To provide a preliminary comparison between the EERC process and existing direct liquefaction processes, product slurry produced during solubilization (Step 2) and polishing (Step 3) steps (i.e., without the Step 1 pretreatment) was catalytically hydrotreated to equilibrium based upon hydrogen uptake. The hydrotreatment was performed in this manner to define the practical upper limit of the products' hydrotreatability. The results were positive, and further tests were performed incorporating the pretreatment step (Step 1). Steps 1 through 3 (pretreatment, solubilization, and polishing) were performed in an integrated fashion. The products were catalytically hydrotreated to demonstrate the maximum hydrotreatability of the solubilized slurry and to provide products that could be compared to the products of existing processes.

The results of the EERC's research indicated that additional studies to develop this process more fully were justified. Two areas were targeted for further research: 1) determination of the recyclability of the solvent used during solubilization and 2) determination of the minimum severity required for hydrotreatment of the liquid product. The current project was funded to investigate these two areas.

PROJECT OBJECTIVES

The project objectives are to determine both 1) the recyclability of the solvent used during solubilization and 2) the minimum hydrotreatment severity required to upgrade the liquid product of the multistep EERC process.

The project is being performed as two tasks. The first task consists of ten solvent recycle tests in which lignite is solubilized via the pretreatment, solubilization, and polishing steps. The product of these three steps is combined with a vehicle solvent, and the resulting stream distilled to remove water, solubilization solvent, and oxygenated light coal-derived liquids. The water is then separated from the light solvent stream, and the solubilization solvent is reused as the solubilization solvent for the next recycle test. The analyses of the products of the tests are used to characterize the recycle solvent stream and to calculate mass and material balances.

The second task consists of a series of twelve hydrotreatment tests at various conditions. The tests will be performed according to a statistically designed experimental matrix to enable the identification and evaluation of the most effective low-severity hydrotreatment conditions. Analyses of the products of these tests will be used to characterize the hydrotreated product and to calculate mass and material balances.

This paper discusses only the results of the Task 1 recyclability tests performed to date.

PROGRAM APPROACH

Task 1 consists of ten multistep tests. In the first test, feed coal and solubilization solvent were pretreated and solubilized. The product of the solubilization step was polished with additional solvent, combined with a hydrogen-donor vehicle solvent, and distilled to remove water, solubilization solvent equal to the amount added in the polishing step, and oxygenated light coal-derived liquids (CDLs). If hydrotreatment had been part of this task, the bottoms from this distillation would have gone to the hydrotreatment step. The distillation overheads were further distilled to separate the water from the solubilization solvent and light CDLs. The solubilization solvent was recycled to the pretreatment and polishing steps for the next test. This sequence is being repeated until ten multistep tests have been performed, each utilizing the solubilization solvent removed in the distillation of the previous test. To date, five tests have been completed.

The purpose of this task is to monitor both the changes occurring in the solubilization solvent as it is recycled in the multistep process and the changes in product slate resulting from the recycle of the solvent. Analyses were selected to enable this information to be determined. The feed coal was subjected to moisture, ash, and elemental (C, H, N, and S) analyses, while the solubilization solvent undergoes ash, Karl Fischer water, elemental (C, H, N, and S), THF solubility, and ASTM D1160 distillation analyses. Oxygen contents are determined by difference. Liquid products are analyzed using the same analyses as were applied to the solubilization solvent. Gaseous products are analyzed by gas chromatography. Changes in the recycled solubilization solvent stream are determined by speciation of this stream using mass spectroscopy (MS) analysis. Complete speciation was scheduled to be performed after the first,

third, seventh, and tenth multistep tests. Complete mass and material balances are being performed for all multistep tests.

ACCOMPLISHMENTS

Preparation of a Composite Solvent

During development of the multistep process, it was found that different solvents were more effective in different steps. A hydrogen-donating solvent is needed during the pretreatment and solubilization steps, while phenolic solvent is needed during the polishing step. Providing these solvents at appropriate times during the previous testing was not difficult since no attempt was made to recycle any of the solvent. The multistep process is of virtually no practical value if it must be performed in a batch mode on a commercial scale; therefore, a solvent must be procured that meets the requirements of each step, yet is recyclable.

The original process development work was performed using hydrogenated coal-derived anthracene oil (HAO61) in the polishing and solubilization steps and cresylic acid (POH) in the polishing step. A composite solvent was prepared from these materials as follows. The HAO61 was distilled to remove a middle fraction equal to 13.4 wt% of the HAO61 stream. (Removing this middle fraction makes it easier to separate the HAO61 into light and heavy fractions for use in different parts of the process.) The light fraction of the HAO61 was defined as the material that distilled over at an overheads' temperature of about 464 K (191°C) or less at a pressure of 7.7×10^3 N/m^2 (1.12 psi). It made up 33.8 wt% of the total HAO61 stream. The light fraction of the HAO61 was combined with an equal part of cresylic acid to form the pretreatment/ solubilization solvent. Additional light material was added to the polishing step. Following polishing, the HAO61 heavy fraction (the material that did not distill at 479 K [206°C] and 7.2×10^3 N/m^2 [1.04 psi]) was added to the product slurry to serve as the vehicle solvent for the hydrotreatment step. The entire mixture was distilled to remove water, POH, HAO61 light fraction, and light CDLs produced from the coal. The water is separated from the light organics, which are then recycled back to the pretreatment and polishing steps. The overall solvent scheme is summarized in the block diagram shown in Figure 1.

The Task 1 testing began following preparation of the composite solvent and distillations performed to determine that the solvent could be reproducibly fractionated into the light and heavy fractions.

Test Description

For each test, the following run sequence was performed. Freedom lignite was slurried with the solubilization solvent (which consisted of a 50:50 mixture of POH and HAO61 light fraction for the first test and recycle solvent for the other tests) in a 2:1 solvent-to-coal ratio. The feed slurry was cold-charged to the reactor. The autoclave was charged with CO and H_2S, which serves as the reaction promoter. The reactor was heated to a temperature of approximately 423 K (150°C) and a pressure of about 9.65×10^6 N/m^2 (1400 psig) for the pretreatment, which lasted 30 minutes. The temperature and pressure were then increased to about 648 K and 2.414×10^7 N/m^2 (375°C and 3500 psig, respectively) for 60 minutes. (All pressures are at

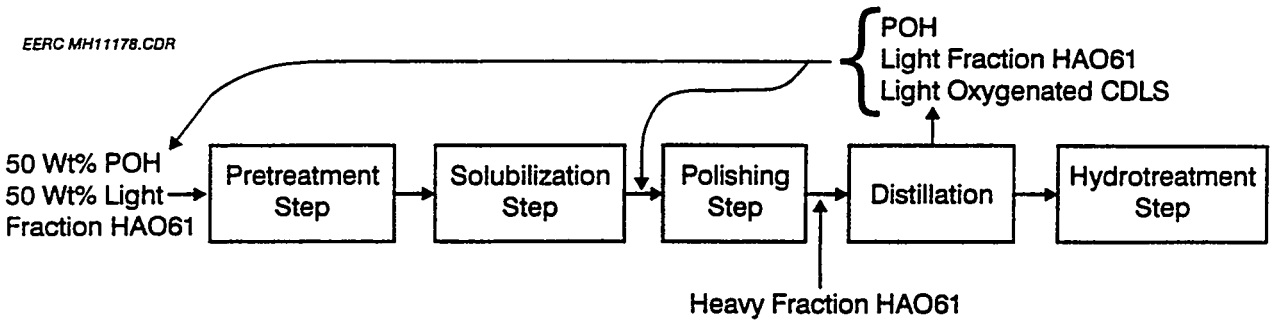

Figure 1. Block diagram showing the location of various solvent fractions during the multistep direct liquefaction process.

reaction temperature and are equivalent to 6.898×10^6 N/m^2 [1000 psig] at room temperature.) The unit was quenched and the product recovered and sampled.

The solubilized product slurry was then charged to a preheated autoclave containing start-up solvent and H_2. The unit was operated at reaction conditions of 713 K and 3.10×10^7 N/m^2 (440°C and 4500 psig) for 20 minutes during the polishing test. The reaction was quenched and the product collected and sampled.

The polished product slurry was combined with HAO61 heavy fraction (which would serve as the vehicle solvent for the product going into the hydrotreatment step) and then distilled. The water was removed first, and a light oil fraction was collected as the overhead material resulting from distillation at 8.2×10^3 N/m^2 (1.19 psig), an overhead temperature of 471 K (198.2°C), and a pot temperature of 494 K (221°C). After samples were taken for analysis, the light oil fraction was used as the feed solvent for the next test.

The conditions at which Tests 1 through 5 were performed are summarized in Table 1.

Discussion of Results

The first two tests went as planned. An electrical power outage unexpectedly occurred prior to the distillation step during Test 3. The equipment was preliminarily tested to be sure that it still operated, but the pressure transducer calibration was not tested. Because it was no longer in calibration, the distillation was not performed at the correct conditions, and approximately 20% of the light organics remained in the bottoms. This changed the composition of the recycle organics used as the solvent in the Test 4 feed slurry.

The material balances for Tests 1 through 5 are presented in Table 2. These data show that recoveries for the gas and liquid fractions for each of the steps are similar. The liquid balance for the pretreatment/solubilization step ranged from 91.0% to 91.7%. The polishing step liquid balance ranged from 97.2% to 97.7%. Overall mass balances for the pretreatment/ solubilization step ranged from 96.0% to 99.3%, for the polishing step 98.2% to 99.2%,

TABLE 1

Run Conditions for Task 1, Tests 1 Through 5

	Test Number				
Processing Step	1	2	3	4	5
Pretreatment	N602	N607	N611	N614	N617
Temp., K	425	426	424	425	422
Pressure, $N/m^2 \times 10^6$	9.7	9.6	9.7	9.8	10.1
Time, min	35	30	30	30	30
Gas	CO	CO	CO	CO	CO
Additive	H_2S	H_2S	H_2S	H_2S	H_2S
Solubilization	N602	N607	N611	N614	N617
Temp., K	650	650	646	645	645
Pressure, $N/m^2 \times 10^6$	24.0	24.3	24.5	23.7	23.4
Time, min	60	60	60	60	60
Polishing	N603	N609	N612	N615	N618
Temp., K	714	713	707	710	711
Pressure, $N/m^2 \times 10^6$	31.8	31.3	31.5	29.6	27.6
Time, min	20	20	20	20	20
Gas	H_2	H_2	H_2	H_2	H_2
Additive	Feed Solvent	RS-606[a]	RS-610	RS-613	RS-616
Distillation[b]	N606	N610	N613	N616	N620
Temp., pot, K	494	492	492	494	494
Pressure, $N/m^2 \times 10^6$	0.008	0.008	0.008	0.008	0.008

[a] Recycle solvent from distillation step of prior test.
[b] Water was removed first; listed conditions indicate the cutoff point for separation of light organic materials from the hydrotreatment step feed.

and for the distillation step 97.9% to 99.6%. The consistency of the mass balances for each step proves that the system is operationally stable. The fact that the mass balances are at least 95% indicates that adequate amounts of material were collected for analysis and subsequent tests and that the data, therefore, reliably describe the process.

The solvent balance from the Test 3 distillation was reduced because some of the distillable material was not collected. After calibration of the pressure transducer during Test 4, the Test 3

TABLE 2

Mass and Material Balances for Task 1, Tests 1 Through 5

	Gas Balance, %	Liquid Balance, %	Overall Mass Balance, %
Test 1			
Pretreatment/ Solubilization	122.6	91.4	96.0
Polishing	169.5	97.3	98.2
Distillation	NA[a]	NA	97.9
Test 2			
Pretreatment/ Solubilization	135.8	91.7	98.6
Polishing	197.9	97.3	98.7
Distillation	NA	NA	98.7
Test 3			
Pretreatment/ Solubilization	140.9	91.7	99.0
Polishing	205.6	97.7	99.2
Distillation	NA	NA	97.9
Test 4			
Pretreatment/ Solubilization	132.1	91.6	98.7
Polishing	220.0	97.2	99.1
Distillation	NA	NA	98.1
Test 5			
Pretreatment/ Solubilization	131.8	91.0	99.3
Polishing	196.1	97.2	99.0
Distillation	NA	NA	99.6

[a] Not applicable.

TABLE 3

Distillate Yields and Solvent Balances for Task 1, Tests 1 Through 5

Test No.	Hydrotreatable Liquid Basis[b]	Solubles, wt% maf[a] Gas Basis[c]	Solvent Yield, wt% maf	Solvent Balance, %
1	76.90	72.54	42.01	116.42
2	80.50	78.88	68.17	127.75
3	77.42	73.55	46.27	118.57
4	73.79	70.03	13.67	105.47
5	80.20	77.99	17.12	106.80

[a] Weight percentage of moisture- and ash-free coal fed to the system.
[b] Yield calculated from liquid stream mass balance data.
[c] Yield calculated by subtracting the gas yield from unity.

distillation was repeated and the recovery results used to calculate the actual Test 3 solvent balance. This value is shown in Table 3, which summarizes the solvent balance and yields of hydrotreatable solubles and distillate for Tests 1 through 5. As the table shows, solvent balances of over 115% were attained for Tests 1 through 3. The lower balances shown by Tests 4 and 5 are probably due to the improper recycle solvent composition. The additional material removed during the redistillation of the Test 3 hydrotreatment feed was added to the recycle solvent stream that will be used in the Test 6 feed slurry.

The yields of hydrotreatable soluble material noted in Table 3 were calculated two different ways: from the liquid stream mass balance data and by subtracting the gas yield from unity. The reliability of the data is high since the numbers are similar and exhibit a consistent 4% difference between values calculated by both methods.

During analysis it was noted that some light organic material was removed with the aqueous phase during distillation. This material is phenolic in nature and makes up about 10% to 16% of the aqueous stream. The organics were gravity-separated and added to the recycle solvent stream that will be used in the Test 6 feed slurry. The organics will be separated from the aqueous stream and added to the recycle solvent during the remaining tests.

CONCLUSIONS

- The process remained both operationally and chemically constant, even though the recycle solvent composition was abruptly changed and some of the light solvent was not returned to the recycle stream.
- This work was performed using a composite solvent that had not been previously used in the multistep process. Although the solvent was prepared using information gathered during previous process development work, it is possible that, as it recycles, the solvent will not remain hydrogen-enriched enough to be optimally effective in the pretreatment and

solubilization steps. If not enough hydrogen is available, light organic material could be removed from the hydrotreated product stream and recycled to the pretreatment step.

FUTURE PLANS

The Task 1 solvent recyclability tests and the Task 2 hydrotreatment severity tests will be completed. The next step in the process development would be optimization of the process on a batch scale, followed by one or more continuous demonstration tests.

COAL-OIL COPROCESSING AT HTI

Development and Improvement of the Technology

DOE Contract No. DE-AC22-94PC91036

(September 1994 - September 1997)

R.H. Stalzer
L.K. Lee
J. Hu
A. Comolli

Hydrocarbon Technologies, Inc.
PO Box 6047
New York & Puritan Avenues
Lawrenceville, NJ 08648

COAL AND GAS CONVERSION CONTRACTORS' REVIEW CONFERENCE

AUGUST 29-31, 1995

INTRODUCTION

Co-Processing refers to the combined processing of coal and petroleum-derived heavy oil feedstocks. The coal feedstocks used are those typically utilized in direct coal liquefaction: bituminous, subbituminous, and lignites. Petroleum-derived oil is typically a petroleum residuum, containing at least 70 W% material boiling above 525°C. The combined coal and oil feedstocks are processed simultaneously with the dual objective of liquefying the coal and upgrading the petroleum-derived residuum to lower boiling (< 525°C) premium products. HTI's investigation of the Co-Processing technology has included work performed in laboratory, bench and PDU scale operations.

The concept of co-processing technology is quite simple and a natural outgrowth of the work done with direct coal liquefaction. In direct coal liquefaction, a feed coal slurry is produced by mixing pulverized coal with a process-derived recycle oil. This slurry allows the coal feedstock to be pumped and preheated to reaction conditions. The concept of coprocessing is to replace the process-derived recycle oil with an external, petroleum-derived residue which also needs to be upgraded. This eliminates costs and equipments associated with preparation and handling of the recycle slurry oil and should, therefore, reduce the cost of liquid fuels from coal.

A 36 month program to evaluate new process concepts in coal-oil coprocessing at the bench-scale was begun in September 1994 and runs until September 1997. Included in this continuous bench-scale program are provisions to examine new improvements in areas such as: interstage product separation, feedstock concentrations (coal/oil), improved supported/dispersed catalysts, optimization of reactor temperature sequencing, and in-line hydrotreating. This does not preclude other ideas from DOE contracts and other sources that can lead to improved product quality and economics.

Direct Coal Liquefaction Technology Background: Hydrocarbon Technologies, Inc. (HTI) has a very strong background and experience in performing research and development in catalytic direct coal liquefaction technology. The personnel of HTI have conducted research on coal liquefaction for more than 25 years. During this time, they have evaluated both thermal-catalytic and catalytic-catalytic coal liquefaction configurations with several alternative reactor designs and process operating conditions. A simplified flow diagram of a catalytic two-stage direct coal liquefaction (CTSL) technology is shown in *Figure 1*. This research work has led to important findings which significantly increased liquid yields, improved product quality, and improved process economics. The following process changes led this to improved performance:

- Staging coal liquefaction reactions
- Lower temperature and higher residence times
- Low-High and high-low temperature mode of operations in Catalytic Processing
- Heavier (343°C$^+$) boiling recycle solvents
- Coal concentration in feed slurries increased from ca. 30 W% to ca. 53 W%
- Deep coal cleaning
- Continuous sulfiding for low-rank, low-sulfur coals
- In-Line hydrotreating
- Use of synthesis gas in first stage instead of pure H_2
- Use of interstage product separation
- Combined processing of coal, resid, waste oils and plastics

With all these process improvements, the CTSL Process, in an extinction recycle mode of operation, provides a much better overall performance (for both bituminous and sub-bituminous coals) than the H-Coal Process, developed in the early 1980's (*Table 1*).

Coal/Oil Co-Processing Technology Background: HTI's approach to coal-oil coprocessing uses a two-stage reaction system with either extrudate catalyst in both reactors or a combination of a dispersed and a supported catalyst in the reactor stages. A simplified process flow-diagram for coal-oil coprocessing is shown in *Figure 2*. So far, HTI's personnel have been involved in a significant number of coprocessing research, development, and pilot-scale demonstration projects. A total of about 450 days of experience operating coal-oil coprocessing programs in continuous bench-scale units (25 kg/day throughput) has been accumulated. The distribution of this experience as per the types of feedstocks is shown in *Table 2*. This bench-scale operating experience has helped them build a bench-scale database covering not only feed coals and oils with varying properties but also a range of operating conditions and process configurations with the corresponding data on process performance. Coal and residuum conversions as high as 97 and 93 W% maf feed, respectively, have been achieved (*Table 3*) with C_4-525°C distillate yields of above 80 W% maf feed. Significant metal and heteroatom removals have also been obtained. All these achievements have improved the overall economics of coal liquefaction via coal-oil coprocessing. At present, coprocessing promises to be 25-30 % more economical than direct coal liquefaction, thus making noticeable headway towards reducing the cost of liquid fuels from coal to below $25 per barrel.

Low/High Temperature Staging and Interstage Separation: One of the prime factors that limits the capacity of a reaction train in ebullated-bed reactors, and therefore adds to product cost, is the velocity of the gas passing through a reactor. The higher this gas velocity, the greater is the gas holdup and consequently the lower is the effective reactor liquid volume. Reactor train sizing is performed by setting the gas velocity at the maximum operable level. This determines the reactor diameter and the required reaction severity determines the height. *Table 4* provides an illustration of hydrogen management options for two-stage reactor configurations. It is assumed that one unit of hydrogen is consumed in the reaction and that 4 units are supplied to the reactors to maintain adequate hydrogen partial pressure. Cases 1 and 1A are for equal reactor temperatures while cases 2 and 2A are for low/high temperature staging. The A cases include the use of an interstage separator between the first and second reactor. Previous experience has shown that for a two-stage system operating at equal temperatures approximately 75-80% of the hydrogen is consumed in the first stage. The low and high temperatures are selected such that 50% of the hydrogen is consumed in each stage.

In cases 1 and 1A, where 80% of the hydrogen is consumed in the first stage, 80% of the fresh hydrogen is supplied to the first stage. This results in a total supply of 3.2 units to the first stage and either 3.2 or 0.8 units to the second stage, depending on whether or not the interstage separator is used to remove all the first stage gases. In cases 2 and 2A, where 50% of the hydrogen is consumed in the first stage, 50% of the fresh hydrogen is supplied to the first stage. This results in a total supply of 2.0 units to the first stage and either 3.5 or 2.0 units to the second stage, depending on whether or not the interstage separator is used to remove all the first stage gases. For equal reactor temperatures the limiting gas velocity is 3.2 with or without the use of interstage separation. For

low/high temperature staging the limiting gas velocity is 2.0 with interstage separation (3.5 without separation). Temperature staging with interstage separation could yield a maximum increase in capacity per reaction train of 60% (3.2/2.0=1.60).

Coal/Oil Coprocessing Synergy: Process synergy is an oft discussed but little understood aspect of coal/oil coprocessing. Process synergy, in terms of enhanced 525°C+ conversion, has been identified in coal/oil coprocessing from batch reactivity screening. It is more difficult to directly detect the synergy in bench scale operations as different modes of operation are employed in coal only liquefaction as opposed to oil only processing. It is possible to infer synergy on coprocessing bench operations with a few assumptions. If it is assumed that the conversion at 10 W% coal is a good representation of oil only operation and that the conversion at 40 W% coal provides an upper limit on conversion for coal only operation, inferences can be made regarding process synergy. As *Figure 3* shows, conversion at 20, 33 and 40 W% coal is significantly higher than would be expected if there was no synergy. At 33 and 40 W% coal, the conversion is 6 W% higher than would be expected.

The other aspect of process synergy in coal/oil coprocessing is demetallization by solids. Petroleum derived oil feedstocks contain metals contaminants, primarily nickel and vanadium, at concentrations as high as 500-1500 wppm. In oil only processing, these metals deposit on the catalyst as metal sulfides permanently poisoning the catalyst. The higher the level of metals in the feed, the higher the rate of catalyst deactivation. In coprocessing a large portion of the metals are deposited in the product solids. As can be seen in Figure 4, which shows the metals concentration in the product solids over the course of a test, these concentrations increase with catalyst age. Over the course of this test 99% of the metals were removed from the liquid product. Of this demetallization, over 90% occurred on the coal solids.

OBJECTIVES

The overall objective of this proposed research and development program is to further develop and improve coal/oil co-processing technology with an emphasis on better integration to existing refinery operations. Improvements can be realized in terms of increased selectivity to distillate products, improved product quality and increased reactor space velocity. These improvements will lead directly to improved economics and the potential for early commercialization of direct coal liquefaction technology. The specific objectives of this program are:

- To enhance co-processing reaction rates through utilization of improved catalysts and optimization of the first- and second-stage temperatures.
- To perform catalyst activity screening, including new high activity ebullated-bed catalysts, dispersed catalysts and combinations of extrudate and dispersed catalysts.
- To study reactant/product and coal-derived liquid/petroleum-derived residuum solubility ranges over a range of coal loadings in this reactor and process configuration.

- To maximize liquid product yields and product quality in an optimized two-stage co-processing system with in-line hydrotreating.

- To assess and optimize the operation of catalytic two-stage coal/oil co-processing technology, operating with interstage separation.

- To provide guidance to ongoing research by performing economic assessments of proposed modifications to the reactor configurations.

PROJECT STATUS

Microautoclave Test Program: The microautoclave unit is composed of two tubular reactor bombs which are mechanically shaken in a heated, fluidized sand bath. The reactors are charged with specific amounts of materials and can be pressurized to 13.5 MPa or greater. The bombs are plunged into a sand bath maintained at a predetermined temperature, then agitated for a specified amount of time. After reaching the desired temperature, the bombs are removed, plunged into a water bath for cooling, and the contents analyzed.

This part of the program serves as the initial screening of new catalyst types, coal/oil combinations, and operating conditions as they affect the reactivity. The microautoclave provides a very rough indication of relative reactivities. Gram quantities of feedstock, diluent and catalyst are charged to the microautoclave reactor. Information can be obtained on 525 °C+ conversion via thermogravimetric analysis, to simulate product distillation, and on coal conversion via extraction with tetrahydrofuran (THF) and ash analysis. In this program, the following microautoclave determinations, approximately 70-80 tests, are planned:

- Co-Processing Feedstock Reactivity - 2 coals and 3 oils will be evaluated (6 feedstock combinations). Reactivity will be evaluated at constant operating conditions (432 °C and 90 minutes residence time) for coal concentrations of 0, 10, 30, 50 and 100 % coal. A total of 25 tests are planned, including repeats and duplicates.

- Effect of Hydroaromatic Solvent Addition on Oil Reactivity - Solvents rich in hydroaromatics will be added to a selected petroleum feedstock to help elucidate process synergy effects in a hydrocracking atmosphere. 10 tests are planned.

- Product Reactivity - Co-Processing vacuum bottoms product reactivity will be evaluated for selected products which represent a range of conversion levels over a range of severity. 15 tests are planned.

- Alternative Catalyst Screening Evaluation - Alternative extrudate catalysts (such as high activity supported hydrocracking catalysts for heavy resids, noble metal-based supported catalysts, etc.) and catalyst systems (dispersed and dispersed/extrudate) will be screened. Dispersed catalysts (based on iron, molybdenum, tin, and vanadium) developed in-house at HTI will be tested in this program. 20 tests are planned.

The first set of microautoclave test are presently in progress. The performance of dispersed catalysts in coprocessing will be compared to that of a supported catalyst, AKZO AO-60, on the basis of 525°C+ conversion. Molyvan A (or L) and $Mo/Fe_2O_3/SO_4$, developed at HTI, will be employed in these microautoclave runs. The effect of catalyst concentration on the product yield (THF soluble and cyclohexane soluble) will be investigated. The hydroaromatic solvents, FCC decant oil and coal-derived oil, will be used to help elucidate process synergy effects in a hydrocracking atmosphere.

Laboratory Scale CSTR Test Program: A continuous two-stage gradient-less, catalytic, stirred autoclave reactor system commonly known as the Robinson-Mahoney reactor system (Unit 245), was recently modified by the HTI scientists to change the internals, especially the catalyst baskets' configuration, to better simulate ebullated bed operation. The modified two-stage CSTR system, now known as the Lee-Faupel-Canas (LFC) reactor system, has two 1000 cc reactors in series and can handle feed rates in the range of 5 to 25g per day. It can operate at temperatures up to 454°C and pressures up to 20.3 MPa. HTI has developed an internally propelled fluid-bed catalyst basket to increase the catalyst loading to a level that more closely simulates an ebullated bed. The flow-patterns and mixing-behavior very closely approach those in a fully ebullated-bed system. It is used for catalyst testing, feedstock screening, and evaluation of process improvements. It can be used as a single-stage or two-stage system with coal slurry or oil feedstocks. This part of the program evaluates the best results obtained from the microautoclave program using a continuous stirred autoclave reactor system, LFC reactor.

Run 1 will provide a baseline operation at conditions selected to tie in to existing bench-scale co-processing data base. It will also confirm operating procedures for coal slurry processing in this unit. Runs 2-4 will evaluate catalysts. Catalysts selected will be based on HTI experience with new high activity hydrocracking catalysts and results from microautoclave catalyst screening study. Two high activity extrudate catalysts will be selected for testing. One test will be devoted to a dispersed catalyst or dispersed/extrudate catalyst test. These tests will be performed in two segments, an initial 3-day catalyst break-in condition, followed by 7-days of operation at a severity representative of projected commercial operations.

Runs 5-6 will be performed to optimize operating conditions for low/high temperature two-stage operation. The preferred catalyst system from the catalyst screening task will be used. Multiple operating conditions, lasting 3-4 days will be evaluated. Run No. 7 will be carried out to study the interstage separation of products. Since the LFC system has no provisions for interstage sampling, this test condition will be simulated by performing two single-stage runs. Products from the initial segment of the run will be cut to remove low boiling materials prior to feeding to the second segment.

The first LFC test is just starting up using a New Mexico coal from the McKinley Mine and a California heavy oil. This baseline test investigates the effect of adding a hydroaromatic solvent, FCC decant oil and a coal-derived liquid, on coal conversion, 524°C+ conversion and on product quality. The initial and final conditions of this test are identical so that catalyst deactivation can also be evaluated. The operating conditions have been selected to provide a tie point to HTI's previous experience in coprocessing.

Bench Scale Test Program: The two continuous bench scale units at the R & D center, designated by the numbers 227 and 238, consist of two-stage reactors each in series and can be operated to exhibit either plug-flow or CSTR kinetics. These reactors are each 2000 cc in volume, with a nominal diameter of one-inch and can be operated either as ebullated catalyst beds or simply as back-mixed reactors with unsupported dispersed slurry catalyst. It is also possible to close-couple the two bench systems in such a way that more than two reactors can be used at the same time if the objectives of the run demand such a configuration. Each unit has two reactors in series with reactor temperatures controlled by electrically-heated fluidized sand baths. The reactors are close-coupled as the effluent from stage one flows directly into stage two without product separation. Provisions can be made to add an interstage separator to unit 227. The units are fully integrated in terms of providing coal slurry mixing, feed preheat, reaction and product separation/recovery as part of the continuous operation. Both units are capable of operating at temperatures up to 485°C and pressures as high as 20.3 MPa. They can process coal, coal/oil, oil only feed, as well as other hydrocarbon mixtures

This part of the program represents the focal point for all of the process improvements identified by economic screening and the smaller scale experimental work. As the bench-scale products can be completely characterized, and interstage samples can be obtained commercial performance can be projected.

Run 1 will evaluate in-line hydrotreating. The objective of adding in-line hydrotreating is to produce co-processing products which can be processed in existing refineries with no separate processing prior to refining. This will improve the acceptability of co-processing to refiners and allow introduction of co-processing to conventional refineries. The in-line hydrotreating of the process distillates (IBP-399°C) from HTI's direct coal liquefaction bench-scale and PDU-scale units has been successful in producing net distillates with high H/C atomic ratios (> 1.8) and very low amounts of heteroatoms (less than 10 ppm of nitrogen and sulfur). The advantage of such a processing is that the feed-stream to the hydrotreater is already at a high temperature and contains sufficient partial pressure of hydrogen for further refining and heteroatom removal. During coprocessing Bench-Run No. 1, an in-line hydrotreater with a fixed-bed of conventional Ni-Mo/Al_2O_3 trilobe catalyst will be employed and the effect of temperature will be studied over a range of 363-379°C. It is also planned that an in-line hydrotreater will be made an integral part of bench-scale processing for the subsequent bench runs. This test is planned for August 1995.

Run 2 will use an improved catalyst. The catalyst, whether extrudates in both stages or a combination of dispersed/extrudate systems, will be based upon the results of catalyst-screening carried out in the microautoclave and CSTR systems. In general, the supported extrudate catalysts will be the high activity resid hydrocracking catalysts based on Ni-Mo or Co-Mo on alumina, while the dispersed catalysts will be based on iron and/or molybdenum.

Run 3 will be performed with low/high temperature staging. So far, most of the continuous bench-scale and PDU-scale co-processing operations at the HTI R & D facility have been carried out in two equal-temperature, catalytic, ebullated-bed reactor stages. The optimization of reactor temperature profiles for direct coal liquefaction led to a fully catalytic two ebullating-bed system with low temperature first stage for recycle solvent generation by hydrogenation and a higher temperature

second stage for upgrading of the first stage products by hydrocracking. Low-high reactor temperatures will be in the range of 413-427°C for the first stage and between 441-449°C for the second stage reactor.

Run 4 will determine the effects of interstage separation. Separation of light distillates and off-gases between the reactor stages has been employed successfully during our ongoing catalytic multistage direct coal liquefaction program. In this process configuration, the feed stream entering the second stage reactor is more concentrated in the reactive components and has a higher hydrogen partial pressure. Thus, a distinct kinetic advantage is obtained. The interstage hot separator will be maintained at around 343°C during Run 4, and the effects of feed space velocity and reaction severity on overall process performance will be studied.

Run 5 will study the thermal/catalytic configuration with dispersed catalyst in the first stage back-mixed thermal reactor. In this run, a combination of a dispersed and an extrudate supported catalyst will be used, i.e., the first stage will have a high surface area, fine dispersed catalyst, while the second stage will be an ebullated-bed reactor with a supported catalyst. The performance data obtained during this run will be compared with that from one of the earlier bench runs employing a catalytic-catalytic reactor system.

With the exception of Run 5, which is for 12 days, each run is scheduled for 15-days at target operating conditions. The total bench-scale program includes 72 operating days at target conditions. A typical bench-scale operation of 15 days will include evaluation of multiple operating conditions. A minimum length of evaluation for a single condition is 3 days. Depending upon specific operating conditions some conditions will be maintained for 4-6 days. A 15-day run will usually evaluate 3-5 conditions.

Material balances are preformed each day of the bench-scale operation. Typical material recoveries are in the range of 98-102 %. Coal conversion is calculated each day except for transition days, where a given operating condition is being changed. Normalized yields and conversions are typically calculated 2 or more times per condition, depending upon the length of the condition.

TABLE 1. CTSL PROCESS PERFORMANCE IMPROVEMENTS				
Coal	Illinois (Bituminous)		Wyoming (Subbituminous)	
Process	H-Coal	CTSL	H-Coal	CTSL
Coal Conv., W% MAF	94	97	91	93
524°C$^+$ Conv., W% MAF	73	94	75	89
C_4-524°C Liquid Yield				
W% MAF Coal	51	78	48	66
Bbl/Ton Coal	3.3	5.0	3.1	4.3

TABLE 2. COAL/OIL COPROCESSING TECHNOLOGY BENCH-SCALE EXPERIENCE (OPERATING DAYS)									
Feedstock (Oil)	Cold Lake	Lloydmin.	Maya	Kuwait	Orinoco	Hondo	Shengli	Assam	Total
Coal	Canada	Canada	Mexico	Kuwait	Venezuela	US	China	India	
Lignan (Canada)		35							35
Westerholt (Germany)	29								29
Ohio (US)	82		15		24				121
Illinois (US)				5					5
Taiheiyo (Japan)			25						25
New Mexico (US)						21			21
Texas Lignite (US)	3		105		4	3			115
Black Thunder (US)	5								5
Forestburg (Canada)	41								41
Yanzhou (China)							25		25
Assam (India)								24	24
Total	160	35	145	5	28	24	25	24	446

TABLE 3. HRI COAL/OIL COPROCESSING TECHNOLOGY SUMMARY OF BENCH-SCALE DATABASE		
COAL FEEDSTOCK PROPERTIES	**MINIMUM**	**MAXIMUM**
Ash, W% Dry Coal	3.9	17.5
H/C Atomic Ratio	0.68	1.03
O/C Atomic Ratio	0.05	0.24
Sulfur, W%	0.3	4.7
OIL FEEDSTOCK PROPERTIES		
°API Gravity	1.8	10.5
H/C Atomic Ratio	1.36	1.54
Sulfur, W%	0.6	5.7
Ni+V, Wppm	11	982
W% 525°C	68	94
OPERATING CONDITIONS*		
W% Coal Feed	10	67
Space Velocity	0.8	2.4
Temperature, °C		
First Stage	400	440
Second Stage	400	440
Recycle/Feed Ratio	0	1.15
525°C+ in Recycle, W%	0	70
PROCESS PERFORMANCE		
525°C+ Resid Conversion, W%	59	93
Coal Conversion, W%	81	97
HDS, W%	66	98
HDN, W%	40	88
C_4-525°C Yield, W%	55	83
C1-C3 Yield, W%	3	9
Hydrogen Consumption, W%	2	5

* The preferred operating conditions include: 25-40 W% coal in feed, a space velocity of 1.0, first and second stage reactor temperatures in the range of 430-440°C with no recycle.

TABLE 4. HYDROGEN MANAGEMENT IN TWO-STAGE REACTOR SYSTEMS				
Case	1	1A	2	2A
Hydrogen Consumed				
Reactor 1	0.8	0.8	0.5	0.5
Reactor 2	0.2	0.2	0.5	0.5
Total	1.0	1.0	1.0	1.0
Hydrogen Supply to Reactor 1	**3.2**	**3.2**	**2.0**	**2.0**
Hydrogen Supply to Reactor 2				
From Reactor 1	2.4	0.0	1.5	0.0
Fresh	0.8	0.8	2.0	2.0
Total	**3.2**	**0.8**	**3.5**	**2.0**

FIGURE 1. HTI'S CATALYTIC TWO-STAGE COAL LIQUEFACTION PROCESS

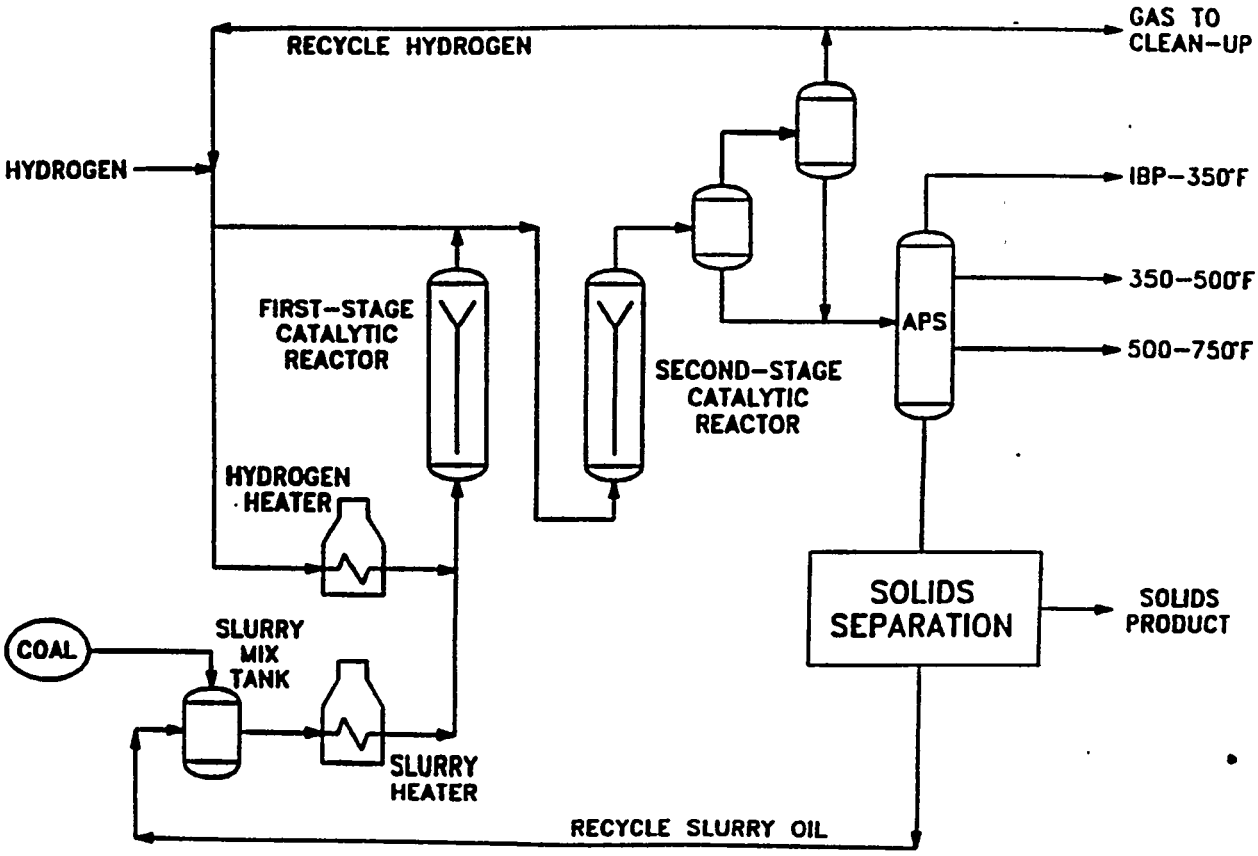

FIGURE 2. HTI'S CATALYTIC TWO-STAGE COAL/OIL COPROCESSING TECHNOLOGY

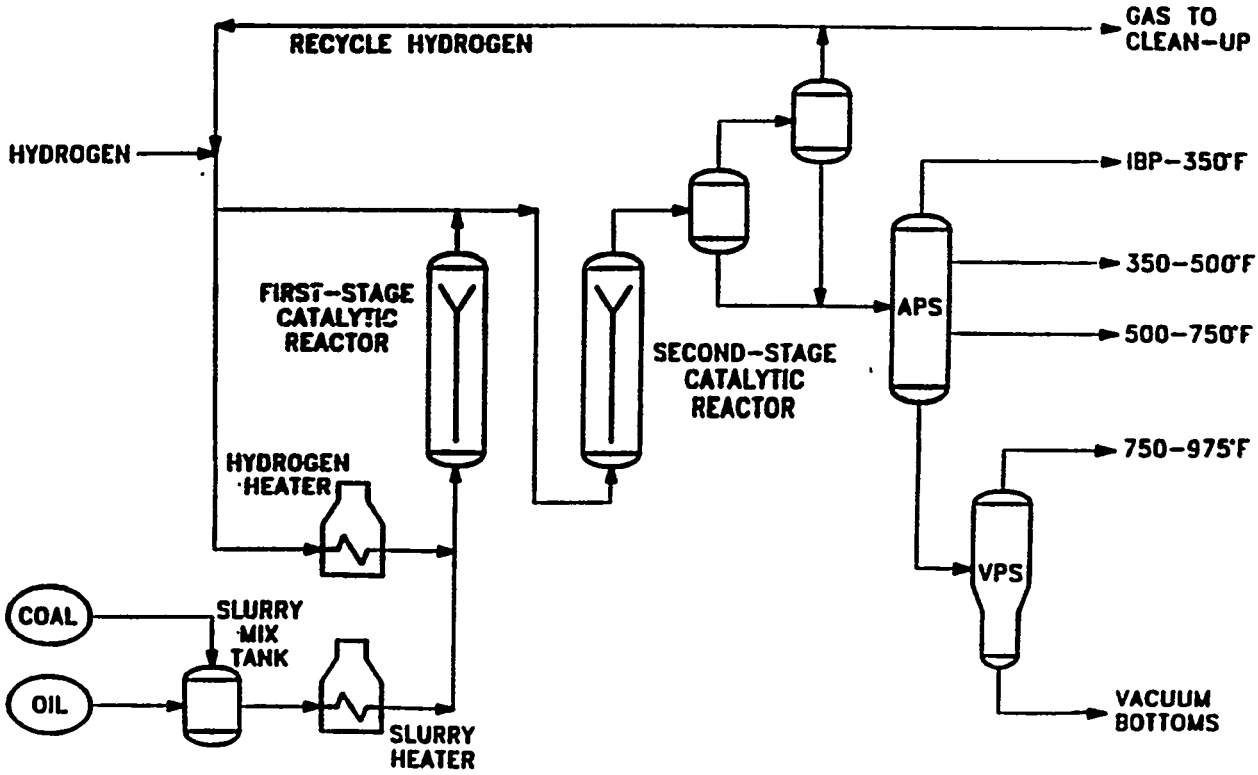

FIGURE 3. COAL/OIL COPROCESSING SYNERGY ON 524 C+ CONVERSION

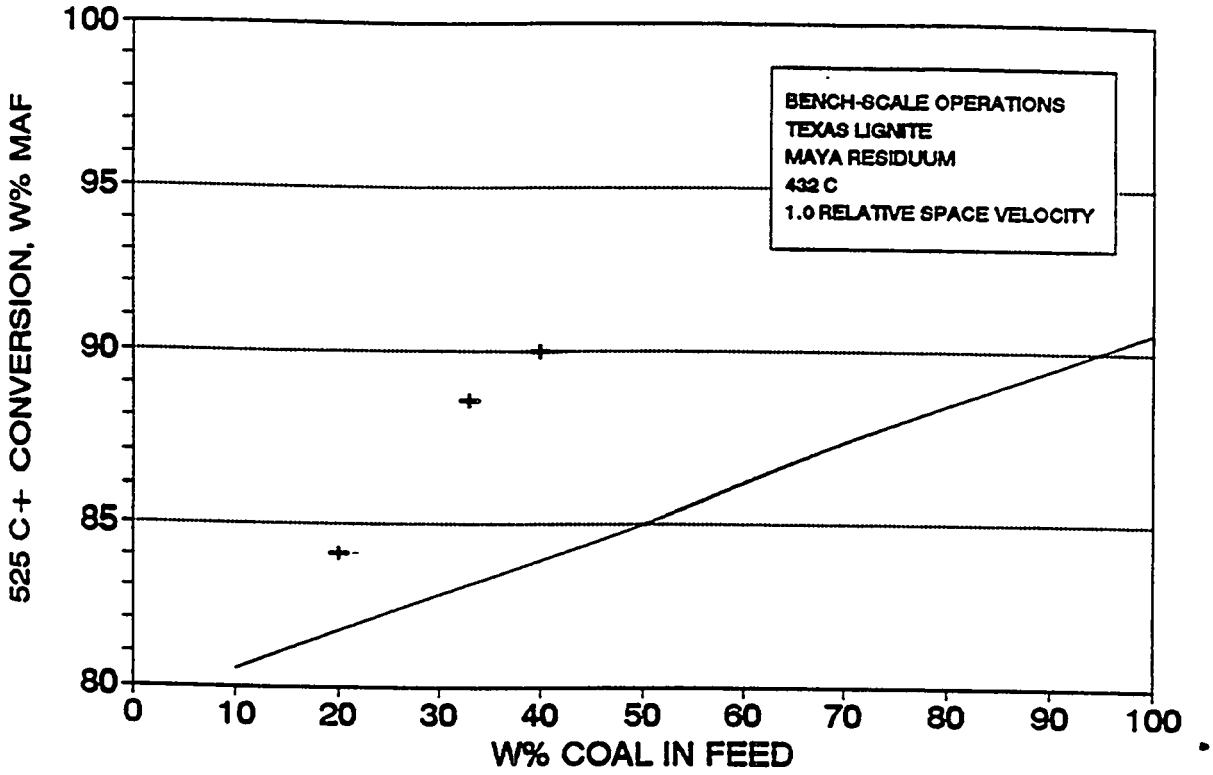

FIGURE 4. COAL/OIL COPROCESSING METALS CONCENTRATION IN PRODUCT SOLIDS

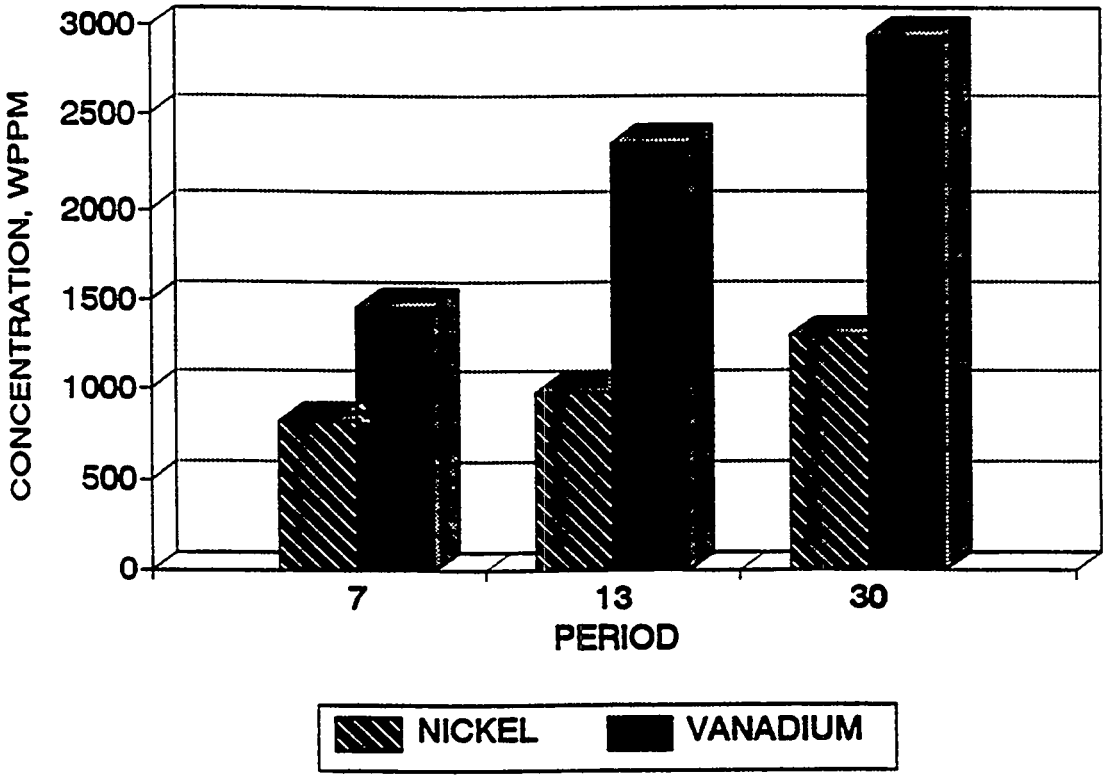

DEASHING OF COAL LIQUIDS WITH CERAMIC MEMBRANE MICROFILTRATION AND DIAFILTRATION

Bruce Bishop and Robert Goldsmith

CeraMem Corporation
12 Clematis Avenue
Waltham, MA 02154

Contract Number: DE-AC22-92PC92149

Period of Performance: August 4, 1992 - September 30, 1995

Introduction

Removal of mineral matter from liquid hydrocarbons derived from the direct liquefaction of coal is required for product acceptability. Current methods include critical solvent deashing (Rose® process from Kerr-McGee) and filtration (U.S. Filter leaf filter as used by British Coal). These methods produce ash reject streams containing up to 15% of the liquid hydrocarbon product.

Consequently, CeraMem proposed the use of low cost, ceramic crossflow membranes for the filtration of coal liquids bottoms to remove mineral matter and subsequent diafiltration (analogous to cake washing in dead-ended filtration) for the removal of coal liquid from the solids stream. The use of these ceramic crossflow membranes overcomes the limitations of traditional polymeric crossflow membranes by having the ability to operate at elevated temperature and to withstand prolonged exposure to hydrocarbon and solvent media. In addition, CeraMem's membrane filters are significantly less expensive than competitive ceramic membranes due to their unique construction. With these ceramic membrane filters, it may be possible to reduce the product losses associated with traditional deashing processes at an economically attractive cost.

Membrane Background

General Description of Crossflow Membrane Processes

The process for removal of solids from coal derived liquids in this program is crossflow microfiltration (MF). This is a pressure driven membrane process in which particulate and colloidal materials are removed from a feed stream (See Figure 1). In microfiltration, the feed stream is pumped over the membrane surface with a transmembrane pressure differential in the range of 20 to 100 psi. The crossflow velocity is generally 100 to 10,000 times the "perpendicular" velocity or filtration velocity. Retained matter is removed from the system as a fluid concentrate. The surface shear at the membrane surface controls the build-up of a filter cake (or membrane foulant layer) so that, in principle, a steady sate filtration rate is attained. The process is to be contrasted with dead-ended filtration in which no crossflow is present and a filter cake builds continuously as filtrate is removed.

MF is generally employed for removal of submicron particulate and colloidal matter which would rapidly blind surface filters. Also, MF replaces diatomaceous earth precoat filters because of greater product recovery and the elimination of waste disposal of a voluminous spent precoat cake.

MF can be used in a diafiltration process to increase the recovery of liquid or soluble products from a particulate containing stream. In diafiltration, a solvent is added to the fluid concentrate to dilute the solids so that the fluid can be refiltered to remove additional product in the filtrate along with some of the added solvent. Several cycles of this process can be used such that essentially all the product in the feed stream is removed and the concentrate consists of solids and solvent. Additional processing of the permeate and/or concentrate may be necessary in order to remove the solvent depending on the application.

Description of CeraMem's Ceramic Crossflow Membrane Technology

CeraMem is one of several commercial suppliers of liquid crossflow ceramic membrane modules which utilize a porous ceramic monolith as a membrane support. However, CeraMem is unique in its approach, described below, in utilizing a very high membrane surface area support structure in each modular element.

Ceramic Monoliths as Membrane Supports. CeraMem's technical approach to construction of ceramic membrane modules is based on the use of porous honeycomb ceramic monoliths as membrane supports. These high surface area, low cost materials have been developed for and are widely used as catalyst supports for automotive catalytic converters. The most commonly available material is cordierite. Cell (i.e., feed passageway) "areal densities" in the honeycomb structure range from 9 to 1400 cells per square inch of monolith frontal area (cpsi), and can have cell geometries of round, square, or triangular. The porosity of the materials can range from about 30% to 50% with mean pore diameters of 3 μm to 35 μm. The monoliths themselves can be extruded in various cross sections such as rounds, ovals, or squares. Cross sections up to 13" and lengths up to 36" are extruded on a commercial scale by Corning, Inc.

Membrane Application to the Ceramic Support. CeraMem forms microfiltration and ultrafiltration membranes on the monolith by slip casting porous coatings of ceramic particles on the cell wall surfaces of the passageways, followed by drying, and then sintering to bond the particles to each other and the honeycomb support. Most membranes have more than one coating layer, constituting a multilayer, asymmetric ceramic membrane. The initial layers are relatively thick (75-100 μm) and consist of large particles to cover the pores of the support material. Subsequent layers are thinner to minimize flow resistance and consist of finer particles to form finer pore sizes. A schematic diagram of a multilayer membrane is shown in Figure 2.

Mode of Use As Membrane Supports/Housing and Seal Design Concept. Each monolith has hundreds to thousands of parallel passageways that run from one face to the opposite end face (Figure 3). During processing, the feed stream to be treated is introduced under pressure at one end of the module, flows through the passageways over the membrane, and is withdrawn at the downstream end of the module. Material which passes through the membrane (permeate) flows into the cell walls of the monolith. The combined permeate from all the passageways flows

toward the periphery of the monolith support, and is removed through an integral, pressure-containing "skin" at the exterior of the monolith.

There is a technical limitation to use of monolith supports as described above. Due to the long and tortuous path through which the permeate must flow to get to the outside pressure containing skin, there can be a large pressure drop for permeate flow. Depending on membrane resistance and process conditions, the only passageways from which permeate can be effectively removed are often those in an annular ring adjacent to the monolith skin. This limitation generally restricts the diameter of monoliths than can be used to approximately one inch.

CeraMem has developed mechanical modifications to monoliths to overcome this limitation, and one version is used commercially for membrane modules of approximately six inches in diameter. These mechanical modifications create permeate conduits within the monolith which conduct permeate from the interior of the monolith to an external permeate collection zone. Figure 4 depicts one form of these mechanical modifications. In this case, slots are cut into one end (or both) of the monolith, and the ends of these slots are sealed. At the opposite end of the monolith, the ends of the cells opening into the slots are sealed in a like manner. Many sealants can be used, but the preferred materials are similar to that from which the monolith is made. After sealing the slots at both ends of the monolith, the monolith is coated with membrane. During operation, feed is pumped through the module, and permeate flows through the membrane into the monolith cell walls. The permeate from any cell in the monolith flows no more than a few cell layers before it arrives at a low pressure permeate conduit. When the conduit is reached, the permeate flow turns toward the end of the monolith containing the slots. Upon reaching the slots, the permeate flow turns 90° and flows into a permeate collection zone.

This approach to removing permeate from the inside of a large diameter monolith results in high surface area modules with very high membrane packing densities. As a result, several advantages are derived from this unique membrane construction. First, since most of the cost of manufacturing ceramic membranes is labor, the cost of producing high surface area membrane elements is relatively low allowing CeraMem to sell membranes at much lower prices per square foot than other ceramic membranes and at prices competitive to polymeric membranes in some cases. Also, with the high surface area filter elements fewer elements are needed in any one system thereby minimizing the amount of associated hardware including housing and seals.

At present, the conduit configuration described above has been commercialized for crossflow liquid applications, using elastomeric boot seals in stainless steel housings, at temperatures up to 200°C. This design, however, is not readily amenable to sealing at higher temperatures due to the temperature limitation on the elastomer boot seal. CeraMem has developed high temperature membrane modules for use in petroleum-based feed stream processing at temperatures up to 350°C on a developmental basis and believes that commercial, full size filter elements with housings and seals capable of operating at higher temperatures are possible.

Proposed Technical Approach

The approach proposed for this program to deash the coal liquid bottoms entails two steps. The first step is ash concentration with crossflow MF. Residual oil, containing ash, is pumped

through a ceramic membrane system operating with a transmembrane pressure of about 20-80 psi. If the feed material is generated at ambient pressure, the filtrate will be recovered at ambient pressure. If the feed is pressurized to retain volatiles, then both the concentrate and the filtrate from the membrane unit will be pressurized. The system pump provides the required crossflow velocity through the membrane elements. This concentration process produces two product streams. The filtrate, free of suspended particulates, may be further processed through the liquefaction reactors to increase product yield. The second stream is the solids containing concentrate. The suspended particulates level in the concentrate can be expected to range from about 20 to 30%. After concentrating the bottoms to this solids level, 55-76% of the liquid fraction can be recovered as filtrate if the starting mixture contains 10% solids. Additional processing of the concentrate is necessary in order to extract most of the remaining residual oil.

To increase overall oil recovery, the concentrate can be treated by diafiltration. In this process, shown schematically in Figure 5, a volatile solvent (e.g., a distillate product generated within the coal liquefaction process) would be added to the concentrate and the diluted concentrate would be further processed by crossflow MF.

Diafiltration serves to displace the resid from the concentrate with solvent. Therefore, the final concentrate from the diafiltration section consists primarily of suspended particulates and solvent. While diafiltration could be used to recover essentially all of the resid from the ash-reject stream, there will be an economic optimum for the degree of diafiltration actually employed. The diafiltration filtrate would be flashed or distilled to recover solvent for recycle. The diafiltration concentrate would be dried to recover solvent for recycle.

Project Technical Objectives

This program is directed towards development of an improved process for de-ashing and recovery of coal-derived residual oil: the use of ceramic membranes for high-temperature microfiltration and diafiltration. Using laboratory scale ceramic membrane modules, samples of a coal-derived residual oil containing ash will be processed by crossflow microfiltration, followed by solvent addition and refiltration (diafiltration). Recovery of de-ashed residual oil will be demonstrated. Data from this program will be used to develop preliminary estimates for production system capital and operating costs that will be used to assess economic feasibility.

A first objective of this program is to demonstrate technical feasibility of crossflow microfiltration (MF) for removal of mineral matter from a coal derived residual oil. A second objective is to demonstrate technical feasibility of diafiltration of MF concentrate using a hydrocarbon solvent.

Experimental Materials and Procedures

Two types of ceramic membranes were tested in coal liquids filtration. These lab scale membrane modules were approximately 12 inches long and 1 inch in diameter and had 1.5 ft^2 of membrane area. The passageways were square and approximately 0.07 inches on a side. The two membranes tested had separation layers consisting of 0.05 μm diameter pore size titania and 0.01 μm diameter pore size silica. Ceramic end rings were bonded onto each end of the module

so that it could be sealed into stainless steel housings. The seal between the housing and module was a graphite packing seal used successfully in previous hydrocarbon testing.

The coal liquid and diluent used in these tests were obtained from Hydrocarbon Research, Inc. in Princeton, NJ. The coal liquid was a reactor liquid flash vessel bottoms (O-43) from a recent HRI liquefaction run (Run Number 260-004-49-T). The diluent was petroleum based, hydrotreated start-up oil (HRI Number L-809).

The process tests were performed at Imperial Oil, Ltd. in Sarnia, Ontario Canada. Imperial Oil had a high temperature crossflow test system designed for liquid hydrocarbon testing. The test system was capable of heating feeds to temperatures of about 300°C, feed stream crossflow of up to 6 gpm, and membrane inlet pressures of up to about 100 psig. The system could process the liquids in both recycle mode and batch concentration mode. In recycle mode, the permeate was recycled back to the feed tank resulting in no change in solids concentration in the feed stream. In the batch concentration mode, the permeate was diverted to an alternate vessel resulting in an increase in solids in the feed material.

Two general sets of tests were conducted on one batch of coal liquid. The flash drum bottoms were diluted from approximately 15% total suspended solids to about 10% solids. Solids concentrations were determined by a THF insolubles test according to a procedure obtained from Consol, Inc. First, filtration tests at constant solids concentration were performed to determine the effects of membrane type, temperature, pressure, and crossflow velocity. Based on the results of these initial tests, the membrane type and process conditions for the batch concentration of the coal liquid to about 20% solids was determined. After this initial batch concentration was performed on the diluted flash drum bottoms, four additional dilutions and concentrations were performed at the same process conditions. Samples of feed and permeate from each cycle were taken and analyzed for THF insoluble solids. These results and the recording of masses of each amount of liquid added to or sampled from the feed tank or permeate stream were used to estimate the amount of residual oil left in the concentrate at the end of each cycle. Due to the very similar boiling point curves of the petroleum-based start-up oil and the coal derived liquid, distillation could not be used to directly determine the concentration of residual oil in the concentrate samples.

Experimental Results

Membrane Type Evaluation

Initial process flux characterization experiments were conducted with the two different membrane module types using the diluted coal liquid bottoms. The feed was charged into the system along with one of the membrane modules and the feed was heated in recycle over the course of two days to 265°C. Permeate flux was then measured over the course of several hours at 265°C, 240°C, and 200°C. Transmembrane pressure was 80 psig and the crossflow was about 6 gallons per minute (gpm). Permeate samples were analyzed for non-THF soluble solids. The same process was repeated for the second membrane type. The data for both membrane types are included in Table 1.

Several clear observations can be made concerning the data. First, the 0.01 μm and 0.05 μm membranes were very different in terms of process flux. The 0.05 μm membrane had a very good crossflow process flux of over 200 kg/m^2/h which was a factor of twenty higher than the 0.01 μm membrane. Second, the process flux appeared to be strongly dependent on temperature between 200°C and 265°C. Third, non-THF soluble solids retention was very high for both types of membranes.

Based on the membrane evaluation tests, the 0.05 μm pore size titania membrane was selected for further testing to evaluate the effects of various process parameters on membrane flux performance. The purpose of these parametric tests was to determine the process conditions for subsequent concentration/diafiltration process runs.

Table 1.
Ceramic Membrane Performance in De-ashing of Coal Liquids

Evaluation	0.01 μm Silica		0.05 μm Titania	
Process Flux	Temperature (°C)	Flux (kg/m^2-hr)	Temperature (°C)	Flux (kg/m^2-hr)
	265	11	265	223
	240	5	240	198
	200	1.3	200	98
Solids Retention	> 99.9%		> 99.7%	

Process Variable Evaluation

The data recorded during the process variable evaluation experiments is shown in Table 2. In this table, the permeate flux level is shown to increase by 17% with an increase in temperature from 200°C to 270°C. This increase appears to be small compared to the anticipated increase based on the data obtained earlier in the project (Table 1). Data obtained on a 0.05 μm pore size titania membrane showed an increase of about 120% from 200°C to 265°C. However, the flux performance at about 265°C in both cases was almost the same, 220-225 kg/m^2-hr. The cause for this observation is probably that the first set of data were obtained by heating the feed directly to 265°C then measuring flux performance as the temperature decreased over the course of about 5 hours. In the parametric tests, the 200°C data was taken first and then the feed was heated to 269°C overnight before the flux data at high temperature was taken. If membrane fouling is occurring over time (see below), then the effect of temperature will appear to be enhanced in the first case. Both membrane fouling and temperature decrease will decrease flux thereby making the low temperature flux in the first set of data look very low. In the second case, the high temperature data will have been taken after a longer processing time and the ultimate flux rate due to temperature will not be measured due to membrane fouling. Consequently, the increase in flux due to increased temperature in the parametric test was

tempered by time effects possibly as a result of adsorption of materials onto the titania membrane during processing.

The effect of time is more clearly shown in Table 2 between that data taken at 22 hours and 27 hours. With a very small reduction in temperature, the flux falls off by about 45%. It appears that membrane fouling possibly by adsorption of material onto the membrane or plugging of the pores by very fine colloidal material is occurring. The effect of membrane fouling is to reduce permeate flux over long periods of time as flux inhibiting material (foulants) is brought to the membrane via permeation flow. As long as there are foulants in the feed material and they can attach to or plug the membrane, flux will decrease. Membrane modifications or process changes (e.g., feed pretreatment) can have a significant impact on the degree of fouling and should be studied before commercial systems are designed. While membrane fouling is an important process characteristic, it does limit the usefulness of the parametric studies.

Table 2
Coal Liquid Deashing Parametric Studies Using Titania Membrane

Elapsed Time (hrs)	Crossflow (gpm)	Temperature (Deg C)	Average Pressure (psi)	Differential Pressure (psi)	Permeate Flux (kg/m^2-hr)
1.1	5.9	195	77.5	3	193.1
Filter element and feed material slowly heated overnight with no permeate flow.					
22.1	5.8	269	74.0	8	225.7
27.0	6	254	76.0	8	122.8
Transmembrane pressure decreased after 27 hours and allowed to stabilize for four hours.					
31.1	5.9	254	37.5	9	76.8
46.5	6	254	39.0	4	80.2
51.5	5.8	254	38.5	3	67.0
Crossflow decreased after 51.5 hours and allowed to stabilize for 2.5 hours.					
54.3	4	243	39.5	3	56.4
70.7	4	243	37.5	3	45.7

The next process variable evaluated was pressure across the membrane. It can be seen in Table 2 that the permeate flux fell off about 40% with a 50% reduction in the pressure. A large decrease in flux level with reduced membrane driving force is typical for microfiltration applications. However, it is unclear how much membrane fouling contributed to this effect. The relative stability of the flux level over the next 20 hours indicated that the rate of membrane fouling was decreasing. This may occur due to membrane conditioning (i.e., reduction in

adsorption sites) and/or a reduction in the amount of foulant in the feed material. Since the experiment is being run with a single batch of material, the foulant could be stripped out of the fluid and onto the membrane. The rate of membrane fouling would decrease as the amount of foulant remaining in the feed is decreased.

Lastly, the effect of crossflow on membrane flux performance was investigated. The effect of crossflow in some applications can be large due to the sweeping action of the fluid across the membrane removing flux inhibiting materials from the membrane surface. As can be seen in Table 1, a 33% decrease in crossflow seemed to cause a 16% decrease in flux. Once again, membrane fouling may have contributed to the observation.

Based on the results of the parametric tests, the process conditions chosen for the concentration/diafiltration runs were those that maximized process flux. These conditions were 270°C, 80 psig inlet pressure, and 6 gpm crossflow.

Diafiltration Process Evaluation

Data from the concentration/diafiltration runs is summarized in Figure 6, 7, and 8 and Table 3. Process flux data from concentration runs 1, 3, and 5 are shown in Figures 6, 7, and 8, respectively. The data is presented using a linear trend line through the flux data points. The trend line is used to give a general guide to the fall off in flux during concentration and is not curve fit to the data which would better indicate the function for flux fall off. The flux data does indicate that each of the concentration run fluxes was fairly similar to each other. This may have been due to the use of start-up oil which is similar to the liquid in the atmospheric bottoms. Use of a lower molecular weight solvent that would need to be pressurized at process temperature but would allow for relatively easy removal from the concentration and permeate by flashing would probably give different results. The overall flux rate is very encouraging. Flux levels for typical crossflow applications range from 20 to 200 l/m^2-hr. Considering the high viscosities and solids concentrations in these streams, the flux levels are very good. This will have a large impact on reducing the number of filters required in a commercial system.

Data in Table 3 includes the measured solids concentration of feed and concentrate samples for each concentration run as well as the calculated amount of residual coal-derived oil in each sample. As can be seen, the amount of concentration that can be obtained with these membrane filters under these process conditions is about 20% solids. Over the course of these concentration runs, most of the residual oil has been extracted from the bottoms. It was calculated that 23% of the oil was removed from the bottoms after 3 dilution/concentration runs while 7% of the residual oil was removed from the bottoms after 5 dilution/concentration runs. This data will be helpful in evaluating the process design and process economics.

Preliminary Process Approach and System Economics

There are many possible locations for a crossflow membrane system to be located in a direct liquefaction process design. These include (1) after the liquefaction reactors, (2) after the atmospheric distillation column, and (3) after the vacuum distillation column. If the system is placed after the reactors, the system will be expensive due to the high temperature and pressure

Table 3
THF Insoluble Solids and Residual Oil Concentrations of Each Process Cycle

	Concentration Runs				
Property	Number 1	Number 2	Number 3	Number 4	Number 5
Feed Solids Conc.	7.2%	9.4%	8.7%	7.8%	7.8%
Retentate Solids Conc.	29.4%	22.1%	17.1%	16.5%	18.8%
Retentate* Residual Oil Conc. (Calc)	62.1%	40.3%	22.8%	11.3%	6.8%

* Residual oil concentration in concentrate calculated on a diluent-free basis. This assumes that in an actual process the diluent would be flashed off leaving only solids and residual oil.

conditions as well as the large volume of liquid to be processed. As a result, CeraMem has performed some preliminary analyses of membrane systems after the atmospheric distillation column with the permeate going to distillate recycle and the dried concentrate going to a gasifier for make-up hydrogen production. In this case the vacuum still and the Rose® unit would be replaced. CeraMem has also looked at replacing the Rose® unit directly by taking the vacuum still bottoms as the feed.

Based on process flows in a 75,000 barrel per day (15,000 tons of coal per day) coal liquefaction plant obtained from Mitre Corporation (McLean, VA) and a permeate flux of 90 liters per square meter per hour, CeraMem has estimated the size and cost of ceramic membrane crossflow diafiltration systems for each scenario. Placing the filtration system after the atmospheric still will require the treatment of a larger process flow, thereby requiring a larger system. Each system would require an estimated 1,535 to 2,500 membrane modules and cost $18,000,000 to $26,000,000. Operating costs (power and membrane replacement) for this type of system is estimated to be about $3,000,000 to $5,000,000. Placing the system after the vacuum still and just replacing the Rose® unit will require a system with an estimated 1,120 to 2,100 modules. The cost for such a system is estimated to be $15,000,000 to $22,000,000 with an annual operating cost of about $2,000,000 to $4,000,000. These estimates do not include associated equipment and further work is required to better define these cost estimates; however, these costs appear to be attractive considering the costs of the vacuum still and Rose® solids removal system for a plant of this size. For example, the capital cost of the Rose® unit for a plant of comparable size has been estimated to be approximately $33,400,000 [1].

Conclusions

Based on work performed to date, CeraMem concludes that 0.05 μm nominal pore size titania membrane crossflow filters can efficiently filter diluted atmospheric flash drum bottoms with excellent solids removal (> 99%) and high fluxes at 270°C (100 to 200 lmh). In addition, a diafiltration process can be designed around these filters. If a relatively volatile diafiltration solvent can be found that is (1) soluble in the coal liquid and (2) capable of being recycled after flashing it off the permeate and concentrate streams, a potentially cost effective MF membrane diafiltration system can be developed.

Future Plans

CeraMem plans on working with Mitre Corporation on further refining the cost estimates for MF membrane diafiltration systems integrated into a direct coal liquefaction process plant. If these costs look attractive, CeraMem believes that additional research to find appropriate diafiltration solvents and experiments on fresh coal liquids from a direct liquefaction process development unit such as the one at HRI would be warranted.

References

1. S. Poddar, P. Adler, and S. Kramer, "Direct Coal Liquefaction - Capital Cost and Economics for Low Rank Coal Design." Proceedings of the Coal Liquefaction and Gas Conversion Contractor's Review Conference, pp. 1-17, September 7-8, 1994.

Acknowledgements

The authors would like to acknowledge the help of Pietro Perrone who participated in some of the experimental and data analysis tasks, Scott Armstrong and Imperial Oil, Ltd. who conducted the process experiments, and Susan Brandes and Consol, Inc. who helped perform some of the analytical measurements. The authors would also like to thank David Gray of Mitre Corporation, Geoff Kimber of the University of Kentucky, and Al Comolli of HRI for their help. Lastly, the help of our DOE PETC representatives Sally Kornfeld and Harold Chambers as well as the funding of the program under DOE Contract Number DE-AC22-92PC92149 is appreciated.

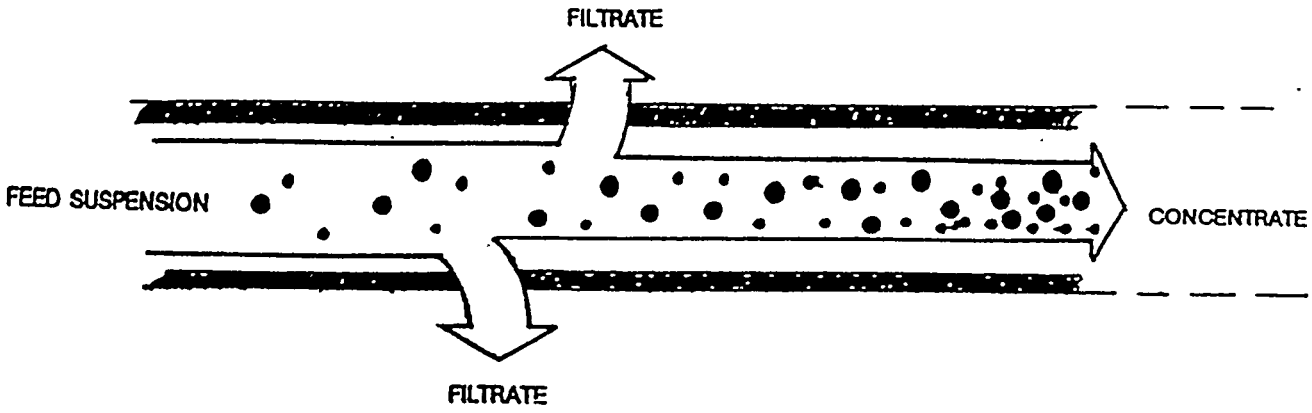

Figure 1. Crossflow Filtration Schematic

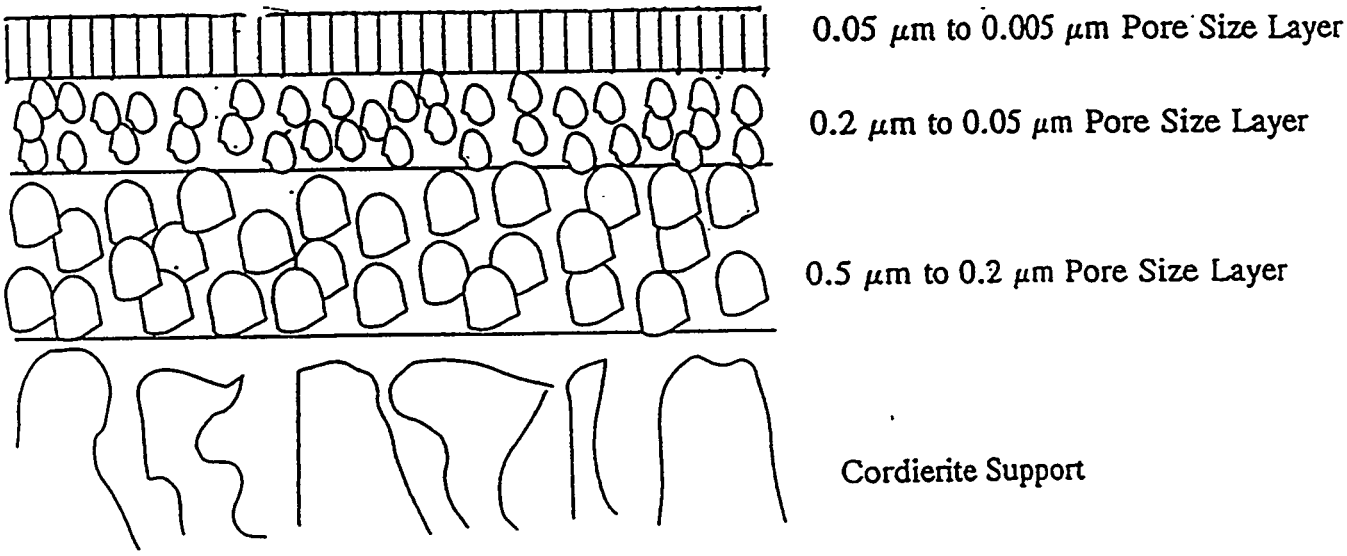

Figure 2. Schematic of Multilayer, Asymmetric Ceramic Membrane

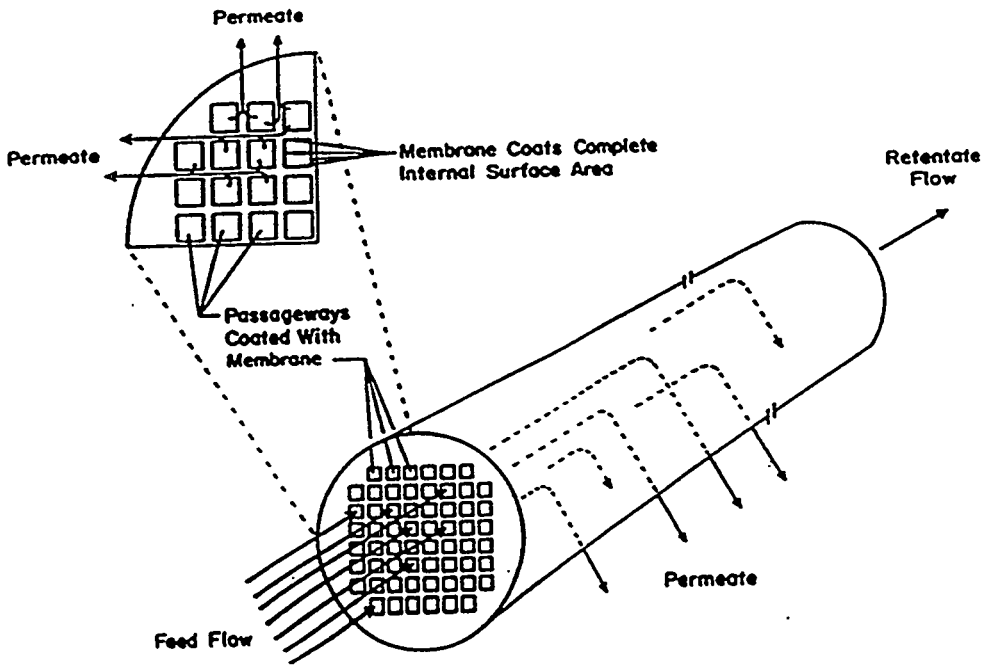

Figure 3. Lab Scale Permeate Flow Schematic

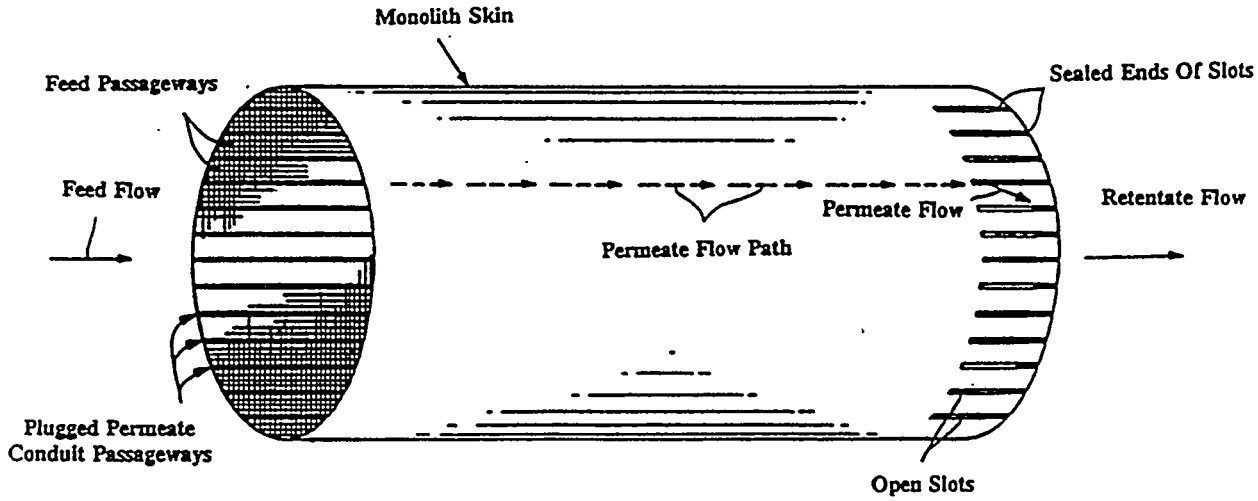

Figure 4. Full Size Permeate Flow Schematic with Permeate Conduits

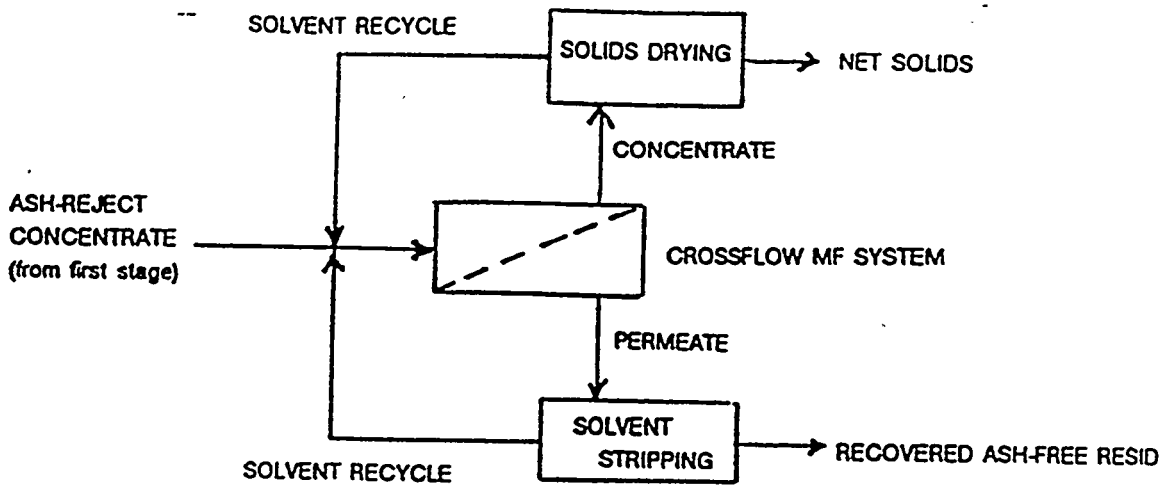

Figure 5. Proposed Deashing Process Using Microfiltration and Diafiltration

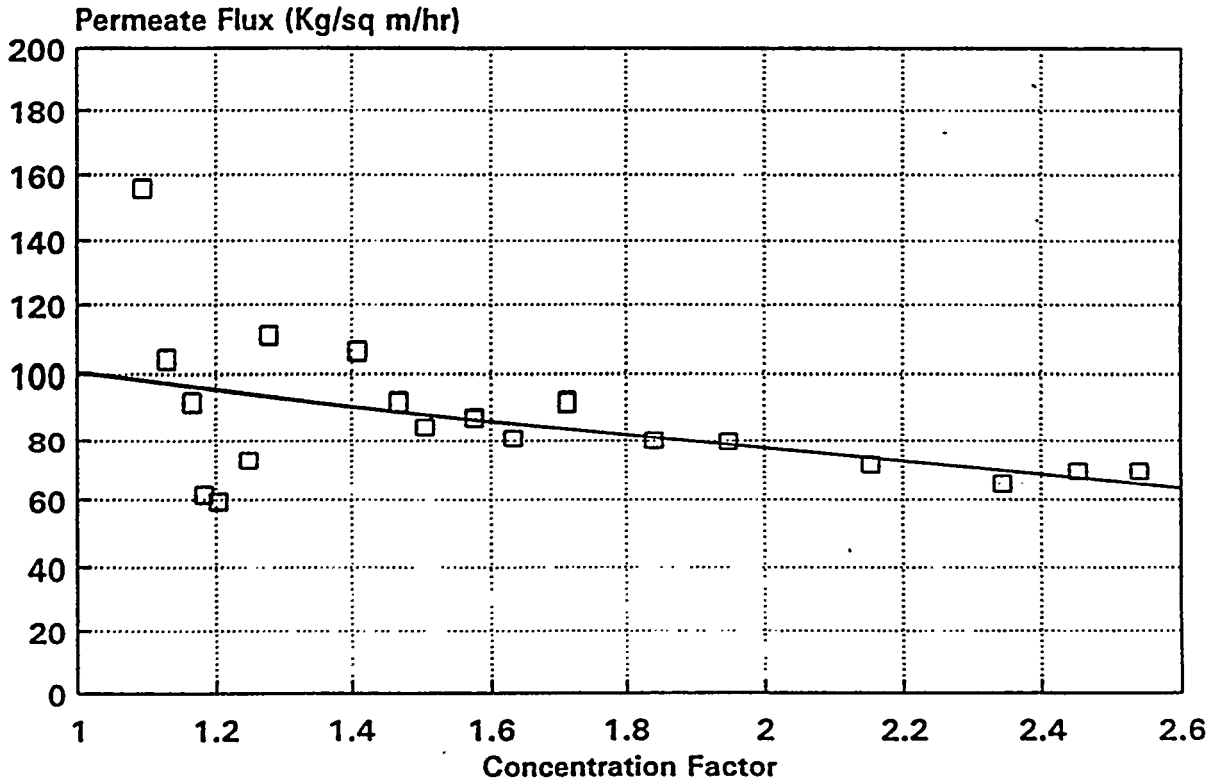

Figure 6. Coal Liquid Process Flux Versus Concentration in Run 1

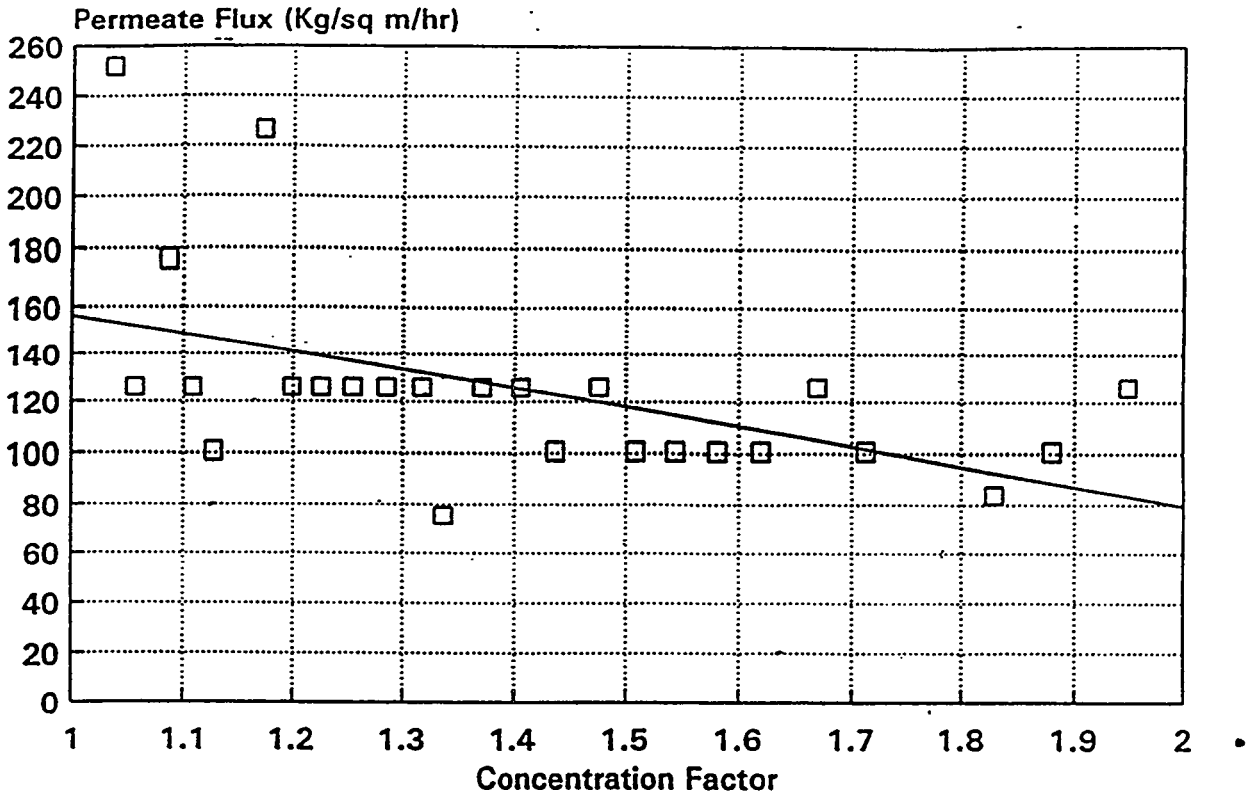

Figure 7. Coal Liquid Process Flux Versus Concentration in Run 3

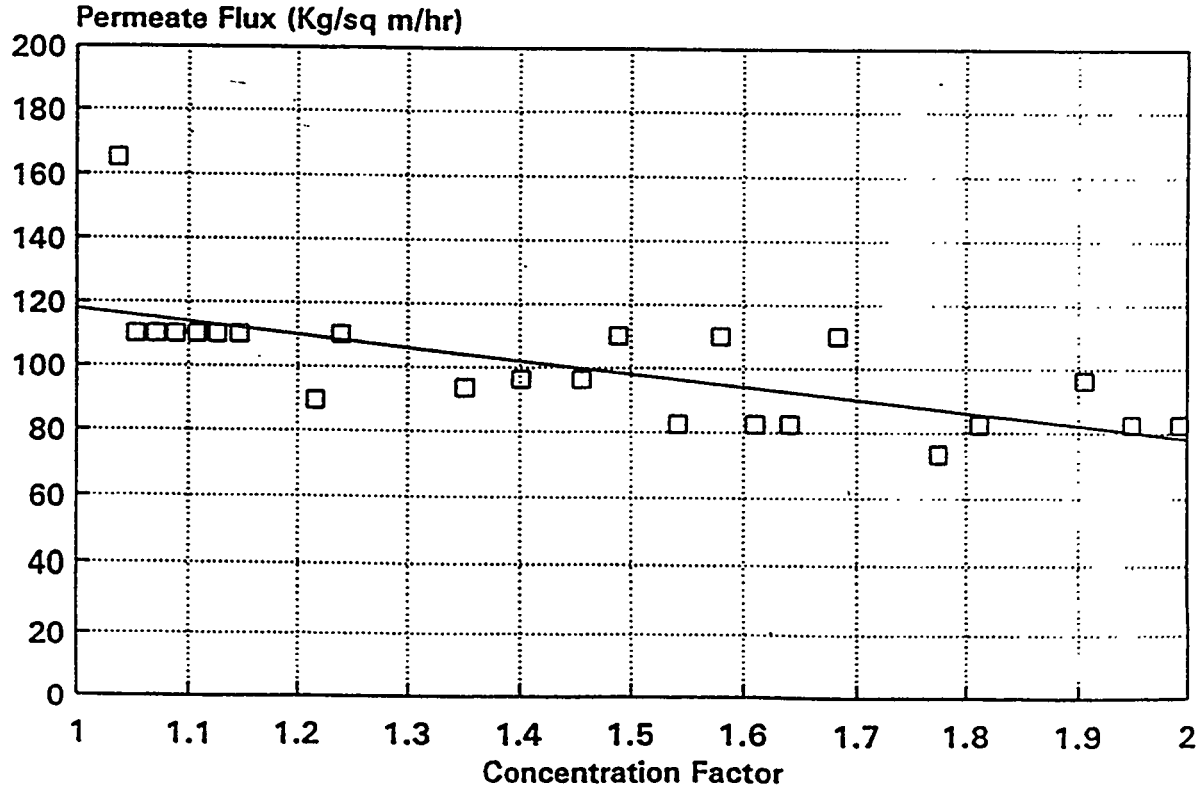

Figure 8 Coal Liquid Process Flux Versus Concentration in Run 5

ION EXCHANGE AND ADSORPTION ON LOW RANK COALS FOR LIQUEFACTION

Karl S. Vorres
Chemistry Division, Building 211
Argonne National Laboratory
Argonne, IL 60439

For Presentation at the
COAL LIQUEFACTION AND GAS CONVERSION
CONTRACTOR'S REVIEW CONFERENCE

Westin William Penn Hotel
Pittsburgh, Pennsylvania
August 29-31, 1995

Contract Number: FWP 49618

Period of Performance: June 1, 1994 - May 31, 1995

OBJECTIVE:

The objectives of this program involve the study of the catalysis of liquefaction of low rank coals. Ion exchange and adsorption techniques are being used or modified to incorporate catalytically active metals into coal samples. Relative oil yields will be determined by Sandia National Laboratory and PETC collaborators to establish the effectiveness of the catalyst incorporation techniques.

INTRODUCTION:

This report describes work done over the past 12 months of an ongoing project. A report describing earlier work was included in the Proceedings of the previous Contractors Meeting (1).

Ion Exchange and Adsorption

A number of techniques are being explored to place catalytically active materials on coal to facilitate direct liquefaction. Catalysts capable of liquefaction as small particles are being developed to permit maximum conversion at minimum cost. Additional motivation is due to a reduced need to recover active materials and the associated cost.

A variety of forms of iron catalysts are being developed in other research groups and are being reported at this meeting.

Other approaches have included the use of cation-exchanged catalysts. The hoped-for advantages include: close contact with the coal surface for good catalytic activity, more limited dosage required because of the close contact, and reduced need to recover the catalyst (particularly if it is an iron oxide).

A related technique is adsorption of anions. Some metals like molybdenum form oxy-salts such as molybdates. The active metal is present in the anion form and requires a different surface site than a cation for attachment to the coal surface. In addition the chemical nature of the metal is altered by surrounding

it with oxide ions in the molybdate complex. A technique has been developed for reproducibly placing the molybdate ions on the surfaces of coal particles (2). An equivalent procedure has not been developed for iron and the success of various efforts to ion-exchange iron has not been uniform.

A part of this work has involved an effort to understand the environment around the coal particle in an aqueous system so that better ion-exchange procedures may follow. The environment can be characterized in terms of the slurry pH of the coal sample. The pH affects the feasibility of ion exchange. Sudden shifts to alkaline values would cause precipitation of hydroxides rather than the exchange with surface sites that is desired.

The coal slurry pH is one of several tests used to characterize coals. A recipe is generally used. The typical recipe (3,4) involves taking one gram of coal for each two grams of water, mixing well, letting the mixture stand for 30 minutes and measuring the pH. Several things are implied in this procedure. The ratio of coal to water is specified and gives a fairly thick material, but not as thick as used in slurry pipelines and feed to burners for boilers. The time period of 30 minutes before measurement implies some reaction(s) are taking place and that a steady state or equilibrium may be reached after the 30 minute period.

A part of this study will explore the changes around coal in an aqueous environment and establish pH ranges during reasonable time periods of value in commercial processing.

Direct Liquefaction Studies

This project has used ion exchange and the related adsorption techniques to place catalytic materials on low rank coal samples. The samples have been sent to other laboratories for treatment to evaluate liquefaction potential. The efforts over time of Drs. Frances Stohl at Sandia National Laboratory, Christine Curtis at the University of Alabama and Anthony Cugini at PETC are much appreciated.

EXPERIMENTAL APPROACH

Ion Exchange - Slurry pH

An Orion Model EA940 pH meter was used with an Accumet pH electrode. The electrode was calibrated with standard commercial buffers of pH 4, 7 and 10. A two point method was used depending on the range of pH values involved in the experiment. Typically calibration was done at pH 7 and 10. Distilled and de-ionized water was used.

The coal samples were taken from the Argonne Premium Coal Sample Program set. Both -100 and -20 mesh samples were used. Water/coal ratios of 2-32 to 1 were obtained by mixing an ampule of 5 grams of -100 or 10 grams of -20 mesh coal with varying amounts of water. For some experiments a polyethylene plug (machined to fit inside the pyrex beaker and center the electrode in a snug-fitting hole) was used to limit the access to the atmos-

phere. For deaerated water experiments, the water was prepared by bubbling a stream of nitrogen through the stirred water for a minimum of 30 minutes. In one experiment, nitrogen gas was passed over the coal-containing equipment in a plastic enclosure. A magnetic stirrer was used in a number of experiments. Figure 1 is a schematic of the experimental apparatus.

At the beginning of a run, the pH electrode was placed in the weighed amount of water and data taking was initiated. Stirring was begun. Sealed ampules were opened, weighed, added to the water, and mixed with a glass stirring rod or magnetic stirrer. Stirring continued if the magnetic stirrer was used. Data were recorded on a IBM microcomputer at 15-20 second intervals. The computer data were analyzed using Lotus 123.

Several beaker materials and sizes were used to evaluate the effects of these parameters.

For comparison with the coal samples a series of oxide materials related to the mineral species in the coal, pyrite and graphite were also run.

A static measurement procedure is used for soil samples (3). The usual procedure calls for the addition of a weighed quantity of coal and water (1:2), stirring well, and measurement of the pH of the liquid above the settled coal after a time period of one half hour.

Liquefaction

The application of catalytic metals by ion exchange has been described in detail earlier (1). The technique involves the sieving of a -20 mesh sample to obtain -20+200 mesh material. This material is then rinsed with distilled water to remove adhering fine material. The moist slurry is transferred to a 50 ml burette equipped with a coarse fritted glass at the lower end of the markings. Initially a 0.10 N acid solution is used to elute the acid exchangeable material. The elution is followed with a series of pH and ion-selective electrodes for Ca, Na and K. The pH decreases and the eluted ion concentration decreases as the acid rinsing is near completion. A distilled water wash is used to remove the acid and provide a pH range of value for the ion exchange. Since some calcium was observed on the washing with water, the process is typically repeated through several cycles.

Following the coal preparation, the slurry is removed from the burette. A solution of known cation concentration is poured over the sample and allowed to stand for a period of several days. The solution is sampled and analyzed for the cation of interest. The change in concentration is related to the cation loading on the coal sample.

CURRENT STATUS - RESULTS AND DISCUSSION

Slurry pH

A typical result for a Wyodak subbituminous coal is shown in Figure 2. Initially the pH decreases as the water is stirred and affected by the atmosphere. As the coal is added the pH increases to a maximum value and then slowly decreases again. This general behavior pattern has been observed for most of the coal samples. The maximum pH value could be used to characterize the samples.

Table 1 gives the maximum pH values for different coal samples with measurements taken in a pyrex beaker, and magnetically stirred at the same setting.

Table 1. Maximum pH Values for Argonne Premium Coal Samples

Coal	Mesh	Max pH
ND	-100	9.626
WY	-100	8.925
IL	-100	9.752
UT	-100	9.717
WV	-20	7.735
PI	-100	9.785
UF	-100	9.298
PO	-100	9.417

For static runs (recipe type) and 2/1 water/coal ratio, the shape of the pH vs time plot is that of a parabola on its side with an asymptotic approach up to a limiting pH. The parabolic shape implies a diffusion limited change through a growing barrier.

The diffusion appears to be related to dissolution of CO_2 in water and formation of bicarbonate ions as well as hydronium ions with consequent decrease in pH.

The observation in some cases of an increase in pH appears to be related to a reaction of some species, such as an inorganic oxide, with water at the surface. Hydronium ions may be attracted to the oxide surface, leaving hydroxide ions free to increase the pH.

The initial decrease is believed to be due to the dissolution of carbon dioxide from the air, formation of carbonic acid, and ionization to provide hydronium and bicarbonate ions. The increase on addition of coal involves an interaction with the surface accessible to the water. This interaction consumes hydronium ions. The final slow decrease in pH may be again due to interaction with the carbon dioxide in the air.

The initial reaction with of different coals of varying ranks gives a series of maximum pH values. The value of the maximum pH does not correlate with the coal carbon content or other organic elemental components.

Effects of Variables

A series of runs with Illinois #6 (IL) indicated the effects of several variables and produced a range of values for the maximum pH. A number of variables were observed to determine if they were significant: container material, water/coal ratio, particle size, stirred/not stirred, aerated/deaerated water, and nitrogen environment.

Container Material

For the -20 mesh sample run in 250 ml pyrex beakers, the maxima were in the range 9.79, the same as if a stainless steel beaker was used instead (250 ml). These results were obtained for a high stirring speed. If the stirring speed was reduced the pH values were reduced to 9.73-9.75.

Particle Size

However, for the -20 mesh sample with a water/coal ratio of 4, the pH range was lower, 9.61-9.76, with a value of 9.53 for the stainless steel beaker. The high values were obtained when the magnetic stirrer was off in the early stages of the run. Stirring introduced a limitation to the maximum pH, probably due to the incorporation of carbon dioxide from the atmosphere.

Water Aeration or Deaeration

Aerating or de-aerating the water had little effect on the maximum pH as both gave 9.72. Interestingly, a sample which had no gas bubbled through gave pH 9.67.

Gas Environment

The run with equipment blanketed with nitrogen and de-aerated water gave the pH 9.76 which was higher than other stirred runs.

Stirring Speed

The effect of stirring speed was notable at low coal concentrations. Apparently, more rapid stirring gives a higher maximum pH.

Mixture aging

Samples were set aside for several days after initial measurements. pH measurements were repeated with stirring. An IL-20 sample had been measured to peak at 8.98 and decline in pH to about 8.53 after 73 minutes. After 7 days the static pH measurement dropped to 7.61. On stirring as before, the pH again increased to a maximum value of 8.00 before decreasing to 7.94 over about 3 hours. The reaction that increases the pH appears to be aided by stirring. The attrition of particles and exposure of fresh surfaces, including minerals would be consistent with this observation. The fresh mineral surfaces could react with hydronium and release hydroxide to increase the pH. The slow and limited subsequent pH decline reflects the near saturation with CO_2 and equilibrium between CO_2, bicarbonate and other ions in

the system. The suggested mechanism is also consistent with the earlier observation of the release of a suspension of clay material from a Wyodak sample after several cycles of acid and water washing. Perhaps chemical comminution by water develops cracks over time, which stirring propagates, leaving a tougher core after peeling off softer material. If so, then the overall rate might be combination of linear rate of exposing new surface from stirring and parabolic one from diffusion into particles. The observation of a slow decrease in pH over time with stirring implies that the addition of CO_2 with subsequent concentrations in the system has a greater effect on the pH than the particle attrition and interaction with new surface. However after standing for several days there is always some initial increase in pH with time after stirring.

The stirring is intended to quickly wet the hydrophobic coal particles so that they will be suspended in the slurry rather than remain on the surface of the mixture. The waiting period before the measurement implies a dynamic situation and an approach to a steady state pH value. Several reactions are apparent from the changes which have been observed.

The wetting involves an interaction with the surface of the coal particles. The effect on pH includes at least dissolution of soluble acidic or basic species, interaction with surface acidic or basic functional groups, interaction with acidic or basic surface sites or areas. Oxidation can change the surface of the mineral as well as the organic parts of the coal, and can be expected to affect the pH. Some of these potential effects may be deduced from changes in the progression of pH with time for a sample.

Other Materials - Inorganic Oxides, Graphite

In an effort to understand the reason for the increase in pH on the addition of coal to water, a series of materials were stirred with water. These materials included a series of insoluble inorganic oxides related to those found in the mineral matter of coal: alumina, titania, silica, calcium carbonate and clay. In addition pyrite was examined. A non-inorganic oxide, graphite, was also studied because it was somewhat similar to the organic material in the coal.

All of the inorganic insoluble oxides gave a slurry pH profile similar to the coal. After the water was equilibrated and stirred, the oxide was added. The pH immediately rose sharply and then slowly declined. This implies that the observed coal slurry pH behavior could be due to the mineral matter alone. Figure 3 shows a typical slurry pH profile for $CaCO_3$.

The pyrite behavior, from a sample which had been in a reagent bottle for some time was quite different. The pH dropped sharply on addition of the pyrite to the water. This implies that the pyrite sample had aged. The outward appearance was typical of the material in a fresh state, and was free flowing. The acid evolution implied a surface oxidation of the sample. The coal samples apparently did not have significant amounts of oxidized pyrite in them. Figure 4 shows a slurry pH profile for pyrite.

It was apparent that graphite did not behave like the coal either, unless it was assumed that the behavior was like an extremely high rank coal. The pH dropped on addition of the graphite in a manner similar to the pyrite. Figure 5 shows a slurry pH profile for graphite.

These observations taken together would indicate that the pH may be due to the effect of various insoluble inorganic oxide mineral constituents in the sample.

Liquefaction

Samples were prepared for a series of WY materials. These included:

WY Mo loaded 1.045 % on moist or 1.45 % on dry coal
WY Fe loaded 0.89 % on moist coal
WY acid and water washed, no catalyst loading for comparison
WY water washed, no catalyst loading for comparison
WY Mo + Fe loaded, 1.45% Mo + 0.053 % Fe on dry coal
WY + Fe loaded 0.71 % Fe on moist coal
WY + Mo loaded 0.126 % Mo on moist coal

These samples have been sent to Sandia National Laboratory for evaluation.

ACCOMPLISHMENTS & CONCLUSIONS:

Application of molybdenum by anion exchange has been successful using the technique developed by Schroeder (2). The ability to apply iron depends on the pH of the system which in turn is affected by environmental variables which are being studied.

The measured pH value of a given coal slurry will depend on the parameters of the experiment, including water/coal ratio, stirring speed, particle size, and coal rank.

The pH of a slurry of insoluble oxides gives a sharp increase on the addition of the oxide to water. Conversely, the addition of pyrite or graphite showed a decrease of pH on their addition to the water.

The addition of coal to water produces a series of pH changes. Initially, the drop in pH corresponds to the addition of carbon dioxide to the slurry. A subsequent increase appears to be related to inorganic constituents in the coal. A long term decrease in pH is assumed due to continued interaction with carbon dioxide.

The maximum pH depends on the interaction of the concentration of carbon dioxide, and the concentration of the mineral matter in the slurry.

PLANS:

The results of liquefaction runs will be learned as they are completed at Sandia National Laboratory. The results with iron loaded samples will be of special interest because of the lower cost of this material and the lower environmental concern.

Alternate means of ion exchange of iron onto coal samples will be explored to optimize the application of this catalyst. Control of pH and exchange of other cations for calcium etc. before addition of iron are initial approaches for the application of iron.

ACKNOWLEDGMENT:

The author gratefully acknowledges the support of the U. S. Department of Energy, Office of Fossil Energy for financial support, and the staff at the Pittsburgh Energy Technology Center for help with this program.

REFERENCES:

1. Ion Exchange and Adsorption on Low Rank Coals for Liquefaction, K. S. Vorres, Proc. Coal Liquefaction and Gas Conversion Contractor's Review Conf., Pittsburgh, PA Sept. 7-8, **1994**, pp 223-238

2. K. Schroeder, Preprints, Am. Chem. Soc., Fuel Chem. Div., 38 (2) 512 1993)

3. Methods of Soil Analysis, Part 2, Chemical and Microbiological Properties, ed. C. A. Black, Amer. Soc. of Agronomy, Madison, WI 1965, pp. 915-920.

4. Chap. 5, pp. 260, in The Science of Victorian Brown Coal, D. J. Brockway and R. S. Higgins, ed. R. Durie, 1992

Figure 1- Apparatus Schematic

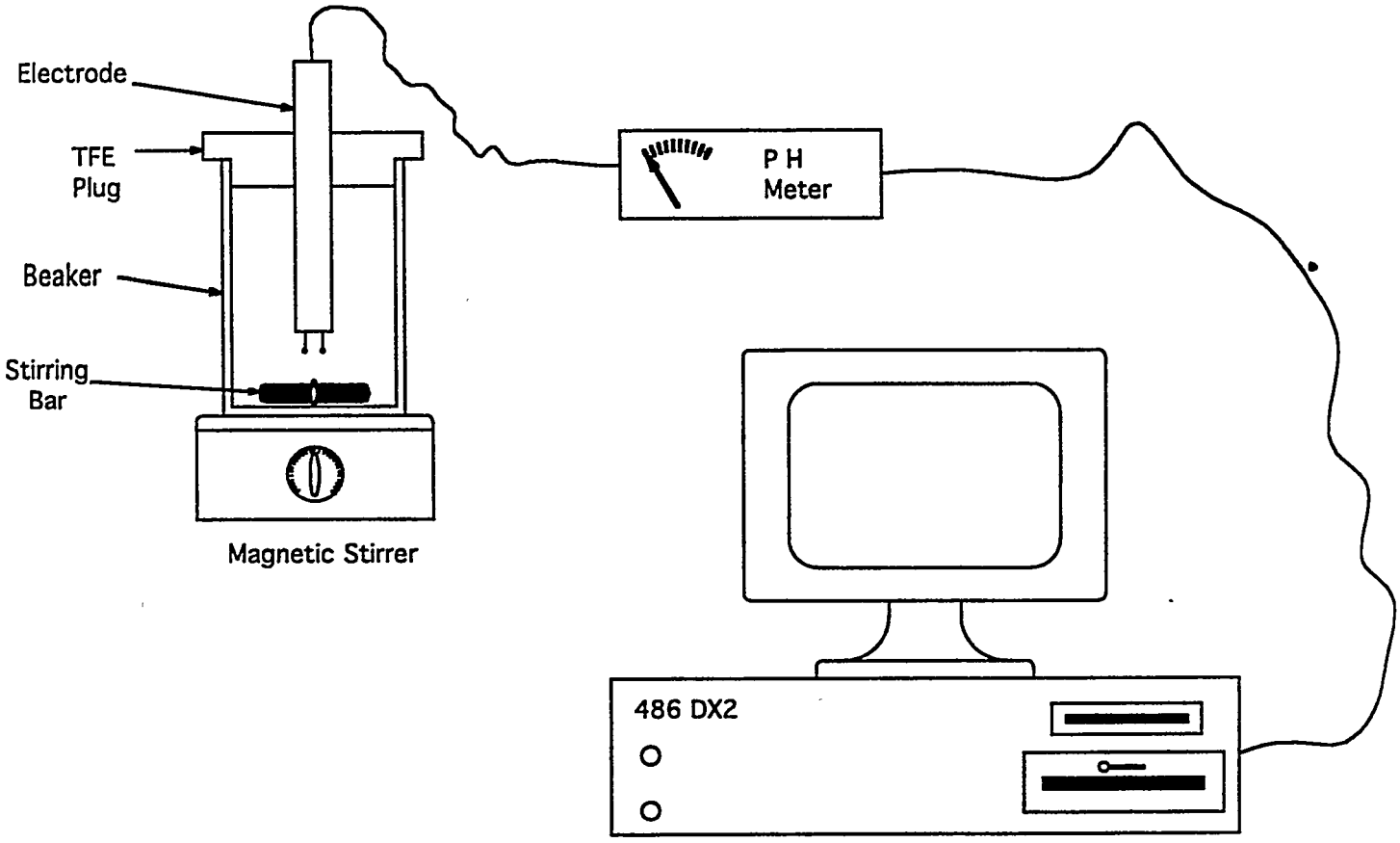

Fig. 2. Wyodak −20 mesh Slurry pH

5/31/95

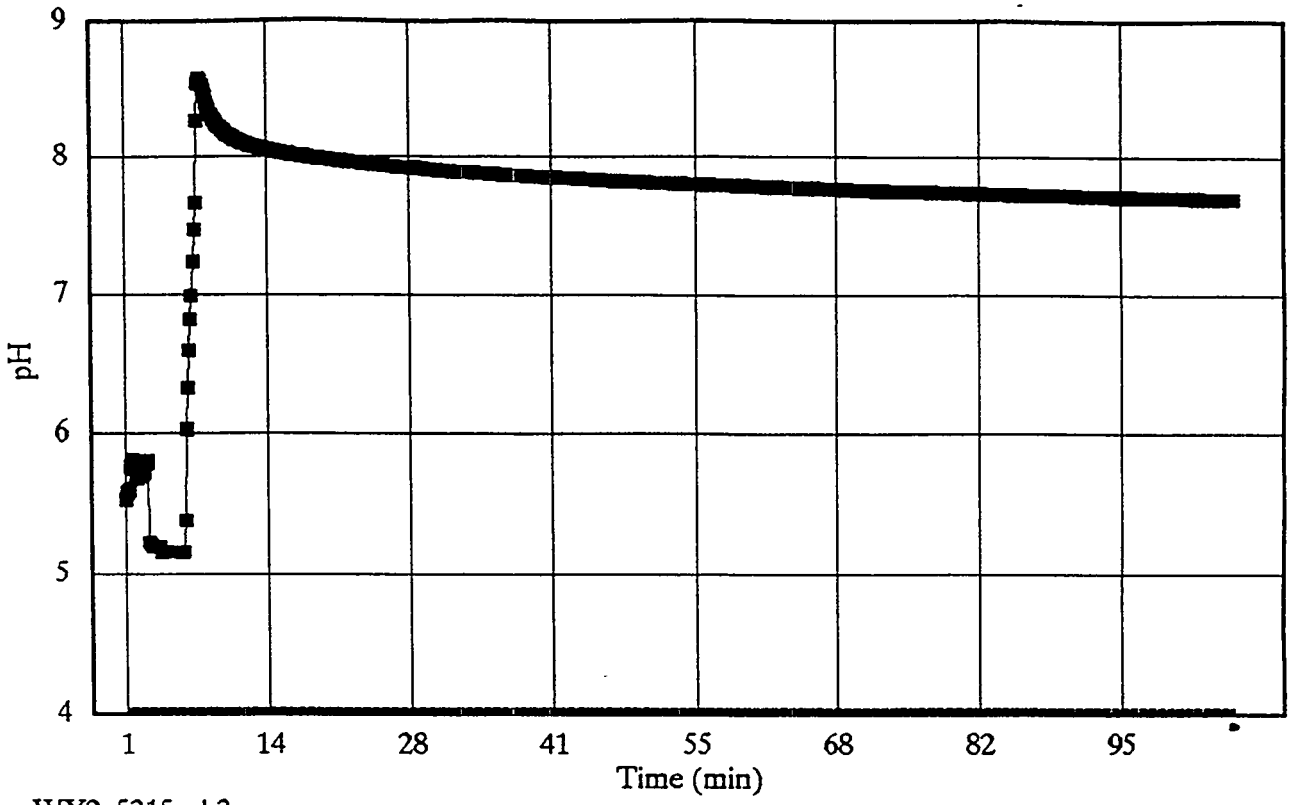

WY2_5315.wk3
pH 2

Fig. 3 CaCO3 Slurry pH

5/22/95

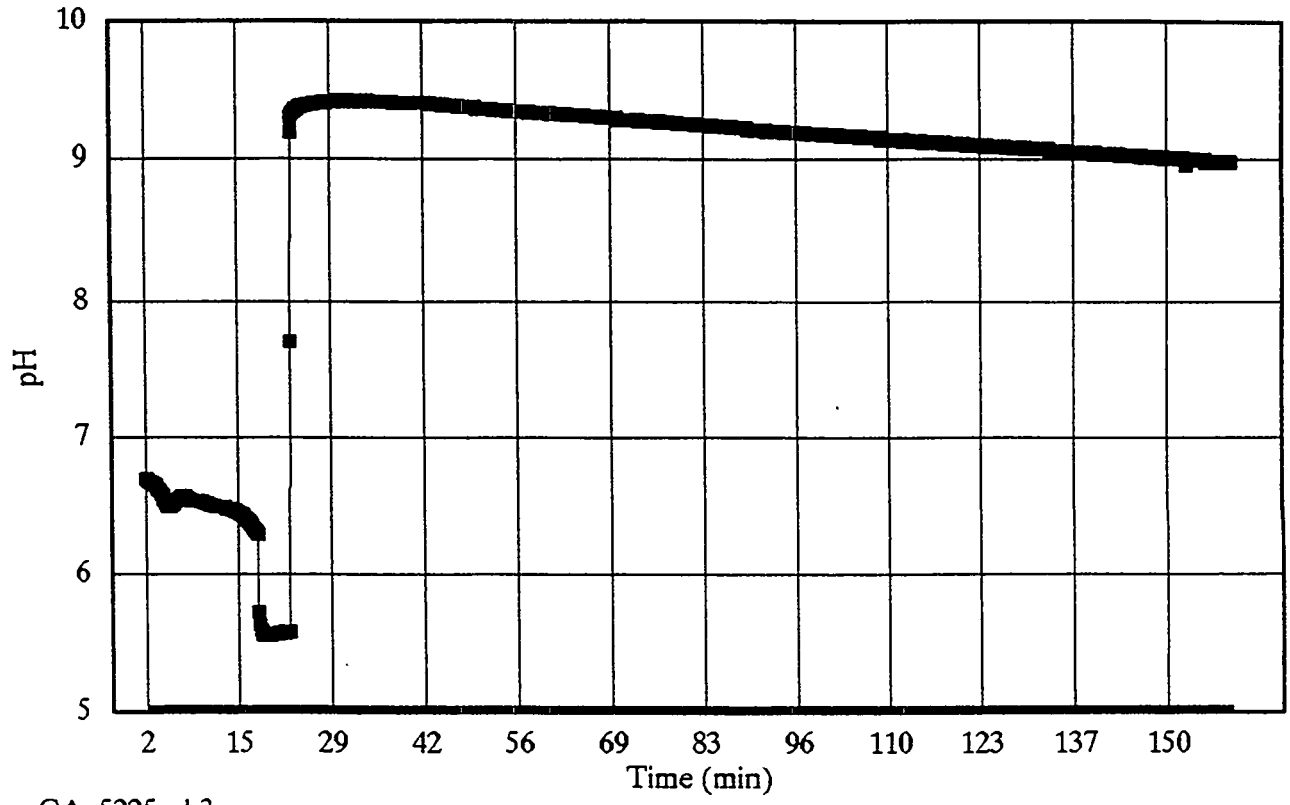

CA_5225.wk3
pH 2

Fig. 4 Pyrite slurry pH

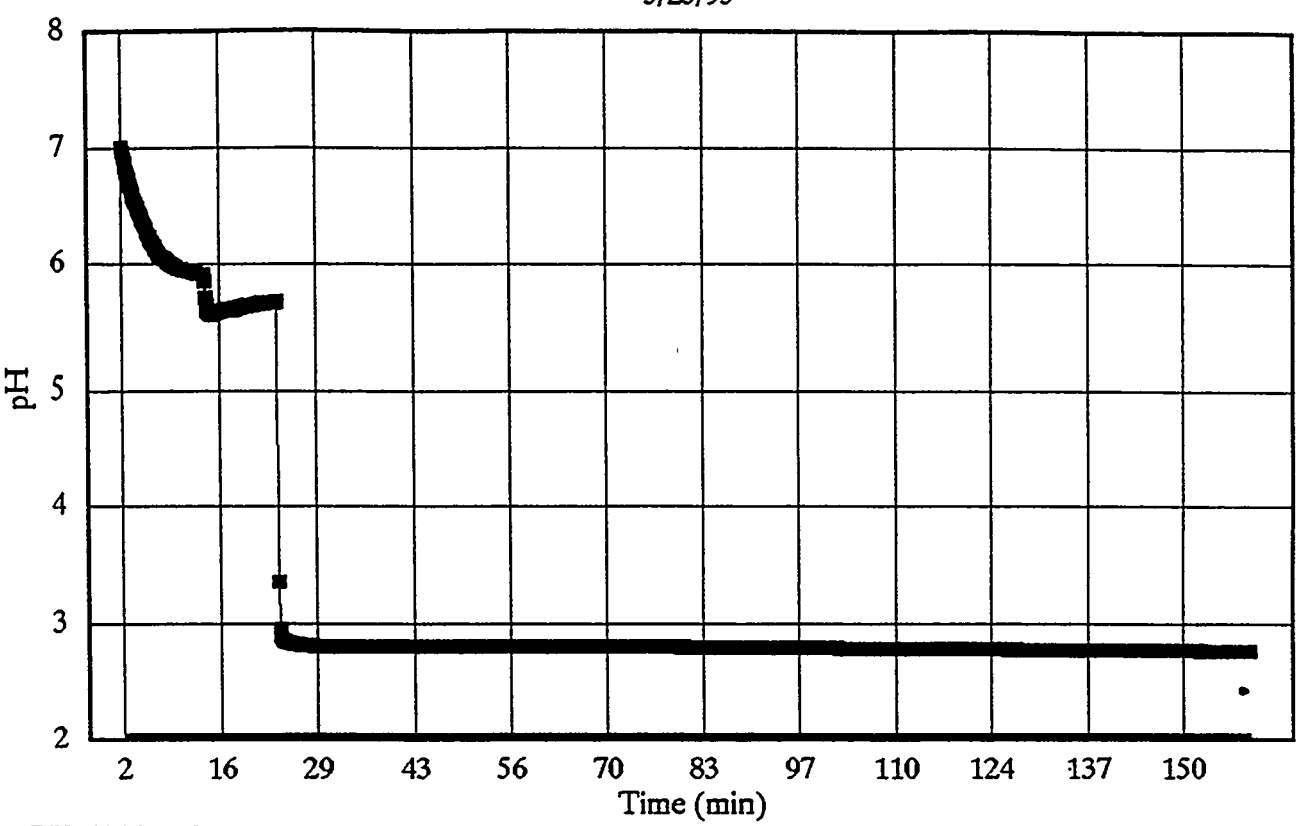

PY_5255.wk3
pH 4

Fig. 5 Graphite slurry pH

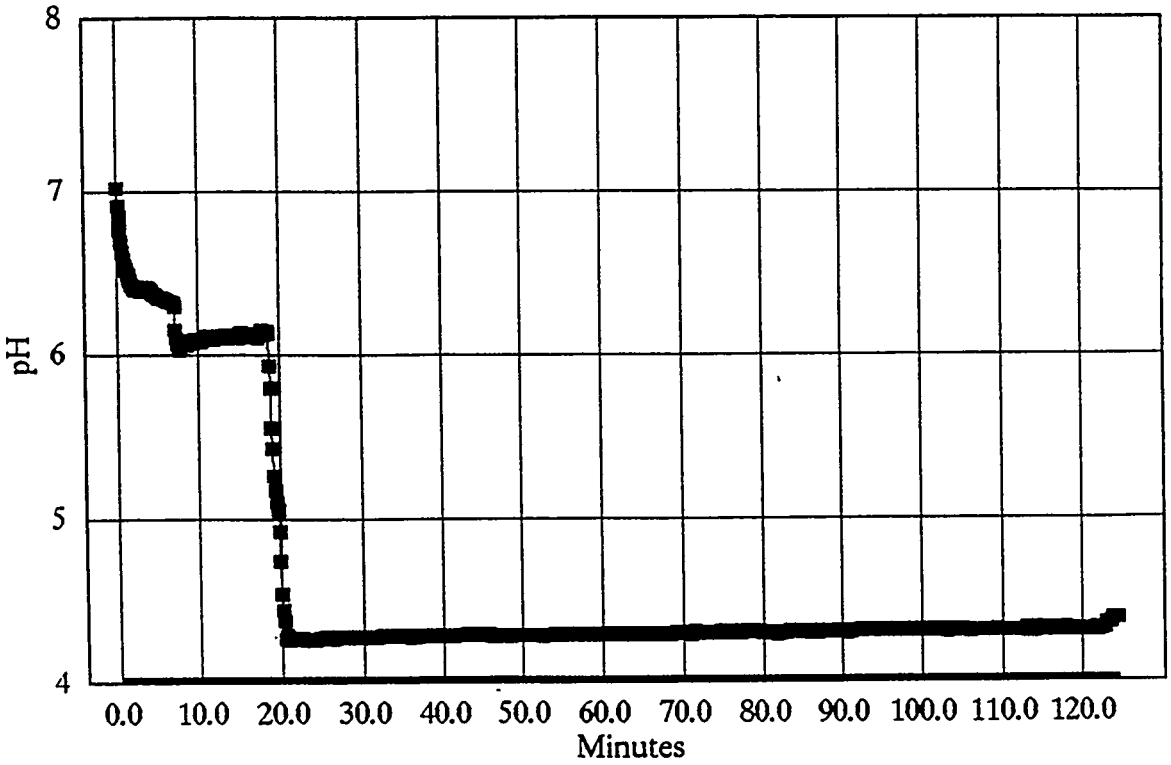

GR1025A4.wk3
pH 5

INDIRECT LIQUEFACTION

RATIONALE FOR CONTINUING R&D IN INDIRECT COAL LIQUEFACTION

David Gray and Glen Tomlinson
The MITRE Corporation
7525 Colshire Drive
McLean, Va 22102

Contract No: Sandia National Laboratories Contract AL-4159
Period of Performance: July 1994-October 1995

OBJECTIVE:

The objective of this analysis is to use the world energy demand/supply model developed at MITRE to examine future liquid fuels supply scenarios both for the world and for the United States. This analysis has determined the probable extent of future oil resource shortages and the likely time frame in which the shortages will occur. The role that coal liquefaction could play in helping to alleviate this liquid fuels shortfall is also examined. The importance of continuing R&D to improve process performance and reduce the costs of coal-derived transportation fuel is quantified in terms of reducing the time when coal liquids will become competitive with petroleum.

ACCOMPLISHMENTS AND CONCLUSIONS:

At the last World Energy Congress meeting in 1992[1], MITRE presented a world energy demand model that was used to estimate total commercial world energy demand to the year 2100. Several future world energy demand scenarios were developed. These scenarios assume that developing countries with low energy consumption per capita but high growth rates in per capita energy consumption, will mimic the rates of change of energy demand that countries ahead of them already experienced in their development progression. The analysis shows that there is an excellent correlation between average annual change in commercial energy (commercial energy is all traded energy but excluding traditional fuels like fuelwood, charcoal, bagasse etc.) use per capita and average energy consumption per capita. This correlation was used to calculate the per capita energy use for each country in the world for each year from the present to 2100. The total world energy demand was then calculated by multiplying these per capita energy consumptions by the population of each country projected to 2100.

This methodology resulted in the world energy demand estimates shown in Figure 1. The upper curve assumes no further efficiency improvements than the present, the lower curve

assumes that future energy conversion and end-use efficiencies will continue to improve in the coming century. It is assumed that, after 33 years, existing equipment is replaced by new equipment saving 33 percent of the energy. This 33 year cycle continues for another two cycles of continuing efficiency improvements saving an additional 16.6 and 8.3 percent per cycle. These assumptions are consistent with historical improvements. The result of these cumulative efficiency improvements reduces the world commercial energy demand from 2,090 quads in the no-improvement upper curve case to about 1,050 quads, a three-fold increase over the present world energy demand.

Other analysts and organizations have estimated future world energy demand using various models, and the MITRE estimate is in good agreement with Holdren,[2] Greenpeace[3] and the U.S. Environmental Protection Agency (EPA).[4] The average of the EPA *Rapidly and Slowly Changing World Cases* gives a total world demand of 1,050 quads by the year 2100, in exact agreement with this analysis.

The hypothetical world energy demand scenario shown in Figure 1 estimates that, by 2100, demand may be three times the current demand. How can this demand be satisfied with known energy resources? To answer this, it is necessary to determine the world resource of oil and natural gas, and to make an assumption concerning the availability of nuclear power. Based on estimates from the United States Geological Survey (USGS)[5], the world ultimate resource of conventional oil is estimated to be the sum of the remaining reserve of 1103 billion barrels and the mean of the undiscovered resource of 583 billion barrels to give a total of 1.7 trillion barrels or about 10,000 quads. Because estimates for natural gas are less certain, two ultimate resource levels were assumed. These were: 10,000 quads[6] (10,000 trillion cubic feet TCF) and twice this resource (20,000 quads). Further, it was assumed that there would be no new starts for current technology nuclear plants after the year 2000. Figure 2 shows depletion curves for these resources. Any number of different depletion curves could be investigated, but the point illustrated is, that by 2100, oil and natural gas are essentially depleted. For the high gas assumption, there is still a gas resource remaining, although by 2100 even that is in rapid decline. Not shown in Figure 2 is a resource for coal. Coal availability worldwide is enormous with estimates ranging from 45,000 quads[7] for proved reserves in place, to 240,000 quads[8] for total resource in place. This represents between 500 and 2000 years supply of coal at current usage rates.

Having established the conventional fossil energy supply resource for the world and having estimated a hypothetical world energy demand scenario, these can be superimposed to produce a world energy demand/supply scenario of the type shown in Figure 3. In this scenario, it is assumed that the oil, gas, and present day nuclear follow the depletions shown in Figure 2, coal use remains constant at the present level, and hydroelectric potential triples between now and the year 2100. The area designated as *21st century* in Figure 3 represents

the energy shortfall not satisfied by conventional fossil, present day nuclear, and hydroelectric. For this *constant coal use scenario,* this shortfall would have to be supplied by a combination of 21st century nuclear energy technologies and renewable or sustainable energy technologies.

Figure 3 shows that before the year 2030, demand on world oil is such that supply cannot keep pace, and world oil supply starts to decline. This scenario is conservative by assuming that world oil use is essentially constant from the present to 2030. Recent data shows that world oil use is increasing. According to International Energy Agency (IEA)[9] estimates, worldwide consumption of petroleum increased by 1.1 million barrels per day to 68.2 MMBPD in 1994. IEA further estimates that total world demand will increase again by 1.1 MMBPD in 1995 to 69.3 MMBPD. The largest demand increase will occur in Asia (7.6 MMBPD). IEA further estimates that world oil demand will increase to 77 MMBPD by the year 2000, and 92.5 MMBPD by 2010. If oil use does in fact increase significantly worldwide instead of remaining essentially constant as depicted in Figure 3, then demand pressures will hasten the imbalance of oil supply and demand causing the decline to occur before the year 2030.

The U.S. currently produces about 17 quads annually of domestic crude oil and natural gas liquids (NGL) and this production is expected to continue its decline in the future. Figure 4 shows a resource depletion scenario for oil, natural gas, and power from current nuclear plants from the present to the year 2100. These depletion curves are based on the EIA[1] assumptions to the year 2010, and on MITRE energy model assumptions thereafter. The resource base used in this analysis is 136 billion barrels of conventional oil, 1300 TCF of natural gas and for NGL it is assumed that the present rate of production equal to 12 percent of natural gas production on a thermal basis is continued. It is assumed that nuclear energy from current technologies phase out over the time period shown. Justification for using these resource amounts comes from several sources. The Oil Resources Panel[10] in 1992 led by W.L. Fisher, estimated that the U.S. Oil Resource base was between 99 billion barrels (for existing technology at $20/bbl) to 204 billion barrels (for advanced technology at $27/bbl). These resources are the sum of proved reserves, reserve growth in existing fields, and undiscovered resources. The Oil and Gas Journal[11] in a recent article quoting the new U.S. Geological Survey estimates states that "land and state waters of the U.S. contain technically recoverable volumes of 112.6 billion bbl of oil and 1,073.8 tcf of conventional and unconventional gas". The DOE Office of Oil and Gas[12] uses 136 billion bbls as the U.S. resource base. This quantity of oil is made up of the following categories: proved reserves (23 billion barrels oil (BBO)), expected reserves with field development using existing technology (29 BBO), advanced recovery potentials (23 BBO), new reserves through existing exploration technology (37 BBO), new reserves with advanced exploration technology (16 BBO), and advanced recovery potential from discoveries (8 BBO). For

natural gas, an average of several independent estimates has been used. These estimates are described in detail in a 1994 article in the Oil and Gas Journal[13].

Imports must be used to make up the shortfall in consumption and this analysis considers two import scenarios that may be applied to the U.S. energy situation from now till 2050. The first scenario assumes that the current U.S. consumption equal to 26 percent of total world petroleum consumption continues out to the year 2050. In this scenario, after about the year 2025, petroleum supply starts to decline because of worldwide supply inadequacies. The second scenario assumes that the quantity of oil that the U.S. can import is proportional to its GDP compared to the total world GDP. As the total world GDP increases due to increasing economic prosperity, so the U.S. percentage of total world GDP declines and thus the level of oil imports declines correspondingly. In this case, the decline is more rapid than the prior assumption of 26 percent of world oil consumption. The point is that the U.S. may not be able to keep on increasing its level of imports continuously without limit.

It is now necessary to turn to expected demand for energy in the U.S. in the future. Figure 5 shows two demand scenarios superimposed on the previously discussed supply scenarios. The higher demand scenario is taken from the EIA Annual Energy Outlook 1995[14] to the year 2010. The essentially constant demand scenario is from the MITRE energy model. If the EIA scenario is correct and U.S. imports are limited by GDP considerations, then a shortfall in required petroleum over domestic plus imports would occur before the year 2005. This shortfall would become significant by 2010. If the constant demand scenario is correct and imports are GDP limited, then a shortfall begins at 2015 and becomes significant (about 7 quads or 3.5 million barrels per day) in the year 2030. If imports are limited by 26 percent of total world consumption, the shortfall in 2030 would be about 1 million barrels per day. The probable situation may lie between these two scenarios, with a resulting shortfall in petroleum between 1 and 7 million BPD in 2030.

This shortfall in conventional petroleum could be supplied in part by utilizing non-conventional heavy oils and bitumens, extraction and use of immobile remaining oil, and by converting coal into liquid fuels. The heavy oil resource worldwide is estimated to be over 600 billion barrels, but very little of this is domestic. Most of this occurs in South America, the former Soviet Union, and Canada. In the U.S. the resource occurs in California and Alaska. The Alaskan resource may be difficult to recover since it is under the permafrost and the California resource is relatively small. Heavy oils are characterized by their low API gravity (<20API), high viscosity, high sulfur and nitrogen content, high asphaltene content, and very high metals content. These oils are so heavy that they must be mined or extracted using steam injection or other tertiary recovery methods. Refining of these heavy oils, that are predominantly residual material, when technically feasible, is expensive and requires sophisticated resid hydrocracking technologies. In contrast liquids from coal conversion

technologies are easier to refine because they are either high quality diesel fuel (cetane of 75) and high quality low-aromatic gasoline such as are obtained from indirect liquefaction, or all-distillate, low sulfur and nitrogen liquids as obtained from direct liquefaction.

As mentioned above, this potential shortfall in petroleum in the 2005-2030 time frame, depending on the above assumed scenarios, could in part be made up by converting coal into high quality transportation fuels. If coal conversion technologies are to play a role in alleviating this potential world liquid fuel supply problem by or before the year 2030, then the technologies must be in a state of readiness for commercial deployment. From a technology standpoint, typical lead times for the introduction of new energy technologies can be in the order of 10 to 15 years even when the technologies are in a state of readiness for commercial deployment. For coal conversion technologies, considerable research and development still needs to be undertaken to achieve this state of technology readiness. In addition to preparing the technologies for deployment, continuing R&D can substantially reduce the cost of coal-derived fuels by improving process performance. Commercial deployment of technologies to produce fuels from coal should begin before the year 2015 in order for them to make a significant contribution to alleviating the liquid fuels shortfall in 2030.

Since the transportation sector would be the predominant user of petroleum, transportation fuels that meet the strict environmental regulations expected to be in force in the next century would be needed. These fuels can be made from domestic coal resources by both indirect and direct liquefaction technologies. Presently the cost of fuels from coal using these technologies is too high to compete with petroleum at $17-18/bbl. The cost of coal-derived fuels have been significantly reduced by R&D since the early 1980s, and continued R&D is likely to reduce the cost so that they are competitive with petroleum in the range of $25-$28 per barrel.

Technologies to convert coal to high quality liquid transportation fuels can be either indirect or direct. Indirect liquefaction uses gasification technology to produce a synthesis gas from coal, and this gas is cleaned and passed over catalysts to make either hydrocarbons or oxygenates. The important point to understand is that coal-derived liquids from indirect liquefaction are high quality, zero heteroatom, paraffinic gasoline and diesel components requiring minimal refining.

DOE contracted Bechtel[15] to develop a conceptual commercial designs of indirect coal liquefaction facilities to produce refined liquid transportation fuels from both Illinois and Wyoming coals. These designs were based on current technology that include Shell coal gasification and slurry-phase Fischer-Tropsch (SFT) technologies. The Shell technology has been demonstrated at a 200 TPD pilot facility in Texas, and a full-scale commercial facility

has recently been completed in the Netherlands for production of electric power in an Integrated Coal Gasification Combined Cycle (IGCC) facility. The SFT technology is being developed by DOE and Air Products at the Laporte Alternative Fuels Development Unit (AFDU), by Exxon, and by SASOL in South Africa.

The Bechtel baseline design represents the current state of the technology and the costs associated with this baseline are in the order of $34 per barrel crude oil equivalent (COE) for a conceptual commercial plant processing about 28,000 tons per day of Illinois coal and producing about 72,000 BPSD of refined gasoline and diesel fuels. This baseline is a snapshot of the current state of the technology, but the technology is emerging and is therefore at an immature level of process development. Considerable R&D needs to be conducted to bring this promising technology to maturity. R&D is also needed to consolidate the current conceptual baseline technology. Proof-of-concept (POC) testing of system components is necessary to verify the performance assumed in the conceptual baseline design, especially in the areas of slurry Fischer-Tropsch synthesis and product refining. Also, component integration is needed to verify continuous operation of the complete system from coal to products.

The main areas where R&D can make the greatest contribution to reducing the costs of this technology are in improving the SFT system and in reducing the cost of synthesis gas production from coal. For the SFT system, more active catalysts, combined with improvements in the performance of the slurry reactor system, have the potential to significantly reduce the costs of fuels. The cost of synthesis gas production is a significant element in the total cost of production of fuels from coal using indirect liquefaction, therefore reducing the cost of this component will impact the cost of fuels. This can potentially be achieved by improving the air separation system. Ceramic membrane systems currently in the early stages of development by Amoco, ANL, and APCI, could significantly reduce both the costs and the energy required for oxygen production and hence will reduce synthesis production costs.

Table 1 shows the current elements of cost for the baseline indirect conceptual commercial plants, and the estimated reduction of costs that can be achieved by further R&D in the product refining, SFT, and synthesis gas production areas. It is estimated that costs of transportation fuels can be reduced from about $34 per barrel crude oil equivalent to $27 per barrel by about the year 2010 by continuing R&D in this area.

Figure 6 shows the estimated impact of this continued R&D on the time that the costs of fuels from indirect liquefaction will be competitive with the world oil price (WOP). This Figure shows the WOP estimate of the EIA[14] from the present to the year 2010. After 2010, the WOP is extrapolated linearly to the year 2035. With no further R&D other than that

necessary to consolidate the present technology base, the COE cost of indirect liquids will remain at the Bechtel baseline cost of about $34 per barrel. The cost of indirect liquids would then only be competitive with the projected WOP in the year 2030, where the no R&D line and the WOP line intersect. With continuing R&D, and with the expected resulting cost reductions detailed in table 2, the cost of indirect liquids will be reduced to about $27 per barrel. Thus, transportation fuels from indirect liquefaction will be competitive with the WOP by about 2015 compared to 2030; 15 years earlier than if no further R&D was conducted.

This 15-year grace period, provided by the cost reductions as a result of further R&D, is very important if coal-derived fuels are to make a timely contribution to the potential shortfall in liquid fuels in the U.S. that was discussed earlier. If it is accepted from the earlier discussion that this liquid fuels shortfall will occur in the 2025-2030 time frame, and the magnitude of this shortfall is between 1 and 7 quads, then between 1 and 7 quads of fuels from coal should be available by 2030. This would be the case if the construction of commercial plants can be started by about 2012. This start date for construction would be feasible if coal-derived fuels were to be competitive with the WOP by the year 2015 as discussed earlier. On this construction schedule, about 15 indirect liquefaction plants could be in production by 2030, producing over 2 quads of transportation fuels from domestic resources of coal. However, if no further R&D were conducted and the cost of coal-derived fuels remained at about $34 per barrel, then commercial plant construction would not start until the year 2030, too late to make any timely contribution to the shortfall in fuel demand by 2030.

Indirect coal liquefaction technology is not necessarily limited to producing an all-liquid product slate. Plants that coproduce both transportation fuels and electric power have great potential. The synthesis gas from coal gasification after purification can be passed once-through the SFT reactors, and the unconverted tail gas can be sent to gas turbines for power production. This configuration eliminates the costly FT recycle section of the plant, and produces two valuable products, power and fuels. Depending on the location, additional coproducts such as hydrogen, alcohols, and chemicals can be produced with the power and fuels. Configurations can also be developed that would allow load following capabilities if needed. With power priced at break even cost, the resulting COE cost of liquid fuels is reduced by 25 percent compared to the baseline liquids-only plant using a once-through F-T configuration with coproduction of electric power.

Production of high quality transportation fuels from U.S. coal will be a domestic industry that will employ engineering and construction people, plant operators, coal miners, and indirect manpower. It has been estimated that the total number of jobs that would be created by the proposed one million barrel per day industry is approximately 330,000.

Indirect coal liquefaction is an example of how coal can be cleanly converted from solid fuel to a clean synthesis gas, and this gas is transformed into clean, zero sulfur, ultra-low aromatic gasoline, diesel and oxygenated fuels. Byproducts of this process are elemental sulfur, ammonia, and a non-leachable slag. Although the process is essentially non-polluting, carbon dioxide is emitted during the transformation of coal to liquid hydrocarbon fuels. There is concern that anthropogenic carbon dioxide may be responsible, in part, for global climate change, and, if coal is to be used as a resource to produce liquid fuels, will the resulting carbon dioxide emissions be significantly increased in the U.S.? Figure 7 shows an energy mix that will result in no further increase in carbon dioxide emissions in the U.S. over the present. This shows that, because of the decrease in oil and gas, coal use can be increased substantially (by about 7 quads) after 2015 with no net increase in carbon dioxide emissions. If all of this additional coal were to be used for production of liquid fuels, then this would represent about 2 million barrels per day of coal-derived fuels.

References:

1) Gouse, S.W., D.Gray, G.C. Tomlinson, D.L. Morrison. *Potential World Development through 2100: The Impacts on Energy Demand, Resources, and the Environment,* World Energy Council Journal, December 1992.
2) Holdren, J.P. *Energy in Transition,* Scientific American pp 157-163, Sept 1990.
3) *Energy Without Oil,* Greenpeace International, March 1993.
4) *Policy Options for Stabilizing Global Climate,* published by Hemisphere Publishing Corporation, 1990, Editors, Lashof and Tirpak, U.S. EPA.
5) 14th World Petroleum Congress, Norway, May 1994, Assessment of USGS.
6) Masters, C.D., *Oil and Gas- Where in the World and Why?,* 8th V.E. McKelvey Forum on Mineral and Energy Resources, Houston, Tx, Feb 1992.
7) World Resources Institute 1994-5, *People and the Environment,* published by WRI in collaboration with UNEP and UNDP, Oxford University Press, 1994.
8) World Reserves Survey 1987, published by IGT, 1989.
9) Oil and Gas Journal, Jan 30, 1995, p 70./ OGJ May 9, 1994.
10) *An Assessment of the Oil Resource Base of the United States Oil Resources Panel,* Report prepared for U.S. DOE by Bureau of Economic Geology, The University of Texas at Austin, and the National Institute for Petroleum and Energy Research. DOE/BC-93/1/SP October 1992.
11) *Partial U.S. Oil, Gas Resource Volumes Termed Astonishing,* Oil and Gas Journal, March 6, 1995, p 84
12) DOE/BPO TORIS, 1992; BEG/NIPER, 1992; DOE/FE OGPT, 1995.

13) Fisher William, L. *How Technology has Confounded U.S. Gas Resource Estimators,* Oil and Gas Journal Oct 24, 1994, p.100
14) Annual Energy Outlook 1995. Energy Information Administration January 1995.
15) *Baseline Design/Economics for Advanced Fischer-Tropsch Technology,* report prepared by Bechtel/Amoco for DOE under contract DE-AC22-91PC90027, Oct 1994.

ACKNOWLEDGMENT:

This work, performed at the MITRE Corporation, was supported by Sandia National Laboratories under contract number DE-AC-04-94AL95000.

TABLE 1: ESTIMATED COST IMPACT OF CONTINUED R&D ON INDIRECT LIQUEFACTION

Elements of Cost $MM	Baseline 18,550tpd	Increased Plant 27,863 tpd	Improvements in Product Refining	Improvements in F-T Synthesis	Improvements in SynGas Production
Coal Handling	143	207	207	207	207
Gasification	703	1,018	1,018	1,018	1,018
Air Separation	322	466	468	468	323
Gas Cleaning/ByProduct Recovery	135	195	195	195	195
Fischer-Tropsch Synthesis	223	331	354	190	190
Synthesis Gas Recycle Loop	278	403	427	352	352
Product Refining	144	209	129	131	131
ISBL Field Cost	1,948	2,829	2,798	2,561	2,416
Power Generation	83	119	78	103	254
OSBL Field Cost	336	488	490	478	481
Total Field Cost	2,367	3,436	3,366	3,142	3,151
Total Plant Cost	2,950	4,283	4,195	3,916	3,927
Total Capital	3,181	4,620	4,529	4,228	4,231
Refined Product Cost	$/BBL	$/BBL	$/BBL	$/BBL	$/BBL
Capital	25.60	24.79	23.85	21.85	21.87
Coal	10.16	10.16	9.97	9.79	9.79
Catalyst	1.96	1.98	1.94	1.91	1.91
Other O&M	5.83	5.48	5.40	4.90	4.92
Power	1.24	1.24	2.01	1.28	-2.04
RSP	44.79	43.65	43.17	39.73	36.45
COE	35.49	34.35	33.87	30.43	27.15
Plant Output Barrels per year	15,796,097	23,691,630	24,133,433	24,592,583	24,590,739

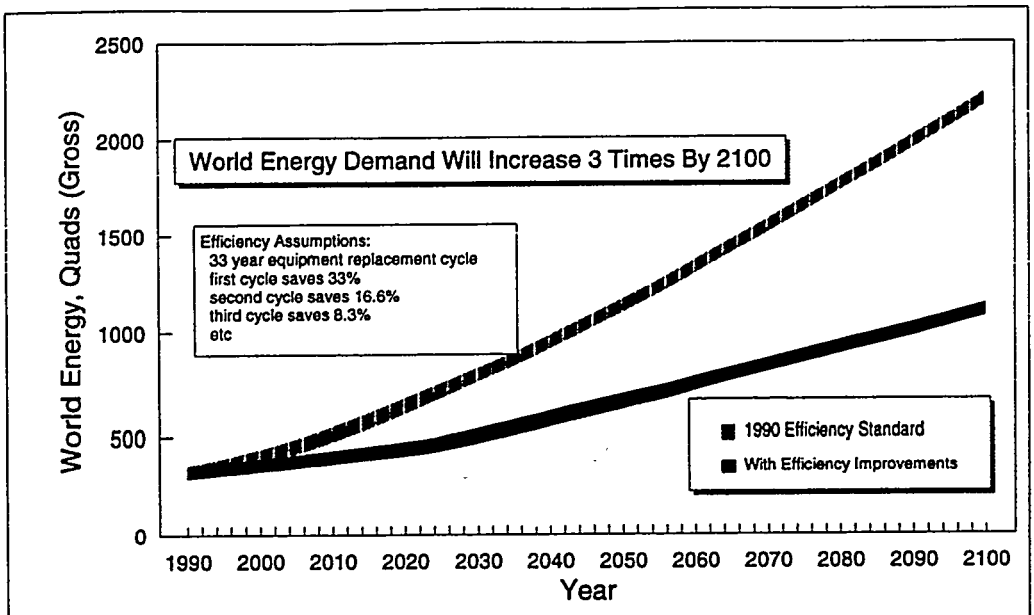

Figure 1: World Energy Demand Projections

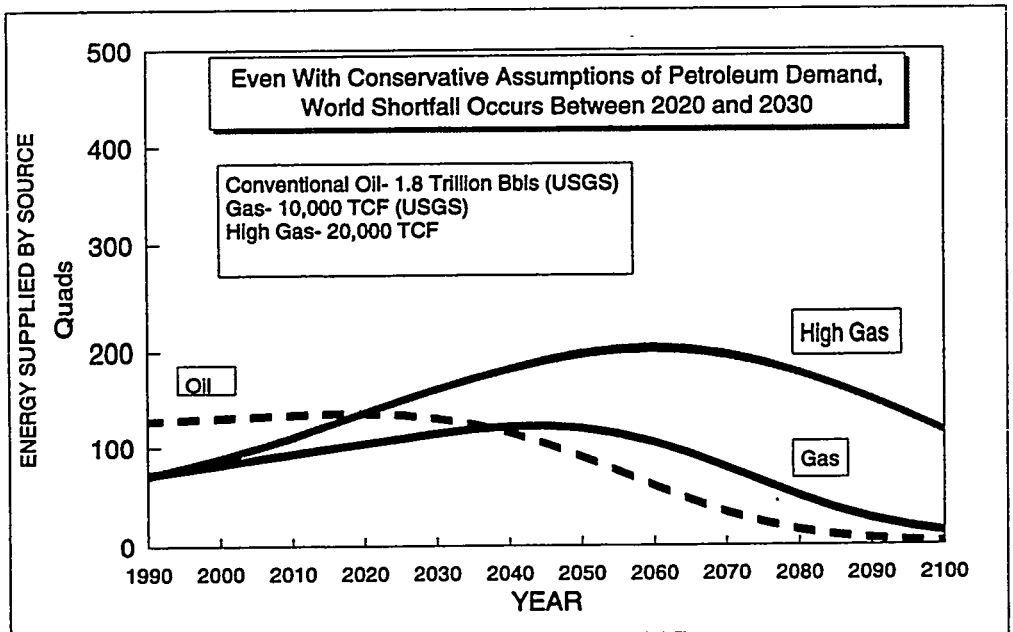

Figure 2: Depletion Curves for World Resources

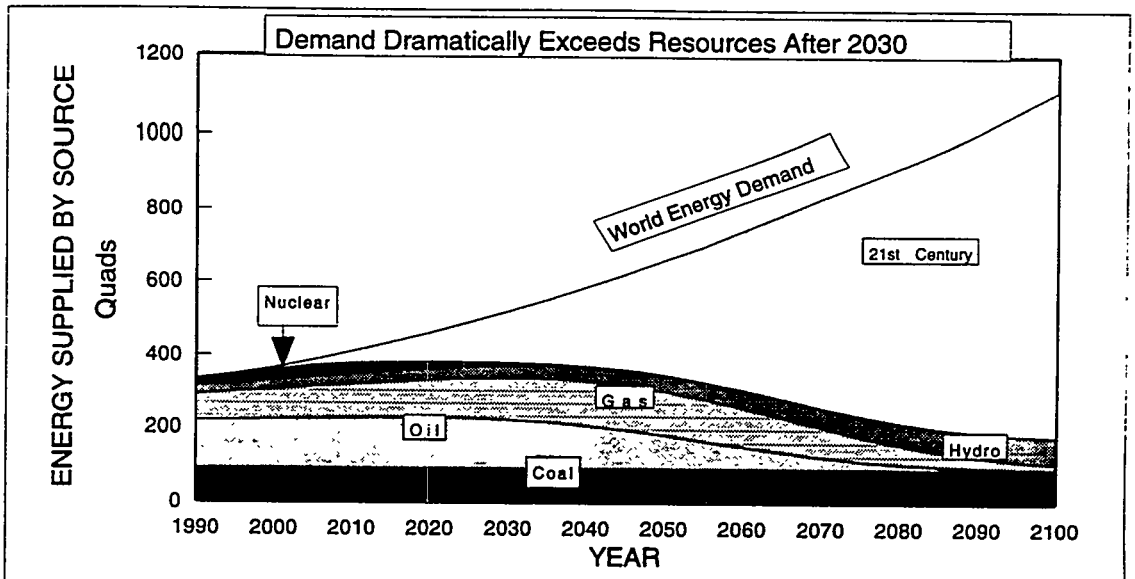

Figure 3: World Energy Mix for Nominal Oil and Gas With Constant Coal Use

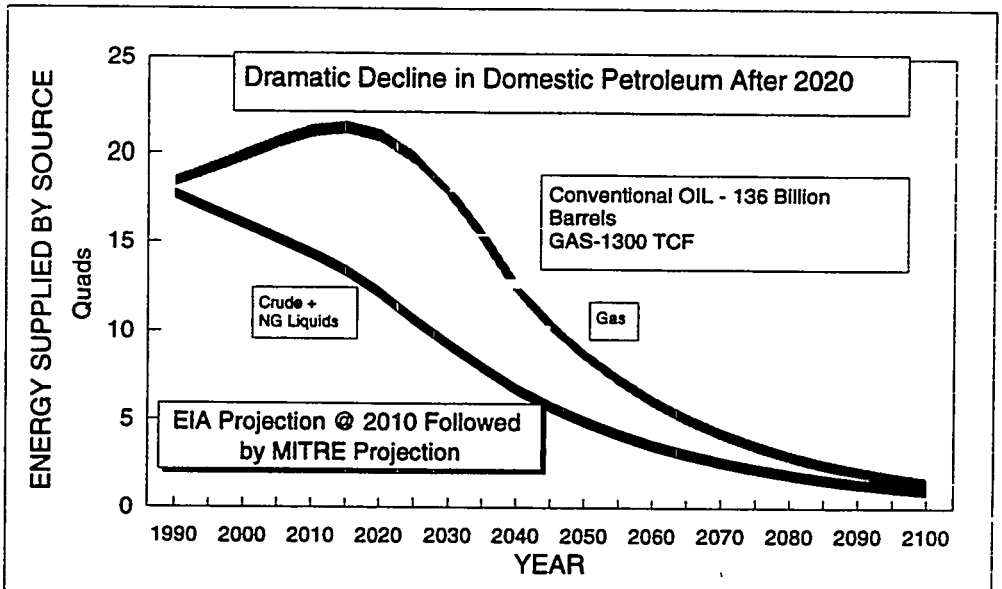

Figure 4: Depletion Curves for U S Domestic Oil and Gas

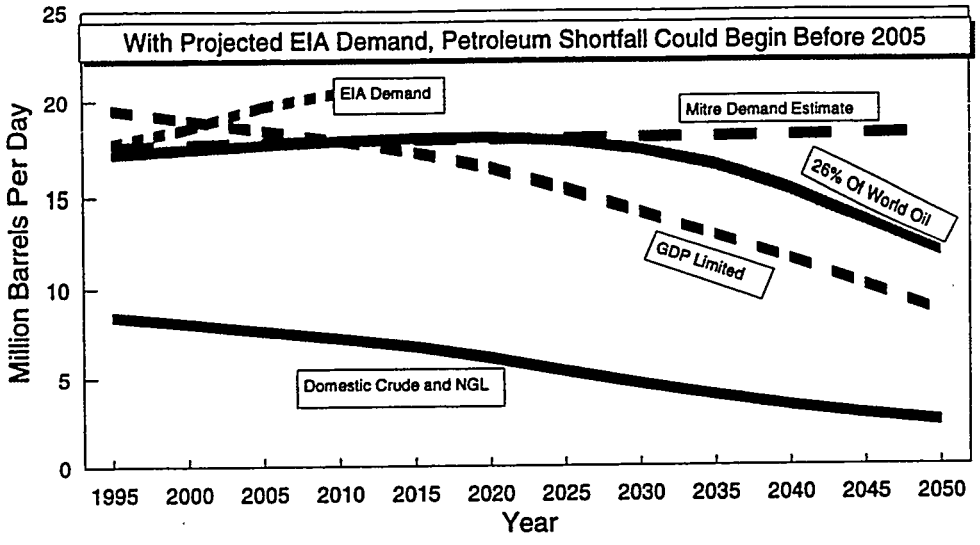

Figure 5: U S Oil Supply And Demand Scenarios

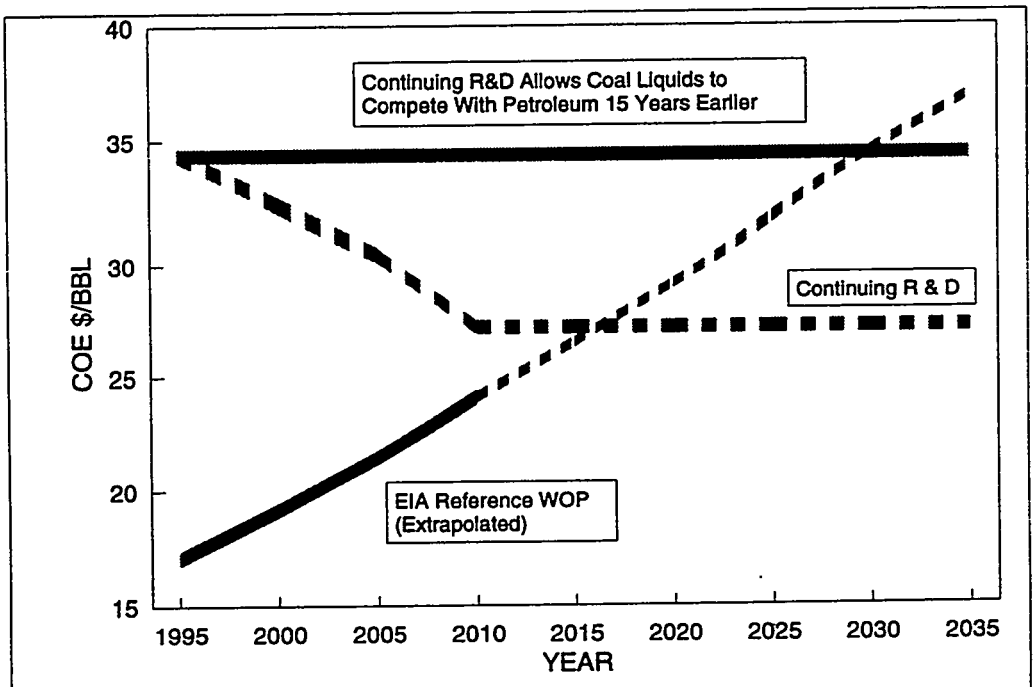

Figure 6: Cost Impact of R&D in Indirect Liquefaction

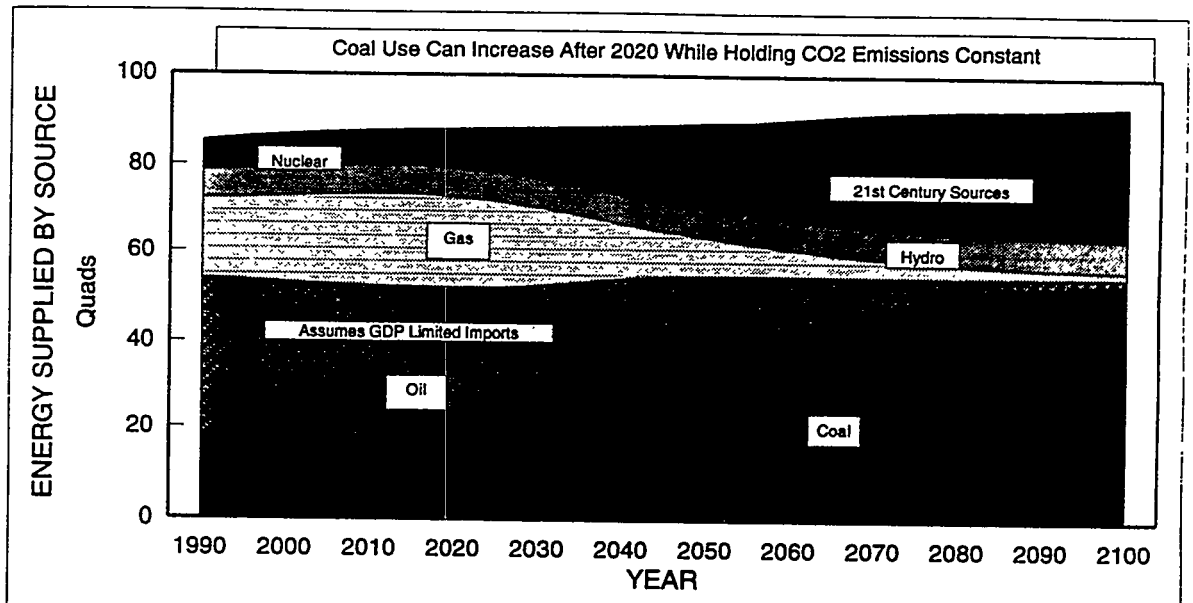

Figure 7: U S Energy Mix For Constant Carbon Dioxide Emissions

1995 COAL LIQUEFACTION AND GAS CONVERSION CONTRACTORS' REVIEW CONFERENCE

Title: Technology Development for Iron Fischer-Tropsch Catalysts

PI (Authors): Robert J. O'Brien, Ajoy Raje, Robert A. Keogh, Robert L. Spicer, Liguang Xu, Shiqi Bao, Ram Srinivasan, Deborah J. Houpt, Sivaraj Chokkaram, and Burtron H. Davis

Institution/Organization: Center for Applied Energy Research, University of Kentucky

Contract Number: DE-AC22-94PC94055

Period of Performance: October, 1994 - May, 1995

Objective:

The objective of this research project is to develop the technology for the production of physically robust iron-based Fischer-Tropsch catalysts that have suitable activity, selectivity and stability to be used in the slurry phase synthesis reactor development. The catalysts that are developed shall be suitable for testing in the Advanced Fuels Development Facility at LaPorte, Texas, to produce either low- or high-alpha product distributions. Previous work by the offeror has produced a catalyst formulation that is 1.5 times as active as the "standard-catalyst" developed by German workers for slurry phase synthesis. In parallel, work will be conducted to design a high-alpha iron catalyst this is suitable for slurry phase synthesis. Studies will be conducted to define the chemical phases present at various stages of the pretreatment and synthesis stages and to define the course of these changes. The oxidation/reduction cycles that are anticipated to occur in large, commercial reactors will be studied at the laboratory scale. Catalyst performance will be determined for catalysts synthesized in this program for activity, selectivity and aging characteristics.

Accomplishments & Conclusions:

Task 1.0. Development of Optimum Promoter Levels for Low- and High-Alpha Catalysts

The goal of this task is to identify and optimize procedures for the preparation of iron-based catalysts that combine high activity, selectivity and life with physical robustness.

The powder sample of RJO-181 (30 wt.% Fe_2O_3/SiO_2) was used for the evaluation of the microhardness test for defining attrition resistance. Cold molds using epoxy hardeners were used to prepare the specimens. After imbedding the particles in the epoxy, they were allowed to harden. Then the epoxy molds were polished.

Several particles were photographed in the optical microscope. Using a MICROMET-4 hardness tester, the microhardness measurements were made. The specimen was mounted onto the hardness tester, and a load of 25 gm was used to make the Vicker's indentation on the particles, which are 10 to 50 microns in size. The indentations were so large that they covered the entire particles. Hence, a load of 10 gm (the minimum load available) was used to make the indentations on several individual particles embedded in the epoxy mold. After making the indentations the specimen was mounted on the optical microscope and the diagonal distances of the indentations were measured. The average value of about 50 indentations was taken for measuring the Vicker's hardness, which was calculated to be 40 kg/mm. According to the ASTM standards, this number indicates that the material under investigation is very soft. The value of 40 is not accurate, as the hard epoxy under the particles can also take part of the load. This introduces additional uncertainty to the calculated value. Comparison of this value to other materials indicate that the iron oxide catalyst particles are very soft.

Task 2.0. Definition of Preferred Pretreatment for Both Low- and High-Alpha Catalysts

The goals of this task are to define the preferred treatment, to define the role of Cu and K during the pretreatment on activity and selectivity and to define the chemical and physical changes which occur during the preferred pretreatment.

Activation of the 100Fe/4.4Si/0.71K catalyst with synthesis gas was unsuccessful. Carbon monoxide conversion slowly increased to 12% and then stabilized after 92 hr. In a previous study, this catalyst showed high activity and productivity when pretreated with CO at 270°C, 175 psig for 24 hr: carbon monoxide conversions were found to exceed 90% for up to 300 hr of synthesis.

It was decided to determine the affect that a CO treatment would have on the inactive catalyst. After 92 hr of synthesis, the hydrogen flow was stopped and the catalyst was exposed to CO at 270°C, 175 psig, 2.0 L/hr-g(Fe) for 24 hr. Following the CO treatment, H_2 flow was resumed and the activity of the catalyst was found to rapidly increase to 84% CO conversion within 26 hr. The ultimate activity of the catalyst was similar to when it was pretreated with CO (Figure 1). The selectivity and productivity were also similar.

Powder X-ray diffraction analysis suggests that the catalyst was reduced to Fe_3O_4 during activation with synthesis gas; however, only a small amount of χ-Fe_5C_2 was formed. Treatment of the catalyst with CO for 24 hr increased the χ-Fe_5C_2 and ϵ'-$Fe_{2.2}C$ content at the expense of the Fe_3O_4. During the synthesis following the CO treatment, the peaks corresponding to ϵ'-$Fe_{2.2}C$ increased while the χ-Fe_5C_2 seemed to remained constant. Peaks corresponding to Fe_3O_4 were the most intense throughout the run. These findings are very similar to those found when the catalyst was pretreated with CO. Based on these preliminary results, it appears that the increase in activity when the inactive catalyst was treated with CO can be correlated with the formation of χ-Fe_5C_2 and/or ϵ'-$Fe_{2.2}C$.

Promotion with Cu is considered to aid the reduction of iron Fischer-Tropsch catalysts and would, based on the above, seem likely to increase the activity of the 100Fe/4.4Si/0.71K catalyst when activated in synthesis gas. The activity of the 100Fe/4.4Si/2.6Cu/0.71K catalyst following activation with synthesis gas was determined. The activity was substantially higher due to the Cu promotion; however, the catalyst never achieved the activity of the CO pretreated 100Fe/4.4Si/0.71K catalyst. It is interesting that the activity increased steadily from 26% to 51% CO conversion during the 200 hr the catalyst was run. In general CH_4 and C_2H_6 selectivity should be low at low CO conversion; however, promotion with Cu seemed to increase the CH_4 and C_2H_6 selectivity to the same level as when the catalyst was run at high conversion. Powder X-ray diffraction data show more intense χ-Fe_5C_2 and ϵ'-$Fe_{2.2}C$ carbide peaks for the Cu promoted catalyst than the catalyst with no Cu. This tends to support the finding that some iron carbide must be present for reasonable activity to be achieved. During the run, the amount of χ-Fe_5C_2 seemed to remain constant; however, the ϵ'-$Fe_{2.2}C$ peaks increased. It is tempting to correlate the increase in activity during the run with the increase in ϵ'-$Fe_{2.2}C$; however, a previous Mössbauer study with the CO pretreated 100Fe/4.4Si/0.71K catalyst showed no correlation between the amount of ϵ'-$Fe_{2.2}C$ or χ-Fe_5C_2 and activity.

Bukur reported high activity when synthesis gas activation ($H_2/CO=0.68$ at 280°C, 1 atm) was used on a precipitated iron catalyst promoted with K and Cu (1). In addition, Soled et al. report high activity for a Cu/K promoted iron-zinc catalyst activated in the slurry phase with a synthesis gas with $H_2/CO=2.0$ at 270°C and 75 psig (2). Kölbel successfully activated a K/Cu promoted precipitated iron catalyst with synthesis gas ($H_2/CO=0.67$ to 0.77) in a slurry phase demonstration plant (3). The catalyst was treated with the synthesis gas at a formation temperature ranging from 15°C to 30°C above the final operating temperature. The CO_2 production was monitored and the activation was considered complete a few hours after the CO_2 production reached its asymptotic limit. The temperature of the reactor was decreased to the operating temperature and the synthesis was begun. Kölbel considered the formation temperature to be critical; if it is too high the catalyst will deactivate due to carbonization and if it is too low the catalyst will not activate. It is possible that the activation temperature used in the present study was too low to completely activate the catalysts. It is also possible that the presence of silicon could have had a detrimental affect on the activation. Bukur reports that silica inhibits the reduction of Fe_2O_3 to iron carbides by CO (4). A similar affect would be expected with synthesis gas.

Activation with synthesis gas at 270°C and 175 psig ($H_2/CO=0.7$) is ineffective for a precipitated catalyst with molar composition of 100Fe/4.4Si/0.71K. The low activity achieved by synthesis gas activation may be related to the lack of bulk χ-Fe_5C_2 and/or ϵ'-$Fe_{2.2}C$ as seen by XRD. Promotion with Cu increased the extent of reduction of the catalyst and thereby substantially increased the activity of the catalyst when activated in synthesis gas; however Cu promotion did not increase the activity to the same level as when the catalyst is activated with CO. Promotion with silicon may

inhibit the reduction of the catalyst to an active state when synthesis gas is used during the activation procedure.

Syngas activation was carried out on catalysts with the following compositions in atomic % relative to iron: 100Fe/3.6Si/0.71K and 100Fe/3.6Si/2.6Cu/0.71K. Catalysts were loaded into a 1 L CSTR and mixed with a C_{30} oil to give a 10 wt % catalyst slurry. The reactor was pressurized to 13 atm under a flow of syngas (H2/CO=0.7, 3.1 NL h^{-1} g^{-1}(Fe)) and then heated to 270°C at 2°C/min. These conditions were maintained throughout the runs. A comparison of syngas conversion for the two runs is shown in Figure 2. The 100Fe/3.6Si/0.71K catalyst was inactive and had a total syngas conversion of only 18% after 92 hr on stream. Promotion with Cu increased the activity of the catalyst considerably. The syngas conversion for the 100Fe/3.6Si/2.6Cu/0.71K catalyst increased throughout the run and finally reached 50% before the reactor was shutdown due to loss of reactor solvent. X-ray diffraction shows that the 100Fe/3.6Si/0.71K catalyst was composed of Fe_3O_4 while the more active 100Fe/3.6Si/2.6Cu/0.71K catalyst was composed of a mixture of Fe_3O_4 and the carbides: χ-Fe_5C_2 and ϵ'-$Fe_{2.2}C$. Mössbauer spectroscopy also shows that the 100Fe/3.6Si/0.71K catalyst was composed of only Fe_3O_4 during the run. In general, the Cu promoted catalyst was composed of approximately 76% Fe_3O_4, 4% of some superparamagnetic component and 20% ϵ'-$Fe_{2.2}C$. These results are consistent with published results that Cu facilitates the reduction of iron oxide to an active state.

The affect of temperature (270°C or 300°C), pressure (13 atm or 1 atm) and gas composition (H_2/CO=0.7, 0.1 or 0) on the activation of precipitated iron catalysts with the compositions 100Fe/3.6Si/0.71K and 100Fe/4.4Si/1.0K was studied. In general, it was found that activation with H_2/CO=0.7 at 13 atm resulted in poorly active catalysts (CO conversion <20%) when activated at either 270°C or 300°C. Decreasing the H_2/CO ratio to 0.1 and activating at 13 atm and 270°C resulted in an activity intermediate between activation in pure CO or H_2/CO=0.7. This suggested that when activating iron catalysts with syngas it is desirable to have a low partial pressure of H_2. In fact, when the catalysts are activated with synthesis gas (H_2/CO=0.7) at 1 atm and 270°C or 300°C conversions comparable to activation with CO are obtained. No pressure affect was seen when the 100Fe/4.4Si/1.0K catalyst was activated with CO at 270°C and 13 atm or 1 atm. X-ray diffraction analysis of the catalysts following activation show that catalysts with low activity (those activated with syngas at 13 atm) are composed of only Fe_3O_4 while those with high activity (those activated with syngas at 1 atm or CO) are composed of a mixture of Fe_3O_4, χ-Fe_5C_2 and ϵ'-$Fe_{2.2}C$ (Figure 3). These results and the results mentioned above indicate that the formation of some iron carbide is necessary for high FTS activity. However, based on previous Mössbauer spectroscopy experiments, we know that the activity of iron catalysts is not related to the amount of iron carbide present. These results indicate that a surface carbide is the active phase.

The influence of H_2 partial pressure on syngas activation can be explained as follows. Based on XRD and Mössbauer spectroscopy results we know that CO or syngas pretreatment of precipitated iron catalysts will rapidly reduce the catalyst to

Fe_3O_4. According to the competition model proposed by Niemantsverdriet (5), surface carbon from dissociated CO can then do three things: become a carbonaceous layer, migrate into the bulk of the catalyst to form iron carbide or be hydrogenated to methyl or methylene groups which participate in the FTS. When an iron catalyst is activated with CO, the surface carbon can only become a carbonaceous layer or form a carbide which is presumed to be necessary for high FTS activity. In the case of syngas activation, H_2 is also present so hydrogenation of the surface carbon can take place. This causes a competition between carbide formation and hydrogenation. At high H_2 partial pressures the hydrogenation of the surface carbon occurs faster than carbide formation so only relatively inactive Fe_3O_4 is formed.

Iron catalysts that have high FTS activity contain bulk iron carbide and some amount of excess carbon. Pretreatment of the 100Fe/3.6Si/0.71K catalyst with CO at 270°C and 13 atm for 24 hr yields a highly active catalyst and yet produces about twice as much carbon as needed for the formation of Fe_5C_2. It is of interest to determine the role of this carbon in the FTS and determine its morphology.

Task 4.0. Catalyst Testing

The goals of this task are to operate the eight CSTRs, measure catalyst performance, determine the stable phases that exist during synthesis at low and high conversions and to determine the rates of interconversion of iron oxide and carbide.

A low alpha catalyst (4.4 atomic % Si relative to Si + Fe, 0.5 wt.% K, relative to K + Fe_2O_3) has been run for over 2000 hours (Figure 4) with a starting CO conversion of approximately 90%. Over this time period, the conversion decreased by 0.76% per week. This meets or surpasses the goal of 90% conversion and a decline in CO conversion of 1%/week.

The previously unexplained loss and re-establishment of activity has been found to be due to the lowering of the liquid level in the reactor. The conversion data shown in Figure 5 clearly show the loss of activity when rewax (wax from the reactor) was collected on a daily basis in the first 500 hours of the run. When the sampling of the rewax was stopped the activity recovered to approximately the initial level. Repeating this cycle produced a loss and gain of activity again. From these data, it was suggested that removing the reactor wax lowered the liquid level by physically removing the wax material and thus allowed more of the lighter material including the start-up oil to be removed from the reactor. After most of the start-up oil was removed and the reactor contained a sufficient amount of FTS wax, the reactor liquid level became stabilized and sampling of the reactor wax could be done without affecting the activity.

The kinetics of the Fischer-Tropsch synthesis was studied over the best low-alpha catalyst developed so far at the CAER to provide optimum reaction conditions for the utilization of this catalyst. Conversion data were obtained over the catalyst for a wide range of conversion levels (15-85%). The partial pressures and reaction rates

of the reaction components were calculated from the analysis of the reaction products. A number of possible reaction rate expressions were tested with the experimental data and an optimum reaction rate expression was developed for this catalyst.

Several kinetic studies have been carried out over iron-based catalysts as evidenced in the literature (6-9). The studies have been over fused iron catalysts as well as precipitated iron catalysts. From the nature of the reaction rate expressions developed, it can be clearly seen that a consensus is lacking in the literature. Especially important is the role played by water and/or carbon dioxide in the suppression of the reaction rate at higher synthesis gas conversions.

The Fischer-Tropsch reaction was carried out in a 1-liter stirred tank slurry reactor. The catalyst used is a precipitated iron catalyst (62 wt.% Fe) containing 4.4 atomic percent silicon and 0.5 wt.% potassium. The iron catalyst containing silicon (5.09 g) was placed in the reactor with 290 g of C_{28} paraffin and 0.0159 g of potassium was added in the form of potassium tertiary-butoxide. The reactor pressure was built up to 175 psig under CO atmosphere and subsequently heated to 270°C at a rate of 2°C/min. Pretreatment of the catalyst was carried out at 270°C, 175 psig using CO at a flow rate of 13.345 NL/hr for 24 hours. Subsequently synthesis gas flow was started at a H_2/CO ratio of 0.67. About two days were required before the catalyst reached steady state as evidenced by the constant conversion of synthesis gas. Subsequently, the space velocity of the synthesis gas was varied between 5 and 70 and conversions of CO, H_2, and the formation of various products were measured with a period of approximately 24 hours at each space velocity. The H_2/CO ratio of the feed synthesis gas was kept constant at 0.67 at all the space velocities. Periodically during the run, the catalyst activity was measured at pre-set "standard" conditions to check for catalyst deactivation. The conversions of CO, H_2 and synthesis gas are calculated from the inlet and outlet flow rates of these components from the reactor

Since the reactor used is a continuous-flow stirred tank reactor (CSTR), the reaction rates of disappearance of CO and H_2 and the rates of formation of products are obtained directly from the observed conversions. Further the reaction rates are uniform throughout the reactor as the partial pressures of the reactants and products are uniform throughout the reactor.

The partial pressures of the various components in the reactor are calculated from their mole fractions in the reactor outlet stream. Here the condensed product liquid in the condensers must be taken into account. Hence the composition of the product liquids is measured and averaged over the total mass balance period to obtain the moles per hour of the liquid products so as to compare the results with the composition of the uncondensed gas from the on-line gas chromatographs and thus obtain the mole fractions of each product and unconverted reactant in the vapor phase in the reactor.

The reaction run lasted for approximately 12 days. The catalyst activity at pre-set standard conditions during this run remained practically constant during the

course of the reaction run. The experimental error in the measurement of percentage conversion is about 2%.

Figure 6 shows the conversions of CO, H_2 and total conversion of CO and H_2 with space time in the reactor. The change in the percent conversion is much faster at low space times than it is at higher space times. Further at low space times the conversion of H_2 is greater than the conversion of CO while at higher space times the situation is reversed. The total CO and H_2 conversion at which the conversions of both CO and H_2 become equal is about 67%.

As expected, the partial pressures of CO and H_2 decrease with space time while the partial pressures of CO_2 and hydrocarbons increase with space time. The partial pressure of water initially increases with space time and then decreases indicating that it is an intermediate. This is also as expected since the water gas shift reaction consumes water formed from the Fischer-Tropsch synthesis.

The rate of disappearance of H_2 decreases with space time as does the rate of formation of water. The rate of disappearance of synthesis gas is approximately constant at small space times and then decreases monotonically with increasing space time. Both the rate of disappearance of CO and the rate of formation of CO_2 pass through a maximum with increasing space time.

It is of interest to note the relative conversions of CO and H_2 as the space time in the reactor is increased. The conversion of H_2 is greater than the conversion of CO at low space times while the reverse is true at higher space times. At a total synthesis gas conversion of between 65-70%, the H_2/CO ratio of the product gas is equal to the H_2/CO ratio of the incoming synthesis gas. This implies that at higher conversions, H_2 is being formed faster by the water gas shift reaction than it is being depleted by the formation of hydrocarbons.

The partial pressure of water over this catalyst is approximately constant over the entire range of synthesis gas conversions studied. Further, its partial pressure is smaller than the partial pressures of the other reaction components especially at high conversion levels. This implies that the catalyst used is a good water gas shift catalyst and converts the greater amounts of water formed by the Fisher-Tropsch reaction at high synthesis gas conversions.

The reaction rates of formation of products and disappearance of reactants are used to calculate the rate of the Fischer-Tropsch reaction and the rate of the water gas shift reaction from:

$$-r_{WGS} = R_{CO_2} \qquad (1)$$

$$-r_{FT} = (-r_{CO}) - r_{CO_2} \quad (2)$$

These rates are plotted as a function of total synthesis gas conversion in Figure 7. As shown in this figure, the rate of the Fischer-Tropsch reaction is always greater than the rate of the water gas shift reaction. However, at high conversions of synthesis gas (above 55%) the rate of the water gas shift reaction closely approaches the rate of the Fischer-Tropsch reaction. Up to about 55% conversion the rate of the Fischer-Tropsch reaction is approximately constant after which it monotonically decreases. In contrast, the rate of the water gas shift reaction passes through a maximum with increasing synthesis gas conversion.

Carbon monoxide can get converted to either hydrocarbons (Fischer-Tropsch) or carbon dioxide (water gas shift). Since hydrocarbons are the more desirable products, it is of interest to see how the fraction of CO converted to hydrocarbons varies with the total synthesis gas conversion. This is plotted in Figure 8 and shows that the fraction of CO converted producing hydrocarbons decreases as the total synthesis gas conversion increases. This implies that at higher synthesis gas conversions a larger amount of CO is being converted to the undesirable product CO_2, and not to hydrocarbons.

An important conclusion to be drawn from this is that it would be more desirable to carry out the Fischer-Tropsch synthesis at intermediate conversions and have either two reactors in series or operate a single reactor with recycle. At intermediate conversions the fraction of CO being converted to the undesirable product CO_2 is lower. Further, the exit gas from the reactor has about the same H_2/CO ratio as that of the inlet gas to the reactor so that the second reactor or the recycle stream would have the same H_2/CO ratio as the first reactor.

The experimental data obtained in this study also allow us to test the various reaction rate expressions proposed in the literature for Fischer-Tropsch synthesis over iron-based catalysts. For the purpose of testing these rate expressions against the experimental data they are rearranged so as to obtain a linear relationship. The experimental data are then plotted according to this linear relationship to determine if a straight line gives a good fit to the data obtained. None of the proposed rate expressions in the literature are able to give a good fit to the data obtained in this study. However, a reaction rate expression which represents the experimental data well is given below:

$$-r_{CO+H_2} = k\, P_{CO}\, P_{H_2} / (1 + K_{CO} P_{CO}) \quad (3)$$

Rearranging this expression, we get:

$$P_{CO}\, P_{H_2} / -r_{CO+H_2} = (1/k) + (K_{CO}/k)\, P_{CO} \qquad (4)$$

Figure 9 shows the fit of the experimental data to the rearranged rate expression. A reasonably good fit is obtained. This rate expression differs from the proposed rate expressions in the literature in that there is no inhibition of the rate by the reaction products (water and/or CO_2) and no competition between the adsorption of CO and the reaction products (water and/or CO_2). A possible reason for this difference in the case of one of the reaction products, water, is the low and almost constant partial pressures of water obtained over this catalyst at all the space velocities studied. Hence any effect of water on the reaction rate would appear to be low since its partial pressure does not vary much. However, this explanation does not hold for the other reaction product, namely carbon dioxide. In this case, the partial pressure of CO_2 varies considerably with space velocity. Hence it can be concluded that CO_2 does not influence the reaction rate over the catalyst used in this study.

The Fischer-Tropsch synthesis has been studied over the best low-alpha catalyst developed at the CAER. A wide range of synthesis gas conversions were obtained by varying the space velocity. The experimental results show that: (i) the rate of the water gas shift reaction is lower than the rate of the Fischer-Tropsch reaction at low conversions (< 60%) whereas it closely approaches the rate of the Fischer-Tropsch synthesis at high conversions, (ii) the fraction of CO converted to hydrocarbons is higher at low and intermediate conversions whereas it is smaller at high conversions, (iii) the H_2/CO ratio of the product gas is equal to the H_2/CO ratio of the inlet synthesis gas at an intermediate conversion level of 67%. These findings suggest that it would be beneficial to carry out the reaction at intermediate conversions. This would result in an optimum use of CO to produce hydrocarbons rather than CO_2. High overall conversions can be obtained by either using a second reactor or recycling the product gas using a single reactor. If the intermediate conversion in a single pass is maintained at 67% there would be no need to adjust the H_2/CO ratio of the recycle stream or the feed to the second reactor as the product gas from a single pass would have the same H_2/CO ratio as the feed synthesis gas.

The optimum reaction rate expression for synthesis gas conversion has been developed for this catalyst:

$$-r_{CO+H_2} = k\, P_{CO}\, P_{H_2} / (1 + K_{CO} P_{CO}) \qquad (5)$$

The rate expression shows that CO is strongly adsorbed on the catalyst and that the reaction products such as water and CO_2 do not inhibit the reaction rate.

Plans:

Future work with Cu promotion will be focused on its affect on the kinetics of the Fischer-Tropsch Synthesis and on the activity of catalysts operating in a high alpha mode. Previous work has shown that promotion with Cu has little affect on the activity or selectivity of the 100Fe/3.6Si/0.71K catalyst when pretreated with CO at 13 atm and 270°C followed by FTS conducted at 13 atm, 270°C with $H_2/CO=0.7$ (3.1 NL h^{-1} g^{-1}(Fe)). However, under these conditions the CO conversion is very high (>90%) and the true promotional benefits of Cu might not be evident. Decreasing the CO conversion of the catalyst by operating at higher space velocities might give a better indication of the affect Cu has on the activity of iron FTS catalysts. In addition, the affect of Cu on H_2 activation needs to be explored. Additional work will focus on obtaining Mössbauer data for the catalysts activated with syngas at 1 atm to see if the catalyst compositions are similar to those obtained for CO activation. In addition, characterization of the 100Fe/4.4Si/1.0K catalyst activated with H_2 will be done.

In addition, future catalyst studies will emphasize the study of high-alpha catalysts and the preparation of catalysts with various hardness values. Work will continue on defining attrition for FT catalysts.

REFERENCES

1. Bukur, D. B., Lang X., Rossin, J. A., Zimmerman, W. H., Rosynek, M. P., Yeh, E. B., and Li, C., Ind. Eng. Chem. Res. **28**, 1130, (1989).
2. Soled, S. L., Miseo, S., Iglesia, E., Fiato, R. A., 1992. U.S. Patent 5,100,856.
3. Kölbel, H. and Ralek, M., *Catal. Rev.-Sci. Eng.* **21**, 225 (1980).
4. Bukur, D. B., Lang, X., Mukesh, D., Zimmerman, W. H., Rosynek, M. P. and Li, C., *Ind. Eng. Chem. Res.* **29**, 1588 (1990).
5. Niementsverdriet, J. W. and van der Kraan, A. M., *J. Catal.*, **72**, 385 (1981).
6. Anderson, R.B. in "Catalysis" Vol. IV, Emmett, P.H., Ed., Rheinhold, New York (1956).
7. Atwood, H.E. and C.O. Bennett, I&EC Proc. Des. Dev., 18, 163 (1979).
8. Huff, G.A. and C.N. Satterfield, I&EC Proc. Des. Dev., 23, 696 (1984).
9. Ledakowicz, S., H. Nettlehoff, R. Kokuun and W-D. Deckwer, 24, 1043 (1985).

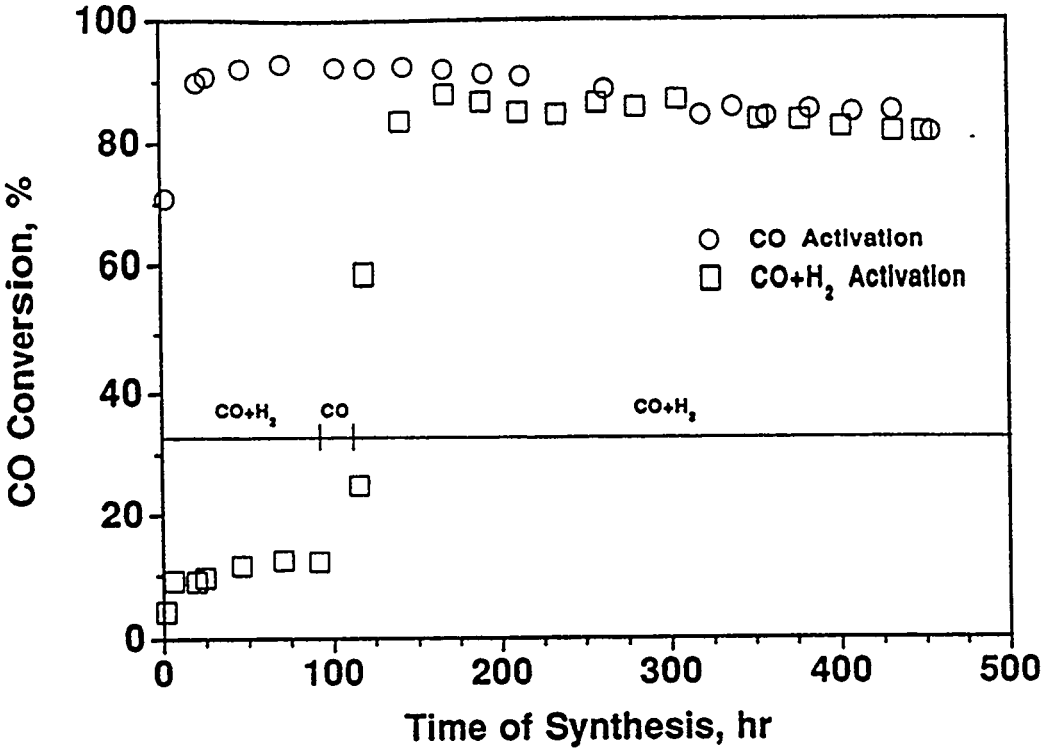

Figure 1. Comparison of the CO conversion vs. time of synthesis for the 100Fe/4.4Si/0.71 K catalyst when activated in CO and $CO+H_2$ (H2/CO=0.7) at 270°C and 175 psig.

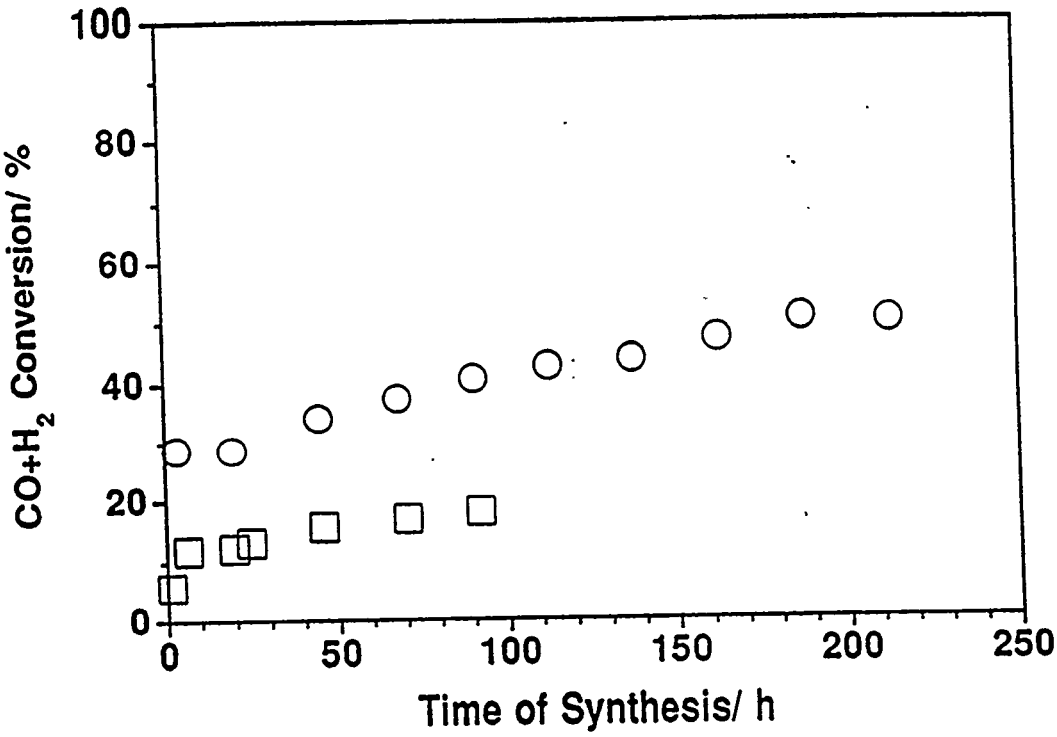

Figure 2. Affect of Cu promotion on synthesis gas activation. O- 100Fe/3.6Si/2.6Cu/0.71K and □- 100Fe/3.6Si/0.71K. Activation and synthesis conditions: 270°C, 13 atm, $H_2/CO=0.7$, s.v.=3.1 NL h^{-1} g^{-1}(Fe).

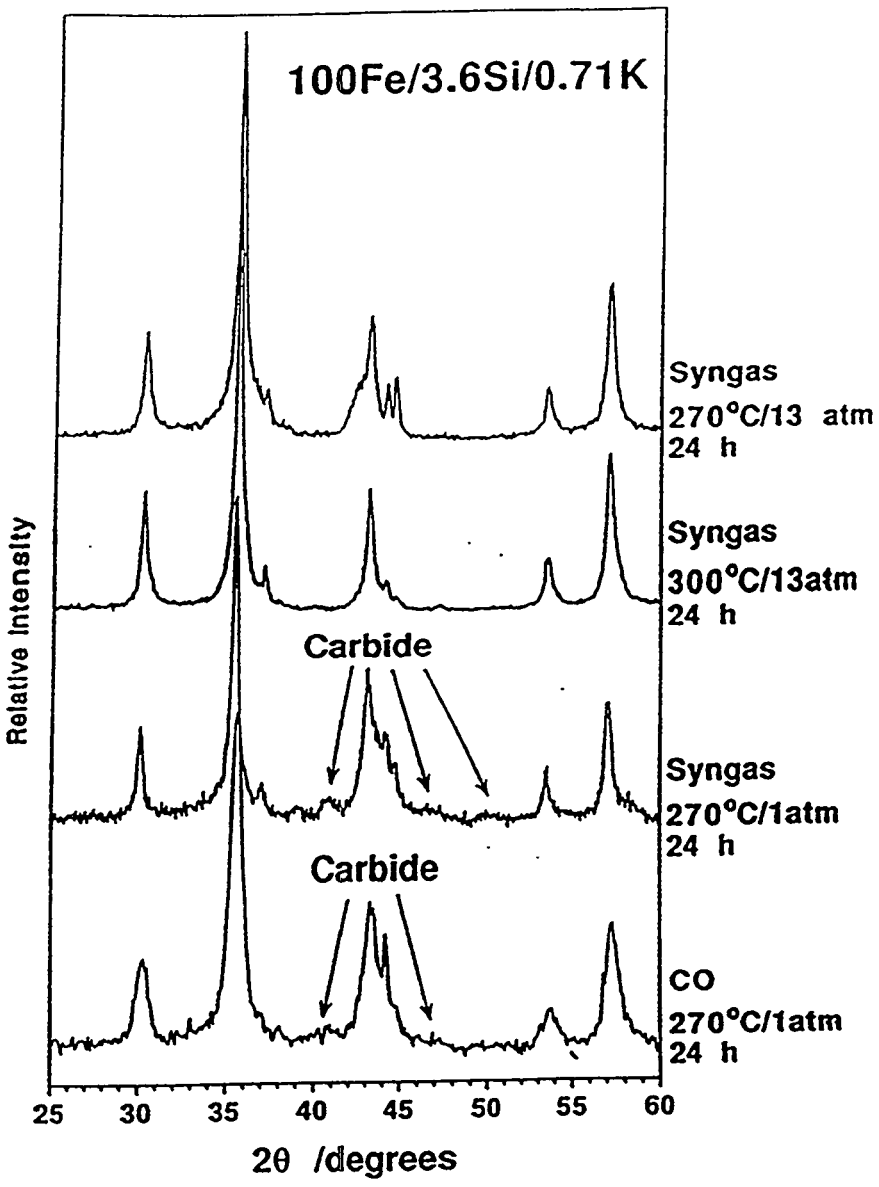

Figure 3. Comparison of X-ray diffraction results for the 100Fe/3.6Si/0.71 K catalyst activated with $H_2/CO=0.7$ at 13 atm. or 1 atm.

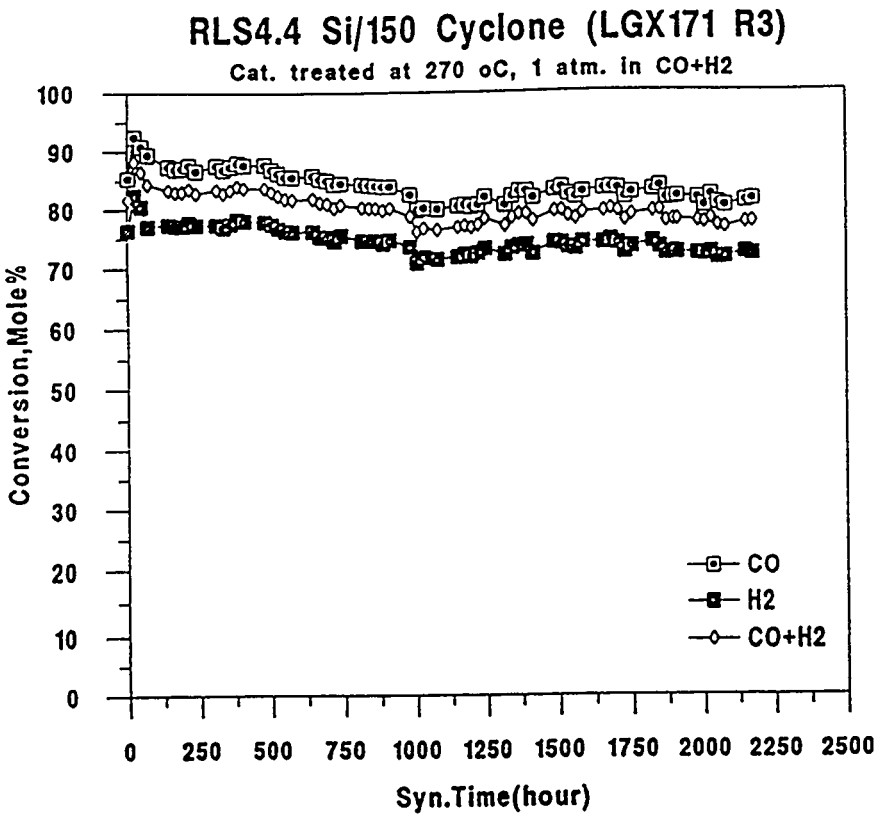

Figure 4. Long term activity test which shows a decline in conversion of 0.76 %/week.

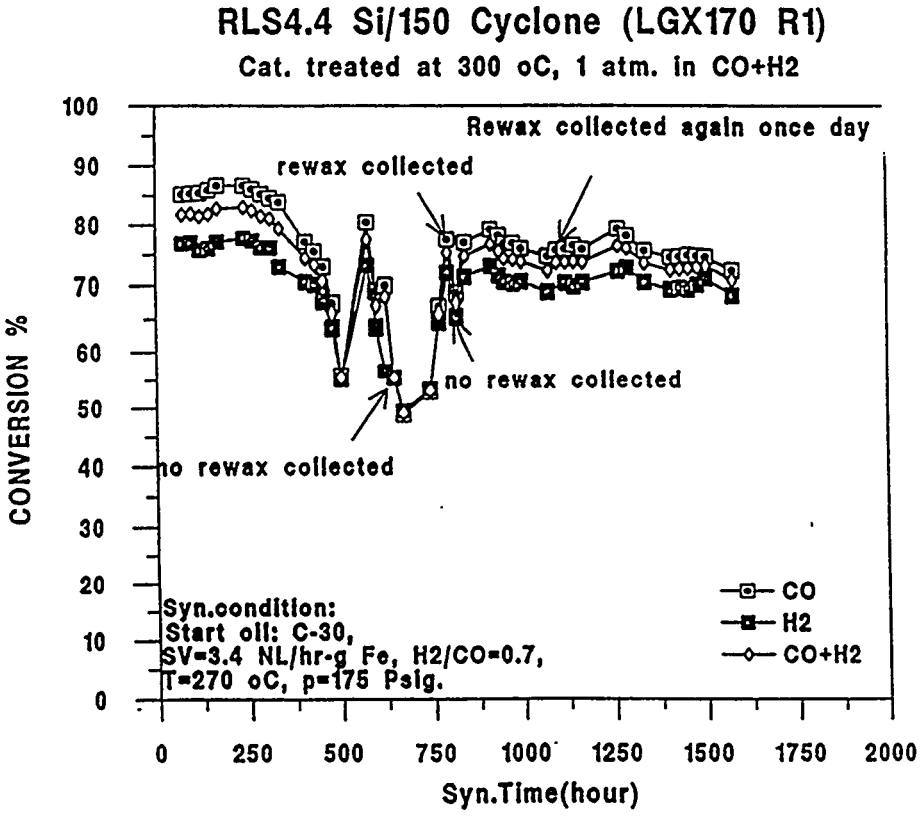

Figure 5. The effect of reactor wax collection on conversion.

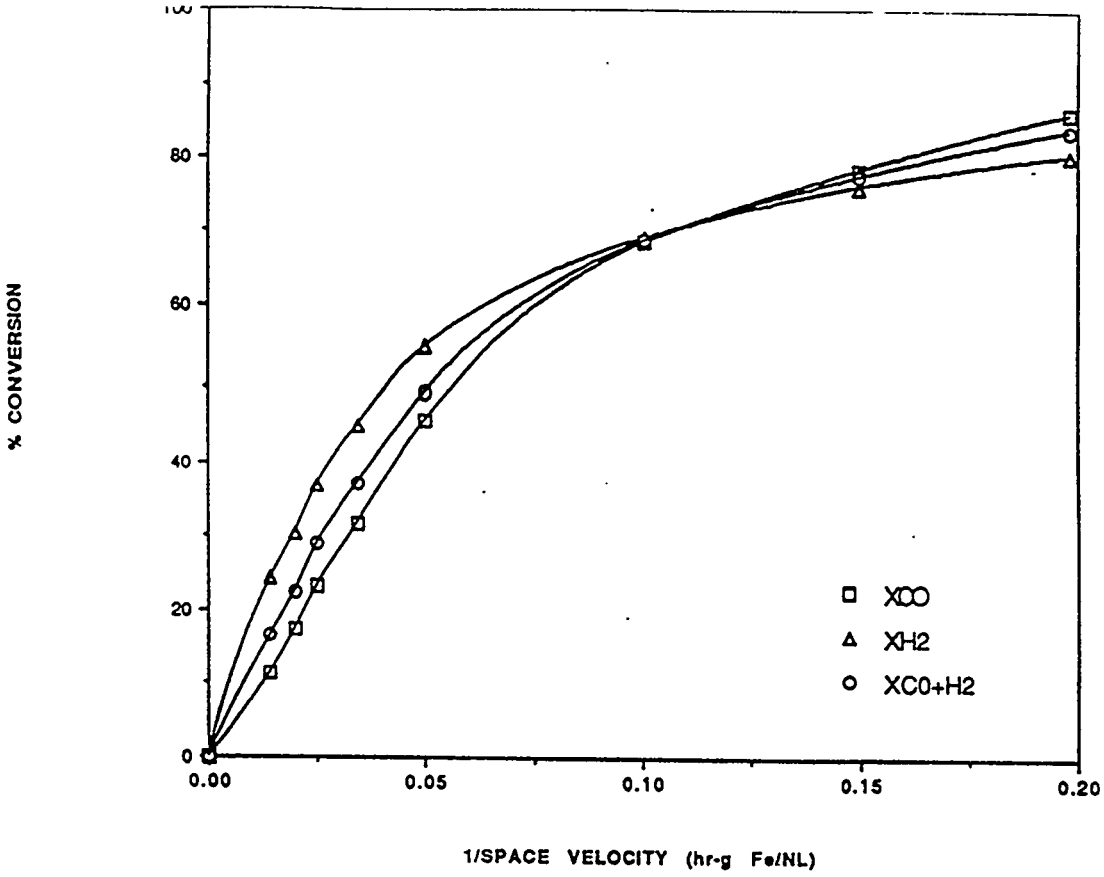

Figure 6. Conversions of reactants versus space time.

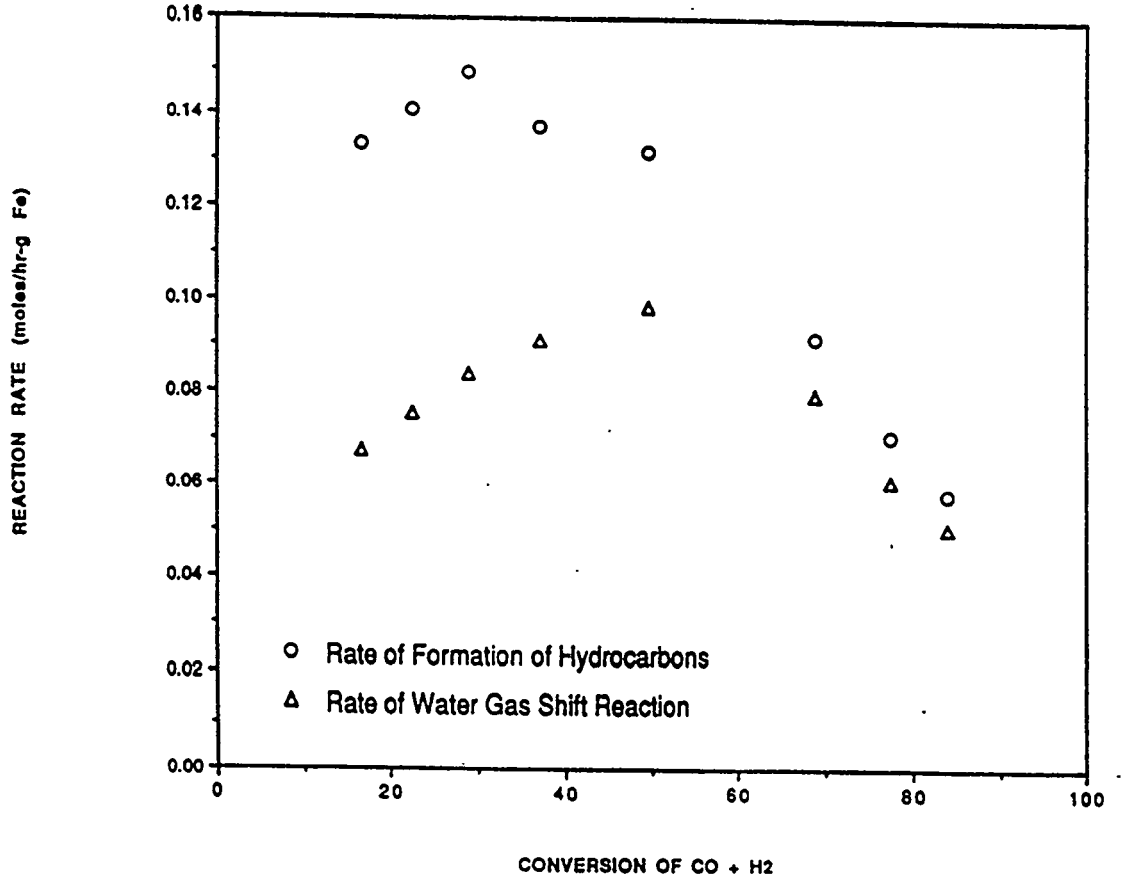

Figure 7. Rates of Fischer-Tropsch and water gas shift reactions.

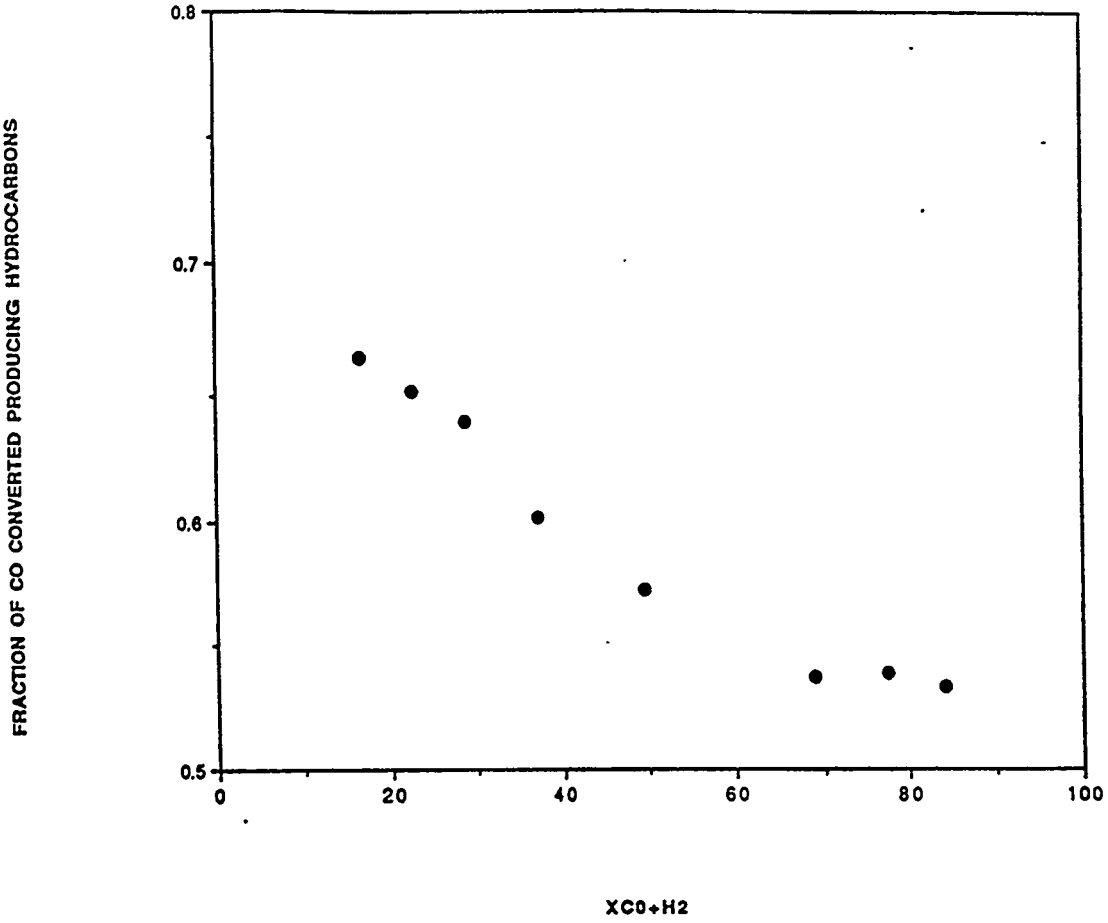

Figure 8. Fraction of CO converted to hydrocarbons.

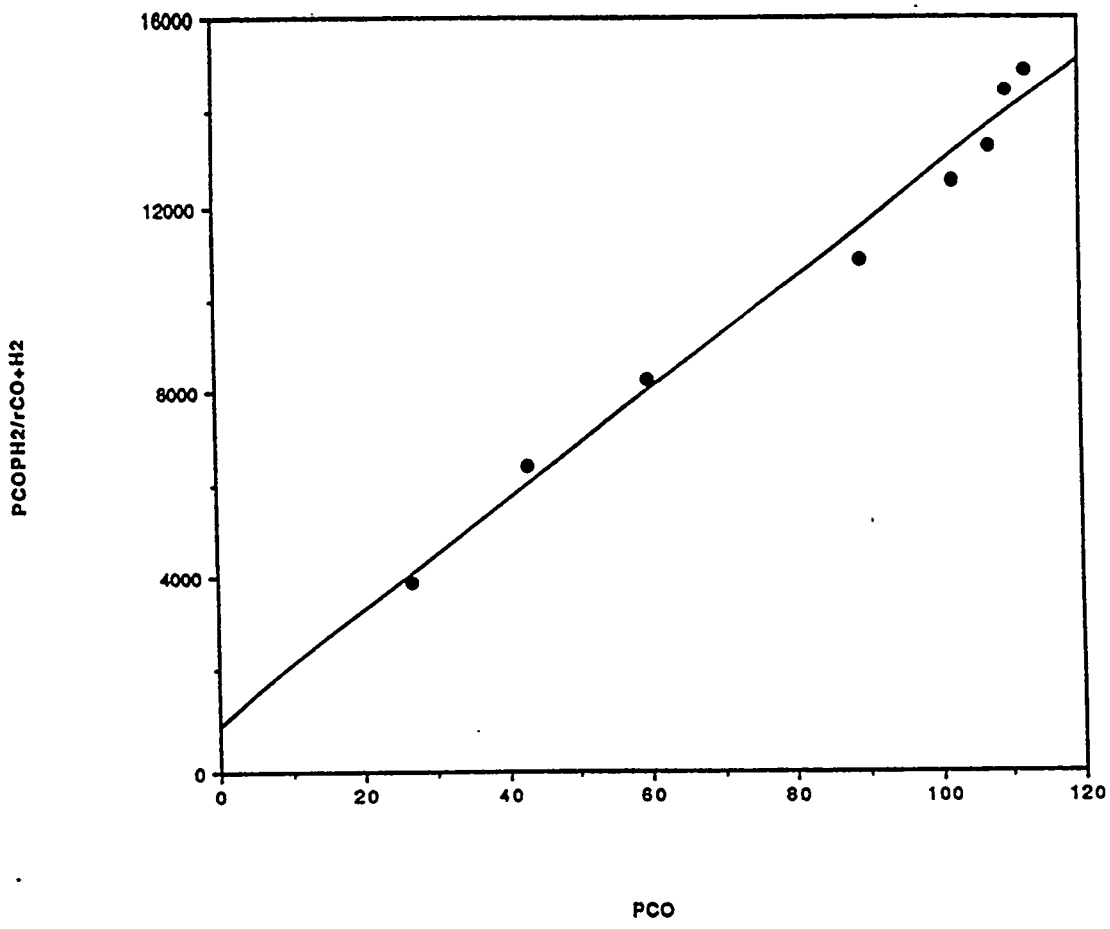

Figure 9. Test for reaction rate expression.

Title: **PREPARATION OF FISCHER-TROPSCH CATALYSTS FROM COBALT/IRON HYDROTALCITES**

Authors: B. H. Howard, J. J. Boff, M. F. Zarochak, and M. A. McDonald

Institution: U. S. Dept. of Energy, Pittsburgh Energy Technology Center

P. O. Box 10940, Pittsburgh, PA 15236

Period of Performance: October 1, 1993- September 30, 1995

ABSTRACT

Compounds with the hydrotalcite structure (hydrotalcites) have properties that make them attractive as precursors for Fischer-Tropsch catalysts. A series of single-phase hydrotalcites with cobalt/iron atom ratios ranging from 75/25 to 25/75 has been synthesized. Mixed cobalt/iron oxides have been prepared from these hydrotalcites by controlled thermal decomposition. Thermal decomposition at temperatures below 600 °C typically produced a single-phase mixed metal oxide with a spinel structure. The BET surface areas of the spinel samples have been found to be as high as about 150 m^2/g. Appropriate reducing pretreatments have been developed for several of these spinels and their activity, selectivity, and activity and selectivity maintenance have been examined at 13 MPa in a fixed-bed microreactor.

OBJECTIVES

The immediate objectives are to explore the catalytic properties of Fischer-Tropsch (FT) catalysts prepared from hydrotalcites and to understand the structure underlying these properties. The ultimate objective is to prepare FT catalysts with adequate activity, selectivity, and longevity for bubble column reactors.

APPROACHES

Introduction

Mixed metal oxides are important in many catalytic applications, both as catalysts and supports. The precursors used in the syntheses of mixed metal oxides are known to influence the physical and chemical properties of the resulting mixed metal oxides. Precursors commonly used for the preparation of these oxides include mixed metal hydroxides and carbonates coprecipitated from basic solution. Materials with a hydrotalcite-like structure, commonly referred to as hydrotalcites after one of the best known minerals of this structural group, have received much attention recently as precursors for catalytic applications. Examples include catalysts for methanol synthesis containing Cu, Zn, Cr, and Al (1,2,3) and catalysts for FT synthesis containing Co, Cu, Zn, and Cr(4).

Hydrotalcites have a layered structure similar to clays. The structure, illustrated in Figure 1, resembles that of the mineral brucite, $Mg(OH)_2$. It consists of stacks of brucite-like metal hydroxide sheets in which substitution of trivalent metal cations for divalent metal cations within the sheets results in a net positive charge. The positive charge is balanced in the structure by an additional layer of hydrated anions between the brucite-like sheets. A generalized formula for hydrotalcite-like compounds can be

written as:

$$[M_{1-x}^{2+}M_x^{3+}(OH)_2]^{x+}A_{x/n}^{n-}\cdot zH_2O$$

where M^{2+} and M^{3+} can be a variety of metals with appropriate ionic radii. The charge compensating anion is also variable with the ionic radius of the charge compensating anion being of only minor importance because the layer separation can adjust to accommodate size differences. Examples are as follows:

M^{2+} = Mg, Ni, Zn, Co, Fe, Cu, etc.

M^{3+} = Al, Cr, Fe, etc.

A = CO_3, OH, SO_4, CrO_4, $V_{10}O_{28}$, etc.

There are many naturally occurring minerals having this structure. These minerals typically have the ideal stoichiometry:

$$M_6^{2+}M_2^{3+}(OH)_{16}CO_3\cdot 4H_2O$$

Compounds with the hydrotalcite structure have several characteristics that make them valuable as precursors for FT catalysts. Among these is the ability of the structure to accommodate a variety of potentially useful transition metals in a single lattice and the ability to control the synthesis conditions to yield a high surface area material upon decomposition to a spinel phase. Furthermore, Co-containing and Fe-containing spinel phases have shown good activity and selectivity for FT synthesis and, when judiciously prepared and pretreated, have the potential for the physical stability required of a slurry FT catalyst.

This research examines the potential of hydrotalcites as precursors for the preparation of slurry Co/Fe FT catalysts. We report results from the initial phase of this work, the preparation of Co/Fe hydrotalcite samples and their thermal decomposition to spinel phases of intermediate-to-high surface area. We also report the initial results of studies defining appropriate reducing pretreatments for the spinels and their subsequent FT activity and selectivity in a fixed-bed microreactor. Finally, addition of promoters will likely be needed to improve various properties of the catalyst. We therefore report synthesis and thermal decomposition of Co/Fe hydrotalcites also containing typical FT catalyst promoters such as Cu or Al, as well as TPR results of some of these samples.

Experimental

The hydrotalcites in this study were prepared by a precipitation in base of the appropriate metal salts. The specific conditions used for the syntheses were varied to yield single-phase, well-crystallized hydrotalcites when possible. An aqueous solution of metal salts was prepared that contained the required ratio of metals for the target hydrotalcite, typically with a total metal concentration of about 0.5 M. The metal salt solution was added dropwise to an aqueous base that typically had an initial concentration of about 1 M. Concentrations were varied for some experiments. Potassium bases were used in most experiments because potassium is typically used to promote iron FT catalysts and additional potassium will be impregnated in many of these spinel samples before their use as catalysts. Thus, trace amounts of potassium retained in a hydrotalcite precursor are less likely to affect the

behavior of the catalyst than are trace amounts of sodium from sodium bases. Additions were usually done at 25°C with magnetic stirring. The pH was monitored during the syntheses. Usually, at the end of the addition, the temperature of the slurry was increased to about 60°C. The slurry was aged, typically for 18 hours, at elevated temperature to promote hydrotalcite formation. After the aging period the product was isolated by filtration, washed, and dried at 50°C. Hydrotalcites were thermally decomposed in air at various temperatures between 125 and 1000°C, usually for 2.5 hours, to determine what mixed metal oxide(s) would be formed.

The phases resulting from the hydrotalcite syntheses and the thermal decompositions were determined by means of x-ray diffraction (XRD). Chemical analyses for K, Na, Al, Co, Fe and Cl in these samples were requested but results were not available when this report was written. Morphologies of these materials were studied with scanning electron microscopy (SEM). Surface areas of the mixed oxides were measured by application of the BET method to N_2 physisorption isotherms. The reduction characteristics of the mixed metal oxides were investigated by means of temperature programmed reduction (TPR) with 10% H_2 in argon, 10% CO in helium, or 5% H_2 / 5% CO in argon. For each TPR experiment, approximately 50 mg of spinel was loaded in a quartz U-tube mounted in an Altamira Instruments AMI-1 unit. Each sample was typically heated at 5 °C min^{-1} in a total gas flow rate of 60 sccm. An Ametek mass spectrometer was used for gas analysis. Catalytic reaction studies were done with 0.3-1.5 g of sample loaded in a fixed-bed stainless steel reactor. The wax product was collected in a hot trap operated at 150 °C, liquid aqueous and oil products were collected in a cold trap operated at 20 °C, and the outlet gas stream was analyzed on-line with a Hewlett-Packard 5730 gas chromatograph.

Results and Discussion- Fe/Co

A stepwise strategy was used to develop the hydrotalcite syntheses. First, the hydrotalcite compositional range attainable for Co (II) with Fe (III) was determined. Then, the use of Fe (II) to increase the iron content of the hydrotalcite lattice was investigated.

Cobalt (II) nitrate and iron (III) nitrate were used as starting materials for the first part of the synthesis study. Potassium bicarbonate solution at an initial concentration of 1.25 M was used as the base. Hydrotalcite formation with Co (II) to Fe(III) atom ratios ranging from 80/20 to 25/75 was attempted in this series of experiments. The results are shown in Table 1. With this method well-crystallized, single-phase hydrotalcites could be prepared with Co (II) to Fe (III) atom ratios from 75/25 to 50/50. At lower cobalt contents some poorly crystallized iron (III) hydroxide was produced along with hydrotalcite and, at higher cobalt contents, some cobalt carbonate was produced. The starting pH for a synthesis was about 8. During the addition of metal salt solution, the pH typically dropped below 7 and a pinkish-tan slurry formed. As the slurry was aged and heated to 60°C, the pH rose to about 9 accompanied by a change in color to a darker reddish-brown, usually indicating formation of the hydrotalcite.

A number of experiments were conducted in an attempt to increase the iron content of the hydrotalcite lattice. Table 2 outlines several of the more successful experiments and the resulting compounds. In all experiments in this series metal chloride salts were used instead of the nitrate salts in order to inhibit the rate of Fe^{2+} oxidation in solution. Several of the syntheses were based on the work reported by Uzunova *et al.* (5). The M^{3+} required for a stable hydrotalcite lattice was provided by the oxidation of

some of the Fe (II) to Fe (III) through contact with atmospheric oxygen during the synthesis. The result of this set of experiments was the extension of the hydrotalcite cobalt to iron ratio to 25/75.

Figure 2 shows XRD patterns for Fe/Co hydrotalcites prepared by the two methods. A peak due to a $CoCO_3$ impurity is visible just above $2\Theta = 30°$ in the pattern for 75Co25Fe hydrotalcite. The large shoulders near the first two peaks in the pattern for 33Co67Fe are likely due to the lack of uniformity in the stacking pattern of the layers. The peaks are noticeably broader for the 25Co75Fe hydrotalcite, indicating smaller crystallite sizes.

The thermal decomposition behavior of several Co/Fe hydrotalcites was examined. The most extensive decomposition study was done for an intermediate composition hydrotalcite with an atom ratio of 67Co to 33Fe, which was decomposed in air at temperatures between 125 °C and 1000 °C. The samples were heated quickly by placing them in a muffle furnace that was already at the desired decomposition temperature and holding them at temperature for 2.5 hours. The results are shown in Table 3. It was found that a spinel phase, referred to as spinel A, was the only crystalline compound present following decomposition at temperatures of 200 to 600°C. Decomposition at 700°C produced a second spinel, spinel B, which was the dominant phase after decomposition at 800°C. Decomposition at 900°C yielded only spinel B, and decomposition above 1000°C began to decompose spinel B to cobalt oxides. The surface areas for these samples decreased from 153 to 18 m^2/g as decomposition temperature increased from 300 °C to 700 °C. This loss of surface area was probably due to a loss of internal particle porosity because no evidence for sintering or for other changes in particle morphology was apparent in SEM. Hydrotalcites with other Co to Fe ratios showed similar behavior. However, for some high iron hydrotalcites two spinels were always present after decomposition. It was also found that slower heating of a sample to the decomposition temperature influenced the relative amounts of the spinels formed.

Table 4 shows the BET surface areas for spinels resulting from decomposition of Fe/Co hydrotalcites at 500 and 600 °C. Decomposition at the lower temperature (500 °C) produced higher surface area materials, as shown previously for the 67Co33Fe spinels. It also appears that the iron-rich spinels, 33Co67Fe and 25Co75Fe, had higher surface areas than spinels of intermediate or cobalt-rich composition. The higher surface area is consistent with the smaller crystallite sizes seen for the parent hydrotalcites in Figure 2. The higher surface area likely reflects the different preparation method used for synthesis of these materials and does not imply any inherent difference in the surface area of iron-rich Co/Fe spinels.

Conditions for the reducing pretreatment needed to convert spinel samples to FT catalysts were investigated. Figure 3 shows the TPR of the 25Co75Fe spinel in 10%CO/He. The major feature is a CO uptake peak occurring slightly above 300 °C. This likely represents reduction and carbiding of the spinel. The decrease in the m/z = 28 signal at temperatures above ~340 °C likely reflects deposition of surface carbon on the catalyst rather than any further reduction of the bulk oxide. A fresh spinel sample was given an isothermal treatment resembling the conditions of this TPR peak. This was done at 260 °C in pure flowing CO for 20 h. This treatment produced a material consisting of several carbide and metallic phases and no oxide phases; the XRD pattern showed two clear patterns of phases that are isostuctural with α-Fe and with iron χ-carbide. The relative amounts of the constituent phases and their exact compositions have not yet been determined. This CO-treated material had a BET surface area of 59 $m^2\ g^{-1}$, similar to that of the parent spinel.

Table 5 summarizes the results of FT synthesis with the 25Co75Fe spinel given the isothermal CO treatment as a pretreatment. The yield of light hydrocarbon (C_1-C_5) synthesis measured after 28.8 h is typical for FT catalysts under these conditions. This yield decayed 30% after an additional day on stream. A great deal of free carbon accumulated on the catalyst during these 49.5 h of synthesis, consistent with deactivation due to excess surface carbon deposition. The H_2/CO usage ratio seen after 28.8 h of synthesis was higher than would be expected for a typical Fe FT catalyst; the water-gas shift reaction is far from equilibrium even at the reactor outlet.

The last row in Table 5 shows the yield of CO conversion to all products except H_2O and CO_2. This value is the integrated yield calculated from each on-line gas analysis and from analysis of the oil and wax fractions obtained for the entire 49.5 h of experiment. Figure 4 shows the overall carbon number distribution ("Anderson-Schulz-Flory" plot) for these integrated data. Gas make (C_1-C_5) approached 30% of the product, corresponding to a low "α" value. The probability of carbon chain growth did increase for heavier carbon numbers; a linear regression of the C_{20}-C_{35} fraction gave $\alpha = 0.82$. The oil product (not shown in tables or figures) was over 50% olefins and 14% alcohols.

Results And Discussion- Addition of Cu and Al modifiers

Copper (II) addition to the hydrotalcite lattice was initially attempted by substituting copper (II) nitrate for part of the cobalt (II) nitrate using the same synthesis method. (Copper is frequently added to precipitated iron catalysts to facilitate reduction.) The atom ratio was 20 Cu(II) / 40 Co(II) / 40 Fe(III). The % Cu was much higher than typically used for FT promotion, and was used so that any undesired phases produced during the synthesis could be detected and identified by XRD. The initial synthesis attempt resulted in primarily hydrotalcite with a trace of malachite, $Cu_2CO_3(OH)_2$. Lowering the base concentration from 1.25 M to 1.0 M eliminated the malachite contamination of the single phase hydrotalcite. Similar results have been obtained with Fe-rich hydrotalcites prepared with solutions of Co(II)/Fe(II)/Fe(III) chlorides; up to 12 metal% Cu has been added to the hydrotalcite lattice under these conditions. Copper can therefore be introduced into the Co/Fe hydrotalcite lattice in concentrations much higher than have typically been needed in FT catalysis.

Other results have shown the feasibility of Al substitution in the Co/Fe hydrotalcite lattice. Hydrotalcites with compositions of 75Co25Al and 75Co20Fe5Al were prepared and thermally decomposed. Table 6 shows BET surface areas of 75Co(25-x)Fe(x)Al spinels. Although Al substitution to the lattice increased the surface area, thermal decomposition still yielded a spinel powder that was coarser than the relatively fine 75Co25Fe spinel.

TPR studies with 10% H_2/ Ar were done on each of the samples listed in Table 6. Figure 5 shows the results. The 75Co25Al sample required temperatures well above 600 °C for thorough reduction, in contrast to the 75Co25Fe spinel, which was completely reduced at 430 °C. The intermediate composition, 75Co20Fe5Al, showed intermediate behavior, requiring temperatures of at least 500 °C for nearly complete reduction.

PLANS

The major portion of hydrotalcite synthesis is complete. The focus of this work has shifted to catalytic reaction of pretreated spinels and to characterization of these catalysts.

ACKNOWLEDGEMENTS

The authors gratefully acknowledge N. E. Johnson for helpful discussions during this project. B. H. Howard acknowledges support for this research provided under Contract # DE-AC05-760R00033 between the U. S. Department of Energy and the Oak Ridge Institute for Science and Education.

DISCLAIMER

Reference in this report to any specific commercial product, process, or service is to facilitate understanding and does not necessarily imply its endorsement or favoring by the United States Department of Energy.

REFERENCES

1. Fornasari, G.; D' Huysser, H.; Mintchev, L.; Trifirò, F.; Vaccari, A., *J. Catal.* **1992**, *135*, 386.
2. Riva, A.; Trifirò, F.; Vaccari, A.; Mintchev, L.; Busca, G., *J. Chem. Soc., Faraday Trans. 1* **1988**, *84(5)*, 1423.
3. Busetto, C.; Del Piero, G.; Manara, G.; Trifirò, F.; Vaccari, A., *J. Catal.* **1984**, *85*, 260.
4. Fornasari, G.; Gusi, S.; Trifirò, F.; Vaccari, A., *Ind. Eng. Chem. Res.* **1987**, *26*, 1500.
5. Uzunova, E.; Klissurski, D.; Mitov, I.; Stefanov, P., *Chem. Mater.* **1993**, *5*, 576.

Table 1. Results of Co(II)/Fe(III) hydrotalcite preparations using metal nitrates

Co (II)	Fe (III)	Resulting Phases
80	20	HTC + trace $CoCO_3$ + trace unidentified
75	25	HTC + trace $CoCO_3$
67	33	HTC
50	50	HTC
33	67	HTC + minor $Fe(OH)_3$
25	75	HTC + $Fe(OH)_3$

HTC = hydrotalcite

Table 2. Use of Fe(II) to increase iron content of hydrotalcite prepared with metal chlorides

Co (II)	Fe (II)	Base	Start pH	Result
25	75	$KHCO_3$	8.0	HTC + trace $Fe(OH)_3$
25	75	$KHCO_3 + K_2CO_3$	8.9	Goethite + $CoCO_3$
33	67	$KOH + K_2CO_3$	12.8	HTC
25	75	$KOH + K_2CO_3$	12.8	HTC

HTC = hydrotalcite

Table 3. Thermal decomposition of 67Co33Fe hydrotalcite

Temperature (°C)	Phase	Surface area m^2/g
50	HTC	-
125	HTC + amorph	-
200	Spinel A	-
300	Spinel A	153
400	Spinel A	95
500	Spinel A	57
600	Spinel A	29
700	Spinel A + B	18
800	Spinel A + B	-
900	Spinel B	-
1000	Spinel B + CoO + Co_3O_4	-

Table 4. Surface areas of Co/Fe spinels

Co	Fe	Other	BET Surface area ($m^2.g^{-1}$), for samples decomposed at: 500 °C	600 °C
100	---	---	---	---
75	25	---	52	30
67	33	---	57	29
50	50	---	---	34
33	67	---	---	47
25	75	---	76	---
25	75	K*	60	---

* Spinel impregnated with 3.0% K_2CO_3

Table 5. Fischer-Tropsch synthesis with 25Co75Fe spinel*

Time (h)	28.8	49.5
Conversions (%)		
H_2	~27	---
CO	~15	---
H_2/CO usage ratio	~1.2	---
Space-time yield of C_1-C_5 (g / kg / h)	106	73
Space-time yield, CO converted to organic products (g CO / kg / h)	313	

* Pretreatment conditions: CO, 20 h, 3.35 WHSV, 260 °C, 0.13 MPa
Reaction conditions 0.71 H2/CO, 3.52 WHSV, 260 °C, 1.32 MPa

Table 6. Surface areas of Co/Fe/Al Spinels

			BET Surface Area ($m^2 g^{-1}$), samples decomposed at:	
Co	Fe	Al	500 °C	600 °C
75	25	---	52	30
75	---	25	81	---
75	20	5	66	---

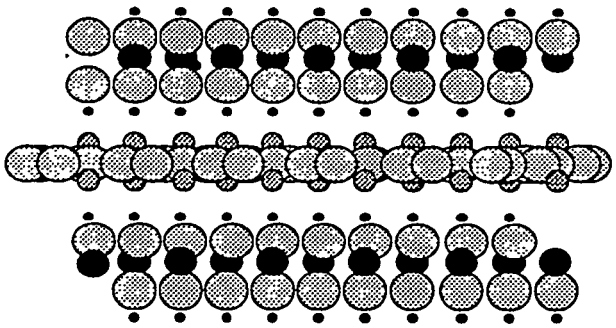

$$[M^{2+}_{1-x} M^{3+}_{x} (OH)_2] A^{n-}_{x/n} \cdot mH_2O$$

M^{2+} = Mg, Zn, Ni, Co, Mn, Cu, ...

M^{3+} = Al, Fe, Cr, Mn, Co, ...

A = CO_3^{2-}, SO_4^{2-}, OH^-, ...

◆ **Example:** $Mg_6 Al_2 (OH)_{16} CO_3 \cdot H_2O$ (Hydrotalcite)

Figure 1. Layered structure of the hydrotalcite-like compounds

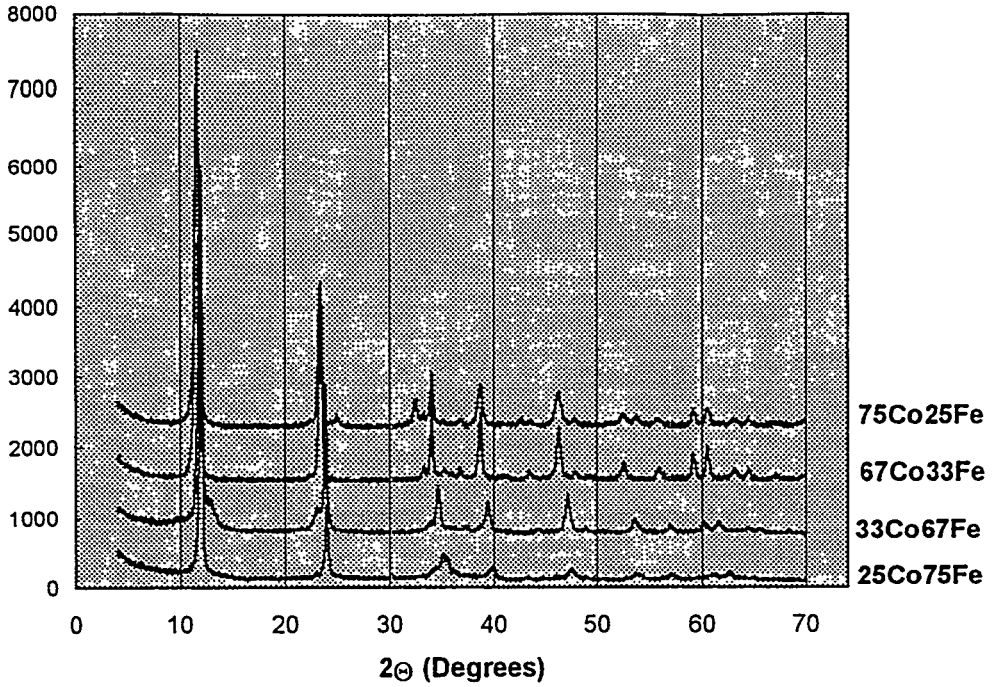

Figure 2. X-ray diffraction patterns of Co/Fe hydrotalcites

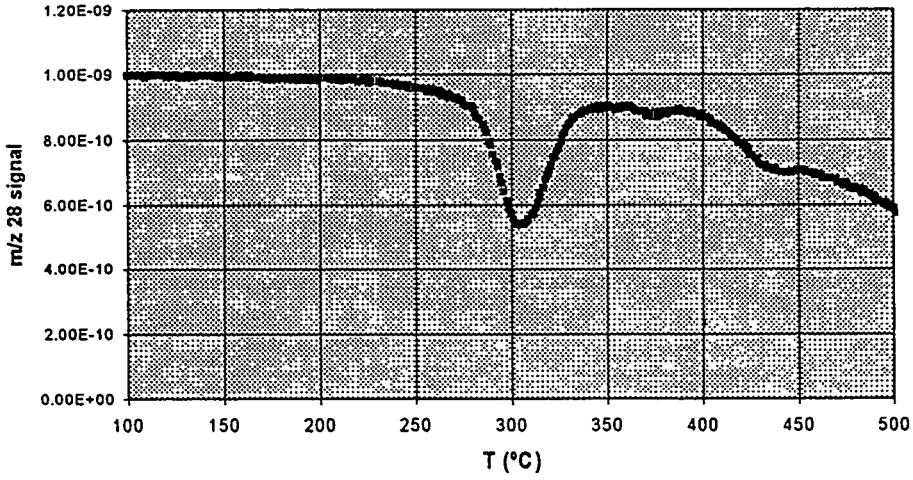

Figure 3. Temperature-programmed reduction of 25Co75Fe spinel in 10% CO/ He at a heating rate of 5 °C min^{-1}

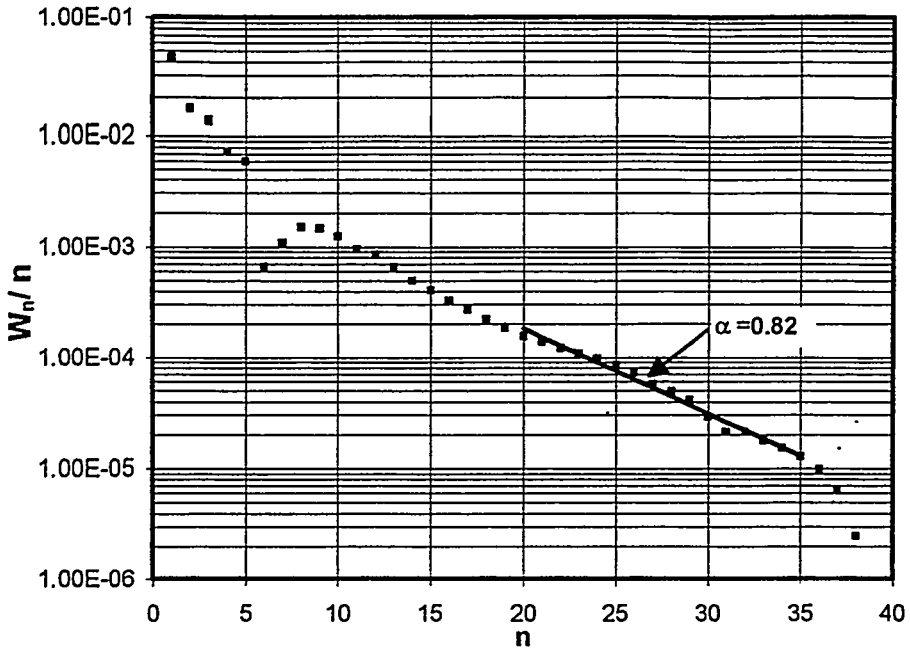

Figure 4. Distribution of carbon chain lengths ("Anderson-Schulz-Flory" plot), 25Co75Fe. (The discontinuity for C_6-C_8 reflects the fact that on-line gas analysis was not made for these products.)

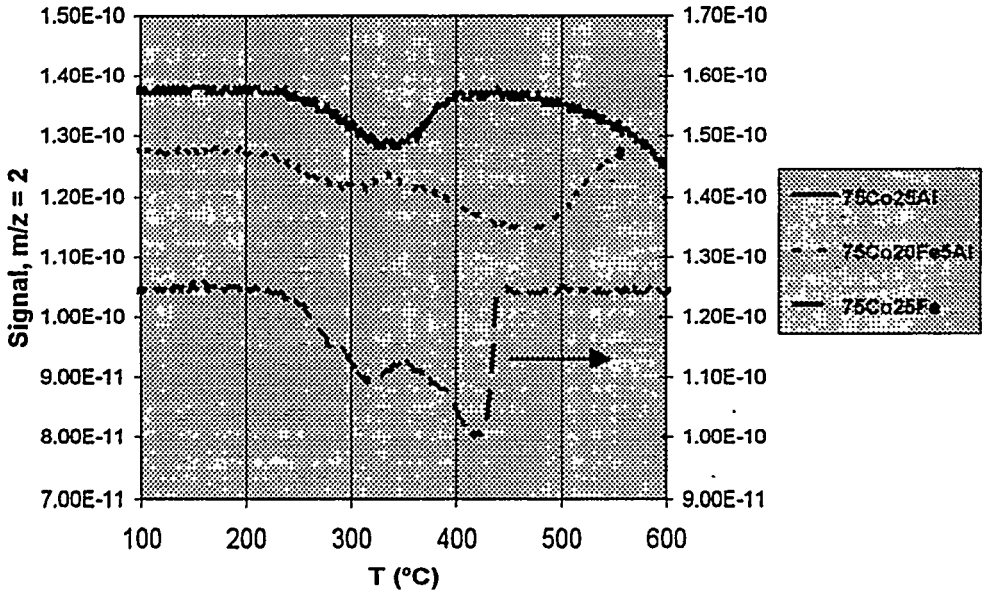

Figure 5. Temperature-programmed reduction of Co/Fe/Al spinels in 10% H_2/Ar at a heating rate of 5 °C min^{-1}

Title:	Morphological Transformations During Activation and Reaction of an Iron Fischer-Tropsch Catalyst
PI (Authors):	Nancy B. Jackson[1], Steven Kohler[1], Mark Harrington[1], Allen Sault[1], Abhaya K. Datye[2], Mehul D. Shroff[2], and Dinesh S. Kalakkad[2]
Institution/Organization:	[1]Sandia National Laboratories, Albuquerque, NM 87185 [2]University of New Mexico, Albuquerque, NM 87131
Contract Number:	DE-AC04-94AL85000
Period of Performance:	10/1/94-9/30/95

Objective

The purpose of this project is to support the development of slurry-phase bubble column processes being studied at the La Porte Alternative Fuel Development Unit. This paper describes the aspects of Sandia's recent work regarding the advancement and understanding of the iron catalyst used in the slurry phase process. A number of techniques were used to understand the chemical and physical effects of pretreatment and reaction on the attrition and carbon deposition characteristics of iron catalysts. Unless otherwise stated, the data discussed below was derived from experiments carried out on the catalyst chosen for the summer 1994 Fischer-Tropsch run at LaPorte, UCI 1185-78-370, (an L 3950 type) that is 88% Fe_2O_3, 11% CuO, and 0.052% K_2O.

Experimental

The catalyst used in this study was precipitated from an iron sulfate precursor and spray - dried. The CO used was Matheson research purity 99.99% and was further purified to remove carbonyls by passing it through a column containing glass beads heated to 600 K, an ascarite column and a 7 μm Swagelok particle filter. H_2 and He were UHP 99.999% Alphagaz and Argyle, respectively. The He was further purified by passing it through an AllTech Oxy-Trap. The O_2 used in passivation was Big 3 UHP 99.993%. The GC He was Argyle UHP 99.999%. The reactor was a differential fixed bed reactor consisting of a quartz glass U-tube with a bulb in which a known weight of catalyst (approximately 1 g.) was placed over a quartz wool plug. The reactor was enclosed by an electrically heated Griffin-Type Series-O heating mantle (750 W) and the catalyst temperature was monitored and controlled by a thermocouple connected to a PID controller which maintained the temperature to within 2 K of the set temperature. The gas flow rates were set and controlled by Tylan FC-260 mass flow controllers calibrated for the specific gases used and were maintained to within 1 sccm for helium and 0.1 sccm for the other gases.

In all the studies, approximately 1 gram of the as-received catalyst was loaded into a tubular, fixed-bed reactor. Different batches were activated under different activation conditions. These were:

a. CO (containing 3% Ar as internal standard) - 20.6 sccm, 543 K, 2 h.
b. H_2:CO - 3.5:5.2 sccm, 543 K, 2h.
c. H_2:CO - 3.5:5.2 sccm (FTS reaction mixture with $H_2/CO = 0.7$), 523 K, 2 h.
d. H_2 - 20 sccm, 543 K, 100 h
e. H_2 - 20 sccm, 723 K, 15 h

After activation, reactions were carried out over the catalyst samples in the same reactor tube at 523 K with $H_2/CO = 0.7$ and a total gas flow rate of 8.7 sccm (H_2:CO/Ar=3.5:5.2 sccm) at a pressure of 630 Torr (normal atmospheric pressure in Albuquerque). Samples were collected at different points along the experiment including the just-activated sample, activated and used for FT reaction for 10 hours, and activated sample used for FT reaction for 45 hours. Before switching the flowing gases from the activation mixture to the reaction mixture, the reactor was cooled to room temperature and extensively purged with helium. In the case of the syngas activation, the first two hours of the reaction run were considered the activation step.

The samples were removed from the reactor after careful and highly controlled passivation. This involved cooling the sample to room temperature, purging with He and exposing to small amounts of O_2 in a stream of flowing He until a final content of 20% was reached. The completion of the passivation process was marked by the occurrence of a small exotherm (typically 2-3 K) in the catalyst bed and the subsequent return to room temperature. The sample was then removed and stored in a glass vial for further characterization tests. To assess the efficacy of the passivation step, we examined a catalyst that was reduced in H_2 at 673K and was transformed into metallic Fe and subsequently passivated. TEM images showed a thin film of magnetite after air exposure, which was no more than 1-2 nm thick. The passivation-grown magnetite film was crystalline and therefore easy to distinguish from the amorphous carbon films that resulted from use of the catalyst in the FT environment.

The product gases were analyzed in a Varian 3400 Gas Chromatograph (GC) and the peak areas were integrated by a Varian 4270 integrator. Analyses were done with a Thermal Conductivity Detector (TCD) with He as a reference gas for the detector. The CO feed stream had 3% Ar as an internal standard so that the conversion of CO could be directly measured. The column used was a 80/100 0.125" x 15' stainless steel column with Supelco Carboxen^{TM} 1000 packing.

The catalyst microstructures were studied by both scanning and transmission electron microscopy using a Hitachi S-800 SEM, JEOL JEM 2000FX TEM (3.0 Å point resolution) and a JEM 2010 TEM (1.9 Å point resolution). For the TEM, the sample was mounted on a copper grid with holey carbon. The grids were dipped into the sample and the excess sample was shaken off. No solvents were used at any stage of the process.

Surface areas were measured using the B.E.T. method using a Micromeritics ASAP 2000 instrument. Carbon content was measured with a Perkin-Elmer 2400 CHN Elemental Analyzer to quantify carbon content of the catalyst samples. This involved oxidizing the samples at 1000 K and measuring the amount of CO_2 formed. Powder X-ray diffraction (XRD) patterns obtained done on all the samples in order to estimate the relative amounts of phases present. Since no internal standard was used in these experiments, the peak area serves only as a qualitative measure of the amount of each phase present. However, determination of peak areas permits a better estimate of the carbide peak since it overlaps with one of the magnetite peaks.

All X-ray photoelectron spectroscopy (XPS) and Auger electron spectroscopy (AES) experiments were performed in an ultra-high vacuum (UHV) chamber coupled to an atmospheric pressure reaction cell. This apparatus is identical to one described elsewhere except that facilities for X-ray photoelectron spectroscopy (XPS) and ion scattering spectroscopy (ISS) have been added. All XPS and AES results were obtained from samples treated in situ in the reaction cell and transferred into UHV without exposure to air. Detailed treatment procedures are described in reference AES was performed using a Perkin-Elmer Model 15-155 cylindrical mirror analyzer, with excitation of

the Auger process provided by a 3 keV, 4 μA, 100 μm diameter electron beam generated by a coaxial electron gun mounted within the analyzer. Details of data collection and manipulation are provided elsewhere[1]. XPS was performed with a VG Microtech CLAM2 hemispherical analyzer operated at a pass energy of 50 eV and a slit width of 4 mm. A 600W Al Kα X-ray source oriented 50° away from the analyzer lens axis provided primary excitation. The XPS energy scale was calibrated by measuring the positions of the Cu 2p3/2 (932.7 eV) and Cu 3p (75.1 eV) peaks from the copper sample holder[2]. Both XPS and AES data are plotted by drawing straight lines between individual data points without any smoothing or curve fitting. XPS peak assignments are based on comparison of peak shapes and binding energies with accepted literature values for metallic iron and iron oxides, as summarized by Kuivila, et al.[3] while AES lineshape analysis is based on reference[4].

Results

The rate of CH_4 formation is plotted in Figure 1 and is used as an indicator of the FTS activity of these samples. It is seen that activation in CO produces the most active catalyst. The activity of the two samples activated in synthesis gas approach one another over time, however the catalyst activated at 543 K is active more quickly than the catalyst activated at 523 K. What is not indicated on Figure 1, are the CH_4 formation rates for the H_2 treated samples. Neither H_2-treated sample demonstrated any Fischer-Tropsch activity.. The sample reduced in H_2 at 543 K produced some CO_2 upon reaction with synthesis gas, but the sample reduced in H_2 at 723 K did not even produce CO_2. We have not quantified any hydrocarbons other than CH_4 since our GC system was not set up for this purpose. We were able to detect C_2 and C_3 in small amounts, but the peaks were extremely broad under our experimental conditions. We also detected hydrocarbon oils when the catalyst was removed after reaction. These oils accumulated at the bottom of the quartz U-tube reactor, but were not quantified. The CH_4 formation rate is therefore the only indicator of FT activity of this catalyst.

CHN Analysis

Table 1 shows the results of CHN analysis used to determine the weight percent carbon as a function of activation and reactions. (The calculated carbon content for the various carbide phases are 6.7% in Fe_3C, 7.9% in χ-$Fe_{2.5}C$, 8.9% in ε'-$Fe_{2.2}C$, and 9.7% in ε-Fe_2C.)

Table 1. Carbon Content (wt%) as a function of activation and reaction. (Rxn T=523 K)

TYPE	ACTIVATION	SHORT REACTION	LONG REACTION
CO/543 K	3.1	6.85	10.6
CO&H_2/523 K	0.2	1.6	5.1
CO&H_2/543 K	0.6	2.3	5.3
H_2/543 K	0	n/a	3.6

XRD Analysis

X - ray powder diffraction patterns of the CO - activated sample after activation, and after 10 and 45 hours of FT synthesis show that it is predominantly magnetite with a small amount of carbide after the activation step. See Table 2. It gradually transforms almost completely into carbide after exposure to syngas at 523 K for 45 hours. The prominent magnetite peaks are seen at the following 2θ values: 30°, 35.5°, 43°, 53.5°, 57°, and 62.7°. The carbide peak at around 43° was found to overlap with the magnetite peak at the same 2θ value. Since we did not use an internal standard, direct quantification of the amounts of various phases present was not possible. We have therefore used the peak area for most intense reflection for each phase as a qualitative measure of

the amount of that phase. For the carbide phase, this was only possible after the area of the magnetite peak at that same 2θ value (scaled with respect to the most intense reflection) was first subtracted. The samples that were activated in synthesis gas were also initially found to be predominately magnetite and after reaction had increasing amounts of carbide present.

Table 2. Analysis of XRD Patterns

Treatment	Ratio of XRD peak at 35.5° to that at 43°	Carbide X 100 (Carbide+Magnetite)
CO activation 543K 2 h	2.12	36.0
activation + 10 h CO/H_2	0.99	70.1
activation + 45 h CO/H_2	0.00	100.0
CO/H_2 activation 523 K 2 h	3.33	0.00
activation + 10 h CO/H_2	2.43	26.8
activation + 45 h CO/H_2	1.21	63.4

BET Surface Area

The surface areas were determined by a multi-point BET isotherm and are listed in Table 3. The as-received sample had a BET surface area of 27 m^2/g. Activation of the sample causes a significant increase in surface area for the CO activated sample. With increasing times on stream, the BET surface areas of all three samples tend to converge and are only marginally different from the initial surface area. While the surface areas, by themselves, do not provide any indication for the changes in catalyst morphology, the electron micrographs reveal major structural rearrangement to be occurring as the sample is activated and used for F-T synthesis.

Table 3. BET surface area (m^2/g)

TYPE	ACTIVATION	SHORT RXN.	LONG RXN.
H_2/543 K	5		
CO/543 K	44.22	33.59	23.17
FTS/523 K	31.76	28.25	24.35

Surface Analysis

For the freshly calcined sample, XPS detects Fe_2O_3 as the sole iron phase present. In addition, copper, potassium, and small amounts of magnesium are observed on the catalyst surface. Since we are unaware of any intentional addition of Mg to the catalyst, it must be assumed that the Mg arises from minor impurities introduced during catalyst synthesis. XPS (Fig. 2) and AES (Fig. 3) spectra were also taken after each activation treatment. After both CO and syngas activation treatments, a single Fe $2p_{3/2}$ XPS peak is observed at a binding energy of 710.8 eV. The position of this peak, coupled with the absence of any shakeup features between 715 and 720 eV, unambiguously identifies magnetite as the primary phase detected in both cases. No evidence is seen for metallic iron or iron carbide phases, which would appear near 707 eV, or carbidic carbon, which would appear at ~283 eV. While the XPS result for syngas activation is in complete agreement with XRD and TEM, the absence of any carbide following CO activation is surprising given that XRD and TEM detect carbide. Based on past measurements of mixed iron carbide/oxide phases with this instrument, carbide levels as low as 4-5% should be detectable, leading to the conclusion that no more than 2-3% of the total surface iron detected is present as carbide following CO activation at 543K for 2 h. AES supports the XPS analysis, showing a two peak structure in the Fe(MVV) region between 40 and 55 eV, characteristic of iron oxides[5]. Furthermore, the O(511 eV)/Fe(703 eV) ratios are lower than expected for Fe_2O_3, and the relative

sizes of the three Fe(LMM) peaks at 598, 651, and 703 eV are intermediate between those of Fe_2O_3 and metallic iron[5]. Taken together, this information supports assignment of the Auger spectra for the CO and syngas activated samples to magnetite.

In order to assess the ability of XPS to detect iron carbide in these catalysts, a sample of the catalyst after hydrogen activation and FT synthesis for 45 h was analyzed by XPS. Even though XRD (Table 2) and TEM (see below) show that more than half the iron in this sample is carbided, XPS detects no carbide whatsoever. TEM shows that the carbide particles are covered by 3-4 nm amorphous carbon films, which undoubtedly severely attenuate the Fe 2p carbide signal and prevent its detection in the presence of magnetite. In support of this argument are the results of a depth profiling experiment in which the sample was bombarded with 5 kV Ar^+ ions at a current density of 1 $\mu A/cm^2$ for 1 h. Following this treatment, shoulders appeared in both the Fe 2p and C 1s regions at energies of 707 eV and 283 eV, respectively, much as observed by Reymond et al.[6] This result is a clear indication of the presence of carbide buried beneath a second phase. We will return to this point later in the discussion section.
XPS and AES detect small amounts of carbon on both the CO and syngas activated samples, with C 1s binding energies and C(272 eV) Auger peak shapes characteristic of graphitic carbon[5]. While Fig. 3 shows a larger carbon signal for the CO activated sample than the syngas activated sample, this result was not reproducible, possibly due to uncertainties in sample temperature measurements discussed in reference 4. It is clear, however, that carbon levels increase with activation time for both treatments. Although no carbidic carbon is seen by either XPS or AES, it is probable that graphitic overlayers on the carbide phase severely attenuate the carbide signals, as described above for attenuation of the Fe 2p carbide signal, and thereby prevent their detection.

XPS and AES of the hydrogen activated sample show nearly complete reduction to metallic iron. The Fe $2p_{3/2}$ binding energy of 707 eV, and the single Fe(MVV) Auger peak at 47 eV are clear indicators of metallic iron. A small shoulder at ~710 eV on the Fe $2p_{3/2}$ peak and subtle differences between the Fe(MVV) lineshape of the activated sample and that of metallic iron[4] indicate the presence of some residual oxide. Note that the presence of a relatively large O(511 eV) peak cannot be taken as a direct indicator of iron oxidation since a fraction of the oxygen is associated with potassium[4]. Detailed Fe(MVV) lineshape analysis[4] suggests that 35 to 45% of the O(511 eV) signal is due to iron oxides while the remainder is associated with potassium.

In addition to demonstrating iron reduction during hydrogen activation, the XPS and AES results also show the appearance of large amounts of sulfur on the surface and growth of the potassium signal relative to iron. The growth of the potassium signal is attributed to the loss of surface area during reduction, which increases the potassium coverage. The appearance of sulfur is attributed to migration of sulfate impurities in the catalyst to the catalyst surface. Rough quantitative analysis shows that the observed S(152 eV)/Fe(703 eV) ratio corresponds to approximately one monolayer of sulfur. Since sulfur is a well known poison for FT synthesis, this result suggests that complete reduction of this catalyst in hydrogen would result in little or no FT synthesis activity. This prediction is in agreement with our reactivity studies where reduction of the catalyst at 543 K for a week with 35 sccm of H_2 or at 723 K with 20 sccm of H_2 for 15 hours resulted in a catalyst that was completely inactive for FT synthesis.

Transmission Electron Microscopy

Fig. 4 shows a typical image of the primary particles that make up the spherical agglomerates of the UCI catalyst. These particles are single crystals of a-Fe_2O_3 as confirmed by electron diffraction[7]. These single crystals have a characteristic contrast consistent with the presence of

voids within the single crystal matrix. The circular features exhibit a characteristic light/dark contrast with changes in focus which is typical of voids. These voids do not disrupt the crystal structure since the lattice fringes go through them. In subsequent discussions, we refer to this microstructure as the "swiss-cheese" morphology.

Sample microstructure after activation

A 2 hr CO activation of 1 g of catalyst with 20 sccm of CO at 543 K transformed the a-Fe_2O_3 into Fe_3O_4 plus small amounts of carbide. The presence of the carbide was deduced from electron diffraction and is consistent with the results from XRD and CHN analysis. We find that the carbide is always covered with a surface film which we attribute to amorphous carbon. Activation in the syngas mixture for 2 h at 523 K shows no carbide but only magnetite. In these images, the presence of magnetite is seen by electron diffraction as well as by the presence of regions with remnants of the "swiss-cheese" morphology of the original hematite catalyst. Activation in H_2 for 15 hours at 723 K of 1 g of catalyst transformed the sample to α-Fe as confirmed by XRD and electron diffraction. A thin film of oxide formed on the surface of the sample during the controlled passivation in the reactor. Electron diffraction showed a faint ring indicating the presence of polycrystalline magnetite. This oxide film was different in appearance from the magnetite resulting from the phase transformation of hematite which retained the "swiss-cheese" morphology. Furthermore, the crystallinity of the film helped to distinguish it from the amorphous and graphitic carbon that forms during exposure to syngas or to CO.

Sample microstructure after activation and 10 hour reaction

After a short reaction period, sample morphologies are quite different. The CO-activated sample shows a much greater degree of transformation into carbide, while the syngas activated sample shows a smaller extent of carbide formation. The carbide particles grow out of the magnetite as nodules on the surface (For example, Fig. 5). This phase transformation starts to break up the initial single crystal "swiss-cheese" morphology by outgrowth of the carbide phase. The carbide particles are invariably covered by a surface film while the magnetite surface is clean. We attribute these surface films to amorphous carbon formed during reaction.

Sample microstructure after activation and 45 hour reaction

After a 45 hour reaction, all samples show significant amounts of carbide formation, although the FT activated samples still have some magnetite present. The CO activated sample shows very small traces of magnetite. A common feature in all samples, irrespective of the nature of the activation treatments or the extent of the reaction, is the occurrence of 3-4 nm thick films of amorphous carbon *only* on the carbide particles. See Fig. 6. The magnetite phase, where present, is not covered by any overlayers. With electron and X - ray diffraction, it is not possible to distinguish between the various carbide phases since they all had primary diffraction peaks extremely close to each other. The major peak from the carbide formed in our samples is a broad reflection centered around a 2q value of 43°. In the TEM images, carbide grains appear as small crystallites showing d spacings of ~2Å. For this reason, we have chosen to label the carbide phase as a single iron carbide without reference to its precise stoichiometry.

The role of activation

When iron catalysts are exposed to FT synthesis reaction environments, the catalysts transform from hematite into one or more carbides, regardless of the activation step. The activation process controls the rate of the transformations. The single crystals of hematite first transform into magnetite retaining the characteristic "swiss cheese" morphology. This step is relatively facile and is complete within 2 hours at 543 K for all activation treatments. We have shown that this

transformation can occur at lower temperatures[7]. The subsequent transformation from magnetite to carbide is slow and depends on the activation environment. The carbide phase forms as small nodules on the surface of the magnetite with the phase transformation proceeding slowly into the bulk. The breakdown of the original single crystals is brought about by this phase transformation.

Based on the rate of CH_4 formation, which we consider to be an indication of FT activity, we find the CO activation to be the most effective method for activating the catalyst. Activation in CO transforms the hematite into magnetite and small amounts of carbide at the end of the 2 hour activation step. With CO/H_2 activation under mild conditions, we see only magnetite and the catalyst shows no initial FT activity, although some CO_2 is formed. When syngas activation was performed at 543 K, we did see evidence of initial FT activity and the presence of carbide. However, the subsequent activity as a function of time is very similar to that of the sample activated at 523 K.

These morphological transformations involve a major breakdown of the single crystal hematite particles into smaller crystallites of carbide, but there is no corresponding increase in the BET surface area, which remains at ~27 m^2/g (the surface area of the as-received catalyst). The hematite crystals are platelets about 1 μm long, 0.3 μm wide and approximately 40-50 nm thick. The surface area can be calculated as follows:

$$S = \frac{2LW + 2(L+W)d}{\rho LWd}$$

$$S \approx \frac{2}{\rho d}$$

when $d << L, W$

Based on these equations, a BET surface area of 27 m^2/g corresponds to a thickness of about 15 nm for particles of density 4.7 g/cm^3 (from helium pycnometry). However, the observed thickness of the crystallites is about 40-50 nm, which is greater than the calculated value. The discrepancy is probably due to the "swiss cheese" morphology of the single crystals which may serve to enhance the surface area beyond the value calculated from the geometry of the particles.
During reaction, the hematite breaks down into carbide crystallites that are 20-30 nm in diameter. The surface area of the catalyst after reaction (21-24 m^2/g) is not very different from the original surface area. This surface area is consistent with spherical particles of diameter 38-34 nm and density 7.4 g/cm^3 (carbide), in agreement with particle sizes observed by HRTEM. The BET surface area does not change significantly as the catalyst is activated and used for reaction. Since the BET surface area includes contributions from the oxide and carbide phases along with the possibility that the surface carbon overlayers are porous, the BET surface area does not serve as a good indicator of catalyst activity.

The nature of the active phase
Our results indicate that the magnetite is not catalytically active, but transformation of the magnetite into carbide is a prerequisite to obtain FT activity. This is seen in the lack of initial methane formation on the sample activated in syngas at 523 K which had only magnetite at the end of the activation step. The CO activated sample was the only one that contained some carbide, and it shows a significant methane formation rate immediately after introduction of the syngas mixture. On the syngas activated samples, the rate of methane formation is seen to increase commensurate with the slow increase in carbide formation as seen in the TEM images, by XRD, and from the amount of carbon in the sample as measured by bulk CHN analysis.

Based on the TEM and XRD results, we cannot specify the stoichiometry of the carbide phase that is formed on our catalyst. If the active phase was c-$Fe_{2.5}C$, we would expect to see approximately 7.9 wt% carbon in the sample. After a 10 hour reaction with the CO activated sample, we have 6.85 wt% C and the sample still contains some magnetite as seen by XRD and TEM. The peak activity for methanation is achieved at this point. Therefore, our data would be consistent with the c-$Fe_{2.5}C$ being the active phase in these catalysts. The CO-activated sample showed some deactivation after 45 hours which was accompanied by an increase in carbon content. This suggests that carbonaceous layers were deposited on the sample which slow down reaction, as seen in TEM images.

The initial low activity of the catalysts activated in syngas can be related to smaller extents of carbide formation. Even after 45 h on stream the syngas activated sample contains 5.1 wt% C, which suggests that the sample has still not completely transformed into the carbide. This observation is confirmed by TEM and XRD which show larger amounts of magnetite present on these samples than for the CO-activated sample. The amount of carbon seen by bulk elemental analysis and the extent of carbide formation seen by TEM and XRD was the lowest in the case of the isothermal syngas reaction at 523K. This suggests that the higher temperature 543K treatment is necessary to accelerate the solid state transformation from magnetite into carbide.

Our conclusion that the transformation of magnetite into carbide is necessary to obtain FT synthesis activity in iron catalysts is consistent with the competition model proposed by Niemantsverdriet et al.[89] This model states that the initial low activity of metallic iron is due to rapid diffusion of carbon atoms into the iron to form carbide, thereby removing carbon atoms from the surface and rendering them unavailable for FT reactions. As bulk carbiding approaches completion, the rate of diffusion of carbon decreases and the amount of carbon available on the surface for FT reactions increases. Within this model, the bulk carbide is not necessarily the active phase, but carbide formation must occur before the catalyst surface can retain enough carbon to become active. Similar arguments can explain the effects of the magnetite to carbide transformation on the FT activity of the catalyst studied in this work. The syngas-activated catalyst consists primarily of magnetite, which is inactive for FT. Upon exposure to the syngas mixture, first magnetite forms, then CO is consumed mainly by conversion of magnetite to carbide. Once carbide is formed, any additional CO dissociation results in the formation of active carbon on the carbide particle surfaces or deposition of inactive graphitic carbon overlayers. Consequently, FT activity increases with the extent of transformation of magnetite into carbide. For the CO activated catalyst, carbide formation has already occurred to some extent prior to introduction of syngas, and the surfaces of these precarbided particles are active for FT synthesis immediately upon introduction of the syngas mixture. Ultimately, the buildup of inactive, graphitic carbon on the carbide particle surfaces inhibits the FT reaction and activity begins to decrease, resulting in the observed maximum in FT activity. Based on the TEM and activity results and the proposed model, nothing can be said about the nature of the active sites on the surface of the carbide particles, except that the formation of bulk carbide is necessary before the active site can be formed.

After performing FT synthesis on an unreduced iron oxide catalyst, Kuivila, et al.[10] observed 22% carbide in the bulk by Mössbauer spectroscopy, but only ~3% carbide on the surface by XPS, and therefore concluded that a sub-surface carbide phase had formed beneath a magnetite surface layer. Based in part on this result, they conclude that magnetite is the active phase for FT synthesis. Reymond, et al[6] also observed substantial amounts of carbide by XRD, but little or no carbide by XPS. Our observation of a 3-4 nm thick carbon layer on the carbide phase, but not on the

magnetite, allows a reinterpretation of the data in these two papers that does not require the counterintuitive concept of carbide formation beneath an oxide layer. In the presence of this carbon layer, the Fe 2p photoelectrons from the carbide would be attenuated by a factor of exp(-d/l) = 0.07 to 0.13, where l = 1.5 nm is the attenuation length of Fe 2p photoelectrons and d = 3 to 4 nm is the carbon layer thickness. Since the magnetite signal is unattenuated (no carbon buildup occurs on the magnetite phase), a bulk composition of 22% carbide would result in an apparent surface composition of only ~2-4% carbide as measured by XPS, exactly as observed by Kuivila, et al[10] and consistent with our results and the qualitative results of Reymond, et al[6]. Thus, measurement of low carbide signals by XPS cannot be interpreted to mean that carbide is absent from the catalyst surface, and therefore not an important phase in FT synthesis. Indeed, the difficulties involved in using XPS to detect carbide in the presence of oxide means that for partially carbided iron catalysts, XPS is not likely to shed any light on the chemical state of iron at the surface of the carbide particles. For a fully carbided catalyst, however, where the entire Fe 2p signal arises from the carbide particle surfaces, XPS could still prove useful in elucidating the nature of the iron at the surface of the particles.

The conclusion of Kuivila, et al.[10] that magnetite and not carbide is catalytically active also contradicts their findings of lower, but not zero, FT activity of the metallic Fe catalyst. The metallic Fe catalyst has undoubtedly no magnetite to start with. In their experiments, the CO turnover frequency seems to correlate well with the extent of carbide formation in agreement with our observations that methanation activity follows the increase in carbide content.

High-pressure, Slurry-phase Iron Catalysts

All the above samples were taken from a 1 atm reaction, which may not represent the morphologies found at industrial conditions. In order to gain insight to the morphological changes of an iron catalyst under more realistic conditions we obtained samples of a Fe/4.4Si/O.71K catalyst from Prof. B. H. Davis, University of Kentucky that were subjected to FT synthesis in a slurry phase reactor for progressively increasing lengths of time. The reaction was carried out at 543 K and 175 psig with H_2/CO=0.7 and a total space velocity of 2.0 nL h^{-1} g^{-1} (Fe). The samples were extracted after varying lengths of time ranging from 6.33 h to 456 h. Although there was no initial activation treatment for the catalyst, after 93 h of FT reaction, H_2 flow was stopped and CO flow was increased to of 2.0 nL h^{-1} g^{-1} (Fe). This was done for 22 h after which the original conditions were restored. The conversion increased significantly after the intermediate CO flow. Two samples were studied by TEM. The first, #RJO-177A, was taken from the reactor after 6.33 h on stream. The second sample, #RJO-177G, was taken from the reactor after 192.5 h on stream, about 80 h after the CO activation. This second sample, #RJO-177G, showed an activity of about four times that of the first sample.

The TEM of RJO-177A shows crystallites having an average diameter of 10 nm. The particle surfaces are mostly clean, i.e., free of carbon overlayers, however high resolution views indicate an occasional particle surrounded by overlayers of graphitic carbon. The diffraction pattern corresponds to the magnetite phase although the spotty nature of the diffraction ring pattern indicates larger crystals of magnetite. If the carbide phase is present, it is not possible to conclusively establish its existence since the various iron carbide phases have d-spacings around 2A which overlap with the (400) plane of Fe_3O_4. The TEM of RJO-177G, Fig. 7, showed the presence of a large number of crystallites which are covered by surface overlayers. The diffraction pattern shows rings consistent with magnetite although it is diminished in intensity compared to the pattern found for RJO-177A.

Because of the amount of graphitic carbon found in close proximity to magnetite in RJO-177G, it is not clear whether this catalyst reacted at higher pressures contains a greater amount of magnetite than the samples reacted at 1 atm or whether there was a passivation problem with these catalysts. This will be pursued further.

Conclusions

We have studied the role of various phases that are formed when an iron oxide catalyst is activated for the Fischer-Tropsch synthesis reaction. Our study shows that during activation, the iron oxide transforms from hematite to magnetite and finally into an iron carbide phase. As the carbide content of the catalyst increases, we see the development of FT activity as measured by the rate of methane formation and CO consumption. Neither magnetite nor hematite were found to have any FT activity. Based on this correlation between carbide formation and activity, we conclude that carbide formation is necessary before iron FT catalysts can exhibit any activity. The exact nature of the surface phase on which the reaction takes place remains elusive, however, due to an inability of surface sensitive techniques such as XPS to penetrate an amorphous carbon film which forms on the carbide particles during FT synthesis. These amorphous carbon films may hinder diffusion of the reactants to the catalyst surface, leading to eventual deactivation of the catalyst after long periods of reaction, and providing an explanation for the observation that the catalyst activity first increases and then starts to fall while the carbide content is still increasing. The formation of the carbide phase activates the catalyst while the simultaneous build-up of carbon on the carbide leads to deactivation. The phase transformations in the catalyst play an important role in determining the activity, attrition resistance, and deactivation of this catalyst. Activation of this precipitated catalyst transforms single crystals of hematite to smaller crystallites of carbide. While the transformation from hematite to magnetite is extremely rapid, the magnetite to carbide transition is much slower under the conditions of temperature and pressure employed in our study. As carbon deposits on the carbide particles, it serves to further pry the carbide particles apart.

Comparison of the various activation treatments indicates that CO activation is able to transform the iron oxide catalyst most rapidly into the carbide phase, and thereby results in the most active catalyst. H_2 reduction to metallic iron may not necessarily be desirable since it causes the sulfur impurities to segregate to the catalyst surface. The slowest activation was seen in syngas at reaction temperature (523 K), suggesting that activation at 543 K may be necessary to obtain higher catalyst activities at short times.

---

[1] Sault, A. G., *J. Catal.*, **140**, 121 (1993)

[2] Joint Committee for Powder Diffraction Standards, pub: JCPDS, International Center for Diffraction Data.

[3] Kuivila, C.S., Butt, J. B. and Stair, P. C., *Appl. Surface Sci.*, **32**, 99 (1988).

[4] Sault, A. G. *Appl. Surface Sci.*, **74**, 249 (1994).

[5] Davis, L.E., McDonald, N. C., Palmberg, P. W. Riach, G. E., and Weber, R. E., "Handbook of Auger Electron Spectroscopy." Perkin-Elmer Corp., Eden Prairie, MN 1978.

[6] Reymond, J. P. , Meriaudeau, P. and Teichner, S. J., *J. Catal.*, **75**, 39 (1982).

[7] Shroff, M. D., Kalakkad, D. S., Coulter, K.E., Kohler, M.S., Harrington, Jackson, N. B., Sault, A. G., and Datye, A. K., *J. Catal., in press.*

[8] Niemantsverdriet, J. W., van der Kraan, A. M., van Kijk, W. L., and van der Baan, H. S., *J. Phys. Chem*, **84**, 3363 (1980).

[9] Niemantsverdriet, J. W., van der Kraan, A. M., *J. Catal.*, **72**, 385 (1981).

[10] Kuivila, C. S., Stair, P. C., and Butt, J. B., *J. Catal.*, **118**, 299 (1989).

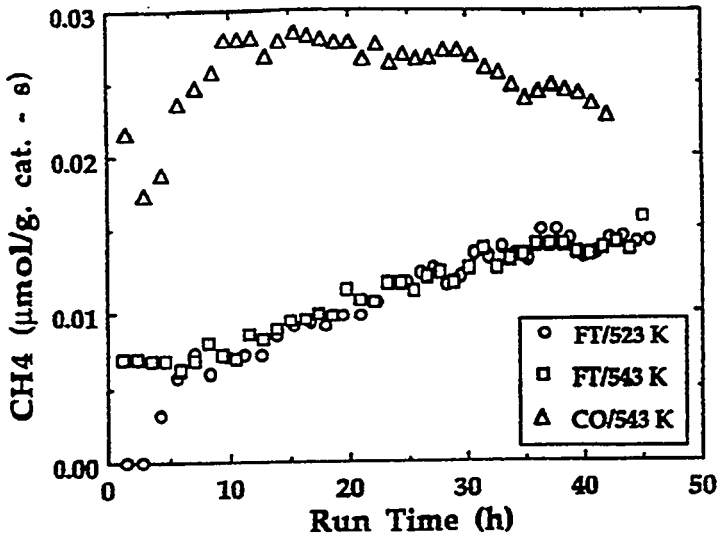

Figure 1. CH_4 formation during FT synthesis over time with various activation treatments.

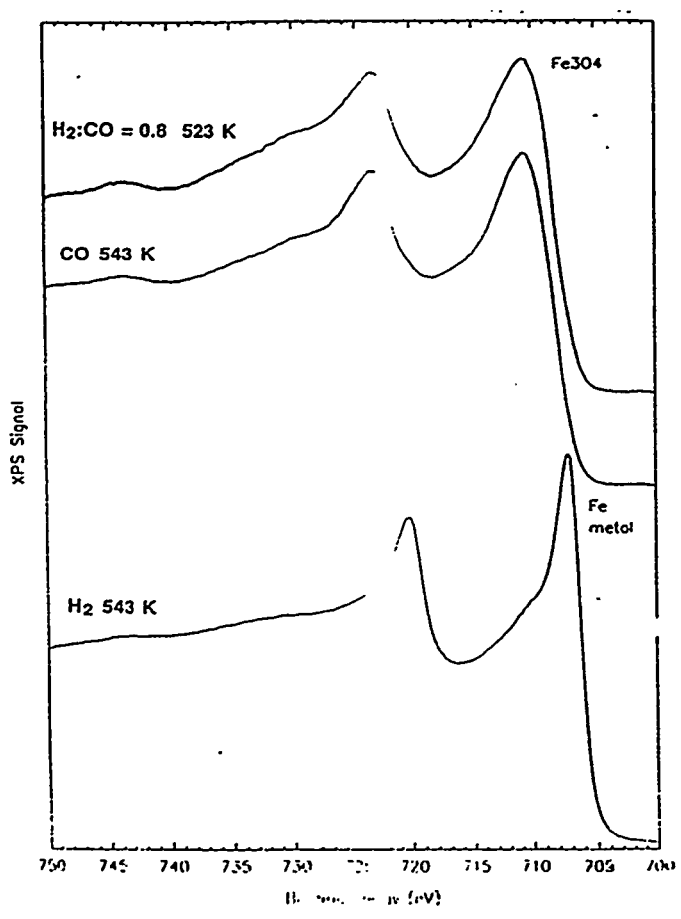

Figure 2. XPS of iron catalyst following three different activations.

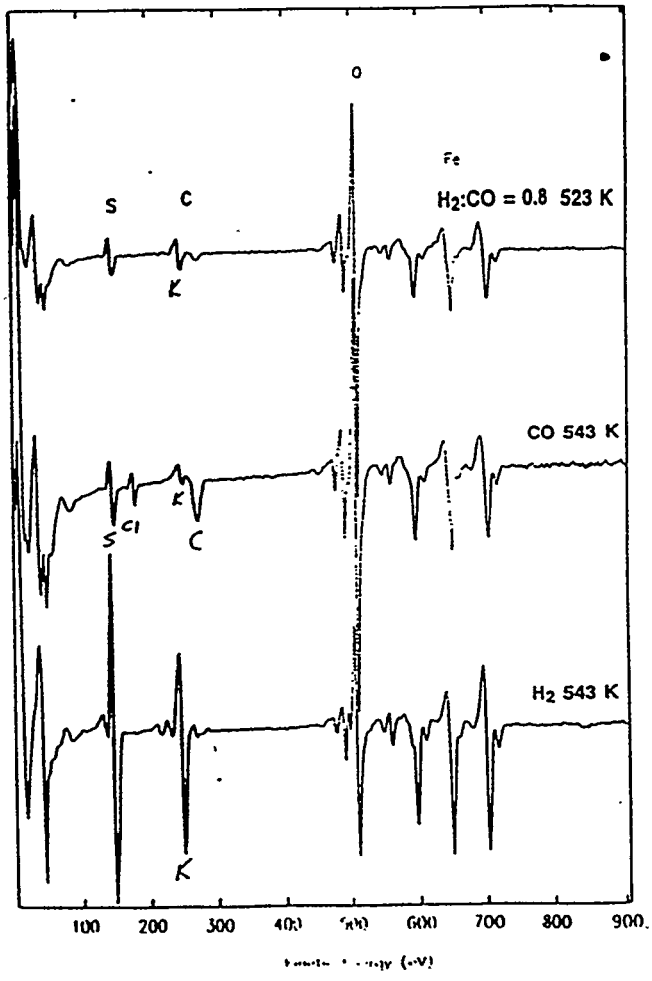

Figure 3. Auger spectra taken after three different activations.

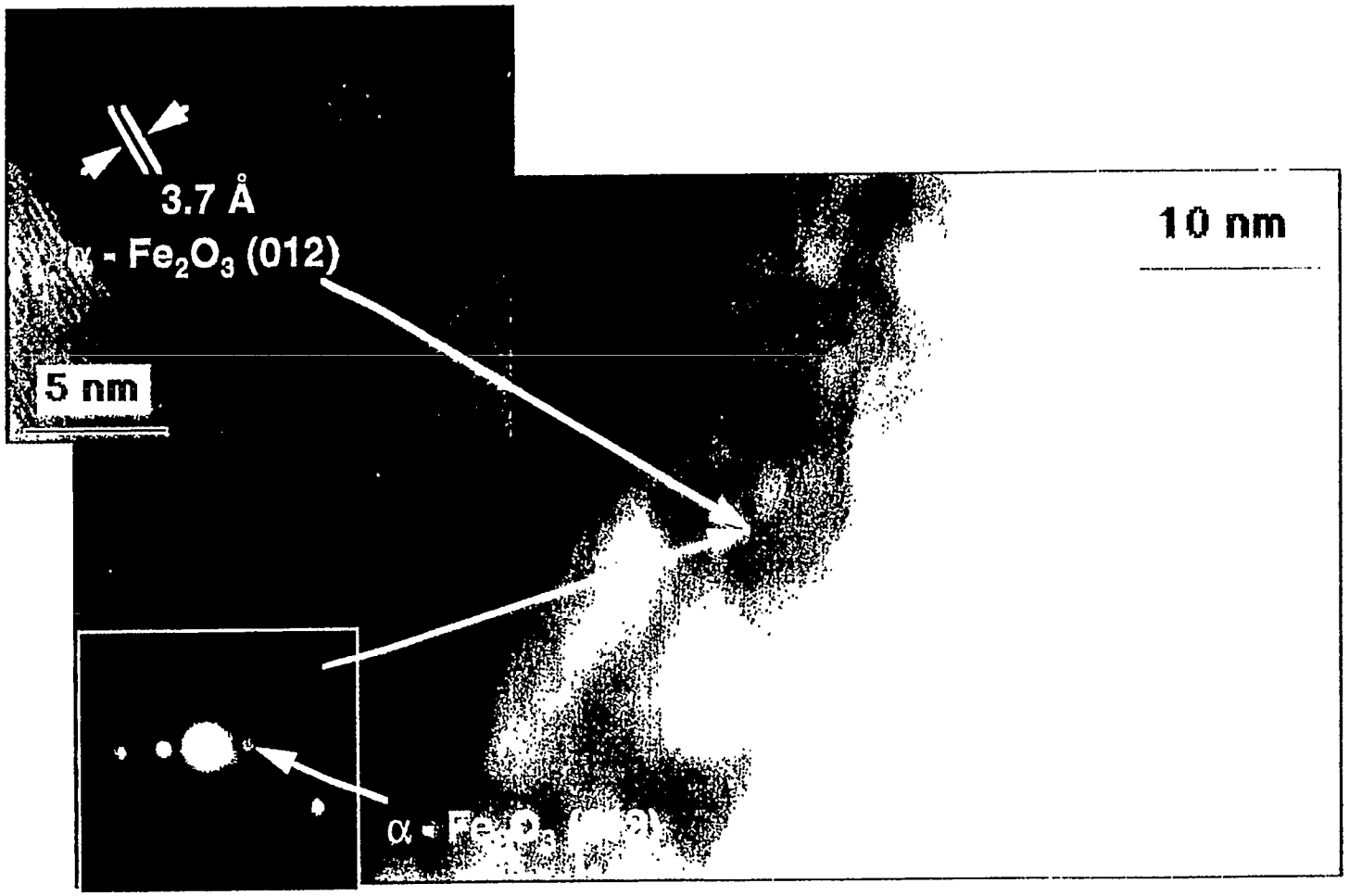
3.7 Å
α - Fe2O3 (012)
5 nm
10 nm

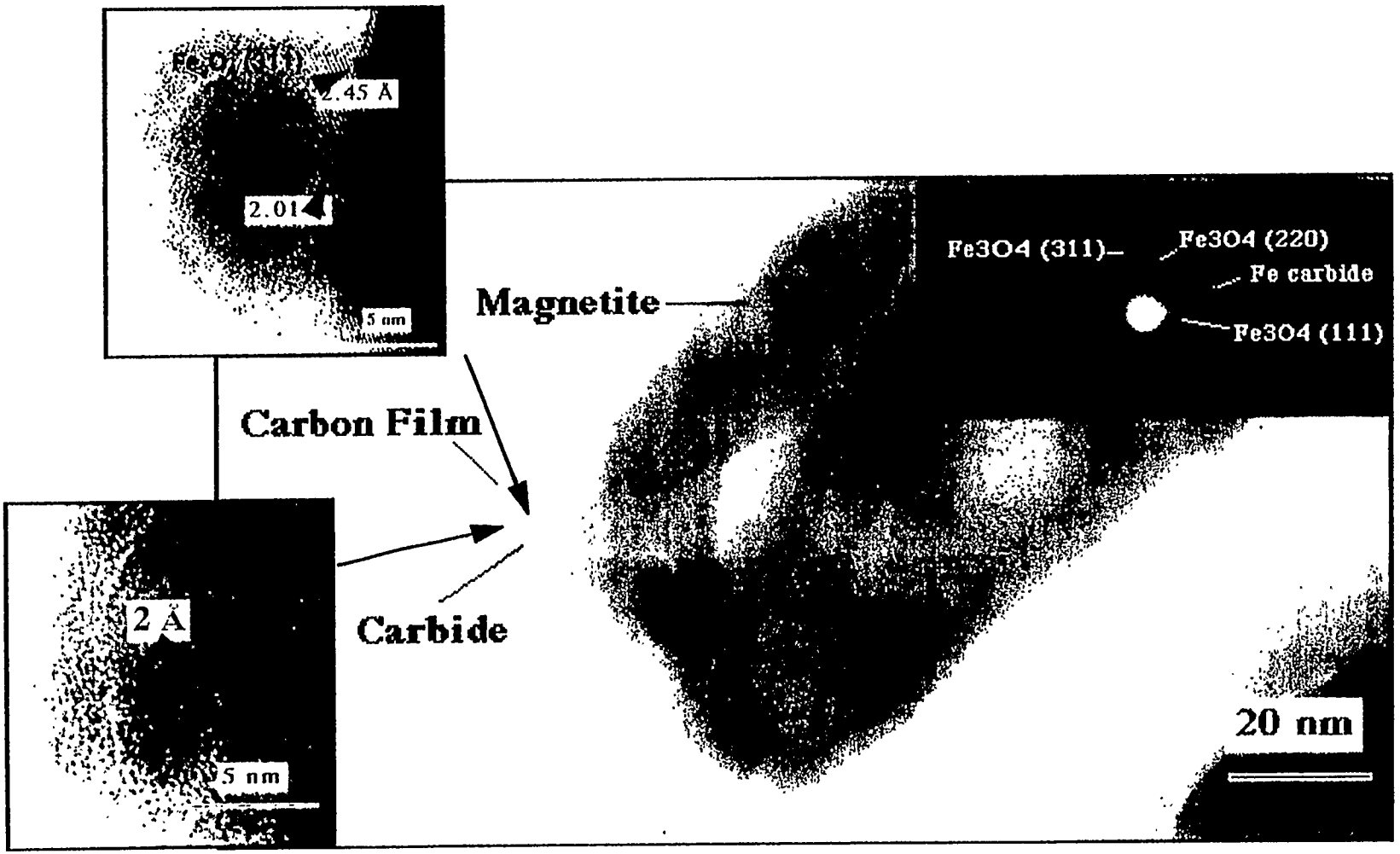
2.45 Å
2.01
5 nm
Magnetite
Carbon Film
Carbide
2 Å
5 nm
Fe3O4 (311)
Fe3O4 (220)
Fe carbide
Fe3O4 (111)
20 nm

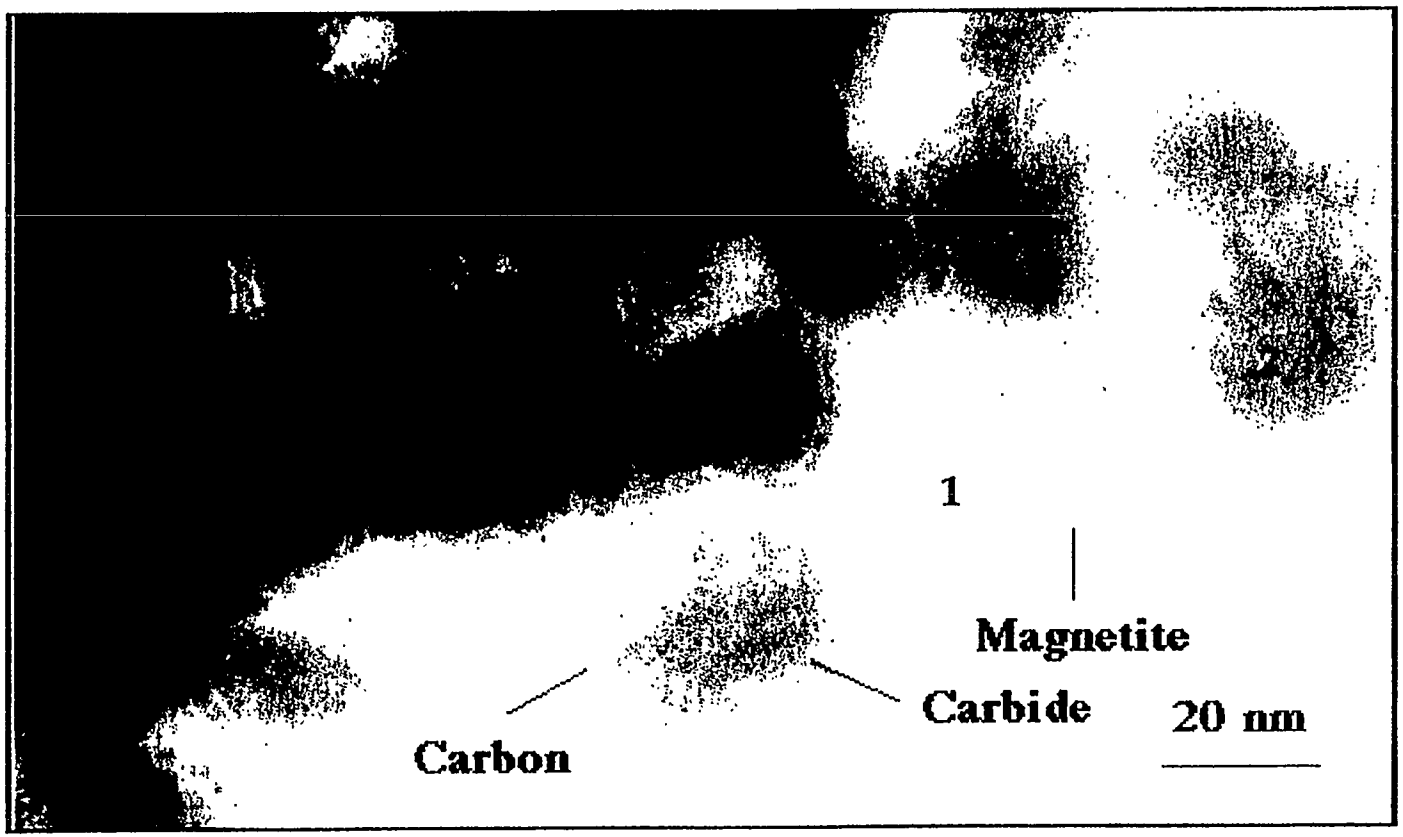
1
Magnetite
Carbide
Carbon
20 nm

Fig. 7

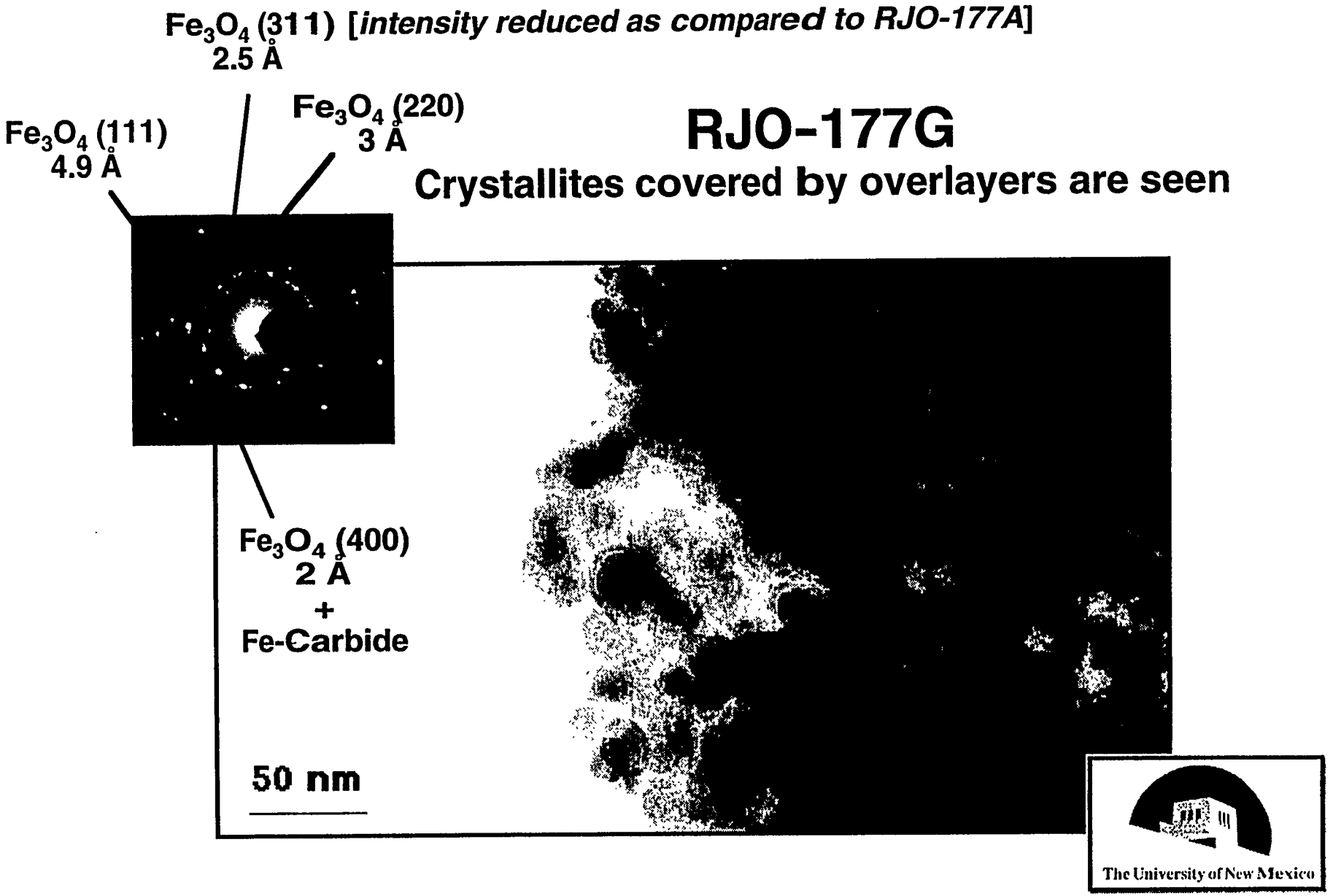
Fe_3O_4 (311) [*intensity reduced as compared to RJO-177A*]
2.5 Å
Fe_3O_4 (111)
4.9 Å
Fe_3O_4 (220)
3 Å
RJO-177G
Crystallites covered by overlayers are seen
Fe_3O_4 (400)
2 Å
+
Fe-Carbide
50 nm
The University of New Mexico

DEVELOPMENT OF MODIFIED FT (MFT) PROCESS

Jinglai Zhou, Zhixin Zhang, Wenjie Shen, Bijiang Zhang
Institute of Coal Chemistry, Chinese Academy of Sciences,
P. O. Box 165, Taiyuan, 030001, CHINA

ABSTRACT

Two-Stage Modified FT(MFT) process has been developed for producing high-octane gasoline from coal-based syngas. The main R & D are focused on the development of catalysts and technological process. Duration tests were finished in the single - tube reactor, pilot plant (100T/Y), and industrial demonstration plant (2000T/Y). A series of satisfactory results has been obtained in terms of operating reliability of equipments, performance of catalysts, purification of coal - based syngas, optimum operating conditions, properties of gasoline and economics etc. Further scaling - up commercial plant is being considered.

INTRODUCTION

China has abundant resource of coal, but that of oil and natural gas is insufficient in comparison with the large populetion. The coal production has been growing rapidly in recent years. At present, over 75% of the total energy consumption in economical activities and daily life is derived from coal. Air pollution is becoming an increasingly serious problem in many urban areas. On the other hand, in some regions, e. g. in Shanxi province, transpotation is the limiting factor of coal production. Growing demand for synfud and availability of cheap coal provide good opportunity for the development of synfuel technologies. It is considered as a comprehensive solution of the above problems, a urgent need and also of long term singnificance.

Fischer - Tropsch Synthesis (FTS) is one of the most important way to produce liquid fuel from syngas, which was already commercialized in South Africa (SASOL). However, the composition of product in FTS is very complicated, and the fraction of gasoline with unsatisfactory quality in product is limited.

China had experience in FTS. In the 50's, an intensive R&D of FTS were finished. Unfortunately, the programme was interrupted after pilot scale tests

because of rapid growth of petroleum production in China.

Since 1980, the catalysts and process research on FTS was resumed in many institutes and Universities. Based on the above studies, ICC,CAS (Institute of Coal Chemistry, Chinese Academy of Sciences) has succeeded in combining FTS catalyst and zeolite catalyst into an integrated two - stage process for producing high - octane gasoline, i. e. Modified FT Synthesis (MFT) process, which has been approved and being funded by the chinese government as state key projects during the 7th and 8th five - year plan. This report has briefly summarized the major results of R & D in MFT process.

MODIFIED FT (MFT) PROCESS

I . FT Synthesis

It is well known that in the conventional FTS the performance of gasoline obtained were not good on quality and quantity. Table 1 illustrated the typical product composition of conventional FTS, Which has the disadvantages :

* Very complicated product distribution. (mainly $C_1 \sim C_{50}$)
* Low gasoline fraction. ($<40\%$)
* Poor quality of gasoline (octane No. <70)
* Miscellaneous & complicated upgrading process of product.
* Only suitable to large scale commercialization.

I . Development of MFT Process

In order to overcome these shortages, we have successfully developed a two - stage Modified FT Synthesis (MFT) process for producing high - octane gasoline with high yield, which showed much better performance than any other one- stage hydrocarbon synthesis from syngas.

1. Principle and Procedure

Figure 1 showed a simplified block flow diagram of MFT process. The purified coal - based syngas is first passed through the 1st - Stage reactor (single - or multi - tube fixed bed) containing Fe - based catalysts for convertional FTS, and then the product effluents therefrom seperated the wax fraction flows into the 2nd - Stage reactor (adiabatic fixed bed) filled with a zeolite catalyst, where a number of reactions, such as cracking, isomerization, cyclization, aromatization and conversion of oxygenates to hydrocarbons etc, take place. The product hydrocarbons coming out of the 2nd-reactor is enrichened with gasoline fraction. The tail-gas, a part of which is recycled, can be used for town-gas. The aqueous phase product was drained off without environmental pollution

treatment.

Since the exothermic heat of 1st - stage FTS is so considerable, a high velocity fixed bed operated with tail - gas recycle was used to remove the large heat of reaction and to redistribute the temperature along the catalyst bed smoothly.

2. Technological Features

The major features of MFT process are as follows:

— Distribution of product hydrocarons ($C_1 \sim C_{50}$) can be highly confined to gasoline fraction ($C_5 \sim C_{11} > 70\%$) with higher yield

— The high - octane gasoline can be used as motor fuel satisfactorilly.

— It is simple and easy to operate at mild conditions.

— The product can be adjusted into different available fractions, such as gasoline, hard wax and towngas.

— It is suitable to small or middle scale commercialization.

DEVELOPMENT OF CATALYSTS

I. Fe - based Catalyst (1st-stage)

In the early studies, a spherical fused - Fe catalyst with higher activity was developed for the 1st-stage use and run over 1000 hrs both in lab and industrial size single tube fixed bed reactor. The fused - Fe catalyst can be easily prepared and more applicable to fluidized bed reactor.

Comparing with the fused catalyst, the precipitated - Fe catalyst shows higher activity and better stability. Furthermore, it can be directly pretreated with syngas at mild conditions, which led the catalyst to have a potential advantage for commercial use. Table 2 summerized the performance of Fused - and Precipitated - Fe Catalyst in MFT process.

I. Zeolite catalysts (2nd - Stage)

Several types of zeolites have been synthesized for the 2nd-stage in both bench scale (5L, 100L) and industrial size ($1M^3$) autoclaves. The structure and properties were also characterized as shown in Table 3.

OPERATION AND RESULTS OF MFT PROCESS

A series of test units has been used for R & D of MFT process. Many sets of 5 - 10ml fixed bed microreactor, gradientless reactor, 100 - 200ml model units, and 2 - 5L single tube reactors were used for catalyst evaluation, kinetics, process development and reactor engineering etc. We also constructed a pilot

the comparing results of pilot and industrial demonstration plant in detail.

INDUSTRIAL DEMONSTRATION PLANT

The industrial demonstration plant(2000T/Y) was constructed in 1993 at a small synthetic ammonia plant and being in operation for in 1994 more than 1700 hrs to demonstate the performance at commercial operating conditions.

As expested, the performance of demonstration plant was very satisfactory , and no siginficant scale-up effects have been observed. Product selectivity, gasoline yield, and quality are similar to those of the bench unit and pilot plant. The gasoline with octane number more than 90 contains no detectable impurities such as sulfur, nitrogen, oxygenates etc. It has passed quality screencing and in-vehicle tests and given satisfactory performance as commercial gasoline. Table 6—9 summerized the data for demonstration plant.

Ⅰ. Syngas(water gas)

1. Production

The syngas was supplied by the ammonia plant, where water gas was procuced by a moving bed gasifier using anthracitic coal. This gasifier is manufactured in China at low cost, and workers are familiar with this technology.

2. Clean up

A major cost when using coal raw material for syngas generation is the need to remove sulfur and other poisons. The AMISOL Process (Absorption of Alcohol-Amine Solvent) was used to remove the H_2S,COS,CS_2 and CO_2 etc. A home made deoxidizer was used for removing the trace amount of oxygen in syngas. The residual total sulfur compounds is less than 1mg/NM^3 syngas, while the oxygen content can be less than 10ppm, which satisfied the limit of catalysts.

Ⅱ. Pretreatment of Precipitated—Fe catalyst

The precipited-Fe catalyst was pretreated with syngas at mild conditions. From characteristics and performance of catalyst, it can be found that direct pretreatment with syngas was simple and beneficial to the formation of iron carbides, which led the catalyst to have higher activity and good stability. In prospect, the catalyst will have a potential advantage for comercialization.

Ⅲ. Effects of Technological Parameters on Catalyst Performance

1. The Effect of Temperature on Catalyst Performance

Fig. 2. shows the temperature effect on catalyst performance. It indicated that the CO conversion increases significantly with increasing temperature.

2. The Effect of Syngas Space Velocity on Catalyst Performance

Results of space velocity traverse are shown in Fig. 3. As shown in Figure, the CO conversion and yield of liquid fuel fall with increasing space velocity, However, the Space-Time-yield (STY) of fuel increases at the first and then fall down with increasing space velocity and a maximum value could be found at GHSV=500hr^{-1}.

3. The Effect of Receyle Ratio of Tail-gas/Syngas on Reaction Performance

Results in Table 10 show that the fuel yield increases significantly with increasing recycle ratio of tail-gas/syngas due to the increment of H_2 conversion and usage ratio of H_2/CO. The results implied that the recycle of tail-gas restrains the Water-Gas Shift Reaction and results in effective use of syngas.

Ⅳ. Kinetics & Reactor Design

1. Kinetics

For process design and reactor scale - up, kinetics of FTS on two types of precipitated catalysts were tested in an internally recycled gradientless reactor in the induserial operation ranges. For two types of catalysts (Fe/Cu/K, Fe/Mn/K), the following rate expression gave the best fit, i. e.

$$-R_{(H_2+CO)}=kP_{H_2}P_{CO}/(P_{CO}+bP_{H_2O})$$

Where the k is the kinetic constant and b is a function of temperature, i. e. $k=k_0\exp(-E/RT)$, $b=b_0\exp(-\Delta H/RT)$, $E=50-70$Kj/mol, $\Delta H=55-75$Kj/mol. The apparent activation energy of indicated that the internal diffusion is probably existent for the catalysts. While the value of ΔH implied that water is more strongly adsorbed on the catalyst surface than that of CO.

The kinetics of the Water-Gas-Shift reactron was also investigated. The models were obtained as fallows and the activation energy was ~120kJ/mol.

$$R_{CO_2}=K_w(P_{CO}P_{H_2O}-P_{CO_2}P_{H_2}/K_{eq})/(P_{H_2O}P_{CO}+bP_{H_2O})$$

2. Reactor Model and Tests Verify

By using one and two-dimensional pseudo-homogeneous reactor mathematical models, effects of operating conditions on the temperature profiles and CO conversions were investigated intensively. The mathematical model was also used to predict the performance of different commercial reactor designs.

- **Axial Temperature Profile**

Figures 4—6 describe the axial temperature distributions along the catalyst bed for the simulation of pilot plant and industrial demonstration reactor. As can be seen from the figures, calculations results showed good agreement with these obtained insite with a maximum mean error of 4℃. However, the data for one-dimensimal model is somewhat higher than that of two-dimensional model due to

the negelet of radial transfer resistance.

• Radial Temperature Profile

The radial temperature profiles for simulating of single-tube, pilot plant and demonstration reactors are shown in Figure 7. The curves calculated from the two-dimensional model indicated that radial temperature difference for three scale reactors are all less than 7℃. However, the case for industrial reactor is somewhat higher than the others, which expected as scaling-up.

• CO Conversion

Effects of operating variables on CO conversions were also studied. Briefly, the CO conversion increases significantly with the temperature rise. As can be seen from Figure 8, the CO conversions for three scale reactors were all increased straightly along the catalyst beds. This trend in CO conversions implied that the temperature distribution for the entirebed is uniform, and thus, the reactor could be operated smoothly. Furthermore, the calculated conversions are very closed to the measured data with a maximum error of 15%.

V. Summerized Points

The results of pilot and demonstration plant may be summarized:

— The experimental equipments of plant are simple, good operation, easy control, and no significant scale-up effects have been observed.

— The higher velocity fixed bed and good heat transfer may form a uniform temperature profile in 1st-stage multi-tube reactor.

— The performance of catalysts for two stages, in terms of activity, selectivety, strength and regeneration etc. are rather convincing.

— The gasoline product with Octane Number of more than 90 is unleaded and chemically similar to gasoline made from crude oil.

— The purification of coal-based syngas (residual total sulphur componds: < 1mg/Nm^3, O_2: <10ppm) was satisfactory for the catalysts.

ECONOMICS

I. Economical Analysis for Demonstration Plant

Based on the data of demonstration plant, a economical analysis is summerized in Table 11. As shown in the table considering the lower price of gasoline in China, the Fuel-Wax-Towngas joint production will be a good economic option.

I. Economical Projection for Commercial Plant

According to the situation of China, combining to the gasoline and FT wax market predictions, a commerical plant of MFT should be chosen to reconstruct

gasoline in China, the Fuel-Wax-Towngas joint production will be a good economic option.

I. Economical Projection for Commercial Plant

According to the situation of China, combining to the gasoline and FT wax market predictions, a commerical plant of MFT should be chosen to reconstruct an operating towngas plant or ammonia plant with available coal gasification and purification systems. A brief economcal projection for the first case is shown as Table 12.

CONCLUDING REMARKS

Energy is the most important issue facing modern China. Shortage in erergy supply is one of the limiting factors of economical growth at present. Since China is a developing country, the technologies appropriate to China should be

- Suitable for chinese coal with wider range.
- Affordable for smaller enterprises
- Simple process and easy operable

The MFT technology developed by ICC, CAS is one of the more efficient process for the purpose, which has been reached the stage of industrial demonstration plant. A scaling-up commercial plant is beeing considered at present.

In the meantime, attempts are being made to explore the international cooperation on the coal conversion technology, especially for MFT process. Furthemore, a pilot plant base was constructed for scaling-up new coal conversion processes. The base is open to other organizations at home and abroad. We believe that international academic exchange programme will be helpful for the development of clean coal technology in China as well as in the world.

ACKNOWLEDGMENT

The authors gratefully acknowledge the support of this work by Chinese Academy of Sciences, State Science & Technology commission, and State Planning Commission as the State-Key Projects in the 5-year plan (1980-1995)

Table 1. Typical Product Compositions of Conventional FT Synthesis (SASOL)

Process Features	Fixed - Bed (ARGE)	Fluidized - Bed (SYNTHOL)
HC Distribution (%)		
Methane	5	10
LPG (C_2-C_4)	13	33
Gasoline (C_5-C_{12})	22	39
diesel ($C_{13}-C_{19}$)	15	5
Wax (C_{20}^+	41	6
Oxygenated compounds	4	7

Table 2. A comparison results of Fused and Pptd - Fe in MFT process

Catalysts	Pptd - Fe/Zeolite			Fused - Fe/Zeolite		
Reaction Temp. (℃)*	235/300	230 - 233/300	260 - 265/320	250/310	260/320	275/300
H_2/CO (feed)	2	2	1.3 - 1.4**	2	2	1.5 - 1.7**
Recycle ratio (R)	0	3.4	3.0	0	3.5	3
CO conv. (%)	92.4	88	84.6	90	85.0	70
Usage ratio (H_2/CO)	0.97	1.6	1.26	0.7	1.7	1.4
HC Distribution (%)						
CH_4	7.19	4 - 4.5	7.26	9 - 16	14.0	10
C_2	2.9	0.7	1.66	7 - 10	8.5	6
C_3-C_4	14.4	16	9.53	10 - 15	22.5	24.0
C_5^+	75.5	72 - 80	81.54	60 - 74	55.0	60

Table 3. Physico - Chemical Characteristics of Zeolites

SiO_2/Al_2O_3	60 - 70
Na_2O (%)	0.1 - 0.5
Surface Area (M^2/g)	400 - 500
Pore Capacity (CC/g)	0.18 - 0.21
Adsorbed Amount (%)	
N - hexane	10 - 14
Cyclo - hexane	5 - 8
H_2O	7 - 9

Table 4. Major Results for Different Scake of MFT

1st-reactor Catalyst volume(V_1)	Fixed bed 10ml	Recyde fixed 200ml	Recycle fixed 5L	Pilot multi—tubes 0.3M^3	Demonstration Multi-tubes 7.2M^3
Time-on-stream (hr)	7560	>500	>500	>1500	>1000
P(MPa)	2.5	2.5	2.5	2.5	2.5
GHSV(hr^{-1})	500	510	500	350—450	400—520
T_r(T_1/T_2℃)	250—270/300	255/300	260—265/295	265/300	265—270/310—330
H_2/CO (feed)	2*	2*	1.3—1.5**	1.3—1.5**	~1.5**
Recycle Ratio	0	~3.5	3.0	3.0	3.0~3.5
CO conv. %	75—80	86	85	81	70—79
HC distribution(wt%)					
CH_4	12—15	10—12	10—12	13—15	10—13
C_2	2—5	3—4	2—5	4—6	3—4
C_{3-4}	17—20	18—20	17—19	15—20	24—28
C_5^+	60—65	64—70	64—71	59—68	55—63

* Syngas: $(CO+H_2)\geq 95\%$ prepared by cracking of Methanol,

** Coal-based Syngas(watergas): $(CO+H_2)\geq 85\%$

Table 5. Major Specifications and Results of MFT Pilot and Demonstration Plant

Plant	Pilot	Demonstration
Feed rate of syngas (M^3/hr)	150	3,600
Capacity of gasoline (T/Y)	100	2,000
1st - Stage Synthesis Reactor		
Reactor type	Multi - tube	Multi - tube
Reactor size	Φ26×4,000mm×155	Φ32×7,000mm×1320
Catalyst volume (m^3)	0.3	7.2
2nd - Stage Reforming Reactor		
Reactor type	Adiabatic	Adiabatic
Reactor size	Φ420×3,740mm	Φ1,600×12,500mm
Catalyst volume (m^3)	0.538	10.8
Time—on—stream(hrs)	1549	956
Operating Conditions		
Temp. 1st - stage (℃)	250 - 260	260 - 270
2nd - stage (℃)	310 - 330	330 - 350
Pressure (Two Stage) (Mpa)	2.5	2.5
GHSV (Hr^{-1})	400	~500
H_2/CO (Feed*)	1.44	1.5
Recycle Ratio	3 - 4	3
CO Convesion (%)	82.1	72
H_2/CO Usage Ratio	1.31	1.31
HC Distribution (Wt%)		
C_1	6.20	12.63
C_2	3.84	3.17
C_{3-4}	17.78	21.54
C_5^+	72.12	62.66

* Coal - based syngas (water gas): $(CO+H_2)\% \approx 85\%$

Table 6. Properties of Gasoline of MFT Demonstration Plant

№		1		2	
1. group composition(%)		100.0		100.00	
Aromatics		40.35		40.26	
N—paraffins		10.12		9.96	
Iso—paraffins		34.21		34.65	
Cyclo—paraffins		10.17		9.07	
Oleffins		1.15		1.91	
Unknown		4.00		4.16	
2. Carbon Number Distribution(%)		100.00		100.00	
~C_5		18.12		19.31	
C_6		19.77		19.98	
C_7		24.51		25.54	
C_8		25.42		24.71	
C_9		8.84		7.38	
C_{10}		2.73		2.19	
C_{11}		0.18		0.15	
$\geqslant C_{12}$		0.43		0.74	
3. Aromatics composition(%)					
C_6(benzene)		3.20		4.22	
C_7(xylene)		30.09		33.93	
C_8		46.34		45.23	
C_9		15.39		12.92	
durene	C_{10}	0.52	4.88	0.45	3.60
the others		4.36		3.15	
C_{11}		0.09		0.1	

Table 7. Composition of Aqueous Phase Product of MFT Demonstration Plant

composition(%)	1	2	3
Methanol	0.0021	0.0663	0.0120
Ethanol	0.0183	0.0105	0.0204
N—propanol	0.0019	—	0.0002
$\sum^{*}$	0.0324	0.0928	0.0475

* The others are H_2O

Table 8. Typical Composition of Syn—gas and Tail—gas of MFT Demonstration Plant

Gas	H_2	CO	N_2	CO_2	CH_4	C_2^0	C_3^0	C_4^0	C_{5-6}^0	H_2/CO	$CO+H_2$(%)
feed	52.72	34.72	11.06	0.2	1.30	—	—	—	—	1.52	87.44
Tail	44.11	15.76	10.10	14.2	10.27	0.96	2.16	1.69	0.75	2.79	59.87

Table 9. Propeties of FT Wax Produced from MFT Demostration Plant

Sample	Demonstr. Plant FT wax	Sasol FT wax(H_1)	Rubrchemie FT wax(hard)
Colour	White	White	White
Hardness	hard	hard	hard
Penetrometer number(25℃)	<5	<1	4.0
Drop point(℃)	111℃±1	—	99
Setting point(℃)	100℃±1	>94.5	90
Soluble acid and alkali	no	—	—
Acid number	—	<0.1	<0.1

Table 10. The Effect of Recycle Ratio of Tail—gas/Feed—gas on Reaction Performance

Recycle ratio(R)	0.31	3.0
CO conv.(%)	73.55	74.78
H_2 conv.(%)	52.72	62.7
C_5^+ g/NM^3($CO+H_2$)	59.0	90.7
Usage ratio H_2/CO	1.13	1.35

Table 11. Economic Analysis for Demonstration Plant

• Basis:			Full-Towngas joint production	Fuel-Wax-Towngas Joint production
Input:	Coal	(Ton/Y)	10000	
	Electricity	(KWH/Ton)	4426	
	Steam	(Ton/hr)	1	
	Water	(Ton/hr)	90	
output:	Gasoline	(Ton/Y)	1940	1261
	Wax	(Ton/Y)	—	700
	Residum	(Ton/Y)	60	39
	Town gas	(NM_3/Y)	1111×10^4	1111×10^4
• Capital investment		(RMB*)	25million	
• capital	Costs			
	Gasoline	(RMB/Ton)	2415	
	Wax	(RMB/Ton)	13600	
	Residuum	(RMB/Ton)	800	
	Town gas	(RMB/NM^3)	0.60	
• Total output value		(RMB/Y)	784×10^4	1571×10^4
• After-Tax profit		(RMB/Y)	62.4×10^4	529×10^4

Table 12. Economic Projection for Commercial Plant*

Input:	Syngas	$60,535NM^3/hr$
Output:	gasoline	18640T/Y
	wax	10543T/Y
	Towngas	$17448NM^3/hr$
	Residiuum	983T/T
Total investment		1.0 Billion RMB
Revenue		0.98 Billion RMB
After-Tax profit		0.406 Billion RMB
Payout		4.7 year

* Based on the Reconstruction of a Operating Towngas Plant

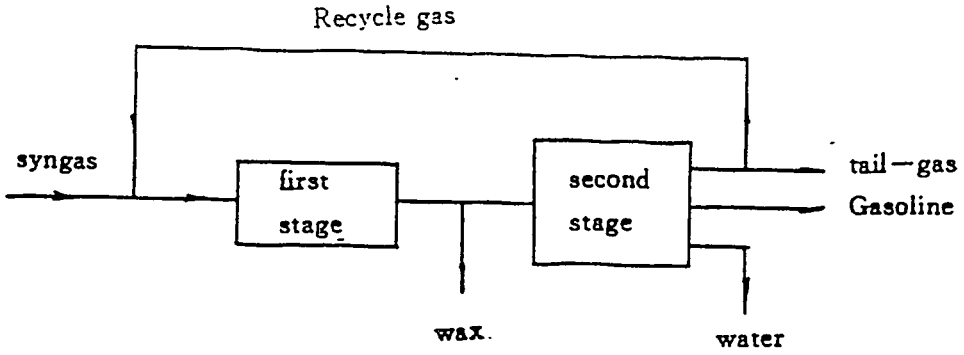

Fig. 1. Simplified Block Flow Diagram of MFT process

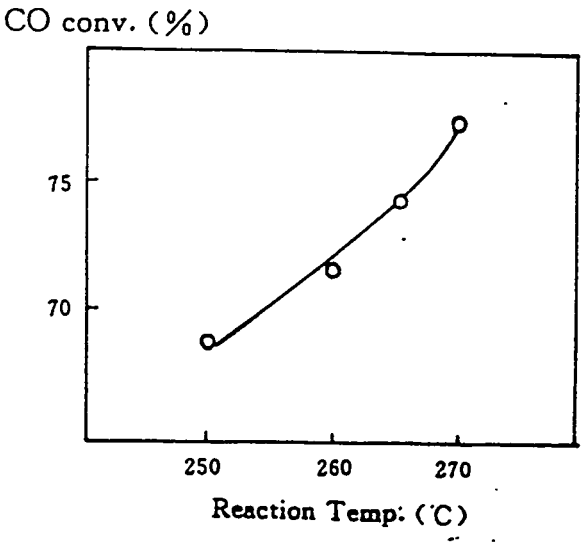

Fig. 2. The effect of reaction temprature on catalyst performance

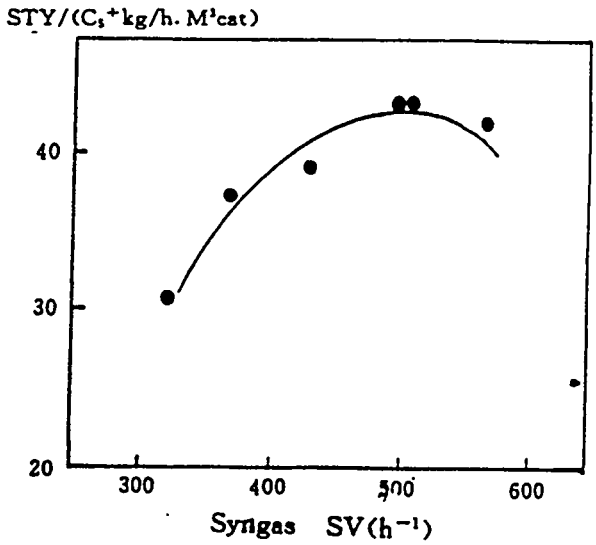

Fig. 3. The effect of Syngas space velocity on reaction results

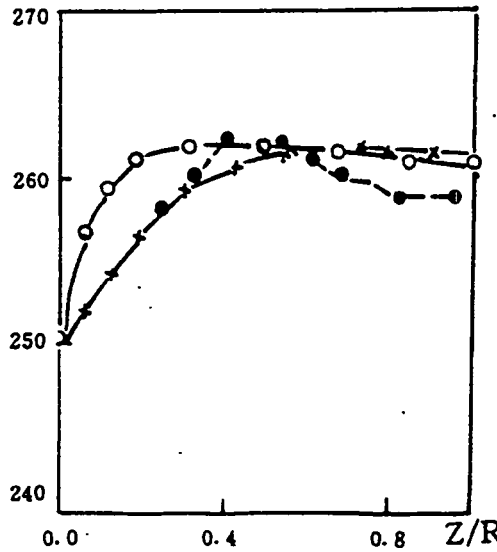

D_t=32mm, R_l=7.0m, SV=500hr^{-1}, T_0=250℃, T_w=255℃, R_N=3.0

○ Data from one-dimensionol model

× Data from two-dimensionol model

● Data measured insite

Fig. 4. Axial temperature profile for single-tube Simulation

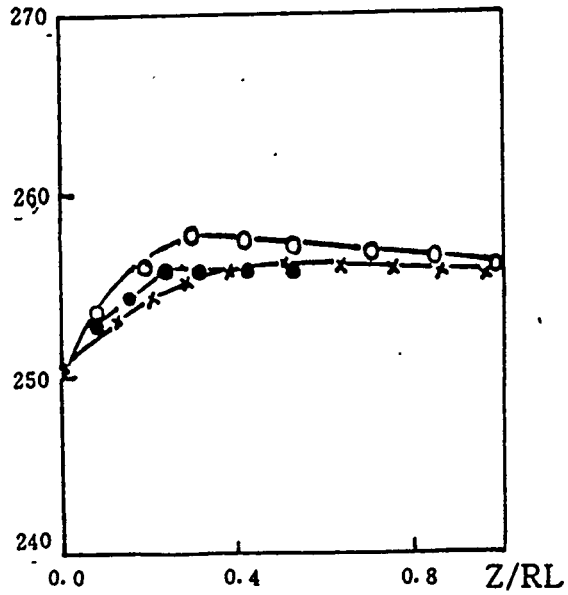

Fig. 5. Axial temperature profile for pilot plant
D_t=26mm, R_L=4.0m, SV=425hr^{-1}, T_0=T_w=250℃,
R_N=3.5. others see figure 4.

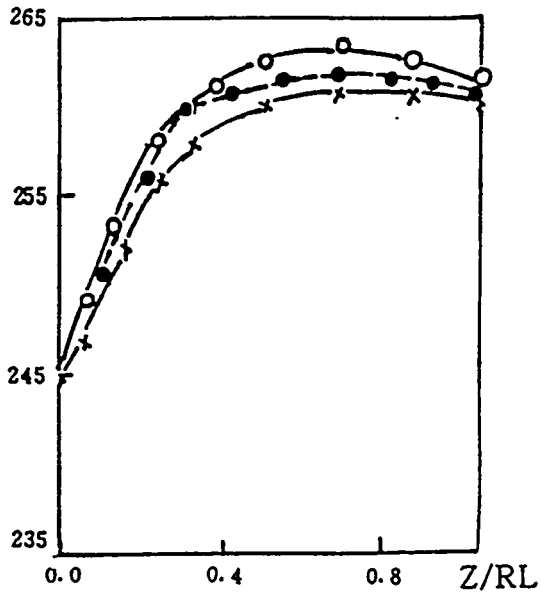

Fig. 6. Axial temperature profile for industrial reactor
D_t=32mm, R_L=7.0m, SV=324hr^{-1}, T_0=T_w=245℃,
R_N=3.3. others see figure 4.

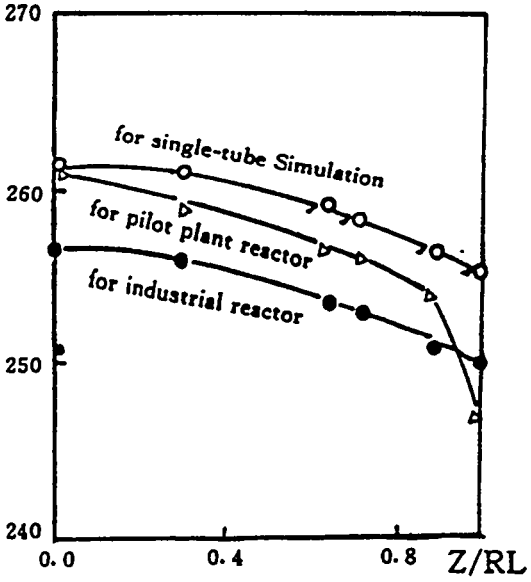

Figure 7 Radial temperature profile

operation voriables see figure 4-6.

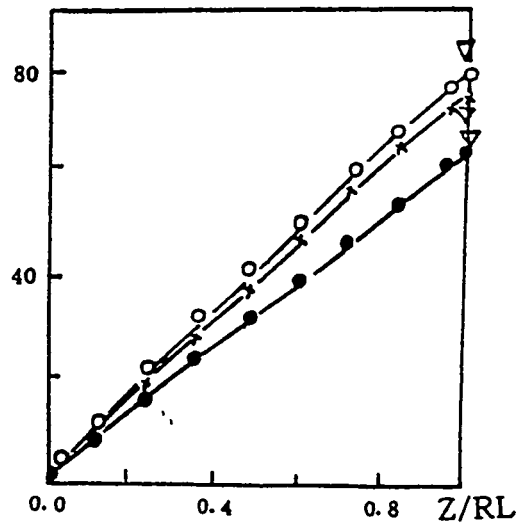

Figure 8 CO conversions along the catalyst bed

×Pilot plant
○ Industrial demonstration plant
△ measured data
Operation condition can see figures 4 to 6

SIMULATION MODELS AND DESIGNS FOR ADVANCED FISCHER-TROPSCH TECHNOLOGY

Gerald N. Choi, Sheldon J. Kramer and Samuel S. Tam
(Bechtel Corporation San Francisco, CA)
Joseph M. Fox III (Consultant)

CONTRACT NUMBER; DE-AC22- DE-AC22-91PC90027

PERIOD OF PERFORMANCE: September 26, 1991 to February 28, 1996

ABSTRACT

Process designs and economics were developed for three grass-roots indirect Fischer-Tropsch coal liquefaction facilities. A baseline and an alternate upgrading design were developed for a mine-mouth plant located in southern Illinois using Illinois No. 6 coal, and one for a mine-mouth plant located in Wyoming using Powder River Basin coal. The alternate design used close-coupled ZSM-5 reactors to upgrade the vapor stream leaving the Fischer-Tropsch reactor. ASPEN process simulation models were developed for all three designs. These results have been reported previously.

In this study, the ASPEN process simulation model was enhanced to improve the vapor/liquid equilibrium calculations for the products leaving the slurry bed Fischer-Tropsch reactors. This significantly improved the predictions for the alternate ZSM-5 upgrading design. Another model was developed for the Wyoming coal case using ZSM-5 upgrading of the Fischer-Tropsch reactor vapors. To date, this is the best indirect coal liquefaction case. Sensitivity studies showed that additional cost reductions are possible.

INTRODUCTION

This study is conducted under an extension of DOE Contract No. DE-AC22-91PC90027, entitled "Baseline Design/ Economics for Advanced Fischer-Tropsch Technology. This program previously has:

- Developed a baseline design and two alternate designs for indirect coal liquefaction using advanced Fischer-Tropsch (F-T) technology. The baseline case used Illinois No. 6 Coal and conventional petroleum refinery technology for product upgrading. ZSM-5 treatment of the F-T reactor vapor stream was studied as an alternate product upgrading scheme. Another alternate case used Wyoming Powder River Basin coal. All schemes contain a wax hydrocracker.

- Determined the capital cost, operating costs and utility requirements for the above three cases.

- Developed ASPEN Process Flowsheet Simulation (PFS) Models for the above cases and a discounted-cash flow (DCF) economics spreadsheet model. Product valuation is based on a linear programming (LP) analysis of the refinery which will process the liquefaction products

into finished products. In concert, these closely-coupled models constitute a research tool which DOE can use to plan, guide, and evaluate its ongoing and future research and commercialization programs for the production of transportation fuels by indirect coal liquefaction.

- Performed preliminary sensitivity studies to examine the effects of key independent process variables and economic assumptions on the baseline case using the ASPEN PFS model.

Details concerning the overall design basis, process selection, and costs were reported at a previous DOE/PETC contractor's conference[1]. The PFS model development, the F-T product valuation study, and the simulation model results were presented in three separate papers last year[2-4].

This paper describes recent enhancements to the ASPEN PFS model which improved the predictions for the alternate ZSM-5 product upgrading case. This enhanced model then was used to study the effects of using ZSM-5 upgrading for Wyoming Powder River Basin coal.

PROCESS DESIGN

Overall Plant Configuration

Figure 1 is a block flow diagram showing the overall F-T process configuration for the baseline design case. The OSBL area is not shown. The ISBL plant contains three areas.

1. Area 100 - Syngas Production -- In the baseline design case, synthesis gas is generated in Shell gasifiers from ground, dried coal. The raw syngas is washed in a wet scrubber followed by single-stage COS/HCN hydrolysis and cooling, acid gas removal, and sulfur polishing. Area 100 also includes the sour water stripper and sulfur recovery plants. Because of the lower sulfur content of the Wyoming coal, Rectisol, instead of an inhibited amine, is used in the acid gas removal step, and the COS/HCN hydrolysis step is not required.
2. Area 200 - The Fischer-Tropsch Synthesis Loop -- The F-T synthesis loop includes F-T synthesis, CO2 removal, recycle gas compression and dehydration, hydrocarbon recovery by deep refrigeration, hydrogen recovery and autothermal reforming processing steps. The hydrocarbon recovery unit includes oxygenates wash columns which are not required when the F-T reactor vapor product is upgraded in the ZSM-5 reactors.
3. Area 300 - Product Upgrading -- In the baseline case, this area contains eight processing steps; 1) wax hydrocracking, 2) distillate hydrotreating, 3) naphtha hydrotreating, 4) naphtha reforming, 5) C4 isomerization, 6) C5/C6 isomerization, 7) C3/C4/C5 alkylation, and 8) saturated gas processing and product blending. The hydrocracked and hydrotreated naphthas are catalytically reformed to produce an aromatic gasoline blending component. The lighter materials are isomerized and alkylated to produce a high quality gasoline blending stock. Purchased butanes are required to alkylate all the available olefins.

   In the ZSM-5 upgrading case, this area only contains four processing steps; 1) wax hydrocracking, 2) C4 isomerization, 3) C3/C4/C5 alkylation, and 4) saturated gas processing and product blending. In addition, this case produces sufficient butanes so that extra butanes are available for sale.

These F-T liquefaction facilities produce C3 LPG, a C5 - 350 F gasoline blending component, and a 350 - 850 F combined light and heavy distillate. As mentioned above, the ZSM-5 upgrading case also produces some butanes for sale. Liquid sulfur is the primary byproduct. The

hydrocarbon products contain no significant sulfur or nitrogen because of the nature of the Fischer-Tropsch reaction. Oxygen is reduced to less than 30 ppmv in the hydroprocessing steps. Olefins are saturated to low residual levels in both the gasoline and distillate products. There are virtually no aromatics in the distillate. The diesel portion of the distillate has a high cetane number (about 70), and the jet fuel and heavy distillate fractions have low smoke points. However, they do have relatively high pour points which must be carefully controlled. In the baseline case, the gasoline product is a mixture of C3/C4/C5 alkylate, C5/C6 isomerate and catalytic reformate. It is basically a raw gasoline with almost an 89 clear (R+M)/2 octane number.

Reactor Design

The F-T slurry reactor essentially is a bubble column reactor in which the slurry phase is a mixture of molten wax and catalyst. The synthesis gas provides the agitation necessary for good mixing and mass transfer of the reactants and products between the two phases. The slurry reactor design was chosen over a fixed bed reactor based on an earlier DOE sponsored Bechtel study[5,6]. The design is based on the slurry F-T reactor data from Mobil's two-stage pilot plant studies for the DOE[7]. These results are the basis for development of the yield correlations contained in the F-T slurry bed computer model used in this study[8].

In this reactor model, vapor and liquid product streams are continuously removed. In the baseline case, this vapor stream is cooled for hydrocarbon recovery before entering the carbon dioxide removal step. The heavy liquid stream goes to the hydrocarbon recovery area wherein all the hydrocarbon products are fractionated and sent to the appropriate product upgrading plant. All the C6 and heavier hydrocarbons in either the vapor or liquid streams are recovered and upgraded to useable products irrespective of the stream in which they leave the slurry bed F-T reactor. Thus, the accuracy of the vapor/liquid flash calculation is not a critical issue.

MODEL ENHANCEMENTS

In the alternate ZSM-5 upgrading case, the entire vapor stream leaving the slurry bed Fischer-Tropsch reactor passes through the ZSM-5 oligomerization reactor before cooling and hydrocarbon recovery. Consequently, in this case, it does make a difference in which stream the heavier hydrocarbon products leave the slurry bed F-T reactor. In the original ASPEN PFS model, individual normal paraffins and 1-olefins through C19 and a single lumped C20+ wax pseudocomponent were used to represent the F-T reaction products. From Schultz-Flory theory, the average carbon number of the C20+ wax can be calculated[8]. The normal boiling point and gravity of the C20+ wax pseudocomponent were determined based on its calculated average carbon number by extrapolating the properties of normal paraffins and 1-olefins assuming that 70% of the wax has a single olefinic bond. These properties (1032 F ABP, 38.6 API gravity, and a 618 MW) were then used as input to the ASPEN pseudocomponent property estimation procedures.

An examination of the model predictions of the amount of material leaving the slurry bed reactor in the vapor and liquid streams for the ZSM-5 case was made to see if the model was making a reasonable prediction of the amount of hydrocarbons leaving in the vapor stream. It predicted that 4804 lbs/hr or about 77% of the C18 material was leaving in the vapor stream, and 3716 lbs/hr or about 68% of the C19 material was leaving in the vapor stream. By simple extrapolation, one would expect about 2500 lbs/hr of the C20 material to leave in vapor stream.

However, the model predicted that only 1128 lbs/hr of the C20 and heavier material was leaving in the vapor stream. Thus, it was easy to conclude that this model is underpredicting the amount of C20 and heavier material leaving the F-T reactor in the vapor phase and the lumping of all the C20 and heavier material into a single C20+ wax pseudocomponent is the cause.

Additional components through C29 were added to improve the vapor/liquid equilibrium predictions at the F-T slurry bed reactor conditions of 488 F and 325 psia. Individual components were added for normal eicosane and 1-eicosene since they both were available in the standard ASPEN PLUS data bank. Although the ASPEN PLUS data bank contains data for the normal praffins through C30, it does not contain pure component physical property data for any olefinic compounds above C20. The API *Technical Data Book - Petroleum Refining* and other standard data compilations do not contain such data either. Thus, in an effort to minimize the number of components in the simulation, a single pseudocomponent was used to represent the olefin/praffin mixture at each carbon number from C21 up to and including C29.

At each carbon number for a mixture of 70 mole% 1-olefins and 30 mole% normal paraffins, the normal boiling point and API gravity of the C21 through C29 olefin/paraffin pseudocomponents were estimated by extrapolating the property differences between the 1-olefin and the corresponding normal paraffin. These properties and the calculated molecular weight were then used as input to the ASPEN pseudocomponent property estimation procedures. In this new situation, the wax pseudocomponent is the C30 and heavier material. Using the same methodology as before, the properties of the C30+ wax were estimated (1128 F ABP, 36.4 API gravity, and a 743 MW) and used as input to the ASPEN pseudocomponent property estimation procedures. Thus, eleven additional components were added to the ASPEN simulation model, and the wax pseudocomponent was redefined to be the C30 and heavier material (although the actual wax production still is considered to be the C20 and heavier material).

Examination of the results from this simulation showed that 715 lbs/hr or about 17% of the C28 material left the F-T reactor in the vapor stream, and 571 lbs/hr or about 14% of the C29 material left in the vapor stream. Furthermore, this model predicted that only 228 lbs/hr of the C30+ wax was leaving in the vapor stream. From a simple extrapolation of the C28 and C29 vapor flows, one would expect about 400 lbs/hr of C30 in the vapor alone. Thus, the model still underpredicts the amount of wax leaving in the vapor stream, but now to a much lesser extent.

Therefore, another approach was used to correct this underprediction without adding additional components. Figure 2 shows an extrapolation of the amount of each carbon number component in the vapor stream as a function of carbon number. This figure shows that about another 30 components are needed to reduce the weight in the vapor of a given carbon number component to below 1 lb/hr. As shown in this figure, the weight in the vapor decreases exponentially with increasing carbon number. Thus, using the average boiling point of the wax in the vapor/liquid equilibrium calculations always will underpredict the amount of wax in the vapor.

From Figure 2 the expected weight in the vapor of the C30 through C50 components is 2762 lbs/hr, and that of the C30 through C60 components is 2803 lbs/hr. Therefore, it was decided to use an effective boiling point for the C30+ wax pseudocomponent rather than the calculated average boiling point to better reproduce its vapor/liquid behavior at the F-T reactor conditions since this behavior is controlled by the lightest portion of the C30+ wax. This effective boiling point being defined as that which produces an amount of vapor equal to that predicted by Figure 2 for the C30+ material. By trial an error, it was found that reducing the average boiling point of

the C30+ wax by 154 Fahrenheit degrees (to produce an effective boiling point of 974 F) results in 2834 lbs/hr of the C30+ wax component leaving the F-T reactors in the vapor stream.

Thus, an enhanced PFS model was developed which contains eleven new components, and a revised C30+ wax component which uses an effective boiling point that is 154 Fahrenheit degrees below that which would be calculated based on the average boiling point of the C30+ wax. This enhancement was incorporated in all the ASPEN PFS indirect coal liquefaction models.

COMPARISON OF MODELS

Table I compares the results from the original ASPEN simulation model with those from the enhanced model for the baseline case with Illinois No. 6 coal. As expected, there is little difference between the two models. Any differences are well within the accuracy of the experimental data upon which the models are based. Also contributing to these slight differences is a switch from ASPEN/SP software in which the original models were developed to ASPEN PLUS software which is used for the enhanced models.

The preliminary Crude Oil Equivalent (COE) prices shown at the bottom of the table are based on the 1995 EIA forecast with a 75% owners equity. Table II shows the basic economic parameters used for these COE calculations in which margins are used to relate the product values to the calculated COE. The COE values are included in Table I only to show that the differences between the two models truly are insignificant in terms of the COE.

Table III compares the results from the original ASPEN simulation model with those from the enhanced model for the ZSM-5 upgrading case using Illinois No. 6 coal. As a result of the revision, there are significant differences between the results from the two models. In the original model, 1,128 lbs/hr of C20+ wax left the F-T reactor in the vapor stream and was processed in the ZSM-5 reactors. In the enhanced model, the flow rate of the C20+ wax material increased to 18,614 lbs/hr. As a result, the total amount of C7+ material processed in the ZSM-5 reactors increased by about 12% to 163,214 lbs/hr, and the hydrocarbon feed to the wax hydrocracker was reduced by 16,489 lbs/hr. These, changes increased the performance difference between the ZSM-5 case and the baseline design case since the effect of ZSM-5 reactor is increased.

Compared to the baseline design case, the ZSM-5 upgrading case radically alters the F-T product distribution and makes more gasoline, butanes, and LPG and less distillate. The gasoline blending stock is of a higher quality[3]. The differences between these two designs previously has been discussed in detail[4], and will not be repeated here. However, with the enhanced model, the differences are somewhat greater and result in a 0.1 $/bbl reduction in the COE.

ZSM-5 UPGRADING OF THE ALTERNATE WYOMING COAL

The primary design differences between the base Wyoming Powder River Basin coal case and the baseline design case are a consequence of the coal properties, although location also is important. Wyoming coal contains less sulfur and has a higher moisture content. It has to be dried from the as-received moisture content of 31 to 8 wt% moisture before gasification as compared to drying the Illinois No. 6 coal from 8.6 to 2 wt% moisture. The lower sulfur content necessitates a Rectisol process rather than an amine guard treating system for sulfur removal. Water availability and cost and the availability of skilled labor also were considered in developing the Wyoming

base case. Consequently, there are significant design changes in the syngas production area and the offsite water treatment plant for the Wyoming location. Reference 4 provides a detailed comparison between the base Wyoming coal case and the baseline Illinois No. 6 coal case.

Because reference 4 showed an economic incentive for both the ZSM-5 upgrading case (Illinois No. 6 coal) and the Wyoming coal case over the baseline case, a ZSM-5 upgrading Wyoming coal case was developed using the enhanced model. In this case a ZSM-5 reactor processes the vapor products from the F-T reactor and converts the olefins, C7+ paraffins and oxygenates to isoolefins, isoparaffins, naphthenes, and aromatics. This eliminates the catalytic reforming, C5/C6 isomerization, naphtha hydrotreating, and distillate hydrotreating plants in the Area 300 Product Upgrading Section. C4 isomerization and alkylation are still required, but the yield of alkylate is increased, and no butanes have to be purchased. The F-T wax stream is processed in the same manner as the base case by mild hydrocracking.

Table IV compares the two Wyoming coal cases. The differences are similar to those for the Illinois coal cases except that the Wyoming ZSM-5 coal case purchases more power than the base case. The ZSM-5 case has a higher gasoline to distillate ratio. Since the F-T reactor is run at a 50% wax yield in both cases, the product yield differences are due entirely to the conversion of the F-T distillate to naphtha in the ZSM-5 reactor. These upgrading reactions produce more light ends which, in turn, increases the C3 LPG, butanes and alkylate yields. The COE for the Wyoming coal ZSM-5 upgrading case is 2.8 $/bbl below that of the base case. This reduction is about 0:25 $/bbl less than that for the corresponding Illinois No. 6 coal cases.

SENSITIVITY STUDIES

Previously, the ASPEN PFS model was used to study the sensitivity of the baseline Illinois No. 6 coal design to coal feed rate, F-T syngas conversion per pass, wax yield, and several F-T slurry bed reactor design variables[4]. This paper reports the effects of coal feed rate and wax yield for the Wyoming coal ZSM-5 upgrading design. The base conditions are 19,789 tons/day of dry Powder River Basin coal and 70.5% hydrogen conversion/pass (corresponding to a 83.5% syngas conversion/pass) at a 50 wt% wax yield.

Effect of Design Plant Capacity

The effect of plant capacity on the overall capital investment of the facility is exponential with an average cost-capacity exponent of 0.92 over the range from 10,000 to 60,000 tons/day of dry ROM coal. This exponent is high because the plant contains many parallel processing trains. At the base case coal feed rate, most of the Area 100 and 200 plants are at their maximum size and have multiple trains. For each processing plant, the PFS model calculates the required number of duplicate trains from the total plant throughput.

Table V shows the overall liquefaction plant inputs and outputs as a function of design capacity. As expected, the COE decreases as the capacity increases. Figure 3 shows that doubling the plant capacity will reduce the COE by about 1.7 $/bbl. However, this plant will have a dry ROM coal feed rate of almost 40,000 tons/day and cost almost 5,900 million dollars. It will produce just over 100,000 bbls/day of C3 and heavier hydrocarbons.

Effect of Design Wax Yield

The F-T reactor simulation model is designed to simulate operations at wax yields between 10 and 75 wt% wax. The effect of wax yield between 30 and 75 wt% wax was studied by varying the F-T reactor temperature between 503 and 468 F. Table VI summarizes the results. Below a wax yield of about 30 wt%, insufficient butanes are available to alkylate the olefins, and butanes have to be purchased. The Wyoming coal ZSM-5 upgrading model is not designed to handle this situation. Above about a wax yield of 68 wt%, the model predicts that excess isobutane is going to the alkylation unit, and some reprogramming is necessary to correctly handle this situation. As currently structured, the model slightly overpredicts the plant cost for these cases.

As the wax yield increases, less gasoline and more distillate are produced. At a 30 wt% wax yield, the gasoline to distillate ratio is 4.7, and at a 75 wt% wax, it decreases to 0.96. Also, as the wax yield increases, the character and the quality of the gasoline changes dramatically. At a 30 wt% wax yield, the gasoline contains just over 28% alkylate, 19 wt% aromatics, 8 wt% olefins, and has an (R+M)/2 octane number of about 76. At a 75 wt% wax yield, the gasoline contains about 14% alkylate, 11 wt% aromatics, 4 wt% olefins, and has an (R+M)/2 octane number of about 71. These gasoline quality changes are the result of two factors. At low wax yields, more hydrocarbon products leave the F-T reactor in the vapor phase and are upgraded to isoparaffins. isoolefins, naphthenes and aromatics. Some cracking also occurs producing more butanes and light olefins in the ZSM-5 reactor. Thus, more alkylate is produced. As the wax yield increases, less material is upgraded in the ZSM-5 reactors, and more wax is processed in the wax hydrocracker. The wax hydrocracker produces both distillate and a lower octane gasoline blending component which has very low aromatic and olefin contents. As a result of these competing forces, more C4 and heavier hydrocarbons are produced as the wax yield increases. However, the propane yield decreases at a greater rate so that there is a slight loss in the yield of C3 and heavier hydrocarbons as the wax yield increases.

Figure 4 shows the effect of wax yield on the COE. These COEs were calculated using a constant delta between the gasoline and crude oil price[3]. They do not account for the changing quality of the gasoline as a function of wax yield. Reducing the wax yield from the design case of 50 wt% to 30 wt% reduces the COE by about 0.5 $/bbl.

CONCLUSIONS AND RECOMMENDATIONS

All the ASPEN PLUS PFS models for indirect Fischer-Tropsch coal liquefaction have been enhanced to better characterize the vapor/liquid equilibrium predictions of the F-T product at reactor conditions. This enhancement did not change the model predictions for the baseline design case which uses conventional technology to upgrade the F-T wax. However, it changed the predictions for the cases where the F-T vapors are upgraded using ZSM-5 catalyst since more material now leaves the F-T reactors in the vapor phase. Parametric studies have shown that conditions other than those of the base case may be more economically attractive. Additional product upgrading schemes are being studied. One uses the ZSM-5 reactor to upgrade the low quality hydrocracked naphtha. Another involves substituting a fluid catalytic cracking unit for the wax hydrocracker and using the additional C4 through C7 olefins to make ethers for use as gasoline blending components.

Additional LP studies should be done to further define the product values; especially for a situation like that of the wax yield study where the gasoline quality changes dramatically as the wax yield changes.

ACKNOWLEDGMENT

Bechtel, along with Amoco who was the main subcontractor for a major portion of this study, expresses our appreciation to the DOE for both financial funding and technical guidance.

REFERENCES

1. Choi, G. N., Tam, S. S., Fox, J. M., Kramer, S. J. and Marano, J. J., "Baseline Design/ Economics for Advanced Fischer-Tropsch Technology", DOE/Proceedings of The Coal Liquefaction and Gas Conversion Contractors' Review Conference, September 27-29, 1993.
2. Choi, G. N., Tam, S. S., Fox, J. M., Kramer, S. J. and Rogers, S., Process Simulation Model for Indirect Coal Liquefaction using Slurry Reactor Fischer-Tropsch Technology", Symposium on Alternative Routes for the Production of Fuels, ACS National Meeting, Washington, D. C., August 21-26, 1994.
3. Marano, J. J., Choi, G. N. and Kramer, S. J., "Product Valuation of Fischer-Tropsch Derived Fuels", Symposium on Alternative Routes for the Production of Fuels, ACS National Meeting, Washington, D. C., August 21-26, 1994.
4. Choi, G. N., Tam, S. S., Fox, J. M., Kramer, S. J. and Marano, J. J., "Process Design Simulation Models for Advanced Fischer-Tropsch Technology", DOE/Proceedings of The Coal Liquefaction and Gas Conversion Contractors' Review Conference, September 7-9, 1994.
5. Fox, J. M., "Slurry vs. Fixed-Bed Reactors for Fischer-Tropsch and Methanol", 1990 Topical Report - DOE Contract No. DE-AC22-89PC89876.
6. Fox, J., M., "Fischer-Tropsch Reactor Selection", *Catalysis Letters* 7 (1990) 281-292.
7. Kuo, J. C., "Slurry Fischer-Tropsch/Mobil Two-Stage Process of Converting Syngas to High Octane Gasoline", DOE Contract No., DE-AC22-80PC30022, Final Report, June 1983; and "Two-Stage Process for Conversion of Synthesis Gas to High Quality Transportation Fuels", DOE Contract No. DE-AC22-83PC60019, Final Report, October, 1985.
8. Fox, J. M. and Tam, S. S., "Correlation of Slurry Reactor Fischer-Tropsch Yield Data",*Topics in Catalysis* 2,(1-4), 285-300 (1995).

Figure 1
INDIRECT COAL LIQUEFACTION BASELINE STUDY
OVERALL PROCESS CONFIGURATION

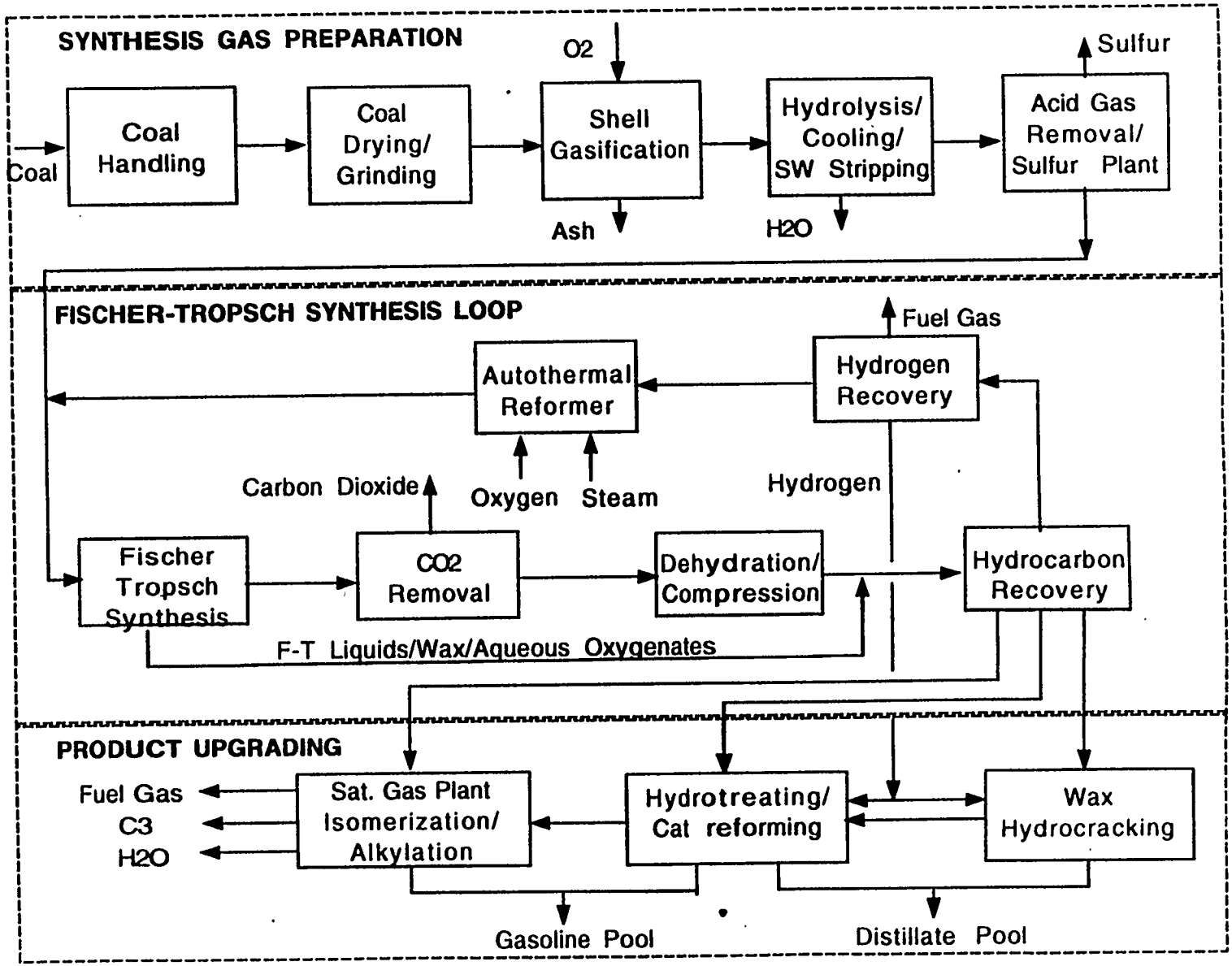

Figure 2
Weight in Vapor vs. Carbon Number

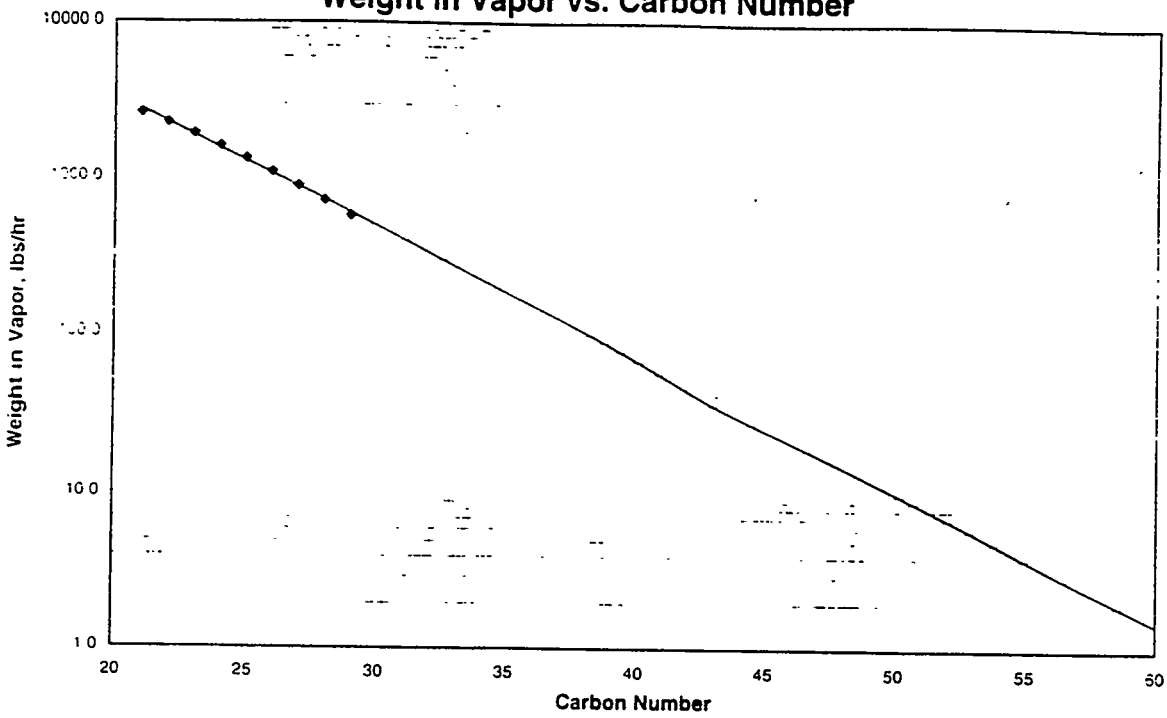

Figure 3
Effect of Design Plant Capacity on COE

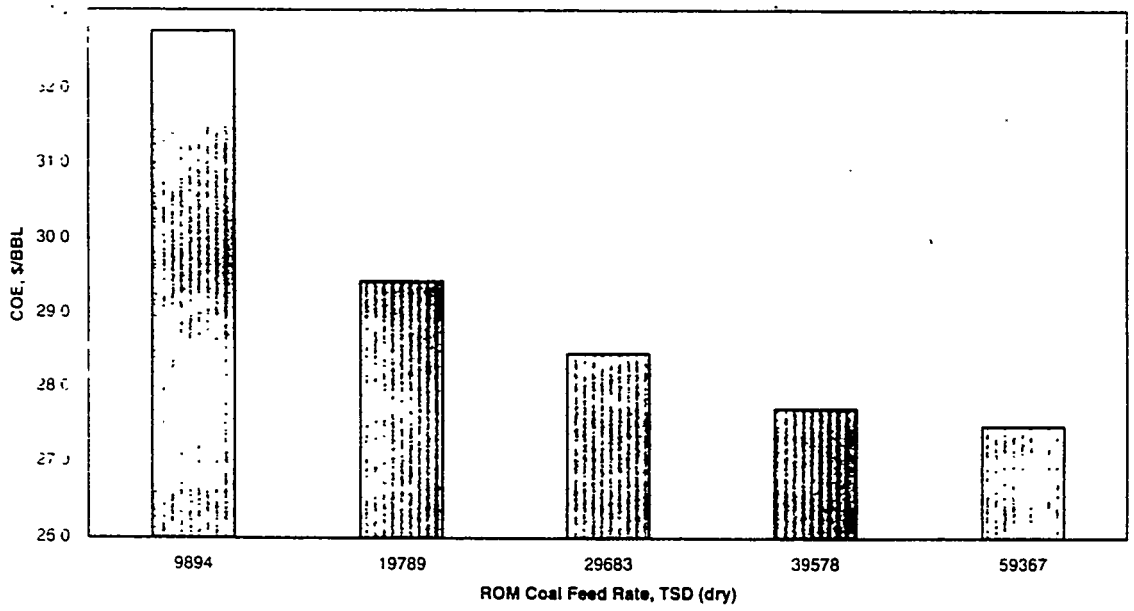

Figure 4

Effect of Wax Yield on COE

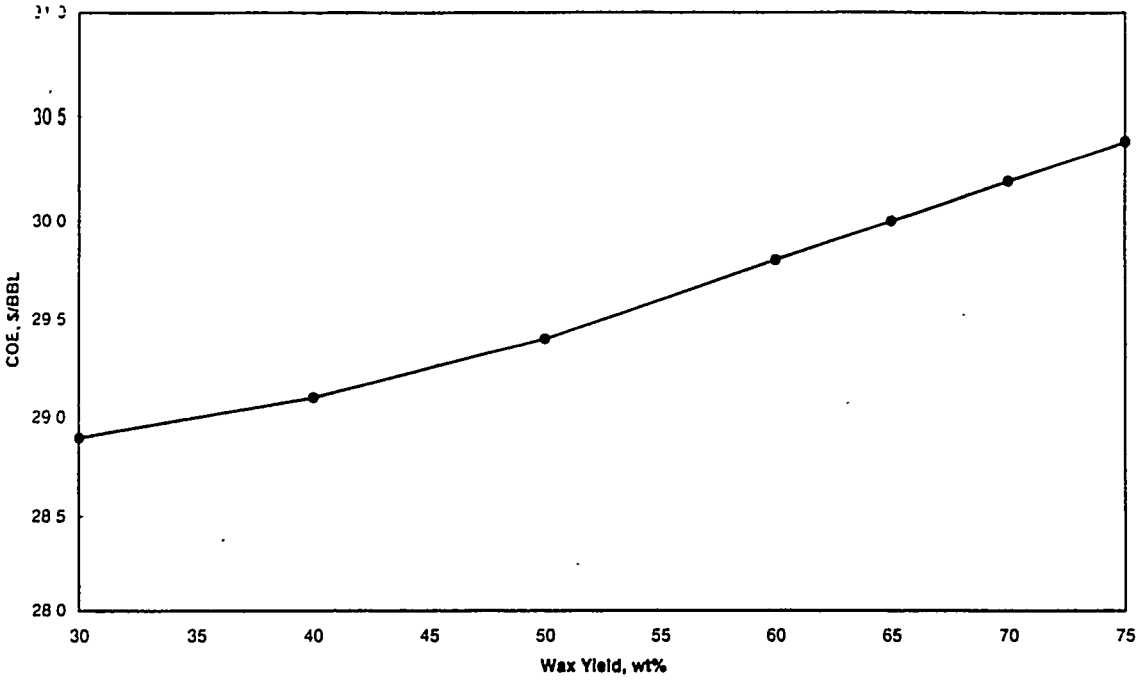

TABLE I

Comparison of the ASPEN Models for the Baseline Design Case

	Original Model	Enhanced Model	Difference
ROM Coal Feed Rate, TSD (MF)	18575	18575	0
Slag Production Rate, TSD (MF)	2244	2244	0
Electricity Purchase, MEGA-WH/SD	1304.5	1303.8	-0.7
Raw Water Make-up, MMGSD	14.460	14.460	0
Gasoline Production, BSD	23952	23943	-9
Distillate Production, BSD	24681	24686	5
Liquid Propane Production, BSD	1923	1922	-1
Mixed Butanes Production, BSD	-3121	-3110	11
Sulfur Production, TSD	560	560	0
No. of Operators and Maintenance Workers	1088	1088	0
Total Installed Capital, $MM	2963.5	2963.8	0.3
Catalyst and Chemicals, $MM	31.1	31.1	0.0
Crude Oil Equivalent Price, $/BBL	35.8	35.8	0.0

File: PAPER895/Baseline

TABLE II

Economic Parameters

Coal Cost, $/ton (31 wt% moisture)	4.5
LPG Price, $/bbl	12.3
N-Butane Price, $/bbl	14.5
Sulfur Price, $/ton	60
Electricity, cents/KWH	5
Plant Life, years	25
Depreciation, years	10
Construction Period, years	4
Owner's Cost, % of initial capital	5
Owner's Initial Equity, %	75
Bank Interest Rate, %/year	8
General Inflation, %/year	3.1
Escalation Above General Inflation, %/year	
Coal	0.8
Crude Oil	2.4
Electricity	0.3
Federal Income Tax, %	34
State and Local Taxes, %	0
Maintenance and Insurance, % of initial capital	1
Labor Overhead Factor, % of salary	40
On-Stream Factor, %	90.8
Percent Plant Operational in	
First Year	100
Second Year	100
Third Year	100

File: PAPER895/TAB2

TABLE III

Comparison of the ASPEN Models for the ZSM-5 Upgrading Case

	Original Model	Enhanced Model	Difference
ROM Coal Feed Rate, TSD (MF)	18575	18575	0
Slag Production Rate, TSD (MF)	2244	2244	0
Electricity Purchase, MEGA-WH/SD	1194.8	1262.0	67.2
Raw Water Make-up, MMGSD	14.460	14.436	-0.024
Gasoline Production, BSD	30317	31255	938
Distillate Production, BSD	16820	15858	-962
Liquid Propane Production, BSD	2509	2623	114
Mixed Butanes Production, BSD	886	998	112
Sulfur Production, TSD	560	560	0
No. of Operators and Maintenance Workers	1024	1024	0
Total Installed Capital, $MM	2901.1	2897.2	-3.9
Catalyst and Chemicals, $MM	30.7	31.4	0.7
Liquid Feed to the Wax Hydrocracker, Mlbs/hr	290.0	273.5	-16.5
Crude Oil Equivalent Price, $/BBL	32.8	32.7	-0.1

File. PAPER895.XLS/Alternate

TABLE IV

Comparison of the ZSM-5 Upgrading Model for the Wyoming Coal Case with the Base Wyoming Coal Design Case

	Base Western Coal Design Case	Western Coal ZSM-5 Upgrading Case	Difference
ROM Coal Feed Rate, TSD (MF)	19789	19789	0
Slag Production Rate, TSD (MF)	1747	1747	0
Electricity Purchase, MEGA-WH/SD	2111.7	2198.4	86.8
Raw Water Make-up, MMGSD	9.803	9.573	-0.230
Gasoline Production, BSD	23756	31026	7270
Distillate Production, BSD	24466	15772	-8694
Liquid Propane Production, BSD	1907	2613	706
Mixed Butanes Production, BSD	-3101	980	4081
Sulfur Production, TSD	108	108	0
No. of Operators and Maintenance Workers	1190	1126	-64
Total Installed Capital, $MM	3149.0	3075.0	-74.0
Catalyst and Chemicals, $MM	21.3	21.5	0.2
Total C3+ Hydrocarbons, BSD	47028	50391	3363
Total C4+ Hydrocarbons, BSD	45121	47778	2657
Crude Oil Equivalent Price, $/BBL	32.2	29.4	-2.8

File: PAPER895.XLS/WestZSM-5

TABLE V

Sensitivity Study - Effect of Design Plant Capacity
Wyoming Coal ZSM-5 Upgrading Case

ROM Coal Feed Rate, TSD (MF)	9894	19789	29683	39578	59367
Slag Production Rate, TSD (MF)	874	1747	2621	3494	5241
Electricity Purchase, MEGA-WH/SD	1099.2	2198.4	3297.6	4396.8	6595.3
Raw Water Make-up, MMGSD	4.787	9.573	14.36	19.146	28.719
Gasoline Production, BSD	15513	31026	46539	62051	93077
Distillate Production, BSD	7886	15772	23658	31544	47317
Liquid Propane Production, BSD	1307	2613	3920	5227	7840
Mixed Butanes Production, BSD	490	980	1470	1960	2940
Sulfur Production, TSD	54	108	163	217	325
No. of Operators and Maintenance Workers	685	1126	1636	2074	3087
Total Installed Capital, $MM	1667.8	3075.0	4494.0	5870.0	8758.6
Catalyst and Chemicals, $MM	10.8	21.5	32.3	43.0	64.6
Total C3+ Hydrocarbons, BSD	25196	50391	75587	100782	151174
Total C4+ Hydrocarbons, BSD	23889	47778	71667	95555	143334
Crude Oil Equivalent Price, $/BBL	32.7	29.4	28.5	27.7	27.5

File: PAPER895.XLS/feedrate

Table VI

Sensitivity Study - Effect of Wax Yield
Wyoming Coal ZSM-5 Upgrading Case

Wax Yield, Wt%	30	40	50	60	65	70	75
ROM Coal Feed Rate, TSD (MF)	19789	19789	19789	19789	19789	19789	19789
Slag Production Rate, TSD (MF)	1747	1747	1747	1747	1747	1747	1747
Electricity Purchase, MEGA-WH/SD	2009.4	2115.1	2198.4	2282.8	2327.7	2379.8	2441.2
Raw Water Make-up, MMGSD	9.758	9.658	9.573	9.493	9.454	9.413	9.371
Gasoline Production, BSD	38696	34743	31026	27580	25942	24356	22814
Distillate Production, BSD	8162	12148	15772	19158	20782	22366	23917
Liquid Propane Production, BSD	3432	3001	2613	2258	2090	1930	1777
Mixed Butanes Production, BSD	259	556	980	1352	1520	1671	1811
Sulfur Production, TSD	108	108	108	108	108	108	108
No. of Operators and Maintenance Workers	1146	1129	1126	1129	1129	1129	1129
Total Installed Capital, $MM	3074.9	3076	3075	3089.6	3099.3	3108.7	3120.8
Catalyst and Chemicals, $MM	21.6	21.6	21.5	21.5	21.5	21.5	21.5
Total C3+ Hydrocarbons, BSD	50549	50448	50391	50348	50334	50323	50319
Total C4+ Hydrocarbons, BSD	47117	47447	47778	48090	48244	48393	48542
Gasoline Properties:							
(R+M)/2 Octane Number	76	75	74	74	73	72	71
Aromatics, wt%	19.2	17.8	16.2	14.4	13.3	12.1	10.8
Olefins, wt%	8.0	7.1	6.5	5.8	5.3	4.8	4.2
Alkylate Production, BSD	11025	9054	7161	5436	4627	3851	3104
Percent Alkylate in Gasoline	28.5	26.1	23.1	19.7	17.8	15.8	13.6
Crude Oil Equivalent Price, $/BBL	28.9	29.1	29.4	29.8	30.0	30.2	30.4

File: PAPER895.XLS/waxyld

Low-Temperature Superacid Catalysis: Reactions of *n*-Butane and Propane Catalyzed by Iron- and Manganese-Promoted Sulfated Zirconia

Tsz-Keung Cheung, Julie L. d'Itri, Friederike C. Lange, and Bruce C. Gates

Department of Chemical Engineering and Materials Science
University of California
Davis, CA 95616

DOE Contract Number DE-AC22-93PC92116

Contract to: University of Delaware
Subcontract to: University of California at Davis

Period of Performance: August, 1994-June, 1995

ABSTRACT

The primary goal of this project is to evaluate the potential value of solid superacid catalysts of the sulfated zirconia type for light hydrocarbon conversion. The key experiments catalytic testing of the performance of such catalysts in a flow reactor fed with streams containing, for example, *n*-butane or propane.

Fe- and Mn-promoted sulfated zirconia was used to catalyze the conversion of *n*-butane at atmospheric pressure, 225-450°C, and *n*-butane partial pressures in the range of 0.0025-0.01 atm. At temperatures <225°C, the significant reactions were isomerization and disproportionation; in the range of 225-300°C, these reactions were accompanied by cracking; at temperatures >350°C, cracking and isomerization occurred. Catalyst deactivation, resulting at least in part from coke formation, was rapid. The primary cracking products were methane, ethane, ethylene, and propylene. The observation of these products along with an ethane/ethylene molar ratio of nearly 1 at 450°C is consistent with cracking occurring, at least in part, by the Haag-Dessau mechanism, whereby the strongly acidic catalyst protonates *n*-butane to give carbonium ions. The rate of methane formation from *n*-butane cracking catalyzed by Fe- and Mn-promoted sulfated zirconia at 450°C was about 3×10^{-8} mol/(g of catalyst · s); for comparison, the rate of cracking of *n*-butane catalyzed by HZSM-5 under these conditions was estimated to be 1×10^{-8} mol/(g of catalyst · s) [as determined by extrapolation of the data of Krannila *et al.*, *J. Catal. 135*, 115 (1992).] . This comparison suggests that the catalytic activity of the promoted sulfated zirconia at 450°C is about the same as that of the zeolite, although its activity for *n*-butane isomerization and disproportionation at temperatures <100°C is orders of magnitude greater than those of zeolites. Thus the indication of superacidity of the promoted sulfated zirconia does not extend to high temperatures. The results raise questions about the nature of the presumed superacidity: perhaps the acidic sites responsible for the low-temperature catalytic performance of (promoted) sulfated zirconia do not exist at the higher

temperatures; alternatively, the low-temperature reactions may involve catalyst functions other than the acidic function.

Iron- and manganese-promoted sulfated zirconia was also tested for conversion of propane at 1 atm, 200-300°C and propane partial pressures in the range of 0.01-0.05 atm. At 250°C, catalysis was demonstrated, as the number of propane molecules converted was at least 1 per sulfate group after 16 days of operation in a continuos flow reactor. Propane was converted in high yield to butanes, but the conversions were low, for example being only a fraction of a percent at a space velocity of 9.1×10^{-7} mol/(g of catalyst · s) and 250°C. Coke formation was rapid. The observation of butanes, pentanes, and methane as products is consistent with Olah superacid chemistry, whereby propane is first protonated by a very strong acid to form a carbonium ion. The carbonium ion then decomposes into methane and an ethyl cation which undergoes oligocondensation reactions with propane to form higher molecular weight alkanes. The results are consistent with the identification of iron- and manganese-promoted sulfated zirconia as a superacid.

INTRODUCTION

Solid superacids offer the prospect of practical new catalysts for paraffin conversion at low temperatures, at which the equilibria favor branched products. Most reports of paraffin conversion catalyzed by solid acids concern high-temperature reactions, e.g., cracking. Cracking of *n*-butane and of isobutane are good test reactions for strong-acid catalysts because they require strong acidity and give simple product distributions (*1-3*). The product distributions provide mechanistic information about reactions proceeding through carbocation intermediates. For example, the cracking of *n*-butane at low conversions catalyzed by HZSM-5 at about 500°C gives methane, propylene, ethane, ethylene, butenes, and H_2 in nearly equimolar amounts, implying the occurrence of the Haag-Dessau carbonium ion cracking mechanism (*1,4*). At higher conversions, the product distribution is more complex, including high yields of propane and indicating classical carbenium ion cracking (*1,4,5*).

Sulfated zirconia is a sufficiently strong acid to catalyze the conversion of *n*-butane at temperatures as low as room temperature (*6*). Promotion of this catalyst with Fe and Mn increases the activity by 2-3 orders of magnitude; promoted sulfated zirconia has been referred to as the most strongly acidic non-halide solid acid (*7*). At temperatures <100°C, this promoted catalyst is selective (>90%) for isomerization, also giving disproportionation products (*7-9*); however, deactivation is rapid. Addition of platinum to sulfated zirconia catalysts reduces the rate of deactivation (*10*).

One objective of the research reported here was to use *n*-butane conversion to characterize Fe- and Mn-promoted sulfated zirconia catalysts over a wide range of temperatures to allow a comparison of its performance with that of conventional solid acid catalysts such as zeolites. This work is the first characterization of promoted sulfated zirconia as a cracking catalyst. Another objective was to test the performance of this catalyst for propane conversion.

EXPERIMENTAL METHODS

Materials. Gases (Liquid Carbonic) included diluent N_2 (99.998%) and a mixture consisting, for example, of 1.0 mol% *n*-butane in N_2, which was found by gas chromatography to contain <0.0002 mol% isobutane impurity. The catalyst preparation is described elsewhere (*8*).

Briefly, the catalyst was made by incipient wetness impregnation of sulfated zirconium hydroxide (Magnesium Elektron, Inc.) with nitrates of iron and manganese, followed by calcination in static air as the temperature was increased from 30 to 500°C at 2.7°C/min and then held at 500°C for 3 h. The catalyst surface area was 90 m^2/g; it contained 1.0 wt% Fe, 0.5 wt% Mn, and 1.8 wt% S.

Catalytic Reaction Experiments. The butane conversion experiments were carried out with apparatus and methods described in the earlier report (*8*). The reaction took place in a tubular flow reactor packed with catalyst particles, and products were analyzed with an on-line gas chromatograph. Experiments were done with a feed of *n*-butane diluted with N_2. The *n*-butane partial pressures were low (0.0025 to 0.01 atm) to minimize catalyst deactivation. Conversions were typically low, as a major goal was to measure primary products of cracking and estimates of reaction rates. The temperature was varied from 225-450 °C. The pressure was atmospheric.

Experiments were done similarly for propane conversion. The reaction conditions were as follows: temperature, 200, 250, or 300°C; pressure, 1 atm; mass of catalyst, 0.5-2.0 g; inverse space velocity, (1-6) x 10^6 (g of catalyst · s)/(mole of propane fed); propane partial pressure, 0.01, 0025, and 0.05 bar; and run length, 4 h to 16 days.

RESULTS

Butane Conversion. At reaction temperatures < 225°C, only few products were formed from *n*-butane, predominantly isobutane, in agreement with earlier observations (*7-9*). In the temperature range 225-275°C, both isomerization and disproportionation occurred, and the selectivity to isomerization products (based on the gas-phase products only) was about 80% or greater, and the molar C_3/C_5 ratio was always >1. Low selectivities for formation of cracking products were observed under these conditions. At temperatures >350°C, the products were methane, ethane, ethylene, propane, propylene, isobutane, and traces of isobutylene, *trans*-2-butene, *cis*-2-butene, and 1-butene. At these temperatures, the cracking products predominated, and no C_{5+} products were observed by the gas chromatographic analysis. A summary of the conversions of *n*-butane to individual products at 400°C is given in Table 1. The selectivity for isomerization decreased with increasing temperature. Reaction was accompanied by rapid formation of carbonaceous deposits, as evidenced by the change in catalyst color from rust to black.

Thus, the following classification summarizes the reactions observed, except for formation of carbonaceous deposits:

Low temp. 25 to 225°C	Intermediate temp. 225 to 275°C	High temp. 350 to 450°C
isomerization + disproportionation	disproportionation + isomerization + cracking	cracking + isomerization

Rapid catalyst deactivation characterized the high-temperature *n*-butane reactions catalyzed by Fe- and Mn-promoted sulfated zirconia. As shown in Fig. 1, the overall conversion of *n*-butane at temperatures in the range 350-450°C decreased rapidly with time on stream. The major product was carbonaceous deposits. We infer that these deposits were responsible for at

least part of the catalyst deactivation. The lack of steady-state operation with the deactivating catalyst complicates the interpretation of these data.

The conversions to propane, propylene, and isobutane are expressed as a function of time on stream are illustrated in Figs. 2-4. The conversions are normalized to represent butane equivalents, so that the conversion to each product is multiplied by the number of carbon atoms in the product divided by 4. The fact that the conversions do not total one is an indication of the formation of carbonaceous deposits. These data indicate how the product distribution changed with reaction temperature. The onstream time profile representing the conversion of *n*-butane to methane (not shown) is similar in shape to that characterizing the total conversion (Fig. 1). These conversions at each temperature decreased rapidly with time on stream as a consequence of catalyst deactivation. However, conversion of *n*-butane to methane, extrapolated to zero on stream time, increased with increasing temperatures >225°C at each of the observed space velocities [6.8×10^{-8} to 2.7×10^{-7} (mol of *n*-C_4)/(s · g of catalyst)]. At 150°C, no methane was observed. At 225°C, methane was detected only for the first 2 h on stream. At 275°C, methane was observed at 5 h on stream, and the selectivity for methane formation exceeded 5% of the gas-phase products.

The pattern of cracking to give ethane and ethylene in the temperature range 225- 450°C was also similar to that characterizing the total conversion (Fig. 1). No C_2 products were observed at 150°C. At 225°C ethane was observed for 5 h, but ethylene was observed only at the shortest time on stream (5 min). Both ethane and ethylene were observed at temperatures in the range of 275-450°C.

Small amounts of C_4 olefinic products (typically a few parts per million) were formed at a temperature of 450°C (data not shown). At the shortest time on stream (5 min), no isobutylene, 1-butene, *cis*-2-butene, or *trans*-2-butene was observed; however, the selectivities for formation of these C_4 olefinic products increased as a function of time on stream. Isobutylene was the first C_4 olefin observed as a function of time on stream (at approximately 0.5 h). Subsequent injections contained the other C_4 products, formed at conversions 2- to 3-fold less than isobutylene.

Selectivities to individual products (based on gas-phase analyses only) are shown as a function of conversion in Fig. 5 for reaction at 225°C. These data represent variously deactivated catalysts, but there is little effect of the degree of deactivation on the selectivity-conversion plots. The data, extrapolated to zero conversion (Fig. 5), show that the selectivity for formation of methane and ethane exceeded zero at 225°C.

At 450°C, the conversion of *n*-butane extrapolated to zero onstream time was as much as almost 100%, and ethylene was formed. Similar selectivity vs conversion plots for reaction at 450°C (not shown) are consistent with the conclusion that methane, ethane, ethylene, and propylene are primary products, as the selectivities determined by extrapolation to zero conversion are nonzero. However it is not clear from the data whether propane or isobutane is a primary product.

As a measure of the formation of carbonaceous deposits, the percentage of the carbon lost to non gas-phase products is plotted as a function of *n*-butane conversion in Fig. 6. The percentage of carbon loss extrapolated to zero conversion of *n*-butane was approximately zero, indicating that the carbonaceous deposits were not primary products.

The data of Fig. 7 show that the ethane to ethylene molar ratio approached 1 after approximately 0.5 h on stream in the temperature range of 350 to 450°C. At shorter times on stream this ratio was greater than one, being about 2.5 at the first injection, taken at 0.08 h on stream.

Both the ratio of methane to ethane and the ratio of methane to (propane + propylene) increased with increasing temperature in the range 225-450°C (Table 3), consistent with thermodynamics. The ratio of methane to ethane remained virtually constant as a function of time on stream, but the ratio of methane to C_3 products was higher at shorter times on stream (i.e., approximately 1-2 h).

The data presented in Fig. 8 represent conversions estimated by extrapolation to zero time on stream. Because the catalyst deactivation was rapid, the errors associated with the extrapolation are large, possibly as much as ±100%, especially at the highest temperatures. However, as shown in Fig. 8, a linear correlation was obtained for the conversion of *n*-butane into each of the products methane, ethane, and ethylene as a function of inverse space velocity in the range of 0 to 1.2×10^{7} (g of catalyst · s)/(mol of *n*-C_4 feed). Thus, these data give rough estimates of differential conversions and hence reaction rates (slopes) for the undeactivated catalyst. The rates of methane, ethane, and ethylene formation at 450°C and a *n*-butane partial pressure of 0.0025 atm are about 3.0×10^{-8}, 3.5×10^{-8}, and 1.9×10^{-8} mol/(g of catalyst · s), respectively.

Similarly, extrapolated conversions at various inverse space velocities (most data not shown) were used to make rough estimates of reaction rates for formation of individual products. The estimates of rates of formation of methane and ethane show about the same pattern as shown by the *n*-butane conversion as a function of time on stream in the range 350-450°C. The same trend was also observed for ethylene, except for the sample taken at 5 min on stream.

The approximate rates of formation of methane, ethane, and ethylene increased with increasing temperature in the range of 350 to 450°C. The apparent activation energies, estimated from the temperature dependence of the rate data extrapolated to zero time on stream, were found to be 10-15 kcal/mol for each of these products (Table 4). The estimates are rough because of the uncertainty of the extrapolation caused by the rapid deactivation.

Propane Conversion. The definitions for propane conversion are analogous to those stated for butane. Carbonaceous deposits formed from propane on the surface of the promoted sulfated zirconia, but they were not accounted for in the calculations of conversion. These deposits formed on the surface of the material at all investigated temperatures, and the color changed from rust to gray or black.

The gas-phase products formed from propane at 200°C were methane, butanes, and pentanes. The conversion to gas-phase products increased for the first hour on stream (the induction period), followed by a period of declining conversion. At 250 and at 300°C, the products included ethane, ethylene, propylene, and the products observed at 200°C. The propane conversion at 300°C was at most 0.6%. A plot of propane conversion at 250°C at the end of the induction period as a function of inverse space velocity (figure 2) is nearly linear, suggesting that the conversion was differential. Thus the slope of the line is taken as an approximation of the reaction rate, i.e. 3×10^{-10} mol/(g of catalyst · s).

The change in product distribution with time on stream at 200°C is shown in figure 3. The initially formed gas-phase products were mostly methane and butanes. The selectivity to butanes initially increased with time on stream and then declined slowly as the selectivity to pentanes increased. Concomitantly, the selectivity to methane declined rapidly with time on stream. The selectivity to butanes was greatest at the lowest temperatures. After the induction period, typical selectivities to butanes at 200°C were about 85% and those at 300°C were about 15%.

The ratio of methane to ethylene in the gas-phase products at 250°C is shown in figure 4. This ratio was approximately 1 as the conversion approached zero; however, it deviated significantly from unity when the conversion was higher than 0.09%.

The flow reactor experiment at 250°C was continued with a constant feed flow rate for 16 days. The conversion profile as a function of time on stream was similar to that observed at 200°C, and conversion was proceeding when the experiment was terminated. If we assume that the number of catalytic sites is the same as the number of sulfate groups, then these data demonstrate that the number of turnovers (propane molecules converted per catalytic site) was 1.0 ± 0.1 and that the reaction was catalytic. However, the number of turnovers per site estimated in this way from the data obtained at 200°C was only 0.12 ± 0.02 when the experiment was terminated after 5 days of operation.

DISCUSSION

Butane Conversion. The data confirm the acidic character of the promoted sulfated zirconia catalyst. The product distributions are those of acid catalysis, and the occurrence of butane reaction at temperatures <100°C and the onset of cracking at about 225°C indicate that the catalyst was strongly acidic. Low-temperature *n*-butane conversion data suggest that it is a superacid (*7*). The strong acidity was confirmed by temperature-programmed desorption of benzene from the catalyst (*11*).

This is, to our knowledge, the first observation and quantification of catalytic cracking of *n*-butane at temperatures as low as 225°C. The results demonstrate that the catalyst has a high activity for this reaction. However, the approximate rate of cracking to give methane at 450°C observed in this work with the promoted sulfated zirconia catalyst, 3×10^{-8} mol/(g of catalyst · s), is about the same as that observed by Krannila *et al.* (*1*) with HZSM-5 catalyst, 1×10^{-8} mol/(g of catalyst · s). This estimate of the methane formation rate for HZSM-5 was obtained by extrapolating the reported kinetics parameters (*1*) to the reaction conditions used for the Fe- and Mn-promoted sulfated zirconia.

Thus there is no evidence of unusually high activity of the promoted sulfated zirconia at the highest temperatures investigated. It has also been shown that the activity of the promoted sulfated zirconia for neopentane cracking at 450°C is not much higher than those of the unpromoted sulfated zirconia and USY zeolite (*12*). Perhaps the catalyst had been substantially deactivated before any measurements could be made at this temperature, or perhaps the catalytic sites responsible for low-temperature *n*-butane isomerization were destroyed by treatment at the higher temperatures. Alternatively, we suggest that the catalytic properties at the lower temperature may be associated with properties other than just acidity. The roles of iron and manganese in the catalyst remain to be determined.

The identification of methane, ethane, and ethylene as primary products of cracking, combined with the observation that ethane and ethylene were formed in equimolar amounts, leads to the suggestion that *n*-butane cracking catalyzed by the promoted sulfated zirconia proceeded via the Haag-Dessau mechanism (*4*). According to this mechanism, which predominates in the cracking of *n*-butane catalyzed by HZSM-5 at 426-523°C and at low conversions (*1*), the *n*-butane is protonated directly by the catalyst to give carbonium ions, which collapse to give equimolar amounts of methane and propylene, ethane and ethylene, and H_2 and butenes. The carbonium ions are regarded as transition states (*1,13*). The product distribution observed in this work is not as simple as that predicted by the Haag-Dessau mechanism, but the

observation of the primary products and of equimolar yields of ethane and ethylene suggests its occurrence.

We infer that secondary reactions also occurred. The least reactive primary products were methane, ethane, and ethylene, and these are the ones that were observed to form as expected for the Haag-Dessau mechanism. In contrast, the other products are relatively more reactive and converted into secondary products. For example, the olefinic products are readily protonated to give carbenium ions, which undergo a variety of hydride transfer and cracking reactions. Even in *n*-butane cracking at the lowest conversions catalyzed by HZSM-5, the product distribution was not quite that corresponding to the primary products formed by the Haag-Dessau mechanism (*1*); the deviations from this simple product distribution were attributed to secondary reactions, especially of propylene. At higher conversions, cracking via the classical carbenium ion mechanism also occurred, giving, for example, high selectivities to propane.

In summary, because the product distribution in *n*-butane conversion catalyzed by promoted sulfated zirconia at the higher temperatures was sufficiently different from that predicted for the simple Haag-Dessau mechanism, we are not able to resolve quantitatively the primary from the secondary reactions, nor are we able to determine the relative importance of cracking proceeding via carbonium ions relative to that proceeding simply through carbenium ions.

The HZSM-5 catalyst used by Krannila et al. (*1*) underwent negligible deactivation, whereas the catalyst used in this work deactivated rapidly, as is typical of cracking catalysts. The lack of deactivation of HZSM-5 is related to the lack of coke formation in the zeolite pores as a consequence of restricted transition state shape selectivity (*14*). The catalyst used in this work deactivated rapidly, and the carbonaceous deposits might have been responsible for almost all of the catalyst deactivation.

There is evidently no prospective practical advantage to using the promoted sulfated zirconia catalysts for cracking. However, the data indicating the occurrence of the Haag-Dessau mechanism of *n*-butane cracking catalyzed by the promoted sulfated zirconia as well as by HZSM-5 suggest that measurements of the rate of this reaction might provide a useful basis for comparison of various catalysts. Rastelli et al. (*2*) advocated this test reaction in 1982. The Haag-Dessau mechanism requires protonation of an extremely weak base by the catalyst. Thus, presuming that the rate of *n*-butane cracking is determined by the rate of protonation, we suggest that the rate of *n*-butane cracking under conditions of Haag-Dessau cracking might be an easily measured criterion of the acid strength of solid acids. Successful application of the test reaction would require successful extrapolation to determine the activities of the fresh catalysts.

Propane Conversion. Because the rates of reaction were so low, the data were sufficient to demonstrate catalysis only for propane conversion at 250°C after 16 days of operation. The data taken at 200°C may represent noncatalytic reactions. However, the estimate of the number of turnovers/site is regarded as conservative, because the number of sulfate groups is considered to be an upper limit of the number of active sites and the amount of propane converted into carbonaceous deposits is not included. Thus the data do not rule out the occurrence of catalysis at 200°C.

Olah et al. (*15*) investigated the conversion of alkanes, for example, propane in the temperature range of -78 to 150°C in the presence of excesses of liquid superacids in a Teflon-lined stainless steel bomb. The superacid was diluted with the weakly nucleophilic SO_2ClF. With propane, they observed protolysis of C-H and, predominantly, C-C bonds, leading to the

formation of methane, ethane, H_2, and carbenium ions. Subsequent oligocondensation led to the formation of higher alkylcarbenium ions.

The products observed by Olah et al. (*15*) for propane conversion were also observed in the present work. The presumed analogy to Olah superacid chemistry implies that the solid superacid protonates propane to initiate its conversion. Thus the results are consistent with the earlier conclusion that the iron- and manganese-promoted sulfated zirconia is a superacid.

Furthermore, the ratio of methane to ethylene, which approaches 1 in the limit of zero conversion at 250°C, is consistent with protonation of propane as an initial reaction step to give carbonium ions (presumably transition states) that collapse into methane and ethyl cations (or into H_2 and *s*-propyl cations), so that the primary cracking products methane and ethylene are formed in equimolar amounts. The lack of data for H_2 leaves open the question of the ratio of H_2 to propylene, which would also be expected to approach 1 in the limit of zero conversion.

Cracking and dehydrogenation of alkanes via protonation has been demonstrated by Haag et al. catalyzed by zeolites at temperatures of 400-550°C (as mentioned above). For example, Krannila et al. (*1*) observed equimolar yields of ethane and ethylene formed from *n*-butane in the limit of zero conversion. The observation of a comparable cracking product distribution (with a much less reactive molecule) in our work at a temperature as low as 250°C is consistent with the suggestion that the promoted sulfated zirconia is a much stronger acid than the zeolites.

The observed formation of butanes and pentanes from propane at the lower reaction temperatures is consistent with oligocondensation chemistry proceeding via carbocation intermediates. Olah et al. (*15*) pointed out that almost all low-molecular-weight alkanes are converted with increasing temperature into stable carbocations, e.g. *t*-butyl cations, in the presence of a superacid. Our observation of butanes as products is consistent with the formation of *t*-butyl cations and hydride abstraction to form isobutane; isomerization would give *n*-butane. At longer times on stream, pentanes were observed, and these can also be accounted for by oligocondensation reactions. The data are explained by the reaction network of Fig. 9, which is based on Olah chemistry.

The similarities in the product distributions observed in this work and in the work of Olah et al. (*15*) with reactions in superacid solutions lead to the postulate that the chemistry on the surface was analogous to that in superacid solutions. But the differences in the experimental conditions were significant, leaving the fundamental issues distinguishing solution and solid superacid chemistry and catalysis largely unresolved.

CONCLUSIONS

Fe- and Mn-promoted sulfated zirconia is an active catalysts for the cracking of *n*-butane. At low *n*-butane partial pressures, primary cracking products, methane and ethane, were observed at temperatures as low as 225°C. The observation of these products along with an ethane/ethylene molar ratio of 1 at 450°C is consistent with cracking occurring by a Haag-Dessau carbonium ion cracking mechanism. High concentrations of propane indicate that cracking via a classical carbenium ion mechanism also occurs. The fact that this catalyst is active for isomerization, disproportionation, and cracking and the relative rate at which these reactions occur is highly dependent on temperature greatly complicates unraveling the mechanism of cracking. Catalyst deactivation is rapid.

Propane is converted into butanes and pentanes in the presence of iron- and manganese-promoted sulfated zirconia at temperatures of 200-300°C. The observation of these products accompanied by methane suggests that the reactions are initiated by protonation of propane to

form a carbonium ion which collapses into methane and ethyl cation, followed by oligocondensation of the ethyl cation with propane. The product distribution is consistent with Olah superacid chemistry; the chemistry has been demonstrated to be catalytic at 250°C, but it may not be catalytic at lower temperature.

PLANS

In the future, this investigation will emphasize the reactions of *n*-butane and of isobutane catalyzed by iron- and manganese-promoted sulfated zirconia, as the *n*-butane isomerization is evidently the reaction for which this class of catalyst holds the most promise of practical application, motivated by the need for isobutane and from that isobutylene for MTBE synthesis for high-octane clean-burning gasoline. The promoted catalyst is evidently the best in prospect for this reaction. Future experiments with emphasize higher pressures of reactant than have been investigated so far, and the data will include those of practical value, including measures of kinetics and catalyst stability and regenerability.

REFERENCES

1. Krannila, H., Haag, W. O., and Gates, B. C., *J. Catal.* **135**, 115 (1992).
2. Rastelli, H., Lok, B. M., Duisman, J. A., Earls, D. E., and Mullhaupt, T., *Can. J. Chem.. Eng.* 60, 44 (1982).
3. Lombardo, E. A., and Hall, W. K., *J. Catal.* **112**, 565 (1992).
4. Haag, W. O., and Dessau, R. M., Proc. 8th Int. Congr. Catal. (Berlin), 1984, Vol. 2, p. 305, Dechema, Frankfurt am Main, 1984.
5. Corma, A., and Wojciechowski, B. W., *Catal. Rev.--Sci. Eng.* **27**, 29 (1985).
6. Hino, M., and Arata, K., *J. Chem. Soc., Chem. Commun.*, 851 (1980).
7. Hsu, C-Y., Heimbuch, C. R., Armes, C. T., and Gates, B. C., *J. Chem. Soc., Chem. Commun.*, 1645 (1992).
8. Cheung, T.-K., d'Itri, J. L., and Gates, B. C., *J. Catal.*, **151**, 464 (1995).
9. Jatia, A., Chang, C., MacLeod, J. D., Okubo, T., and Davis, M. E., *Catal. Lett.* **25**, 21 (1994).
10. Iglesia, E., Soled, S. I., and Kramer, G. M., *J. Catal.* **144**, 238 (1993).
11. Lin, C-H., and Hsu, C-Y., *J. Chem. Soc., Chem. Commun.*, 1479 (1992).
12. Cheung, T.-K., d'Itri, J. L., Lange, F. C., and Gates, B. C., *Catal. Lett.* **31**, 153 (1995).

Lercher, J. A., van Santen, R. A., and Vinek, H., *Catal. Lett.* **27**, 91 (1994).

14. Haag, W. O., and Chen, N. Y. in "Catalyst Design, Progress and Perspectives," L. L. Hegedus, ed., Wiley, New York, 1987, p. 163.
15. Olah, G. A., Halpern, Y., Shen, J., Mo, Y. K., *J. Amer. Chem. Soc.*, **95**, 4960 (1973).

TABLE 1

Distribution of Products in Cracking of *n*-Butane Catalyzed by Fe- and Mn-Promoted Sulfated Zirconia at 400°C[a]

Product	Conversion of *n*-butane to product (%)		
	Extrapolated to zero time on stream[b]	1 h on stream[c]	2 h on stream[d]
Methane	18	1.3	1.2
Ethane	19	2.4	1.5
Ethylene	8.2	2.4	1.5
Propane	15	1.5	0.74
Propylene	0.15	0.18	0.27
Isobutane	1.8	0.38	0.28

[a] Mass of catalyst, 1.5 g; feed *n*-butane partial pressure, 0.0025 atm; total feed flow rate, 80 ml (NTP)/min.
[b] Total conversion, 95%.
[c] Total conversion, 8%.
[d] Total conversion, 6%.

TABLE 2

Product Molar Ratios from *n*-Butane Cracking Catalyzed by Fe- and Mn- Promoted Sulfated Zirconia[a]

Temperature (°C)	Molar Ratio in Product	
	$CH_4/(C_3H_8 + C_3H_6)$[b]	CH_4/C_2H_6[c]
225	0.04	0.55
275	0.21	0.61
350	0.70	0.71
400	0.98	0.80
450	1.39	0.91

[a] Feed *n*-butane partial pressure, 0.0025 atm; total feed flow rate, 80 ml (NTP)/min.
[b] Taken at 3 h time on stream.
[c] At a given temperature, this ratio was nearly constant as a function of time on stream.

TABLE 3

Approximate Kinetics Parameters Characterizing *n*-Butane Cracking Catalyzed by Fe- and Mn-Promoted Sulfated Zirconia[a]

Product	k_0 preexponential factor (mol/(s · g of catalyst · atm)	E_A apparent activation energy (kcal/mol)
Methane	0.13	13.3
Ethane	0.09	12.6
Ethylene	0.012	11.1

[a] Calculated on the basis of assumed first-order kinetics; feed *n*-butane partial pressure, 0.0025 atm; total feed flow rate, 80 ml (NTP)/min.

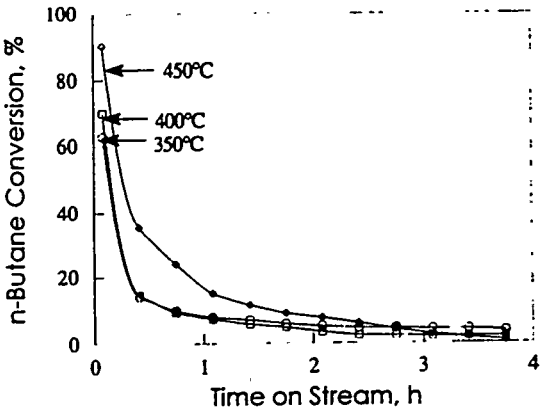

FIG. 1. Effect of reaction temperature on *n*-butane conversion to gas-phase products and coke catalyzed by Fe- and Mn-promoted sulfated zirconia. Feed *n*-butane partial pressure, 0.0025 atm; total feed flow rate, 80 ml (NTP)/min; catalyst mass, 1.5 g.

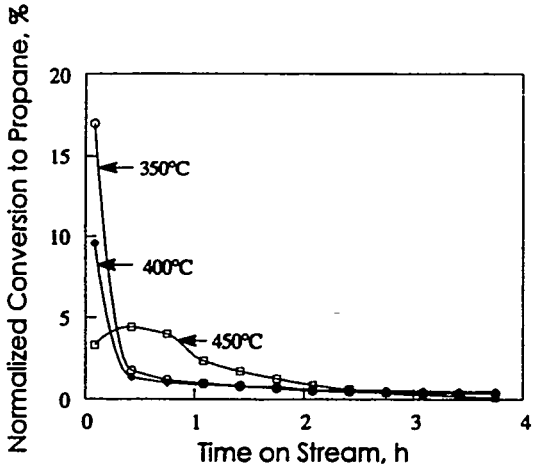

FIG. 2. Effect of reaction temperature on conversion to propane from *n*-butane reaction catalyzed by Fe- and Mn-promoted sulfated zirconia. Feed *n*-butane partial pressure, 0.0025 atm; total feed flow rate, 80 ml (NTP)/min; catalyst mass, 1.5 g.

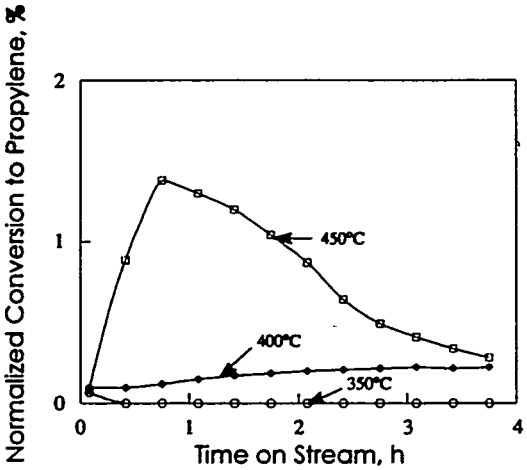

FIG. 3. Effect of reaction temperature on conversion to propylene from *n*-butane reaction catalyzed by Fe- and Mn-promoted sulfated zirconia. Feed *n*-butane partial pressure, 0.0025 atm; total feed flow rate, 80 ml (NTP)/min; catalyst mass, 1.5 g.

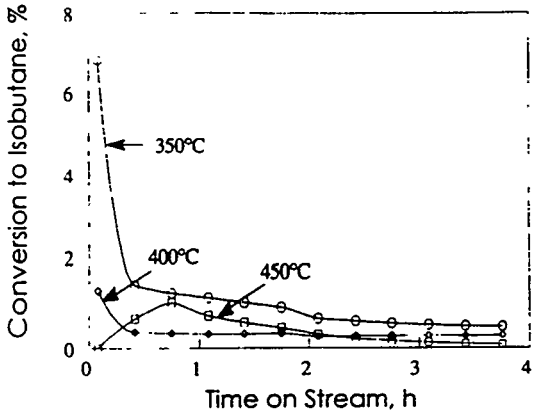

FIG. 4. Effect of reaction temperature on conversion to isobutane from *n*-butane reaction catalyzed by Fe- and Mn-promoted sulfated zirconia. Feed *n*-butane partial pressure, 0.0025 atm; total feed flow rate, 80 ml (NTP)/ min; catalyst mass, 1.5 g.

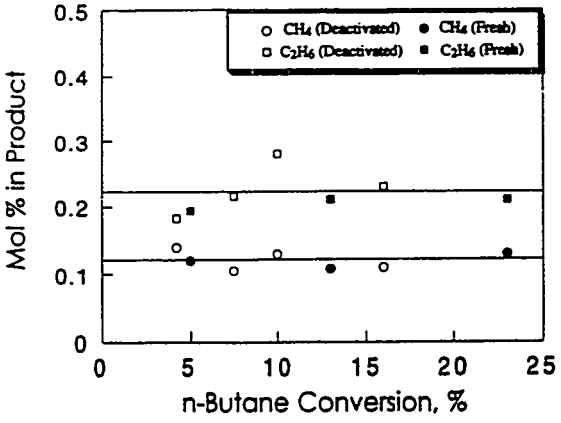

FIG. 5. Selectivity for formation of methane and ethane in *n*-butane reaction catalyzed by Fe- and Mn-promoted sulfated zirconia at 225°C. Data are based on analysis of the gas-phase products and do not account for carbonaceous deposits. Feed *n*-butane partial pressure, 0.01 atm; total feed flow rate, 80 ml (NTP)/min.

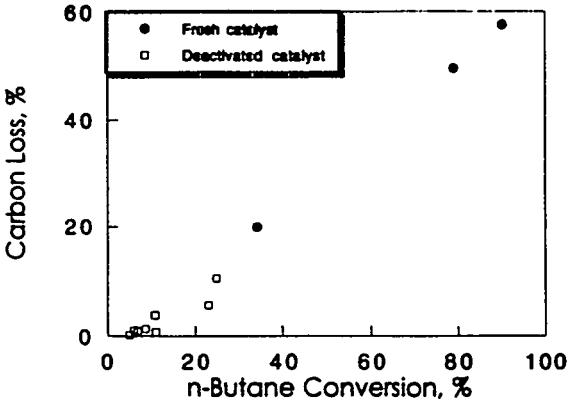

FIG. 6. Percentage of carbon loss in the gas phase effluent stream for *n*-butane reaction catalyzed by Fe- and Mn-promoted sulfated zirconia at 450°C. Feed *n*-butane partial pressure, 0.0025 atm; total feed flow rate, 80 ml (NTP)/min.

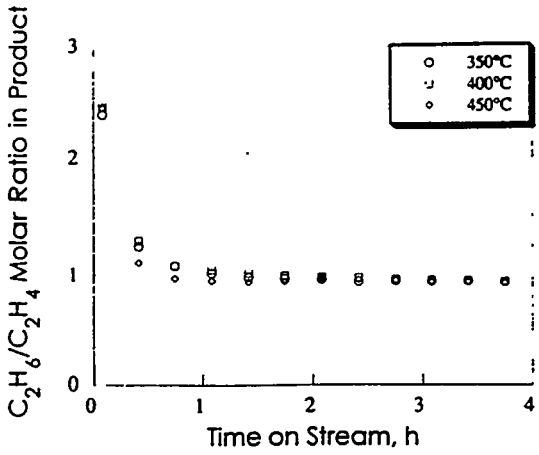

FIG. 7. Effect of reaction temperature on the ethane to ethylene ratio in the products of *n*-butane conversion. Feed *n*-butane partial pressure, 0.0025 atm; total feed flow rate, 80 ml (NTP)/min; catalyst mass, 1.5 g.

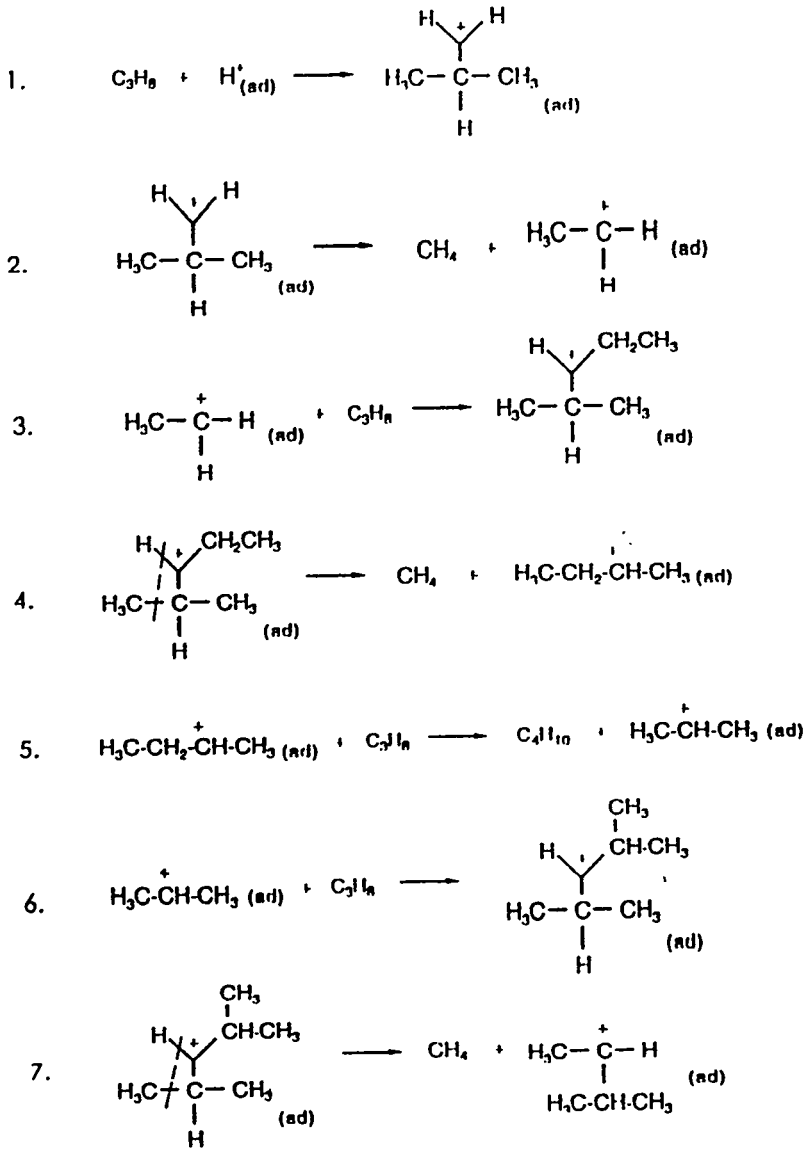

Fig. 8. Reaction network postulated for propane conversion in the presence of iron- and manganese-promoted sulfated zirconia. The dashed lines represent bond cleavages.

ALCOHOL SYNTHESIS IN A HIGH-TEMPERATURE SLURRY REACTOR

George W. Roberts, Marco A. Marquez and M. Shawn McCutchen

Department of Chemical Engineering
North Carolina State University
Box 7905
Raleigh, NC 27695-7905

Contract Number: DE-AC22-90PC90043

Period of Performance: 25 September 1990 - 31 December 1995

SUMMARY

Objective:

The overall objective of this contract is to develop improved process and catalyst technology for producing higher alcohols from synthesis gas or its derivatives. Recent research has been focused on developing a slurry reactor that can operate at temperatures up to about 400°C and on evaluating the so-called "high pressure" methanol synthesis catalyst using this reactor.

Accomplishments and Conclusions:

A laboratory stirred autoclave reactor has been developed that is capable of operating at temperatures up to 400°C and pressures of at least 170 atm. The overhead system on the reactor is designed so that the temperature of the gas leaving the system can be closely controlled. An external liquid-level detector is installed on the gas/liquid separator and a pump is used to return condensed slurry liquid from the separator to the reactor. In order to ensure that gas/liquid mass transfer does not influence the observed reaction rate, it was necessary to feed the synthesis gas below the level of the agitator.

The performance of a commercial "high pressure" methanol synthesis catalyst, the so-called "zinc chromite" catalyst, has been characterized over a range of temperature from 275 to 400°C, a range of pressure from 70 to 170 atm., a range of H_2/CO ratios from 0.5 to 2.0 and a range of space velocities from 2500 to 10,000 sL/kg.(catalyst),hr. Towards the lower end of the temperature range, methanol was the only significant product. At the highest temperatures, the methanol synthesis reaction was close to equilibrium. However, there were significant quantities of methane, dimethyl ether and olefins in the product at these temperatures. Formation of higher alcohols was insignificant, although small amounts of isobutanol were detected at the highest temperatures and pressures, with 10 mole percent CO_2 in the feed gas.

Plans:

The next phase of this research will be devoted to modifying the "high pressure" methanol synthesis catalyst to increase the production of higher alcohols and to decrease the production of methane and ethane. The initial approach to this objective will involve adding alkali metals such as cesium to the commercial catalyst.

INTRODUCTION

The synthesis of higher (C_2^+) alcohols from mixtures of H_2 and CO (synthesis gas) has been an active area of research for the last several decades, and continues to be an important element of the Department of Energy's indirect coal liquefaction program. Table 1 summarizes the types of catalysts that have been studied for this reaction.

TABLE 1
HIGHER ALCOHOL SYNTHESIS CATALYSTS

	Water Gas Shift Activity?	
	Yes	No
Anderson-Schulz-Flory Product Distribution	Molybdenum Sulfide (+ promoters) Cu/Co/Cr (IFP)	Rhodium, other Group VIII metals
Non Anderson-Schulz-Flory Product Distribution	Methanol Synthesis: Cu/ZnO ZnCrO	None

The synthesis gas that is produced by modern, thermally-efficient coal gasifiers has a H_2/CO ratio in the range of 0.5 to 1. With such a feedstock, it is advantageous to use a catalyst that has some water-gas shift (WGS) activity since H_2 is the limiting reactant for alcohol synthesis at these ratios. When the H_2/CO ratio approaches or exceeds 2, as it can when synthesis gas is manufactured from natural gas, substantial WGS activity is not desirable since this reaction now causes a loss of the limiting reactant, CO.

Heydorn et al (1) and Minahan and Nagaki (2) have pointed out the advantages associated with an alcohol synthesis process that produces roughly one mole of methanol (or ethanol) and one mole of a 2-methyl alcohol such as isobutanol or 2-methyl 1-butanol. Such a product distribution could lead to the production of established octane enhancers such as methyl tertiary butyl ether (MTBE), ethyl tertiary butyl ether (ETBE) and tertiary amyl methyl ether (TAME), with relatively small amounts of methanol, ethanol, propanol, etc. that would have to be sold as by-products. By definition, the catalysts that produce an Anderson-Shulz-Flory distribution of

products cannot approach this target. However, some modified methanol synthesis catalysts have yielded product distributions in which methanol and isobutanol are the predominant products (1,2,3,4,5,6). None of these catalysts are completely satisfactory either because the molar rate of methanol formation has exceeded that of isobutanol formation by a substantial amount, and/or because the overall rate of alcohol formation has been low.

The synthesis of alcohols, particularly C_2^+ alcohols, is highly exothermic. Excellent temperature control is essential to good selectivity, long catalyst life and, in the case of methanol synthesis, to high conversions because of the reversibility of the reaction. The slurry reactor provides an essentially isothermal environment, on both the scale of the reactor and the scale of the catalyst particle. Therefore, this type of reactor has received a great deal of attention for methanol synthesis (7), for dimethyl ether synthesis (8) and for the synthesis of C_2^+ alcohols. A cesium-promoted Cu/ZnO methanol synthesis catalyst, a modification of the so-called "low pressure" methanol synthesis catalyst, has been demonstrated in a slurry bubble column reactor at the Department of Energy's Alternate Fuels Development Unit in La Porte, Texas (1).

Most of the studies of alcohol synthesis and related reactions (e.g., 9) that have been carried out in slurry reactors have been at temperatures below about 310°C . There are several reasons for this temperature limit. First, most of the previous work has involved catalysts, such as the Cu/ZnO "low pressure" methanol synthesis catalyst, that lose activity rapidly above about 300°C (7). Second, as will be discussed in more detail below, the liquids that have been used to slurry the catalyst are thermally unstable in the presence of high partial pressures of H_2 at temperatures significantly in excess of 300°C.

The specific objectives of the work described in this paper were to extend the operating range of slurry reactors for alcohol synthesis to a temperature of about 400°C, and to characterize the performance of a commercial, high-pressure methanol synthesis catalyst in a slurry reactor at temperatures up to 400°C. This research is intended to set the stage for the synthesis and evaluation of catalysts for the production of C_2^+ alcohols that are derived from this "zinc chromite" methanol synthesis catalyst.

EQUIPMENT

A schematic diagram of the equipment employed is shown in Figure 1. Gases are fed from cylinders through activated carbon traps to remove impurities and then through mass flow controllers to measure and control the flow rate. The mixed gas is compressed to the desired pressure, typically in the range of 70 to 200 atm., and the compressed gas is passed through another activated carbon trap specifically to remove any iron and/or nickel carbonyl that may have formed during and after compression. The gas is then fed into a 300 $cm.^3$ Autoclave Engineers stirred autoclave reactor. The gas leaving the reactor passes into a gas/liquid separator that contains a cooling coil. The temperature of the gas/liquid separator is carefully regulated. The gas then passes through a back pressure regulator that controls the reactor pressure. After leaving the regulator, the gas passes through heated lines to prevent condensation and through a wet test meter to measure the gas flow rate. Samples of the reactor feed and effluent are

periodically diverted to a dual column gas chromatographic system containing a Carboxen 1000 column followed by a thermal conductivity detector and a Poroplot Q column followed by a flame ionization detector. The former system is used to measure the fixed gases, H_2, N_2, CO, CO_2 and H_2O. The organic species are measured on the second system.

Several features of the equipment merit further discussion: the carbonyl traps, the overhead system and the location at which gas is fed into the stirred autoclave reactor.

Carbonyl Traps

Iron and nickel carbonyl are known to poison both types of methanol synthesis catalyst, even at very low concentrations (7,10,11). Two types of trap have been employed to remove these volatile species from the feed gas, a low-temperature adsorptive trap, typically containing activated carbon (12,13), and a high-temperature catalytic trap, in which the carbonyls are decomposed and the metal is deposited on the catalyst at a temperature of about 300°C. Only the former type of trap should be used at the CO partial pressures that are typical of methanol synthesis. Thermodynamic calculations have shown that high-temperature traps are relatively ineffective at high CO partial pressures, and can even result in the formation, rather than the destruction, of metal carbonyls. Moreover, the iron and nickel that are deposited on the catalyst might lead to the formation of large quantities of carbon through catalysis of the Boudouard reaction.

Overhead System

At the high reactor temperatures employed in this research, the vapor pressure of the inert liquid that is used to suspend the catalyst can be appreciable. Therefore, the quantity of liquid that is condensed in the overhead system and returned to the stirred autoclave can be significantly greater than with, for example, a liquid-phase methanol synthesis reactor that operates in the region of 250 to 300°C. Unless the hydraulics of the overhead system are carefully designed, some of the condensed liquid can fill the gas/liquid separator and overflow through the back pressure regulator. Simple gravity return of the condensed liquid may not be sufficient to avoid this loss. Three important features of the actual overhead system are not shown in Figure 1. First, an ultrasonic liquid level sensor is mounted on the exterior of the gas/liquid separator to provide a warning in the event that the liquid level in the separator reaches a position that is high enough to threaten liquid loss through the back pressure regulator. Second, a high-pressure piston pump is used to return condensed liquid from the separator to the reactor. These two features have permitted the overhead system to be operated reliably over long periods of time without any significant mechanical loss of the slurry liquid.

Under certain circumstances, it may be necessary to operate the overhead system at a relatively high temperature in order to avoid condensing and returning a high-boiling product or a product that has a high partial pressure in the reactor effluent. When the effluent temperature from the gas/liquid temperature is sufficiently high, a small loss of the slurry medium as vapor can occur. For long periods of operation, the

cumulative loss of slurry medium by this mechanism can be significant. Therefore, the actual overhead system is equipped with a high pressure pump to return slurry liquid that is condensed downstream of the back pressure regulator to the reactor, or to feed fresh slurry liquid in lieu of returning low-pressure condensate.

Feed Location

Figure 2 shows the results of two sets of experiments designed to determine the optimum agitation rate and gas-feed location. These experiments were carried out with BASF S3-86 "low pressure" (Cu/ZnO) methanol synthesis catalyst. The methanol productivity is defined as the rate of methanol production per unit weight of catalyst (g. moles of methanol/kg. catalyst, hr.) at a standard set of operating conditions: reactor temperature - 250°C; total pressure - 51 atm.; feed composition - 35 mole % H_2, 51% CO and 14% CO_2, and; gas hourly space velocity (GHSV) - 5000 sL/kg.,hr. Two feed gas locations were tested in each experimental set: 1) through a dip tube that extended into the slurry, and; 2) directly into the "headspace" above the liquid. The data has been normalized by dividing each data point by the catalyst productivity at infinite stirrer speed, as determined by extrapolating the data in each set that was obtained with the feed through the dip tube to infinite stirrer speed. The basis for the abscissa, the reciprocal stirrer speed raised to the 2.2 power, is a publication by Yagi and Yoshida (14) showing that the k_La for the reactor depends on stirrer speed raised to this power.

Only the data obtained with the gas feed introduced below the level of the agitator (designated "extended dip tube" in Figure 2) showed no dependence on the agitation rate. This is strong evidence that gas/liquid mass transfer had no significant influence on the overall reaction rate. The data for the "short dip tube", which terminated about 1 cm. above the agitator, shows a strong dependence of catalyst productivity on agitation rate, suggesting that gas/liquid mass transfer influenced the overall reaction rate to a significant extent. The effect of agitation rate was present even at the highest stirrer speed, 2500 rpm. However, the data extrapolated to essentially the same productivity that was measured in the run with the extended dip tube.

The manufacturer of the stirred autoclave reactor recommends feeding gas into the headspace above the liquid. The "dispersimax" agitator in the reactor has a hollow shaft and the blades at the bottom of the shaft are designed to draw gas down the shaft from the headspace, creating bubbles in the shear field of the agitator. The two runs that were done with this feed location exhibited a significant effect of agitation rate. Moreover, neither "headspace" run extrapolated to a normalized productivity of 1 at an infinite stirrer speed. Apparently, the "headspace" feed location has a deficiency that is more than just an insufficient value of k_La. One possible explanation of the failure of the data for the two "headspace" feed runs to extrapolate to a normalized productivity of 1 is that gas by-passing occurred.

The "extended dip tube" has been used for all runs with the "zinc chromite", "high pressure" methanol synthesis catalyst. The stirrer speed has been varied on several occasions, with no noticeable effect on catalyst productivity.

RESULTS AND DISCUSSION

Liquid Stability Testing

The literature (15,16,17) suggests that the "zinc chromite", "high pressure" methanol synthesis catalyst is typically run at temperatures of 350 to 410°C in commercial, fixed-bed methanol synthesis reactors. Moreover, the research that has been carried out to date on the addition of alkali metals to this catalyst in order to shift the product distribution towards the higher alcohols (e.g., 3,4,5) has involved similar temperatures. Therefore, a target operating temperature of 375°C was set for slurry reactor operation and a series of tests was carried out to evaluate the stability of various liquids in the presence of H_2 at this temperature.

The stability of a liquid was evaluated in two phases. First, a "thermal" stability test was carried out by charging a measured amount of the liquid to the stirred autoclave reactor, pressurizing to the range of 54 to 68 atm. with hydrogen, heating to 375°C, continuously sparging hydrogen through the liquid and holding the system at these conditions for about three days. Catalyst was not present in the reactor during this test. The gas leaving the reactor was analyzed periodically by gas chromatography to determine whether any hydrocarbons were present, and, if so, their identities and concentrations in the sampled gas. At the end of the test period, the liquid remaining in the reactor was measured and a number of analytical tests were carried out, including molecular weight, density, refractive index and nuclear magnetic resonance (NMR) spectroscopy.

Table 2 shows the performance of four different liquids in this testing protocol.

TABLE 2
RESULTS OF THERMAL STABILITY TESTING OF VARIOUS LIQUIDS

Liquid	Run Duration[1] (hr.)	Molecular Weight Reduction (%)	Rate of Liquid Loss (wt. % of initial charge/hr.)	
			Maximum	Steady-State
Drakeol 34	69	35	1.2	0.10
Durasyn 180	65	86	1.8	0.12
A	71	Pending	0.44	0.044
B	73	Pending	0.095	0.0040

1 - at a temperature of 375°C, H_2 pressure of 60 to 70 atm. and H_2 flow rate of 3.8 sL/min.

Liquids A and B were much more stable than either Drakeol 34 or Durasyn 180, as indicated by both of the rates of hydrocarbon loss in the effluent gas stream. NMR analyses (^1H and ^{13}C) were carried out on samples of Liquids A and B taken from the reactor at the end of the thermal stability test and on samples of the original liquids for comparison. There was no evidence of hydrocracked products in the final sample of

Liquid B. However, there were traces of compounds that could have resulted from hydrocracking in the final sample of Liquid A. Because the stability of Liquid B appears to be higher than that of Liquid A, the former has been used exclusively to date in slurry reactor operation.

Performance of Commercial Catalyst

A commercial high pressure methanol synthesis catalyst (Zn-0312 T1/8) was obtained from Engelhard Corporation in a reduced and stabilized form. The catalyst contained 60 wt. % Zn and 15 wt. % Cr, with ZnO and $ZnCr_2O_4$ detectable by x-ray diffraction. The as-received BET surface area was 145 m^2/g. The catalyst was ground and sieved to -120 mesh. All runs were made with a 20 wt. % slurry of catalyst in Liquid B. The catalyst was activated in-situ by: pressurizing the reactor to 69 atm. with N_2 and heating it to 130°C while sparging N_2 through the slurry; heating from 130 to 300°C at about 40°C /hr. with a sparge gas consisting of 5% H_2 in N_2; heating to 375°C at 25°C/hr. while progressively increasing the hydrogen mole fraction in the sparge gas from 0.05 to 1, and; holding at 375°C with a pure H_2 sparge until no water was present in the gas leaving the reactor.

A series of experiments was conducted at a total pressure of 69 atm., temperatures in the range of 300 to 375°C and gas hourly space velocities (GHSV) between 1500 and 10000 sL/kg.,hr. The feed was a mixture of H_2 and CO, with H_2/CO ratios between 0.5 and 2. A typical operating pressure for a methanol synthesis process based on the "zinc chromite" catalyst is about 300 atm. (15,16,17). The equilibrium concentration of methanol decreases as the pressure is decreased. In order to limit the amount of methanol formed in a higher-alcohols process, it seems reasonable to presume that the pressure would be lower than that used for methanol synthesis. An operating pressure of 69 atm. was chosen for the initial series of runs in order to characterize the performance of the "zinc chromite" catalyst in a slurry reactor at conditions that might be reasonably characteristic of a higher-alcohols process, and were not likely to lead to the formation of excessive amounts of methanol.

Figure 3 shows the product distributions that were obtained in two runs at 375°C, 5000 sL/kg.,hr. GHSV and H_2/CO ratios of 0.5 and 1. Methanol was the only alcohol detected in the outlet stream. Dimethyl ether (DME) was the only other oxygenate present in significant quantities. DME probably formed by the condensation of two molecules of methanol, a reaction that is catalyzed by mildly acidic surfaces such as γ-alumina (8). A portion of the product, slightly less than 10 % of the carbon atoms, was C_2 through C_4 olefins. Olefin formation in these quantities has not been reported previously for this type of catalyst in research carried out in gas-phase, fixed bed reactors. However, the formation of C_2 through C_4 alcohols has been reported. It is tempting to speculate that the olefins that were observed in this run may have resulted from the dehydration of the corresponding alcohol. It has been reported that the dehydration of isobutanol to isobutene is catalyzed by the same kind of acidic materials that catalyze the formation of dimethyl ether from methanol (9). The formation of about 15% methane plus ethane is a negative feature of the performance of this catalyst.

The production of a large quantity of CO_2 demonstrates that the catalyst has a substantial activity for the water-gas shift reaction, as suggested by Table 1. The water

produced by the formation of alkanes, olefins and dimethyl ether was shifted to CO_2 and H_2 essentially quantitatively.

The product distributions at the two different H_2/CO ratios are similar except for the higher relative amount of methanol and the lower relative amount of CO_2 at the higher ratio. Both changes are conceptually reasonable; the 1:1 H_2/CO ratio should increase the rate of methanol formation because it is closer to the stoichiometric ratio, and should decrease the driving force for the water-gas shift reaction.

Figure 4 shows the product distribution at a H_2/CO ratio of 1 and at a lower space velocity of 1500 sL/kg.,hr. The most pronounced change is the increase in the ratio of dimethyl ether to methanol. This is probably the result of the factor of three increase in contact time, which permitted a higher conversion of methanol into DME.

Figure 5 compares the product distribution at 375°C with that at 300°C, for a GHSV of 5000 sL/kg.,hr. and a H_2/CO ratio of 0.5. At the lower temperature, methanol is the only product that is formed in substantial quantities. The formation of hydrocarbons is substantially lower, as is the formation of dimethyl ether. The small quantity of CO_2 that is produced does not necessarily indicate that the shift activity of the catalyst is substantially diminished at 300°C. The reactions that result in the formation of water, i.e., hydrocarbon formation and DME formation, do not occur to any substantial extent at 300°C. The low rate of water formation, compared to the rate at 375°C, limits the amount of CO_2 that can be formed.

The experimentally measured rate of methanol production is compared to the rate that would be observed if chemical equilibrium were achieved in Figure 6. The "equilibrium" catalyst productivity is calculated by assuming that the methanol synthesis reaction is in equilibrium in the gas stream leaving the reactor, thus defining the methanol production rate. At 375°C and 350°C, the measured and theoretical rates are reasonably close, which suggests that the presence of the liquid has not had a significant inhibiting effect on the activity of the catalyst. On the contrary, the close approach to equilibrium at a temperature of 350°C is somewhat surprising. It has been reported (15) that the effectiveness factor of the pelleted commercial catalyst is only about 0.7 in the temperature range from 370 to 410°C. Thus, the surprising low-temperature activity of the catalyst in the slurry reactor may be associated with a reduction in the resistance to pore diffusion as a result of the much smaller particle size of the catalyst in the slurry reactor.

As the reactor temperature is further decreased, the actual catalyst productivity decreases to a relatively small fraction of the equilibrium productivity. However, at 300°C, the lowest temperature investigated, the methanol productivity of the catalyst was higher than it was at any of the higher temperatures. This reflects the fact that the reaction equilibrium becomes more favorable as the temperature decreases. For comparison, the methanol productivity obtained with the "zinc chromite" catalyst at 300°C is one-quarter to one-fifth of the productivity obtained with the Cu/ZnO catalyst at 250°C at otherwise comparable conditions.

Figure 7 shows the effect of space velocity and H_2/CO ratio on the methanol productivity at a temperature of 300°C. As expected, the reaction rate increases as the H_2/CO ratio is increased from 0.5 to 2 and as the space velocity is increased.

The experiments described above required about fifteen days of continuous reactor operation. The liquid in the reactor at the end of this period was analyzed to

determine whether any degradation had taken place. Some of the data is still pending. However, there was no decrease in the molecular weight. The conversion and product distribution were measured periodically during the run at a standard set of conditions: 375°C, 5000 sL/kg.,hr. GHSV and a H_2/CO ratio of 1. The results are shown in Figure 8. There is no trend with time in the rate of paraffin production, there is a modest increase in the rate of methanol formation and the rates of olefin and DME production decrease with time. The BET area of the catalyst that was recovered at the end of the run was about 110 $m^2/g.$, about 25% lower than the "fresh" value.

One of the disappointing features of the data presented above is the lack of a substantial rate of C_2^+ alcohol formation. However, it was theorized that the olefin formation that was observed may have resulted from the dehydration of the corresponding alcohol. Therefore, in a subsequent series of experiments, 10 mole percent CO_2 was added to the feed gas in order to suppress the water-gas shift reaction, increase the concentration of water in the reactor and shift the alcohol dehydration reaction to the left. This experiment resulted in the production of very small amounts of isobutanol, which lends some credence to the alcohol dehydration theory.

CONCLUSIONS

The studies reported above are significant in several respects. First, operation of the slurry reactor at 375°C, with no apparent degradation of the slurry liquid and with what appears to be a reasonable level of catalyst activity, represents a significant extension of the operating temperature range of this type of reactor. A number of operating and equipment problems associated with the overhead system had to be overcome before reliable operation was possible.

The "zinc chromite" catalyst showed some promising performance features. First, the commercial version of this catalyst appears to be compatible with slurry reactor operation in that a high level of activity was observed, there was no catastrophic deactivation of the catalyst over the course of two weeks of continuous operation, and the catalyst did not appear to cause any degradation of the slurry liquid. Second, some features of the product distribution at 375°C are encouraging, particularly the formation of substantial quantities of dimethyl ether and olefins. The high production rates of methane and ethane are a negative element of the performance of this catalyst, which will have to be addressed in future research.

REFERENCES

1. Heydorn, E. C., Schaub, E. S., Stein, V. E. E., Underwood, R. P. and Waller, F. J., "Recent Progress on Syngas Conversion to Isobutanol", paper presented at U. S. Department of Energy, Pittsburgh Energy Technology Center Coal Liquefaction and Gas Conversion Contractor's Review Conference, Pittsburgh, PA, September 7-8, 1994

2. Minahan, D. M. and Nagaki, D. A., "Heterogeneous Catalytic Process for Alcohol Fuels from Syngas", paper presented at U. S. Department of Energy, Pittsburgh Energy Technology Center Coal Liquefaction and Gas Conversion Contractor's Review Conference, Pittsburgh, PA, September 7-8, 1994

3. Riva, A., Trifiro, F., Vaccari, A., Busca, G., Mintchev, L., Sanfilippo, D. and Manzatti, W., "The Promoting Role of Cr and K in Catalysts for High-Pressure and High-Temperature Synthesis", *J. Chem. Soc., Faraday Trans. 1*, **83**, 2213-2225 (1987)

4. Tronconi, E., Lietti, L., Groppi, G., Forzatti, P. and Pasquon, I., "Mechanistic Kinetic Treatment of the Chain Growth Process in Higher Alcohol Synthesis", *J. Catal.*, **124**, 376-390 (1992)

5. Tronconi, E., Lietti, L., Forzatti, P. and Pasquon, I., "Higher Alcohol Synthesis over Alkali Metal-Promoted High-Temperature Methanol Catalysts", *Applied Catalysis*, **47**, 317-333 (1989)

6. Vedage, G. A., Himelfarb, P. B., Simmons, G. W. and Klier, K., "Alkali-Promoted Copper-Zinc Oxide Catalysts for Low Alcohol Synthesis", *ACS Symp. Series*, **279**, 295-312 (1985)

7. Roberts, G. W., Brown, D. M., Hsiung, T. H. and Lewnard, J. J., *Ind. Eng. Chem. Res.*, **32**, 1610 (1993)

8. Brown, D. M., Bhatt, B. L., Hsiung, T. H., Lewnard, J. J. and Waller, F. J., *Catalysis Today*, **8**, 279 (1991)

9. Armstrong, P. A., Bhatt, B., Heydorn, E. C. and Toseland, B. A., "Isobutanol Dehydration: A Key Step in Producing MTBE from Syngas", paper presented at U. S. Department of Energy, Pittsburgh Energy Technology Center Coal Liquefaction and Gas Conversion Contractor's Review Conference, Pittsburgh, PA, September 27-29, 1993

10. Supp, E., "Technology of Lurgi's Low Pressure Methanol Process", *Chemtech*, July (1973), 430-435

11. Satterfield, C. N., *Heterogeneous Catalysis in Industrial Practice (2nd Edition)*, McGraw-Hill, 447 (1991)

12. Bhatt, B. L., Golden, T. C. and Hsiung, T. H., "Adsorptive Removal of Catalyst Poisons from Coal Gas for Methanol Synthesis", *Separation Science and Technology*, **26**, 1559-1574 (1991)

13. Golden, T. C., Hsiung, T. H. and Snyder, K. E., "Removal of Trace Iron and Nickel Carbonyls by Adsorption", *Ind. Eng. Chem. Res.*, **29**, 502-507 (1991)

14. Yagi, H. and Yoshida, F., "Gas Absorption by Newtonian and Non-Newtonian Fluids in Sparged Agitated Vessels", *Ind. Eng. Chem., Process Des. Dev.*, **14**, 488-493 (1975)

15. Pasquon, I. and Dente, M., "Heat and Mass Transfer in Methanol Synthesis - Optimum Operating Conditions of the Reactors", *J. Catal.*, **1**, 508-520 (1962)

16. Strelzoff, S., "Methanol: Its Technology and Economics", *Chem. Eng. Prog. Symp. Series*, No. 98, **66**, 54-68 (1970)

17. Stiles, A. B., "Methanol, Past, Present and Speculation on the Future", *AIChE Jnl.*, **23**, 362-375 (1977)

Figure 1

STIRRED AUTOCLAVE PROCESS FLOWSHEET

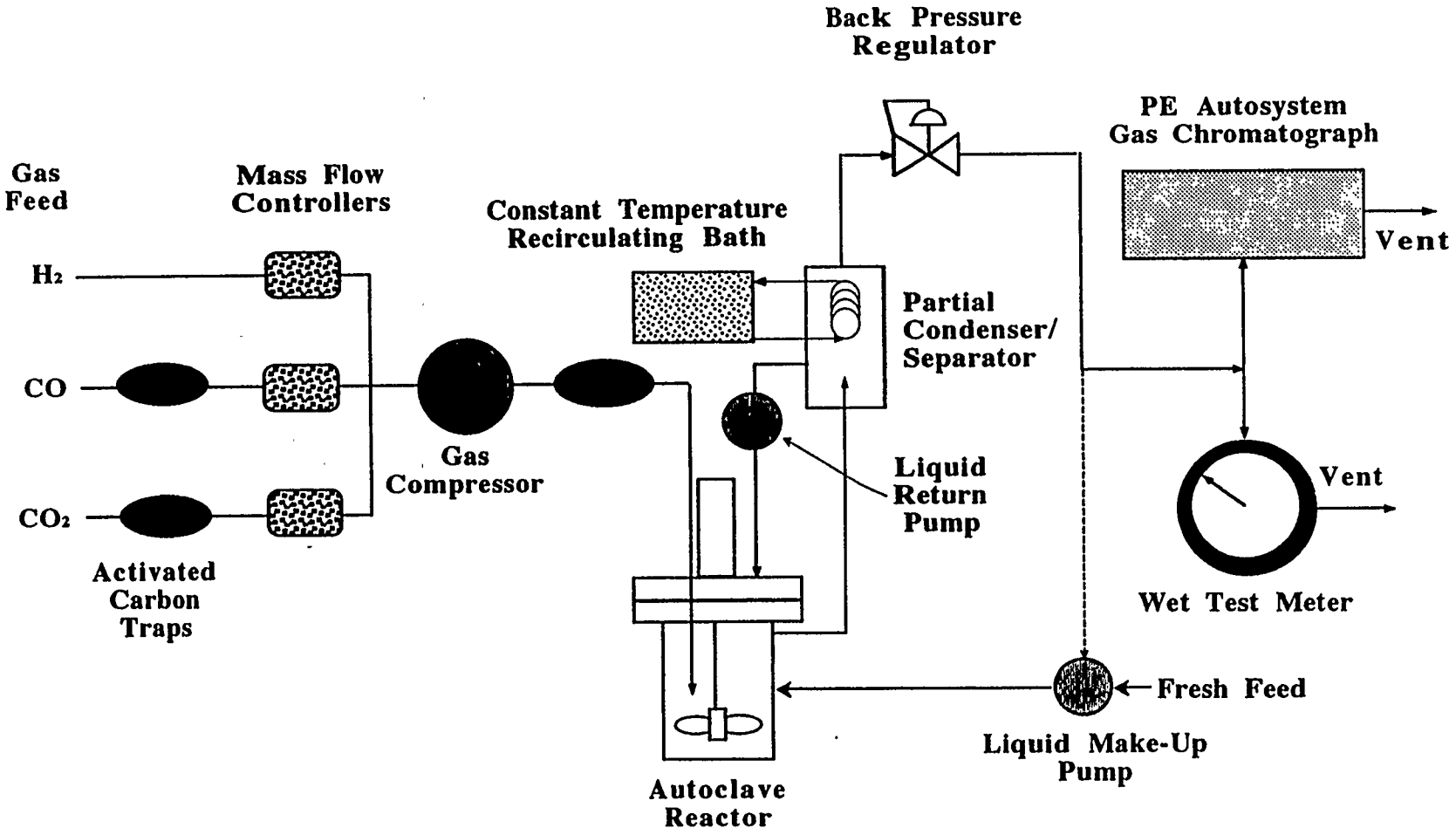

Figure 2

Effect of Reactor Gas Feed Configuration on Catalyst Performance

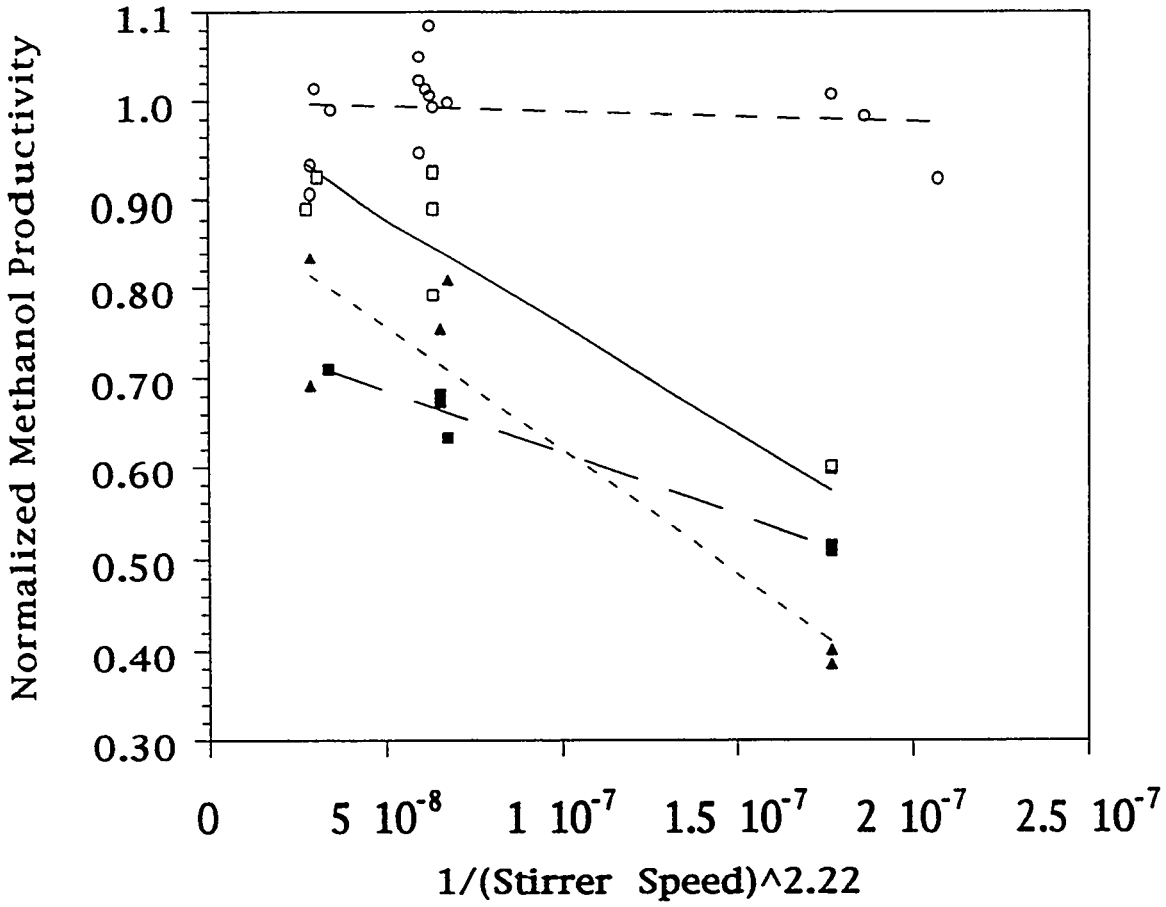

Figure 3

Effect of H_2/CO Ratio on Product Distribution
(5000 GHSV, 68 atm, 375°C)

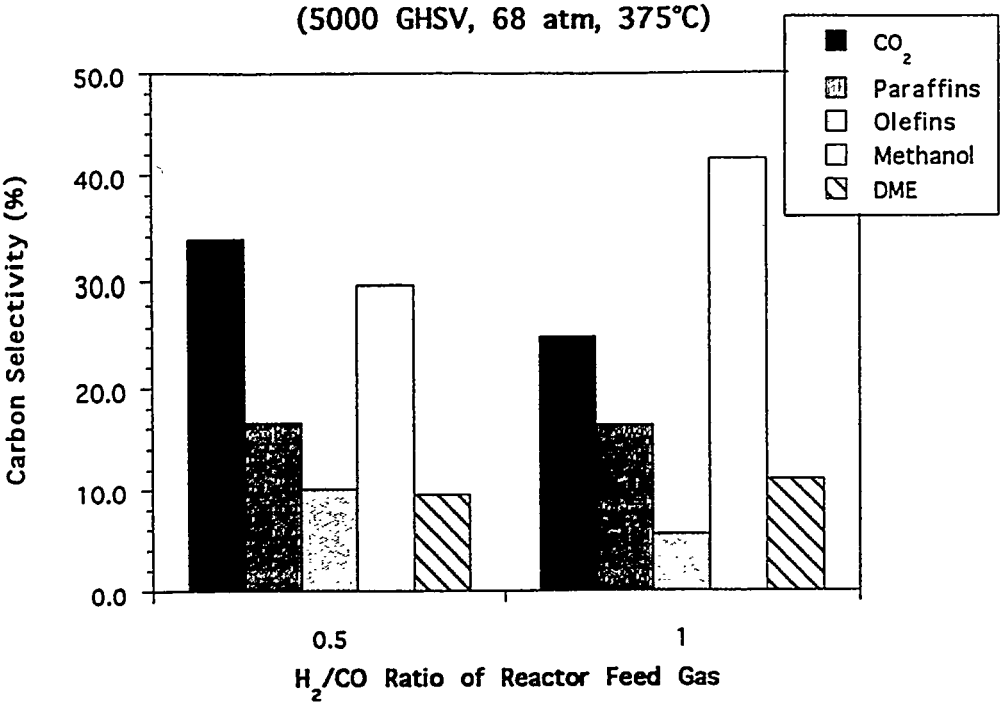

Figure 4

Product Distribution for ZnCrO Catalyst
(1500 GHSV, 375°C, 68 atm, H_2/CO = 1)

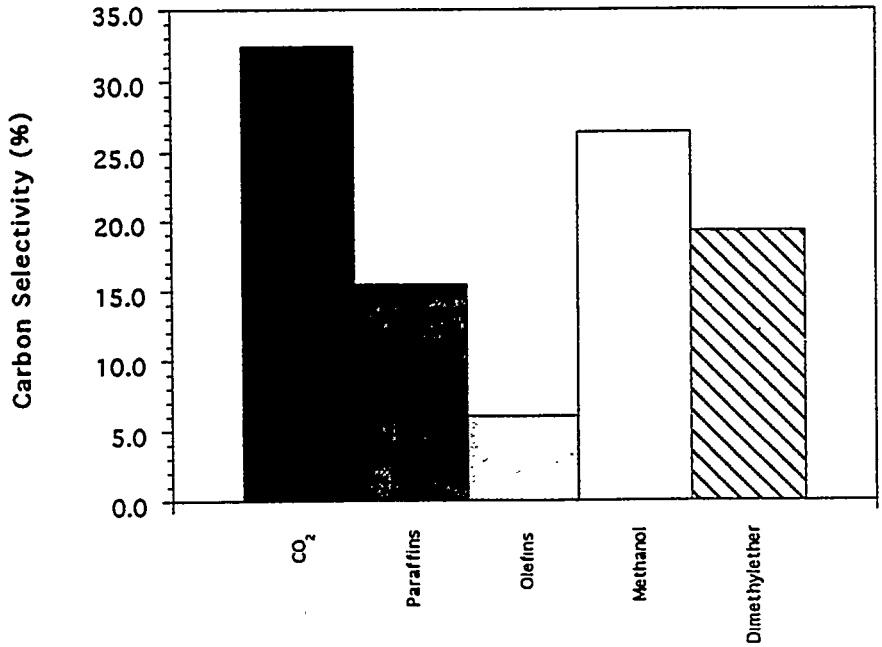

Figure 5

Effect of Temperature on Product Distribution
(5000 GHSV, 68 atm, $H_2/CO = 0.5$)

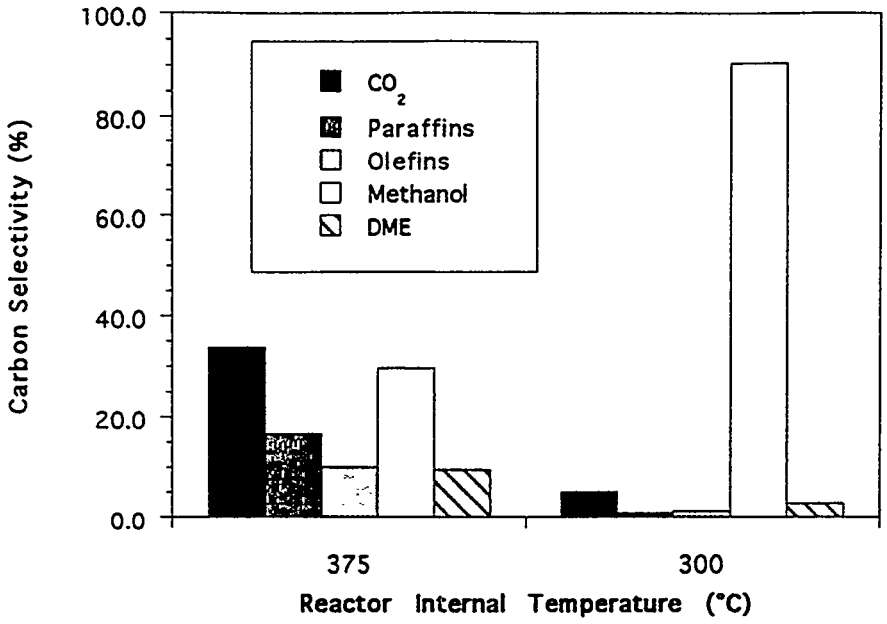

Figure 6

Effect of Temperature on Methanol Production
(5000 GHSV, 68 atm, $H_2/CO = 0.5$)

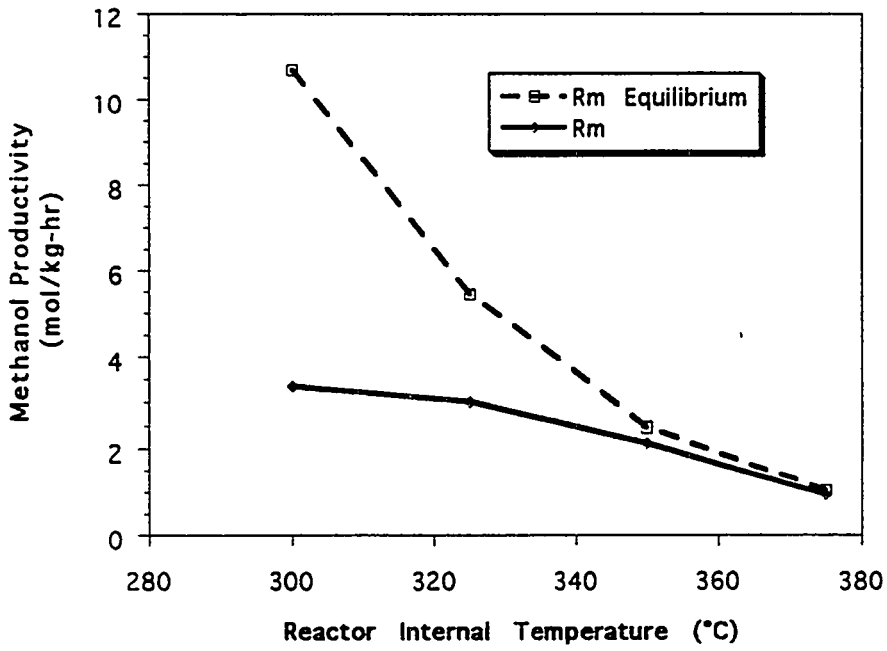

Figure 7

Effect of GHSV, H_2/CO Ratio on Methanol Production (300°C, 68 atm)

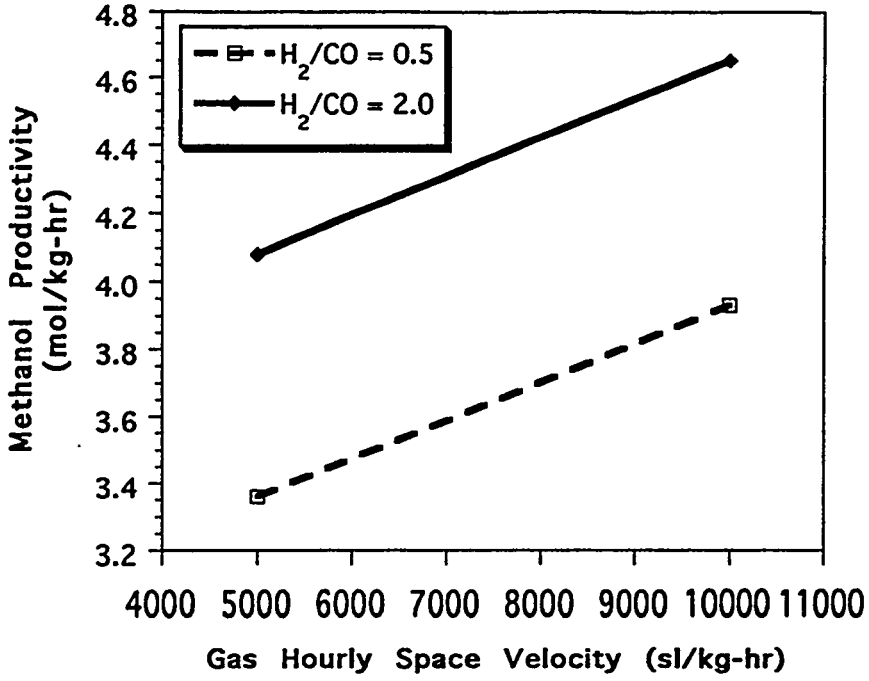

Figure 8

Catalyst Activity Versus Run Time (375°C, 5000 GHSV, $H_2/CO = 1$)

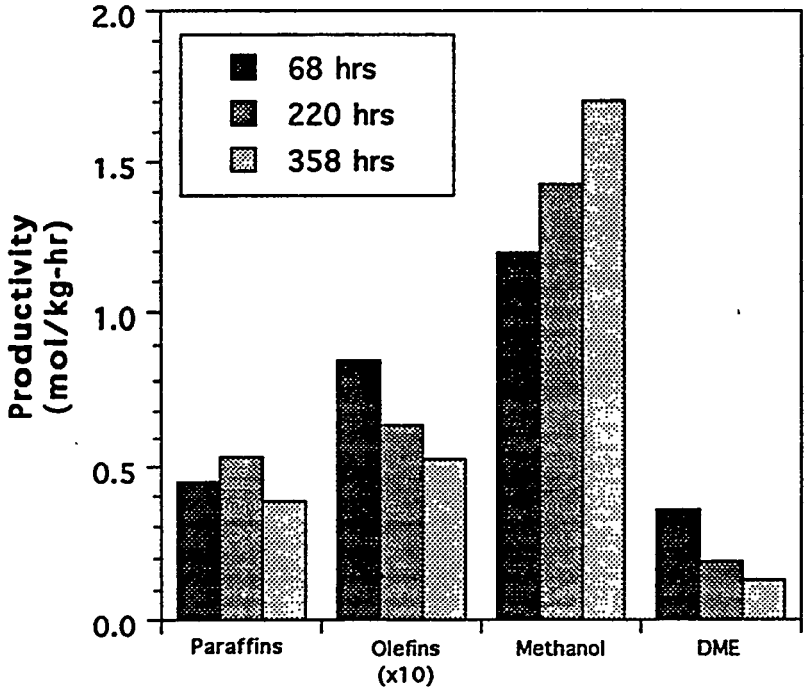

HETEROGENEOUS CATALYTIC PROCESS FOR ALCOHOL FUELS FROM SYNGAS

D.M. Minahan and D.A. Nagaki

Union Carbide Corporation

DOE COAL LIQUEFACTION AND GAS CONVERSION
CONTRACTORS REVIEW CONFERENCE
August 29-31st 1995, Pittsburgh, PA

CONTRACT NO. DE-AC22-91PC90046
Period of Performance: 01/92 to 12/95

OBJECTIVE This project is focused on the discovery and evaluation of novel heterogeneous catalyst for the production of oxygenated fuel enhancers from synthesis gas. Catalysts have been studied and optimized for the production of methanol and isobutanol mixtures which may be used for the downstream synthesis of MTBE or related oxygenates.

ACCOMPLISHMENTS We have studied higher alcohols synthesis (HAS) from syngas; the alcohols that are produced in this process may be used for the downstream synthesis of MTBE or related oxygenates. This work has resulted in the discovery of a catalyst system that is highly selective for isobutanol compared with the prior art [1]. The catalysts operate at high temperature (400°C), and consist of a spinel oxide support (general formula AB_2O_4, where $A = M^{2+}$ and $B = M^{3+}$), promoted with various other elements. These catalysts operate by what is believed to be an aldol condensation mechanism, giving a product mix of mainly methanol and isobutanol. In this study we report the effect of product feed/recycle (methanol, ethanol. n-propanol, isopropanol, carbon dioxide and water) on the performance of 10-DAN-55 (spinel oxide based catalyst) at 400°C, 1000 psi, GHSV = 12,000 and syngas (H_2/CO) ratio = 1:2 (alcohol addition) and 1:1 (carbon dioxide and water addition). We have also examined the effect of operation at high temperatures and pressures on the performance of an improved catalyst formulation.

Effect of Methanol Feed

There is little or no effect of methanol addition on higher alcohol synthesis with 10-DAN-55, a representative spinel oxide catalyst: this is illustrated in figure 1.

The methanol synthesis reaction is essentially at equilibrium over the catalysts used here. The equilibrium:

$$CO + 2H_2 = CH_3OH$$

lies heavily to the left-hand side at 400°C and above, thus the vast majority of the methanol feed reverts back to syngas. Methanol feed/recycle is thus not a viable option for boosting higher alcohol production.

Effect of Ethanol Feed
The effect of ethanol addition on the performance of 10-DAN-55 has been examined. Test conditions were 1000 psi 400°C, GHSV=12000 and syngas (H_2/CO) ratio = 1:2. The results are summarized below and in figure 2:

		Ethanol Feed		
	no EtOH	EtOH 29 g/kg-hr	EtOH 70 g/kg-hr	EtOH 127 g/kg-hr
Sel. Total Alcohols (%)	84	77	72	68
Total Alcohol Rate (g/kg-hr)	115	115	135	147
Methanol Rate (g/kg-hr)	48	41	42	38
Ethanol Rate (g/kg-hr)	0	0	0	6
n-Propanol rate (g/kg-hr)	0	-	19	28
Isopropanol rate (g/kg-hr)	0	2	5	8
Isobutanol Rate (g/kg-hr)	57	60	69	68
MeOH/i-BuOH mole ratio	3.3	2.7	2.4	2.2
Hydrocarbon rate (g/kg-hr)	14	22	34	45

The isobutanol rate increases by a modest 19% over the range studied. Significant quantities of n-propanol and isopropanol are observed as more ethanol is added. The methanol/i-butanol ratio falls from 3.3 to 2.2. Feeding a large excess of ethanol (~500 g/kg-hr) results in a doubling in the isobutanol rate, but with concurrent formation of large amounts of ethane.

Effect of n-Propanol Feed
The effect of n-propanol addition on the performance of 10-DAN-55 has been examined. Test conditions were 1000 psi, 400°C, GHSV=12000 and syngas (H_2/CO) ratio = 1:2. The results are summarized in the following table and in figure 3.

Addition of small amounts of n-propanol to the syngas feed appears to qualitatively improves the performance; the isobutanol rate doubles on the first incremental addition (isobutanol rate rises from 38 g/kg-hr to 75 g/kg-hr) and the methanol/i-butanol ratio falls from 5.8 to 2.7.

Further addition of up to 236 g/kg-hr of isopropanol results in an additional increase in the isobutanol rate to 138 g/kg-hr (MeOH/i-BuOH ratio = 1.3). The hydrocarbon rate also increases and propane is the major hydrocarbon product. The overall rate is increased by a factor of 4 over the range studied. n-Propanol addition is more effective than ethanol addition in boosting the isobutanol rate.

The isopropanol rate is not significantly affected by the addition of n-propanol. The methanol rate falls with n-propanol addition and no ethanol is seen, suggesting that there is no back reaction to lighter alcohols from n-propanol.

	n-Propanol Feed			
	no n-PrOH	n-PrOH 25 g/kg-hr	n-PrOH 110 g/kg-hr	n-PrOH 236 g/kg-hr
Sel. Total Alcohols (%)	67	70	72	72
Total Alcohol Rate (g/kg-hr)	97	131	143	192
Methanol Rate (g/kg-hr)	54	50	44	44
Ethanol Rate (g/kg-hr)	0	0	0	0
n-Propanol rate (g/kg-hr)	3	6	3	9
Isopropanol rate (g/kg-hr)	0	0	0	1
Isobutanol Rate (g/kg-hr)	38	75	93	138
MeOH/i-BuOH mole ratio	5.8	2.7	1.9	1.3
Hydrocarbon rate (g/kg-hr)	27	35	37	52

Effect of Isopropanol Feed

The effect of n-propanol addition on the performance of 10-DAN-55 has been examined. Test conditions were 1000 psi, 400°C, GHSV=12000 and syngas (H_2/CO) ratio = 1:2. The results are summarized below and in figure 4:

	Isopropanol Feed			
	no i-PrOH	i-PrOH 29 g/kg-hr	i-PrOH 106 g/kg-hr	i-PrOH 225 g/kg-hr
Sel. Total Alcohols (%)	72	67	61	58
Total Alcohol Rate (g/kg-hr)	107	119	120	146
Methanol Rate (g/kg-hr)	54	51	43	39
Ethanol Rate (g/kg-hr)	0	0	0	0
n-Propanol Rate (g/kg-hr)	5	7	11	16
Isopropanol Rate (g/kg-hr)	0	0	4	17
Isobutanol Rate (g/kg-hr)	48	61	61	75
MeOH/i-BuOH mole ratio	4.5	3.3	2.8	2.1
Hydrocarbon rate (g/kg-hr)	25	36	49	69

Addition of small amounts of isopropanol to the syngas feed appears to qualitatively improves the performance; the isobutanol rate increases by 27% on the first incremental addition (isobutanol rate rises from 48 g/kg-hr to 61 g/kg-hr) and the methanol/i-butanol ratio falls from 4.5 to 3.3.

Further addition of up to 225 g/kg-hr of isopropanol results in isopropanol breakthrough and an additional increase in the isobutanol rate to 75 g/kg-hr (MeOH/i-BuOH ratio = 2.1). The hydrocarbon rate also increases and propane is the major hydrocarbon product.

Interestingly, the n-propanol rate also increases modestly, perhaps suggesting some pathway exists for conversion of isopropanol to n-propanol. The methanol rate falls with isopropanol addition and no ethanol is seen, suggesting that there is no back reaction to lighter alcohols from isopropanol.

Effect of Carbon Dioxide Feed

The effect of carbon dioxide addition on the performance of 10-DAN-55 has been examined. Test conditions were 1000 psi, 400°C, GHSV=12000 and syngas (H_2/CO) ratio = 1:1. The results are summarized below and in figure 5:

	Carbon Dioxide Feed (%)			
	No CO2	3% CO2	6% CO2	No CO2
Sel. Total Alcohols (%)	83	89	89	84
Total Alcohol Rate (g/kg-hr)	192	137	107	165
Methanol Rate (g/kg-hr)	108	102	90	103
Ethanol Rate (g/kg-hr)	1	2	0	0
Isopropanol rate (g/kg-hr)	0	0	0	0
n-Propanol rate (g/kg-hr)	18	12	6	12
Isobutanol Rate (g/kg-hr)	64	21	11	51
MeOH/i-BuOH mole ratio	7	19	33	8
Hydrocarbon rate (g/kg-hr)	23	9	6	18

Addition of carbon dioxide to the syngas feed adversely affects the performance of a spinel oxide catalyst; the total alcohol rate falls by 44% and the isobutanol rate by 83% on addition of 6% carbon dioxide. In concert, the methanol rate decreases by a modest 17%, such that the methanol/i-butanol ratio rises from 7 to 33.

It should be remembered that the water gas shift (WGS) equilibrium must be taken into account when viewing these results, as these materials are excellent WGS catalysts. The equilibrium

$$CO + H_2O = CO_2 + H_2$$

lies to the right under the reaction condition employed here (Keq = 8), so the effect of carbon dioxide on catalyst performance cannot be disentangled from that of water: the introduction of carbon dioxide to the system will automatically result in an increase in the water content of the gas mixture.

Effect of Operation at Higher Temperatures and Pressures
We have tested 16-DMM-68, an improved formulation over 10-DAN-55, at elevated temperatures (>400°C) and pressures (>1000 psi). GHSV was held constant at 12000 and the syngas (H_2/CO) ratio was also held constant at 1:1. The results are summarized below:

	T = 400°C P = 1000 psi	T = 400°C P = 1500 psi	T = 440°C P=1180 psi	T = 440°C P = 1500 psi
Sel. Total Alcohols (%)	84	86	54	64
Total Alcohol Rate (g/kg-hr)	233	407	159	304
Methanol Rate (g/kg-hr)	119	248	35	99
Ethanol Rate (g/kg-hr)	0	7	0	0
Isopropanol rate (g/kg-hr)	0	0	0	0
n-Propanol rate (g/kg-hr)	12	21	15	27
Isobutanol Rate (g/kg-hr)	102	130	109	179
MeOH/i-BuOH mole ratio	4.7	7.6	1.3	2.2
Hydrocarbon rate (g/kg-hr)	26	37	94	112
Conversion (%)	14	24	23	28

The data show that the catalyst is most effective for higher alcohol synthesis (HAS) at elevated temperatures and pressures. Note that the *combination* of high temperature and high pressure is required for optimal higher alcohol formation:

	Methanol Synthesis	Hydrocarbon Formation	Higher Alcohol Synthesis
High temperature	- -	+ +	+
High Pressure	+ +	- -	+

CONCLUSIONS:

- Methanol feed/recycle is not a viable option for higher alcohol production.

- Ethanol feed is moderately effective for boosting isobutanol activity: the isobutanol rate increases by a modest 19% over the range studied. A large amount of ethanol is converted to ethane. There is no back reaction to methanol.

The inhibition of higher alcohol synthesis by carbon dioxide has been observed in other HAS catalyst systems [1]. This observation is explained by assuming that water rather than carbon dioxide inhibits HAS by competing for adsorption with the intermediate C_1 species on the catalyst surface, preventing the homologation reactions from proceeding. Methanol formation is thus not as sensitive to the water/carbon dioxide equilibrium and, in addition, the mechanism proposed for methanol synthesis involves carbon dioxide as an intermediate. The extra water produced via the WGS equilibrium may help to drive the alcohol equilibrium back to the left, viz.:

$$n\,CO + 2n\,H_2 = C_nH_{2n+1}OH + (n-1)\,H_2O$$

An advantage of carbon dioxide addition is that the rate of hydrocarbon formation is suppressed in an even greater extent such that the selectivity to total alcohols shows a modest increase from 83% to 89%. The extra water produced via the WGS equilibrium may also help to drive the hydrocarbon equilibrium back to the left, viz.:

$$n\,CO + (2n+1)\,H_2 = C_nH_{2n+2} + n\,H_2O$$

or perhaps water helps to titrate acid sites on the catalysts responsible for hydrocarbon formation. The catalyst recovers slowly after stopping the addition of carbon dioxide - see figure 6. Normally, a change in process parameters and alcohol feeds results in a new steady state within 4-8 hours, but on turning off the carbon dioxide feed, the catalyst is still returning to pre-carbon dioxide feed performance after 48 hrs. This suggests some surface intermediate is being slowly lost, perhaps carbonate.

An initial boost in methanol formation is also seen on removing the carbon dioxide feed and is reflected in a transient increase in the methanol/isobutanol mole ratio - see figure 7. It appears that the carbon dioxide released on decomposition of the surface carbonate layer formed by carbon monoxide addition enhances methanol formation, suggesting that carbon dioxide is an intermediate in methanol synthesis over these catalysts.

Effect of Water Feed

The effect of carbon dioxide addition on the performance of 10-DAN-55 has been examined. Test conditions were 1000 psi, 400°C, GHSV=12000 and syngas (H_2/CO) ratio = 1:1.

Addition of water to the syngas feed adversely affects the performance of a spinel oxide catalyst 10-DAN-55; the total alcohol rate falls by 44% and the isobutanol rate by 86% on addition of up to 490 g/kg-hr of water. In concert, the methanol rate decreases by only 17%, resulting in an increase in the methanol/i-butanol ratio from 8 to 48.

These results are essentially identical to those obtained through carbon dioxide addition. The introduction of water to the system will automatically result in an increase in the carbon dioxide content of the gas mixture through the WGS equilibrium, which, under the reaction conditions employed here, lies heavily on the side of carbon dioxide.

ESCA analysis of the spent catalyst, after water addition, indicates the formation of a carbonate layer on the catalyst surface, supporting this hypothesis. The WGS activity is a plus, as it is less expensive to remove carbon dioxide from the recycle stream by extraction than water via distillation.

• n-Propanol feed is more effective than ethanol feed, with the rate increasing by a factor of 4, and only a small increase in propane formation up to surface saturation. There is no back reaction to lighter alcohols from n-propanol.

• Isopropanol is as effective as ethanol in boosting the isobutanol rate, but a large amount is hydrogenated to propane. Interestingly, the n-propanol rate also increases modestly: perhaps suggesting some pathway exists for conversion of isopropanol to n-propanol. There is no back reaction to lighter alcohols from isopropanol.

• Addition of carbon dioxide to the syngas feed adversely affects catalyst performance; the total alcohol rate falls by 44% and the isobutanol rate by 83% on addition of 6% carbon dioxide. An advantage of carbon dioxide addition is that the rate of hydrocarbon formation is suppressed so that the selectivity to total alcohols shows a modest increase from 83% to 89%.

• The catalyst recovers slowly from the carbon dioxide addition, suggesting some surface species is formed in the presence of carbon dioxide, probably carbonate. Carbon dioxide released on decomposition of the surface carbonate layer enhances methanol formation, suggesting that carbon dioxide is an intermediate in methanol synthesis over these catalysts.

• Addition of water to the syngas feed adversely affects catalyst performance in a manner that mirrors the effect of carbon dioxide addition. These results are essentially identical to those obtained through carbon dioxide addition. This can be explained by the production of carbon dioxide via the water-gas-shift equilibrium.

• ESCA analysis of the spent catalyst, after water addition, indicates the formation of a carbonate layer on the catalyst surface, supporting this hypothesis. The WGS activity is a plus, as it is less expensive to remove carbon dioxide from the recycle stream by extraction than water via distillation.

• Operation at higher temperatures *and* higher pressures is optimal for higher alcohol synthesis, with isobutanol rates as high as 179 g/kg-hr at 440°C and 1500 psi.

FUTURE PLANS

• Catalyst formulation optimization through changes in both support and promoters.

• Surface analysis of catalysts to uncover structure/property relationships

REFERENCES

1. P. Forzatti, E. Tronconi and I. Pasquon, Catal.Rev.-Sci.Eng, 33(1&2), 109-168 (1991)

ACKNOWLEDGMENTS The authors would like to acknowledge the following people for their help during the course of the work: Jerome Hornbuckle for catalyst preparation, Paul Ruppert for catalyst testing and reactor modification, and Duane Dombek and Jim Schreck for helpful discussions.

FIGURE 1

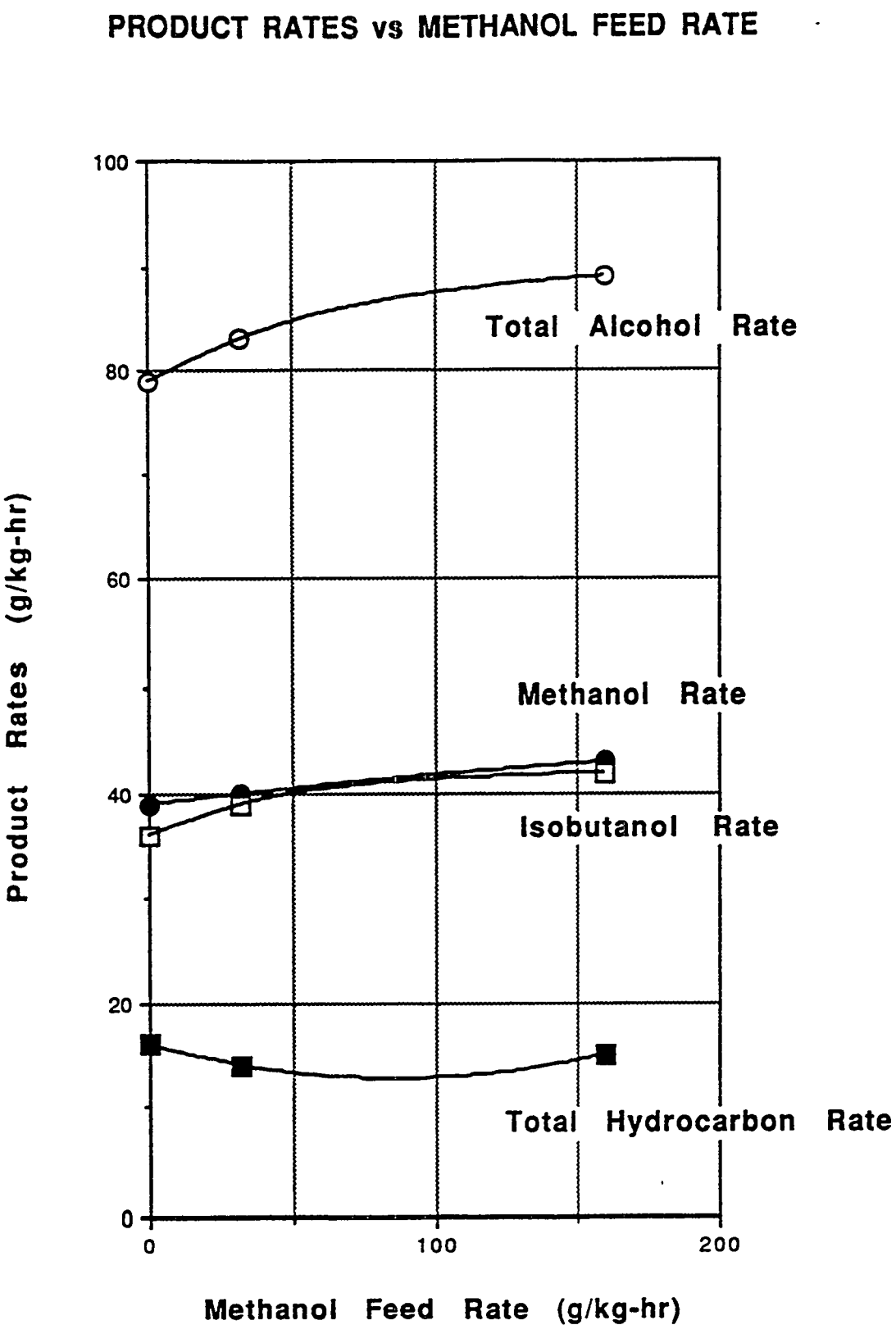
PRODUCT RATES vs METHANOL FEED RATE
Product Rates (g/kg-hr)
100
80
60
40
20
0
0
100
200
Methanol Feed Rate (g/kg-hr)
Total Alcohol Rate
Methanol Rate
Isobutanol Rate
Total Hydrocarbon Rate

FIGURE 2

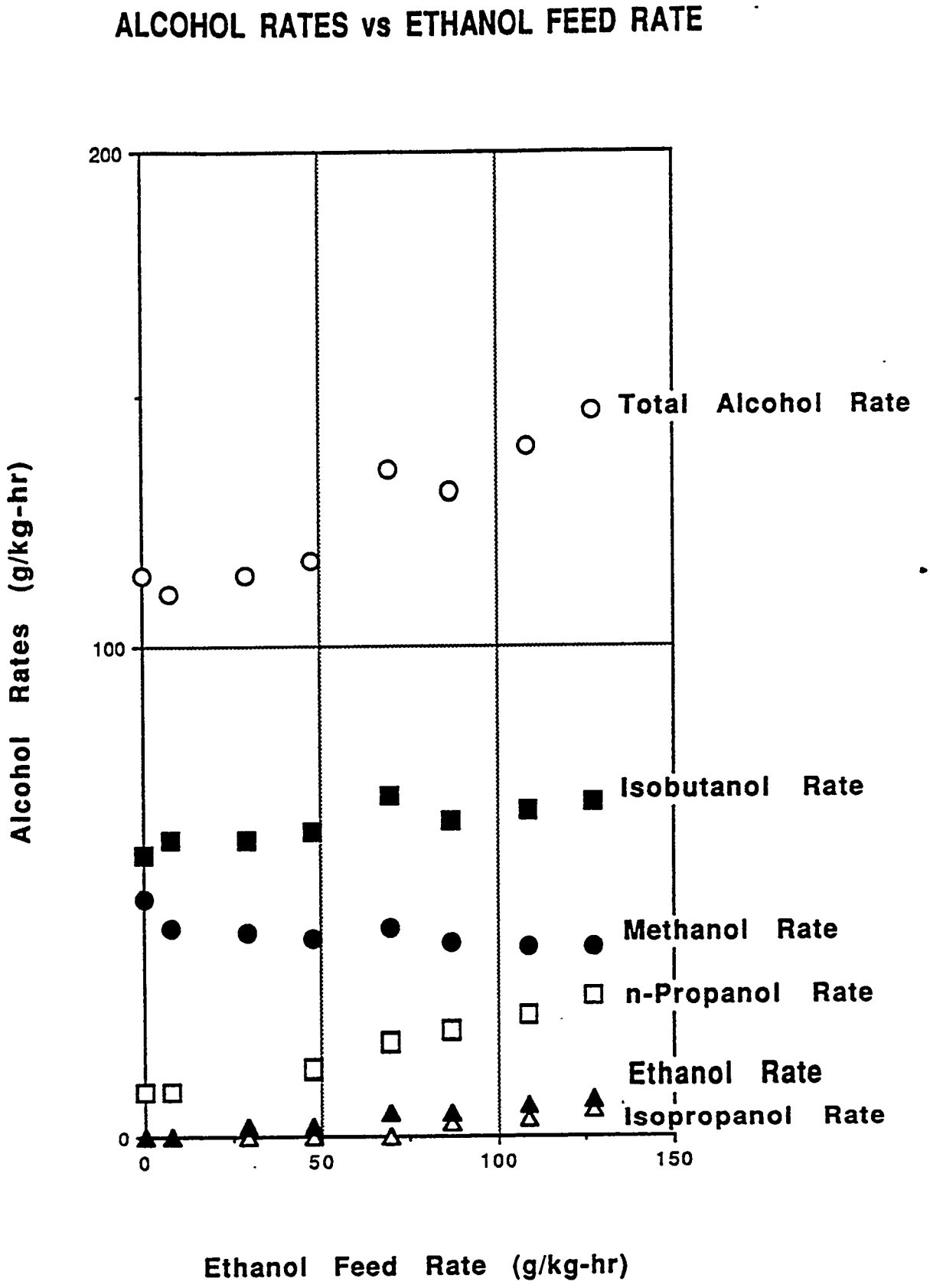
ALCOHOL RATES vs ETHANOL FEED RATE
Alcohol Rates (g/kg-hr)
200
100
0
0
50
100
150
Ethanol Feed Rate (g/kg-hr)
Total Alcohol Rate
Isobutanol Rate
Methanol Rate
n-Propanol Rate
Ethanol Rate
Isopropanol Rate

FIGURE 3

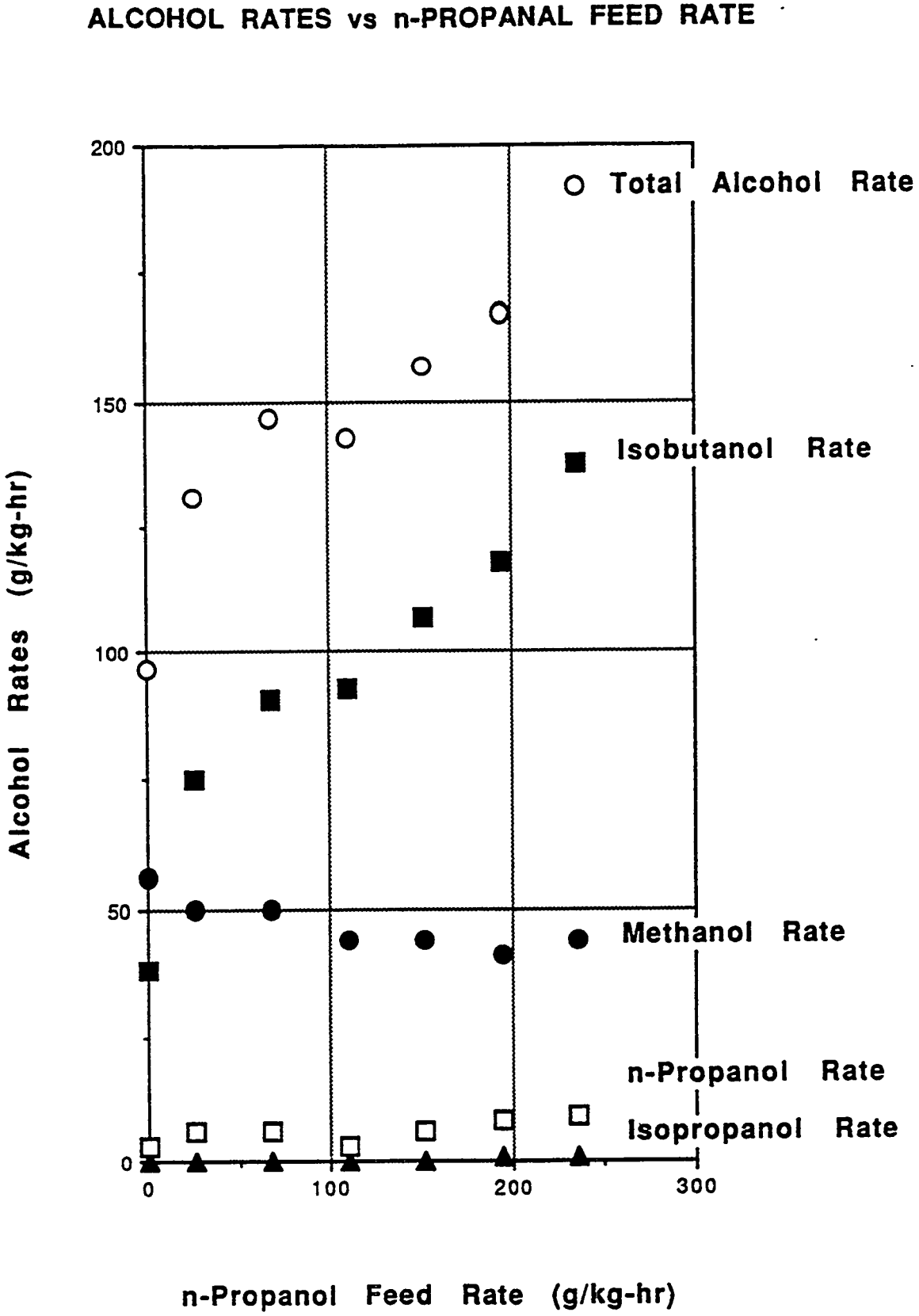
ALCOHOL RATES vs n-PROPANAL FEED RATE
Alcohol Rates (g/kg-hr)
200
150
100
50
0
0
100
200
300
n-Propanol Feed Rate (g/kg-hr)
Total Alcohol Rate
Isobutanol Rate
Methanol Rate
n-Propanol Rate
Isopropanol Rate

FIGURE 4

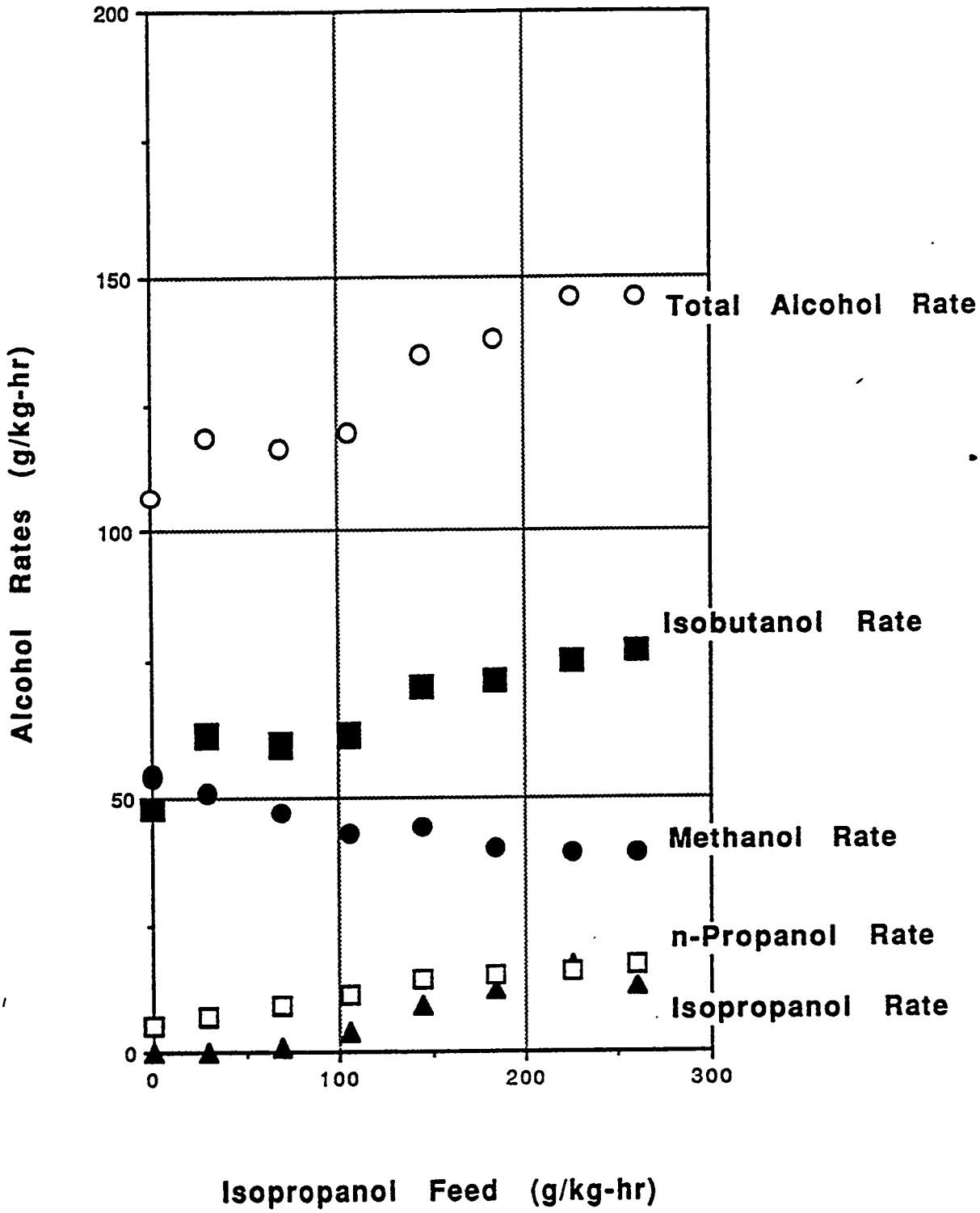
ALCOHOL RATES vs ISOPROPANOL FEED RATE
Alcohol Rates (g/kg-hr)
200
150
100
50
0
0
100
200
300
Isopropanol Feed (g/kg-hr)
Total Alcohol Rate
Isobutanol Rate
Methanol Rate
n-Propanol Rate
Isopropanol Rate

FIGURE 5

PLOT OF ALCOHOL RATES vs
ADDITION OF CARBON DIOXIDE TO FEED

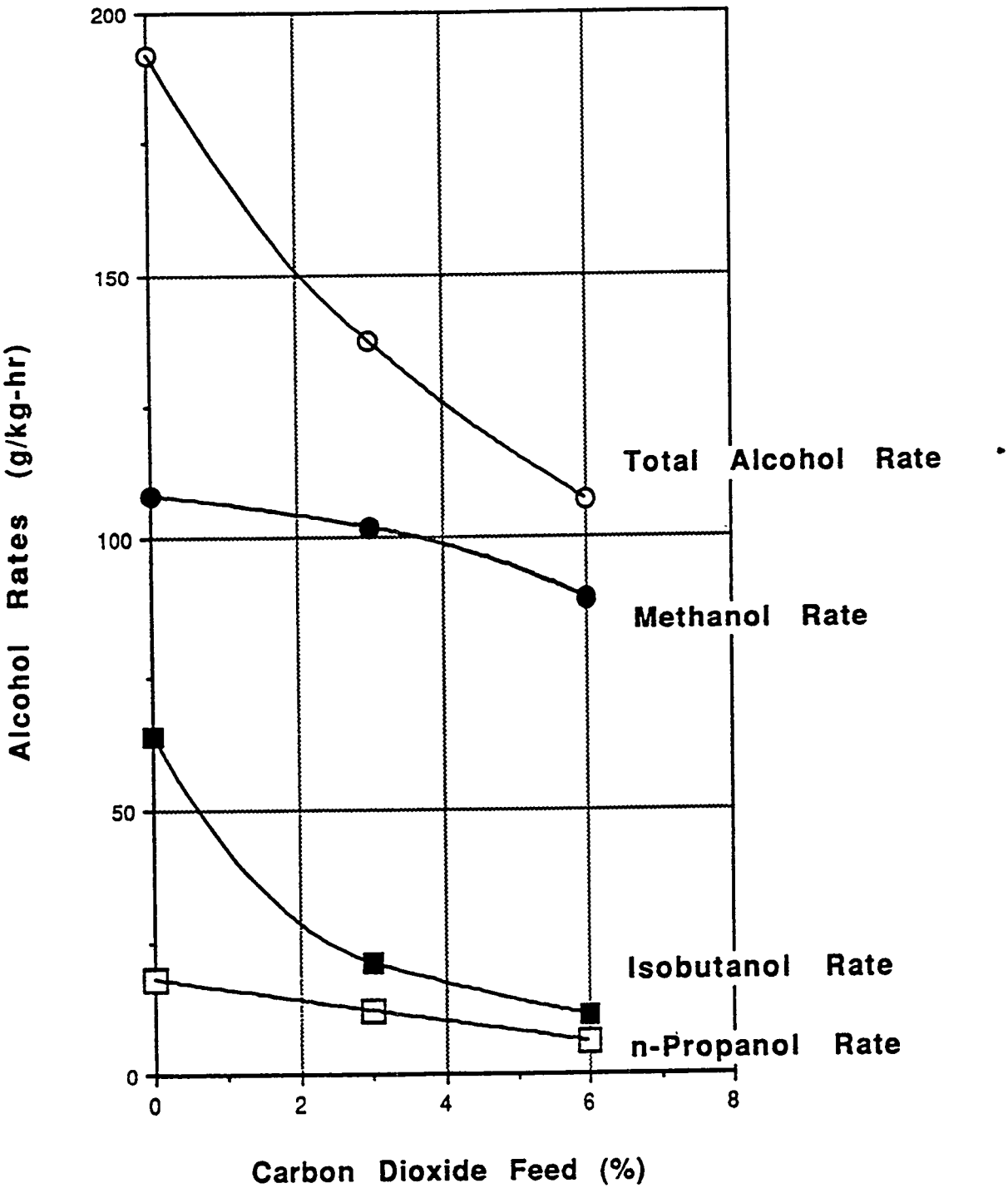

FIGURE 6

PLOT OF ALCOHOL RATES vs TIME AFTER REMOVAL OF 6% CARBON DIOXIDE FROM FEED

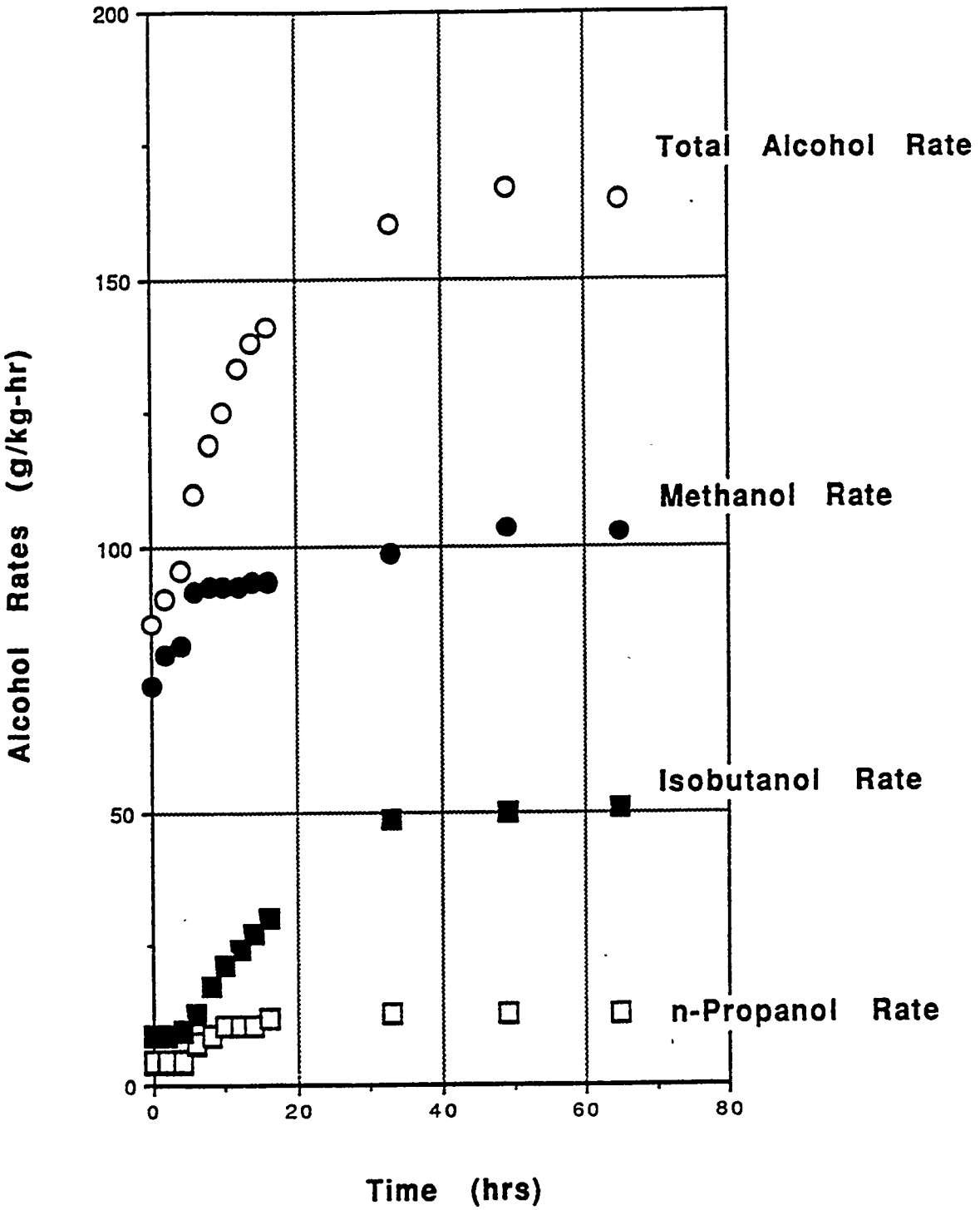

FIGURE 7

PLOT OF MeOH/i-BuOH MOLE RATIO vs TIME AFTER REMOVAL OF 6% CARBON DIOXIDE FROM THE FEED

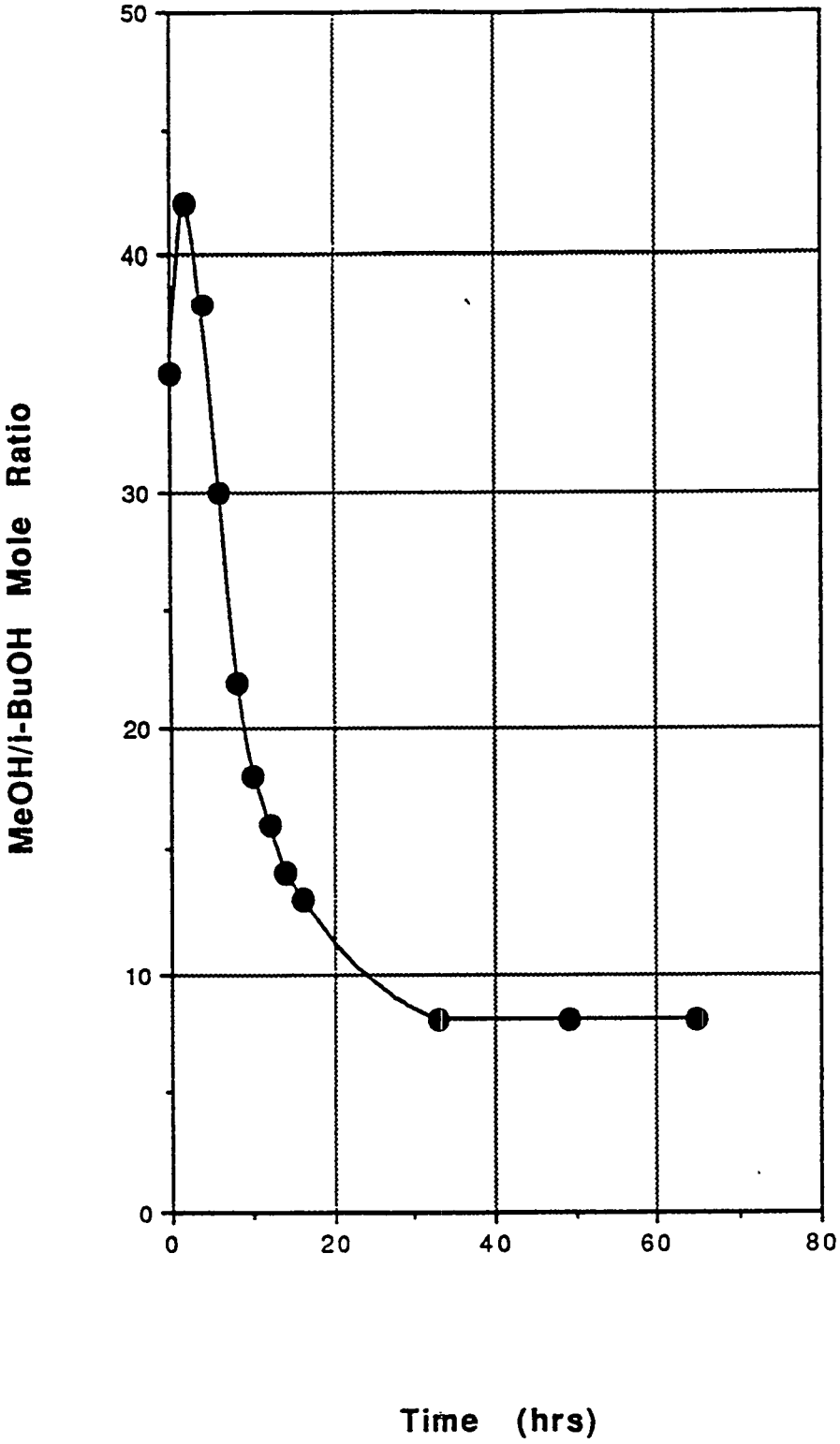

The Economic Production of Alcohol Fuels from Coal-Derived Synthesis Gas

E. L. Kugler, D. B. Dadyburjor, R. Y. K. Yang, Z. Y. Liu, X. Li, L. Feng, E. Zubovic, J. L. Petersen*, M. R. Close*, J. A. Shaeiwitz, R. Turton, W. B. Whiting, R. W. Maier, J. E. Saymansky** and T. F. Torries**

Departments of Chemical Engineering, Chemistry* and Resource Management**, West Virginia University, Morgantown, WV 26506

Contract Number: DE-AC22-91PC91034

Period of Performance: July 1, 1994- May 31, 1995

I. OBJECTIVES

The objectives of this project are:

1. to discover, study and evaluate novel heterogeneous catalytic systems for the production of oxygenated fuel enhancers from synthesis gas. Specifically, alternative methods of preparing catalysts are to be investigated, and novel catalysts, including sulfur-tolerant ones, are to be pursued. (Task 1)

2. to explore, analytically and on the bench scale, novel reactor and process concepts for use in converting syngas to liquid fuel products. (Task 1)

3. to simulate by computer the most energy efficient and economically efficient process for converting coal to energy, with primary focus on converting syngas to fuel alcohols. (Task 2)

4. to develop on the bench scale the best holistic combination of chemistry, catalyst, reactor and total process configuration integrated with the overall coal conversion process to achieve economic optimization for the conversion of syngas to liquid products within the framework of achieving the maximum cost effective transformation of coal to energy equivalents. (Tasks 1 and 2)

5. to evaluate the combustion, emission and performance characteristics of fuel alcohols and blends of alcohols with petroleum-based fuels. (Task 2)

2.2 Catalyst Testing Units

Two computer controlled reactors were used for catalyst testing. One unit is used exclusively for testing sulfide catalysts whereas the other unit is used to test carbides and nitrides. Each unit has 4 gas feed lines independently controlled with mass flow controllers and one liquid feed line controlled by an HPLC pump. The units are designed to operate from atmospheric pressure to 1500 psig and with reactor temperatures up to 500°C. Operating conditions are set directly from the computer and data are logged at operator-determined intervals. Each unit uses a Hewlett Packard 5890 gas chromatograph for on-line product analysis. The product is sampled immediately below the reactor with a gas sampling valve at reactor operating pressure and at a minimum temperature of 250°C. Each unit is controlled by the commercial software package InTouch[tm] by Wonderware and the gas chromatograph is controlled by Hewlett Packard Chemstation[tm] software. All programs operate from the same computer in a multitasking MS Windows[tm] environment. A figure for this unit was provided in our 1994 report (1).

Catalysts are tested in small, plug-flow reactors typically loaded with 0.5 g of catalyst and 3 g of crushed quartz. The screening procedure for sulfide catalysts is to pretreat the catalyst at 400°C with a 10% H_2S in H_2 mixture. After 1 hr presulfiding, the catalyst is purged with H_2 and the temperature lowered to 200°C. The system is then pressurized to 750 psig and the gas flows adjusted to 25 sccm H_2 and 25 sccm CO. The reaction temperature is ramped from 200 to 400 to 200°C at a rate of 10 °C/hr. Reaction product is sampled at 2 hr intervals.

The product is analyzed with a Hewlett-Packard 5890 gas chromatograph with a flame-ionization detector for hydrocarbon and alcohol analysis and a thermal conductivity detector for inorganic gas analysis. Flow from the sampling valve below the plug-flow reactor passes through the gc injector and is split between two columns: a 30' x 1/8" HayeSep D_B packed column and a 20m x 0.10mm J&W DB-WAX capillary column, temperature programmed from 40 to 230°C. The HayeSep D_B column provides quantitative analysis for N_2 (internal standard), CO, CO_2, H_2O. H_2 is separated but cannot be measured satisfactorily. The DB-WAX column separates all of the C_1-C_5 alcohols and groups all of the C_1-C_6 hydrocarbons as a single peak. This DB-WAX column provides excellent product analysis for catalysts that produce only alcohols and light hydrocarbons as we observe with MoS_2. However, aldehydes, ketones, ethers and heavy hydrocarbons also elute with the alcohols. Complicated product mixtures cannot be identified by gas chromatography alone.

The gc analysis with two columns in parallel is a significant advance beyond our prior analysis with a single Porapak Q packed column. Last year we could separate the inorganic gases, methanol and C_1-C_3 hydrocarbons by temperature programming from -60 to 250°C. However, we could not distinguish C_{4+} hydrocarbons from C_{2+} alcohols. With the current method, C_1-C_8 hydrocarbons are cleanly separated from all of the alcohol peaks.

II. ACCOMPLISHMENTS

1. Introduction

This is a joint project between West Virginia University and Union Carbide Chemicals & Plastics. The project has two parts. Task 1 focuses on catalyst evaluation and reaction engineering; Task 2 is studying process synthesis and fuel evaluation. This paper emphasizes the work at WVU on objectives 1 and 3: discovery, study and evaluation of molybdenum based catalysts for producing fuel alcohols from syngas, and computer simulation of the most economically efficient process for producing fuel alcohols.

In the period since the September 1994 review meeting, Task 1 has evaluated over 100 catalysts for alcohol fuels production while Task 2 has developed seven new economic cases where fuel alcohols are either the primary product or the byproduct of a power generation facility.

2. Experimental

2.1 Catalyst Preparation

Three methods of catalyst preparation have been used in this program. These are described below.

Vapor Phase Reaction Volatile metal carbonyls are decomposed in an H_2S or ammonia atmosphere to produce high-surface-area sulfides and nitrides. The reactor tube temperature is operated in the range of 300 to 1100°C. This method works well for producing both molybdenum and molybdenum-iron catalysts. Catalysts are in the form of fine powders.

Pore Volume Impregnation Incipient-wetness impregnation with salts or organometallic compounds was used to prepare supported catalysts. The catalyst precursor is then decomposed in a controlled atmosphere to produce the desired sulfide, nitride or carbide phase. Catalysts are in the form of the support material, either as a powder or a preformed pellets.

Solid State Synthesis Solid-state synthesis by combining the appropriate elements and heating at high temperature in a controlled atmosphere was used to prepare molybdenum sulfide chevrel phase catalysts. The following chevrel phase materials have been prepared by this technique: $HoMo_6S_8$, $SmMo_6S_8$, $AgMo_6S_8$, $InMo_6S_8$, $Cu_{3.2}Mo_6S_8$, $Fe_{1.5}Mo_6S_8$, $Ni_{1.6}Mo_6S_8$, $Co_{1.6}Mo_6S_8$ and $K_XMo_2S_3$. Catalysts were produced as powders.

2.3 Titration of MoS_2 Reaction Sites

Oxygen chemisorption on molybdenum sulfide catalysts has been measured by a Micromeritics 2700 pulse chemisorption unit. In our measurement procedure, a catalyst sample is first reduced and sulfided in a flowing 10% H_2S in H_2 mixture at 400°C for 1 hour, then purged for 1/2 hour in helium at the same temperature. After sulfiding, the sample is cooled in flowing helium to -78°C where O_2 gas is added in small doses and the adsorption is measured with a thermal conductivity detector.

3. Results

3.1 Synthesis of Vapor Phase Reactor Catalysts

The primary method of catalyst preparation was vapor phase reaction of molybdenum carbonyl, $Mo(CO)_6$, in ammonia to produce nitrides or in hydrogen sulfide to produce sulfides. Figure 1 shows a diagram of the apparatus used. The heated zone of the reactor is 18 inches long. A detailed drawing of the injector is shown in Figure 2. Injector #1 is the original design. However, extensive carbonyl decomposition occurred at the inlet of the furnace and on the reactor walls so that product yields were often in the range of 40-50%. Injector #2 shows the current design. The outside wall of the reactor tube is swept with a laminar flow of inert gas to keep the reacting carbonyl away from the tube wall. The injector is also water cooled into the heated zone. This reduces the reaction zone from 18 to 10 inches, but keeps carbonyls below their decomposition temperatures until they are abruptly heated. The improved injector design increased product yields to 80-100%.

The effect of decomposition reactor conditions on MoS_2 products is shown in Table 1. The temperature of the furnace was increased from 300 to 900°C in preparing a series of catalysts. Samples prepared at 300°C showed a low yield of recovered product, its surface area was low, and the x-ray diffraction powder pattern described a poorly crystalline structure. On raising the decomposition temperature to 500°C, the product yield increased to from 27 to 83%, the surface area increased from 21 to 76 m^2/g, and the x-ray diffraction pattern started to show the characteristic lines of MoS_2. On raising reaction temperature from 500 to 900°C, the product yield increased to 98%, the surface area remained nearly constant at 66-78 m^2/g and the x-ray diffraction lines became larger and more defined, showing an increase in MoS_2 crystallinity. The percentage sulfur in the product increased with increasing decomposition temperature. The stochiometric amount of sulfur in MoS_2 is 40.06%. Samples from 300 and 400°C decompositions were sulfur deficient, suggesting that oxygen or carbon from the $Mo(CO)_6$ was present in the low temperature product. Samples produced at 500°C were nearly stochiometric. Samples produced above 500°C showed excess sulfur. This excess sulfur probably comes from the decomposition of H_2S into hydrogen and elemental sulfur.

In its current design, the vapor phase reactor is able to produce a consistent, high-surface-area MoS_2 product with 83-98% yield. This MoS_2 has been used as the basic starting

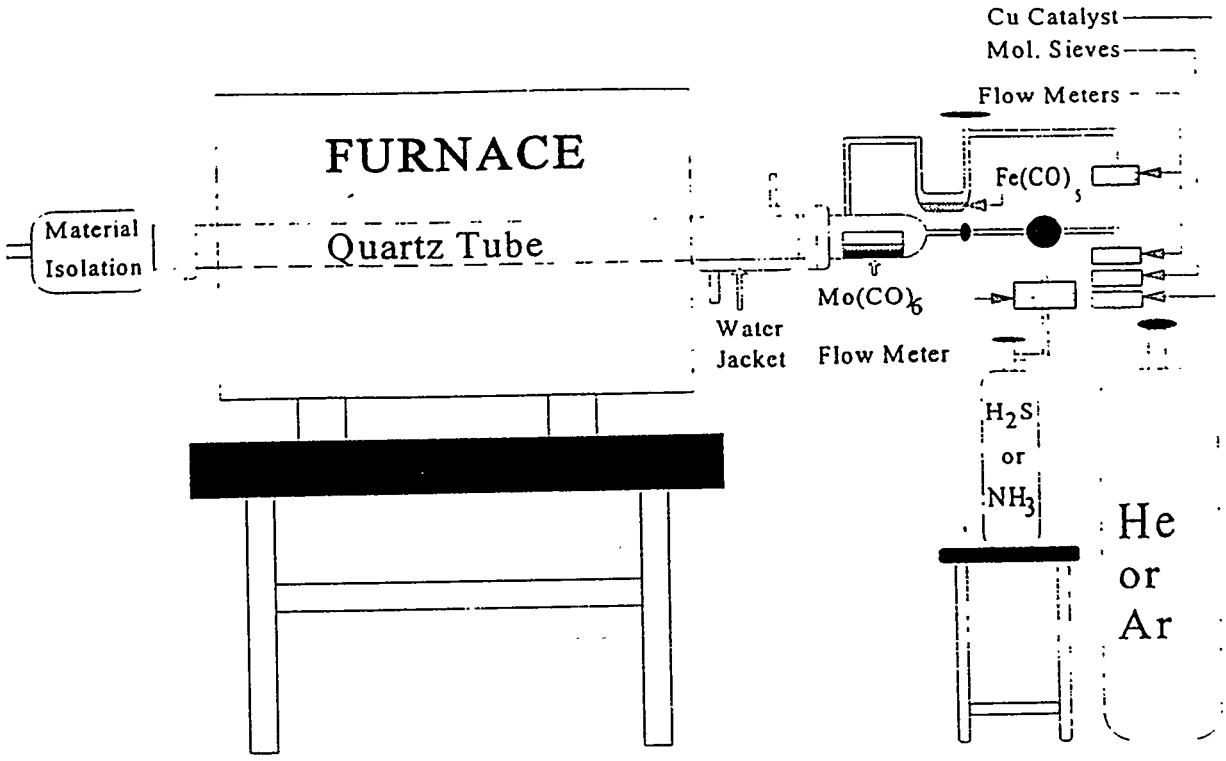

Figure 1: Vapor phase catalyst synthesis reactor for preparing molybdenum or molybdenum-iron sulfides and nitrides.

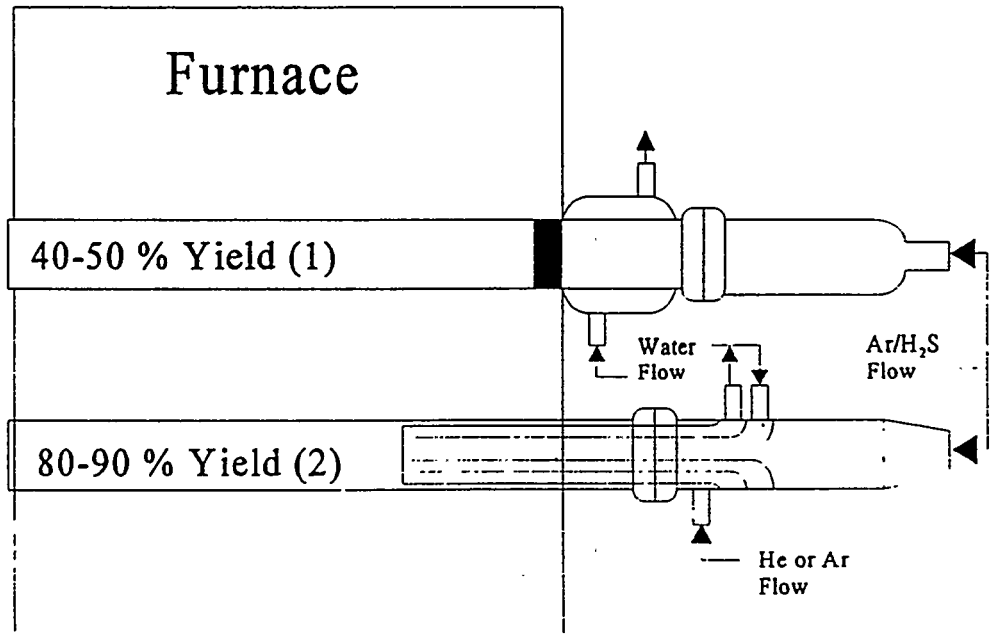

Figure 2: Detail of injector showing (1) original design and (2) improved design.

Table I Correlation of Furnace Temparature and Physical Properties for MoS_2 Catalysts Prepared by the Thermal Decomposition of $Mo(CO)_6$ and H_2S using injector #2.

Ref #	T_f[1]	T_{Mo}[1]	T_{wj}[1]	Ar_i[1]	Ar_o[1]	H_2S rate (ml/min)	Yield %	XRD	Surface Area	Sulfur %
2MRC128A	300	98-99	85	220	700	11	26.7	Broad-26	21.4	22.6
2MRC129A	400	98-99	85	220	700	11	N/A	Broad-27	47.3	22.4
2MRC115A	500	98-99	85	220	700	11	82.7	Broad-18	76.53	37.85
2MRC116A	600	98-99	85	220	700	11	88.6	MoS_2	75.44	42.61
2MRC116C	700	98-99	85	220	700	11	95.0	MoS_2	77.96	45.95
2MRC118A	800	98-99	85	220	700	11	94.6	MoS_2	72.53	45.56
2MRC119A	900	98-99	85	220	700	11	98.2	MoS_2	66.15	46.03

T_f Furnace Temperature, °C
T_{Mo} Temperature of $Mo(CO)_6$, °C
Twj Water Jacket Temperature, °C
Ar_i Argon Flow, Inner Tube, sccm
Ar_o Argon Flow, Outer Tube, sccm
XRD X-ray Diffraction Characteristics
SA BET Surface Area, m^2/g

material for alkali-promoted vapor phase reactor (VPR) catalysts. The form as a fine powder is well suited for a slurry reactor, but must be combined with a binder (silica) and compressed into pellets for testing in our plug-flow, catalyst screening units.

3.2 Titration of Reaction Sites on MoS_2

Carbon supported molybdenum sulfide catalysts have also been prepared in this study. The carbon support is a hard, 20-40 mesh solid that is well suited for reactor studies. Similar catalysts for alcohol synthesis have been reported previously by researchers at Dow Chemical Company (2).

With supported molybdenum sulfide catalysts, it is important to know how much of the surface is active component and how much is support. Tauster and coworkers (3) have reported that active sites on molybdenum sulfides can be titrated by oxygen chemisorption. We have studied O_2 adsorption over a series of carbon supported molybdenum sulfides where the molybdenum concentration was varied from 0 to 30%. All of the samples were prepared by a pore-volume-impregnation technique using ammonium heptamolybdate solutions. These samples were then sulfided and tested using our standard oxygen chemisorption procedure. The results of these tests are shown in Figure 3.

The O_2 chemisorption was observed to increase linearly with increasing molybdenum concentration from 0 to 6%. The adsorption then goes through a broad plateau with little change in O_2 uptake with increasing molybdenum sulfide concentration. The maximum occurred at about 12%, suggesting that adding more molybdenum beyond that concentration does little to increase the number of active sites.

Alkali must be added to molybdenum sulfide catalysts to produce alcohols. Adding potassium to molybdenum in a 1:1 molar ratio causes O_2 adsorption to increase from about 50 to 250 umoles/g. This is not due to an increase in the number of reaction sites since potassium on carbon alone will adsorb about 200 umoles/g. This latter result shows that some potassium is reduced to its metallic form on the carbon support during pretreatment with H_2S/H_2, then reacts with O_2 to form a potassium oxide. Reduction of potassium to its metallic form is not expected for oxide supported materials.

The difficulty with potassium reacting with oxygen on carbon supported molybdenum sulfides has been used to our advantage. We have found that CO adsorption at -78°C can be used to measure the molybdenum sulfide sites on a potassium promoted catalyst. After CO adsorption, O_2 adsorption can then be used to measure the amount of reduced potassium. The amount of CO adsorption appears to correlate with catalyst activity.

3.3 Catalyst Screening Studies

In the experimental section, we stated that one catalyst testing unit is used exclusively for sulfide catalysts whereas the other testing unit is used exclusively for carbides and nitrides.

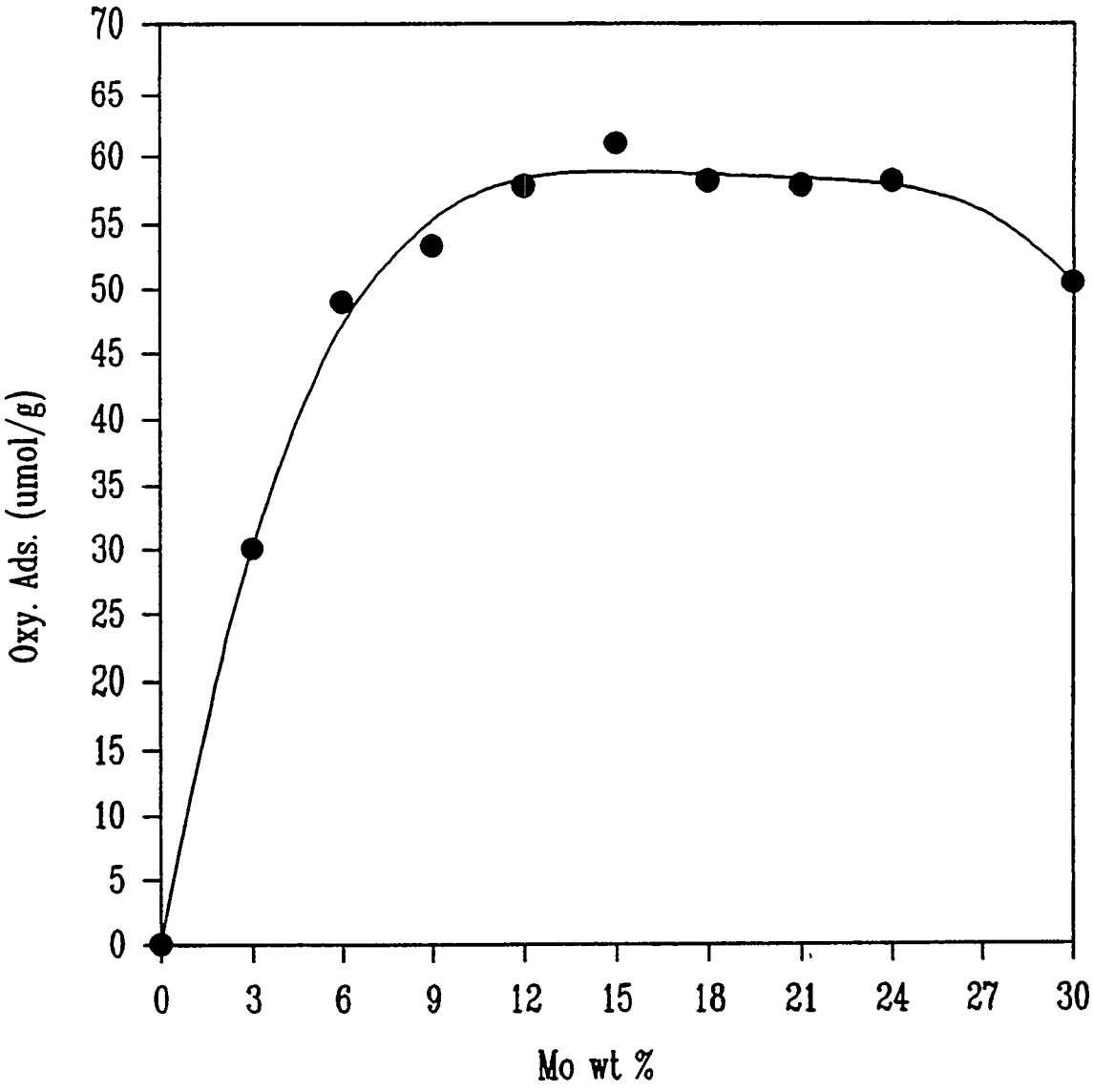

Figure 3: Change in O_2 chemisorption with molybdenum concentration for carbon supported MoS_2 catalysts.

In this section, we will only describe the results with sulfide catalysts. Many of the molybdenum carbides and nitrides tested are very active for CO conversion, but made many products other than alcohols and straight-chain hydrocarbons. Most of these products could not be identified by gas chromatography alone. A gas chromatography-mass spectrometry system has been ordered to improve product identification. Progress with carbide and nitride catalysts will be described in a future report.

Molybdenum sulfide studies were begun with the mixed metal chevrel phase catalysts. A listing of materials screened is in Section 2.1, Solid State Synthesis. Catalytic results showed that the 9 chevrel molybdenum sulfides studied had such low catalytic activities, that it was difficult to distinguish the catalytic reaction products from the background activity of the stainless steel reactor. No further work is planned for chevrel phase catalysts.

Vapor phase synthesis MoS_2 was found to have high activity for alcohol catalysis. Figure 4 shows results from a screening study with a potassium promoted molybdenum sulfide, $K_{0.7}$ MoS_2. The catalyst was screened from 200 to 400 to 200°C by changing the temperature at a rate of 10 °C/hr and sampling the product stream at 2 hour intervals. Reaction pressure was 750 psig with a standard-condition space velocity of 6000 l/ kg catalyst/ hr. The top section of Figure 4 shows the space-time yield for alcohol and hydrocarbon products. The open symbols are for increasing ttemperature, the filled symbols for decreasing temperature. The alcohol production rate reached a maximum near 200 g product/ kg catalyst/ hr. The selectivity to alcohols at this maximum rate was over 80%. The selectivity to higher alcohols on a CO_2 free, weight basis is over 40% on both increasing and decreasing temperatures. The criteria we use for judging a promising catalyst is 100 g/kg/hr alcohol production, with 50% selectivity to alcohols and 20% selectivity to higher alcohols. Vapor phase reaction MoS_2 materials promoted with potassium exceeded this criteria 2-fold.

The alcohol product distribution of this $K_{0.7}$ MoS_2 catalyst is shown in Figure 5. Data for decreasing temperatures is plotted, showing mole % at the top and wt % at the bottom of the figure. Looking at the mole % distribution data, the selectivity to methanol is seen to continuously decrease with increasing temperature. This effect probably has two causes. Methanol reacts to form higher alcohols through secondary reactions, so that as the absolute concentration of methanol increases, more of it reacts to form ethanol, decreasing its selectivity. The second effect is probably thermodynamic in origin, since methanol formation is less favored at higher temperatures. Similar behavior in selectivity is observed for ethanol. A maximum in selectivity is observed near 375°C. This maximum is probably caused by secondary reactions, producing higher alcohols or hydrocarbons. Selectivity to n-propanol and n-butanol grow to significant values as the selectivity to ethanol reached its maximum.

The lower section of Figure 5 shows how the selectivities to methanol, higher alcohols and hydrocarbons change with temperature on a weight basis. At the maximum in higher

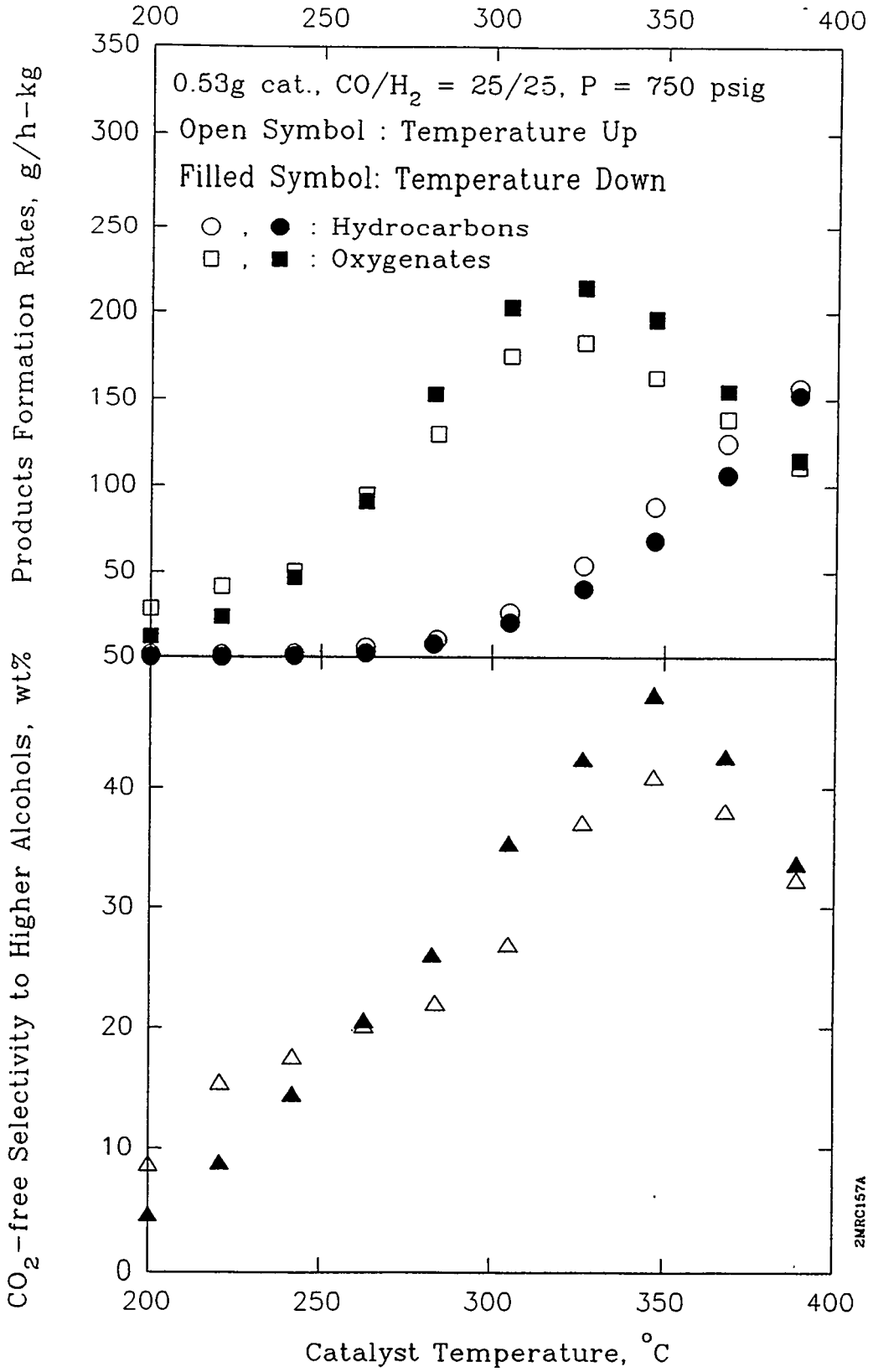

Figure 4: Product formation rates and alcohol selectivity for $K_{0.7}$ MoS_2 VPR catalyst tested at 750 psig and 6,000 l/kg/hr space velocity.

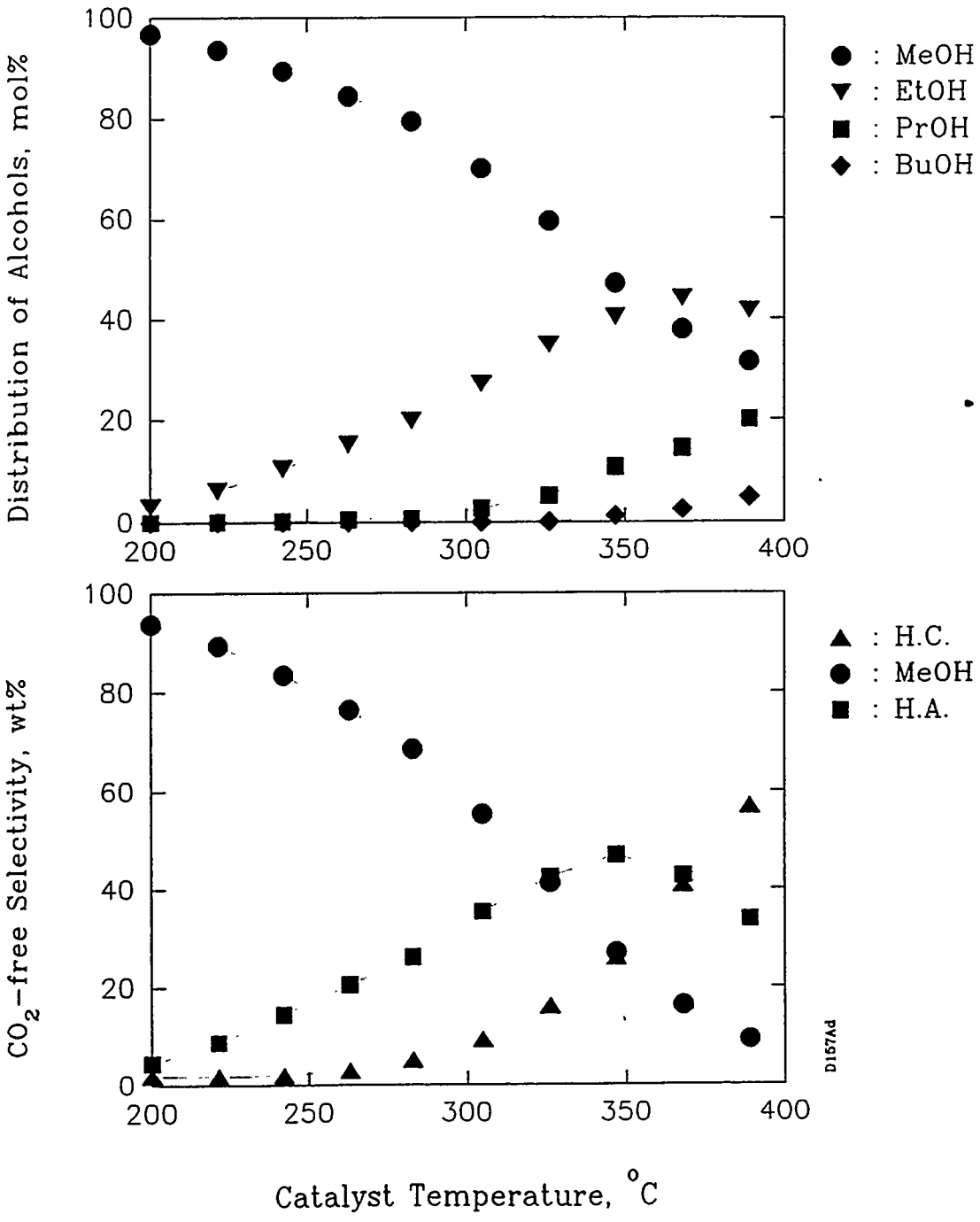

Figure 5: Alcohol selectivity of $K_{0.7}$ MoS_2 VPR catalyst at same conditions as Fig. 4.

alcohol selectivity, product concentrations are nearly 50% higher alcohols, 25% methanol and 25% hydrocarbons.

Similar performance is noted with vapor phase synthesis catalysts promoted with cesium or rubidium. A series of catalysts was prepared with similar concentrations of alkali on a molar basis: $K_{0.7}MoS_2$, $Cs_{0.7}MoS_2$ and $Rb_{0.7}Mos_2$. The performance the potassium promoted sample was presented in Figures 4 and 5. The catalysts promoted with rubidium and cesium also had space-time yields of approximately 200 g/kg/hr and similar selectivities. The promoter level for potassium is believed to be near optimum. Optimum values are not known for the other two alkali promoters.

Data supporting hydrocarbon and alcohol formation by secondary reactions is presented in Figure 6. A molybdenum-cobalt-potassium on carbon catalyst with molar ratios of 1-0.3-1 was run isothermally at 350°C and 750 psig. During the initial 16 hr period, the space velocity was constant at 6,000 l/kg/hr. The rate of alcohol conversion was nearly constant at 160 g/kg/hr while the rate of hydrocarbon formation decreased initially, then leveled out below 40 g/kg/hr. The space velocity was then increased to 12,000 l/kg/hr. Increasing the flow rate increased the rate of alcohol formation but decreased the selectivity to hydrocarbons and higher alcohols. Increasing the space velocity decreases the residence time and decreases secondary reaction products. The same effect is observed when the space velocity is increased to 18,000 and 21,600 l/kg/hr, further supporting the hypothesis that higher alcohol formation involves secondary reactions of methanol product.

3.4 Process Synthesis Computer Modeling

The goal of Task 2 is to simulate, by computer, energy efficient and economically efficient processes for converting coal to energy (fuel alcohols and/or power). The first step for Task 2 was to develop computer simulations of alternative coal to syngas to linear higher alcohol processes, to evaluate and compare the economics and energy efficiency of these alternative processes, and to make a preliminary determination as to the most attractive process configuration. Seven cases were developed using different gasifier technologies, different methods for altering the H_2/CO ratio of the syngas to the desired 1.1/1, and with the higher alcohols as the primary product and as a by-product of a power generation facility. Texaco, Shell, and Lurgi gasifiers were used as to gasify coal, and steam reforming of natural gas, sour gas shift conversion, or pressure swing adsorption was used to alter the H_2/CO ratio of the syngas. In addition, a case using only natural gas was prepared in order to facilitate comparison between coal and natural gas as a source of syngas.

There are significant differences between the production costs for processes converting coal to syngas to higher alcohol fuel additives for cases involving Texaco, Lurgi, and Shell gasifiers, between cases involving natural gas reforming or sour gas shift conversion to alter the H_2/CO ratio, and for different plant capacities. The best case is one of the hybrids, a Shell gasifier with natural gas.

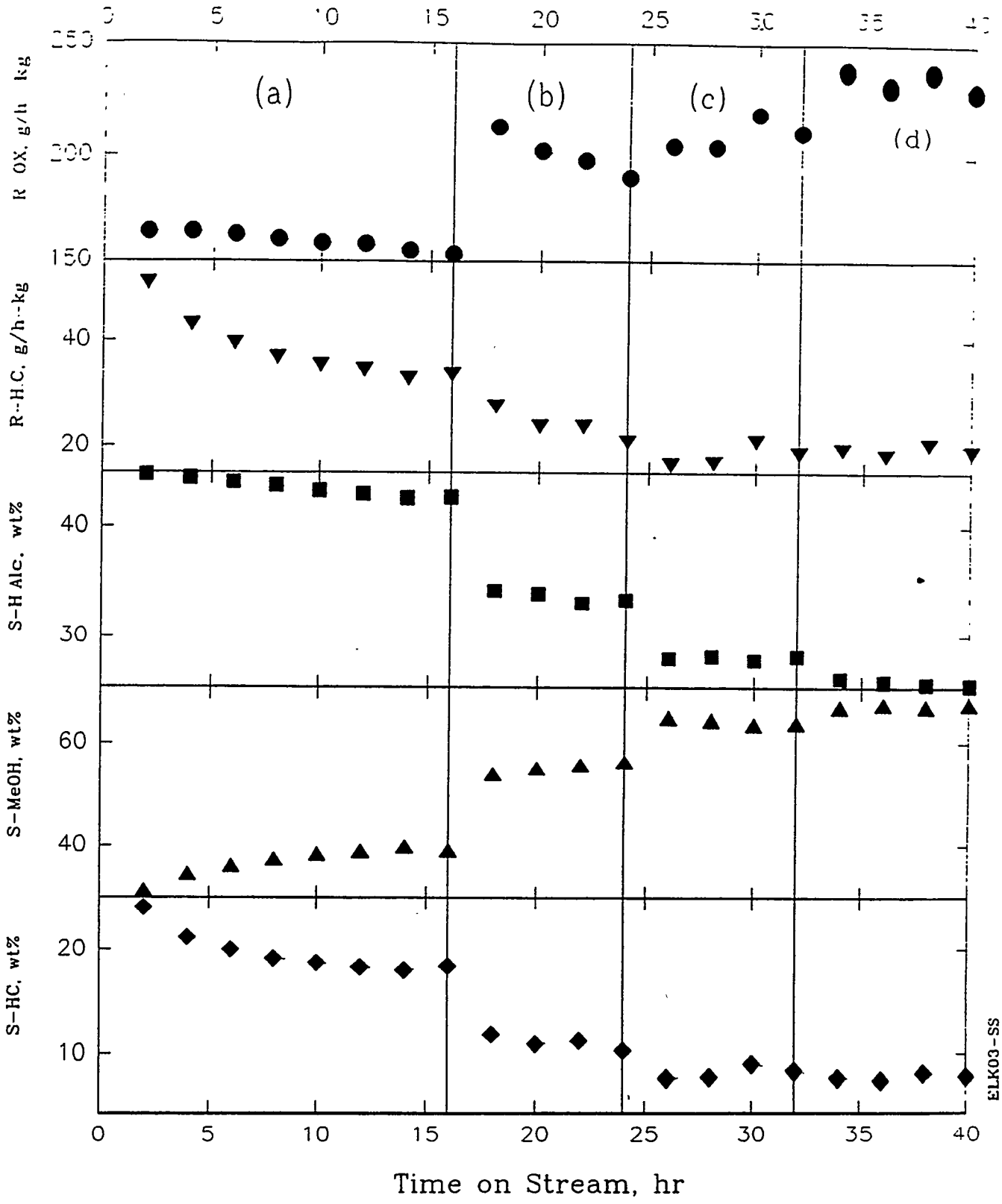

Figure 6: Performance of carbon supported Mo-Co-K catalyst at increasing space velocities: (a) 6,000; (b) 12,000; (c) 18,000; (d) 21,600 l/kg/hr. Catalyst tested at 350°C and 750 psig.

Production of 5.1 billion liters/yr (32 MM bbl/yr) of alcohol fuels from coal is considered the maximum feasible process scale. As expected, there are economies of scale favoring larger-scale over smaller-scale processes. However, there appear to be diminishing economies of scale above this plant size.

Production of higher alcohol fuel additives from natural gas is more economical than production from coal at any scale at current or predicted natural gas prices. Production of higher alcohol fuel additives from coal and natural gas hybrids may be as economical as production from natural gas at West Virginia natural gas prices ($3.00/MM BTU). However, if the natural gas and hybrid cases were compared at scales consistent with the same net power produced, the manufacturing cost for the natural gas case would be significantly lower than that for the hybrid cases. Furthermore, if a plant life of 10 years were used, which is more typical in the chemical process industry, then all of the manufacturing costs for the cases using coal gasification would increase, making natural gas the clearly superior option.

Since capital and operating costs are estimated on the basis of conventional technology, equipment, processes, and environmental controls, it is possible that future emission control requirements could significantly increase capital and operating costs of all coal-based processes described.

The manufacturing cost of the alcohol derived from natural gas is a strong function of the natural gas price. The capital costs are lower for these cases than they are for the coal-based cases. Thus, raw material costs for the natural gas cases are a larger portion of the total annualized cost.

The cost of producing syngas from coal or from coal and natural gas is currently greater than or equal to producing it from natural gas only. This is primarily a result of the high capital investment for the gasifier and accompanying cryogenic oxygen plant. This higher investment outweighs the benefit of using a cheaper raw material, coal. The only way for coal based processes to be more competitive than natural gas under all conditions is either for the relative price of coal and natural gas to change or for a major development to occur in coal gasification technology. Price variations would have greater impact on the natural gas reference cases, since raw material costs for these cases are a larger portion of the total annualized cost. Therefore, the competitiveness of the coal-based cases would be enhanced more by increases in the price of natural gas than by decreases in coal cost.

III PLANS

Molybdenum sulfide catalysts have been found to meet our criteria for more detailed study. Kinetic studies in a continuous, stirred-tank reactor are planned to measure rate constants and predict the best operating conditions for this type of catalyst. One catalyst testing unit will be used for this work.

Molybdenum carbides and nitrides have been found to be very active catalysts but make a complicated product mixture that has been very hard to identify. Most of these products are believed to be oxygenates. We have ordered a gc/ms to measure the mass spectra of the compounds that are separated in the gas chromatograph. This will be installed on-line with our carbide and nitride catalyst testing unit, so that small concentrations of product can be analyzed. The main feature of this instrument will be chemical ionization capability. This will produce molecular ions that should allow identification of product compound classes. Traditional electron impact ionization in a mass-spectrometer at 70 eV causes such extreme fragmentation that unknown molecules are very hard to identify. Catalyst screening of carbides and nitrides will continue with the goal of identifying promising catalysts for alcohol synthesis.

IV REFERENCES

1. E. L. Kugler, D. B. Dadyburjor, R. Y. K. Yang, J. L. Petersen, M. R. Close, Z. Y. Liu, X. Li, A. Subramanian and K. Hammerbeck, Proceedings of the Coal Liquefaction and Gas Conversion Contractors' Review Conference, Pittsburgh, PA, 281-292, 1994

2. C. B. Murchison, M. M. Conway, R. R. Stevens and G. J. Quarderer, Proceedings of the 9th International Congress on Catalysis, Calgary, Alberta, 626-633, 1988

3. S. J. Tauster, T. A. Pecoraro and R. R. Chianelli, J. Catalysis **63**, 515 (1980)

1995 COAL LIQUEFACTION AND GAS CONVERSION CONTRACTORS' REVIEW CONFERENCE

Title: **Slurry Phase Synthesis of Oxygenates with Nanometer Particle Catalysts**

Authors: **D. Mahajan, J. Wegrzyn and A. Goland**

Organization: **Brookhaven National Laboratory**
P. O. Box 5000
Upton, New York 11973-5000

Contract Number: **DE-AC02-76CH00016**

Period of Performance: **July 1, 1994 - June 1995**

Objective: The purpose of this initiative is to ultimately develop an economically viable route to isobutanol by catalytic conversion of synthesis gas derived from coal or natural gas.

Introduction

Methyl t-butyl ether (MTBE), an oxygenated fuel-additive, is manufactured according to Reaction 1:

$$H_3C\text{-}OH + H_3C\text{-}\underset{\displaystyle CH_3}{\overset{\displaystyle |}{C}}\text{=}CH_2 \rightarrow (H_3C)_3C\text{-}O\text{-}CH_3 \qquad (1)$$

Due to increasing demand, MTBE at 10.9 x 10^9 Kg and methanol at 4.8 x 10^9 Kg ranked #9 and #21 in top 50 chemicals produced in the United States in 1993. A shortage of methanol will be met by six natural gas-based plants planned to be built in the next few years. But supply of isobutylene, normally recovered from refineries as a by-product, could become a problem if non-refinery sources are not found or developed. Catalytic transformation of coal or natural gas to isobutanol (dehydration of this molecule produces isobutylene) is a viable option. This approach involves two steps: 1) conversion of coal via gasification and natural gas via steam reforming or partial oxidation (POX) to synthesis gas, 2) catalytic transformation of generated syngas to desired products. The latter step is essentially hydrogenation of carbon monoxide (CO) and both oxygenates as well as hydrocarbons are potential products:

$$CO \xrightarrow[Catalyst]{H_2} Oxygenates \xrightarrow{(H_2?)} Hydrocarbons \qquad (2)$$

Thermodynamically, hydrocarbon synthesis being more exothermic is favored but catalytical processes exist to intercept less exothermic oxygenates. Due to higher temperature operation in direct synthesis of higher oxygenates, any improved product selectivity is invariably attained at the expense of hydrocarbon formation. The subject of CO hydrogenation is recently reviewed (1).

For synthesis of higher alcohols, the following reaction stoichiometries are of interest:

$$n\ CO + 2n\ H_2 \rightarrow C_nH_{2n+1}OH + (n-1)\ H_2O \quad (3)$$

$$(2n-1)\ CO + (n+1)\ H_2 \rightarrow C_nH_{2n+1}OH + (n-1)\ CO_2 \quad (4)$$

Except for C_1(MeOH), all alcohols yield H_2O and/or CO_2 as byproducts. Synthesis of higher alcohols, directly from synthesis gas, is favored at higher temperatures but at the expense of selectivity. Approaches used in some of the DOE Indirect Liquefaction programs are covered(2). These and other known catalytic systems include Pd-Li/CeO_2 (3), Rh-Ti/SiO_2 (4), supported NiO (5), MoS_2-based (2), modified Cu (2), Fe-Cu Ruhrchemie catalysts (6), modified CO-Cu IFP (7), and variations thereof (1,2). Specifically, production of isobutylene directly from syngas and isobutanol dehydration to isobutylene have been evaluated (8). Higher alcohol synthesis is typically carried out by either modified Fischer-Trospch (F-T) synthesis or modified methanol synthesis catalysts. The most likely operating mechanisms are as follows:

- Linear alcohols are produced via classical CO insertion mechanisms to form carbon-carbon bond dictated by Anderson-Schulz-Flory (ASF) distribution followed by hydrogenation.

- Isoalcohols are produced via aldol condensation.

Irrespective of the catalyst employed, a highly selective synthesis of isobutanol still remains elusive. Our attempt to design a new catalyst system is based on the following strategy:

1. A successful development of LPMeOH process for synthesis of methanol from synthesis gas (9) demonstrates that slurry phase operation provides an excellent heat management option. A parallel can be drawn with liquid phase homogeneous catalysis where a uniform isothermal operation is routinely achieved.

2. To enhance catalyst lifetime and productivity, dispersed catalysts have been evaluated for direct coal liquefaction(8). A few reports have also appeared in the use of ultrafine particle (UFP) catalysts for F-T synthesis (10). Our work (11) with a slurried Fe UFP catalyst suggested the following:

- A commercial Fe UFP catalyst (α-Fe_2O_3 with mean particle diameter (MPD) = 3 nm, and surface area (SA) = 255 $m^2.g^{-1}$) obtained from Mach-1 Inc., was active at 220°C for F-T synthesis. But the reactor was devoid of CO_2 suggesting no water-gas-shift (WGS) activity.

- On volumetric basis, space-time-yield (STY) was higher with Mach-1 compared to that with standard UCI catalyst (MPD = 32.5 μm and SA = 232 $m^2.g^{-1}$).

- EXAFS and Mössbauer characterization of a quenched catalyst sample during the F-T run with Mach-1 at 200°C showed no carbide phase. The phase was found to be 100% magnetite (Fe_3O_4).

- Though oxygenates accounted for only up to 13 wt% of the aqueous phase, linear alcohols (C_1 - C_4) accounted for > 90% of the oxygenated fraction.

3. The F-T reaction can be effected at a lower temperature with Co based catalyst (8). But due to its price, Fe remains the metal of choice. For higher alcohols synthesis, Fe has been evaluated. Razzaghi et al studied Fe/SiO_2 with promoters and obtained selectivity up to 22% to higher linear alcohols (12). This yield was too low to be of commercial interest. In another study with an iron catalyst, alcohols yield of 45% (primary aliphatic alcohols) at ~200°C is claimed. The hydrocarbons formed in this reaction were primarily olefins (13). Mechanistic studies on Co-Cu or MoS_2 indicate that higher alcohols are formed through the reaction of a C_n hydrocarbon entity with a C_1 oxygenated species (1). In another study synthesis of methanol and higher alcohols by Rh indicated that this system is selective for C_2 oxygenates. Arakawa et al have shown a relationship between turnover (TO) frequency of CO conversion and Rh dispersion with Rh/SiO_2 (14).

The aforementioned discussion relevant to slurry phase operation, particle size dependence, C-C bond formation led us to tailor a UFP system capable of enhanced oxygenates synthesis. Our approach to isobutanol synthesis involves the following:

- Initially, Fe UFP (MPD <100 nm) catalyst precursor is to be utilized. Co UFP will follow.
- Slurry phase operation is preferred for heat management and to enhance catalyst/solvent interaction.
- A typical high molecular weight hydrocarbon solvent mixed with a high boiling oxygenated solvent is used as a reaction medium. Ultimately, hydrocarbon solvent will be eliminated. Solvent is to act as an agglomeration inhibitor.
- Slurry-phase operation limits operating temperature to T<280°C. The upper temperature limit drops even further with oxygenated solvent.
- To take advantage of the CO_2 oxidizing atmosphere, runs are to be conducted in the absence of water-gas-shift (WGS) activity. The presence of CO_2 is to be utilized to control Fe oxidation state.
- Base addition is designed to 1) promote C-C coupling to enhance C_4 yield, 2) acts as an agglomeration inhibitor.

- Cocatalysts may be added to promote isomerization and dehydration to produce isobutylene from synthesis gas in one-step.

For this work, the following systems will serve as a guide. It is to be noted that these systems operate in packed-bed reactors.

1. The most studied system is an alkali metal-modified traditional methanol synthesis catalyst. A variation of this catalyst is being evaluated by APCI (8). At P<12Ma, t<310°C with syngas (H_2/CO = 1/4-4/1), maximum rate is 37 and 7 g/Kg.h for iBuOH and t-BuOH respectively. It is suggested that favorable conditions for isobutanol synthesis are 1) low H_2/CO ratio, 2) low CO_2, 3) high T.

2. A multimetal Pd-based catalyst developed in Keim's laboratory at the Technical University of Aachen claims 59 wt% isobutanol selectivity and productivity of 1500 g/Kg h at <450°C and P~10 MPa.

Initially, our emphasis is on maximizing C_1 - C_4 alcohols with an iron catalyst.

Experimental

Two commercially available nanometer size unsupported Fe_2O_3 catalyst precursors were obtained as samples in 1 lb each quantity from the vendors: 1) Mach-1 (MPD=3nm; SA=255 $m^2.g^{-1}$; and 2) BASF (MPD = 20 - 80 nm; SA = 16-20 $m^2.g^{-1}$; density (d) = 0.05 $g.mL^{-1}$; d = 5.25 $g.mL^{-1}$) from BASF. Since Co-based nanometer size catalyst precursors are not readily available, these materials will be generated at BNL via sonolysis of cobalt complexes. The sonication technique will be described in a future publication. Ethylflo-164, a C_{30} hydrocarbon solvent, was obtained from Ethyl Corporation. All chemicals were purchased from Aldrich and premixed syngas of varied composition was purchased from Scott Specialty Gases. All gaseous and liquid reactants and products were analyzed on a PE8500 gas chromatograph in FID and TCD modes. A full mass balance was carried-out on each run. The Fe_2O_3 samples were stored in a glove box to avoid water contamination prior to reduction.

For catalyst screening, a 0.5L AE Zipperclave batch CSTR was modified (Figure 1). The unit is rated at 13 MPa @230°C. For catalyst evaluation, the BNL bench-scale continuous unit fitted with a 1L AE CSTR was modified for oxygenates synthesis (Figure 2). The unit is rated at 40 MPa @340°C.

Results and Discussion

The utilization of both Mach-1 and BASF catalysts in F-T synthesis has been described previously (8, 15). Of interest is the aqueous phase composition of these runs to determine concentration of oxygenates. The total C_1-C_4 values were 5.8, 8.4, 6.0, 13.4, 1.9 wt% respectively for Runs 1-5 as shown in Table 1. These values accounted for >90 wt% of all oxygenates in the aqueous phase. Though the absolute C_1-C_4 values are even smaller with

maximum alcohols produced at 4 wt% with MACH-1, the value was even smaller (0.6 wt%) with BASF. Since our measurements show that MACH-1 is predominately in the Fe_3O_4 phase and preliminary EXAFS and Mössbauer data show quenched BASF catalyst in several mixed phases, our approach to modify Fe oxidation state to maximize alcohols production becomes relevant. To further this concept, catalyst screening was carried-out in the batch reactor. Four runs were completed to establish boundary conditions.

Run OXY #0-Blank: A 10% triglyme/90% Ethylflo-164 solvent mixture (125 mL) was loaded. The reactor was heated under syngas (66% H_2/34% CO) for 2 hours. The reactor was cooled and 124 mL liquid was collected. Mass balance error was set at $<\mp 1\%$.

Run OXY #1: The desired reaction is intended to be carried-out at a lower temperature. The formation of $Fe(CO)_5$ and thus loss of Fe at lower temperatures (<200°C) is of concern. To address this issue, 5 mmol $KHCO_3$ base and 125 mL 90% Ethylflo-164/10% Triglyme solvent mixture were loaded into the batch reactor. After adding 10 mmol $Fe(CO)_5$ (Fe/base = 2/1), the reactor was pressurized with 300 psig syngas (H_2/CO = 66%/34%). In one hour at 170°C and 341 psig, gas analysis showed 5.7 vol % CO_2 (15 mmol). The expected CO_2 from $KHCO_3$ decomposition was 5 mmol. An extra 10 mmol CO_2 needs to be accounted for. The final black slurry (0.7 wt% Fe + base) suggested $Fe(CO)_5$ decomposition at 170°C. Syngas consumed was small at <10 mmol. No further analysis was carried-out. (Table 2).

Run OXY #2: In this run, $Fe(CO)_5$ was replaced with 1g Fe BASF (α-Fe_2O_3) catalyst precursor and slurried with base in the solvent mixture as described in Run OXY #1 (Fe/base ~ 1.2). Under 329 psig syngas at 170°C, CO_2 increased to 1.5 vol % in 0.7 hour and the final value in 1.6 hours was 1.7 vol % (4.3 mmol). The measured CO_2 suggested complete $KHCO_3$ decomposition (theoretically maximum CO_2 = 5 mmol). Only ~ 10 mmol syngas was consumed. The initial orange fine powder (α-Fe_2O_3) became slightly darker suggesting incomplete reduction of α-Fe_2O_3 at 170°C (Table 3).

Run OXY#3: A negligible amount of syngas (66% H_2/34% CO) was consumed when 1.0 g α-Fe_2O_3 BASF catalyst and 10 mmol KOMe were slurried in 90% Ethylflo-164/10% Triglyme solvent and heated at 170°C for 1.7 h. Only ~1 mmol CO_2 was measured and the final slurry was dark red suggesting incomplete reduction of the BASF catalyst even with a strong base (Table 4).

The data from Runs OXY#2 and #3 show that base reduction of α-Fe_2O_3 at 170°C is not appropriate to yield reduced Fe catalyst. But this method works well when starting with $Fe(CO)_5$ to generate $Fe^{(0)}$.

Run OXY#4. The strategy is to modify Fe catalyst in a CO_2 -rich atmosphere to enhance yield of C_1-C_4 alcohols. To establish a baseline, this run was done in the continuous unit. The run procedure was as follows:

- Reduced catalyst for 24 hours at 280°C under CO.
- Set T = 240°C.

- Added balanced syngas to establish baseline hydrocarbons synthesis.
- Replaced syngas with CO_2-rich syngas.

The BASF catalyst precursor was reduced by slurrying 5 wt% catalyst material in Ethyleflo-164 and heating under 100 psig CO (0.2L/min) to 280°C. The temperature was held at 280°C for 24 hours. At this time, with pressure at 100 psig, the temperature was decreased to 220°C, flow rate was adjusted to 0.7 L/min and syngas (H_2/CO = 66%/34%) was introduced. No conversion was observed in the first 1.5 h. On raising the temperature to 240°C, gas conversion was 8% (at 0.5 L/min flow rate) for 17 h. At 19 h total time, balanced syngas was replaced with CO_2-rich syngas (64%H_2/25%CO)/11%CO_2). Gas conversion initially increased to 16% but then quickly decreased to <5%. The data in Table 5 indicates: 1) The observed 8% conversion at 240°C was far below the previously collected reference F-T data. In the reference run, BASF catalyst (~5 wt%) was reduced under CO at 280°C and its F-T activity was evaluated at 240°C, 100 psig, 0.88 L./min (4.6 $NL.gFe^{-1}.h^{-1}$). Gas conversion peaked at 44% in 24 hours and then slowly decreased to 38% at 144 h. For comparison, the reference F-T run yielded 44% conversion at 19 h whereas gas conversion was 8% in the present run, 2) At 8% conversion, addition of CO_2-rich syngas caused conversion to surge to 16% but value quickly decreased to <5% after 4 h, 3) The aqueous phase contained 7 vol % C_1-C_4 n-alcohols. These alcohols constitute >90% of all oxygenates produced, 4) Considering that the desired condition likely to enhance oxygenates with CO_2-rich gas is the absence of water-gas-shift (WGS) activity, this condition was not attained in Run OXY#4.

The above observations still failed to explain irreproducibility of gas conversion values. An examination of catalyst reduction procedure revealed that in Run OXY #4, the reactor was pressurized with CO during warm-up (to 280°C) whereas in the reference run (high conversion), N_2 was utilized during reactor warm-up. Instead of further investigating this effect, the original procedure was adopted during subsequent runs. No elaborate higher hydrocarbon analysis was conducted on liquids from Run #4.

Run OXY#5. In this run, BASF catalyst was reduced according to the procedure described for OXY#4 except that during reactor warm up, N_2 was used. At 280°C, N_2 was replaced with CO. The CO_2 value dropped from 10.5 vol % at 0.7 h to 1.2 vol % in 20 h at which time the catalyst was assumed to be >90% reduced.

Since the ultimate goal is to drive the reaction at the lowest possible temperature, the data were collected at 240, 220, 200°C. Initially, the temperature was reduced to 240°C, CO was replaced with balanced syngas (H_2/CO = 66%/34%) and flow rate was adjusted to 0.6 L/min to establish a baseline. At 1 h, gas conversion was 4% that steadily increased to 14% in 4 h at which time flow was decreased to 0.4 L/min. Gas conversion increased to 45% in 29 h. At 29.2 h, CO_2-rich gas was introduced. The conversion was 40% at 47 h (a steady-decrease in 18 h) and CO_2 in the exit gas increased from 12% at 29 h (with 66% H_2/34% CO syngas) to 22.2% at 47 h (with 64% H_2/25% CO/11% CO_2). The temperature was further reduced to 220°C at 48 h. Gas conversion remained stable at ~28% (28-30.5%) in the 26 h run time at 220°C. The only parameter varied during this period was stirring speed (500 rpm

between 52 to 70 h). At 70 h, the reactor was pressurized to 510 psig and operated in batch mode. The pressure decreased from 510 to 318 psig in 0.6 h. The reactor was left in batch mode for 73 h with pressure dropping to 185 psig. On repressurization to 510 psig, the pressure dropped to 325 psig in 18.5 h. The temperature was further decreased to 200°C and in continuous-mode operation at 100 psig, 8% conversion was recorded at 170 h (including 91.5 h batch-mode operation). The reactor was cooled to room temperature after 170 h. The data are shown in Table 6.

The data in Table 6 indicate that CO conversion was 40%, ~30%, and 8% respectively at 240, 220, and 200°C with the BASF catalyst. At these temperatures, CH_4 values were: 2.6%, 0.6%, 0.03%. CO_2 was 12% (240°C at 29 h) with 0%CO_2 incoming syngas), 22.2% (240°C at 47 h) with 11% CO_2 containing syngas (assuming 11.2% was a contribution from WGS reaction), 13.7% (220°C at 70 h) with only 2.7% from WGS activity). Since the last value of 21.2% at 170 h was taken after only 3.5 h at 200°C after the run was in batch-mode from 91.5 h this value may be high. The net 2.7% CO_2 value at 70 h shows some WGS activity at 220°C and the true intended conditions were not attained.

The collected hydrocarbons and aqueous phases were 23 mL and 72 mL respectively. Since the aim of this project is to enhance oxygenates production, the aqueous phase was analyzed to yield the following: MeOH (0.5 mL), EtOH (3.4 mL), PrOH (0.9 mL) and BuOH (0.3 mL) with C_1-C_4 alcohols at 5.9 vol % accounting for >90% of all oxygenates produced. The overall selectivity to alcohols was 18 vol % corresponding to the alcohols/hydrocarbon ratio of about 1/6. This value is higher than that reported earlier from our laboratory with balanced syngas. Considering that the ultimate catalyst system is yet to be formulated, our approach to synthesize alcohols with Fe-based catalyst appears promising.

Accomplishments and Conclusions

From the runs completed so far the following conclusions are noteworthy:

- Since thermodynamic equilibrium conditions are normally not attained during planned runs, a 0.5L AE batch CSTR (T < 230°C; P < 13 MPa) was selected for catalyst screening. This has now been replaced with a 0.3L Parr batch CSTR (T<350°C P < 13 MPa). This method is quick, inexpensive and very efficient. The selected catalyst can be then fully evaluated in the continuous unit.

- Two commercially available nanometer scale catalysts were selected (Mach-1 and BASF). All Co-based catalysts will be generated via sonolysis.

- To set boundary limits several batch runs were conducted:

    - The formation of $Fe(CO)_5$ and thus loss of Fe is of concern at intended lower temperatures of operation. The data from Run OXY#1 suggest that $Fe(CO)_5$ fully decomposed even under syngas (66% H_2 /34% CO) at 170°C to form a dispersed black slurry.

- A slurried BASF α-Fe_2O_3 did not fully reduce with $KHCO_3$ at 170 °C. Even with a stronger base KOMe, the reduction was incomplete. A slow syngas consumption was noted in both cases.

- A baseline run (Run OXY#4) conducted with reduced BASF catalyst in continuous mode showed somewhat enhanced gas consumption with CO_2-rich syngas. The problem with attaining baseline catalytic activity (gas conversion: 44% for reference versus 8% attained in this run) made added CO_2 effect unclear (Run OXY#4).

- The data from Run OXY#5 indicate that the catalyst reduction procedure is critical to achieving baseline activity. The adopted procedure involves slurrying BASF material in Ethylfo-164 solvent, heating to 280°C for 24 h before starting the actual run. Just by substituting CO with N_2 during warm-up, conversion dropped from 45% to 8% at 240°C (Runs OXY #4 and #5).

- With syngas containing 11%CO_2, conversion was 40% in 18 h at 240°C. A 5% drop (from 45 to 40%) during this period was not conclusively attributed to added CO_2.

- The measured CO_2 was 13.7% at 220°C. Considering syngas at the inlet contained 11% CO_2, a net 2.7 % is attributed to WGS reaction. Obviously, a desired condition of no WGS activity was close but not met.

- The oxygenates constituted 5.9 vol % of the aqueous phase. The selectivity to C_1-C_4 alcohols was 18 vol %. This is promising considering that all the intended modifications to the Fe catalyst system have not been implemented.

Future Direction

The selected approach utilizes 1) nanometer particles of Fe or Co in a slurry-phase, 2) CO_2-rich syngas, 3) added compatible base to enhance yield of oxygenates and effect the reaction at a lower temperature of T < 240°C.

The selected Fe catalyst is unusual in that it is unsupported. Considering that Fe_3O_4 is anticipated to be the predominant phase, the addition of an oxygenated solvent becomes important to avoid agglomeration. If this system is successful, these and other features of the working system may find application in Fischer-Tropsch catalysis. As for enhancing alcohols yield, several baseline runs are now underway to establish the fate of added C_1-C_4 alcohols under reaction conditions to eliminate the possibility of secondary reactions. The target is to first match and then exceed the reported 45 wt% C_1-C_4 alcohols yield with a base modified Fe catalyst. This will be the subject of a forthcoming publication. These planned runs are intended to achieve our goal of enhancing C_1-C_4 alcohols yield with an Fe catalyst. This will be followed by enhancement of C-C bond formation to increase yield of C_4 alcohols.

References

1. Hindermann, J.P., Hutchings, G.J. and Kiennemann, A. *Catal. Rev.-Sci. Eng.* 35(1), 1-127 (1993)

2. *Proceedings of the PETC Contractors' Review Conference*, Vol. II. Pittsburgh, PA, September 27-29, 1993.

3. Diagne, C., Idriss, H., Hindermann, J.P. and Kiennemann, A. *Appl. Catal.* 51, 165 (1989) and references therein.

4. Ichikawa, M. And Fukushima, T. *J. Chem. Soc. Chem. Commun.* 321 (1985).

5. Uchiyama, S., Obayashi, Y., Shibata, M., Uchiyama, T., Kawata, N., and Konishi, T. *J. Chem. Soc. Chem. Commun.* 1071 (1985).

6. *German Patent 1, 103, 315 (1961)* assigned to Ruhrechmie.

7. Sugier, A. And Freund E. *U.S. Patent* 4,291,126 (1978).

8. *Proceedings of the PETC Contaractors' Review Conference*, Pittsburgh, PA, September 7-8, 1994.

9. LaPorte Liquid-Phase Methanol Process Development Unit: Continued Operation in Liquid-Entrained Catalyst Mode. *EPRI Report AP-5050*, Februray 1987.

10. Itoh, H., Tanabe, H. and Kikuchi, E. *Appl. Catal.* 47 L1(1989) and references therein.

11. Mahajan, D., Kobayashi, A. and Gupta, N. *J. Chem. Soc. Chem. Commun.*, 795-6 (1994).

12. Razzaghi, A., Hindermann, J.P. and Kiennemann, A. *Appl. Catal.* 13, 193 (1984).

13. Through reference: Energy Alcohols. C.B. von der Decken. *Kernforschungsanlage Jülich GmbH.* November 1987.

14. Arakawa, H., Takeuchi, K., Matsuzaki, T., and Sugi, Y. *Chem. Lett.* 1607-10(1984).

15. Mahajan, D. And Pandya, K. Symposium on Alternate Routes for the Production of Fuels. Division of Fuel Chemistry. *208th ACS National Meeting*, Washington, D.C. August 21-24, 1994.

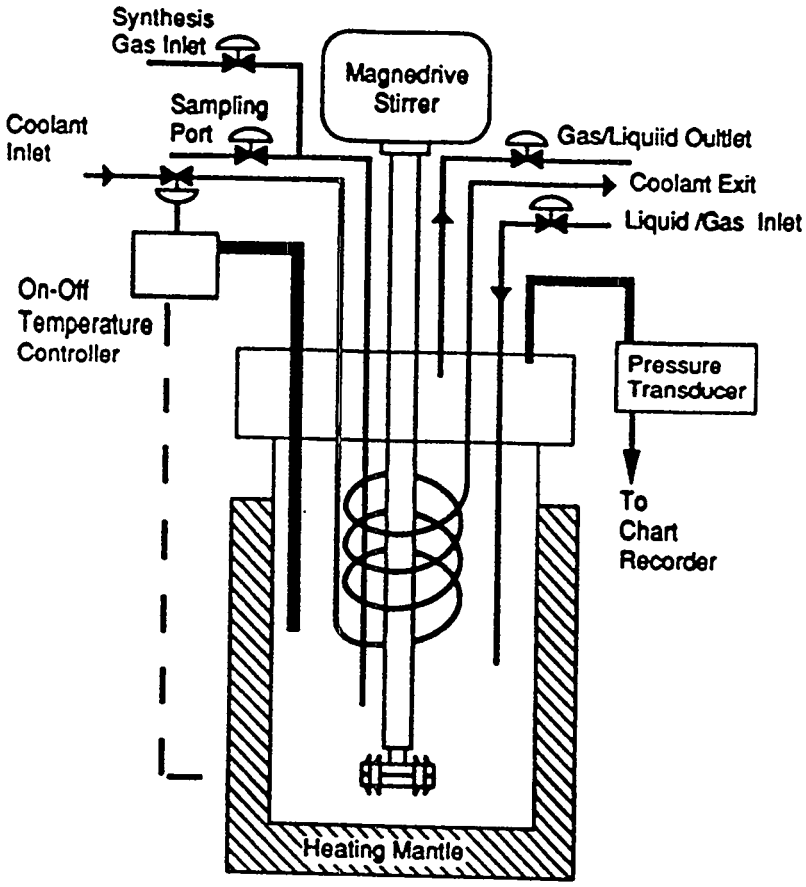

Figure 1. AE Zipperclave Reactor used in Batch Studies

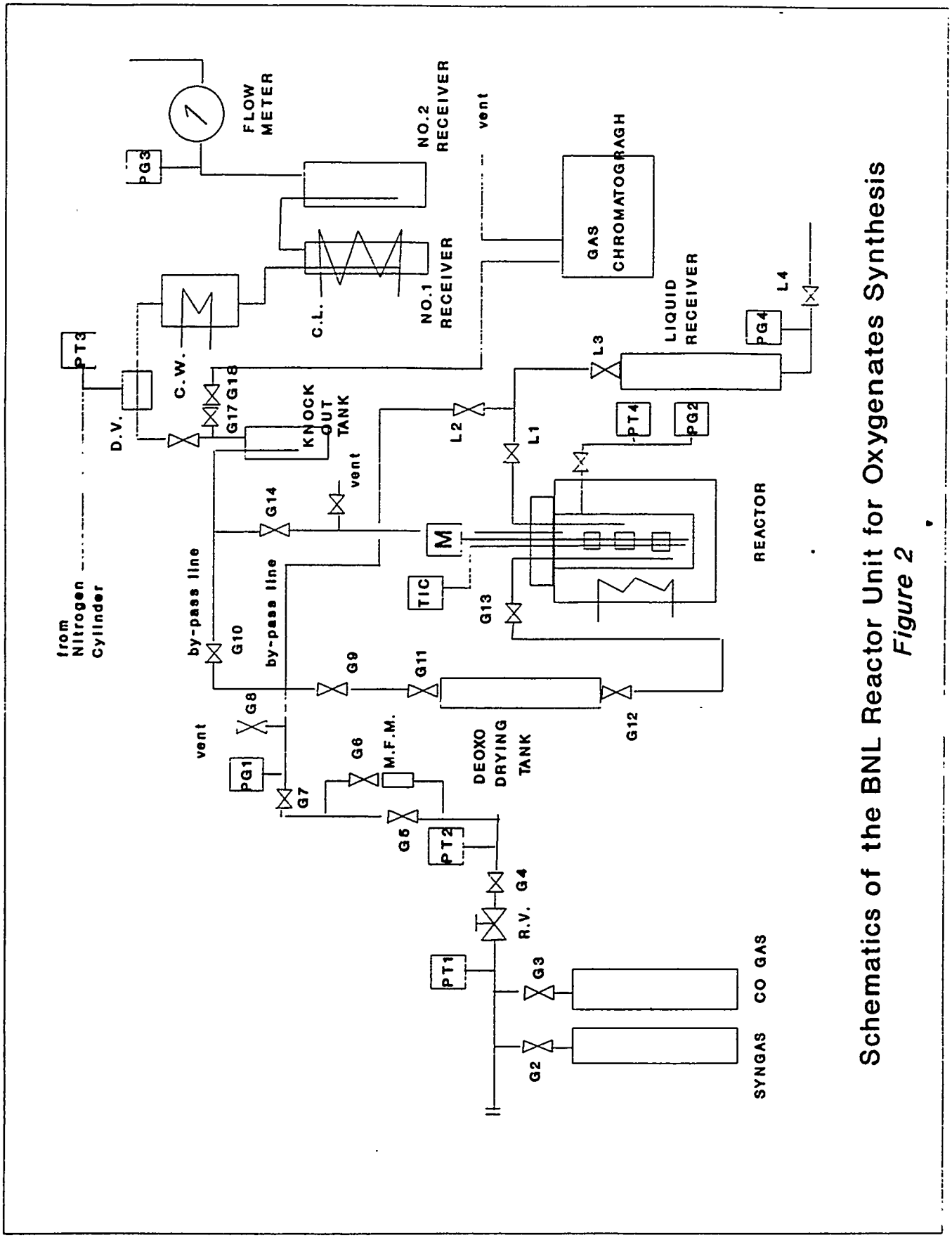

Schematics of the BNL Reactor Unit for Oxygenates Synthesis

Figure 2

Table 1
Alcohols Composition in Aqueous Phase[a]

Run	Catalyst	T,°C	% Aqueous Phase	ROH, wt% C_1	C_2	C_3	C_4
1	Mach-1	220	56	0.9	2.0	2.3	0.6
2	Mach-1	240	47	1.9	3.8	1.9	0.8
3	Mach-1	260	36	1.1	2.4	2.0	0.5
4[b]	Mach-1	220/260	32	3.2	4.8	3.8	1.6
5	BASF	240	29	0.3	1.1	0.3	0.2

[a] Data from reference F-T runs.
[b] Syngas: H_2/CO = 1/1, in this run. In all other runs, 2/1 gas was used.

Table 2
Run OXY #1 in Batch Mode

Run Conditions

Catalyst precursor: $Fe(CO)_5$ = 10 mmol
Solvent: 90% Ethylflo-164/10% Triglyme = 125 mL
Base: $KHCO_3$ = 5 mmol
Syngas: 66% H_2/34% CO
T: 170°C
P: 341 psig @ T
On-line time: 1.0 h

Data

Initial Solution = yellow homogeneous
Final Solution = Black slurry
CO_2 = 15 mmol
Syngas Consumed = 10 mmol

Table 3
Run OXY #2 in Batch Mode

Run Conditions

Catalyst precusor: BASF (α-Fe_2O_3) = 1.0 g
Solvent: 90% Ethylflo-164/10% Triglyme = 125 mL
Base: $KHCO_3$ = 5 mmol
Syngas: 66% H_2/34% CO
T: 170°C
P: 341 psig @ T
On-line time: 1.6 h

Data

Slurry: Initial = Reddish
Final = Dark red
CO_2 = 5 mmol
Syngas consumed ≈ 10 mmol

Table 4
Run OXY #3 in Batch Mode

Run Conditions

Catalyst precursor: BASF (α-Fe_2O_3) = 1.0 g
Solvent: 90% Ethylflo-164/10% Triglyme = 125 mL
Base: KOMe = 10 mmol
Syngas: 66% H_2/34% CO
T: 170°C
P: 303 psig @ T
On-line time: 1.7 h

Data

Initial/Final solution: Dark red slurry
CO_2 ≈ 1 mmol
Syngas consumed: negligible

Table 5
Data Summary of Run OXY#4

Run Conditions and Data

Catalyst: Reduced BASF Fe
Stirring Speed = 250 rpm

Time h	T °C	P psig	Flow Rate L/min	Initial Syngas			Final Gas				Gas Conv. %
				$\%H_2$	%CO	$\%CO_2$	$\%H_2$	%CO	$\%CO_2$	$\%CH_4$	
1.5	220	100	0.7	66	34	0	64.6	36.4	0.4	0.04	0
19	240		0.5				62.2	31.9	1.3	0.4	8
23				64	25	11	64	22.5	10.2	0.5	16
24		300	0.4				62.3	21.7	12.3	0.5	20
41							63.5	20.5	13.9	0.4	<5

Mass Balance

Initial Slurry Weight = 310g
Final Slurry Collected - 307g
Liquid Collected in Tank #1 = 39g = 42 mL
Hydrocarbons = 6.5 mL
Aqueous = 35.5 mL

Aqueous Analysis (35.5 mL)

MeOH = 1%
EtOH = 4%
n-ProH = 1.2%
n-BuOH = 1%

Table 6
Data Summary of Run OXY#5

Run Conditions

Catalyst: Reduced BASF
Stirring Speed: 250 rpm

Time h	T °C	P psig	Flow Rate L/min	Initial Syngas			Final Gas				Gas Conv. %
				$\%H_2$	%CO	$\%CO_2$	$\%H_2$	%CO	$\%CO_2$	$\%CH_4$	
1	240	100	0.6	66	34	0					4
4			0.4				62.7	28.8	1	0.7	14
21							65.2	17.7	11.7	2.7	39
21.5											42
29							64.6	16.5	12.0	2.6	45
29.2				64	25	11					
47							62.1	10.6	22.2	2.1	40
48.5	220										
52[a]											28
70[a]							63.5	17.6	13.7	0.6	29
75[b]		500									31
166.5[b]	200	100									
170							56.8	22.8	21.2	0.03	8

[a]Stirring speed was 500 rpm
[b]Reactor in batch mode for 68 h under 500 psi which dropped to 185 psig. See text.

ETHANOL AND OTHER OXYGENATEDS FROM LOW GRADE CARBONACEOUS RESOURCES

O.S. Joo, K.D. Jung, S.H. Han and S.J. Uhm*
Korea Institute of Science and Technology
P.O.Box 131, Cheongryang, Seoul, Korea. Fax# 822-968-1924

Abstract

Anhydrous ethanol and other oxygenates of C2 up can be produced quite competitively from low grade carbonaceous resources in high yield via gasification, methanol synthesis, carbonylation of methanol and hydrogenation consecutively. Gas phase carbonylation of methanol to form methyl acetate is the key step for the whole process. Methyl acetate can be produced very selectively in one step gas phase reaction on a fixed bed column reactor with GHSV over 5,000. The consecutive hydrogenation of methyl or ethyl acetate produce anhydrous ethanol in high purity. It is also attempted to co-produce methanol and DME in IGCC, in which low grade carbonaceous resources are used as energy sources, and the surplus power and pre-power gas can be stored in liquid form of methanol and DME during base load time. Further integration of C2 up oxygenate production with IGCC can improve its economics. The attempt of above extensive technology integration can generate significant industrial profitability as well as reduce the environmental complication related with massive energy consumption.

Introduction

In this presentation, gas conversion will be focused as a mean of clean energy development. There have been many research efforts on higher alcohol synthesis from syn gas which is produced from low grade carbon sources. The major draw back from the results of the research efforts is selectivity of the products. Two approaches will be presented for the purpose: one is ethanol synthesis and another one is dimethyl ether synthesis from syn gas. Increasing attention has been paid to ethanol as a potential oxygen carrier and octane booster in gasoline. However, the ethanol price is the major obstacle to be used for such purpose. Currently, ethanol is produced by fermentation or ethylene hydration. Therefore, ethanol from such process is too expensive to be used in gasoline without government subsidies such as tax benefit. Indeed, this problem is the hottest issue among the end users and the manufacturers particularly grain producers. A number of routes from C1 to ethanol have been proposed by the several major research groups from industries during last decade or so in the light of the importance as oxygen carrier in gasoline. Three meaningful routes of these alternative approaches will be discussed briefly to review the back ground in this field. Direct synthesis of ethanol from syn gas has been studied in vapor phase reaction over supported transition metal catalyst under severe reaction conditions(1-4). Only alcohol mixture which contains mostly methanol and 40 - 50% of ethanol at most can be obtained even under high reaction pressure of 1,800 - 2,000 psi. Second one is methanol homologation to ethanol using cobalt-ruthenium halide under even higher reaction pressure of 4,000 - 5,000 psi(5-6). The selectivity to ethanol is 60 - 80% which is higher than the direct synthesis. However, the mixture product includes other alcohols and their acetate ester. In any cases, the reaction conditions are severe and the purity of the ethanol is rather low. The last one is hydrogenolysis of methyl or ethyl acetate which is produced from esterification of acetic acid with methanol or ethanol(7-9). Since expensive acetic acid is used as starting material and esterification of the acetic acid with methanol removing equivalent amount of water is involved, the manufacturing cost is very high. To improve the above processes, an alternative route is presented to produce ethanol from cheap low grade carbon resources such as coal, natural gas and even bio mass. The first step to utilize such low grade carbonaceous resources is gasification to produce syn gas. The commercially amenable chemical process from syn gas is methanol synthesis at this time and the process is one of the best established chemical technology. Therefore, methanol is taken as common starting

material from a well established technology. There have been many reports on C2 chemical synthesis from C1. But, there are very few reactions which can convert C1 to C2 selectively in reasonably good yields. Methanol carbonylation is the only commercial process to make C2 from C1 selectively in high yield. However, the current commercial process of methanol carbonylation is conducted in liquid phase which entails severe corrosion problem and large quantity acetic acid recycle as solvent. In this work, the gas phase methanol carbonylation has been successfully conducted to make acetic acid as well as methyl acetate selectively with high productivity. Particularly, methyl acetate can be produced selectively in one step in the gas phase carbonylation and make it possible to produce anhydrous ethanol and other oxygenate chemicals quite competitively to be used as commodity chemicals. Further more, DME was reported as an excellent substitute for diesel fuel(11). The performance test showed excellent results with respect to emissions, efficiency and noise. Large scale DME production instead of methanol being integrated with IGCC will be discussed here to enhance economic of DME production as well as IGCC.

Ethanol Production

To improve the current ethanol synthesis, methanol carbonylation is employed as a key step to make C2 chemicals from C1 most selectively. The C2 chemical intermediate in this process is methyl acetate which is hydrogenated to ethanol subsequently. The schematic diagram of the process from methanol to ethanol is shown in the Fig. 1. In the process, 2 moles of methanol are taken as feed stock to form 1 mole of methyl formate and 2 moles of hydrogen. The methyl formate formed by dehydrogenation of methanol can be decomposed to one mole of methanol and CO which are introduced consecutively into methanol carbonylation reactor in gas phase to form methyl acetate. The methyl acetate formed is reduced by the hydrogen, which is produced from the methanol dehydrogenation reaction, to produce one mole of ethanol and methanol correspondingly. The methanol is recycled to the carbonylation reactor. As the result, one mole of ethanol is produced from 2 mole of methanol.

-Methanol carbonylation in gas phase

The methanol carbonylation has been done commercially in liquid phase to produce acetic acid in presence of rhodium catalyst and iodide promoter such as methyl iodide. It is highly desirable to do the carbonylation in gas phase since the liquid

phase reaction accompanies serious problems such as corrosion and side reactions due to extensive residence time under severe reaction conditions. There have been several reports on gas phase carbonylation of methanol. However, they have not been successful with catalyst life time in the gas phase carbonylation due to deactivation and fast elusion of the active species from the support. KIST has developed a noble method to prevent the catalyst elusion from the support and maintain the longevity of the catalyst for long time during the gas phase carbonylation.

$$CH_3OH + CO \longrightarrow CH_3COOCH_3 + CH_3COOH + H_2O$$

The reaction has been conducted in a fixed bed column with 100% conversion and high selectivity toward acetic acid and methyl acetate in the ratio of from 15/85 to 85/15 under relatively mild conditions. The product ratio is freely controllable within the range shown above by simple change of the reaction conditions. This catalytic system showed high activity and low corrosion problem. It enables that the gas phase carbonylation is very useful for practical application to produce C2 chemicals such as acetic acid and methyl acetate from C1. In this presentation, methyl acetate is the main concern and will be discussed extensively. As the result, C2 compounds can be prepared successfully starting from CO and methanol which can be achieved readily from low grade carbonaceous resources such as coal and natural gas employing well established commercial technology.

-Ethanol from methyl acetate

Once the methyl acetate is obtained with a competitive cost, the ester can be readily hydrogenolized to produce ethanol using copper based catalyst.

$$CH_3COOCH_3 + H_2 \xrightarrow[Cu\text{-}ZnO]{220^\circ C,\ 500psi} CH_3CH_2OH + CH_3OH$$

As indicated above, hydrogenolysis of methyl or ethyl acetate to produce ethanol have been patented and reviewed extensively (7-9). However, the process has been left as uneconomic one to produce ethanol from rather expensive acetic acid until now. KIST has developed a one step noble process in a simple fixed bed column to produce methyl acetate with very competitive cost from methanol and carbon monoxide which can be readily obtained from low grade carbonaceous resources via well established gasification technologies. Hydrogenation of methylacetate was performed in gas phase to produce 1:1 mixture of ethanol and methanol in the

presence of copper based catalysts. Commercially available catalysts showed good activities, but they need rather vigorous reaction conditions. The catalysts which have been developed at KIST were examined under the conditions of 220°C, 500psi, and H_2/CH_3COOCH_3=5/1(fig. 2). The selectivity was high and part of the ethanol formed reacted with methyl acetate to produce ethyl acetate as a major by-product under the reaction conditions with low conversion.

-Other C2 up oxygenate chemicals from methyl acetate
Methyl acetate is further carbonylated to produce acetic anhydride which is used in production of cellulose acetate from cellulose. Transesterification of methyl acetate with corresponding alcohols, which can be conducted rather simply in a reactive distillation column, can produce acid free alkyl acetates competitively without generating water which causes reversible reaction to give carboxylic acid in the product. The competitive production of methyl acetate can improve the economic of vinyl acetate process via methyl acetate carbonylation which has been studied extensively by many research groups. Some of the potentially important chemical reactions starting from methyl acetate are shown in the following chemical equations.

- $CH_3COOCH_3 + CO \longrightarrow CH_3COOCOCH_3$
- $CH_3COOCH_3 + ROH \longrightarrow CH_3COOR + CH_3OH$
- $CH_3COOCH_3 + CO/H_2 \longrightarrow CH_3COOCH{=}CH_2$
- $CH_3COOCH_3 \longrightarrow CH_3CH_2COOH$

The value added chemical production from methanol could improve the economics of IGCC through further integration with the processes involved.

DME Production for Further Integration in IGCC

Due to fast depletion of high grade energy source, more and more attention has been paid to first low grade energy source such as coal, natural gas and other low grade carbonaceous resources. Power generation from the first low grade energy source is very popular in the light of low cost. However, this kind of power generation entails environmental implication and intrinsic problem of power peak control due to power demand fluctuation. More specifically, the usage of low grade carbonaceous

resources for power generation requires gasification first and the gas product, which is known as syn gas(CO/H_2), must be cleaned from SOx and NOx. The syn gas prepared is ready to be burned in the gas turbine to produce electricity and the heat in the gas is used to generate steam which is used in the steam turbine consecutively to generate electricity further. As indicated above, the power generation burning low grade carbonaceous resources particularly coal has an intrinsic problem of peak management due to the power demand fluctuation. It is attempted to alleviate the inefficiency of the power generation due to the power demand fluctuation combining with methanol plant, where the surplus power and pre-power-gas can be stored into a storable and transportable liquid of methanol(fig. 3). If 10% of the average energy is transformed into a liquid chemical such as methanol at a power plant with a capacity of 500Mw burning 3230,000 ton/year, 109,000 ton/year of methanol can be produced. This way, the surplus energy can be stored in an ideal chemical form of methanol which can be used readily as desired. It is widely recognized that the methanol is the building block of C1 to open a new era of chemical industry for the future starting from low grade carbonaceous resources including even renewable biomasses. The methanol from such an integrated technology combining energy and chemical mass commutation is significantly cheaper than from regular methanol plant. The integration of the related technologies, which is known as IGCC(Integrated Gasification Combined Cycle electric power generation), has been extensively studied by many expert groups in this field to find sound economic feasibility of the approach(10). However, commercialization of the IGCC to generate power and chemical mass has not been practiced yet due to massive large scale integration of broad technologies. When the IGCC is commercialized, there will be a major change in chemical technologies starting from methanol. Since the economic of the ethanol production depends heavily on the cost of methanol and CO, methanol and CO from IGCC will improve the cost of ethanol production great deal(fig. 4). In such case, ethylene from ethanol dehydration would be quite popular with a small scale merit. Further more, CO2, which is considered to be the major cause of the green house effect, can be recycled as energy storage media in the mimesis of natural photo synthesis. It is obvious that hydrogen, which can be produced from abundant water on the earth utilizing solar energy or waste energy, will be the future energy source. The hydrogen produced will be stored in CO2 via appropriate catalysis to form methanol which is feasible with currently available technologies. Methanol synthesis from carbon dioxide has the intrinsic problem of water formation which is the cause of unfavorable equilibrium limit. However, we have managed to over come the limitation through multi stage synthesis loop to meet the optimum CO2/CO/H2 ratio for the feed gas. Further more, any organic refuses

which can be gasified could also be put into the cycle through gasification to alleviate environmental implication.

It has been reported that DME is a clean fuel which shows excellent engine performance replacing diesel fuel which is known as the major urban pollution source(11). If DME could be used as clean urban fuel replacing diesel, large volume of DME should be produced. The large scale DME production from pre-power syn gas produced in a power plant as a mean of power peak control during the base load time could supply reasonably cheap clean fuel for the urban transportation eliminating the heavy initial investment for syn gas generation. The investment breakdown of a methanol plant shows that more than 50% of the initial investment is for syn gas preparation. DME synthesis from pre-power syn gas of IGCC could be advantageous to methanol synthesis which has unfavorable thermodynamic limitation. In the reaction the formation of DME is favored to that of methanol under the given reaction conditions. It has been found that one through conversion of the syngas in the lab. scale is more than 80% under 1,500 psi at 240 C with the space velocity of 10,000/hr. The power peak control problem will be alleviated by further integration with relevant chemical technology such as DME production from the pre-power gas. Since coal will be major organic energy sources replacing oil, clean coal technology come to our attention increasingly. Therefore, IGCC will be the common power generation technology in the near future, and DME will even be produced from any low grade carbon sources such as biomass and organic refuses from our daily life. It would be also highly desirable to convert these organic refuses to syn gas and DME clean fuel for the urban transportation. Further more, DME could be produced instead of methanol as a mean of hydrogen storage in CO2 as described above.

Conclusion

It can be concluded that the integration of the technologies in power generation and chemical mass production is highly desirable to develop alternative clean energy sources and other chemical raw materials from low grade carbon sources such as coal and natural gas replacing oil. Further more, it is essential to develop clean technology to avide with the nature on this planet. Ethanol and DME are know as good oxygenated chemical compounds to be used as clean fuel or additive. The methanol carbonylation in gas phase can provide an excellent process to produce anhydrous ethanol. The integration of these kind of technologies can alleviate the high cost of clean technology. Our effort in the further integration of the related

technologies will realize the dream of clean environment and promote the development of alternative energy and chemical sources in near future.

References

1. Ph. Courty, J.P. Arlie etal. Hydrocarbon Processing, 105, November 1984.
2. USP 4,122,110 24 October 1978, assigned to IFP.
3. USP 4,162,202, assigned to Union Carbide.
4. GB 1,547,687, assigned to IFP.
5. UK 2,053,915, assigned to BP.
6. USP 4,239,924, assigned to Gulf Oil.
7. Barry Juran, Richard V. Porcelli, Hydrocarbon Processing, 87, October 1985.
8. PCT WO 83/03409 13 October 1983, assigned to Davy McKee.
9. UK patent GB 2 162 172 A, 29 January 1986, assigned to Davy McKee.
10. EPRI Report AP-3109, June 1983.
11. Kapus, P., Ofner, H., Development of Fuel Injection Equipment and Combustion System for DI Diesel Engines Operated on DME, SAE Paper 950062, 1995.

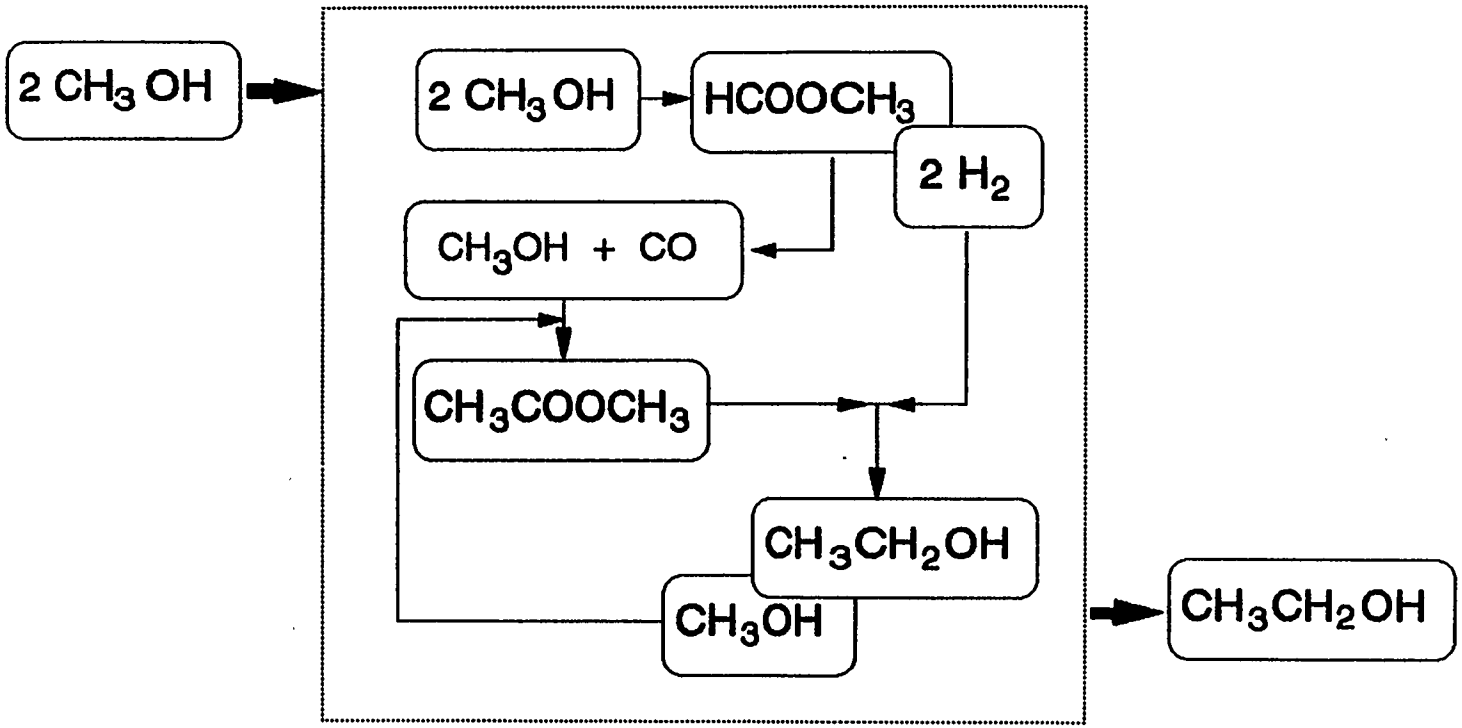

Figure 1. The schematic diagram of the process from methanol to ethanol.

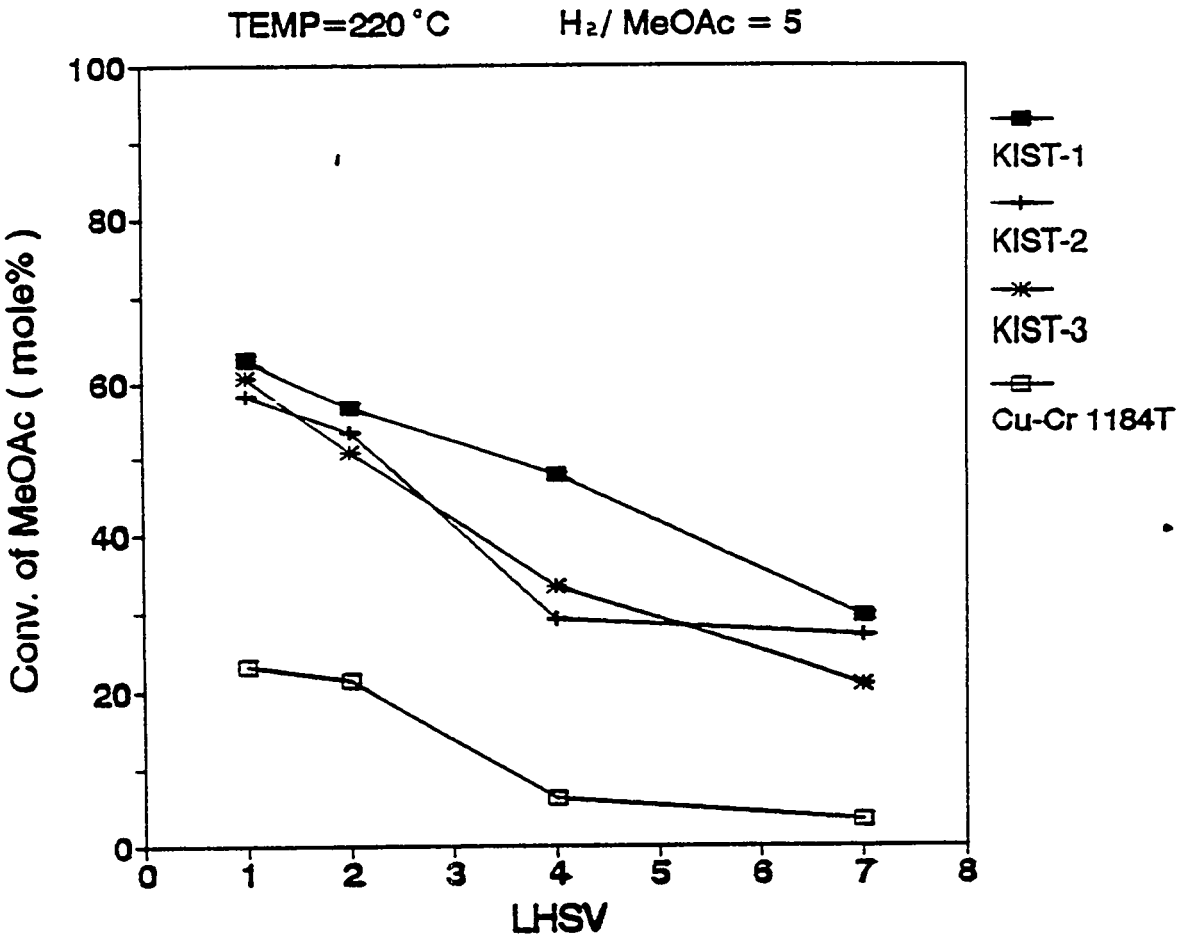

Figure 2. Hydrogenolysis of methyl acetate on various catalysts.

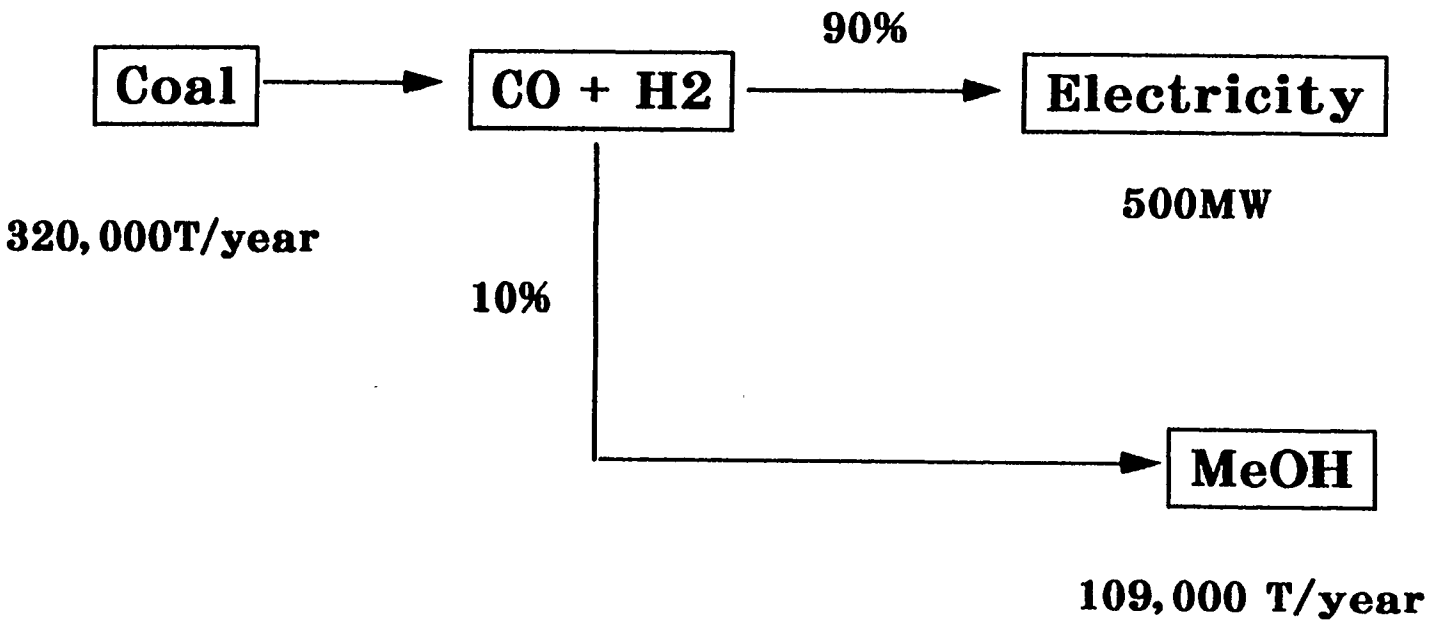

Figure 3. Integrated gasification combined cycle

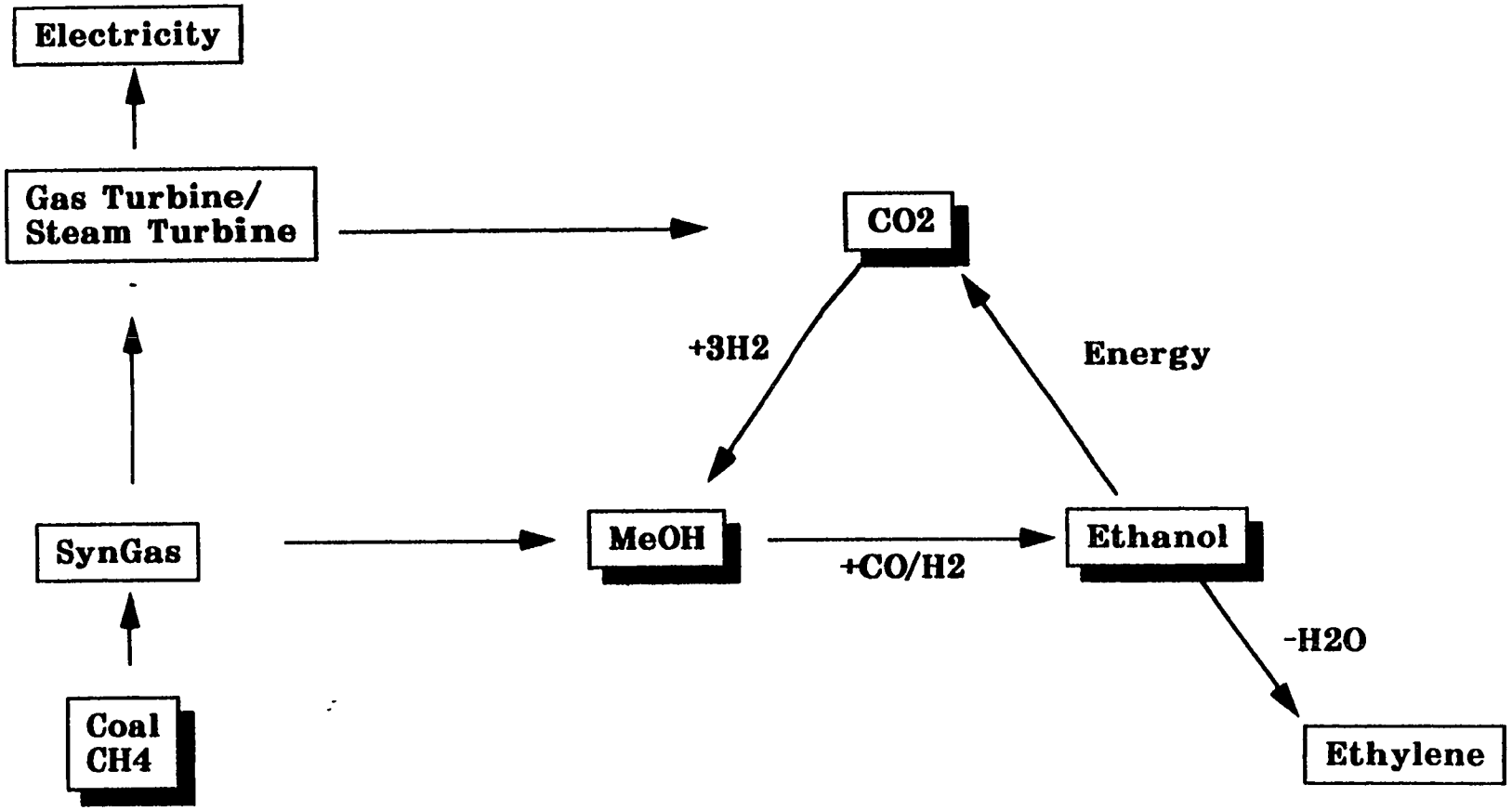

Figure 4. Future energy and chemicals digram based on CO_2, H_2 and CO.

Catalyst Activity Maintenance Study for the Liquid Phase Dimethyl Ether Process

X. D. Peng, B. A. Toseland and R. P. Underwood

Air Products and Chemicals, Inc.
7201 Hamilton Boulevard
Allentown, PA, 18195-1501

DOE Contract number: DE-FC22-94 PC93052
April 1994 to May 1995

OBJECTIVES

The co-production of dimethyl ether (DME) and methanol from syngas is a process of considerable commercial attractiveness. DME coproduction can double the productivity of a LPMEOH process when using coal-derived syngas [1]. This in itself may offer chemical producers and power companies increased flexibility and more profitable operation. DME is also known as a clean burning liquid fuel; Amoco and Haldor-Topsoe have recently announced the use of DME as alternative diesel fuel [2]. Moreover, DME can be a interesting intermediate in the production of chemicals such as olefins and vinyl acetate [3].

The current APCI liquid phase dimethyl ether (LPDME) process utilizes a physical mixture of a commercial methanol synthesis catalyst and a dehydration catalyst (e.g., γ-alumina). While this arrangement provides a synergy that results in much higher syngas conversion per pass compared to the methanol-only process, the stability of the catalyst system suffers. The present project is aimed at reducing catalyst deactivation both by understanding the cause(s) of catalyst deactivation and by developing modified catalyst systems. This paper describes our current understanding of the deactivation mechanism.

ACCOMPLISHMENTS

1. Introduction

Catalyst stability for LPMEOH, which uses only a methanol catalyst, is compared to that of a liquid phase dimethyl ether (LPDME) process, which uses a physical mixture of the same methanol catalyst and a γ-alumina (80:20 weight ratio) in Figure 1. Catalyst stability for a liquid phase dehydration experiment which uses γ-alumina only is also shown. All runs were carried out in a 300 cc slurry phase autoclave using powdered catalysts. The syngas used in both LPMEOH and LPDME run simulates that derived from a Shell-type gasifier. A 10% methanol in N_2 feed gas was used for the dehydration run.

For the LPMEOH and LPDME runs, the stability of the catalysts is expressed in terms of the apparent reaction rate constants (normalized to the initial values), calculated from the rate expressions shown in Figure 1. The subscript *m* refers to the methanol synthesis reaction, *d* to the methanol dehydration reaction, and *appr.* stands for the approach of the reaction to equilibrium, respectively. This methanol rate expression is the same as developed for the LPMEOH process while the dehydration rate expression was newly obtained by regression of the kinetic data of LPMEOH and LPDME experiments. They serve as a good semi-quantitative kinetic tool in the domain of the reaction conditions used in our experiments. For the dehydration run, the normalized DME productivity was used to describe the stability of the alumina.

Figure 1: Catalyst deactivation in different liquid phase processes

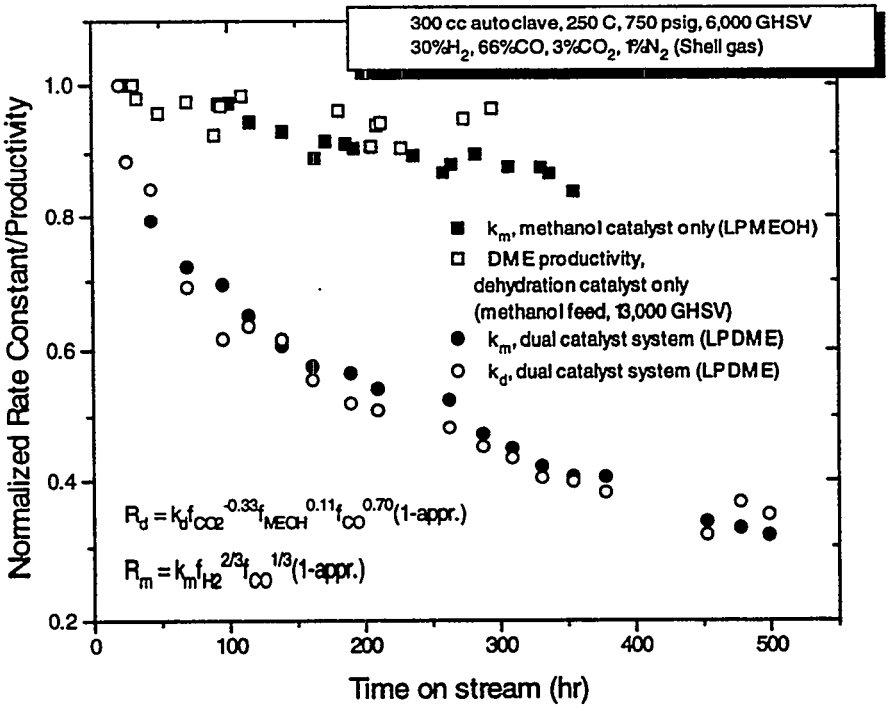

Both the methanol catalyst and the alumina are much less stable under the LPDME conditions than under LPMEOH conditions. Both catalysts undergo rapid deactivation for the first 80 hr or so, followed by a slow, continuous deactivation as long as the reaction proceeds. Although a stable productivity could be maintained in a commercial LPDME process by on-line catalyst withdrawal and addition, a stable catalyst system is still a preferred and ultimate solution to the problem. The work in the past year has gained a good understanding of the deactivation mechanism. Continuing work is focused on developing solutions to the rapid deactivation.

2. Investigation of the Possible Causes

Four major differences between the LPDME and the LPMEOH process have been identified. Each could be responsible for the catalyst deactivation under LPDME conditions.

First, the DME concentration is much higher in LPDME, e.g., typically 6% vs. <0.1% for LPMEOH. DME has been reported to disintegrate the texture of methanol catalyst [4]. It may also serve as a source of coke formation on the dehydration catalyst.

Secondly, the water concentration in LPDME is higher than that in LPMEOH due to the dehydration reaction. The water concentration depends upon syngas composition. It ranges from 0.15% to 1.3% in LPDME compared to LPMEOH (0.06%-0.2%). Hydrothermal sintering has long been known as a deactivation mechanism for methanol catalysts. The high water concentration may also deactivate the alumina by hydrating the alumina surface.

Thirdly, heavy oxygenates form under LPDME conditions. These heavy oxygenates can lead to coke formation which leads to the loss of the dehydration activity.

Finally, the physical/chemical interaction of alumina with the methanol catalyst could be a source of catalyst deactivation.

Based on these considerations, experiments were designed to investigate these possible causes individually. Each of these experiments is discussed below.

2.1. DME

DME was eliminated as the cause of methanol catalyst deactivation by cofeeding DME with syngas in an otherwise standard LPMEOH run. The experiment was conducted by first running methanol synthesis in a 300 cc autoclaves for 150 hr to establish a baseline. No alumina was present in the system. At 150 hr, the supplemental N_2 in the feed gas was replaced with DME at the same feed rate. The DME concentration in the reactor during this period, approximately 5 mol%, is typical of that observed during DME synthesis using the dual catalyst system.

The methanol production rate as a function of time is shown in Figure 2. Initial introduction of DME resulted in no change in the methanol production rate or the product distribution. This indicates that, at these conditions, the presence of DME has no influence on the kinetics of methanol synthesis. Most significant is the fact that the rate of decrease of the methanol activity during DME addition is comparable to that prior to the injection. This deactivation rate is much lower than rate of deactivation observed during LPDME synthesis using the dual

catalyst system. Thus, DME, per se, has no direct negative effect on the stability of the methanol catalyst.

Figure 2: Effect of DME addition on methanol catalyst stability
250 °C, 750 psig, GHSV=6,000 std.lit./kg-hr, Shell-type gas

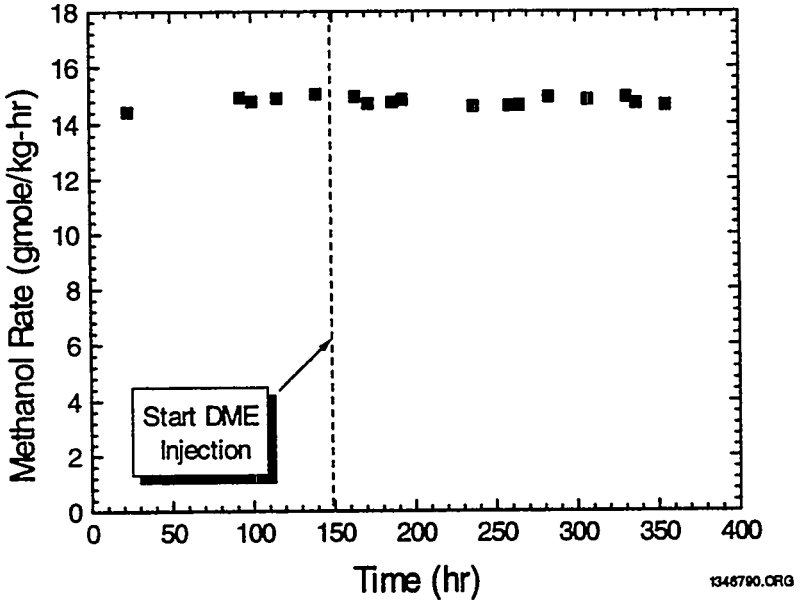

2.2. Water

The water level in both LPMEOH and LPDME reactions depends on the composition of the feed gas owing to the water gas shift reaction. This phenomenon prevents comparison at exactly the same conditions. However, one can run the two reactions at a similar water levels by using H_2-rich gas for LPMEOH and CO-rich gas for LPDME. The results of two experiments using this approach is shown in Fig. 3. It can be seen that, although the water levels in the two experiments are similar, the methanol catalyst is much less stable in the LPDME run. Thus, we infer that water, per se, is not the cause of the higher deactivation in the LPDME process. Although hydrothermal sintering is a known cause of methanol catalyst deactivation, it cannot be used as an explanation for the fast deactivation of the methanol catalyst under LPDME conditions.

2.3. Coking

Coke formation has been known to cause the deactivation of acidic catalysts such as alumina. Methanol and DME are unlikely the precursors of coke formation on the alumina surface under the temperature of LPDME reaction (250 °C), as the dehydration run using the alumina by itself and methanol as feed gas at 250 °C exhibited no sign of catalyst deactivation (Fig. 1). However, some heavier oxygenates, such as C2-C4 alcohols, methyl formate and acetate, and,

Figure 3: Stability of the methanol catalyst in LPMEOH and LPDME runs with a similar water concentration

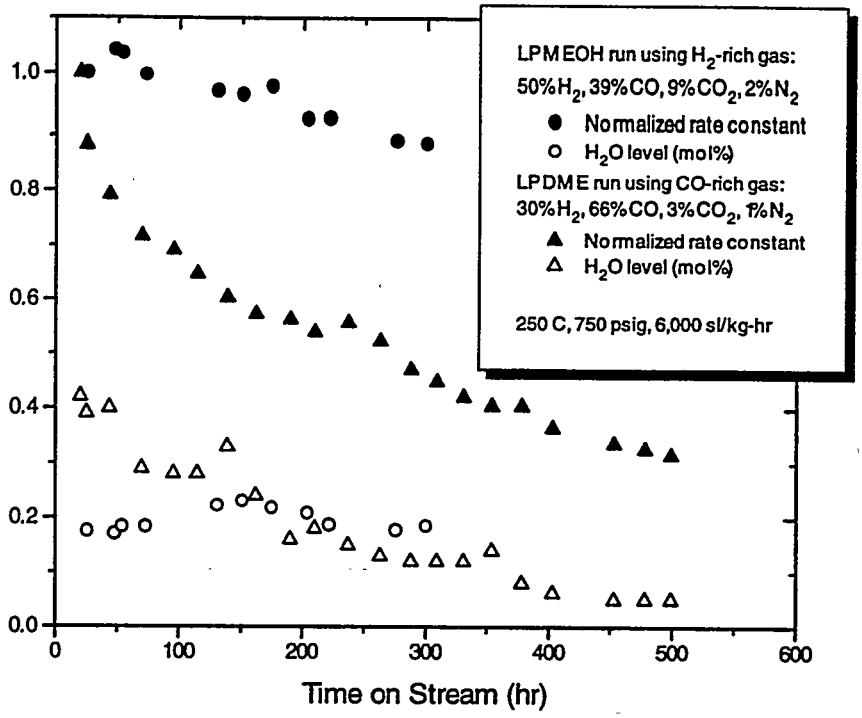

possibly, some nonvolatile species, are formed under LPDME conditions. These are possible coke precursors. Coke analysis of the alumina sample used in a LPDME run is difficult because the catalyst system contains well-mixed powders of the two catalysts of < 100 μm in size . A spent alumina pellet sample has been generated from a LPDME run using Robinson-Mahoney basket internals and pelletized methanol catalyst and alumina. At the present time, the coke analysis is obscured by the presence of residual slurry fluid (a hydrocarbon based mineral oil) in the sample. Therefore, the possibility of coking is as yet unresolved. Better extraction methods are being developed.

2.4. Alumina

The following experiment was designed to see if the presence of alumina per se results in the deactivation of the catalyst system. The standard catalyst mixture consisting of 80 wt.% of the methanol catalyst and 20 wt.% of the γ-alumina was loaded into a 300 cc autoclave. Following a normal catalyst reduction (using 2% H_2 in N_2), this catalyst system was left under flowing reduction gas (2% H_2 in N_2, 50 sccm/min.) at 250 °C for 117 hours with normal stirring. The activity of the catalyst system was then measured using the simulated Shell-type syngas to see if holding the two catalysts together at 250 °C had any effect on their activity. Since this scheme avoids exposure of the catalyst system to syngas and reaction products during the holding period, any effect can be attributed to the presence of alumina.

The activity of this catalyst mixture is compared in Figure 4 with that of a similar catalyst mixture from a normal LPDME life run. Merely holding the methanol catalyst together with the alumina at 250 °C for 117 hours resulted in a 55% drop in the methanol equivalent productivity. (The methanol equivalent productivity is defined as the methanol productivity plus 2 times of the DME productivity.) Judging by the rate constants calculated from the above mentioned methanol synthesis and methanol dehydration rate expressions, the methanol synthesis rate constant dropped by 68%, and the dehydration rate constant by 62%. This experiment was repeated. As shown in Fig. 4, the observation is reproducible. These results clearly indicate that there is a strong interaction between the methanol catalyst and the γ-alumina that deteriorates both catalysts. As will be discussed later, in a counter experiment deactivation of the methanol catalyst is low when the catalysts are not held in intimate contact.

Figure 4: The effect of the alumina on the stability of the catalyst system

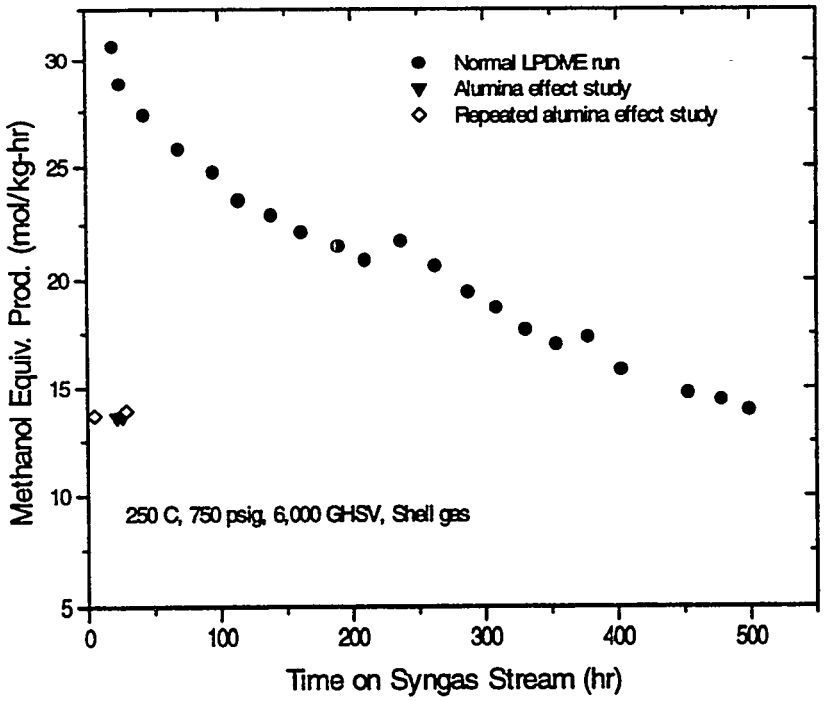

Ideally, one would like to use a inert gas such as nitrogen or helium for the holding period. However, a previous experiment has shown that the methanol catalyst, when loaded by itself, deactivates irreversibly under flowing nitrogen (APCI zero grade) at 250 °C. In contrast, holding the methanol catalyst by itself at 250 °C under 2% H_2 in N_2 did not effect catalyst activity. Therefore, the reduction gas was used in the current alumina effect study. Since the normal LPDME run has a reducing atmosphere (high H_2 and CO concentration), it is plausible to say that the mechanism that is responsible for catalyst deactivation in the alumina effect study is also responsible for the catalyst deactivation under

the LPDME conditions. If there is any difference, it is the greater drop in the activity under the reduction gas (55% in methanol equivalent productivity) as compared to that under LPDME conditions (33%) for a similar length of time. This suggests that the interaction is more severe in the absence of the LPDME products.

3. Mechanistic Investigation

3.1. The nature of the interaction between the two catalysts

Figures 5 and 6 display the activity of methanol catalyst and dehydration catalyst, respectively, as a function of time on stream for two catalyst systems: the methanol catalyst plus γ-alumina and the methanol catalyst plus a ZnO-modified γ-alumina. The rate expressions described previously were used to calculate the rate constants. The methanol rate constant was adjusted to make the comparison between different catalyst systems on an equal basis. All the data were obtained under the standard conditions, i.e., 250 °C, 750 psig, 6000 GHSV, Shell-type gas, and a methanol-to-dehydration catalyst ratio of 80:20.

Figure 5: Methanol synthesis rate constant as a function of time on stream for different catalyst systems

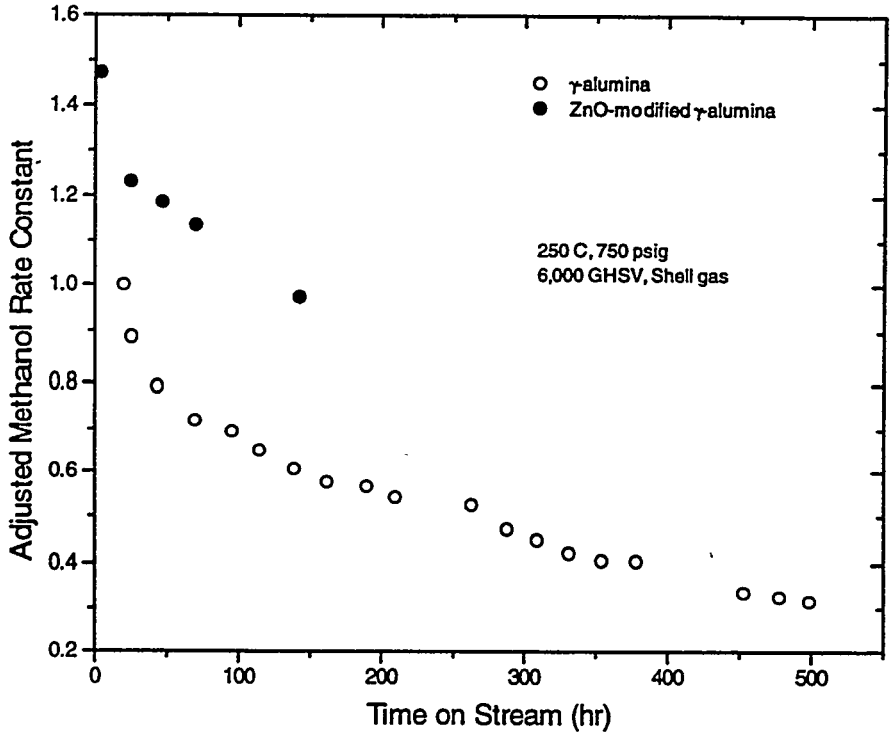

Figure 6: Dehydration rate constant as a function of time on stream for different catalyst systems

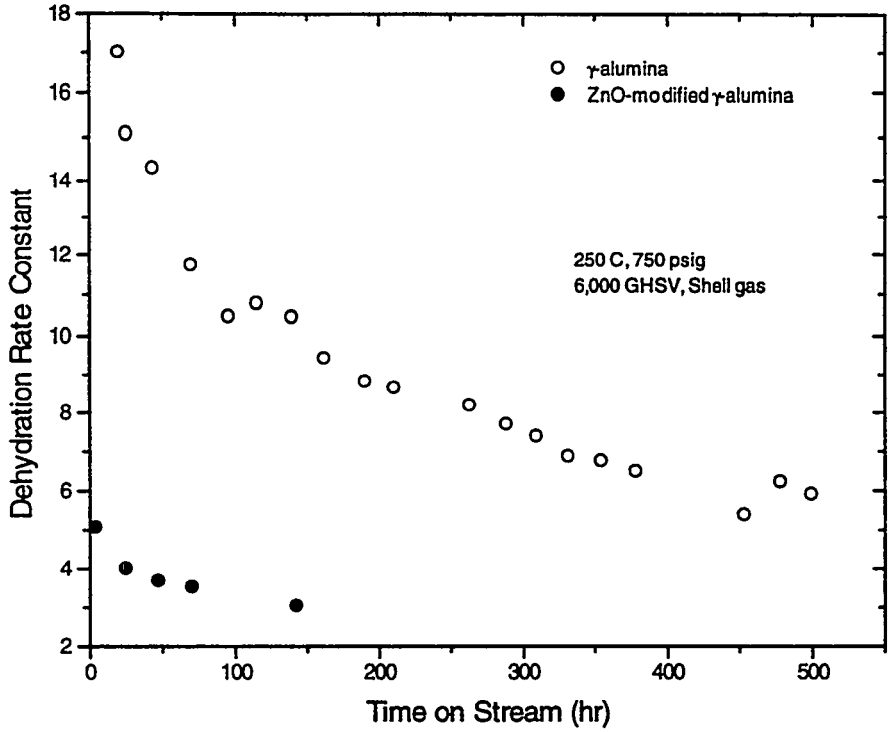

As shown in Figs. 5 and 6, the deactivation of both the methanol catalyst and the dehydration catalysts can be divided into two stages: a *initial*, fast deactivation followed by a stage of slower but continuous, *long term* deactivation. The division between the initial and long term deactivation is where the deactivation rate becomes almost constant. For the catalyst system containing virgin alumina, the initial deactivation period stops at ca. 80 hr on stream. For the system containing ZnO-modified alumina, it stops at ca. 40 hr. As discussed below, different mechanisms are operational behind these four different modes of catalyst deactivation.

A normal LPDME run in the lab starts with reduction of the methanol catalyst in the presence of a dehydration catalyst in the slurry. Apparently, the initial deactivation of the methanol catalyst occurred during the reduction, as suggested by the different initial activities of the same methanol catalysts in different catalyst systems (Fig. 5). Rapid deactivation continues into the early period when the system was on syngas stream. The magnitude of the initial deactivation and the length of this period appears to be a function of the acid strength of the dehydration catalyst. Figure 7 displays the initial deactivation of the methanol catalyst, measured by the methanol synthesis activity at 80 hours on syngas stream, as a function of different dehydration catalysts. Among them, the ZnO-modified γ-alumina possesses the weakest acidity since ZnO is a base. The silica alumina used in this study has the strongest acidity. It has exhibited higher activity toward isobutanol dehydration than γ-alumina in this lab. As

shown in Fig. 7, the initial deactivation of the methanol catalyst increases with increasing acid strength of the dehydration catalyst. This trend holds true for the other dehydration catalysts we have tested, including, other silica alumina, zeolitic materials, γ-alumina calcined and modified differently.

Figure 7: Correlation between the initial deactivation of the methanol catalyst and the acidity of dehydration catalysts

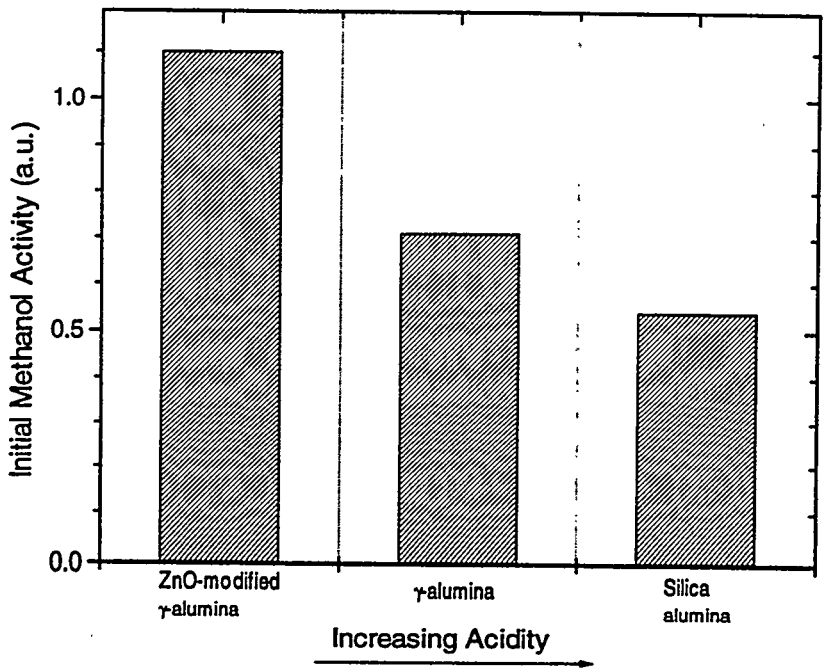

The long term deactivation of the methanol catalyst is not directly related to the acidity of dehydration catalysts. As shown in Figs. 5 and 6, although the two dehydration catalysts have different acidity, as indicated by the different dehydration activity, the deactivation rate of the methanol catalyst is similar for these two catalyst systems. A similar long term deactivation rate was also observed for the catalysts systems containing other dehydration catalysts mentioned above. This rate is ~ 0.082% hr^{-1}, a factor of 2 greater than that of the methanol-only system (0.045% hr^{-1}).

The pattern of the initial deactivation of dehydration catalysts varies from one system to another. In general, the deactivation occurs during the period of catalyst reduction and continues to the early hours on syngas stream. The strong acid sites appear to deactivate in this period. Moreover, the experiments using zeolitic materials demonstrate that the Brønsted acid sites deactivate very fast under LPDME conditions, dropping to a residual activity within 50 hours, regardless of the acid strength.

The long term deactivation of dehydration catalysts does not follow any clear pattern. The deactivation rate varies from one system to another. The higher dehydration activity, i.e., greater acidity, does not necessarily results in faster deactivation of the dehydration catalyst, or vice versa.

In summary, among the four different modes of catalyst deactivation, the initial deactivation of both methanol and dehydration catalysts is related to the acidity of the dehydration catalyst. The long term deactivation of both catalysts are not directly related to the acidity of dehydration catalysts. While the long term deactivation of the methanol catalyst exhibits a similar deactivation rate for different dehydration catalysts, the long term deactivation of dehydration catalysts does not follow a simple pattern.

The initial deactivation of the methanol catalyst is possibly *driven by the acid-base interaction* between the two catalysts, since it correlates with the dehydration activity (Fig. 7). Among the possible mechanisms are the inter-catalyst mass transfer and inter-catalyst solid state reaction. For instance, ion exchange could take place between Cu- and Zn-containing species from the methanol catalyst and the protons on the dehydration catalyst. Or the deactivation could be due to a reaction between ZnO (a base) in the methanol catalyst and the acid sites on a dehydration catalyst. The same acid-base interaction may also be responsible for the initial deactivation of dehydration catalysts. However, as discussed before, this deactivation could also be compounded by coke formation.

The mechanism for the long-term deactivation of both methanol and dehydration catalysts is not clear. For one thing, it is not directly related to the dehydration activity. The long term deactivation may still be due to inter-catalyst mass transfer or solid state reactions, but not likely acid-base in nature. For example, the migration of Zn- and Cu-containing species from the methanol catalyst to dehydration catalysts can be *driven by the concentration gradient* of these species between the methanol catalyst and dehydration catalysts. Note that most of the metal oxides tested as dehydration catalysts are also good catalyst supports with dispersing capability for metal, metal oxides, and salts, and the dispersing capability is not necessarily related to the acidity of the materials.

3.2. The role of the intimate contact between the two catalysts in the catalyst deactivation

The *driving force* discussed above alone may not be surficient to deactivate the catalysts. Unless the slurry fluid serves as mass transfer medium, the *intimate contact* between the two catalysts is necessary to provide the time and area for the mass transfer or/and reaction to take place. One can envision that the solid state reaction between the two catalysts can only occur when they touch each other and remain that way for a long enough time. The migration goes from the outer surface to the inner surface, requiring both contact time and area of the two catalysts. Under the slurry phase operation conditions, this intimate contact

can be provided by the collision between the catalyst particles, the attachment of small particles to the large ones, and the agglomeration of small particles. Collision and attrition continuously generate particles of smaller and smaller size, resulting in large and fresh (therefore active) contact area. This speculation is supported by the results from the following experiment.

This experiment was conducted using Robinson-Mahoney basket internals built to fit into a 300 cc autoclave. Methanol catalysts and alumina pellets were mixed together and loaded into the basket. The basket was submerged in a mineral oil in the autoclave and kept stationary during the run, while the oil was agitated to provide the mixing. The purpose of the R-M experiment is two fold. First, individual methanol catalyst and alumina samples can be obtained at the end of the run because it is easy to separate pellets. These samples were analyzed to elucidate the deactivation mechanism. Secondly, one would like to see if the change in the physical features of the reactor set-up would result in different deactivation behavior.

The reaction rate was mass transfer limited because of the use of pelletized catalysts. Therefore, the activity and stability of the catalyst system could only be checked in a subsequent run using the standard slurry phase operation conditions. For these runs, the spent pellets were ground into powders and re-loaded into the autoclave, now without the basket, to measure the activity. Two R-M runs were performed, one with a on-stream time of 500 hr, the other 120 hr. The activity of the spent catalysts from these two runs is listed in Table 1, along with that from a standard LPDME run (powdered catalysts). Again the rate expressions described above were used to calculate the rate constants.

Table 1: The activity of the spent catalysts from the LPDME runs using Robinson-Mahoney basket internals. Reaction conditions: 250 °C, 750 psig, Shell-type gas.

Run	MEOH Cat. :Al_2O_3	Time on Strm (hr)	MEOH Equiv. Prod. (mol/kg-hr)	Concentration (%) MEOH	DME	Rate Constant k_m	k_d
1st R-M run	82.2:17.8	508	28.1	1.59	6.13	2.7	10.7
2nd R-M run	80:20	127	27.1	2.74	4.87	3.1	7.0
Standard run	81.3:18.7	20	30.7	1.01	6.95	3.0	17.0
		115	23.6	0.83	4.89	1.9	10.8
		499	30.7	0.49	2.67	1.0	5.9

Some differences can be seen between the two R-M runs. Mainly, the sample from the second run exhibits higher methanol activity and lower dehydration activity. This difference is likely due to the experimental error in determining the actual ratio of the two catalysts in the ground samples. Given the experimental error, the same conclusion can be drawn from the two R-M runs. Judging by the rate constant, the spent methanol catalysts from the R-M runs have about the same activity as the fresh methanol catalyst in the standard run, and much higher activity than the methanol catalyst at a similar time on stream in the standard run. Therefore, both R-M runs indicate that the methanol catalyst is

stable under the R-M set-up. The dehydration catalyst deactivates in the R-M runs by 37-59%. Since the longer time on stream did not result in greater deactivation in the dehydration activity, it can be concluded that the deactivation of the dehydration catalyst occurred only in the earlier stage of the run (< 127 hr). That is, there is no long term deactivation of the dehydration catalyst under the R-M set-up.

Note that the Robinson-Mahoney reactor differs from a standard slurry phase reactor in that it does not have certain physical features of a slurry phase reactor such as mixing, powdered catalysts, and collision between catalyst particles. As described above, these features are likely to provide the intimate physical contact between the two catalysts, leading to catalyst deactivation by inter-catalyst mass transfer or/and inter-catalyst solid state reaction. In other words, without the intimate physical contact between the two catalysts, the methanol catalyst could be stable and the dehydration catalyst would not suffer long term deactivation.

The alumina suffered a initial deactivation even under the R-M set-up. This deactivation could be due to either inter-catalyst mass transfer or coking. If the inter-catalyst mass transfer is the reason, the slurry fluid must have served as the mass transfer medium. And apparently the methanol catalyst has some "free" Zn- and/or Cu-containing species to spare before its activity starts to suffer.

4. Progress in Solving the Problem

According to our current understanding of the deactivation mechanism, the problem can be solved by eliminating either the driving force for the inter-catalyst mass transfer/reaction or the intimate physical contact between the two catalysts. Efforts and progress are being made in both these directions.

Figures 8a and b provide an example how the stability of the catalyst system can be improved by reducing the driving force of the interaction between the two catalysts. In this example, the alumina was treated with a Si-containing compound to remove the strong acid sites. It can be seen from Fig. 8a that the modified alumina results in a much smaller initial deactivation of the methanol catalyst, or a 30% higher methanol synthesis activity. The long term stability of the methanol catalyst, however, is not improved by the modification.

The initial activity of the Si-modified alumina is lower than the virgin alumina due to the reduction in the number of acid sites by silica passivation. However, its long term deactivation rate is much lower than that of the virgin alumina. The combination of the high initial activity of the methanol catalyst with the slow long term deactivation of the dehydration catalyst results in a higher methanol equivalent productivity after the catalysts were on stream for 50 hr (Fig. 8b), as compared to the standard system (the methanol catalyst plus virgin γ-alumina).

Figure 8: The stability of the LPDME catalyst system: Si-modified γ-alumina vs. virgin γ-alumina

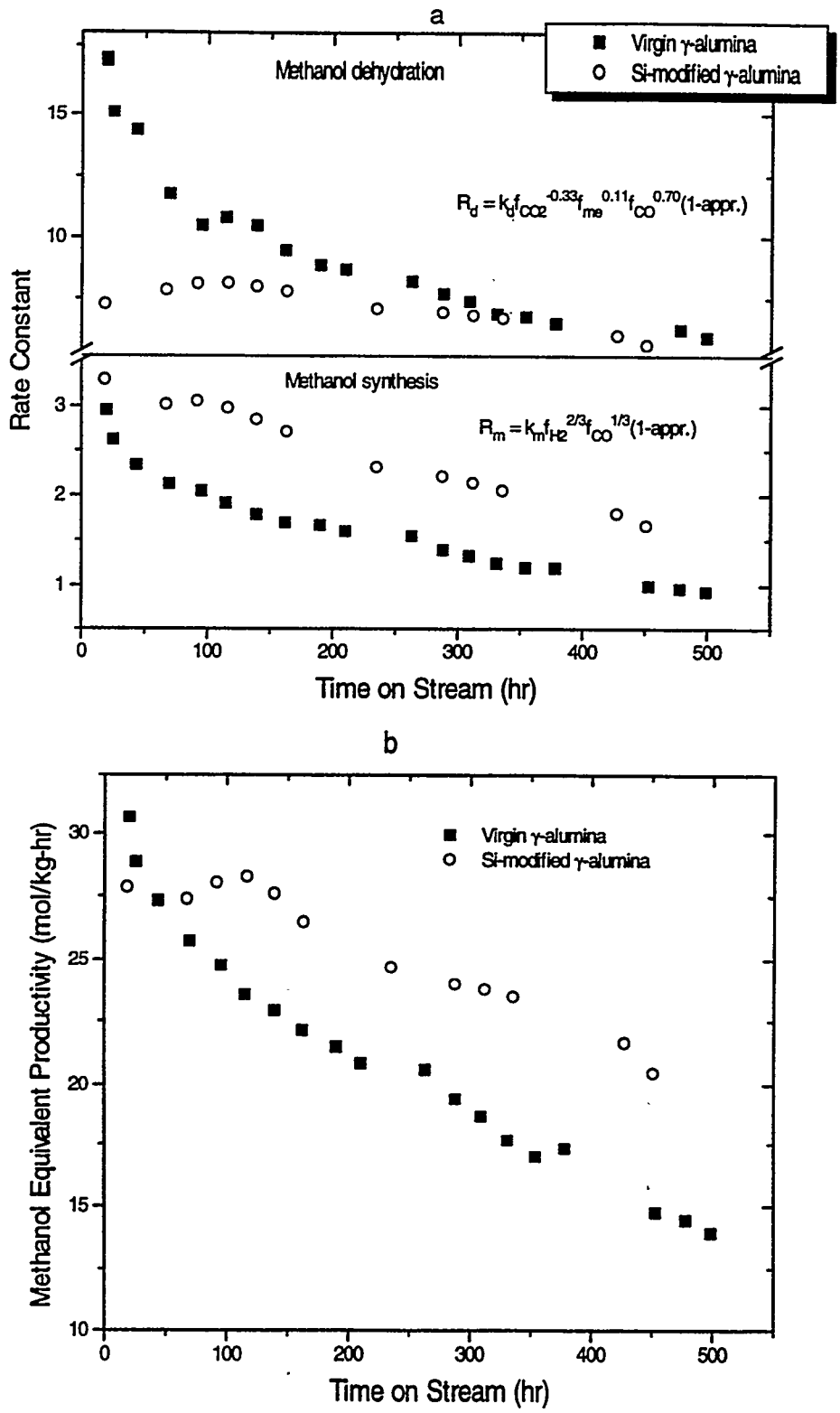

The rate of decrease in the productivity is also smaller, with a slope of 0.019 vs. 0.027 for the standard catalyst system, a 30% of improvement. The stability of this catalyst system is not all that could be desired because of the poor long term stability of the methanol catalyst.

CONCLUSIONS

This investigation shows that high level of water and DME under the LPDME conditions has no direct effect on the deactivation of the catalysts. An interaction between methanol and dehydration catalysts has been identified as the cause of the deactivation of both catalysts. In the initial stage, this interaction is predominantly associated with the strong acid sites on the dehydration catalyst, resulting in a fast, initial deactivation of the methanol catalyst and the elimination of the strong acid sites on the dehydration catalyst. The slower, long term deactivation of both catalysts are not directly related to the acid-base properties of the catalyst system, but to an interaction of yet uncertain nature. The initial deactivation of the methanol catalyst can be avoided by passivating the strong acid sites on a dehydration catalyst. Furthermore, except for the initial deactivation of the dehydration catalyst, both catalysts can be stable if the intimate contact between them can be avoided. Efforts and progress are being made to improve the stability of the catalyst system based on this understanding.

REFERENCES

1. B. Bhatt, DOE Topical Report under Contract No. DE-AC22-90PC89865, 1992.

2. A. M. Rouhi, C&E News, May 29, 1995, p. 37.

3. B. A. Toseland, R. P. Underwood, and F. J. Waller, Proceedings of 1994 DOE Contracts' Review Conference, p. 307.

4. M. Kuczynski, Ph.D. Thesis, University of Twente, Netherlands, 1986.

SYNTHESIS OF ACRYLATES AND METHACRYLATES FROM COAL-DERIVED SYNGAS

James J. Spivey[1], Makarand R. Gogate[1], Ben W. L. Jang[1], Eric D. Middlemas[2], Joseph R. Zoeller[2], Gerald N. Choi[3], and Samuel S. Tam[3]

[1]Research Triangle Institute, Research Triangle Park, NC 27709
[2]Eastman Chemical Company, Kingsport, TN 37662
[3]Bechtel, San Francisco, CA 94119

CONTRACT NUMBER DE-ACC22-94PC94065

PERIOD OF PERFORMANCE 10-1-94 to 9-30-97

BACKGROUND

Acrylates and methacrylates are among the most widely used chemical intermediates in the world. One of the key chemicals of this type is methyl methacrylate. Of the 4 billion pounds produced each year, roughly 85% is made using the acetone-cyanohydrin process, which requires handling of large quantities of hydrogen cyanide and produces ammonium sulfate wastes that pose an environmental disposal challenge. There is a clear need to develop a process that is both environmentally benign and cost-competitive. In addition, the use of coal-derived syngas to synthesize this high-value chemical allows this abundant domestic resource to be utilized more productively.

The U.S. Department of Energy and Eastman Chemical Company are sharing the cost of research to develop an alternative process for the synthesis of methyl methacrylate from syngas. Research Triangle Institute is focusing on the synthesis and testing of active catalysts for the condensation reactions, and Bechtel is analyzing the costs to determine the competitiveness of several process alternatives. The overall process to generate methyl methacrylate consists of three steps: (1) dehydrogenation *or* partial oxidation of methanol to produce formaldehyde:

$$CH_3OH \quad <==> \quad HCHO + H_2 \qquad (1a)$$
$$CH_3OH + \tfrac{1}{2} O_2 \quad <==> \quad HCHO + H_2O \qquad (1b)$$

(2) condensation of formaldehyde with a propionate (which, in turn, is derived from C_2's) to produce methacrylic acid, and (3) esterification of methacrylic acid with methanol to produce methyl methacrylate. The third step, esterification, is well-established and does not pose a challenge for process demonstration and development. The focus of this project is on the first two steps.

The keys to a successful process are (a) a catalyst for the synthesis of the propionate from C_2-feedstocks (such as ethylene), and (b) balancing the production of formaldehyde (from methanol) with the condensation reaction. Step (b) is to be carried out in a slurry reactor

into which methanol, oxygen (for reaction (1b)), and the propionate are introduced. The methyl methacrylate product is drawn off as a vapor. The advantages of slurry reactor include a nearly isothermal operation and flexibility of catalyst type. Commercially, a bubble column slurry reactor would be used, allowing a significantly higher catalyst-slurry loading, and minimizing power consumption and moving agitator parts.

Results thus far show that the catalysts for the condensation of formaldehyde and the propionate are key to selectively producing the desired product, methacrylic acid, with a high yield. These condensation catalysts have both acid and base functions and the strength and distribution of these acid-base sites controls the product selectivity and yield. We are developing a predictive relationship between the acid-base nature of the catalysts and the yield of methacrylic acid/methyl methacrylate.

OVERALL CHEMISTRY FOR METHYL METHACRYLATE SYNTHESIS

The synthesis of methyl methacrylate involves the following three steps:

(1) Synthesis of a propionate, in this case, propionic acid or propionic anhydride.
(2) Condensation of propionate with formaldehyde to produce methacrylic acid.
(3) Esterification of methacrylic acid with methanol to produce methyl methacrylate.

Two processes, one via propionic acid and one via propionic anhydride, are shown below, including a comparison of the current and novel routes (developed in this effort by Eastman Chemical) to produce the propionate (Step (1), above).

Methyl Methacrylate Synthesis Via Propionic Acid

Step 1. Synthesis of Propionic Acid

$H_2C{=}CH_2$ + CO + H_2 ==> CH_3CH_2CHO (1)
(ethylene) (hydrogen) (propionaldehyde) **... current**

CH_3CH_2CHO + $\frac{1}{2}\ O_2$ ==> CH_3CH_2COOH
(propionaldehyde) (oxygen) (propionic acid)

$H_2C{=}CH_2$ + CO + H_2O ==> CH_3CH_2COOH **... novel** (2)
(ethylene) (water) (propionic acid)

Step 2. Condensation of Propionic Acid with Formaldehyde

$EtCO_2H$ + HCHO ==> $CH_2{=}C(CH_3)COOH$ + H_2O (3)
(propionic acid) (formaldehyde) (methacrylic acid) (water)

Step 3. Esterification of Methacrylic Acid with Methanol

$CH_2=C(CH_3)COOH + CH_3OH \Longrightarrow CH_2=C(CH_3)COOCH_3 + H_2O$ (4)
(methacrylic acid) (methanol) (methyl methacrylate) (water)

Methacrylic Acid Synthesis Via Propionic Anhydride

Step 1. Synthesis of Propionic Anhydride

$2\ EtCO_2H + Ac_2O \Longleftrightarrow AcOH + (EtCO)_2O$ **... current** (5)
(propionic acid) (ac. anhydride) (ac. acid) (pr. anhydride)

$EtCO_2H + CO + H_2C=CH_2 \Longrightarrow (EtCO)_2O$ **... novel** (6)
(propionic acid) (ethylene) (pr. anhydride)

Step 2. Condensation of Propionic Anhydride with Formaldehyde

$(EtCO)_2O + HCHO \Longrightarrow CH_2=C(CH_3)COOH + EtCO_2H$ (7)
(pr. anhydride) (formaldehyde) (methacrylic acid) (pr. acid)

Step 3. Esterification of Methacrylic Acid with Methanol

$CH_2=C(CH_3)COOH + CH_3OH \Longrightarrow CH_2=C(CH_3)COOCH_3 + H_2O$ (4)
(methacrylic acid) (methanol) (methyl methacrylate) (water)

Note that reaction (7) produces both methacrylic acid and propionic acid in equimolar amounts. The propionic acid this produced would react further with formaldehyde (reaction (3)) to produce a second mole of methacrylic acid, which is then esterified (reaction (4)).

SYNTHESIS OF PROPIONATES

Minimizing the cost of propionate synthesis, and therefore that of methyl methacrylate (MMA), is a key part of the research since the first step in the generation of methacrylates is the generation of the propionate. Work thus far has focused on the development of a new highly active, low-cost, proprietary catalyst for this process which may replace existing catalysts, which are based upon either expensive Pt group metals (i.e., Rh) or the highly toxic nickel carbonyl. The initial focus has been the development of a propionic anhydride process based on the following reaction:

$$EtCOOH + H_2C=CH_2 + CO \Longrightarrow (EtCO)_2O \quad (8)$$

The process is also amenable to the production of propionic acid and its esters using a similar chemistry. Typically, the reaction (8) above is performed at a pressure of 400-1000 psig and temperature of 140-200°C using a gas mixture consisting of ethylene and carbon monoxide which contains ca. 5-10% hydrogen (to maintain the catalyst in an active state).

The reaction has been observed to run at rates as high as 5-6 moles/L-h. However, at these high reaction rates, the reaction is mass transfer limited with the existing equipment. Most reactions in this study are run at slower reaction rates (typically in the range of 0.5 to 2.5 moles/L-h) to avoid this limitation. The reaction is carried out in a batch autoclave with a ratio of propionic acid to catalyst of 300-1200:1. Reaction rates are constant with time until conversions of 75-85% are achieved at which time the reaction rate decreases.

In-Situ Spectroscopic Probes. In-situ spectroscopic probes indicate the simultaneous presence of the following three catalyst phases under reaction conditions:

M-CO, M-X^-, and MX_2

where M = catalyst and X = an anionic component. Further studies indicate that the dominant phases, M-CO and M-X^-, are in equilibrium with each other as indicated in reaction (9) below:

$$M\text{-}CO + X^- \;\text{<==>}\; M\text{-}X^- + CO \qquad (9)$$

In the absence of hydrogen, the entire catalyst is rapidly oxidized to MX_2, but the equilibrium mixture of reduced species is regenerated by the addition of hydrogen. Although the reaction proceeds in the absence of hydrogen, it is quite sluggish, and it usually stops prior to reaching high conversions.

Byproduct Determination. The reaction to form propionic anhydride is generally very selective, giving small quantities (<2%) of ethyl propionate, which is likely to be eventually converted to propionic anhydride in a continuous process. However, closer examination of byproducts by GC-MS reveals the presence of small quantities of 3-(4-hexanonyl) propionate (EtC(=O)CH(OOCEt)Et) and 5-ethyl-1-hydro-2-furanone (or an olefinic isomer thereof). These byproducts provide key insights into the reaction mechanism since both of these species represent reactions of a propionyl radical ($Et(CO)^\cdot$). The first product is coupling of the propionyl radical to form 3,4-hexanedione. The dione is a oxidant, and can be reduced by the components of the catalytic system to give 3-(4-hexanonyl) propionate, ultimately forming MX_2.

Kinetics. Kinetic studies have been run in the range of 0.5 to 2.5 moles/L-h to avoid the mass transfer related complications. To maintain consistent gas compositions in the head space of our reactor, a system equipped with a gas purge is used for the kinetic studies. We obtained the reaction rate orders on the catalyst level (M, in reaction (9) above), and the partial pressures of CO, EtX, X^-, hydrogen, and ethylene. These rate orders are:

Component	Experimental Reaction Order
M	0.62
EtX	0.54
X^-	1.00
CO	- 1.12
hydrogen	0.05* (*still under investigation).
ethylene	0.06

Mechanism. The mechanism of propionic anhydride formation from carbon monoxide, ethylene, and propionic acid has been formulated as follows:

$$^{\bullet}M(CO)^{-} + HX \quad ==> \quad ^{\bullet}M(CO)^{-}H + I^{-} \qquad (10)$$

$$^{\bullet}M(CO)^{-}H + H_2C{=}CH_2 \quad ==> \quad (Et\text{-}M\text{-}CO)^{\bullet} \qquad (11)$$

$$(Et\text{-}M\text{-}CO)^{\bullet} + CO \quad ==> \quad (EtCO\text{-}M\text{-}CO)^{\bullet} \qquad (12)$$

$$(EtCO\text{-}M\text{-}CO)^{\bullet} + X^{-} \quad <==> \quad ^{\bullet}(EtCOM\text{-}X)^{\bullet} + CO \qquad (13)$$

There is some evidence for the hydride process also since when the reaction is run in the absence of hydrogen, it is spontaneously evolved. If our catalyst follows the pathways described for catalysts such as Ir and Rh, it is likely that there are several pathways generating the catalyst-ethyl complex operating simultaneously (see P.R. Ellis, J.M. Pearson, A. Haynes, H. Adams, N.A. Bailey, and P.M. Maitlis, *Organometallics*, **13**, 3215(1994) and references cited therein.)

Refinements to the Kinetic and Mechanistic Model. Several probe reactions have been used to study the mechanism of the propionate synthesis catalyst. These studies are important in minimizing the cost of the propionate synthesis, and therefore that of MMA. Typical methylcyclopentanyl radical forming probes failed since isomerization of the olefinic-halide substrates was more rapid than the free radical initiation process. However, benzyl bromide proved to be a good probe. Using stoichiometric quantities of M(CO)X and benzyl bromide in diglyme and in absence of added CO, bibenzyl is the major product (from radical coupling). Equally important, significant quantities of phenylacetates, particularly benzyl phenylacetate and $PhCH_2CO_2CH_2CH_2OCH_2CH_2OCH_3$ (from reaction with solvent), are produced.

The presence of bibenzyl indicates that there are free radicals generated, but the presence of phenylacetates indicates that the free radicals may (and probably do) subsequently interact with the metal carbonyl complexes. This suggests that carbonylation of the radical likely occurs by subsequent attachment to a metal carbonyl, and not by direct carbonylation of the free radical as initially proposed since benzyl radicals are known to be refractory to direct carbonylation.

CONDENSATION CATALYSIS

Catalyst Synthesis. The synthesis of methyl methacrylate in one reactor depends on an active and selective catalyst for the condensation of formaldehyde with either propionic acid [reaction (3)] or propionic anhydride [reaction (7)]. The literature on the synthesis of methacrylic acid deals with the condensation of propionic acid and methyl propionate with formaldehyde [2, 4-8], and *not* with propionic anhydride. Because the anhydride route (a) does not prouce water (which can degrade the product and kinetically inhibit the reaction) and (b) produces a more easily separated product mix, initial efforts have focused on the catalytic condensation of propionic *anhydride* with formaldehyde [1]. However, the activity and selectivity of the catalysts developed here for the condensation of the anhydride must be compared to those for the acid to deteremine if the anhydride route [reactions (5)-(7) and (4)] is competitive with the conventional acid route [reactions (1)-(4)]. All the catalysts developed here are currently a matter of *patented proprietary information.*

Reported work on the condensation of propionic acid with formaldehyde can be divided into polymetal oxide catalysts, and other metal oxides on inert and active supports like the alkalized aluminas and silica-aluminas. Research on polymetal oxides is summarized in Table I.

Table I. Condensation of Propionic Acid with Formaldehyde on Polymetal Oxide Catalysts

Catalyst[1]	Atomic Ratio	Temp (deg C)	Yield (mol%)[2]
M_1-M_2-M_3	1/1.0	330	38
M_1-M_2-M_3	1/2/1.2	340	3
M_1-M_2-M_3	1/2/2.2	330	51
M_1-M_2-M_3	1/2/5.5	290	28
M_1-M_2-M_3	1/2/5.5	290	36
M_1-M_2-M_3	1/2/6.5	310	41
M_1-M_2-M_3	1/2/3.5	310	26
M_1-M_2-M_3	1/2/4.4	290	19
M_1-M_2-M_3	1/2/3.3	300	27
M_1-M_2-M_3	1/2/3.3	320	14

[1]M_1-M_2-M_3 are combinations of metal oxides; [2]Yield (mol%) of methacrylic acid based on charged HCHO, i.e., mole of methacrylic acid in the product/mole of HCHO charged x 100%; feed rates PA:HCHO:N_2 = 30-15-350 mmol/h; space velocity 448 cc/h/g-cat.

Based on Table I, at a 2:1 mole ratio of charged propionic acid to formaldehyde, the maximum yield of methacrylic acid based on charged HCHO is about 50%. [At the 2:1 feed ratio of propionic acid to formaldehyde, this corresponds to a 25% yield based on propionic anhydride charged.] The conversion of HCHO under these conditions is about 80%.

Catalysts other than poly metal oxide catalysts have also been tested for the condensation of propionic acid and formaldehyde. Results are summarized in Table II.

Based on Table II, the maximum yield of methacrylic acid based on charged HCHO is ca. 60% (corresponding to 30% yield based on charged propionic acid). Maximum conversions of propionic acid and formaldehyde are ca. 40% and 70%, respectively. However, unlike the results shown in Table I, these results are for a wide range of space velocities.

Table II. Catalyst Performance for Condensation of Propionic Acid with Formaldehyde, Supported Metal Catalysts

Catalyst	PA/HCHO[1] mol ratio	PA Conv. (%)	HCHO Conv. (%)	MAA Yield mol% on PA	MAA Yield mol% on HCHO
M/SiO_2	10	-	68.0	5.4	54.3
M/SiO_2	1.0	34.0	39.0	24.1	24.1
M/SiO_2	1.0	24.1	-	13.3	13.3
M/SiO_2	1.5	32.1	-	10.0	29.3
M/Al_2O_3	0.5	27.3	-	23.3	11.7
M_1+M_2/SiO_2	0.5	33.7	-	27.8	13.9
M_1+M_2/SiO_2	1.5	40.7	61.3	31.5	47.2
$M_{1x}M_{2y}$	2.0	38.1	-	31.3	62.4
$M_{1x}M_{2y}$	1.4	40.0	-	33.1	44.8

[1]PA = propionic acid, HCHO = formaldehyde, MAA = methacrylic acid. Reaction Conditions ca.: T = 300-350 °C, N_2(carrier)/PA mol ratio = 10-20.

These results provide a basis of comparison for catalysts developed in this work for thecondensation of propionic *anhydride*. Again, catalysts developed here are subject of *patented proprietary information.* The catalysts shown in Table III were studied here for the condensation of the anhydride. The catalysts from groups A, B, C, F, and G were prepared by the incipient wetness technique [3, 9]. The catalysts from groups D were prepared by co-precipitation. Catalysts from group E were synthesized by gel precipitation.

TABLE III. Summary of Condensation Catalysts for MAA Synthesis

Catalyst Group	Support	Additive(s)
A	Alumina	metals
B	Aluminosilicates	metals
C	Silica	metals
D	Silica	mixed metals
E	Titania	mixed metals
F	Silica	mixed metals
G	Magnesia	mixed metals

Characterization of Condensation Catalysts. The catalysts have been analyzed for metal content by inductively coupled plasma - optical emission spectrometry (ICP-OES). The catalysts from groups D, E, and F are observed to be amorphous, based on x-ray powder diffraction. The B.E.T. - N_2 surface area on a typical polymetal oxide synthesized in our laboratory is ca. 96 m^2/g. Pore size distribution and average pore size determination is currently in progress. This polymetal oxide is used to generate the reaction rate data, in terms of methacrylic acid yield and reactant conversions, summarized in Table V.

Catalyst Testing. The catalysts were tested for their condensation activity in a bench-scale gas-phase microreactor system. All tests thus far have been made on the condensation of propionic anhydride with formaldehyde, reaction (7) above. The reaction conditions are:

- T = 400 °C and 300 °C
- P = 2 atm
- F/W = 290-1200 cc/h/g-cat

A flow diagram of microreactor system is shown in Figure 1.

Results at 400 °C showed that propionic anhydride undergoes significant decarboxylation, forming carbon dioxide and 3-pentanone (diethyl ketone), as reported in the literature. Other results at 400 °C showed that our proprietary catalysts are active for methacrylic acid synthesis. Initial tests at 300°C have focused on a polymetal oxide catalyst with a specified atomic ratio. The results are summarized in Table IV . [Further tests on the catalysts are planned, including long term runs to examine the possible effect of changes in surface acidity on methacrylic acid yield.] The maximum yield of methacrylic acid, based on HCHO, is 77% at 290 cc/h/g-cat. At 1200 cc/h/g-cat, the yield on the same basis is 65%.

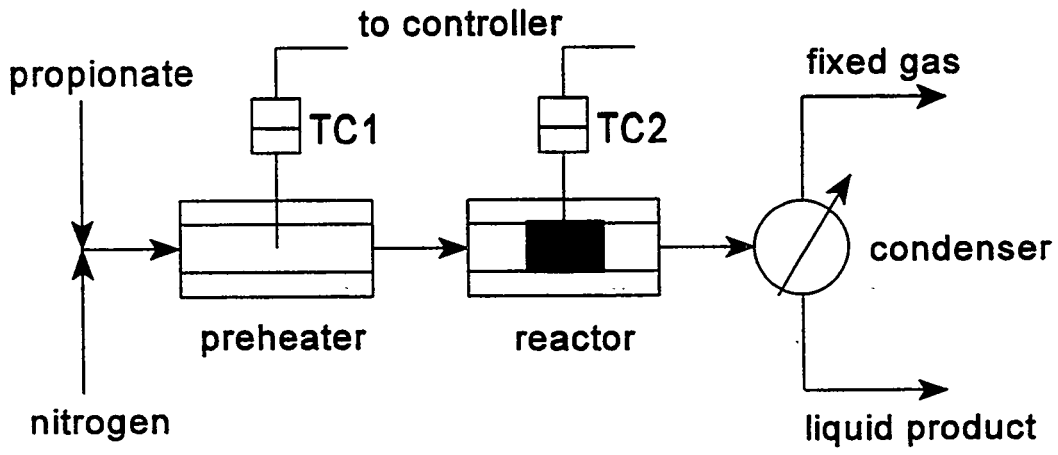

Figure 1. Schematic of Experimental Microreactor System.

Table IV. Condensation of Propionic anhydride with Formaldehyde[1]

Space velocity, cc/h/g-cat	PA Conv.[2]	MAA yield[3]	MAA yield[4]	MAA rate[5]	C balance on liquid products[6]
480	42.6%	36.4%	16.7%	0.868	83.5%
290	44.8%	76.8%	36.4%	1.251	88.2%
1200	43.8%	65.3%	30.6%	0.887	79.3%
900	28.2%	30.1%	14.1%	1.226	86.7%

[1]Reaction conditions: T = 300 C, P = 2 atm (30 psi in-house nitrogen), mole flow rates of propionic anhydride:formaldehyde:nitrogen = 40:20:220 mmol/h.
[2]Propionic acid conversion, (mol PAC out - 2 x mol PAN in) / (2 x mol PAN in) x 100.
[3]MAA yield based on charged HCHO, i.e., mol MAA/mol charged HCHO x 100.
[4]MAA yield based on charged propionic anhydride
[5]MAA rate, gmol/kg cat. h.
[6]The carbon balance reported here accounts for only the liquid products collected in a condenser downstream of the reactor. CO, CO_2, and unreacted formaldehyde are detected in the exit gas also, but are not quantified here.

A comparison of the results reported in the literature for the condensation of propionic acid and those for the anhydride in this study are shown in Table V.

Table V. Comparison of Catalysts for Condensation of Propionic Acid and Anhydride[1]

Space velocity, cc/h/g-cat	Catalyst (atomic ratio for M_1-M_2-M_3)	Temp, °C	PA/HCHO	PAA/ HCHO	MAA yield, based on HCHO	MAA yield, based on PA	MAA yield, based on PAA
448	x_1-x_2-x_3	330	2:1	---	51	25	---
NA	x_1-x_2-x_3	300-350	10:1	---	54	5.4	---
290	x_1-x_2-x_3	300	---	2:1	77	---	36
1200	x_1-x_2-x_3	300	---	2:1	65	---	31

[1]PA=propionic acid, PAA=propionic anhydride, MAA=methacrylic acid

These results, for catalysts that have not been fully characterized or optimized, show that yields of methacrylic acid from propionic anhydride are comparable and in some cases even superior to those reported in the literature for the acid. The yields do not approach, yet, to those likely needed for a commercially practical process, however. Further improvements in the yield, selectivity, and long-term activity are possible after a complete catalyst characterization and optimization, particularly in terms of the acid-base properties. These crucial studies constitute the focus of ongoing research effort.

SUMMARY

The development of a syngas-based process for the synthesis of methyl methacrylate depends on:

- the development of a cost-competitive process for the propionate. We have focused on the anhydride because of it produces a more easily separated product mix and eliminates a mole of water, which is a kinetic inhibitor.
- the development of an active and selective condensation catalyst for the anhydride.

Experimental results show that:

- the synthesis of propionic anhydride (via the acid) can be achieved using homogeneous catalysts for the reaction of ethylene, CO, and steam. The reaction appears to be a free radical process and hydrogen is needed to maintain the catalyst in a reduced state.
- the condensation of the anhydride can be catalyzed by catalysts based on those reported for the condensation of the acid, with comparable yields. Further improvements in these yields are needed for the process to produce methyl methacrylate to be commercially viable.

- We are developing a novel environmentally-benign cost-competitive process for the synthesis of methacrylates from syngas.
- Propionic anhydride is selected as the target propionyl intermediate moiety.
- The direct synthesis of propionic anhydride from propionic acid and ethylene (and hydrogen in some cases) is the most promising and economical route for propionic anhydride synthesis.
- Several amphoteric and acid catalysts have been tested in a bench-scale microreactor system for their activity in methacrylic acid synthesis from propionic anhydride and formaldehyde. The yield of methacrylic acid is 77% (based on charged HCHO) and a space velocity of 290 cc/h/g-cat, and 65% at 1200 cc/h/g-cat, which is comparable to that reported in the literature for the condensation of the acid.

REFERENCES

1. "Synthesis of Acrylates and Methacrylates from Coal-derived Syngas", Vol. 1 Proposal PRDA DE-RA-22-94PC94052, Submitted to U.S. DOE, June 20, 1994.
2. Ai, M, Personal Communication, 1995.
3. O.H. Bailey, R.A. Montag, and J.S. Yoo, *Applied Catalysis A: General*, **88** (1992) 163-177.

4. Ai, M., *J. Catal.*, **124** (1990) 293.

5. Ai, M., *J. Catal.*, **116** (1989) 231.

6. Katsumoto, K. and Marquis, D.M., U.S. Patent 4 132 670, Assigned to Chevron Research Co., 1979.

7. Schneider, R.A., U.S. Patent 3 864 280, Assigned to Chevron Research Co., 1975.

8. Ai, M., *Bull. Chem. Soc. Jpn.*, **63** (1990) 199.

9. Turk, B., Personal Communication, 1995.

TITLE: HYDRODYNAMIC MODELS FOR SLURRY BUBBLE COLUMN REACTORS

PI: Dimitri Gidaspow

STUDENT(s) Mitra Bahary, Ph.D. December 1994 and
Yuangxiang Wu, Ph.D. Candidate

INSTITUTION: Illinois Institute of Technology
Department of Chemical Engineering
IIT Center
Chicago, IL 60616
(312) 567-3045

GRANT NO. DE-FG22-94PC94208

PERIOD OF PERFORMANCE: June 1994 to June 1995

OBJECTIVE: The objective of this investigation is to convert our "learning gas-solid-liquid" fluidization model into a predictive design model. This model is capable of predicting local gas, liquid and solids hold-ups and the basic flow regimes: the uniform bubbling, the industrially practical churn-turbulent (bubble coalescence) and the slugging regimes. Current reactor models incorrectly assume that the gas and the particle hold-ups (volume fractions) are uniform in the reactor. They must be given in terms of empirical correlations determined under conditions that radically differ from reactor operation. In the proposed hydrodynamic approach these hold-ups are computed from separate phase momentum balances. Furthermore, the kinetic theory approach computes the high slurry viscosities from collisions of the catalyst particles. Thus particle rheology is not an input into the model.

WORK DONE AND CONCLUSIONS:
The IIT hydrodynamic model computes the phase velocities and the volume fractions of gas, liquid, and particulate phases. Model verification involves a comparison of these computed velocities and volume fractions to experimental values.

- A combination of X-ray and gamma-ray densitometers was used to measure the solids and the liquid volume fractions in a two dimensional bed in the bubble coalesced regime. There is a reasonable agreement between preliminary theoretical computations for an asymmetric distributor and the experiments.
- A high resolution micro-imaging/measuring system apparatus was used to measure instantaneous and time averaged particle velocities. The fluctuations of particle velocities around their average were found to be approximately Mawellian. The measured time averaged velocities compare reasonably well with the predicted velocities for an asymmetric distributor used in this study.

- A Brookfield viscometer was used to measure the "apparent" bed viscosity in two three-phase fluidized beds. The viscosities were also calculated from measurements of particle oscillations (granular temperature) using a high resolution micro-imaging/measuring system. To obtain these viscosities a dense phase kinetic theory formula derived in D. Gidaspow's book ("Multiphase Flow and Fluidization. Continuum and Kinetic Theory Descriptions," Academic Press, 1994) was used. There is an excellent agreement between the macroscopically measured viscosities using a Brookfield viscometer and those computed from particle fluctuations and collisions using kinetic theory.
- This comparison of viscosities computed from particle collisions and measured macroscopically and related viscosity measurements of gas-solid flow in a pipe, obtained by 3 methods, to be reported at the Miami 1995 AIChE meeting validates the proposed kinetic theory approach.
- Our computer code was modified to include reactions. A numerical simulation of synthesis of methanol in a G-L-S slurry reactor based on Air Products' LaPorte's Run E-2-B (1987) was carried on our HP700 Work-Station. We have computed the observed catalyst distribution and methanol production.
- After a discussion with DOE and Air Products representatives in late January 1994, we modified our computer code for computation with gas rather than liquid as a continuous phase to simulate Air Products RUN E-8.1 (1991). The results of this simulation presented in this paper show that the model predicts close to the experimentally observed gas-hold-up and the methanol production.

INTRODUCTION

Gas-liquid-solid fluidization systems are used in a variety of applications such as resid hydroprocessing, coal liquefaction or methanol production from syntheses gas in the presence of catalyst, biological wastewater treatment and fermentation (Fan, 1989). Overall three-phase fluidized bed behavior, bubble motion and breakage have been experimentally studied by a number of researchers (Fan, 1989; Kim et al., 1985; Henrickson and Ostergaard, 1974). Shah, et al. (1982) have reviewed flow regimes: bubble flow, slug flow, and churn-turbulent flow, depending on the column diameter and the superficial gas velocity. However, recent reviews by Fan (1989), Tarmy and Coulaloglou (1992) show that there exist no hydrodynamic models for three-phase fluidized beds in the literature.

In this paper a three fluid model is presented that predicts the gas, liquid and solid hold-ups (volume fractions) and flow patterns in the bubbly and in the industrially important churnturbulent (bubble coalesced) regimes. The input into the model can be either particulate viscosities as measured with a Brookfield viscometer, or derived using the mathematical techniques of kinetic theory of granular flows pioneered by Savage (1983), Jenkins and Collaborators for particulate flows without an interstitial fluid. The kinetic theory is described in three chapters in a book by Gidapow (1994).

HYDRODYNAMIC MODEL

The physical principles used are the laws of conservation of mass and momentum for the gas, the liquid and the solid phases, as shown in Table 1. The constitutive equations for the stress are shown in Table II.

COMPARISON OF COMPUTATIONS TO IIT EXPERIMENT

The hydrodynamic model was used to compute gas-liquid-solid flows in the dispersed and in the free bubbling regions (Gidapow, et al. 1994). A two dimensional bed shown in Figure 1 was constructed at IIT to operate in the dispersed flow regime. Figure 2 shows bubble coalsence in the bed and Figure 3 shows the computed time average volume fractions of 800 μm glass beads. The computations were made for an asymmetric distributor depicted in Figure 3. A combination of X-ray and gamma ray densitometers were used to obtain the hold up.

A digital camera technique was developed to measure particle velocities. It involves a measurement of a particle streak on a computer monitor for a millisecond time interval (Baharry, 1994). Figure 6 shows a typical measured velocity distribution. A fit of the data to a Maxwellian or normal probability distribution gives the mean and the fluctuating velocity distributions. Figure 7 gives a comparison of these values to the computed velocities.

PARTICULATE VISCOSITY FROM KINETIC THEORY

The variance obtained from data such as depicted in Figure 6 gives the granular

temperature. Gidaspow (1994) reviews this theory. Table 3 shows a comparison of the computed viscosity using the measured granular temperature and the theoretical formula to the viscosity obtained from a Brookfield viscometer. The agreement is excellent.

REACTION MODEL

A reaction model for production of methanol using an approach similar to that described in the Vikings System (1993) report was added to the hydrodynamic computer code. The first computer run described in our first quarterly report involved a simulation of early Air Products systems in which a liquid flowed continuously through the reactor like the IIT experiment described in the previous section. Our computations agreed with Air Products methanol production. We had also computed solids hold-up that agreed with data obtained at Air Products using a nuclear gauge. Since the new Air Products design involves no liquid recirculation but is like a batch system with only gases entering and leaving the reactor, we changed our hydrodynamic model to operate with gas as a continuous phase. We simulated Run E8. of Air Products and Chemicals (1991).

Table 4 shows the reaction model. Figure 8 depicts the grid used. The obstacles shown represent heat exchangers. At this stage we assumed isothermal operation. Typical flow patterns are shown in Figure 9. Figure 10 gives the computed time average area averaged liquid, gas and solids volume fractions. The gas solid-up is close to that reported by Air Products (1991). Table 5 shows a good comparison of IIT's simulation to Air Products data for Run E8.1. Figure 11 shows the time and area averaged gas profiles along the reactor height.

ACKNOWLEDGEMENT

This work was partially supported by the National Science Foundation, grant No. CTS-9305850.

REFERENCES CITED:

Air Products and Chemicals, Inc., "Liquid-Entrained Catalyst Operations at LaPorte Methanol Process 1984-1985", Final Report to DOE for Contract No. DE-AC-22-81PC300019 (1987)

Air Products and Chemicals, Inc., "Liquid Phase Methanol LaPorte Process Development Unit: Modification, Operation, and Support Studies", Draft Report to DOE for Contract No. DE-AC22-87PC90005 (1991).

Air Products and Chemical, Inc., "Synthesis of Dimethyl Ether and Alternative fuels in the Liquid Phase from Coal-Derived Synthesis Gas", Topical Report to DOE for Contract No. DE-AC222-90PC89865 (1992).

Baha: ry, M. (1994) Experimental and Computational Studies of Hydrodynamics of Three-phase Fluidization, Ph.D Thesis, Illinois Institute of Technology, Chicago, Illinois.

Fan, L.S. (1989). Gas-Liquid-Solid Fluidization Engineering, Butterworths, Boston.

Gidaspow, D. (1994). Multiphase Flow and Fluidization. Continuum and Kinetic Theory Descriptions. Academic Press, Boston.

G.H. Graff, J.G.M. Winkelman, E. J. Stamhuis and A.A.C.M. Beenachers, "Kinetics of the Three-Phase Methanol Synthesis, "Chem. Eng. Sci., Vol. 43, No. 8, P2161-68 (1988)

Henriksen, H.K., and Ostergaard, K. (1974). On the Mechanism of Large Bubbles in Liquid and Three Phase-Fluidized Beds. Chem. Engng. Sci., 29, 626.

Hetzler and Williams, (1969). Fluidized Bed Viscosity and Expansion, Correlated With Glass Forming liquid Model, I & EC Fund., 666-677.

Jenkins, J.T., and Savage, S.B. (1983) A Theory for the Rapid Flow of Identical, Smooth, Nearly Elastic, Spherical Particles. J. Fluid Mech., 130, 187-202

Kim, S.D., Baker, C.G.J and Bergougnou, M.A. (1975). Phase Holdup Characteristics of Three Phase Fluidized Beds, Can. J. Chem Engng., 53, 134.

Savage S.B. Granular Flows at High Shear Rates. Theory of Dispersed Multiphase Flows (ed. R.E. Meyer). Academic Press, 39-358 (1983).

Seo, Y.C. and Gidaspow, D. "An x-ray gamma-ray Method of Measurement of Binary Solids Concentrations and Voids in Fluidized Beds. I & EC Research, 26 1622-1628 (1987).

Shah, Y.T., B.G. Kelkar and S.P. Godbole, "Design Parameters Estimations for Bubble Column Reactors," AIChE J. 28, 353-379 (1982).

Tamry, B.L. and C.A. Coulaloglou, "Alpha-Omega and Beyond. Industrial Veiw of Gas/Liquid/Solid Reactor Development," Chem. Eng. Science, 47, 3231-3246 (1992).

Viking Systems International Report to DOE/PETC (1993) "Design of Slurry Reactor for Indirect Liquefaction Applications."

Table 1 Conservation Equations

Continuity Equation for phase k (=g, l, s)

$$\frac{\partial}{\partial t}(\varepsilon_k \rho_k) + \nabla \cdot (\varepsilon_k \rho_k \mathbf{v}_k) = m_k$$

Momentum Equations

(a) Gas Phase (Continuous Phase)

$$\frac{\partial}{\partial t}(\varepsilon_g \rho_g \mathbf{v}_g) + \nabla \cdot (\varepsilon_g \rho_g \mathbf{v}_g \mathbf{v}_g) = -\nabla p + \rho_g \mathbf{g} + \sum_{m=\ell,s} \beta_{gm}(\mathbf{v}_m - \mathbf{v}_g) + \nabla \cdot [\tau_g] + m_g \mathbf{v}_g$$

(b) Liquid and Solid Phases k (=l, s) (Dispersed Phases)

$$\frac{\partial}{\partial t}(\varepsilon_k \rho_k \mathbf{v}_k) + \nabla \cdot (\varepsilon_k \rho_k \mathbf{v}_k \mathbf{v}_k) = -\nabla P_k + \frac{\varepsilon_k}{\varepsilon_g}(\rho_k - \sum_{m=g,\ell,s} \varepsilon_m \rho_m)\mathbf{g} + \sum_{m=g,\ell,s,m\neq k} \beta_{km}(\mathbf{v}_m - \mathbf{v}_k) + \nabla \cdot [\tau_k] + m_k \mathbf{v}_k$$

Table 2 Drag Coefficients, Shear Stresses, Solid Pressure. k = l, s

For $\varepsilon_g < 0.8$, (based on Ergun equation)

$$\beta_{gk} = \beta_{kg} = 150\frac{(1-\varepsilon_g)\varepsilon_k \mu_g}{(\varepsilon_g d_k \psi_k)^2} + 1.75\frac{\rho_g \varepsilon_k |\mathbf{v}_g - \mathbf{v}_k|}{\varepsilon_g d_k \psi_k}$$

For $\varepsilon_g > 0.8$, (based on empirical correlation)

$$\beta_{gk} = \beta_{kg} = \frac{3}{4} C_D \frac{\rho_g \varepsilon_k |\mathbf{v}_g - \mathbf{v}_k|}{d_k \psi_k} \varepsilon_g^{-2.65}$$

$$\beta_{\ell s} = \beta_{s\ell} = \frac{3}{2}\alpha_{\ell s}(1+e)\frac{\rho_s \rho_\ell \varepsilon_s \varepsilon_\ell |\mathbf{v}_\ell - \mathbf{v}_s|}{\rho_s d_s^3 + \rho_\ell d_\ell^3}(d_s + d_\ell)^2$$

$$\tau_g = \varepsilon_g \mu_g \left\{ [\nabla \mathbf{v}_g + (\nabla \mathbf{v}_g)^T] - \frac{2}{3}\nabla \cdot \mathbf{v}_g \mathbf{I} \right\}$$

$$\tau_k = \mu_k [\nabla \mathbf{v}_k + (\nabla \mathbf{v}_k)^T] - \frac{2}{3}\mu_k \nabla \cdot \mathbf{v}_k \mathbf{I}$$

$$\nabla P_k = G(\varepsilon_k)\nabla \varepsilon_k$$

Where

$$C_D = \begin{cases} \frac{24}{Re_k}(1 + 0.15 Re_k^{0.687}) & Re_k < 1000 \\ 0.44 & Re_k > 1000 \end{cases}$$

$$Re_k = \frac{\rho_g \varepsilon_g |\mathbf{v}_g - \mathbf{v}_k| d_k \psi_k}{\mu_g} \qquad e = 0.9999 \qquad \alpha_{\ell s} = 0.5$$

$$G(\varepsilon_k) = 10^{8.76\varepsilon_k - 0.27} \quad (\text{dynes/cm}^2) \qquad \mu_s = 5.0\varepsilon_s$$

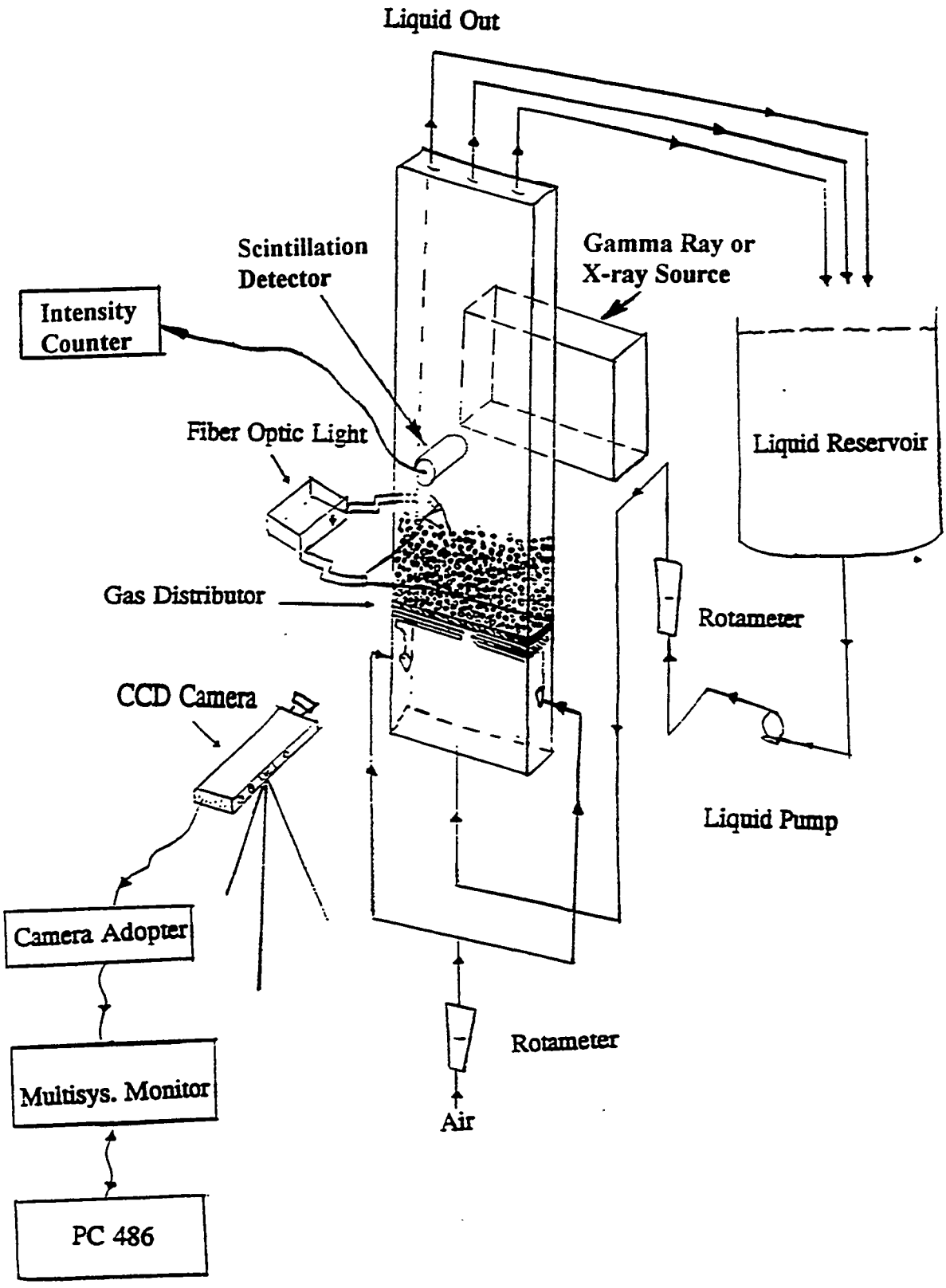

Figure 1 Three Phase 2-D Bed Apparatus at IIT

Table 3 Viscosity Measurements

$$\mu_s = \frac{2\mu_{dil}}{(1+e)g_0}\left[1+\frac{4}{5}(1+e)g_0\varepsilon_s\right]^2 + \frac{4}{5}\varepsilon_s^2\rho_s d_s(1+e)g_0\left(\frac{\theta_s}{\pi}\right)^{1/2}$$

where: $\mu_{dil} = \frac{5\sqrt{\pi}}{96}\rho_s d_s\sqrt{\theta_s}$ $\quad g_0 = \left[1-\left(\frac{\varepsilon_s}{\varepsilon_{s,max}}\right)^{1/3}\right]^{-1}$

ε_s	g_0	$\theta_s(cm^2/s^2)$ Velocity Measurement	μ_s(poise) Velocity Measurement	μ_s(poise) Brookfield Viscometer
0.346	5.39	845	4.26	4.359
0.272	4.03	435	2.947	3.125

Fig. 2 Photograph of Bubble Coalescence in a G-L-S Fluidized Bed (V_g=3.37 cm/s, V_l=2.03 cm/s)

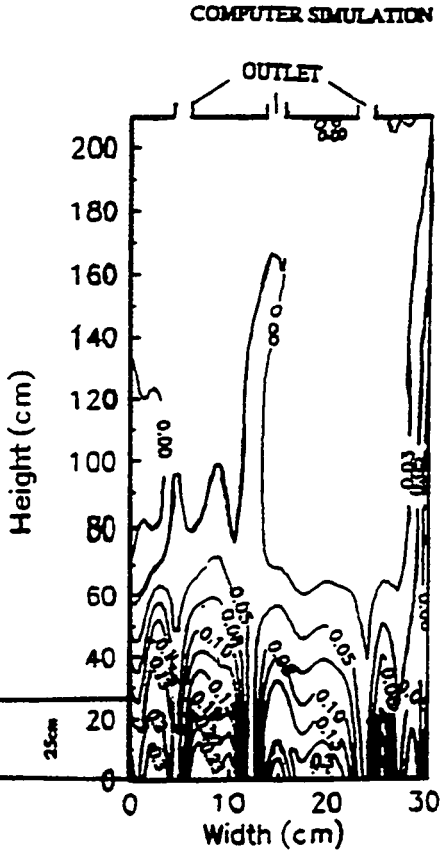

Fig. 3 Computed Time Average Volume Fraction Contours for Solid Phase.

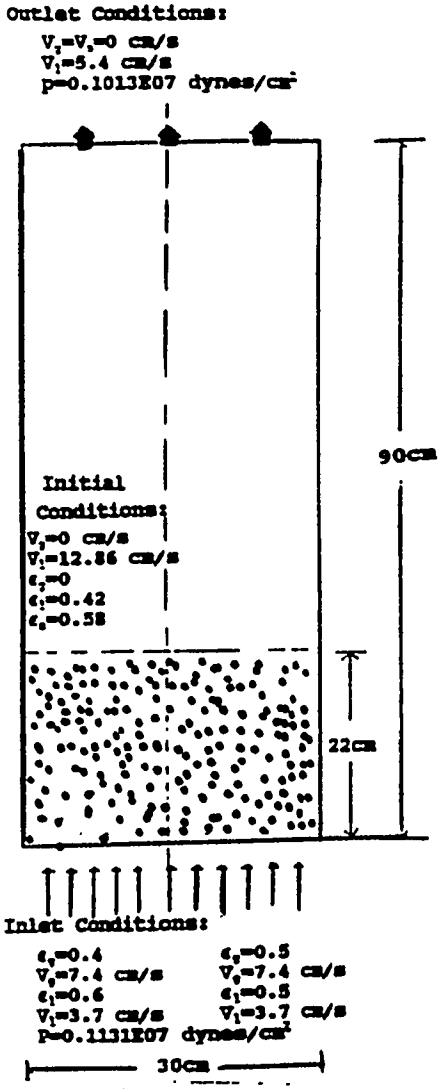

Asymmetric

Fig. 4 System for Simulation of Three Phase Fluidized with Dimensions and Conditions

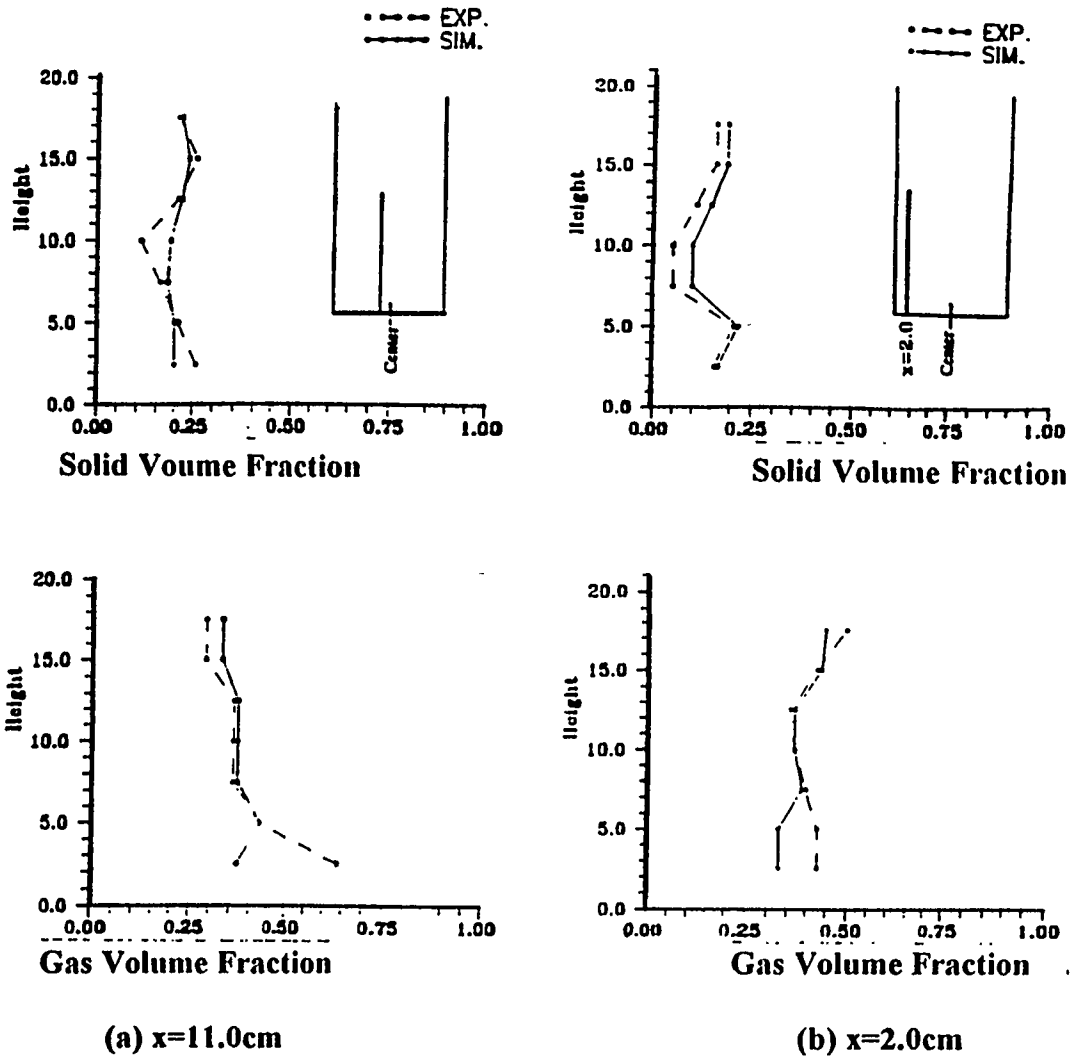

Figure 5 Comparison of Computed and Experimental Time Average Volume Fractions at (a) x=11.0cm and (b) x=2.0cm.

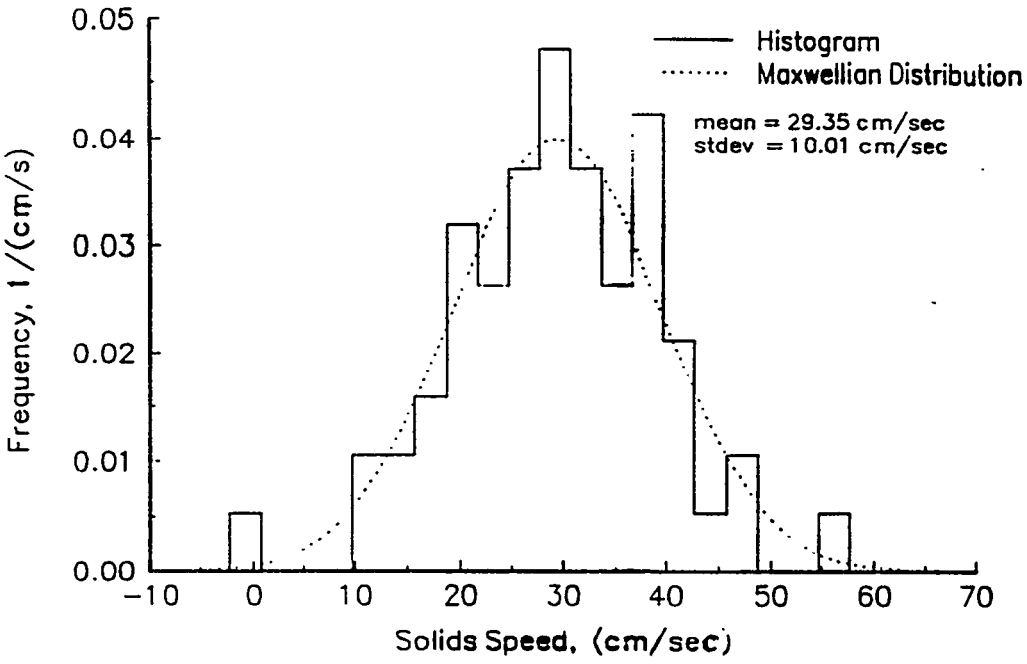

Fig. 6 Distribution of mean solid speed at x=4 cm and y=4.5 cm for liquid-solid-gas system with V_l=4 cm/s and V_s=3.36 cm/s.

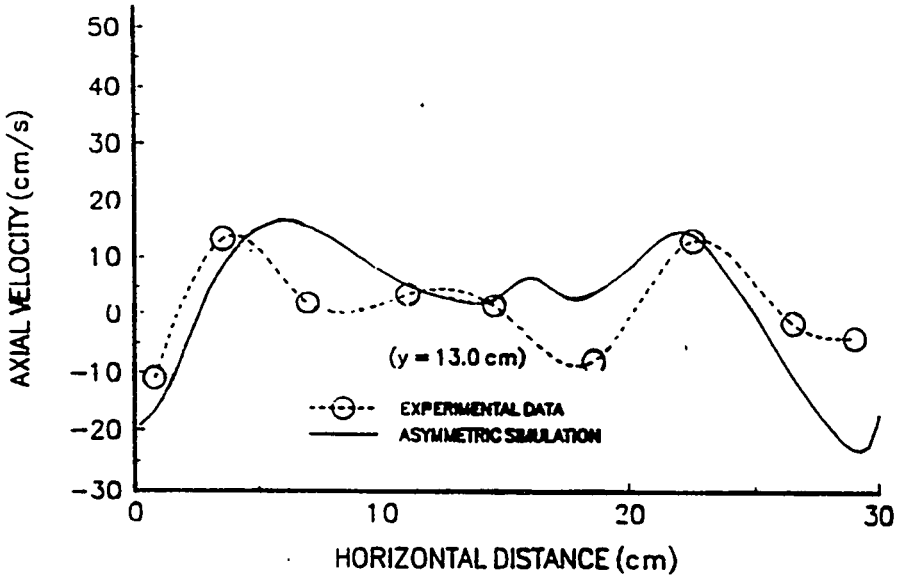

Fig. 7 Comparison of experimental and computed results for solid velocity profile at y=13 cm.

Table 4 Reaction and Species-Balances

$$CO + 2H_2 = CH_3OH$$

Overall rate expression:(Air Products 1992)

$$r = K \cdot f_{CO}^{1/3} \cdot f_{H_2}^{2/3} \left(1 - \frac{f_{MEOH}}{K_{eq} f_{CO} f_{H_2}^2} \right)$$

Mass transfer between gas and liquid:

$$R_i = K_{\ell i} a \left(C_i^{g\ell} - C_i^{\ell} \right)$$

$$K_{\ell i} a = 0.3 \rightarrow 1.3 \quad (1/s) \text{ (Ledakowicz 1984 and Viking 1993)}$$

Henry's law and constants (Graaf 1988):

$$C_i^{g\ell} = \frac{f_i}{H_i}$$

$$H_{CO} = 0.175 \exp(638 / RT)$$

$$H_{CO_2} = 0.402 \exp(-6947 / RT)$$

$$H_{H_2} = 0.0782 \exp(4875 / RT)$$

$$H_{CH_3OH} = 1.49 \exp(-17235 / RT)$$

Species balance in gas phase:

$$\frac{\partial}{\partial t}(\varepsilon_g \rho_g y_i) + \nabla \cdot (\varepsilon_g \rho_g v_g y_i) = \frac{\alpha_i \varepsilon_s \rho_s M_i r}{3.6 \times 10^6} - \varepsilon_\ell M_i R_i$$

Species balance in liquid phase:

$$\frac{\partial}{\partial t}(\varepsilon_\ell \rho_\ell x_i) + \nabla \cdot (\varepsilon_\ell \rho_\ell v_\ell x_i) = \varepsilon_\ell M_i R_i$$

$$\sum y_i = 1 \qquad \sum x_i = 1$$

$i =$	CO	H_2	CH_3OH	N_2	CO_2
$\alpha_i =$	−1	−2	1	0	0

Table 5 Comparison of IIT's Simulation and LaPorte's RUN E-8.1

	CO Conv. (%)	ε_g gas holdup	slurry height (inches)	total catalyst (kg)	CH_3OH (gmol/hr/kg)	net CH_3OH (TPD)
Simulation	14.24	26.9	215	740	16.93	9.62
RUN E-8.1	13.50	29.5	200	567	20.50	10.03

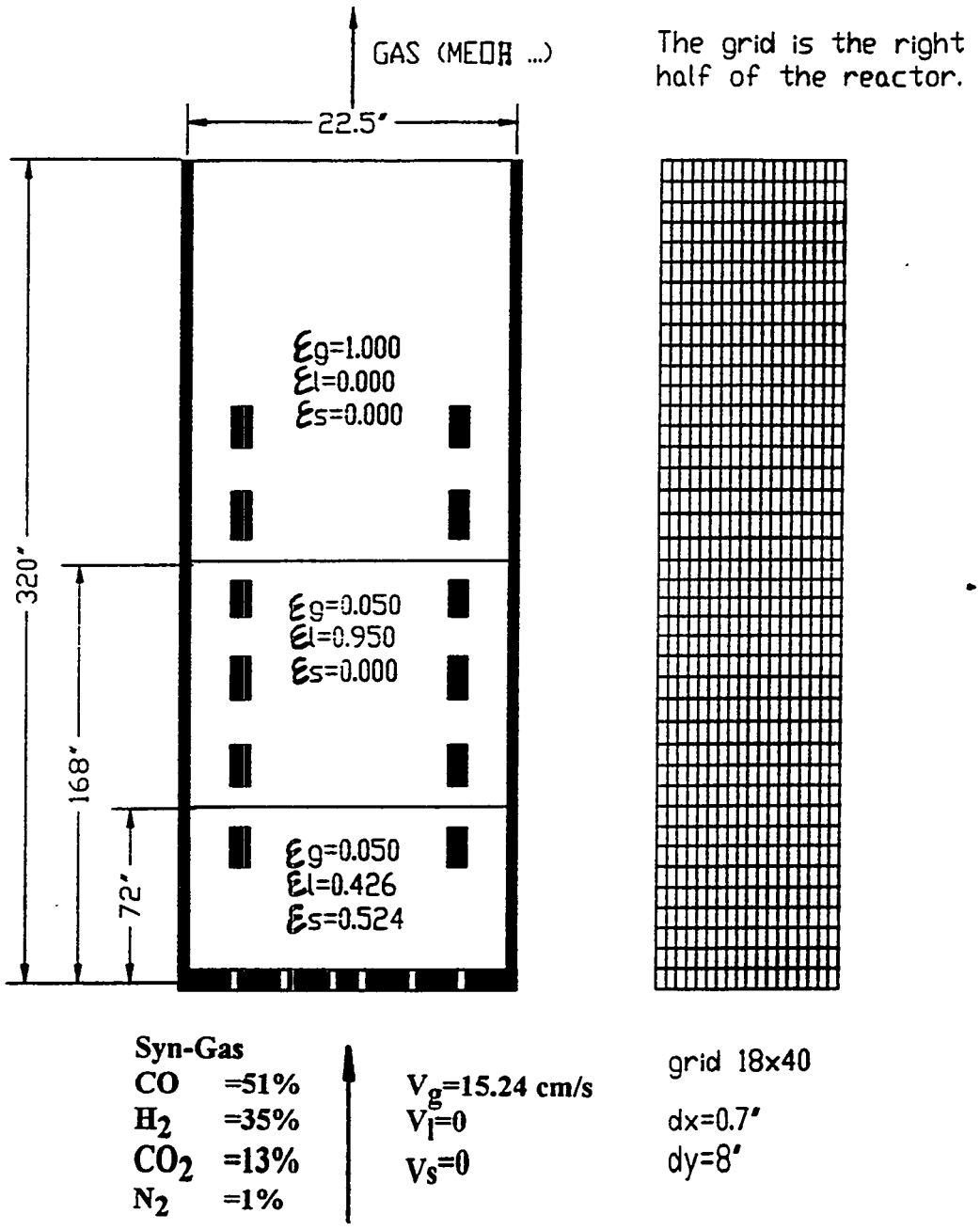

Fig. 8 Reactor and Grid with Inlet and Initial Conditions

(P=753.2 psig, T=250.3 ^{o}C, $d_p = 50\mu m$, $\rho_s = 3.011\ {}^{g}/_{cm^3}$, $\rho_\ell = 0.70025\ {}^{g}/_{cm^3}$)

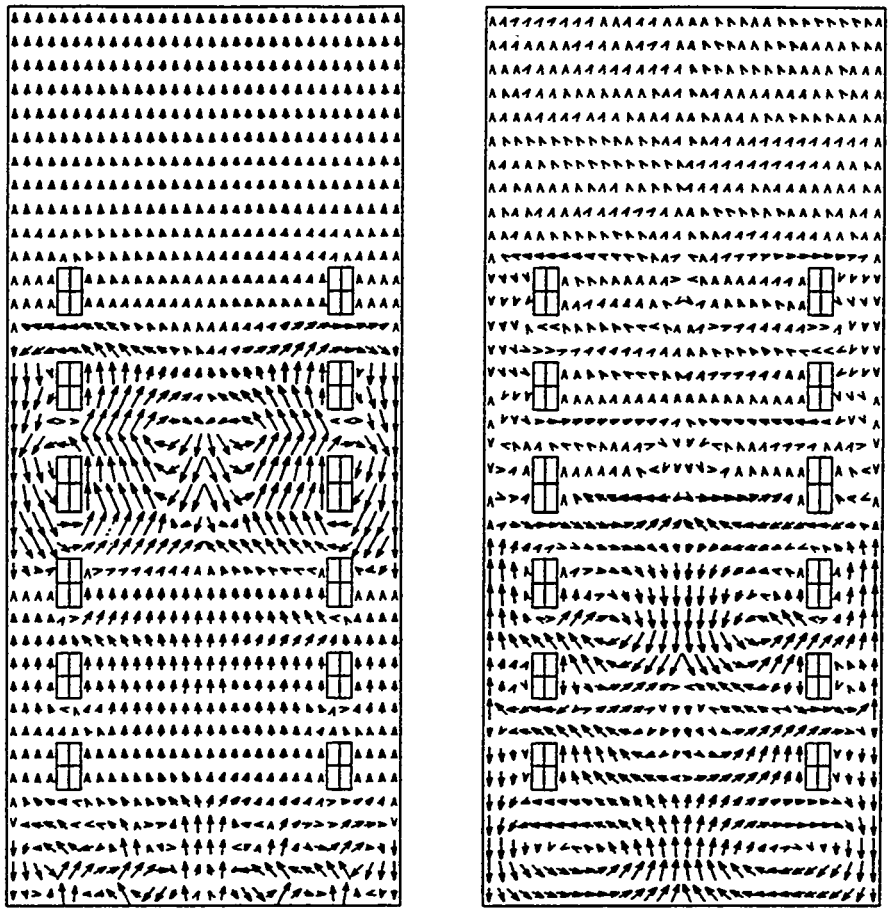

Time = 1 second Steady State

Figure 9 Gas Transient Flow Pattern.

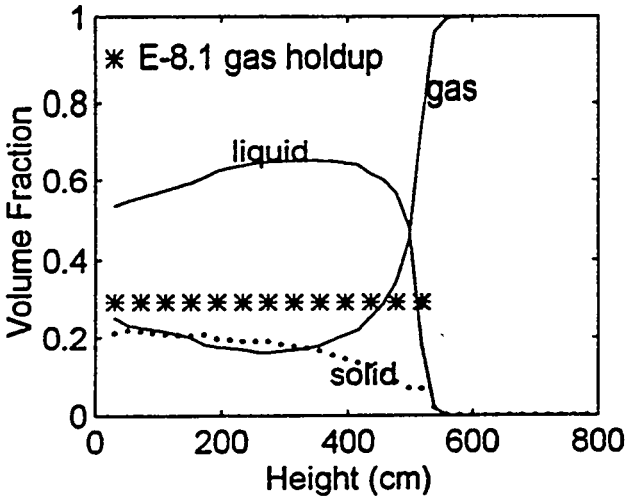

Fig 10 Time average g-l-s volume fraction profiles

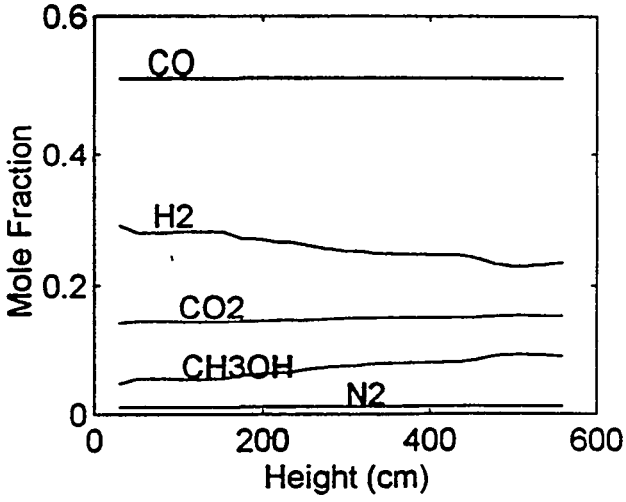

Fig 11 Time average gas composition profiles

NOTATION:

a	interfacial area per unit volume (cm^2/cm^3)
C_i^{ℓ}	concentration of i in bulk liquid phase
$C_i^{g\ell}$	concentration of i in g-l interface
C_D	drag coefficient
d_k	diameter of solid particle or liquid droplet
e	restitution coefficient
f_i	fugacity of i
H_i	Henry's constant of i
K	reaction kinetic coefficient
K_{eq}	reaction equilibrium constant
$K_{\ell i}$	mass transfer coefficient of i in liquid phase
m_k	rate of generation of phase k
M_i	molecular weight of i
P	pressure
r	rate of reaction
R_i	rate of mass transfer
Re_k	Reynolds number
T	temperature
v	velocity
x_i	weight fraction of i in liquid phase
y_i	weight fraction of i in gas phase

Greek letters:

α_i	stoichimetric coefficient of i
β	frictional coefficient
ε	volume fraction
ρ	density
μ	viscosity
θ	granular temperature
τ	shear stress
ψ	sphericity of particle or droplet

Subscripts:

g, ℓ, s	gas, liquid, solid respectively
i	species
k	solid or liquid phase

TITLE: Flow Patterns in a Slurry-Bubble-Column Reactor Under Reaction Conditions

PI (AUTHORS): B. A. Toseland, D. M. Brown, B. S. Zou, M. P. Dudukovic

INSTITUTION/ORGANIZATION: Air Products and Chemicals, Inc.
Washington University, St. Louis

CONTRACT NUMBER: DE-FC22-94PC93052

PERIOD OF PERFORMANCE: June 1994 — August 1995

OBJECTIVE: Understand Flow Patterns in SCBB

ABSTRACT

The gas and liquid radioactive tracer response curves obtained in an industrial bubble column reactor of height to diameter ratio of 10 are analyzed and the suitability of the axial dispersion model for interpretation of the results is discussed. The relationship between the tracer concentration distribution and measured detector response is calculated. It is found that the liquid can be considered well mixed and that the response of the soluble gas tracer (Ar-41) is possibly dominated by the dissolved gas. The one dimensional axial dispersion model cannot match all the experimental observations well and the flow pattern of the undissolved gas cannot be determined with certainty.

INTRODUCTION

Radioactive tracers have been used to study flow and mixing in bubble columns (Field and Davidson, 1980; Air Products and Chemicals, 1990; Tarmy et al., 1982; Nalitham and Davies, 1987). Model-supported interpretation of tracer data allows extraction of parameters for design and scale up and is a necessary addition to visual inspection of data. The axial dispersion model is most frequently used for interpreting tracer data. The above cited studies either ignore gas absorption or assume that the gas tracer is instantaneously equilibrated between the gas and the liquid phase. The standard gas-phase model, however, needs modification to account for gas solubility (Joseph and Shah, 1986). Moreover, Vermeer and Krishna (1981) demonstrated the presence of a bi-modal bubble size distribution in the churn- turbulent regime. This distribution is not accounted for in the dispersion type model. However, no general model that can be fitted to tracer data was presented. Shetty and Kantak (1992) developed a two-bubble-class model and matched some data reported in the literature. Unfortunately, their model requires a large number of independently measured parameters which were not available in the present study.

The purpose of this study was to scrutinize the tracer data collected while conducting a reaction in a 0.57 m i.d. bubble-column, assess the extent of backmixing in the liquid and gas phases, and test the ability of the models to consistently match experimental observations. Dispersion models, being the simplest and most popular, were tried first. Follow-up work will use other models. A simple model for radiation measurements is also discussed to assess the errors in measuring tracer curves.

EXPERIMENTAL

The Alternate Fuels Development Unit (AFDU) at LaPorte, Texas owned by the United States Department of Energy (DOE) is a stainless steel bubble-column reactor with an internal diameter of 0.57 m and a possible liquid height of 7.62 m (Air Products and Chemicals, 1990). The stationary slurry phase is a powdered catalyst suspended in

a hydrocarbon oil. Gas bubbles through the slurry via a sparger. Oil disengages from the gas in a space above the liquid, and gas exits from the reactor through the top of the column.

The tracer curves were measured by ICI TracerCo of Houston, Texas. Ar-41, used as the gas phase tracer, was introduced into the feed line upstream of the vessel. Tests were performed in a reacting system. Manganese oxide was the liquid tracer since the particle size ($< 45\mu m$) was small enough to mimic the liquid flow (Air Products and Chemicals, 1990).

The flow distribution within the reactor was monitored by four rings of four detectors. The four detectors of each ring are evenly distributed around the circumference of the reactor. Detector rings were located at 30.5 cm, 149.9 cm, 337.8 cm and 482.6 cm vessel elevations. The liquid level during tracer studies was at 546.1 cm elevation. During the vapor studies, additional detectors were placed on the feed inlet and reactor overhead piping. During the liquid studies these detectors were repositioned at 200.7 cm and 292.1 cm elevations.

The reactor temperature was 300 $°C$, pressure was 2.7 atm. The reaction was the dehydration of isobutanol to isobutylene and water. Conversion was nearly complete so that the number of moles of gas almost doubled in the reactor. Gas holdup data taken by means of nuclear density gauge clearly shows the effect of the expanding gas flow. The particular example used later has a superficial gas velocity of 7.01 cm/s and an average gas holdup of 0.20.

INTERPRETATION OF TRACER DATA

The residence time distribution (RTD) theory (Duduković, 1986; Nauman, 1987) suggests that the parameters of a suitable model be found by minimizing some measure of the error between model predictions and experimental data. Closed form expressions for the most popular models for the impulse response mixing cup concentration at the reactor outlet are available to be matched to the data. The difficulties with interpreting industrial data arise mainly from two factors: 1) tracer input is not always an instantaneous pulse or it is not made at the reactor inlet; 2) measurements do not capture the mixing cup concentration and are often performed on the reactor itself, not at its outlet. Finally, the model may be too simplistic in nature to match all of the observed features. Space limitations do not allow us to address all of the above issues here. It may be noted that in this study the duration of the tracer injection was of the order of a few seconds, so that the input can be considered instantaneous. The relationship between radiation measurements and tracer concentration is discussed below because this important issue seems to be overlooked in the studies reported so far.

Distortions due to Radiation Measurements

The radiation signals measured by the scintillation detectors are affected by the solid angle subtended by the cylindrical detector, the distance between the radiation source and the detector, the attenuation and buildup factors (Tsouflanidis, 1983). Establishing the relationship between the measured radiation signals and the instantaneous three dimensional concentration distribution of the emitting tracer can only be done via tomography. However, the spatial range from which a detector receives most of its signal can be assessed. We consider a single detector in the bubble column and assume a uniform tracer distribution throughout the column, as is the case at the end of the liquid tracer

experiment.

The schematic is shown in Fig. 1. The bubble column is considered as divided into many compartments. The radiation from each compartment which is received by the detector is calculated. We denote d_M as the distance traveled through the gas-liquid mixture, d_S as the distance through stainless steel and d_A as the distance through air. We assume that the detector receives the radiation signal both on its front flat circular face (diameter = 5.1 cm) and on the cylindrical side face (length = 5.1 cm).

The total detector counting rate resulting from a point source inside the bubble column is:

$$N_t = e^{-\mu_M d_M}(1 + a_1\mu_M d_M e^{b_1\mu_M d_M})e^{-\mu_S d_S}(1 + a_2\mu_S d_S e^{b_2\mu_S d_S})\frac{A\epsilon S}{4\pi(d_M + d_S + d_A)^2} \quad (1)$$

where A is the area of the part of the detector which can be directly irradiated by the point source, ϵ is the detector efficiency. Other symbols are defined in the nomenclature, together with their default values.

The results of the radiation calculation are also shown in Fig. 1. The calculated radiation measurement is normalized so that the radiation measurement from the closest compartment equals to 1. The recorded intensity from a compartment which is 38 cm away from the detector is less than 1% of the recorded intensity from the closest compartment, with the source strength being the same. Those compartments whose distances from the detector are less than 56 cm contribute 90% of the total radiation intensity so that the large number of compartments far away form the detector do no swamp the signal.

Only the response of the detectors located around the vessel outlet pipe is approximately proportional to the tracer cross sectional average concentration. The signals received by the detectors located around the vessel (see Fig. 1) are mainly proportional to the amount of tracer present in a hemisphere about 15.2 cm in radius centered at the flat face of the detector. The detectors in the study were shielded on the sides, i.e., partially collimated, but the basic conclusion that the region close to the detector face influences the response most still holds. One can also show that the radiation signal at a given elevation is broader than the corresponding cross sectional concentration at the same elevation. This broadening is severe for systems close to plug flow and nonexistent for a completely back-mixed system. Since, as will be shown below, our bubble column is well mixed, this broadening is not a major factor.

Liquid Tracer

Liquid tracer is introduced at the 175.3 cm elevation close to the reactor wall at one side of the column. Detector responses at all elevations indicate lack of symmetry in the response which is the least severe at the 482.6 cm elevation. Therefore, the model prediction is fitted to the normalized response at 482.6 cm elevation. A one dimensional dispersion, with a constant dispersion coefficient in a batch liquid, is assumed with instantaneous tracer injection at the 175.3 cm elevation and cross-sectional average concentration measurement at the 482.6 cm elevation.

The liquid phase dispersion coefficient was obtained by matching the model predicted response to the detector response at the 482.6 cm elevation and a value of D_L=3,244 (cm^2/s) was found to yield the best fit. Figure 2 shows that the match between the model and data is reasonable. The dispersion coefficient of 3,244 (cm^2/s) at the inlet gas superficial velocity of 7 (cm/s) is about twice as large as the values predicted by typical

correlations (Fan, 1989) for the same diameter column. Since gas volume doubles due to reaction, liquid dispersion coefficients of the order of 2,000 (cm^2/s) are predicted by correlations at the doubled inlet superficial gas velocity. It is possible that additional liquid backmixing arises from in-situ gas generation.

The large value of the liquid dispersion coefficient indicates that the liquid is almost completely mixed. The characteristic liquid mixing time is of the order $L^2/D_L = 92$ seconds. Figure 2 also indicates that liquid mixing is complete in about 1.5 minutes.

Gas Tracer

A thorough literature search was carried out to locate transient models which deal with churn-turbulent regime of operation of bubble columns. It is found that no model is readily applicable to our tracer data, for the reason that either the model is incomplete or the required data is incomplete. Since the axial dispersion model with interphase mass transfer can to some extent simulate the behavior of bimodal bubble size distribution in churn turbulent regime by assuming that the small bubbles behave the same as the adsorbed tracer, this model is chosen as our first attempt to quantify the tracer data.

Gas tracer is introduced in the inlet pipe and monitored at the wall along the reactor length and in the exit pipe. Our task was to determine whether a one dimensional dispersion model can fit the observed measurements along the reactor length. Versions of the dispersion model that assumed equilibration between gas and liquid or a completely backmixed liquid were unable to match the experimental results. The most sophisticated dispersion model included argon solubility. The following equations describe the gas and liquid mass balance for the tracer when interphase mass transfer resistance is also considered:

$$D_G\frac{\partial^2 C_G}{\partial z^2} - \frac{U_G}{\epsilon_G}\frac{\partial C_G}{\partial z} + k_l a(HC_L - C_G) = \frac{\partial C_G}{\partial t} \tag{2}$$

$$D_L\frac{\partial^2 C_L}{\partial z^2} - \frac{\epsilon_G}{\epsilon_L}k_l a(HC_L - C_G) = \frac{\partial C_L}{\partial t} \tag{3}$$

The following boundary and initial conditions are used:

$$t = 0, \quad C_L = 0; \quad C_G = 0 \tag{4}$$

$$z = 0, \quad \frac{\partial C_L}{\partial z} = 0; \quad \frac{U_G}{\epsilon_G}C_G = D_G\frac{\partial C_G}{\partial z} + \frac{U_G}{\epsilon_G}\delta(t) \tag{5a}$$

$$z = L, \quad \frac{\partial C_L}{\partial z} = 0; \quad \frac{\partial C_G}{\partial z} = 0 \tag{5b}$$

It is assumed that the detector response is proportional to $\epsilon_L C_L(z,t) + \epsilon_G C_G(z,t)$. A similar model was presented and solved by Laplace transform by Van Vuuren (1988). Here we used a NAG (Numerical Algorithm Group) differential equation solver to get the time domain solution.

We assumed backmixing in the reactor gas space above the liquid level and that the outlet response is proportional to the exit mixing cup concentration for the gas. Radial uniformity of the tracer injection was adequate so that averaged responses of the detectors in the ring at a given elevation were used for comparison with model predictions.

Table 1: Parameter estimation using detectors at different elevations

	D_G (cm^2/s)	$k_l a$ (1/s)	H
30.5 cm	5789	0.1810	5.993
149.9 cm	6043	0.3016	4.676
337.8 cm	5626	0.1838	6.013
482.6 cm	5789	0.3055	5.032

There were three floating parameters: H, D_G, $k_l a$, while the measured mean values of gas and liquid holdup were used in the model together with the liquid dispersion coefficient determined earlier from tracer data.

The present model does not fare any better than the simpler models, as illustrated in Figure 3. Further attempts at curve fitting using different weights for the liquid and gas tracer concentrations in equation (9) for the detector response or accounting properly for the radial holdup distribution did not improve the consistency of the estimated parameters. This leads to the conclusion that the axial dispersion model with constant dispersion coefficients cannot match the observed gas tracer data.

Examination of the data at different elevations (Fig. 3) shows that the peak of the response shifts only slightly to larger times at higher elevations and that the spread of the curve does not increase much with elevation. This indicates that the response is mainly generated by the dissolved tracer in the liquid which is pretty well mixed. This is confirmed by the fact that the peak of the response occurs much later than the mean transit time for the undissolved gas, $\epsilon_G z/\overline{u}_G$. For example, for the detector at 149.9 cm elevation the mean gas transit time is less than 4 seconds while the response peak occurs at close to 20 seconds. The same pattern is observed for the detectors at all other elevations and at no detector is an early peak observed at the time corresponding to the mean transit time of the undissolved gas at that elevation. CARPT (Computer Automated Radioactive Particle Tracking) measurements (Devanathan, 1991) indicate that at conditions used in this study maximum liquid recirculation velocity could be of the order of 100 (cm/s). This implies that the tracer particle at the reactor centerline could transverse the whole liquid height in less than 6 seconds.

If we assume that the gas tracer input, instead of a delta function, is a response of a well mixed region given by:

$$f(t) = \frac{U_G}{\sqrt{U_G/(12\pi D_G)}} \exp\left(\frac{-(3-U_G t)^2}{12 D_G/U_G}\right) \tag{6}$$

This could be expected if rapid mixing and gas liquid transfer occurred in the sparger zone, then a good agreement between model predictions and data is possible as shown in Fig. 4. A consistent set of parameters is obtained (Table 1). Recomputing model predictions based on average parameter values still provides a good agreement between measured and modeled responses at all elevations. Theoretical justification for using this particular forcing function cannot be offered at present and work regarding this issue is in progress.

The parameter values listed in Table 1 are reasonable. The Henry's constant is close

to the value of calculated by Air Products, the volumetric mass transfer coefficient is close to the range of 0.1 to 0.2 (s^{-1}) predicted by most correlations (Fan, 1989), and the gas phase dispersion coefficient is well within the range of 1,000 to 20,000 (cm2/s) indicated by correlations (Fan, 1989). The gas phase Peclet number is of order one, and indicates that the gas phase is well mixed. This, however, may be an artifact of the model as liquid response dominates.

The overall gas phase tracer response in the outlet pipe are matched by assuming plug flow or complete backmixing in the gas space above the slurry level. It is found that the mixing pattern above the slurry level is bounded by the above two limits, but not close to either side.

CONCLUSIONS

The liquid, in our cigar shaped bubble column with the aspect ratio (L/D) of 10 and operated in churn turbulent regime, is well mixed. Complete mixing is achieved in about 90 seconds which is much shorter than the characteristic reaction time. Conversion predictions based on a well mixed compartment are therefore justified. The gas phase tracer runs cannot be interpreted satisfactorily based on the axial dispersion model. Very high backmixing of the dissolved gas is indicated but no conclusions can be reached regarding the flow pattern of the undissolved gas. The existence of symmetrical responses by detectors located in a ring at the same axial reactor elevation indicate presence of axial symmetry but is not sufficient proof of the lack of radial tracer concentration gradients. Only tracer injection close to the wall can reveal the existence of radial nonuniformities.

For the purpose of reactor modeling the tracer tests indicate that the industrial bubble column investigated here is close to a single well mixed tank which was the assumption made in calculating reactor performance.

NOMENCLATURE

A	area of the detector which can be reached by radiation, cm^2
a_1, b_1, a_2, b_2	coefficients for Berger equation, a_1 =1.30, b_1=0.027, a_2 =1.27, b_2=0.032
C_G, C_L	gas and liquid phase tracer concentrations, $mole/l$
D_G,D_L	gas and liquid phase dispersion coefficients, cm^2/s
d_A, d_M, d_S	radiation traveling distance in air, slurry and stainless steel, cm
$f(t)$	forcing function at the inlet.
H	Henry's law constant
L	liquid level in the bubble column, cm
N_t	total detector counting rate
k_la	mass transfer coefficient, $1/s$
S	source strength in a compartment = 1 (any units)
U_G	superficial gas velocity, cm/s
z_i	liquid tracer injection point, cm
δ	Dirac delta function.
ϵ	detector efficiency
ϵ_L, ϵ_G	liquid and gas holdups
μ_M, μ_S	attenuation coefficients, $\mu_M = 4.2 \times 10^{-2}$ $1/cm$, $\mu_S = 0.468$ $1/cm$

REFERENCES

Air Products and Chemicals Inc. and Chem Systems Inc. A Report to DOE Contract No. DE-AC22-87PC90005, August, 1990.

Devanathan, Doctoral Dissertation, Washington University, 1991.

Field, R. W.; Davidson, J. F. Trans IChemE, Vol. 58, 228, 1980.

Joseph, S.; Shah, Y. T. Can. J. Chem. Eng. Vol. 64, 380, June, 1986.

Nalitham, R. V.; Davies, O. L. Ind. Eng. Chem. Res. 1987, Vol. 26, 1059-1066.

Nicholas Tsoulfanidis. "Measurement and Detection of Radiation", Hemisphere Publishing Corp., 1983.

Shetty, S. A.; Kantak, M. V. AIChE J. Vol. 38, No. 7, 1013, 1992.

Tarmy, B. L.; Chang, M.; Coulaloglou, C. A.; Ponzi, P. R. I. Chem. E. Symposium Series, No. 87, 303, 1982.

Vermeer, D. J.; and Krishna, R. Ind. Eng. Chem. Process Des. Dev. Vol. 20, 475, 1981.

Van Vuuren, D. S. Chem. Eng. Sci. Vol. 43, No. 2, 213, 1988.

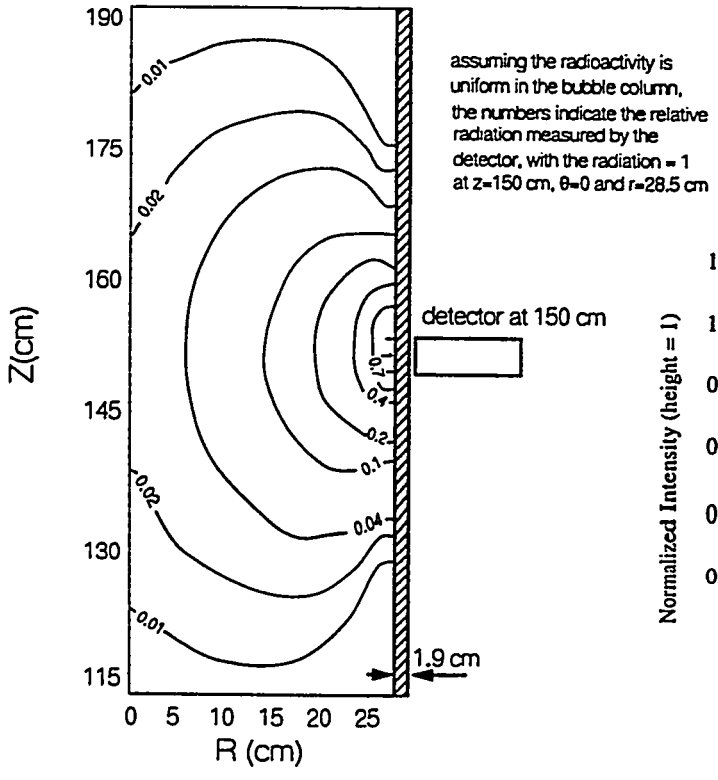

Figure 1: Schematic of the Radiation Measurement Calculation

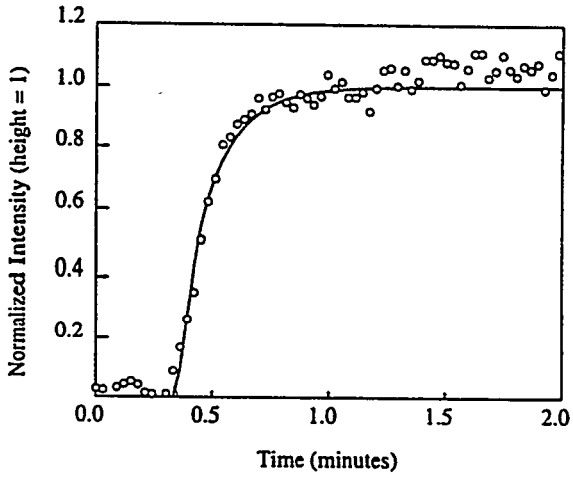

Figure 2: Time domain curve fitting for liquid tracer

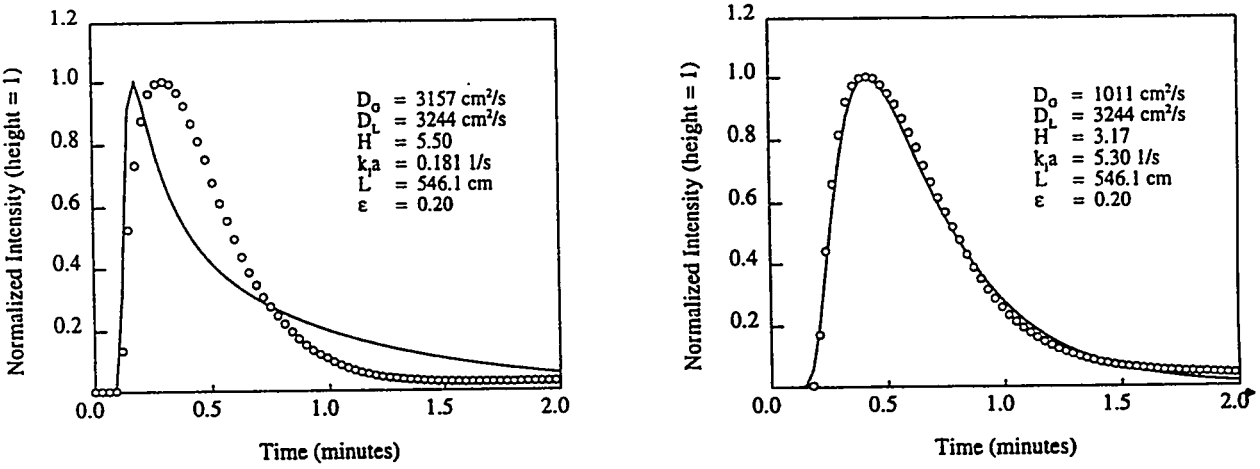

Figure 3: Time domain matching of the responses at different elevations using Dirac delta input function. A: 149.9 cm; B: 482.6 cm

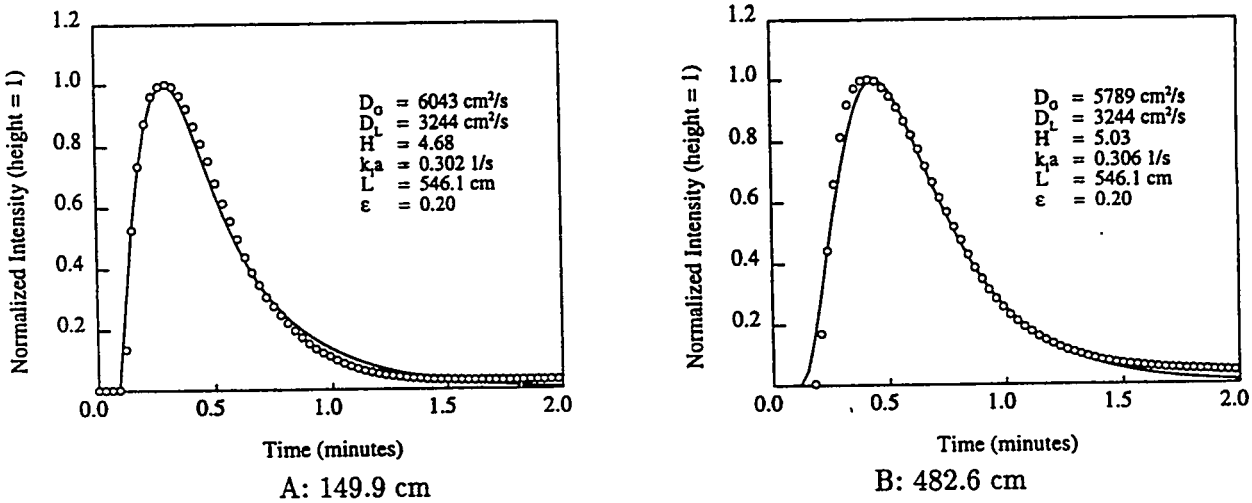

Figure 4: Time domain matching of the responses at different elevations using an exponential decaying input function. A: 149.9 cm; B: 482.6 cm

List of Figure Captions

Figure 1. Schematic of the Radiation Measurement Calculation.

Figure 2. Time Domain Curve Fitting for Liquid Tracer.

Figure 3. Time Domain Matching of the Responses at different Elevations Using Dirac Delta Input function.
A: 149.9 cm; B: 482.6 cm

Figure 4. Time Domain Matching of the Responses at Different Eleveations Using an Exponential Decaying Input Function.
A: 149.9 cm: B 482.6 cm

FISCHER-TROPSCH SLURRY REACTOR MODELING

Y. Soong, I. K. Gamwo, F. W. Harke,
A. G. Blackwell, and M. F. Zarochak

U.S. Department of Energy
Pittsburgh Energy Technology Center
P.O. Box 10940
Pittsburgh, PA, 15236-0940

For Coal Liquefaction and Gas Conversion Contractors' Review Conference,
Pittsburgh, PA, August 29-31, 1995

FISCHER-TROPSCH SLURRY REACTOR MODELING

Y. Soong, I. K. Gamwo, F. W. Harke, A. G. Blackwell, and M. F. Zarochak

U.S. Department of Energy
Pittsburgh Energy Technology Center
P.O. Box 10940
Pittsburgh, PA 15236-0940

ABSTRACT

This paper reports experimental and theoretical results on hydrodynamic studies. The experiments were conducted in a hot-pressurized Slurry-Bubble Column Reactor (SBCR). It includes experimental results of Drakeol-10 oil/nitrogen/glass beads hydrodynamic study and the development of an ultrasonic technique for measuring solids concentration. A model to describe the flow behavior in reactors was developed.

The hydrodynamic properties in a 10.16-cm diameter bubble column with a perforated-plate gas distributor were studied at pressures ranging from 0.1 to 1.36 MPa, and at temperatures from 20 to 200 °C, using a dual hot-wire probe with nitrogen, glass beads, and Drakeol-10 oil as the gas, solid, and liquid phase, respectively. It was found that the addition of 20 wt% glass beads in the system has a slight effect on the average gas holdup and bubble size.

A well-posed three-dimensional model for bed dynamics was developed from an ill-posed model. The new model has computed solid holdup distributions consistent with experimental observations with no artificial "fountain" as predicted by the earlier model. The model can be applied to a variety of multiphase flows of practical interest.

An ultrasonic technique is being developed to measure solids concentration in a three-phase slurry reactor. Preliminary measurements have been made on slurries consisting of molten paraffin wax, glass beads, and nitrogen bubbles at 189 °C and 0.1 MPa. The data show that both the sound speed and attenuation are well-defined functions of both the solid and gas concentrations in the slurries. The results suggest possibilities to directly measure solids concentration during the operation of an autoclave reactor containing molten wax.

INTRODUCTION

The application of three-phase SBCR systems for coal liquefaction processing is receiving considerable attention. Slurry-bubble-column Fisher-Tropsch (F-T) reactors have many advantages over other types of F-T reactors. Among them are good temperature control of the F-T reaction, the ability to utilize a low H_2/CO ratio synthesis gas, and low mass-transfer resistances.

The important hydrodynamic parameters in the operation of a SBCR are the gas bubble size, holdup, and flow regimes. Hydrodynamic measurements in two-phase systems have been reviewed by several authors (1,2); however, the majority of these studies has been limited to the air-water system. Hydrodynamic measurements using molten wax (typical slurry medium) as the liquid medium are rather limited (3-6). Different hydrodynamic behaviors (e.g., Sauter mean bubble diameter, gas holdup) have been reported in these studies for waxes of similar physical properties. As indicated by Bukur et al.(3), despite similar physical properties among the waxes studied, they showed dissimilar hydrodynamic behaviors. Additional experimental data is clearly required on the hydrodynamic behavior of SBCR

systems using the operating conditions and liquid-phase media of F-T slurry reactors. This information is necessary for a reliable design and scale-up of F-T slurry reactors.

Recently, a three-dimensional hydrodynamic model to describe flow in a bubbling fluidized column with a circular jet was developed. The code was able to predict three-dimensional effects such as a maximum in time-averaged porosities above the jet entrance. However, solid distributions in the free board consistently displayed a "fountain" artifact that was not observed experimentally. It was found that the equation system possesses potential complex-valued characteristics and hence is ill-posed as an initial-value problem (7,8). The above model is modified to a well-posed model referred to as model B (9). The new three-dimensional model has predicted solid holdup distributions with no artificial "fountain." This is consistent with the experimental observations.

To design and efficiently operate a SBCR, the degree of dispersion of the solid (catalyst) in the SBCR must be understood and controlled. The catalyst concentration along the column greatly affects the operation of the SBCR. Measurements must be made under reaction conditions to fully understand the influence of various reaction, reactor, and catalyst parameters on the catalyst concentration profile in the reactor and the effect of catalyst distribution on the overall conversion and product selectivity. A recent method involving the measurement of ultrasound transmission in a slurry-phase stirred-tank reactor offers the possibility of using the ultrasonic technique for the measurement of solids concentration in a SBCR (10). When the velocity of sound in a liquid (1324 m/sec at 25°C for kerosene) is significantly different from that in a solid (5968 m/sec at 25°C for fused silica), a time shift and an amplitude change in the sound wave relative to those for the pure liquid can be detected when solid particles are present. The solids concentration in a slurry reactor can be determined by measuring the amplitude and time shift of an ultrasonic pulse in the slurry medium. The development of this ultrasonic technique will permit the measurement of catalyst concentration during reaction in a SBCR.

The objectives of this project are to study the hydrodynamics in a hot-pressurized SBCR, develop experimentally verified hydrodynamic models, and a diagnostic technique for the direct measurement of slurry concentrations in SBCR. The ultimate goal is to develop a data base which would provide reliable estimates of hydrodynamic parameters relevant to design and operation of the Fischer-Tropsch (F-T) slurry reactors.

EXPERIMENTAL FACILITIES

A schematic diagram of our SBCR is reported elsewhere (11). The unit consists of two stainless steel columns, each of which has an internal diameter of 10.16 cm and a height of 244 cm. The column in which the hydrodynamic studies were conducted has 12 different axial locations for data collection. Experiments were conducted in batch-mode operation (continuous flow of gas and a stationary liquid). The local gas holdup, bubble diameter, bubble velocity, and bubble size distribution were measured by inserting a dual hot-wire probe horizontally into the column at any of the 12 positions and moving it to the desired radial position. The details of the dual hot-wire probe and an integrated data acquisition and analysis system have been described elsewhere (11). The experiments were conducted at temperatures ranging from 20 to 200 °C, at pressures from 0.1 to 1.36 MPa, and at superficial gas velocities of up to 9 cm/sec with the Drakeol-10 oil as the liquid-phase medium, nitrogen as the gas-phase medium, and 20 wt% of glass beads (80 ± 5 microns in diameter) as the solid-phase medium.

The detail of the 2.5-liter autoclave reactor used for the ultrasonic investigation was reported elsewhere (11). Nitrogen bubbles were introduced through a sintered frit at the bottom of

the reactor. The nitrogen flow was controlled electronically to a maximum of 400 mL/min by a mass-flow controller. Glass beads (80 ± 5 microns in diameter) were used as the solid in the slurry. The solids concentration (solid weight/liquid weight) was varied from 1 to 25 wt% for each nitrogen flow in the reactor. Molten paraffin wax (Fischer Scientific, P-22) at a temperature of 189 °C was used as the liquid medium. Experiments were conducted at 0.1 MPa. Ultrasonic pulses were generated using lithium niobate transducers at a frequency of 2.5 MHz. The transducer and receiver were mounted directly inside a metal delay line which was screwed into a fitting inside the reactor wall. Ultrasonic measurements were made by using a computer-based TestPro system manufactured by Infometrics Inc.

RESULTS AND DISCUSSIONS

HYDRODYNAMIC STUDY

Figure 1 shows the effect of gas superficial velocity on axial gas holdups on the nitrogen/Drakeol-10 oil/glass beads (20 wt%) system in the bubble column at ambient conditions. At gas velocity up to 4.36 cm/sec, the axial gas holdup profiles in the column were rather uniform; however, at gas velocity of 5.26 cm/sec, there was a noticeable change in the gas holdup at height of 150 cm above the gas distributor. At a higher gas velocity of 7.05 cm/sec, axial gas holdup increases significantly in the column. It increased from 0.06 at the bottom of the column to 0.72 at the top of the column.

Figure 2 illustrates the Sauter mean bubble diameters versus the superficial gas velocity on the nitrogen/Drakeol-10 oil/glass beads (20 wt%) system in the bubble column at ambient conditions. As shown in Figure 2, the Sauter mean bubble diameters were approximately 2 cm for most superficial gas velocities. The Sauter mean bubble diameters were affected by the distance above the gas distributor, when the superficial gas velocity changed from 5.26 to 7.05 cm/sec. A significant change on the Sauter mean bubble diameter was observed along the axial direction of the column, it increased from 2 cm at the bottom to 9.6 cm at the top of the column. The presence of solids in the bubble column reactors further complicates the flow pattern. As reported by Matsura and Fan (12), similar to two-phase bubble columns, three main flow regimes can be distinguished in the system, namely the homogeneous, heterogeneous, and slug flow regimes. Results from Figures 1 and 2 can be combined to describe the flow regimes. At low gas velocities, smaller than 4 cm/sec, the homogeneous bubble regime exists. The transition from homogeneous bubbling to slug regime may occur for gas velocities ranging from 4 to 6 cm/sec. The slug flow occurred for gas velocity above 6 cm/sec.

Figure 3 shows the effect of 20 wt% glass beads on the Sauter mean bubble diameter in nitrogen/Drakeol-10 oil system in the bubble column at ambient conditions. The results were obtained at the same conditions except that one was collected in a two-phase system and the other in a three-phase system. The Sauter mean diameter decreased slightly after the addition of 20 wt% of glass beads in the system.

Figure 4 illustrates the effect of 20 wt% glass beads on the Sauter mean bubble diameter on the nitrogen/Drakeol-10 oil system in the bubble column at 200 °C and 1.36 MPa. The results were again obtained at the same conditions except one was collected in a two-phase system and the other in a three-phase system. The Sauter mean diameter collected from the two-phase system was approximately the same as that obtained from the three-phase system. However, at higher gas velocities, 6 cm/sec or higher, the Sauter mean diameter obtained from the three-phase system was higher than that collected from the two-phase system. The Sauter mean bubble diameter profiles in the bubble column were rather uniform at both conditions. Thus, one can infer that the superficial gas velocity did not have any

effect on the Sauter mean bubble diameter at the above conditions.
Figure 5 shows the effect of 20 wt% glass beads on the average gas holdup for experiments conducted at ambient conditions. The average gas holdup was found to increase linearly with increasing superficial gas velocity. It can be seen from the data that the addition of 20 wt% glass beads in the system has only a slight effect on the observed average gas holdup. Our results are consistent with the results reported in the literature, i.e., the presence of solid generally decreases the gas holdup. Joosten et al. (13) observed that the gas holdup values at high solids concentrations (>15%) are lower and gas bubbles are larger, so bubble coalescence apparently takes place at a higher frequency. Several authors (14-16) concluded that an increase in solids concentration generally decreases the gas holdup, but the effect becomes insignificant at high gas velocity (>0.1 m/sec). Chabot and de Lasa (17) conducted the three-phase studies using a zinc-copper oxide catalyst (dp = 12.5 μm) suspended in a paraffin oil. They concluded that, in general, the presence of small solid particles reduces the gas holdup, due to an increase in the slurry viscosity. The influence of the solid is higher at lower superficial gas velocities, decreasing gradually with increasing gas velocity, and becomes imperceptible at the highest gas velocity studied (14.7 cm/sec). Due to the scare of data at higher gas velocities, we were not able to confirm our results with those in the literature.
Figure 6 illustrates the effect of 20 wt% glass beads on the average gas holdup in nitrogen/Drakeol-10 oil system in the bubble column at 200 °C and 1.36 MPa. Again, the results were obtained at the same conditions except one was collected in a two-phase system and the other in a three-phase system. The average gas holdup collected from the two-phase system was approximately the same as that obtained from the three-phase system. However, under the higher gas velocities conditions, 6 cm/sec or higher, the average gas holdup obtained from the three-phase system was higher than that collected from the two-phase system. Inconsistencies in the solids effect on gas holdup were also reported in the literature. Kuo (4) reported that when a very low (2 wt%) catalyst loading was used with Mobil reactor wax, the gas holdup at 260 °C and 0-6 cm/sec superficial gas velocity was about 9% lower than that obtained without any catalyst. A different picture was described by Bukur et al. (18) based on the experiments with iron-oxide particle suspended in FT-300 wax. The addition of 0-5 μm solid particles increased gas holdup and the 20 wt% concentration had the maximum effect in the small column. The addition of particles (20-44 μm) in the large column (0.21 m) increased the gas holdup at ug < 0.04 m/sec and had no effect at ug > 0.08 m/s.

MATHEMATICAL MODEL

The well-posed model, i.e., one possessing all real characteristics was first given by Rudinger and Chang (19) who analyzed non-steady one-dimensional two-phase flow. Saltanov (20) solved such a problem for steady two-dimensional supersonic flow over an airfoil. Lyczkowski (21) generalized the Rudinger-Chang equations.
The fundamental differences between the ill- and well-posed models appear in the phases momentum and the drag coefficient. In the well-posed model, all pressure drops are in the gas-phase momentum equations. The drag coefficient is modified to satisfy Archimedes' principles (9) and the usual minimum fluidization relationship as given by Kunii and Levenspiel (22). The differential equations and constitutive relations are written below. In the following equations, R=1 for the rectangular coordinates; R=r for the symmetric cylindrical coordinates, where r is the radial coordinate.

Continuity equation for phase k (= g, s)

$$\frac{\partial}{\partial t}(\epsilon_k \rho_k) + \frac{1}{R}\nabla\cdot(R\,\epsilon_k \rho_k \vec{v}_k) = 0 \qquad (1)$$

$$\sum_k \epsilon_k = 1.0 \qquad (2)$$

Gas-phase momentum equation k = (g; l ≠ g)

$$\frac{\partial}{\partial t}(\epsilon_g \rho_g \vec{v}_g) + \frac{1}{R}\nabla\cdot(R\,\epsilon_g \rho_g \vec{v}_g \vec{v}_g) =$$

$$-\nabla p_g + \epsilon_g \rho_g \vec{g} + \frac{1}{R}\nabla\cdot(R\bar{\bar{\tau}}_g) - \tau_{g0}\frac{1}{R}\nabla R \qquad (3)$$

$$+ \sum_{l=1}^{N} \beta_{gl}(\vec{v}_l - \vec{v}_g)$$

Gas-phase stress

$$\bar{\bar{\tau}}_g = \epsilon_g \mu_g[\nabla\vec{v}_g + (\nabla\vec{v}_g)^T] - \frac{2}{3}\epsilon_g \mu_g \frac{1}{R}\nabla\cdot(R\vec{v}_g)\bar{\bar{I}} \qquad (4)$$

$$\tau_{g0} = 2\epsilon_g \mu_g \frac{1}{R}\vec{v}_g\cdot\nabla R - \frac{2}{3}\epsilon_g \mu_g \frac{1}{R}\nabla\cdot(R\vec{v}_g) \qquad (5)$$

Solids-phase momentum equation k (=s; l≠s)

$$\frac{\partial}{\partial t}(\epsilon_s \rho_s \vec{v}_s) + \frac{1}{R}\nabla\cdot(R\epsilon_s \rho_s \vec{v}_s \vec{v}_s) =$$

$$\epsilon_s \rho_s \vec{g} + \frac{1}{R}\nabla\cdot(R\bar{\bar{\tau}}_s) - \tau_{s0}\frac{1}{R}\nabla R - \sum_{l=1}^{N} \beta_{sl}(\vec{v}_l - \vec{v}_g) \qquad (6)$$

Solids-phase stress

$$\bar{\bar{\tau}}_s = -p_s\bar{\bar{I}} + 2\epsilon_s \mu_s \bar{\bar{S}}_s \qquad (7)$$

$$\tau_{s0} = -p_s + 2\epsilon_s \mu_s[\vec{v}_s\cdot\frac{1}{R}\nabla R - \frac{1}{3R}\nabla\cdot(R\vec{v}_s)] \qquad (8)$$

Deformation rate

$$\bar{\bar{S}}_s = \frac{1}{2}[\nabla\vec{v}_s + (\nabla\vec{v}_s)^T] - \frac{1}{3R}\nabla\cdot(R\vec{v}_s)\bar{\bar{I}} \qquad (9)$$

Solid-phase pressure

$$p_s = p_s(\epsilon_s) \qquad (10)$$

and

$$\nabla p_s = G(\epsilon_s)\nabla \epsilon_s \tag{11}$$

with

$$G(\epsilon_s) = 10^{(8.76\epsilon_s - 1.33)} \ dynes/cm^2 \tag{12}$$

Gas-solid drag coefficients

for $\epsilon_g \leq 0.8$, (*based on Ergun equation*)

$$\beta = 150\frac{\epsilon_s^2 \mu_g}{\epsilon_g^2 d_p^2} + 1.75\frac{\rho_g \epsilon_s |\vec{v}_g - \vec{v}_s|}{\epsilon_g d_p} \tag{13}$$

for $\epsilon_g > 0.8$, (*based on empirical correlation*)

$$\beta = \frac{3}{4} C_d \frac{\epsilon_g \epsilon_s \rho_g |\vec{v}_g - \vec{v}_s|}{d_p} \epsilon_g^{-1.65} \tag{14}$$

$$C_d = \begin{cases} \dfrac{24}{Re_p}[1 + 0.15 Re_p^{0.687}], & for\ Re_p \leq 1{,}000 \\ 0.44 & for\ Re_p > 1{,}000 \end{cases} \tag{15}$$

where

$$Re_P = \frac{\epsilon_g \rho_g |\vec{v}_g - \vec{v}_s| d_p}{\mu_g} \tag{16}$$

Equation of state

$$\rho_g = \frac{p_g}{RT} \tag{17}$$

$$\rho_k = \rho_s \quad for\ k \neq g. \tag{18}$$

The well-posed hydrodynamic code was used to simulate the flow in a fluidized column with a circular jet. The column cross sections were 40 cm by 3.81 cm. The jet nozzles were

1.27 cm O.D copper tubing. Air is supplied by three separate streams: two for the air plenum supplying air to fluidize the bed particles, and one for the air jet. The computation was done in one quarter of the bed due to the assumption of symmetry in both the X and Y directions. The solid material was Ottawa Sand with actual density of 2610 kg/m^3, a settled bulk density of 1562 kg/m^3, and a mean particle diameter of 503 μm. The minimum fluidization velocity was 25.9 cm/s and the packed-bed voidage was 0.45. The nonuniform finite difference grids used in the computation are shown in Figure 7. Numerical error that arises in the solution of the Navier-Stokes equations when a nonuniform mesh is used was minimized by proper assignment of cell sizes $(\Delta_{i+1}/\Delta_i) \leq 1.25$ which provided maximum accuracy and minimum computation time. The total number of grids was 14x38x8 (4256 nodes). The time step Δt was 10^{-5} second during the first second of the simulation and 4 x 10^{-5} up to 2 seconds. The computer code was run on a CRAY supercomputer.

The solid holdup distributions predicted by the ill-posed model (previous version (23)) and the well-posed model (present version) are compared with a sketch of the experiment results in Figure 8. It clearly shows that the well-posed model predictions are consistent with the sketch of the experiment. Thus, we have cured the ill-posedness of the initial value problem as evidenced by the disappearance of the artificial fountain.

ULTRASONIC INVESTIGATION

Figure 9 shows the change in the amplitude ratio of the transmitted ultrasonic signals A/A_o in the reactor as a function of nitrogen flow at 189 °C. A and A_o are the amplitudes of the transmitted signals with and without the presence of nitrogen, respectively. Figure 9 also indicates that the amplitude ratio is approximately an inverse exponential function of the nitrogen flow. When a sound wave strikes the boundary between two different media and the acoustic impedances of the two media are different, part of the acoustic energy will be reflected and some will be transmitted. Acoustically, the impedance's of two media will determine the transmission of the wave from one medium to another and the amount of reflection of sound at the boundary between two media. If the impedances of two media are widely separated, e.g. nitrogen and paraffin wax, then most of the energy is being reflected back in the first medium (paraffin wax) with little transmission into the second medium (nitrogen). It can be assumed that the ultrasonic pulse cannot penetrate through much of the nitrogen-paraffin wax interface in the current experimental frequency due to the acoustic impedance mismatch of this combination. Since the ultrasound beam cannot penetrate nitrogen bubbles that lie in its path, the amount of attenuation of the ultrasound beam by nitrogen bubbles is proportional to the amount of gas in the form of bubbles present in the path. We also estimated the bubble sizes to be around 2 mm in the path between the transducer and the receiver within the range of flow studied. The decreasing of A/A_o as the nitrogen flow increased appears related to the nitrogen bubbles. Chang et al. (24) measured void fractions up to 20% in bubbly air-water two-phase flow using an ultrasonic transmission technique. Their results showed that the transmitted ultrasonic signal could be approximated by the exponential relationship :

$$A/A_o = \exp [-f(d_b)\, \epsilon] \qquad (19)$$

where ϵ is the void fraction and $f(d_b)$ is a function dependent on the Sauter mean diameter. This correlation shows that the A/Ao ratio has exponential relationship with both the void fraction and a function dependent on the bubble diameter. The effect of air bubble diameter on A/Ao ratio was found to be significant where A/Ao decreased with increasing bubble size. Bensler et al. (25) also conducted the measurement of interfacial area in bubbly flows in air-water systems by means of an ultrasonic technique. Their observations showed that the

transmitted ultrasonic signal could also be expressed by the exponential-relationship :

$$A/A_o = \exp [\Gamma x/8\ S(kd_b/2)] \qquad (20)$$

where Γ is the volumetric interfacial area, x is the travel distance in the path, S is the scattering coefficient, k is the wave number of the ultrasonic wave which surrounds the bubble, and d_b is the Sauter mean bubble diameter. Equation (20) shows that the A/Ao ratio has exponential relationship with the interfacial area and the scattering cross section which is a function dependent on both the bubble radius and the wave number of the ultrasonic wave surrounding the bubble. Our observations of A/Ao in the nitrogen/paraffin wax system are in qualitative agreement with those reported by Chang et al. (24) and Bensler et al. (25). The decreasing A/Ao ratio as the nitrogen flow increased in Figure 9, may be attributed to the combination of the void fraction, bubble size and the scattering cross section. Figure 9 also illustrates the effect of the nitrogen flow on the transit time, t_b. It was approximately 140.25 μsec at all nitrogen flows. It is evident that the transit time was unaffected by the nitrogen flow within the current experimental conditions. The results indicate that only the amplitude and not the transit time of the ultrasonic signal are affected by the nitrogen flow rate in the reactor within the current experimental conditions. Chang et al. (24) also reported that the amplitude of the transmitted sound pulses depends significantly on the number of bubbles; however, the transit time does not change with the void fraction. Our results obtained from the nitrogen/molten wax system are similar to those of Chang et al. (24) for the air/water system.

The solids concentration in a three-phase slurry has a significant effect on both amplitude ratio and transit time, t_b, of an ultrasonic signal. Figure 10 shows the effect of solids concentration on the amplitude ratio of the transmitted ultrasonic signal A/A_o (A and A_o are the transmitted signals with and without the presence of solids, respectively) in the autoclave at a constant temperature of 189 °C and with a constant stirring speed and without nitrogen flow. A/A_o decreases with increasing solids concentrations. Figure 10 also presents the effect of the solids concentration on the transit time, t_b. It was approximately 140.25 μsec with no solids; however, it decreased to approximately 139.25 μsec as the solids concentration increased to 25 wt%. In general, the amplitude of the transmitted ultrasonic signals and transit time decreased as the solids concentration increased. When an ultrasonic pulse is sent across the slurry reactor, the amplitude of the pulse is reduced when it strikes a solid in the slurry because the pulse is partially scattered and absorbed. Scattering is often the predominant form of attenuation in heterogenous materials. It occurs when some of the ultrasonic wave incident upon a discontinuity in a material, for example, solid particle, is scattered in directions which are different from that of the incident wave. The unscattered pulse is transmitted through the solid to the receiver. The amplitude of the transmitted portion of the pulse is measured by the receiver located on the opposite side of the autoclave. The more particles present in the path, the less transmitted pulse will be detected. The amplitude ratio of the pulse is inversely proportional to the quantity of solid particles present in the path. Therefore, the measured amplitude of the sound wave transmitted through a slurry mixture is expected to be a strong function of the concentration of solids. The transit time decreased as the solids concentration increased in the reactor. Since sound waves travel at a much faster velocity in the solid (5571 m/sec for fused silica at 189 °C) than in the paraffin wax (943 m/sec at 189 °C), the transit time of the transmitted ultrasonic pulse should depend on the quantity of solid particles present in the path. The higher the concentration of solid particles are present in the path, the shorter the transit time would be observed.

Figure 11 shows the effect of solids concentration on the transit time as a function of

nitrogen flow. The solids concentration has a significant effect on the transit time at a constant flow of nitrogen of 100 mL/min: it was approximately 140.20 μsec at 2 wt%, decreased to approximately 139.79 μsec as the solids concentration increased to 15 wt%, and decreased further to approximately 139.27 μsec as the solids concentration increased to 25 wt%. As discussed earlier, sound waves travel at a much faster velocity in the solid than in the paraffin wax, the transit time of the transmitted ultrasonic pulse should depend on the quantity of solid particles present in the path. The higher the concentration of solid particles present in the path, the less the transit time would be observed. We speculate that the decrease of transient time as the solids concentration increased is due to the number of solid particles present in the path. It was interesting to note that the presence of nitrogen bubbles affect the transit time. For most cases, the presence of more nitrogen bubbles causes a slightly decreased in transient time. It should be noted that the principal effect of the nitrogen bubbles is to improve the suspension of the beads, thereby increasing the attenuation and decreasing the transit time over the values obtained with the stirrer alone. Separate tests with the stirrer and nitrogen bubbles in the absence of beads confirm that their presence alone causes no effects on the transit time (Figure 9). Figure 11 further illustrates the fractional change in transit time $\Delta t/t_o$ ($\Delta t = t_a - t_b$) as a function of solids concentration under different nitrogen flows. The fractional change in transit time (time ratio) increased as the solids concentration increased. The results illustrated in Figure 11 can be described by a simple model in which it is assumed that the presence of solid particles in the path of the sound wave reduces the transit time because the sound velocity in the solid is faster than that in the liquid. If the solid particles are assumed to be randomly distributed, the time ratio $\Delta t/t_o$ is related to the concentration fraction ω by the equation.

$$\Delta t/t_o = \alpha\, \omega^{1/3}(1 - v_l/v_s) \qquad (21)$$

Here α is a constant for particles of a given composition and v_l and v_s are the speed of sound in the liquid and solid, respectively. A derivation of this equation is given elsewhere (26). The above equation, which predicts that the time ratio should be dependent upon solids concentration, is approximately the case in experiments presented here for solids well-suspended in the liquid phase. However, it is clear that the functionality of the predicted dependence on solids concentration does not adequately describe the data. The observed dependence is closer to a linear rather than a cube root dependence on ω. This discrepancy is perhaps not surprising because equation (21) is only expected to be true for $\omega << 1$, and this condition is violated over the range of solids concentration investigated here. It should be noted that the simple model (assuming that the ultrasound wave can transmit through the nitrogen bubble) predicts that the number of nitrogen bubbles in the liquid should increase the transit time, because the speed of sound in nitrogen is less than that in the liquid. This increase will not be observed in the current experimental set-up due to the acoustic impedance mismatch, and will not affect our measurements. The signal that we measured was not transported through the nitrogen and therefore showed no change in transit time with increasing nitrogen flow.

In concentrated systems, multiple scattering is important, i.e. a significant proportion of the energy scattered from one particle is incident upon neighboring particles (27). The velocity of the sound and attenuation depends on particle size as well as concentration under this condition (28). Two important parameters - the ultrasound wave number, k, and the radius of the particle, a - are often utilized to describe the ultrasound propagation and attenuation. For this study, the ka range is around 1.3. As indicated previously, the bubble size was around 2 mm. A slight change in the transit time (velocity) observed with the presence of more nitrogen bubbles is probably due to the improved suspension. The theoretical

ultrasonic propagation of polystyrene spheres in water and glass spheres in epoxy systems has been studied by Anson and Chivers (28). Although their systems are not the same as in this study, their theoretical approaches - an effective medium approach, and a multiple scattering approach - can be applied to further theoretical study. The results from our study are in qualitative agreement with those previously reported by Okamura et al., (10). Our results with molten wax similar to the previous results from the nitrogen/water/glass beads system (26). However, our previous results for the nitrogen/water/glass beads system give larger values of time ratio at a given solids concentration fraction than our current nitrogen/paraffin wax/glass beads data. A possible explanation of this discrepancy could be that the geometry of our previous apparatus and nitrogen/water/glass bead system differs considerably from that employed here. In general, both the amplitude and the fractional change of transit time (or time ratio) were affected by the variation of solids concentrations. It appears that the time ratio depends mainly on the solids concentration. The variation of nitrogen flow has little effect on the observed fractional change of transit time (or time ratio) within the flow conditions studied.

We have noticed that the temperature of the paraffin wax has a significant effect on the ultrasonic signal. The effect of P-200 wax temperature on ultrasonic measurement under the conditions of a constant stirring speed and no gas flow in the autoclave reactor is plotted in Figure 12. It shows that the measured transit time and amplitude ratio become significantly influenced by the P-200 wax temperature. The increasing transit time and decreasing amplitude ratio as the temperature increased are probably due to the change in densities and other physical properties in the paraffin wax which result in the variation of the ultrasonic signal with temperatures. Based on these results, it can be concluded that the ultrasonic technique with some modifications has potential applications for solids concentration measurements in three-phase slurry reactors.

SUMMARY

Based on the three-phase experimental hydrodynamic studies, we can tentatively conclude that the addition of 20 wt% glass beads in the system has a slight effect on the average gas holdup and bubble size.

A well-posed three-dimensional hydrodynamic model was developed from a previous ill-posed model. The new model has shown reasonable solid holdup distributions in the column. The artificial "fountain" incorrectly predicted by the ill-posed model has been resolved. The program can be used for liquid-solids flows and with some modifications for gas-liquid-solids flows. The code is undergoing improvements such as extension to multisize particles, finite element, and parallelization to speed up running time.

The results presented in this study led to the conclusion that both the amplitude and the transit time of an ultrasonic signal are influenced by the variation of solids concentration in molten paraffin wax. The variation of nitrogen flow has little influence on the observed transit time within the conditions studied. The ultrasonic technique with some modifications has potential applications for solids concentration measurements in three-phase slurry reactors at elevated operating temperature.

ACKNOWLEDGEMENTS

The authors appreciate the help from R. R. Anderson and C. E. Taylor. I. K. Gamwo would like to acknowledge the support of the U.S. Department of Energy through ORISE.

NOMENCLATURE

D_{32}	Sauter mean diameter
C	Fluctuating velocity of particle
e	Coefficient of restitution
g	Gravity
g_0	Radial distribution function
[I]	Unit tensor
P	Pressure
q	Flux vector of fluctuating energy
t	Time
v	Velocity vector
a	Bubble or particle radius, m
A	Amplitude of the transmitted signal
A_o	Amplitude of the transmitted signal in the absence of nitrogen and solid
k	The wave number (k) of the ultrasonic wave which surrounds the bubble or particle
$f(d_b)$	A function dependent on the Sauter mean diameter
t_a	Arbitrary first distinct zero crossing time in liquid, s
t_b	Arbitrary first distinct zero crossing time in the presence of solid in slurry, s
t_o	Arbitrary travel time of the sound wave between the transmitter and the receiver in the absence of solid in slurry, s
v_l	Speed of sound in liquid, m/s
v_s	Speed of sound in solid, m/s
Δt	Equals $(t_a - t_b)$, s
$\Delta t/t_o$	Time ratio
x	The travel distance in the path, m
S( )	The scattering coefficient

Greek Letters

ν_l	Kinematic viscosity of liquid
ϵ_g	Gas holdup
σ_l	Surface tension
$ß_{km}$	Interphase momentum transfer between phase k and phase m
γ	Collision energy dissipation
ϵ	Volume fraction
$3/2\Theta_s$	Fluctuation energy
κ	Conductivity of fluctuating energy
μ	Shear viscosity
μ_s	Shear viscosity x volume fraction of solids
ξ_s	Bulk viscosity x volume fraction of solids
ξ	Bulk viscosity
ρ	Density
τ	Stress
α	A constant for particles at a given composition
ω	Solids concentration fraction
Γ	The volumetric interfacial area

Subscript

dil	Dilute

g Gas phase
k Phase k
l Liquid phase
m Phase m
s Solid phase

REFERENCES

1. S. C. Saxena, D. Patel, D. N. Smith, and J. A. Ruether, Chem. Eng. Comm., 63, 87 (1988).
2. Y. T. Shah, B. K. Kelkar, S.P. Godbole, and W. D. Deckwer, AIChE J., 28, 353 (1982).
3. D. B. Bukur, J. G. Daly, and S. A. Patel, AIChE J., 36, 93 (1990).
4. J. C. Kuo, DOE Final Report, DE-AC22-83PC60019 (1985).
5. E. S. Sanders, E. L. Ledakowicz, and W. D. Decker, Can. J. Chem. Eng., 64, 133 (1986).
6. W. D. Deckwer, Y. Loiisl, A. Zaldi, and M. Ralek, Ind. Eng. Chem. Process. Des. Dev., 19, 699 (1980).
7. R. W. Lyczkowski, D. Gidaspow, C. W. Solbrig and E. D. Hughes, Nucl. Sci. and Eng., 66, 378 (1978) .
8. I. K. Gamwo, Y. Soong, D. Gidaspow and R. W. Lyczkowski, Proc. 13th Int. Conf. on Fluidized Bed Combustion, Vol. 1, pp. 297-303, ASME, (1995).
9. J. X. Bouillard, R. W. Lyczkowski, and D. Gidaspow, AIChE J., 35, 6, 908, (1989).
10. S. Okamura, S. Uchida, T. Katsumata, and K. Iida, Chem. Eng. Sci., 44, 196 (1989).
11. Y. Soong, J. J. Boff, F. W. Harke, A. G. Blackwell, and M. F. Zarochak, Proc. Coal Liquef. and Gas to Liq. Contr. Rev. Conf., 897 (1994).
12. A. Matsura and L. S. Fan., AIChE J., 30, 894 (1984)
13. G. E. H. Joosten, J. G. H. Schilder, and J. J. Jansen, Chem. Eng. Sci. 32, 563 (1977).
14. Y. Kato, A. Nishiwaki, T. Fukuda, and S. Tanaka, J. Chem. Eng. Japan., 5, 112, (1972).
15. Y. M. Kato, and A. Nishiwaki, Int. Chem. Eng., 12, 182 (1972).
16. H. Hammer, Int. Chem. Eng. 21, 173 (1981).
17. J. Chabot., and H. I. de Lasa, AIChE Annual meeting, Nov 1-6, 1992, Miami, FL
18. D. B. Bukur, J. G. Daly, and S. A. Patel, DOE Report, DE-AC22-86PC90012, (1990).
19. G. Rudinger, and A. Chang, Physics of Fluids, 7, 1747 (1964).
20. G. A. Saltanov, 1972, Supersonic Two-Phase Flow, Moscow, USSR
21. R. W. Lyczkowski, AIChE Symp. Ser., 75 (174):165-174, (1978).
22. D. Kunii, and O. Levenspiel, 1969, Fluidization Engineering, Wiley, NY.
23. Gidaspow, D., and Ding, J., DOE Report, DOE-PC-89769, March 1990.
24. J. S. Chang., Y. Ichikawa, G. A. Irons., E. C. Morala.,and P. T. Wan, Measuring Techniques in Gas Liquid Two-Phase Flows, Delhaye, J.M. and Cognet, G., Eds, Springer-Verlag, 319 (1984).
25. H. P. Bensler., J. M. Delhaye., and C. Favreau., Proc. ANS National Heat Transfer Confer. 240 (1987).
26. Y. Soong., I. K. Gamwo, A. G. Blackwell, R. R. Schehl, and M. F. Zarochak, Chem. Eng. J. (1995) in press.
27. D. McClements, J. Adv. Colloid Int. Sci. 37, 33 (1991).
28. L. W. Anson., and R. C. Chivers., J. Acoust. Soc. Am. 85, 535 (1989).

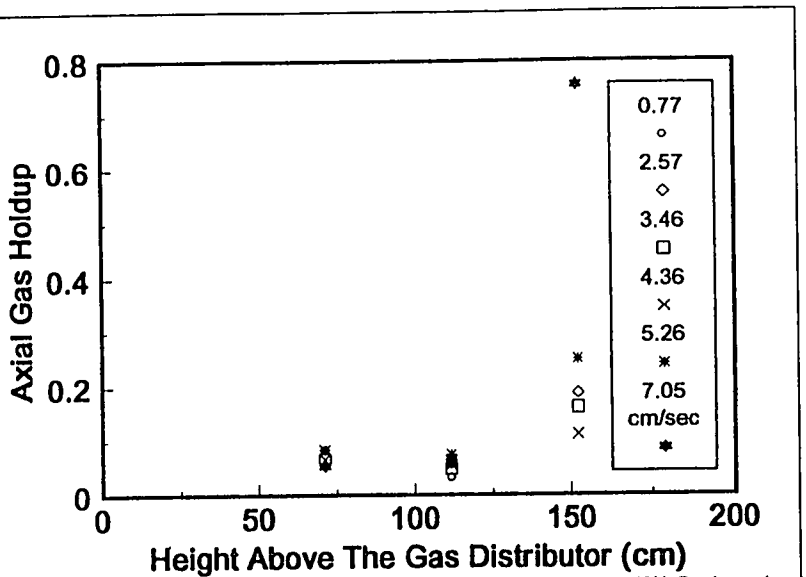

Figure 1. Effect of SFGV on Axial Gas Holdup in N2/Oil/Beads (20 wt%) System at Ambient Condition.

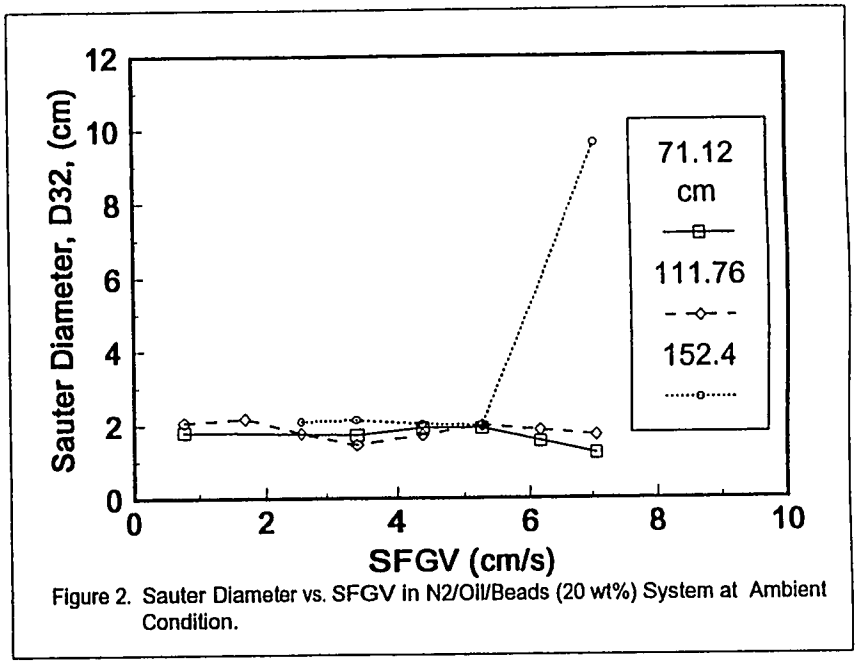

Figure 2. Sauter Diameter vs. SFGV in N2/Oil/Beads (20 wt%) System at Ambient Condition.

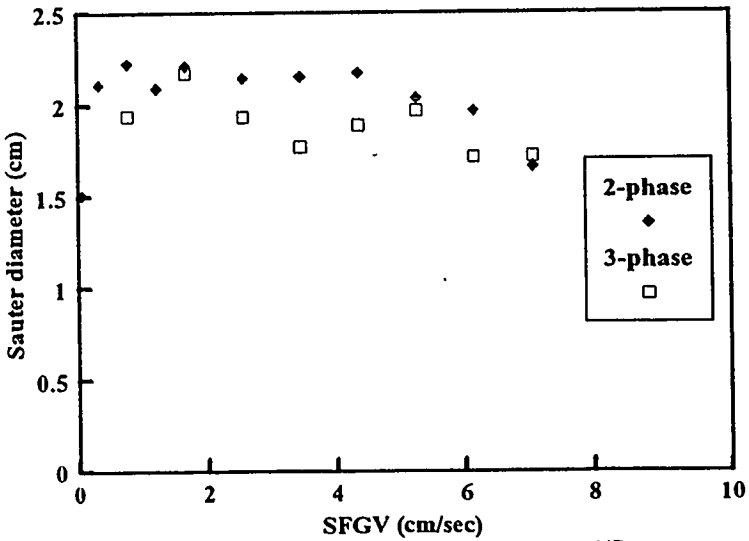

Figure 3 Effect of Solids and SFGV on Bubble Size at 20 °C and 0.1 MPa.

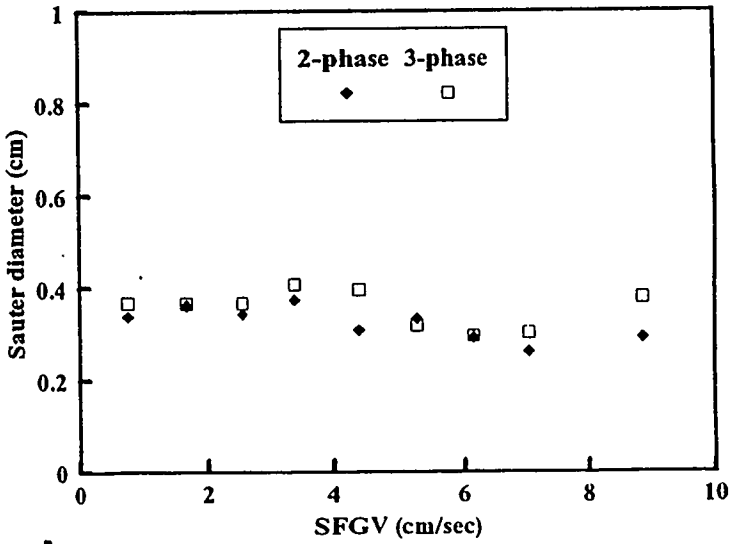

Figure 4. Effect of Solids and SFGV on Bubble Size at 200 °C and 1.36 MPa

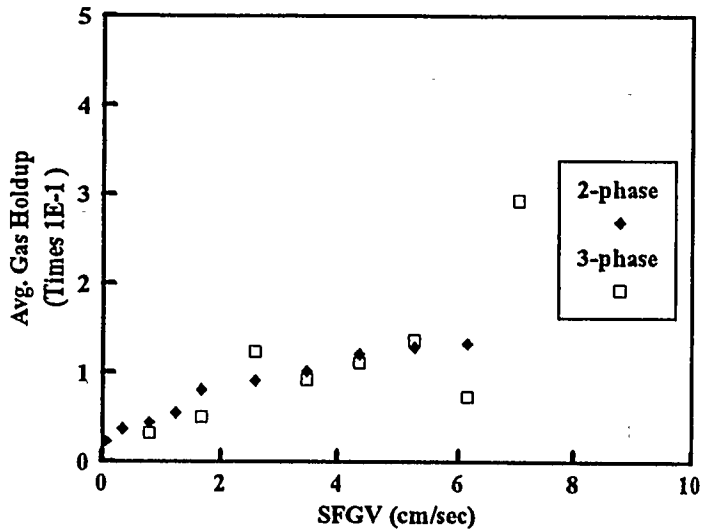

Figure 5. Effect of Solids (20wt%) and SFGV on Gas Holdup at 20°C and 0.1 MPa

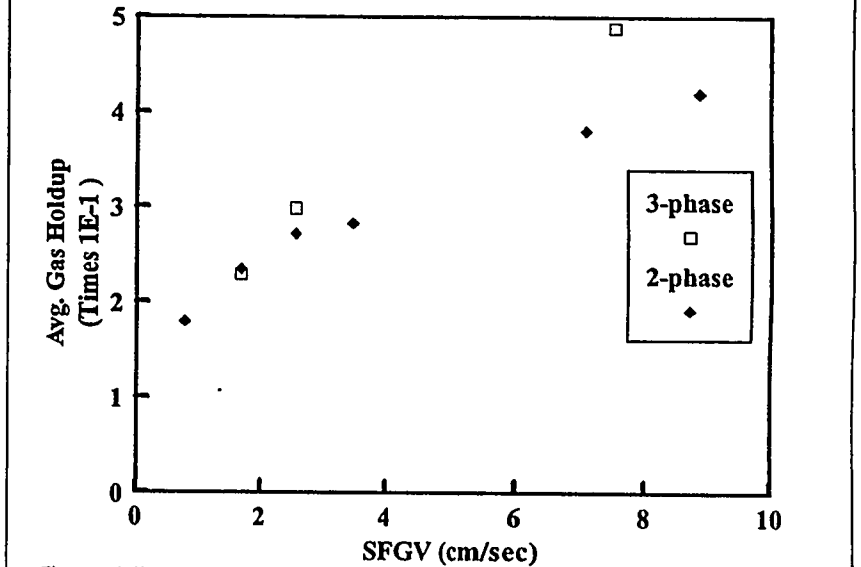

Figure 6. Effect of Solids (20wt%) and SFGV on Gas Holdup at 200°C and 1.36 MPa

DX min = 0.3175 cm
DY min = 0.3175 cm
DZ min = 2.1 cm

DX max = 3.0 cm
DY max = 0.635 cm
DZ max = 5.0 cm

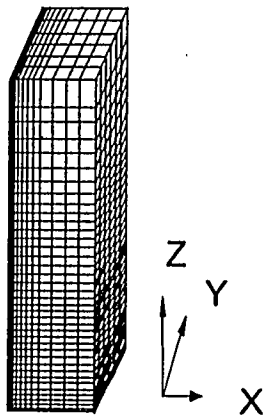

Figure 7. Finite Difference Cells.

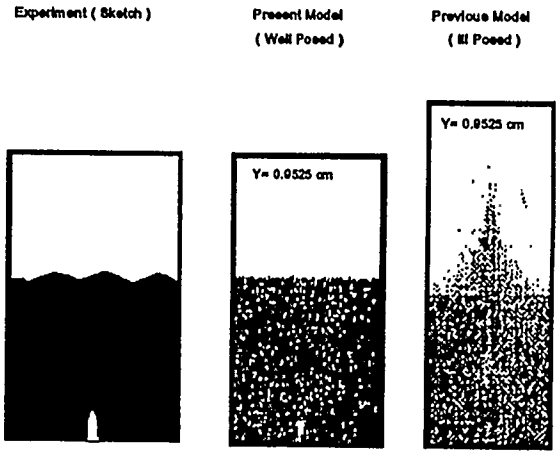

Figure 8. Comparison of Well-Posed and Ill-Posed Models Results with the Experiment (Sketch)

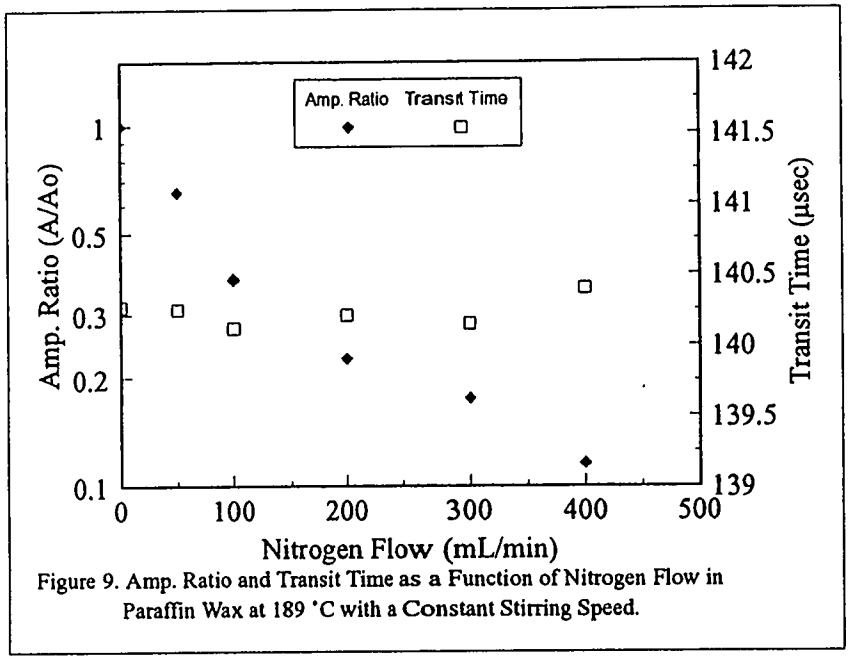

Figure 9. Amp. Ratio and Transit Time as a Function of Nitrogen Flow in Paraffin Wax at 189 °C with a Constant Stirring Speed.

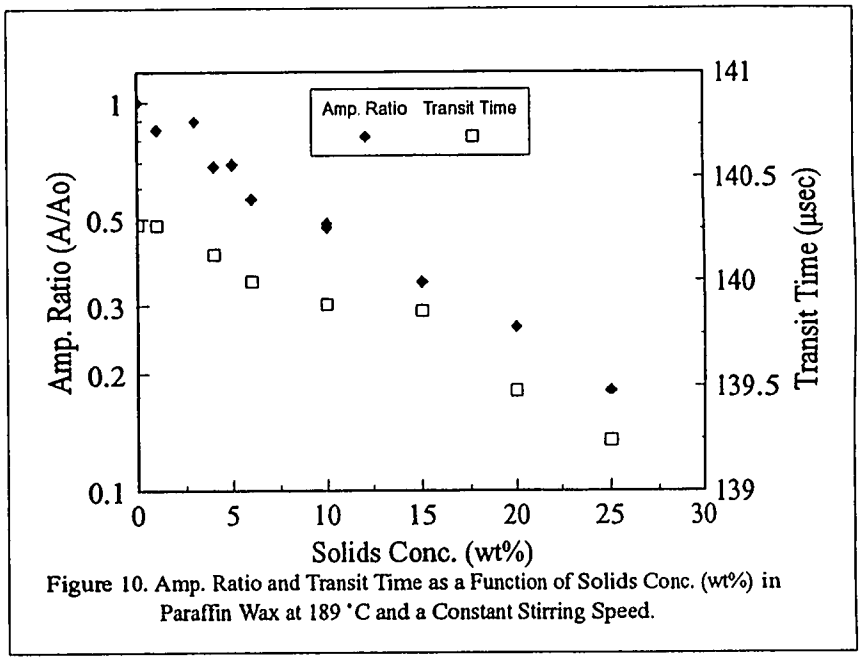

Figure 10. Amp. Ratio and Transit Time as a Function of Solids Conc. (wt%) in Paraffin Wax at 189 °C and a Constant Stirring Speed.

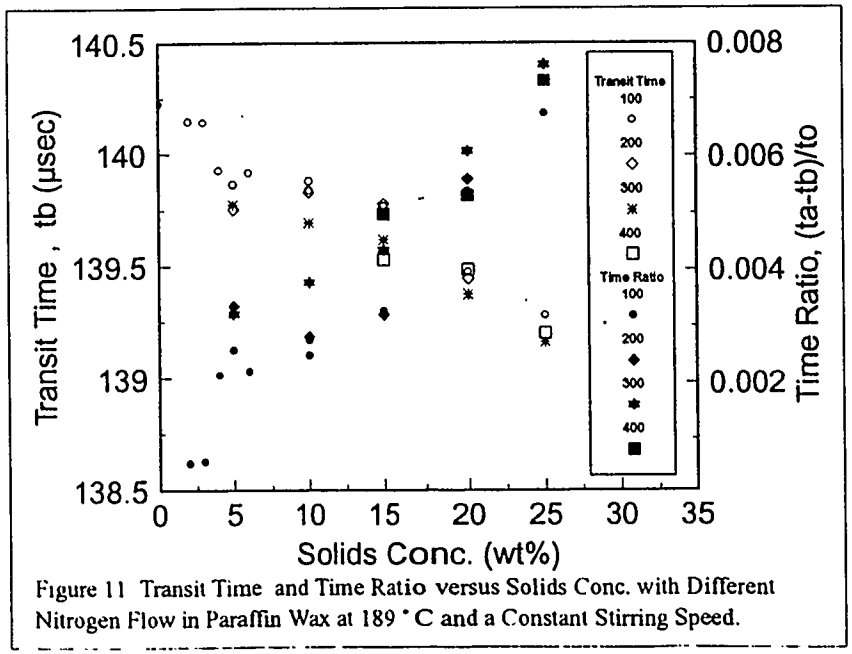

Figure 11 Transit Time and Time Ratio versus Solids Conc. with Different Nitrogen Flow in Paraffin Wax at 189 °C and a Constant Stirring Speed.

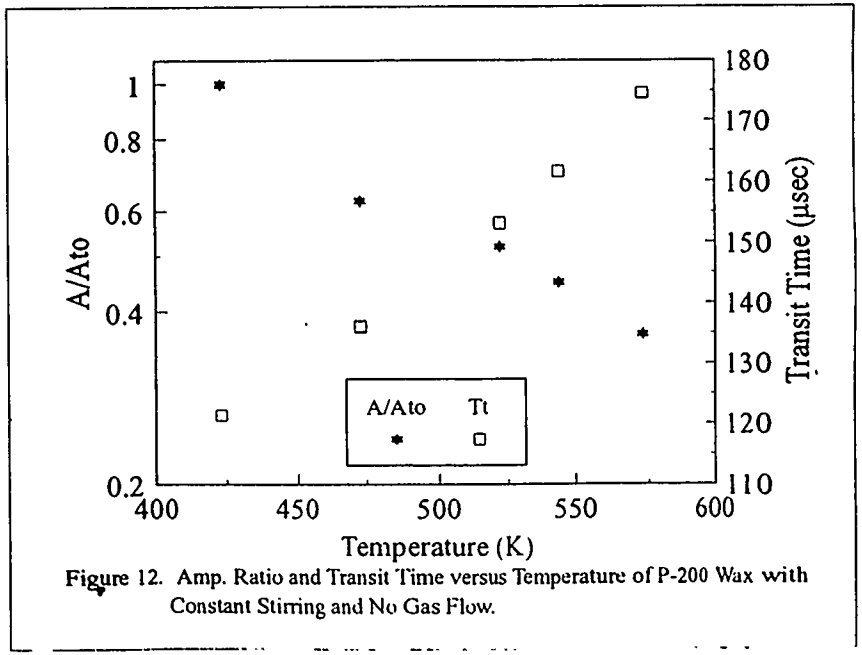

Figure 12. Amp. Ratio and Transit Time versus Temperature of P-200 Wax with Constant Stirring and No Gas Flow.

Title: INFLUENCE OF LIQUID MEDIUM ON THE ACTIVITY OF A LOW-ALPHA FISCHER-TROPSCH CATALYST

PI (Authors): Robert J. Gormley, Michael F. Zarochak, Paul W. Deffenbaugh*, and K.R.P.M. Rao**

Institution/Organization: U.S. Department of Energy/PETC, (*Gilbert/Commonwealth, Inc.) and (**University of Kentucky, CFFLS)

Period of Performance: Oct. 1, 1994 to Sept. 30, 1995

For: DOE Coal Liquefaction and Gas Conversion Contractors' Review Conference, Pittsburgh, Pa., Aug. 29-31, 1995.

OBJECTIVE

The purpose of this research was to measure activity, selectivity, and the maintenance of these properties in slurry autoclave experiments with a Fischer-Tropsch (FT) catalyst that was used in the "FT II" bubble-column test, conducted at the Alternative Fuels Development Unit (AFDU) at LaPorte, Texas during May 1994. The catalyst contained iron, copper, and potassium and was formulated to produce mainly hydrocarbons in the gasoline range with lesser production of diesel-range products and wax. The probability of chain growth α was thus deliberately kept low, hence the name "low-α" catalysts. Principal goals of the autoclave work have been to find the true activity of this catalyst in a stirred tank reactor, unhindered by heat or mass transfer effects, and to obtain a steady conversion and selectivity over the approximately 15 days of each test. This would typically require that activity be unaffected by variations of the initial wax medium or by increasing the weight % catalyst loading in the slurry. Nevertheless, slurry autoclave experiments have demonstrated a dependence on initial wax medium and on weight % catalyst loading. We report research attempting to clarify these effects. The reaction experiments were correlated with the results of Mossbauer spectroscopic analysis of the iron catalyst composition. These reactor tests were conducted using most of the same run parameters as those used in the AFDU bubble column reactor.

Slurry autoclave testing of a "low-α" catalyst in heavier waxes also allows insight into operation of larger slurry bubble column reactors. The hydrodynamic properties of the slurry liquid should, under these conditions, resemble the properties in a reactor containing either a "high-α" catalyst or a "lower-α" catalyst initially charged with a typical FT wax. (After a short time, the heavier wax products from a "high-α" catalyst displace the initial wax.) Thus, the stability of reactor operation in these experiments, particularly at loadings exceeding 20 weight %, suggests the likely stability of operations on a larger scale.

APPROACHES

The catalyst was prepared at United Catalysts Inc. (UCI). The catalyst contained 86.6% by weight Fe_2O_3, 12.5% CuO, and 0.05% K_2O. There was also 0.37% sulfur present as an impurity. The catalyst was formed by spray drying and no binder was added. The agglomerates were submicron to 60 microns in diameter, and broke down further inside the reactor.

Either 36.5 g (9 weight % catalyst in slurry wax) or 86.6 g (23 weight %) of catalyst were added initially to 290 or 370 g of wax in the reactor. One of three different waxes were loaded initially in the reactor: purified n-octacosane, (C_{28}), a heavier wax composed of linear polyethylene chains (Polywax-655) made by Petrolite Corporation or another heavy wax obtained from Allied-Signal, #AC1702, which had its lightest compounds distilled off at the University of Kentucky, CAER. All the tests were conducted in a 1-L Autoclave Engineers (AE) stirred tank reactor with either the original hollow shaft and stirrer or with a larger diameter hollow shaft and stirrer obtained from Pressure Products Industries (PPI). Figure 1 shows the internals of the reactor. Gas was introduced through a 1/8" tube at the bottom of the reactor while stirring was maintained at 1000 rpm (except where otherwise noted). Other experimental details are given in our previous work [1,2,3].

The catalyst was activated in 1.4 L CO/g Fe hr at 270° C and 1.31 MPa for 22 hours. The synthesis was conducted for up to 15 days at 1.31 MPa and 270° C, using a H_2/CO ratio of 0.70. The flowrate was 2.4 L syngas/g Fe hr. The volatile liquid products were collected continuously in a trap maintained at 20° C and vaporized wax was collected in a 200° C trap, while the heavier wax products remaining in the reactor were sampled for analysis. Samples for Mossbauer analysis of catalyst composition were obtained from these reactor samples. The gaseous products were analyzed every 24 hours by an on-line gas chromatographic (GC) system. A material balance based on weights of reactants and products was calculated for each 24-hour period. From this, the conversions and selectivities were determined. Mossbauer analyses gave the iron composition present in the catalyst at various points in the tests [4].

CURRENT STATUS

One initial wax tested was purified $C_{28}H_{58}$, n-octacosane. The higher flow rate used in the experiment with high weight % catalyst caused rapid loss of wax from the reactor and a substantial decrease in the reactor liquid level. The conversions are shown in figure 2. Approximately 71 grams of 270 grams of n-octacosane loaded initially was lost by the end of 75 hours. It is assumed that the drop off in conversion was related to the loss of liquid from the reactor.

In order to limit the loss of reactor wax in experiments with "low

α" catalysts, other heavier waxes were considered for the initial medium, some commercially prepared and some from F-T reactors. Use of heavier waxes required the development of a new method for wax analysis. This is because the gas chromatograph used at this laboratory for wax analysis was not a high temperature apparatus and could only elute peaks up to a carbon number of 42, although many of the waxes considered had a significant weight % exceeding C_{42}. The new method was to dissolve the starting waxes in solvent as before, but then spike the solution with a known weight of a branched C_{19} compound, and inject the spiked liquid onto the chromatographic column. The weight % values for compounds $\leq C_{42}$ can then be obtained from the internal standard. The weight %'s $\leq C_{42}$ determined for each prospective wax are given in Table 1, along with the average carbon number if known. Polywax-655, with a nominal average carbon number of C_{48}, has 25.9 % of wax $\leq C_{42}$ and is clearly much heavier than n-octacosane. It resembles an FT wax, with straight, but only even carbon number chains. It is similar to an end-of-test Mobil wax from a "high-α" FT run (CT256-4+7), which has 24.3 % C_{18}-C_{42}. The Allied-AC1702 wax had very little hydrocarbon $\leq C_{42}$. The distillation by Burt Davis' group at Kentucky CAER [5] yielded the heaviest wax seen in this study.

The F-T synthesis was conducted at 10 % wt catalyst with three different initial waxes. In figure 3, the effect of initial wax composition on (H_2+CO) conversions is shown. The most stable conversions resulted when the lightest wax, n-octacosane was used. When the heavier Polywax-655 was used, the conversions were initially as high but decreased to 60 % in 13 days. When the heaviest wax, distilled Allied-AC1702 was used, conversions were initially lower and decreased to 60 % in 12 days. These results with the Allied wax matched results previously reported at Kentucky CAER [5]. Clearly the wax medium affected the conversion. However, two other parameters were varied in these tests. The Autoclave Engineer's shaft and stirrer, rather than the PPI shaft and stirrer, were used for the test in n-octacosane. Only 290 grams, rather than 370 grams, of initial wax was loaded of distilled Allied wax.

To ensure that the trend in figure 3 was due to the effect of initial wax, the test in n-octacosane was repeated with the PPI stirrer and shaft. These conversions are shown in figure 4 and can be compared to those shown in figure 3. The conversions in n-octacosane were similar to those in the initial test in n-octacosane with the A.E. shaft and stirrer. They would likely have remained steady above 80% out to 300 hours. The test in distilled Allied wax was repeated but with 370 grams rather than 290 grams of wax, and there was some small improvement in conversion. Perhaps this was due to the increased residence time of the bubbles compared with the test in 290 grams. There was again the same trend of a sharp drop in conversion with the two heavier waxes.

Chao and Lin [6] report solubilities of reactants and product gases

in four waxes: C_{28}, C_{36}, Sasol Arge wax, and Mobil-CT-256-7 FT wax. The solubilities of the gases H_2, CO, CH_4, CO_2, and C_2H_6 are shown in Table 2. The waxes are shown in order of increasing carbon number. Solubilities do decrease as the wax becomes heavier. Solubilities in Mobil wax (average carbon number 61) are 70-75 % those in C_{28} wax.

One might propose a simple model which states that: because the solubilities of the reactant gases are lower in a heavier wax than in a lighter wax, the conversions would be proportionately lower. This would assume a simple first-order reaction rate. It would be assumed that the number of active sites are constant no matter what wax is used. Figure 5 plots actual data in C_{28} wax, and two "guesses" for reaction behavior in the heavier waxes in which the C_{28} data is corrected for lower solubilities. This simple model clearly does not work. It predicts lower activity throughout the life of a run, while figures 3 and 4 show that the initial conversions in the three waxes are nearly the same, while the deactivation rates are different.

This raises the question of what is causing the timing and severity of the deactivation among the different waxes. Mossbauer spectroscopy was used to identify iron phases on samples withdrawn from the reactor at various times during the activation and syntheses for several tests. Figure 6 shows the results of the test conducted in Polywax-655. After 22 hours of activation in CO, the iron oxide was converted to 81 % χ-carbide. After 6 days of synthesis some of the χ-carbide has converted back to Fe_3O_4, perhaps due to the presence of oxidizing product gases. The χ-carbide has reached a steady value of 50%, while the other 50% is made up of Fe_3O_4 and super-paramagnetic particles (probably composed of α-FeOOH). In previous work [4] it was proposed that the level of conversion is related to the amount of χ-carbide formed during activation and is best when the χ-carbide starts high, at 80% to 90%, and then is converted to include some Fe_3O_4. A poorer form of the catalyst is found in activations that yield a moderate amount of χ-carbide, say 50%, which grows to a higher amount during synthesis. Our Mossbauer results indicate that catalysts are being activated to the same extent in either the C_{28} or the Polywax media after the 22 hour activation (carbiding) period. However, in the distilled Allied wax, the catalyst was carbided to a lesser extent, 64% after activation. It reached only 42% during synthesis. Whether this has any correlation with the deactivation rate is not yet known.

In one other way, the activations in the three waxes were not totally identical. The cumulative amounts of CO_2 made from CO during the 22 hour activations were different. The legend in figure 4 shows these differences as a theoretical percentage. If all the Fe_2O_3 had been converted to χ-carbide and if all the CuO had been converted to Cu, the amount of CO_2 produced would have been equal to a certain number of moles which was called 100%. In C_{28} wax, where CO is most soluble, 250% of the theoretical CO_2 was made

in carbiding and carbon formation. However, in the Polywax-655 and the distilled Allied wax, only 150% of the theoretical CO_2 was made. So the catalyst activated in C_{28} wax might have had a greater amount of surface carbon produced. Whether this had any influence on the drop in conversion rate is not yet known. (Latest tests show these results may be an artifact of the experiments.)

The rate of the water gas shift (WGS) reaction ($H_2O + CO \rightarrow H_2 + CO_2$) decreased along with the overall rate of syngas conversion. It is difficult to separate the influence of each reaction on the other. The decrease in the WGS conversion may be influencing the decrease in the FT conversion since the WGS reaction may be catalyzed by different sites than is the F-T reaction, perhaps by Fe_3O_4 versus χ-carbide sites. Or both reactions may be decreasing simultaneously. The apparent shift constant, R, begins near the equilibrium value of 62 for the WGS reaction in each of the three waxes. At this point, most of the oxygen from dissociated CO leaves as CO_2 rather than as H_2O. The shift constant decreases as syngas conversion decreases. Figure 7 shows an increase in the grams of water produced per day at lower conversions. Therefore the partial pressure of water in the reactor is actually increasing significantly over time for the heavier waxes, but not for the C_{28} wax.

Koenig et al. [7] reported FT conversions and Anderson-Schulz-Flory (ASF) distributions on iron foils with and without potassium and with and without water vapor added. They concluded that catalyst sites promoted with potassium "are more stable with respect to oxidation (deactivation) by water than unpromoted sites." They did not speculate whether the WGS sites are the same as the FT catalytic sites. This catalyst clearly has very few sites promoted with potassium compared with other previously tested FT catalysts. The catalyst may be subject to a more rapid deactivation by water than those FT catalysts with higher loadings of potassium. However, one must then explain why more water would be formed in the case of the heavier waxes.

Figures 8 and 9 show the effect of stirrer speed on conversion, using 11 weight % catalyst in Allied wax. This technique tests for gas/liquid or film mass transport limitations. Rpm's and flows were varied in the same test. Figure 8 shows that at 1.5 times the baseline flow, the conversion dropped as stirrer speed went below 500 rpm. This behavior was expected. In going from the baseline stirrer speed of 1000 rpm to 1200 rpm, the conversion reached a plateau. There can then be said to be no apparent gas/liquid or film mass transfer limitations in this wax. A few days of test were run at the normal flow, shown in figure 9, where the conversions were up near 85% and again there was little change in going from 1000 rpm to 1200 rpm. This, however, does not rule out all mass transfer or diffusion limitations in the heavier waxes.

In figure 10, conversions are plotted for a loading of 19 weight % of the LaPorte FT-II catalyst in 370 grams of Polywax-655.

Conversions started high, near 83 %, and decreased to 60 % by the end of 7 days. This decrease was more severe than that seen for 9 weight % catalyst in Polywax-655. Only a cumulative total of 5 grams of Polywax-655 was lost over 8 days for the figure 10 results. Therefore the loss of a sufficient liquid level cannot be blamed for this sharp decrease, as was suggested for the figure 2 results. How much of this drop in conversion was due to the use of a heavier wax and how much was due to additional mass transfer limitations at the higher weight loading and higher flow still need to be determined.

PLANS

The reasons for the conversions' deactivation in Polywax-655 and Allied wax still need to be explored. We also plan to retest this catalyst at a high weight loading with the C_{28}, light wax. This retest will involve modifying the unit to allow daily addition of C_{28} wax to the reactor to maintain the liquid level. If wax addition is successful at 10 weight % catalyst loading, we will go to $\geq$20 weight % catalyst loading and hope to obtain a steady conversion lasting about 15 days.

CONCLUSIONS

In general, Polywax-655 and distilled Allied wax have the same advantage over n-octacosane in their slow rate of leaving the reactor at high flows. Conversions using these two heavier waxes, however, show more of a decrease over time than conversions in n-octacosane. Reasons for these trends still need to be understood. Catalysts with 0.05 wt% K_2O could be very sensitive to the partial pressure of water present in the reactor.

REFERENCES

1. "A Study of Iron Fischer-Tropsch Catalysis," M.F. Zarochak and M.A. McDonald, 7th DOE Indirect Liquefaction Contractors' Review Meeting, Pgh. Pa., Dec. 8-9, 1987.

2. "Slurry Phase Fischer-Tropsch Catalysis," R.J. Gormley and M.F. Zarochak, 11th DOE Indirect Liquefaction Contractors' Review Meeting, Pgh. Pa., Sept. 3-5, 1991.

3. "Testing Low-Alpha Fischer-Tropsch Catalysts," R.J. Gormley and M.F. Zarochak, P.W. Deffenbaugh, and K.R.P.M. Rao, DOE Coal Liquefaction and Gas Conversion Contractors' Review Conference, Pgh. Pa., Sept. 7-8, 1994.

4. "Mossbauer Spectroscopy Study of Iron-based Catalysts used in Fischer-Tropsch Synthesis," K.R.P.M. Rao, F.E. Huggins, G.P. Huffman, B. Davis, R.J. O'Brien, R.J. Gormley, and D.B. Bukur, ACS National Meeting, Div. of Fuel Chem., Anaheim, CA, Apr. 2-7, 1995.

5. "Technology Development for Iron Fischer-Tropsch Catalysts,"

B.M. Davis, F.L. Tungate, L. Xu, R.L. Spicer, D.J. Houpt, R.J. O'Brien, R. Lin, D.R. Milburn, S. Chokkaram, and K. Chary, DOE Coal Liquefaction and Gas Conversion Contractors' Review Conference, Pgh. Pa., Sept. 27-29, 1993.

6. "Synthesis Gas Solubility in Fischer-Tropsch Slurry," K.C. Chao and H.M. Lin, Purdue Univ., Final Report to U.S. Dept. of Energy, Contract No. DE-AC22-84PC70024, July 20, 1987.

7. "The influence of water and of alkali promoter on the carbon number distributions of Fischer-Tropsch Products Formed over Iron Catalysts," L. Koenig, J. Gaube, W Meisel, P. Gutlich, W. Gerhard, and C. Plog, Ber. Bunsenges. Phys. Chem., 91, 116-121, 1987.

The authors would like to acknowledge: Richard Anderson, Bob Ferrence, Joseph Hackett, and Donald Martello for analytical support; the Gilbert-Commonwealth technicians: Ed Smerkol, Jim Barnhart and Ray Rokicki for conducting the experiments, Art Blackwell for preparing the reactor drawing and Mark McDonald for editing assistance.

LIQCONPA.956

Table I

GAS CHROMATOGRAPHIC ANALYSES OF COMMERCIAL OR F-T WAXES

WAX	WT % < C_{42}	REPORTED AVG C #
N-OCTACOSANE	100.0 %	PURE C_{28}
DRAKEOL-10	-	$C_{30,??}$
ETHYLFLO-164	-	$C_{30,40}$
C_{36} H_{74}	104.0 %	C_{36}
POLYWAX-500	59.2 %	C_{36}
SASOL-7-91	49.2 %	C_{43} OR 47
ETHYLFLO-170A	40.4 %	$C_{40,50}$
LAPORTE-I–ROSE-383A	37.9 %	
POLYWAX-655	25.9 %	C_{47}
MOBIL-CT256-4+7	24.3 %	C_{61} OR 85
ALLIED-AC1702	7.9 %	
DIST. ALLIED-AC1702	3.4 TO 5.4 %	

All spiked with tetra Me-C_{15}, and dissolved in CS_2 or decalin

Table II

GAS SOLUBILITIES IN DIFFERENT WAXES *

MOLES GAS / KG WAX @ 300 ° C , 2.0 MPa

GAS	$C_{28}H_{58}$	$C_{36}H_{74}$	SASOL (Arge) Avg. C No.= 43	MOBIL CT-256-7 Avg. C No. = 61
H_2	0.155	0.133	0.130	0.111
CO	0.182	0.161	0.161	0.130
CH_4	0.288	0.254	0.247	0.208
CO_2	0.352	0.316	0.305	0.271
C_2H_6	0.504	0.463	0.409	0.350

* Chao and Lin, Purdue U., Final Report DE-AC22-84PC70024, 1987.

MODIFIED REACTOR
WITH LARGER HOLLOW SHAFT / STIRRER FOR GAS RECYCLE

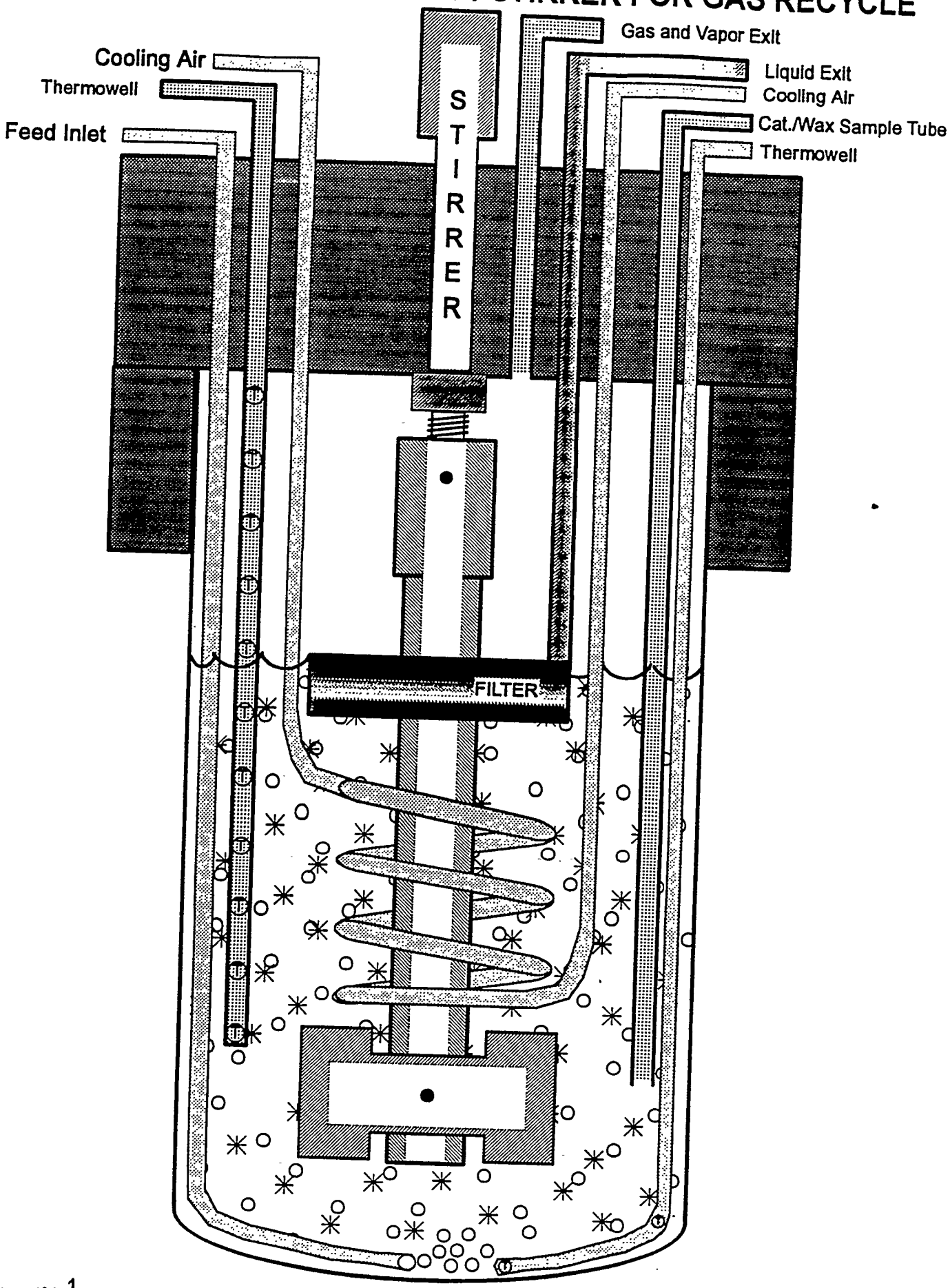

Figure 1

CONVERSIONS FOR 23 WT % LaPorte II CATALYST in 290 gm C28 WAX

Increased Wt % with proportionately higher flow

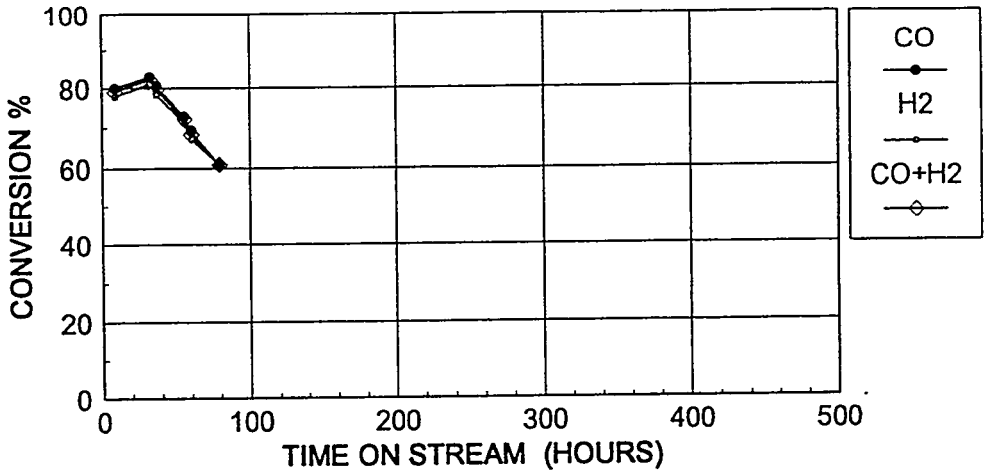

PETC TEST S3-09, A.E. STIRRER, 7 HR CO ACTIVATION
CUMULATIVE WAX LOST = 71 GM

Figure 2

EFFECT OF INITIAL WAX COMPOSITION ON CONVERSION 9 OR 11 Wt % LaPorte II Catalyst

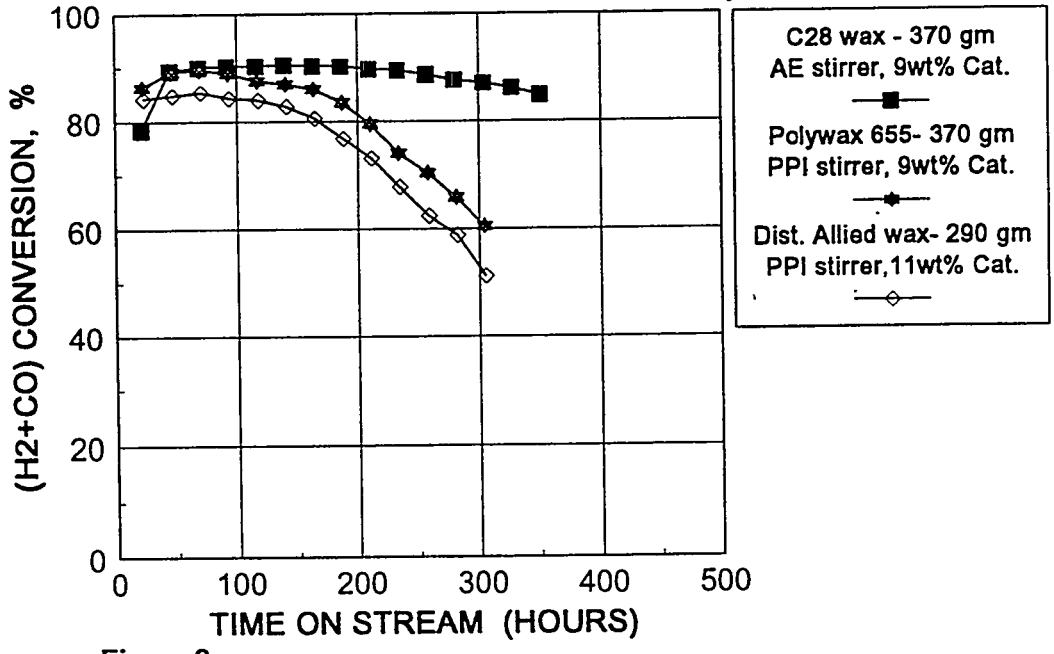

Figure 3

EFFECT OF INITIAL WAX ON USE OF CO IN ACTIVATION
9 Wt % LaPorte II Catalyst, PPI Stirrer, 370 gm Wax

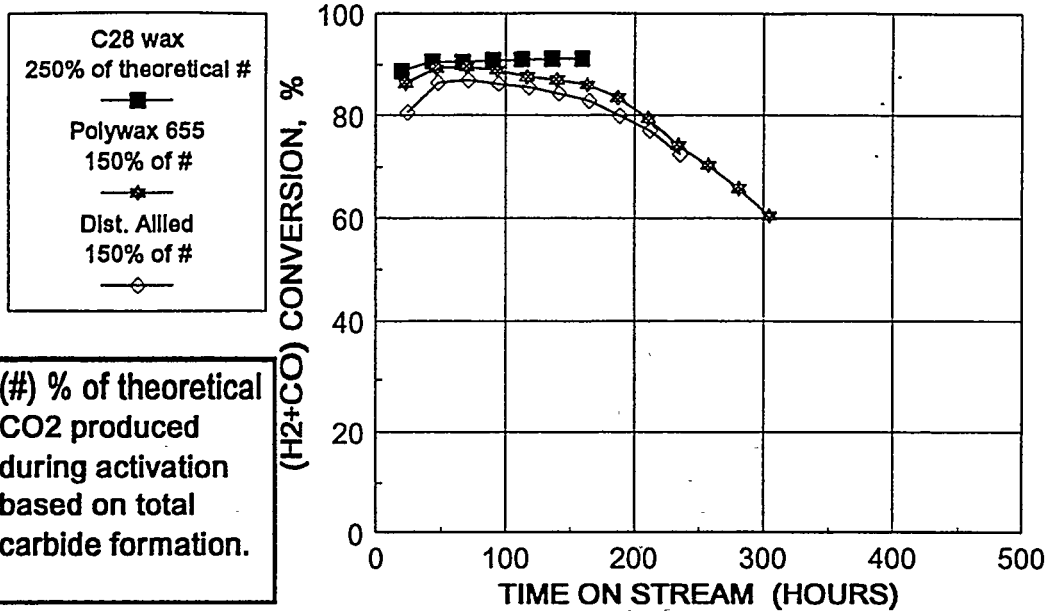

Figure 4

H2 + CO CONVERSIONS, EXPECTED IN HEAVIER WAXES
9 Wt % La Porte II Catalyst in 370 gm Wax

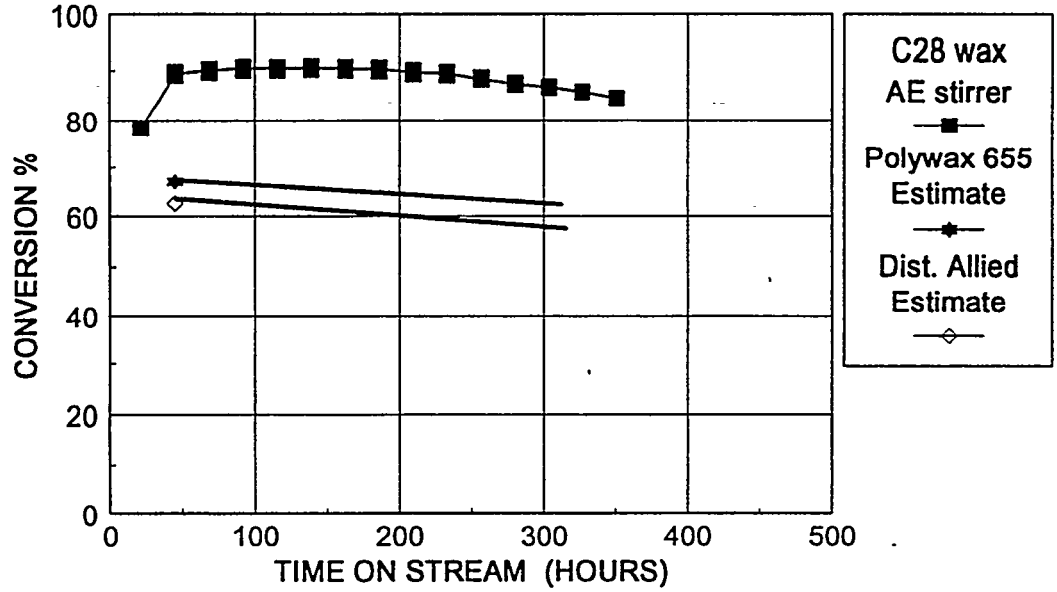

Figure 5

MOSSBAUER SAMPLES - 9 WT % CAT. IN POLYWAX

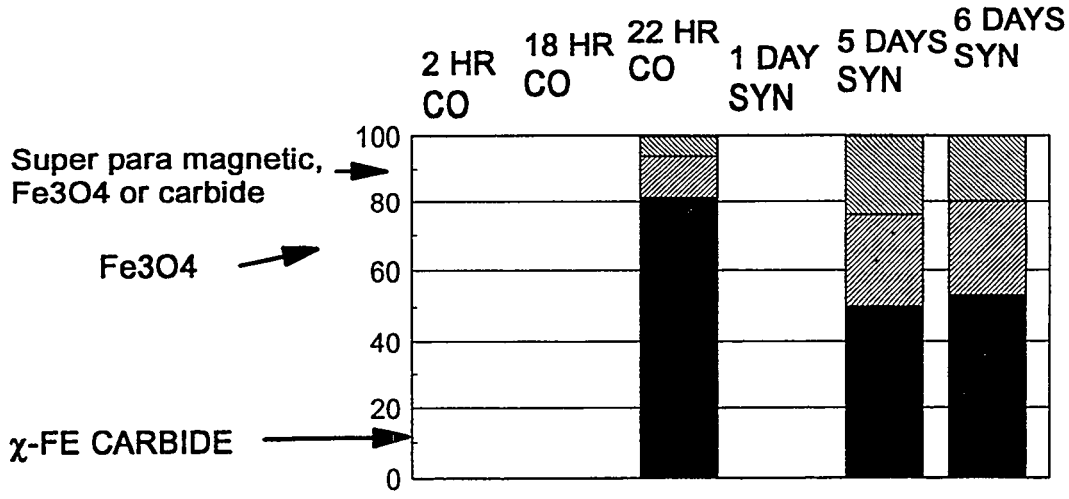

	2 hr CO	18 hr CO	22 hr CO	1DAY SYN	5 DAYS SYN	6DAYS SYN
chi carbide			81		50	53
Fe3O4			13		26	27
SPM Fe3O4 (or carbide)			6		24	22
epsilon carbide			0		0	0

Figure 6

WATER VAPOR IN PRODUCT STREAM ; DIFFERENT WAXES
9 OR 11 Wt % LaPorte II Catalyst

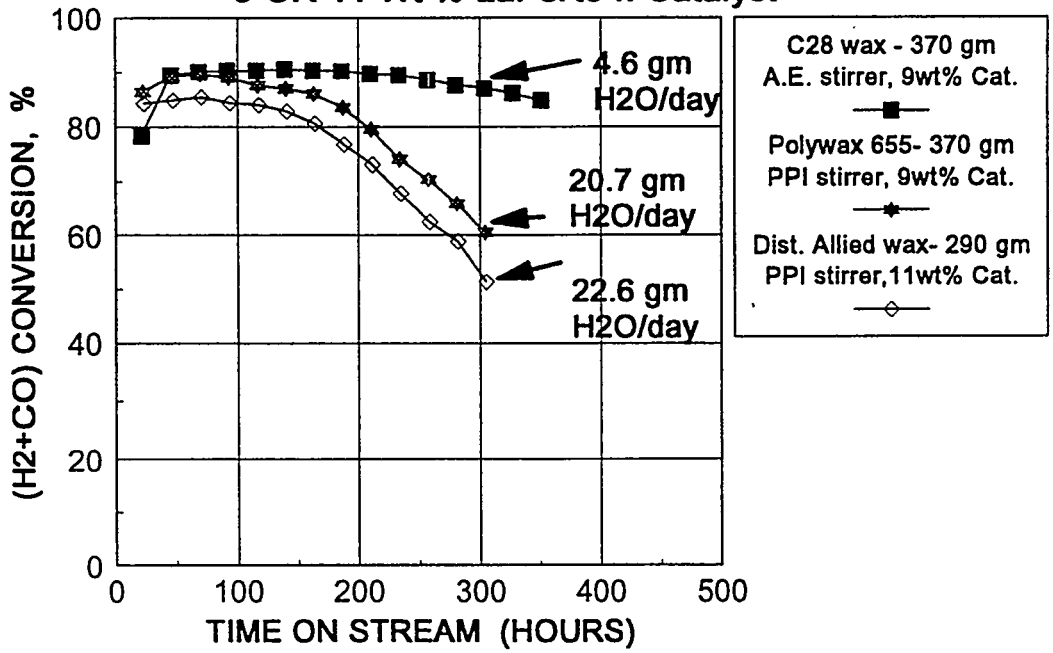

Figure 7

EFFECT OF STIRRER SPEED ON CONVERSION
with SYNGAS FLOW = 1.5 X Normal

11.2 WT % LaPorte II Cat. in 290 gm Dist. Allied Wax

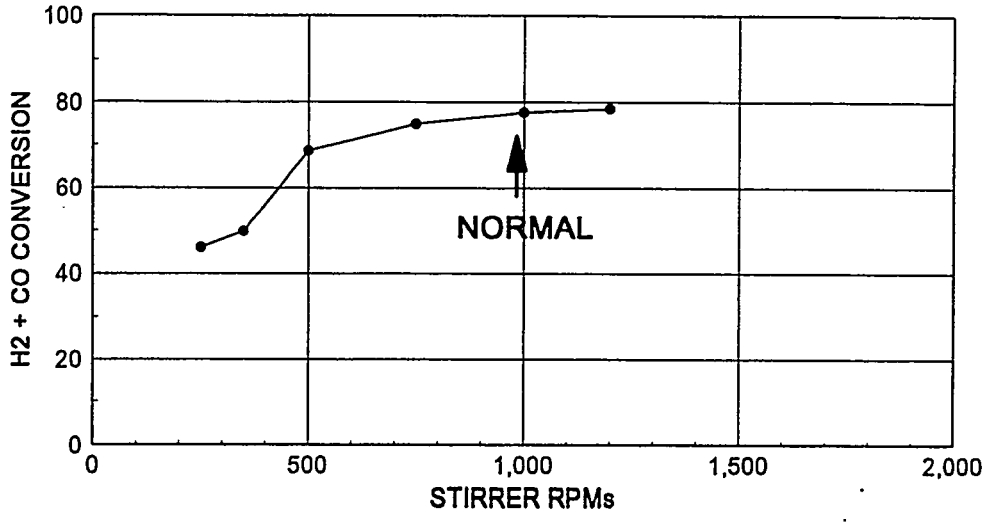

Figure 8

EFFECT OF STIRRER SPEED ON CONVERSION
with SYNGAS FLOW = 1.0 X Normal

11.2 WT % LaPorte II Cat. in 290 gm Dist. Allied Wax

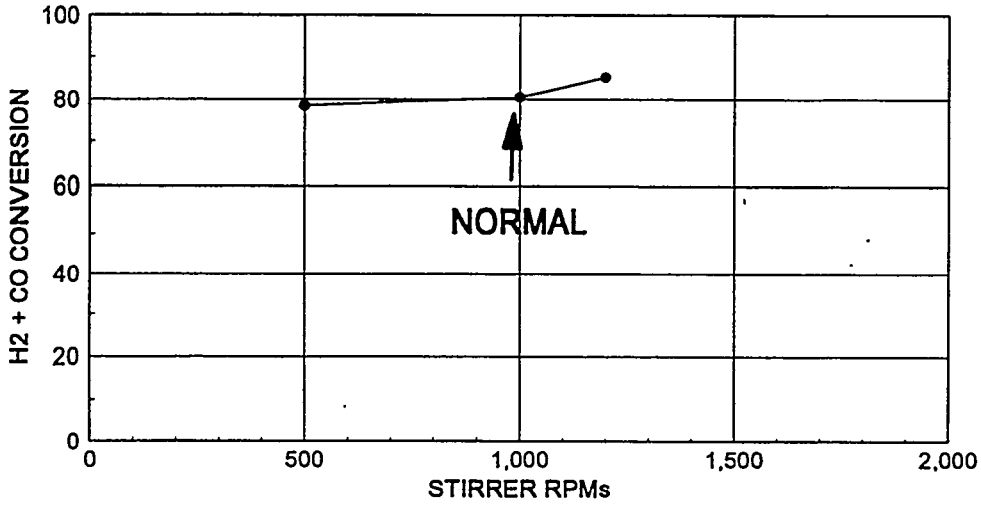

Figure 9

CONVERSIONS FOR 19 WT % LaPorte II CATALYST in 370 gm POLYWAX-655

Increased Wt % with proportionately higher flow

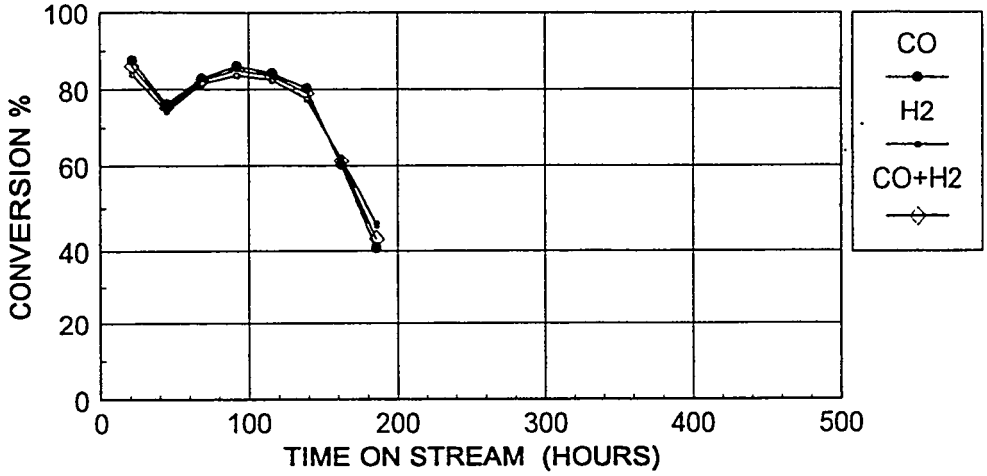

PETC TEST S3-14 , PPI STIRRER, 22 HR CO ACTIVATION
CUMULATIVE WAX LOST= 5 GM

Figure 10

TITLE: MÖSSBAUER STUDY OF IRON-CARBIDE GROWTH AND FISCHER-TROPSCH ACTIVITY

PIs (AUTHORS): K.R.P.M. Rao, F.E. Huggins, and G.P. Huffman, R.J. Gormley[1], R.J. O'Brien[#], and B.H. Davis[#]

INSTITUTION/ORGANIZATION:

University of Kentucky, 341, Bowman Hall, Lexington, KY 40506-0059 and [#]Center for Applied Energy Research, Lexington, KY 40511, [1]Department of Energy, Pittsburgh, PA 15236

CONTRACT NUMBER: DE-AC22-93PC93066

PERIOD OF PERFORMANCE: Jan 12, 1994 - Jan 11, 1997

OBJECTIVE: The objective of the project is to develop an understanding of the catalytic conversion of synthesis gas into liquid products through a determination of the phases, structure, and particle-size distributions of the iron-based catalysts, as measured by Mössbauer and XAFS spectroscopies. Relationships that exist between process conditions and the iron-bearing phases in the catalyst are investigated in the present studies.

ACCOMPLISHMENTS AND CONCLUSIONS: The present studies indicate that the presence of carbides is essential but not a sufficient condition for good FT activity. It is shown that the nature of growth of carbides during pretreatment and FT synthesis is correlated with the FT activity.It is also shown that the pressure at which the catalyst is activated affects the carbide phase formation. The liquid medium used for the FT synthesis is shown to alter the phase distribution. Heavy wax medium gave rise to less carbide as compared to light wax medium.

ABSTRACT: There is a need to establish a correlation between the Fischer-Tropsch (FT) activity of an iron-based catalyst and the catalyst phase during FT synthesis. The nature of iron phases formed during activation and FT synthesis is influenced by the nature of the gas and pressure apart from other parameters like temperature, flow rate etc., used for activation. Mössbauer investigations of iron-based catalysts subjected to pretreatment at two different pressures in gas atmospheres containing mixtures of CO, H_2, and He have been carried out. Studies on UCI 1185-57 (64%Fe_2O_3/5%CuO/1%K_2O/30% Kaolin) catalyst indicate that activation of the catalyst in CO at 12 atms. leads to the formation of 100% magnetite and the magnetite formed gets rapidly converted to at least 90% of χ-Fe_5C_2 during activation. The FT activity was found to be good at 70-80% of (H_2+CO) conversion. On the other hand, activation of the catalyst in synthesis gas at 12 atms. leads to formation of Fe_3O_4 and it gets sluggishly converted to χ-Fe_5C_2 and $\acute{\varepsilon}$-$Fe_{2.2}C$ during activation and both continue to grow slowly during FT synthesis. FT activity is found to be poor.

Pretreatment of the catalyst, 100Fe/3.6Si/0.71K at a low pressure of 1 atms. in syngas gave rise to the formation of χ -Fe_5C_2 and good FT activity. On the other hand, pretreatment of the catalyst, 100Fe/3.6Si/0.71K at a relatively high pressure of 12 atms. in syngas did not give rise to the formation any carbide and FT activity was poor.

INTRODUCTION: Pretreatment of iron catalysts is an important step in the development of an efficient catalyst. It affects the distribution of iron phases that are formed during the pretreatment and changes that take place during synthesis. It is controlled by the type of gas, temperature (T), pressure (P) and gas space velocity (S.V.) used. The FT activity and possibly selectivity are related to the iron phases present in the catalyst; however the role of any specific phase on the FT synthesis is not yet clearly understood.

Mössbauer characterization of two iron based catalysts, viz., UCI 1185-57 (64%Fe_2O_3/5%CuO/1%K_2O/30% Kaolin) and UCI 1185-149 (57.2Fe/9.3Cu/0.05K) has been carried out with a view to identify and quantify the different iron phases that are present in the activated and spent catalysts and study their influence on Fischer-Tropsch (FT) synthesis. The catalysts were activated in (i) CO and (ii) H_2/CO (syngas) and then subjected to FT synthesis.

EXPERIMENTAL:

(I) ASSOCIATION OF CARBIDE PHASE WITH FT ACTIVITY

CO-ACTIVATED UCI 1185-57 CATALYST: The UCI 1185-57 catalyst (64%Fe_2O_3/5%CuO/1%K_2O/30% Kaolin) was ramped to 270°C @1.5°C/min under CO atmosphere at 175psig and maintained at 270°C in CO for 24hrs with a flow rate of 2.0nL/hr/g-Fe at 175psig. It was then subjected to FT run with a syngas of H_2/CO=0.7 at 270°C, with a space velocity=3.4nL/hr/g-Fe at 175psig. The catalyst samples were withdrawn at various times during pretreatment and FT synthesis. The phase distribution determined is shown in Fig.1. The phases formed consist of magnetite, chi-carbide and a superparamagnetic phase (spm phase) which is an oxide. χ-Fe_5C_2 phase, to the extent of 90%, is formed rapidly during the 24hrs of activation in CO.

SYNGAS-ACTIVATED UCI-1185-57 CATALYST: The UCI 1185-57 catalyst was preheated in He up to 200°C at 2.0°C/min at 150psig and then to 280°C, at 7.0°C/min. and held for 12hrs. The FT synthesis was carried out in (H_2+CO)=0.7 with a flow rate of 2.5nL/hr/g-Fe at 265°C and 200psig. The catalyst samples were withdrawn at various times during pretreatment and FT synthesis. The phase distribution determined is given in shown in Fig.2. As compared to the CO pretreatment, activation in synthesis gas, leads to slow growth of χ-carbide and é-carbide at the expense of Fe_3O_4. The carbides are formed in proportion to the pretreatment and synthesis duration in addition to magnetite, some substituted magnetite and a small fraction of superparamagnetic phase which is an iron oxide.

The hematite is converted into magnetite (Fe_3O_4) during heating the catalyst in CO up to 270°C in 2hrs 43 min. The magnetite is rapidly converted into χ-Fe_5C_2 during further pretreatment under CO at 270°C and 175psig. The conversion is 90 % at the end of 24hrs of pretreatment. The remaining 10 % of magnetite is converted into superparamagnetic (spm) phase. Low temperature (12°C) measurement on one of the used catalyst has revealed that the spm phase is magnetite. During FT synthesis part of the χ-Fe_5C_2 (~25%) gets converted back to Fe_3O_4 and spm phase, possibly due to oxidation by the water generated during WGS reaction. However, after about 20 hrs of FT synthesis χ-Fe_5C_2, Fe_3O_4 and the spm phase reach equilibrium values. The FT activity is also maintained at an equilibrium value of ≈70% (H_2+CO) conversion.

It was found that the activity of the catalyst was better when activated in CO than in synthesis gas. As compared to the CO pretreatment, the synthesis gas pretreatment leads to a slow growth rate of χ-Fe_5C_2 and é-$Fe_{2.2}C$ at the expense of Fe_3O_4 and ≈ 30% (H_2+CO) conversion at the end of 24 hrs of activation. The χ-Fe_5C_2 and é-$Fe_{2.2}C$ continue to grow during FT synthesis while Fe_3O_4 continues to decrease indicating that magnetite is getting converted into carbides, a trend which is opposite to that seen in the case of CO-activated catalyst as shown in

Fig.1 where the total carbide formed is plotted. It may be noted that there is no ε-$Fe_{2.2}C$ formed during either pretreatment or FT synthesis in the present case of CO pretreated catalysts.

The variation of the ($CO+H_2$) conversion for the two types of pretreatment is shown in Fig. 3. The ($CO+H_2$) conversion is maintained at ≈70% in the case of CO pretreated catalyst when the χ-Fe_5C_2 is maintained at ≈65% and the magnetite at 35%. On the other hand, in the case of synthesis gas pretreated catalyst, the conversion is ≈ 60% during activation for a relatively short time and drops to ≈ 30% at the start of FT run and continues to be low. The carbides were formed during activation and continue to grow throughout FT run at the expense of magnetite. The growth of carbides even during FT synthesis might imply that reduction of the catalyst is not complete during activation in synthesis gas.

The rapid formation of the carbide in the case of CO pretreated catalyst may possibly imply that the surface of the catalyst is clean and that the CO gas is able to penetrate the catalytic surface and give rise to the rapid formation of the carbide and FT activity. On the other hand, sluggish formation of the carbides in the case of syngas pretreated catalyst might imply that the catalytic surface is covered with some inactive or graphitic carbon which slows down the formation of carbides and diminishes the FT activity.

We have also carried out Mössbauer investigations on the low α catalyst, UCI 1185-149, 57.2Fe/9.3Cu/0.05K (from 2nd and 3rd batch) subjected to pretreatment in (i) CO and (ii) H_2/CO. The pretreatment and FT synthesis conditions and the phase distribution determined are given in Tables I to II.

CO-ACTIVATED UCI 1185-149 (2nd batch) (57.2Fe/9.3Cu/0.05K):

UCI 1185-149 (2nd batch) catalyst was pretreated in CO at 270°C, 175 psig, for 22hrs in 1.4 nL CO/g-Fe hr. FT synthesis was carried out in distilled Allied-Signal heavy wax with 9% catalyst loading at 270°C, 175psig, 2.4 nL syngas/g-Fe hr, at 1000rpm.

The activation is not complete during pretreatment. As can be observed from the Table I, the χ-carbide continues to grow during FT synthesis and the FT activity which was initially high at 84% of (H_2+CO) conversion decreases rapidly with increasing time on stream. This might imply the presence of some inactive or graphitic carbon on the surface of the catalyst.

SYNGAS-ACTIVATED UCI 1185-149 (2nd batch) (57.2Fe/9.3Cu/0.05K): UCI 1185-149 (2nd batch) catalyst was pretreated in H_2/CO at 280°C, 175 psig, for 14hrs in 1.4 nL CO/g-Fe hr. FT synthesis was carried out in C28 wax with 9% catalyst loading at 270°C, 175psig, 2.4 nL syngas/g-Fe hr, at 1000rpm. In this case also the activation is not complete during pretreatment. As can be observed from the Table II, the χ-carbide continues to grow during FT synthesis and the FT activity which was initially low decreases still further with increasing time on stream. It may be noted that the FT activity is low even when the χ-Fe_5C_2 present in the spent catalyst is as much as 91%. This indicates that the absolute amount of χ-Fe_5C_2 present in the catalyst may not be significant for FT activity. The slow growth of carbide observed might imply the possible deposition of some inactive carbon on the surface.

(II) INFLUENCE OF LIQUID MEDIUM ON THE CARBIDE PHASE FORMATION:

The UCI 1185-149 (3rd batch) catalyst under the same conditions of activation and FT synthesis except for the liquid medium used gave rise to different amounts of carbide depending up on the nature of the medium. Lighter wax gave relatively larger amounts of chi-carbide compared to the heavier wax during FT synthesis as shown in Tables III and IV. Although the

initial activity is high in both the cases, the deactivation is rapid in the case of the catalyst containing lesser amount of carbide.

(III) INFLUENCE OF PRESSURE USED FOR ACTIVATION:

SYNGAS ACTIVATION OF AN IRON CATALYST AT LOW PRESSURE VS HIGH PRESSURE:

The pressure at which an iron catalyst is activated in syngas has a profound effect on the phase distribution and consequently on the FT activity. When the catalyst 100Fe/3.6Si/0.71K (atomic ratio) was activated in syngas at 12 atms for 24hrs @ 270°C, 3.4nL/hr-g(Fe), $H_2/CO=0.7$ no carbide was formed even when the activation was continued for 93 hrs. as shown in Table V. However, activation of the the same catalyst in CO (after 93hrs. of activation in syngas) only for 22hrs leads to the formation of 33% of χ-carbide and the FT activity increased to about 88% at TOS=77.5hrs. The FT activity does not correlate with the bulk carbide present.

Adding Cu to the catalyst did not improve carbide formation under similar activation conditions as can be seen from Table VI. The FT activity was low at about 10% of (H_2+CO) conversion at the end of 24 hrs of TOS.

Activation of 100Fe/3.6Si/0.71K (atomic ratio) in syngas at 1 atms gave rise to 41% of χ-carbide and the FT activity of the catalyst was high at about 85% of (H_2+CO) conversion at the end of 24hrs of TOS as shown in Table VII .

CONCLUSIONS: It is shown that the presence of χ-carbide in a catalyst is essential for good FT conversion but may not be a sufficient condition.. It may not be the amount of χ-carbide that is significant but the formation of the carbide during activation period seems to be important for good FT activity. The above results imply a correlation between the growth rate of carbide formed during activation and the FT activity. Rapid and complete formation of χ-Fe_5C_2 during activation may indicate that the catalyst surface is clean and conducive for good FT activity. Large amounts of χ-Fe_5C_2 present in spent catalysts may not necessarily indicate good FT conversion as has been observed in the present Mössbauer studies.

It is observed that in the case of CO activation the carbide content increases during activation and decreases during FT synthesis resulting in good FT activity. On the other hand in the case of syngas activation under high pressure the carbide formation is slow and incomplete during activation and continues to grow during synthesis resulting in poor FT activity. Activation in syngas at low pressure gives rise to χ-Fe_5C_2 during activation and decreasing amounts of χ-Fe_5C_2 during FT synthesis leading to good FT activity.

It is possible that the active surface species form only under conditions that are also favor bulk carbide formation. The FT activity results suggest that this surface is more stable than the bulk carbide.

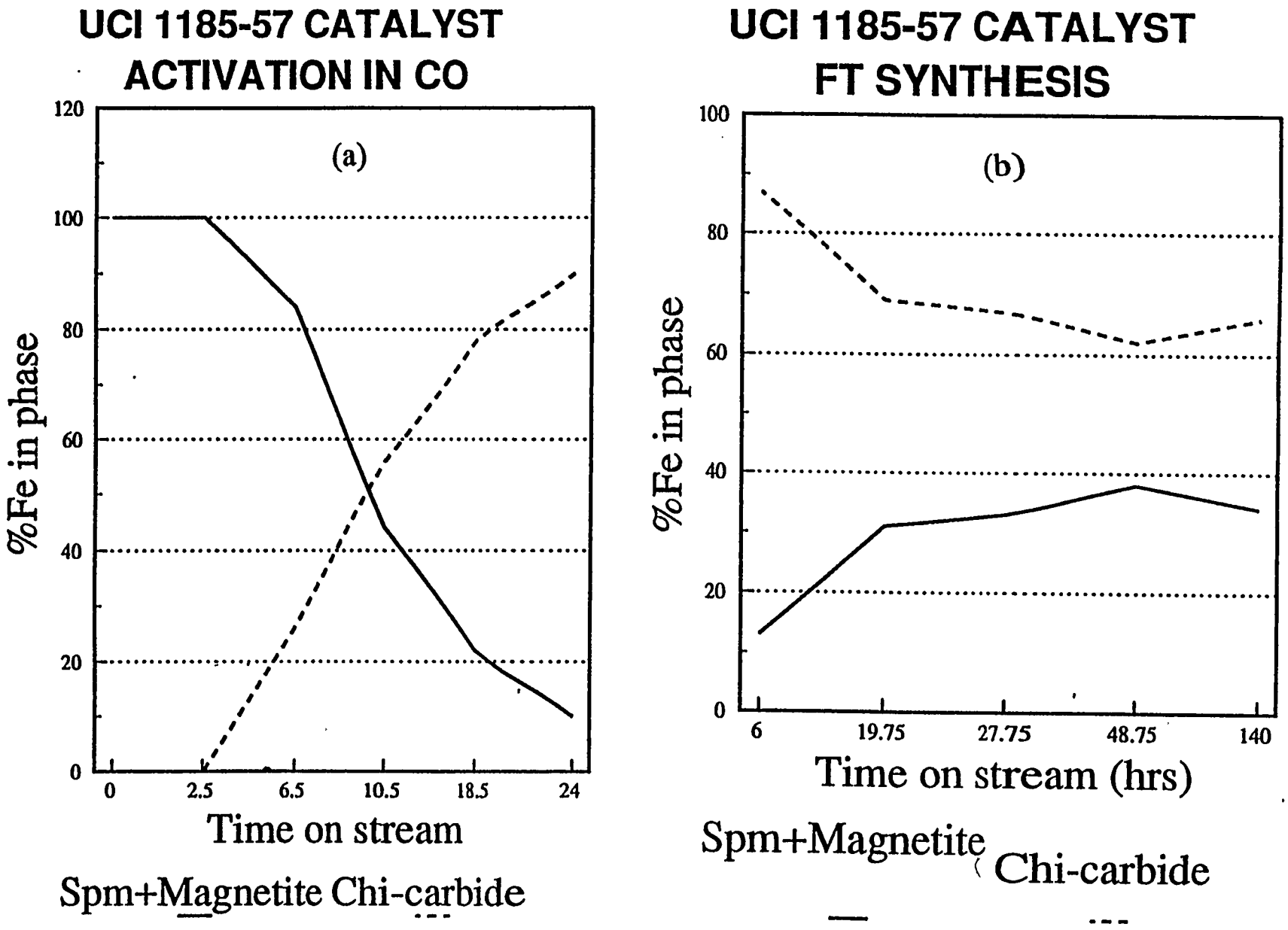

Fig. 1 Iron phase distribution in the catalyst UCI 1185-57 vs TOS
(a) during activation in CO and (b) during FT synthesis

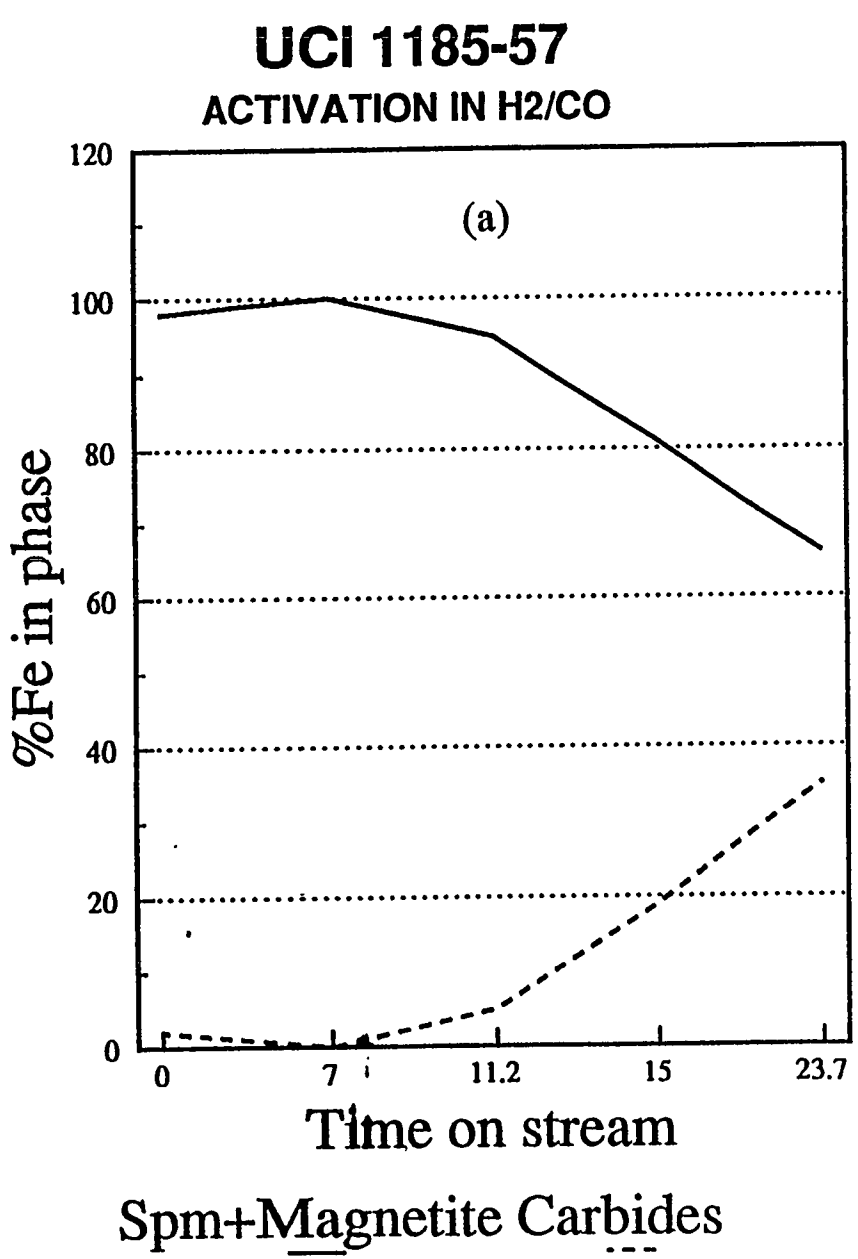

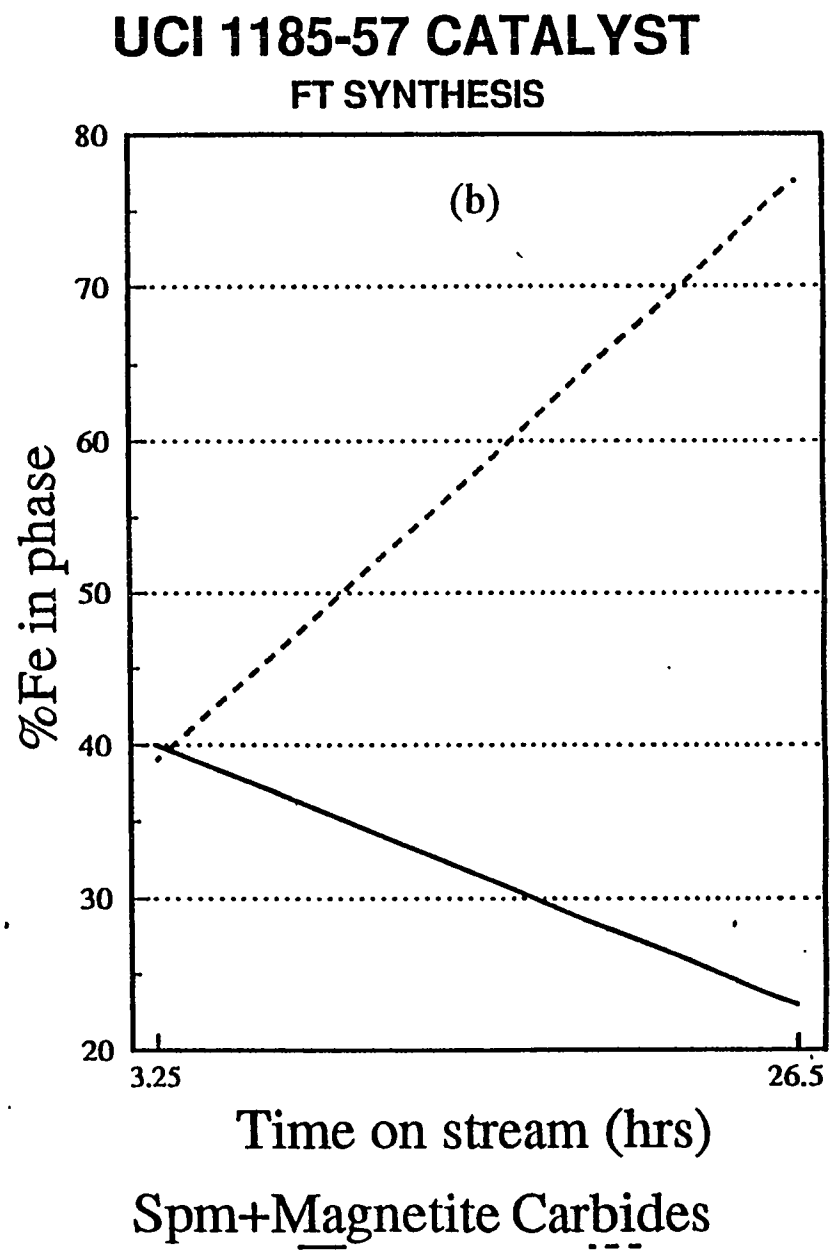

Fig.2 Iron phase distribution in the catalyst UCI 1185-57 vs TOS
(a) during activation in syngas and (b) during FT synthesis

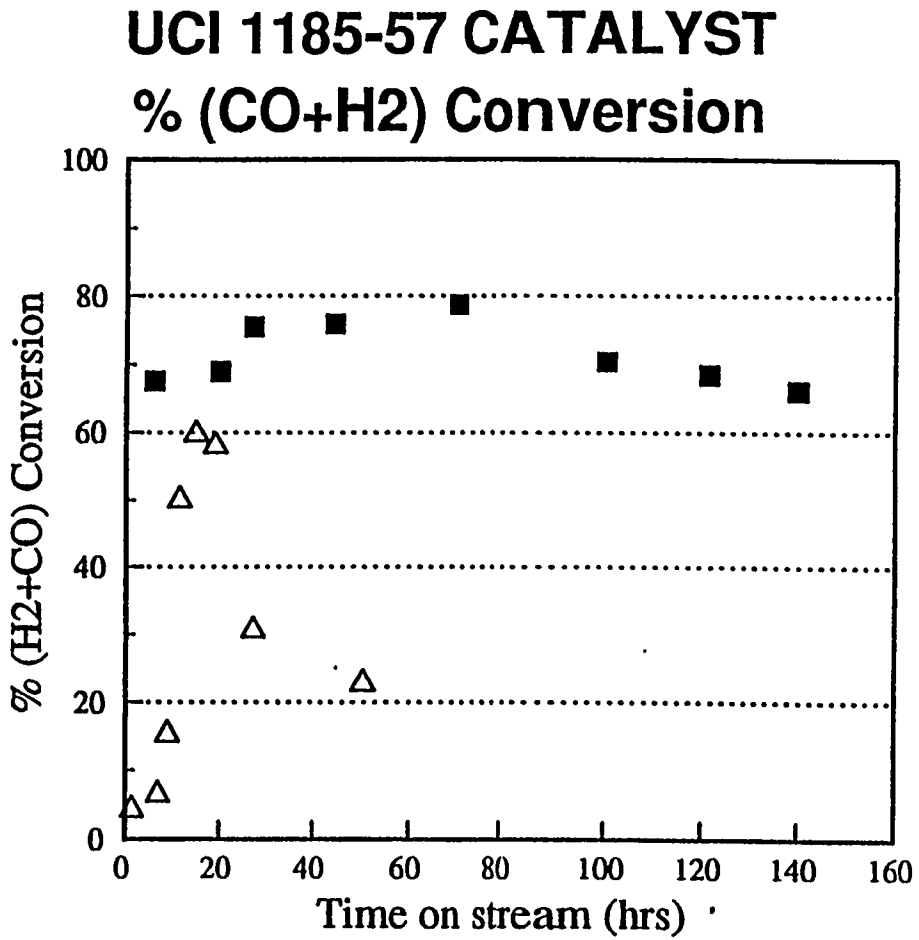

Fig.3 (H2+CO) conversion dependance on pretreatment

Table I

Catalyst: UCI 1185-149-2nd (57.2Fe/9.3Cu/0.05K)
Activated in CO at 270°C, 175psig,22hr, 1.4nL/hr-gFe
FT synthesis conditions: H_2/CO=0.70, 270°C, 175psig,2.4nL/hr-gFe
9% catalyst loading in distilled Allied-Signal heavy wax of 370gms.

SAMPLE	χ-Fe_5C_2	Fe_3O_4	Spm	(H 2+CO) Conversion %*
FT run TOS=84hrs	40	37	23	84.0
FT run TOS=235hr	60	30	10	67.7
FT run TOS=305hr	68	27	5	51.2

* Catalyst preparation and FT synthesis runs were carried out at PETC, Pittsburgh

In the case of CO activation, increasing carbide content during FT synthesis gives rise to decreasing FT activity as can be seen from the above table.

Table II

Catalyst: UCI 1185-149-2nd (57.2Fe/9.3Cu/0.05K)
Activated in syngas at 270°C, 175psig,22hr, 1.4nL/hr-gFe
FT synthesis conditions: H_2/CO=0.70, 270°C, 175psig,2.4nL/hr-gFe
9% catalyst loading in C-28 light wax of 370gms.

Sample	χ-Fe_5C_2	Fe_3O_4	Spm phase	(H2+CO)* conversion
Activated for 14hrs	36	48	16	--
FT run TOS=26hrs	84	14	2	16
FT run TOS=9hrs	91	7	2	6

* Catalyst preparation and FT runs were carried out at PETC,Pittsburgh

In the case of syngas pretreatment, increasing carbide content during synthesis gave rise to low FT activity as can be seen from the above table.

Table III

Catalyst: UCI 1185-149-3rd ((57.2Fe/9.3Cu/0.05K):
Activated in CO at 270°C, 175psig,22hr, 1.4nL/hr-gFT

9% loading in C28, n-octacosane, light wax of 370gms.
Synthesis conditions: H_2/CO=0.70, 270°C, 175psig,2.4nL/hr-gFe

FT synthesis in light wax

Sample@	χ-Fe_5C_2	Fe_3O_4	Spm phase	ϵ-$Fe_{2.2}C$	%(H_2+CO) conversion*
Activated for 2hr	---	82	6	12	--
Activated for 18hr	77	21	2	---	--
Activated for 22 hr	86	12	2	---	--
FT run TOS=19.5	58	15	27	---	89
FT run TOS=43 hr	56	16	28	---	91
FT runTOS=90 hr	65	20	15	---	91
FT runTOS=160 hr	56	21	23	---	91

Table IV

FT synthesis in a heavy wax

Catalyst: UCI 1185-149-3rd ((57.2Fe/9.3Cu/0.05K): 9% loading in distilled Allied-Signal wax of 370gms.
Activated in CO at 270°C, 175psig,22hr, 1.4nL/hr-g
FT synthesis conditions: H_2/CO=0.70, 270°C, 175psig,2.4nL/hr-gFe

Sample	χ-Fe_5C_2	Fe_3O_4	Spm phase*	ϵ-$Fe_{2.2}C$	% (H_2+CO) conversion *
Activation for 2hrs	---	88	6	6	--
Activation for 9.5h	54	37	9	----	--
Activation for 22h	64	27	9	---	--
FT run TOS=24h	42	30	28	---	81
FT runTOS=47.5h	39	34	27	---	48
FT run TOS=94.5h	37	40	23	---	86

*The Spm phase i.e. superparamagnetic phase is likely to be α-FeOOH as revealed by low temperature measurements on UCI 1185-149-3rd catalyst subjected to CO activation and 24hrs of FT synthesis.

Table V

Activation carried out at high pressure (12 atms):

Catalyst: 100Fe/3.6Si/0.71K (atomic % relative to Fe)

Initial Activation in syngas at 12 atms, 270°C, $H_2/CO=0.7$, S.V.=3.4 nL/hr/g(Fe)

Synthesis conditions: 270°C, 175 psig, 3.4nL/hr-g(Fe), $H_2/CO=0.7$

Catalyst	Spm-phase	Fe_3O_4	χ-Fe_5C_2	% Conversion*
Syngas:TOS=6.33h	75	25	-	9.2
Syngas:TOS=24.0h	31	69	-	9.7
Syngas:TOS=46.0h	11	89	-	11.5
Syngas:TOS=93.0h	-	100	-	12.2
CO: TOS=22.0h	9	58	33	25
Syngas:TOS=26.5h	15	60	25	59
Syngas:TOS=77.5h	18	63	19	88
Syngas:TOS=198.0h	13	67	20	86
Syngas:TOS=341.0h	11	63	26	81

*Catalyst preparation and FT runs were carried out at CAER, University of Kentucky

Table VI

Pretreatment carried out at high pressure (12 atms):

100Fe/3.6Si/2.6Cu/0.71K (atomic % relative to Fe)
Activation in Syngas at high pressure (12 atms): 270°C, $H_2/CO=0.7$, S.V.=3.4 nL/hr/g(Fe),24hrs
Synthesis conditions: 270°C, 175 psig, 3.4nL/hr-g(Fe), $H_2/CO=0.7$

Catalyst	Spm-phase	Fe_3O_4	χ-Fe_5C_2	% (H_2+CO) Conversion*
TOS=4.33h	19	81	-	26
TOS=21.0h	10	90	-	26
TOS=45.0h	14	86	-	32
TOS=113.7h	3	82	15	43
TOS=214.5h	4	76	20	51

*Catalyst preparation and FT runs were carried out at:
CAER, University of Kentucky

Table VII

Pretreatment carried out at low pressure (1 atms):
Catalyst: 100Fe/3.6Si/0.71K (atomic % relative to Fe)
Activation conditions: 270°C, 1 atm., $H_2/CO=0.7$, S.V.=3.4 nL/hr/g(Fe),24hrs
Syntheisis conditions: 270°C, 13 atm., $H_2/CO=0.7$, S.V.=3.4 nL/hr/g(Fe)

Sample@	χ-Fe_5C_2	Fe_3O_4	Spm phase	% (H_2+CO) conversion *
Activated for 24hrs	41	32	27	----
FT run TOS=24hrs	36	40	24	82.0
FT run TOS=48hrs	31	47	22	83.0
FT run TOS=95hrs	33	48	19	79
FT run TOS=218hrs	26	50	24	75
FT run TOS=384hrs	20	60	20	69

GAS CONVERSION

FABRICATION AND CHARACTERIZATION OF DENSE CERAMIC MEMBRANES FOR PARTIAL OXIDATION OF METHANE*

U. Balachandran, B. Ma, J. T. Dusek, J. J. Picciolo,
R. L. Mieville, and P. S. Maiya
Energy Technology Division
Argonne National Laboratory
Argonne, IL 60439

and

M. S. Kleefisch and C. A. Udovich
Amoco Research Center
Naperville, IL 60566

June 1995

For presentation at the Coal Liquefaction and Gas Conversion Contractors' Review Conference, August 29–31, 1995, Pittsburgh, PA.

*Work at Argonne National Laboratory is supported by the U.S. Department of Energy, Pittsburgh Energy Technology Center, under Contract W-31-109-Eng-38.

FABRICATION AND CHARACTERIZATION OF DENSE CERAMIC MEMBRANES FOR PARTIAL OXIDATION OF METHANE

U. Balachandran, B. Ma, J. T. Dusek, J. J. Picciolo,
R. L. Mieville, and P. S. Maiya
Energy Technology Division
Argonne National Laboratory
Argonne, IL 60439

and

M. S. Kleefisch and C. A. Udovich
Amoco Research Center
Naperville, IL 60566

INTRODUCTION

A significant reduction in the cost of syngas would have a major effect on the future direction of fuel and chemical production. Syngas production accounts for up to 60–70% of the total cost of most integrated systems that produce chemical and hydrocarbon liquids. Syngas is also a major source of hydrogen, which is in ever-increasing demand for the removal of pollutants from fossil fuels.

A recent innovation [1,2] that could bring down the production cost of syngas is the use of ceramic membranes in a partial oxidation mode or in a combined mode of partial oxidation and steam reforming. In this review, we offer a technology that is based on dense ceramic membranes and that uses air as the oxidant for methane conversion reactions, thus eliminating the need for an expensive oxygen plant. Oxygen separation plants are the single most costly item in the production of syngas by partial oxidation.

Certain ceramic materials exhibit both electronic and ionic conductivities (of particular interest is oxygen-ion conductivity). These materials transport not only oxygen ions (functioning as selective oxygen separators) but also electrons back from the reactor side to the oxygen/reduction interface. No external electrodes are required and if the driving potential of transport is sufficient, the partial-oxidation reactions should be spontaneous. Such a system will operate without an externally applied potential. Oxygen is transported across the ceramic material in the form of oxygen anions, not oxygen molecules.

Recent reports in the literature suggest that dense ceramic membranes made of these mixed conductors can successfully separate oxygen from air at flux rates that could be considered commercially feasible, and thus can have the potential to improve the economics of methane conversion processes [1-11].

One such class of mixed conductors is the perovskites, which are oxides based on the structure of the cubic-lattice mineral perovskite, $CaTiO_3$ [12]. Partial substitution of a higher-valency cation (donor-dopant) for a lower metal ion results in two types of charge compensation, namely, electronic and ionic, depending on the partial pressure of oxygen in equilibrium with the oxides [13,14]. The charge compensation in acceptor-doped oxides (i.e., substituting a divalent cation for a trivalent cation) is by electronic holes at high oxygen pressures, but by oxygen-ion vacancies at low pressures [10,15]. Ion vacancies are the pathways for oxide ions; therefore, oxygen flux can be increased by increasing the amount of acceptor-dopant. Reported oxygen flux values [1-3,10,11] for perovskites tend to follow the trends suggested by the charge compensation theory. Although not all of the mixed oxides we have made are perovskites, the suggested mechanism outlined above is believed to hold true for other similar oxides.

EXPERIMENTAL

Several LaSrFeCo mixed oxides (designated as SFC) of different stoichiometries (see Table 1) are made by solid-state reaction of the constituent cationic salts. Most of the performance evaluation has concentrated on SFC-2, a nonperovskite mixed oxide [16]. All of the oxide powders were made by mixing appropriate amounts of $La(NO_3)_3$, $SrCO_3$, $Co(NO_3)_2 \cdot 6H_2O$, and Fe_2O_3 and then grinding the mixture in isopropanol with ZrO_2 media for 15 h. After drying, the mixtures were calcined in air at 850°C for 16 h with intermittent grinding. After final calcination, the powders were ground with an agate mortar and pestle to an average particle size of ≈7 μm. The resulting powders were characterized by X-ray diffraction (XRD), scanning electron microscopy, and thermogravimetric analysis (TGA), and analyzed for particle-size distribution.

The powder was made into a slip that contained a solvent, dispersant, binder, and plasticizer. Membrane tubes were fabricated by extruding the slip to an outside diameter of ≈6.5 mm, lengths up to ≈30 cm, and wall thicknesses of 0.25-1.20 mm. The tubes were sintered at ≈1200°C for 5-10 h in stagnant air.

Table 1. Mixed-oxide designations

Designation	Formula
SFC-1	$La_{0.2}Sr_{0.8}Fe_{0.6}Co_{0.4}O_x$
SFC-2	$SrFeCo_{0.5}O_x$
SFC-3	$Sr_7Fe_{6.5}Co_{3.5}O_x$
SFC-4	$Sr_2Fe_3O_x$
SFC-5	$Sr_7Fe_{10}O_x$
SFC-6	$Sr_2Fe_{3.1}O_x$
SFC-7	$SrFe_{1.2}Co_{0.5}O_x$
SFC-8	$SrFe_{0.8}Co_{0.2}O_x$

Mechanical properties of the finished material were measured by conventional methods, i.e., bulk density was measured by the Archimedes principle; flexural strength, in a four-point bending mode; fracture toughness, by a single-edge notch method [17]; and Young's modulus, shear modulus, and Poisson ratio, by ultrasonic methods [18]. The thermal expansion coefficient was measured with a dilatometer.

The ceramic materials were evaluated for performance in a quartz reactor system, shown in Fig. 1. The reactor supports the ceramic membrane tube with Pyrex hot seals, a design that creates an isothermal environment for the ceramic tube. To facilitate reactions and equilibration of gases in the reactor, an Rh-based reforming catalyst is loaded adjacent to the tube. Gold wire mesh is wrapped around the tube to prevent solid-state reactions between the catalyst and the ceramic. Feed gas and effluents were analyzed by gas chromotography.

Samples were prepared for conductivity and diffusional measurements by compressing the constituent powders at 1.2×10^3 MPa into pellets 21.5 mm in diameter and ≈3 mm thick. Pellets were sintered in air at ≈1200°C for 5 h; they were then cut into small bars. The bulk densities of samples were ≈95% of their theoretical values.

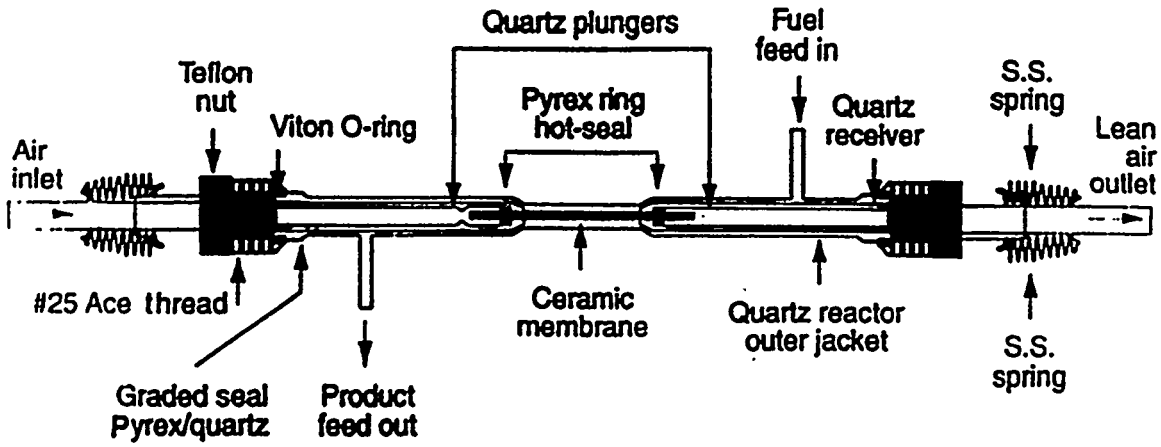

Fig. 1. Schematic diagram of ceramic membrane reactor.

Platinum wires were used as probes in the four-probe conductivity measurement. Specimen resistance was measured with an HP 4192A LF impedance analyzer. For measurement of oxygen ion conduction, yttria-stabilized zirconia (YSZ, with 8 mol% Y_2O_3) was used for the electron (hole) blocking electrode [19].

The oxygen diffusion coefficient was measured by a relaxation method. The sample was subjected to a sudden change in oxygen partial pressure, and ionic conductivity was then monitored as a function of time and temperature [20].

RESULTS AND DISCUSSION

SFC-1 tubes survived only a few minutes when operated as a conversion reactor at 850°C; they then broke into several pieces. XRD patterns of the original SFC-1 samples were recorded at 850°C in Ar-O_2 gas mixtures. The phase behavior of SFC-1 in 1 and 20% O_2 is shown in Fig. 2. In an oxygen-rich atmosphere (20% O_2), the material was a cubic perovskite. However, once the oxygen partial pressure dropped below 5%, the cubic phase transformed to an oxygen-vacancy-ordered phase. New peaks appeared in the XRD pattern, as seen in Fig. 2 (1% O_2). It is important to note that this material expanded substantially after the phase transition, as can be seen from the change in the position of the Bragg peak near 32° in Fig. 2. Evidently, this peak in the oxygen-vacancy-ordered phase (in 1% O_2) shifted to the low-angle (larger d-spacing) side of the corresponding peak in the cubic perovskite phase (in 20% O_2).

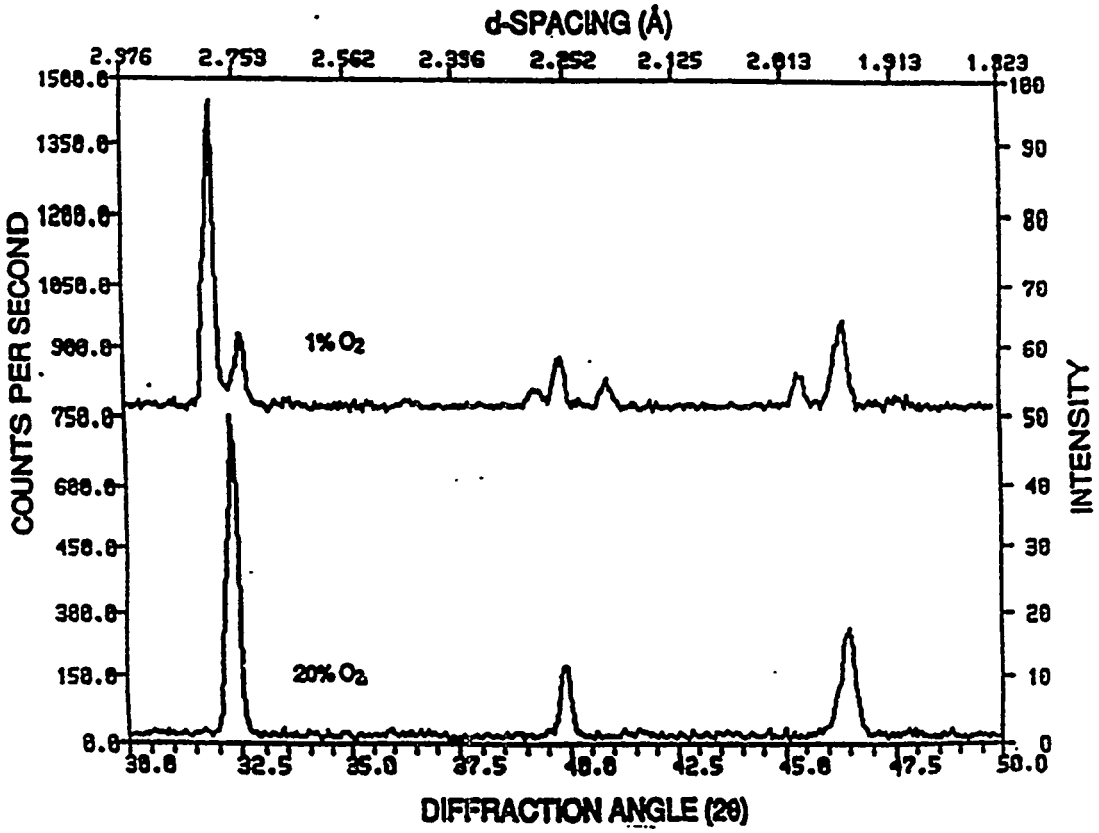

Fig. 2. XRD of SFC-1 at 850°C in 1% and 20% O_2 (balance is Ar).

Detailed TGA [21] showed that the oxygen content x of the SFC-1 sample in 1% O_2 was ≈0.1 lower than that in a sample in 20% O_2. Dependence of the unit cell volume on the oxygen content of the sample has been established by comparing lattice parameters. For example, the volume of the primitive perovskite cell V_p is 57.51 Å^3 for x = 2.67 and 59.70 Å^3 for x = 2.48. These results show that this material expands as oxygen is removed. Such behavior suggests that an electronic effect is predominant in influencing the specific volume; otherwise, a simple size effect would cause the lattice to shrink. By linear interpolation of the above results, we predict that a decrease in x of 0.1 will result in an increase of ≈2% in V_p.

Both XRD and TGA data [21] give a clear picture of the state of SCF-1 under reaction conditions. When the membrane tube is in use, high oxygen pressure is maintained outside the tube and low oxygen pressure is maintained inside the tube. Before the tube is brought to high temperature, oxygen distribution is uniform.

Upon heating, the tube material begins to lose oxygen that was incorporated during the fabrication process. Moreover, the material on the

inner wall loses more oxygen than that on the outer wall. As a result, a stable oxygen gradient is generated between the outer and inner walls. It follows that the material, depending on its location in the tube, may contain different phase constituents. It is probable that the inner zone, with less oxygen, contains more ordered oxygen vacancies and hence is less oxygen-permeable.

The most remarkable factor, and one that can cause tube fracture, appears to be lattice mismatch between the materials on the inner and outer walls of the tube. The difference in composition between the inner and outer zones leads to an expansion of 2%, which is equivalent to thermal expansion caused by a 333°C temperature increase.

In comparison, SFC-2 exhibited remarkable structural stability at high temperature, as shown in Fig. 3. No phase transition was observed in this material as oxygen partial pressure was changed. Furthermore, the Bragg peaks stayed at the same position regardless of the oxygen partial pressure of the atmosphere. This structural stability of SFC-2, when compared with that of other mixed oxides, is reflected in its physical and mechanical properties, as shown in Table 2.

In all cases, SFC-2 shows above-average strength, especially in fracture toughness, which is the ability of a material to resist crack propagation.

Figure 4 shows the probability of failure vs. flexural strength (Weibull statistics) for SFC-2 [22]. The Weibull modulus was 15, indicating only moderate scatter in the strength data. Measured room-temperature properties were used to develop failure criteria for the membranes under actual reaction conditions in a plant where methane is expected to be at higher pressures. Figure 5 shows the computed allowable external pressure on SFC-2 as a function of tube wall thickness. These calculations were based on assumptions that the tensile strength is ≈0.67 times the flexural stress and that the compressive strength of SFC-2 is greater than its tensile strength by a factor of 8. These results suggest that this ceramic material can withstand reasonable stresses that might occur in a commercial reactor. Tubes made of this material, unlike those made of SFC-1, are not expected to fracture under reactor conditions.

Differences between SFC-2 and SFC-8 are observed in their electronic and ionic conductivities (Table 3) relative to those of other materials of this same type (19, 23-27). It is clear that SFC-2 is unique in that its ratio of ionic to electronic conductivity is close to unity.

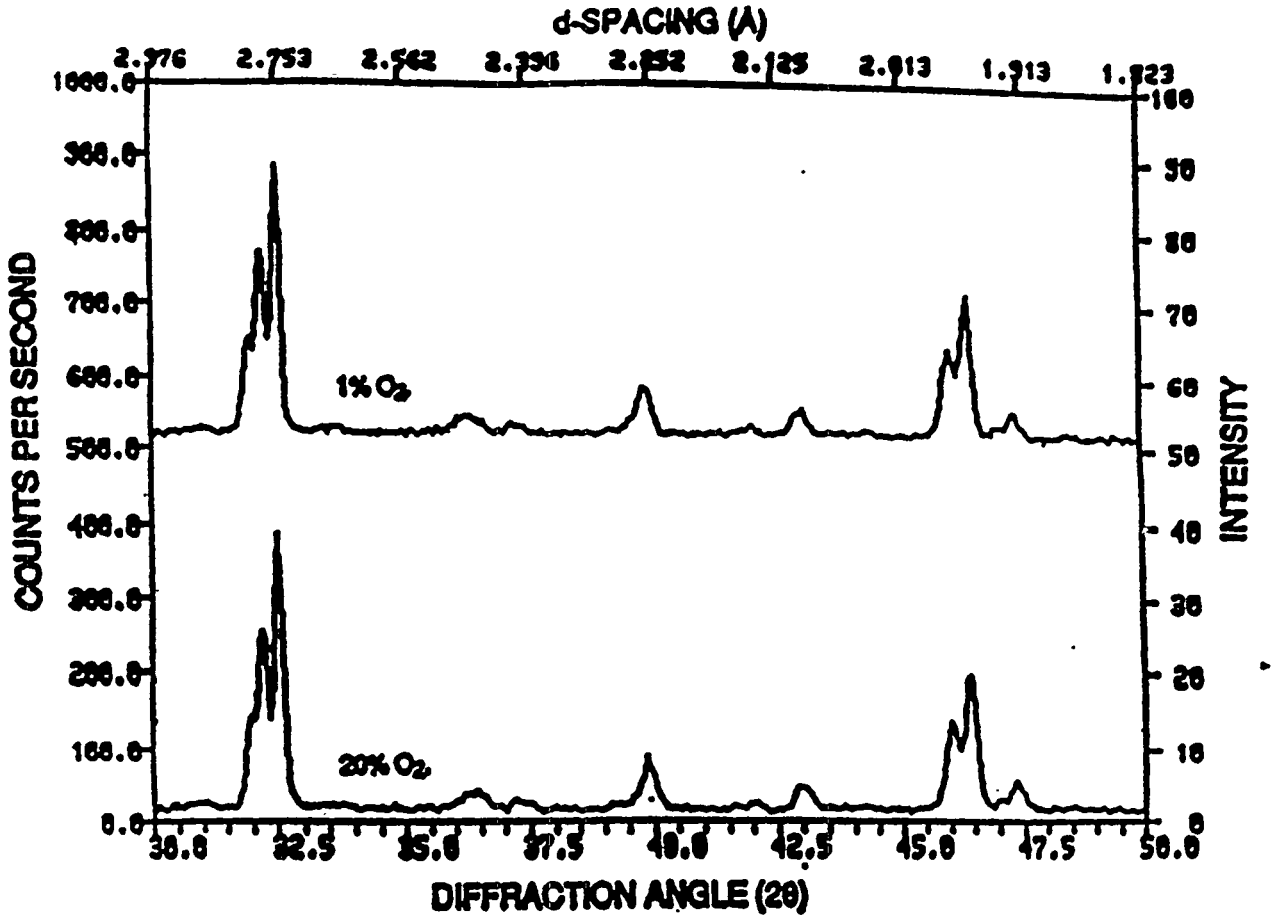

Fig. 3. XRD of SFC–2 at 850°C in 1% and 20% O_2 (balance is Ar).

Table 2. Physical and mechanical properties of ceramic membrane material

Property	$SrFeCo_{0.5}O_x$ (SFC-2)	$SrFe_{1.2}Co_{0.5}O_x$ (SFC-7)	$Sr_2Fe_3O_x$ (SFC-4)	$Sr_7Fe_{10}O_x$ (SFC-5)	$Sr_2Fe_{3.1}O_x$ (SFC-6)	$Sr_7Fe_{6.5}Co_{3.5}O_x$ (SFC-3)
Percent of theoretical density	93	97	87	80	94	92
Flexural strength, MPa	81 ± 16	65 ± 35	80 ± 20	78 ± 27	83 ± 11	89 ± 16
Fracture toughness, $MPa\sqrt{m}$	2.04 ± 0.06	1.68 ± 0.09	1.02 ± 0.05	1.10 ± 0.08	1.33 ± 0.13	1.42 ± 0.04
Young's modulus, GPa	124 ± 3	85 ± 4	110 ± 2	99 ± 2	134 ± 52	120 ± 1
Shear modulus, GPa	48 ± 1	35 ± 1	43 ± 1	39 ± 1	52 ± 1	47 ±1
Poisson ratio	0.30	0.20	0.27	0.28	0.29	0.28

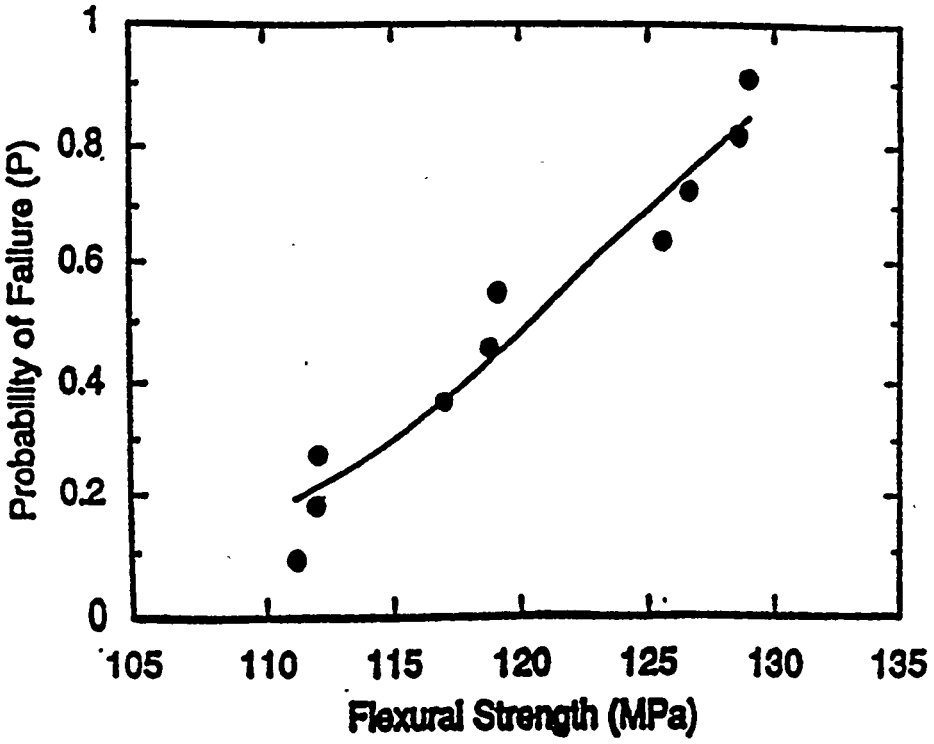

Fig. 4. Probability of failure vs. flexural strength for SFC–2 (Weibull modulus = 14.5).

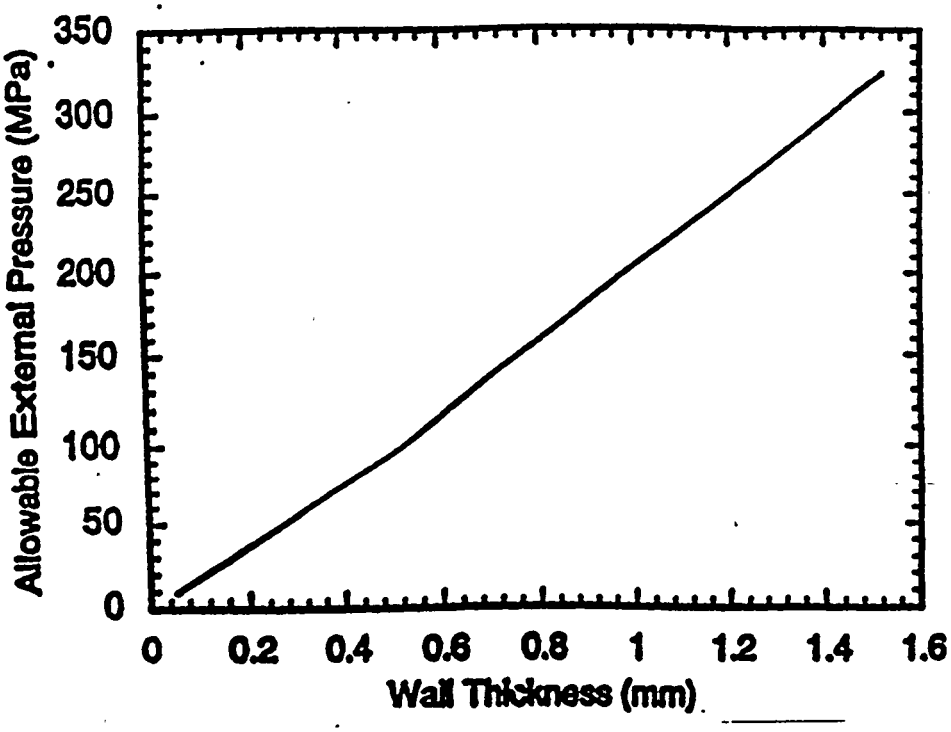

Fig. 5. Allowable external pressure on SFC–2 tubes as a function of wall thickness (O.D. = 6.40 mm).

Table 3. Conductivities of (La,Sr)(Fe,Co)O_X systems, measured in air at 800°C

Sample	Electronic σ_{el} ($S \cdot cm^{-1}$)	Ionic σ_i ($S \cdot cm^{-1}$)	Method for Measuring σ_i	Ref.
SFC-2	10	7	4-terminal, YSZ electron block	19
SFC-8	76	4	4-terminal, YSZ electron block	19
$La_{0.6}Sr_{0.4}Co_{0.2}Fe_{0.8}O_3$	300	0.01	4-terminal, YSZ electron block	23
$La_{0.6}Sr_{0.4}Co_{0.2}Fe_{0.8}O_3$	300	0.003	2-terminal, electron block	24
$La_{0.8}Sr_{0.2}Co_{0.8}Fe_{0.2}O_3$	600	15	4-terminal, YSZ electron block	25
$La_{0.8}Sr_{0.2}Co_{0.8}Fe_{0.2}O_3$	250	0.10	4-terminal, YSZ electron block	26
$La_{0.75}Sr_{0.25}FeO_3$	50	0.03	$^{18}O/^{16}O$ exchange	27

Furthermore, limited SFC-2 diffusion data, obtained from the time-relaxation method [20], indicate that transport of oxygen ions is associated with an activation energy of 0.89 eV. This finding is consistent with the high diffusion coefficient of 9×10^{-7} cm^2 s^{-1} at 900°C.

Performance in generating syngas is demonstrated in Fig. 6, which shows conversion data obtained with an SFC-2 membrane tube at 850°C for ≈70 h. As shown, methane conversion efficiency is >98%, and CO selectivity is 90%. Measured H_2 yield is approximately twice that of CO, as expected.

The role of the catalyst in the transport of oxygen across the membrane of an SFC-2 tube was tested without the reforming catalyst. The results from a run of ≈350 h are shown in Fig. 7. The feed gases are the same as before. In the absence of a catalyst, the oxygen that was transported through the membrane reacted with methane and formed CO_2 and H_2O. As seen in Fig. 8, methane conversion efficiency was ≈35% and CO_2 selectivity was ≈90%. Under our operating conditions, measured oxygen flux was ≈0.3 std $cm^3/cm^2/min$. Figure 8 shows the result of a reactor run made under more severe conditions and in the presence of a catalyst for >500 h. Conversion

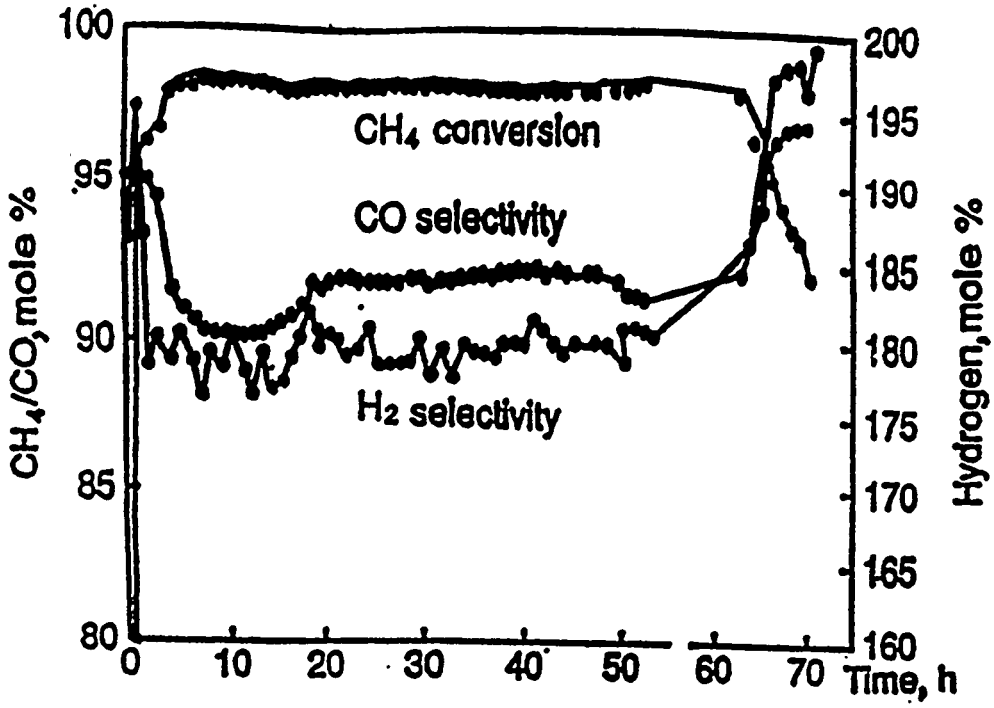

Fig. 6. Methane conversion and CO and H_2 selectivities in SFC–2 membrane reactor with reforming catalyst. Conditions: feed, 80% CH_4, 20% Ar; flow, 2.5 cm^3/min; temp., 850°C; pressure 1 atm; membrane surface area, 10 cm^2.

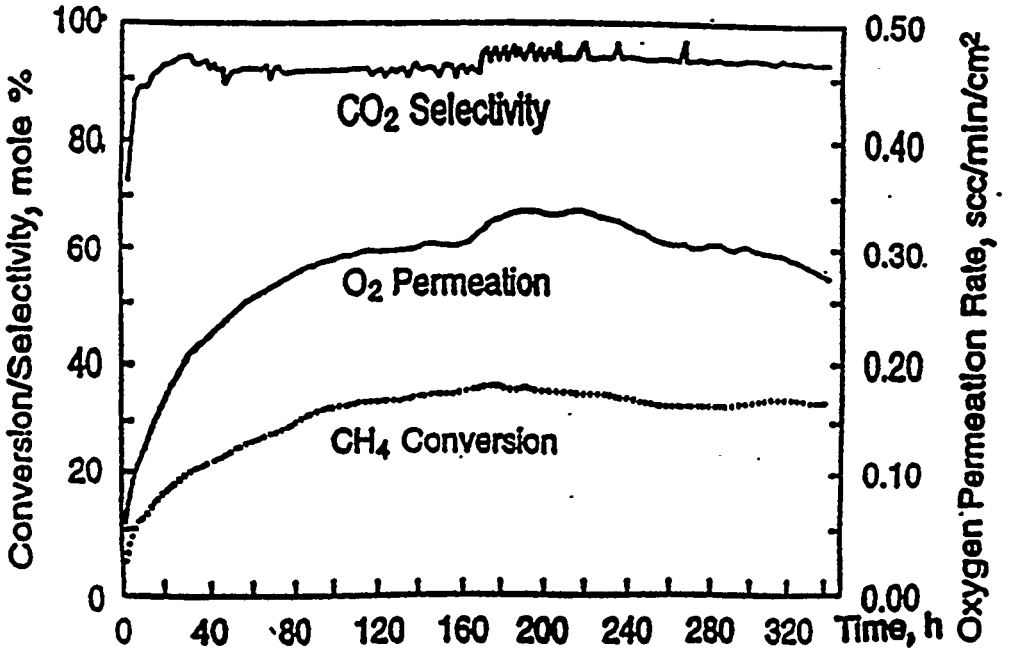

Fig. 7. Methane conversion and CO_2 selectivity and O_2 permeation in SFC-2 membrane reactor without reforming catalyst. Conditions: same as in Fig. 6.

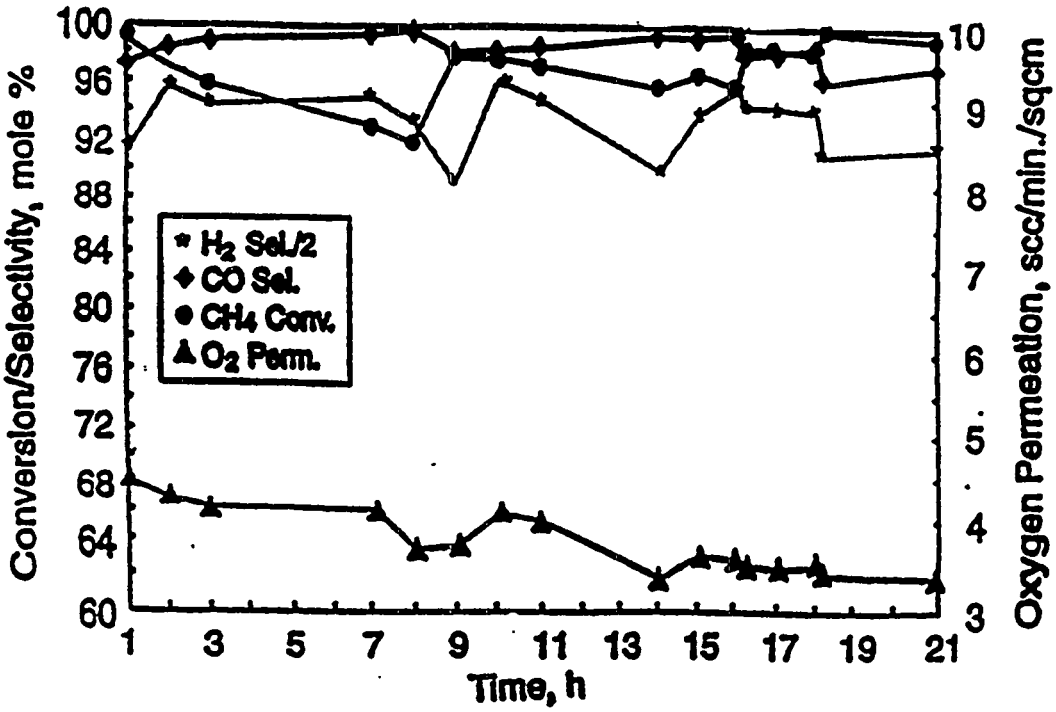

Fig. 8. Methane conversion and CO and H_2 selectivities and O_2 permeation in SFC–2 membrane reactor with reforming catalyst. Conditions: feed, 80% CH_4, 20% Ar; flow, 20 cm^3/min; temp., 900°C; pressure 1 atm; membrane surface area, 8 cm^2.

and selectivities are similar to those of the 350–h run but the oxygen flux was one order of magnitude greater. Some small deactivation in oxygen permeation rate was observed.

Further confirmation of the stability of this membrane tube is shown in Fig. 9, which shows reactor results over a period of 1000 h. The feed during this period was a typical mixture expected in a commercial recycling feed, namely methane, CO, CO_2, and H_2. Throughout the run, methane conversion was high. A small decline in oxygen permeation was observed. However, this high oxygen flux is consistent with the high diffusion coefficient of 9 x 10^{-7} cm^2 s^{-1} that was measured by the time–relaxation method [20].

A further run of 1000 h, seen in Fig. 10, was made with a methane/argon feed. During this run, the temperature was changed several times. To compensate for the resulting change in reaction rate, the feed

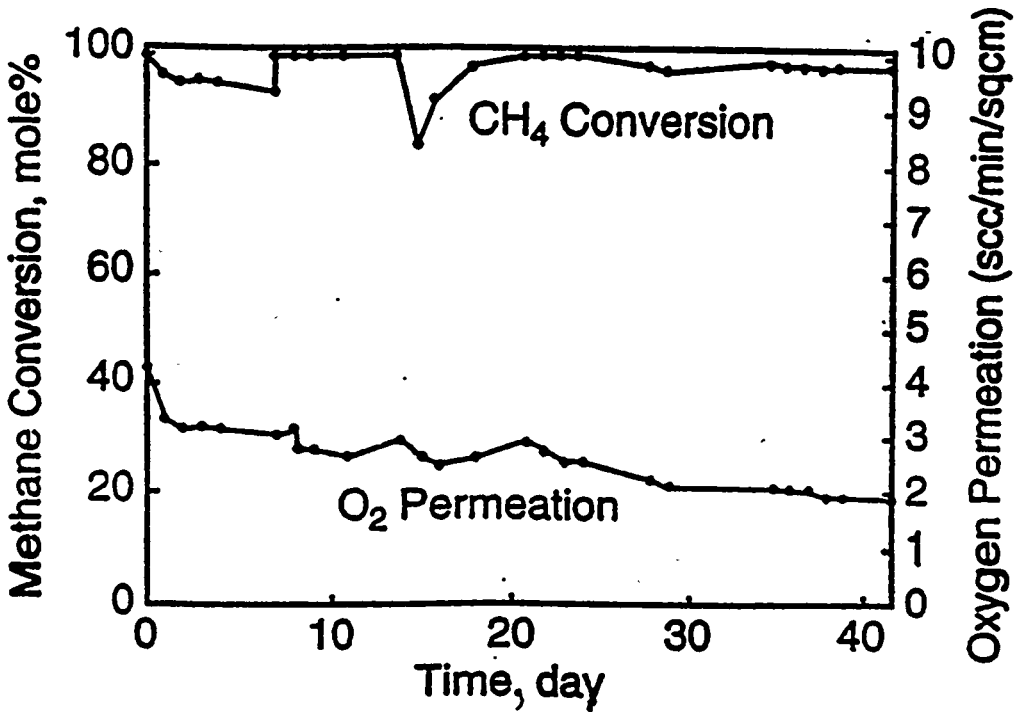

Fig. 9. Methane conversion and O_2 flux for a mixed feed. Conditions: feed, 80% CH_4, 20% Ar; temp., 900°C; pressure 1 atm; catalyst, 1.5 g; membrane surface area, 8.4 cm^2.

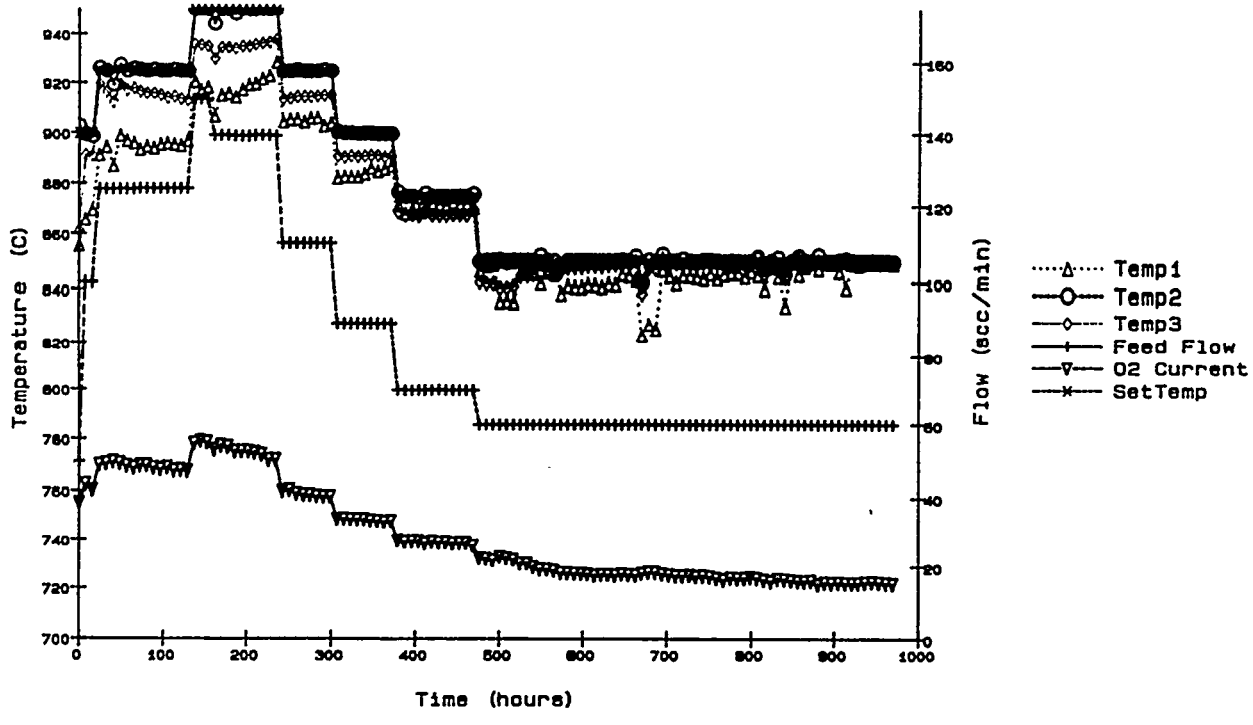

Air=1.2 l/m, Pres=~1atm, Membrane SA=4.4sqcm, Wall=.75mm, Cat=2.5g

Fig. 10. Temperature profile and O_2 current in membrane.

flow rate was altered accordingly. The selectivity to CO during the entire run remained >98%. Oxygen permeability followed the changes in temperature and feed flow.

Application of the oxygen permeability data obtained from simple geometry such as tubes to large-scale reactor configurations requires an oxygen transport model across the ceramic membrane. Recently, an oxygen transport equation was developed [28] on the basis of the phenomenological theory of diffusion to describe the effects of temperature, membrane thickness, and driving force on oxygen flux. It is shown that the oxygen permeability observed in reactor experiments can be adequately described by

$$J_{O^{2-}} = \frac{1}{2}\frac{D_{eff}c_{O^{2-}}}{L}\ln\left(\frac{p^{I}_{O_2}}{p^{II}_{O_2}}\right)$$

where $J_{O^{2-}}$ is the oxygen flux across a thin wall tube of wall thickness, D_{eff} is the effective diffusion coefficient of oxygen in species, $c_{O^{2-}}$ is the concentration of oxygen ions in the material, and $p^{I}_{O_2}$ and $p^{II}_{O_2}$ are the oxygen partial pressures on the air and methane side, respectively.

Thermodynamic calculations were made [28] to calculate the oxygen partial pressure on the methane side, assuming that all of the oxygen transported through the tube is consumed in the conversion of methane to syngas. The permeablity data obtained from the reactor in combination with the model (see Fig. 11) yielded

$$D_{eff} = 4.37 \exp\left(\frac{-156{,}000}{RT}\right) \text{cm}^2/\text{s}.$$

where the activation energy of 156 kJ/mole is within the range of values reported [29] for La-based nonstoichiometric perovskite structure oxides. The experimentally observed results of the oxygen flux agree within 25% of the predicted, as seen in Fig. 12.

CONCLUSIONS

Mixed-conducting ceramic materials have been produced from mixed-oxide systems of the La-Sr-Fe-Co-O (SFC) type, in the form of tubes and bars. Thermodynamic stability of the tubes was studied as a function of oxygen partial pressure by high-temperature XRD. Mechanical properties of

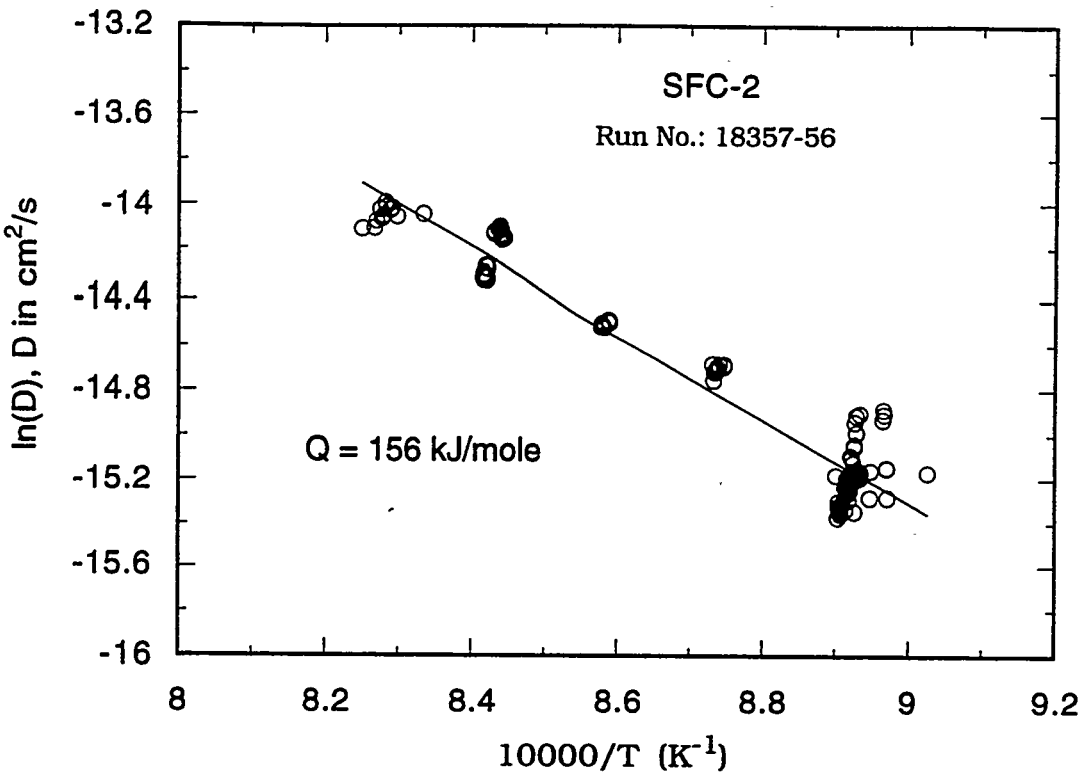

Fig. 11. Temperature dependence of O_2 diffusivity in SFC–2.

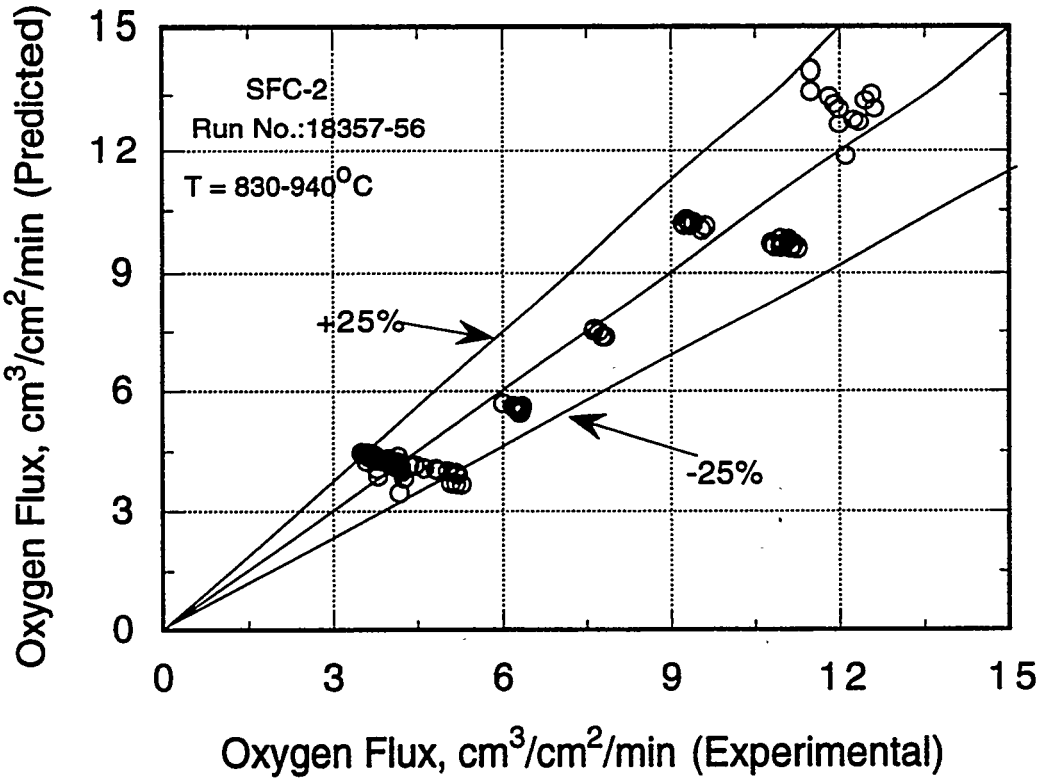

Fig. 12. Predicted O_2 flux vs. experimentally determined O_2 flux.

the SFC–2 material were adequate for reactor use. Electronic and ionic conductivities showed that SFC–2 is unique in that its ratio of ionic to electronic conductance is close to unity.

Performance of the membrane tubes was good only with SFC–2. Fracture of other SFC tubes was the consequence of an oxygen gradient that introduced a volumetric lattice difference between the inner and outer walls. SFC–2 tubes provided methane conversion efficiencies >99% in a reactor and have operated successfully for >1000 h.

ACKNOWLEDGMENTS

Work at Argonne National Laboratory is supported by the U.S. Department of Energy, Pittsburgh Energy Technology Center, under Contract W-31-109-Eng-38.

REFERENCES

1. Y. Teraoka, H. M. Zhang, S. Furukawa, and N. Yamozoe, *Chem. Lett.*, **1985**, 1743, 1985.

2. Y. Teraoka, T. Nobunaga, and N. Yamazoe, *Chem. Lett.*, 503, 1988.

3. T. J. Mazanec, T. L. Cable, and J. G. Jr. Frye, *Solid State Ionics*, 53, 1992.

4. A. C. Bose, J. G. Stigel, and R. D. Srivastava, "Gas to Liquids Research Program of the U.S. Department of Energy: Programmatic Overview," paper presented at *Symp. on Alternative Routes for the Production of Fuels*, American Chemical Society National Meeting, Washington, DC, Aug. 21-26, 1994.

5. U. Balachandran, S. L. Morissette, J. T. Dusek, R. L. Mieville, R. B. Poeppel, M. S. Kleefisch, S. Pei, T. P. Kobylinski, and C. A. Udovich, in *Proc. Coal Liquefaction and Gas Conversion Contractors Rev. Conf.* (S. Rogers et al., eds.), Vol. 1, pp. 138-160, U.S. Department of Energy, Pittsburgh Energy Technology Center, Pittsburgh, PA, Sept. 27-29, 1993.

6. T. L. Cable, European Patent EP 0438 902 A2, July 31, 1991.

7. E. A. Hazbun, U.S. Patent 4,791,079, Dec. 13, 1988.

8. K. Omata, S. Hashimoto, H. Tominaga, and K. Fujimoto, *Appl. Catal.*, **52** (1989) L1.

9. U. Balachandran, S. L. Morissette, J. J. Picciolo, J. T. Dusek, R. B. Poeppel, S. Pei, M. S. Kleefisch, R. L. Mieville, T. P. Kobylinski, and C. A. Udovich, in *Proc. Int. Gas Res. Conf.* (H. A. Thompson, ed.) pp. 565-573, Government Institutes, Inc., Rockville, MD, 1992.

10. T. M. Gur, A. Belzner, and R. A. Huggins, J. Membrane Sci., **75**, 151, 1992.

11. T. L. Cable, European Patent EP 0 399 833 Al, Nov. 28, 1990.

12. R. D. Evans, An Introduction to Crystal Chemistry, Cambridge University Press, Cambridge, England, 1964.

13. N. G. Eror and U. Balachandran, *J. Solid State Chem.* **40**, 85, 1981.

14. U. Balachandran and N. G. Eror, *J. Phys. Chem. Solids*, **44**, 231, 1983.

15. N. G. Eror and U. Balachandran, *J. Amer. Ceram. Soc.*, **65**, 426, 1982.

16. U. Balachandran, M. Kleefisch, T. P. Kobylinski, S. L. Morissette, and S. Pei, International Patent WO94/24065, Oct. 1994.

17. W. F. Brown, Jr. and J. E. Strawley, ASTM STP 410, Philadelphia, PA, 1967.

18. J. Kraütkramer and H. Kraütkramer, Ultrasonic Testing of Materials (Springer–Verlag, New York, 1983).

19. B. Ma, J.–H. Park, U. Balachandran, and C. U. Segre, "Electronic/Ionic Conductivity and Oxygen Diffusion Coefficient of the Sr–Fe–Co–O System," Materials Research Society Spring Meeting, San Francisco, CA, April 17–21, 1995.

20. B. Ma, U. Balachandran, J.–H. Park, and C. U. Segre, submitted to *Solid State Ionics.*, 1995.

21. S. Pei, M. S. Kleefisch, T. P. Kobylinski, J. Faber, C. A. Udovich, V. Zhang–McCoy, B. Dabrowski, U. Balachandran, R. L. Mieville, and R. B. Poeppel, *Catal. Lett/*, **30**, 201, 1995.

22. W. Weibull, *J. Appl. Mech.*, **293**, 18, 1951.

23. H. U. Anderson, C. C. Chen, L. W. Tai, and M. M. Nasrallah, in *Proc. 2nd Intl. Symp. on Ionic and Mixed Conduction Ceramics* (T. A. Ramanarayaman, W. L. Worrell, and H. L. Tuller, eds.) pp. 376-387, The Electrochem. Soc., Pennington, NJ, 1994.

24. C. C. Chen, M. M. Nasrallah, and H. U. Anderson, submitted to *J. Electrochem. Soc.*, 1994.

25. W. L. Worrell, P. Han, and J. Huang, in *High Temperature Electrochemical Behavior of Fast Ion and Mixed Conductors* (F. W. Poulsen, J. J. Bertzen, T. Jacobson, E. Skou, and M. J. L. Ostergood, eds.), Risø National Laboratory, Roskilde, Denmark, 1993) pp. 461-466.

26. Y. Teraoka, H. M. Zhang, K. Okamoto, and N. Yamazoe, *Mater. Res. Bull.*, **23**, 51, 1988.

27. T. Ishigaki, S. Yamauchi, K. Kishio, J. Mizusaki, and K. Fuek, *Solid State Chem.*, **73**, 179, 1988.

28. P. S. Maiya, M. S. Kleefisch, J. T. Dusek, R. L. Mieville, U. Balachandran, and C. A. Udovich, paper for presentation at the 1st Intl. Conf. on Ceramic Membranes, 188th Mtg. of the Electrochem. Soc., Inc., Chicago, IL, October 8–13, 1995.

29. S. Carter, A. Selcuk, R. J. Chater, K. Kajda, J. A. Kilner, and B. C. H. Steele, *Solid State Ionics*, **53–56**, 597, 1992.

Title: Oxidative Coupling of Methane Using Inorganic Membrane Reactor.

PI(Authors): Y.H.Ma,W.R.Moser, A.G.Dixon, A.M.Ramachandra,Y.Lu and C.Binkerd.

Institution: Worcester Polytechnic Institute, Worcester, MA.

Contract Number: DE-AC-92PC92113

Period of Performance: 1994-1995.

Objective:

The goal of this research is to improve the oxidative coupling of methane in a catalytic inorganic membrane reactor. A specific target is to achieve conversion of methane to C_2 hydrocarbons at very high selectivity and relatively higher yields than in fixed bed reactors by controlling the oxygen supply through the membrane. A membrane reactor has the advantage of precisely controlling the rate of delivery of oxygen to the catalyst. This facility permits balancing the rate of oxidation and reduction of the catalyst. In addition, membrane reactors minimize the concentration of gas phase oxygen thus reducing non selective gas phase reactions, which are believed to be a main route for formation of CO_x products. Such gas phase reactions are a cause for decreased selectivity in oxidative coupling of methane in conventional flow reactors. Membrane reactors could also produce higher product yields by providing better distribution of the reactant gases over the catalyst than the conventional plug flow reactors.

Accomplishments and Conclusions:

Introduction

The aim of the experimental studies in this project was to investigate the effect of controlling the oxygen feed supplied for the methane coupling reaction. C_2 hydrocarbons, ethane and ethylene, which form as a result of methane coupling, have a higher affinity for gas phase oxygen than methane. Thus both the reactant CH_4 and the intermediate products (C_2 hydrocarbons) convert into the complete oxidation products CO and CO_2. Hence, it is advantageous to regulate the supply of one of the reactants along the length of the catalyst bed to maximize the yield of the intermediate products. Research efforts were aimed at porous Vycor membrane reactors that were used to study oxidative coupling of methane under a variety of experimental conditions. Using tubular porous Vycor membranes in a shell and tube type of reactor, gas flow was metered in from the high pressure shell side into the catalyst packed tube side of these membrane reactors.

A second avenue of research was the study of oxygen conducting perovskite materials, their synthesis and characterization. These materials are also intended to be used in shell-and-tube membrane reactors. A third research focus was the development of a novel radial flow catalytic membrane reactor. Methane coupling was also investigated in this reactor configuration. Modeling work which aimed at predicting the observed experimental trends in porous membrane reactors was also undertaken in this research program.

Reactor Performance Comparisons

Experimental studies were made with porous Vycor membrane reactors and conventional non-porous packed bed reactors operating under identical conditions. Figure 1(a) shows the C_2 selectivities in the porous Vycor membrane reactor and the quartz non-porous reactor operated at the same contact time (experimental parameters are listed in Table 1). C_2 selectivities were consistently higher in the Vycor membrane reactor over the temperature range 700°C-800°C, compared to the non-porous quartz tube reactor. With increasing temperature, the non-selective gas phase methane conversion to CO_x products increased. Hence the C_2 selectivity decreased as reaction temperature went up. The overall C_2 yields were about the same in both reactor configurations as shown in Figure 1(b). The membrane reactor has an overall C_2 yield of 11%, while the quartz tube fixed bed reactor has 10% C_2 yield at the same conditions. Due to the necessity of larger reactor volumes in porous membrane reactors, higher levels of methane conversions have not been achieved. A larger bed cross-section is not desired as that would increase methane loss to non-selective reactions on the shell side. Total methane conversions for the two reactor systems are shown in Figure 1(c) for the reactors. The higher conversions seen for the quartz tube fixed bed reactor however, are mainly caused by the deep oxidation to CO_x products as seen by the low values of C_2 selectivity at the corresponding temperatures for this reactor configuration. Figure 1(d) shows a conversion versus selectivity plot that compares the performance of the Vycor membrane reactor with the co-feed non-porous reactor. At the same level of conversion, membrane reactors yield higher C_2 selectivity. Conditions of equal methane conversions were obtained at different reaction temperatures for the two reactors. The higher C_2 selectivity in the membrane reactor shows that for the methane coupling reaction, regulating the supply of oxygen along the length of the packed bed is beneficial for C_2 product formation.

TABLE 1. Experimental Conditions for VYCOR membrane reactors

Experimental. Parameter	Set 1	Set 2
Helium Flow rate	200 ml/min	100 ml/min
Methane Flow Rate	40ml/min	20.3ml/min
Oxygen Permeate	20ml/min	10.2ml/min
Shell side Pressure	65 psi	30 psi
Reactor Bed Length	12 cms	6 cms
Catalyst loading	2.4 gms	1.2 gms
Temperature Deviation	10°C	5°C
Temperature range	650°C-850°C	650°C-800°C

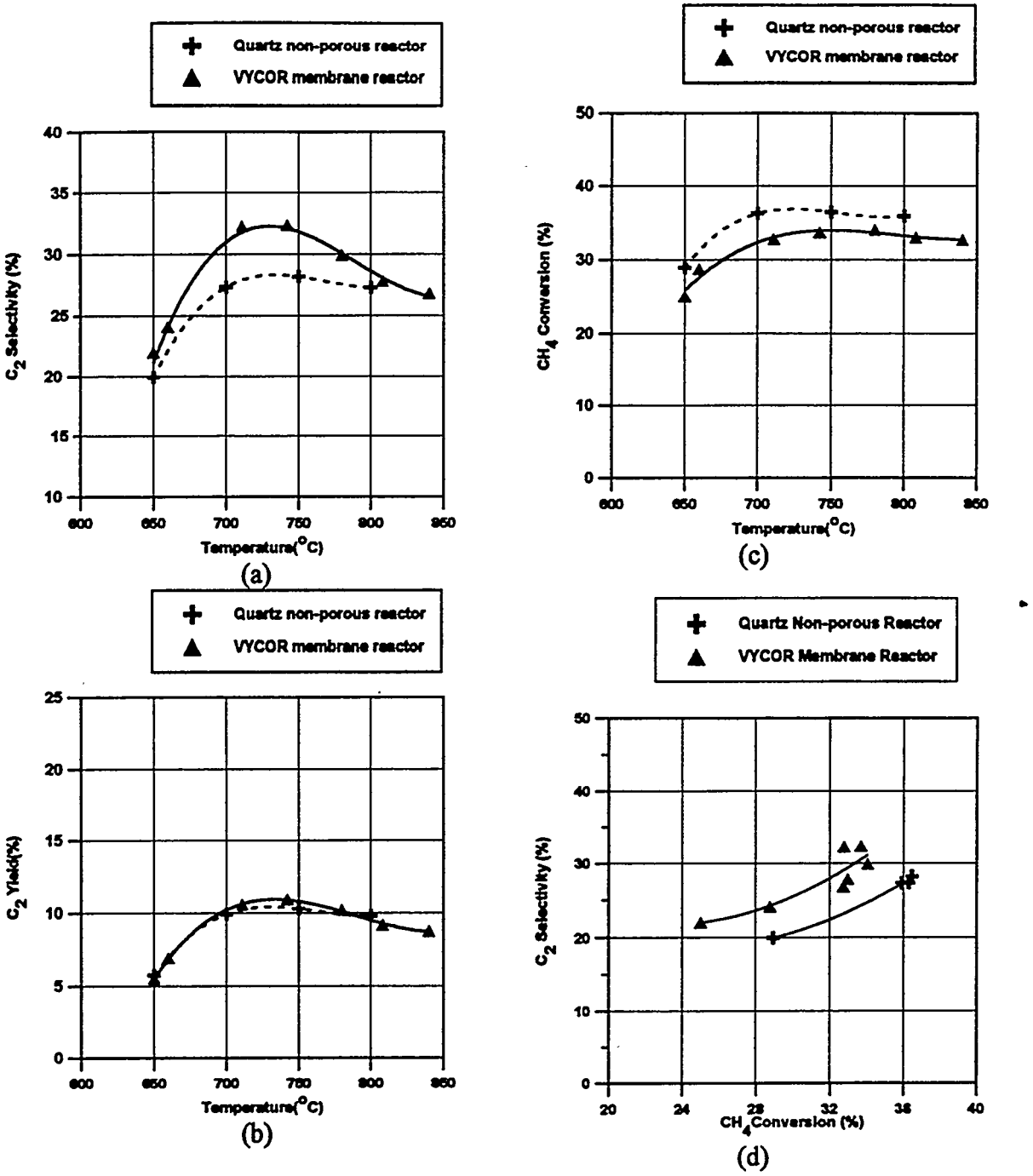

Figure 1. Comparison of (a) C_2 selectivities (b) C_2 yields, and (c) CH_4 conversions from porous Vycor membrane reactor and co-feed, non-porous quartz reactor. (d) conversion vs. selectivity plot. where the different conversions were obtained at different reaction temperatures.

Methane coupling under varying methane to oxygen feed ratios

The VYCOR membrane reactor was operated at various methane to oxygen feed ratios to study the effect of the variations in methane and oxygen concentrations on the methane coupling reaction. The catalyst (Sm_2O_3) was packed on the tube side of the

membrane reactor and a constant flow of oxygen permeated from the shell to the tube side. The methane flow on the tube side was varied to change the methane to oxygen ratio. Figures 2 shows the effect of the changing methane to oxygen ratio at various reaction temperatures. It was seen that highest C_2 yields were obtained at a methane to oxygen ratio of 2.0, where both the CH_4 conversions and C_2 selectivities were optimal. Similar trend was observed at other temperatures. A majority of our studies on methane coupling were done at the methane to oxygen ratio of 2.0 and in the temperature range of 650°C to 850°C, thereby exploring the active thermal range of the coupling reaction.

Methane coupling under oxygen rich conditions

These studies were aimed at exploring the effects of conducting the methane coupling experiments under conditions where the oxygen conversion was far from complete. Since we were investigating a reactor system that operates on the principle of metering the oxygen supply, it was necessary to study the reaction under conditions where the oxygen was present in an excess.

Figure 3 shows a comparison of the methane conversion with reaction temperature from porous VYCOR membrane reactors under oxygen rich and oxygen lean environments, run at equivalent flow conditions and at a methane to oxygen ratio of 0.5. Oxygen lean conditions result in almost complete conversion of oxygen, limiting the amount of methane that can be converted to between 40% and 60%. Though this limitation on methane conversion was overcome under oxygen rich conditions, a decline in C_2 selectivity was observed as shown in Figure 3. These results indicate that metering the oxygen flow through porous membrane reactors is beneficial to the methane coupling reaction when most of the oxygen supplied to the catalyst bed is used up before exiting the reactor. This was ascertained by carrying out similar experiments at various methane to oxygen ratios as shown in Table 2.

Table 2. Performance of Vycor membrane reactor under O_2 rich conditions.

CH_4/O_2	Methane Conversion	Oxygen Conversion	C_2 Selectivity	C_2 Yield
2.0	20%-25%	40%-90%	30%-20%	5%-10%
1.0	10%-30%	30%-60%	20%-15%	2%-5%
0.5	90%-100%	40%-50%	10%-2%	2%-5%

Metering methane flow in membrane reactors

Since oxygen was the competing reactant for methane coupling as well as for methane deep oxidation, most of the experimental work done earlier in this project involved metering in oxygen flow through the porous membrane tube of the reactor. Due to the higher affinity of C_2 hydrocarbons over methane for oxygen, metering in oxygen flow was counter-productive in the lower part of the catalyst bed and detreimental to C_2 selectivity.

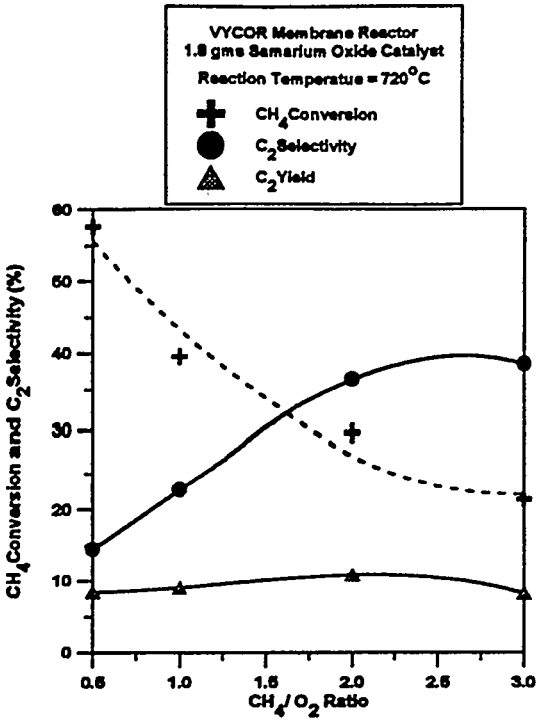

Figure 2. Effect of varying methane to oxygen ratio in Vycor membrane reactor.

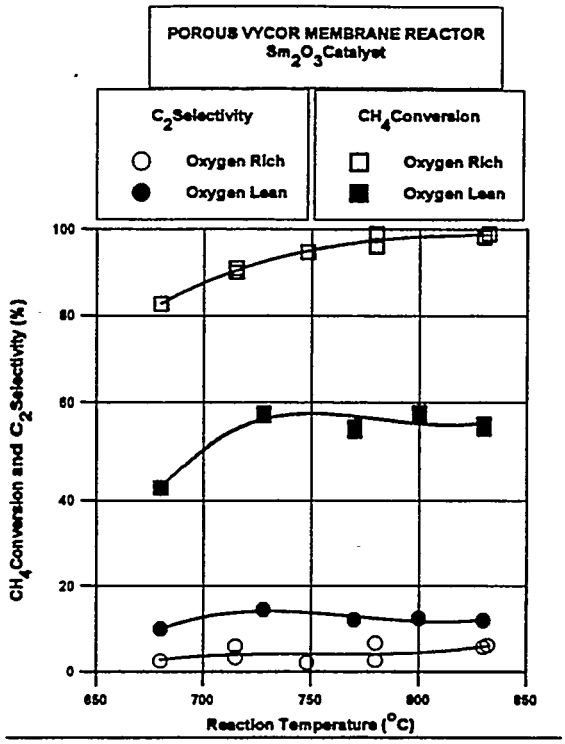

Figure 3. CH_4 conversion and C_2 selectivity in Vycor membrane reactors operated under O_2 rich and O_2 lean conditions.

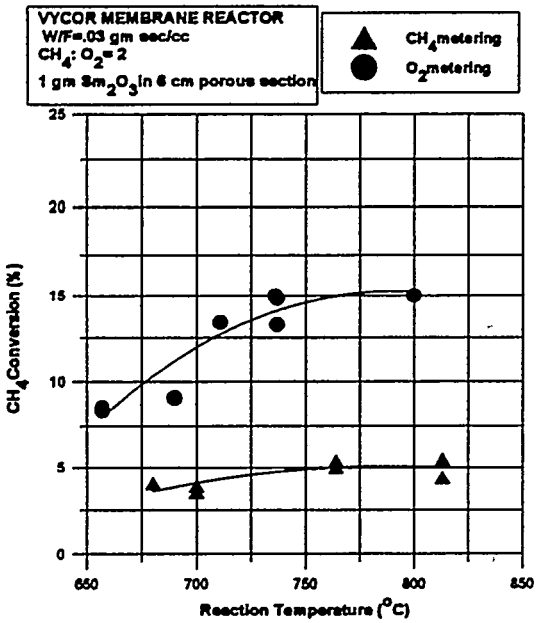

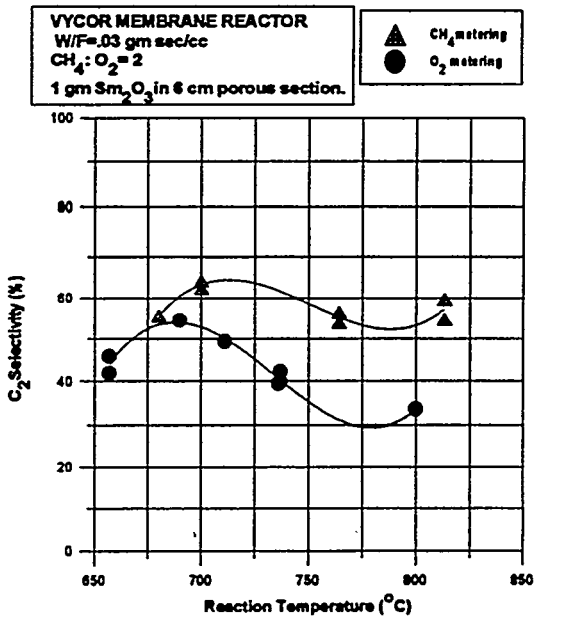

Figure 4. Comparison of (a) CH_4 conversions, and (b) C_2 selectivities in Vycor membrane reactors under O_2 and CH_4 metering.

The following experiments were performed to test the effect of metering methane flow into a flowing stream of oxygen. Since the C_2 products that were produced in the earlier sections of the reactor bed were susceptible to oxidation, these experiments of

metered methane flow were aimed at improving the overall C_2 selectivity. The Vycor membrane reactor was run in a configuration where pure methane was fed to the shell side while oxygen mixed with helium diluent was fed in the tube side (catalyst packed inside the tube). Methane permeate flow for methane metering was equal to the oxygen permeate flow for the oxygen metering experiments and all these experiments were run at an overall methane to oxygen ratio of 2.0.

Figure 4(a) compares the methane conversions and Figure 4(b) compares the C_2 selectivities in these experiments with those of oxygen metering at equivalent flow conditions. An improvement in the overall C_2 selectivities was obtained as expected, as compared to the earlier studies which were run with oxygen on the shell side. Lower methane conversions, however, offset the higher selectivities, resulting in very low C_2 yields.

Modeling Studies

Oxidative coupling of methane involves a series-parallel reaction scheme where methane and oxygen are consumed in parallel reactions resulting in the formation of desired C_2 products and the undesired CO_x products. The C_2 products could further react with oxygen to form CO_x products through complete oxidation. The reaction scheme is as follows :

$$CH_4 + O_2 \xrightarrow{k1} C_2H_4$$

$$CH_4 + O_2 \xrightarrow{k2} CO_x$$

$$C_2H_4 + O_2 \xrightarrow{k3} CO_x$$

Modeling studies of the methane coupling reaction incorporated the above three reactions and the kinetics parameters from Tung and Lobban [1]. A theoretical fit was obtained for the methane coupling experimental data in the quartz non-porous fixed bed reactor as shown in Figure 5(a). The experimental data obtained at various reaction temperatures, at a constant methane to oxygen ratio of 2.0 were fitted with the kinetic model. Figure 5(a) shows that the theoretical fit is in good agreement with the experimental data. Using the parameters obtained from this fit of the model to the fixed bed reactor data, and the experimental conditions of the VYCOR membrane reactor experiments, the model predicted trends in methane conversion and hydrocarbon selectivity and yield in membrane reactors. A reasonably good agreement was obtained between the predicted model trends and experimental results with the VYCOR membrane reactors as shown in Figure 5(b). The model is being further refined by incorporating other kinetic schemes to predict the trends of the methane coupling reaction in VYCOR membrane reactors obtained under different sets of experimental conditions.

Oxygen Conducting Materials : Perovskites

One of the proposed avenues of research was the synthesis of dense membrane reactors, where the dense membranes are made of materials that allow only the permeation of oxygen across the membrane. Perovskites of rare earths like Sr, La, Ce and Yb in combination with group VIII elements like Fe and Co are known to permit oxygen conduction through their bulk. Litereature reports also suggest that the oxygen that is

conducted through these materials is not molecular oxygen, but rather an oxygen anion. This research thus aims at not only looking for materials that would conduct oxyge and are catalytically active for methane coupling, but also aims at changing the chemistry of the methane coupling reaction by bringing in oxygen in a form that is not molecular oxygen. Research efforts on the synthesis and characterization of these perovskites are discussed next.

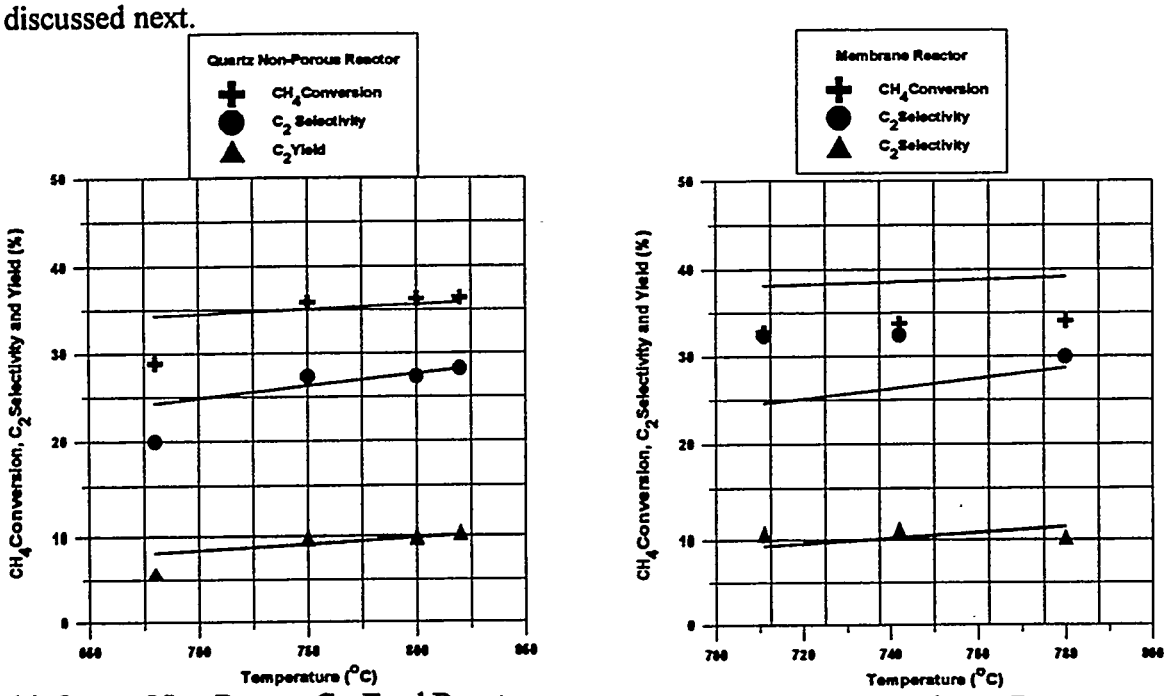

(a) Quartz Non-Porous Co-Feed Reactor (b) Porous Vycor Membrane Reactor

Figure 5. Comparison of model predictions for CH_4 conversions and C_2 selectivities in porous VYCOR membrane reactors with experimental data. (Solid line shows the predicted trend).

Perovskite Synthesis

The oxygen conducting perovskite, $Sr_{0.8}La_{0.2}FeO_3$, was synthesized by both the conventional solution precipitation technique as well as by the cavitation technique. Synthesis by cavitation was accomplished in the Microfluidizer which produces nanometer size particles of the perovskite. KOH and NH_4OH were used as precipitating agents in the Microfluidizer and the perovskite was precipitated from a mixture of the corresponding metal nitrates, while being subjected to cavitational forces. Water and 2-Propanol were used as solvents in both the conventional and the Microfluidizer synthesis techniques. The perovskites were characterized using XRD, DSC and TGA.

The synthesized perovskite was subjected to high temperature calcinations at progressively higher temperatures. XRD analysis of the calcined materials showed that the Microfluidizer-synthesized $Sr_{0.8}La_{0.2}FeO_3$ showed the characteristic perovskite peaks at a calcination temperature of 590°C when KOH was used as the precipitating agent, in both water and 2-Propanol media. Figure 6 shows the XRD spectra from $Sr_{0.8}La_{0.2}FeO_3$ samples that were prepared using the different methods, precipitating agents and solvents, and calcined at 590°C. The materials prepared by using NH_4OH did not show the perovskite structure under XRD for the calcination temperature of 590°C. This was

probably due to phase separation of strontium oxide during synthesis, since strontium oxide does not easily precipitate from NH_4OH.

Characterization of Perovskites

$Sr_{0.8}La_{0.2}FeO_3$ prepared both by the conventional and the cavitation techniques showed reversible exotherms on the DSC spectrum at 150°C and 350°C only when KOH was used as the precipitating agent in 2-Propanol medium. Using KOH in water resulted in the perovskite structure as evidenced by XRD, but this material did not show the reversible DSC exotherms. Since such reversible exotherms occur when a material undergoes structural or polymorphic changes, it is likely that the material prepared in 2-Propanol resulted in perovskites with a defect structure in which there was a measurable energy difference between the two polymorphic forms as evidenced by the reversible exotherms at 150°C and 350°C as shown in Figure 7.

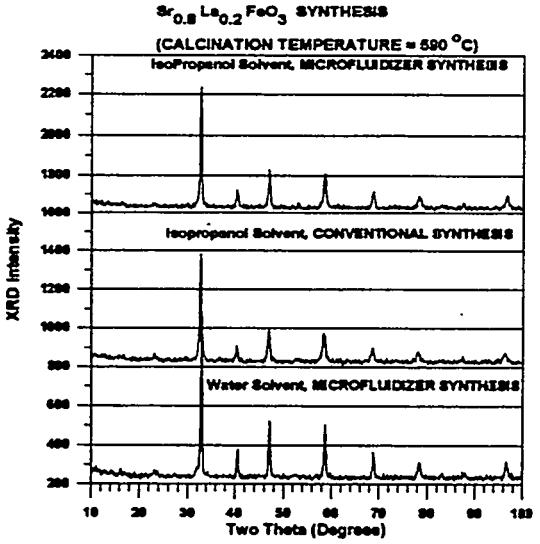

Figure 6. XRD Spectra from samples of the $Sr_{0.8}La_{0.2}FeO_3$ prepared by the conventional and the cavitation techniques.

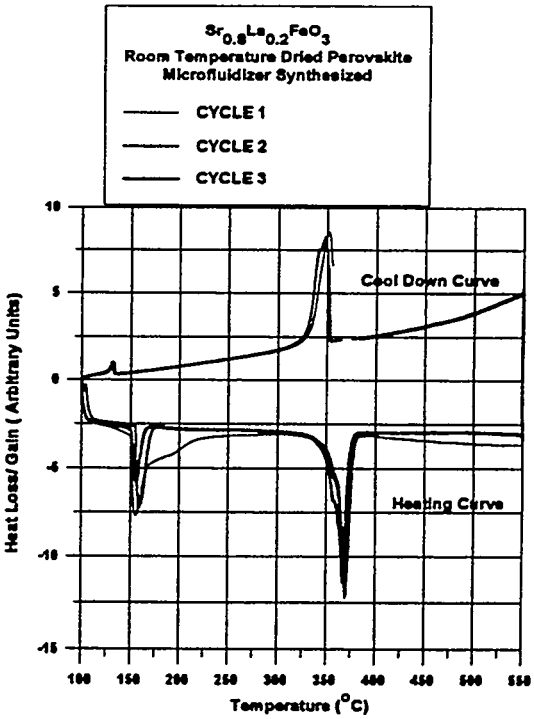

Figure 7. DSC spectra from a sample of $Sr_{0.8}La_{0.2}FeO_3$ showing the reversible exotherms and endotherms.

Comparison of catalytic activity of the perovskites

Methane coupling activity of the synthesized perovskite materials was tested by using these materials as catalysts in a quartz tube fixed bed reactor. Blank reactor experiments were performed in the non-porous quartz tube reactor at standard flow conditions typically used for the methane coupling experiments. Methane to oxygen ratio was maintained at 2.0, with a 10% oxygen dilution in helium. Methane conversions were found to be less than 5% over the temperature range 650°C to 850°C, indicating that the contribution from the quartz chips and the reactor tube walls was minimal.

Two perovskites, $Sr_{0.8}La_{0.2}FeO_3$ and $SrCe_{0.8}Yb_{0.2}O_3$ were tested for their catalytic activity towards methane coupling by packing the materials in fixed bed non-porous reactor. The performance of both perovskites was compared with that of Sm_2O_3 over the temperature range of study. Figure 8(a) compares the methane conversions by all three materials, $Sr_{0.8}La_{0.2}FeO_3$, $SrCe_{0.8}Yb_{0.2}O_3$, and Sm_2O_3 operating under identical flow conditions. Catalyst loading of about 1gm was used for all these experiments. The catalyst was mixed with quartz chips and packed in the quartz tube, making up a 10 cm reaction zone. Over the entire temperature range of study, both the perovskite materials showed constant activity and stability over several hours on-line. Methane conversions were significantly higher than the blank reactor conversion of 5%. Over the entire temperature range studied, samarium oxide had 5-10% higher methane conversions than both the perovskites. $SrCe_{0.8}Yb_{0.2}O_3$exhibited higher conversions than the $Sr_{0.8}La_{0.2}FeO_3$.

Figure 8(b) compares the C_2 selectivities of the three materials. Of the two perovskites, $Sr_{0.8}La_{0.2}FeO_3$ acts as a deep oxidation catalyst with very low C_2 selectivities, and no significant hydrocarbon yields. C_2 selectivity of $SrCe_{0.8}Yb_{0.2}O_3$ lies midway between that of samarium oxide and $Sr_{0.8}La_{0.2}FeO_3$.

Although these studies were done using the perovskite materials in packed beds and not as membranes, the catalytic results suggest that the use of $Sr_{0.8}La_{0.2}FeO_3$ as a dense membrane material would be disadvantageous. We would like to synthesize dense membranes from materials that exhibit oxygen conductivity at elevated temperatures, while, at the same time, are good methane coupling catalysts, so that they would not lower the overall C_2 selectivity of the reactor. $SrCe_{0.8}Yb_{0.2}O_3$ is a more promising candidate since it has both methane coupling activity as well as oxygen conducting ability. Though literature reports do not indicate very high oxygen conductivity of this material, changes in relative compositions of cerium and yitribium are postulated to enhance the oxygen flux transported through the material. Hence, other compositions of this family of perovskites could serve as a potential candidate for dense membrane synthesis. Further work involving synthesis and catalytic testing of different compositions as well as other prospective materials is underway.

Fabrication of supported thin films of perovskite

In parallel with the research on dense membrane materials, work was also oriented toward finding a robust way of making thin films of the perovskite materials. Thus, while on one hand, we are looking for a good catalyst/oxygen conductor, on the other hand, we are working on supports and structural stability. A spray technique was developed to synthesize a perovskite dense membrane supported on porous alumina substrates. A 2000 Angstrom pore size α-alumina was used as the support material. Nitrates of metals constituting the perovskite which serve as precursors for perovskite formation were deposited on top of the support using the spray technique. The perovskite precursors deposited as a thick layer on top of the support. The perovskite structure evolved after the 1200°C treatment, but the film developed cracks. To achieve crack-free films and improve adhesion with the support, modifications of porous alpha alumina supports as well as microporous gamma alumina membranes were done as described below.

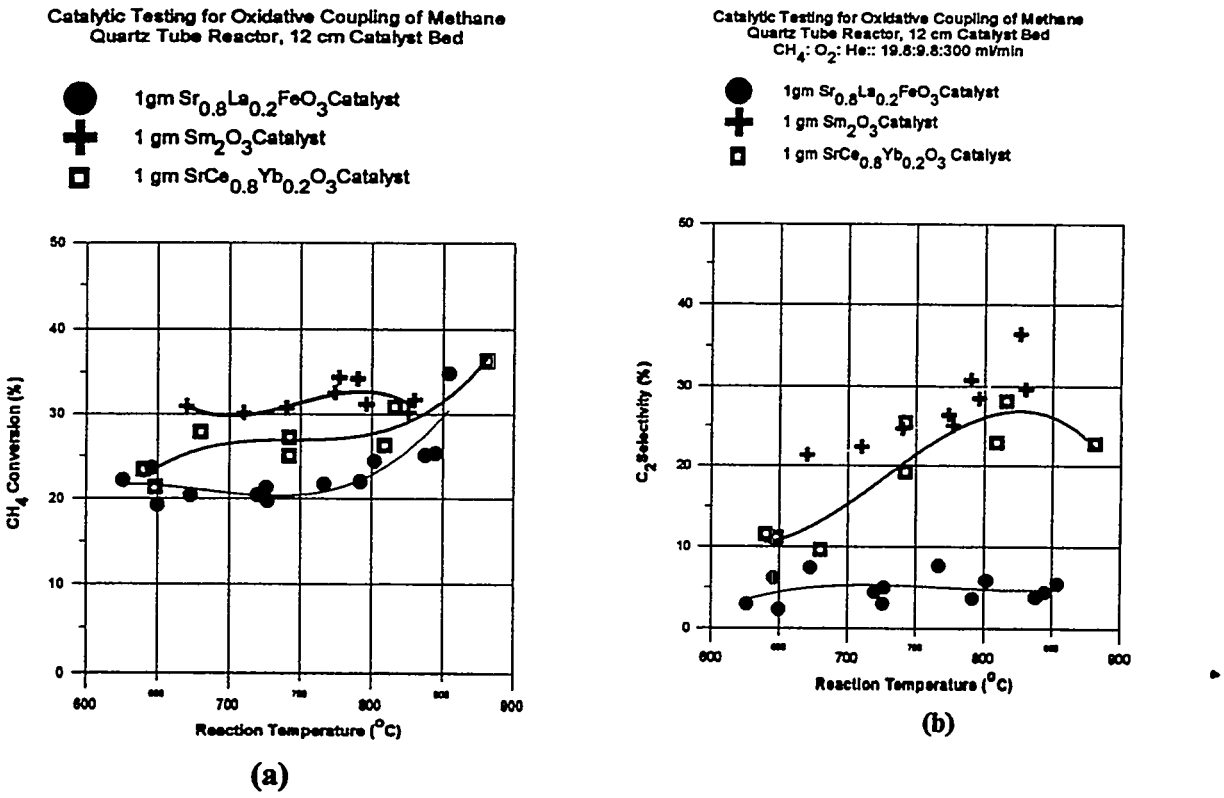

Figure 8. Comparison of (a) CH_4 conversions and (b) C_2 selectivities of the perovskites and Sm_2O_3 under identical operating conditions.

Modification of porous gamma alumina membranes

Experiments were performed to stabilize the gamma alumina top layer of the 40 Angstrom pore size alumina membranes since commercially available gamma alumina membranes were unstable at temperatures above 700°C. The stabilization process involved treating gamma alumina membranes with lanthanum nitrate solution, followed by repeated calcinations, to form lanthanum aluminate on the gamma alumina. The unmodified gamma alumina had higher permeance after calcination at 900°C, due to pore opening and loss of stability. The modified gamma alumina membrane showed lowered permeance and good thermal stability. Permeance increased only slightly after 50 hours at 900°C, indicating good stability of the modified membrane. The lower permeance of the lanthanum modified alumina, as compared to the unmodified alumina, indicated that either a partial pore blockage or a change in morphology had occurred in the alumina substrate. An oxygen conducting perovskite ($Sr_{0.8}La_{0.2}FeO_3$) was deposited on the modified gamma alumina membrane by solution deposition technique. The perovskite caused a lowering of permeance to gas flow at room temperature indicating that partial pore filling had occurred. XRD analysis of the deposit showed it to have the perovskite structure. Experiments are underway to achieve complete pore closure and to make high temperature oxygen conduction measurements through these dense membranes.

Pore filling of porous alpha alumina membranes.

Another approach taken to develop perovskite thin films was by filling up the pores in large pore diameer support material. By progressively narrowing the pore size with a different material, it was hoped that a more robust thin film membrane could be synthesized. Alpha alumina membranes with large pores (1.2 micron pore diameter) were used as the starting material. A high pressure technique based on *cavitation* effects in fluids was used to synthesize nanometer size particles. The nitrates of lanthanum and aluminum are subjected to high pressure (20,000 psig) in the presence of ammonium hydroxide in a specialized apparatus called the *Microfluidizer* to produce nanometer sized grains of $LaAlO_3$ with a particle size of 0.5 microns. $LaAlO_3$ synthesized in the Microfluidizer has been studied by XRD to determine phase purity with increasing temperature of calcination as shown in Figure 9. A comparison with the JCPDS line spectra of $LaAlO_3$ showed that the perovskite structure formed after the 900°C calcination. On the basis of these results, the porous alpha alumina discs containing the $LaAlO_3$ gel produced in the Microfluidizer were calcined at 900°C.

Lanthanum aluminate nanoparticles produced in the Microfluidizer were deposited inside the 1.2 micron pores of the alpha alumina substrate, partially filling the pores of the membrane. $LaAlO_3$ showed better adhesion to the alpha alumina support at high temperature, probably due to the fact that they have similar thermal expansivity. Figure 10 shows the change in gas permeance in the pore-filled alumina as a function of increasing number of pore fillings. The figure compares the gas permeance achieved in the pore blocked alumina with that of 40 Angstrom pore diameter gamma alumina and the 40 Angstrom pore diameter Vycor.

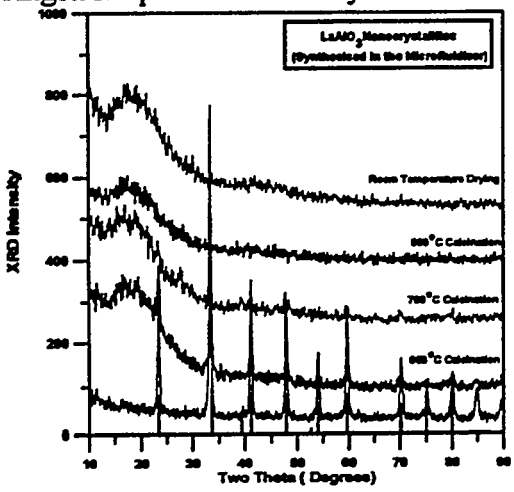

Figure 9. XRD patterns of $LaAlO_3$ synthesized in the Microfluidizer showing evolution of crystallinity with increasing temperature of calcination.

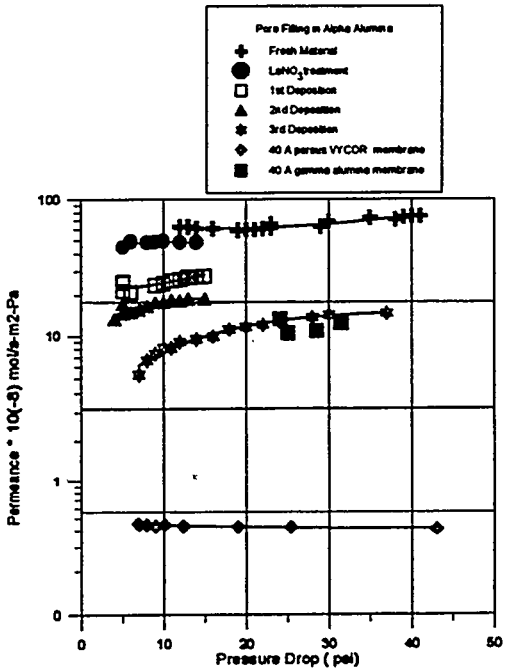

Figure 10. Comparison of gas permeance in pore-filled alumina with increasing number of fillings.

Methane Coupling in Radial Flow Catalytic Membrane Reactor.

The third proposed avenue of membrane reactor research was the study of porous catalytic membrane reactors. The following work aims at using a porous membrane that is also catalytically active for methane coupling. Reactant gases flowing through the membrane pores are brought in contact with the methane coupling catalyst deposited inside the membrane pores in this catalytic membrane reactor.

Recent literature reports indicate that external mass transfer limitations present during highly reactive methane coupling catalytic reactions detrimentally affect methane conversion and total C_2 production rates. External mass transfer limitations can be reduced by increasing the linear velocity of reactant gases over the catalyst. By using porous catalytic membranes of different pore diameters and by varying the flow rates of reactant gases passing through the catalytic membrane, one can regulate the contact time of the reactant gases with the active catalyst in the membrane pores. The combined effect of membranes coated with the active catalyst and the reactor flow configuration was postulated to minimize external mass transfer limitations. The result was expected to maximize the overall efficiency of methane coupling.

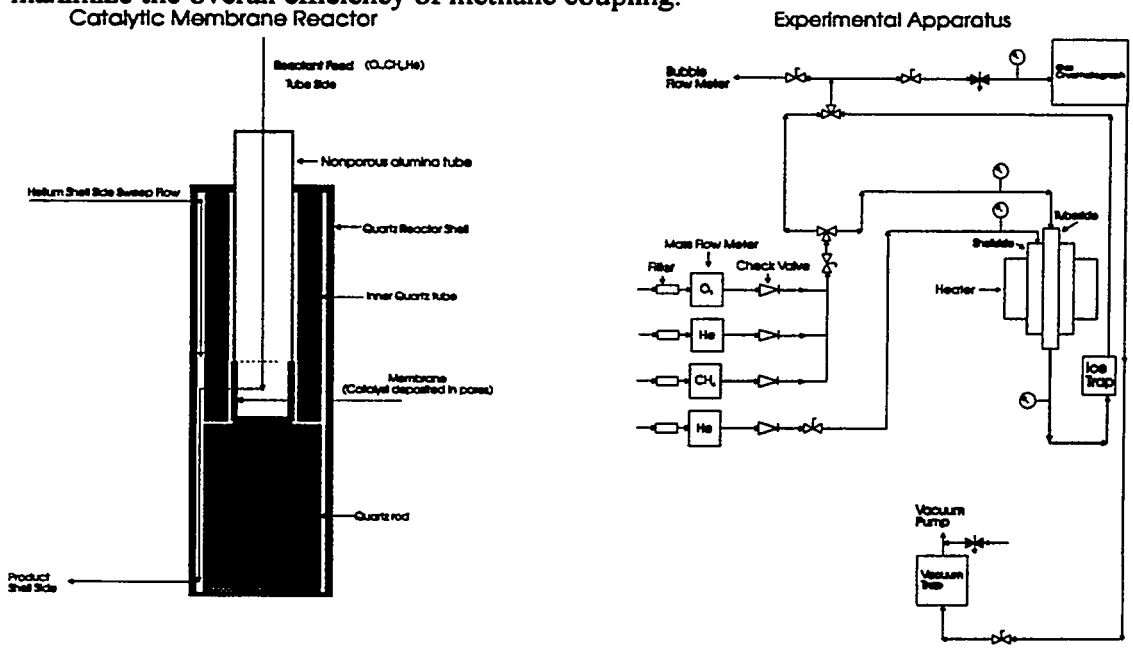

Figure 5. (a). Cross section view of the catalytic membrane reactor and (b). Schematic of the experimental setup of a catalytic membrane reactor.

As detailed in the cross section of the catalytic membrane shown in Figure 11(a), the catalytic membrane reactor provides the experimental capability to research the effects of high reactant linear velocities. Figure 11(b) shows a schematic of the experimental setup. Large pore size (0.02 μm to 2 μm pore size) alpha alumina membranes were used to form these catalytic membranes. The reactant gas mixture of oxygen, methane and helium diluent was fed in the tube side of the catalytic membrane reactor. All the gas was forced out of the membrane pores into the shell side of the membrane reactor. The free volume on both the tube side and the shell side of the membrane reactor was filled with quartz rods and quartz chips to minimize the gas phase reaction contribution. A small

helium sweep flow was maintained on the shell side to prevent back mixing on the shell side. Methane coupling occurs inside the membrane pores as the reactant gases pass from the tube side to the shell side of the membrane reactor. The product gases mixed with the helium sweep gas and exited on the shell side of the catalytic membrane reactor. The exit stream was then sent through a water trap and then through the sample loop for GC analysis.

The catalytic membrane which acts as the tube of the shell-and-tube membrane reactor was constructed by welding together a porous membrane tube and a non-porous alumina tube with a high temperature ceramic glaze. The end of the membrane tube not welded to the non-porous segment was blocked off and sealed with a high temperature glaze. This welding procedure minimized the length of the porous alpha alumina membrane to be used in the reactor setup. Porous membrane tubes with a standard length of 2.6 cm and of different pore diameters, (0.02 μm, 0.1 μm, 0.2 μm, 0.5 μm, 2.0 μm), made of both alpha alumina and zirconia have been used for these studies. In all cases, blank reactions have been run in each reactor to establish the base-line conversions of the empty reactor. As shown in Figure 12, the conversion of methane was negligible over the range of flow rates used for the experimental study. Methane conversion was less than two percent for total feed flow rates greater than 150 ml/min at reaction temperatures of 750°C to 850°C. The reactivity of the blank porous membrane tubes for all pore sizes was minor.

Oxidative coupling of methane was carried out in the radial flow membrane reactor in the temperature range of 750°C- 900°C. The membrane reactors chosen for the catalytic studies were of pore diameters of 2.0 μm, 0.2 μm, and 0.02 μm. By covering the range of two orders of magnitude, these experiments were designed to study the effect of membrane pore size on the reactor performance for oxidative coupling of methane.

The catalyst was impregnated as samarium nitrate into the membrane top layer using a vacuum solution deposition technique. High temperature calcination converted the nitrate into samarium oxide and rendered it active for methane coupling. X-ray digital mapping of the porous membrane cross-section revealed high intensity of samarium in the active catalyst within the toplayer. This is advantageous, since the reactant gas mixture would be expected to pass through most of the membrane support without contacting the catalyst on the walls of the support, until it entered the top layer, in which the pore diameter is accurately known. A summary of the reaction conditions is given in Table 3.

The stability of both the reactor and the catalyst was investigated by keeping the membrane reactor on-stream in excess of 100 hours. Results indicated only relatively minor catalyst deactivation over a six day period as shown in Figure 13. Methane conversions and C_2 selectivities were relatively unchanged even after 125 hours on-line. This indicates that there was no loss in catalytic activity either due to catalyst poisoning or from loss in catalyst surface area due to sintering.

Figure 14 shows the experimental results for the 2.0 μm, 0.2 μm, and 0.02 μm pore diameter reactors. The 2.0 μm and 0.2 μm pore diameter tubes show similar results with a trend showing higher CH_4 conversions, and lower total C_2 selectivities with decreasing flowrates (WHSV). Lower contact times result in lower CH_4 conversions and higher total C_2 selectivities. The 0.02μm pore diameter tube shows constant and lower

total C_2 selectivities in comparison to the larger pore diameter tubes over the entire flow range.

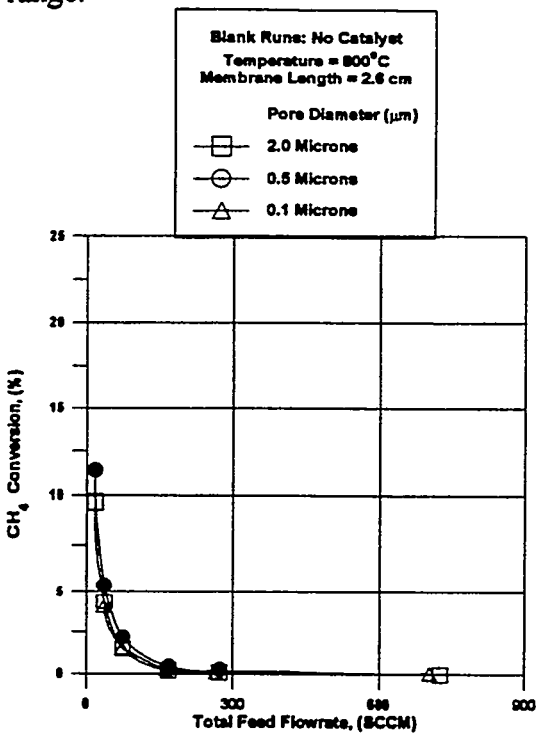

Figure 6. Blank Reactor Conversion Data at 800°C.

Figure 7. Stability test for the Sm_2O_3 catalyst in the radial flow membrane reactor.

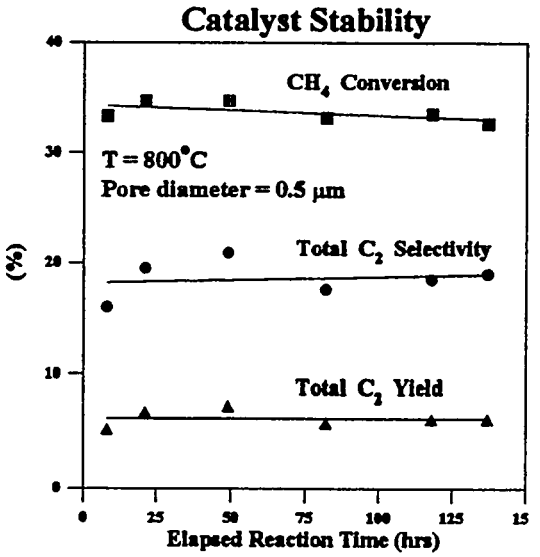

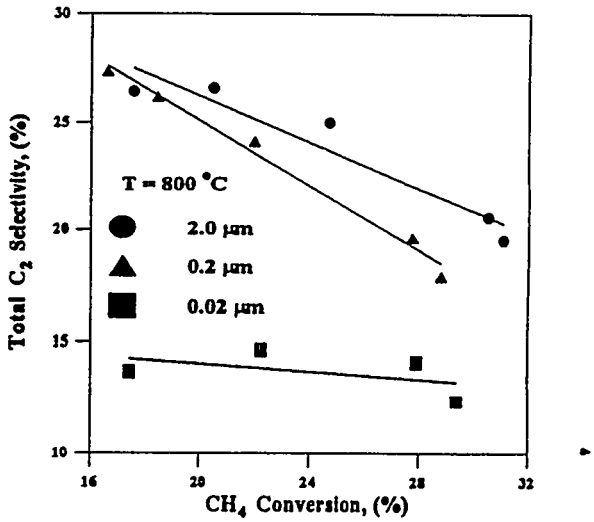

Figure 8. Reactor performance of different pore diameter membranes used in radial flow reactor.

Table 3. Experimental conditions for the catalytic membrane reactor.

Temperature	700°C - 850°C
Feed	$CH_4 : O_2 : He = 2 : 1 : 10$
Flowrate	200 - 2000 cc/min
Catalyst Weight	Sm_2O_3, 100 mg
Support materials	α - Al_2O_3, ZrO_2
Membrane Dimensions	Tubular membrane, 7 mm ID, 10 mm OD Length = 26 mm
Toplayer	Thickness = 30 μm
Toplayer Pore Diameters	α - $Al_2O_3 \Rightarrow d_p$ = 2.0, 0.5, 0.2 μm $ZrO_2 \Rightarrow d_p$ = 0.02 μm

The observed results are believed to be the result of the characteristic flow regime for each membrane pore size. Table 4 shows the results of calculations at reaction conditions for the relationship between the molecular mean free path and pore radius. The results reveal that the smallest pore size tube (0.02 μm pore diameter) is clearly in the Knudsen flow regime where molecule-wall collisions are predominant. As the pore size increases the flow behavior changes to viscous flow where the benefits of higher total C_2

selectivities are observed. Evidence in the literature [2] shows C_2 products to have approximately 5-10 times greater affinity for the catalyst active sites than CH_4. It is believed that the lower C_2 selectivity for the smallest pore size is due to the more intimate contact of the C_2 products with the active sites on the pore walls, with the result being further oxidation. These initial reactor investigations show a trend of increasing methane coupling performance with larger pore sizes.

These results provide insight into the general understanding of the oxidative coupling of methane. The fact that coupling in the Knudsen flow regime resulted in lower C_2 selectivities at the same degree of conversion, when compared to the viscous flow experiments, suggests that at the conditions of the experimental study, it is not advantageous to have a porous catalyst of high surface area. The flow regime in high surface area catalysts is predominantly Knudsen inside the catalyst pores and would therefore be disadvantageous for methane coupling.

Table 4. Flow regimes [l = molecular mean free path, r = pore radius]
Temperature = 800°C ; Pressure = 1 atm

Pore Diameter (μm)	Knudsen Number (Kn) = λ/r	Flow Regime
2.0	0.2	Viscous
0.2	2.0	Transition
0.02	20	Knudsen

Conclusions

Methane coupling experiments showed that under equivalent conidtions, C_2 selectivities were 10% higher in the membrane reactors as compared to the conventional co-feed non-porous reactors in the temperature range 650°C to 850°C. Studies involving variation of methane to oxygen ratios showed that both the methane conversions and C_2 selectivities were high at a methane to oxygen ratio of 2.0. Experiments run at conditions where the oxygen conversion was less than 100% resulted in lowered C_2 selectivity and higher methane conversions because of oxygen availability. Experiments involving metering of methane flow from the high pressure shell side into a mixture of oxygen and helium on the catalyst packed tube side showed that improved hydrocarbon selectivity is overshadowed by a lowered methane conversion. These results indicate that metering the oxygen flow through porous membrane reactors is beneficial to the methane coupling reaction when most of the oxygen supplied to the catalyst bed is used up before exiting the reactor. Modeling studies focused on fitting the experimental results obtained in VYCOR membrane reactors with a simplified kinetic model. The parameters for the fit were obtained by using the experimentally obtained values of methane conversions and C_2 selectivities and yields from fixed bed reactor experiments. The trends in experimental data on methane conversions, and C_2 selectivities and yields agreed reasonably well with the predicted trends of the model.

Oxygen conducting perovskites have been synthesized using conventional as well as cavitation techniques and characterized by XRD, TGA and DSC. $Sr_{0.8}La_{0.2}FeO_3$, an oxygen conducting perovskite that was synthesized in the Microfluidizer showed interesting DSC and TGA spectra that indicated a change in the crystal structure at

relatively moderate temperatures of 150°C and 350°C. Perovskites of lanthanum, strontium and iron oxides which form good oxygen conductors showed very poor methane coupling activity in comparison to the commonly used methane coupling catalyst, samarium oxide. Hence, a dense membrane reactor that employs this material for metering oxygen flow for methane coupling might inherently cause very low hydrocarbon selectivities. On the other hand, perovskites of the strontium-cerium-yitribium series showed moderate activity for methane coupling, which lay between that of samarium oxide and the La-Sr-Fe oxides. Since these Sr-Ce-Yb-oxides also show moderate oxygen conduction properties, they might be better choices as potential candidates for dense membranes in membrane reactors.

Experiments aimed at modifying the porous alumina included stabilization of gamma alumina and pore filling of alpha alumina supports. The lanthanum modified alumina exhibited lower permeance as compared to the unmodified alumina, indicating that either a partial pore blockage or a change in morphology had occurred in the alumina substrate. A high pressure technique based on *cavitation* effects in fluid was used to synthesize nanometer size $LaAlO_3$ particles which were deposited inside the 1.2 micron pores of the alpha alumina substrate. A lowering of gas permeance was achieved, wherein gas permeance decreased with increasing number of pore fillings.

Catalytic results of the high temperature oxidative coupling of methane in radial flow membrane reactors indicate an interesting observation in regard to oxidative coupling of methane. By exploring the reactor performance in membranes of pore diameters of 2.0 μm, 0.2 μm, and 0.02 μm, the effect of the flow regime on the methane coupling activity can be postulated. The lower pore (0.02 μm) diameter membrane reactor showed much lower hydrocarbon selectivity than the other two membrane reactors. Theoretical calculations indicate the flow regime in this 0.02 μm membrane reactor to be in the Knudsen region, in contrast to the higher pore diameter membrane reactors where the flow is predominantly viscous flow. This suggests that high surface area catalysts, where the flow inside the catalyst pores is in the Knudsen regime, do not offer big advantages for oxidative coupling of methane.

References

1. Web-Yuan Tung and Lance L. Lobban, *Ind. Eng. Chem. Res.*, **31**, 1621-1625 (1992).
2. Cherrak, A., Hubaut, R., Barbaux, Y., *J. Chem. Soc. Faraday Trans.*, **88**, (21), 3241-3244, (1992).

Plans:

Radial flow catalytic reactors will be used for studying methane coupling under varying experimental conditions and the reactor performance will be compared with a conventional non-porous fixed bed reactor operating under the same experimental conditions. In addition, comparison studies of CH_4 conversion rates and C_2 selectivites in the radial flow catalytic membrane reactor and the conventional co-feed packed bed reactor, will be investigated.

Methane coupling activity of materials that are oxygen conducting will be expanded to identify candidates for dense membrane synthesis. Dense membrane reactors will be used for methane coupling studies.

The modeling work will be continued to predict the trends of various process parameters and the predicted trends will be compared to our experimental data on the oxidative coupling of methane in the porous VYCOR packed bed membrane reactors. The kinetic scheme used in the modeling studies will be improved to include kinetics specific to samarium oxide catalyst.

TITLE:	PLASMA CONVERSION OF METHANE INTO HIGHER HYDROCARBONS AT SURFACES
PI (AUTHORS):	W. M. SACKINGER* AND V. A. KAMATH**
INSTITUTION/ORGANIZATION:	*OBELISK HYDROCARBONS (ALASKA) LTD. **UNIVERSITY OF ALASKA FAIRBANKS
CONTRACT NUMBER:	INVITED PAPER
OBJECTIVE:	PRODUCTION OF SYNTHETIC MISCIBLE GAS AND SYNTHETIC CRUDE OIL FROM METHANE FEEDSTOCKS

1. Introduction.

Natural gas is widely abundant, is easily withdrawn from reservoirs, is commonly produced as an associated gas along with crude oil production, and is found in many geologic settings as a resource separate from oil. A much larger fraction of the natural gas may be produced from a gas reservoir, as compared with a crude oil reservoir. However, natural gas is normally transported by pipeline, and the energy throughput of such a pipeline is perhaps only 20% to 30% of the throughput of an oil pipeline of the same size and cost. Gas is difficult to transport in moderate quantities at low cost, as it must either have a special pipeline or must be liquified into LNG, shipped in cryogenic LNG tankers, and regasified at the destination. It has been difficult to make use of methane as a fuel for transportation vehicles. The chemical stability of methane has made it difficult to convert it directly into conventional hydrocarbon fuel mixtures, and has also impeded its use as a feedstock for petrochemical production. Consequently, the economics of natural gas production and distribution have been rather different from the economics of oil. Nevertheless, the usage of natural gas for more than simple heating or electricity generation would be accelerated by development of technology which could convert natural gas into hydrocarbon liquids. Particularly with the growth of the "newly-developing economies" of the world, the need for liquid fuels is expected to grow very much more rapidly than in the recent past. Improvements in the standard of living in these emerging economies of the world are crucially dependent upon the availability of liquid fuels at modest prices. In this paper, we discuss the direct conversion of natural gas to higher hydrocarbon liquids by using energetic plasma interactions with surfaces.

2. Use Of Plasma Interactions With Surfaces

If neutral methane is ionized, and the ions are accelerated beyond the energy of about 15 eV, then when they collide with other methane neutrals, the C-H bonds are broken (Winters 1975) and chemical combinations take place. Historically, methane plasmas have been used to produce carbon, and to produce acetylene. Building higher hydrocarbons requires more than merely high ion energy; there must be a high probability of interaction, and the collision of three or more carbon-containing molecules and/or ions must be commonplace. A control of the recombination of the ions with neutrals is important.

A methane-based plasma initially contains methyl ions of several types, along with hydrogen ions, electrons, and methane and hydrogen neutrals. Electrons, ions, and neutrals will each be at different temperatures, generally, but at higher pressures with frequent interactions, the charged particles will deliver kinetic energy (below the threshold for ionization) to the neutrals, and much of this energy will be lost to the ambient and to the walls of the enclosure. Simultaneous multi-particle collisions in the volume of a plasma are extremely unlikely.

It has been shown that hydrogen ion bombardment of carbon-containing surfaces can produce all of the carbon-containing gases up to C_3 (deVries et al. 1984; Brown et al. 1982). We have extended this approach in our experiments. We have not made use of catalysts, high temperatures, or high pressures. Using low pressures, any kind of surface, and locally intense regions of high energy density associated with ionic impact, we have shown that in a time interval of a few picoseconds, methane ions and neutrals combine on the surface to form a wide spectrum of higher hydrocarbon molecules and ions. Some of these are ejected from the surface and can participate in additional reactions of the same type on adjacent surfaces. Kinetic energy is continually added to ions after they are created, and their energies quickly exceed the threshold values needed to ionize methane and thus allow the random creation of higher hydrocarbons. The technology is not highly selective; many output product gases and liquids should be expected. A traditional separation of them may be necessary for certain downstream chemical applications, but perhaps will be minimal for hydrocarbon fuel applications. The basic technology involves the use of an array of many small tubes, which are co-parallel and provide a large surface area for interactions. The direction defined by the axes of the tubes is co-parallel with a component of a superimposed electric field.

A pressure of gas is maintained at a low enough value so that an ion, once created, can acquire an energy greater than 15 eV, without a significant probability of an energy-transferring collision with a neutral gas molecule in the ambient. When such an ion strikes the inside wall of a tube, it will locally excite the neutral molecules on the surface, and a variety of chemical conversions will take place.

In our experiments, over 1.3 million tubes were used, arranged in a microchannel plate array, with each tube nominally 12 micrometers in diameter. The phenomenon can be explained most easily with reference to a single tube such as is shown in Figure 1a. Methane molecules are adsorbed on the walls of the tube from the ambient partial pressure of methane, which may be in the range of 0.4 Pa to 100 Pa or more. Electron and ion flow is possible without a significant number of collisions with neutrals in the volume above the surface. Ionization may initiated by using a suitable photoemissive, field emissive, radioactive or thermionic source outside of the tube, and the electrons from such a source are accelerated with a low voltage towards the end of the tube, where they strike the interior walls at grazing incidence and produce secondary electrons, ions, and other products. Secondary electrons cascade along the tube, acquiring energy from the electric field and striking the walls further down the tube, where more electrons and ions are generated. Positive ions are accelerated in the direction opposite that of the electrons, and strike the walls of the tube, producing electrons, ions, emitted neutrals, and chemical reactions. The ions produced at the walls of the tube are accelerated by the electric field, and acquire energy. Striking the neutrals which are adsorbed along the walls of the tube, the ions deliver most of their energy to the upper layers of atoms, allowing them to form new chemical combinations and to be released from the surface, either in ionic or in neutral form.

Some of the newly-formed neutrals are deposited upon the opposite wall of the tube, and are available for further ion-impact-stimulated chemical reactions. Newly-formed ions are accelerated by the electric field and then strike the walls of the tube further downstream (in the ionic flow direction), initiating another ion-impact-stimulated chemical reaction there. There is a statistical distribution of emission energies, emission angles, number of ions emitted, the number of neutrals emitted, and the ratios of chemical species produced, in each impact event. Therefore, there is a distribution of trajectory length, impact energy and angle of incidence for successive ion impact events. The energy delivered to the excited surface region will be a statistical process. One of the effects is the rapid chemical conversion of methane to higher hydrocarbons at the impact sites; There will also be a more gradual transfer of some of the residual ion energy into heat energy. Consideration of the energetics should be part of any development of a commercially feasible device.

Molecular dynamics models, developed by other researchers, (Johnson 1989; Johnson and Sundquist 1992) may be used to predict an excited region some 30 nanometers wide, 30 nanometers deep, and up to 1000 nanometers in length, for grazing incidence ions. Many ions and neutrals are emitted from a single event, as the energy required for separation of the product species from the surface (0.05eV to 0.2 eV)is small in comparison with the available ion impact energy (15eV to 200 eV). Rough surfaces

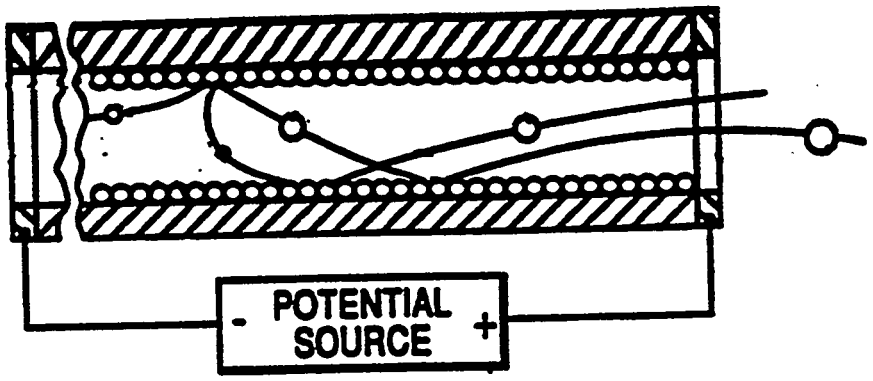

Figure 1a. Electronic conversion of methane by electron-impact reduction, electron-stimulated desorption of ions, and ion-impact-stimulated chemical combination and desorption at inside surface of a single tubular microchannel.

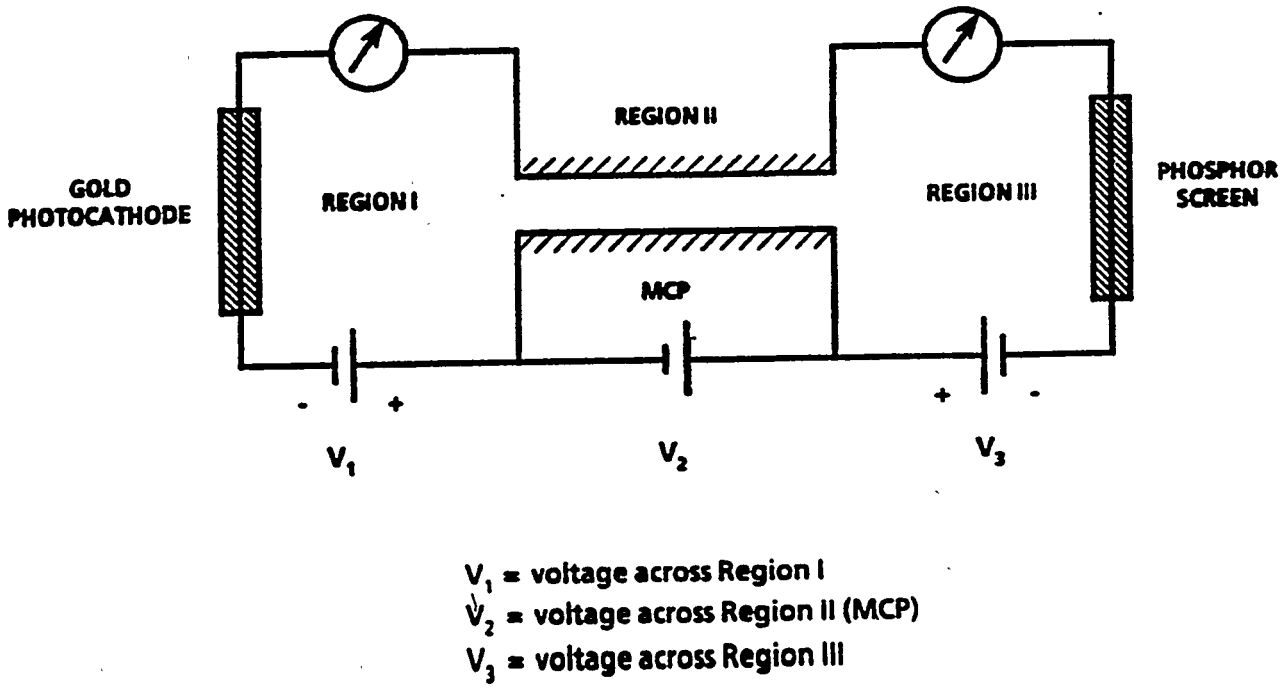

Figure 1b. Electrical circuit arrangement for methane conversion using microchannel plate (MCP) channel array.

are involved, and excited zones are irregular in shape. The time of emission is in the range of 5 picoseconds, and takes place long before thermalization of the residual amount of incident ion energy. The process is very fast, and chemical conversion and escape of products takes place long before a Maxwellian distribution of the residual energy is achieved. Thermal driving forces are not significantly involved in the chemical conversion. The fraction of incident ion energy which is slowly degraded into thermal energy, however, will be one factor determining the energy consumption of an operating device, and may place an upper limit on the specific conversion per unit area of surface. There are numerous choices for substrate materials, some of which can function at very high temperatures.

The electrical connections shown in Figure 1b were originally used in the first set of experiments, to check the electron gain of the microchannel plate. An additional invention of a related device in this family (Sackinger, Morgan, and Airey, 1992) makes use of an array of dynodes, rather than a microchannel plate. This second dynode-based device has not yet been experimentally investigated. It uses the same principles of plasma interaction with surfaces with an improved geometry involving construction from metal sheets. A higher electric field provides the required ion acceleration at a higher ambient gas pressure. The dynode-based device can be produced at a lower cost, is capable of a very high operating temperature, and will be included in future experimental programs.

3. Experimental Results

Conversion of methane into higher hydrocarbons was noted in <u>every</u> case when the electric field was above 4 volts/diameter (333 volts/millimeter). Thirty-two experiments were conducted, and have been reported elsewhere (Sackinger, Kamath, Morgan, and Airey, 1993). A summary of the most significant cases are discussed below, denoted as Cases 1,2,3,5,7, and 8 (see Table I).

Several batch and continuous methane conversion experiments were conducted at pressures ranging from 3.3×10^{-10} kPa to 0.113 kPa, using a demountable, stainless steel, ultra-high-vacuum (UHV) system. This consisted of the following major components: 1) an image tube sub-assembly containing a microchannel plate (MCP) assembly, a gold photocathode, a phosphor screen, and electrical feedthroughs; 2) a floating high-voltage supply, with three output voltages; 3) an ammeter; 4) an UV light source (mercury lamp); 5) a large VacIon pump with a UHV valve and ion gauge; 6) a gas leak valve for gas injection; 7) a mass specrometer assembly; 8) a VacSorb pump with shutoff valve and down-to-air valve; 9) a capacitance gauge for pressure measurement.

Prior to the start of the conversion experiments, several precautionary and calibration steps were followed which included: a) Bake out the system overnight at 250°C for wall outgassing; b) Helium leak tests to ensure that there were no leaks at flanges and joints; c) Electron scrubbing of the MCP to remove gas adsorbed from the atmosphere; d) Measurement of the resistance of the MCP; e) Voltage-Current relationship for the photocathode-to-MCP region; f) Calibration of the UV filters for varying input current to the MCP; g) Measurement of the electron gain of MCP at different voltages; h) Calibration of the mass specrometer system; i) Measurement of conductance of the gas leak valve.

In the batch experiments, the initial conditions were: 1) a thoroughly-pumped system at the ultra-high-vacuum level of 1.3×10^{-10} kPa; 2) no electric field applied to the MCP. The VacIon pump was then isolated from the system by closing the UHV valve, and the residual gas background spectrum was recorded. Gas was next injected into the main chamber through the leak valve, and that valve was closed after the desired pressure level was reached. The input methane background specrum was recorded. The conversion process was then started by applying voltage to all three regions as shown in Figure 1b and turning on the UV light source. The mass spectra were recorded very frequently, for accurate tracking of the kinetics of the conversion process. The mass spectra recorded at various times were then analyzed to compute composition of the gas in the main test chamber.

For the experiments reported in Table I, three MCP's were used in cascade, so that the effective length of each channel was 120 diameters or 1.44 millimeters. The pressures in the main chamber for the experiments ranged between 1.35×10^{-4} kPa to 1.13×10^{-1} kPa. The voltage in the Region 1 between the

TABLE I

Rate of Conversion, % Conversion and Selectivity of Methane to Various Hydrocarbons During Batch Methane Conversion Experiments

							% Selectivity to Various Hydrocarbons				
Case No.	Input Gas Used	Time (min)	Pressure (kPa)	MCP Voltage (Volt/dia)	Methane Conversion Rate (gmole/sec)	% Methane Conversion	C_2	C_3	C_4	C_5	C_6
1	$^{12}CH_4$	164	1.13×10^{-1}	Variable*	4.90×10^{-9}	29.5	47.2	13.7	18.5	7.8	12.8
2	$^{13}CH_4$	1446	8.96×10^{-2}	Variable*	1.13×10^{-9}	24.2	67.9	14.3	10.8	0.1	6.9
3	$^{13}CH_4$	1352	7.8×10^{-2}	Variable*	1.74×10^{-8}	24.5	67.2	19.3	8.6	0.3	4.6
5	$^{13}CH_4$	1125	3.88×10^{-3}	5	4.09×10^{-12}	22.7	88.0	3.2	8.8	0.0	0.0
7	$^{13}CH_4$	1232	4.00×10^{-4}	12.5	1.65×10^{-12}	19.8	85.6	7.5	2.7	0.6	3.3
8	$^{13}CH_4$	1125	3.46×10^{-4}	8.33	2.23×10^{-13}	11.4	81.6	6.8	7.2	1.0	3..4

*Low density plasma with glow discharge

electron source and the MCP was set at 30 volts and in the Region 3 between the MCP and the phosphor screen was set at 0 volts in all experiments. The electric field across the set of MCP's was varied from 0 to 15 volts / diameter (or 0 to 1250 volts/millimeter). The mass spectrometer was separated from the main chamber by a low-conductance leak valve for the high pressure experiments.

Experiments at the highest pressures, which we shall discuss as cases 1, 2, and 3, were in the category in which a glow discharge was initiated between the fixture and the chamber walls, as well as within the MCP, for MCP voltages above 3 volts/diameter. These are discussed because they resulted in a substantial conversion of methane into higher hydrocarbons, and they illustrate the situation when a time-variable voltage may be beneficial.

For case 1, operated at a pressure of 1.13×10^{-1} kPa, an evolution of the mass spectra is displayed as Figure 2, indicating the progressive production of higher hydrocarbons, at least as high as C_8. Since the mass spectrometer detected mass partial pressures only up to 100 a.m.u., the presence of hydrocarbons above C_8 was not definitively detected, but their presence cannot be ruled out, especially since the major (most probable) fragment of such large molecules is listed as appearing in the range of < 100 a.m.u.. We consider the presence of hydrocarbons up to C_{14} as being a possibility, but in quite small quantities. The statistics of ionic impacts seems to favor production of C_2, followed by C_3, C_4, C_5, C_6, C_8, and C_7, in that order. Consideration of case 2, which was conducted at a slightly lower pressure of 8.96×10^{-2} kPa, showed rapidly-varying conversion in the initial 100 minutes. (Most of it was an increase in higher hydrocarbons plus hydrogen). During the time used for the initial scanning of the mass spectrum after conversion had started, it is likely that the quantities of converted gases were increasing. Based on these rapidly-rising quantities, we have the qualitative impression that a continuous-flow conversion device would have an appreciable conversion in throughput times of the order of seconds or fractions of seconds. Over time intervals of the order of hours, in this batch experiment, there was a gradual conversion of methane and a diminishing level of ethylene. The relative proportions of ethane, ethylene, and acetylene are a function of time. At a pressure of 7.8×10^{-2} kPa, case 3 showed conversion into hydrogen and into roughly comparable levels of acetylene, ethylene, and ethane. A very long batch experiment, it showed continuous conversion over 1367 minutes, with about an order of magnitude difference in each of the product spectrum partial pressures of C_2, C_3, C_4, and C_6, respectively.

At lower pressures, the glow discharge between the fixture and the chamber wall was not initiated. Thus it was possible to have a series of different fixed voltage values on the MCP. These experiments may be discussed as cases 5, 7, and 8. The important summary parameters are presented in Table I. The two values of low electric field, which were 5 and 8.33 volts/diameter, in cases 5 and 8, were intended to explore the categories of products associated with near-threshold operations. In both cases, isotopic methane was used as the feedstock, but there was a mixed residual layer of ^{12}C, ^{13}C, H and D from earlier experiments. Thus, the presence of H_2 in both the initial and final stages of both experiments was very obvious. The formation of C_2 hydrocarbons is favored, after the very long time of this batch experiment, as compared with larger hydrocarbons.

The relatively-high value of electric field of 12.5 volts/diameter was explored in case 7. A relatively low pressure, 4×10^{-4} kPa, was used. As reported in detail in our earlier work (Sackinger, Kamath, Morgan, and Airey, 1993), the C_4 production dominated over the C_3 production. The molecules containing a large and odd- number of carbon atoms, C_5 and C_7, were only produced at low levels. The reason for this may be that the ion impact energies available at such a value of electric field are only sufficient to commonly activate 1 or 2 or 3 carbon atoms which are bonded to the surface. An incoming hydrogen ion would thus contribute to the formation of C_1, C_2, or C_3 species, in order of decreasing probability; an incoming methyl ion would contribute to the formation of C_2, C_3, and C_4 species, in order of decreasing probability. This suggests that C_2 species would be most prominent, and if the C_4 category is the next most probable, it might be explained by a two-sequence process, which may take place during a fraction of those ion impact events. In this case and in most other cases, it was noticed that the residue from earlier experiments, in which ^{12}C was used, was converted during the ion impact experiments, into new methane, carbon dioxide, ethane, and ethylene made from this residual carbon. This more detailed

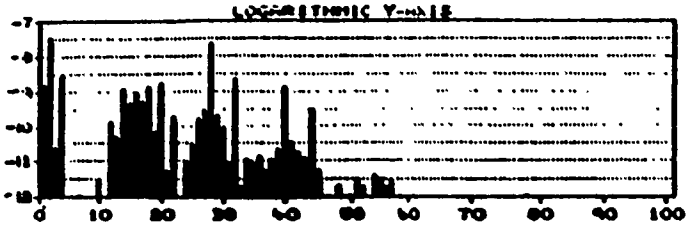

a) t = 0 min (Background Spectrum)

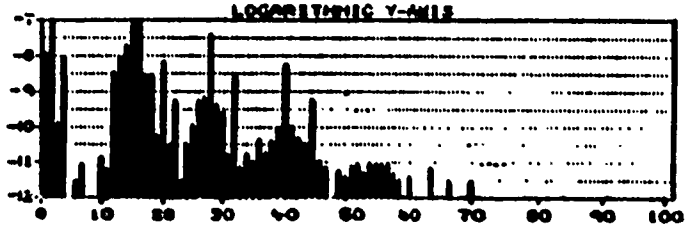

b) t = 39 min (CH_4 Injection)

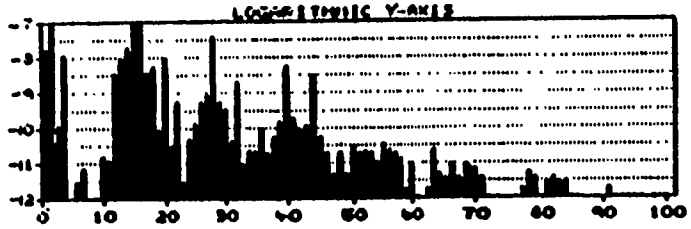

c) t = 95 min

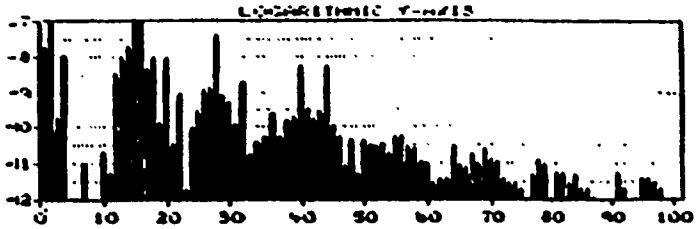

d) t = 130 min

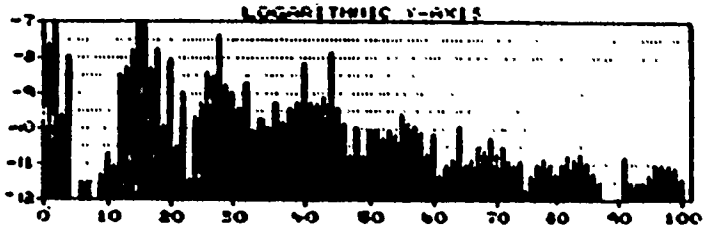

e) t = 170 min

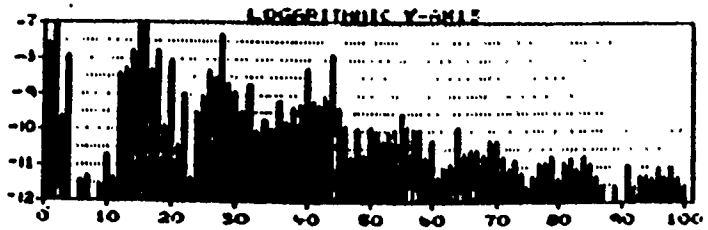

f) t = 203 min (Final Spectrum)

Figure 2. Evolution of mass spectra as a function of time during case 1, at a pressure of 0.113 kPa, indicating progressive conversion of methane to higher hydrocarbons up to at least C_8.

data (Sackinger, Kamath, Morgan, and Airey, 1993) proved that hydrocarbons containing one, two, and even six residual carbon atoms can be produced and released from the surface by ionic impact.

Case 8 was conducted at a low pressure (3.46×10^{-4} kPa), and at an intermediate value of electric field strength, 8.33 volts/diameter. The decrease in methane and the increase in hydrogen were most obvious in the first part of the experiment, but continued throughout. A rapid growth in C_2H_2 and in C_2H_4 took place in the first 69 minutes, and the C_3 and C_4 gases also increased in that initial time interval. Oddly enough, the level of C_2H_6 remained near the background level throughout the 1200 minutes of the experiment. It was only after 250 minutes that increases were seen in the levels of C_5H_8 and C_3H_8, both of which contain an odd number of carbon atoms. Near the end of the experiment, there was a slow growth in most components, but a slow decrease in C_3H_6, C_6H_6, and C_5H_8. Such slowly-varying concentrations must be related to the presence of some of the initially-formed higher hydrocarbons at the ion impact sites later in the experiment, and the subtile details of how such larger hydrocarbons are transformed when impacts of hydrogen ions and methyl ions occur. In this experiment, the hydrogen neutrals and the methyl neutrals were over 1000 times more numerous than the higher hydrocarbons, so it is a reasonable assumption that the dominant ion impact events were with ions from these two species. One hypothesis may be presented for the production of molecules containing an odd number of carbon atoms, involving the impact of a methyl ion and one resident C_2 neutral, along the lines $[C + C_2] \longrightarrow C_3$. However, the presence of some unsaturated hydrocarbons of all carbon-numbers, early in the experiment, means that at this value of electric field intensity, multiple combinations of carbon ions and neutrals were taking place at each ion impact interaction event with the surface. Therefore, at this value of electric field strength, the presence of products such as C_2 on the surface is not a necessary condition for the full spectrum of higher hydrocarbons to be generated, but it may assist in the generation.

Examination of the summary of these cases, shown in Table I, shows the following summary facts. Percentage of methane conversion was remarkably in the 20%-30% range in cases 1, 2, 3, 5, and 7. Conversion clearly requires an electric field strength of 5 volts/diameter or more. Selectivities for C_2 are greatest for low electric fields, at 5 volts/diameter. Production of a rich spectrum including up to at least C_6 is the case for high electric field intensities, in the range 8 - 15 volts/diameter. Maximum mass throughput and conversion is at the highest pressures combined with higher voltages. The practical reason for using higher pressures is to reduce the transverse size of the plasma converter, for a given required mass throughput, and thus perhaps reduce the cost of the plasma converter as well. Subsequent compression stages would also involve less equipment cost.

In Figure 3, the trend of increase in mass conversion per second with increasing pressure is depicted. This is a plot on log-log coordinates of the methane conversion rate, in gram-moles/second, vs. the pressure, in kPa, for many of the cases. If there were only one mechanism responsible for the reaction, one would expect a straight line to be drawn through these points. The cluster of points in each pressure regime, in the vertical direction, expresses the fact that the choice of electric field strength affects the conversion rate. The obvious increase in the conversion trend from the 0.001 kPa region to the 0.1 kPa region may be explained by the viewpoint that the number of active ion impact events per unit length of the MCP, per second, is increasing nonlinearly. This may be because there are ions created by some of the collisions in the volume, as well as the fraction of ions created by the collisions at the surface. The implications are that higher operating pressures will lead to greater methane conversion rates, until the point is reached for which the ions created in the volume are unable to acquire sufficient energy from the electric field to cause the desired conversion when they strike the surface. Application of a higher electric field will cause this saturation of conversion to take place at still higher pressures. Therefore, higher pressures and higher electric fields should be one of the objectives of future experimental programs. Obviously, a glow discharge will be initiated within the MCP during such experiments. The extinction of the glow discharge within the MCP by the high gas pressure will be a sign of saturation of the conversion process. It may be noted that, at atmospheric pressure, one study has found that a corona discharge may be initiated in methane at an electric field strength of 2230 volts/millimeter. Since the electric field of 1250 volts/millimeter has already been demonstrated, and conversion has taken place, the possibility of carefully-designed fixtures, electric field intensities of 2200 volts/millimeter, and near-atmospheric pressures of methane, should be on the agenda for the future experimental program. Such an operating

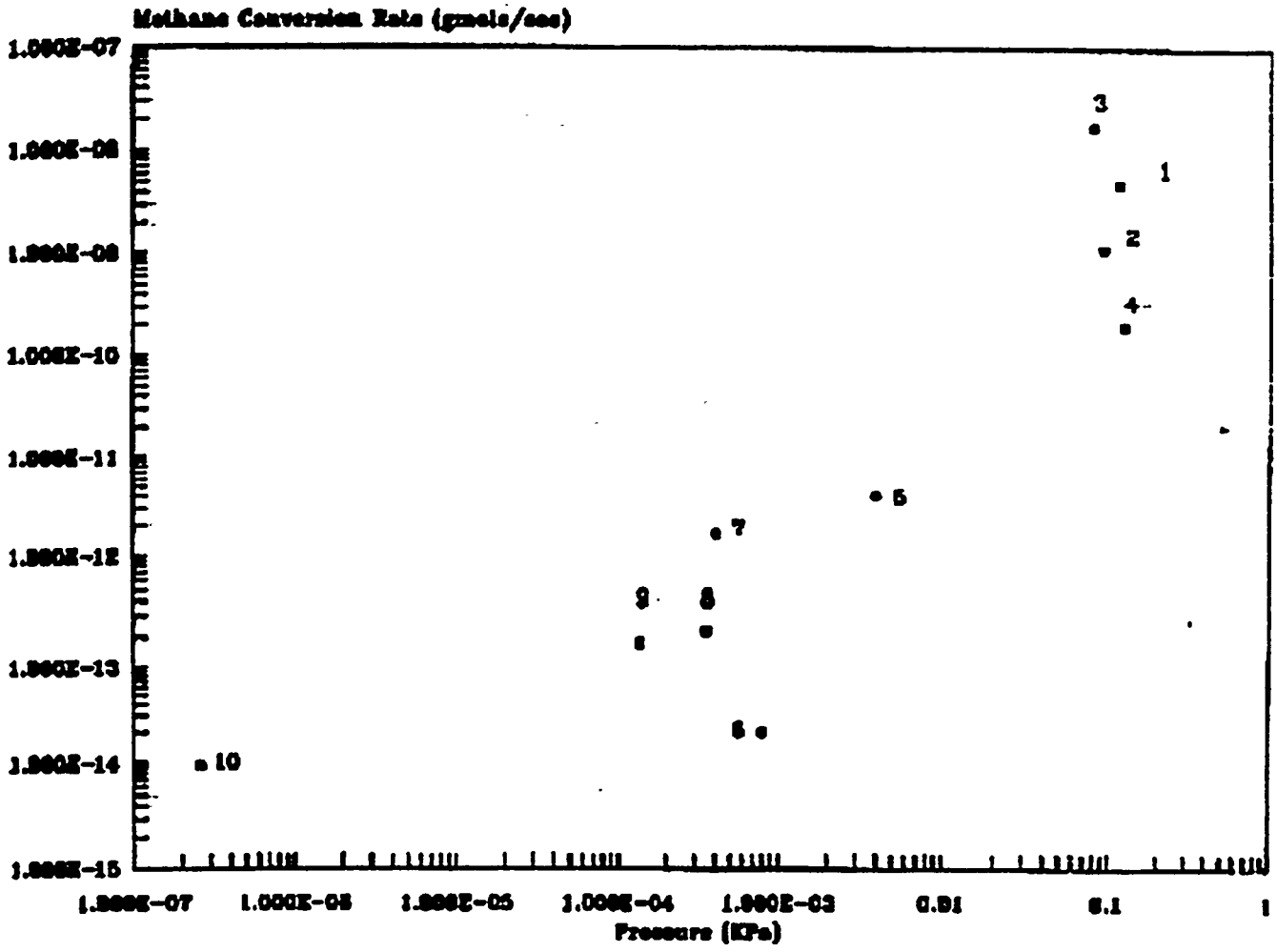

Figure 3. Log-log plot of methane conversion rate (gram-moles/second) vs. pressure, for ten experiments, showing a nonlinear increase in conversion rate as pressure increases, which is attributed to the increasing effect of ion interactions with the surface.

regime would be expected to produce a full spectrum of hydrocarbons, if one extrapolates the previous results, and would have the possibility of high throughput rates. Attention must be given to the diameter of the microchannels, as well, since that will affect the flow rate of the methane into and through the channels, and therefore the actual in-situ pressure within the microchannels.

4. Economic Aspects of Future Commercialization.

In order to determine the commercial applicability of this technology, the construction costs for units capable of producing much larger quantities, in the range 10 tonnes/day to 1000 tonnes/day, need to be estimated. Normally, such a task is done by first constructing one or several units of intermediate size, or "pilot-production- sized-units". Therefore, estimates of the cost and the conversion spectrum of large, continuous-flow units are necessarily based only upon parameters known at this time.

A practical alternative to MCP may be offered at large scale, by the metallic dynode structure for the conversion of methane into higher hydrocarbons, which is a related invention by Sackinger, Morgan, and Airey (1992). This provides for the conversion to take place when ions strike the metallic dynodes. The dynodes can be made in several geometrical formats, such as an array of tubes, or an array of slats as is found in a 'Venetian blind' structure, or an array of holes punched in a flat metal plate.

The costs of such metallic dynodes are little more than the costs of the metal from which they are made, and thus there is the prospect of large dynodes being fabricated at low cost. We estimate that the metal-dynode version of the device would contain many dynodes, but the main cost would be in the provision of the electrical feedthrough sub-assembly, and the labor involved in mounting the dynodes in a position in which they were hermetically-sealed to the wall of the enclosure. The operating life of such dynode-based devices is expected to be of the order of 10 years, as there is no need for electron emitters with limited life; field emitters or ß-emitters can provide the electrons needed for initiation of the plasma. It should also be noted that no dynode-based device has yet been tested, to establish its conversion efficiency.

Conversion of methane into higher hydrocarbons, plus hydrogen, requires the addition of energy, due to the different chemical bonding of the products. This may be calculated in kilowatt-hours, for each kilogram of product. However, the hydrogen is made available and can be burned, yielding energy which can help supply the energy for the reaction. This can be summarized as follows:

Product	**Energy Needed**	**Energy available From Burning Hydrogen**
C_2H_6	0.3735	-3.4468
C_2H_4	1.2997	-6.4351
C_2H_2	2.5885	-8.9648
C_3H_8	0.4872	-6.7431
C_3H_6	1.1002	-9.6561
C_3H_4	1.6495	-12.263
C_4H_{10}	0.5420	-9.9982
C_4H_8	1.0619	-12.874

The conversion of the hydrogen into electrical power, however, has an efficiency which may be in the range of 50%. The delivery of the electrical power to the electrical load representing the device also means that only 50% of the power from the generator may be made available for the reaction. In addition, there will be some energy lost to the subsurface materials, in the form of heat. The actual energy needed in each practical situation will depend upon the mix of output products, and is expected to be supplied primarily by the burning of the hydrogen produced, along with the burning of methane as required. As for the cost, the equipment cost is the most important, and can be estimated to be $0.01 per kilowatt-hour. The consumption of the electricity for the dynode-version is expected to be lower, as there is no continuous leakage current. The electrical power costs are expected to be in the range of $10 to $40 per tonne ($0.19 to $0.77 per MSCF) of methane converted depending on the product formed.

We note that the feedstock costs vary with the location, and are as low as $25 per tonne in the oilfield (or perhaps even less, if the gas is not marketable!). The natural gas costs in a consumer location vary with time, but can be as high as $200 per tonne if the pipeline costs are high, or if LNG is used as part of the transportation chain. It therefore appears that the most prominent low-cost location for the use of this technology is in the oilfield, where the gas may be today undeliverable, but where a higher hydrocarbon use (e.g. for miscible-gas injection into a reservoir) exists.

5. Some Possible Applications.

In one application, which is quite related to the Alaskan oil production effectiveness, the possibility is considered of converting the lean residue gas in the Prudhoe Bay gas handling facility into miscible gas injectant (C_2 to C_4) and TAPS compatible liquids (C_4 and higher). Miscible gas generated from this process can be used for improving oil recovery from Prudhoe Bay, Kuparuk River, West Sak and other smaller oil fields. The TAPS compatible liquids produced from this process can be transported through the existing oil pipeline (TAPS). Figure 4 shows projected annual production from the West Sak heavy oil reservoir by applying a miscible flooding process (Patil,1995). Thus, West Sak oil which is currently not being produced can help offset the decline in oil production from the Alaskan North Slope. Since natural gas is abundant on the Alaskan North Slope and is currently not marketable this seems to be one of the locations where the most favorable economics could be expected for this kind of technology.

For those oilfields in other parts of the world where there is presently no gas separation plant, the feedstock could be the natural mixture of CH_4, C_2H_6, C_3H_8, C_4H_{10}, with the C_5-and-higher hydrocarbons sent into the oil production stream. This feedstock would be enriched in C_2, C_3, and C_4 by the plasma device, and C_5, C_6, C_7, C_8 would also be produced. The presence of C_2H_4 and C_2H_2 in the output stream from the plasma device would open the possibilities for petrochemicals. This kind of conversion into petrochemical feedstocks could take place after pipelining, as well as before, as it may be most economic to position the petrochemical factories in locations where the petrochemical products can reach the consumers by normal overland transportation. The location of this completely-sealed type of ethylene production facility in regions of high population density, however, would not have the social disadvantages commonly associated with older ethylene units. However, it is also feasible to position the ethylene and propylene production units at the gas field. Tankers or pipelines may be used to carry the ethylene to downstream locations elsewhere.

A use which is simple in concept is to simply convert the natural gas of any gas field, or the produced gas of any oil field, into C_5 or larger molecules, with this kind of technology, and send it into the existing crude oil stream to be refined and utilized just as crude oil is today. Thus, the natural gas need not be reinjected, which has a cost. It need not be flared, which is done today in some offshore locations. This is essentially a method for the better use of the natural gas fossil energy resource. The negative value of wellhead natural gas which must today, by law, be reinjected, may be compared with the "API" value of the higher hydrocarbon liquids produced, which can be considerable. This offers an economic margin for the production of such liquids from natural gas, directly, using the plasma conversion process.

In relation to refining, the concept is to use this technology to try to upgrade the heavy residue oils coming from the refining of low-API crude oil. These oils, nominally selling for less than crude oil itself, are only sold into a very limited market, such as for power stations in locations near a refinery, or near a marine terminal, as they are difficult to move by pipeline. They fall outside the normal range of definition of transportation fuels, and are much thicker than lubricating oils. However, they will certainly vaporise at the temperatures and pressures used in the plasma-based units, and they may be combined with a methane or a natural gas feedstock to allow the plasma to produce a larger quantity of intermediate-range hydrocarbons than would be possible with a methane or natural gas feedstock alone. This category of processes can also be viewed as a cracking of the heavy oils using methyl ions and hydrogen ions in the plasma device. One would expect this to produce a very wide range of alkanes and olefins. The presence of petrochemical feedstocks in the output, for this category of experiments, should also be expected. The economics of this type of conversion would require that the margin available between the price of these heavy fuels, and the price of motor fuels, would be approximately the same as

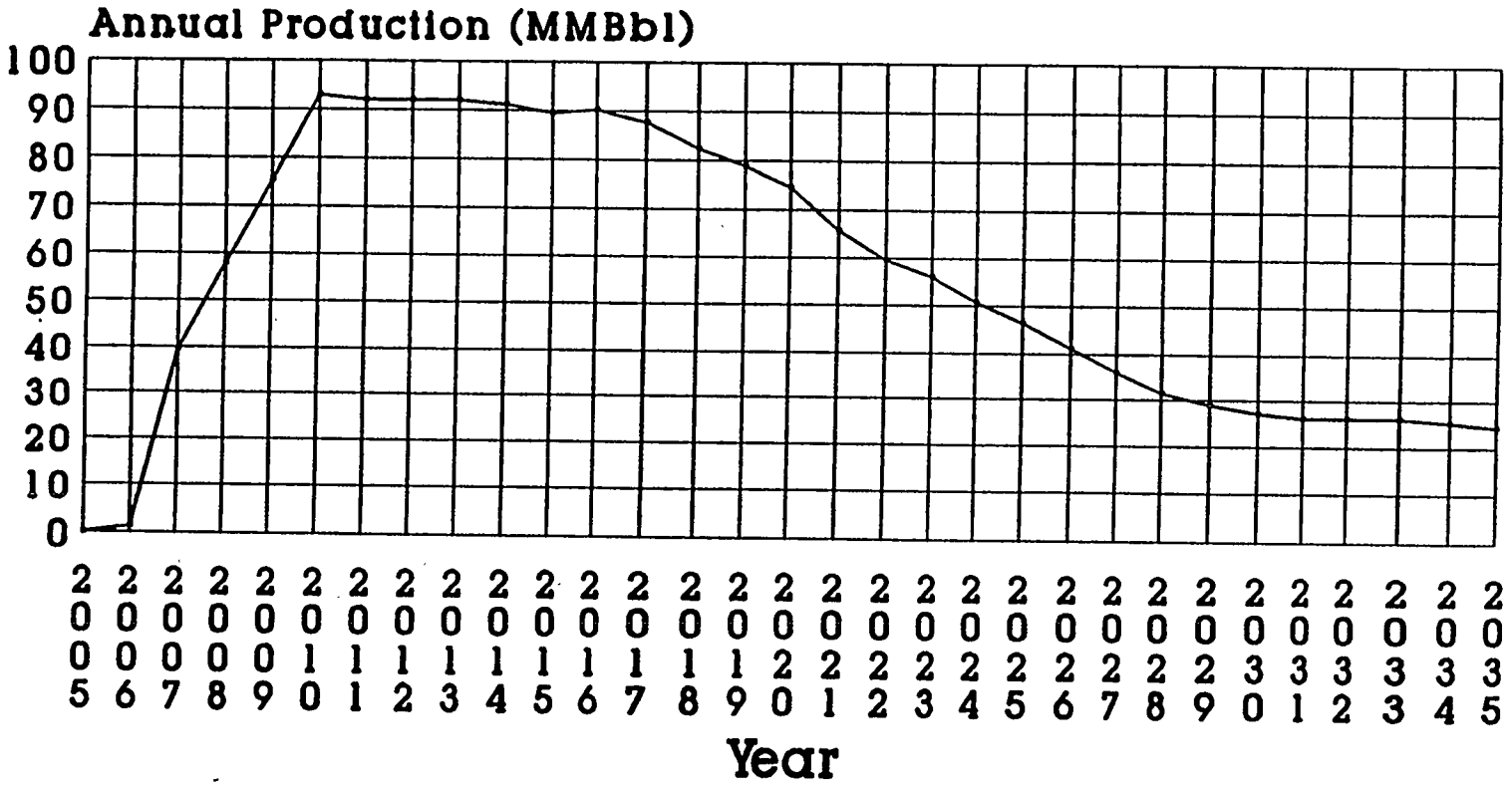

Figure 4. Projected annual heavy oil production from the West Sak heavy oil reservoir, Kuparuk River Unit, North Slope, Alaska by application of a miscible flooding process (after Patil 1995).

the marginal cost of operating the plasma conversion equipment. If this proves to be the case, then the use of plasma conversion in this segment of the petroleum industry would lead to a greater supply of gasoline and other transport fuels.

6. Conclusions

Experiments have been described in which a methane plasma is created, and the resulting methyl and hydrogen ions have been accelerated within a microchannel array so that they interact with neutral methane molecules on the inside surfaces of the microchannels. No catalysts are used, and the device operates at room temperature. Impact energies of the ions are in the range of 15 ev to greater than 100 ev, and the energy delivered in the interaction at the surfaces has caused the production of larger hydrocarbon molecules, such as C_2H_2, C_2H_4, and C_2H_6, along with C_3, C_4, C_5, C_6, C_7, and C_8 molecules. Conversion effectiveness is greater at higher pressure, due to the increased ionic activity. The yield of the higher hydrocarbons depends upon the external voltage used, and voltage can be used as a control parameter to adjust the output mixture proportions. In batch experiments, the selectivity for C2 has varied from 47% to 88%, and selectivity for C_6 was up to 12.8%. Other hydrocarbon selectivities also span a wide and useful range. The costs of production of the plasma conversion devices are projected to be quite low, and the technology appears to be commercially and economically feasible.

7. Recommendations For Future Development.

The feasibility of this category of conversion technology has been established. The economics, and the details of the implementation for high levels of throughput which would be needed in a production situation, remain to be established. Since Phase I, already completed, was a sequence of many batch experiments at sub-gram levels, it is appropriate to target Phase II at the level of 10 kilograms per day of throughput, and make experiments on a continuous-flow basis. Several types of experiments are planned, including those which vary the electrical voltage over all possible ranges, and which vary the pressure from the established values in Phase I, to higher pressures which would lead to a larger throughput for a given device cross-sectional area. The two fundamental parameters, pressure and electrical voltage settings, will be varied in every future experiment. Phase II is planned for 24 months duration. Phase III, set to build up to the level of 10 tonnes per day, is planned for 36 months duration.

Plasma conversion technology may be quite useful in those oilfields where there is presently no methane separation plant. The feedstock in such locations could be the natural mixture of CH_4, C_2H_6, C_3H_8, C_4H_{10}, with the higher hydrocarbons sent into the oil production stream. In such an application, this feedstock would be enriched in C_2, C_3, and C_4 by the plasma device, and C_5, C_6, C_7, C_8 would also be produced.

For experiments to examine these applications, in Phase II, we would expect to use feedstocks of CH_4, $^{13}CH_4$, C_2H_6, $^{13}C_2H_6$, various mixtures of $CH_4 + C_2H_6 + C_3H_8$, and natural gas (from Alaska and many other locations, to be supplied by cooperating industrial partners), natural gas without water, natural gas without water and without carbon dioxide. Output spectra would be monitored and recorded with the GC/MS equipment.

A second part of the Phase II program, a downstream application, is intended to consider some of the possible applications of this technology to refining and petrochemical feedstock production. As is evident from the Phase I results, production of ethylene, acetylene, and propylene is quite possible for certain ranges of voltage and pressure. Since this kind of technology is inherently statistical in nature, all possible product gases may be expected, but the more useful ones may be increased in quantity by proper choice of voltage, and can be separated out with low-temperature, low-pressure separation stages. The economics of the process will be connected with the costs for construction and operation of such separation equipment, as well as with the plasma-based stages themselves.

To use this technology to try to upgrade the heavy residue oils coming from the refining of low-API crude oil, we intend to combine them with a methane or a natural gas feedstock to allow the plasma

to produce a larger quantity of intermediate-range hydrocarbons than would be possible with a methane or natural gas feedstock alone. This category of experiments can also be viewed as a cracking of the heavy oils using methyl ions and hydrogen ions in the plasma device. One would expect this to produce a very wide range of alkanes and olefins. Many possible mixtures are candidates for feedstocks, and certainly one should try some very precisely-known mixtures of two or three alkanes, as well as the practical mixtures which are representative of normal refinery residual outputs, which would be supplied by cooperating industrial partners. The presence of petrochemical feedstocks in the output, for this category of experiments, should also be expected.

In the plans described above, the several types of converter geometries using plasma would be tested, including the microchannel types, and the various configurations of the dynode types. Therefore, at least twenty such units would be constructed to span the most important variations in construction geometry.

8. References

1. Brown, W. L., Lanzerotti, L. J., and Johnson, R. E., " Fast Ion Bombardment of Ices and Its Astrophysical Implications", *Science*, **218**, pp. 525-531 (1982).

2. deVries, A. E., Pedrys, R., Haring, R. A., Haring, A., and Saris, F. W., " Emission of Large Hydrocarbons from Frozen CH_4 by keV Proton Irradiation", *Nature*, **311**, p. 39 (1984).

3. Johnson, R. E., *J. Phys.* **C 2**, p. 251 (1989).

4. Johnson, R. E., and Sundqvist, B. U. R., " Electronic Sputtering: From Atomic Physics to Continuum Mechanics", *Physics Today*, **45**, 3, pp. 28-36 (March 1992).

5. Patil, S. L., *Resource Development of Alaska North Slope Fields and Its Impact on Trans Alaska Pipeline System*, M.S. Research Project Report, University of Alaska Fairbanks, (April 1995).

6. Sackinger, W. M., Kamath, V. A., Morgan, B. L., and Airey, R. W., *Natural Gas Conversion To Higher Hydrocarbons Using Plasma Interactions With Surfaces*, Geophysical Institute, University of Alaska Fairbanks, Report to U.S.D.O.E., Grant No. DE-FG21-90MC27420, (December 1993).

7. Sackinger, W. M., Morgan, B. L., and Airey, R. W., *Electrical Device for Conversion of Molecular Weights Using Dynodes*, U. S. Patent No. 5,141,715 (August 25, 1992).

8. Winters, H. F., " Dissociation of Methane by Electron Impact", *J. Chemical Physics*, **63**, 8, pp. 3462-3466 (15 October 1975).

Magnesium Carbide Synthesis From Methane and Magnesium Oxide - A Potential Methodology for Natural Gas Conversion to Premium Fuels and Chemicals

Alexander F. Diaz, Anthony J. Modestino,
Jack B. Howard, Jefferson W. Tester, and William A. Peters

Energy Laboratory and Department of Chemical Engineering
Massachusetts Institute of Technology
Cambridge, MA 02139

US DOE/PETC-MIT Contract No. DE-AC22-92PC92111
Period of Performance: October 1, 1992 - September 30, 1995

Paper to Appear in
Proceedings of the U.S. DOE Coal Liquefaction and
Gas Conversion Contractors' Review Conference, (Gas-to-Liquids Session)
Westin William Penn Hotel
Pittsburgh, Pennsylvania
August 29-31, 1995

Magnesium Carbide Synthesis From Methane and Magnesium Oxide - A Potential Methodology for Natural Gas Conversion to Premium Fuels and Chemicals

Alexander F. Diaz, Anthony J. Modestino,
Jack B. Howard, Jefferson W. Tester, and William A. Peters

Energy Laboratory and Department of Chemical Engineering
Massachusetts Institute of Technology
Cambridge, MA 02139

US DOE/PETC-MIT Contract No. DE-AC22-92PC92111
Period of Performance: October 1, 1992 - September 30, 1995

1. Executive Summary

Pseudo-stoichiometric (i.e. non-catalytic) reactions of methane with low-cost, recyclable, alkaline earth metal oxides at temperatures above 2100 K

$$3\ CH_4 + CaO \rightarrow CaC_2 + 6\ H_2 + CO \quad (1)$$

$$5\ CH_4 + 2\ MgO \rightarrow Mg_2C_3 + 10\ H_2 + 2\ CO \quad (2)$$

indicate technical and economic promise for upgrading natural gas to solid metal carbides that can be stored, transported, and hydrolyzed to acetylenes:

$$CaC_2 + 2\ H_2O \rightarrow Ca(OH)_2 + C_2H_2\ \text{(acetylene)} \quad (3)$$

$$Mg_2C_3 + 4\ H_2O \rightarrow 2\ Mg(OH)_2 + C_3H_4\ \text{(MAPD, i.e. methylacetylene/propadiene)} \quad (4)$$

The acetylenes can subsequently be converted to premium liquid fuels and petrochemicals. The overall goal of the present project is to develop new scientific and engineering knowledge for improved technical and economic assessment of Reactions (1) and (2) as bases for gas-to-liquids upgrading. One specific objective is to assess the technical feasibility of achieving high conversions of CH_4 to Mg_2C_3 via Reaction (2) in a thermal plasma.

A series of scoping runs was conducted wherein MgO was reacted with CH_4 in a magnetically rotated d.c. arc discharge plasma reactor, yielding solid products which evolved C_2H_2 and C_3H_4 upon hydrolysis. The results of these runs strongly indicate that a breakthrough has finally been achieved in that synthesis of magnesium carbides from MgO and CH_4 in the arc discharge reactor has been demonstrated.

2. Introduction

Diversification of the raw materials base for manufacturing premium fuels and chemicals offers U.S. and international consumers economic and strategic benefits (Longwell, 1993). Extensive reserves of natural gas in the world provide a valuable source of clean gaseous fuel and chemical feedstock. Assuming the availability of suitable conversion processes, natural gas offers the prospect of improving flexibility in liquid fuels and chemicals manufacture, and thus, the opportunity to complement, supplement, or displace petroleum-based production as economic and strategic considerations require. Many attractive deposits of natural gas are remotely located from key market sites. In order to utilize this remote resource commercially, natural gas must be transported to the market from the production site either via extensive pipeline distribution networks under pressure or in specially designed ocean-going tankers as liquefied natural gas at low temperatures. Due to the state in which it exists at normal conditions, natural gas has a low energy content per unit volume compared to petroleum or coal. This relatively low energy density contributes to elevated transportation costs which exclude significant quantities of gas from commercial exploitation. Thus, there is considerable interest in developing new approaches to the volumetric energy densification of natural gas to enhance its marketability.

The composition of natural gas varies from reservoir to reservoir but the principal hydrocarbon constituent is always methane (CH_4). With its high hydrogen-to-carbon ratio, methane has the potential to produce hydrogen or hydrogen-rich products. However, methane is a very chemically stable molecule and, thus, is not readily transformed to other molecules or easily reformed to its elements (H_2 and carbon). With the interest in upgrading natural gas to "value-added" products, several technologies for methane conversion to liquid fuel and chemical precursors currently exist at various stages of scientific and technological development. In many cases, further research is needed to augment selectivity to desired product(s), increase single-pass conversions, or improve economics (e.g. there have been estimates of $50/bbl or more for liquid products) before the full potential of these methodologies can be realized on a commercial scale. With the trade-off between gas conversion and product selectivity, a major challenge common to many of these technologies is to simultaneously achieve high methane single-pass conversions and high selectivity to desired products.

2.1 Motivation for Present Study

Prior work at MIT (Kim, 1977; Kim *et al.*, 1979) has demonstrated that, by reacting methane with calcium oxide (CaO) in a laboratory-scale rotating direct current (d.c.) arc reactor, high (>95%) methane single-pass conversions to molecular hydrogen (H_2) and calcium carbide (CaC_2) can be obtained, according to the reaction:

$$3\,CH_4 + CaO \rightarrow CaC_2 + 6\,H_2 + CO \qquad (1)$$

Hydrogen can be used as a fuel in thermal processes and in fuel cells to generate electricity at efficiencies which may approach 60%. It finds wide applications in petroleum refining (and could be used extensively in coal liquefaction) to improve fuel quality, e.g. by increasing hydrogen-to-

carbon ratio and lowering the fuel content of pollutant precursors such as sulfur, nitrogen, and heavy metals. Mixtures of H_2 and carbon monoxide (CO) in various proportions are known as synthesis gas which is valuable as a fuel. By various catalytic processes, synthesis gas can be upgraded to a wide range of premium products, e.g. liquid fuels, methanol, and waxes, many of which are manufactured from petroleum. Calcium carbide, which exists as a solid at dry ambient conditions, is a particularly attractive product with significant commercial benefits in the present context: (a) being a solid, it can be separated from the gaseous products of Reaction (1) relatively easily; (b) it has an equivalent heating value (based on acetylene - see Reaction (3)) of about 8700 BTU/lb and thus, like low-rank coal, can be stored and transported over long distances at reasonable cost; and (c) by well-established hydrolysis processes, it can be converted to acetylene (C_2H_2) by the reaction:

$$CaC_2 + 2\ H_2O \rightarrow Ca(OH)_2 + C_2H_2 \qquad (3)$$

Acetylene is a reactive raw material that can be converted to a diverse array of organic chemicals and to high-grade liquid fuels.

In the light of the success of the previous work by Kim (1977) *et al.* (1979), there is incentive to investigate comparable reactions of methane with other alkaline earth metal oxides. In particular, magnesium oxide (MgO) undergoes analogous reactions to produce hydrogen, carbon monoxide and magnesium sesquicarbide (Mg_2C_3) and/or magnesium dicarbide (MgC_2). Thermodynamic calculations imply that the sesquicarbide is strongly favored over the dicarbide above 2000 K. Of interest is the fact that magnesium is the only alkaline earth metal known to form a sesquicarbide, which, upon hydrolysis, yields methylacetylene (C_3H_4), providing a route for C_1-to-C_3 conversion. Furthermore, methylacetylene offers a potential route to benzene by condensation/dehydrocyclization. Concepts for synthesizing magnesium sesquicarbide from magnesium oxide and methane, with further upgrading of the sesquicarbide to C_3 hydrocarbons by hydrolysis, are described by Peters and Howard (1990; 1993). Earlier experimental work by Kim (1977) *et al.* (1979), together with preliminary cost estimates (Peters and Howard, 1989), indicate that the metal carbide route for methane upgrading offers sufficient potential for good thermal efficiency and favorable economics to warrant further systematic study.

2.2 Description of Proposed Methane Upgrading Approach

In the proposed approach, methane would be reacted, essentially stoichiometrically (rather than catalytically), with relatively low cost and recyclable alkaline earth metal oxides such as calcium oxide (quicklime), magnesium oxide (magnesia) or mixtures of the two (calcined dolomite) to achieve very high (approaching 100%) conversion to hydrogen, carbon monoxide and the corresponding alkaline earth metal carbide, according to the reactions:

$$3\ CH_4 + CaO \rightarrow CaC_2 + 6\ H_2 + CO \qquad (1)$$

$$5\ CH_4 + 2\ MgO \rightarrow Mg_2C_3 + 10\ H_2 + 2\ CO \qquad (2)$$

In order to carry out Reactions (1) and (2), the high chemical stability of methane would be overcome under high severity conditions, i.e. high temperature (>2000 K), in an electrical arc discharge (thermal plasma) reactor or in a purely thermal (i.e. non-plasma) reactor.

The carbides produced are solids at dry ambient conditions. Thus, they could be more readily separated during processing and would be more attractive for storage and transport. Their value as fuel precursors and chemical intermediates is further enhanced when, upon reaction with water, they yield the valuable hydrocarbon gases acetylene and methylacetylene:

$$CaC_2 + 2\ H_2O \rightarrow Ca(OH)_2 + C_2H_2 \text{ (acetylene)} \quad (3)$$

$$Mg_2C_3 + 4\ H_2O \rightarrow 2\ Mg(OH)_2 + C_3H_4 \text{ (MAPD, i.e. methylacetylene/propadiene)} \quad (4)$$

Reactions (3) and (4) are expected to produce acetylene and methylacetylene in high purity. Thus, the carbide approach may exhibit simpler and lower cost separation and purification steps than those needed in alternative processes for acetylene manufacture. Acetylenes can be upgraded to a wide range of chemicals or to premium-value liquid hydrocarbon fuels.

CaO and MgO for reuse in Reactions (1) and (2) can be regenerated by heating $Ca(OH)_2$ and $Mg(OH)_2$, respectively, and subsequently recycled back to the process, according to:

$$Ca(OH)_2 \rightarrow CaO + H_2O \quad (5)$$

$$Mg(OH)_2 \rightarrow MgO + H_2O \quad (6)$$

A conceptual process wherein Reaction (1) [or (2)] is carried out under thermal plasma conditions followed by low temperature Reaction (3) [or (4)] to produce CO, H_2 and C_2H_2 (or C_3H_4) is estimated to have a reasonably high thermal efficiency. In the ideal case of perfect heat integration where the plasma provides only the endothermicity of Reaction (1) or (2) and where CH_4 is used to generate electricity for driving the plasma reactor at 33% efficiency, Table 1 shows that the process thermal efficiencies are about 60%, which compare well with the 60% thermal efficiency of commercial H_2 production by steam reforming of CH_4 (Gary and Handwerk, 1984).

Table 1. Estimated Process Thermal Efficiency of Methane Conversion in a Thermal Plasma[a]

Product LHV as a Percentage of Total Input CH_4, i.e. CH_4 Converted to Products or Used to Manufacture Electricity to Run Plasma[b]

Reaction[c]	H_2	CO	C_2H_2	C_3H_4	Total
(1) and (3)	32	6	28		66
(2) and (4)	29	7		22	58

[a] Assumes perfect heat integration so the plasma supplies only endothermicity of Rxns (1) or (2).
[b] Methane is assumed to be converted to electricity at 33% efficiency.
[c] All chemical reactions are assumed to proceed to 100% completion.

2.3 Objective of Research Supported by U.S. DOE/PETC

The major goal of this research is to develop new scientific and engineering knowledge bases for assessing the technical and economic promise of converting methane to alkaline earth metal carbides for subsequent production of acetylenes, chemicals and premium-value liquid hydrocarbon fuels. A specific objective is to determine the technical feasibility of converting CH_4 and MgO to Mg_2C_3, H_2 and CO, according to Reaction (2), under thermal plasma conditions to achieve high single-pass CH_4 conversions and strong selectivity to these three products.

3. Experimental Section

A laboratory-scale electrical arc discharge (thermal plasma) reactor is used to carry out Reaction (2) and will be utilized to systematically investigate the effects of variations in thermal plasma operating conditions on the conversion of methane to metal carbides.

3.1 Description of Experimental Apparatus and Procedure

The experimental apparatus, shown in Figure 1, consists of a plasma generator system, a mechanical powder feeder, a post-plasma cooling chamber for thermally quenching the plasma effluent, and a sample collection system. The plasma generator system is composed of an arc discharge d.c. plasma torch as the reactor, a high frequency oscillator (for initiating the arc), a control console and an AIRCO d.c. power supply unit rated by the manufacturer at up to 83 kW and capable of providing open circuit output voltages of 80, 160 and 320 volts.

The heart of the plasma reactor, shown schematically in Figure 2, consists of a cylindrical graphite cathode (¾ in. O.D. by 1½ in. long) and a cylindrical graphite anode (1 in. I.D. by 2½ in. O.D. by 4 in. long). The top of the anode is counterbored to a depth of 2 in. to accommodate: (a) an annular boron nitride shield (1 in. I.D. by 1½ in. O.D. by ½ in. long) to electrically insulate the upper end of the anode from the cathode; and (b) a replaceable annular graphite insert (1 in. I.D. by 1½ in. O.D. by 1½ in. long). The insert (b) allows for convenient replacement of that section of the anode most subjected to arc impingement. The top 2½ in. of the outside wall of the anode are threaded so that the anode can be mounted by screwing it into a water-cooled brass support piece. This anode holder is held between the top flange of the cooling chamber and a nylon cap by three screws that secure the cap to the flange (Figure 2). The nylon cap is thermally insulated from the anode by a flat disk of low density alumina, and from arc radiation by an annular insert of high density alumina. This cap supports a water-cooled copper cathode extension piece, indented and threaed at its lower end to mount the graphite cathode tip. Gas, or a mixture of gas and entrained powdered solids (e.g. MgO), is introduced axially to the plasma arc via a 1/8 in. thick by ¾ in. I.D. annular space between the cathode and the anode (Figure 2).

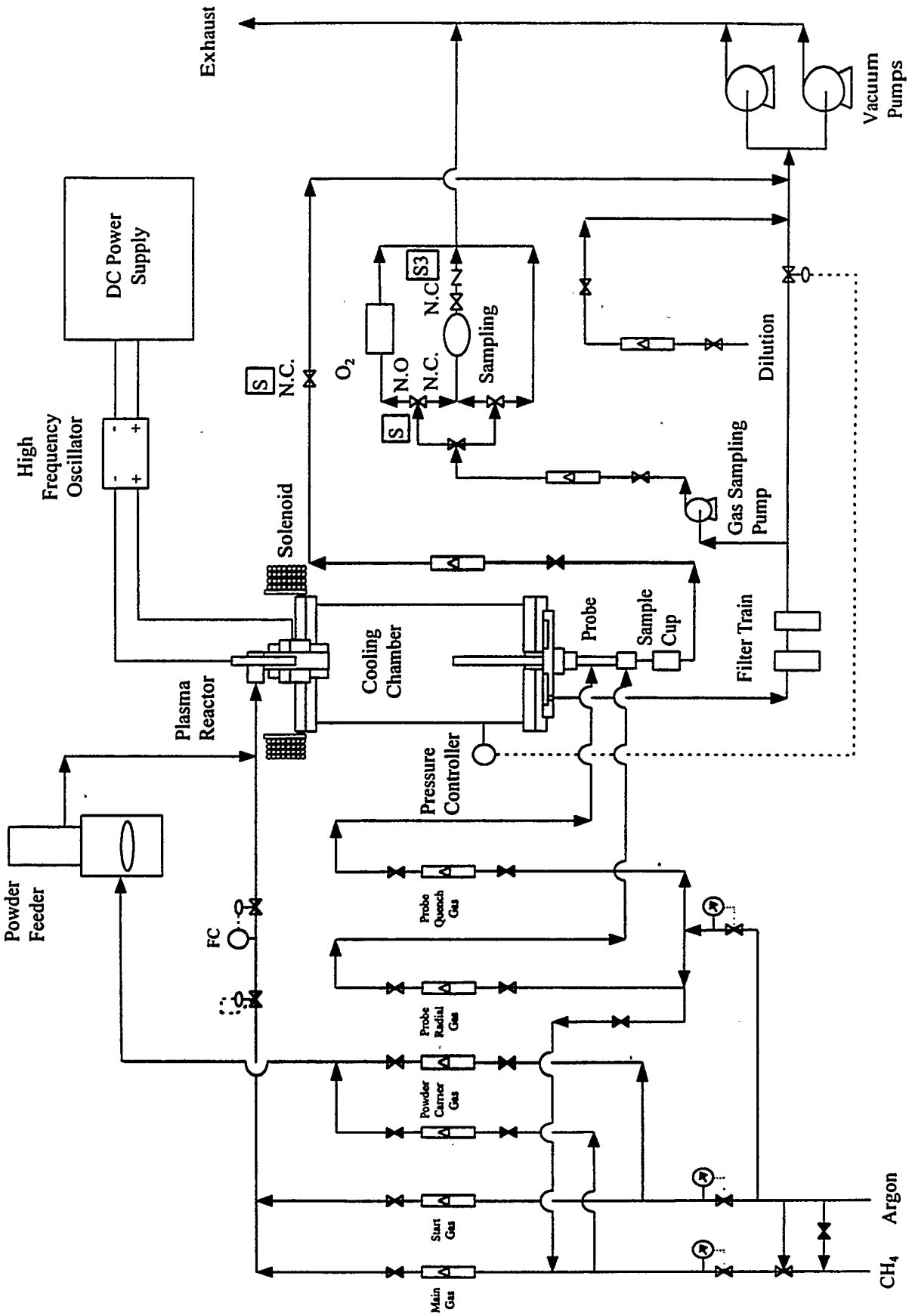

Figure 1. Process Flow Diagram

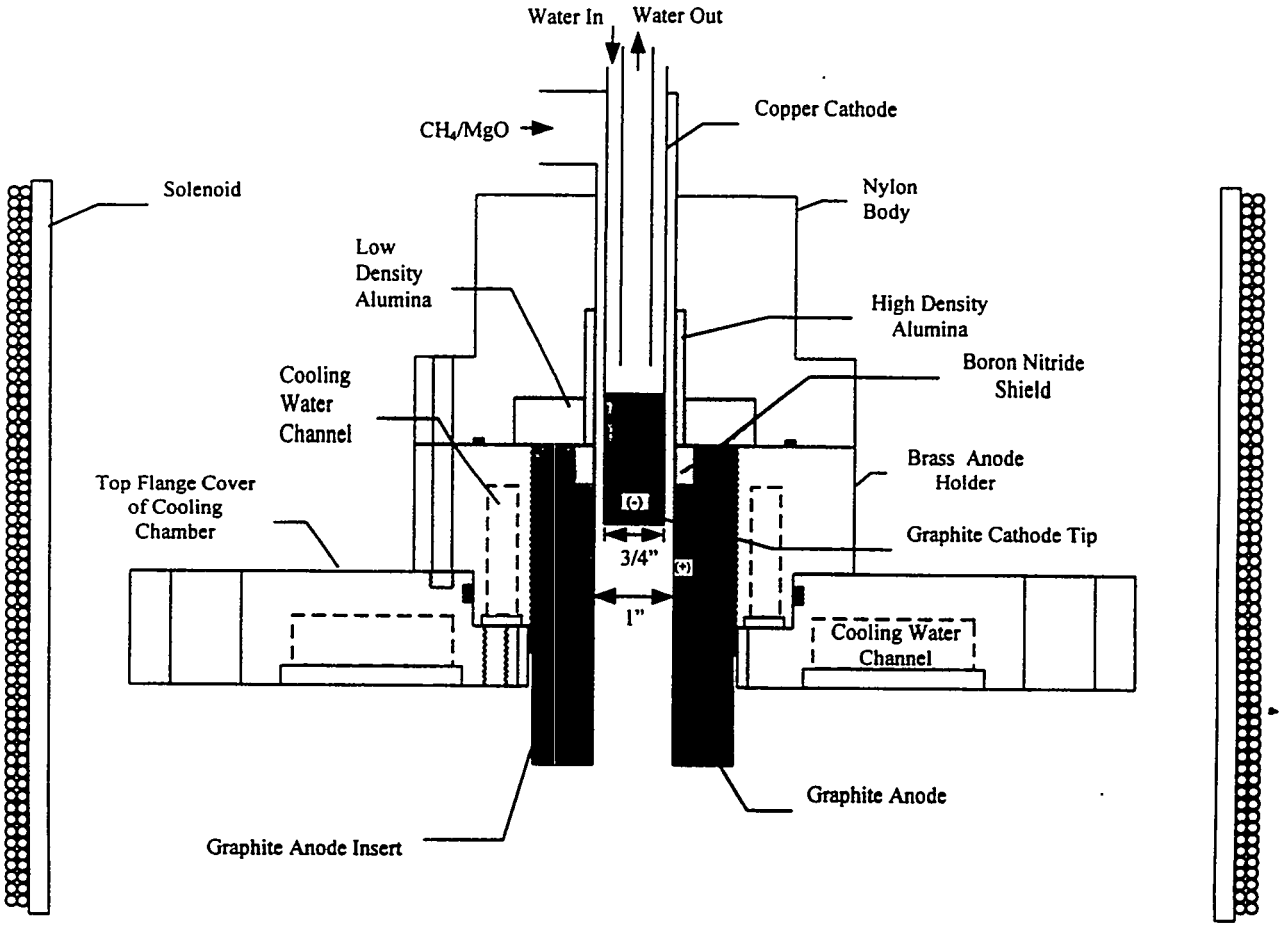

Figure 2. Schematic Representation of Plasma Reactor

Using a solenoid, a magnetic field is applied perpendicular to the arc current, inducing in the charged particles a velocity component perpendicular to their original direction of travel. Consequently, the path of charged particles moving in a plane perpendicular to the magnetic field will curve. However, the mean free path of the particles remains practically unaltered. One effect is that the electric conductivity of the plasma becomes more anisotropic under these conditions (Gross *et al.*, 1969), resulting in a better confined plasma.

Powder is delivered with argon as carrier gas to the reactor gas inlet using a Miller Thermal, Inc. Model 1270 mechanical wheel-type powder feeder. The plasma reactor is mounted on top of a steel, cylindrical, post-plasma cooling chamber, with a water-cooled wall. This chamber helps cool the plasma effluent and facilitates rapid quenching and recovery of solid and gaseous reaction products. Using two vacuum pumps, the gaseous products are aspirated from this chamber through a sintered disc at the chamber bottom and a filter train downstream of the chamber. The pumps exhaust to a ventilation stack.

The product quenching and collection system consists of a movable, water-cooled and gas-quenched cylindrical collection probe mounted at the bottom of the cooling chamber. This probe is designed so that the distance of separation between the end tip of the plasma "flame" and the entrance to the probe can be adjusted. Solid samples are collected on a sintered stainless steel

filter cup located downstream of the probe. The rest of the solid effluent from the reactor is collected on the sintered disc at the chamber bottom and on the filters downstream of the chamber (Figure 1). Gas samples from the chamber are collected with a sampling pump in a sample bulb.

In scoping runs performed to investigate the viability of Mg_2C_3 synthesis, an argon plasma was first established at a flowrate of 1 cfm (ambient temperature). Powder feeding was then initiated 30 seconds later. MgO powder entrained in 9 cfh (ambient temperature) of argon was introduced at a feed rate of 12 g/min into the plasma. After a few seconds of establishing powder feeding, the argon feed gas to the plasma was gradually switched to methane until the feed gas was 100% methane. On average, this switchover to methane was complete within three minutes of initiation of the argon plasma and an operating (100% methane) plasma could be sustained long enough to carry out the desired experiments.

3.2 Analysis of Solid Products

A small fraction of the solids was collected in the sampler downstream of the probe while most of them were deposited on the sintered stainless steel disc at the bottom of the cooling chamber. These solid were analyzed for the presence of carbides indirectly by measuring the acetylene/methylacetylene evolved upon hydrolysis, using a Hewlett-Packard 5830A gas chromatograph (GC) with a flame ionization detector and a helium carrier gas. A few milligrams of the solid product were placed inside a vial which was then fitted with a septum. Distilled water was injected into the vial to hydrolyze the solid. A 0.5 ml aliquot of the headspace gas above the hydrolyzed sample was injected into the GC. The analysis consisted of aliquot injection onto a Graphpak column at 10°C, followed by a 6.5 minute wait. After this time had elapsed, the C_2 species eluted, and the remainder of the aliquot was switched onto a Porapak-T column. At this point, the GC oven temperature was increased at a rate of 30°C/min to 50°C and there held to a final time of 28 minutes to complete the analysis.

4. Results of CH_4/MgO Scoping Runs

The results of two scoping runs are presented. In the first run, the arc voltage and current ranged from 125 to 135 volts and between 200 and 400 A, respectively. The voltage and current were fluctuating so greatly that taking a reading proved to be very difficult. The pressure in the cooling chamber, which was to be maintained at 760 mm Hg, rose above 1000 mm Hg upon initiation of the argon plasma. Manual attempts to control it at below 760 mm Hg proved futile. In the second run, the arc voltage ranged from 80 to 100 volts and the current from 250 to 450 A. The pressure build-up problem in the cooling chamber was addressed with the installation of a filter cartridge with a larger surface area downstream of the chamber. Thus, chamber pressure was successfully maintained below 760 mm Hg.

4.1 Scoping Run No. SR-M-1: "Breakthrough" Run

GC analysis of the headspace above both unhydrolyzed and hydrolyzed solid samples collected from this run revealed the presence of significant quantities of C_3H_4 and C_2H_2, i.e. in percentage, not ppm, levels. In addition to C_3H_4 and C_2H_2, which together, comprised more than 90% of the

gas sample, various other hydrocarbons such as CH_4, C_2H_4, C_2H_6, C_3H_8, C_3H_6, and C_4's were detected. Significant bubble formation accompanied by a distinct smell was observed upon hydrolysis of the solid samples in an open atmosphere. To test the hypotheses that other hydrocarbons are methane pyrolysis products and that they were carried out of the reactor adsorbed onto the carbides or soot particles, the solid samples were subjected to various kinds of treatment including heating, vacuum degassing and combinations thereof. Table 2 summarizes the results of the GC analyses of the headspace above these samples.

Table 2. Summary of GC Analyses of Headspace above Solid Samples

Source of Sample	Treatment of Solids Before Hydrolysis[a]	Hydrolysis[b]	Amount of HC[c]	% C_3H_4 + C_2H_2[d]	C_3H_4: C_2H_2 Ratio
Downstream Probe	None	Yes	+	96	1:2
Cooling Chamber Bottom	Heated to 100°C for 5 min	No	+	95	1:2
Cooling Chamber Bottom	Heated to 100°C for 5 min; Vacuum degassed @ ambient T	No	-	78	1.5:1
Cooling Chamber Bottom	Heated to 100°C for 5 min; Vacuum degassed @ ambient T	Yes	+	87	1.5:1
Cooling Chamber Bottom	Vacuum degassed @ ambient T	No	-	89	1:1
Cooling Chamber Bottom	Vacuum degassed @ ambient T	Yes	+	e	1:1
Cooling Chamber Bottom	Vacuum degassed @ 120°C overnight	No	-	e	e
Cooling Chamber Bottom	Vacuum degassed @ 120°C overnight; heated to 100°C for 10 min	No	-	77	1:3
Cooling Chamber Bottom	Vacuum degassed @ 120°C overnight; heated to 100°C for 10 min	Yes	+	74	3:1

[a] Treatment was intended to allow any adsorbed gases to escape from the solids prior to withdrawing samples of the headspace gas for GC analysis.

[b] Bubbling was visible in all hydrolysis cases.

[c] Amount of Hydrocarbons detected: (+) significant; (-) minimal.

[d] Corresponds to uncorrected area count. GC calibration to be performed in future runs.

[e] Data not available.

No quantification of the carbide yield was done in this study because the sampling was done cumulatively, i.e. sampling was done throughout the entire run. In what is envisioned to be a better-controlled experimental run, sampling will be performed only when fully developed flows of methane and MgO are established. Nevertheless, the study provided several insights. First, the

observation of bubble formation on hydrolysis is a strong indication of the formation of magnesium carbides. Figures 3 and 4, which are the GC analyses of the headspace above pre- and post-hydrolysis solid samples, respectively, show strong increases in hydrocarbon formation after hydrolysis. Second, heat treatment of the solid samples seems to increase the yield of C_3H_4 relative to C_2H_2, which suggests that MgC_2 (which hydrolyzes to C_2H_2) is being converted to Mg_2C_3 (which hydrolyzes to C_3H_4) upon heating. Third, although C_3H_4 and C_2H_2 are the major gaseous products of hydrolysis, the detection of other hydrocarbons upon hydrolysis may be indicative of other hydrolysis reactions taking place or of desorption of hydrocarbons generated earlier by methane pyrolysis. The latter could arise by displacement of hydrocarbons sorbed on soot or carbide surfaces, or by release of trapped hydrocarbons due to disintegration of the carbides during chemical reaction.

Because detection of acetylenes from hydrolysis of the solid products is an indirect method of carbide identification, X-ray diffraction analysis was performed as a direct identification technique. Figure 5 shows the X-ray diffraction pattern of the solid sample from the bottom of the cooling chamber. Peaks represent actual data while vertical lines represent the carbide spectral pattern. The diffraction pattern reveals three peaks matching MgC_2 and two peaks matching Mg_2C_3. Although the complete diffraction patterns for MgC_2 and Mg_2C_3 show several other lines, the absence of peaks coresponding to these lines in the present specimens may reflect the small size of the crystals in the sample.

4.2 Scoping Run No. SR-M-2: Run with Lower Chamber Pressure Build-up

The difficulty of controlling the chamber pressure in the MgO/CH_4 run described above was due to clogging of the sintered stainless steel disc at the bottom of the chamber. A 5μ filter cartridge with a larger area was therefore installed downstream of the cooling chamber. With this configuration, another scoping run with MgO/CH_4 was performed.

Upon withdrawal of the probe from the chamber, some solid particles dislodged from the probe glowed instantaneously upon exposure to the ambient atmosphere. When the cartridge filter was removed, the solids in the cartridge likewise glowed once exposed to the atmosphere. This strongly suggests that the solid products are carbides that reacted with moisture in the air, exothermically forming acetylenes which, because of the elevated temperatures arising from localized heating of the specimens, were able to ignite instantaneously in the presence of oxygen. Samples of the reactor solids that had exhibited this instantaneous glowing behavior were hydolyzed. GC analysis of the headspace above these hydrolyzed samples revealed very little CH_4, C_3H_4 and C_2H_2 (and no other hydrocarbon). This would suggest that the hypothesized hydrolysis of reactor solids (i.e. magnesium carbides) upon exposure to the moist atmosphere proceeded virtually to completion leaving little or no carbides to generate acetylenes upon controlled hydrolysis in the septum vial. It should also be noted that the rapid and instantaneous reaction may be attributed to the small particle size of the carbides. The solids in the filter cartridge are presumably between 5 and 100 μ, and even smaller particles may be sorbed on these. In future experiments, particle sizes will be determined more quantitatively by electron microscopy.

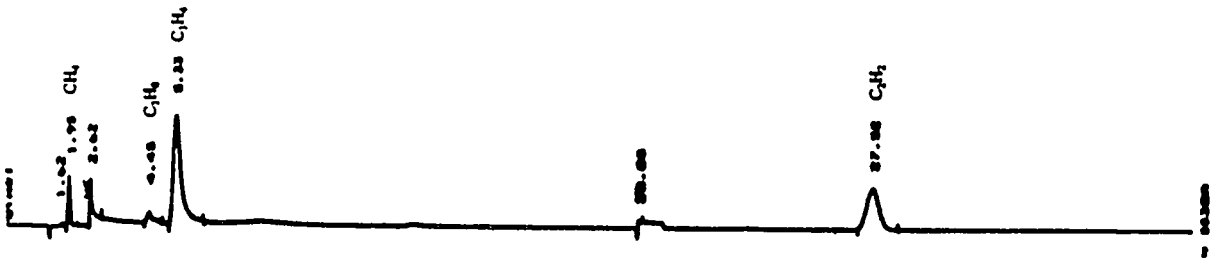

Figure 3. GC Analysis of Headspace Gas Above Unhydrolyzed Solid Sample Heated to 100°C for 5 minutes; Vacuum Degassed at Ambient T 0.5 ml Sample Gas Injection

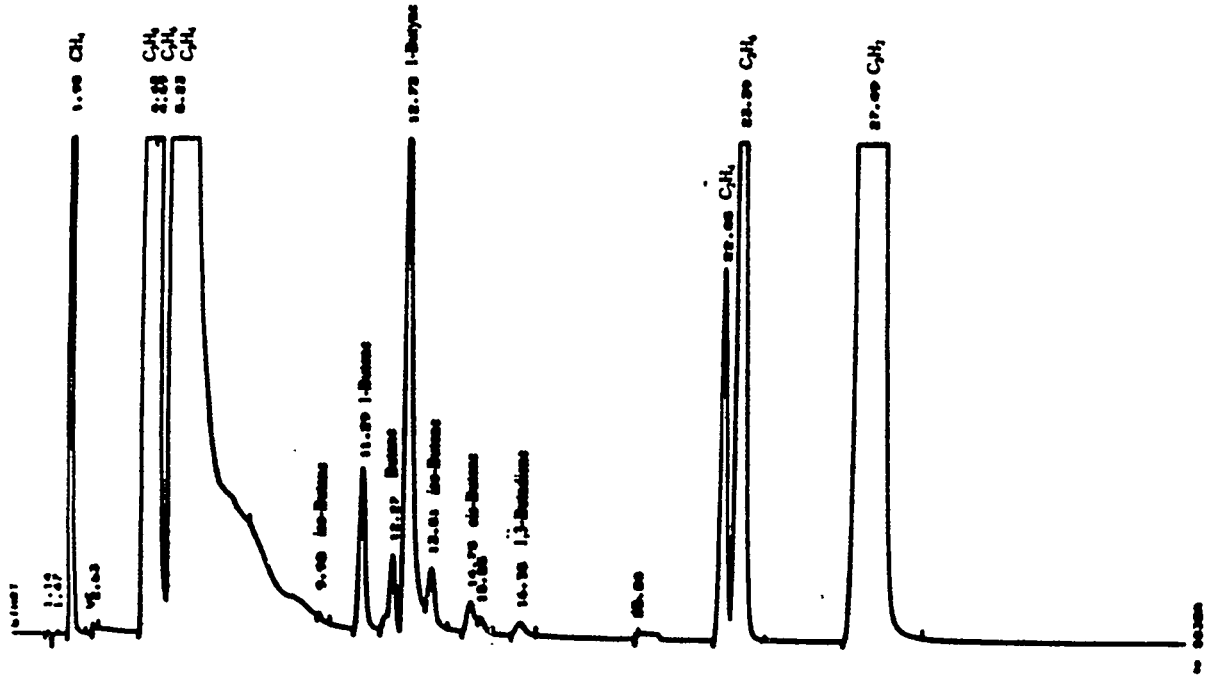

Figure 4. GC Analysis of Headspace Gas Above Hydrolyzed Solid Sample Heated to 100°C for 5 minutes; Vacuum Degassed at Ambient T 0.5 ml Sample Gas Injection

Figure 5. X-ray Diffraction Pattern of Solid Sample From Chamber Bottom

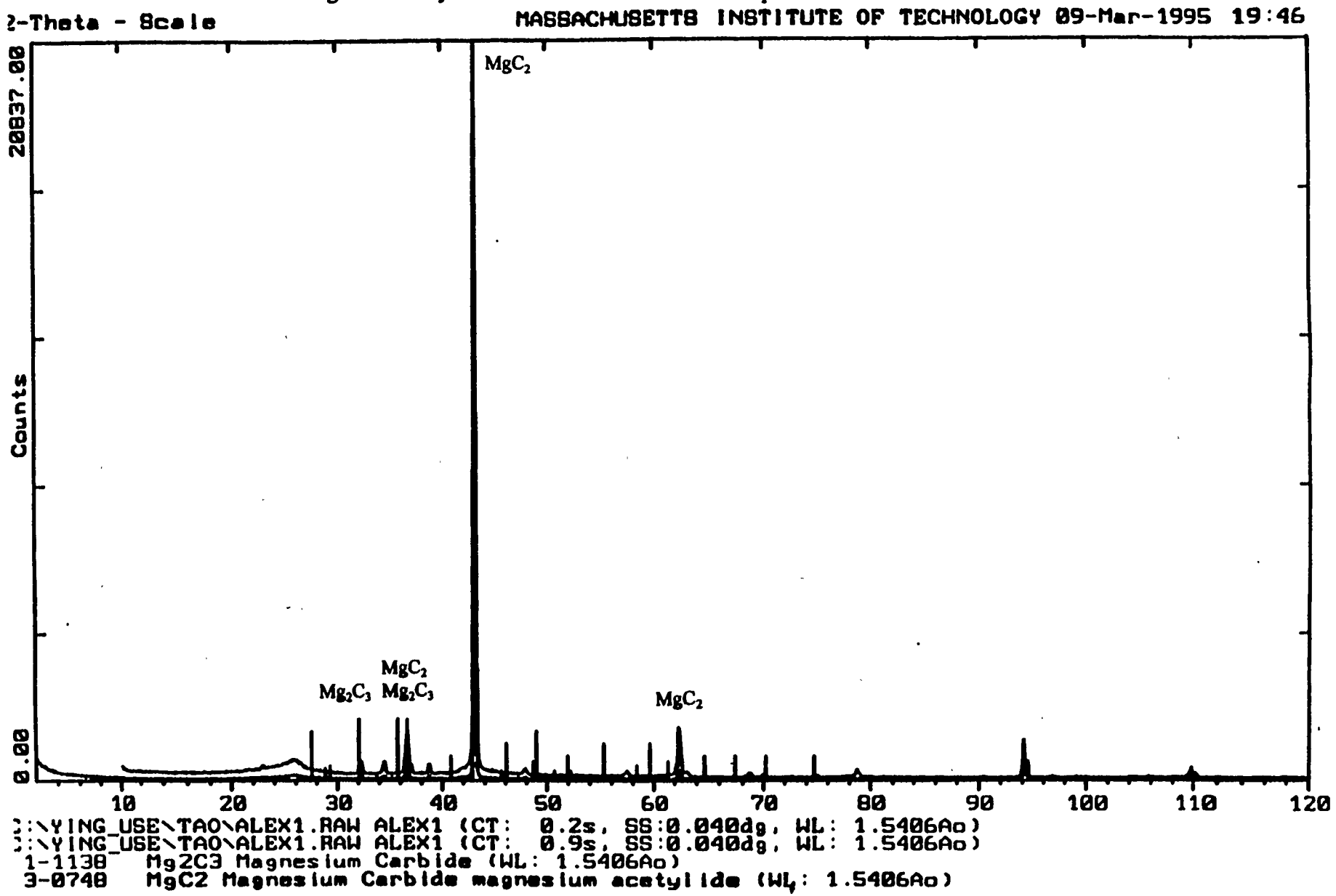

5. Conclusions

Based on the results of the scoping runs, there appears to be strong indications that a breakthrough has finally been achieved in that synthesis of magnesium carbides from MgO and methane in the arc discharge reactor has been demonstrated.

6. Future Plans

In preparation for a systematic study of carbide formation in the rotating arc reactor, the experimental apparatus had to be upgraded to allow for improved characterization of the process conditions. A sampling scheme that allows solid and gas sampling only during a period of the run time when the flows of methane and MgO are fully established was implemented using solenoid valves actuated according to a prescribed time sequence by an automatic control system. An automatic pressure controller was installed to maintain the chamber pressure at 760 mm Hg and a data acquisition system was installed so that arc voltage and current can be recorded on a computer. In addition, analytical techniques are being explored for quantifying carbide yields and for more detailed chemical and physical characterization of the solid products.

In the planned study, methane conversion, product yields and, to the extent feasible, products global formation rates will be measured in the plasma reactor as affected by independent variations in operating conditions of practical interest such as average temperature, power input, apparent average residence time, quench time, CaO/CH_4 and MgO/CH_4 ratios, initial particle size of CaO and MgO, methane partial pressure and partial pressure of a diluent such as hydrogen.

7. Acknowledgements

Financial support for this research by the U.S. Department of Energy Pittsburgh Energy Technology Center under Contract No. DE-AC22-92PC92111 is gratefully acknowledged, as is the keen interest in this work shown by the DOE Technical Project Officers, Dr. Arun C. Bose and Mr. George Cinquegrane. We also acknowledge Mr. Jason Pride, Mr. John Cremin, Dr. Joseph Marr, and Prof. Adel Sarofim for their helpful contributions.

8. References

1. Gary, J.H. and G.E. Handwerk, *Petroleum Refining Technology and Economics*, Second Edition, p. 207, Marcel Dekker, New York, (1984).

2. Gross, B., B. Grycz and K. Miklossy, "Plasma Technology", American Elsevier Publishing Company, Inc., New York (1969).

3. Kim, C.S., "Formation of CaC_2 from CaO and 'Nascent' Carbon Species in a Rotating-Arc Reactor", Sc.D. Thesis, Department of Chemical Engineering, MIT, Cambridge, MA, (1977).

4. Kim, C.S., R.F. Baddour, J.B. Howard and H.P. Meissner, "CaC_2 Production from CaO and Coal or Hydrocarbons in a Rotating-Arc Reactor", *Ind. Eng. Chem. Process Des. Dev.* **18**, 323-328, (1979).

5. Longwell, J.P., "Diversification of Raw Materials for Domestically Produced Transportation Fuels", *Energy & Fuels* 7, 23-26, (1993).

6. Peters, W.A. and J.B. Howard, "Methane Conversion Illustrated by Examples of Applications to Conversion of Remote Natural Gas to Hydrogen and to Transportable Solids and Liquids with Preliminary Cost Estimates, Technical Assessments, and Critical Research Needs", MIT Energy Laboratory Report, MIT, Cambridge, MA, April (1989).

7. Peters, W.A. and J.B. Howard, "Method for Methane Conversion", United States Patent No. 4,921,685, May 1, 1990; 15 Claims, Assigned to MIT.

8. Peters, W.A. and J.B. Howard, "Method for Methane Conversion", United States Patent No. 5,246,550, September 21, 1993; 10 Claims, Assigned to MIT.

Title: Light Hydrocarbon Gas Conversion Using Porphyrin Catalysts

Authors: Margaret C. Showalter, John A. Shelnutt

Institution/ Organization: Fuel Science Department, Sandia National Laboratories

Contract Number: FEW-4262

Period of Performance: October 1994 - September 1995

Objective:

The objective of this project is to develop novel catalysts for the direct conversion of natural gas to a liquid fuel. The current work investigates the use of biomimetic metalloporphyrins as catalysts for the partial oxidation of light alkanes to alcohols.

Accomplishments and Conclusions:

Background. Enzymes such as the cytochromes P450 are known to catalyze the partial oxidation of unactivated alkanes to alcohols. Analysis of these natural systems indicates structural features needed to create a biomimetic catalyst which will mimic the enzyme's high catalytic activity and selectivity. Metalloporphyrins have been reported to catalyze the oxidation of light alkanes to alcohols under mild conditions using molecular oxygen as the oxidant without the need for added co-reductant (Paulsen, D.R., Ullman, R., Soane, R.G., Closs, G.L., *J. Chem. Soc., Chem. Commun.* **1974**, 186. Ellis, Jr., P.E., Lyons, J.E., Symp. Oxygen Activation in Catalysis, ACS, April 22-27, 1990. European Patent Appl. No. 88304455.4, 1988). We are developing more active and selective catalysts for this process, toward the goal of obtaining a catalyst which is active enough to convert methane to methanol. We are using computer-aided molecular design (CAMD) in conjunction with activity testing to develop improved metalloporphyrin catalysts. Our stepwise approach to catalyst development involves first using CAMD techniques to design potential porphyrin catalysts, followed by the synthesis and characterization of promising catalysts, and finally subjecting these catalysts to bench scale activity testing. Catalyst testing experiments give insights into important structure-activity relationships which are used to evaluate and refine our modeling tools so that better catalysts can be developed.

In the previous year, we described a series of dodecaphenyl substituted iron porphyrin catalysts which had two desired structural features: 1) a substrate binding cavity and 2) a systematic variation of the redox potential of the Fe center caused by increasing numbers of fluorine substituents. We have found that placing large numbers of bulky substituent groups, such as phenyl groups, around the periphery of a porphyrin macrocycle causes a nonplanar distortion of the macrocycle which creates a rigid shallow cavity adjacent to the metal center. It

was predicted that this cavity would promote substrate binding and trap reactive intermediates adjacent to the metal center, although a deeper, more well defined cavity is required to fully realize these beneficial properties. This "micro-reactor" environment would thus improve catalyst activity and might also influence selectivity. We also predicted that highly substituted porphyrins such as our iron dodecaphenylporphyrin catalysts would have improved stability relative to traditional planar porphyrin catalysts because there is considerable steric hindrance to bifacial approach of two porphyrin molecules, thus inhibiting bimolecular catalyst destruction. Electron withdrawing groups were substituted on the phenyl rings of iron dodecaphenyl-porphyrin to create a series of catalysts, FeF_xDPPCl where x = 0, 20, 28, 36, with a range of overall electron depletion at the metal center. This catalyst series is unique because the bulky phenyl substituents create a nonplanar distortion leading to the formation of a cavity, as discussed above. In addition, these catalysts maintain this same shape across the series, even with the addition of fluorine substituents. In most other investigations of the effect of electron withdrawing substituents on metalloporphyrin catalyst activity, the addition of electron withdrawing groups to the porphyrin macrocycle has been accompanied by a change in the degree of porphyrin nonplanarity. Our unique catalyst series allowed us to study the effect of increased electron depletion of the metal center isolated from significant structural variation.

The FeF_xDPPCl catalyst series was tested in the oxidation of isopentane by molecular oxygen. For comparison, we also tested the commercial planar catalyst $FeF_{20}TPPCl$. This reaction was very selective for the production of alcohols. We observed the predicted trend -- catalytic activity increased with the degree of fluorination for the FeF_xDPPCl series. However, the overall activity of the FeF_xDPP catalysts was much lower than that of the planar catalyst, $FeF_{20}TPPCl$, despite the built-in cavity of the DPP catalysts. Furthermore, we observed that the porphyrins tested as oxidation catalysts degraded completely after several hours, even when the reactor was charged with a large amount of catalyst. Such rapid catalyst deactivation is in conflict with literature reports which indicate that metalloporphyrin catalysts in this type of reaction are stable for much longer time periods, some even for days (Ellis, P.E., Jr., Lyons, J.E., *Catal. Lett.* **1989**, *3*, 389 and Lyons, J.E., Ellis, P.E., Jr., *Catal. Lett.* **1991**, *8*, 45). Our catalysts were stable at the temperatures and pressures used in catalyst testing. Catalyst degradation was only observed in the presence of a reactive alkane substrate. This indicates that some species formed in the course of the oxidation reaction is responsible for the catalyst degradation. The short life of our catalysts, a problem in itself, also prevented us from making adequate comparisons for our designed catalysts. Although the amount of alcohol produced by $FeF_{20}DPPCl$ was substantially less than the amount produced by $FeF_{20}TPPCl$ under identical experimental conditions, we did not know if this was an indication that the DPP catalyst is less active, less stable, or a combination of both. One would expect similar activities and stabilities for the two catalysts based on the degree of electron depletion of the porphyrin by the substituents. (Charge depletion can be estimated from the sum of the Hammett σ constants of the substituents, and $FeF_{20}DPPCl$ is predicted to be more active and stable or less active and stable depending on whether *meta* or *para* constants are used, respectively.)

Conclusions which can be drawn from our previous testing with the FeF_xDPP series are as follows: The importance of adding electron withdrawing substituents to alter the redox potential of the metal center was validated by the trend of increasing activity with increased degree of fluorination observed for this structurally homologous series. The catalysts were less stable than expected. However, if the reaction proceeds via a radical autooxidation mechanism,

this is not surprising. Thc concept of steric bulk preventing bimolecular catalyst destruction would be more applicable to a P450-like mechanism and to bulkier porphyrin catalysts than those investigated here. Any enhancement of the catalyst activity or selectivity by the cavity adjacent to the metal center was unable to be verified when O_2 is used as the oxidant. Rapid catalyst decomposition makes it impossible to definitively determine whether or not the pocket provides any beneficial effect. If it does, it is small enough to be canceled out by the poor stability and small differences in porphyrin charge depletion. In any case, molecular modeling suggests that a more enclosed cavity is required to achieve radical trapping, promote substrate binding, and prevent bimolecular degradation reactions.

Current Progress. Our previous attempts to measure the activity of Sandia-developed porphyrins as alkane oxidation catalysts have been hampered by rapid catalyst decomposition and low apparent activities. Furthermore, such low activities are inconsistent with results reported by other research groups, including scientists at Sun Co. At the invitation of Drs. James Lyons and Paul Ellis, Margaret Showalter traveled to the Sun Co. to test some of the Sandia catalysts in the Sun reactors. In this collaborative effort, two different Sandia porphyrins and one Sun porphyrin, shown in Figure 1, were tested side-by-side using a catalyst screening experiment developed at Sun for isobutane conversion. There are three major differences in the Sun procedure and the procedure used previously at Sandia. First, catalyst testing at Sandia has been performed in teflon-lined stainless steel reactors, while the reaction vessel employed at Sun is a glass aerosol tube. Second, the scientists at Sun have found that when the axial ligand coordinated to the metalloporphyrin is OH, the reaction is usually easier to initiate than when the ligand is Cl. Thus Sun prefers to screen potential catalysts as the OH form; however the porphyrins tested at Sandia have had Cl as the ligand. Before traveling to Sun, one of the Sandia catalysts to be tested was converted from the Cl-porphyrin to the OH-porphyrin. Finally, isopentane is the substrate used for screening at Sandia, since this alkane is a liquid and is thus simple to handle in the laboratory. However, the Sun researchers typically screen oxidation catalysts with isobutane as the substrate.

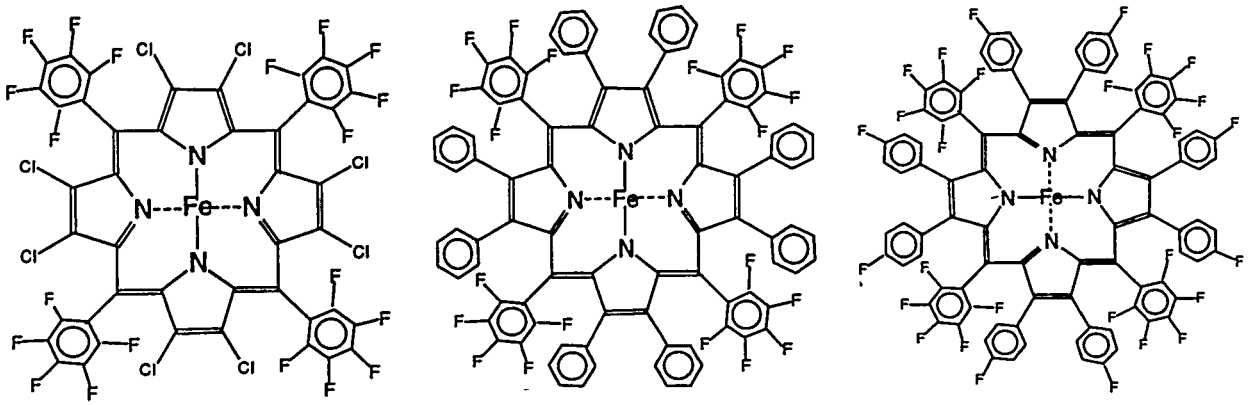

Figure 1. Structures of porphyrins tested at Sun Co.; -OH and -Cl indicate the axial ligand, not shown in the structure. The numbers in parenthesis are the predicted activities for identical axial ligands relative to the Sun-OH catalyst based on the sum of the Hammett para substituent constants).

Table 1. Summary of Reactions Performed at Sun Co.

Catalyst ID	mmol catalyst	T (°C)	O2 uptake (mmol)	Turnovers*	Visual observations
Sun-OH	0.013	60	25.4	1950	deep brown, constant color
Sandia1-OH	0.012	60	13.3	1100	initially dark red, lighter at 2.5 hr, continued lightening to reddish-orange
Sandia1-OH	0.017	80	14.5	850	initially dark red, lighter at 1hr, continued lightening to reddish-orange
Sandia2-Cl	0.013	80	0	0	no reaction, remained dark brown throughout

Reaction solutions contained catalyst and 7g isobutane in 25ml benzene. Solutions were heated while stirring for 6 hours under 100 psi of O_2. *Defined as mmol O_2 consumed /mmol catalyst.

Table 1 summarizes the experiments performed. The Sun-OH catalyst, which they had previously determined to be very active and robust, performed as expected. Oxygen uptake continued throughout the course of the reaction and no noticeable change in the deepness of color occurred. The Sandia1-OH catalyst performed well initially, taking up O_2 at a rate comparable to the Sun-OH catalyst. However, after a couple of hours, the Sandia1-OH solutions were noticeably lightened and oxygen consumption slowed. Eventually the solutions lightened to pale reddish-orange and O_2 uptake stopped. This lightening happened more quickly in the 80°C reaction. UV/Visible spectroscopy on the reacted Sandia1-OH samples indicated that there was

Figure 2. Plot of oxygen consumption over time.

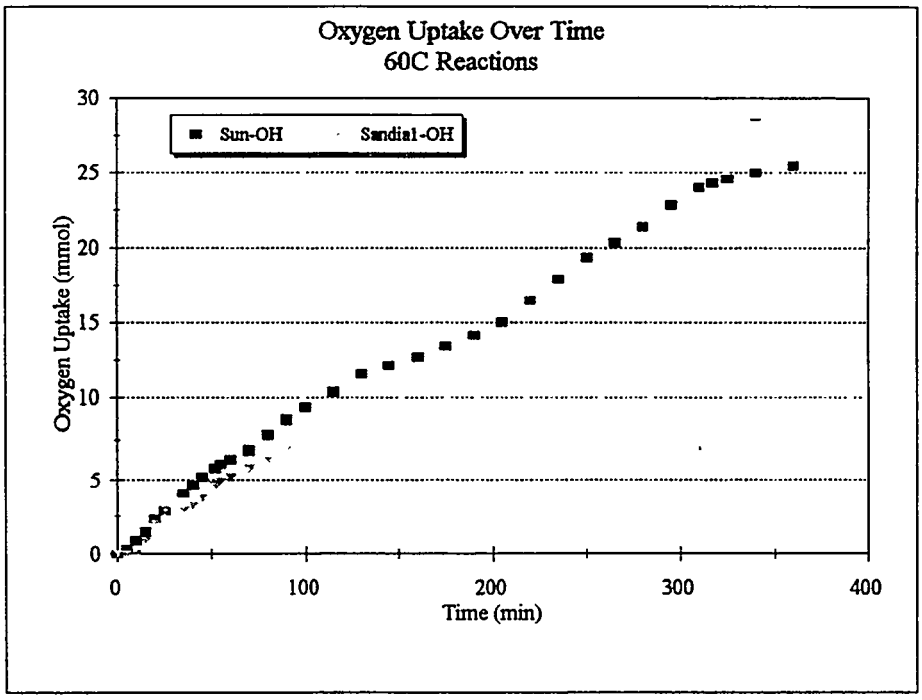

no porphyrin left in these pale solutions. Thus, the turnovers achieved by the Sandia1-OH catalyst are lower because this porphyrin did not persist in the solution for the entire 6 hour run. Figure 2 shows O_2 uptake with time for the 60°C reactions, which gives a graphical indication of relative reactivity. Note that initially, the Sandia1-OH catalyst consumed oxygen at a rate comparable to the Sun-OH catalyst, but O_2 usage by the Sandia1-OH catalyst leveled off as the catalyst decomposed. Although the Sandia1-OH catalyst is not as stable as desired, this catalyst was more active and stable than previous experiments at Sandia using the Cl salt and isopentane had indicated.

GC was used to analyze the liquid products formed in these reactions. The only products formed in significant quantities were tertiary butyl alcohol (TBA, the desired product) and acetone, which results from cleavage of the isobutane substrate. The ratio of TBA to acetone is 9:1, thus the selectivity for the desired product is excellent. Approximately 90% of the measured oxygen uptake can be accounted for by these two products.

The Sandia2-Cl catalyst was unreactive, even though the higher temperature of 80°C was used for this compound. This lack of reactivity is consistent with previous observations at Sun that iron porphyrin chlorides are often difficult to initiate. Catalyst testing to date at Sandia has been done with Cl porphyrins, and this warrants change. However, the problem we had had at Sandia was not that the porphyrin did not react at all, but rather that once the reaction was initiated, the porphyrin was short-lived. We had also found that temperatures of 100°C were required. This higher temperature is high enough to cause the relatively unreactive Cl to react, but catalyst decomposition is probably also accelerated by this higher temperature. High activities for the Cl catalysts previously reported by Sun are probably the result of incomplete conversion to the chloride form.

In summary, the initial activity of the Sandia1-OH catalyst was comparable to that of Sun-OH, one of Sun's best catalysts; however the Sandia material is not as robust (as predicted on the basis of the Hammett constants, see Table 1). The measured activity of the Sandia1-OH catalyst was significantly higher as tested at Sun than in previous experiments at Sandia. The Sandia2-Cl catalyst was completely unreactive under the mild conditions used. In the future, axial Cl should be avoided to facilitate easier catalyst screening; conversion to the azide or hydroxide complex will be used to promote catalysis. The glass-tube reactors utilized at Sun provide a quick, easy, reliable method for screening oxidation catalysts, and have the added advantage of allowing visual observation of the reaction in progress.

Since the visit to Sun, we have constructed a glass tube reactor in our laboratory at Sandia which is essentially identical to those used at Sun. We also added an additional pressure gauge to the teflon lined steel reactors, so that we can more accurately monitor and control the pressure. In an attempt to apply some of the insights gleaned from the collaborative work with Sun, we passed commercial $FeF_{20}TPPCl$ through a column of activated alumina to exchange the axial Cl ligand. (The material obtained from the column is a mixture of hydroxide and μ-oxo dimer). We then used this porphyrin to catalyze the oxidation of isopentane. However, we found that even with the non-Cl porphyrin, a temperature of 100°C was needed for the reaction to proceed, and the catalyst was consumed quickly at this temperature. When isobutane was used as the substrate, the reaction proceeded at 80°C, catalyst decomposition was minimal, and turnovers comparable to those reported by Sun were obtained. Thus it appears that the choice of alkane substrate is as important as the axial ligand of the catalyst in obtaining results consistent with those published by Sun. The lower activity with isopentane than with isobutane is unexpected

and this result needs to be understood. Also, there does not appear to be any inherent problem with the teflon reactors, as we once believed. We can get excellent catalytic turnovers with minimal catalyst degradation in these reactors when isobutane is used as the substrate and the axial ligand of the porphyrin is not Cl.

An interesting facet of this chemistry is that the catalyst turnovers (amount of oxygenated products/amount of catalyst) are dependent on the initial catalyst concentration, as shown in Figure 3. Such a phenomenon may indicate that true catalytic rates can not be determined under these experimental conditions. In fact, for the higher catalyst concentrations plotted in Figure 3, the amount of oxygenated products produced was essentially the same. Thus a doubling of catalyst concentration leads to a halving of the turnovers calculated. To obtain true catalytic activities we need to be operating under conditions for which doubling the amount of catalyst doubles the product produced. Therefore, it is critical to be very careful when comparing catalysts which have not been tested under identical conditions.

Figure 3. Plot of catalyst turnovers vs. amount of catalyst for a series of $FeF_{20}TPP$ catalyzed isobutane reactions.

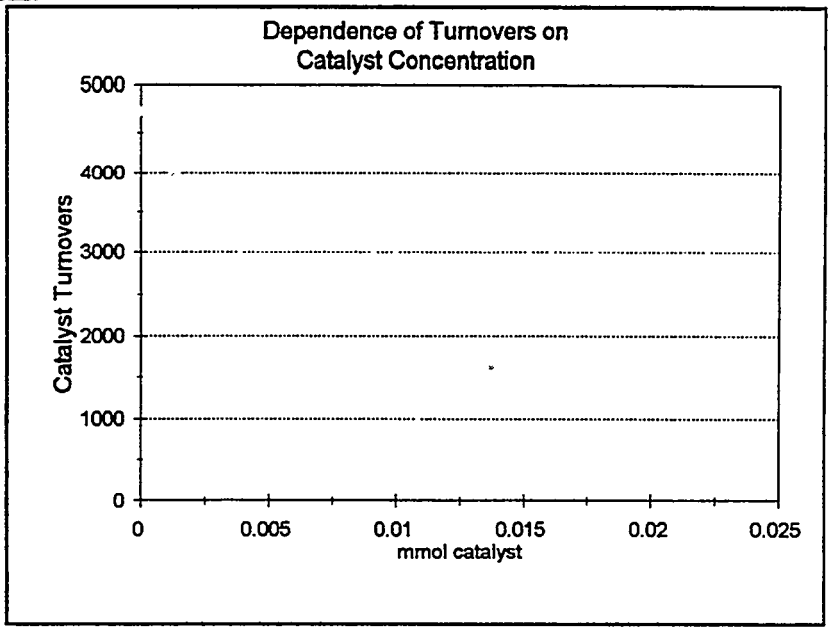

Synthesis has begun on a new class of highly substituted metalloporphyrin catalysts. These new catalysts are also based on the parent iron dodecaphenylporphyrin (FeDPP). However, we are pursuing a different route to charge deplete the porphyrin ring. Synthesis of porphyrins becomes problematical when highly electron withdrawing substituents are present. Therefore, we have devised a method of assembling the porphyrin macrocycle with less electron-withdrawing substituents (pyridyl) and then converting the substituents to highly electron withdrawing ones (pyridinyl). In order to improve the catalyst stability and activity, in the new class of dodeca-substituted iron porphyrins some or all of the phenyl rings are replaced by pyridyl or pyridinyl groups. Representative catalysts of this type are shown in Figure 4, along with their activity number relative to Sun-OH (Figure 1). Quaternizing the N of the substituent pyridyl groups greatly enhances the electron withdrawing effect on the Fe center. The Hammett constant for phenyl, perfluorophenyl, 4-pyridyl, and 4-pyridinyl groups are-0.01, 0.41, 0.83, and >1.30,

respectively. Furthermore, these ionic groups provide a site for anchoring the catalyst molecules to an inorganic support such as silica and alumina, thus enhancing catalyst stability and providing a means for easy recovery of the catalyst.

Activity testing of these pyridyl porphyrins requires changing our experimental protocol. These cationic porphyrins will not be soluble in the benzene currently used for homogeneous testing experiments, so they will first be applied to an inorganic support. We are currently developing suitable procedures for preparing and testing such a heterogeneous catalyst using the commercially available iron(III) chloride tetra(N-methyl-4-pyridinyl)porphyrin tetratosylate (predicted activity relative to Sun-OH: 1.49) supported on silica. Preliminary tests show this supported catalyst to be active under the same conditions as the homogeneous catalysts. This is the first demonstration that this supported catalyst is active when O_2 is used as oxidant. This shift from homogeneous to heterogeneous catalysis is significant because heterogenous catalysts are likely to be better suited to the conversion of a gaseous substrates in flow reactors. We anticipate that this new class of porphyrins will also exhibit enhanced activity and stability.

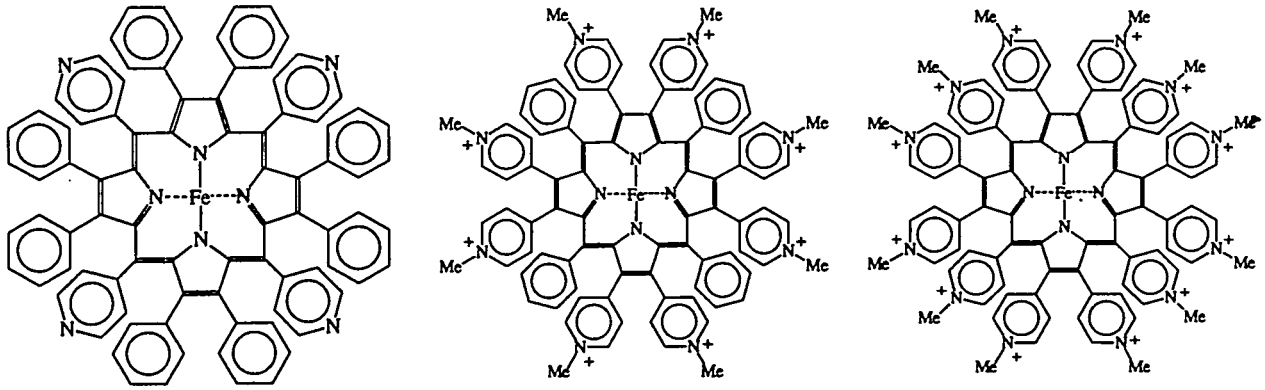

Iron tetrapyridyl-octaphenylporphyrin (0.93, >1.47 for N-Me derivative)

Iron tetraphenyl-octa(N-methylpyridinyl)porphyrin (>2.98)

Iron dodecapyridinylporphyrin (>4.48)

Figure 4. Pyridyl and N-methyl pyridinyl porphyrins based on parent dodecaphenylporphyrin structure. Counter ions are not shown. (Predicted activities relative to Sun-OH catalyst in Figure 1.)

In addition to the synthesis of these new catalysts, we are also making progress in the synthesis of more stable and active porphyrins in the fluorinated dodecaphenyl series. The most fluorinated of this series tested to date is F_{36}. However, recent progress in synthesis using the Susuki reaction may soon yield F_{40}DPP and F_{60}DPP. The fully fluorinated F_{60} material will be particularly interesting to test since all possible H's in the parent FeDPP will be replaced by F. It is possible that part of the instability of the previously tested catalysts in the FeDPP series is due to the presence of CH bonds on the substituent groups which are susceptible to attack by radical intermediates. The F_{60}DPP catalyst, in addition to being the most electron deficient of the series, will not have any CH bonds.

Molecular design studies are underway to engineer catalyst with deeper cavities that are easily synthesizible. These catalysts are also based on the dodeca-substituted porphyrins, including the 2- and 3-pyridinyl analogs of the catalysts shown in Figure 4.

Plans:

We will continue the development of an experimental protocol for testing the catalytic activity of supported porphyrin catalysts using a heterogeneous material prepared from a commercial tetrapyridyl porphyrin. Once we have demonstrated the ability to reproducibly prepare and test the supported catalyst, we will be ready to test the new pyridyl porphyrins that are currently being synthesized. We anticipate having several of these new porphyrins available for testing before the end of this report period.

Once the additional fluorinated DPP catalysts, F_{40}DPP and F_{60}DPP, become available, we will test these materials using the optimized homogeneous process discussed in this paper. These materials may also be available in testable quantities this summer.

This work was supported by the United States Department of Energy under Contract DE-AC04-94AL85000.

1995 Coal Liquefaction and Gas Conversion Contractors Review Conference

Methyl Chloride Via Oxyhydrochlorination of Methane: A Building Block for Chemicals and Fuels from Natural Gas

Ronda L. Benson, Scott S.D. Brown, Steven P. Ferguson, and Robert F. Jarvis, Jr.

Dow Corning Corporation, Silicon Methyl Intermediates Research, US Hwy 42, Carrollton, Kentucky 41008.

Contract : DE-AC22-91PC-91030 (DoE)
5091-222-2300 (GRI)

Period of performance : October 1, 1991 to September 30, 1995.

Objectives :

The objectives of this program are to (a) develop a process for converting natural gas to methyl chloride *via* an oxyhydrochlorination route using highly selective, stable catalysts in a fixed-bed, (b) design a reactor capable of removing the large amount of heat generated in the process so as to control the reaction, (c) develop a recovery system capable of removing the methyl chloride from the product stream and (d) determine the economics and commercial viability of the process.

Approach :

The general approach has been as follows: (a) design and build a laboratory scale reactor, (b) define and synthesize suitable OHC catalysts for evaluation, (c) select first generation OHC catalyst for Process Development Unit (PDU) trials, (d) design, construct and startup PDU, (e) evaluate packed bed reactor design, (f) optimize process, in particular, product recovery operations, (g) determine economics of process, (h) complete preliminary engineering design for Phase II and (i) make scale-up decision and formulate business plan for Phase II.

Background :

Methyl chloride (CH_3Cl) is an important feedstock for the silicone industry. It is also used as an intermediate in the manufacture of other chlorocarbons, agrochemicals, methyl cellulose, quaternary ammonium salts and as a solvent in the production of butyl rubber (Figure 1). In 1992, CH_3Cl consumption in the US was reported to be around 850 million lbs. for these applications[1], although the actual consumption was probably higher than this. Currently, CH_3Cl is derived from methanol, however, the demand for methanol in the US is currently higher than the available domestic supply. As a result, methanol prices have exhibited a high degree of variance recently. Oxyhydrochlorination (OHC) technology utilizes domestic natural gas as a feedstock and thereby provides a reliable, low cost source of CH_3Cl that is independent of methanol. Considerable savings are believed to be achievable *via* the application of this technology.

OHC is a key step in a potential gas-to-liquid fuels process. Currently, two approaches exist for converting natural gas to liquid hydrocarbon fuels, namely the Methanol-To-Gasoline (MTG) and the

Fischer-Tropsch (FT) routes. Both of these processes begin with the production of Synthesis Gas from methane which is a high temperature, endothermic, and costly operation. The OHC process reacts natural gas, oxygen and hydrogen chloride (HCl) in the presence of a specialized catalyst to produce primarily CH_3Cl and some methylene chloride (CH_2Cl_2). These chlorohydrocarbons may then be fed to a fixed bed reactor where they are oligomerized to liquid hydrocarbon fuels (Figure 2)[2]. Data from the Department of Energy's Pittsburgh Energy Technology Center (PETC) show that a mixture of CH_3Cl and CH_2Cl_2 can be converted over ZSM-5 zeolite without undue carbon deposition[3]. Unconverted methane and other light hydrocarbons may be recycled and the HCl recovered, thus improving the economics of the process. Despite the need for special materials of construction, OHC appears to be an attractive alternative to either the MTG or the FT process.

Methyl chloride usage

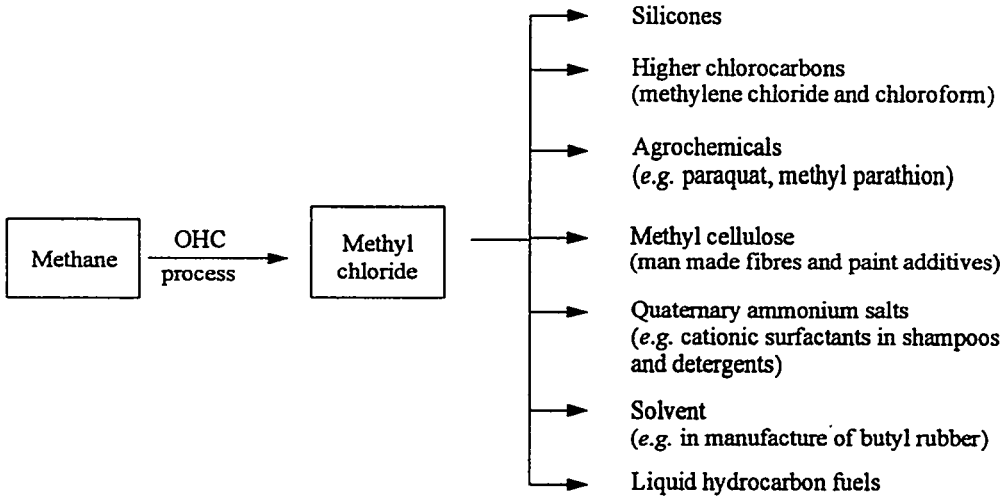

Figure 1.

Gas to liquid fuels process

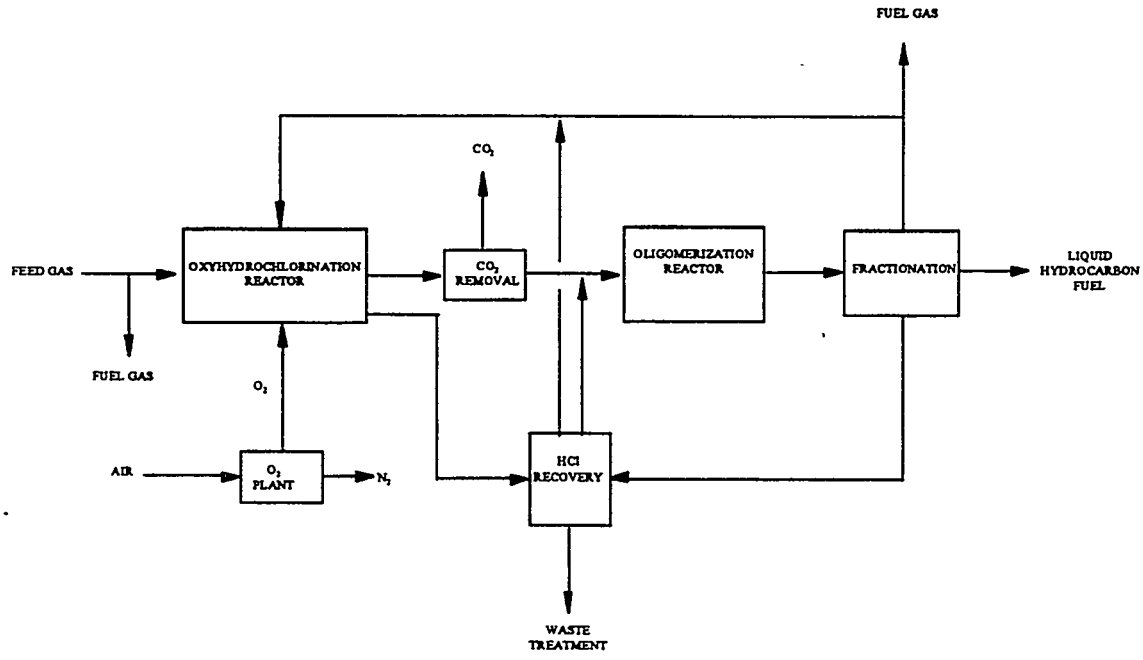

Figure 2.

The activation energy of the primary OHC reaction is 121 $kJmol^{-1}$ (Figure 3) and the overall reaction is highly exothermic with an enthalpy of reaction equal to 157 $kJmol^{-1}$. Secondary chlorination reactions to produce CH_2Cl_2, chloroform ($HCCl_3$) and carbon tetrachloride (CCl_4) also occur with similar activation energies. An additional complication is that methane and chlorinated product can undergo combustion reactions to give carbon monoxide (CO) and carbon dioxide (CO_2). Although the activation energies for these combustion reactions are somewhat higher than for chlorination, the enthalpies of reaction for combustion are significantly higher. Thus, once initiated, the combustion process is difficult to control. Selectivity is a function of temperature, and to minimize undesirable side reactions and maximize CH_3Cl formation, adequate heat transfer and excellent temperature control of the process are essential. Careful selection of the catalyst can also assist in optimizing selectivity.

Oxyhydrochlorination Chemistry

Primary Reaction	ΔE(kJ/Mol)	ΔH(kJ/Mol)
$CH_4 + HCl + 1/2\ O_2 \Longrightarrow CH_3Cl + H_2O$	121	-157
Subsequent Chlorination Reactions		
$CH_3Cl + HCl + 1/2\ O_2 \Longrightarrow CH_2Cl_2 + H_2O$	126	-153
$CH_2Cl_2 + HCl + 1/2\ O_2 \Longrightarrow CHCl_3 + H_2O$	126	-149
$CH_3Cl + HCl + 1/2\ O_2 \Longrightarrow CCl_4 + H_2O$		-142
Combustion Reactions		
$CH_4 + 3/2\ O_2 \Longrightarrow CO + 2\ H_2O$	225	-500
$CH_4 + 2\ O_2 \Longrightarrow CO_2 + 2\ H_2O$	240	-781
$CH_3Cl + O_2 \Longrightarrow CO + H_2O + HCl$	187	-343
$CH_3Cl + 3/2\ O_2 \Longrightarrow CO_2 + H_2O + HCl$	197	-624

Figure 3.

Accomplishments:

The OHC process can be considered as five individual processing steps, *i.e.* (1) natural gas purification and feed, (2) reaction, (3) reactor effluent recovery, (4) HCl recovery, and (5) CH_3Cl purification. The developmental effort associated with this project has been focused primarily on the reaction and reactor effluent recovery since the remaining steps are well understood and routinely operated within Dow Corning.

The construction of a Process Development Unit (PDU) was deemed necessary since adequate heat removal and high gas velocities were not achievable in a smaller lab reactor. Catalyst development studies, however, have continued on a lab scale (see below).

The PDU was built in an existing tower consisting of three 20'x20' floors at Dow Corning's Carrollton, Kentucky manufacturing site. Capital expenditure for the PDU totaled $3.2 million. The PDU utilizes a PC-based Camile data acquisition and process control system comprised of approximately 149 I/O points with intrinsically safe wiring. A schematic of the PDU is shown in Figure 4.

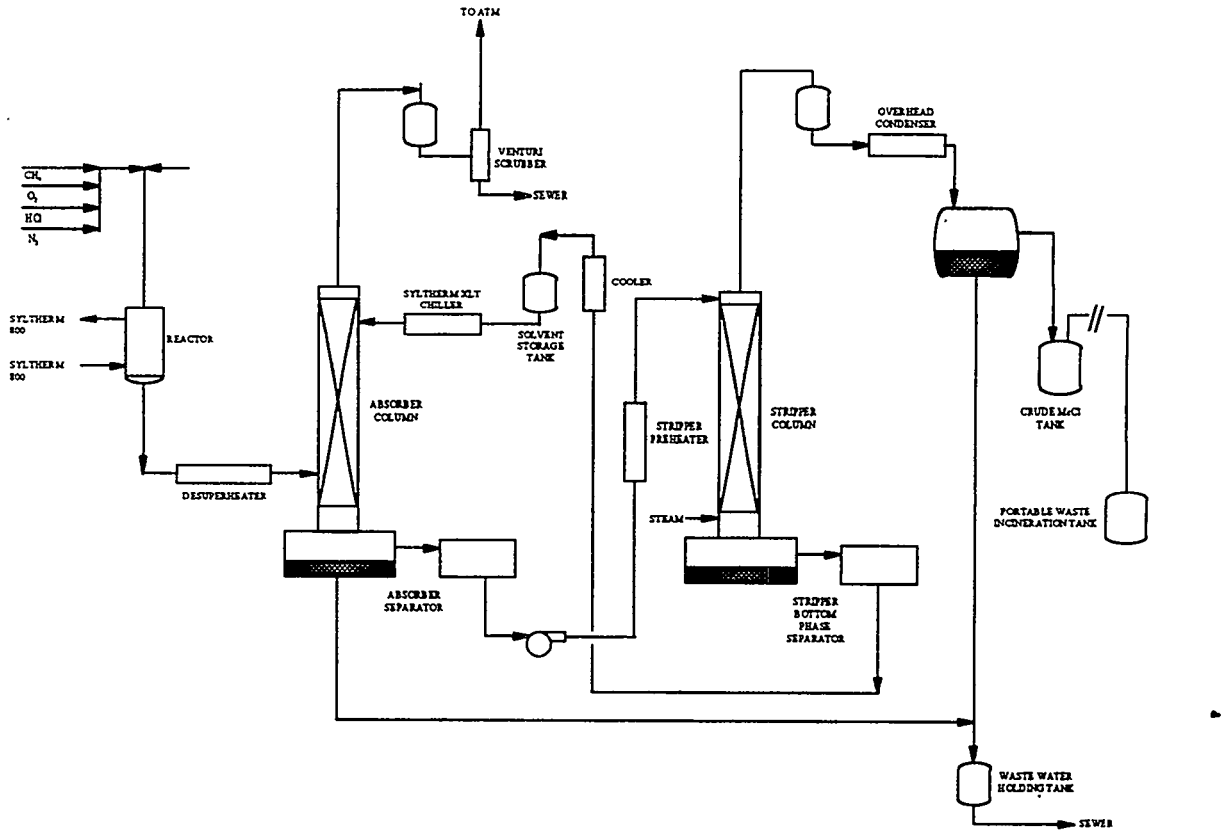

Figure 4.

PDU dimensions

Details of the key process units are summarized in Table 1 below.

Table 1.

Unit	Size/specification	Principal materials of construction
Reactor	Shell and tube design, 19 tubes 0.5"x72"	Hastelloy C
Desuperheater	Shell and tube design, 4 tubes 0.5"x60"	Hastelloy C
Absorber column	4"x120", 3/4" ceramic Intalox packing	Glass-lined
Sylthern® 800 heat exchanger	70 kW heater/ 95,750 BTU/h cooler	Carbon steel
Sylthern® XLT chiller	6 ton chiller	Carbon steel/ Hastelloy C
Stripper column	4"x120", 3/4" ceramic Intalox packing	Glass-lined
Phase separators	Various dimensions	Glass-lined

Reactor Design

In the reactor, methane (CH_4) reacts with HCl and O_2 over a supported metal catalyst at between 280°C and 350°C and 1-50 psig to form CH_3Cl. By-products from the reaction include CH_2Cl_2, H_2O, various combustion products and, to a lesser extent, $CHCl_3$ and CCl_4. A large heat transfer area per volume of catalyst bed is necessary to relieve the exotherms exhibited by the OHC process. Heat transfer coefficients and Aspen™ calculations suggest that a shell and tube reactor design, with catalyst in the tube and Syltherm® 800 heat exchange fluid on the shell side, would be adequate. A reactor containing 19 tubes (0.5" diameter, 72"' long) was constructed with enough heat transfer area to tolerate a heat duty of up to 95,750 Btu/h. The reactor is constructed from Hastelloy C since this material has served well in the lab reactor. The selectivity of the reaction is maximized by (a) limiting the CH_4 conversion to <25%, (b) maintaining high gas velocities which minimize heat and mass transfer limitations and (c) maintaining excess CH_4 in the feed. Excess CH_4 in the reactor feed is also important for maximizing HCl efficiency/conversion. High HCl conversion not only eliminates the need for HCl recovery but also minimizes corrosion problems elsewhere in the PDU.

Reactor Effluent Recovery

Product recovery is difficult given the low conversion of CH_4 and several technologies were initially considered. Membrane separation was discounted on the basis of cost (mainly associated with corrosion resistant compressors) and the lack of a readily available membrane capable of the separation. Pressure swing absorption operating at a high pressure differential would also require expensive compressors and was, therefore, rejected. Absorption and Steam Stripping (AST) appeared to be the best economic approach for product recovery. The advantage of AST over other processes is that it can be operated without high pressure. Reactor effluent is scrubbed in an absorber column with a refrigerated, non-volatile oil in a packed tower where direct contact condensing and gas absorption occurs. The desired recovery is achieved through careful selection of packing height, temperature and L/G ratio. The column operates adiabatically. Absorber bottoms are allowed to separate and the organic phase is fed to the top of the stripper column. Product condensables are removed from the oil with high pressure steam. Regenerated oil exits the stripper, is refrigerated and returned to the absorber column. Stripper overheads, steam, and chlorocarbons are condensed and routed to a second phase separator. The crude chlorocarbons are collected for analysis in the PDU but in a commercial process these would be sent to a distillation column where pure CH_3Cl would be collected overhead while crude methylene chloride would be accumulated in the bottoms. Recovery of >98% CH_3Cl is possible using this absorber/stripper technology.

At the start of this project, AST had not been demonstrated before and an oil with suitable properties had not been identified. Ideally the oil would be non-volatile, acid resistant, possess a high affinity for CH_3Cl, have low viscosity at low temperatures and be thermally stable. It is important that the oil selected has a high affinity for CH_3Cl as this is influential in the determination of L/G, which in turn, has a dramatic impact on the capital cost of the process. Several oils were evaluated before Multitherm™ fluid was selected. Multitherm™ is a hydrogenated dimer of iso-decene (average molecular weight = 272), with a vapor pressure of < 1mm Hg at 21°C. CH_3Cl solubility was found to be approximately 13% by wt. at 0°C and 15 psig. No degradation of the oil was observed after repeated exposure to HCl at elevated temperature.

A study was completed to determine CH_3Cl removal efficiency as a function of CH_3Cl loading on the absorption column. Different ratios of methyl chloride to nitrogen were fed to the column while keeping the total volumetric flow rate constant. Solvent flow rates and system pressure were varied while column temperature was kept constant at 0°C. Table 2 lists % CH_3Cl in the feed, the ratio of liquid to gas mass flow rate (L/G), pressure and associated CH_3Cl removal efficiencies.

Table 2.

% CH_3Cl in feed	L/G	Pressure (psig)	% CH_3Cl removed
10	20	30	80.6
15	20	30	83.9
20	20	30	87.9
25	20	30	93.1
30	20	30	98.5
10	20	40	93.0
15	20	40	93.8
20	20	40	94.9
25	20	40	96.6
30	20	40	96.7
10	30	30	98.9
15	30	30	99.3
20	30	30	99.5
25	30	30	99.6
30	30	30	99.8
35	30	30	99.9
40	30	30	99.9

(Total volumetric flowrate of CH_3Cl and N_2 = 165 ml/min. STP)

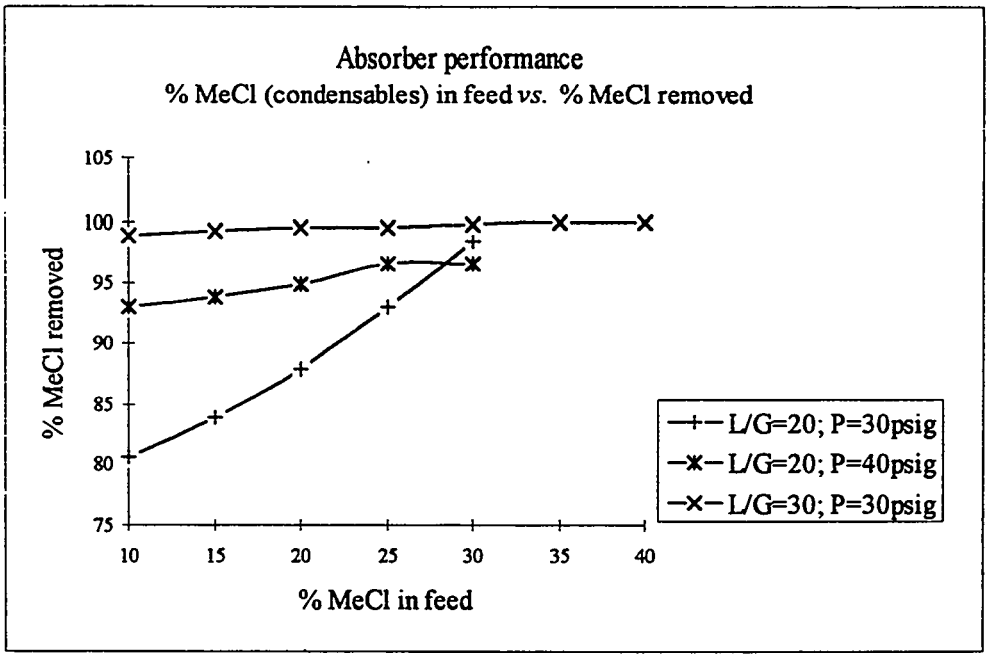

Figure 5.

The data show that, at a given pressure and L/G, more CH_3Cl will be removed by the absorber column as the percentage of CH_3Cl in the feed is increased. An increase in pressure and L/G also facilitates CH_3Cl recovery. Under the conditions used, CH_3Cl condenses and, in effect, the absorber operates both as an absorber and as a direct contact condenser.

Problems were initially encountered when the PDU absorber column was operated at temperatures below 0°C due to water, which is carried over from the solvent storage tank, freezing and blocking the column. Reliable flow is possible, however, with a column temperature of between 5°C and 10°C and CH_3Cl recovery trials were completed to evaluate absorber and stripper performance prior to introducing reactants into the unit.

Pressure Effects

Typically, as pressure is increased, the selectivity of the OHC reaction increases for a given methane conversion. For example, Figure 6 shows a typical set of data for a Cu/La/Li catalyst on an alumina support. The reaction was conducted at 0, 30 and 40 psig and CH_4 conversion was kept constant at approximately 15%. The percentage of CH_3Cl in the product stream increases from 72% to 85% over this pressure range. In order to keep methane conversion constant, the temperature was reduced from 340°C to 310°C as the pressure was increased from 0 psig to 40 psig.

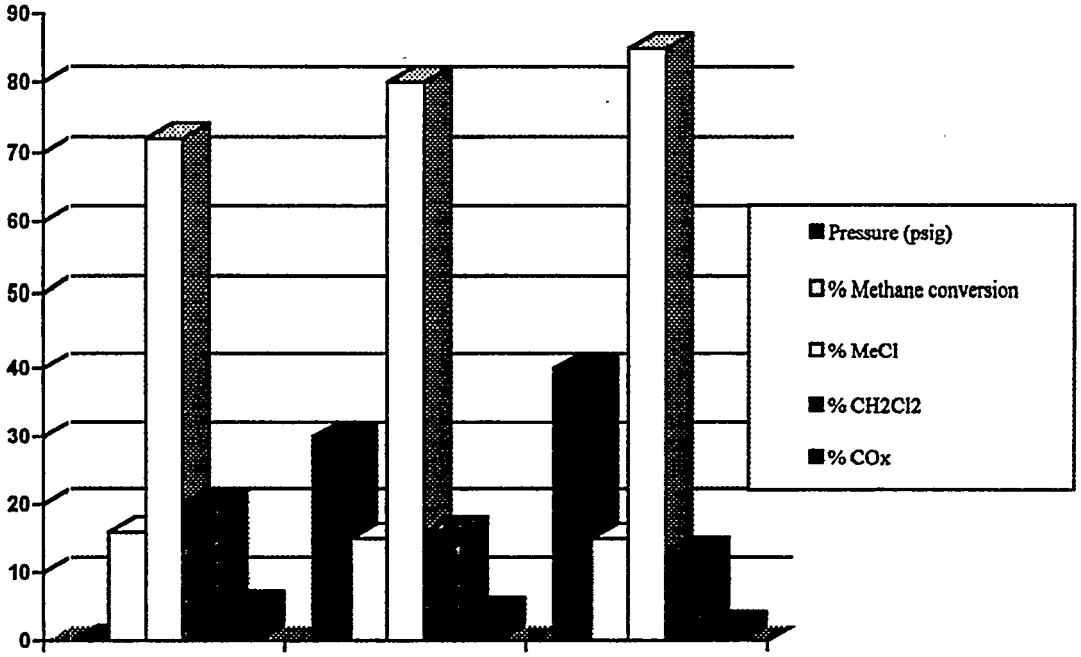

Figure 6.

Temperature Effects

Typically, OHC catalysts display the same pattern of decreased selectivity with increased methane conversion and/or increased temperature. Figure 7 shows a typical set of data for a Cu/La/Li catalyst on an alumina support. As the temperature is increased from 315°C to 340°C, methane conversion increases from 11% to 23%. HCl conversion similarly increases from 34% to 83%. The percentage of CH_3Cl in the product stream, however, decreases from 77% to 57% over this temperature range whereas the amounts of methylene chloride and combustion products increase.

Figures 6 and 7 demonstrate the impact that pressure and temperature have on the OHC reaction. Much of the work that will be performed on the PDU will be aimed at optimizing these process conditions for maximum CH_3Cl production.

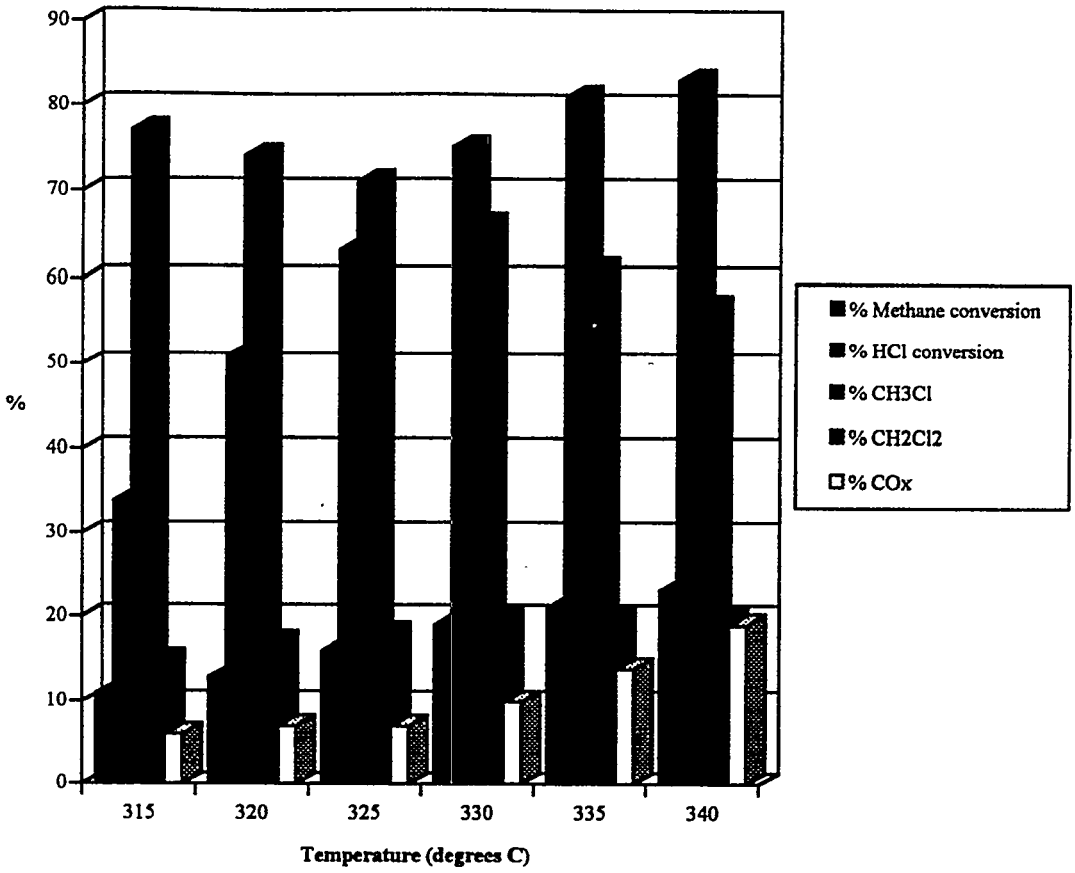

Figure 7.

Catalyst Development

Work in this area has focused upon optimization of metal-support-promoter combinations to enhance selectivity and catalyst activity. Traditionally, catalysts used for OHC chemistry usually contain copper, although iron and cobalt have been reported as being useful[4]. The copper is generally deposited on an oxide support such as silica or alumina. Potassium chloride or lanthanum chloride may be used as promoters in the system. The precursor materials used for the metal deposition, the impregnation technique, and catalyst preparation all have a major impact on the resulting catalyst. Many experiments have been conducted within Dow Corning to explore the effect that metal type, metal loading, temperature, feed ratio, *etc.* have upon catalyst performance. The results obtained have provided much information concerning catalyst performance although studies have been limited in that reactions are mass transfer limited (sufficient gas velocities are not generated in the lab to overcome this) and the reactor is not operating isothermally (insufficient heat transfer capabilities). Future studies on the PDU, which does not suffer these problems, will allow better evaluation of new and existing OHC catalysts.

The mechanism originally suggested by Deacon for oxychlorination involves the following steps :

$$2CuCl_2\ (s) \rightleftharpoons Cu_2Cl_2\ (s) + Cl_2\ (g)$$
$$Cu_2Cl_2\ (s) + 1/2\ O_2\ (g) \rightleftharpoons CuO.CuCl_2\ (s)$$
$$CuO.CuCl_2\ (s) + 2HCl\ (g) \rightleftharpoons 2CuCl_2\ (s) + H_2O\ (g)$$

Scheme 1.

Work by Allen[5] and Ruthven[6] has substantiated this mechanism through various kinetic studies. Kenney[7] reports first order kinetics for O_2 and zero or negative order kinetics for Cl_2 and suggests the following redox mechanism:

$$2Cu^{2+} + 2Cl^- \rightleftharpoons 2Cu^+ + Cl_2 \quad \text{(fast)}$$
$$2Cu^+ + 1/2\ O_2 \rightleftharpoons 2Cu^{2+} + O^{2-} \quad \text{(slow)}$$
$$O^{2-} + 2HCl \rightleftharpoons H_2O + 2Cl^- \quad \text{(fast)}$$

Scheme 2.

In the above reaction scheme, the thermal dissociation of $CuCl_2$ is in equilibrium and the oxidation of CuCl to $CuCl_2$ is rate determining. Figure 8 shows a simple OHC catalyst system formed by impregnation of silica with 2% by wt. $Cu(CH_3CN)_4^+PF_6^-$. At 340°C, the overall activity for this catalyst is low, with methane conversion less than 5%, using a CH_4:O_2:HCl reaction stoichiometry of 4:1:1.3. This is well below the desired CH_4 conversion of 20%.

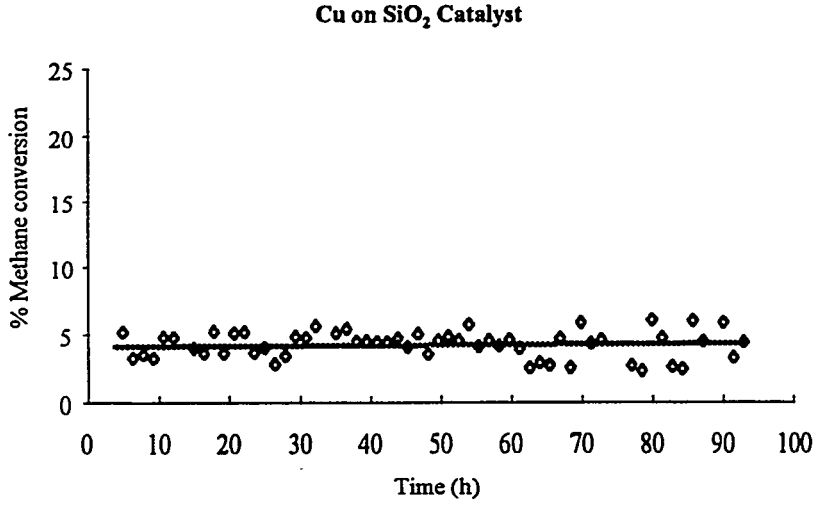

Figure 8.

By adding lanthanum chloride as a promoter, catalyst activity can be dramatically increased from below 5% to approximately 20% CH_4 conversion (Figure 9). Unfortunately, over a 200 h. period catalyst activity declines to less than half of the original activity. The conditions employed were identical to those used in Figure 8. The enhanced reactivity is thought to be due to the acceleration of the rate-controlling oxidation of the Cu^+ species in the mechanism described above. The addition of $LaCl_3$ raises the pre-exponential factor in the rate constant without affecting the activation energy. It is also possible that the lanthanum competes effectively with copper for available chloride, thereby releasing more copper for oxychlorination.

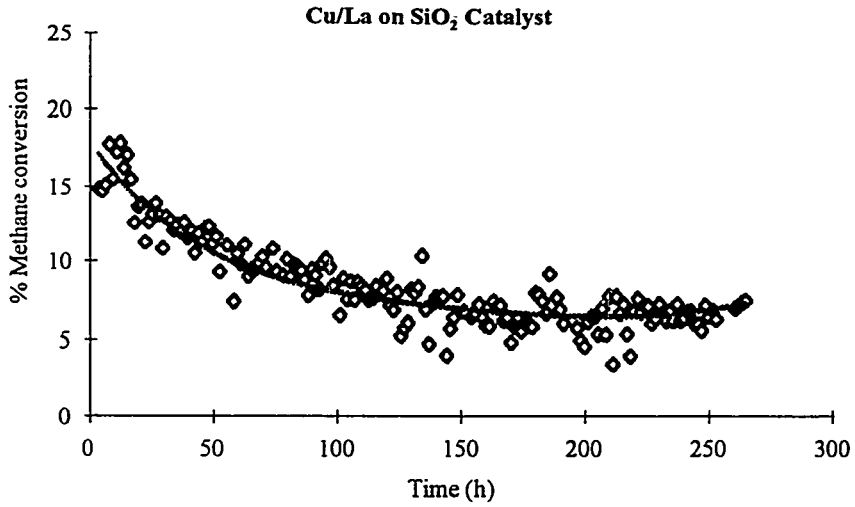

Figure 9.

Figure 10 shows the impact of adding a lithium promoter to the copper catalyst using the same conditions as described above. In this case, catalyst activity is increased to around 10% CH_4 conversion. Again, over a 200 h. period, catalyst activity decreases to half the original value. Non-dissociated CuCl or Cu_2Cl_2 are both volatile and not readily oxidized. The formation of these species can account for low reactivity and poor catalyst stability. Villadsen[8] has reported that upon addition of KCl to copper chloride-based OHC catalysts, cuprous complexes with the following structure are formed :

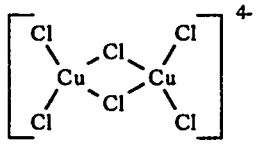

These species are readily oxidized to the oxygen-bridged analogue, which in turn, reacts with HCl to form $(Cu_2Cl_6)^{2-}$ and/or $(CuCl_4)^{2-}$ complexes. These complexes may be reduced to Cu^+ with concomitant evolution of chlorine, thus bringing greater reactivity to the system. Figure 10 suggests that similar behavior is observed with LiCl. Catalyst stability, however, is still clearly an issue in this case.

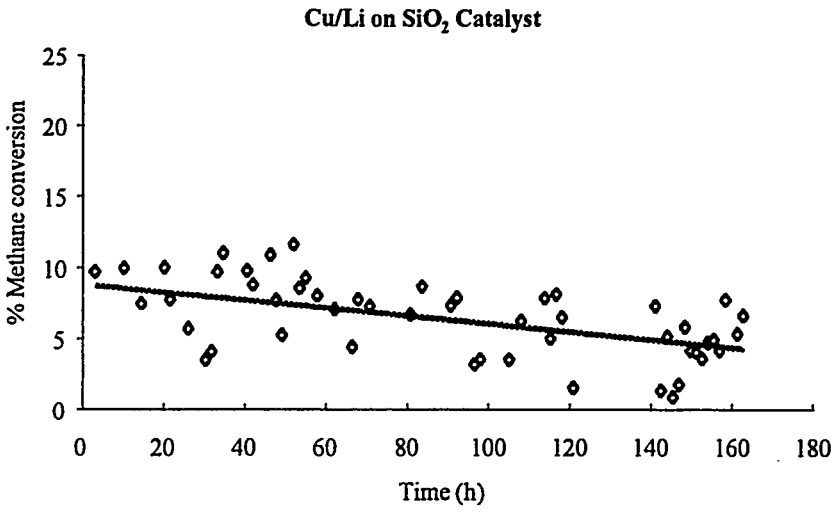

Figure 10.

The best results are obtained when all three metals, *i.e.* Cu, La and Li are present (Figure 11). Such a catalyst shows almost 20% CH_4 conversion and has greater stability than Cu/La alone (Figure 9). $LaCl_3$ is expensive and to reduce the overall cost of the catalyst, a mixed lanthanide starting material was subsequently used without adversely affecting performance.

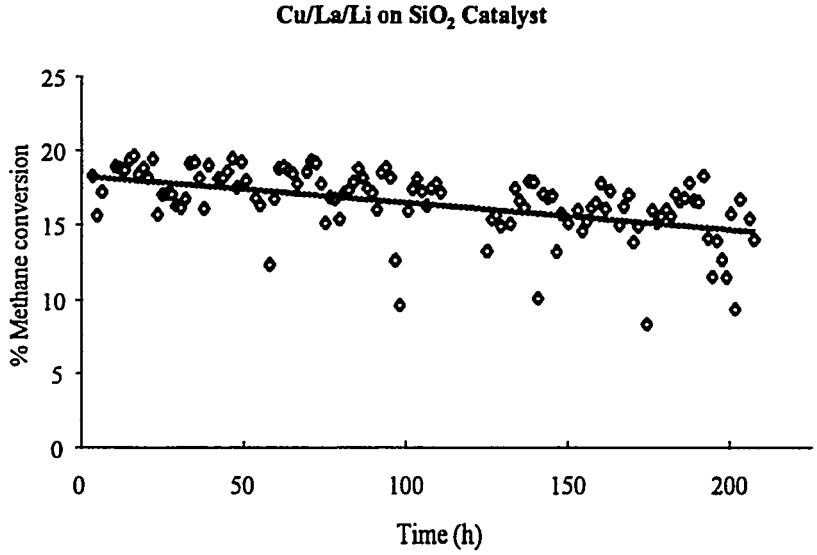

Figure 11.

Support Effects

Results have shown that catalysts made using alumina as the support exhibit greater stability compared to silica analogues (Figures 11 and 12) due to the stronger interaction between copper and alumina[9]. Pre- and post-reaction catalysts were characterized to determine chemical and physical properties. The principle techniques used were BET surface area measurements; thermal gravimetric analysis (TGA) to determine volatility and thermal stability; X-ray photoemission spectroscopy (XPS) to determine the chemical state of the metal loading; Scanning Auger spectroscopy (SAM) to map compositional gradients

of the elements on the catalyst surface; Scanning Electron Microscopy (SEM) to determine microscopic morphology of metal crystallites and X-ray diffraction measurements (XRD) to determine the extent of crystallinity. SEM clearly showed a difference between an alumina- and a silica-supported catalyst. Micrographs for the alumina system showed little or no change in metal distribution before and after reaction whereas the silica analogue showed significant crystallite growth on the surface after reaction. At OHC reaction temperatures, the catalyst is not held strongly to the silica surface and migration of the metal through the bed takes place, resulting in reduced catalyst life. The catalyst illustrated in Figure 14 represents the best performance achieved to date and is the catalyst that will be used in extended PDU trials.

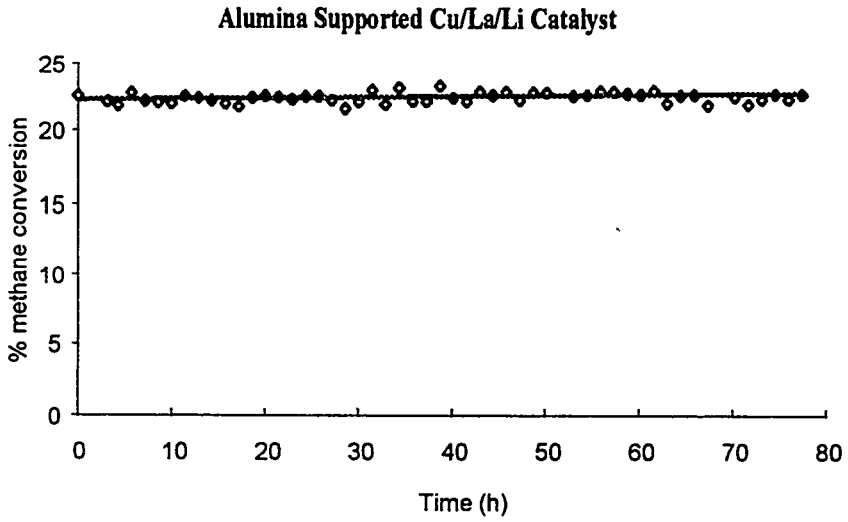

Figure 14.

It should be noted that catalyst support also affects the selectivity of the reaction. As already mentioned, selectivity toward CH_3Cl tends to decrease as CH_4 conversion increases. Figure 13 shows data collected for two catalysts which are identical in all respects except for the nature of the support. For a given conversion, the alumina-supported catalyst shows a higher percentage of oxygenates in the product stream.

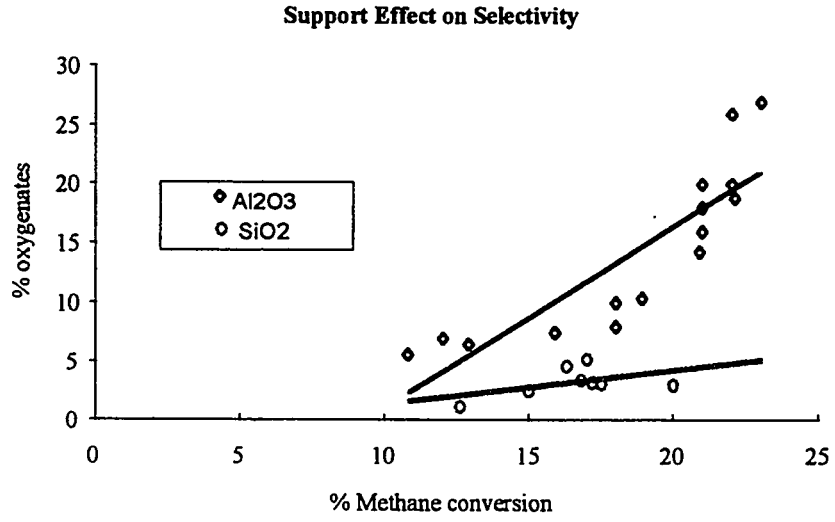

Figure 13.

The data presented above were generated using pure methane as the feed to the OHC reactor. The PDU and the lab reactor are currently using natural gas, which contains up to 4% of higher alkanes, as the feed. In this case, many more by-products are possible and catalyst performance is significantly changed. Studies are in progress to fully understand this system.

Conclusions :

Process Engineering

- OHC technology demonstrated in laboratory has been successfully taken to PDU scale
- Construction of the PDU has been completed
- The system has been successfully operated at pressure
- The Syltherm® 800 and Syltherm® XLT chiller systems have been fully tested
- The Solvent loop and hydraulics have been tested
- Absorber/stripper hydraulics have been evaluated
- CH_3Cl recovery runs have been successfully completed
- The FTIR on-line analyzer has been installed and commissioned
- The best catalyst to date has been identified, manufactured and loaded into the PDU
- The PDU has been successfully started up
- CH_3Cl has been produced and recovered in the PDU

Catalyst Development

- A catalyst containing Cu, La, and Li has been developed which shows good reactivity, selectivity and stability
- Cu is essential for catalysis but La and Li enhance reactivity
- An alumina support gives greater catalyst stability than silica but selectivity is reduced somewhat

The technology described herein is the subject of two patent applications.

Future work :

Much additional work remains to be done to render this technology commercially viable. On the PDU, designed experimentation will be used to optimize process conditions for maximum CH_4 conversion, CH_3Cl selectivity and CH_3Cl recovery. The effects of corrosion will also have to be closely monitored and, where possible, eliminated. Extended reaction runs are planned to determine catalyst lifetime under process conditions. The economics of the process will be determined once mass balances and operating costs are fully understood. Finally, the effects of operating the PDU using natural gas as opposed to pure methane will be examined.

As far as the catalyst is concerned, further studies of promoter and support effects are underway. It is also hoped that through a more detailed and sophisticated characterization of various OHC catalysts that a better understanding of the mechanism can be obtained.

Acknowledgments :

The authors would like to thank Bruce Crum (Catalyst development), Mike Diaz, Jeff Hale, Jay Hein, Scott Kleman, Cory Knutson, and Keith Toole (PDU start-up team).

This project was partially funded by the DoE, GRI and Texas Gas.

References:

1) The Freedonia Group, Inc., October 1993.
2) J.M. Fox, T.P Chen, and B.D. Degen, *Chem. Eng. Prog.*, 1990, **86**,42.
3) R.D. Srivastava, P. Zhou, G.J. Stiegel, V.U.S. Rao, and G. Cinquegrane, in "Catalysis", Ed. J.J. Spivey, *The Royal Society of Chemistry, Cambridge*, Volume 9, 1992.
4) C.E. Taylor and R.P. Noceti, *Proc. Int. Cong. Cat.*, 1988, **2**, 990.
5) J.A. Allen and A.J. Clark, *J. Appl. Chem. (London)*, 1966, **16**, 327.
6) D.M. Ruthven and C.N. Kenney, *Chem. Eng. Sci.*, 1968, **23**, 981.
7) C.N. Kenney, *Catal. Rev. Sci. Eng.*, 1975, **11**(2), 197.
8) J. Villadsen and H. Livbjerg, *Catal. Rev. Sci. Eng.*, 1978, **17**(2), 203.
9) E.M. Fortini, C.L. Garcia, and D.E. Resasco, *J. Catal.*, 1986, **99**, 12.

1995 COAL LIQUEFACTION AND GAS CONVERSION CONTRACTORS REVIEW CONFERENCE

TITLE: GASOLINE FROM NATURAL GAS BY SULFUR PROCESSING

PI(AUTHORS): **Erek J. Erekson**
Frank Q. Miao

INSTITUTION/ORGANIZATION: **Institute of Gas Technology**
1700 S. Mount Prospect Road
Des Plaines, IL 60018-1804

CONTRACT NO.: DE-AC22-93PC92114

PERIOD OF PERFORMANCE: **June 24, 1993 to June 23, 1996**

OBJECTIVE:

The overall objective of this research project is to develop a catalytic process to convert natural gas to liquid transportation fuels. The process, called the HSM (Hydrogen Sulfide-Methane) Process, consists of two steps that each utilize a catalyst and sulfur-containing intermediates: 1) converting natural gas to CS_2 and 2) converting CS_2 to gasoline-range liquids. Experimental data will be generated to facilitate evaluation of the overall commercial viability of the process.

ACCOMPLISHMENTS & CONCLUSIONS

Catalysts have been found that convert methane to carbon disulfide in yields up to 98%. This exceeds our target of 40% yields for the first step. The best rate for CS_2 formation was 132 g CS_2/kg-cat-h. The best rate for hydrogen production is 220 L H_2 /kg-cat-h. A preliminary economic study shows that in a refinery application hydrogen made by the HSM technology would cost $0.25-$1.00/1000 SCF.

INTRODUCTION

Natural gas is an abundant resource in various parts of the world. The major component of natural gas is methane, often comprising over 90% of the hydrocarbon fraction of the gas. The expanded use of natural gas as fuel is often hampered because of difficulties in storage and handling a gaseous fuel. This is especially true for natural gas in remote areas such as the north slope of Alaska. It is desirable to convert natural gas to more valuable liquids. The successful implementation of this process would decrease dependence on imported oil for transportation fuels.

There are two commercialized methods for converting natural gas to gasoline range liquids.

1) Fischer-Tropsch synthesis
2) Mobil's MTG process.

Each has two basic steps:

1. Removal of sulfur compounds (H_2S, COS and mercaptans with sulfur adsorbing guard beds to prevent breakthrough of sulfur to the catalysts).
2. Steam reforming to make synthesis gas which requires 2 moles of superheated steam for every mole of methane.

In Fischer-Tropsch synthesis, the third step is the conversion of synthesis gas to hydrocarbons. In Mobil's MTG process, the third step is methanol synthesis and an additional step of methanol conversion to gasoline liquids is required. The commercial steps listed above; i.e., steam reforming, methanol synthesis, or Fischer Tropsch synthesis, require the removal of sulfur compounds present in natural gas down to less than 0.1 ppm. This additional gas clean-up step means extra cost, but it is necessary because the catalysts are quickly poisoned by sulfur compounds.

IGT is developing the HSM Process, a two-step process that uses H_2S as a reactant to convert natural gas to gasoline-range liquids. Sulfur, which has been considered as a poison, is used as a reactant in the HSM process. This process of methane conversion utilizes H_2S to convert methane to CS_2. Then CS_2 plus hydrogen can be catalytically converted to gasoline range hydrocarbons. All of the H_2S generated during the CS_2 to gasoline reaction is recycled. This

process does not require steam reforming nor the manufacture of hydrogen. This process is actually a net producer of hydrogen.

There are two main reactions involved in this process:

$$1) \quad CH_4 + 2\,H_2S \rightarrow CS_2 + 4\,H_2 \qquad (1)$$

$$2) \quad CS_2 + 3\,H_2 \rightarrow [\text{-}CH_2\text{-}] + 2\,H_2S \qquad (2)$$

The process is a net H_2 producer, and H_2S is recycled. So the overall process would be:

$$3) \quad CH_4 \rightarrow [\text{-}CH_2\text{-}] + H_2 \qquad (3)$$

As we began this project, we found no other references to catalysts for the methane-hydrogen sulfide. The second reaction has been demonstrated by researchers at Mobil Corporation[1] and will be studied during this project. A schematic diagram of the process is shown in Figure 1.

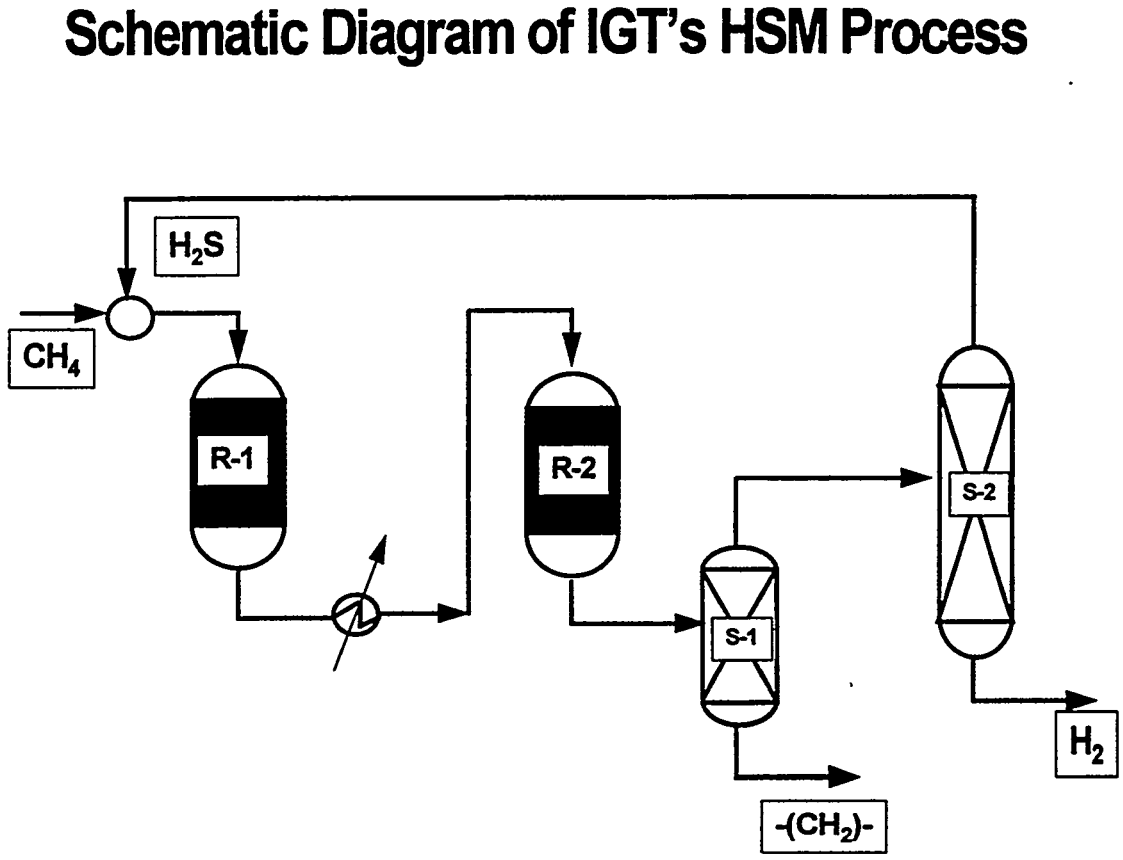

Figure 1. SCHEMATIC DIAGRAM OF HSM(HYDROGEN SULFIDE-METHANE)PROCESS

EXPERIMENTAL

Figure 2 shows the schematic diagram of catalysis reactor system. The feed gas hydrogen sulfide, nitrogen and methane flow rates are controlled by mass flow controllers(Brooks Instruments 5850). The gas flow rates are calibrated by a dry test meter(SINGER, American Meter Company). The gas from mass flow controllers are mixed before flowing into a custom made quartz adapter. There are two openings in the adapter. One is for mixed feed gas; the other is for a ceramic thermowell. The feed gas flows through the adapter into 42 inch long, 22 mm I.D. by 25 mm O.D. quartz reactor. The joint which connects with adapter and quartz reactor were sealed by TFE sleeve. There are three indents around quartz reactor at 26 inch from the top. The catalyst is held above the indents. The temperature of catalyst reactor were measured by a type R high temperature thermocouple which protected by 1/4 inch O.D. ceramic thermowell. The heat was provided by a 2 inch I.D. 32 inch long split tube high temperature furnace with maximum temperature 1540 °C. (Series 3420, APPLIED TEST SYSTEMS, Inc.). The product gas from the catalyst reactor flows into a condenser. The condenser is placed into an ice bath. There is a sample point just after the reactor before the condenser. Gases are analyzed by GC. Before going to the vent gases are scrubbed by a solution of 6M Sodium hydroxide and 30% Hydrogen peroxide. The total product gas flow rate was measured by a wet test meter(Precision Scientific Co.) before being release into the vent system.

Gas samples were analyzed by Gas Chromatograph (HP5890) with a thermal conductivity detector (TCD) and a flame photometric sulfur detector (FPD). A 1/8-inch diameter 10-ft long HayeSep C 80/100 column(SUPELCO Inc.) was used for gas separation. In order to measure hydrogen in the TCD detector, Argon was used as the carrier gas.

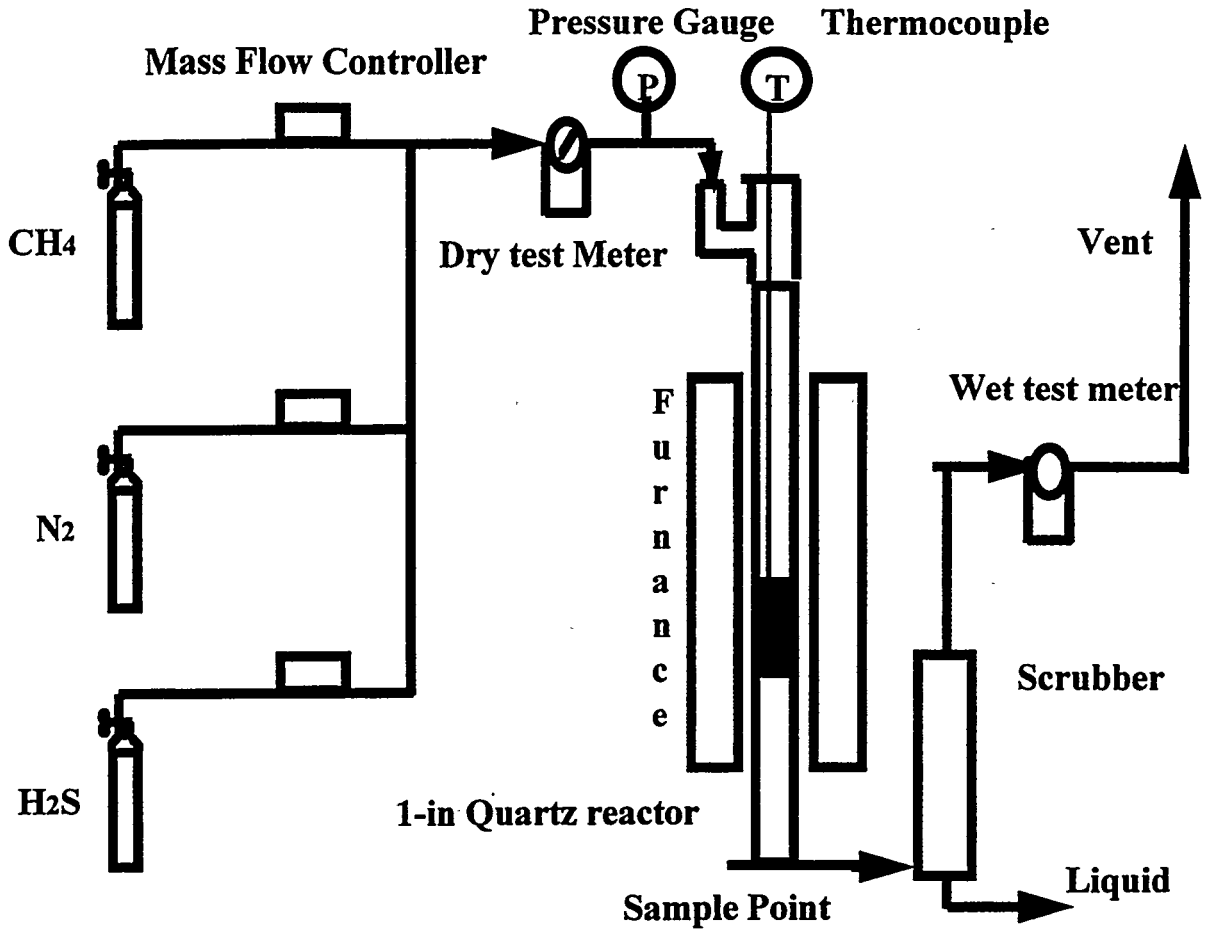

Figure 2. SCHEMATIC DIAGRAM OF EXPERIMENTAL TEST UNIT

RESULTS AND DISCUSSION

Task 1. Catalyst Preparation (SMP Funded)

The purpose of this task is to prepare the catalysts according to both conventional and IGT proprietary methods for evaluation in the reactions studied in Tasks 2 through 5. Ten batches of sulfur processing catalysts have been prepared.

Task 2. Experimental Studies of the H_2S Decomposition Reaction

This Task was completed before the last review meeting. The purpose of this task is to evaluate catalysts for the following reaction:

$$2\,H_2S \rightarrow S_2 + 2H_2 \qquad (4)$$

Catalysts that have activity for this reaction will likely have good activity for reaction 1. We used this reaction as an indicator for screening catalysts for Task 4.

Task 3. Carbon Deposition Studies

This task was completed before the last review meeting. As we develop a catalyst for the conversion of $CH_4 + H_2S$, we want a catalyst that does not become deactivated by carbon deposition. In the temperature range that we will be testing, carbon formation is thermodynamically possible. We designed a group of tests to see if some carbon deposition occurred, whether the catalyst can be regenerated, and whether CS_2 would be formed from the carbon on the catalyst surface. The catalysts that performed well in being regenerated after carbon deposition also performed well in Task 4, the production of CS_2 and hydrogen.

Task 4. Experimental Studies of the Methane/Hydrogen Sulfide Reaction

The objective of this task is to develop a group of catalysts for the direct conversion of methane and hydrogen sulfide to carbon disulfide and hydrogen. The task is divided into two parts. During the first part, ten catalysts were prepared and evaluated. A group of the best catalysts will be identified. The optimum operating conditions will also be determined. In the second part of this task, the most promising catalysts will be tested under the best operating conditions for sustained periods of time.

A group of ten catalysts have been evaluated in over 155 runs. The best catalysts for producing CS_2 are shown in Figures 3 and 4. The best conditions for CS_2 yields are an H_2S/CH_4 ratio of 4, temperature 1100°C, and a residence time of 1.2 seconds. These runs used a nitrogen diluent.

We evaluated catalyst IGT-MS-103 for sustained activity. The results of an 8 hour sustained run are shown in Figure 5. There is no indication of deactivation during this run.

Catalyst IGT-MS-105 also showed high yields of CS_2. This catalyst will also be tested for sustained catalyst activity.

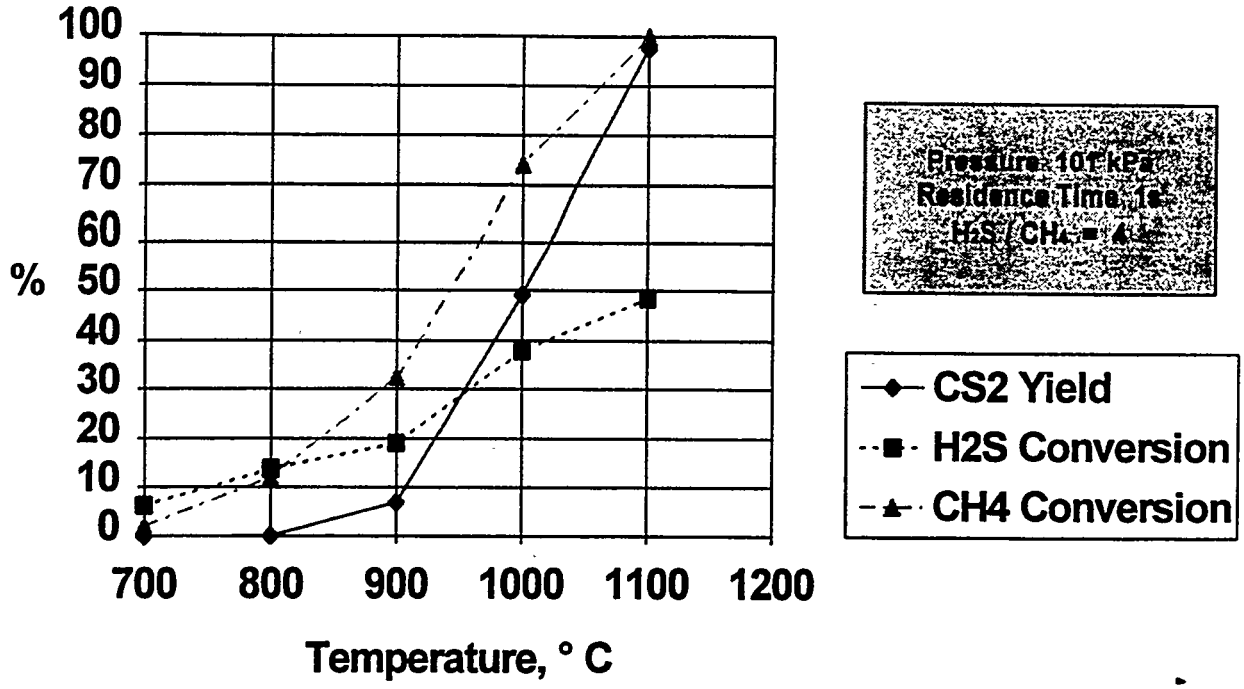

Figure 3. CS_2 YIELDS AND REACTANT CONVERSION FOR IGT-MS-103

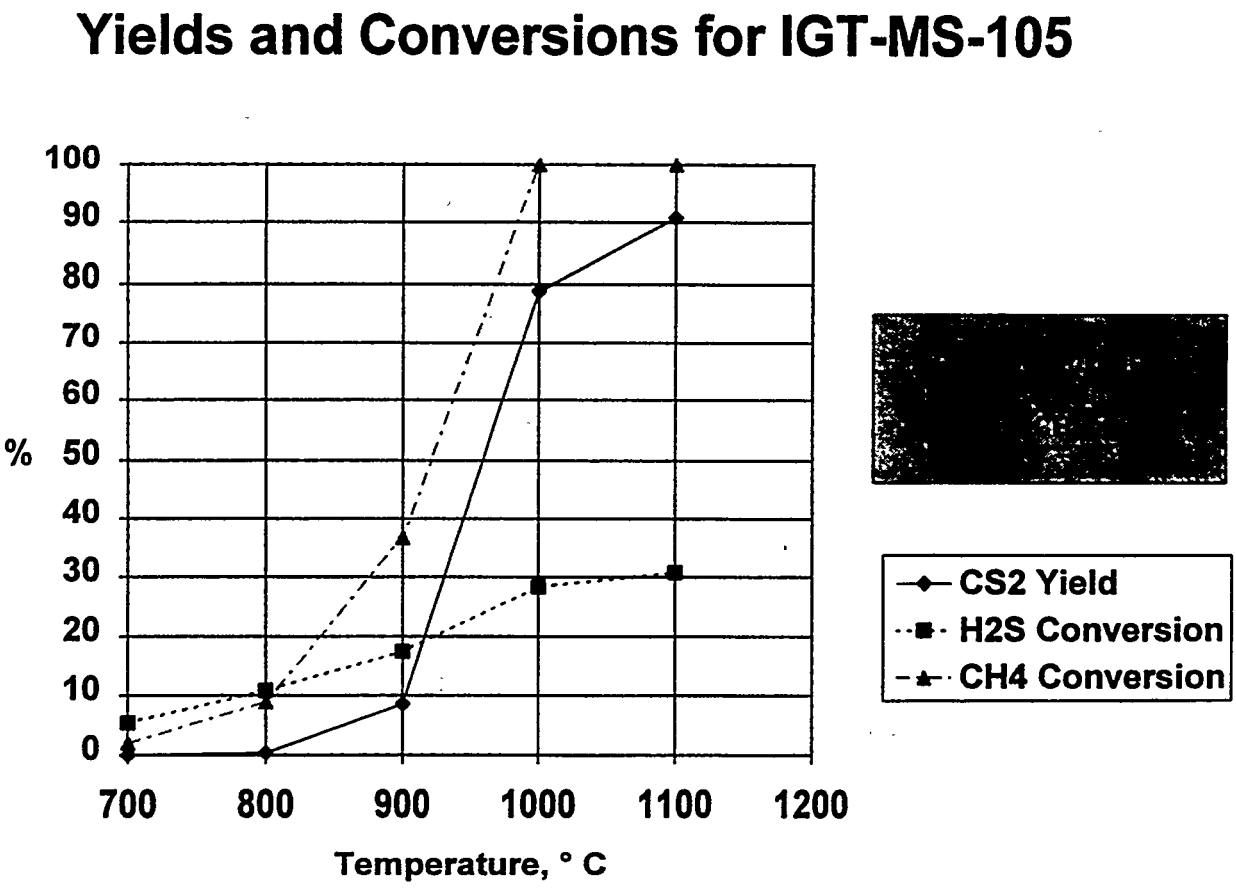

Figure 4. CS_2 YIELDS AND REACTANT CONVERSION FOR IGT-MS-105

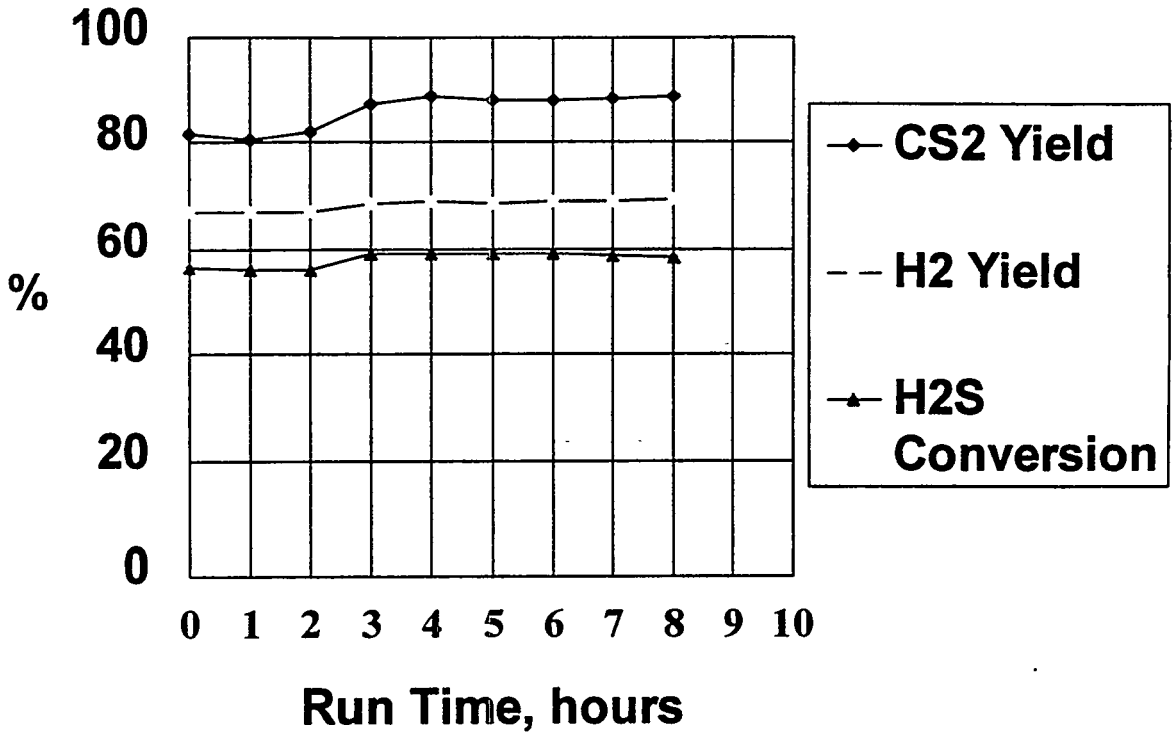

Figure 5. CS_2 AND H_2 YIELDS AND H_2S CONVERSION FOR EXTENDED RUN

In addition to using the HSM process for making gasoline range liquids, we have been investigating the use of reaction 1 alone for use in a refinery situation where H_2 is valuable and H_2S is converted to sulfur in a Claus unit. Reaction 1 would use methane, but it would convert H_2S into hydrogen and a sulfur compound that can be used as a feedstock for sulfuric acid. We have performed a preliminary economic evaluation that shows that hydrogen produced by the HSM technology would cost \$0.25 to \$1.00/ 1000 SCF depending on the price of CS_2. These results are encouraging, and we will be investigating this potential application further.

Task 5. Experimental Studies of CS_2 to Liquid Hydrocarbons

Under this task, a group of catalysts will be developed for the reaction:

$$CS_2 + 3H_2 \rightarrow -[CH_2]- + 2\,H_2S$$

The optimum operating conditions will be determined. The best catalyst will be tested in relatively long duration time to determine catalyst's long-term activity, stability as well as selectivity for above reaction. Work in this task is planned.

Task 6. Proof-of-Concept Testing

For this task, the best catalysts from Task 4 and the best catalysts from Task 5 will be tested in combination to demonstrate that these two steps can be used in combination to make gasoline range liquids from methane. Work in this task will begin after completing Task 4.

FUTURE PLANS

Catalysts will be tested in Task 4 for activity with a refinery type H_2S stream. Such a stream would be coming from an acid gas removal unit and would contain significant amounts of CO_2. The goal here is to see if these catalysts can achieve high conversion of $H_2S + CH_4$ to hydrogen. We will be evaluating this process for application in a refinery situation. We also plan to search for more active and selective CS_2 hydrogenation catalysts. A demonstration of both steps is planned as part of this project.

ACKNOWLEDGMENT

This work was supported by the U.S. Department of Energy, Pittsburgh Energy Technology Center, Pittsburgh, Pennsylvania under Contact No. DE-AC22-93PC92114, and IGT's Sustaining Members Program(SMP), Project #80023.

REFERENCES

1. C.D.Chang, US patent #4,543,434, Sep.24, 1985

PHOTOCATALYTIC CONVERSION OF METHANE TO METHANOL

Charles E. Taylor, Richard P. Noceti, and Joseph R. D'Este
U.S. Department of Energy
Pittsburgh Energy Technology Center
P.O. Box 10940
Pittsburgh, PA 15236-0940

INTRODUCTION

Methane is produced as a by-product of coal gasification. Depending upon reactor design and operating conditions, up to 18% of total gasifier product may be methane. In addition, there are vast proven reserves of geologic methane in the world. Unfortunately, a large fraction of these reserves are in regions where there is little local demand for methane and it is not economically feasible to transport it to a market. There is a global research effort under way in academia, industry, and government to find methods to convert methane to useful, more readily transportable and storable materials. Methanol, the initial product of methane oxidation, is a desirable product of conversion because it retains much of the original energy of the methane while satisfying transportation and storage requirements. A liquid at room temperature, methanol could be transported to market utilizing the existing petroleum pipeline and tanker network and distribution infrastructure. Methanol may be used directly as a fuel or may be converted to other valuable products (*i.e.,* other transportation fuels, fuel additives, or chemicals). Currently, the direct oxidation of methane to methanol suffers from low methane conversion and poor methanol selectivity. A process for the direct oxidation of methane to methanol, in high yield and with high selectivity, is desirable.

Investigation of direct conversion of methane to transportation fuels has been an ongoing effort at PETC for over 10 years. One of our current areas of research is the conversion of methane to methanol, under mild conditions, using light, water, and a semiconductor photocatalyst. The use of three relatively abundant and inexpensive reactants, light, water, and methane, to produce methanol, is attractive. Research in our laboratory is directed toward applying the techniques developed for the photocatalytic splitting of water[1,2] and the photochemical conversion of methane.[3,4]

OBJECTIVE

A long-term goal of our research group is the exploration of novel pathways for the direct oxidation of methane to liquid fuels, chemicals, and intermediates. The use of three relatively abundant and inexpensive reactants, light, water, and methane, to produce methanol is attractive. The products of reaction, methanol and hydrogen, are both commercially desirable, methanol being used as is or converted to a variety of other chemicals, and the hydrogen could be utilized in petroleum and/or chemical manufacturing.

BACKGROUND

It has been reported that methane may be converted to methanol, in a strictly photochemical reaction, by first sparging it through a heated (~90°C) water bath in order to saturate it with water vapor and then exposing it to ultraviolet light at a wavelength of 185 nm in a quartz photochemical reactor. The proposed reaction pathway, shown in Scheme 1, suggests initial production of hydroxyl radical. This radical may then react with a methane molecule to produce methyl radical. In the preferred reaction, the methyl radical then reacts with another water molecule to produce methanol and hydrogen.

Catalytic photolysis of water to hydrogen and oxygen occurs during irradiation of liquid water with visible light at wavelengths longer than 410 nm in the presence of an insoluble solid (Scheme 2).[3] The photolysis sequence of interest initially produces a hydroxyl radical through the reaction of water in the presence of a doped tungsten oxide photocatalyst and an electron transfer molecule, methyl viologen dichloride hydrate. The proposed mechanism invokes the coupling of two hydroxyl radicals to form hydrogen peroxide, which then decomposes to hydrogen and oxygen.

By combining these reactions, it should be possible to react hydroxyl radicals, generated with the photocatalyst and electron transfer reagent, with methane to produce methyl radicals. In our proposed reaction pathway (Scheme 3), methyl radicals react with an additional water molecule to form methanol and hydrogen.

Previous research by our group has confirmed literature reports[1,2] that it is possible to photolyze methane, saturated with water vapor, to produce methanol and hydrogen. In a modification of the above experiment, we were also able to photolyze methane sparged through a photochemical reactor filled with water. Recently, we began investigating the photocatalytic conversion of methane in water.

EXPERIMENTAL

The reactor, a commercially supplied quartz photochemical reaction vessel, was fitted to meet the needs of this research (Figure 1). This included use of a Teflon-coated magnetic stirring bar in the reactor, a fritted glass sparger, a nitrogen line used to cool the UV lamp, and an injection port. Deionized water was distilled prior to use.

The semiconductor photocatalysts were synthesized following a modification of the procedure in the literature[4]. Four dopants, copper, lanthanum, platinum, and a mixture of copper and lanthanum, were selected for study. After sintering, the catalyst is suspended, by mechanical stirring, in water (~750 mL) containing an electron-transfer reagent, methyl viologen dichloride hydrate. A mixture of methane (5 mL/min) and helium (16 mL/min) is sparged through the photocatalytic reactor. Helium is used as an internal standard for on-line analysis of the reactor effluent. Temperature of the reaction is maintained at ~94°C by circulation of heated (~120°C) silicon oil in the outer jacket of the reactor. Irradiation is accomplished by a high-pressure mercury-vapor quartz lamp. The spectral characteristics and energy output of the lamp are displayed in Figure 2. The

outer surface of the lamp is cooled by a stream of nitrogen gas, while the lamp's immersion well is cooled by a flow of tap water. The gaseous products of reaction are analyzed on-line and in real-time by a quadrupole mass spectrometer. Liquid products are condensed from the gas stream at 0°C and analyzed by gas chromatography.

RESULTS

The first series of experiments were conducted with no catalyst in the reactor. During these experiments, an unexpected temperature dependance of the reaction was observed; photoconversion of methane decreased sharply with temperature and was not observed below ~70°C (Figure 3). Several experiments were performed where the temperature of the reactor was allowed to cycle between 60°C and 95°C. In all experiments, as the temperature of the reactor decreased, conversions of methane and the production of methanol decreased. The effect was reversible; when the reactor temperature increased above ~70°C, conversion of methane and the production of methanol increased.

The drop in reactor temperature in the above experiments was a result of the cooling water for UV lamp overpowering the capacity of the external circulating heater. The cooling water, supplied from the tap, is circulated through the UV lamp immersion jacket. When the UV lamp is turned on, the cooling water flow also begins, removing heat from the lamp and, unavoidably, the reactor, resulting in relatively large temperature excursions. Replacement of the heater with one of larger capacity, addition of a nitrogen cooling line, and a decrease in water flow permitted control of temperature to within 1°C throughout the reaction.

Four doped tungsten oxide catalysts were synthesized and used in this study. The catalysts were analyzed by scanning electron microscopy (SEM), energy dispersion spectroscopy (EDS), x-ray diffraction (XRD), and electron spectroscopy for chemical analysis (ESCA). For all catalysts except the platinum-doped tungsten oxide, these techniques were not able to detect any differences between the tungsten oxide as received and the unsintered-doped oxide because the level of doping, ~4 atom percent, is below the detection limits of these instruments. The sintering process produced differences that were detectable by SEM and XRD. After sintering, XRD data show the doped tungsten oxides to be more crystalline than the unsintered materials as evidenced by the separation of a broad diffraction peak into two separate peaks having 2-theta values of 28.8° and 42.0° (Figure 4). Analysis of the sintered, doped tungsten oxides by SEM revealed that the sintered materials contained larger crystallites with smoother edges.

SEM and EDS analysis of the platinum-doped tungsten oxide photocatalyst after sintering showed the presence of platinum particles on the surface of the tungsten oxide. Figure 5 is a "back-scatter" photomicrograph of the sintered, platinum-doped tungsten oxide photocatalyst (the bright spheres are platinum). Analysis of the sintered platinum-doped tungsten oxide by ESCA (Figure 6) revealed that the platinum on the surface is Pt^0.

The catalysts were tested for their ability to catalytically photolyze water prior to their use in the methane conversion experiments. We were able to reproduce photolysis results reported in the literature[4] using these catalysts under similar conditions.

Figure 7 shows the results of an typical photocatalytic methane conversion experiment. Methane conversions are ~4% with hydrogen and methanol as the main products of reaction. Gas chromatographic analysis (Figure 8) of the liquid product, condensed at 0°C, revealed the presence of methanol and acetic acid. The peak at 41.854 minutes in the GC trace was not able to be identified. Further analysis, in an attempt to identify the component by GC-MS, was not possible due to the low concentration of products in the trap. The products were diluted by water carried over from the reactor by the helium that is used as an internal standard.

As noted previously, the proposed reaction sequence of interest initially produces hydroxyl radical which then reacts to produce methanol. To test the validity of this sequence, a 30% solution of hydrogen peroxide, a good source of hydroxyl radicals, was injected into the reactor during photocatalytic methane conversion. Figure 9 shows the results typical of the peroxide injection experiments. After peroxide injection, conversion of methane increases from ~4% to ~10%. Methanol production increases 17 fold, and carbon dioxide increases 5 fold, along with modest increases in hydrogen and carbon monoxide.

CONCLUSIONS

We have reproduced the results reported in the literature for both methane photolysis and catalytic photolysis of water. In experiments that combine elements of both systems, methane and water have been converted to methanol, hydrogen, and acetic acid by a doped semiconductor photocatalyst at temperatures of ~94°C and atmospheric pressure. Conversion of methane and the production of methanol are augmented by the addition of hydrogen peroxide, indicating that hydroxyl radical is an intermediate.

FUTURE PLANS

Research during the next fiscal year will be focused on developing the photocatalyst. Studies on the effect of radical propagation/initiators on the reaction will also investigated.

ACKNOWLEDGMENT

We would like to acknowledge the technical assistance of Richard R. Anderson, John Baltrus, J. Rodney Diehl, Elizabeth A. Frommell, Neil Johnson, Donald V. Martello, and Joseph P. Tamilia.

DISCLAIMER

Reference in this report to any specific commercial product, process, or service is to facilitate understanding and does not necessarily imply its endorsement or favoring by the United States Department of Energy.

REFERENCES

1. Ogura, K.; Kataoka, M. *J. Mol. Cat.* **1988**, *43*, 371-79.
2. Ogura, K.; Migita, C.T.; Fujita, M. *Ind. Eng. Chem. Res.* **1988**, *27*, 1387-1390.
3. Ashokkumar, M.; Maruthamuthu, P. *J. Mat. Sci. Lett.* **1898**, *24*, 2135-2139.
4. Maruthamuthu, P.; Ashokkumar, M. *Int. J. Hydrogen Energy* **1989**, *14(4)*, 275-277.

SCHEME 1. Catalytic Photolysis of Water

(1) $La/WO_3 \xrightarrow[\lambda \geq 410\ nm]{h\nu} e^-_{CB} + h^+_{VB}$

(2) $e^-_{CB} + MV^{2+} \longrightarrow MV^{\bullet +}$

(3) $h^+_{VB} + H_2O \longrightarrow H^+ + {\bullet}OH$

(4) $MV^{\bullet +} + H^+ \longrightarrow \frac{1}{2} H_2 + MV^{2+}$

(5) $2{\bullet}OH \longrightarrow H_2O_2 \longrightarrow \frac{1}{2} O_2 + H_2O$

MARUTHAMUTHU, P.; ASHOKKUMAR, M.; GURUNATHAN, K.; SUBRAMANIAN, E.; SASTRI, M.V.C. *INT. J. HYDROGEN ENERGY* 1989, *14(8)*, 525-8.

SCHEME 2. Photochemical Conversion of Methane

(1) $H_2O \xrightarrow[\lambda \geq 185\ nm]{h\nu} H_2 + \frac{1}{2} O_2$

(2) $H_2O \xrightarrow[\lambda \geq 185\ nm]{h\nu} \frac{1}{2} H_2 + {\bullet}OH$

(3) $CH_4 + {\bullet}OH \longrightarrow CH_3{\bullet} + H_2O$

(4) $CH_3{\bullet} + H_2O \longrightarrow CH_3OH + \frac{1}{2} H_2$

OGURA, K.; KATAOKA, M. *J. MOL. CATAL.* 1988, *43*, 371-9.

SCHEME 3. Photocatalytic Conversion of Methane

(1) $La/WO_3 \xrightarrow[\lambda \geq 410\ nm]{h\nu} e^-_{CB} + h^+_{VB}$

(2) $e^-_{CB} + MV^{2+} \longrightarrow MV\bullet^+$

(3) $h^+_{VB} + H_2O \longrightarrow H^+ + \bullet OH$

(4) $MV\bullet^+ + H^+ \longrightarrow \frac{1}{2} H_2 + MV^{2+}$

(5) $CH_4 + {}^\bullet OH \longrightarrow CH_3\bullet + H_2O$

(6) $CH_3\bullet + H_2O \longrightarrow CH_3OH + \frac{1}{2} H_2$

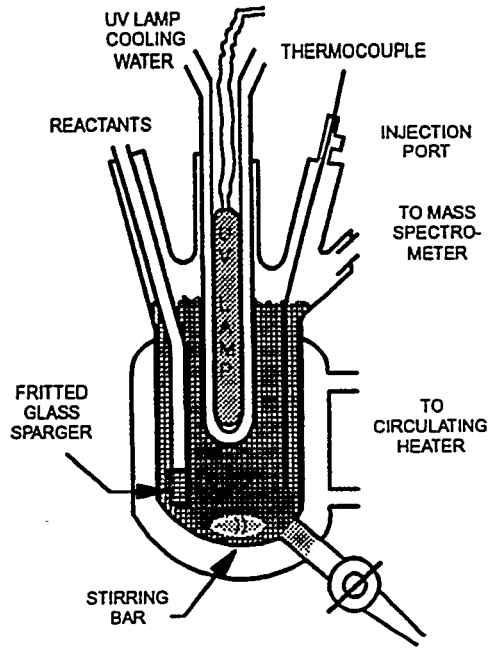

FIGURE 1. Schematic of Photocatalytic Reactor

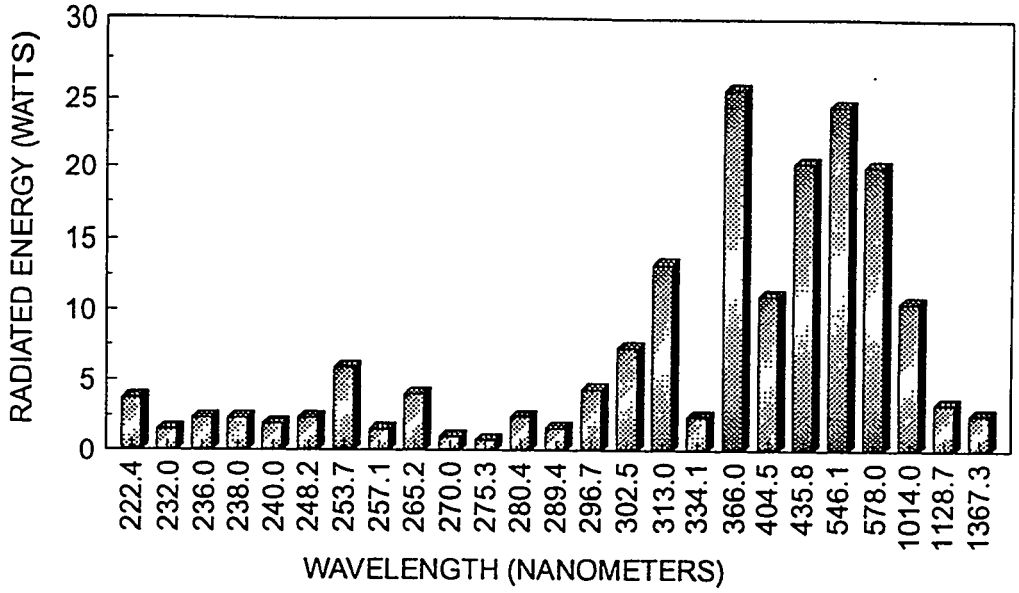

FIGURE 2. High-Pressure Quartz Mercury-Vapor Lamp Spectral Energy Distribution

Ace Glass Inc. Data Sheet

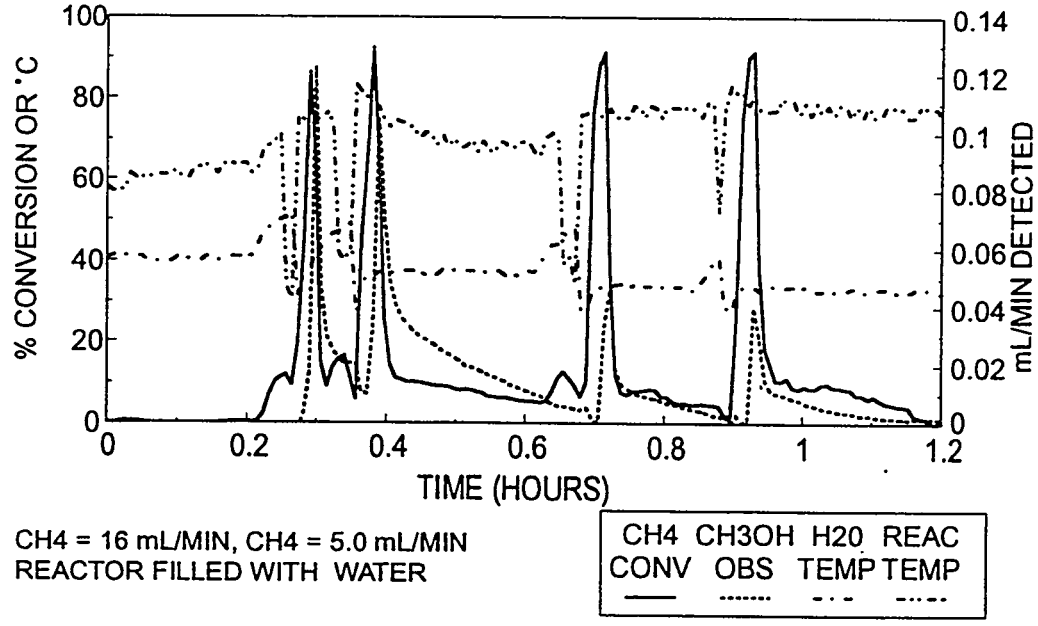

FIGURE 3. Temperature Dependence of Methane Photoconversion Reaction

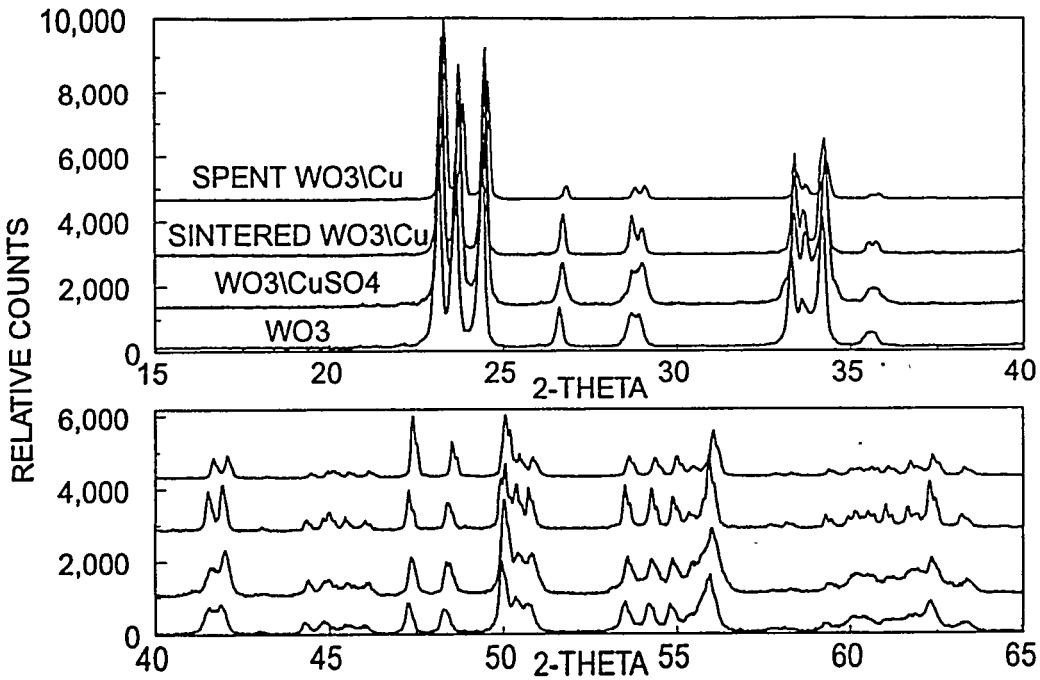

FIGURE 4. X-ray Spectra of Copper-Doped Photocatalysts

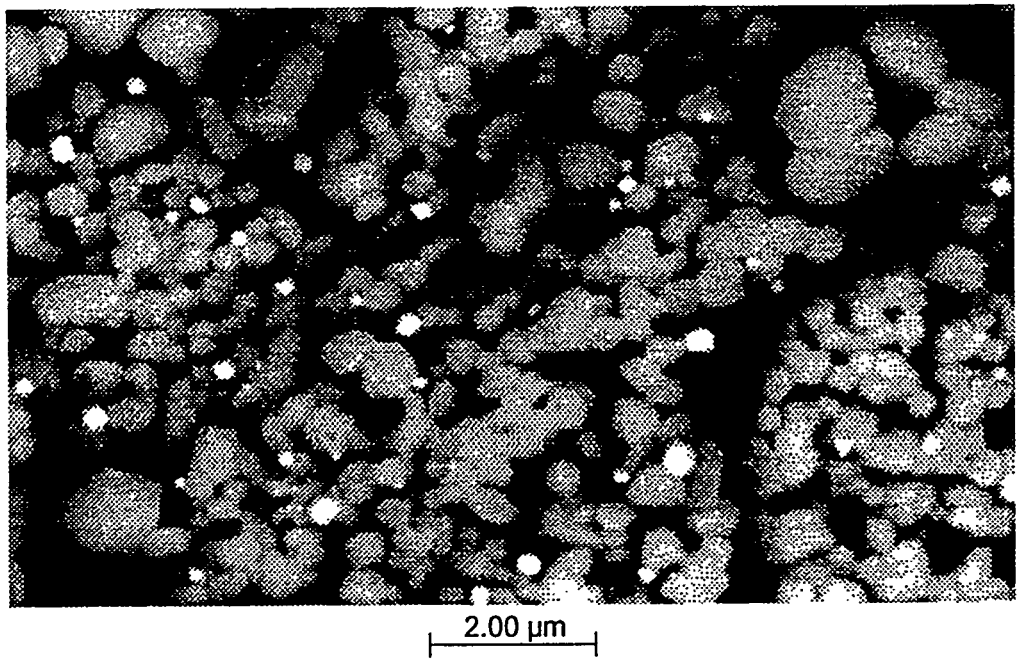

FIGURE 5. Backscatter SEM of WO_3\Pt Photocatalyst

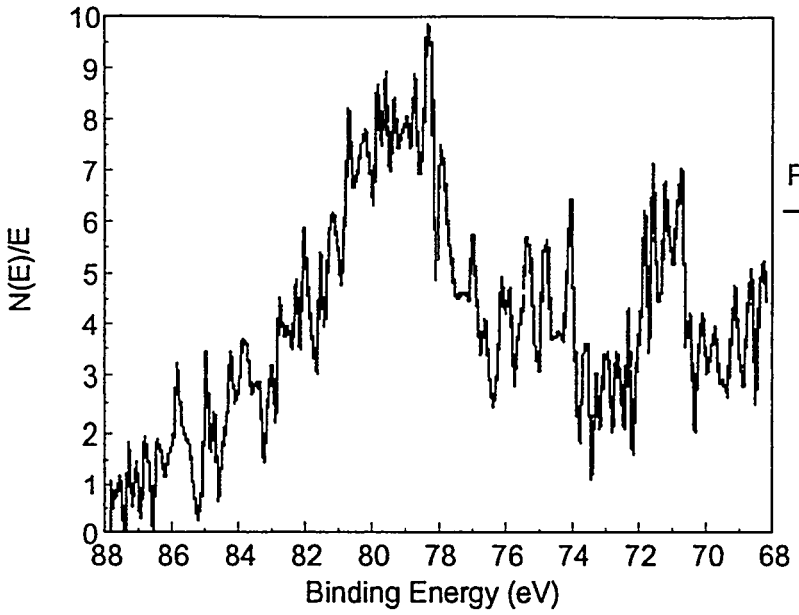

FIGURE 6. ESCA Survey of WO_3\Pt Photocatalyst

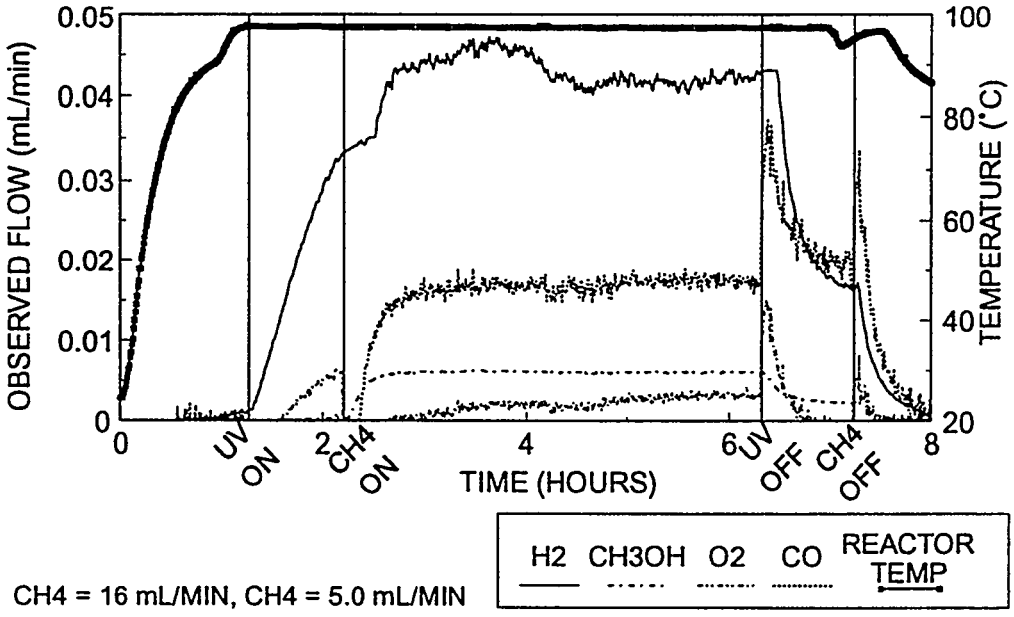

FIGURE 7. Typical Results of Photocatalytic Methane Conversion

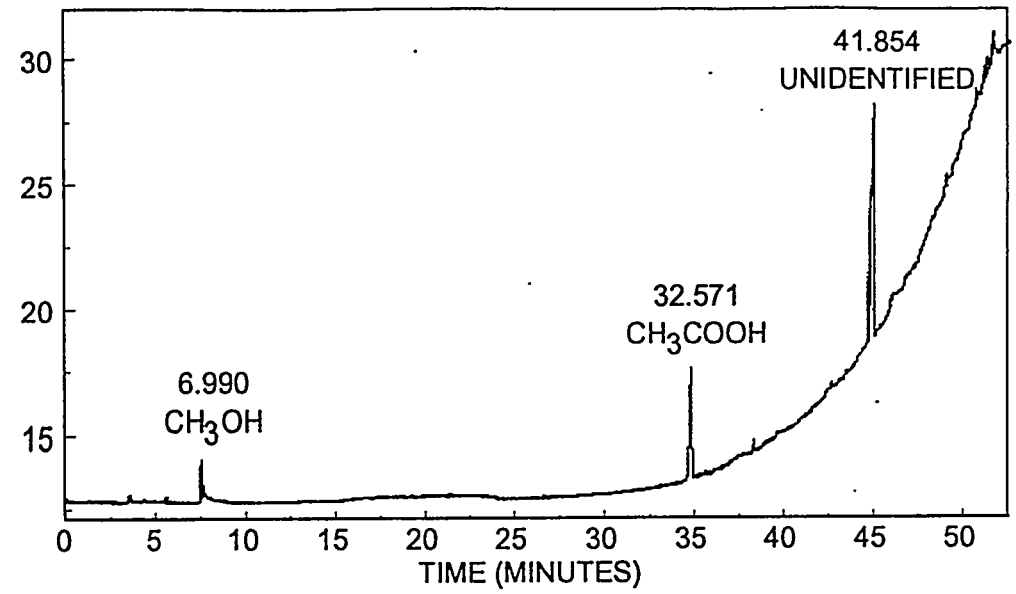

FIGURE 8. GC of Condensed Liquid Product

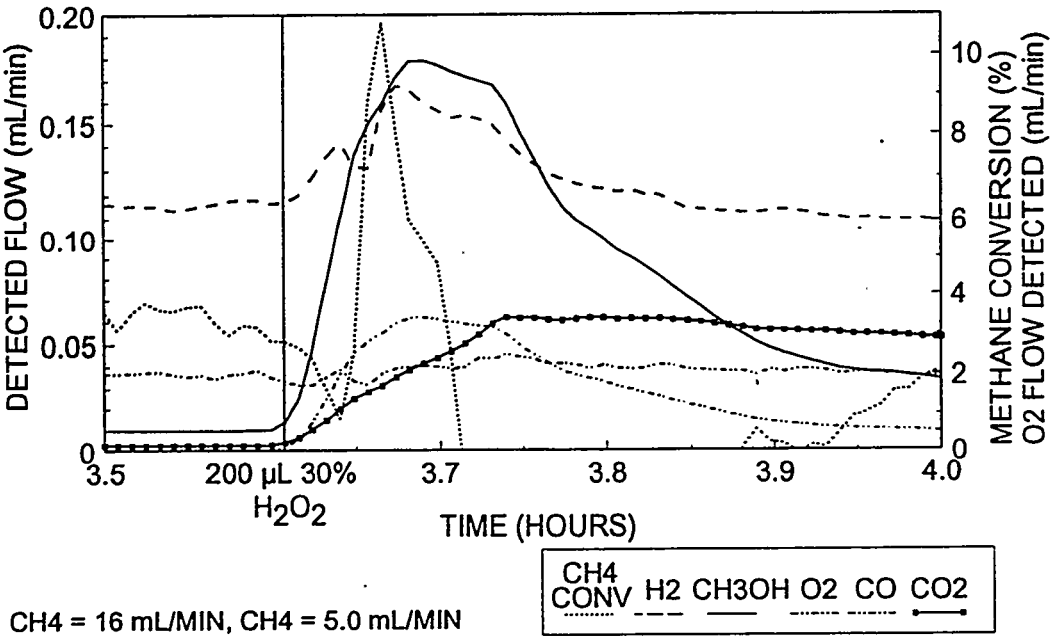

FIGURE 9. Results of Hydrogen Peroxide Addition

TITLE: THE DIRECT AROMATIZATION OF METHANE

PI (AUTHORS): G. Marcelin, R. Oukaci, R. A. Migone, and A.M. Kazi

INSTITUTION: Altamira Instruments
149 Delta Drive
Pittsburgh, PA 15238

CONTRACT NUMBER: DE-22AC-92PC92109

PERIOD OF PERFORMANCE: July 1, 1994 - May 31, 1995

OBJECTIVE: The thermal decomposition of methane shows significant potential as a process for the production of higher unsaturated and aromatic hydrocarbons when the extent of the reaction is limited. Thermodynamic calculations have shown that when the reaction is limited to the formation of C_2 to C_{10} products, yields of aromatics can exceed 40% at temperatures of 1200°C. Preliminary experiments have shown that cooling the product and reacting gases as the reaction proceeds can significantly reduce or eliminate the formation of solid carbon and heavier (C_{10+}) materials. Much works remains in optimizing the quenching process and this is one of the goals of this program. We are also studying means to lower the temperature of the reaction as this will result in a more feasible commercial process due to savings realized in energy and material of construction costs. The use of free-radical generators and catalysts will be investigated as a means of lowering the reaction temperature thus allowing faster quenching. It is highly likely that such studies will lead to a successful direct methane to higher hydrocarbon process.

ACCOMPLISHMENTS AND CONCLUSIONS: During the first two years of this project, a quench reactor system was designed and constructed and a study of the effect of process variables on methane conversion and product selectivities was carried out.

During this last period, significant work has focussed on evaluating the effect of free-radical initiators on methane pyrolysis. Most of the work dealt with a study on the effect of ethane addition on reaction rates and selectivities. Effects of temperature, space velocity, ethane/methane ratio, reaction quenching, quench water flow rates, and reactor configuration were investigated. In addition, studies of initiation of pyrolysis by a solid surface using a variety of catalysts have been started.

Significant reduction in the pyrolysis temperature was observed both in the cases of assisted pyrolysis by the addition of a free-radical initiator, as well as when pyrolysis was initiated on a catalyst surface.

EXPERIMENTAL PROCEDURE

Axial Temperature Profile in the Pyrolysis Reactor

The quench-reactor system designed for this study was described in previous conference proceedings [1]. A new quench reactor has been installed for studying the pyrolysis in presence of a catalyst. As before, this reactor will consist of two concentric tubes. However, as opposed to the quench reactor used in previous studies, in this reactor methane and other gases flow in the inner tube whereas quench water flows in the annular space between the two tubes. This configuration is more practical than the previous one to load the catalyst into the quench reactor.

The reactor axial temperature profile has been measured under a 500 Scc/min flow of nitrogen. A movable, high temperature resistant, mineral-insulated, Alloy 6000 thermocouple was used. The thermocouple was placed inside the reactor and displaced over the entire length. Measurements were taken both in the presence and absence of a quench water flow.

Methane Pyrolysis in the Presence of a Free Radical Initiator

Ethane was used as a free radical initiator. The addition of ethane was first studied in the absence of quench water. The pyrolysis experiments were carried out at temperatures between 800°C and 1100°C. Methane and ethane flow rates of 500 -1000 Scc/min and 24 - 49 Scc/min were used, respectively.

The assisted pyrolysis by addition of a free-radical initiator was further investigated in the presence of quench water. Ethane was again used as the free-radical initiator. The pyrolysis experiments were carried out at temperatures between 850°C and 1100°C. Methane and ethane flow rates of 200-475 Scc/min and 8-42 Scc/min were used, respectively. The quench water flow rate was maintained at 250 ml/hr for all the assisted pyrolysis experiments. In addition to the effect of quench water on methane pyrolysis in the presence of a free-radical initiator, the effects ethane-methane ratio and space velocity were also investigated.

Pyrolysis of Ethane

Since ethane was used as free radical initiator it was of interest to find out its pyrolysis activity and product distribution in the absence of methane. Ethane pyrolysis was therefore investigated under conditions similar to the one used for methane pyrolysis. The reaction was carried out under 42 Scc/min and 500 Scc/min flow of ethane and helium, respectively. Helium flow was used to keep the space velocity of ethane comparable to the experiments where it was added to methane as a free radical initiator.

Catalytic Pyrolysis

Pyrolysis in the presence of a variety of catalysts including quartz chips, SiC, α-alumina, and barium manganese hexaaluminate ($BaMnAl_{11}O_{19}$) have been studied. Quartz chips were used to see the effect of an additional inert surface on the methane conversion. The selection of other catalysts was based on the basis of their moderate surface area and structural stability at the temperature of interest, up to 1200°C. Moreover, they are relatively inert to reduction during the methane activation step.

So far, the studies have only been performed using a straight quartz tube, i.e.,in the absence of any quench water flow. Catalytic pyrolysis was carried out at temperatures between 800 and 1100°C. Methane flow rates of 500-1000 Scc/min, and 0.5 to 1.0 g of catalyst were used. The effect of addition of free radical initiator during catalytic pyrolysis was also studied. In the latter experiments, the ethane flow rate was maintained between 24-49 cc/min.

RESULTS AND DISCUSSION

Axial Temperature Profile in the Pyrolysis Reactor

(i) Without quench

The heating zone of the furnace is 24 inches long surrounded by the heavy insulated material. The lower 9 inches of the reactor tube inside the heating zone were shielded with quartz insulation. The thermocouple used for the furnace temperature controller is located in the middle of the furnace (i.e. 12 inches from either end of the heating zone). Figure 1 depicts the axial temperature profile in the quartz tube with 500 Scc/min of nitrogen flow

and with the furnace temperature controller set at 1050°C. As a result of heat loses from the top and bottom, there was a slight temperature drop at the ends. The drop was much more significant for the lower three inches of the reactor, possibly because of the small draft of air leaking through the insulation into the furnace from the bottom. The section of the reactor between 4 and 16 inches from the top end of the heating zone was quite uniformly heated and was very close to the furnace temperature controller set point.

(ii) With quench

Figure 2 shows the axial temperature profile in the reactor tube under the various quench water flow rates with the remaining conditions similar to one described above. For all water flows, the temperature profile for the upper half part of the reactor tube was somewhat similar to the one obtained in the absence of quench. As expected, in the lower half of the furnace, the temperature dropped faster than observed in the absence of quench and decreased more rapidly with increasing water flow. It dropped to even below 100° C (not shown in the Figure) at the outlet of the furnace casing, i.e.,at 28 inches from the top. This section of the reactor in the immediate vicinity of the reactor which was not heated previously is now heat wrapped even when not introducing quench water.

Using this reactor configuration, i.e.,with the reaction zone in the inner tube and the quench water flowing on the outside, in the annular space between the two tubes, water flow rates as low as 250 ml/hr resulted in a substantial decrease in the gas temperature.

Free Radical Initiator Addition

Table 1 summarizes the results on the effect of ethane addition on methane pyrolysis runs conducted without and with quench water. Results for the run 93-1 and 93-2 show the methane conversions for the unquenched pyrolysis in the absence of ethane in the feed at 1100 and 1050°C, respectively. As mentioned earlier, ethane was used as a free radical initiator for the methane pyrolysis reaction. Addition of ethane to the methane feed was first studied in the absence of quench water flow (Runs with prefixes 91 and 92 in Table 1). Some of the runs were repeated for reproducibility checks. Significant methane conversion was observed at temperatures as low as 850°C. At 1100°C the methane conversions were around 40%.

Figure 3 shows the effect of temperature on methane conversion and the product selectivity for major analyzable products for the methane + ethane pyrolysis. At

temperatures below 950°C,the major pyrolysis products were ethylene and propylene. With an increase in pyrolysis temperature the selectivity was somewhat shifted toward benzene and acetylene. At 1050°C and 1100°C, benzene and ethylene were the main analyzable product. Figure 4 shows a similar plot for the minor analyzable products. Apparently, with an increase in the pyrolysis temperature, the product selectivity for all of the minor products passed through a maxima. Figure 5 shows the effect of temperature on the total carbon (i.e. from methane and ethane) and the product yields.

Runs 87-1, 87-2, 87-3 were performed to evaluate ethane pyrolysis rates and the product distribution under similar conditions used for unquenched methane pyrolysis. To maintain the ethane space velocity in the reactor close to the one used when it was added to the methane feed, 42 ml/min of ethane feed were mixed with He flowing at 500 ml/min. It is evident from the results that, as compared to methane, ethane is far more reactive for pyrolysis since, even at 850°C, 91% of it was converted. The selectivity for "tar" was relatively higher and at all temperatures it was ≥ 55%. Only a very small fraction of ethane had cracked to methane. Most of it was dehydrogenated to ethylene, acetylene or converted into "tar". Benzene was formed only in trace amounts.

The results of the quenched methane pyrolysis experiments conducted with and without ethane addition are also included in Table 1 (Runs with prefixes 95 and 96, respectively). As with the unquenched reaction, methane conversion with quenching was negligible at temperatures below 1100°C (see runs, 93-2, 94-1, 96-1 and 96-2 in Table 1) in the absence of a free radical initiator. The non-assisted methane pyrolysis was measurable only at 1100°C. However, the temperature range of interest was lowered to 850 - 1100°C in the case of ethane addition to the feed (runs 95-1 to 95-4). As expected, the methane conversions were lower at all temperatures than those obtained without reactor quenching at similar temperatures. However, the "tar" selectivities and yields were much lower than those obtained without quenching.

Table 2 summarizes the results of the investigation of the effect of ethane-to-methane ratio at relatively low space velocities (runs 96-4 - 102-4). It appears that as the C_2/C_1 ratio was increased, the methane conversion reached a maximum at around C_2/C_1(x100) of 4.5. Further increases in ethane flow rate do not seem to improve the methane conversion and may even be having a negative effect. Higher "tar" yields were obtained at the highest C_2/C_1 ratio.

Table 3 illustrates the effect of space velocity on methane conversion and the product selectivity for the methane + ethane pyrolysis at 1050°C and constant C_2/C_1 ratio. Ethane conversion, almost complete at temperatures above 950°C, was unaffected by

changes in reaction conditions. Methane conversion, on the other hand, was very sensitive to changes in space velocity. However, increases in methane pyrolysis rates with decreasing space velocities resulted mainly in increases in "tar" selectivity and yield. The yields of aromatics and C_2-C_{10} products in generals was not much affected by changes in space velocity.

Catalytic Pyrolysis

A catalytic pyrolysis process was expected to be initiated by a solid surface at lower temperatures. The preliminary results of pyrolysis in the presence of a variety of catalysts including quartz chips, SiC, α-alumina, and barium manganese hexaaluminate ($BaMnAl_{11}O_{19}$) are summarized in Table 4. Before testing solids which were expected to have some catalytic activity, the very first few runs were performed to find out the effect of an additional inert surface on the pyrolysis activity. Runs 79-1, 79-2, 79-3, and 80-1 showed the effect of temperature on unquenched pyrolysis of methane in the presence of quartz chips in the reactor. The result indicate that the additional surface from the quartz chips did not have any positive effect on the pyrolysis activity. At temperatures below 1050°C, there was almost no methane conversion. Similar observations were made in the absence of quartz chips, thus indicating that their presence did not modify the pyrolysis process.

Runs 81-1, 81-2 and 81-3 showed the effect of addition of ethane (a free-radical initiator) on the pyrolysis of methane in the presence of quartz chips. The runs were performed at 950°C and under different methane and ethane flows. In all cases a measurable amount of methane was converted, but the conversions were very low and did not change significantly with the amount of ethane in the feed. In all cases, the selectivity towards "tar" was significant.

Similar studies were performed using the three other catalysts including SiC, α-Al_2O_3, and $BaMnAl_{11}O_{19}$ (BET surface 4.5 m^2/g) characterized by the run numbers with prefixes 82, 83, and 84, respectively. The results for all three catalysts were quite similar. In the absence of ethane in the feed, at temperatures $\leq$ 950°C, the methane conversion was $< 1\%$ in all the cases, except for Run No. 82-1. At 1050°C, the methane conversion for the three catalysts varied between 6-10% and the selectivity toward "tar" was > 35 %. In Run No. 82-1, even at 900°C a methane conversion of 21.3 % was observed. It is possible that SiC was very active even at 850°C and deactivated after the first run. This could explain why its higher activity was not evident in the subsequent higher temperature runs.

CONCLUSIONS

Assisted pyrolysis has been performed by the addition of ethane as a free-radical initiator. The effects of temperature and methane and ethane flow rates has been investigated without reaction quenching. Measurable amounts of methane were converted at temperatures as low as 850°C, and the major pyrolysis products were ethylene and propylene at temperatures below 950°C. At higher pyrolysis temperatures, the selectivity shifted toward benzene and acetylene.

The effects of temperature, space velocity, and ethane/methane ratio, in the presence of quench water, have been addressed. Reaction quenching resulted in lower conversions than without quenching, but also in significantly lower yields of "tar-like" products. High C_2/C_1 ratios and low space velocities result in significant increases in the "tar-like" products yields. Very low ethane concentrations were required to initiate methane pyrolysis at lower temperatures without a major negative effect on product selectivities.

The initiation of pyrolysis by a solid surface using a variety of catalysts has also been investigated. The preliminary results indicate that a significant reduction in the pyrolysis temperature may be obtained in the presence of some catalysts. However, the selectivity towards "tar" was significant in most cases. The reaction conditions have to be optimized in order to improve the selectivities towards valuable products.

FUTURE PLANS

In the remaining time before the end of this project, we expect to conclude the experimental work on the assisted pyrolysis by addition of a free-radical initiator. We will also continue the investigation of the initiation of pyrolysis by a solid surface using a variety of catalysts.

REFERENCES

(1) G. Marcelin, R. Oukaci, and R.A. Migone, "Direct Aromatization of Methane", Proceedings: Coal Liquefaction and Gas Conversion Contractors Review Conference (1994).

Table 1. Effect of Ethane Addition on Methane Pyrolysis with and without Quenching

Run No.	Temp. (°C)	Methane		Ethane		Carbon Selectivities (%)		
		Flow (ml/min)	Conv. (%)	Flow (ml/min)	Conv. (%)	Benzene	C_2-C_{10}	"Tar"
87-1	850	0[1]	-	42	91.0	T	41.2	58.8
87-2	950	"	-	"	99.3	2.2	45.0	55.0
87-3	1100	"	-	"	100.0	0.6	39.2	60.8
91-4	850	475	9.2	"	61.5	0.1	84.5	15.5
91-3	950	"	9.9	"	96.8	5.0	76.5	23.5
91-1	1050	"	17.1	"	98.6	24.1	72.8	27.1
91-2	1100	"	42.9	"	99.1	17.6	40.4	59.6
92-1	1050	"	24.1	"	98.9	21.5	61.4	38.6
92-2	1100	"	39.1	"	99.3	14.9	33.3	66.7
93-1	1100	"	13.7	0	-	22.1	70.6	29.4
93-2	1050	"	< 2	"	-	x	x	x
94-1	1050	"	< 1	"	-	x	x	x
95-2[2]	1100	"	19	42	99	25.2	60.7	39.3
95-1[2]	1050	"	7.9	"	98	23.0	80.0	20.0
95-4[2]	950	"	2.7	"	94	3.4	79.9	20.3
95-3[2]	850	"	<1	"	42	x	x	x
96-5[2]	1100	"	4	0	-	13.3	88.0	12.0
96-2[2]	1050	"	<1	0	-	x	x	x
96-1[2]	950	"	<1	0	-	x	x	x

1 He = 500 cc/min; T = Trace amounts; x = Cannot be analyzed accurately

2 Quenched reaction: Quench water flow rate = 250 ml/hr.

Table 2. Effect of Ethane/Methane Ratio on Methane Pyrolysis[1]

Run No.	96-4	102-4	102-1	102-2
Methane Flow (ml/min)	200	200	200	200
Ethane Flow (ml/min)	0	9	18	36
C_2/C_1 (x100)	0	4.5	9	18
Methane Conv. (%)	1.4	17	16	13
Ethane Conv. (%)	-	98	99	99
Total C Conv. (%)	1.4	24	29	39
Selectivities				
Ethylene	x	14.1	14.7	13.7
Acetylene	x	8.1	9.4	7.5
Aromatics	x	23.9	24.3	22.9
C_2-C_{10}	x	51.0	54	47.5
Tar	x	49.0	46	52.5
Yields[1]				
Ethylene	x	3.4	4.3	5.3
Acetylene	x	2.0	2.8	2.9
Aromatics	x	5.8	7.1	8.9
C_2-C_{10}	x	12.3	15.9	18.5
Tar	x	11.9	13.5	20.5

1. T = 1050°C; Quench water flow rate = 250 ml/hr.
2. Yields are calculated based on total carbon conversion.

x Cannot be analyzed accurately.

Table 3. Effect of Space Velocity on Methane Pyrolysis in the Presence of Ethane[1]

Run No.	95-1	102-3	102-1
Methane Flow (ml/min)	475	300	200
Ethane Flow (ml/min)	42	26	18
C_2/C_1 (x100)	8.8	8.7	9.0
Methane Conv. (%)	8	13	16
Ethane Conv. (%)	98	99	99
Total C Conv. (%)	22	27	29
Selectivities			
Ethylene	27.7	17.7	14.7
Acetylene	18.5	11.2	9.4
Aromatics	23.4	25.4	24.3
C_2-C_{10}	80.0	59.8	54
Tar	20.0	40.2	46
Yields[2]			
Ethylene	6.1	4.7	4.3
Acetylene	4.1	3.0	2.8
Aromatics	5.2	6.8	7.1
C_2-C_{10}	17.7	16.0	15.9
Tar	4.4	10.8	13.5

1. T = 1050°C; Quench water flow rate = 250 ml/hr.
2. Yields are calculated based on total carbon conversion.

Table 4. Effect of Catalyst Surface on (Unquenched) Pyrolysis Initiation

Run No.	Temp. (°C)	Catalyst	Methane		Ethane		Carbon Selectivities (%)		
			Flow (ml/min)	Conv. (%)	Flow (ml/min)	Conv. (%)	Benzene	C_2-C_{10}	"Tar"
79-1	900	quartz[1]	1000	<1	0	-	x	x	x
80-1	950	"	"	<1	"	-	x	x	x
79-2	1000	"	"	<1	"	-	x	x	x
79-3	1050	"	"	3.7	"	-	1.3	30.7	68.0
81-1	950	"	"	1.7	42	100	1.3	57.0	43.0
81-2	"	"	475	4.4	42	"	8.2	62.4	37.6
81-3	"	"	"	5.1	21	"	5.1	54.1	45.9
82-1	900	SiC[1]	"	21.3	0	-	0	0	100
82-2	950		"	<1	"	-	x	x	x
82-3	1000		"	1.1	"*c4a$b100g2P	-	0	59.2	40.8
82-4	1050		"	6.21	"	-	9.3	47.1	52.9
82-5	950	"	"	4.25	42	100	7.2	48.3	51.7

1. Approx. 1 g
x Cannot be accurately analyzed

Table 4. Effect of Catalyst Surface on (Unquenched) Pyrolysis Initiation (Contd.)

Run No.	Temp. (°C)	Catalyst	Methane		Ethane		Carbon Selectivities (%)		
			Flow (ml/min)	Conv. (%)	Flow (ml/min)	Conv. (%)	Benzene	C_2-C_{10}	"Tar
83-1	900	α-Al_2O_3[1]	475	<1	0	-	x	x	x
83-2	950	"	"	<1	"	-	x	x	x
83-3	1000	"	"	1.0	"	-	x	x	x
83-4	1050	"	"	5.7	"	-	11.7	67.9	32.1
83-5	950	"	"	7.0	42	100.0	9.6	61.3	38.7
83-6	800	"	"	2.7	"	29.8	0	55.2	44.8
83-7	850	"	"	4.3	"	66.8	0.3	44.3	55.7
84-1	850	$BaMnAl_{11}O_{19}$[2]	"	<1	0	-	x	x	x
84-2	950	"	"	<1	"	-	x	x	x
84-3	1050	"	"	9.6	"	-	10.2	45.3	54.7
84-4	950	"	"	6.1	42	100.0	0.5	34.2	65.8
84-5	850	"	"	6.0	"	73.9	10.1	60.4	39.6

1. Approx. 1.0 gm
2. Approx. 0.5 gm

x Cannot be analyzed accurately

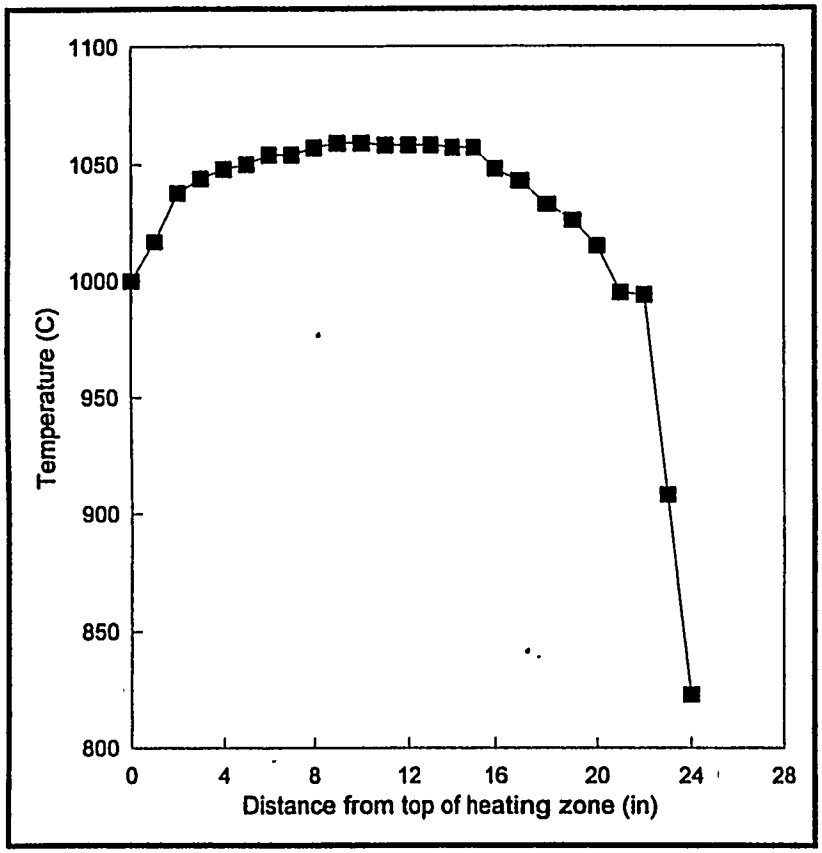

Figure 1. Axial temperature profile in the pyrolysis reactor in the absence of quench water flow (Nitrogen flow = 500 ml/min; Furnace temperature controller setpoint = 1050°C)

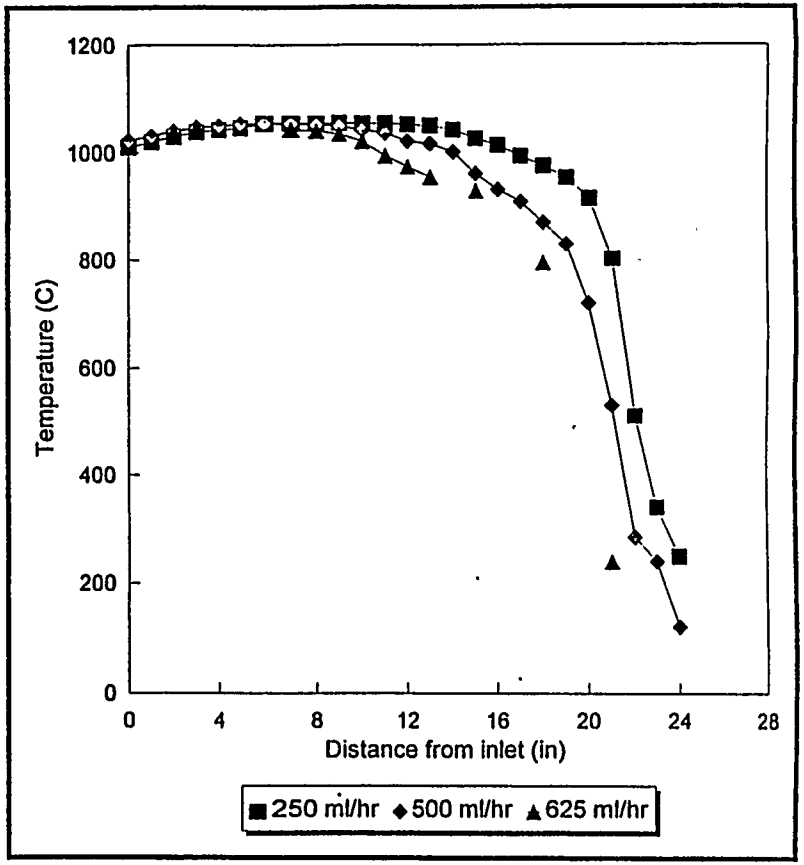

Figure 2. Axial temperature profile in the pyrolysis reactor at different quench water flow rates (Nitrogen flow = 500 ml/min; Water flow = as indicated on the plot; Furnace temperature controller setpoint = 1050°C)

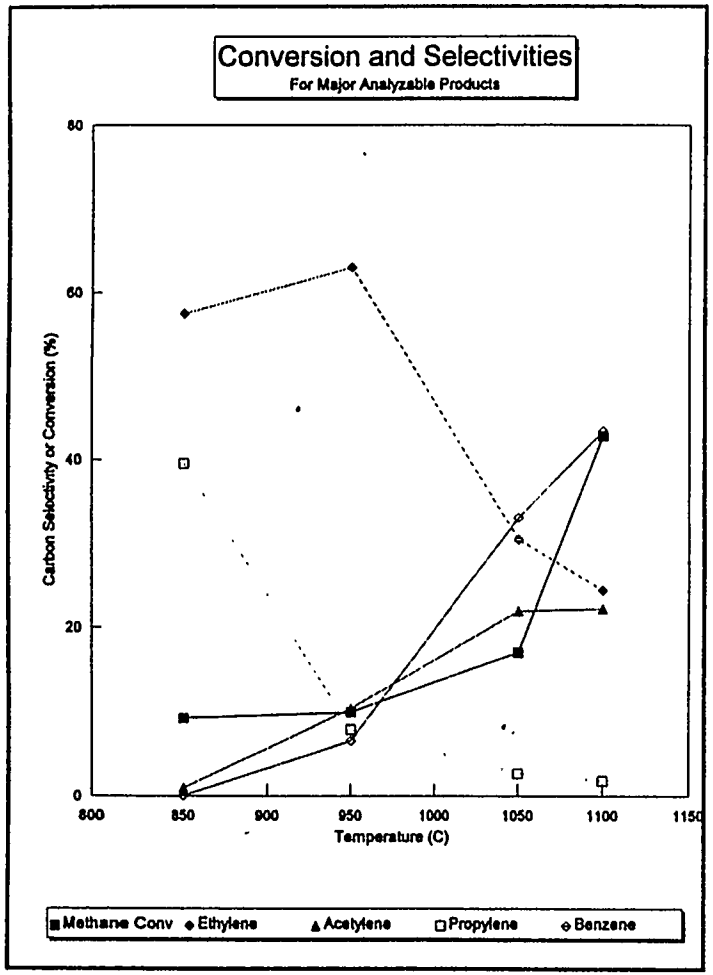

Figure 3. Effect of temperature on methane conversion and selectivities for major analyzable products of methane + ethane unquenched pyrolysis. (Methane flow = 475 ml/min, Ethane flow = 42 ml/min)

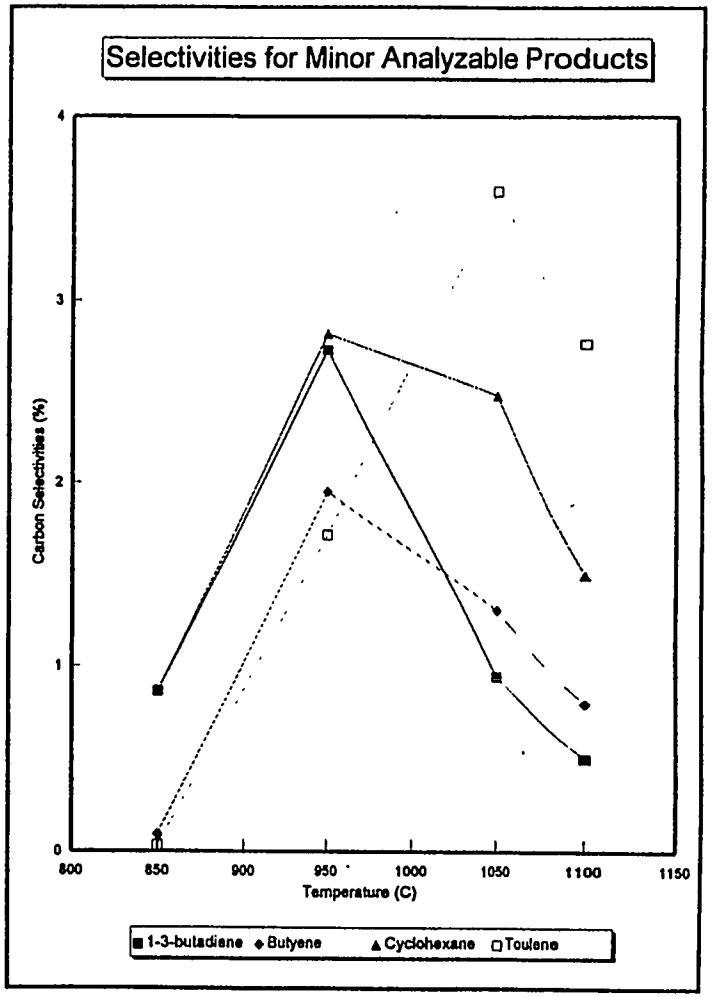

Figure 4. Effect of temperature on selectivities for minor analyzable products of methane + ethane unquenched pyrolysis. (Methane flow = 475 ml/min, Ethane flow = 42 ml/min)

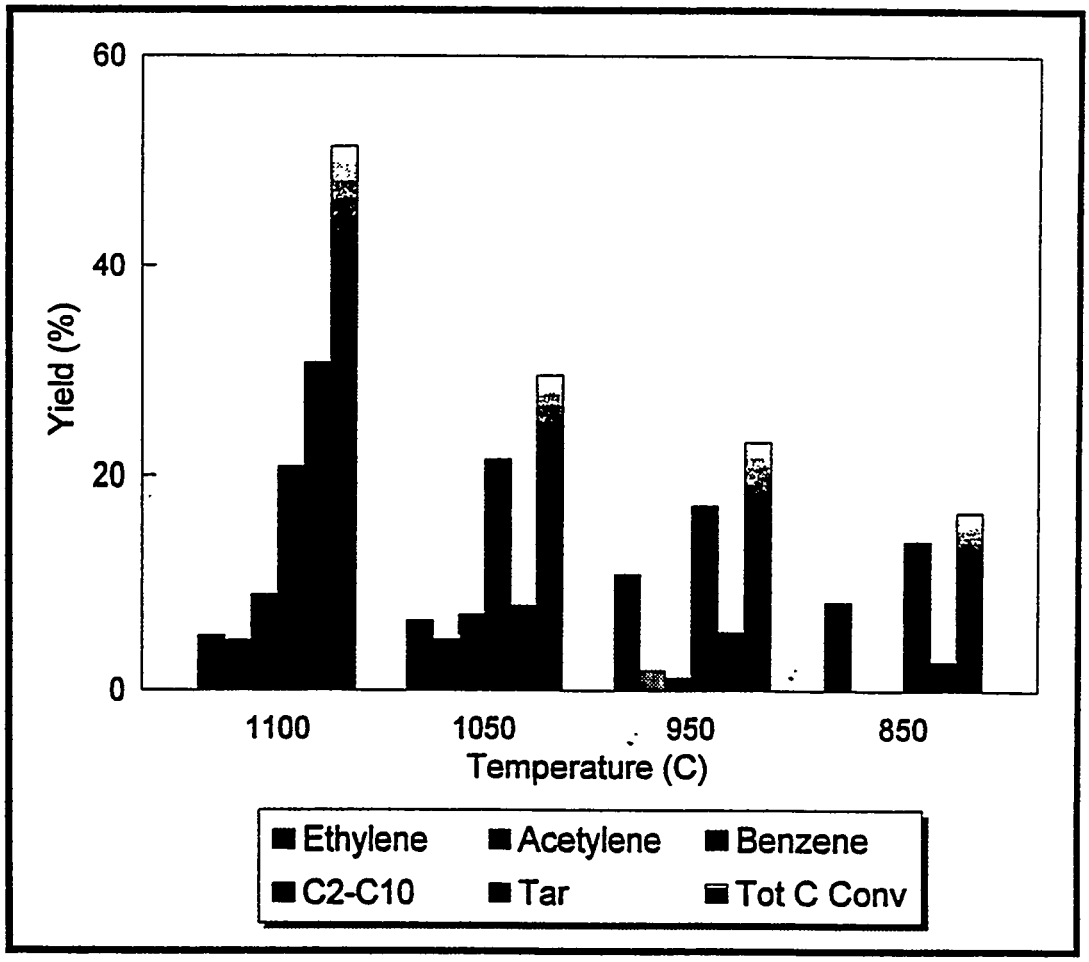

Figure 5: Effect of temperature on the product yield for the unquenched pyrolysis of methane + ethane (Methane flow = 475 ml/min, Ethane flow = 42 ml/min)

TITLE: Development of Vanadium-Phosphate Catalysts for Methanol Production by Selective Oxidation of Methane

PI: Robert L. McCormick*

INSTITUTION: Department of Chemical Engineering and Petroleum Refining
Colorado School of Mines
Golden, CO 80401-1887

CONTRACT NUMBER: DE-AC22-92PC92110

PERIOD OF PERFORMANCE: September 28, 1992-March 31, 1997

OBJECTIVE:

The United States has vast natural gas reserves which could contribute significantly to our energy security if economical technologies for conversion to liquid fuels and chemicals were developed. Many of these reserves are small scale or in remote locations and of little value unless they can be transported to consumers. Transportation is economically performed via pipeline, but this route is usually unavailable in remote locations. Another option is to convert the methane in the gas to liquid hydrocarbons, such as methanol, which can easily and economically be transported by truck. Therefore, the conversion of methane to liquid hydrocarbons has the potential to decrease our dependence upon oil imports by opening new markets for natural gas and increasing its use in the transportation and chemical sectors of the economy. In this project, we are attempting to develop, and exploring for new catalysts capable of direct oxidation of methane to methanol.

The specific objectives of this work are:

- To determine the activity and selectivity of vanadium phosphate catalysts in methane oxidation.
- To utilize promoters and catalyst supports to improve oxygenate yield relative to the base case catalysts.
- To provide a preliminary understanding of the catalytic mechanism and how promoters and supports actually effect catalytic properties.
- Use the information obtained to prepare advanced catalysts which will be tested for activity, selectivity, and stability.

* Phone: 303 273-3967. Fax: 303 273-3730. Internet: rlmccorm@mines.colorado.edu.

- Develop a simplified methanol production process flowsheet based on these advanced catalysts.

The basic premise of this project is that $(VO)_2P_2O_7$ (vanadyl pyrophosphate or VPO), a catalyst used commercially in the selective oxidation of butane to maleic anhydride, can be developed as a catalyst for selective methane oxidation. Supporting this idea are published reports indicating moderate to high selectivity in oxidation of ethane,[1] propane,[2] and pentane,[3] as well as butane[4] to various oxygenates. Thus, VPO appears to have a unique catalytic functionality for selective activation of alkanes. Methane oxidation is a much more difficult reaction to catalyze and it is expected that considerable modification of VPO will be required for this application. It is well known that VPO can be modified extensively with different promoters and in particular that promoters can enhance selectivity and lower the temperature required for butane conversion.[5] A key problem in methane selective oxidation is that, at the high temperatures typically required for methane activation, the selective reaction products are rapidly converted to carbon oxides.

Background on Vanadyl Pyrophosphate

Vanadyl pyrophosphate is prepared from V_2O_5 and phosphoric acid. The most active and selective catalysts are obtained using organic solvents such as a mixture of *iso*-butyl and benzyl alcohols and anhydrous phosphoric acid.[4,6] Excess phosphorus is generally employed in the reaction mixture. The catalyst precursor obtained from reaction of these materials under reflux is $VO(HPO_4)\cdot 0.5H_2O$ which has a layered structure. The use of organic solvents and excess phosphorus is thought to lead to a desirable crystalline face exposure and to the development of disorder in the layer stacking through entrapment of benzyl alcohol molecules between the layers.[7,8] This procedure may also introduce anion vacancies.[9]

The catalyst precursor is then converted to vanadyl pyrophosphate by heating under a variety of gas environments. The precursor undergoes a topotactic transformation such that structural disorder in the precursor is preserved in the active phase.[10] Strong Lewis acid sites on the surface of VPO

---

[1] Michalakos, P.M., Kung, M.C., Jahan, I., Kung, H.H. J. Catal. 140 226 (1993).
[2] Ai, M. J. Catal. 101 389 (1986).
[3] Busca, G., Centi, G. J. Am. Chem. Soc. 111 46 (1989).
[4] Centi, G., Trifiro, F., Ebner, J.R., Franchetti, V.M. Chem. Rev. 88 55 (1988).
[5] Hutchings, G.J. Appl. Catal. 72 1 (1991).
[6] Cavani, F. and Trifiro, F. Chemtech April, pp. 18 (1994).
[7] Busca, G., Cavani, F., Centi, G., Trifiro, F. J. Catal. 99 400 (1986).
[8] Horowitz, H.S., Blackstone, C.M., Sleight, A.W., Teufer, G. Appl. Catal. 38 193 (1988).
[9] Cornaglia, L.M., Caspani, C., Lombardo, E.A. Appl. Catal. 74 15 (1991).
[10] Johnson, J.W., Johnston, D.C., Jacobson, A.J., Brody, J.F. J. Am. Chem. Soc. 106 8123 (1984).

are responsible for initial alkane activation.[11] It has been proposed that this Lewis acidity is caused by lattice defects or strain initiated by the disorder in stacking of the layered structure.[7,11] However, equilibrated catalysts (used for at least 200 hours) exhibit a lower degree of structural disorder but a higher level of strong Lewis acidity compared to freshly activated catalysts[12] indicating that the source of the strong Lewis acidity is not well understood. One hypothesis is that anion vacancies are introduced through the use of organic solvents and excess phosphorus. These vacancies are the source of both disorder in the stacking plane and the strong Lewis acidity. After many hours on stream the disorder in the layer stacking is eliminated but the anion vacancies remain. After the activation process some carbon is present on or in the catalyst which may also contribute to structural disorder or to the active site structure.[3,13] The P:V ratio of the active catalyst is typically about 1.05, assuming some excess phosphorus was present, regardless of the starting P:V ratio.[8] Most or all of the excess phosphorus is found on the surface where the P:V ratio has been found to be closer to 2. This observation lead to a model of the VPO surface consisting of pendant pyrophosphate groups.[14]

Catalyst Development Approach

One approach to catalyst development that we are taking is directed at increasing the strength of the strong Lewis acid sites by enhanced strain or disorder in the layer stacking. Presumably this will also alter the nature of the anion vacancies more directly responsible for Lewis acidity. Surface acidity is being measured by FTIR of chemisorbed bases. By increasing Lewis acid site strength it is hoped that the temperature required for methane activation can be lowered resulting in improved activity and selectivity. A second approach involves addition of promoters to alter the metal-oxygen bond strength and the oxidation activity of the catalyst. These approaches, and others, are being investigated through a combination of catalyst activity measurements and characterization of catalyst surface and bulk properties.

In this paper we describe baseline methane oxidation activity and catalyst characterization results for conventionally prepared VPO, a catalyst prepared under conditions known to enhance disorder in the layers, and a Zn promoted catalyst. These results provide a general idea of the type of work being performed under this contract. Results of other approaches including modification of the VPO surface through various ion exchange and doping

---

[11] Busca, G., Centi, G., Trifiro, F., Lorenzelli, V. J. Phys. Chem. 90 1337 (1986).
[12] Comaglia, L.M., Lombardo, E.A., Anderson, J.A., Garcia Fierro, J.L. Appl. Catal. 100 37 (1993).
[13] Pepera, M.A., Callahan, J.L., Desmond, M.J., Milberger, E.C., Blum, P.R., Bremer, N.J. J. Am. Chem. Soc. 107 4883 (1985).
[14] Ebner, J.R., Thompson, M.R. Catal. Today 16 51 (1993).

procedures and preparation of VPO on various supports will be presented at the Contractors Review Conference.

ACCOMPLISHMENTS & CONCLUSIONS:

Over the past year our main accomplishment has been to set up a new laboratory and bring equipment for catalyst synthesis, catalyst characterization, and activity studies on line. Additionally, we have begun to employ these facilities to examine vanadyl pyrophosphate and novel modifications of this material. Specific equipment brought on line includes:

- Apparatus for catalyst synthesis, drying, and activation.
- Diffuse reflectance infrared cell for studies of surface acidity and surface reactions via spectroscopy of chemisorbed molecules.
- Catalytic microreactor and gas chromatograph analytical system.

These facilities have been used to examine the surface acidity and oxidation activity of several catalysts. Activity for oxidation of methane and methanol has been examined for VPO prepared using the *iso*-butyl/benzyl alcohol method. A modified catalyst prepared in the presence of tetraethyl orthosilicate (TEOS) has been studied in methane oxidation. Addition of TEOS has been shown to disrupt the VPO layered structure resulting in exposure of more active surface and producing a more active butane oxidation catalyst.[8] A Zn promoted catalyst has also been prepared and characterized. Zn is added to many commercial butane oxidation catalysts and is thought to increase the rate of butane oxidation, possibly by enhancing the rate of oxygen incorporation into the catalyst.[15]

An interesting observation in this work has been the formation of small amounts of methanol and formaldehyde from methane at atmospheric pressure and temperatures from 350 to 450°C. The observation of more than a trace of methanol at these relatively mild conditions appears to be somewhat surprising based on previous literature reports.[16]

Catalyst Preparation

$(VO)_2P_2O_7$. V_2O_5 (15.0 g) was suspended in a solution of 90 ml of *iso*-butyl alcohol and 60 ml of benzyl alcohol. The solution was stirred and heated under reflux for 3 hours. A black solution was formed. The solution was cooled to room temperature and left stirring overnight. Then *ortho*-phosphoric acid (anhydrous, 19.4 g) was added and the solution was heated under reflux for an additional 2 hours. A blue suspension formed. This suspension was filtered,

[15] Takita, Y., Tanaka, K., Ichimaru, S., Ishihara, T., Inoue, T., Arai, H. J. Catal. 130 347 (1991).
[16] Brown, M.J., Parkyns, N.D. Catal. Today 8 305 (1991).

washed in water, and dried at 150°C overnight. A light blue precipitate recovered.

$(VO)_2P_2O_7$-TEOS Modified. After Horowitz and coworkers,[8] V_2O_5, (15.0 g), *ortho*-phosphoric acid (anhydrous, 19.4 g), and tetraethyl orthosilicate (9.2 ml) were added to a solution of 90 ml *iso*-butyl alcohol and 60 ml of benzyl alcohol. This solution was heated under reflux for 6 hours. A light blue precipitate was then filtered from the solution, washed with water, and dried overnight at 150°C.

9%Zn-$(VO)_2P_2O_7$. V_2O_5(15.24 g) and $ZnCl_2$(1.0 g) were suspended in a mixture of *iso*-butyl alcohol(90 ml) and benzyl alcohol(60 ml). The suspension was stirred under reflux for 3 hours and then overnight at room temperature giving an almost black suspension. *Ortho*-phosphoric acid(20.8 g) was added and the suspension stirred under reflux for 1hour giving a light blue suspension. Benzyl alcohol(*ca.* 50 ml) was added to the cooled suspension which was then filtered, washed with *iso*-butyl alcohol, ethanol, acetone and air dried. A portion of the solid was then dried in a stream of air at 140°C giving a blue-gray solid.

Conversion of the dried catalyst precursors to the active phase was performed in ceramic boats placed in a quartz tube furnace under a stream of air or 1.5% butane in air. The temperature was gradually increased from room temperature through 125°C (40 min.), 350°C (40 min.) and finally 400°C where it was held for 24 hours. Large amounts of maleic anhydride were deposited at the quartz tube outlet during activation in butane/air mixtures. Catalyst samples for kinetic studies were pelletized at 15,000 psi. The resultant pellets were crushed in a mortar and pestle and sieved to 1.4 x 0.7 mm.

Catalyst Characterization

X-Ray powder spectra were recorded using a Rigaku controlled powder camera using a 2 theta step size of 0.05°. Infrared spectra were recorded on a Bio-Rad FTS-40 spectrometer in the FT mode using an MCT detector with 2 cm^{-1} resolution. Typically 1032 scans were recorded from KBr discs or, for adsorption studies, using a heatable diffuse reflectance cell.

For infrared studies of adsorbed acetonitrile, a portion of the activated catalyst was ground in a steel Wiggle-Bug mill for 60 s. This material was then transferred to the heatable cell of a Harrick diffuse reflectance attachment and enclosed in a dome containing KBr windows. The sample was typically conditioned in a flow of He by heating to 400°C, holding the temperature for 30 min., and then cooling to 27°C and holding that temperature for 30 min. The He flow was then saturated with the required anhydrous base for 10 min. after which time the sample was purged with He for a further 10 min. The sample was then heated to various temperatures for 10 min. and spectra recorded.

Figure 1 shows x-ray diffraction data for the region of the (001) reflection in the catalyst precursors ($VO(HPO_4)\cdot 0.5H_2O$). The (001) reflection serves as an indication of the order and spacing of the layers in this layered structure.[7] It is evident that precursor preparation in the presence of TEOS has resulted in broadening of this peak indicating increased disorder (FWHM=0.9 for TEOS versus 0.55 for regular VPO). A very slight broadening may also be evident for the Zn promoted precursor. Figure 2 presents similar data for catalysts prepared from these precursors by activation in air. Here, the (200) reflection indicates degree of disorder in the layer stacking. Both the catalyst prepared with TEOS and the catalyst promoted with Zn exhibit broadening of this peak (FWHM=1.60 and 1.50, respectively versus 1.35 for regular VPO) indicating enhanced disorder relative to unmodified vanadyl pyrophosphate.

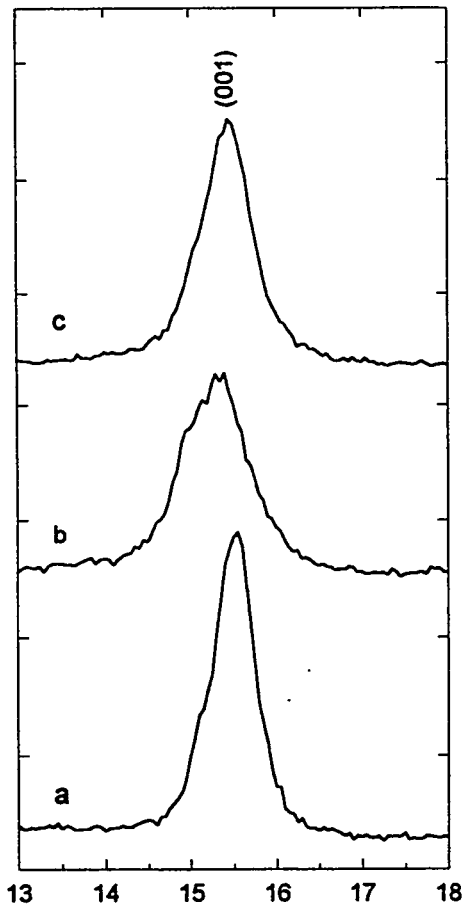

Figure 1. X-ray diffraction results for catalyst precursors, (001) reflection for a)$VO(HPO_4)$-$0.5H_2O$, b)TEOS modified, c) Zn promoted.

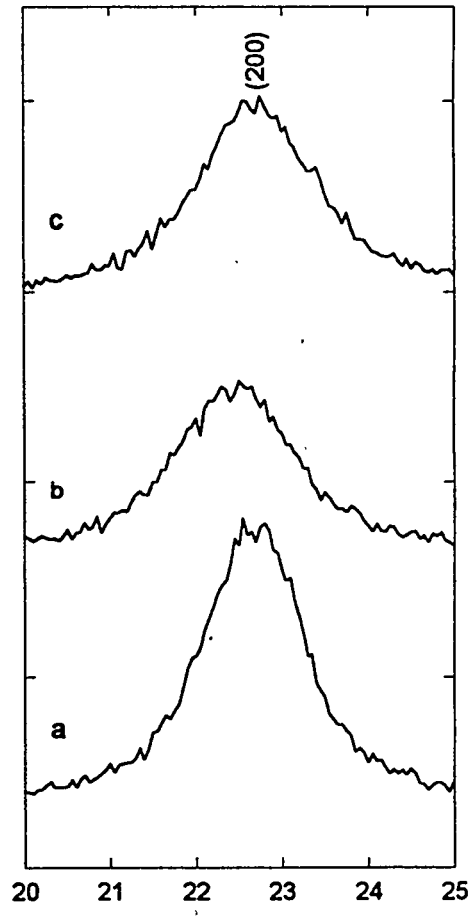

Figure 2. X-ray diffraction results for air activated catalysts, (200) reflection for a)vanadyl pyrophosphate, b)TEOS modified catalyst, c) Zn promoted catalyst.

We have hypothesized that enhanced disorder in the catalyst layer stacking will lead to enhanced Lewis acidity. Surface acidity has been investigated via

infrared spectra of chemisorbed acetonitrile. This weak base has a high specificity for the very strong Lewis sites which have been linked to activity in butane oxidation.[11] Spectra of acetonitrile on these catalysts are shown in Figure 3. The doublet at roughly 2325 and 2300 cm^{-1} is caused by acetonitrile adsorbed on very strong Lewis acid sites.[17] The peak at 2260 cm^{-1} and much of the intensity at 2300 results from hydrogen bonded or liquid acetonitrile. Spectrum (a) was taken after heating to 120°C to remove this non-chemisorbed material and this procedure resulted in improved peak resolution. The band at 2327 is clearly an indication of very strong Lewis acid sites and they appear to

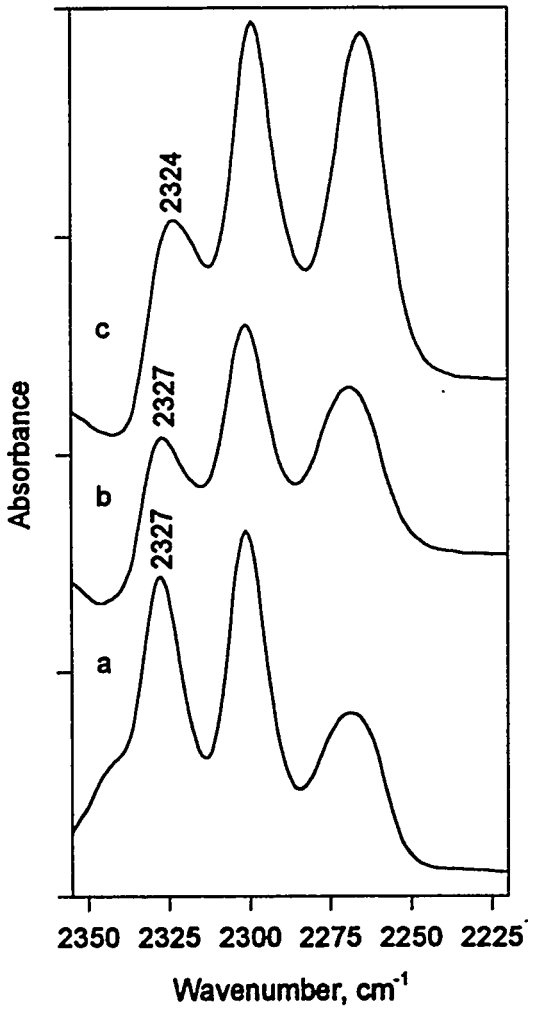

Figure 3. DRIFTS results for acetonitrile chemisorbed on air activated a)vanadyl pyrophosphate, b)TEOS modified catalyst, c)Zn promoted catalyst.

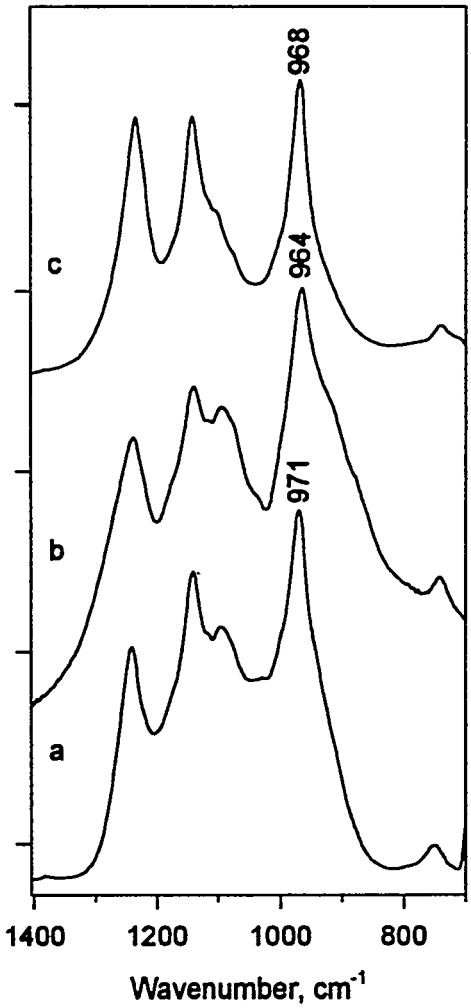

Figure 4. Transmission IR results for air activated a)vanadyl pyrophosphate, b)TEOS modified catalyst, c)Zn promoted catalyst.

[17] Knozinger, H., Krietenbrink, H. JCS Faraday 1 71 2421 (1975).

be similar on all three catalysts. This method of surface characterization will be refined to allow some distinction of differing acid site strengths to be made. Also, the use of other weak bases (including pyridine) will provide other measures of acid strength as well as Bronsted to Lewis site ratios. The number of acid sites will be measured thermogravimetrically in future work.

Figure 4 presents infrared spectra of the air activated catalysts. The V=O stretch for the unmodified catalyst is observed at 971 cm^{-1}. For the TEOS modified and Zn promoted catalysts this band is at 964 and 968 cm^{-1}, respectively. Takita and coworkers[18] have shown that promoters which lead to a reduction in the wavenumber of the V=O stretch also produce catalysts with enhanced butane oxidation activity. The V=O stretch has shifted significantly for the TEOS modified catalysts suggesting that higher activity is to be expected.

Oxidation Activity Studies

Reactivity studies conducted to date include blank (empty) reactor studies of methane and methanol oxidation, methane and methanol oxidation over air activated VPO, and methane oxidation over butane activated VPO and TEOS modified VPO. Experiments have been conducted in 7.75 mm (3/8") stainless steel or in 4 mm i.d. quartz tube reactors. At temperatures below 500°C no significant difference in activity or selectivity was observed for the two reactor materials. At higher temperatures lower selectivities are obtained in steel presumably because of wall catalyzed oxidation of CO, methanol, and formaldehyde. Carbon balances were better than ±5% for all data reported and better than ±2% for most runs. Catalytic methane oxidation tests employed a GHSV of 1400, and this is within the range used for butane oxidation over VPO catalysts.[4]

Results of blank methane and methanol oxidation tests are shown in Table 1. At atmospheric pressure no methane conversion was observed at temperatures as high as 600°C. A somewhat surprising result is the lack of significant methanol conversion at atmospheric pressure and temperatures up to 550°C. In vanadium phosphate catalyst development we are endeavoring to convert methane at temperatures of 500°C and below. These blank reactor results suggest that gas phase reactions are not important at atmospheric pressure in this temperature range. Oxidation of methane and methanol did occur at higher pressures. Methane oxidation results are generally in agreement with those reported in the literature.[16] Non-catalytic methanol oxidation produced primarily carbon oxides although formaldehyde and methane were also observed.

[18] Takita, Y., Tanaka, K., Ichimaru, S., Mizihara, Y., Abe, Y., Ishihara, T. Appl. Catal. A: General 103 281 (1993).

Table 1. Results of Non-Catalytic Oxidation of Methane and Methanol in Quartz Lined Reactor.

(GHSV=8000@NTP))

Temperature, °C	Feed Composition (balance He)			Pressure, atm	Percent Conversion	Percent Selectivity				
	$\%O_2$	$\%CH_4$	$\%CH_3OH$			CO	CO_2	HCHO	CH_3OH	CH_4
400	10	20	0	6.8	0	0	0	0	0	–
450	10	20	0	6.8	0	0	0	0	0	–
450	10	20	0	15.3	0	0	0	0	0	–
500	10	20	0	5.1	0.06	0	100	0	0	–
500	10	20	0	6.8	0.11	78.1	21.8	0	0	–
500	10	20	0	10.2	0.81	5.3	16.6	0	78.0	–
500	10	20	0	15.3	31.1	63.4	23.3	0.89	12.3	–
525	10	20	0	6.8	45.8	55.6	18.2	0	26.2	–
525	10	20	0	10.2	56.4	65.3	16.1	0.25	18.3	–
550	10	20	0	1	0	0	0	0	0	–
550	10	20	0	5.1	1.3	21.2	37.8	0	40.9	–
550	10	20	0	6.8	49.5	61.7	24.3	0	13.9	–
600	10	20	0	1	0	0	0	0	0	–
525	10	0	20	1	0.2	14.1	53.9	31.9	0	0
525	10	0	20	5.1	96.5	49.0	50.3	0	0	0.7
550	10	0	20	1	0.2	22.2	12.8	0	0	64.8
550	10	0	20	5.1	80.3	84.2	10.4	0.86	0	4.4

Figure 5 reports methane conversion as a function of temperature for several catalyst preparations at a CH_4:O_2 ratio of 25:1. The TEOS modified catalyst is slightly more active at lower temperatures. Butane activation had little effect on catalyst activity relative to air activation. A similar plot is shown in Figure 6 for CH_4:O_2 ratio of 10:1. Higher conversions are observed than at 25:1 and the TEOS modified catalyst is much more active. Recall that TEOS/VPO exhibited a V=O stretch shifted 7 cm^{-1} relative to the unmodified catalyst. This weakening of the V=O bond had indeed resulted in a more active catalyst.

These catalysts also exhibited significantly different selectivity behavior. Air activated VPO produced almost exclusively CO as the reaction product although traces of methanol and formaldehyde were observed. Butane activated VPO, on the other hand, produced CO, CO_2, and *low yields of formaldehyde and methanol.* Examination of the literature on catalytic methane partial oxidation (in particular the reviews of Brown and Parkyns[16] and of Pitchai and Klier[19]) suggests that to obtain methanol, previous researchers had to operate at lower oxygen content, higher temperature, and higher pressure or use nitrous oxide rather than dioxygen. Under similar conditions to those employed here methanol is rarely observed, even in trace quantities.[16,20]

[19] Pitchai, R., Klier, K. Catal. Rev.-Sci. Eng. 28 13 (1988).
[20] Spencer, N.D. and Pereira, C.J. J. Catal. 116 399 (1989).

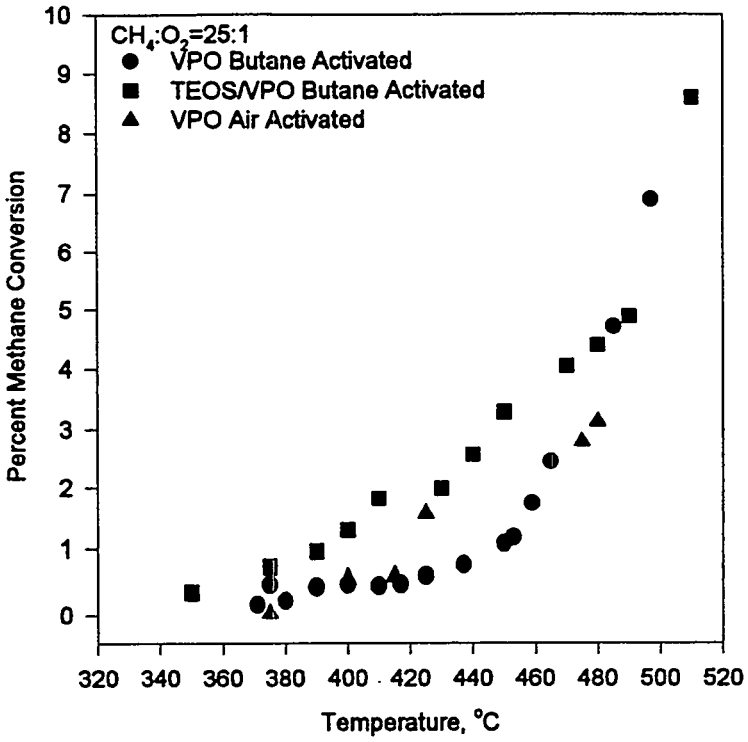

Figure 5. Methane conversion as a function of temperature, GHSV=1400.

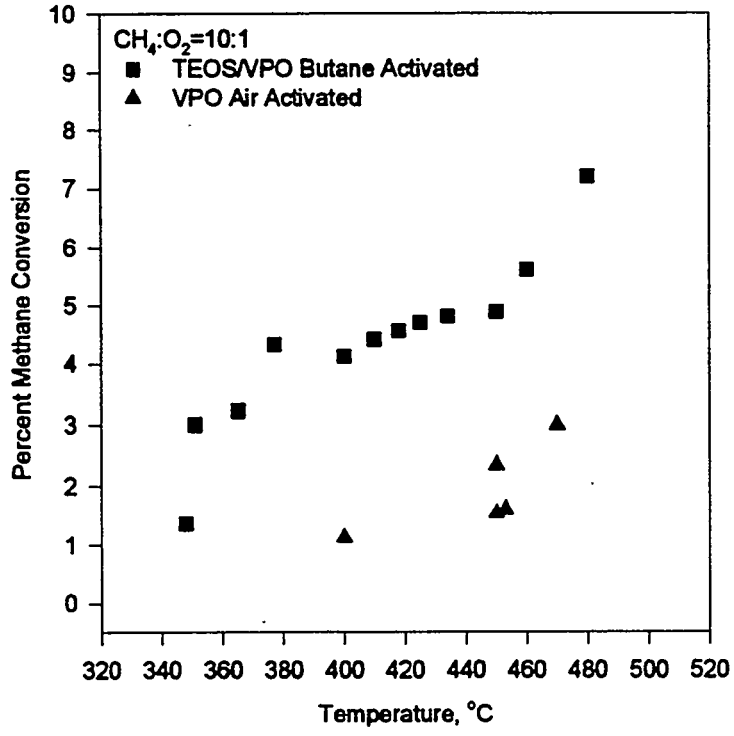

Figure 6. Methane conversion as a function of temperature, GHSV=1400.

The slightly more active TEOS modified catalyst produced only CO and CO_2 as reaction products. Additionally, the selectivity behavior was much different for this catalyst as shown in Figure 7. For TEOS/VPO, CO is by far the major product at relatively high conversions. For butane activated VPO, CO and CO_2 occur at roughly 40 and 60% selectivity, respectively. Much more data will be required to fully understand important kinetic and mechanistic aspects of methane oxidation over these catalysts. Future plans include acquisition of data over a much broader range of conditions and improvements to the reactor design and analytical system.

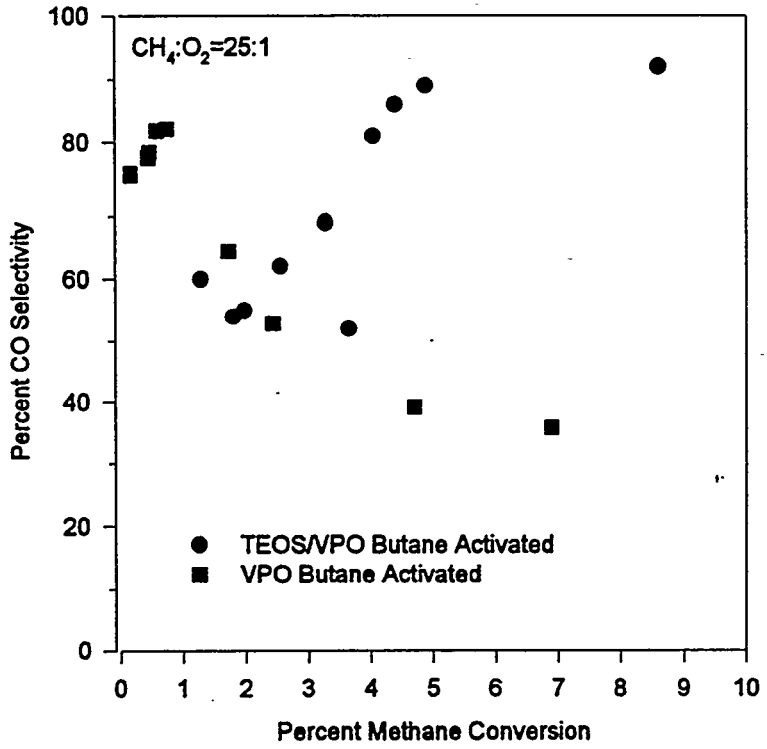

Figure 7. Carbon monoxide selectivity versus methane conversion for two catalysts. GHSV=1400.

Finally, a series of methanol oxidation tests was conducted over air activated VPO. The results are shown in Table 2. Vanadyl pyrophosphate is a highly active catalyst for methanol conversion to dimethyl ether (DME). DME formation is believed to be catalyzed exclusively by Bronsted acid sites and not by Lewis acid sites.[21] Smaller amounts of formaldehyde, methane, and methyl formate (MF) were also observed. Formaldehyde and methyl formate are oxidation products of methanol and DME, respectively. The selectivity of the catalyst in methanol conversion is remarkable in that under most conditions carbon oxides are very minor products. The data in Table 2 indicate that for the formation of oxidation products higher temperatures or pressures are required. Attempts to

[21] Klier, K., Herman, R.G. Coal Liquefaction and Gas Conversion Contractors' Review Conference, Pittsburgh, September 7-8, (1994).

perform methanol oxidation at higher temperatures using this reactor configuration resulted in reactor runaway. This indicates that at temperatures above about 350°C methanol oxidation is facile with carbon oxides as the most likely products.

Table 2. Results of methanol oxidation over air activated vanadyl pyrophosphate.

(Feed containing 70% He, GHSV=12,000@NTP)

Temperature, °C	Methanol/ Oxygen	Pressure atm	Percent Conversion	Percent Selectivity					
				CO	CO_2	DME	HCHO	MF	CH_4
250	0.3	1	27	0	0	93	0	0	7
300	3.1	1	31	2	0	77	19	0	2
250	9.9	1	10	0	0	93	0	0	7
350	10.8	1	45	1	0	80	17	0	2
250	1.4	5	7	7	0	63	30	0	0
250	3.1	5	12	1	5	94	0	0	0
300	2.3	5	31	6	1	92	0	0	1
350	2.7	5	65	26	1	73	0	0	0
300	15.3	5	18	2	1	94	0	2	1
250	1.1	10	6	0	4	95	0	0	1
300	2.1	7	20	12	1	86	0	0	1
250	13.9	10	7	2	2	90	5	0	1
350	8.7	10	44	10	1	86	1	2	0

The activity/selectivity results reported above indicate that VPO is an active catalysts for methane oxidation. The catalyst is unusual in that methanol is observed as a minor reaction product at atmospheric pressure and at relatively high oxygen partial pressure compared to previous studies. The desired reaction product, methanol, is also easily converted over this catalyst. A catalyst development approach suggested by these results is to modify the surface so that methanol conversion is inhibited. Because DME is the main product from methanol at lower temperatures, removal of the surface Bronsted acid sites by ion exchange with an alkali metal is an obvious approach.

PLANS:

Future plans for the project involve improvements in experimental techniques and synthesis of more novel catalysts followed by testing for activity and selectivity in methane oxidation. Improvements to experimental methods include:

- Surface site characterization using infrared spectroscopy. Improved procedures for obtaining spectra of acetonitrile and pyridine are being developed. Additional surface probe molecules will also be investigated.
- Measurement of acid site density. A thermogravimetric method for measurement of the number of acid sites will be developed.
- Catalyst activity testing. Improved reactors and analytical methods are tested on a regular basis and this will continue. In particular, quantitative analysis of formaldehyde and methanol observed in products has not been obtained although peaks for these materials are easily seen in the GC trace.

A number of new catalysts based on the approaches outlined above as well as catalysts based on other approaches will be prepared and tested. In particular, a number of preparations involving intercalation or pillaring of the vanadyl pyrophosphate layered structure are planned. Modification of the oxidation functionality by several different promoters will be investigated. Direct modification of the vanadyl pyrophosphate surface through ion exchange and reaction also appears to be a promising approach. For example, ion exchange of acidic or basic hydroxyl groups appears feasible and may dramatically effect activity and selectivity.[22] The results reported above strongly suggest attempting to remove surface Bronsted sites by ion exchange. Finally, in preliminary work we have developed practical procedures for preparing supported vanadyl pyrophosphate. Catalyst supports provide enhanced surface area and can interact strongly an with oxide or phosphate active phase. Catalysts based on each of these approaches will be characterized and tested in the microreactor system.

As time and funds allow, other experiments will also be performed. These include butane oxidation tests to verify that we are using *bona fide* vanadyl pyrophosphate and because some of the novel catalysts may be interesting for this application. Also, pulsed reactor testing could be performed to provide information on the performance of the catalyst in the absence of gas-phase oxygen. If activity and selectivity are adequate, a process using the catalyst as an oxygen carrier might be developed.

[22] Centi, G., Golinelli, G., Busca, G. J. Phys. Chem. 94 6813 (1990).

AR - LIQUEFACTION

TITLE: **The Role of the Resid Solvent in Coprocessing**

PI (AUTHORS): Christine W. Curtis

INSTITUTION/ORGANIZATION: Auburn University

CONTRACT NUMBER: DE-AC22-91PC91055

PERIOD OF PERFORMANCE: September 1991 to September 1995

OBJECTIVE: The objective of this project is to determine the role of petroleum resid in coprocessing of coal and resid. The question being asked is whether the resid is a reactant in the system or whether the resid is a merely a diluent that is being simultaneously upgraded? To fulfill the objective the hydrogen transfer from model compounds, naphthenes that represent petroleum resids to model acceptors is being determined. The specificity of different catalytic systems for promoting the hydrogen transfer from naphthenes to model acceptors and to coal is also being determined. In addition the efficacy of hydrogen transfer from and solvancy of whole and specific resid fractions under coprocessing conditions is being determined.

ACCOMPLISHMENTS & CONCLUSIONS:

The objective of this research was to evaluate the role of the resid in the coprocessing of coal and petroleum resid. An effective means of determining whether resid participates in the reactions at coprocessing conditions is to use model systems and trace their reaction pathways. The research performed in this study evaluated the hydrogen donability of a naphthenic compound perhydropyrene, a compound type prevalent in resids that are hydrogen-rich. Model species were also used as acceptors that represented the aromatic aspect of coal. The model acceptors that were used were anthracene and phenanthrene. In addition, coprocessing reactions using whole resids and resid fractions with coal and with a model acceptor were performed to evaluate hydrogen transfer and the solvancy ability of the resids.

Perhydropyrene has been used previously as a model donor representing resids.[1,2] In a N_2 atmosphere, perhydropyrene donated hydrogen to anthracene, increased the conversion of coal to THF soluble material, and reduced retrogressive reactions of petroleum resid in both thermal and catalytic reactions. Reactions of a number of hydrogen donor compounds such as cyclic olefins, hydroaromatic compounds, and naphthenes like perhydropyrene under equivalent reaction conditions showed that perhydropyrene had the least propensity for hydrogen donation among those compounds in both N_2 and H_2 atmospheres.[2] Since the naphthenic content of resids is significant, understanding how resids and their naphthenic content react in coal-resid coprocessing is important even though naphthenes exhibited the least hydrogen donating propensity of any of the hydrogen donors tested. In the current study, the model perhydropyrene was used to represent petroleum resid and was reacted individually and with model acceptors primarily in a H_2 atmosphere to simulate coprocessing reaction although some reactions were performed in N_2 to provide a reference point.

The model acceptors that were used included anthracene and phenanthrene, both of which are aromatic and represent molecules typically found in coal. Anthracene and phenanthrene have been

used as coal model compounds and evaluated according to their ability to accept hydrogen from either a model donor or molecular hydrogen.[3-8] Hydrogenation reactions of anthracene and phenanthrene were performed at temperatures of 325 °C[3] and 400 °C[4-8] for 60 min with a hydrogen pressure of 5 to 9.8 MPa at ambient temperature. Different catalysts were used by the researchers including $NiMo/Al_2O_3$, $NiCl_2$, and sulfided $NiMo/Al_2O_3$ at loadings of 10 to 15 % on a reactant charge basis. MoNaph has been used extensively in coal and resid coprocessing reactions.[9-15] The catalyst used in this study was a slurry phase catalyst molybdenum naphthenate (MoNaph) which was added directly to the reactor contents along with excess sulfur.

The objective of the research involving coal and resid was to determine the role of resid in the coprocessing of coal and resid: basically, is resid serving as a reactant reacting with and trasferring hydrogen to coal to produce a product or is resid serving as a diluent for coal that is simultaneously upgraded? Coprocessing reactions were performed using three different resids, Maya, FHC-623, and Manji, each of which have different characteristics in terms of the amount of asphaltenes, metals such as Ni and V, and saturates containing naphthenes. These resids were used as either whole resid, hexane solubles of the resid, or the saturate fraction of the hexane soluble fraction. The resids and resid fractions were used in coprocessing reactions with coal and with the model acceptor, anthracene. The purpose of performing these reactions was to determine if hydrogen donation was occurring from the whole resid or resid fraction to the coal or anthracene. A second purpose was to determine the effect of the resid composition on its ability to solvate coal. Two bituminous coals, Pittsburgh No. 8 and Blind Canyon, were used in this study. The amount of coal conversion to THF solubles achieved in thermal and catalytic coprocessing reactions was determined and correlated to the type of resid fraction used. In the resid reactions with anthracene, the amount of conversion of anthracene to partially saturated products was determined and the amount of H_2 accepted by anthracene was calculated to evaluate the hydrogen donating ability of the resids.

Experimental

Materials. The chemicals used in the model experiments included anthracene (ANT, 99%), phenanthrene (PHEN, 98+ %), dihydrophenanthrene (DHPN), hexahydrophenanthrene (HHPN) biphenyl, dihydroanthracene (DHA) hexahydroanthrancene (HHA), pyrene (PYR), hexahydropyrene (HHP), and perhydropyrene (PHP). These chemicals were obtained from Aldrich Chemical Company and were used as received. The slurry phase catalyst, molybdenum naphthenate (MoNaph, 6 wt % Mo), was obtained from Shepherd Chemical Company and was used as received. Sulfur added to the catalytic reactions was introduced as elemental sulfur and was obtained from Aldrich. The solvent used to recover the reaction products was HPLC grade THF from Fisher Scientific Company.

The coals used in the coprocessing reactions were Pittsburgh No. 8 obtained from the Argonne Premium Coal Sample Bank and Blind Canyon (DECS-17) bituminous coal from the Penn State Coal Sample Bank. The coal was 200 mesh and was dried before being used.

The resids used in the coprocessing reactions were Maya and FHC-623, both supplied by Amoco. The resids were used as either whole resids, hexane soluble fractions or saturate fractions of the resid in the coprocessing reactions. The fractions were produced by fractionating into hexane solubles and insolubles, and then taking the hexane soluble fraction and separating the saturates by preparative liquid chromatography. The procedure involved dissolving 5 g of hexane soluble material into 20 ml of cyclohexane and the eluting the solution through a packed silica gel column. The solution was eluted with 150 ml of cyclohexane and the eluent collected was the saturated fraction

after evaporation of the solvent. The compositions of the resids and resid fractions are given in Table 6. The carbon, hydrogen, nickel, and vanadium contents were measured by Galbraith Laboratory, Knoxville, TN. The sulfur content was determined using a Leco Model SC 32 sulfur analyzer. The MoNaph catalyst was in the same manner as in the model reactions used.

Reaction Procedures for Model Systems. The model reactions were conducted for 30 min in stainless steel tubular microreactors with a volume of ~20 mL. Each reaction was duplicated. The reactors were charged with the model reactants and with H_2 at 3.4 or 8.7 MPa at ambient temperature. When reacted individually, the model donor or model acceptors were added at ~ 0.1 g each of the donor or acceptor. When the donor and acceptor were charged simultaneously at a 1:1 weight ratio, each reactant was charged at 0.05 g, but when the weight ratio charged was 5:1, then 0.1 g of donor and ~ 0.02 g of acceptor were added. The reactions were performed at two different temperatures: 400 and 440 °C. The reactors were situated horizontally in a heated sand bath and were agitated at 400 cpm during the reaction. The liquid and solid products were removed from the reactor after being washed with 5 mL of THF and recovery obtained is given in the data tables.

Catalytic reactions were performed with MoNaph being charged to the reactors at a loading level of 1000 ppm of Mo on a total reactant charge basis. Elemental sulfur was added to MoNaph reaction in a 3:1 S to Mo ratio since MoS_2 was shown to be produced under these reaction conditions.[14] The catalyst generated in situ at reaction temperature formed finely divided catalyst particles.

The products that were recovered with THF from the reaction were analyzed on a Varian Model 3300 gas chromatograph equipped with an SGE HT-5 column and flame ionization detector. The HT-5 column had a 0.1 μm coating thickness, 0.33 mm in diameter and 25 m in length. The temperature program started at 60 °C with a final temperature of 320 °C and with a program rate of 2.5 °C/min. The temperatures of the injector and detector were 320 and 325 °C, respectively. Biphenyl was used as the internal standard.

Reaction Procedures for Coprocessing Reactions. Catalytic and thermal coprocessing reactions were performed using ~20 cm^3 stainless steel tubular microreactors. For each reaction, approximately 1 g of resid (weighed accurately to 0.0001 g) dissolved in 5 ml of THF was introduced into the reactor. The THF was evaporated by placing the microreactor in a vacuum oven overnight; coal was added to the system after the THF evaporated. In the catalytic reactions, MoNaph was introduced at a loading of 1000 ppm Mo on total reactor charge with a 3:1, S to Mo charge.

The coprocessing reaction conditions were 400 °C, for 30 min, 8.7 MPa H_2 introduced at ambient temperature, with horizontal agitation of 400 cpm. All reactions were duplicated. The reaction products were removed from the reactor by washing with several 10 mL aliquots of THF. The recovery typically obtained from these reactions ranged from 85 to 100% for resid reactions and 82 to 100% for coal and resid reactions. Conversion of the reaction products to THF soluble material was determined.

Results and Discussion

Model Naphthene and Model Acceptor Reactions

The reactions were conducted at liquefaction conditions and in the absence of a solvent. The reaction systems were composed of the model donor and model acceptors reacted individually and

combinatorially under thermal and catalytic conditions. The model donor used in all of this work was perhydropyrene and the two model acceptors were anthracene and phenanthrene.

Reactions of the Model Acceptors. The two model acceptors used in this study had different propensities for accepting H_2 from the naphthenic donor and from molecular H_2. Reactions of anthracene and phenanthrene were performed individually in N_2 and H_2 at 400 and 440 °C and are described in Tables 1 and 2. Reactions of anthracene in N_2 resulted in less than 2% conversion of anthracene to DHA. The source of the hydrogen most likely came from anthracene itself when anthracene dimerized and the released H_2 which hydrogenated anthracene to form DHA.

Coprocessing of coal and petroleum resid is typically performed at temperatures ranging from 400 to 440 °C and under a H_2 pressure of 18 to 20 MPa at reaction temperature. H_2 pressure was used in these model reactions to simulate actual reaction conditions. Therefore, reactions of the two model acceptors were performed in H_2 at temperatures of 400 and 440 °C and at H_2 pressures of 18 to 20 MPa at reaction temperature. (The corresponding pressure at ambient temperature is 8.7 MPa.) The reaction products obtained from anthracene were DHA and THA as verified by GC mass spectrometry; the products from phenanthrene were dihydrophenanthrene (DHPN) and tetrahydrophenanthrene (THPN). The amount of H_2 that was accepted in each reaction is given in the tables by the column headed by the "H_2 accepted" which is the moles of H_2 accepted per 100 moles of acceptor. Comparison of these quantities gives a measure of the amount of H_2 that had been accepted by the given acceptor under specific reaction conditions.

Anthracene was reactive in a thermal reaction with molecular H_2 present, yielding nearly 86% conversion to partially saturated products at both 400 and 440 °C (Table 1). The primary product formed was DHA at 440 °C which accounted for nearly 81% of the product; the minor product was THA which only accounted for about 5% of the product. At 400 °C, the same products were formed although the quantities were somewhat different; a lesser amount of DHA, 67.5%, and greater amount of THA, 18.4%, were formed. The results from these reactions showed that although anthracene conversion remained relatively constant at 400 and 440 °C, the amount of DHA being hydrogenated to THA increased. Therefore, the amount of H_2 accepted per 100 moles of anthracene was greater at 400 °C than at 440 °C.

Phenanthrene, in contrast to anthracene, had a lesser propensity for accepting molecular H_2 at 400 and 440 °C as evidenced by the conversion of phenanthrene being 4.7% and 9.1%, respectively (Table 2). The products from phenanthrene were DHPN and THPN which were produced in equivalent amounts in the 400 °C reaction and in an almost 2:1 ratio of DHPN to THPN in the 440 °C reaction. This lower proclivity for accepting molecular H_2 made phenanthrene the reactant of choice in the reactions with the naphthene perhydropyrene. The donation of H_2 from perhydrophyrene and acceptance of H_2 by the model acceptor would be more apparent when hydrogenation from molecular H_2 was minimized.

These model acceptors were also reacted with the slurry phase catalyst, MoNaph+S, at the same temperatures and pressures as the thermal reactions; the result of these reactions are shown in Table 1 for anthracene and Table 2 for phenanthrene at 400 and 440 °C. Although fairly small increases in the conversion were obtained in the reactions with anthracene and phenanthrene, the catalyst promoted hydrogenation of the model acceptors. For example, the conversion for phenanthrene increased from 4.7 to 9.0% at 400 °C and from 9.1 to 18.7% at 440 °C with the addition of MoNaph+S. Similarly, the conversion of anthrancene increased at both reaction

temperatures; the increase at 400 °C was from 85.9 to 88.6% conversion, while at 440 °C the increase was from 85.8 to 96.9% conversion.

Reaction of the Model Donor. The model donor used in this study was a naphthene, perhydropyrene. Perhydropyrene was used in the current study as a test naphthene molecule to examine if hydrogen transfer occurred between the model naphthene and aromatic species in H_2 and N_2 atmospheres. Perhydropyrene when reacted alone in H_2 and N_2 atmospheres thermally and catalytically at 400 and 440 °C was stable showing almost no reactivity at these conditions (Table 3). At 400 °C in N_2, no conversion of perhydropyrene occurred thermally while with MoNaph+S only 1% conversion to pyrene occurred; the thermal and catalytic conversions of PHP were 0.5% and 5.6%, respectively. At 440 °C in N_2, slightly higher conversion of perhydropyrene occurred. In H_2 at both 400 and 440 °C, perhydrophyrene was stable in noncatalytic reactions yielding at most 3% conversion. The MoNaph+S catalyst promoted conversion.

Reactions of Model Donor and Acceptors. Reactions were performed that combined the model donor perhydropyrene with the model acceptors anthracene and phenanthrene. The reactions of perhydropyrene with anthracene at 1:1 and 5:1 weight ratio under thermal and catalytic conditions are given in Table 1. The moles of H_2 accepted per 100 moles of anthracene or phenanthrene as well as the conversion of anthracene or phenanthrene served as a measure of the activity of the system.

The thermal reaction of perhydropyrene with anthracene at 400 °C and a 1:1 ratio gave a H_2 accepted of 103.9 while the addition of MoNaph+S increased the amount of H_2 accepted to 120.9. Increasing the ratio of perhydropyrene to ANT to 5:1 did not change the amount of H_2 accepted; the H_2 accepted in the thermal reaction was 104.0 while the addition of MoNaph+S increased H_2 accepted to 121.2. The primary product in all of these reactions was DHA, but the addition of MoNaph+S increased the amount of THA produced. These conversion and H_2 accepted values were nearly equivalent to those obtained without perhydropyrene at 400 °C.

Phenanthrene accepted much less donor and molecular H_2 than anthracene at equivalent reaction conditions. For example, when perhydropyrene and phenanthrene were reacted together thermally at a 1:1 and 5:1 ratio at 400 °C, the amount of conversion was 2.9 and 4.6% and the H_2 accepted was 4.4 and 7.4 moles, respectively, as shown in Table 2. The respective values for anthracene ranged from 80 to 95% conversion and 104 to 120 moles of H_2 accepted. The primary product from phenanthrene was usually DHPN with THPN being the secondary product.

Although the reactivity of phenanthrene was much lower than that of anthracene, reactions of phenanthrene with perhydropyrene responded to the presence of perhydropyrene, to change in reaction temperature, and to the type of catalyst used (Table 2). Comparison of the conversion and H_2 acceptance values at two different temperatures but at otherwise equivalent conditions showed that reactions at 440 °C promoted a higher level of conversion and H_2 accepted than those at 400 °C.

Despite the lower reactivity at 400 °C, notable differences in the reactivity were observed in the thermal reactions of phenanthrene and perhydropyrene compared to catalytic reactions containing MoNaph+S. Reactions at 5:1 ratio of donor to acceptor in N_2 at 400 °C showed that a small amount of perhydropyrene donated H_2 to phenanthrene yielding THPN as product. By comparison, the reaction of phenanthrene alone in N_2 at 400 °C did not convert any phenanthrene and, hence, did not yield any hydrogenated product. Thermal reactions at 400 °C in H_2 with a 1:1 ratio of perhydropyrene to phenanthrene converted 2.9% phenanthrene while the 5:1 ratio converted 4.6%. The amount of H_2 accepted gave a corresponding amount of 4.4 and 7.4 moles of H_2 accepted per 100 moles of phenanthrene. The increased amount of naphthene present in the reaction at 400 °C

increased the amount H_2 accepted by phenanthrene, indicating that the increased hydrogen accepted was donated by perhydrophyrene. Hydrogen was released from perhydropyrene since pyrene was formed.

In the catalytic reactions using MoNaph+S, an excess amount of perhydropyrene at 400 °C also increased the amount of phenanthrene conversion and the amount of H_2 accepted by phenanthrene. MoNaph+S promoted hydrogenation of phenanthrene to DHPH and THPN. Comparing the combined donor and acceptor reactions to the acceptor reaction alone showed that perhydropyrene being present in the thermal reaction did not increase either phenanthrene conversion or the amount H_2 accepted. However, the addition of MoNaph+S with perhydropyrene present increased both conversion and H_2 accepted at 400 °C when compared to the catalytic reaction with phenanthrene alone.

Reactions of perhydropyrene and phenanthrene at 440 °C (Table 2) showed an overall higher reactivity than those at 400 °C at corresponding reaction conditions. In N_2 with MoNaph+S at 440 °C, the amount of phenanthrene conversion to DHPN and THPN was 2.2%. The source of H_2 in the reaction was H_2 donated from perhydropyrene. In the reaction perhydropyrene produced pyrene and several partially saturated pyrene compounds, thereby donating 8.9 moles of H_2 per 100 moles of perhydropyrene. In H_2 at 440 °C, the ratio of perhydropyrene to phenanthrene affected the amount of phenanthrene conversion as well as the amount of H_2 accepted. Both the thermal and catalytic reactions at the higher ratio gave larger amounts of these quantities than at the lower 1:1 ratio. The thermal reaction at 440 °C resulted in 9.3 moles of H_2 accepted per 100 moles of phenanthrene at the 1:1 perhydrophrene to phenanthrene ratio and 16.8 moles of H_2 were accepted at the 5:1 ratio. The MoNaph+S catalyst promoted hydrogenation of phenanthrene at both ratios, yielding at the 1:1 ratio 15.8 moles of H_2 accepted by phenanthrene while at the 5:1 ratio 26.2 moles of H_2 were accepted.

Perhydropyrene reacted in these reactions with phenanthrene to form decahydropyrene (DCP), hexahydropyene (HHA), tetrahydropyrene (THP), dihydropyrene (DHP), and pyrene (PYR). When perhydropyrene was reacted alone, at 400 °C only pyrene was produced while at 440 °C with MoNaph + S a wider variety of products were formed (Table 3). Table 4 presents typical product distribution from reactions of perhydropyrene with anthracene. A calculation of the amount of H_2 donated from these products is given in the tables and is designated as the moles of H_2 donated per 100 moles of perhydropyrene or H_2 donated. In the H_2 atmosphere at 400 °C, the amount of H_2 donated from perhydropyrene remained nearly the same except for reactions containing MoNaph+S which increased H_2 donated to 6.3 from 1 to 2 in the thermal reactions. At 440 °C, higher amounts of H_2 were donated from perhydropyrene to the acceptors.

Role of Resid in Coprocessing

Thermal and catalytic coprocessing reactions of coal with whole resid and two resid fractions, hexane solubles and saturates from hexane solubles, were performed to evaluate the effect of solvent composition on solvating Pittsburgh No. 8 and Blind Canyon coal during coprocessing. In addition, these resid fractions were reacted with the hydrogen acceptor, anthracene; the amount of partially saturated products produced from anthracene in thermal and catalytic reactions was determined and the relative hydrogen donating ability of the different resid fractions was evaluated. Slurry phase MoNaph + S was the catalyst used in all of these reactions.

Characterization of the Resids. The resids chosen in this study have quite different compositions; Maya has the highest asphaltene content of 37.1% and less hexane solubles 62.9% than

the other two resids as shown in Table 5. Maya also has the highest Ramsbottom carbon and metals content of Ni and V compared to the other two resids. Fractionating the resids affected the composition of the material produced. When the asphaltenes were separated from both resids by fractionating with hexane and analyzing the hexane solubles, the V content of Maya decreased from 680 to 140 ppm and of FHC-623 from 240 to 93 ppm. The Ni content did not change substantially with the separation indicating that the compounds containing Ni were fairly evenly distributed among all the compound types in the resids. The sulfur content of the whole resids ranged from 3 to nearly 5 %. Solvent fractionation reduced the sulfur content in both Maya and FHC-623 resids. The aromaticity f_a as measured by ^1H NMR decreased for both resids from the whole resid to the hexane solubles to the saturate fraction.

Coprocessing Reactions of Coal and Resid. Coprocessing reactions were performed thermally and catalytically with Pittsburgh No. 8 and Blind Canyon coals using three resids and their resids fractions as solvents as shown in Table 6. Hexadecane served as base line solvent. The coals were also reacted without solvent. Comparison of the reactivity of the coals reacted at equivalent reaction conditions showed that Pittsburgh No. 8 was more reactive than Blind Canyon coal when reacted alone or with hexadecane as the solvent.

Coprocessing reactions of three whole resids and their fractions with Pittsburgh No. 8 and Blind Canyon coals resulted in substantial differences in the coprocessing behavior between the two coals. Compilations of the effect of the catalyst and solvent on the coprocessing reactions are given in Tables 7 and 8. In Table 7, the values for determining the effect of the catalyst were obtained by subtracting the coal conversions obtained in the thermal reactions from those obtained in corresponding catalytic reactions. Positive values indicated that the catalyst increased coal conversion compared to the thermal reaction. In Table 8, the values were obtained by subtracting the coal conversions obtained when reacting coal by itself without a solvent from coal conversion obtained when coprocessing the coal with a solvent. The addition of hexadecane increased Pittsburgh No. 8 coal conversion by 12 and 13% in both thermal and catalytic reactions; whereas, in reactions with Blind Canyon coal the addition of hexadecane only increased coal conversion by 3 to 5 %.

The slurry phase catalyst MoNaph + S was equally effective in the reactions of both coals with the whole resid and saturate fraction. However, the catalyst was much more effective in the reaction of Maya hexane solubles with Pittsburgh No. 8 than with Blind Canyon coal. A similar effect was observed with FHC-623 resid, where the hexane soluble fraction was catalyzed more with Pittsburgh No. 8 than with Blind Canyon coal. The catalytic reaction of FHC-623 whole resid converted Pittsburgh No.8 coal more than Blind Canyon coal although after the asphaltenes were removed the hexane soluble fraction was a more effective solvent in the catalytic reaction with Pittsburgh No. 8 than with Blind Canyon. After the aromatic compounds were removed from the hexane soluble fraction, the FHC-623 saturates were equally effective as solvents in catalytic reaction of both coals. In coprocessing reactions of with Manji resid and its fractions, the resid asphaltenes also appeared to have a direct influence on the resids' ability to convert in catalytic reactions coal. The whole resid was more effective solvent for converting Pittsburgh No. 8 coal while Blind Canyon coal was converted better by Manji hexane soluble fraction.

The composition of the resid solvent had a noticeable effect on the coal conversions in both the thermal and catalytic coprocessing reactions (Table 8). As in evaluating the effect of the slurry phase catalyst, the effect of the solvent was dependent on both the compositions of the resids and the coal. Maya resid, for example, positively affected the coal conversion as a whole resid and as hexane

solubles for both coals; however, the Maya saturates were detrimental to coal conversion for Pittsburgh No. 8 coal giving negative values while for Blind Canyon coal the saturates promoted coal conversion giving positive values of 11 to 12 %. The FHC-623 resid was also a better solvent for Blind Canyon coal than Pittsburgh No. 8. The whole resid gave the largest increase compared to no solvent; the hexane solubles were next followed by the saturates which gave just marginally positive values. In contrast, with Pittsburgh No. 8 coal the thermal reaction with FHC-623 hexane solubles and both thermal and catalytic reactions with FHC-623 saturates were negative. The thermal reaction of Manji whole resids yielded negative values for both coals which indicated that having Manji whole resid present in the reaction was detrimental to coal conversion. The same was true for Manji hexane solubles reacted with Pittsburgh No. 8 while the error involved in the corresponding reaction with Blind Canyon coal precludes any conclusions. The catalytic reaction with Manji whole resid and hexane solubles promoted conversion compared to no solvent being present.

The whole resids and resid fractions had distinctive abilities to convert coal. In the thermal reactions of Pittsburgh No. 8 coal, the whole resids were more effective than the hexane solubles followed by the saturates. In catalytic reactions, both the whole resids and hexane solubles were equally effective for coal conversion, while the saturates were much less effective. A different sequencing of the resid effectiveness was observed in both the thermal and catalytic reactions. The hexane solubles of some of the resids were more effective in thermal and catalytic reactions than the corresponding whole resid. The saturate fractions ranged from being very poor solvents to being similar in solvating ability as the whole resids and hexane soluble fractions.

Evaluation of Hydrogen Transfer from Resids and Resid Fractions to Anthracene. In the above described coprocessing reactions, not only did the whole resids' or resid fractions' composition affect the amount of coal conversion, but the coal's chemistry and reactivity also affected the amount of coal conversion achieved. Therefore, the effect of the resid or resid fraction itself on converting coal was difficult to discern. And, since the resid or resid fractions may serve as both solvating agents and as hydrogen donors to coal, experiments were performed with the whole resid and resid fractions using anthracene as a model acceptor to evaluate the propensity of these resid solvents to transfer hydrogen under coprocessing reaction conditions. Reactions were performed with anthracene alone and with perhydropyrene plus anthracene and hexadecane plus anthracene. These reactions showed the effect of the reaction conditions as well as the effect of having an additional hydrocarbon species present in the reaction. Table 9 presents the H_2 accepted by anthracene in these reactions; H_2 accepted is defined as the moles of H_2 accepted per 100 moles of anthracene.

Thermal reactions of anthracene alone and with the resid, resid fractions and hydrocarbons resulted in less H_2 being accepted by anthracene than in the catalytic reactions. The presence of MoNaph + S promoted hydrogenation of anthracene from molecular H_2 as shown by the increase H_2 accepted from 104.3 to 123.2 when anthracene was reacted alone in molecular H_2. The addition of a hydrocarbon solvent such as hexadecane or perhydropyrene decreased the amount of H_2 accepted by anthracene. The straight chain hydrocarbon, hexadecane, decreased the amount of H_2 accepted more than the naphthene, perhydropyrene. In fact, at a 1:1 ratio perhydropyrene only minimally reduced the amount of H_2 accepted. Two obvious factors affected the amount of H_2 accepted in these reactions: the diluent effect of adding a solvent and the amount of hydrogen that can be released from the solvent and donated to anthracene.

Introduction of Maya whole resid and resid fractions decreased the amount of H_2 accepted in both thermal and catalytic reactions compared to the anthracene alone reaction and the anthracene with perhydropyrene reaction. However, the amount of H_2 accepted was similar to that of the hexadecane reaction. For the Maya reactions, the whole resid and saturate fraction gave similar H_2 accepted in the thermal and catalytic reactions with anthracene while the H_2 accepted in the reactions with the hexane soluble fraction was less in the thermal reaction and more in the catalytic reaction than the other two resid materials. The FHC-623 whole resid and resid fractions gave very similar values for H_2 accepted in the thermal and catalytic reactions.

The diluent factor that reduced the amount of H_2 accepted was apparent in the addition of the whole resids and resid fractions to the anthracene reaction. The composition of the resids and the compatibility between the chemistry of the resid material and the catalyst were also factors that affected the amount of coal conversion achieved in these reactions.

Summary

Determining whether hydrogen donation occurred from perhydropyrene as a representative of a resid naphthene at typical coprocessing conditions was a goal of this investigation. The reactions of the model naphthene perhydropyrene and the model acceptors, anthracene and phenanthrene, clearly showed that different chemical species present in the coal have different propensities for accepting H_2 regardless of its source, molecular or donor. The model naphthene under some circumstances, like in the anthracene reaction, was a positive influence on the reaction, causing the overall amount of H_2 accepted to increase. Catalytic reactions with MoNaph+S also promoted the apparent transfer of H_2 from perhydropyrene to anthracene. Phenanthrene was not as active an acceptor as anthracene. Thermal hydrogenation of anthracene and phenanthrene with molecular hydrogen at 400 °C yielded 85% and 4.7% conversion, respectively. Excess donor model was required to observe a positive effect of the naphthene on the H_2 accepted by the model acceptor.

Coprocessing reactions of coal and petroleum resid and resid fractions showed substantial differences in the amount of conversion obtained in thermal and catalytic reactions depending on the composition of the resid solvent. The presence of the asphaltenes in the whole resid promoted coal conversion by providing a solvent that was conducive to coal conversion. Although catalysis by the slurry phase molybdenum naphthenate catalyst increased conversion for all of the fractions, catalysis improved disproportionately the ability of the hexane soluble fraction of all three resids to convert bituminous coals. Both Pittsburgh No. 8 and Blind Canyon coals' conversions were increased by catalysis although Pittsburgh No. 8 was somewhat more sensitive and yielded relatively higher conversions under catalytic conditions. The addition of a solvent to coal during these reactions resulted in more coal conversion if the solvent promoted coal conversion. The relatively inert hexadecane provided a solvent that helped to disperse the coal and the catalyst when a catalyst was used. The whole resids and most of the hexane soluble fractions promoted coal conversion; however the saturate fraction was usually detrimental to coal conversion. The composition of the resid solvent affected coal conversion and the compatibility between the resid and the catalyst. Hydrogen donation did appear to be a major factor in promoting conversion since the none of the resid materials appeared to promote coal conversion to a significant extent.

References

1. Owens, R.; Curtis, C.W. *Energy Fuels, 8*, 823, 1994.
2. Wang S.L.; Curtis, C.W. *Energy Fuels, 8*, 446, 1994.
3. Salim, S.S. and Bell, A.T. *Fuel*, 1984, Vol 63, April, 469-476.
4. Nakatsuji, Y., Kubo, T., Nomura, M., and Kikkawa, S., *Bulletin of the Chemical Society of Japan*, Vol. 51 (2), 618-624, 1978.
5. Song, C.; Nomura, M. and Ono, T. *Preprint - Am. Chem. Soc. Div. Fuel Chem., 36, 2,* 586-596, 1991.
6. Song, C.; Ono, T.; and Nomura, M. *Bulletin Chemical Society Japan 62,* 630-632, 1989.
7. Fixari, B. and Perchec, P.L., *Fuel*, 1989, Vo. 68, February, 218-221.
8. Miyak, M., Sakashita, H., Norura, M. and Kikkawa, S. *Fuel*, 1982, Vol 61, February, 124-128.
9. Cassell, F.N.; Curtis, C.W. *Energy Fuels, 2,* 1, 1988.
10. Pellegrino, J.L.; Curtis, C.W. *Energy Fuels, 3*, 160, 1989.
11. Kim, H.; Curtis, C.W. *Energy Fuels, 4,* 214, 1990a; Kim, H.; Curtis, C.W. *Energy Fuels, 4,* 206, 1990b.
12. Ting, P.S.; Curtis, C.W.; Cronauer, D.C. *Energy Fuels, 6,* 511, 1992.
13. Kim, H.; Curtis, C.W. *Fuel Sci. Tech Intl. 9*, 229, 1991.
14. Kim, H.; Curtis, C.W.; Cronauer, D.C.; Sajkowski, D.J. ACS Fuel Div. Prep. 34, 4, 1446, 1989.
15. Brannan, C.J.; Curtis, C.W.; Cronauer, D.C. *Fuel Proc. Tech.* in press, 1995.

Acknowledgements

The support of the United States Department of Energy under contract No. DE-AC22-91PC91055 for this work is greatly appreciated.

Table 1. Anthracene at Reactions 400 °C and 440 °C: Reacted Alone and With Perhydropyrene

Reaction Condition	Reactants	Atmosphere	T (°C)	Product Distribution (mol%)			Recovery (%)	ANT Conversion, %	H_2 Accepted H_2 Donated
				ANT[c]	DHA	THA			
Thermal	ANT	N_2	400	98.3±0.17	1.70±0.17	0±0	92.5	1.7	1.7
Thermal	ANT	H_2	400	14.1±0.8	67.5±0.4	18.4±1.2	90.1	85.9	104.3
MoNaph + S	ANT	H_2	400	11.4±0.6	70.0±9.3	26.6±8.6	94.4	88.6	123.2
Thermal	ANT	H_2	440	14.2±0.40	80.9±0.42	4.9±0.82	84.4	85.8	90.75
MoNaph + S[b]	ANT	H_2	440	3.8±0.06	55.8±0.62	40.4±2.1	80.1	96.9	136.58
Thermal	PHP: ANT 1:1	N_2	400	94.0±1.8	6.0±1.8	0.0±0.0	82.5	6.0	6.5±0.7
MoNaph + S	PHP: ANT 1:1	N_2	400	95.4±1.1	3.2±1.2	1.4±0.1	85.2	4.6	6.0±0.9
Thermal	PHP: ANT 1:1	N_2	440	94.4±0.4	4.6±0.1	1.0±0.3	83.8	5.6	6.5±0.7
MoNaph + S	PHP: ANT 1:1	N_2	440	96.3±0.1	3.7±0.1	0.0±0.0	87.1	3.7	4.3±0.3
Thermal	PHP: ANT 1:1	H_2	400	5.9±0.5	84.3±4.5	9.8±4.0	98.2	94.1	103.9
MoNaph + S	PHP: ANT 1:1	H_2	400	3.4±0.8	72.5±5.2	24.1±6.0	96.8	96.6	120.9
Thermal	PHP: ANT 5:1	H_2	400	6.3±2.1	83.4±0.6	10.3±2.7	92.2	93.7	104.0
MoNaph + S	PHP: ANT 5:1	H_2	400	5.3±2.0	68.2±6.5	26.6±4.5	82.9	94.7	121.2

[a] Reaction time = 30 min; 8.7 MPa H_2 or N_2 at room temperature.
[b] MoNaph + S = Mo naphthenate with added elemental S.
[c] ANT = anthracene; DHA = dihydroanthracene; THA = tetrahydroanthracene; H_R = (1 x DHA mol% + 2 x THA mol%) x 100.
[d] Reactant loading: Aproximately 0.05 g of each ANT and PHP in PHP:ANT = 1:1 thermal and catalytic reactions; Approximately 0.02 g of ANT and 0.1 g of PHP in PHP:ANT = 5:1 thermal and catalytic reactions.
Mo naphthenate loading is approximately 0.0017 g = total reactant charge (0.1 g)/ 60, computed according to 1000 ppm MoS_2 and 6 wt% Mo in Mo naphthenate.

Table 2. Phenanthrene Reactions at 400 and 440 °C: Reacted Alone and With Perhydropyrene

Reaction Condition	Reactant	Atmosphere	T(°C)	Product Distribution (mol %)			Recovery (%)	PHEN Conversion (%)	H_2 Accepted[b]	H_2 Donated[c]
				PHEN	DHPN	THPN				
Thermal	PHEN	N_2	400	100±0.0	0.0	0.0	86.6	0.0	0.0	NA[d]
MoNaph	PHEN	N_2	400	100±0.0	0.0	0.0	85.5	0.0	0.0	NA
Thermal	PHEN	H_2	400	95.3±0.7	2.6±0.5	2.1±0.2	83.5	4.7	6.8±0.9	NA
MoNaph+S[b]	PHEN	H_2	400	91.0±0.0	6.0±0.0	3.0±0.1	87.3	9.0	12.0±0.1	NA
Thermal	PHEN	N_2	440	100 ±0.0	0.0	0.0	87.6	0.0	0.0	NA
MoNaph+S	PHEN	N_2	440	100 ±0.0	0.0	0.0	85.3	0.0	0.0	NA
Thermal	PHEN	H_2	440	90.9±1.2	5.9±0.7	3.2±0.5	91.8	9.1	12.3±1.7	NA
MoNaph+S	PHEN	H_2	440	81.3±3.8	12.8±2.4	5.9±1.4	82.0	18.7	24.6±5.2	NA
Thermal	PHP: PHEN 1:1	H_2	400	97.1±0.2	1.5±0.0	1.4±0.2	88.5	2.9	4.4±0.3	1.2±0.1
MoNaph+S	PHP: PHEN 1:1	H_2	400	86.9±2.0	9.0±1.5	4.1±0.5	90.0	13.1	17.2±2.5	6.2±0.0
Thermal	PHP: PHEN 5:1	N_2	400	98.4±0.2	0.0±0.0	1.6±0.2	92.3	1.6	3.2±0.4	3.8±0.0
MoNaph+S	PHP: PHEN 5:1	N_2	400	99.0±0.0	0.0±0.0	1.0±0.0	86.6	1.0	2.0±0.0	3.9±0.0
Thermal	PHP: PHEN 5:1	H_2	400	95.4±0.2	1.8±0.4	2.8±0.8	86.9	4.6	7.4±2.1	1.8±0.0
MoNaph+S[b]	PHP: PHEN 5:1	H_2	400	82.8±0.1	10.7±0.6	6.5±0.1	92.9	17.2	23.7±0.1	6.3±0.0
Thermal	PHP: PHEN 1:1	H_2	440	93.2±1.4	4.4±0.8	2.4±0.6	92.5	6.8	9.3±2.1	0.9±0.1
MoNaph+S	PHP: PHEN 1:1	H_2	440	87.2±1.3	9.9±0.7	2.9±0.6	94.8	12.8	15.8±1.9	7.5±0.1
Thermal	PHP: PHEN 5:1	H_2	440	87.1±1.1	9.0±0.0	3.9±1.2	86.0	12.9	16.8±2.3	8.6±0.1
MoNaph+S[b]	PHP: PHEN 5:1	H_2	440	79.5±3.6	14.9±2.1	5.6±1.5	80.0	20.5	26.2±5.1	10.7±0.6
MoNaph+S	PHP: PHEN 5:1	N_2	440	97.8±0.2	0.5±0.1	1.7±0.7	86.4	2.2	3.9±1.0	8.9±0.1

[a] Reaction Conditions: 30 min; 8.7 MPa H_2 or N_2 introduced at ambient temperature; catalyst loading = 1000 ppm on total reactant charge basis; the total amount of reactant charged is approximately 0.1 g.

[b] Moles of H_2 Accepted per 100 moles of PHEN; H_2 accepted = (2 x THPN mol% + 1 x DHPN mol%) x 100.

[c] Moles of H_2 Donated per 100 moles of PHP; H_2 Donated = (3 x DCP mol% + 5 x HHP mol% + 6 x THP mol% + 7 x DHP mol% + 8 x PYR mol%) x 100.

Table 3. Product Distribution of Perhydropyrene from Thermal and Catalytic Reactions at 400 and 440 °C[a]

Reaction Conditions	Atmosphere	Temperature (°C)	Catalyst Loading (ppm)	Product Distribution (wt%)			Recovery (%)	PHP Conversion (%)
				PHP	PYR	Others		
Thermal	N_2	400	0	100.0±0.0	0.0±0.0	0	85.5	0.0
Mo Naph+S	N_2	400	1000	99.0±0.5	1.0±0.5	0	82.5	1.0
Thermal	N_2	440	0	99.5±0.8	0.5±0.8	0	88.1	0.5
Mo Naph+S	N_2	440	1000	94.4±0.1	1.6±0.4	4.0±0.4	82.6	5.6
Thermal	H_2	400	0	100.0±0.0	0.0±0.0	0	82.1	0.0
Mo Naph+S	H_2	400	1000	99.8±0.0	0.2±0.0	0	78.3	0.2
Thermal	H_2	440	0	97.0±0.0	3.0±0.0	0	87.3	3.0
Mo Naph + S	H_2	440	1000	97.9±0.3	0.4±0.1[c]	1.7±0.2[d]	85.8	2.1

[a] Reaction Conditions: 30 min, 8.7 MPa H_2 introduced at ambient temperature. [b] PHP = perhydropyrene; PYR = pyrene. [c] 0.4±1 is the wt % of HHP.
[d] Other unidentitiable peaks.

Table 4. Product Distributions of Perhydropyrene from Reactions of Anthracene with Perhydropyrene

Reaction Conditions	Catalyst Loading (ppm)	Atmosphere	Reaction Temperature (°C)	Product Distribution (mole %)			Recovery (%)	H_2 Accepted:[e] moles of H_2 Accepted per 100 moles of ANT	H_2 Donated:[f] moles of H_2 Donated per 100 moles of PHP
				PHP	PYR	Others			
Thermal	0	N_2	400	100±0	0	0	87.3	6.0±1.8	0.0±0.0
MoNaph+S	1000	N_2	400	99.6±0.5	0.4±0.5	0	82.0	6.0±0.9	3.2±0.5
Thermal	0	N_2	440	98.1±0.5	1.9±0.5	0	83.8	6.5±0.7	15.2±0.5
MoNaph+S	1000	N_2	440	98.8±0.3	1.2±0.3	0	83.9	4.3±0.3	9.6±0.3

[e] H_2 Accepted = (1 x DHA mol % + 2 x THA mol %) x 100. [f] H_2 Donated = (8 x PYR mol %) x 100.

Table 5. Characteristics of Resids and Resid Fractions

Resid	Fractions (wt %)[a]			Elemental Analysis				Ramsbottom Carbon (wt%)	Metals (ppm)		
	Hexane Solubles	Toluene Solubles	THF Solubles	C	H	H/C	S		V	Ni	Fe
Maya	62.9±1.1	37.1±1.1	0.0	83.4[b]	9.5	1.4	5.2	28.3[b]	660[b]	123	20
Manji	86.1±0.7	13.9±0.7	0.0	85.1[b]	10.8	1.5	2.6	16.2	235	222	22
FHC-623	83.3±1.1	14.9±0.4	1.8±0.8	86.2[c]	10.4	1.5	3.7	NA	240[c]	84	NA

[a] Analyzed, [b] Data provided by Amoco, [c] Analyzed at Galbraith Laboratories, Knoxville, TN.

Table 6. Coprocessing Reactions of Coals and Resids

Reactions	Coal Conversion (%)			
	Pittsburgh No. 8		Blind Canyon DECS-17	
	Thermal	Catalytic	Thermal	Catalytic
Coal	44.8±2.1[a]	61.7±4.2	26.4±0.4	45.3±0.8
Coal + Hexadecane	59.1±4.7	84.9±3.3	31.9±0.6	48.4±1.1
Maya Complete Reaction Matrix				
Coal + Whole Resid	56.2±5.2	89.3±1.1	31.8±2.2	64.0±2.3
Coal + Hexane Solubles	49.2±2.2	82.9±2.2	40.5±0.7	49.2±0.2
Coal + Saturate Fraction	37.2±1.4	59.8±1.4	37.7±1.8	57.7±7.4
FHC-623 Complete Reaction Matrix				
Coal + Whole Resid	68.4±4.1	77.9±1.4	49.2±0.2	72.9±1.4
Coal + Hexane Solubles	44.3±4.4	77.8±6.6	43.6±0.7	63.4±0.6
Coal + Saturate Fraction	29.9±5.1	56.9±5.6	27.7±3.0	53.9±2.1
Manji Complete Reaction Matrix				
Coal + Whole Resid	34.9±4.7	75.8±2.9	23.9±2.5	51.9±2.3
Coal + Hexane Solubles	29.3±0.4	77.5±3.3	50.1±11.2	78.7±3.5
Coal + Saturate Fraction	25.6±0.6	32.7±9.8	9.4±3.3	52.6±1.6

[a] Reaction Conditions: 400 °C, 30 min, 8.7 MPa H_2 introduced at ambient temperature.

Table 7. Increase in Coal Conversion Caused by Slurry Phase Catalysis

	Pittsburgh No. 8 (%)	Blind Canyon DECS-17 (%)
Coal	16.9	18.9
Coal + Hexadecane	25.8	16.5
Maya Reacton Matrix		
Coal + Whole Resid	33.1	32.2
Coal + Hexane Solubles	33.7	8.7
Coal + Saturates	22.6	20.0
FHC-623 Reaction Matrix		
Coal + Whole Resid	9.5	23.7
Coal + Hexane Solubles	33.5	19.8
Coal + Saturates	27.0	26.2
Manji Reaction Matrix		
Coal + Whole Resid	40.9	28.0
Coal + Hexane Solubles	48.2	28.6
Coal + Saturates	14.7	43.2

Ma3. shen2.pap

Table 8. Increase in Coal Conversion Caused by Addition of Solvent

Reactions	Coal Conversion (%)			
	Pittsburgh No. 8		Blind Canyon DECS-17	
	Thermal	Catalytic	Thermal	Catalytic
Coal	–	–	–	–
Coal + Hexadecane	14.3	23.2	5.5	3.1
Maya Complete Reaction Matrix				
Coal + Whole Resid	11.4	27.6	5.4	18.7
Coal + Hexane Solubles	4.4	21.2	14.1	3.9
Coal + Saturates	-7.6	-1.9	11.3	12.4
FHC-623 Complete Reaction Matrix				
Coal + Whole Resid	23.6	16.2	22.8	27.6
Coal + Hexane Solubles	-0.5	16.1	17.2	18.1
Coal + Saturates	-14.9	-4.8	1.3	8.6
Manji Complete Reaction Matrix				
Coal + Whole Resid	-9.9	14.1	-2.5	6.6
Coal + Hexane Solubles	-15.5	15.8	23.7	33.4
Coal + Saturates	-19.2	-21.4	-17.0	7.3

Table 9. Hydrogen Accepted in Reactions with Hydrogen Donors

Reactions	H_2 Accepted[a]	
	Thermal	Catalytic
ANT	104.3	123.2
PHP + ANT (1:1)	103.9	120.9
Hexadecane + ANT (1:1)	89.0	108.8
Maya Whole + ANT (1:1)	95.1	106.9
Maya Hexane Solubles + ANT (1:1)	87.7	111.7
Maya Saturates + ANT (1:1)	95.5	103.5
FHC-623 Whole + ANT (1:1)	96.9	105.4
FHC-623 Hexane Solubles + ANT (1:1)	92.2	106.4
FHC- 623 Saturates + ANT (1:1)	94.9	100.9

[a] H_2 accepted per 100 mol of ANT
[b] Reaction Conditions: 400 °C, 30 min, 8.7 MPa H_2 introduced at ambient temperature.

Ma3. shen2.pap

Title: **Molecular Catalytic Coal Liquid Conversion**

Authors: Leon M. Stock and Shiyong Yang

Organization: Department of Chemistry, The University of Chicago
5735 S. Ellis Ave., Chicago, IL 60637

Contract No.: DE-AC22-91PC91056

Period of Performance: September 27, 1992 - March 26, 1996

Objectives: This research, which is relevant to the development of new catalytic systems for the improvement of the quality of coal liquids by the addition of dihydrogen, is divided into two tasks. Task 1 centers on the activation of dihydrogen by molecular basic reagents such as hydroxide ion to convert it into a reactive adduct $[OH{\cdot}H_2]^-$ that can reduce organic molecules. Such species should be robust withstanding severe conditions and chemical poisons. Task 2 is focused on an entirely different approach that exploits molecular catalysts, derived from organometallic compounds that are capable of reducing monocyclic aromatic compounds under very mild conditions.

Accomplishments and Conclusions:

Task 1 Organic Base-catalyzed Hydrogenation

Introduction

It has been known for a long time that simple basic molecules such as potassium t-butoxide catalyze the hydrogenation of benzophenone [1,2]. Moreover, simple bases such as hydroxide ion and amide ion catalyze the exchange of dideuterium with water and ammonia, respectively [3]. The energy barrier for the exchange of dideuterium with potassium amide in liquid ammonia is less than 5 kcal mol^{-1}, and that for dideuterium exchange in aqueous potassium hydroxide is less than 25 kcal mol^{-1}. Several lines of evidence including the kinetic isotope effects imply that dihydrogen forms an adduct, sometimes referred to as a vander Waals molecule, with hydroxide ion and that exchange occurs within this adduct rather than through free hydride anion. The proposed immediates, the H_3O^- and H_4N^- anions, have been detected in ion cyclotron resonance experiments [4,5], and the nature of the bonding within these species has been investigated theoretically [6]. There are several different structures that differ only modestly in energy content, the most stable ones have long hydrogen-hydrogen bonds, between 0.92 Å and 0.97 Å, compared to 0.73 Å in the dihydrogen molecule. The most stable structures can be described as solvated hydride ions with theoretical binding energies near 20 kcal mol^{-1}. They can rearrange via internal proton motion to dihydrogen complexes, which are 2 to 15 kcal mol^{-1} less stable than hydride adduct. Clearly, the hydrogen-hydrogen bond is greatly weakened in these substances and it is this feature that we sought to exploit for the hydrogenation of aromatic hydrocarbons and coal liquids.

Experimental Section

Hydrogenation of the coal liquid or aromatic hydrocarbon was performed in a Model 4576 HP/HT T316 autoclave system manufactured by Parr Instrument Company. The temperature was controlled by the Model 4842 temperature controller. In a typical experiment, naphthalene (6.4g, 0.05 mole) and freshly distilled hexane (38 ml) were placed in the autoclave, lithium diisopropylamide (0.0125 mole) suspended in hexane (10 wt%, 13.4 ml) was added to the autoclave under dinitrogen. The sealed autoclave was purged with dinitrogen and then with dihydrogen several times to replace the air, before it was filled with dihydrogen at the desired pressure. The mixture was stirred at 200 °C for 18 hrs. The products were isolated in the customary way and the product distribution was determined by GC-MS and ^{1}H NMR.

Results and Discussion

Base-activated hydrogenation of aromatic hydrocarbons

Several different strong bases were tested as catalysts for the hydrogenation of naphthalene. The results, Table 1, indicate that alkali metal *t*-butoxides (sodium *t*-butoxide, potassium *t*-butoxide and lithium *t*-butoxide) do not effect the hydrogenation of naphthalene at 200 °C and 1000 psig of hydrogen in hexane or *t*-butanol as solvent even though potassium *t*-butoxide does reduce benzophenone to benzhydrol [1,2]. We found that the sodium amide and lithium amide can reduce naphthalene in low yield (1.0% for $NaNH_2$ and 7.0% for $LiNH_2$) at 200 °C and 1000 psig of hydrogen. Even more success was realized with lithium organoamides such as lithium diisopropylamide and lithium dicyclohexylamide. They exhibit very effective catalytic activities for the hydrogenation of naphthalene to tetralin in more than 95% yield at 1000 psig and 200 °C for 5 hrs. The reaction proceeds cleanly with no byproducts.

Table 2 shows the results for a series of lithium organoamides as catalysts for the same hydrogenation reaction. The catalytic activities of the lithium organoamides depend importantly on the ligands. For instance, lithium diisopropylamide can catalyze the hydrogenation of naphthalene to tetralin in 100% yield, but lithium diethylamide and dimethylamide provide only 3 to 7% conversion. Thus, the lithium organoamides with larger aliphatic substituents exhibit higher activities than those with small substituents such as lithium diethylamide, lithium dimethylamide or lithium bis(trimethylsilyl)amide. In addition, the catalytic activities of the alkali metal trimethylsilylamides decrease in the order $K^+ > Na^+ > Li^+$ in toluene solution. Potassium bis(trimethylsilyl)amide, like lithium diisopropylamide, is a very active catalyst. However, the yield of tetralin was decreased when sodium bis(trimethylsilyl)amide and lithium bis(trimehylsily)amide were used as the catalysts under the same conditions.

The reaction was also influenced by the amount of the catalyst. The yield of tetralin reaches about 94% when the mole ratio of the substrate to the catalyst was less than 12.5. The yield depends on the hydrogen pressure, but the reaction proceeds very well (80% yield) even when the dihydrogen pressure is reduced to 300 psig.

Lithium diisopropylamide does not dissolve in hexane at room temperature, so a suspension of the catalyst in hexane was used. Indeed, a clear homogeneous solution was observed when the autoclave was opened after the reaction was completed, then a white solid slowly precipitated. The lithium content of the white solid was determined to be between 31 and 38 wt% by a gravimetric method [7] implying that the solid probably was a mixture of LiOH and Li_2O(Li : 37.7% in the 1:1 mixture). This material was produced by the reaction of lithium diisopropylamide with water.

The substitution of dideuterium gas for dihydrogen gas in the catalytic hydrogenation of naphthalene produced highly deuterated tetralin, indicating that the

protons in the reduced aromatic molecule come from the dihydrogen molecules and not the solvents.

Other aromatic hydrocarbons were also investigated. Anthracene was hydrogenated to 9,10-dihydroanthracene in 95% yield and to another unidentified compound in 3% yield. Acridine was converted to 9,10-dihydroacridine in 77% yield and to 9% of another unidentified compound under 1000 psig of hydrogen pressure at 200 °C. At 300 °C, 1-methoxynaphthalene was hydrogenated in 95% yield; the main products are 1,2,3,4,-tetrahydromethoxynaphthalene(63%) and 1,2,3,4-tetrahydronaphthalene(12%).

The results indicate that organoamides, especially lithium diisopropylamide and potassium (trimethylsilyl)amide, are active catalysts for the hydrogenation of bicyclic and polycyclic aromatic hydrocarbons.

Hydrotreating of coal liquids

Coal liquids supplied by The Department of Energy have also been investigated. The results for two bases, lithium diisopropylamide (Catalyst 2) and potassium bis(trimethylsilyl)amide (Catalyst 5), are shown in Table 3. Three experiments with various catalyst loadings were performed with regard to the Catalyst 2. The conversions of the aromatic compounds in the sample were calculated from the decrease in intensity of the absorptions at 321 and 338 nm in UV-Visible spectrum. The conversions reached 82% at 338 nm and 97% at 321 nm when 4 g of Catalyst 2 per 10 g of coal liquids was employed. The elemental analysis for the product obtained under these conditions indicates that the carbon content (89.13%) decreased 0.45 units as the hydrogen content (10.70%) increased 0.62 units. Thus the H/C ratio increased from 1.36 to 1.43.

Catalyst 5 is an even more effective catalyst for the hydrotreating of the coal liquid. VSOH was hydrotreated to form a clear yellow liquid under mild conditions (1000 psig of hydrogen and 200 °C) if 16 mol% of Catalyst 5 was employed. The resonances between 8.0 and 8.3 ppm in ^{1}H NMR spectrum of the product, which are attributed to the protons bonded to aromatic carbon atoms of bi- and tricyclic molecules disappeared as new resonances of protons bonded to aliphatic carbons appeared. In addition, the absorptions at 321 and 338 nm in the UV-Visible spectrum, which are also attributed to the absorptions of polycondensed aromatic hydrocarbons, also completely disappeared, indicating that all the condensed aromatic compounds such as naphthalene derivatives were hydrogenated to the monoaromatic hydrocarbons.

The effects of temperature, catalyst loading as well as hydrogen pressure on the hydrotreating of coal liquids have also been studied. In general, after being hydrotreated, the coal liquid has a lower carbon content and higher hydrogen content than the untreated coal liquid sample.

Task 2 Catalytic Hydrogenation of Aromatic Compounds by Rh Catalysts

Introduction

The advantages of aqueous phase catalysis for hydroformylation and related processes has received considerable scientific scrutiny in recent years. One successful example is the Ruhrchemie/Rhone-Poulenc process in which water-soluble rhodium complexes catalyze the hydroformylation of propene. There are indications that the water, which is used as solvent in the two-phase system, alters the chemistry.

Preliminary research on the use of metal catalysts that was already underway in our laboratory prompted us to consider the use of aqueous systems for the hydrogenation of aromatic compounds in coal liquids.

Results and Discussion

The dimer of chloro(1,5-hexadiene)rhodium is an active catalyst precursor for the hydrogenation of aromatic hydrocarbons and heterocyclic compounds under phase transfer conditions involving tetrabutylammonium hydrogen sulfate (THS) or cetyltrimethylammonium bromide (CTAB) in an aqueous buffer [8]. This catalyst was investigated in more detail in our laboratory using tetralin as the substrate. Table 4 shows the influence of several phase transfer agents on the hydrogenation of tetralin to decalin at [substrate]/[catalyst] = 200/1. It can be seen that the addition of surfactant molecules reduces the activity of the catalyst. The conversion of the tetralin was decreased from 91% to 30% when THS was used. Similar results were obtained for CTAB and other surfactants exhibited even more negative effects on the reaction. It was clear that $[1,5\text{-HDRhCl}]_2$ was a more effective catalyst in the systems which contained low concentrations of the surfactant, and that some surfactants hindered the reaction. It is also noteworthy that $[1,5\text{-HDRhCl}]_2$ does not catalyze the reduction reaction of tetralin when only one of the solvents is used.

The use of buffers as the aqueous phase showed that the pH values and the composition of the buffer both effect the reaction, Table 5. The buffers with same compositions but different pH values and those with same pH value but different compositions all yield different conversions. The high yield (91%) was obtained by using hydion buffer at pH=7.4. In addition, the optimum volume ratios for the aqueous phase to organic phase were in the range 0.3-0.6 with more than 85% of tetralin hydrogenated to decalin under these conditions.

Methylene chloride, chloroform, dimethylethylene oxide alcohols, aliphatic hydrocarbons including hexane, cyclohexane, heptane, and higher homologues were studied. Hexane proved to be the most generally suitable cosolvent.

Other aromatic compounds were also hydrogented with this catalyst system. The reaction process was influenced by the subsituents in the aromatic ring, and the ease of the hydrogenation was found to be in the order benzene, toluene>n-butylbenzene> o-xylene> mesitylene.

Although the catalytic activity of $[1,5\text{-HDRhCl}]_2$ for the hydrogenation of tetralin was very good, the catalyst system had poor stability. The Rh metal aggregated on the wall of the reactor and appeared to be deactivated. We have begun to address this problem. The highest turnover number achieved under the optimum conditions with the [substrate]/[catalyst]=200:1 and the [aqueous phase]/[organic phase]=0.3 was 200. However, we found that small amounts of some surfactants ([surfactant]/[Rh]= 1.0) appear to form an emulsion to stabilize the catalyst without apparently affecting its activity. Under these conditions, the stability of the catalyst was improved greatly. In an experiment that was carried out for eight days, we found the turnover number of the catalyst exceeded 1200.

Our observations suggest that an active, stable catalyst system can be obtained for hydrogenation of monocyclic aromatic compounds under mild conditions. In addition, the noble metal can be separated and recycled. Thus, systems of this kind may prove highly effective for the removal of aromatic compounds from coal liquids.

Future Plans

The research will continue to focus on these two tasks. More work will be done on the rhodium catalyst system to improve its performance and to apply this catalyst system for the hydrotreating of coal liquids. Hydrotreating of coal liquids catalyzed by organic bases will proceed in parallel.

Reference

1. C. Walling and L. Bolyky, *J. Am. Chem. Soc.*, **1961, 83, 2968**
2. C. Walling, and L. Bolyky, *J. Am. Chem. Soc.*, **1964, 86, 3750**
3. C. Dayton and W. Wilmarth, *J. Chem. Phys.*, **1950, 18, 759**
4. J. C. Klingeld, S. Ingemann, J. E. Jalonen and N. M. M. Nibbering, *J. Am. Chem. Soc.*, **1983, 105, 2474**
5. S. C. Ingemann, J. C. Klingeld and N. M. M. Nibbering, *J. Chem. Soc., Chem. Commun.*, **1982,** 1009
6. D. Cremer and E. Koraka, *J. Phys. Chem.*, **1986, 90, 33**; G. Chalasinski, R. A. Kendall and J. Simons, *J. Chem. Phys.*, **1987, 87, 2965**
7. G. A. Simmons, Jr., *J. Ann. Chem.*, **1953, 25, 1386**
8. K. R. Januszklewicz and H. Alper, *Organometallics,* **1983, 2, 1055-1057**

Table 1 The organic bases used in attempts to activate hydrogen for the reduction of naphthalene

Organic Bases	[Substrate]/ [Base] (mole/mole)	Solvent	Conversion (%)
NaOBu-*t*	4:1	Hexane	0
LiOBu-*t*	4:1	Hexane	0
KOBu-*t*	1:2	Hexane	1
	1:2	*t*-BuOH	0
$NaNH_2$	4:1	Hexane	1
$LiNH_2$	4:1	Hexane	7
$LiN[CHMe_2]_2$	4:1	Hexane	100
$LiN[C_6H_{11}]_2$	4:1	Hexane	95

Conditions: Substrate: naphthalene; Solvent: 50 ml; Temperature: 200 °C; Initial H_2 pressure: 1000 psig; Reaction time: 18 hrs.

Table 2 Influence of ligands on the catalytic activity of lithium amides for the hydrogenation of naphthalene to tetralin

$LiNR_2$	[Substrate]/ [$LiNR_2$] (mole/mole)	Solvent	Conversion (%)
$LiN[CHMe_2]_2$	4:1	Hexane	100
$LiN(C_6H_{11})_2$	4:1	Hexane	95
$LiN[CH_2Me_2]_2$	4:1	Hexane	3
$LiNMe_2$	2:1	Hexane	7
$LiN[SiMe_3]_2$	2:1	Hexane	16
$LiN[SiMe_3]_2$	4:1	Toluene	3
$NaN[SiMe_3]_2$	4:1	Toluene	51
$KN[SiMe_3]_2$	4:1	Toluene	100

Conditions: Substrate: naphthalene; Solvent: 50 ml; Temperature: 200 °C; Initial H_2 pressure: 1000 psig; Reaction time: 18 hrs.

Table 3 Hydrotreating of coal liquid(VSOH) with Catalysts 2 and 5

Catalyst	[VSOH]/ [Catalyst] (g/g)	Temperature (°C)	Yield (%)	Conversion(%)		H/C Ratio
				321nm	338nm	
	VSOH	200	95	0	0	1.38
2	10/1	300	82	22	17	1.41
	10/2	300	81	77	62	1.43
	10/4	300	76	97	82	1.43
5	10/1	200	90	48	32	1.40
	10/2	100	92	95	90.0	1.43
		200	87	100	100	1.45
		250	89	100	100	1.49
		300	95	100	100	1.57
	10/4	200	93	100	100	1.57

Conditions: Solvents: Hexane for Catalyst 2 and Hexane-toluene mixture (2/3 v/v) for Catalyst 5; Reaction volume: 50 ml; Hydrogen pressure: 1000 psig at 25 °C; Reaction time: 24 hrs; Catalyst 2: $LiN(CHMe_2)_2$; Catalyst 5: $KN[SiMe_3]_2$.

Table 4 Effect of surfactants on the conversion of tetralin to decalin catalyzed by [1,5-HDRhCl]$_2$ catalyst

No	[Surfactant]/[Rh] (mole/mole)	Yield(%) *Trans*-decalin	*Cis*-decalin	Total
None	–	18	74	91
THS	0.5	12	76	87
	8.0	4	26	30
CTAB	0.5	19	81	100
	1.0	21	79	100
	2.0	18	82	100
	4.0	13	61	73
	8.0	7	37	44
Aliquat 336	1.0	12	66	78
Tween 20	1.0	8	38	45
DSS	1.0	17	83	100

Conditions: Substrate: Tetralin(3.3g, 25.0 mmole) Catalyst: [1,5-HDRhCl]$_2$ (58 mg, 0.126 mmole); [Substrate]/[Catalyst]: 200/1; Solvent: Hexane(30 ml); Buffer(pH=7.4): 20ml, [Aqueous phase]/[Organic phase](v/v): 0.60; Temperature: 25 °C; H_2 pressure: 1 atm.

THS: Tetrabutylammonium hydrogen sulfatre,
CTAB: Cetylmethylammonium bromide,
Aliquat 336: Tricaprylmethylammonium chloride,
DDS: Dodecylsulfate sodium salt.

Table 5 Influence of the buffer as the aqueous phase on the biphase hydrogenation of tetralin to decalin catalyzed by [1,5-HDRhCl]$_2$

No	Buffer (pH, composition)	Yield(%) *Trans*-decalin	*Cis*-decalin	Total
1	Buffer (pH=7.4, Hydrion)	18	74	92
2	Buffer (pH=7.0, Hydrion)	7	32	39
3	Buffer (pH=8.0, Hydrion)	5	33	37
4	Buffer (pH=7.4, phosphate, 0.1M)	6	29	34
5	Buffer(pH=7.4, Phosphate:0.001M, NaCl: 0.138M, KCl: 0.027M, Tween 20: 0.05 % w/v)	4	36	41
6	Buffer(pH=7.4, Trizma saline: 0.05M NaCl: 0.56 %)	3	25	28

Conditions: Substrate: Tetralin(3.3g, 25.0 mmole); Catalyst: [1.5-HDRhCl]$_2$ (58 mg, 0.126 mmole); [Substrate]/[Catalyst]: 200: 1; Solvent: Hexane(30 ml); Buffer: 10 ml; [Aq.phase]/[Org. phase]: 0.30; Temperature: 25 °C; H_2 pressure: 1 atm.

Dispersed Catalysts for Co-processing and Coal Liquefaction

Bradley Bockrath, Derrick Parfitt, Ronald Miller,
Murphy Keller,III, Edward Bittner

Pittsburgh Energy Technology Center

10/94 - 9/95

Objective:

The basic goal is to improve dispersed catalysts employed in the production of clean fuels from low value hydrocarbons. The immediate objective is to determine how the properties of the catalysts may be altered to match the demands placed on them by the properties of the feedstock, the qualities of the desired end products, and the economic constraints put upon the process.

Several interrelated areas of the application of dispersed catalysts to co-processing and coal conversion are under investigation. The first involves control of the selectivity of MoS_2 catalysts for HDN, HDS, and hydrogenation of aromatics. One means of controlling selectivity lies in the manipulation of the morphology of the slab-like particles of MoS_2. The main concern is to gain control of the relative number of edge and rim sites on the catalyst. Rim sites, those located at the juncture of the edge and basal planes, are regarded as active for hydrogenation, while edge sites participate in the direct removal of sulfur (1). A prime example of the later reaction is the conversion of dibenzothiophene to biphenyl and H_2S. A method of preparing MoS_2 catalysts with varying ratios of edge to rim sites will be employed to investigate the importance of controlling the selectivity. The method makes use of published procedures for the exfoliation and restacking of MoS_2. The prepared materials then will be tested in coal liquefaction and as upgrading catalysts using various resids.

A second area of research is the development and use of methods to evaluate dispersed catalysts by means of activity and selectivity tests. A micro-flow reactor has been developed for determining intrinsic reactivities using model compounds, and will be used to compare catalysts prepared in different ways. Micro-autoclaves will also be used to develop data in batch experiments at higher partial pressures of hydrogen.

The third area under investigation concerns hydrogen spillover reactions between MoS_2 catalysts and carbonaceous supports. Preliminary results obtained by monitoring H_2/D_2 exchange reactions with a pulse-flow microreactor indicate the presence of spillover between MoS_2 and a graphitic carbon. A more complete study will be made at a later stage of the project.

Accomplishments & Conclusions:

Exfoliation, that is, the dismantling of multilayered MoS_2 into single layers, has been used to generate interesting new materials (2,3). An extension of this technique has been used to apply exfoliated MoS_2 as a catalyst in the direct liquefaction of coal (4). The first step is the intercalation of MoS_2 with lithium. Briefly, MoS_2 was mixed with n-butyllithium in hexane for two or three days. The resulting lithium intercalated molybdenum sulfide was filtered, dried, and then added to a protic solvent, such as water. The reaction between the protic solvent and the intercalated lithium produced hydrogen gas, effectively blowing the multilayered molybdenum sulfide apart.

$$Li_x \cdot MoS_2 + xH_2O \rightarrow 1/2xH_2 + xLiOH + MoS_2$$

Single-layer exfoliated metal sulfides are reported to stay in suspension for several days due to the formation of a hydroxylated surface. The restacking of the single-layer MoS_2 can be accelerated by the addition of dilute acids. The changes in the stacking dimension of MoS_2 crystallites that occur over the course of exfoliation and reassembly may be conveniently followed using X-ray diffraction. The average crystallite size perpendicular to the plane of the layers may be estimated from the half-width of the (002) line. Measured by this method, the untreated MoS_2 had an average stacking dimension of 375 Å. Examination of the untreated MoS_2 by SEM revealed a wide assortment of slab widths ranging from about 10 μ down to a few hundred angstroms. After exfoliation in water and with restacking induced by drying, the (002) peak was broadened and corresponded to a reduction in the average stacking dimension to 185 Å. The BET surface area was 10.0 m^2/g for the dried material.

The exfoliated MoS_2 catalysts were tested for their activity in microautoclaves using 3 g of a high volatile bituminous coal (hvBc) from Blind Canyon, Utah (DECS-17), 3 g of a coal-derived recycle solvent (Wilsonville distillate V-178), and 0.12 g of elemental sulfur (Fisher) when applicable. The initial H_2 pressure was 6.8 MPa (1000 psi) at room temperature and the loading for the catalysts was 2000 ppm Mo calculated on a weight basis using daf (dry, ash-free) coal. The reaction temperature was 375°C, with a reaction time of 1 or 2 hours.

Table 1 contains results illustrating the various effects of the addition of sulfur, solvent pretreatments, and the technique of catalyst addition in terms of THF conversion, cyclohexane conversion, and the amount of hydrogen taken up. It may be seen that the catalytic performance of a particular sample of MoS_2 may be improved by exfoliation in the presence of coal. A number of variables in the application technique were surveyed. It was found that catalyst application techniques likely to promote a high degree of exfoliation coupled with extensive swelling of the coal

gave better results.

Three basic methods of applying the catalyst to coal were compared. First, the original material was mixed with coal without intercalation or exfoliation. The mixing took place in a binary solvent, 1:1 THF/water, using an ultrasonic bath for 4 h to promote dispersion. Separate experiments demonstrated that mixing in the ultrasonic bath led to higher oil yields than when the catalyst and coal were mixed by hand with a stirring rod. For the sake of consistency, the ultrasonic bath was used even in cases where no catalyst was added to the coal (Exps. 3 & 4). The combined effect of the solvents and ultrasound on coal reactivity when measured in the absence of catalyst is small, as may be seen by comparing the results of Exps. 1 - 4. In the second method, the MoS_2 was exfoliated in water, recovered by drying, then mixed with coal as in the first case. In the third, the intercalated MoS_2 was exfoliated directly in slurries of coal in THF/water or other solvent systems, thus providing greater opportunity for increasing the dispersion of catalyst on a swollen coal structure. All of the coal/catalyst mixtures were then dried and subjected to the microautoclave test.

Comparison of the three methods reveals best results were obtained by conducting the exfoliation and dispersal in a single step (Exp. 14). Once the improvement of using a single exfoliation/dispersal step was realized, several solvent systems were compared for use in this single step. None of the other choices provided performance better than using THF/water.

Table 2 provides results obtained with a longer residence time. Here, a comparison was made with MoS_2 catalysts prepared *in situ* by conventional means. This method involves the deposition of MoS_2 precursors on the coal from solution prior to liquefaction. Impregnation of ammonium heptamolybdate or ammonium tetrathiomolybdate was accomplished by dissolving the salts in THF/water, then mixing the solution with coal for 4 h in an ultrasonic bath in the same manner as used with the particulate MoS_2 catalysts. In this comparison, the method of exfoliation of particulate MoS_2 in THF/water with coal (Exp. 19) gave a somewhat higher cyclohexane conversion and a greater amount of hydrogen uptake than both catalysts derived from the impregnated precursors.

In summary, exfoliation of MoS_2 in the presence of coal has produced a catalyst with good liquefaction performance. The results indicate that for the same amount of catalyst, a combination of reduction in MoS_2 stacking and improved coal/catalyst dispersion is beneficial.

TABLE 1. LIQUEFACTION OF BLIND CANYON BITUMINOUS COAL; ONE HOUR AT 375° C, EXFOLIATION OF MoS_2 WITH COAL PRESENT (EXCEPT AS INDICATED).

Exp.	Catalyst	Dispersing Solvent	Conversion, % daf Coal		H_2 Uptake, psi	Added Sulfur
			THF	Cyclohexane		
1	None	None	75	16	24	yes
2	None	None	70	18	8	no
3	None	THF/H_2O	78	21	31	yes
4	None	THF/H_2O	69	19	14	no
5	MoS_2[1]	THF/H_2O	77	18	56	no
6	MoS_2[2]	THF/H_2O	82	20	96	yes
7	MoS_2[2,3]	THF/H_2O	79	18	98	yes
8	MoS_2[1]	THF/H_2O	87	27	120	yes
9	MoS_2	H_2O	88	26	146	yes
10	MoS_2	EtOH	85	25	148	yes
11	MoS_2	i-PrOH	86	26	141	yes
12	MoS_2	H_2O/i-PrOH	86	27	149	yes
13	MoS_2	THF/i-PrOH	88	28	126	yes
14	MoS_2	THF/H_2O	88	32	160	yes

1 MoS_2 was exfoliated in H_2O, recovered, dried, and dispersed onto coal in a THF/H_2O slurry..

2 MoS_2 was used as received from Aldrich, without exfoliation; material was dispersed onto coal in THF/H_2O slurry.

3 Lithium hydroxide added in equimolar amount with molybdenum.

TABLE 2. LIQUEFACTION OF BLIND CANYON BITUMINOUS COAL; TWO HOURS AT 375° C, COMPARISON OF EXFOLIATED MoS_2 WITH OTHER MOLYBDENUM CATALYSTS.

Exp.	Catalyst	Dispersing Solvent	Conversion, % daf Coal		H_2 Uptake, psi
			THF	Cyclohexane	
15	AHM[1]	THF/H_2O	90	37	176
16	ATTM[2]	THF/H_2O	87	37	181
17	MoS_2[3]	THF/H_2O	89	31	156
18	MoS_2[4]	THF/i-PrOH	90	35	178
19	MoS_2[4]	THF/H_2O	90	40	216

1 Ammonium heptamolybdate.
2 Ammonium tetrathiomolybdate.
3 MoS_2 was exfoliated in THF/H_2O and dried before it was impregnated onto the coal by ultrasonication in THF/H_2O.
4 MoS_2 was exfoliated in the binary solvent system in the presence of coal.

Similar techniques for modifying MoS_2 were used to generate catalysts for use in upgrading a vacuum resid from Hondo crude oil. This application provided different challenges. The reactions crucial to conversion of coal are different in kind from those for HDS or HDN of petroleum resid. The Hondo resid used as a test material was 82% soluble in heptane before treatment. In the case of resid upgrading, major interests lie in the extent of the HDS and HDN reactions in addition to conversion to heptane solubles. In the absence of coal, the solid particulate substrate used to carry the catalyst is missing. Accordingly, the exfoliated, restacked catalysts were mixed directly with the resid. The effect of catalyst promoters is conveniently studied in this way by conducting the exfoliation step in aqueous solutions of $Ni(NO_3)_2$ or $Co(NO_3)_2$. Elemental analyses of the finished catalysts were used to determine the atomic ratios of Co/Mo and Ni/Mo which were 0.61 and 0.66, respectively. Nitrogen contents of the catalysts were negligible, indicating the nitrate counterions are not carried along with the washed materials.

The interlayer distance in the stacking dimension may be estimated from the position of the 002 line. Values for the original MoS_2 and restacked MoS_2 are 6.14 Å, as expected. The interlayer distance for both NiMo and CoMo catalysts was ~11.5 Å. A net expansion of the layered structure is evident from these data. These layer expansions are consistent with the observations of Golub et al. (5). They report the formation of MoS_2 intercalated with nickel or cobalt hydroxide as well as other transition metals.

Recovered catalysts were also examined by XRD. The soluble organic material was first removed by extraction with THF. In the case of exfoliated/restacked MoS_2, the recovered catalyst exhibited properties similar to the fresh catalyst. The stacking dimension was unchanged, 185 Å. The diffraction spectrum still gave evidence of an extensive contribution by a turbostratic structure.

The catalysts prepared with Ni and Co were also recovered. In these cases, the XRD spectra of the original and recovered materials were significantly different. The interlayer distances of the recovered materials were reduced from the former values of ~11.5 Å to 6.14 Å, now consistent with MoS_2. Apparently, the intercalated Ni or Co ions were removed from between the layers during the resid upgrading reaction. In the case of Co, there was also a remarkable growth in crystallite size. Only sharp lines for MoS_2 were apparent, leading to an estimate of an average crystallite size of >1000 Å in both the 002 and 11 planes.

The results from hydrotreatment tests are summarized in Table 3 along with some of the physical properties of these catalysts taken before mixing with the resid.

Table 3. Results of hydrotreatment of Hondo resid at 425° C for one hour, and some catalyst properties.

Catalyst	Heptane extract, wt%	S, wt%	N, wt%	Spins/g x 10^{-17}	Stacking height, Å	Surface area, m^2/g
(Resid)	82	5.1	0.9	--	--	--
None	89	3.5	0.8	--	--	--
MoS_2, as received	93	3.2	0.8	6.0	375	6.2
MoS_2, exfoliated /restacked	95	3.3	0.7	7.1	185	10
$CoMoS_2$	95	2.6	0.7	1.9	110	22
$NiMoS_2$	96	2.2	0.8	9.4	98	6.1

The main difference in performance between the catalysts is in the extent of HDS. Cobalt and especially nickel significantly promote desulfurization. Review of the catalyst properties in Table 3 does not produce a simple, consistent correlation of a property with HDS performance. For example, the surface area of the CoMo catalyst is 3.6 times that of the NiMo catalyst, but the latter exhibits a greater amount of HDS. A correlation between the EPR signal intensity assigned to Mo(IV) and the rate of catalytic conversion of dibenzothiophene for a series of MoS_2 catalysts has been reported [6]. This correlation fails when promoted and unpromoted catalysts in Table 3 are compared. The CoMo catalyst has the lowest EPR signal intensity, but performed quite well in HDS. In contrast to the significant HDS activity, HDN activity is negligible for all catalysts tested here. These preliminary results are encouraging in that a variety of related dispersed catalysts can be prepared for comparative studies, although it is evident that no single physical parameter can be used to correlate with all of the differences in performance.

Evaluation of the intrinsic reactivity and selectivity of dispersed catalysts has been carried out using a micro-flow reactor constructed at PETC (7). An exfoliated/restacked MoS_2 catalyst was prepared by drying after exfoliation in water. This typically leads to a catalyst with a moderate degree of stacking. The catalyst was mixed with sand before it was packed in the stainless steel reactor. The test conditions were 350°C with a H_2 flow of 1.3 mL/min at a gauge pressure of 350 kPa. A solution of 1% dibenzothiophene in tetralin with 0.8% dimethlydisulfide (DMDS) added was pumped through the reactor at various flow rates from 2 to 5 μL/min. DMDS is a convenient source of H_2S, and was added to maintain a constant degree of sulfidation of the catalyst. The recovered products were analyzed quantitatively by gas chromatography. The products included biphenyl, naphthalene

derived from the tetralin solvent, and unconverted dibenzothiophene.

The conversion of dibenzothiophene followed a pseudo-first order rate law over this set of conditions. A plot of the ln of the molar ratio of unconverted dibenzothiophene to the total of dibenzothiophene and its products versus the space time was well fit by a straight line. The rate constant for dibenzothiophene conversion was 4.17×10^{-5} mmol dibenzothiophene/g catalyst·min. This result may be compared with a value determined for a high surface area MoS_2/carbon catalyst (BCP 287, surface area = 262 m^2/g) prepared by A. Cugini (8). Under the same conditions of hydrogen pressure and flow rate but at the lower temperature of 275° C, the rate constant was 2.85×10^{-4} mmol dibenzothiophene/g catalyst·min. The latter catalyst thus had an activity seven times greater although it was measured at a significantly lower temperature. An additional product, phenylcyclohexane, was also found among the products. The appearance of both biphenyl and phenylcyclohexane among the products can be accounted for using the reaction network proposed by Singhal et al. (9). This network includes parallel paths, one that begins with hydrogenation of dibenzothiophene followed by removal of sulfur, and another that results in direct sulfur removal producing biphenyl. From our results it may be seen that two nominally similar MoS_2 catalysts prepared by different methods may be significantly different in both activity and selectivity.

PLANS

The exploration of the use of exfoliated/restacked catalysts for co-processing Hondo resid will be continued. Of prime interest will be the effect of various preparation techniques on the relative amount of sulfur and nitrogen removal. This information may indicate whether controlling MoS_2 particle morphology can result in an optimum reduction in heteroatom content at the least cost in hydrogen. The selectivity for HDS and HDN will be determined for the exfoliated/restacked MoS_2 catalyst now under evaluation in the micro-flow reactor by use of mixtures of dibenzothiophene and quinoline. These data will be correlated with that obtained from the high-pressure microautoclave study with Hondo resid.

REFERENCES

1. M. Daage and R. R. Chianelli, J. Catal., 149 (1994) 414.
2. P. Joensen, R. F. Frindt, and S. R. Morrison, Mater. Res. Bull., 21 (1986) 457.
3. B. K. Miremadi and S. R. Morrison, J. Catal., 103 (1987) 334.
4. B. C. Bockrath and D. S. Parfitt, Catalysis Letters, in press.
5. A. S. Golub, G. A. Protzenko, I. M. Yanovskaya, O. L. Lependina, and Y. N. Novikov, Mendeleev Commun. (1993) 199.
6. B. G. Silbernagel, T. A. Pecoraro, and R. R. Chianelli, J. Catal., 78 (1982) 380.
7. K. T. Schroeder, B. C. Bockrath, and R. D. Miller, Am. Chem.

Soc. Div. Fuel Chem. Preprints, 39(3) (1994) 710.
8. A. V. Cugini, D. V. Martello, D. Krastman, J. P. Baltrus, M. V. Ciocco, E. F. Frommel, and G. D. Holder, Am. Chem. Soc. Div. Fuel Chem. Preprints, 40(2) (1995) 370.
9. G. H. Singhal, R. L. Espino, and J. E. Sobel, J. Catal, 67 (1981) 446.

ACKNOWLEDGEMENTS

The performance of the X-ray diffraction studies and the interpretation of the data by Sidney Pollack and Elizabeth Frommell is gratefully acknowledged, as is the EPR study performed by Robert Thompson and SEM studies performed by Donald Martello. This publication is supported in part by an appointment of DSP to the U.S. Department of Energy Fossil Energy Technology Center administered by the Oak Ridge Institute for Science and Education.

DISCLAIMER

Reference in this work to any specific commercial product is to facilitate understanding and does not necessarily imply endorsement by the United States Department of Energy.

Title: Direct liquefaction of plastics and coprocessing of coal with plastics

PI: G.P. Huffman, Zhen Feng, and Vikram Mahajan, CFFLS, 341 Bowman Hall, University of Kentucky, Lexington, KY 40506-0059

Contract Number: DE-FC22-93PC93053

Period of Performance: May 1, 1994 - April 30, 1995

Objectives: To optimize reaction conditions for the direct liquefaction of waste plastics and the coprocessing of coal with waste plastics.

Accomplishments: As summarized below, significant progress has been made in the current contract year in determining the optimum temperature range, in exploring the effect of hydrogen pressure, in evaluating different solvents, and in the development of new catalysts.

Introduction

In previous work,[1] we have investigated the direct liquefaction of medium and high density polyethylene(PE), polypropylene(PPE), poly(ethylene terephthalate)(PET), and a mixed plastic waste, and the coliquefaction of these plastics with coals of three different ranks. The results established that a solid acid catalyst(HZSM-5 zeolite) was highly active for the liquefaction of the plastics alone, typically giving oil yields of 80-95% and total conversions of 90-100% at temperatures of 430-450 °C. In the coliquefaction experiments, 50:50 mixtures of plastic and coal were used with a tetralin solvent(tetralin:solid = 3:2). Using ~1% of the HZSM-5 catalyst and a nanoscale iron catalyst, oil yields of 50-70% and total conversions of 80-90% were typical.

In the current contract year, we have conducted further investigations of the liquefaction of PE, PPE, and a commingled waste plastic obtained from the American Plastics Council(APC), and the coprocessing of PE, PPE and the APC plastic with Black Thunder subbituminous coal.[2,3] Several different catalysts have been used in these studies.

Experimental Procedure

The feedstock materials used in the work reported in this paper included medium and high density polyethylene (PE), polypropylene (PPE), the APC commingled waste plastic, and a subbituminous coal (Black Thunder). Proximate and

ultimate analyses for the coal and APC waste plastic are shown in Table 1. The experiments used several types of catalysts: a commercial HZSM-5 zeolite catalyst[4], an ultrafine ferrihydrite treated with citric acid(FHYD/CA), a ternary Al/Si/ferrihydrite with Al:Si:Fe=1:1:18 ($FHYD_{0.90}/Al_{0.05}Si_{0.05}$), a coprecipitated SiO_2-Al_2O_3, (Si/Al ≈4) and a coprecipitated SiO_2-Al_2O_3 containing 5% ferrihydrite. All catalysts except the zeolite catalyst were synthesized in our laboratory. For all runs, 1 wt.% of catalyst was added. The preparation, structure, and liquefaction activity of the ferrihydrite catalysts has been discussed in detail elsewhere[5-8].

The liquefaction experiments were conducted in tubing bomb reactors with a volume of 50ml which were shaken at 400 rpm in a fluidized sand bath at the desired temperature. The reaction times were 20-60 min. and the atmosphere in the bomb was either hydrogen or nitrogen (cold pressure 100-800 psi). Usually 5 g of plastic or plastic + coal with 7.5 g of solvent(tetralin and/or waste oil) were charged in the tubing bombs. However, a number of experiments were conducted with plastics alone. The reactor was cooled in a second sand bath, and gas products were collected and analyzed by gas chromatography. The other products were removed from the reactor with tetrahydrofuran (THF) and extracted in a Soxhlet apparatus. The THF solubles were subsequently separated into pentane soluble (oils) and pentane insoluble (PA + AS) fractions. Total THF conversion was determined from the amount of insoluble material that remained (residue). Any added catalyst was subtracted from the residue sample weight.

Results and Discussion

Previously, we have shown that a solid acid catalyst(HZSM-5 zeolite) is highly active for the liquefaction of PE, PPE, and mixed waste plastic.[1] Some interesting new results for PE are shown in Figure 1, where it is shown that oil yields are not strongly dependent on hydrogen pressure. Moreover, the oil yield as determined by pentane solubility is as high under nitrogen as it is under hydrogen. The total conversion(THF soluble) was nearly 100% in all cases. Figure 1 also shows the time dependence of the reaction for PE in the presence of HZSM-5.

Our previous paper[1] examined the coliquefaction of a mixed waste plastic with both a bituminous and a

Table 1.

Proximate[a]	Coal	Plastic
% Ash	6.3	0.5
% Volatile	45.4	98.8
% Fixed Carbon	48.3	0.7
Ultimate[b]		
% Carbon	71.6	84.7
% Hydrogen	4.8	13.7
% Nitrogen	1.5	0.7
% Sulfur	0.5	0.01
% Oxygen	15.2	1.0

a = Dry basis, b = Dry ash free basis.

subbituminous coal. Oil yields of 60-70% and total conversions of over 90% were observed in the presence of both the HZSM-5 catalyst and an iron catalyst(430 °C, 800 psi H_2-cold, 60 min., tetralin solvent). We are currently studying the response of individual plastic resins to various catalysts and conditions in more detail. Some typical results are shown in Figure 2, where the coliquefaction results for a 1:1 mixture of polyethylene(PE) and Black Thunder subbituminous coal are compared to those for a 1:1 mixture of polypropylene(PPE) with the same coal. It is evident that PPE undergoes considerably more synergistic reactions with coal than PE.

Several solvents for plastics liquefaction are being explored. An example of this work is shown in Figure 3. The APC commingled plastic was liquefied in mixtures of tetralin and waste automotive oil; the percentage of waste oil in the mixture is indicated. At 445 °C, the effect of using waste oil rather than tetralin is obviously much greater than the effects of the added catalysts. Presumably, the aliphatic structure of the waste oil is more conducive to dissolution of the plastic than the aromatic tetralin solvent.

Currently, an experimental matrix of temperature, catalysts, pressure, solvent, and time is being explored for the APC commingled plastic. This work will be extended to include additional mixed waste plastics as well as individual resins. Some typical results are shown in Figure 4, where the use of a tetralin solvent is compared to liquefaction with no solvent for both thermal and catalytic reactions. It is evident from both Figure 4 and Figure 3 that the aromatic structure of tetralin, which makes it a good solvent for coal liquefaction, is not the best choice for liquefaction of predominantly aliphatic plastics. It is also seen that the coprecipitated silica-alumina catalysts prepared in our laboratory give somewhat better yields than the commercial HZSM-5 zeolite.

Future Plans

A thorough experimental matrix of time, temperature, and pressure will be explored for liquefaction and coprocessing of the APC plastic with coals of different rank. Additional commingled plastics will also be investigated. The reactions of individual resins will be studied in more detail. A primary goal will be to develop a catalyst system that will be simultaneously effective for both coal and plastics.

References:

1. M.M. Taghiei, Z. Feng, F.E. Huggins, and G.P. Huffman, Energy & Fuels, **1994**, *8*, 1228-1332.
2. G.P. Huffman et al., *ACS Division of Fuel Chem. Preprints, 40(1),* 34(1995).
3. G.P. Huffman, Zhen Feng, F.E. Huggins, and V. Mahajan, to be published in the Proceedings, 1995 ICCS Meeting, Oviedo, Spain.
4. United Catalysts Inc., P.O. Box 32370, Louisville, KY 40232.
5. J. Zhao, Z. Feng, F.E. Huggins, and G.P. Huffman, Energy & Fuels, **1994**, *8*, 38-43.

6. J. Zhao, Z. Feng, F.E. Huggins, and G.P. Huffman, Energy & Fuels, **1994**, *8*, 1152-1153.
7. J. Zhao, Z. Feng, F.E. Huggins, K. Rao, and G.P. Huffman, *ACS Division of Fuel Chem. Preprints, **40(2)**,* 351(1995).
8. J. Zhao, Z. Feng, F.E. Huggins, and G.P. Huffman, to be published in the Proceedings, 1995 ICCS Meeting, Oviedo, Spain.

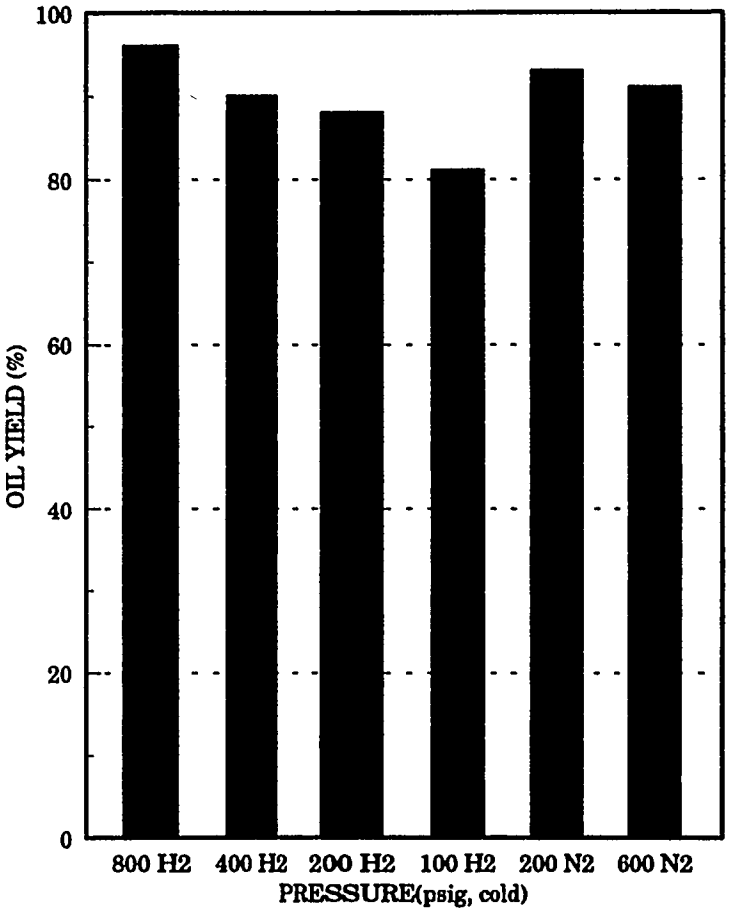

Figure 1. Liquefaction results for MDPE vs. pressure: 430 C, 60 min, 1% HZSM-5, tetralin.

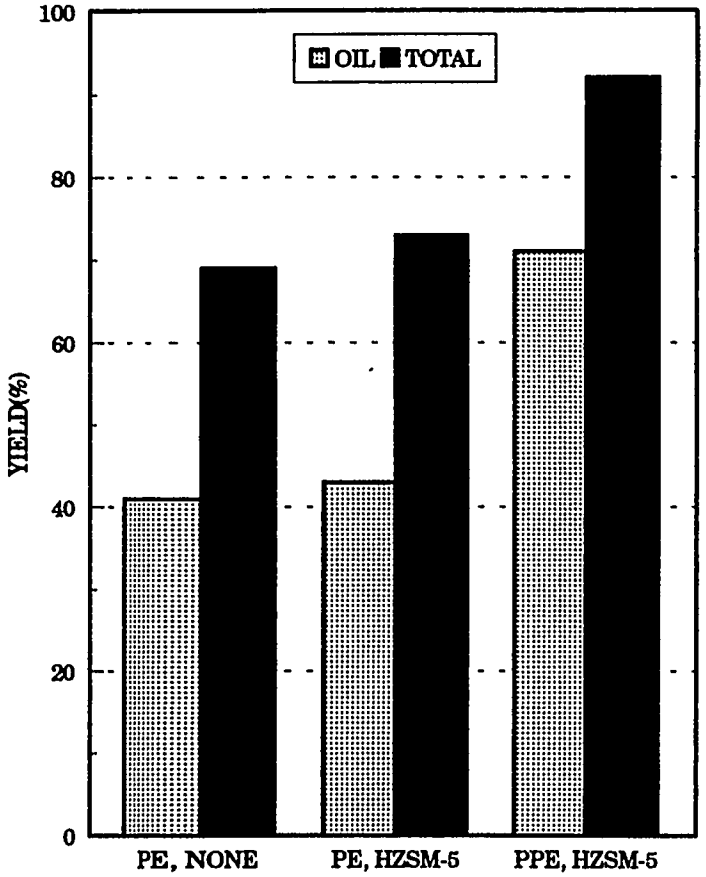

Figure 2. Coliquefaction of coal with PE and PPE: 400 C, 60 min, 800 psig H2(cold), tetralin.

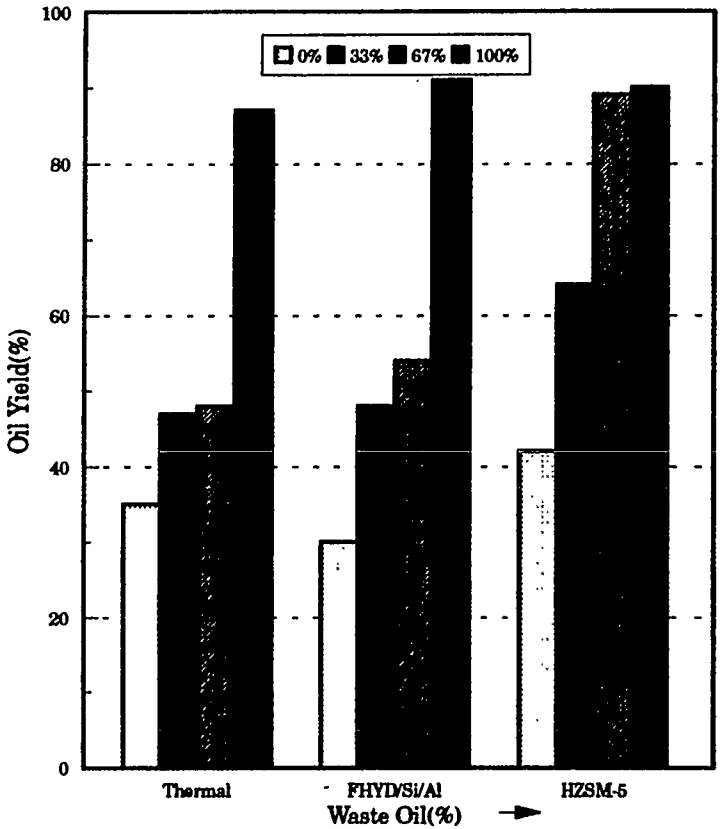

Figure 3. Effect of percentage of waste oil in solvent on oil yields for APC plastic: 445 C, 800 psig H2(cold, 1 wt.% HZSM-5, tetralin.)

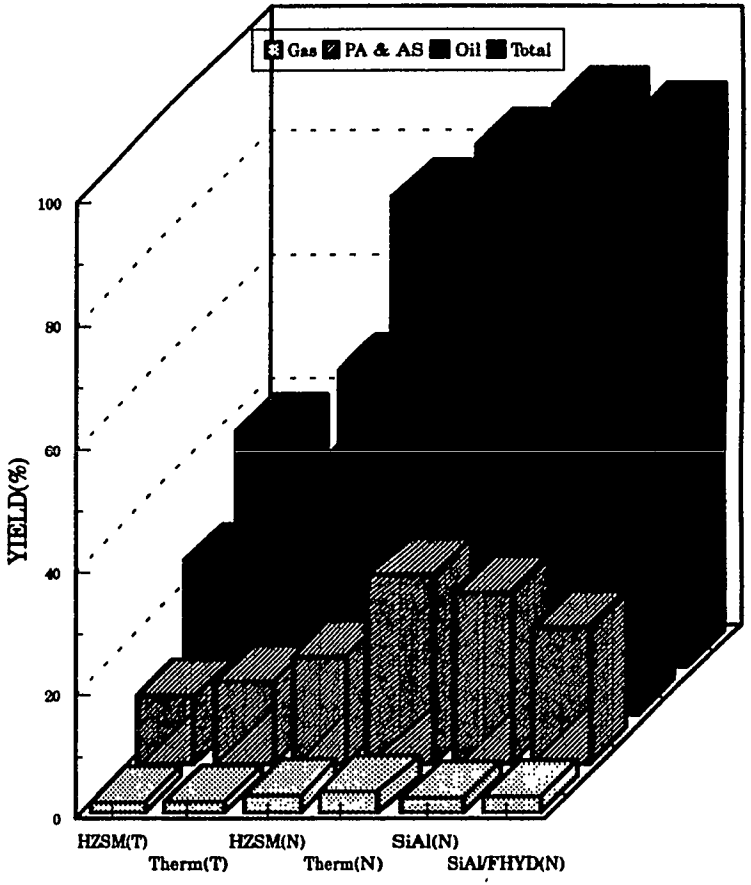

Figure 4. Liquefaction results for commingled plastic: 800 psig H2(cold), 60 min, 430 C: solvent = tetralin(T) or none(N), tetralin.

TITLE: Effect of Hydrogen Pressure on Free Radicals in Direct Coal Liquefaction/Coprocessing

PI (AUTHORS): M. S. Seehra and M. M. Ibrahim

INSTITUTION: Physics Department, West Virginia University, Morgantown, WV 26506-6315

CONTRACT NUMBER: DE-FC22-93PC93053

PERIOD OF PERFORMANCE: May 1, 1994 - April 30, 1995

OBJECTIVE: To investigate the coprocessing of coal with waste tires and commingled plastics and to characterize the relevant catalysts, using high pressure/high temperature in-situ ESR (Electron Spin Resonance) spectroscopy. In this report, we will only concentrate on the recent results from high pressure ESR spectroscopy.

ACCOMPLISHMENTS & CONCLUSIONS:

During this period, we made considerable progress in developing the high pressure capabilities in in-situ ESR spectroscopy and new results carried out in 1000 psi of H_2 gas are presented in this report. In these experiments, we employ sapphire tubes to contain the high pressures at temperatures up to 500°C. Results of the experiments carried out under 1000 psi of H_2 are compared with those under 1000 psi of non-interacting argon and with the earlier experiments in flowing H_2 gas where the volatiles are removed by the flowing gas. In these experiments, the free radical density N of the Blind Canyon coal is measured at each temperature and pressure by double integration of the ESR signal and calibrating it against a standard. The details of our experimental apparatus and procedures have been described in earlier publications [1-3].

In Fig. 1, we show the temperature dependence of the free radical intensity N of Blind Canyon coal under three conditions: in H_2 flow, in 1000 psi of argon (cold) and in 1000 psi of H_2 (cold). In H_2 flow experiments, the volatiles from the coal are swept away by the flowing gas and these volatiles from coal are known to contain ESR active free radicals [4]. The results in Fig. 1 show that in argon atmosphere, N is essentially temperature independent above 200°C suggesting that inert argon suppresses any thermolysis of coal. In 1000 psi of H_2, N is significantly lowered at the lower temperatures as compared to the argon case suggesting significant hydrogenation (capping) of the free radicals. Above 380°C, we observe a dramatic increase in N due to cracking of coal in H_2. In flowing H_2, N values are definitely lower than those compared to 1000 psi of H_2. As indicated above, this result may be due to the fact that the volatiles that are carried away by flowing H_2 have free radicals [4], thus lowering the observed N in flowing H_2.

In Fig. 2, we show the effect of H_2 pressure (up to 500 psi) at a fixed temperature on the free radical intensity N, both with and without a catalyst ($NiMo/Al_2O_3$). For comparison, data from similar experiments carried out in argon gas is also included. The results from both Fig. 1 and Fig. 2 are consistent in that there is clear evidence that hydrogen pressure lowers the free radical intensity N by capping the free radicals. This is an important step in direct coal liquefaction since the free radicals formed during the thermal/catalytic decomposition of coal must be stabilized by transferring hydrogen from gaseous H_2 and/or hydrogen donor solvent. The results presented in Fig. 1 and 2 show that this hydrogenation does indeed occur. In the presence of the catalyst ($NiMo/Al_2O_3$), there is clear evidence of hydrogenolysis since the free radical intensity is enhanced as compared to the case of coal alone even though above about 150 psi of H_2, hydrogenation process takes over. These experiments clearly suggest that hydrogen in the presence of a catalyst promotes cracking of coal in addition to hydrogenation. Thus, in direct coal liquefaction, hydrogen plays the dual role of coal cracking and hydrogenation.

Next we consider the experimental ESR results of the coprocessing of coal with waste tire polymers. In Fig. 3, we show the free radical intensity N versus temperature for the Blind Canyon

coal, and for the coal mixed with Goodyear and Michelin tread in 1:1 ratio in flowing H_2 experiments. It should be noted that the tire treads by themselves do not yield any free radical ESR signal at the temperatures investigated in these experiments. Therefore the observed signals are from the coal alone, but including any catalytic effect of the tire polymers on the coal decomposition/hydrogenation. The results shown in Fig. 3 are interpreted as follows: First, the cracking temperature of coal which equals about 350°C in Fig. 3 is shifted downwards to about 240°C by the action of the tire polymers so that at the liquefaction temperatures (say 350°C-400°C), the free radical intensity of the coal is considerably enhanced by the action of the tire polymers; Second, although the magnitudes of N are different for the Michelin and Goodyear experiments, the observed effects are qualitatively similar for the two cases; and third, the drop in N above 400°C, may be either due to repolymerization of the free radicals or increased hydrogenation produced by the tire polymers.

Further insights into the role of tire polymers in coal coprocessing has emerged from the high pressure experiments with Michelin tire. These results are shown in Fig. 4, along with the data for H_2 from Fig. 3 and the results from experiment in 1000 psi of argon. Here we see a dramatic effect in 1000 psi of H_2 where experiment was repeated three times to confirm the findings. Departures of the data for 1000 psi of H_2 from the other experiments at temperatures around 160°C shows that 160°C may now be considered to be the cracking temperature of coal. Between 160° and 400°C, N continues to increase with temperature in 1000 psi of H_2 and increase in N for this temperature range is nearly three fold. It is indeed amazing that in 1000 psi of argon, N is severely suppressed as temperature increases. These experiments clearly show that in the presence of 1000 psi of H_2, the tire polymers lower the cracking temperature of coal to about 160°C and promote significant decomposition of coal in the temperature range of 160° to 400°C. These results provide insight as to why tire polymers promote enhanced liquefaction [5]. In future experiments, we will be examining the combined effect of a donor solvent and molecular hydrogen in coal/waste tire coprocessing.

In conclusion, the results of in-situ ESR experiments up to 500°C and in H_2 pressures up to 1000 psi show that molecular H_2 caps the free radicals generated in the thermal decomposition of Blind Canyon coal. Furthermore, in the presence of the catalyst ($NiMo/Al_2O_3$) and tire polymers, additional bonds are broken at lower temperatures resulting in enhanced cracking of the coal. Thus, although it is generally accepted that coal liquefaction is a free radical process, our in-situ ESR experiments are providing the first clear evidence for the processes of hydrogenation, hydrogenolysis and catalytic cracking.

PLANS:

In future experiments, we will be examining the effects of donor solvents in direct coal liquefaction/coal-waste tire coprocessing. Experiments are also underway for the investigations of the coprocessing of coal with commingled plastics. Results of these experiments will be reported elsewhere.

REFERENCES:

1. M. M. Ibrahim and M. S. Seehra, Prepr. Pap. - Am. Chem. Soc., Div. Fuel Chem. 37, 1131-1140 (1992).
2. M. M. Ibrahim and M. S. Seehra, Energy Fuels 5, 74-78 (1991).
3. M. S. Seehra and B. Ghosh, J. Anal. Appl. Pyrolysis 13, 209-220 (1988).
4. S. S. Kim, M. L. Jarand, and K. Durai-Swamy, Fuel 61, 1124-1126 (1982).
5. M. Farcasiu and C. M. Smith, U.S. Patent 5,061,363, 1991.

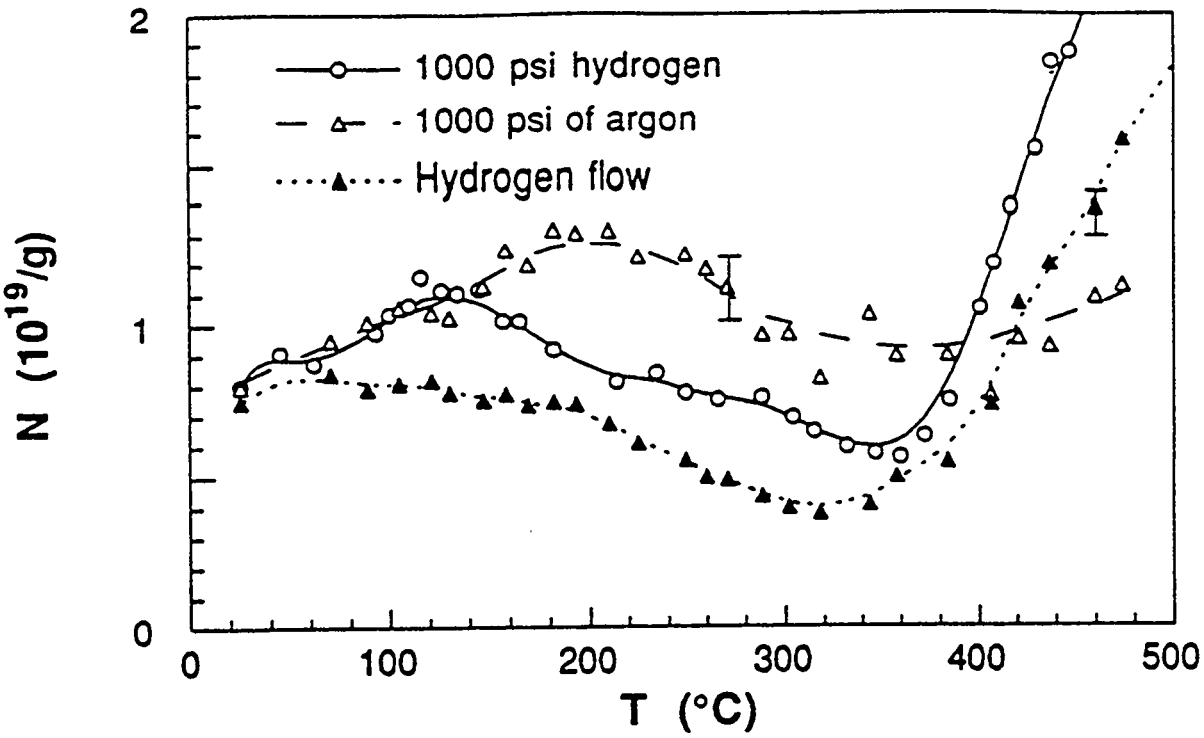

Fig. 1. Variation of N with temperature for coal alone in hydrogen flow and in 1000 psi of hydrogen/argon.

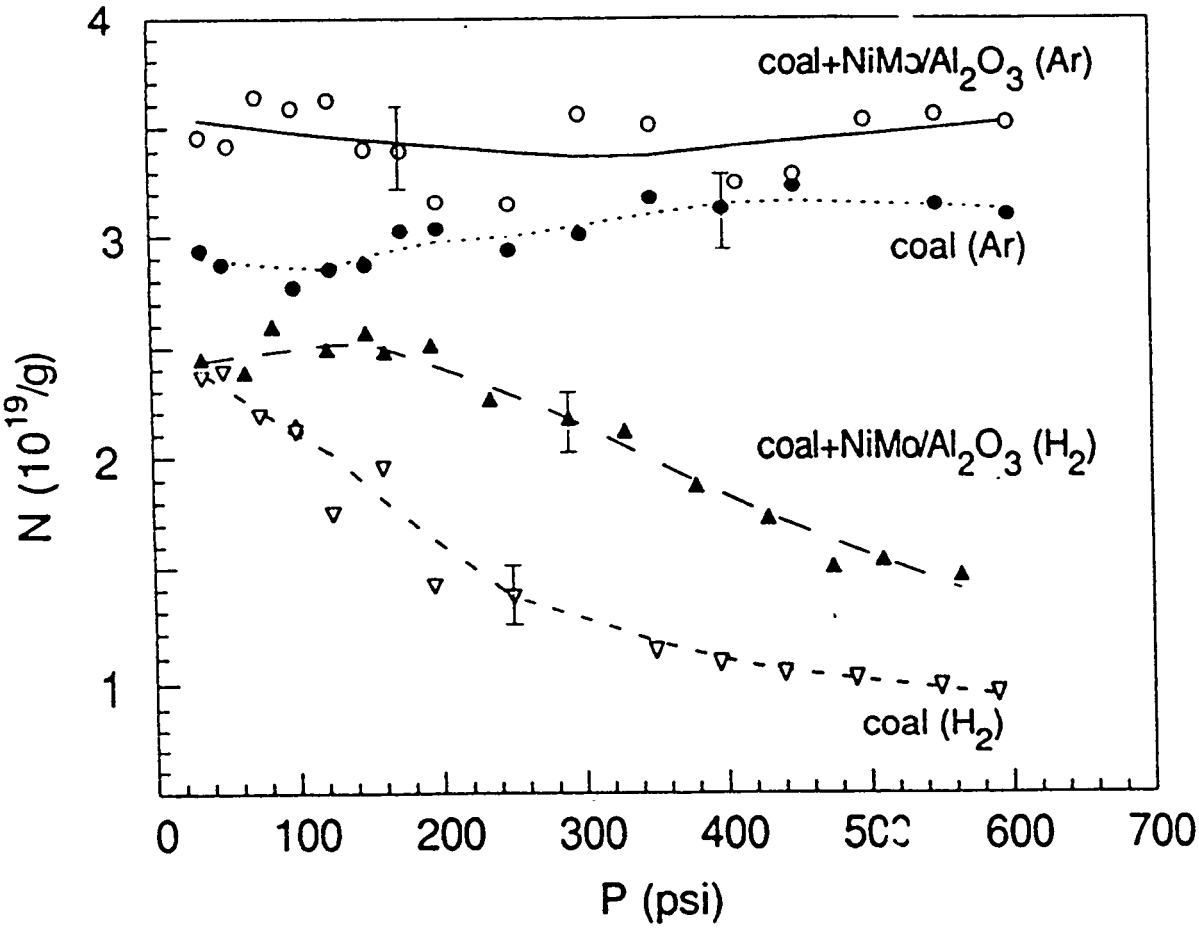

Fig. 2. Variation of the free radical intensity N with pressures of argon and H_2 for Blind Canyon coal and the coal mixed with the $NiMo/Al_2O_3$ catalyst (2.1% loading). The experiments were carried out at 440°C.

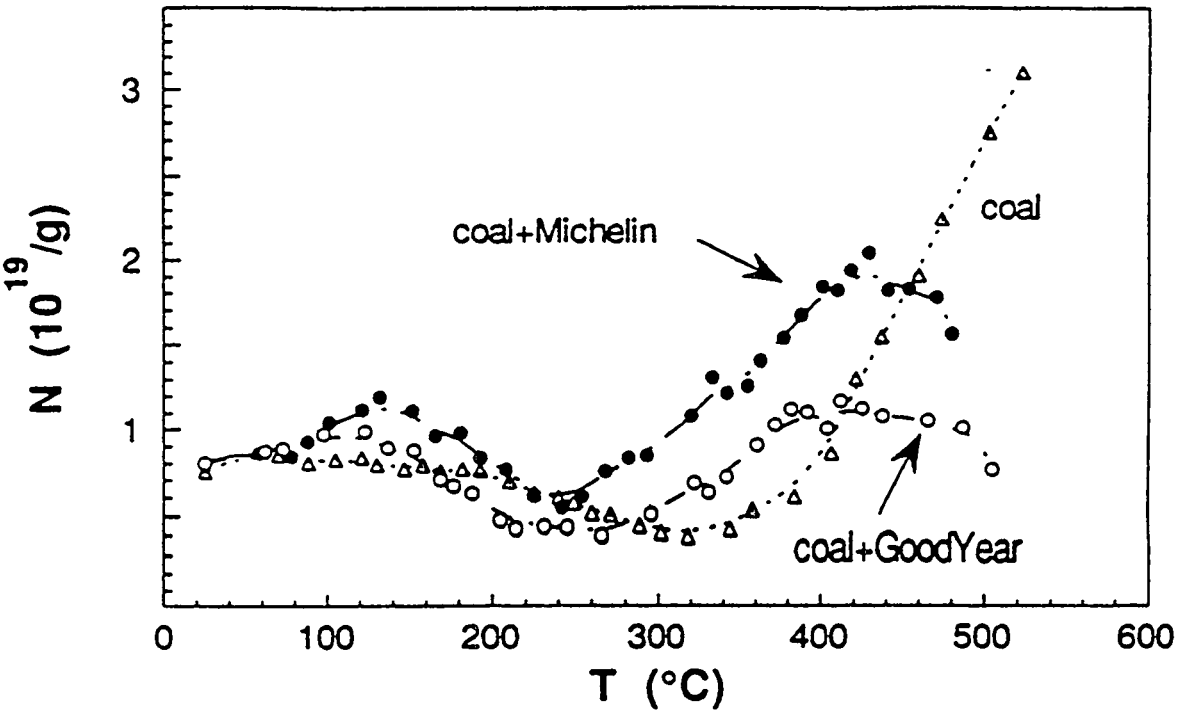

Fig. 3. Variation of N with temperature for coal and coal mixed with tread, for measurements in hydrogen flow.

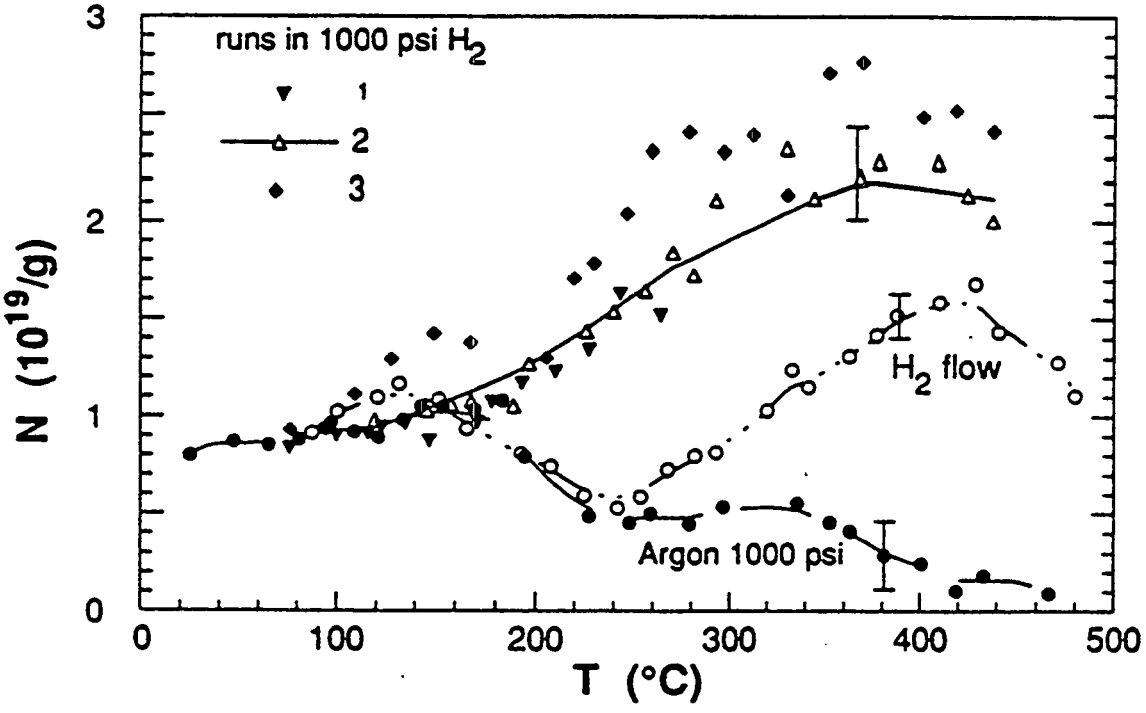

Fig. 4. Variation of N with temperature for coal + tread in hydrogen flow and in 1000 psi of hydrogen/argon.

The Use of Mixed Pyrrhotite/Pyrite Catalysts for Co-Liquefaction of Coal and Waste Rubber Tires

Dady B. Dadyburjor, John W. Zondlo, Ramesh K. Sharma, Jianli Yang, Fang Hu and Barbara Bennett

Department of Chemical Engineering, West Virginia University, P.O. Box 6102, Morgantown WV 26506-6102

Contract Number: DE-FC22-93PC93053

Period of Performance: May 1, 1993 - April 30, 1996

OBJECTIVES

The overall objective of this research program is to determine the optimum processing conditions for tire/coal co-liquefaction. The catalysts used will be our ferric-sulfide-based materials, as well as promising catalysts from other consortium laboratories. The intent here is to achieve the maximum coal+tire conversion at the mildest conditions of temperature and pressure. Specific objectives include an investigation of the effects of time, temperature, pressure, catalyst and co-solvent on the conversion and product slate of the co-liquefaction.

ACCOMPLISHMENTS AND CONCLUSIONS

Introduction

There is now a growing body of research attesting to the technological possibility [1,2] and economic feasibility [3] of co-liquefying waste tire material with coal. While other waste materials such as plastics may show greater short-term viability for co-liquefaction, the long-term advantages of tires as a feedstock include greater homogeneity from type to type, and lower amounts of environmentally flagged constituents such as chlorides.

The majority of the coal samples has been from DECS-6, which is a high-volatile A bituminous coal from the Blind Canyon seam in Utah. Other coals used include DECS-24 (Illinois number 6; bituminous, high-volatile C) and DECS-26 (Wyodak; sub-bituminous B). All coals were sized to -60 mesh. The proximate and ultimate analyses of the coal samples are given in Table I.

Three different tire materials have been tested. The first samples were prepared from a Goodyear Invicta tire, recycled in-house at WVU (Tire-1). Another sample, obtained from the University of Utah, was a recycled tire ground to -30 mesh (Tire-2). The third sample (Tire-3) consists of truck tire, also obtained from the University of Utah. Tire sample sizes were -30 mesh. The majority of the tire samples used this year have been from Tire-2. Analyses of all the tire samples are also given in Table I.

The catalyst tested in this work is based on ferric sulfide as a precursor. Disproportionation of the ferric sulfide results in an intimate mixture of pyrrhotite and pyrite

(and elemental sulfur), and this has been shown to be a very effective catalyst in coal liquefaction [4-6].

For all the data reported below, total conversion was based on the measurement of tetrahydrofuran (THF)-insoluble matter. The asphaltene+preasphaltene yield was found from the measurement of (THF-soluble but) hexane-insoluble matter. For most runs, the gas fraction was measured separately, using gas chromatography. The oil fraction was found by difference. In the case of co-liquefaction experiments, the results are reported on a "coal-alone" basis, *i.e.*, with the effect of the tire subtracted proportionately. This procedure allows us to compare the results of experiments with coal alone directly with the results of coal-plus-tire experiments.

Some of our work in this area has been described in the literature [2,4,7]. Preliminary baseline runs with Tire-1 and DECS-24 indicate:

(1) the organic matter in the tire is almost completely converted to oils, at least after 0.5h at 400°C and 1000 psig (cold) H_2;

(2) there is little effect of H_2 pressure on tire liquefaction;

(3) co-liquefaction of tire and coal results in an increase in asphaltenes produced, with oil and gas yields being unchanged;

(4) co-liquefaction yields depend upon the temperature and the tire-to-coal ratio, but there is little dependence upon the hydrogen pressure, at least after around 500 psi(cold);

(5) the synergism between coal and tire probably arises when the radicals generated from the coal combine with C_{2+} fragments from the tire to produce asphaltenic fractions rather than with other coal radicals to form condensation products;

(6) untreated residue from the tire has no special effect on the conversion or product slate after co-liquefaction

(7) ferric-sulfide-based catalysts generated *in-situ* in the coal can improve conversions and oil yields during co-liquefaction, at loadings as low as 0.5wt% of the coal.

Results of three investigations are reported here. In the first, a statistical design was used so that temperature, pressure and time of liquefaction, coal type, and catalyst loading could be systematically altered over relatively narrow ranges. In the second, a particular coal-tire system was used, and the effects of temperature and tire-to-coal ratio were more extensively investigated. In the third, preliminary work has been started on the pretreatment of the tire residue for use as a possible catalyst during coal liquiefaction.

Effect of Experimental Conditions on Co-liquefaction of a Spectrum of Tire-Coal Pairs

A Box-Behnken statistical design was used. Reactor temperatures ranged from 350-450°C, reaction times from 0.25-1h, and hot hydrogen pressures from 0-2000psi. The total

pressure (hot basis) was kept constant at 2000psi by adding helium as appropriate. No additional solvent was added in this work. Tire-2 was used in this portion of the work. Different coals were used by the two investigators who worked on this portion of the project: one worked with DECS-24 and the other with DECS-26, and both worked with DECS-6 coal. Results were obtained for the total conversion (X), and the yields of asphaltene+preasphaltene (A+P), oil (O) and gas (G). A polynomial fitting procedure was used, with the polynomials including terms of up to second order, including cross terms. The expressions were centered at 400°C, 0.5h, and 1000 psi(hot), approximately the midpoint of the respective ranges. Terms deemed to be statistically insignificant (t ratio less than 2) were dropped.

Results with the common coal alone and the tire alone for the two investigators are summarized in Table II. Even though the actual coefficients in the polynomials of Table II are not identical between the two investigators, the two sets of experimental values (not shown) agree to within 2 percentage points, and the predicted values agree with the corresponding experimental values for each investigator to within 2 percentage points. Hence the results for the two investigators can be considered to be reproducible, and we can therefore compare the results using DECS-6, DECS-24 and DECS-26 with the tire, as obtained by the two investigators.

For DECS-6, the coefficients from Table II indicate that conversion is highly dependent upon temperature, and moderately dependent upon hydrogen pressure. Reaction time only exhibits a slight influence upon conversion. Gas yield is also highly dependent upon temperature, with moderate dependencies upon both pressure and time. Oil yields are highly dependent upon temperature, and moderately dependent upon time. The hydrogen pressure has virtually no effect upon oil production. A+P yields show a reasonable dependence upon all three parameters, with temperature being slightly more important. Based on the coefficients of Table II, the surfaces of Figure 1 show the effect of temperature, time and pressure on the overall conversion, while the surfaces of Figure 2 show the effects of temperature and time on the conversion and product yield for the highest hydrogen pressure.

For Tire-2 alone, the corresponding surfaces are shown in Figure 3. The conversion is highly dependent upon temperature and slightly dependent upon time. Gas yield is highly dependent upon temperature and time. Oil yields seem to follow the same general trend as conversion; a high dependence upon temperature with a slight dependence upon time. A+P yields were too small to be modeled with much confidence. The effect of pressure is not explicitly shown in Figure 3. While conversion is relatively independent of hydrogen pressure, this effect is somewhat more pronounced for oil production, and somewhat greater for gas production.

For DECS-26 coal, Figure 4, conversion shows a strong dependence upon hydrogen pressure and only a moderate dependence upon temperature. A slight dependence upon reaction time is observed. Gas yield exhibits a strong dependence upon temperature, with moderate dependencies upon both pressure and time. Oil yields exhibit a strong dependence upon temperature, moderate dependence upon pressure, and slight dependence upon time. A+P yields show approximately equal dependence upon both temperature and pressure. Reaction time has almost no significance in asphaltene and preasphaltene production.

A quantitative analysis of the results with the coals and the tire (each alone) lead to the following "optimum" conditions for each: 400°C, 1h, 2000 psi for DECS-6; 450°C, 1h, 2000 psi for DECS-26; 450°C, 1h, 1500 psi for DECS-24; and 400°C, 0.5h, 2000 psi for Tire-2. (The values above are the rounded-off values of the parameters. The values corresponding to maximum conversion, maximum oil yield, etc. can be predicted using the polynomial expressions analogous to that in Table II. The parameter values above correspond to conversions and yields within expected error bars of the predicted maximum values.) Co-liquefaction experiments were run under these conditions at values of tire-to-coal ratios, R_{TC}, ranging from 0 to 2. As noted earlier, the results are reported on a "coal-alone" basis.

For DECS-26 and Tire-2, the conversion increases with R_{TC} upto the maximum value used. When DECS-6 coal is used, however, the conversion increases when R_{TC} is equal to 1, but then decreases at $R_{TC} = 2$. In all cases, the incremental conversion corresponds mostly to an increase in the A+P yield. Oil yields are affected slightly. Gas yields are virtually unchanged.

Preliminary results with the ferric-sulfide-based, *in-situ* impregnated catalyst have also been obtained on the DECS-6 and DECS-26 coals with Tire-2. The catalytic runs were made both at a low temperature (350°C) and at the "optimum" temperature for the corresponding coal. The reaction time and hydrogen pressure were kept at the maximum value of their respective ranges. Results (on a "coal-alone" basis) using the coal, catalyst and tire with $R_{TC} = 1$ are compared with those using the coal and catalyst, and those using the coal alone. At the low temperature, the catalyst has little effect on the coal alone. However, at the higher temperature, the catalyst increases the conversion dramatically. For DECS-26, this is due to increasing yields of A+P and gas; for DECS-6, this corresponds to increasing A+P alone. When the tire is added to catalyst-impregnated DECS-26, the conversion increases by approximately 7 percentage points. Interestingly, this is due to changes in oil yield and gas yield. When the tire is added to the impregnated DECS-6 coal, the conversion is 7 percentage points lower than that with the catalyst-impregnated coal alone. However, the conversion is 20 percentage points higher than that with the (unimpregnated) coal plus tire. Clearly the catalyst has a considerable effect, but the effect is somewhat attenuated by the presence of the tire. The product distribution from the impregnated coal-plus-catalyst run is also interesting: the decrease in conversion is almost entirely at the expense of the gas yield. These results are consistent with our preliminary findings regarding the role of the tire and the role of the catalyst in the co-liquefaction.

Effect of Temperature, Tire-to-Coal Ratio, and Catalyst Preparation for a Given Tire-Coal Pair

Results using (uncatalyzed) DECS-6 coal, Tire-2, and mixtures at various values of R_{TC} and various temperatures are summarized in Table III. The conversion of tire increases from 66.5 wt% at 375°C to around 69 wt% at 400 and 425°C. The product is mainly oil. The amount of gaseous product is between 2-4 wt%. The conversion of coal also increases with temperature, from about 27 wt% at 375°C to 37% at 425°C. The increase in conversion is mostly accompanied by an increase in the oil yield, which is nearly double at 425°C (21.5%) than at 375°C (10.2%).

With the addition of tire, the conversion of coal increases, indicating a synergistic effect of tire. The increase was found to be dependent on both R_{TC} and temperature. At 375 and 400°C, the conversion of coal increases continuously with the increase in R_{TC}. However, at 425°C, the conversion is maximum (50%) when R_{TC} = 1. This work, though performed independently of work reported in the previous section, is consistent with the results reported therein.

The effect of catalyst preparation conditions on its activity was also studied. Specifically, Table IV shows the effect of drying temperature on the product slate at 400°C for R_{TC} values of 1 and 2, as well as for the corresponding feed components by themselves. In all cases, the catalyst loading was fixed at 1.67% of the coal. In the coal-alone runs, the conversion of coal decreases slightly as the drying temperature is increased. However, in the co-liquefaction runs, a drying temperature of 150°C is generally beneficial to the activity of the catalyst. The results indicate that the addition of tire is detrimental to the activity of the catalyst, especially when the drying temperature is below 118°C or when R_{TC} = 2. Catalysts used below were dried at 150°C.

Table V shows the effect of liquefaction temperature on the conversion and product yields of catalyzed co-liquefaction. As expected, the conversion of coal in coal-alone runs increases with increase in temperature. The yield of asphaltenes is maximum (40.9%) at 400°C, whereas the yield of oil is maximum (28.3%) at 425°C. This indicates that the asphaltenes are probably converted to oil at 425°C. In the co-liquefaction runs, the conversion of coal is maximum at R_{TC} = 1, after which it either decreases or, at the highest temperature, levels off. At all temperatures, oil yields in co-liquefaction runs are lower than those in coal-alone runs.

As mentioned earlier, the catalyst loading used has been 1.67%, based on coal. However, with the addition of tire to the catalyst-impregnated coal, the total amount of catalyst in the reacting system decreases. In order to study the effect of the catalyst, runs were carried out in which the total amount of catalyst (*i.e.*, based on coal-plus-tire) was kept constant while R_{TC} was varied. This was done by first impregnating coal with catalyst to a loading of 5%, based on coal. Then, appropriate amounts of un-impregnated ("raw") coal and/or tire were added such that the catalyst loading was always 1.67%, based on coal-plus-tire, while R_{TC} was varied. (Earlier results reported in [2] indicate that mixing our catalyst-impregnated coal with "raw" coal results in liquefaction yields undistinguishable from runs where the average amount of catalyst is impregnated on the entire amount of coal.) The results are presented in Table VI. The conversion of coal increases from 65%, in the absence of tire, to 75% in the presence of tire, independent of R_{TC}. The increase in conversion is tied to the increase in the yield of asphaltenes. The results are consistent with our earlier hypothesis on the interaction of the catalyst with tire. When the total amount of catalyst is kept the same, the conversion and product slate are independent of R_{TC}.

Using the Tire Residue as a Reaction Enhancer for Coal Liquefaction

As noted earlier, the residue after liquefaction of tire alone has no particular beneficial effect on coal liquefaction. This was demonstrated [2] by comparing the results of liquefaction of coal plus tire with the results when the feed consisted of coal and the liquid products from

tire liquefaction (*i.e.*, when the residue was absent); no significant change could be seen. However, Consortium colleagues at Auburn and elsewhere have reported (*e.g.*, [8]) that the tire residue, when pretreated, may have catalytic activity towards coal liquefaction. Preliminary runs were made with tire residue obtained in two ways in this work: in an autoclave, and in the conventional tubing-bomb reactor (TBR) used for the other liquefactions. The first method has the potential of generating larger amounts of residue in one run, if scale-up problems can be overcome. In both cases, the tire was reacted under standard liquefaction conditions (SLC): 400°C, 1000 psi H_2 pressure, 0.5h. The product was extracted with THF to obtain the THF-insoluble material as residue. The residue obtained in each case was heat treated at 560°C for 1h under N_2.

The reactivity of the residue itself was checked by heating it under SLC. The amount of THF-soluble material ("conversion") after this process was below 1%. This indicates that the residue is stable under these conditions, *i.e.*, that all reactive species have been removed.

The tire residue, obtained by each of the two methods above, was used in the liquefaction of DECS-6 coal. The liquefaction was also performed under SLC. The residue-to-coal ratio was 0.33, much higher than the loading of the iron-based catalyst above, to ensure that relatively small changes in conversions could be detected.

With the tire residue obtained from the autoclave, the conversion of coal increased from around 35% (without residue) to 48%. The conversion of coal also increased when it was liquefied with the tire residue from the TBR. However, the increase in the latter case was much higher than with the autoclave residue. The exact reason for this difference is not clear. One possibility is that the TBR residue may have been contaminated with the copper anti-sieze lubricant during the washing of the TBR with THF. No such lubricant was used with the autoclave. Alternatively, the different characteristics for heat and mass transfer in the two reactors may be the cause of the different effects. Clearly, further work is needed.

The activity of the residue was also found to depend on the treatment time at 560°C. For example, when the treatment time of the autoclave product was increased to 4h, the conversion of coal increased to 57%. The increase in conversion was mostly accompanied by an increase in the yield of asphaltenes.

Conclusions

Optimum processing conditions for co-liquefaction (temperature, pressure, R_{TC}, catalyst loading) depend upon the nature of the coal and the tire used.

The ferric-sulfide-based, *in-situ* impregnated catalyst improves the coal conversion, but the effect is attenuated by the presence of the tire.

The residue from the tire, if suitably pretreated, may increase liquefaction conversions.

PLANS

The product slate from our co-liquefaction runs has not been adequately characterized to date, except for solubility-based separation into asphaltenes+preasphaltenes, oils and gases. We expect to be working with other members of the Consortium to characterize these products better. We plan to tie the product quality to coliquefaction conditions.

The use of waste oil as a co-solvent in the co-liquefaction of tires and coal presents opportunities both for the removal of an additional waste and for improving liquefaction yields.

We plan to study the effect of pretreatment of the tire residue on its ability to enhance the co-liquefaction reaction. In particular, the problems associated with scale-up of the generation of the residue need to be resolved.

REFERENCES

1. Farcasiu, M., Chemtech **23**, 22 (1993).
2. Liu, Z., J.W. Zondlo and D.B. Dadyburjor, Energy and Fuels **8**, 607 (1994)
3. Gray, D. and G. Tomlinson, Contractors' Review Meeting, Pittsburgh, PA (1994).
4. Liu, Z., J. Yang, J.W. Zondlo, A.H. Stiller and D.B. Dadyburjor, Fuel, accepted (1995).
5. Dadyburjor, D.B., W.R. Stewart, A.H. Stiller, C.D. Stinespring, J.-P. Wann and J.W. Zondlo, Energy and Fuels **8**, 19 (1994).
6. Stansberry, P.G., J.-P. Wann, W.R. Stewart, J. Yang, J.W. Zondlo, A.H. Stiller and D.B. Dadyburjor, Fuel **72**, 793 (1993).
7. Liu, Z., J.W. Zondlo, and D.B. Dadyburjor, Energy & Fuels **9**(4), in press (1995).
8. Curtis, C.W., personal communication (1995).

Table I

Proximate and Ultimate Analyses of Coal and Tires Used.
Coal analyses from Galbraith Laboratories; Tire analyses from Penn State Coal Bank

SAMPLE	H_2O	ASH	VOLATILE MATTER	FIXED CARBON	C	H	N	S
	%	%dry	%daf	%daf	%daf	%daf	%daf	%daf
TIRE-1	0.3	4.7	67.1	32.9	84.3	7.4	<0.5	1.6
TIRE-2	0.4	8.1	71.0	29.0	79.7	7.5	<0.5	1.7
TIRE-3	0.5	7.3	67.1	32.9	81.8	7.3	<0.5	1.4
DECS-6	1.8	6.3	49.0	51.0	81.9	6.3	1.5	0.9
DECS-26	0.8	6.6	48.5	51.5	75.5	6.1	1.0	0.5
DECS-24	---	13.4	47.0	53.0	76.3	5.3	1.3	6.4

TABLE II

Coefficients for X, AP, O, G from two investigators using DECS-6 coal. Coefficients correspond to

$$Y = A_0 + A_T*T + A_t*t + A_P*P + A_{Tt}*T*t + A_{TP}*T*P + A_{tP}*t*P + A_{TT}*T^2 + A_{tt}*t^2 + A_{PP}*P^2$$

where T = (temperature [°C] - 400)/400; t = (time [h] - 0.5)/0.5; P = (H_2 pressure [psig hot] - 1000)/1000

"---" indicates that the term is not statistically significant

Y	A_0	A_T	A_t	A_P	A_{Tt}	A_{TP}	A_{tP}	A_{TT}	A_{tt}	A_{PP}
X (BB)	31.8	7.93	1.75	2.79	-0.837	1.38	2.64	-6.03	---	-1.58
(FH)	32.5	6.09	0.649	3.2	-1.25	---	2.6	-6.22	---	1.04
A+P (BB)	12.7	-2.92	-2.05	1.76	-1.33	0.745	---	-5.8	---	---
(FH)	11.4	-3.72	-2.14	1.88	---	1.23	---	---	-4.85	---
O (BB)	14.7	6.13	2.33	---	---	---	2.52	-2.18	---	---
(FH)	18.3	4.83	1.36	---	---	-1.328	2.45	-3.54	---	---
G (BB)	3.41	4.78	1.93	0.781	1.13	1.21	---	2.01	-0.756	---
(FH)	2.95	4.26	2.29	0.445	1.22	1.39	-0.891	2.79	1.68	1.01

TABLE III

Effect of Liquefaction Temperature (T) and Tire-to-Coal Ratio (R_{TC}) on Product Yields
Other Liquefaction Conditions: 1000 psi(cold) H_2, 0.5h.
Results for tire-coal mixtures on "coal-alone" basis.

	TIRE-2	DECS-6	R_{TC} = 1	R_{TC} = 2
T = 375°C				
X	66.5	27.1	34.1	36.6
A+P	1.1	15.8	25.1	29.8
O	63.2	10.2	7.2	4.3
G	2.2	1.1	1.8	2.5
T = 400°C				
X	69.1	31.4	43.8	44.7
A+P	1.1	15.5	31.8	35.7
O	64.7	14.9	8.2	4.3
G	3.3	2.0	3.8	4.7
T = 425°C				
X	69.5	37.2	50.1	49.8
A+P	1.1	11.0	23.6	28.7
O	64.4	21.5	20.0	12.9
G	4.0	4.7	6.5	8.2

TABLE IV

Effect of Catalyst Drying Temperature on Product Yields
Liquefaction Temperature = 400°C; Other Parameters as in Table III

	DRYING TEMPERATURE, °C			
	25	92	118	150
DECS-6				
X	69.1	67.5	64.9	62.4
A+P	43.6	46.5	42.6	40.9
O	22.3	18.5	20.3	18.8
G	3.3	2.5	2.1	2.8
$R_{TC} = 1$				
X	68.1	61.8	66.4	66.0
A+P	47.8	43.3	44.1	50.2
O	16.2	15.3	20.0	13.4
G	4.2	3.2	2.3	2.4
$R_{TC} = 2$				
X	---	49.8	60.7	60.7
A+P	---	38.4	46.9	46.9
O	---	8.1	10.7	10.7
G	---	3.3	3.2	3.2

TABLE V

Catalytic Liquefaction of DECS-6 Coal and Tire-Coal Mixtures. Catalyst dried at 150°C; Catalyst Loading = 1.67% of Coal; Other Parameters as in Table IV.

	COAL	R_{TC} = 1	R_{TC} = 2
LIQUEFACTION TEMPERATURE = 375°C			
X	32.9	36.0	33.4
A+P	24.4	27.6	27.2
O	7.8	6.9	5.0
G	0.8	1.6	1.2
LIQUEFACTION TEMPERATURE = 400°C			
X	62.4	66.0	60.7
A+P	40.9	50.2	46.9
O	18.8	13.4	10.7
G	2.8	2.4	3.2
LIQUEFACTION TEMPERATURE = 425°C			
X	67.0	78.1	78.1
A+P	32.7	20.2	22.8
O	28.3	15.2	13.8
G	6.1	7.3	5.0

TABLE VI

Effect of R_{TC} on Product Yields. Catalyst Loading = 1.67% of Coal + Tire. Liquefaction Temperature = 400°C. Other Parameters as in Table V.

	DECS-6	R_{TC} = 1	R_{TC} = 2
X	64.6	75.5	75.3
A+P	39.7	53.3	54.2
O	21.8	17.6	16.6
G	3.1	4.6	4.6

Figure 1. Effect of temperature, time and H_2 pressure on conversion of DECS-6 coal

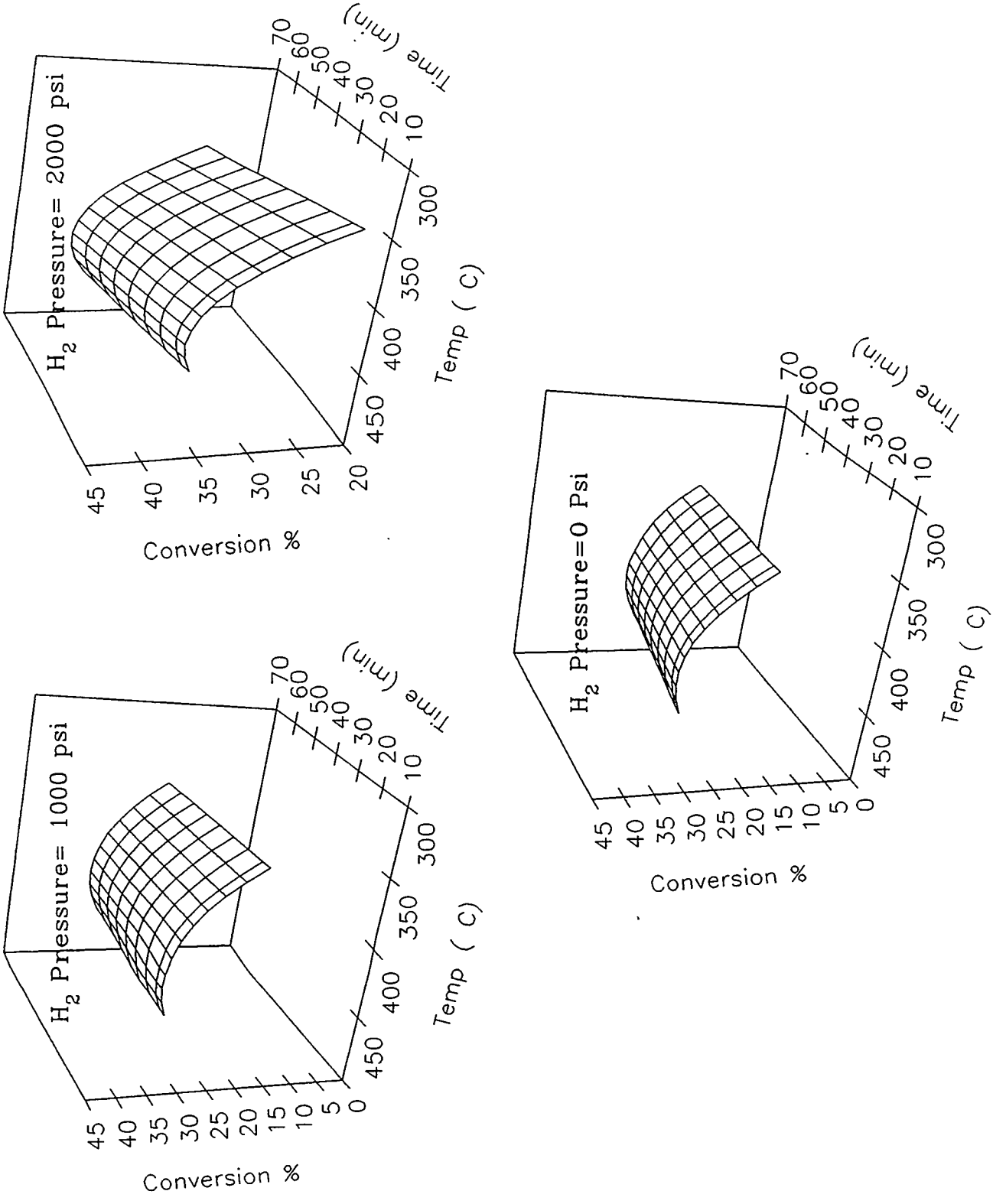

Figure 2. Conversion and product yields for DECS-6 coal at 2000 psi(hot) H_2 pressure.

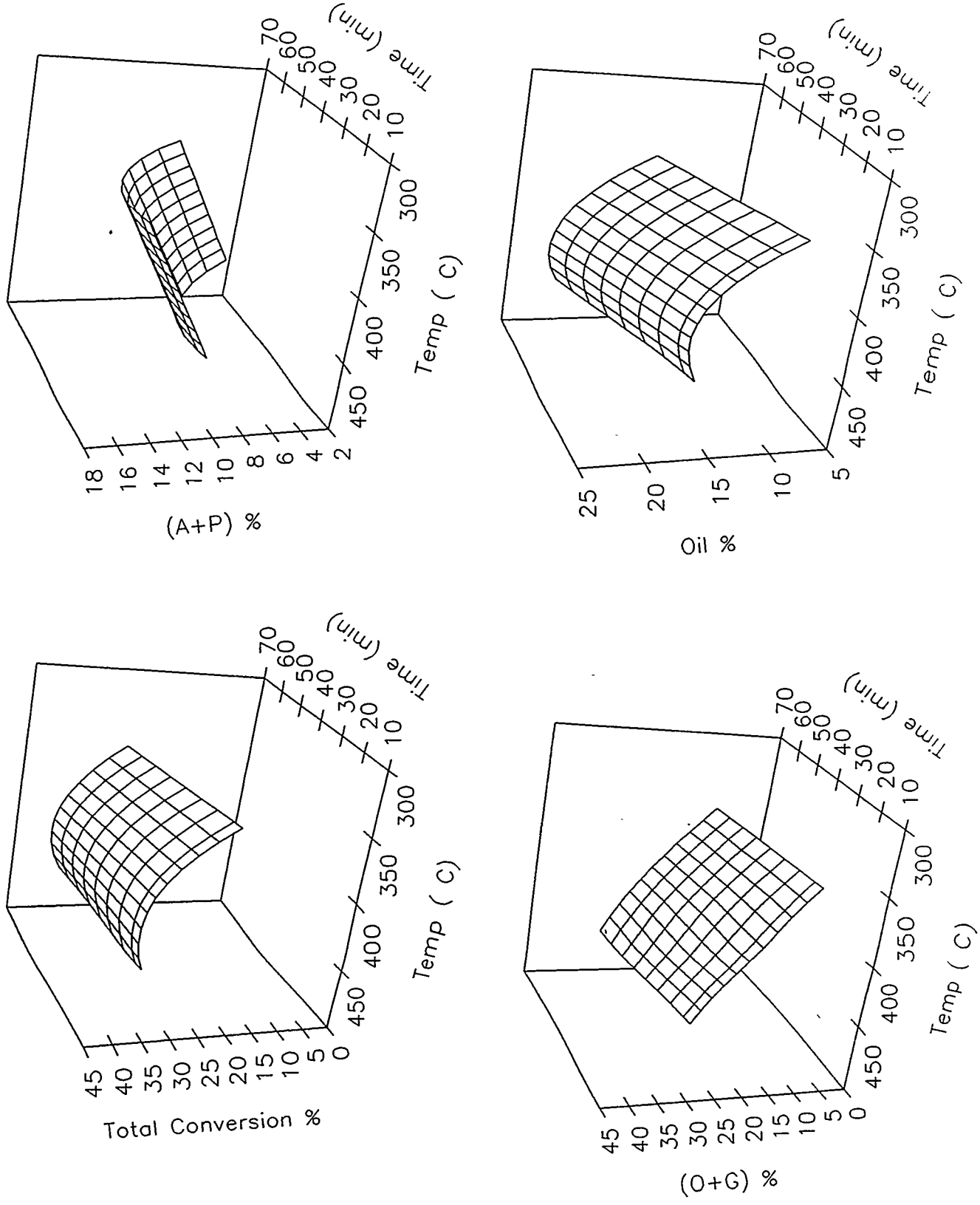

Figure 3. Conversion and product yields for Tire-2 at 2000 psi(hot) H_2pressure.

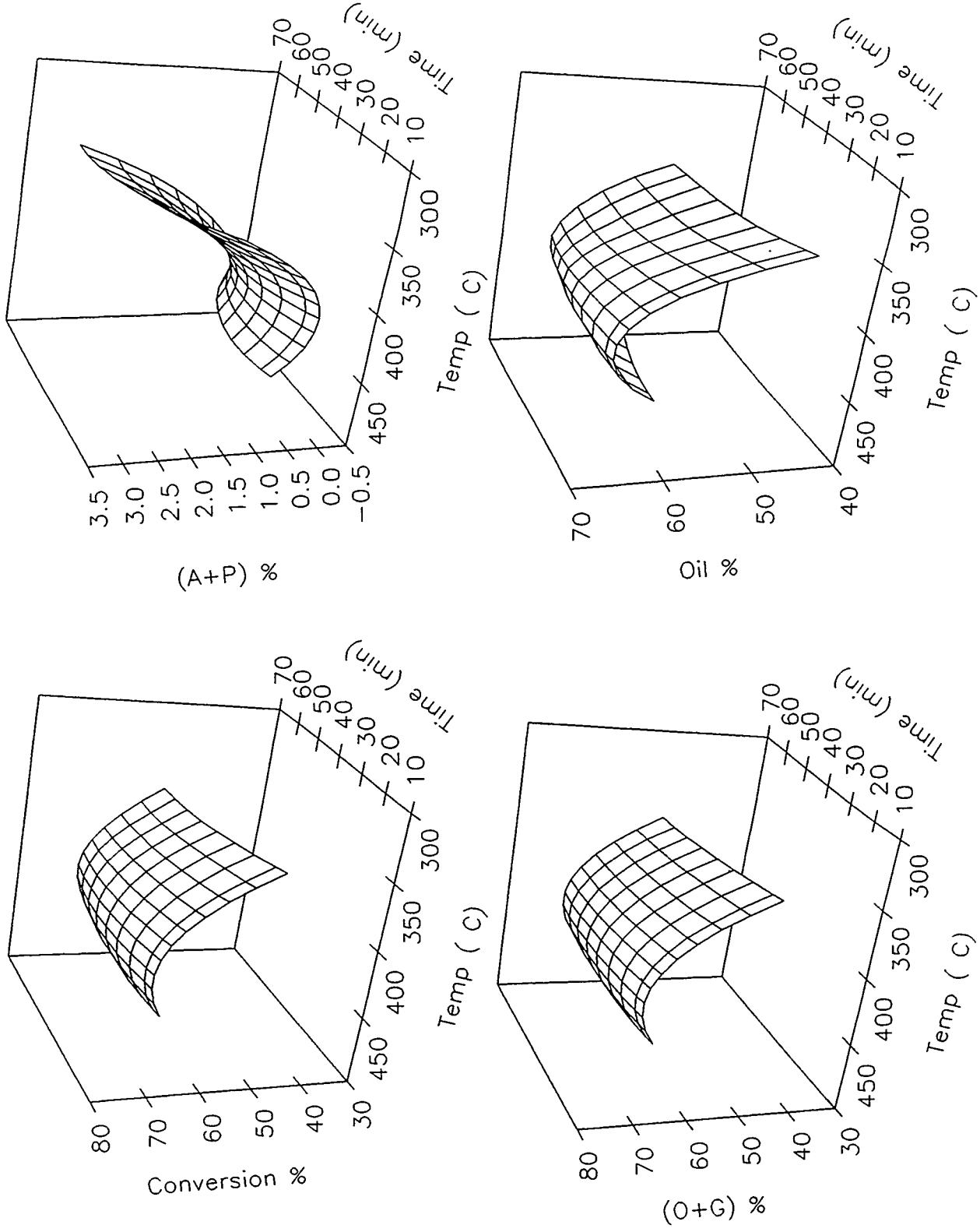

col0695-3

Figure 4. Conversion and product yields for DECS-26 coal at 2000 psi(hot) H_2 pressure.

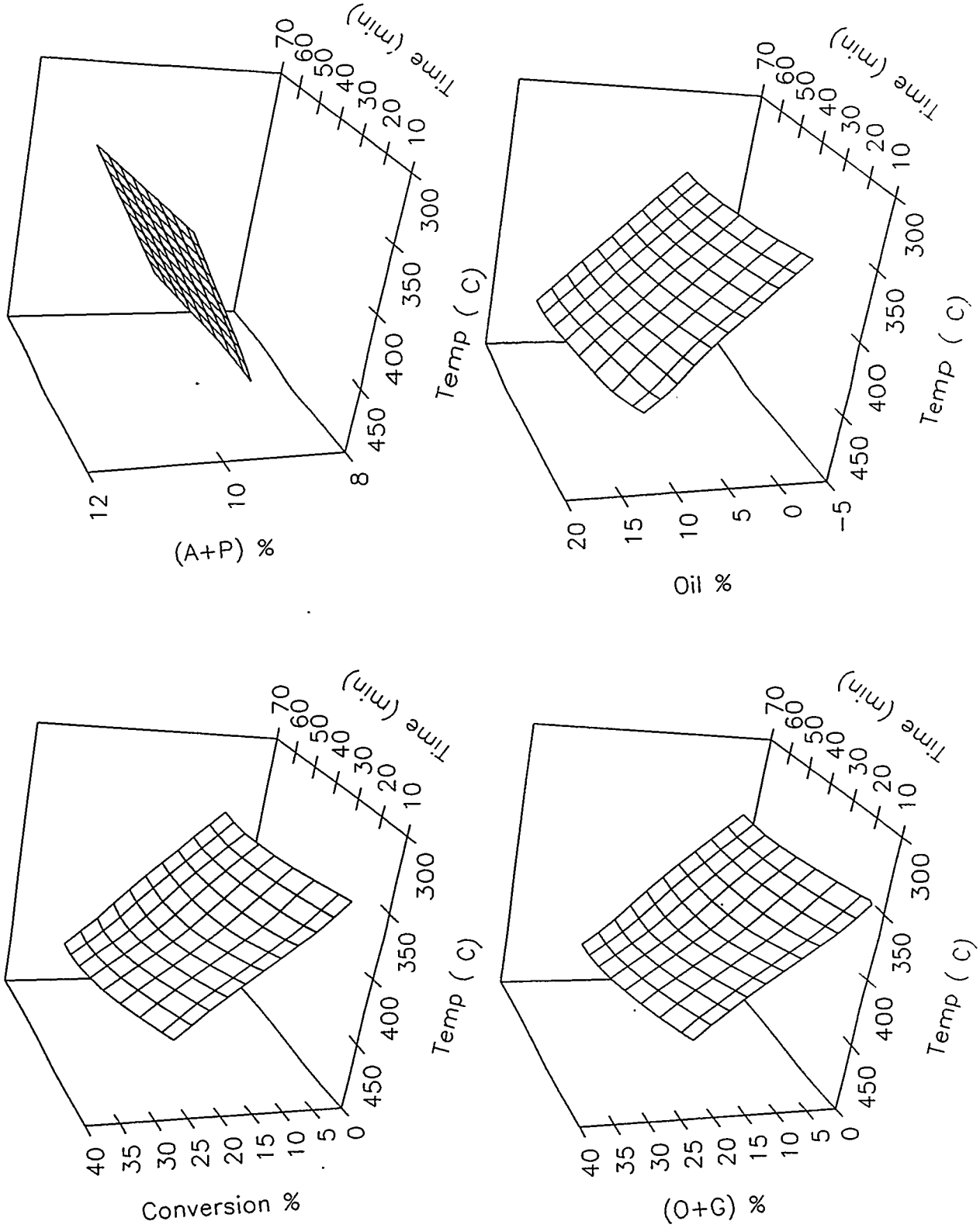

col695-4

Novel Bimetallic Dispersed Catalysts for Temperature-Programmed Coal Liquefaction

-- Hydrodeoxygenation and Hydrocracking of Model Compounds over Mo- and Fe-based Dispersed Catalysts

Chunshan Song, Stephen Kirby, Eckhardt Schmidt, and Harold Schobert

Fuel Science Program
Department of Materials Science & Engineering
Pennsylvania State University
University Park
PA 16802-2303

U.S. DOE/PETC Contract No. DE-AC22-92PC92122

Period of Performance: September 1992-September 1995

Paper to Appear in

Proceedings of 1995 U.S. DOE Coal Liquefaction and Gas Conversion Contractors' Review Conference

August 29-31, 1995

Westin William Penn Hotel, Pittsburgh, Pennsylvania

Accomplishments & Conclusions

Summary

The objective of this project is to explore bimetallic dispersed catalysts for more efficient coal liquefaction. Coal liquefaction involves cleavage of methylene, dimethylene and ether bridges connecting various aromatic units and the reactions of various oxygen functional groups. This paper describes our recent results on 1) hydrodeoxygenation of O-containing polycyclic model compounds using novel organometallic catalyst precursors; and 2) activity and selectivity of dispersed Fe catalysts from organometallic and inorganic precursors for hydrocracking of 4-(1-naphthylmethyl) bibenzyl.

For hydrodeoxygenation, model compound studies were performed using multi-ring systems, or those of comparable molecular weight, to investigate the capabilities of the dispersed catalysts. The model compounds selected include anthrone (carbonyl); dinaphthyl ether (aryl-aryl ether); xanthene (heterocyclic ether); and 2,6-di-*t* -butyl-4-methylphenol (hydroxyl). The catalyst precursors used were $(NH_4)_2MoS_4$ (ATTM), $[Ph_4P]_2[Ni(MoS_4)_2]$ (Ni-Mo1) and $Cp_2Co_2Mo_2(CO)_2S_4$ (CoMo-T2). Reactions were performed in a 22ml capacity microreactor (with 0.5 g model compound under 1000 psi H_2) at 300°C, 350°C and 400°C for 30 minutes.

From the non-catalytic data shown there is a clear order of starting material reactivity : 2,6-di-*t*-butyl-4-methylphenol > anthrone > dinaphthyl ether > xanthene. However, the reactivity order of the oxygen functionalities in the presence of the various catalysts is different. For non-catalytic conditions the order appears to be : carbonyl > aryl-aryl ether » substituted phenol ≈ heterocyclic ether. In the presence of ATTM this sequence changes slightly to : carbonyl > substituted phenol ≈ aryl-aryl ether » heterocyclic ether and for reactions involving CoMo-T2 the reactivity order appears to be : carbonyl > aryl-aryl ether > heterocyclic ether > substituted phenol.

These differences in reactivity order emphasize the effect of the nature of the oxygen functionality on the deoxygenating capabilities of the catalysts and that different catalysts can have different roles in promoting hydrodeoxygenation and reduction, depending on the nature of the starting material. They also highlight the undesirability of phenolic and heterocyclic ether structures in liquefaction systems. Both these structures types are quite unreactive under liquefaction conditions and any reaction has a tendency to form high yields of single-ring phenols.

When applied to coals, these findings suggest that coals differing from each other in the form of which oxygen functional groups are dominant, may show quite different kinds of liquefaction products, depending on which catalyst precursor was chosen.

To examine what determines the activity and selectivity of Fe catalysts for hydrogenation and hydrocracking, various molecular precursors with Fe in different chemical environments have been tested in this work to help understand the influence of precursor structure and the effect of sulfur addition on the activity and selectivity of resulting Fe catalysts in model reactions of 4-(naphthylmethyl)bibenzyl (NMBB). We have examined various precursors, including a thiocubane type cluster $Cp_4Fe_4S_4$, a cyclopentadienyliron dicarbonyl dimer $Cp_2Fe_2(CO)_4$, ferrocene Cp_2Fe, a series of carbonyl precursors including $Fe(CO)_5$, $Fe_2(CO)_9$, and $Fe_3(CO)_{12}$, and superfine iron oxide with average particle size of 30 Å (SFIO). For testing various Fe catalyst precursors, runs with NMBB were carried out in 33 mL reactor using 0.78 mmol NMBB in n-tridecane solvent at 400°C for 30 min, in the presence of a Fe catalyst precursor (2.11 wt% Fe based on NMBB).

The particles from $Cp_2Fe_2(CO)_4$ showed the highest activity among all the precursors examined in the absence of added sulfur. The activity of catalysts from Fe carbonyls decreased with increasing number of irons in the carbonyl compounds: $Fe(CO)_5$ > $Fe_2(CO)_9$ >

$Fe_3(CO)_{12}$; adding sulfur increased their activity but their activities rank the same both with and without sulfur addition. Surprisingly, $Cp_4Fe_4S_4$ exhibited the lowest activity, although it has the S-to-Fe ratio closest to pyrrhotite ($Fe_{1-x}S$, where X= 0 to 0.12) which is thought to be the active phase. The nano-scale SFIO particles performed at an activity level similar to that of $Fe_2(CO)_9$ in the absence of sulfur, but afforded the highest NMBB conversion when S was added. Ferrocene is more effective in hydrocracking reactions of NMBB than the inorganic iron complex $FeSO_4 \cdot 7H_2O$. Sulfur added to iron sulfate had the expected beneficial effect on NMBB conversion. But sulfur added to ferrocene decreased the activity of resulting catalyst. The other iron containing organometallic complex that showed a similar trend in conversion after sulfur addition was $Cp_2Fe_2(CO)_4$. Both complexes have cyclopentadienyl ligands as common features. Another precursor with Cp-functionalities and sulfur in the precursor molecule ($Cp_4Fe_4S_4$) showed very low activity too. There is apparently a negative correlation between the conversion of iron containing complexes and the presence of cyclopentadienyl/sulfur units.

The present results showed that some iron containing catalysts have higher activity in the sulfur-free form, contrary to conventional wisdom. Adding sulfur to Fe precursors with Cp-ligands decreased the activity of the resulting catalyst. This is in distinct contrast to the cases with iron pentacarbonyl and superfine Fe_2O_3, where S addition increased their catalytic activity substantially. A positive correlation between sulfur addition and increased activity can be seen, but a reversed trend between Fe cluster size and hydrocracking conversion could be observed, for carbonyl-type Fe precursors. It is apparent that the activity and selectivity of Fe catalysts for NMBB conversion depends strongly on both the type of ligand environment, the oxidation state and the number of intermetal bonds in the molecular precursor.

Recent Results : Part I

Hydrodeoxygenation of O-containing Polycyclic Model Compounds Using Novel Organometallic Catalyst Precursors.

I-1. INTRODUCTION

Oxygenated compounds are present in virtually all coals [1]. Phenols (and related hydroxyl compounds) have been identified as components of coal-derived distillates [2,3]. Ethers and related compounds, connecting structural units within the coal matrix, have been proposed as sites for the depolymerization of the coal [4] and also ethers, together with carboxyls and phenolics, have been implicated in the facilitation of retrogressive, crosslinking, repolymerization reactions [5,6].

Low-rank coals (i.e. lignites and subbituminous coals) include significantly more oxygen-containing groups than coals of higher rank [7]. With the increase in the extraction of lower rank coals in the U.S. and research into their use as liquefaction feedstocks [5,8,9], the importance of oxygen functionality removal from coal and coal-derived liquids is all the more apparent.

The removal of these functionalities from the distillate products of coal liquefaction can be both complicated and expensive, and often leads to substantial reductions in distillate yields [3]. Therefore, deoxygenation during the liquefaction process would be beneficial. This goal may be attainable with the use of sulphided bimetallic catalysts dispersed onto the coal using an organometallic precursor [10,11].

Model compound studies using multi-ring systems, or those of comparable molecular weight, were performed to investigate the capabilities of these catalysts. The model compounds selected represent a variety of oxygen functionalities, possibly present in coals of differing rank [12-14], contained within polycyclic systems. They include: anthrone (carbonyl); dinaphthyl ether (aryl-aryl ether); xanthene (heterocyclic ether); and 2,6-di-*t* -butyl-4-methylphenol (hydroxyl).

I-2. EXPERIMENTAL

All experiments were performed in a 22 ml capacity microreactor. A 0.5g sample of model compound was loaded into the reactor. Solvent was added in a 1:2 weight ratio to model compound and catalyst precursors were added at 2.46mol% concentration (unless otherwise stated). The catalyst precursors used were $(NH_4)_2MoS_4$ (ATTM), $[Ph_4P]_2[Ni(MoS_4)_2]$ (Ni-Mo1) and $Cp_2Co_2Mo_2(CO)_2S4$ (CoMo-T2).

Air was removed by flushing the reactor three times with H_2 to 1000psi. The reactor was then repressurized to 1000psi H_2. Reactions were performed at 300°C, 350°C and 400°C for 30 minutes. All reactions were carried out in a fluidized sand bath equipped with a vertical oscillator driving at a setting of 55 (~250 strokes per minute). At the end of the reaction the microreactor was quenched in cold water.

Tridecane (0.25g) was added to the microreactor as an internal standard. The microreactor contents were then extracted with acetone and diluted for analysis.

Capillary gas chromatography (GC) connected to a flame ionization detector (Perkin Elmer-8500) and gas chromatography / mass spectrometry (Hewlett Packard-5890) were used for the quantitative and qualitative analysis of the product distribution, respectively.

I-3. RESULTS AND DISCUSSION

Product distributions have been grouped as oxygen-containing and deoxygenated for the purposes of this article. The conversions of anthrone, dinaphthyl ether, xanthene and 2,6-di-*t*-butyl-4-methylphenol are shown in Figures 1-4, and the product distribution of dinaphthyl ether is given in Table 1.

Generally, the addition of any catalyst to a system under the conditions studied increases the total conversion. For example, at 400°C dinaphthyl ether undergoes 26% thermal conversion; this yield is increased to 72% in the presence of ATTM, 88.5% with Ni-Mo1, and 100% using CoMo-T2. However, any improvement in the product quality, especially deoxygenation and ring reduction, in the presence of these catalysts is also important, and the variation of these factors for the different oxygen functional groups will be the main focus of this discussion.

Anthrone

Under non-catalytic conditions anthrone converts to anthracene through thermal reaction of the carbonyl oxygen. Anthracene then reacts further to form a variety of hydrogenated ring species, such as di- and tetrahydroanthracene.

In the presence of ATTM, the formation of oxygen-containing compounds in the products at 350°C and 400°C (substituted naphthols and phenols) suggest hydrogenation of the carbonyl oxygen to a hydroxyl group before extensive conversion to anthracene. Reduction in the yields of these oxygen functionalities in the ATTM reaction at 400°C may indicate the possibility of an increase in the conversion of these species to non-oxygenated products.

Conversion of anthrone to oxygen-free products is increased considerably using the CoMo-T2 catalyst precursor. This implies that CoMo-T2 has the capability to increase the conversion of carbonyls without additional phenol or naphthol production. This may be achieved by either rapid C=O cleavage prior to ring hydrogenation, rapid phenol conversion to oxygen-free products, or by the prevention of initial hydroxyl group formation. From the reactions of 2,6-di-*t*-butyl-4-methylphenol with CoMo-T2, it can be seen that this catalyst, although removing some hydroxyl functionality, does not promote the ready conversion of phenols to non-oxygen containing species.

Variations in the oxygen-free products of anthrone conversion are also apparent for the different catalyst precursors. Ni-Mo1 appears to promote the formation of 1,2,3,4-tetrahydroanthracene (THA), whereas CoMo-T2 demonstrates the facilitation of 9,10-dihydroanthracene (DHA) production. ATTM seems to have equal affinity for the formation of both products. Ni-Mo1 and ATTM both exhibit an increase in the formation of 1,2,3,4,5,6,7,8-

octahydroanthracene (OHA) at 400°C (0% under catalyst-free conditions to 11.8% and 11.3% respectively), which only appears in very low yields with CoMo-T2 (1.5%). This reduction in OHA yield for the CoMo-T2 precursor is comparable to increases in anthracene and DHA production, suggesting selective hydrogenation of the 9- and 10- positions (i.e. the carbonyl carbon).

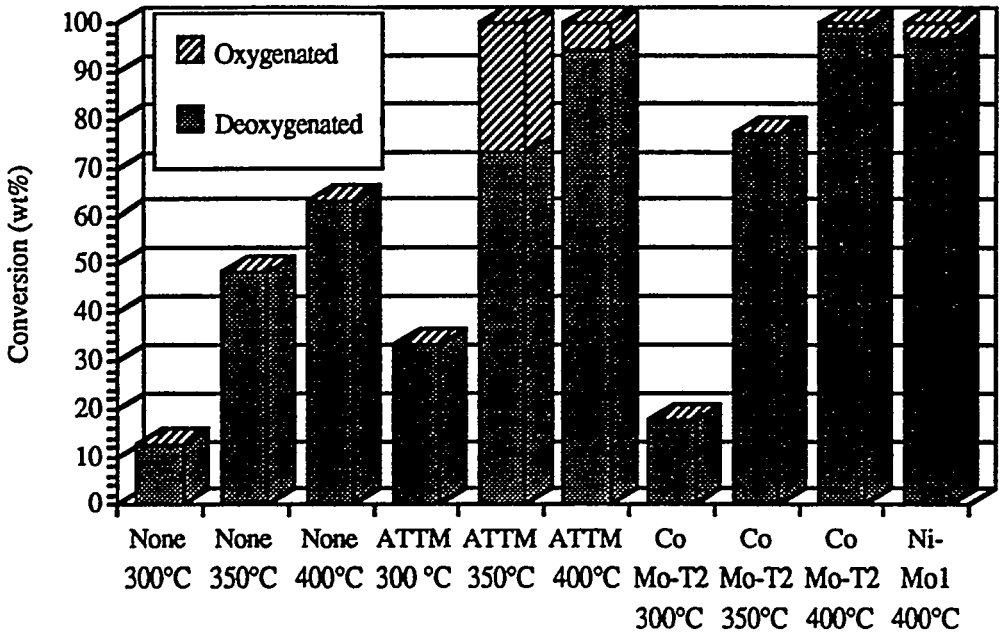

Figure 1. Yield of oxygenated and deoxygenated products of anthrone as a function of temperature and catalyst precursor.

Dinaphthyl Ether

Under non-catalytic conditions naphthalene is the major product of dinaphthyl ether (DNE) hydrogenation, with low yields of 2-naphthol, although total conversion is very small (26%). Oxygen functionality removal is increased in the presence of all the catalyst precursors, although to a lesser extent than for anthrone.

ATTM increases DNE conversion to oxygen-free products (63.6% at 400°C) with the balance of the products being phenols, naphthols (1.8%) and ring-reduced derivatives of the starting material. Phenol and naphthol yields decrease from 350°C to 400°C, again implying that ATTM facilitates hydroxyl group removal.

High conversions to tetralin and naphthalene are achieved in the presence of CoMo-T2 (51.6% and 40.2% respectively at 400°C). Phenols and naphthols are present in larger yields than for anthrone, suggesting the cleavage of a single C-O bond followed by hydrogenation of the phenoxy (or naphthoxy) group. Ring-reduced derivatives of DNE produced at 350°C are absent at 400°C and naphthol yields decrease across the same temperature range. These reductions in oxygen compound yields are accompanied by increases in tetralin, naphthalene and alkylbenzene formation.

The product distributions (O : non-O) of reactions of ATTM, Ni-Mo and CoMo-T2 with DNE (Figure 2 and Table 1) distinctly show the latter precursor to be the most favourable for C-O-C bond cleavage to oxygen-free products.

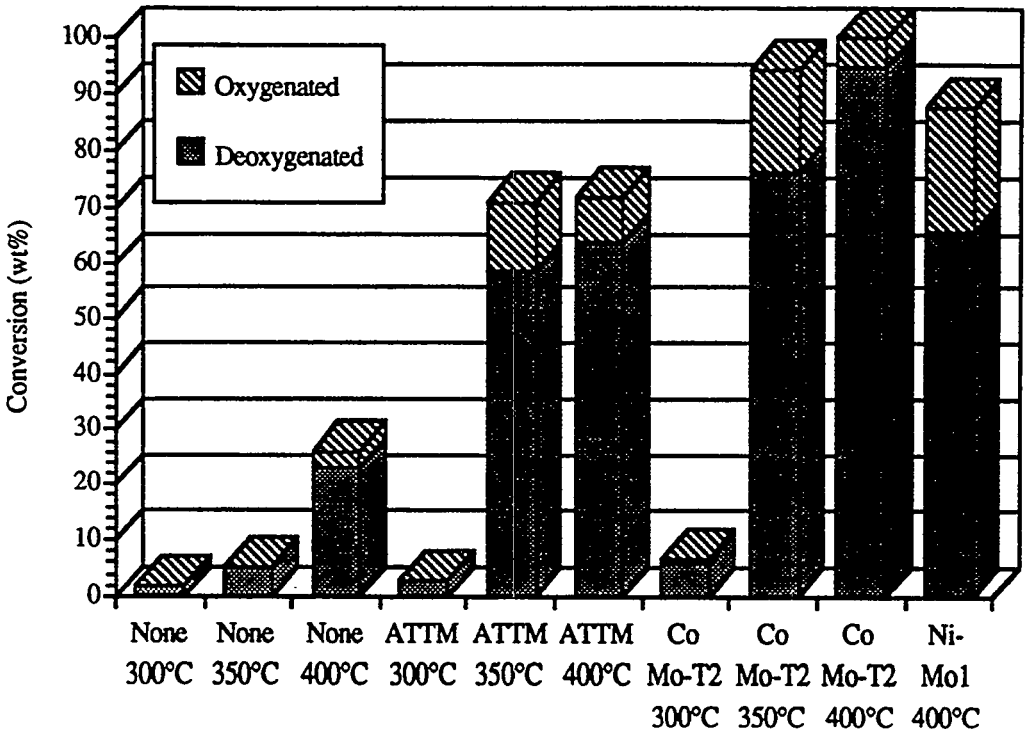

Figure 2. Yield of oxygenated and deoxygenated products from dinaphthyl ether as a function of temperature and catalyst.

Table 1. Product distribution of dinaphthyl ether under liquefaction conditions.

React.temp.(°C)	300	350	400	300	350	400	400	300	350	400
Cat. Precursors	None	None	None	ATTM	ATTM	ATTM	Ni-Mo	CoMo-T2	CoMo-T2	CoMo-T2
Products(wt%)										
Tetralin		1.2		1.3	30.5	24.4	24.6	4.4	47.2	51.6
Naphthalene	1.9	4.1	22.9	1.4	26.1	38.3	39.1	1.9	28.6	40.2
THDNE					7.4	6.3	12.0	0.3	7.5	0.3
OHDNE					1.7		3.2		2.6	
THnaphthol					2.3	1.0	4.1		5.9	3.5
2-Naphthol			3.2		0.6	0.8	2.1	0.3	1.5	0.5
Methylphenol					0.3		0.4		0.6	0.7
Alkylbenzenes					1.9	0.9	2.0		0.5	3.1
Conv. (wt%)	1.9	5.3	26.1	2.7	70.7	71.9	87.6	6.9	94.3	100

Xanthene

In the absence of a catalyst xanthene is totally unreactive. Addition of ATTM or CoMo-T2 produces noticeable reaction at 350°C and 400°C.

At 350°C the products from both precursors are phenols, cycloalkyl- and long-chain alkylbenzenes formed by C-O and C-C bond cleavage. However, at 400°C ATTM produces an increase in oxygen-free products with no increase in phenols, although conversion to non-oxygen containing species is low (24.9%).

Increases in oxygen-free product yields are also achieved with CoMo-T2 at 400°C , but with accompanying increases in phenol formation. This gain in phenols may be attributed to the

formation of short-chain (C1-C2) alkylphenols from longer chain alkylphenols, implying that CoMo-T2 favours C-C cleavage over C-OH.

The comparably large conversion to oxygen-free products and phenols reinforces the ability of CoMo-T2 to cleave ether linkages, and inability to remove hydroxyl groups. However, the low conversions of xanthene illustrate the unreactive nature of the starting material.

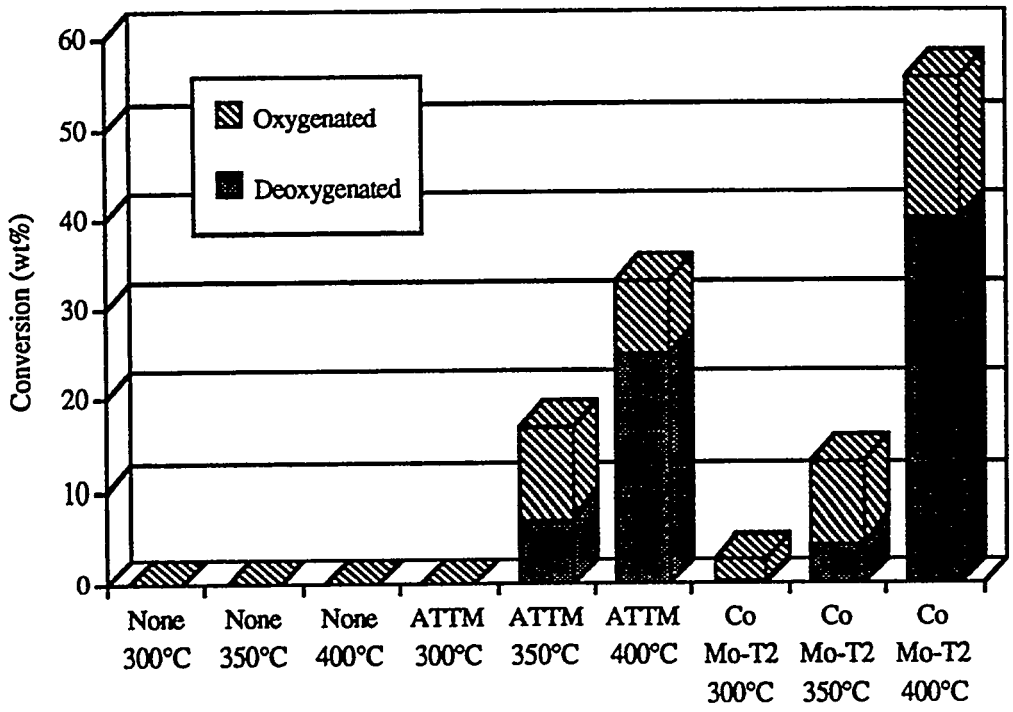

Figure 3. Yield of oxygenated and deoxygenated products of xanthene as a function of temperature and catalyst.

2,6-Di-*t*-butyl-4-methylphenol (DBMP)

Under non-catalytic reaction conditions the conversion of DBMP involves the cleavage of one, or both, of the *t*-butyl groups to produce 2-butyl-4-methylphenol (BMP) and ultimately 4-methylphenol (100% at 400°C). No reaction occurs at 300°C in the absence of a catalyst. When a catalyst is present the removal of the butyl groups becomes more favourable and formation of the above products takes place.

At 350°C with ATTM, almost all the starting material has reacted and only a small portion remains as BMP (13.5%). The major product, 4-methylphenol, then undergoes catalytic hydrogenation and hydroxyl removal to form toluene and methylcyclohexane. At 400°C these reactions proceed to a greater extent, resulting in greater yields of both products (46.5% and 20.2% respectively).

In the presence of CoMo-T2, DBMP appears to lose both butyl groups so rapidly that no 2-*t*-butyl-4-methylphenol is isolated, so 4-methylphenol is the only product at 300°C. At 350°C it exhibits some further conversion to methylcyclohexane (1.6%) and at 400°C toluene and methylcyclohexane are produced.

DBMP is a reactive compound through loss of its butyl groups. However, the hydroxyl group C-OH bond is very resistant to reaction and is only cleaved, to a substantial degree, in the presence of the ATTM precursor. CoMo-T2 removes the OH-group, but only to a small extent.

Investigations using the Ni-Mo1 precursor are not as advanced as those for ATTM and

CoMo-T2. Presentation of these results is planned for future articles.

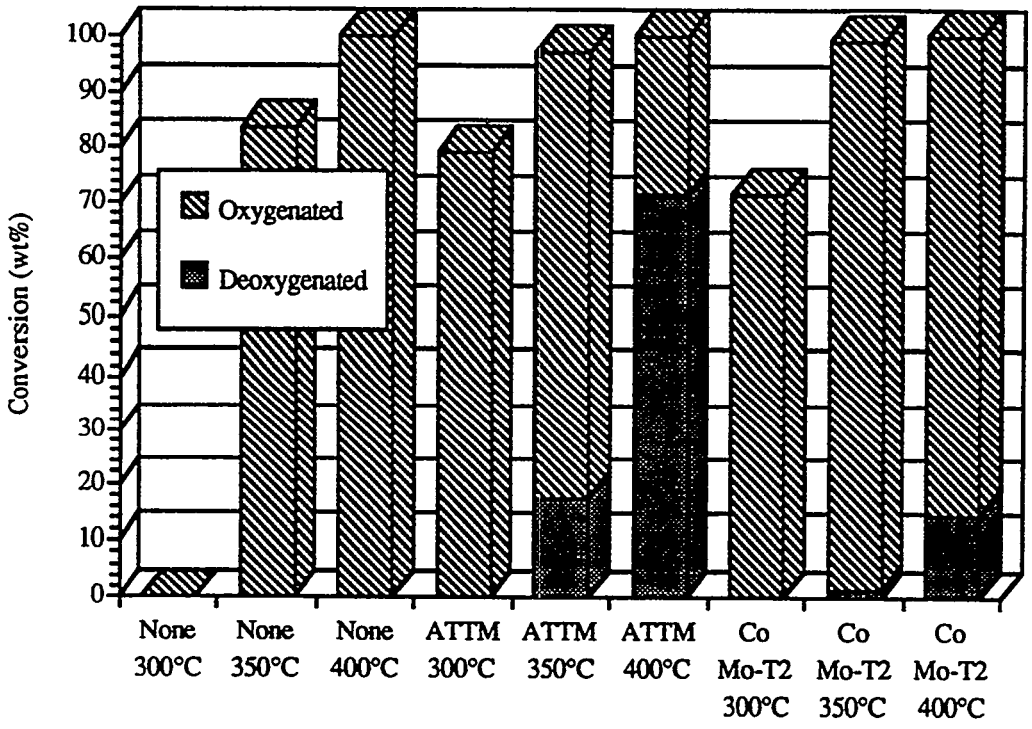

Figure 4. Yield of oxygenated and deoxygenated products of 2,6-di-*t*-butyl-4-methylphenol as a function of temperature and catalyst.

CONCLUSIONS

From the non-catalytic data shown there is a clear order of starting material reactivity : 2,6-di-*t*-butyl-4-methylphenol > anthrone > dinaphthyl ether > xanthene. However, the reactivity order of the oxygen functionalities in the presence of the various catalysts is different. For non-catalytic conditions the order appears to be : carbonyl > aryl-aryl ether » substituted phenol ≈ heterocyclic ether. In the presence of ATTM this sequence changes slightly to : carbonyl > substituted phenol ≈ aryl-aryl ether » heterocyclic ether and for reactions involving CoMo-T2 the reactivity order appears to be : carbonyl > aryl-aryl ether > heterocyclic ether > substituted phenol.

These differences in reactivity order emphasize the effect of the nature of the oxygen functionality on the deoxygenating capabilities of the catalysts and that different catalysts can have different roles in promoting hydrodeoxygenation and reduction, depending on the nature of the starting material. They also highlight the undesirability of phenolic and heterocyclic ether structures in liquefaction systems. Both these structures types are quite unreactive under liquefaction conditions and any reaction has a tendency to form high yields of single-ring phenols.

When applied to coals, these findings suggest that coals differing from each other in the form of which oxygen functional groups are dominant, may show quite different kinds of liquefaction products, depending on which catalyst precursor was chosen.

REFERENCES

1. C. Song, L. Hou, A. K. Saini, P. G. Hatcher and H. H. Schobert, (1993). *Fuel Processing Technology*, **34** 249-276.
2. R. E. Pauls, M. E. Bambacht, C. Bradley, S. E. Scheppele and D. C. Cronauer, (1990). *Energy & Fuels*, **4** 236-242.
3. C. Burgess, (1994). "Direct Coal Liquefaction: A Potential Route to Thermally Stable Jet Fuel", pp. 167.
4. L. Artok, O. Erbatur and H. H. Schobert, (in press).
5. C. Song, H. H. Schobert and P. G. Hatcher, (1992). *Energy & Fuels*, **6** 326-328.
6. M. A. Serio, E. Kroo, S. Charpenay, R. Bassilakis, P. R. Solomon, D. Miller, FA. Satyam, J. Manion and R. Malhotra, (1993). Proceedings of Contractors' Review Conference: "Coal Liquefaction and Gas Conversion": "The Dual Role of Oxygen Functions in Coal Pretreatment and Liquefaction: Crosslinking and Cleavage Reactions", Pittsburgh, PA, 15-44.
7. S. M. Solum, R. J. Pugmire and D. M. Grant, (1989). *Energy & Fuels*, **3** 187-193.
8. C. Song and H. H. Schobert, (1992). *Am. Chem. Soc. Div. Fuel Chem. Prepr.*, **37** 42.
9. L. Huang, C. Song and H. H. Schobert, (1992). *Am. Chem. Soc. Div. Fuel Chem. Prepr.*, **37** 223.
10. C. Song and H. H. Schobert, (1993). "Novel Bimetallic Dispersed Catalysts for Temperature-Programmed Coal Liquefaction", Penn State University DE-AC22-92PC92122-TPR-1.
11. C. Song, D. S. Parfitt and H. H. Schobert, (1993). *Catalysis Letters*, **21** 27-34.
12. L. M. Stock, (1989). *Accounts of Chemical Research*, **22** 427-433.
13. R. Hayatsu, R. E. Winans, R. G. Scott, L. P. Moore and M. H. Studier, (1978). *Fuel*, **57 (2)**, 541.
14. J. H. Shinn, (1984). *Fuel*, **63 (3)**, 1187.

Recent Results : Part II

Activity and Selectivity of Fe Catalysts from Organometallic and Inorganic Precursors for Hydrocracking of 4-(1-Naphthylmethyl) Bibenzyl

II-1. INTRODUCTION

Various iron containing catalysts have been investigated for their use in hydroliquefaction of coal ever since Bergius (1) demonstrated the feasibility of the process. Conventional iron (2,3) catalysts have been widely used either unsupported or as catalysts dispersed directly onto coal. Iron catalysts have generally a lower cost and lower environmental detriment than Mo, Ni and Co catalyst precursors. The search for active high surface area iron particles has become recently an important part in the development of a cost effective direct coal liquefaction process (4,5).

To examine what determines the activity and selectivity of Fe catalysts for hydrogenation and hydrocracking, various molecular precursors with Fe in different chemical environments have been tested in this work to help understand the influence of precursor structure and the effect of sulfur addition on the activity and selectivity of resulting Fe catalysts in model reactions of 4-(naphthylmethyl)bibenzyl (NMBB). We have examined various precursors, including a thiocubane type cluster $Cp_4Fe_4S_4$, a cyclopentadienyliron dicarbonyl dimer $Cp_2Fe_2(CO)_4$, ferrocene Cp_2Fe, a series of carbonyl precursors including $Fe(CO)_5$, $Fe_2(CO)_9$, and $Fe_3(CO)_{12}$, and superfine iron oxide with average particle size of 30 Å (SFIO).

II-2. EXPERIMENTAL SECTION

Runs with NMBB were carried out in 33 mL reactor using 0.78 mmol NMBB in n-tridecane

solvent at 400°C for 30 min, in the presence of a Fe catalyst precursor (2.11 wt% Fe based on NMBB). Carbonyl precursors were purchased from Aldrich. Precursor synthesis and experimental details may be found elsewhere (6). SFIO sample was provided by Mach I Inc. in Pennsylvania. Catalyst samples for BET and XRD analysis were prepared in similar reactors from ca. 1 g precursor and 4 g tridecane at 400 °C under 6.9 MPa H_2 pressure for 30 min. XRD data were obtained from a Scintag I (Scientific Computer and Instruments, USA). Surface area measurements were conducted using a Quantachrome Autosorb I Gas Sorption system.

II-3. RESULTS AND DISCUSSION

Conversion of NMBB

The initial stage of a catalytic reaction involves catalyst activation at elevated temperatures, depending on the type of catalyst precursor. It is known (7-9) that some precursors like metal carbonyls require the addition of sulfur for sufficient activity. There seems (10) to be consensus that the sulfides of the transition metals are more active in catalytic hydroliquefaction than their oxides. The reason for this remains unclear. The activation reaction is difficult to perform and iron carbonyls tend to form less reactive iron carbides and oxides (11) during the activation process. The present results in Tables 2 and 3 revealed several interesting trends. Even the catalysts without sulfur can display certain activity. The particles from $Cp_2Fe_2(CO)_4$ showed the highest activity among all the precursors examined in the absence of added sulfur. The activity of catalysts from Fe carbonyls decreased with increasing number of irons in the carbonyl compounds: $Fe(CO)_5 > Fe_2(CO)_9 > Fe_3(CO)_{12}$; adding sulfur increased their activity but their activities rank the same both with and without sulfur addition.

Table 2. Effect of Fe containing catalyst precursors on NMBB hydrocracking at 400 °C.

Catalyst Precursors	$Cp_2Fe_2(CO)_4$	$Fe(CO)_5$	$Fe_2(CO)_9$	$Fe_3(CO)_{12}$	$Fe(CO)_5$ + S	$Fe_2(CO)_9$ + S	$Fe_3(CO)_{12}$ + S	$Cp_2Fe_2(CO)_4$ +S
Conv, wt %	**62.2**	**45.6**	**24.7**	**22.1**	**61.2**	**51.5**	**45.7**	**21.3**
Prod, mol %								
Benzene	0.6				1.3		0.7	0.9
Toluene	1.6	1.3	0.8	1.5	2.3	2.3	1.9	
p-Xylene	0.5	0.2	0.2	0.3	0.8	0.4	0.7	0.2
Tetralin	8.5	4.2	2.2	2.0	2.6	1.5	2.0	0.3
Naphthalene	38.1	42.8	20.3	23.3	67.8	47.8	46.6	20.4
2-MTHN[a]								
1-MTHN	0.8	0.3	0.4					
2-MN[b]	0.2				1.3	1.1	0.8	0.1
1-MN	2.5	2.6	1.0	1.6	5.3	3.7	3.4	1.1
BB[c]	4.0	3.6	1.6	1.8	7.6	6.7	5.5	1.5
Benzyl-naphthlene	0.3	0.1						0.2
4-MBB[d]	40.1	35.7	20.3	16.2	52.7	41.1	33.6	18.5
TH-NMBB[e]	14.4	0.8	1.4					0.3

[a]Methyltetrahydronaphthalene; [b]methylnaphthalene; [c]bibenzyl; [d]methylbibenzyl; [e]tetrahydro-NMBB.

Surprisingly, $Cp_4Fe_4S_4$ exhibited the lowest activity, although it has the S-to-Fe ratio closest to pyrrhotite ($Fe_{1-x}S$, where X= 0 to 0.12) which is thought to be the active phase. The nano-scale SFIO particles performed at an activity level similar to that of $Fe_2(CO)_9$ in the absence of

sulfur, but afforded the highest NMBB conversion when S was added. Ferrocene is more effective in hydrocracking reactions of NMBB than the inorganic iron complex $FeSO_4 \cdot 7H_2O$ (Table 3). Sulfur added to iron sulfate had the expected beneficial effect on NMBB conversion. But sulfur added to ferrocene decreased the activity of resulting catalyst. The other iron containing organometallic complex that showed a similar trend in conversion after sulfur addition was $Cp_2Fe_2(CO)_4$. Both complexes have cyclopentadienyl ligands as common features. Another precursor with Cp-functionalities and sulfur in the precursor molecule ($Cp_4Fe_4S_4$) showed very low activity too. There is apparently a negative correlation between the conversion of iron containing complexes and the presence of cyclopentadienyl/sulfur units.

Table 3. Effect of Fe precursors with different ligands on NMBB hydrocracking at 400 °C.

Catalyst Precursors	Non-catalytic	Superfine Fe_2O_3	Superfine Fe_2O_3 + S	$FeSO_4$ x 7 H_2O	$FeSO_4$ x 7 H_2O+ S	Cp_2Fe	Cp_2Fe +S	$Cp_4Fe_4S_4$
Conv, wt %	**3.9**	**27.1**	**78.2**	**3.7**	**23.9**	**15.8**	**9.6**	**11.7**
Prod, mol %								
Benzene	0.6	0.2	0.5					2.5
Toluene	0.3	1.3	1.9		1.3	1.6	1.1	
p-Xylene		0.3	0.7					
Tetralin	0.2	3.0	4.0		0.6	0.4	0.3	
Naphthalene	0.6	16.4	64.1	4.5	24.0	13.8	10.3	10.9
2-MTHN[a]			0.2					
1-MTHN		0.5	0.4					
2-MN[b]			1.4					
1-MN			5.8		1.5	5.6	0.5	0.1
BB[c]		1.0	8.9	0.6	2.5	2.6	0.6	0.4
Benzylnaphthlene	0.9							
4-MBB[d]	1.3	17.4	59.6	2.6	19.1	9.4	7.4	10.8
TH-NMBB[e]		7.3	5.5					

[a]Methyltetrahydronaphthalene; [b]methylnaphthalene; [c]bibenzyl; [d]methylbibenzyl; [e]tetrahydro-NMBB.

To better understand the relationship between catalyst composition and catalytic activity, surface area and XRD measurements were carried out. The surface area of freshly generated catalyst particles was measured and the phase identified through X-ray diffraction.

Table 4. BET Surface area and phase of activated catalysts.

Precursor Molecule	**BET Surface area m^2/g**	**Meso Pore Surface Area m^2/g**	**Phase Pattern from XRD**
$Fe(CO)_5$	3.22	3.22	Fe_3O_4
$Fe_2(CO)_9$	7.73	7.73	Fe_3O_4
$Fe_3(CO)_{12}$	17.6	17.6	Fe_3O_4
$Fe(CO)_5$ + S	1.56	1.54	FeS
$Fe_2(CO)_9$ + S	3.58	3.45	FeS
$Fe_3(CO)_{12}$ + S	2.93	2.93	FeS
Ferrocene + S	21.7	20.5	FeS
$Cp_4Fe_4S_4$	11.39	9.33	FeS
Fe_2O_3	228	228	---

Our investigation of in situ generated iron catalyst from organometallic precursor revealed

higher surface areas for pyrrohtite than magnetite particles. From XRD-measurement, it was found that iron carbonyl was transformed at 400 °C into magnetite Fe_3O_4. Sulfur added to $Fe(CO)_5$ yields pyrrohtite as black material. Generally iron sulfides have higher surface areas than magnetite. The effect of sulfur addition to iron carbonyls on the surface area is illustrated in Table 4.

Surprisingly, higher surface areas can be generated from higher iron carbonyl clusters. The BET surface area increases dramatically with increasing number of inter iron bonds. A similar trend can be observed when sulfur is added to the corresponding iron carbonyls. However, pyrrohtite coming from Fe carbonyls has a substantially lower surface area than the analogue generated from ferrocene and sulfur. Even the sparingly soluble $Cp_4Fe_4S_4$ yields after thermal activation higher surface area material than most iron carbonyls which are more soluble in hydrocarbons and are expected to lead to higher dispersion. The XRD-pattern reveals pyrrohtite as main product. This excludes iron carbide as the activity inhibiting material. However, the microstructure can be influenced by minute traces of impurities. Further elemental analysis will help clarify this issue.

Distribution of products from NMBB

Hydrocracking of NMBB yields three product categories that can be explained by the cleavage of the bonds between the aromatic moieties. Those coming from hydrocracking reactions form the major pool of reaction products, followed by hydrogenation and isomerization products. As can be seen from Tables 2 and 3, all iron containing catalyst precursors give a similar ratio of main products. It is apparent that ferrous catalysts cleave NMBB preferably in position α. Increasing conversion leads in most experiments to a proportional increase in the ratio of major products. The following compounds can be found as main products: naphthalene, 4-MBB, bibenzyl and tetralin.

Farcasiu et al. (12-14) suggested a reaction mechanism in which the first stage consists of the formation of a radical cation. The loss of electron density leads to a weakened α-bond which can then be broken relatively easily. This is in contrast to model studies in which phenyl-containing compounds undergo preferably β-cleavage (15).

In the work of Penn and Wang (15) radical cations were generated in the mass spectrometer under a variety of conditions which had little impact on the bond cleavage pathway. Preference for β-cleavage was explained by resonance stabilization of the intermediates. Both intermediates are resonance stabilized. Thermochemical calculations (16) show that reaction pathway β is 30 kcal/mol lower for both neutral and radical cationic species than pathway α. In contrast, neither of the intermediates resulting from bond α cleavage is stabilized. However, in the presence of a catalyst, the major reaction pathway mainly involves the cleavage of bond α.

Possible reaction mechanism

The structure of NMBB influences the cleavage pathway. Catalyst particles act as hydrogen transfer agents and stabilize the intermediate radical. They prevent undesirable recombination of the free radicals to polymeric material. Naphthalene and 4-methylbibenzyl are formed predominately in catalyzed reactions, indicating that bond α in NMBB is the most reactive unit in the Fe-catalyzed runs. However, different ligand environment and oxidation state of the precursor molecule can reverse the observed preference for bond α cleavage (e.g. $MoCl_3$). Related work (17) investigated the reaction mechanism of bond scission of naphthyl-derivatives and proposed the addition of a hydrogen radical to the ipso position of the naphthyl-unit to generate a relatively stable benzylic radical. Our data, as shown in Tables 1 and 2 support the hypothesis that all iron containing catalyst precursors induce preferably the scission of bond α in NMBB. It is believed (18) that strong hydrogenation catalysts show higher selectivity towards α cleavage than less active iron catalysts. High catalytic activity is accompanied by rich hydrogen supply adsorbed on the catalyst surface. Model compounds with aromatic ipso positions are prone to subsequent reactions with hydrogen radicals, leading to hydrogenation products. The less active iron catalysts are not capable of multiple hydrogen transfer during the short contact time between NMBB and model compound. Thus cleavage of NMBB occurs with higher

selectivity. The structure of the catalyst precursors and the sulfur addition affect the reactions on the surface of in situ generated catalysts.

II-4. CONCLUSIONS

Some iron containing catalysts have higher activity in the sulfur-free form, contrary to conventional wisdom. Adding sulfur to Fe precursors with Cp-ligands decreased the activity of the resulting catalyst. This is in distinct contrast to the cases with iron pentacarbonyl and superfine Fe_2O_3, where S addition increased their catalytic activity substantially. A positive correlation between sulfur addition and increased activity can be seen, but a reversed trend between Fe cluster size and hydrocracking conversion could be observed, for carbonyl-type Fe precursors. It is apparent that the activity and selectivity of Fe catalysts for NMBB conversion depends strongly on both the type of ligand environment, the oxidation state and the number of intermetal bonds in the molecular precursor.

ACKNOWLEDGEMENTS

This project is supported by the U.S. Department of Energy, Pittsburgh Energy Technology Center, in Advanced Coal Research Program. Dr. U. Rao is the DOE/PETC Project Manager. Dr. H.H. Schobert and Dr. C. Song are the Co-Principal Investigators at Penn State. The authors wish to express their appreciation to Dr. U. Rao of DOE/PETC for his support of this effort, and to Mach I Inc. for providing the SFIO sample. The authors would also like to thank Mr. R.M Copenhaver for the fabrication of tubing bomb reactors.

REFERENCES

1 F. Bergius and Billiviller, German Patent No. 301, Coal Liquefaction Process, (1919), 231.
2 P.A. Montano, A.S. Bommannavar and V. Shah, Fuel, Vol. 60, (1981), 703.
3 T. Suzuki, H. Yamada, P.L. Sears, and Y. Watanabe, Energy Fuels, Vol. 3, (1989), 707.
4 A.V. Cugini, D. Krastman, R.G. Lett and V. Balsone, Catalysis Today, Vol. 19, (1994), 395-408.
5 F. Derbyshire, Energy and Fuels, Vol. 3 (1989), 273-77.
6 a) E. Schmidt and C. Song, Prepr. Pap. - Am. Chem. Soc., Div. Fuel Chem., No. 35, (1990) 733-737.
b) C. Song, E. Schmidt and H.H. Schobert, DOE Coal Liquefaction and Gas Conversion, Contractors' Review Meeting in Pittsburgh, (September 7-8, 1994), 593-604.
7 O. Yamada, T. Suzuki, J. Then, T. Ando and Y. Watanabe, Fuel Process. Technol., Vol. 11, (1985), 297- 311.
8 T. Suzuki, T. Ando and Y. Watanabe, Energy and Fuels, Vol. 1, (1987), 299-300.
9 L. Artok, A. Davis, G.D. Mitchell and H.H. Schobert, Energy Fuels, Vol. 7, (1993), 67-77.
10 S. Weller, Energy Fuels, Vol. 8, (1994), 415-420.
11 D. Herrick, J. Tierny, I. Wender, G.P. Huffamn and F.E. Huggins, Energy and Fuels, Vol. 4, (1990), 231.
12 M. Farcasiu and C. Smith, Prepr. Pap. - Am. Chem. Soc., Div. Fuel Chem., No. 35, (1990) 404-13.
13 M. Farcasiu and C. Smith, Fuel Processing Technology, No. 29, (1991), 199-208.
14 M. Farcasiu and C. Smith and E.P. Ladner, Prepr. Pap. - Am. Chem. Soc., Div. Fuel Chem., No. 36, (1991), 1869-77.
15 J.H. Penn and J.H. Wang, Energy Fuels, Vol. 8, (1994), 421-425.
16 H.F. Ades, A.L. Companion, K.R. Subbaswamy, Prepr. Pap. - Am. Chem. Soc., Div. Fuel Chem., Vol. 36, (1991) 420-430.
17. J.A. Franz, D.M. Camaioni, M.S. Alnajjar, T. Autrey and J.C. Linehan, Prepr. Pap.-Am. Chem. Soc., Div. Fuel Chem., No. 40, (1995), 203-7.
18. M.T. Klein, C.F. Foley, D.T. Walter and S.M. Casey, Coal Liquefaction and Gas Conversion, Contractors' Review Meeting in Pittsburgh, (September 7-8, 1994), 565-78.

Future Plan

We intend to continue model compound studies on the activity, and selectivity of various bimetallic and monometallic dispersed catalysts under coal liquefaction conditions. The model reactions will cover hydrogenation, hydrocracking, hydrodeoxygenation, hydrodesulfurization, and hydrodenitrogenation.

Title: EVALUATION OF WEST VIRGINIA UNIVERSITY'S IRON CATALYST IMPREGNATED ON COAL

Authors: Frances V. Stohl, Kathleen V. Diegert, David C. Goodnow

Organization: Sandia National Laboratories, Albuquerque, NM 87185-0709

Contract No.: This work was supported by the U.S. Department of Energy at Sandia National Laboratories under contract DE-AC04-94-AL85000.

Period of Performance: January 1992 -

Objective: To evaluate and compare the activities/selectivities of fine-particle size catalysts being developed in the DOE/PETC Advanced Research (AR) Coal Liquefaction program by using standard coal liquefaction activity test procedures.

Accomplishments: Previously reported results have described the standard test procedure developed at Sandia to evaluate fine-particle size iron catalysts being developed in DOE/PETC's AR Coal Liquefaction Program and described the evaluation of several catalysts (commercially available pyrite, University of Pittsburgh's (U. of Pitt.) catalyst, Pacific Northwest Laboratories' (PNL) catalyst) using these procedures. The test uses DECS-17 Blind Canyon Coal, phenanthrene as the reaction solvent, and a factorial experimental design that enables evaluation of a catalyst over ranges of temperature (350 to 400°C), time (20 to 60 minutes), and catalyst loading (0 to 1 wt% on an as-received coal basis). Recent work has focused on the evaluation of West Virginia University's (WVU) iron catalyst that WVU impregnated on DECS-17 Blind Canyon coal. Results showed good activity for this catalyst including the highest amount of 9,10-dihydrophenanthrene (13.2%) observed in a reaction product and a small but significant catalytic effect for heptane conversion (0.5%). Additional experiments are being performed to enable comparison with previously tested catalysts. Tetrahydrofuran (THF) insolubles from selected reactions have been sent to the University of Kentucky for Mossbauer characterization of the iron phases present.

Plans: Ongoing work includes completion of the statistical analysis of WVU's impregnated catalyst and comparison of this catalyst's results with results from previously tested catalysts. Future work will include testing additional catalysts being developed in the AR Coal Liquefaction Program (including catalysts impregnated on Wyodak coal), developing procedures to characterize reaction products, and determining the kinetics of the reactions.

Sandia Project Team: Frances Stohl, Kathleen Diegert, David Goodnow

INTRODUCTION

There are several potential advantages of using cheap, unsupported, fine-particle size (less than or equal 40 nm) catalysts in direct coal liquefaction. These include improved coal/catalyst contact due to good dispersion[1] of the catalyst, and the potential for using low quantities of catalyst (less than or equal to 0.5% based on the weight of coal) because of their very high surface areas. These catalysts could be combined with the coal as either active catalysts or catalyst precursors that would be activated in situ. Research efforts that have been performed to develop fine-particle size, unsupported catalysts for direct coal liquefaction[2] indicate that the use of these catalysts could result in significant process improvements, such as enhanced yields of desired products, less usage of supported catalyst, and possibly lower reaction severities. These improvements would result in decreased costs for coal liquefaction products.

The Advanced Research (AR) Coal Liquefaction Program, which is managed by the United States Department of Energy's Pittsburgh Energy Technology Center (PETC), is funding numerous research efforts aimed at developing these types of catalysts for direct liquefaction. Although most catalyst developers have the capability of testing the performances of the catalysts they develop, it is difficult if not impossible to compare results among researchers because of the different testing procedures used. Therefore, to guide the research and development efforts for these fine-particle size, unsupported catalysts, it is necessary to evaluate each catalyst's performance under standard test conditions so that the effects of catalyst formulations from different laboratories can be compared.

Sandia has previously reported[3] a standard test procedure using a factorial experimental design for the evaluation of fine-particle catalysts. This test has been applied to evaluate several different catalysts including a commercially available pyrite[3], a sulfated iron oxide catalyst[4] from the University of Pittsburgh and several different formulations of a 6-line ferrihydrite[5,6] prepared at Pacific Northwest Laboratories (PNL). This paper will describe the recent results obtained from evaluating West Virginia University's (WVU) iron catalyst that was impregnated on DECS-17 Blind Canyon coal.

EXPERIMENTAL SECTION

Materials. The coal being used in this project is the DECS-17 Blind Canyon coal obtained from The Penn State Coal Sample Bank. It is a high volatile A bituminous coal with 0.36% iron, 0.02% pyritic sulfur, and 7.34% mineral matter (on a dry basis). The particle size is -60 mesh. Sandia sent four packets of this coal to WVU for impregnation with their catalyst. Phenanthrene is used as the reaction solvent.

Microautoclave Reactors. The testing is performed using batch microautoclaves made of type 316 stainless steel components. The total volume of a reactor is 43 cm^3 with a liquid capacity of 8 cm^3. The reactors are loaded with 1.67g coal and 3.34g reaction solvent. If the reaction is catalytic, the catalyst loading will be either 0.5 wt% or 1.0 wt% on an as-received coal basis. The reactors are charged to 800 psig H_2 (cold charge) and heated to reaction temperatures in fluidized-sand baths. Temperatures, pressures and times are recorded with a digital data acquisition system every 30 seconds during the course of the reactions. Following the heating period, the reactors are rapidly cooled to ambient temperature in a water bath and a gas sample is collected. The reaction data is analyzed to determine the actual reaction time and the averages and standard deviations for reaction temperature and pressure. Heat-up times and cooling times are also determined.

Product Workup Procedures. The reaction products are rinsed out of the reactors with tetrahydrofuran (THF). THF and heptane solvent solubilities are measured using a Millipore 142 mm diameter pressure filtration device with air pressurization and Duropore (0.45 micron) filter paper. The filter cakes are rinsed twice with THF or heptane as appropriate. After the filtrations are complete, the filter papers are dried under vacuum at 70°C, cooled to room temperature and weighed to determine the insoluble portions. The THF soluble material is quantitatively sampled for gas chromatographic (GC) analysis, which is used to determine the reaction solvent recovery and composition. The THF is removed from the solubles by rotary evaporation prior to determining the heptane conversion. The quantity of gases

(CO, CO_2, CH_4, C_2H_6) produced in a reaction is calculated using the postreaction vessel temperature and pressure with the ideal gas law and the mole percents in the gas sample as determined using a Carle GC and standard gas mixtures.

Factorial Experimental Design and Analysis. The factorial experimental design (Figure 1) evaluates the effects of three variables at two levels: temperature (350 and 400°C), time (20 and 60 minutes), and catalyst loading (0 and 1 wt% based on as-received coal). With this full factorial experimental design, the experimental results are evaluated for all combinations of levels of the three variables so that 2^3 evaluations are required. Additional reactions are also performed at the center point of this cubic design. An Analysis of Variance (ANOVA) is performed to estimate the effects of the experimental variables and to statistically test their significance. Replication of the experiments is used to estimate measurement error and to reduce its effect on the estimated effects of the variables. Models are constructed using the estimates of the effects of the variables to calculate the expected experimental results for specified sets of reaction conditions[7]. The controlled factors used in the ANOVA are the measured average reaction temperature, measured reaction time, and the actual weight of catalyst used.

Figure 1. Factorial experimental design (temperature = °C, time = minutes, catalyst loading = wt% of as-received coal).

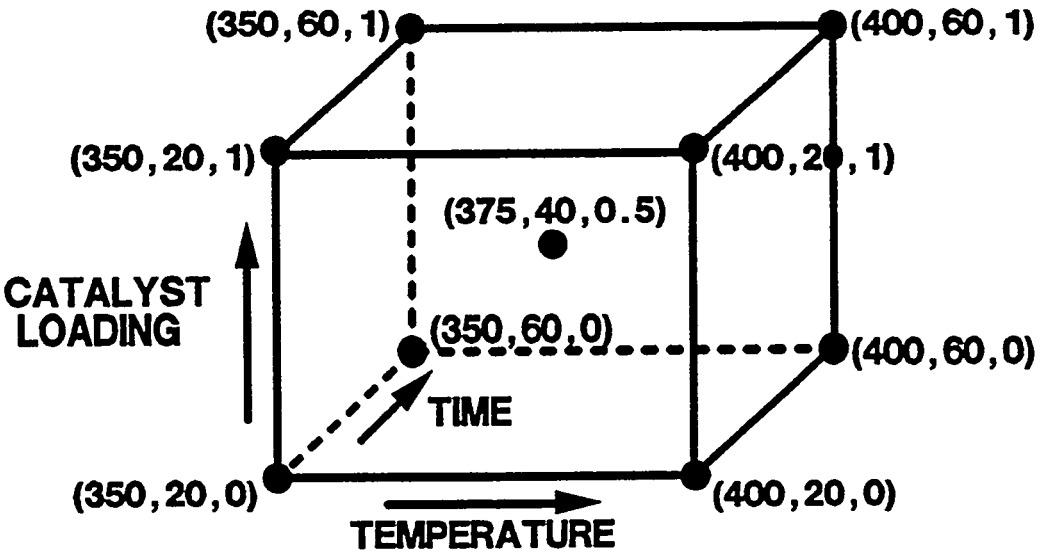

Catalyst. Sandia sent DECS-17 coal samples to D. Dadyburjor for impregnation with an iron catalyst. Calculations were performed by both Sandia and WVU to ensure that the correct amounts of catalyst were impregnated on the coal so that comparisons with other catalysts could be done. Dadyburjor (WVU) supplied Sandia with impregnated coals that had both 1 wt% and 0.5 wt% catalyst loadings on an as-received coal basis. No pretreatment, additives or special handling were required during testing. Impregnated coals were stored under argon to minimize changes with time.

RESULTS and DISCUSSION

Experimental Results of Testing WVU's Impregnated Catalyst. The measured results of testing WVU's impregnated catalyst are shown in Table 1 along with the average reaction temperature, and the actual reaction time. The standard deviation of the reaction temperature is almost always less than or equal to 1°C. Heat-up times are less than or equal to 3 minutes. Table 2 shows the averages and standard deviations for the data in Table 1. Negative values for heptane conversion occur because the values are very close to zero, and the variability is high.

Modeling of Experimental Results. Results of a preliminary statistical analysis of the data with an asterisk in Table 1 are given in Tables 3 and 4. These tables show calculated estimates of the effects of the variables and the interactions among variables over the region bounded by the cubic design, calculated estimates of the mean values of the reaction results at the nine sets of reaction conditions, standard errors of the estimates, the means of the measured values used in this statistical analysis, and R^2 values for the fit of the model to the data. The constant represents the estimate of the reaction results when all variables are at their low levels: temperature = 350°C, time = 20 minutes, and catalyst loading = 0%. The variables with statistically significant effects are listed under the constant; the larger the estimated value, the greater the effect. The estimate of experimental error, which is presented as a standard deviation, accounts for all variability in the data not accounted for by the fixed and random effects of the model. Included in this estimate are variabilities due to measurement, process and material inconsistencies, and modeling inadequacies. The estimates of reaction results at the nine sets of reaction conditions are calculated from the model and can be compared to the means of the measured values. The standard errors of the estimated results are derived from the experimental error, which pertains to a single measurement.

Procedure for Estimating Experimental Results from the Linear Model. To use one of the linear models in Tables 3 or 4 to estimate an experimental result within the cube, first calculate proportional levels for each variable that has a significant effect. For example, to calculate THF conversion for the reaction at 375°C for 40 minutes with 0.5 wt% catalyst:

p_{TIME} = (40 min-20 min)/(60 min-20 min) = 0.5
p_{TEMP} = (375°C-350°C)/(400°C-350°C) = 0.5
p_{CAT} = (0.5 wt%-0 wt%)/(1.0 wt%-0 wt%) = 0.5

These calculated p's are used in the following equation (see Table 3):

$$K + p_{TIME} \cdot a + p_{TEMP} \cdot b + p_{CAT} \cdot c + p_{TIME} \cdot p_{CAT} \cdot d + p_{TEMP} \cdot p_{CAT} \cdot e$$

where K is the estimated constant (24.9%), a is the estimated time effect (5.7%), b is the estimated temperature effect (21.1%), c is the estimated catalytic effect (9.5%), d is the estimated time-catalyst interaction (11.1%), and e is the estimated temperature-catalyst interaction (20.7%). The calculated THF conversion is 51.0% as shown in Table 3. For calculating a result for any point within the region bounded by the cube, the p values will range from 0 to 1. Extrapolation beyond the limits of the cube is usually not recommended.

Results of the modeling (Table 3 and 4) show that temperature has the largest effect on THF conversion (21.1%), followed by the temperature-catalyst interaction (20.7%), the time-catalyst interaction (11.1%), the catalyst effect (9.5%), and the time effect (5.7%). Calculated estimates of the THF conversions for the nine experimental sets of conditions can be compared with the average measured data shown in Table 3. Results show that the largest difference is for the center point of the cube (51.0% versus 63.3%). Modeling the measured heptane conversions shows that temperature (12.1%), the time-temperature interaction (9.6%), time (2.4%) and the catalyst (0.5%) have a statistically significant effect on heptane conversion. This is the first time a catalytic effect was observed for heptane conversion. There is good agreement between the measured and calculated heptane conversions in Table 3. The significant effects for gas yield are temperature (0.73%), the time-temperature interaction (0.42%), and time (0.23%). The 9,10-dihydrophenanthrene (DHP) formed by hydrogenation of phenanthrene during the reaction has the most complicated model with six parameters having significant effects: temperature-catalyst interaction (6.06%), time-catalyst interaction (4.24%), catalyst (1.01%), time-temperature interaction (0.96%), temperature (0.12%), and time (-0.07%). The amount of DHP obtained at 400°C for 60 minutes (13.04%) was the highest amount observed for any catalyst tested so far. The R^2 values for the fits of these models ranged from 0.91 for heptane conversion to 0.98 for the gas yield.

Comparison of Catalysts. A preliminary comparison of results (Table 5) from WVU's impregnated catalyst with results from PNL's catalyst, the U. of Pitt.'s catalyst and pyrite at the highest severity conditions (400°C, 60 minutes) indicates that WVU's catalyst has performed very well. The calculated THF conversion is at least as good as that obtained with PNL's catalyst if not better. WVU's catalyst has also yielded the highest amount of DHP at the highest severity condition; it's about 50% higher than obtained with PNL's catalyst. WVU's catalyst has shown a small but significant catalytic effect (0.5%) on heptane conversion, which has not been seen previously with other catalysts that have been evaluated. These results of the statistical analysis for WVU's catalyst are based on the data in Table 1 that has an asterisk. Since this statistical analysis was performed, some additional reactions have been performed. Therefore, a new statistical analysis of WVU's catalyst will be performed using all the data in Table 1.

Two catalysts in Table 5 (PNL's catalyst and the U. of Pitt.'s catalyst) were analyzed using a baseline with sulfur addition (either 1% or 2% based on as-received coal). For WVU's impregnated catalyst and pyrite, Sandia did not add sulfur to the reactions so the baseline was a thermal reaction. To get a good comparison, among these four catalysts, it is necessary to perform comparisons with the same baseline, i.e. the thermal baseline. This will be done when the statistical analysis of WVU's complete data set in Table 1 is done.

CONCLUSIONS

Results of the evaluation of WVU's iron catalyst that was impregnated on the DECS-17 Blind Canyon coal showed that it is a very good catalyst. At 400°C for 60 minutes, it yielded 93.0% THF conversion, which is as good or better than PNL's catalyst, and it yielded the highest amount of DHP (13.04%) observed in the reaction product indicating significantly better hydrogenation activity than the other catalysts tested. WVU's catalyst also showed a small (0.5%) catalytic effect for heptane conversion, whereas other catalysts tested to date have not shown any catalytic effect for heptane conversion. At 400°C for 60 minutes, THF conversion obtained with PNL's catalyst was 89.4% versus 82.3% with the U. of Pitt.'s catalyst, and 73.4% with pyrite. Analyses of DHP in the reaction products showed that PNL's catalyst gave 8.41% DHP, versus 5.35% for the U. of Pitt.'s catalyst, and 3.88% for pyrite. No catalytic effects have been detected for gas yield. Future work will include completing a statistical analysis of the complete data set in Table 1, comparing all catalysts tested to date using a thermal baseline, testing additional catalysts being developed in DOE/PETC's program, and continuing to evaluate better analytical methods for determining product quality.

REFERENCES

1. Huffman, G. P.; Ganguly, B.; Zhao, J.; Rao, K. R. P. M.; Shah, N.; Feng, Z.; Huggins, F. E.; Taghiei, M. M.; Lu, F.; Wender, I.; Pradhan, V. R.; Tierney, J. W.; Seehra, M. S.; Ibrahim, M. M.; Shabtai, J.; Eyring, E. M.; Energy Fuels 1993, 7, 285-296.
2. Pradhan, V. R.; Tierney, J. W.; Wender, I.; Energy & Fuels 1991, 5, 497-507.
3. Stohl, F. V.; Diegert, K. V.; Energy & Fuels 1994, 8, 117-123.
4. Stohl, F. V.; Diegert, K. V.; Gugliotta, T. P.; Proc. Coal Liquefaction and Gas Conversion Contractors' Review Conf., September 27-29, 1993, Pittsburgh, PA. p. 123-135.
5. Stohl, F. V., Diegert, K. V., Goodnow, D. C., Rao, K. R. P. M., Huggins, F., Huffman, G. P.; Proc. Coal Liquefaction and Gas Conversion Contractors' Review Conf., September 7-8, 1994, Pittsburgh, PA. p. 605-617.
6. Stohl, F. V., Diegert, K. V., Goodnow, D. C.; American Chemical Society Division of Fuel Chemistry Preprints 40 (2), 1995, 335-340.
7. John, P. W. M.; Statistical Design and Analyses of Experiments; MacMillan Co., New York, 1971.

Table 1. Measured experimental results.

	TEMP (°C)	TIME (min)	CAT.	THF CONV. (%)	HEPTANE CONV. (%)	GAS (%dmmf)	DHP(%)
*	350.4	20.5	NO	24.13	2.64	0.29	0.25
*	350.3	20.5	NO	25.01	2.46	0.27	0.23
*	350.3	20.5	NO	27.91	4.85	0.28	0.25
	350.0	20.5	NO	19.93	1.69	0.41	NA
	350.1	20.5	NO	21.92	2.43	0.41	0.18
	350.3	20.5	NO	20.67	NA	0.65	NA
*	350.0	20.5	YES	32.29	-0.80	0.28	1.69
*	350.1	20.5	YES	28.97	-2.56	0.30	1.45
*	349.9	20.5	YES	34.68	-1.46	0.32	1.60
	350.2	20.5	YES	26.97	NA	0.48	1.22
*	350.2	60.8	NO	23.74	0.67	0.59	NA
*	350.2	60.5	NO	24.86	1.08	0.57	0.45
*	350.1	60.5	NO	28.85	5.03	0.49	0.43
*	350.2	60.5	NO	27.54	4.63	0.48	0.47
	350.4	60.5	NO	27.75	6.28	0.67	0.38
	350.6	60.5	NO	26.90	5.09	0.67	0.43
*	350.2	60.5	YES	NA	NA	0.42	5.95
*	350.3	60.5	YES	51.91	3.43	0.50	5.69
*	349.8	60.5	YES	49.09	3.47	0.53	5.27
*	350.4	60.5	YES	52.57	1.79	0.53	5.59
*	375.0	40.5	YES	66.02	8.73	0.73	7.29
*	374.8	40.0	YES	63.09	7.17	0.79	6.38
*	375.1	40.5	YES	60.73	10.47	0.81	6.67
*	400.4	20.5	NO	39.65	10.17	0.84	0.65
*	399.8	20.5	NO	46.61	17.72	1.04	0.68
*	400.1	20.5	NO	41.09	13.09	1.13	0.61
	400.2	20.0	NO	38.74	13.69	1.22	0.63
	400.3	20.5	NO	38.37	12.68	1.13	0.60
*	399.6	20.5	YES	76.98	12.99	0.98	8.10
*	400.0	20.5	YES	77.16	10.51	0.99	8.10
*	400.1	20.5	YES	74.63	12.93	1.20	6.84
*	400.0	20.5	YES	75.35	14.12	0.97	7.43
*	399.5	60.5	NO	54.00	23.83	1.63	1.20
*	400.9	60.8	NO	52.63	19.01	1.68	1.52
*	400.0	60.5	NO	50.69	19.61	1.69	1.11
	399.9	60.5	NO	48.93	20.98	1.87	1.21
	399.7	60.5	NO	46.83	20.95	1.83	1.19
	400.3	60.5	NO	49.52	NA	1.95	1.47
*	400.2	60.5	YES	92.17	30.69	1.63	13.09
*	400.5	60.5	YES	91.68	28.79	1.72	13.37
*	399.9	60.5	YES	91.02	24.75	1.74	13.10
*	399.9	60.5	YES	90.65	29.02	1.57	12.36
	400.3	60.5	YES	91.51	NA	2.02	12.22

* Reactions used in preliminary statistical analysis (see Tables 3 and 4). ** = Not Available.

Table 2. Averages and standard deviations for all reaction conditions and all results in Table 1.

	TEMP (°C)	TIME (min)	CAT.	THF CONV. (%)	HEPTANE CONV. (%)	GAS (%dmmf)	DHP (%)
AVER =	350.2	20.5	NO	23.3	2.8	0.4	0.23
Std Dev =	0.2	0.0		3.0	1.2	0.1	0.001
AVER =	350.1	20.5	YES	30.7	-1.61	0.3	1.5
Std Dev =	0.1	0.0		3.4	0.89	0.1	0.2
AVER =	350.3	60.6	NO	26.6	3.8	0.6	0.4
Std Dev =	0.2	0.1		1.9	2.3	0.1	0.2
AVER =	350.2	60.5	YES	51.2	2.9	0.5	5.6
Std Dev =	0.3	0.0		1.8	1.0	0.0	0.3
AVER =	375.0	40.3	YES	63.3	8.8	0.8	6.8
Std Dev =	0.2	0.3		2.6	1.7	0.0	0.5
AVER =	400.2	20.4	NO	40.9	13.5	1.1	0.6
Std Dev =	0.2	0.2		3.4	2.7	0.1	0.0
AVER =	399.9	20.5	YES	76.0	12.6	1.0	7.6
Std Dev =	0.2	0.0		1.2	1.5	0.1	0.6
AVER =	400.1	60.6	NO	50.4	17.4	1.8	1.3
Std Dev =	0.5	0.1		2.6	8.7	0.1	0.2
AVER =	400.2	60.5	YES	91.4	22.7	1.7	12.8
Std Dev =	0.3	0.0		0.6	12.8	0.2	0.5

Table 3. Results of preliminary statistical analyses for THF and heptane conversion data shown with an asterisk in Table 1.

	THF Conversion (%)			HEPTANE Conversion (%)		
Parameter	Model Estimate	Meas'd Average	Std. Error	Model Estimate	Meas'd Average	Std. Error
Constant*	24.9		2.7	0.3		1.4
Time	5.7		3.1	2.4		1.8
Temperature	21.1		3.1	12.1		1.8
Catalyst	9.5		3.8	0.5		1.2
Time-Temp. Int.				9.6		2.5
Time-Cat. Int.	11.1		4.2			
Temp.-Cat. Int.	20.7		4.2			
Experimental Error	5.4			3.1		
350°C, 20min, 0%	24.9	25.7	2.0	0.3	3.3	1.3
350°C, 60min, 0%	30.6	27.1	2.0	2.7	3.6	2.2
400°C, 20min, 0%	46.0	42.4	3.7	12.5	13.7	3.8
400°C, 60min, 0%	51.7	52.4	1.7	24.4	20.8	2.6
375°C, 40min, 0.5%	51.0	63.3	2.7	10.2	8.8	1.6
350°C, 20min, 1%	34.4	32.0	2.9	0.8	-1.6	0.9
350°C, 60min, 1%	51.2	51.2	1.8	3.2	2.9	1.0
400°C, 20min, 1%	76.2	76.0	1.2	13.0	12.6	1.5
400°C, 60min, 1%	93.0	91.4	0.7	24.9	28.3	2.5
R^2	0.95			0.91		

* Value calculated for a thermal reaction at 350°C for 20.

Table 4. Results of preliminary statistical analyses for gas yields and amounts of DHP in reaction product (based on data with an asterisk in Table 1).

	GAS YIELD (%dmmf coal)			DHP (%)		
Parameter	Model Estimate	Meas'd Average	Std. Error	Model Estimate	Meas'd Average	Std. Error
Constant*	0.27		0.03	0.72		0.60
Time	0.23		0.04	-0.07		0.78
Temperature	0.73		0.04	0.12		0.78
Catalyst				1.01		0.78
Time-Temp. Int.	0.42		0.06	0.96		0.87
Time-Cat. Int.				4.24		0.87
Temp.-Cat. Int.				6.06		0.88
Experimental Error	0.12			1.1		
350°C, 20min, 0%	0.27	0.28	0.01	0.72	0.24	0.01
350°C, 60min, 0%	0.50	0.51	0.05	0.65	0.45	0.02
400°C, 20min, 0%	1.00	1.00	0.15	0.84	0.65	0.04
400°C, 60min, 0%	1.65	1.67	0.03	1.73	1.28	0.22
375°C, 40min, 0.5%	0.86	0.78	0.04	4.07	6.78	0.46
350°C, 20min, 1%	0.27	0.30	0.02	1.74	1.58	0.12
350°C, 60min, 1%	0.50	0.52	0.02	5.90	5.52	0.22
400°C, 20min, 1%	1.00	1.03	0.11	7.92	7.62	0.61
400°C, 60min, 1%	1.65	1.67	0.08	13.04	12.98	0.43
R^2	0.98			0.95		

* Value calculated for a thermal reaction at 350°C for 20 minutes.

Table 5. Calculated results (400°C, 60 minutes).

	THF Conv. (%)	DHP (%)*
1wt%** WVU Impregnated Catalyst***	93.0	13.4
Thermal	51.7	1.73
1wt% PNL Cat. Precursor + 1wt% Sulfur	89.4	8.41
Thermal + 1wt% Sulfur	63.6	2.35
1wt% U. of Pitt. Cat. Precursor + 2wt% Sulfur	82.3	5.35
Thermal + 2wt% Sulfur	63.0	2.43
1wt% Pyrite	73.4	3.88
Thermal	54.9	1.08

* Percent of recovered reaction solvent.
** Weight percent based on as-received coal.
*** Based on preliminary statistical analysis (results with asterisk in Table 1).

EFFECT OF PRETREATING OF HOST OIL ON COPROCESSING

Paul E. Hajdu, John W. Tierney and Irving Wender

Department of Chemical & Petroleum Engineering

University of Pittsburgh

Pittsburgh, PA 15261

Contract Number: DE-AC22-91P91054

Period of Performance: April 1, 1992 through June 31, 1995

OBJECTIVES

The principal objective of this research was to determine if coprocessing performance (i.e., coal conversion and oil yield) could be significantly improved by pretreating the heavy resid prior to reacting it with coal. For this purpose, two petroleum vacuum resids (1000°F+), one from the Amoco Co. and another from the Citgo Co., were used as such and after they had been pretreated by catalytic hydrogenation and hydrocracking reactions. The pretreatments were aimed at improving the host oil by; (1) converting any aromatic structures in the petroleum to hydroaromatic compounds capable of donating hydrogen, (2) cracking the heavy oil to lower molecular weight material that might serve as a better solvent, (3) reducing the coking propensity of the heavy oil through the hydrogenation of polynuclear aromatic compounds, and (4) removing metals and heteroatoms that might poison a coprocessing catalyst. Highly dispersed catalysts, including fine particle Fe- and Mo-based, and dicobalt octacarbonyl, $Co_2(CO)_8$, were used in this study. The untreated and pretreated resids were extensively characterized in order to determine chemical changes brought about by the pretreatments. The modified heavy oils were then coprocessed with an Illinois No.6 coal as well as with a Wyodak coal, and compared to coprocessing with untreated resids under the same hydroliquefaction conditions. The amount of oil derived from coal was estimated by measuring the level of phenolic oxygen (derived mainly from coal) present in the oil products.

INTRODUCTION

The world's supply of petroleum crude is becoming heavier so that the amount of vacuum tower bottoms (resid) has been steadily increasing. Coprocessing of coal with petroleum resid (1000°F+) may be an attractive way of obtaining valuable distillates from these readily available and relatively inexpensive hydrocarbon sources.[1,2,3,4]

In general, petroleum is a poor coal liquefaction solvent and coal conversion in heavy oil in the absence of a liquefaction catalyst is usually less than that achieved in the coal-derived recycle solvent used in conventional liquefaction processes.[5,6] This is mainly because petroleum contains fewer aromatic and hydroaromatic compounds. Some hydroaromatic compounds are known to donate hydrogen and certain polynuclear aromatic compounds shuttle hydrogen atoms during coal liquefaction. Both of these steps are important for bringing about high levels of coal dissolution.

One approach for improving coprocessing coal conversion involves modifying the heavy

oil prior to reacting it with coal. Takeshita and Mochida[7] obtained a coal conversion of 88% with a petroleum pitch that had first been hydrotreated at high pressure over a $Ni/Mo/Al_2O_3$ catalyst. A similar approach was taken by Sato and coworkers[8] who obtained high conversions and high distillable oil yields from a Japanese subbituminous Taiheiyo coal in a tar sand bitumen that was prehydrotreated with a Ni-Mo catalyst. Curtis and coworkers[9,10,11] showed that high levels of coal conversion can be obtained in a host that contained a mixture of both heavy oil and hydrogen donor compounds.

EXPERIMENTAL

Material

This project used two different petroleum vacuum tower resids (1000°F+); one from the Amoco Oil Company the other from the Citgo Oil Company. Properties of the resids are given in Table 1. Experiments were first conducted with the Amoco resid in order to explore reaction conditions required to hydrogenate and hydrocrack a resid, and to evaluate the sensitivity of reaction parameters such as time, temperature and pressure on product yields. The Citgo resid, however, was chosen as the primary heavy oil to test because it came from an identifiable crude oil source, Venezuela. The Amoco resid, on the other hand, was derived from a wide mixture of crude oils from around the world.

Two different coal samples were used; an Illinois No 6 bituminous coal and a Wyodak subbituminous coal. Most of the work was done with the Illinois No 6 coal. Both coals are Argonne premium samples that had been ground to -100 mesh and stored in sealed glass vials. Properties of the coals are listed in Table 2.

Several different finely dispersed catalyst systems were used; Fe_2O_3/SO_4, $Mo/Fe_2O_3/SO_4$, $Mo(CO)_6+Fe(CO)_5$ and Mo naphthenate. The sulfated iron oxides, synthesized in our laboratory, have been previously described and successfully tested in coal liquefaction and coprocessing reactions.[12,13,14] Iron and Mo carbonyls were obtained from Aldrich Chemical Co. and Mo naphthenate, which contained 6% Mo by weight, was obtained from ICN Biomedical Inc. It is known that the iron compounds used in this study are transformed to pyrrhotites ($Fe_{1-x}S$) at reaction conditions in the presence of sulfur, which was supplied in our experiments by adding either H_2S gas or elemental sulfur in excess to the reactants. It is generally accepted that pyrrhotites, along with H_2S gas, function as hydrogenation catalysts. Under similar conditions, the Mo compounds used in this study are transformed to MoS_2, which acts as a catalyst.

A homogeneous catalyst, dicobalt octacarbonyl, $Co_2(CO)_8$, and a 1:1 synthesis gas system was used based on findings that cobalt carbonyl, $Co_2(CO)_8$, can partially hydrogenate polynuclear aromatic compounds at relatively low temperatures, below 250 °C, in the presence of CO and H_2.[15,16]. Project SEACOKE[17], carried out by ARCO, also demonstrated the action of transition metal carbonyls using coal model compounds as well as coal derived liquids.

Petroleum Resid Pretreatment Reactions and Product Workup

The petroleum vacuum resids were pretreated in a well-stirred stainless-steel 300 ml autoclave batch reactor. At the end of the reaction, the reactor was cooled to room temperature and gases were vented and collected for analysis. The reactor was then opened and products were removed by washing with tetrahydrofuran (THF). The THF-washed material was sonicated for 30 minutes and separated into two fractions according to their solubility in THF. The THF-soluble liquid, which contained oil and asphaltenes, was used as the host oil in coprocessing

runs. Asphaltenes are soluble in THF but insoluble in pentane, and oil is soluble in both THF and pentane.

The product workup procedure was later improved by adding an atmospheric distillation step to remove any light (bp<380°F) products directly from the reactor prior to washing with THF. The light oil fraction was recombined with the heaver fraction before being used as a coprocessing host oil.

Products containing $Co_2(CO)_8$ were refluxed for three hours to destroy the carbonyl. To further facilitate removal of cobalt, silica-alumina powder was added to the product mixture prior to filtering.

Coal- Heavy Oil Coprocessing Reaction and Product Workup

Coprocessing experiments were performed in a horizontal, stainless-steel microreactor. The microreactor system has been previously described[12]. At the end of the reaction, the reactor was removed from the sand bath and cooled to room temperature. Gases were vented and collected for analysis; gas production was determined by weight loss. Oil products were recovered by washing the reactor with pentane. Asphaltenes were recovered by washing with THF. The material that was insoluble in both pentane and THF consisted of coke and coal-derived mineral matter. Pentane was removed from the filtered oil by a rotovapor under atmospheric pressure instead of vacuum pressure. This was done to minimize losses of light compounds during this product recovery step. However, under the mild separation condition, a small amount of pentane remained dissolved in the oil. This amount was latter measured by simulated distillation.

Reactant and Product Characterization Techniques

Product gases were analyzed for composition (H_2, H_2S and C1-C5) using an HP 5880A GC. Light pentane-soluble oils (free of ash and asphaltenes) were analyzed for composition with an HP 5890 series II GC/HP 5970 mass selective detector. A boiling curve for pentane-soluble oil samples was estimated using simulated distillation techniques[18] with an HP 5890 series II GC. Product oil and asphaltene samples were analyzed for their hydrogen type and aromatic content by ^1H NMR using a Bruker 3000 MSL spectrometer; samples were prepared in deuterated chloroform with tetramethylsilane for internal reference. Catalytic dehydrogenation[19] was used to measure the "available" hydrogen of untreated resids and pretreated host oils. Available hydrogen was defined as the amount of hydrogen gas evolved when an oil sample was catalytically dehydrogenated at atmospheric pressure in boiling phenanthridine (bp=350°C) for 285 min over a reduced $Pd/CaCO_3$ catalyst. Metal contents (V and Ni) of selected samples were measured by The Pittsburgh Applied Research Corp. using the ICP technique. The elemental composition (C, H, S and N) of selected samples was measured by Galbraith Laboratories Inc. and CONSOL Inc. The phenolic oxygen concentration of pentane-soluble oil samples was measured by CONSOL Inc. using an FTIR method.[20]

RESULTS AND DISCUSSION

Resid Pretreatment Experiments

A critical property of a liquefaction solvent is its ability to supply hydrogen to coal during coprocessing. From pretreatments with the Amoco oil, we found that the available hydrogen content of the pretreated resids was sensitive to pretreatment temperature.

Pretreatment of the Amoco resid at a reaction temperature of 440°C, using Mo naphthenate resulted in a decrease in available hydrogen content. When the same resid was pretreated at a lower temperature of 400°C, using either $Mo/Fe_2O_3/SO_4$ or Mo naphthenate, the available hydrogen content of the starting resid almost doubled.

Four different pretreatments of the Citgo resid were performed around 400°C; one above it and three below it. Conditions for these runs are summarized in Table 3. The first pretreatment, referred to as A, involved cracking the resid at 440°C for two hr with the main objective of reducing molecular weight and removing sulfur and metals. The other three pretreatments, referred to as B through D, involved hydrogenating the resid at temperatures below 400°C where cracking is suppressed. The objective of these runs was to increase available hydrogen.

Properties of the untreated Citgo resid and the four pretreated Citgo host oils are listed in Table 4. The A host oil was lighter, based on wt% of distillate (bp<565°C), than the untreated Citgo resid as well as the other pretreated oils. This was expected due to the higher pretreatment temperature used. The atomic H/C ratio of this host oil was slightly higher than that of the untreated resid and its C/S ratio was higher, indicating that sulfur atoms had been removed. The atomic C/N ratio of A was slightly lower than that of the starting resid, suggesting that nitrogen atoms were not removed. The available hydrogen content of A was slightly higher than that of the untreated resid. The available hydrogen content of the host oils from the mild temperature pretreatments (B, C and D) was much higher than that of the untreated resid and A. The increase in available hydrogen content for the host oil from pretreatments B, C and D was slightly below the amount of hydrogen gas consumed during these runs, indicating significant hydrogen utilization. The atomic H/C, C/S and C/N ratios of the host oils exposed to mild temperature pretreatments were essentially unchanged.

Effect of Host Oil Type and Coal Feed Concentration on Coal Conversion

Coprocessing experiments were conducted in order to evaluate the four pretreated host oils (A, B, C, and D) under thermal (no added catalyst) as well as catalytic conditions. Results of these experiments were compared to base-line runs made with the untreated Amoco and Citgo resids. The bulk of the work was done with Illinois No. 6 coal at the following thermal coprocessing conditions; 425°C, 1000 psig (cold) H_2 and 30 min reaction time. In these runs, the coal-feed concentration was varied from 10 to 50 wt%.

Table 5 lists reaction conditions and results (coal conversion and product yields) for coprocessing experiments made with the Illinois No.6 coal. The data are grouped by host oil type. At baseline reaction conditions (30 min reaction time, 425°C, 1000 psig H_2, host oil:coal feed ratio of 2:1), the Illinois No.6 coal reacted with the untreated Citgo resid, resulting in 74 wt% (maf) of coal converted to THF-soluble products and gases. When the Illinois coal was coprocessed with untreated Amoco resid under the same reaction conditions, 56 wt% of coal (maf) was converted. The fraction of coal converted to gases and soluble products was not measured directly, but was determined by the amount of unconverted THF-insolubles. The following equation was used to calculate coal conversion.

$$Y_T = 100 * [1.0 - \frac{W_i - W_{ash} - W_{cat} - W_{pc}}{W_{maf}}]$$

where,

Y_T = coal conversion, %

W_{ash}, W_{cat}, W_i, W_{maf}, W_{pc} = mass of ash, catalyst, THF insolubles, maf coal, and petroleum coke, g

The low coal conversions obtained with the two untreated petroleum resids illustrate that petroleum is a poor liquefaction solvent, due mainly to its low supply of donatable hydrogen. Increasing the supply of active hydrogen by addition of 2000 ppm of Mo to the Citgo resid, with other reaction parameters held constant, resulted in an increase in Illinois coal conversion, from 74 wt% to 88 wt%. However, the aim of this study was to increase coal conversion by improving the properties of the host-solvent through pretreatment.

Figure 1 shows that the conversions of Illinois No. 6 coal in the host oils that were pretreated at mild reaction temperatures (B, C and D) were higher than levels achieved with the untreated Citgo resid or the host oil from the high temperature pretreatment, A. Coal conversions in the Citgo resid and in A decreased as the concentration of coal in the feed was increased. This trend demonstrates the limited ability of these host oils to bring about coal conversion. On the other hand, coal conversions in B, C and D remained high at all coal loadings tested. Coal conversions in B, C and D were slightly higher than conversions obtained when the coal was catalytically coprocessed in the Citgo resid using either Mo naphthenate (2000 ppm Mo) or $Mo/Fe_2O_3/SO_4$ (2 wt%).

These results demonstrate that the pretreated oils B, C and D are superior to untreated Citgo resid or A to obtain high levels of coal conversion. These results can be rationalized in terms of available hydrogen. The available hydrogen content of B, C and D was higher than that of A or the untreated Citgo resid (Table 4).

Effect of Host Oil Type and Coal Feed Concentration on Product Yield and Quality

Products from coal-heavy oil coprocessing include gases, pentane-soluble oil, asphaltenes, and THF-insoluble coke (excludes coal-derived minerals and, when used, catalyst). Asphaltene yields were determined by difference. Pentane-soluble oil yields were corrected to exclude dissolved pentane, by simulated distillation. We found that product yield was affected by the concentration of coal in the feed. This can be seen in Figure 2, which shows that, for coprocessing runs with host C, oil yield reached a maximum at a coal-feed concentration between 10 % and 33 wt%. With every host oil, asphaltene yields were highest at coal loading of 50 wt%, the highest coal-feed concentration studied. In general, asphaltene yields were lowest at coal-feed concentration where the oil yields were highest; both gas and coke yield remained at a low level and did not change much with coal-feed concentration. These results suggest that high level of oil production is brought about by conversion of asphaltenes (petroleum- or coal-derived) to oils. Furthermore, oil yields appear to be enhanced by the presence of small amounts, less than 33 wt%, of coal. In coprocessing runs made with A, the

oil yield decreased as coal was added to the feed, while asphaltene and coke yield increased.

Distribution of products from coprocessing Illinois coal with untreated Citgo resid and the various pretreated host oils is shown in Figure 3. Based on oil yield, the host oils are ranked in the following order; D > C > untreated Citgo resid > B > A. The differences between the oil yield for D, C and untreated Citgo resid are small; little improvement in oil yield was realized as a result of our pretreatments of the Citgo resid.

Properties of the oil and asphaltene from the various coprocessing runs are listed in Table 6. In general, the product oils had atomic H/C ratios above 1.6, had a low concentration of nitrogen (about 0.3%) and contained a significant amount of oxygen (higher than 1.4%) and sulfur (above 1.5%). Essentially all the oxygen is presumably from the coal. The oil from the coprocessing run with A was the lightest oil produced; over 55 wt% of this oil had a simulated distillation boiling range below 650°F. Oil A was lighter than the other host oils. Product oils from the other coprocessing runs contained over 25 wt% of resid material; over 65 wt% of the oil boiled above 650°F, indicating that only a small fraction of the starting host oil and coal was converted to light distillate products. Further, the fraction of light distillate products that boiled in the gasoline and diesel range remained small at all coal loadings studied.

The asphaltenes had about the same concentration of S and O as the corresponding oils, but were richer in N and contained metals. The asphaltenes had a high aromatic carbon content (over 60 %) and had an average atomic H/C ratio of less than one.

The Amount of Coal Liquids in the Oil Products

The various products from coprocessing of coal and heavy oil are a mixture of coal-derived and petroleum-derived material that cannot easily be separated. To estimate the fraction of coal liquids and petroleum in the pentane-soluble oil products, the phenolic oxygen concentration of oil samples was measured and correlated to the fraction of coal liquid in the products. Since the Illinois coal contains much more oxygen than that of the Citgo resid (Tables 1 and 2) and a significant portion (about half) of oxygen in coal is associated with phenols, it was expected that the phenolic oxygen in the oil was essentially from the coal. The concentration of oxygen as phenolic OH for oils produced by coprocessing Illinois coal with the five Citgo host oils is shown in Figure 4. The data point at zero coal-feed concentration was measured on oil obtained by processing the untreated Citgo resid without coal; all other conditions were the same as those used in the coprocessing runs. From this measurement, we assigned the petroleum-derived oil component an average phenolic oxygen concentration of 0.26 wt%. The two data points at 100 % coal-feed concentration were the phenolic oxygen of the pentane-soluble products from processing Illinois coal in the non-hydrogen donor solvent, diphenylmethane (DPM); all other conditions were the same as those used in the coprocessing runs. The values, which average 1.78 wt%, have been corrected to account for the presence of DPM, and they reflect the estimated phenolic oxygen concentration of the coal-derived oil. As shown in Figure 4, the phenolic oxygen concentration of the oil products fell between the two end points and increased as the concentration of coal in the feed was increased; and the amount of coal liquid in the oils increased as the concentration of coal in the feed was increased.

An estimate of the fraction of coal liquid present in the oils allowed study of the effect of host oil type and coal-feed concentration on the yield of coal-derived and petroleum-derived oils. Using phenolic oxygen concentration, the weight fraction of coal liquid in the oil products was calculated by the following equation.

$$x = \left[\frac{C_t - C_p}{C_c - C_p} \right]$$

where,
x = fraction of coal-derived liquid in oil product
C_c, C_p, C_t = concentration of phenolic-oxygen in coal-derived oil, petroleum-derived oil and oil product, wt%

The equation assumes that the phenolic-oxygen concentration of the coal and petroleum components did not change as a result of interactions between coal and heavy oil during coprocessing. Three oil yield curves for coprocessing runs made with C are shown in Figure 5. The top curve represents the overall oil yield. The yield of coal-derived oil, as measured by phenolic oxygen content, is represented by the lower curve. It starts at zero and ends at 28 wt%. This last point was obtained by processing the Illinois coal in DPM. The yield of petroleum-derived oil is represented by the middle curve. The starting point for this curve was determined by processing the host oil without coal, with all other reaction conditions the same as those used in coprocessing runs. The straight dashed lines drawn between the end points represent the oil yields assuming no interaction between coal and pretreated resid. These lines are simply the linear extrapolation of produced oil yields obtained when the coal and host oil were processed separately. Any deviation of the experimental data points above or below the dashed lines would imply an interaction between coal and host oil which either resulted in an enhancement or reduction in the oil yield.

In coprocessing runs with host C and D (not shown) the presence of small amounts of coal (less that 33 wt%) seemed to enhance the yield of petroleum-derived oil; the data points were above the line. This behavior was also seen in coprocessing runs with the untreated resid. Conversely, the presence of coal with B caused a slight reduction in the yield of petroleum-derived oil, and the yield of oils from A were adversely affected by the presence of coal.

The untreated Citgo resid and oil A had no enhancing effect on the production of coal-derived oil; the data points fell on the dashed line. On the other hand, the resids that were pretreated at mild temperatures (B, C and D) brought about a higher yield of coal-derived oil than were obtained in DPM.

CONCLUSIONS

Certain pretreatments caused the available hydrogen content of the resids to increase, and these pretreated oils became better liquefaction solvents; higher coal conversions were obtained in these oils as compared to untreated resid. However, only a small fraction of the host oil and coal were converted to light distillate products during coprocessing. The yield of product oil with pretreated hosts was about the same as that obtained with untreated resid. Oil and asphaltene yields were strongly affected by the concentration of coal in the feed.

The fraction of coal liquid in the oil products, determined by phenolic oxygen concentration, increased as the amount of coal in the feed was increased. The presence of small amounts, less than 33 wt%, of coal enhanced the yield of oil from the untreated Citgo resid as

well as from oils that were pretreated it mild temperatures. The oil yield from the host that was pretreated at 440°C was adversely affected by the presence of coal.

ACKNOWLEDGMENTS

This project was supported by a grant from the U.S. Department of Energy (DE-AC22-91PC91054). We would also like to thank the EXXON Educational Foundation for their generous support. We are grateful to Genea Lee for her assistance in the dehydrogenation experiments. We would like to thank the Citgo Co. as well as The Amoco Co. for providing the petroleum resid samples, and Argonne Premium Coal Sample Bank for providing coal samples.

BIBLIOGRAPHY

1. Shinn, J.H., Dahlberg, A.J., Keuhler, C.W., and Rosenthal, J.W., "The Chevron Co-Refining Process", presented at the Ninth Annual EPRI Contractors Conference on Coal Liquefaction, Palo Alto, CA, May 1984.

2. Greene, M., Gupta, A., and Moon, W., "LCI's Two-Stage Co-Processing Route: Continuous Bench-Scale Operations", presented at the DOE Direct Liquefaction Contractors' Review Meeting, Pittsburgh, PA, October, 1986.

3. Duddy, J., Panvelker, S., and Popper, G., "HRI's Co-Processing Program", presented at the Fifteenth Annual EPRI Conference on Fuel Science, Pal Alto, CA, August, 1991.

4. Kelly, J.F., Fouda, S.A., Rahimi, P.M., and Ikura, M., 'CANMET Co-Processing: A Status Report", presented at the CANMET Coal Conversion Contractors' Review Meeting, Calgary, Alberta, November, 1984.

5. Cugini, A.V., Lett, R.G., and Wender, I., "Coal/oil Coprocessing Mechanism Studies", Energy and Fuels, Vol. 3, 120-126 (1989).

6. Miller, T.J., Panvelker, S.V., Wender, I., and Tierney, J.W., " Thermal Non-Catalytic Coprocessing of Illinois No. 6 Coal with Maya Resid and Boscan crude", Fuel Processing Technology, Vol.23, 23-38 (1989).

7. Takeshita, K. and Mochida, I., Jap. Pat. 80-45703 (1980)

8. Sato, Y., Yamamoto, Y., Kamo, T., Inaba, A., Miki, K., and Saito, I., "Effect of Hydrotreatment of Various Heavy Oils as Solvent for Coal Liquefaction", Energy & Fuels, Vol 5, 90-102 (1991).

9. Curtis, C.W., Tsai, K.-J. and Guin, J.A., "Effect of Solvent Composition on Coprocessing Coal with Petroleum Residua", Fuel Processing Technology, Vol 16, 87 (1987).

10. Bedell, M.W., Curtis, C.W. and Hool, J.L., "Reactivity of Argonne coals in the presence of cyclic olefins and other donors", Fuel Processing Technology, Vol 37, 1-18 (1994).

11. Owens, R.M. and Curtis, C.W., " An Investigation of Hydrogen Transfer from Naphthenes during Coprocessing", Energy & Fuels, Vol 8, 823-829 (1994)

12. Pradhan, V.R., Hu, J., Tierney, J.W., and Wender, I., "Activity and Characterization of Anion-Modified Iron(III) Oxides as Catalysts for Direct Liquefaction of Low Pyrite Coals", Energy & Fuels, Vol 7, 446-454 (1993).

13. Pradhan, V.R., Herrick, D.E., Tierney, J.W., and Wender, I., "Finely Dispersed Iron, Iron-Molybdenum, and Sulfated Iron Oxides as Catalyst for Coprocessing Reactions", Energy & Fuels, Vol 5, 712-720, (1991).

14. Pradhan, V.R., Holder, G.D., Wender, I., and Tierney, J.W., "Kinetic Modeling of Direct Liquefaction of Wyodak Coal Catalyzed by Sulfated Iron Oxides", I&EC Res. Vol. 31 (1992) 2051-2056

15. Friedman, S., Metlin, S., Svedi, A., and Wender, I., "Selective Hydrogenation of Polynuclear Aromatic Hydrocarbons", J. Org. Chem, Vol 24, 1287, (1959).

16. Wender, I., Levine, R., and Orchin, M., J. Am. Chem. Soc., Vol.72 (1950) 4375

17. ARCO Chemical Company, "Catalytic Hydrogenation of Coal-Derived Liquids", Project SEACOKE, Phase II, Final Rep., Contract No. 14-01-0001-472, Off. Coal Res., U.S. Dept. of Interior, Washington, DC (1966)

18. ASTM Designation: D 2887-89, Annual Book of ASTM Standards

19. Whitcomb, J.H., M.S. Thesis, University of Pittsburgh, 1993.

20. Robbins, G.A., Winschel, R.A., and Burke, F.P., "Phenolic -OH as a Process-Performance Indicator in Two-Stage Liquefaction", Am. Chem. Soc. Div. Fuel Chem. Prepr., 155-163, (1986).

Table 1 Properties of Two Petroleum Resids (1000 °F+)

	Citgo Resid	Amoco Resid
S.G. @ 60°F		1.03
C, wt%	85.4	84.3
H, wt%	10.1	10.2
S, wt%	3.4	4.6
N, wt%	0.8	0.5
O, wt%	0.3	0.4
Atomic H/C	1.42	1.45
V, ppm	555	251
Ni, ppm	110	57
Fe, ppm	12	13
Pentane insolubles, wt%	29	20
Available H/100 C atoms	9.8	
f_a, fraction of total C	0.33	0.32

Table 2 Properties of Argonne Coal Samples

	Illinois No.6	Wyodak
Moisture, wt%	8.0	28.1
Ash, wt%	14.3	6.3
Volatile matter, wt%	35.8	32.2
Rank	hvB	Subbituminous
C, wt% (maf)	77.7	75.0
H, wt% (maf)	5.0	5.3
N, wt% (maf)	1.4	1.1
S, wt% (maf)	2.4	0.5
Cl, wt% (maf)	0.06	0.03
O, wt% (maf)	13.5	18.0
Atomic H/C	0.77	0.85
f_a	0.71	0.62

f_a = Fraction of aromatic carbon, determined by ^{1}H NMR using the Brown and Ladner method (1960).

Table 3 Reaction Conditions and Product Yields for Pretreatments of Citgo Resid

Conditions	Oil-A	Oil-B	Oil-C	Oil-D
Catalyst, concentration	MN, 1000 ppm	MN, 1000 ppm	$Mo/Fe_2O_3/SO_4$, 200 ppm Mo 13000 ppm Fe	$Co_2(CO)_8$ 6.2 wt%
Gas used	H_2	H_2	H_2	CO/H_2 (1:1)
Temperature, °C	440	375	375	135
Pressure (cold), psig	1,000	1,000	1,000	2,000
Time, hrs	2	5	5	2
Gas yield, wt%	25	1	3	0
Liquid yield, wt%	72	97	95	100
Coke yield, wt%	3	2	2	0

MN=Mo naphthenate (6 wt% Mo)

Note: elemental sulfur was added in pretreatments A, B and C in excess of amount needed to sulfide the catalyst.

Table 4 Properties of Citgo Pretreated Host Oils

	Citgo Resid	Oil-A	Oil-B	Oil-C	Oil-D
b.p. <565°C[a], wt%		62.6	29.7	33.3	17.9
b.p. >565°C, wt%		37.4	70.3	66.7	82.1
C, wt%	85.4	85.1	85.9	85.6	84.8
H, wt%	10.1	10.6	10.4	10.8	10.0
S, wt%	3.4	2.2	2.7	2.9	2.9
N, wt%	0.8	0.9	0.9	0.8	0.8
O, wt%	0.3	1.2	0.1	0.0	1.5
Atomic H/C	1.42	1.49	1.45	1.51	1.42
Atomic C/S	67	103	85	79	78
Atomic C/N	124	110	111	125	124
V, ppm	555	393		472	
Ni, ppm	110	67		95	
Available[b] Hydrogen per 100 C atoms	9.9	12.4	16.8	14.0	17.5
wt% H_2 added		1.4	0.5	0.5	0.5

a: b.p. <565°C consists of pentane-soluble oil having a simulated distillation b.p. <565°C (1050°F). b.p. >565°C consists of pentane-insoluble asphaltenes and pentane-soluble oil having simulated distillation b.p. >565°C.

b: Value based on catalytic dehydrogenation.

Table 5 Reaction Conditions and Results of Illinois No.6 Coprocessing Runs (Conditions: 1000 psig (cold) H_2, 30 min reaction time, other conditions shown in table)

Host Oil	Run No.	Cat.	Oil: Coal	Tavg, °C	Pavg, psig	Coal Conv, wt%	Gas yield, wt%	Oil yield, wt%	Asph. yield, wt%	Coke yield wt%
Amoco Resid	69	none	2:1	427	2104	56	10.1	73.1	in oil	16.8
Citgo Resid	85	none	2:1	415	2046	74	3.3	69.4	13.9	8.7
Citgo Resid	87	none	1:1	427	2227	58	6.0	40.4	28.7	17.8
Citgo Resid	119	Fe	2:1	423	1889	81	6.7	70.2	12.3	6.1
Citgo Resid	136	MN	2:1	425		88	5.0	70.0	16.0	4.2
Oil-A	115	none	2:1	425	2097	74	4.7	48.4	34.5	7.6
Oil-A	114	none	1:1	425	2257	71	3.9	40.0	37.3	11.7
Oil-B	96	none	9:1	426	1756	85	4.9	95.1	-4.2	2.8
Oil-B	142	none	4:1	424	1805	85	7.1	78.0	8.3	3.7
Oil-B	91	none	2:1	427	1766	92	6.5	65.0	20.5	3.3
Oil-B	95	none	2:1	428	1790	93	5.1	67.3	19.8	3.0
Oil-B	141	none	1.5:1	424	1844	90	5.8	64.6	19.7	4.2
Oil-B	93	none	1:1	425	1849	89	6.0	46.8	34.8	5.2
Oil-C	100	none	9:1	425	1803	72	10.1	99.0	-16.2	5.6
Oil-C	143	none	9:1	423	1796	89	4.1	68.4	23.4	2.7
Oil-C	144	none	4:1	425	1813	94	3.3	61.3	29.9	2.6
Oil-C	117	none	2:1	425	1915	94	6.7	74.6	9.9	4.1
Oil-C	97	none	2:1	426	1874	93	4.1	46.9	39.9	4.4
Oil-C	145	none	1.5:1	425	1844	89	5.7	43.4	39.4	5.7
Oil-C	98	none	1:1	425	2311	56	6.0	31.0	36.7	19.1
Oil-C	107	none	1:1	425	1890	90	6.5	53.3	27.4	5.6
Oil-D	106	none	9:1	424	1697	86	3.3	71.3	20.7	3.3
Oil-D	118	none	9:1	424	1710	43	6.5	85.0	0.3	6.8
Oil-D	147	none	4:1	424	1777	85	11.3	63.7	17.7	4.5
Oil-D	102	none	2:1	425	1032	88	4.2	78.5	7.7	4.8
Oil-D	137	none	2:1	426	2071	44	13.6	42.4	23.4	16.1
Oil-D	146	none	1.5:1	425	1781	90	5.2	47.5	37.2	4.4
Oil-D	103	none	1:1	426	1764	91	4.3	56.7	27.2	4.7

Fe = Mo/Fe_2O_3/SO_4 (1 wt% Mo)
MN = Mo Naphthenate (6 wt% Mo)
Oil-A= Citgo resid hydrotreated with 1000 ppm Mo naphthenate at 440°C for 2 hrs.
Oil-B= Citgo resid hydrotreated with 1000 ppm Mo naphthenate at 375°C for 5 hrs.
Oil-C = Citgo resid hydrotreated with 2 wt% Mo/Fe_2O_3/SO_4 (1% Mo) at 375°C for 5 hrs.
Oil-D = Citgo resid hydrotreated with 6.2 wt% $Co_2(CO)_8$ and 1:1 H_2:CO at 135°C for 2 hrs.
Asph. = Asphaltenes (determined by difference)

Table 6 Properties of Coprocessing Oil and Asphaltenes (conditions: 425°C, 1000 psig (cold) H_2 , host oil:coal = 2:1, 30 min reaction time)

Properties	Citgo resid + Illinois No.6		Oil-A + Illinois No.6		Oil-B + Illinois No.6		Oil-C + Illinois No.6		Oil-D + Illinois No.6	
	Oil	Asph	Oil	Asph	Oil	Asph	Oil	Asph	Oil	Asph
< 421°F, wt%	13.4		19.5		12.6		9.5		14.2	
421-650°F, wt%	21.0		36.4		16.4		15.5		12.1	
650-1050°F, wt%	38.6		36.9		43.7		39.4		42.4	
1050°F +, wt%	27.0		7.2		27.3		35.6		31.3	
Atomic H/C	1.62	0.35	1.67	0.86	1.66	0.96	1.69	0.86	1.64	0.90
S, wt%	2.3		1.6		1.8	1.8	2.0		2.2	2.2
N, wt%	0.3	2.5	0.2	1.8	0.3	1.8	0.3	1.9	0.3	1.8
O, wt%	1.4		2.7		4.0	3.5	3.0		3.3	2.9
f_a	0.29		0.25	0.74	0.25	0.62	0.22	0.75	0.27	0.66
V, ppm		1015		206				750		
Ni, ppm		204		43				205		

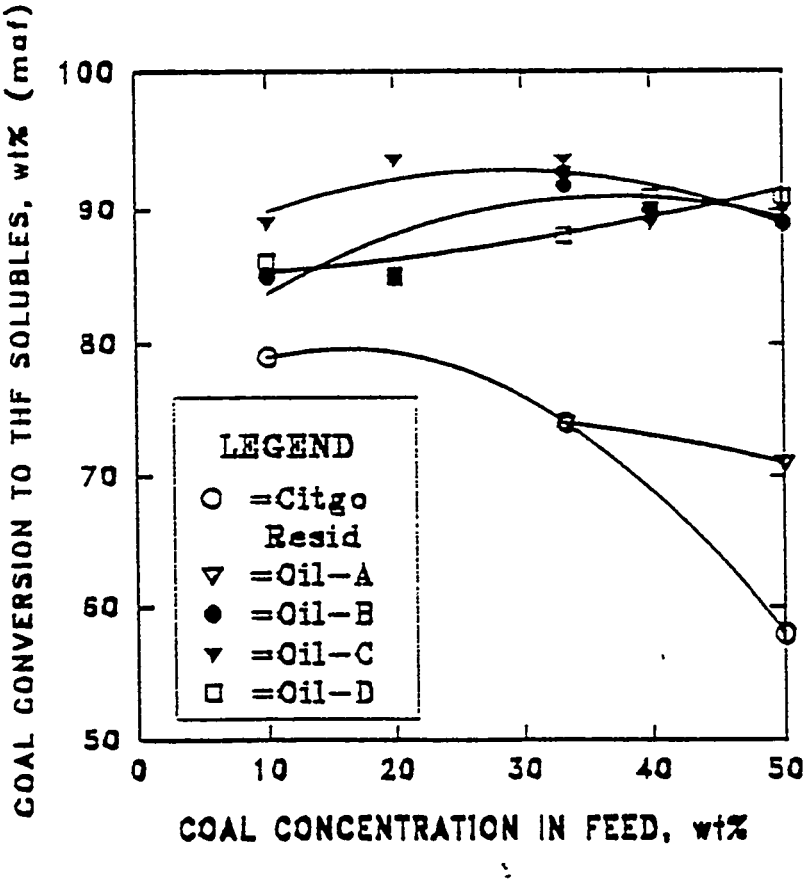

Figure 1 Illinois No.6 Coal Conversions When Coprocessed With Citgo Resid and Pretreated Host Oils (conditions: 425°C, 1000 psig (cold) H_2, 30 min)

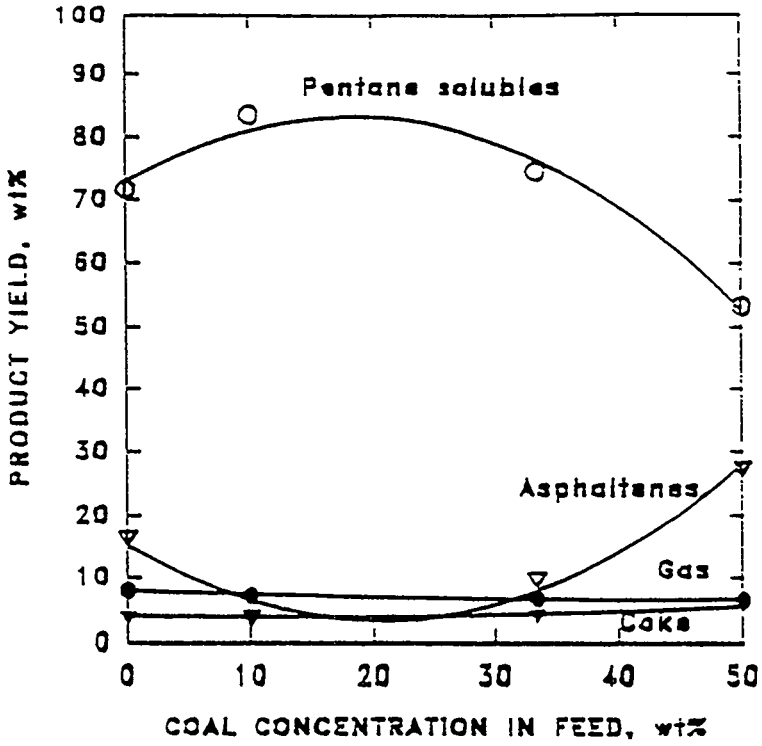

Figure 2 Product Yields from Coprocessing Illinois No.6 Coal and Host Oil-C (conditions : 425°C, 1000 psig (cold) H_2, 30 min)

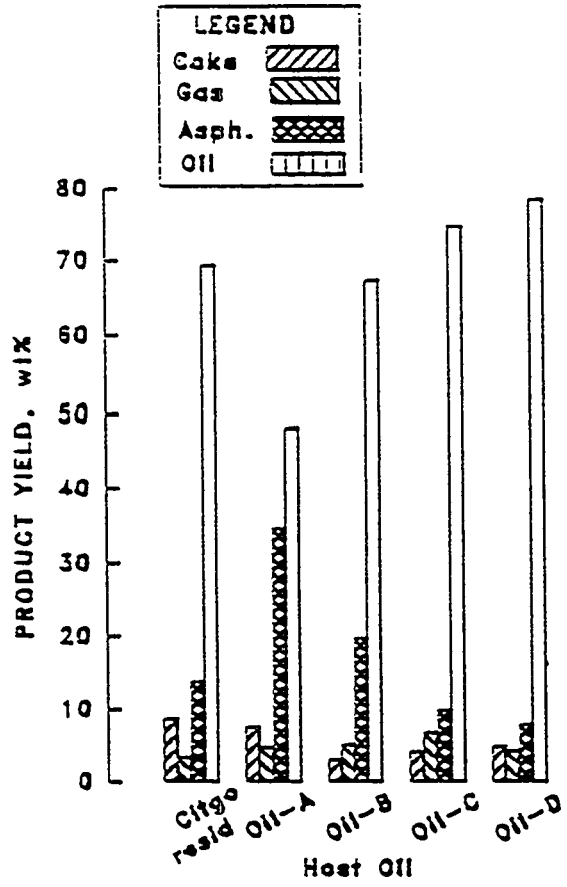

Figure 3 Product Yields from Coprocessing Illinois No.6 Coal and Citgo Host Oils (conditions : 425°C, 1000 psig (cold) H_2, 30 min, host oil:coal=2:1)

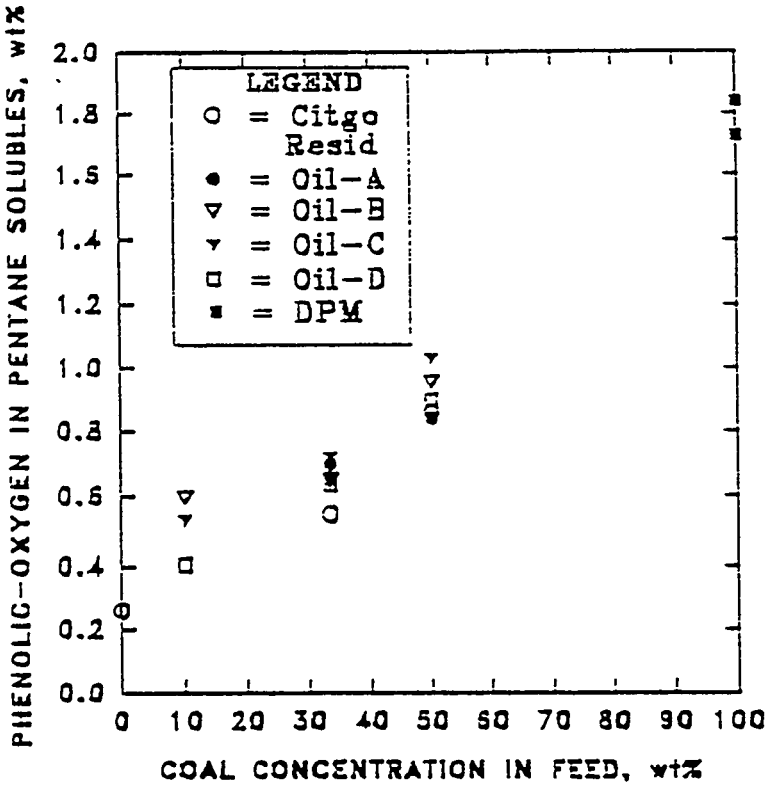

Figure 4 Concentration of Oxygen as Phenolic-OH in Pentane-Soluble Products from Coprocessing Illinois No.6 Coal with the Various Citgo Host Oils

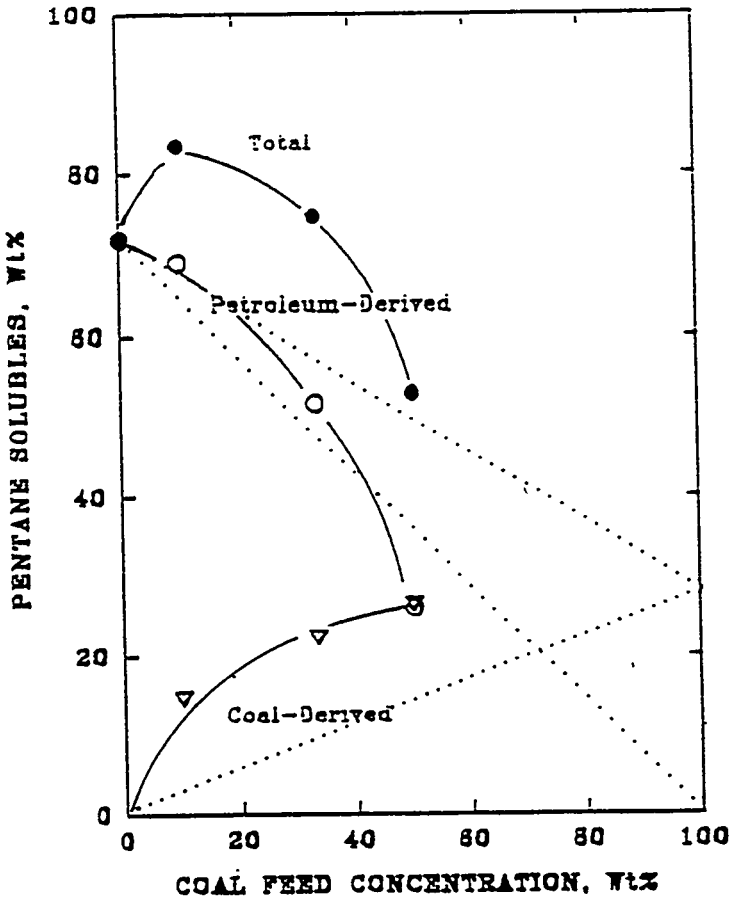

Figure 5 Petroleum-Derived and Coal-Derived Oil Yields from Coprocessing Illinois No.6 Coal with Host Oil-C (conditions: 425°C, 1000 psig (cold) H_2, 30 min)

LIQUEFACTION CHEMISTRY AND KINETICS: HYDROGEN UTILIZATION STUDIES

Kurt S. Rothenberger, Robert P. Warzinski, Anthony V. Cugini, Michael V. Ciocco, and Garret A. Veloski

U. S. Department of Energy, Pittsburgh Energy Technology Center, P. O. Box 10940, Pittsburgh, PA 15236

OBJECTIVE

The objectives of this project are to investigate the chemistry and kinetics that occur in the initial stages of coal liquefaction and to determine the effects of hydrogen pressure, catalyst activity, and solvent type on the quantity and quality of the products produced.

PROJECT OVERVIEW

The project comprises three tasks: (1) Preconversion Chemistry and Kinetics, (2) Hydrogen Utilization Studies, and (3) Assessment of Kinetic Models for Liquefaction. The Hydrogen Utilization Studies work will be the main topic of this report. However, the other tasks will be briefly described here.

The Preconversion Chemistry and Kinetics task focuses on understanding the influence of a catalyst and solvent on the chemistry occurring in the initial phases of the dissolution and liquefaction of coal. Particular emphasis is placed on understanding and controlling retrogressive reactions that lead to high molecular weight, refractory products. Mitigating these reactions could lead to an improved first-stage product requiring less severe upgrading to produce lower molecular weight, more highly saturated products. Catalyst studies with $Mo(CO)_6$ as the catalyst precursor in a solvent-free liquefaction system were designed to investigate the role of the catalyst apart from added solvents in the initial stages of liquefaction. Samples of coal recovered after liquefaction for various periods of time have been subjected to detailed microscopic and chemical characterization to determine the nature of physical and chemical changes that occur. Emphasis is given to understanding the changes occurring in the coal and insoluble residues that precede the formation of soluble products and the role of a catalyst and solvent in preventing retrograde reactions in these processes. Kinetic descriptions of these processes have been developed and are described in several publications and presentations [1,2,3].

Assessment of Kinetic Models for Liquefaction is a new effort that is intended to develop improved kinetic models for evaluating the liquefaction process. The initial stages of this task will consist of an information needs assessment with review of the pertinent literature and discussions with process engineers to understand the limitations of current kinetic models for direct coal liquefaction. Because of the preliminary nature of this task, there have been no publications or presentations to date.

The remainder of this report will be concerned with the Hydrogen Utilization Studies task. It entails an investigation of the effects of solvent type, catalyst activity, and hydrogen pressure on the conversion of coal in first stage coal liquefaction and on the quantity and quality of the products produced. One of the perceived major costs associated with coal liquefaction is the high pressure commonly employed in first-stage catalytic reactors. Reducing the overall pressure significantly could result in considerable savings in the costs associated with coal liquefaction, provided that the hydrogen demands of the system are met. In the first stage of coal liquefaction, hydrogen serves the important functions of capping radical fragments formed from thermal (or other) bond scission reactions and of maintaining a desirable equilibrium between aromatic molecules and their hydroaromatic analogs. Understanding the pathways for hydrogen consumption during this crucial time period would enable one to choose catalysts and conditions that favor desired reactions. In this task, three aspects of hydrogen utilization have been investigated. Gas-phase hydrogen consumption has been monitored as a function of initial pressure, the extent of solvent hydrogenation of simple two-ring aromatic solvents has been determined in the presence of various catalysts, and these measurements have been correlated with coal conversion as determined by solvent fractionation. Several publications and presentations have resulted from this work [4,5,6,7].

EXPERIMENTAL SECTION: Hydrogen Utilization Studies

Materials. Panasol®, a mixture containing mostly alkyl naphthalenes, was obtained from Crowley Chemical Company and used without further purification. Purified grade 1-methylnaphthalene (1-MeNp) from Fisher Scientific Company, found to be 99% pure by gas chromatography, was used without further purification. Blind Canyon coal, DECS-6, from the U.S. Dept. of Energy's Coal Sample Program, was used in these studies. A unique, high surface area, preformed molybdenum catalyst (MoS_2) was prepared at the U.S. Dept. of Energy's Pittsburgh Energy Technology Center (PETC). The catalyst consisted of the recovered solid from a semi-batch, 1-L stirred autoclave reaction of ammonium heptamolybdate, hydrogen sulfide, and Panasol under 17 MPa (2500 psi) hydrogen at 425°C [8]. The catalyst contained 50% C, 30% Mo, and 20% S, and possessed a BET surface area of approximately 250 m^2/g. Aged Akzo EXP AO-60 catalyst, containing Ni-Mo on an Al_2O_3 support, was obtained from Hydrocarbon Technologies, Inc, and ground before use. Shell-324 (S-324), also a Ni-Mo/Al_2O_3 based catalyst, was sulfided before use by reaction with elemental sulfur under 7 MPa (1000 psi) H_2 (cold) at 425°C for 30 minutes in 1-MeNp.

Reactions. Reactions were completed in a stainless steel batch microautoclave reactor system constructed at PETC. The cylindrical reactor portion has a volume of 43 mL, and the total internal volume, including all tubing and connections, is 60 mL. Unless otherwise stated, a normal reaction charge consisted of 6.6 g solvent, 3.3 g coal, catalyst to obtain 3000 ppm metal loading, and 7 MPa (1000 psi) ambient temperature hydrogen gas. The reactor was then attached to the rocker arm (180 cycles / minute) and plunged into a preheated sand bath, where it was heated up to 425°C in 2 to 4 minutes. It was held at temperature in the sand bath for 30 minutes, and then removed and allowed to air cool, typically in less than 5 minutes, to near room temperature.

Sample Workup Procedure and Characterization Scheme. The reaction characterization scheme is diagrammed in Figure 1. The reactor was equipped with an internal thermocouple and a pressure transducer for continuous monitoring of pressure and temperature throughout the run. These were the only measurements that were made while the reaction was in progress. After the reactor cooled to room temperature, it was vented and the vent gas was collected and analyzed by a previously published method [9]. Total hydrogen consumption for the run was calculated based on the difference between initial and final (cold) gas pressure as adjusted for product gas slate. The reactor was rinsed with tetrahydrofuran (THF), and the extracted material was filtered through a 0.45-micron filter under 0.3 MPa (40 psi) nitrogen gas pressure. Coal conversion, or "THF conversion" was calculated from the measured mass of THF insolubles adjusted for catalyst and coal mineral matter as compared to MAF coal. In solvent-only runs, the THF extraction was done to recover the catalyst from the solvent. If coal was present the THF solvent was removed on a rotary evaporator and the remaining material was extracted with heptane solvent. The heptane-insoluble material was used to calculate an "oil conversion," or "heptane conversion." After removal of the solvent, the heptane-soluble material was submitted for a suite of analytical techniques which included low-voltage, high-resolution mass spectrometry (LVHRMS), gas chromatography (GC), ^{1}H and ^{13}C nuclear magnetic resonance (NMR) spectroscopy, and elemental analysis. Normally, LVHRMS data were used both to survey the variety of chemical species in the soluble product and to calculate solvent hydrogenation for the reaction. The GC was used for solvent hydrogenation when special attention to quantitation of particular components was needed. The reported solvent hydrogenation represents the percent of naphthalenes converted to hydrogenated analogs. The NMR and elemental analyses were normally used only for qualitative support for the other data. In solvent-only runs, the heptane extraction was omitted and the THF solubles were submitted for the suite of solvent-analysis methods.

RESULTS AND DISCUSSION: Hydrogen Utilization Studies

Solvent hydrogenation is shown as a function of cold hydrogen gas pressure for an unsupported (MoS_2) and two supported molybdenum catalysts (AO-60 and S-324) in Figure 2. Also shown on the plot is the level of hydrogenation expected for a pseudo-equilibrium distribution of naphthalenes and tetralins as calculated from literature data [10]. As can be seen, all the data lie well below the equilibrium value. Several conclusions can be drawn from the plot. Solvent hydrogenation increases as a function of hydrogen pressure in all cases. This would be expected from both thermodynamic and kinetic arguments. In the absence of coal, solvent hydrogenation is greater with the supported Mo catalysts than with the unsupported catalyst. The experiments were designed to have equal metal loadings for the unsupported and supported comparison, although this does not imply equal accessibility or nature of the metal sites. The results illustrate the relative activities of the synthesized unsupported catalyst as compared to two state-of-the-art supported catalysts in the absence of coal.

Solvent hydrogenation is shown as a function of coal addition in Figure 3. A comparison is made between two types of supported catalysts (AO-60 and S-324) and the

unsupported catalyst (MoS_2). A no-catalyst case is also presented for comparison. The figure shows that in the absence of a catalyst, virtually no solvent hydrogenation is observed, regardless of the amount of coal present. Solvent hydrogenation decreases as a function of coal addition for both the unsupported MoS_2 and the supported catalysts. The unsupported MoS_2 loses about half its initial activity with the addition of 0.2 g coal; the level of activity is similar for a full 3.3 g coal charge. The supported AO-60 loses activity in a more gradual manner, with activity decreased to 50% of the initial value between 0.5 and 1.0 g of added coal. However the activity continues to decrease as more coal is added. With a full 3.3 g charge of coal, the AO-60 has only about 20% of its initial solvent hydrogenation activity, which is equal to the activity of the unsupported MoS_2 under the same conditions. A similar series of experiments (not displayed) shows that the presence of coal also inhibits the dehydrogenation of tetralin.

In Figure 4, baseline data for coal conversion, hydrogen consumption, and solvent hydrogenation are compared to the results for a sequence of microautoclave experiments where the catalyst material was recovered by THF extraction and reused. Although the data expressed in the figure are only for the unsupported MoS_2 catalyst, similar trends were obtained for the supported catalysts. Block "A" shows the baseline solvent hydrogenation and hydrogen consumption for MoS_2 catalyst in a solvent-only system. Block "B" shows the diminution of both of these quantities in a second experiment that contained 0.2 g coal. The catalyst from this experiment was recovered and used to hydrogenate fresh solvent to see if the activity would recover to previous values. As can be seen from the results in block "C", both solvent hydrogenation and hydrogen consumption remained low. This indicates that the diminution observed in "B" was not due to competition from species derived from the coal, but was the result of some permanent modification of the catalyst. The catalyst from "C" was recovered and reused in a third experiment, containing a full 3.3 g coal. As shown in block "D", solvent hydrogenation has been diminished even further. Hydrogen consumption is up, but this is due to the hydrogen requirements of the coal. Coal conversion is nearly identical to the baseline case with fresh catalyst and 3.3 g of coal shown in block "E". The difference in hydrogen consumption between "D" and "E" is most likely due to the difference in solvent hydrogenation, as the recovered catalyst in "D" continues to deactivate toward solvent hydrogenation. Thus the catalyst is still capable of promoting coal conversion (coal conversion in the absence of catalyst is about 50%) although its ability to hydrogenate the alkylnaphthalene has been severely diminished.

Figure 5 shows coal THF and heptane conversions as a function of hydrogen pressure for both the unsupported and supported catalyst systems. A no-catalyst case is shown at two pressures for comparison. All runs contained 3.3 g coal and 6.6 g solvent. It can be seen that conversions are similar for both supported and unsupported catalyst systems at all pressures. Thus any advantage in hydrogenation activity enjoyed by the supported catalysts would appear to have been lost in the presence of coal. With both types of catalysts, THF and heptane conversions increase as a function of hydrogen pressure, although the increase begins to level out at the higher pressures. In spite of the obvious difficulties in promoting contact between solid coal and solid catalyst particles in the reactor, the presence of catalyst in the dissolution stage certainly appears

to aid in conversion, as the THF and heptane conversions at 2.7 MPa (400 psi) with catalyst are somewhat above those obtained at 7 MPa (1000 psi) with no catalyst.

Conclusions. Catalyst activity for coal liquefaction is observed at hydrogen pressures (cold) as low as 2.7 MPa (400 psi). The results imply that significant reductions in operating pressures may be possible with the use of appropriate first-stage catalysts. Catalyst behavior in the initial stages of coal liquefaction then becomes important. The results of Figures 3 and 4 show that some deactivation of both the unsupported and supported catalysts used here takes place in the presence of coal. However, a substantial amount of catalytic activity remains, as evidenced by good coal conversion results following repeated recovery and reuse of catalyst. At this point, it is not known whether the hydrogen reacting with the coal is involved with hydrogenating aromatic rings, or simply capping fragments formed from bond scission. However, the results illustrate that the best catalysts for hydrogenation in solvent-only systems may not enjoy the same advantages in the initial stages of coal liquefaction.

PLANS: Hydrogen Utilization Studies

In the Hydrogen Utilization Studies task, the initial stage of coal dissolution is evaluated by direct measurement of coal conversion using solvent extraction methods. The product quality is evaluated indirectly by probing other facets of the process such as hydrogen consumption and solvent hydrogenation. As the project develops, more direct methods will be developed to measure product quality. For example, a planned series of experiments will compare microautoclave reactions done under different experimental conditions of pressure, catalyst, and solvent quality, but which are known (from previous work) to give similar coal conversion levels. With the "conversion" variable held constant, a detailed examination of the reaction products will be made to determine if the different reaction conditions favor particular products. In addition, work is planned to identify the poisoning agent or agents responsible for the inhibition of solvent hydrogenation, and to determine if the effect on the catalyst is reversible. Finally, the process improvements developed during the microautoclave studies, particularly those based on reducing hydrogen pressure, will be tested on a continuous unit.

ACKNOWLEDGEMENTS

This work was performed while one of the authors (MVC) was under an appointment to the U.S. Department of Energy Fossil Energy Postgraduate Training Program administered by the Oak Ridge Institute for Science and Education.

DISCLAIMER

REFERENCES

1. Warzinski, R.P.; Bockrath, B.C. "Molybdenum Hexacarbonyl as a Catalyst Precursor for Direct Coal Liquefaction", accepted for publication in Prepr. Pap. - Amer. Chem. Soc., Fuel Chem. Div., 1995.

2. Warzinski, R.P.; Cugini, A.V.; Bockrath, B.C. "Comparison of the Means of Introduction of MoS_2 Liquefaction Catalysts on Performance", accepted for publication in Prepr. Pap. - Amer. Chem. Soc., Fuel Chem. Div., 1995.

3. Warzinski, R.P.; Bockrath, B.C.; Irdi, G.A.; Booher, H.B.; Wells, A.W. "Preconversion Chemistry and Liquefaction of Coal in the Presence of a Molybdenum-Containing Catalyst, accepted for publication in Proc. 8th International Conf. Coal Science, 1995.

4. Ciocco, M.V.; Cugini, A.V.; Rothenberger, K.S.; Veloski, G.A.; Schroeder, K.T. "Effect of Pressure on First-Stage Coal Liquefaction with Dispersed Catalysts," Proc., 11th Ann. Pittsburgh Coal Conf., 1, 500-505, Sept 12-16, 1994.

5. Cugini, A.V.; Rothenberger, K.S.; Ciocco, M.V.; Veloski, G.A.; Martello, D.V. "Effect of Pressure and Solvent Quality on First-Stage Coal Liquefaction with Dispersed Catalysts," Am. Chem. Soc., Fuel Chem. Div., Prepr. Pap. **39**(3), 695-701 (1994).

6. Rothenberger, K.S.; Cugini, A.V.; Schroeder, K.T.; Veloski, G.A.; Ciocco, M.V. "Effect of Coal Addition on Solvent Hydrogenation and Coal Conversion in a Model Alkylnaphthalene Solvent," Am. Chem. Soc., Fuel Chem. Div., Prepr. Pap. **39**(3), 688-694 (1994).

7. Cugini, A.V.; Rothenberger, K.S.; Veloski, G.A.; Ciocco, M.V.; McCreary, C. "The Effect of Pressure of First Stage Coal Liquefaction and Solvent Hydrogenations with Supported Catalysts," accepted for publication in Proc. 8th International Conf. Coal Science, 1995.

8. Cugini, A.V.; Krastman, D.; Lett R.G.; Balsone, V.D. Catalysis Today, **1994**, 19(3) 395-408.

9. Hackett, J.P.; Gibbon, G.A. In Automated Stream Analysis for Process Control, Manka, D.P., Ed., Academic Press, 1982; pp 95-117.

10. Frye, C. G.; Weitkamp, A. W. J. Chem. Eng. Data, **1969**, 14(3), 372-376.

Figure 1: Characterization Scheme

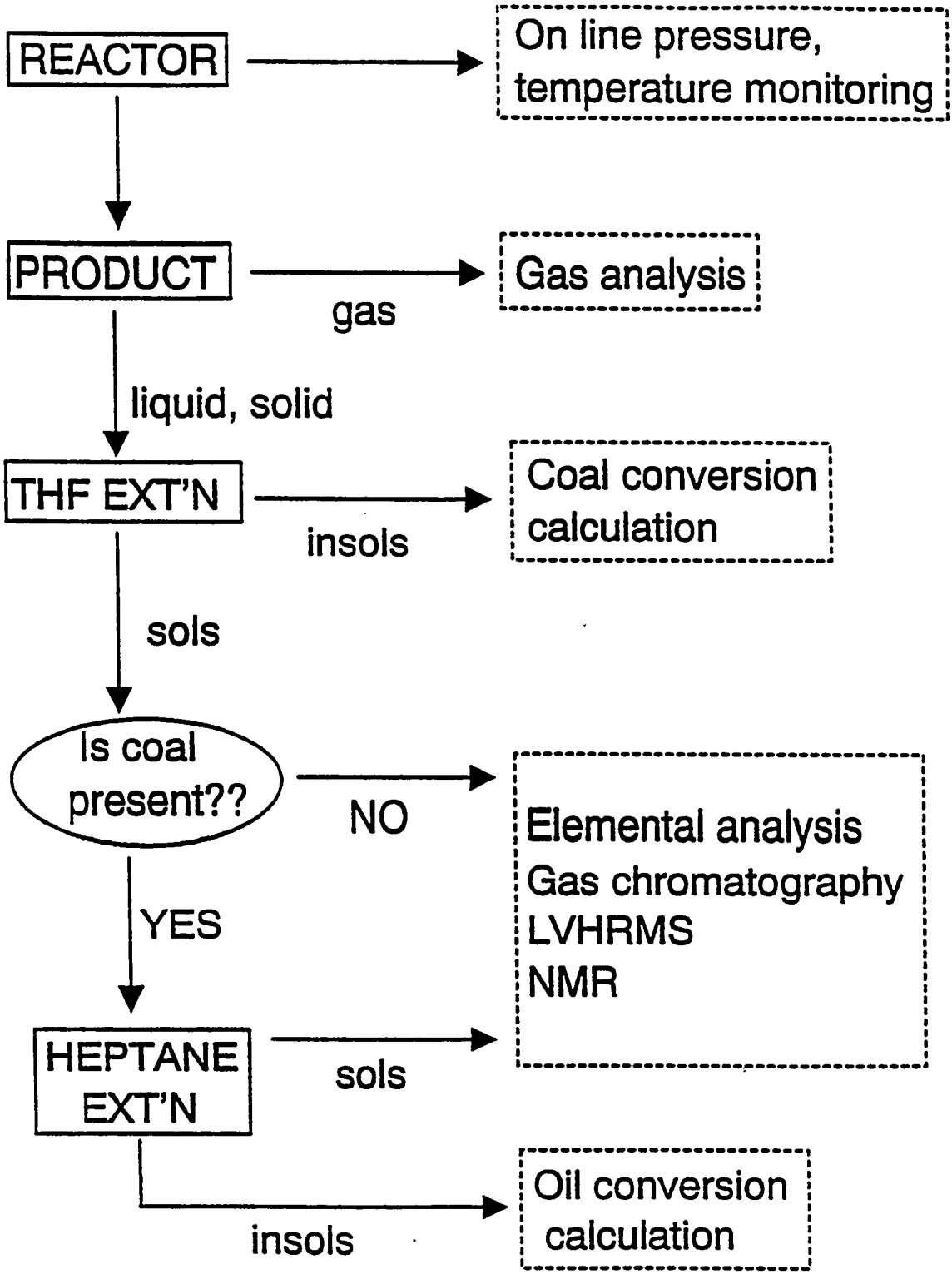

Figure 2: Solvent Hydrogenation as a Function of Hydrogen Pressure (no coal)

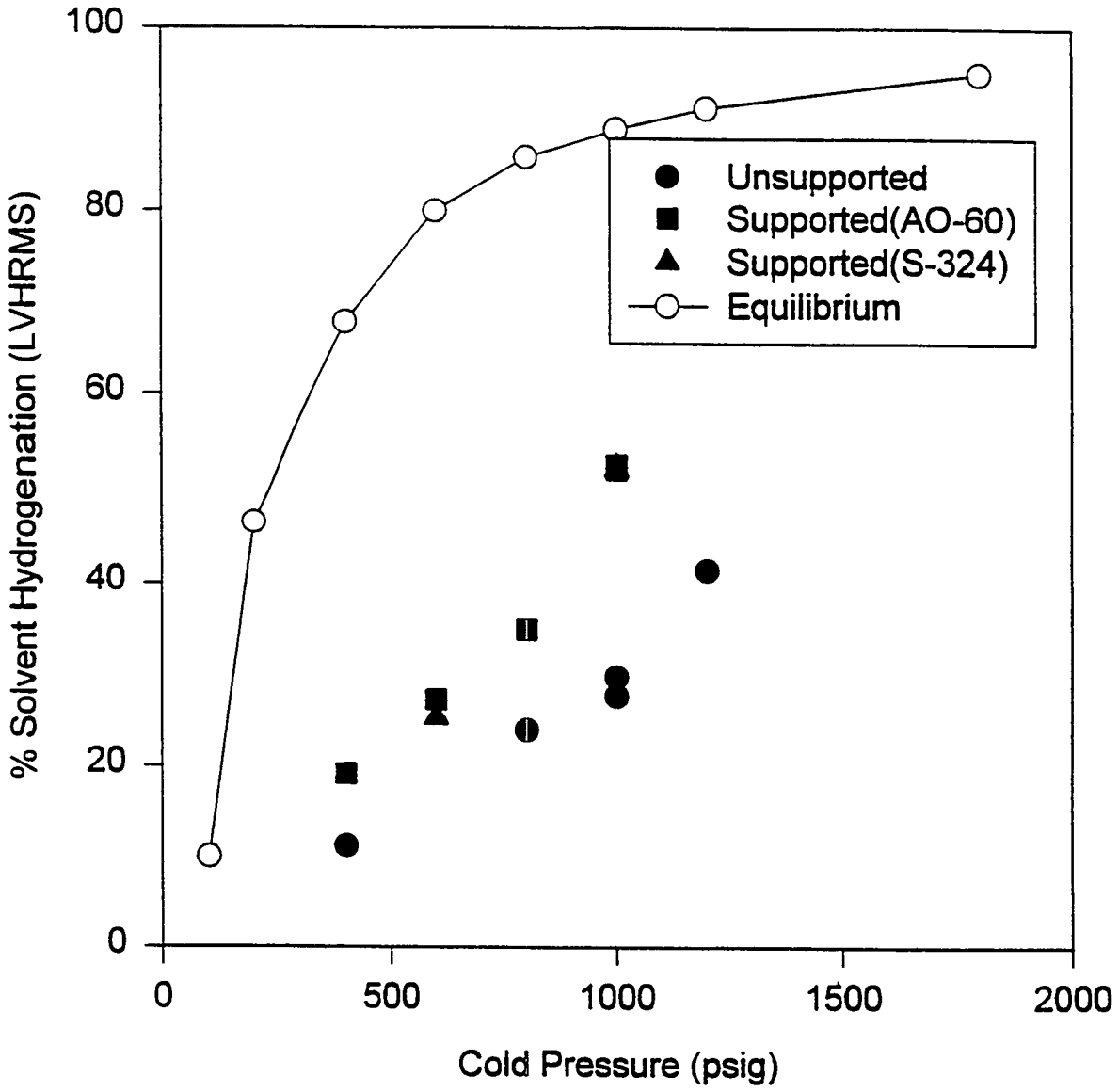

Figure 3: Solvent Hydrogenation as a Function of Added Coal

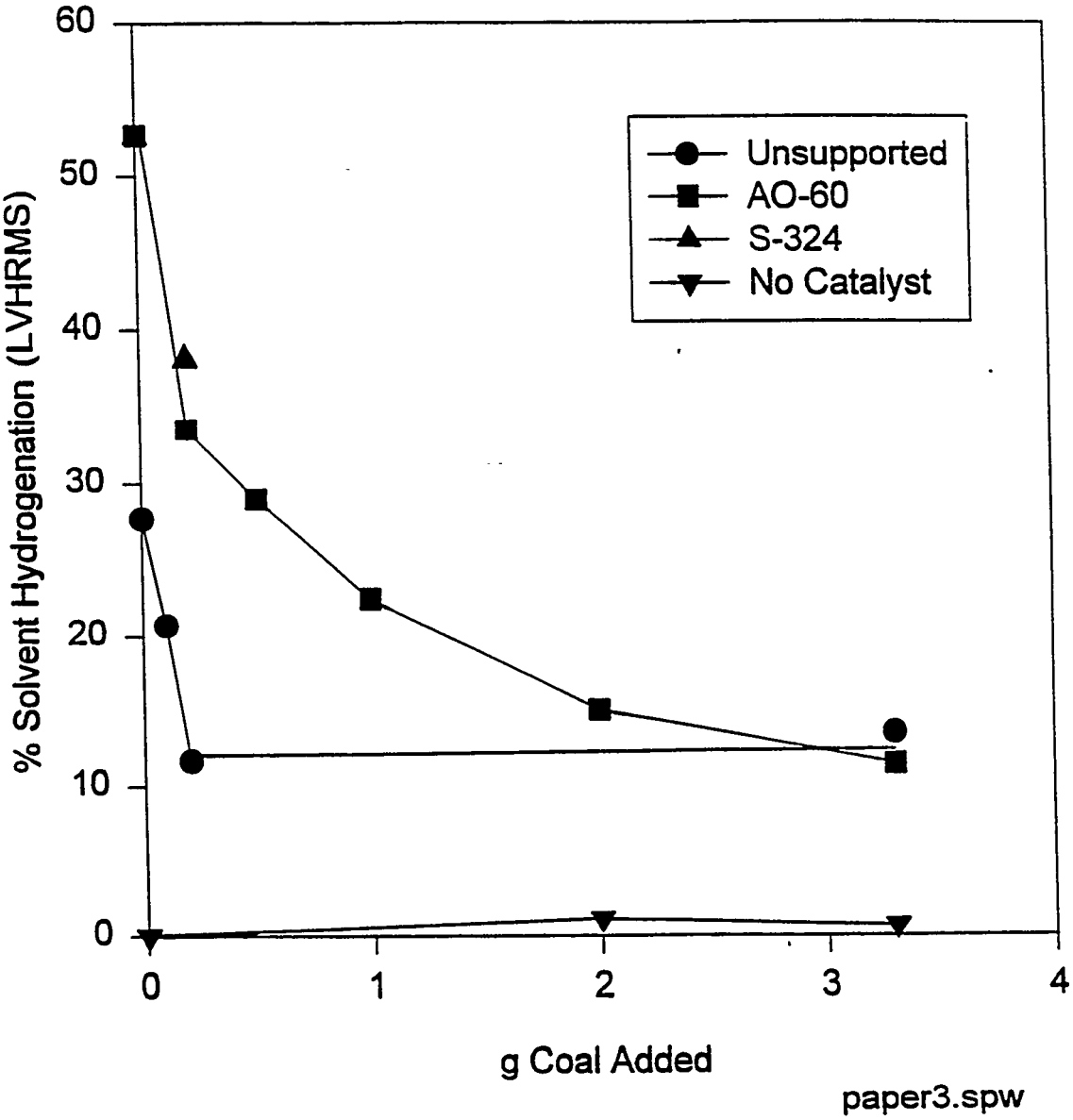

Figure 4: Behavior of Catalyst Exposed to Coal

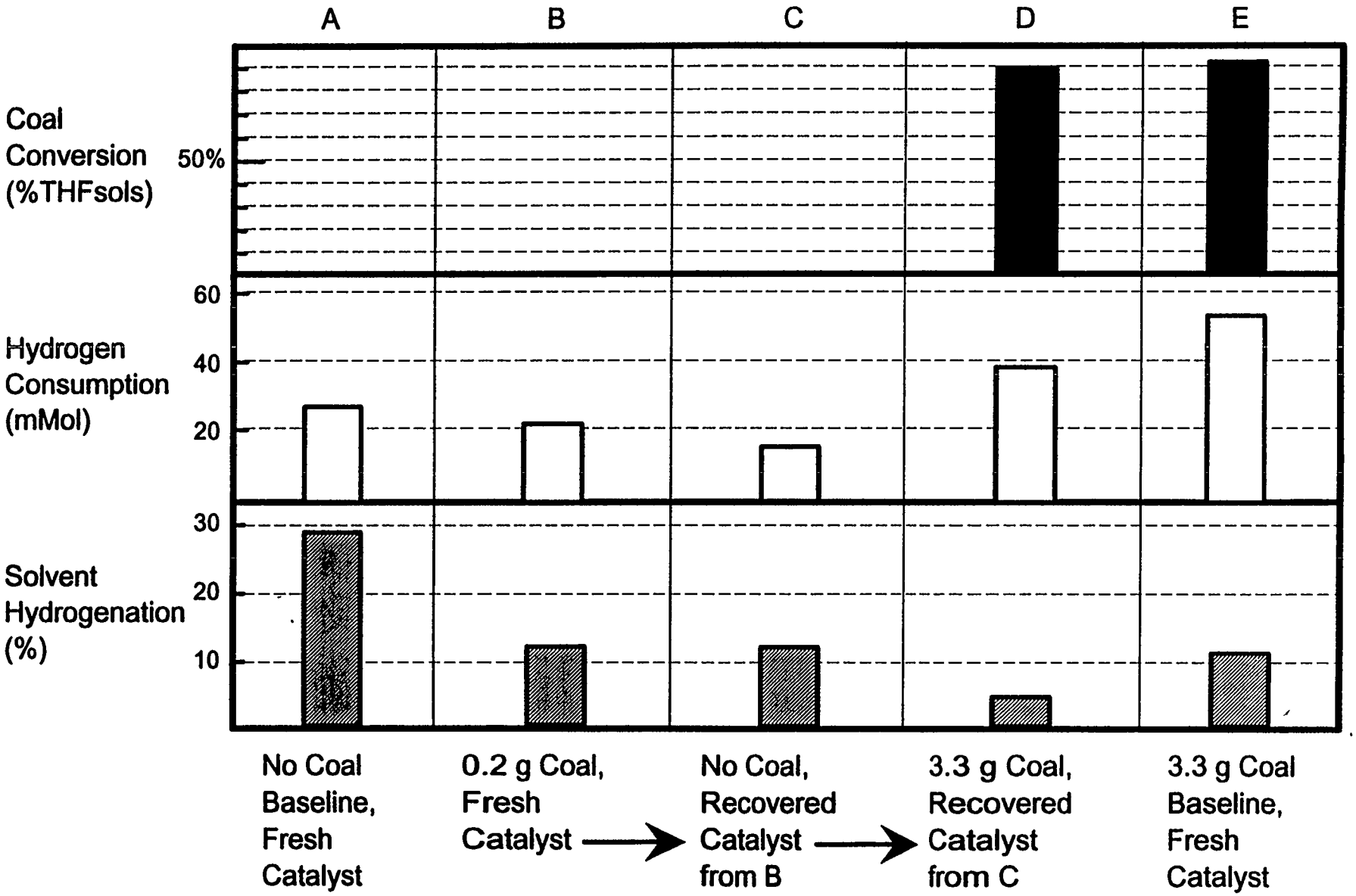

Figure 5: Effect of Pressure and Catalyst Type on Coal Conversion

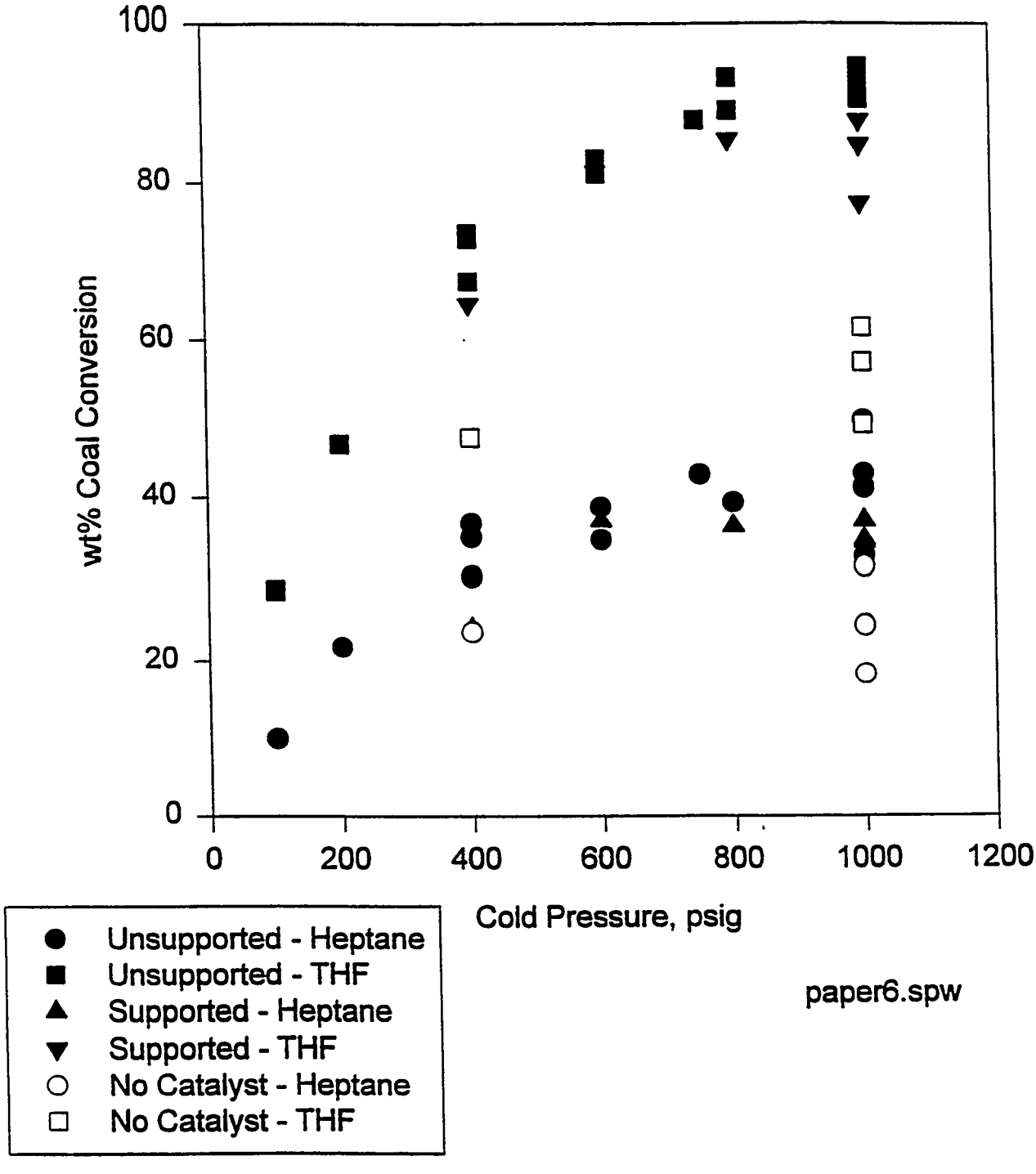

1995 COAL LIQUEFACTION AND GAS CONVERSION CONTRACTORS REVIEW CONFERENCE

Title: Synthesis and Characterization of Fe Colloid Catalysts in Inverse Micelle Solutions

Authors: Anthony Martino, Matthew Stoker, Michael Hicks, Calvin H. Bartholomew, Allen G. Sault, Jeffrey S. Kawola

Organization: Sandia National Laboratories, Albuquerque, NM 87185-0710

Contract No.: DE-AC04-76DP00789

Period of Performance: 10/1/90 - Present

Objective:

Surfactant molecules, possessing a hydrophilic head group and a hydrophobic tail group, aggregate in various solvents to form structured solutions (1-3). In two component mixtures of surfactant and organic solvents (e.g., toluene and alkanes), surfactants aggregate to form inverse micelles. Here, the hydrophilic head groups shield themselves by forming a polar core, and the hydrophobic tails groups are free to move about in the surrounding oleic phase. We have studied the formation of Fe clusters in inverse micelles. Iron salts are solubilized within the polar interior of inverse micelles, and the addition of the reducing agent $LiBH_4$ initiates a chemical reduction to produce monodisperse, nanometer sized Fe based particles. The reaction sequence is sustained by material exchange between inverse micelles. The surfactant interface provides a spatial constraint on the reaction volume, and reactions carried out in these micro-heterogeneous solutions produce colloidal sized particles (10-100Å) stabilized in solution against flocculation by surfactant. We have characterized the clusters with respect to size with transmission electron microscopy (TEM) and with respect to chemical composition with Mossbauer spectroscopy, electron diffraction, and x-ray photoelectron spectroscopy (XPS). In addition, we have tested these iron based clusters for catalytic activity in a model hydrogenolysis reaction. The hydrogenolysis of naphthyl bibenzyl methane is used as a model for coal pyrolysis.

Metal alkoxide reactions (4), the formation of polymer particles (5,6), and the formation of metal (7-12) and semiconductor (13-21) clusters are examples of chemical processes that have been carried out in structured surfactant solutions. The formation of ultra-small metal particles is of particular interest in the area of chemical catalysis. The clusters are high surface area, highly dispersed, unsupported materials. In addition, catalytic enhancement due to unique material properties (i.e. quantum size effects) is possible. Metal clusters prepared by a number of techniques have been studied as potential

catalysts (22). Reactant adsorption and the reactivity in various processes depends strongly on particle size. The effect is not just a matter of surface area, but of a fundamental change in the material's properties as the number of metal atoms per cluster decreases. Pt, Pd, Rh, and Ir particles prepared via inverse micelle techniques (23) have been studied in the hydrogenation and isomerization of but-1-ene (24,25) and the hydrogenolysis and isomerization of hexanes (26). The activity of these catalysts increases when supported, and the selectivity of the colloidal sized particles is a function of the particle size. We are studying iron clusters as potential catalysts in hydrogenation reactions, Fischer-Tropsch synthesis, and coal liquefaction.

Experimental:

Octane and toluene were purchased from Aldrich at 99.9+% purity. Surfactants used include didodecyldimethylammonium bromide (DDAB) from Kodak and butyl-ethylene glycol n-dodecyl ether ($C_{12}E_4$) from Nikkol. Metal salts used include iron(III) chloride hexahydrate from Aldrich and iron(II) tetrafluoroborate hexahydrate from Alfa Chemicals. Lithium borohydride in tetrahydrofuran (2M) was purchased from Aldrich.

Synthesis of Fe Based Colloids: Four different iron samples (FeI, FeII, FeIII, and FeIV) were prepared and studied (Table 1). The reactions and all chemical manipulations are carried out in a glove box under dry, oxygen-free conditions. The synthesis technique is general and specific samples differ only in the type and concentration of salts and surfactant added to the apolar solvents. First, the inverse micelle solutions are prepared by adding surfactant to the solvents (i.e. DDAB in toluene, $C_{12}E_4$ in octane). Then, the metal salts are introduced and the precursor salt solutions are mixed overnight on a stirring plate to assure complete solubilization. Transparent yellow Fe salt solutions are formed. 2M $LiBH_4$/THF solution is directly injected into the salt solutions under rapid stirring to initiate the reduction of iron. The reaction is run at a 3:1 molar ratio of $[BH_4^-]$:$[Fe^+]$. The reacted Fe solutions turn black. The colloids formed in solution are stabilized by surfactant indefinitely.

Further manipulation of the iron in DDAB/toluene solutions produces iron powders. When approximately 15 vol. % methanol is added to the colloidal solution, the surfactant is washed from the colloid surface, and the particles aggregate. A black precipitate forms below a clear and transparent solution after several hours. The precipitate is separated from the solution by centrifugation and washed with methanol. The process is repeated two or three times, and the powder is finally dried (FeIII). We have re-coated the particles with poly(vinylpyrrolidone) (MW = 40,000) by adding the polymer to an iron powder and methanol mixture. The particles remain in solution for days without the

presence of surfactant. Removing the methanol produces Fe particles embedded in PVP powder (FeIV). Replacing surfactant with polymer allows us to control the ratio of stabilizing agent to metal, remove the relatively volatile surfactant for x-ray photoelectron spectroscopy studies, and protect the particles from oxidation during air exposure.

Table 1. Listing of the samples used in this study.

NAME	DESCRIPTION
FeI	0.01M $FeCl_3$, 10 wt. % DDAB/toluene
FeII	0.01M $Fe(BF_4)_2$, 10 wt. % $C_{12}E_4$/octane
FeIII	FeI powder from methanol washing
FeIV	0.03M $FeCl_3$, 10 wt. % DDAB/toluene, re-dispersed with PVP and re-dried

Characterization of the Colloids: Particle size and composition in the colloidal solutions are characterized with transmission electron microscopy (TEM) and electron diffraction. These tests are performed with a Joel 1200EX electron microscope. The colloidal solutions are applied directly on a holy carbon grid, and the solution is wicked away by adsorbent towels under the grid leaving the particles on the grid. Transfer of the particle coated grid into the microscope briefly exposes the sample to air.

Mossbauer spectroscopy is used to determine the composition of the iron in the PVP coated iron powders (FeIV). The Mossbauer Spectrometer (Austin Science) and its operation are described in detail elsewhere (27). The spectra are obtained using a 60 mCi ^{57}Co in palladium foil source and computer fitted to Lorentzian lines with a least-squares optimization procedure. The spectra are corrected during the collection procedure to remove the curved background of instrumental origin, and resonant absorption areas are found from integration of the background curvature-corrected spectra. With the use of an absolute laser velocity calibrator it is possible to measure isomer shifts to within an absolute accuracy of +/-0.005 mm/s. A particle embedded polymer powder was tested under four conditions: at room temperature without air exposure, at room temperature after air exposure, at -183°C, and at -183°C with an applied magnetic field of 11kGauss.

X-ray photoelectron spectroscopy (XPS) is used to determine the composition of the iron particles in solution (FeI), as powders (FeIII), and as powders re-dispersed with PVP in methanol (FeIV). To prepare samples of the surfactant stabilized iron particles suitable for XPS analysis, the surfactant/particle solution is evaporated to concentrate the particles and a drop of the resulting solution is placed on a Ta foil and allowed to evaporate

completely overnight. For analysis of the washed iron powders, the particles are re-dispersed in methanol and a drop of the dispersed solution is placed on a Ta foil and again allowed to dry. Finally, for the particles embedded in PVP, the PVP matrix is dissolved in methanol and a drop of the resulting solution placed on a Ta foil and the methanol evaporated to form a PVP film. All samples are prepared and mounted on a sample holder inside a dry, oxygen free glove box. As with microscopy, transfer of the sample to the XPS chamber requires brief exposure to air. XPS is performed using Al K_α radiation, and an analyzer resolution of 1 eV.

Complexometric experiments were used to determine the extent of reaction of the iron salts upon reduction. 1, 10 phenanthroline forms a complex with ionic Fe^{2+} species that has a distinctive maximum at 530 nm. The peak is followed before and after reaction with UV-visible spectrophotometry (Hewlett-Packard 8452A diode array spectrophotometer) by adding 1, 10 phenanthroline to the Fe salt precursor solutions and reacted Fe colloid solutions. The quantity and nature of the Fe^{2+} species present is determined. Two salt solutions were studied: $FeCl_3$ and $Fe(BF_4)_2$ in 10 wt. % $C_{12}E_4$ / octane.

Finally, BET surface area analysis of the methanol washed iron powder was carried out with a Quantachrome Autosorb-6 surface analysis apparatus.

Naphthyl Bibenzyl Methane (NBM) Hydrogenolysis: Hydrogenolysis testing of NBM has been developed as a model reaction for coal liquefaction (28). We add 100 mg of NBM, 400 mg of the hydrogen donating solvent 9,10 dihydrophenanthrene (9, 10 DHP), and up to 15 wt. % catalyst on an NBM basis to a 10 ml flame sealed glass test tube. If used, 15 mg of elemental sulfur is added. The test tube is sealed under ambient air pressure. The tube is placed in a 400°C sand bath for one hour. Previously, NBM hydrogenolysis has been used to study the selectivity of catalysts for five different cleavage reactions (28). We do not quantify the selectivity of the catalysts used here. Conversion is calculated as the ratio of the molar sum of all products to the initial amount of NBM. The products are worked up in THF and analyzed by gas chromatography. Methanol washed Fe powders were tested as catalysts. These results were compared to the commercial catalyst Shell 324 (12.4 wt. % Mo, 2.8 wt. % Ni on Al_2O_3).

Accomplishments:

Transmission electron micrographs show that the product of the reaction is highly dispersed nanometer sized particles of uniform size and shape (Figure 1). The number average diameter by TEM is 1.5 +/- 0.2 nm (FeI). Fe particle size as determined by TEM shows no discernible trend and is roughly constant in the ranges of 0.001M - 0.01M $FeCl_3$

salt concentration and 1-10 wt. % DDAB in toluene. In this range, the average particle diameter is 2.4 nm. The methanol extracted Fe powder characterized by TEM and BET surface analysis consist of agglomerated particles (FeIII). Large agglomeration structures approximately 100 nm in size are observed. These structures consist of the ultra small particles (approximately 2 nm in diameter) flocculated together. Multi-point BET analysis gives a surface area of 156 m^2/gm for this sample. The degree of re-dispersion upon addition of PVP has not been determined. As the particles are stable in solution for only a couple of days with PVP, it is likely that the degree of dispersion is not as great as after the original reaction in the presence of surfactant.

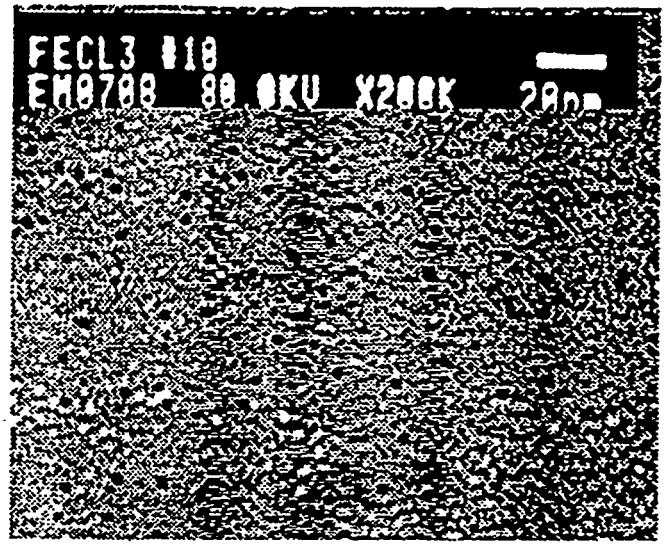

Figure 1. TEM of FeI particles. The number average diameter of the particles shown is 1.5 +/- 0.2 nm.

Mossbauer spectroscopy completed on the particle embedded polymer powder indicates the presence of three different forms of iron (FeIV). The spectrum for the powder at 21°C before exposure to air (Figure 2) is fit with two doublets and a singlet (corresponding Mossbauer parameters are found in Table 2). We assign the first doublet to the presence of fine superparamagnetic particles of FeB, the second doublet to the presence of Fe(II)BO_x, and the singlet to the presence of superparamagnetic Fe metal. On the basis of spectral areas, the iron phases are present at 60, 10, and 30 mole %, respectively with the species order listed above. The mole percentages are based on equal recoil-free fractions of each phase, and this assumption is only approximately correct in the case of small clusters. There is no discernible change in the spectra or fit after the sample is exposed to air. The iron is apparently protected from oxidation by the polymer. The spectrum of the sample at -183°C after exposure to air is quite different from the room temperature spectrum (Figure 3). It appears that the two large peaks in the room

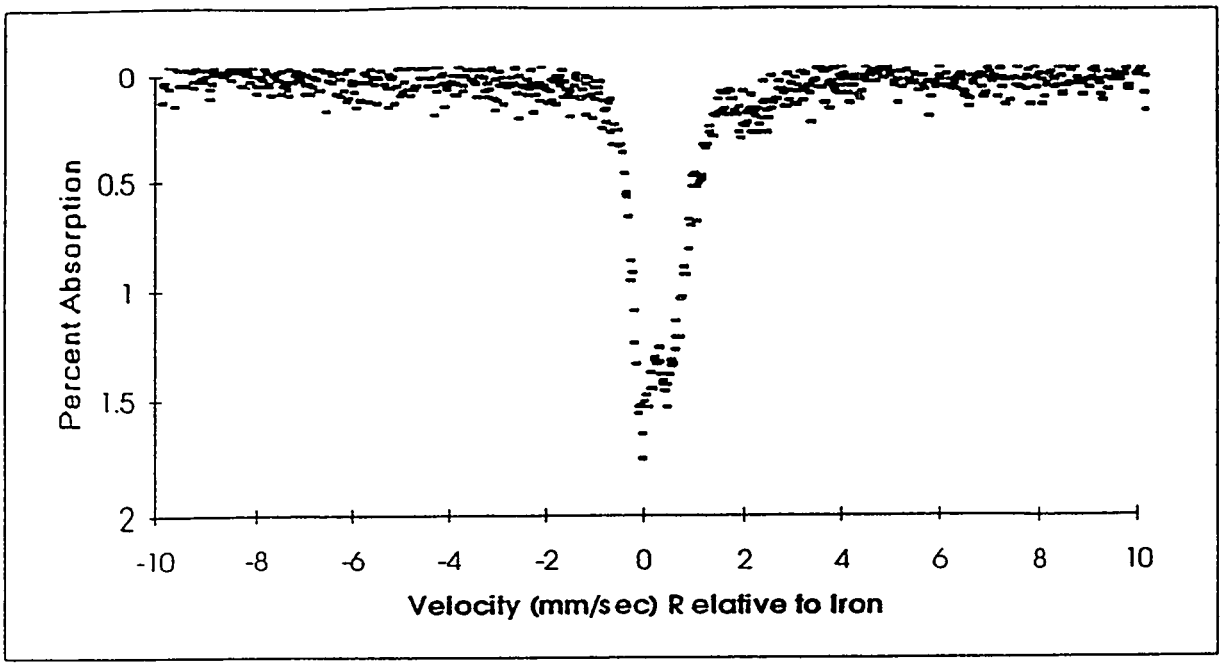

Figure 2. Mossbauer Spectrum of FeIV. T = 21°C. Not exposed to air. Parameters listed in Table 2.

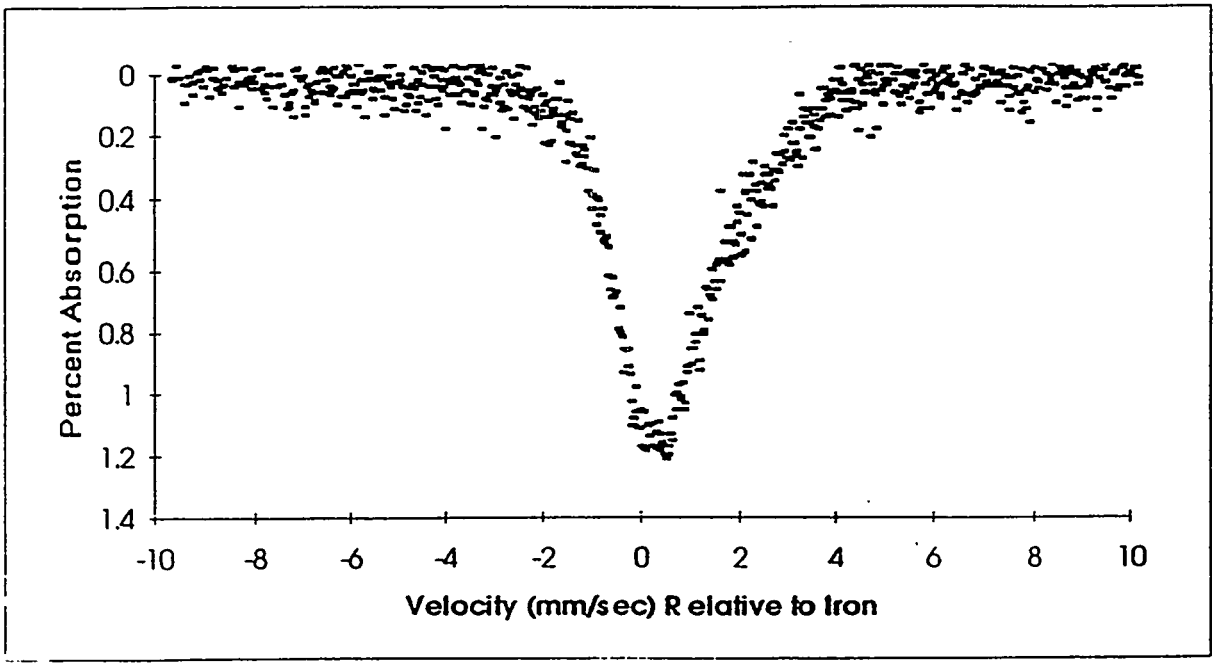

Figure 3. Mossbauer Spectrum of FeIV. T = -183°C. Exposed to air. Parameters listed in Table 3.

temperature spectrum have broadened. The broadened spectrum is fit with a sextet and two doublets (Table 3). The sextet has a magnetic hyperfine splitting of 128 kOe and an isomer shift of 0.35 mm/sec consistent with the presence of superparamagnetic FeB. When a magnetic field is applied to the sample, the spectrum is further broadened.

Table 2. Mossbauer Parameters for FeIV (Figure 2). T = 21°C, sample not exposed to air.

Assignment	Isomer Shift[a] (mm/sec)	Quadrupole Splitting (mm/sec)	Magnetic Hyperfine Splitting (kOe)	% Area
Doublet 1	0.450	0.27	----	60.4
Doublet 2	1.108	2.11	----	10.4
Singlet	-0.136	----	----	29.2

[a]relative to iron

Table 3. Mossbauer Parameters for FeIV (Figure 3). T = -183°C, sample exposed to air.

Assignment	Isomer Shift[a] (mm/sec)	Quadrupole Splitting (mm/sec)	Magnetic Hyperfine Splitting (kOe)	% Area
Sextet	0.98	0.065	94.0	43.5
Doublet	0.29	0.87	----	56.5

[a]relative to iron

Selected area electron diffraction (FeII) and XPS (FeI, FeII, FeIV) give complementary results. Diffraction patterns of particles deposited on the microscope grid are consistent with the presence of α-Fe. The electron diffraction results do not indicate the presence of any crystalline iron oxides, borides, or borates. A diffraction pattern consistent with the presence of crystalline B_2O_3 as a reaction by-product is also detected. XPS of *in-situ* colloids in solution, methanol washed powders, and particle embedded polymer powders detects an undetermined Fe^{2+} species only.

Complexometric experiments indicate that the reaction is complete upon the addition of $LiBH_4$. In the $Fe(BF_4)_2$ precursor solutions, the Fe^{2+} species complexes with 1,10 phenanthroline, and the distinctive peak is observed at 530 nm. The peak is non existent in $Fe(BF_4)_2$ samples after the addition of $LiBH_4$ indicating the reaction goes to completion. In $FeCl_3$ precursor solutions, no complex is formed with the Fe^{3+} species. After reaction, a slight peak at 530 nm is detected indicating some conversion of Fe^{3+} to Fe^{2+} but too little to quantify.

Hydrogenolysis of naphthyl bibenzyl methane (NBM) was tested with the methanol extracted Fe powder (FeIII) with and without sulfur additives and compared with the commercial catalyst Shell 324. In each experiment we monitored the percentage recovery of the reactant NBM and the percentage conversion to products (28) by gas chromatography. In each experiment we also monitored the percentage recovery of the hydrogen donating solvent 9, 10 DHP and the percentage converted to its dehydrogenated form phenanthrene. In an average of six runs, NBM was recovered at nearly 97+/-3% in thermal runs (no catalyst) and no product was obtained (Figure 4). Some NBM was converted to products in thermal runs with added elemental sulfur. Little 9, 10 DHP is dehydrogenated to phenanthrene in the thermal runs. Methanol extracted Fe powder as catalyst decreased the amount of NBM recovered to 87% and to 75% with added S. Product recovery correspondingly increased. In the Fe sample tests, hydrogens are given up to the hydrogenolysis products, and some 9, 10 DHP is dehydrogenated to phenanthrene.

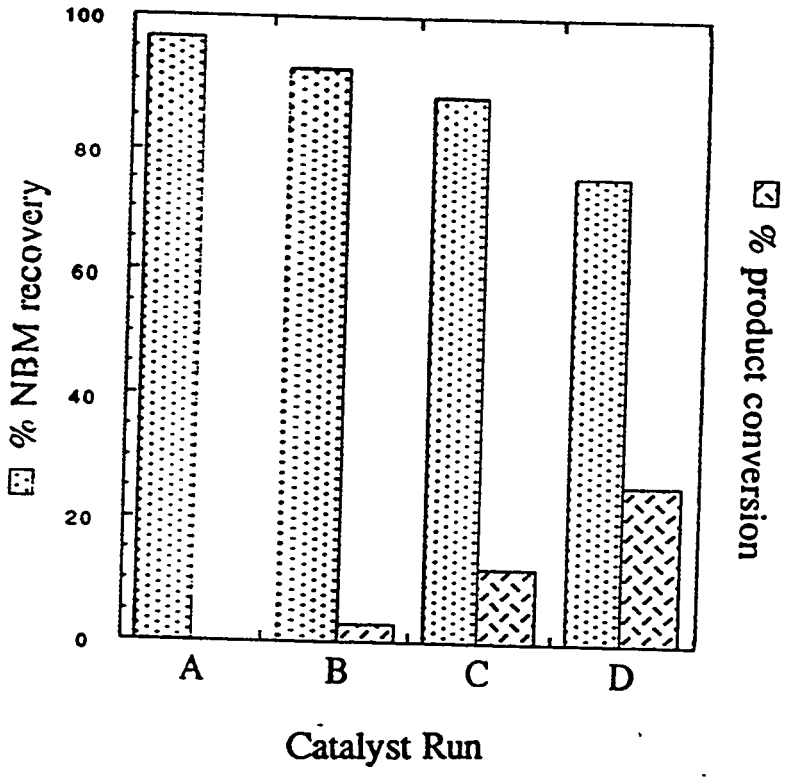

Figure 4. NBM hydrogenolysis results for Fe clusters. (a) The percentage of reactant recovered and percentage converted to product. A = thermal average; B = thermal with elemental S average; C = FeIII (~ 15% active metal basis); D = FeIII with elemental S (~ 15% active metal basis).

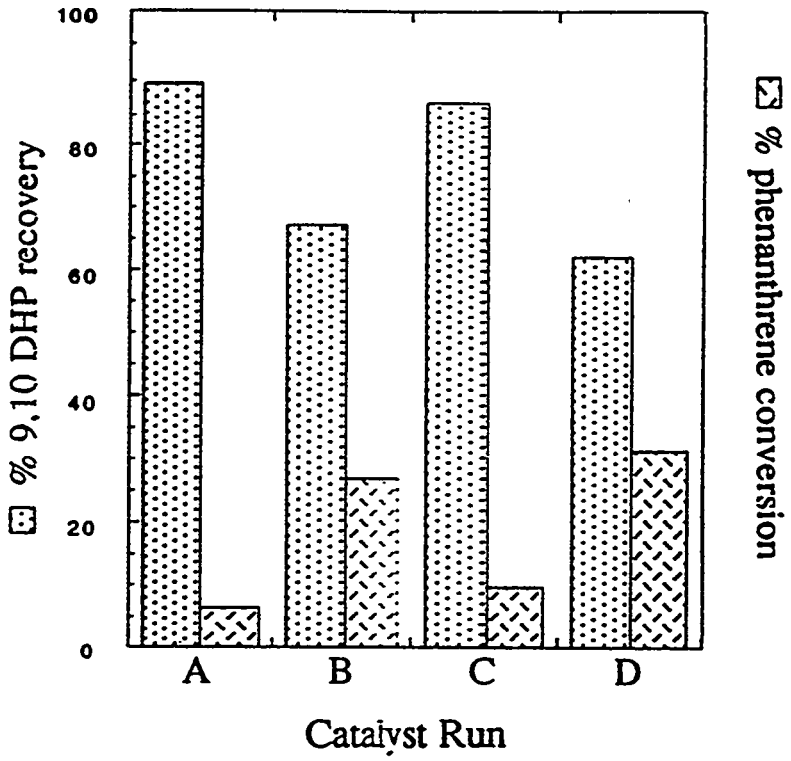

Figure 4. NBM hydrogenolysis results for Fe clusters. (b) The percentage of the hydrogen donating solvent 9, 10 DHP recovered and the percentage dehydrogenated to phenanthrene. A = thermal average; B = thermal with elemental S average; C = FeIII (~ 15% active metal basis); D = FeIII with elemental S (~ 15% active metal basis).

Much higher product yields were obtained with Shell 324 (Figure 5). Higher conversions of 9,10 DHP to phenanthrene are consistent with these higher yields. In order to study the effect of surfactant on catalytic activity, we doped Shell 324 with increasing amounts of DDAB. As the Shell 324:DDAB mass ratio decreases, the trends in reactant recovery and product conversion move back to the thermal results indicating loss of catalytic activity. Initially the conversion of 9, 10 DHP to phenanthrene moves toward the thermal results as well. At the lower Shell 324 : DDAB ratios, however, this trend reverses itself and nearly all of the 9,10 DHP is converted to phenanthrene.

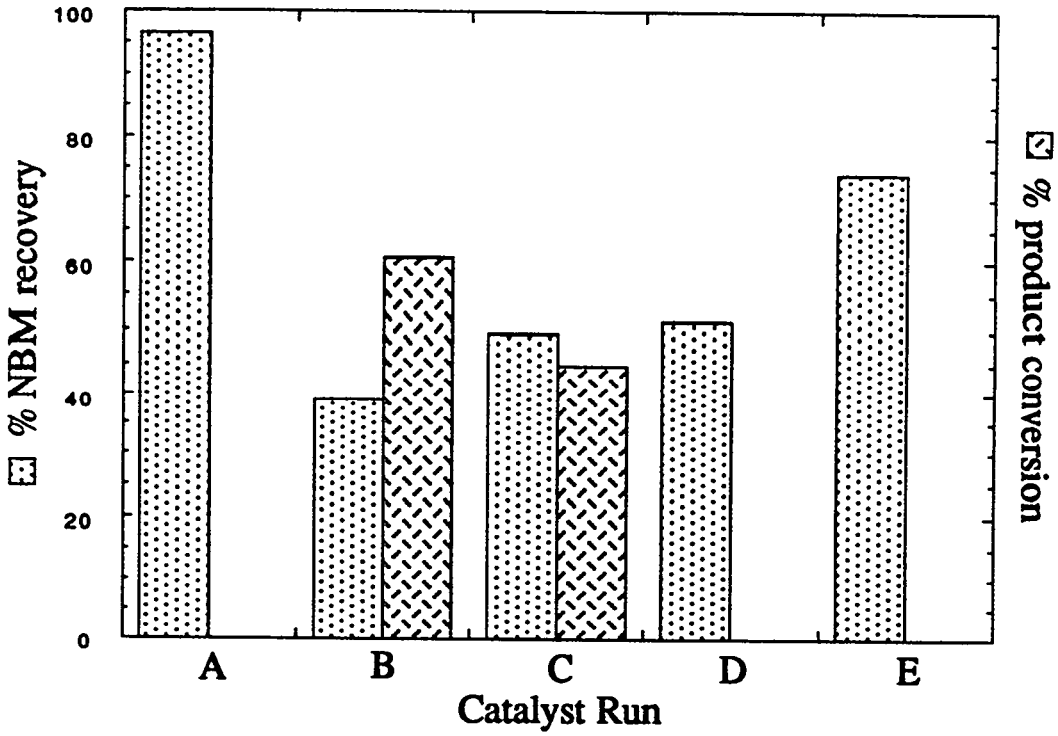

Figure 5. NBM hydrogenolysis results for Shell 324 as a function of DDAB surfactant doping. (a) The percentage of reactant recovered and percentage converted to product. A = thermal average; B = Shell 324; C = Shell 324:DDAB =1:4; D = Shell 324:DDAB = 1:20; E = Shell 324:DDAB = 1:50. Active metal basis ~ 15% for all catalyst runs.

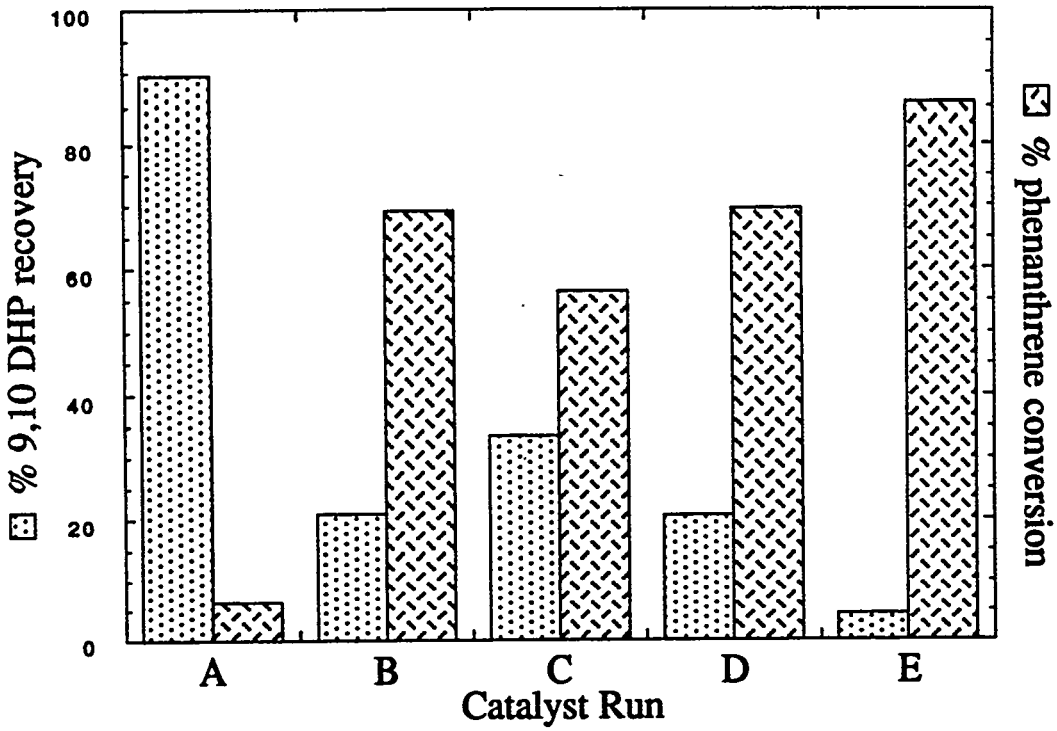

Figure 5. NBM hydrogenolysis results for Shell 324 as a function of DDAB surfactant doping. (b) The percentage of the hydrogen donating solvent 9, 10 DHP recovered and the percentage reduced to phenanthrene. A = thermal average; B = Shell 324; C = Shell 324:DDAB =1:4; D = Shell 324:DDAB = 1:20; E = Shell 324:DDAB = 1:50. Active metal basis ~ 15% for all catalyst runs.

Conclusions:

Introduction of $LiBH_4$ to iron salt containing inverse micelle solutions causes immediate reduction of the salt to form nanometer sized, highly dispersed particles of equal size and shape. $LiBH_4$ enters the surfactant-oil solution and is solubilized within the inverse micelle structure. The reaction is initiated and is sustained through material exchange between inverse micelles. After the particle growth has equilibrated, the surfactant stabilizes the particles and prevents flocculation and precipitation. The final particle size of nanometer sized clusters formed in inverse micelles depends on a complicated nucleation and growth process (29). Inverse micelles effect this process primarily in two ways: (1) diffusion of the reacting nucleation sites and ions is governed by exchange rates between micelles and (2) the critical nucleation size depends inherently on the size of the inverse micelles. Size dependence of metal borides, CdS, and CdSe clusters

produced in inverse micelles has been discussed previously (12-21). The Fe particles synthesized in DDAB/toluene mixtures showed no size dependence by TEM on the salt to surfactant concentration ratio within the range studied.

Mossbauer spectroscopy, electron diffraction, and XPS results indicate three products are formed by the reduction of iron salts with $LiBH_4$ in inverse micelle solutions. Mossbauer spectroscopy detects three phases: FeB, $Fe(II)BO_x$, and metallic Fe in approximate mole percentages of 60%, 10%, and 30%, respectively. Mossbauer results at low temperatures and in the presence of a magnetic field further support the presence of FeB. The spectral broadening is consistent with longer magnetic relaxation times in a superparamagnetic species, and the sextet has a hyperfine field consistent with FeB. In the limit of a sufficiently large magnetic field or at sufficiently low temperatures, the spectrum would resolve into six lines.

Electron diffraction gives strong evidence for the presence of α-Fe, and is consistent with the Mossbauer results showing the presence of metallic Fe. The FeB phase is not detected by diffraction because of relatively weak scattering. It is unlikely that the manipulation of the colloids in solution (tested in electron diffraction) to produce the particles in PVP (tested in Mossbauer) results in the formation of FeB and $Fe(II)BO_x$. Further Mossbauer experiments are planned, however, on particles not manipulated with methanol and PVP.

XPS of *in-situ* colloids in solution, methanol washed powders, and particle embedded polymer powders detects an undetermined Fe^{2+} species. XPS examines only the particles that protrude above the PVP surface as the Fe 2p photoelectrons can only escape from within 3-4 nm of the PVP film surface. The protruding particles are not protected from oxidation upon exposure to air, and the XPS detected phase is likely a mixture of oxidized FeB and α-Fe. The B 1s XPS spectrum confirms the presence of oxidized boron, but does not show any evidence for borides. Metallic iron detected by electron diffraction even though the samples are exposed to air is not detected by XPS. As XPS surveys only particle surfaces, perhaps an oxidized shell surrounds a small core of Fe^0 species (FeB and/or α-Fe).

Hydrogenolysis of NBM indicates catalytic activity with FeIII. A more than linear increase in activity with added S indicates that there is a synergistic effect between the Fe and S.

Catalyst activity of Shell 324 far exceeds the activity of the iron based clusters. Doping Shell 324 with surfactant illustrates the effect of surfactant on catalyst activity. When Shell 324 is doped with surfactant, catalyst activity decreases (Figure 5). The behavior of the hydrogen donating solvent indicates two mechanisms are at work. At low

surfactant concentrations, a decrease in product conversion and a decrease in the amount of 9, 10 DHP dehydrogenated to phenanthrene indicates less activity due to a chemical or steric poisoning of the catalyst. At high surfactant concentrations, we propose that a decrease in NBM conversion and an increase in the amount of 9, 10 DHP dehydrogenated to phenanthrene indicates that the thermal pyrolysis products of the surfactant (observed by GC) scavenge the hydrogens from the donor solvent.

References:

(1) Langevin, D., Accounts of Chemical Research, 21, 255 (1988)
(2) Fendler, J.H., Chem. Rev., 87, 877 (1987)
(3) Henglein, A., Chem. Rev., 89, 1861 (1989)
(4) Jean, J.H. and Ring, T.A., Colloids and Surfaces, 29, 273 (1988)
(5) Paleos, C.M., Chemical Society Reviews, 14, 45
(6) Perez-Luna, V.H., Puig, J.E., Castano, V.M., Rodriguez, B.E., Murthy, A.K., and Kaler, E.W., Langmuir, 6, 1040 (1990)
(7) Barnickel, P. and Wokaun, A., Molecular Physics, 69, 1 (1990)
(8) Gobe, M, Kon-No, K., Kandori, K. and Kitahara, A., Journal of Colloid and Interface Science, 93, 293 (1983)
(9) Kurihara, K., Kizling, J., Stenius, P., and Fendler, J.H., J. Am. Chem. Soc., 105, 2574 (1983)
(10) Nagy, J.B., Gourgue, A. and Derouane, F.G., Preparation of Catalysts III, eds. Grange, P., Jacobs, P.A., Elsevier Science Publishers,193 (1983)
(11) Torigoe, K. and Esumi, K., Langmuir, 8, 59 (1992)
(12) Nagy, J.B., Colloids and Surfaces, 35, 210 (1989)
(13) Lianos, P. and Thomas, J.K., Journal of Colloid and Interface Science, 117, 505 (1987)
(14) Lianos, P. and Thomas, J.K., Chemical Physics Letters, 125, 299 (1986)
(15) Modes, S. and Lianos, P., J. Phys. Chem., 93, 5854 (1989)
(16) Petit, C. and Pileni, M.P., J. Phys. Chem., 92, 2282 (1988)
(17) Petit, C., Lixon, P. and Pileni, M.P., J. Phys. Chem., 94, 1598 (1990)
(18) Motte, L., Petit, C., Boulanger, L., Lixon, P. and Pileni, M.P., Langmuir, 8, 1049 (1992)
(19) Pileni, M.P., Motte, L. and Petit, C., Chem. Mater., 4, 338 (1992)
(20) Robinson, B.H., Towey, T.F., Zourab, S., Visser, A.J.W.G. and van Hoek, A., Colloids and Surfaces, 61, 175 (1991)
(21) Towey, T.F., Khan-Lodhi, A. and Robinson, B.H., J. Chem. Soc. Faraday Trans., 86, 3757 (1990)
(22) Moskovits, M., Annu. Rev. Phys. Chem., 42, 465 (1991)
(23) Boutonnet, M., Kizling, J., Stenius, P. and Maire, G., Colloids and Surfaces, 5, 209 (1982)
(24) Boutonnet, M., Kizling, J., Touroude, R., Maire, G. and Stenius, P., Applied Catalysis, 20, 163 (1986)
(25) Boutonnet, M., Kizling, J., Mintsa-Eya, V., Choplin, A., Touroude, R., Maire, G. and Stenius, P., Journal of Catalysis, 103, 95 (1987)
(26) Boutonnet, M., Kizling, J., Touroude, R., Maire, G. and Stenius, P., Catalysis Letters, 9, 347 (1991)
(27) Neubauer, L.R., Ph. D. Dissertation, Brigham Young University, (1986)
(28) Faracasiu, M.; Smith, C. ACS Preprints Fuel Chemistry Division, 35, 404, (1990)
(29) Steigerwald, M.L. and Brus, L.E., Annu. Rev. Mater. Sci., 19, 471 (1989)

AUTHORS INDEX

AUTHORS INDEX